GROUNDWATER EXPLORATION IN GEOLOGICALLY COMPLEX AND PROBLEMATIC TERRAIN – CASE STUDIES (VOLUME 2)

K Sami • I Neumann • D Gqiba • G de Kock • G Grantham

WRC Report No. 966/2/02

Water Research Commission

Groundwater Exploration In Geologically Complex And Problematic Terrain – Case Studies (Volume 2)

by

K. Sami, I. Neumann, D. Gqiba, G. de Kock, G. Grantham

Council for Geoscience
Private Bag X112
Pretoria 0001
South Africa

Final Report to the Water Research Commission for the Project
"Groundwater Development For Rural Water Supply In Complex And Problematic Terrain: An Assessment Of Geological Controls, Geophysical Exploration Methods And The Quantification Of Exploitation Potential"

Project Leader: K. Sami
WRC Report No.: 966/2/02
ISBN No: 1 86845 863 6

April 2002

EXECUTIVE SUMMARY

1. Background

The Department of Water Affairs and Forestry has identified the provision of sustainable water and sanitation services to all as being one of its top priorities (DWAF, 1994). The challenge of providing developing rural areas in South Africa with sufficient potable water is substantial, especially where settlement is not densely concentrated and the ability to pay is low. The water requirements of these settlements can be met most cost-effectively from groundwater. The provision of these regions with sufficient potable water is complicated by the large backlog in water delivery, which results in pressure for rapid service delivery at the expense of time-consuming groundwater exploration methods.

Previous studies (King, 1997) have shown that some of the greatest water needs occur in regions underlain by fractured basement aquifers with complex hydrogeology and where the exploitation potential of groundwater has been thought to be low due to historically low drilling success rates or the high frequency of low yielding boreholes. Groundwater exploration success rates in these environments have been relatively low due to inappropriate exploration or interpretation methods resulting from an incomplete understanding of the geohydrology.

The current paradigm of groundwater exploration in South Africa, as well as in many other places in Africa, is based on a geophysical approach, where most boreholes are sited on anomalies identified from magnetic or electromagnetic traverses, often with little or no understanding of the structural geology of the target area. In many areas of complex hydrogeology this technique has proved to be unsuccessful for a variety of reasons. Specific causes that have been identified include:

* an inadequate understanding of the occurrence of groundwater and the factors affecting permeability in these terrains, leading to inappropriate exploration planning;
* siting of boreholes on geophysical anomalies without a conceptual understanding of the geological framework and how it affects the geophysical response, or siting boreholes without an adequate interpretation of the geophysical data;
* the use of only one geophysical method, which makes the interpretation of anomalies difficult or unsubstantiated;
* the use of inappropriate geophysical methods for the specific terrain; and
* inappropriate or insufficient quantification of the sustainable yield of boreholes due to inadequate test pumping procedure or analysis methods.

As the demand for groundwater grows and the more obvious aquifers and target features become increasingly exploited, it can be expected that further development will have to consider alternative targets in such problematic and complex fractured geological environments. Significant savings in exploration and especially drilling costs can be realised if success rates could be improved. However, it is essential not to consider exploration in isolation from resource evaluation. If these complex terrain's are to be developed in a sustainable manner, the importance of quantifying groundwater resources will be magnified due to the their low potential.

To improve the borehole success rate in these terrains, and to develop groundwater resources in a sustainable manner, a multi-disciplinary approach is needed. This approach must incorporate:

1) an understanding of the structural geology and its influence on the occurrence of groundwater so that target features can be identified;
2) the identification of appropriate methods and interpretative techniques to delineate target features in the field;
3) and the use of simple yet effective groundwater resource evaluation methods.

The Council for Geoscience undertook this project to re-evaluate the groundwater resources of some of these regions using a rigorous scientific approach, with the objective of establishing a more successful exploration strategy.

A multidisciplinary approach was followed where structural geological mapping, tectonics, strain analysis, LANDSAT image interpretation and geophysical methods were combined to unravel the geodynamics of a region and to identify geological structures where groundwater could be located. These methods include:

1) the identification and categorisation of lineaments observed on LANDSAT using various digital filtering techniques into strike-frequency and strike-length plots to identify preferential structural orientations;
2) structural mapping on a regional scale to identify tectonic processes given the geological and deformation history;
3) structural mapping of joints on an outcrop scale to identify compressional and extensional orientations through strain analysis; and
4) geophysical exploration of identified potential water bearing structures using magnetics, resistivity and electromagnetics.

Data collection for exploration is often costly and time consuming, hence it is important that any proposed techniques be fully analysed to determine their practical viability. Consequently, a financial analysis of the proposed methodology is presented, demonstrating that, although exploration costs of the adopted approach are higher, the ultimate establishment costs per successful water point and the costs of the water are dramatically reduced compared to conventional methods due to greatly improved success rates and significantly higher yields. These results suggest that it is cost effective to undertake groundwater exploration in a scientific manner, whether only successful points are required for hand pumps, or where high yields are required for reticulated motorised schemes.

From these results, a suggested method for exploration has been formulated to assist with undertaking regional exploration programmes.

2. Research Objectives

The primary objective of this project is to investigate the development potential of groundwater in problematic or complex terrain where the demand for water for rural communities is expected to grow, and to develop guidelines for groundwater exploration and development in these environments. The supporting objectives are to:

- investigate the occurrence of groundwater and the geological and structural controls that distinguish high yielding features from those that have low potential;

- evaluate the ability of currently used geophysical methods to distinguish or delineate target features;
- quantify the exploitation potential of groundwater and evaluate methods for estimating sustainable aquifer and borehole yields;
- and to develop guidelines for groundwater exploitation in these environments.

The geological evaluation of target features and the guidelines for groundwater exploration will assist water practitioners with siting boreholes and interpreting geophysical data. Furthermore it will reduce the use of inappropriate geophysical methods and/or the siting of boreholes based on an incorrect geophysical interpretation. This will reduce the frequency of incorrectly sited boreholes and increase the drilling success rate.

The evaluation of methods to estimate sustainable yield will assist consultants and implementing agents with planning pumping tests and recommending pumping rates so that groundwater abstraction does not exceed sustainable yield of the aquifer.

3. Research Areas

Field data is provided from 4 study areas in South Africa. The four research areas were selected on the basis of the following criteria:

The area is densely populated rural region with underdeveloped infrastructure and services and has been identified as a critical water deficit area by DWAF.

Water scarcity is a serious problem and the area and relies mostly on springs, rivers, hand-dug wells and some boreholes. Groundwater would be a preferred water option in the area because of its generally availability even in drought situations and its relatively good quality.

The areas are underlain by fractured bedrock aquifers where success rates and borehole yields have been historically low, yet high yielding holes are present suggesting that suitable hydrogeological target features do exist.

The areas which have been studied include: the Natal Metamorphic Province of the KwaZulu-Natal south coast in the vicinity of Mapumulo; regions underlain by thick Dwyka Group rocks inland of the south coast in the vicinity of Harding; the greenstone belt of the Barberton Supergroup in the vicinity of Tjakastad, and the basement rocks and greenstones of the Limpopo Mobile Belt in the vicinity of Alldays.

4. Dwyka Group

The area of investigation is situated immediately north of the Transkei border, about 12 km southeast of Harding in KwaZulu-Natal. Water demand in the study area is primarily for domestic purposes and partly for small-scale agricultural activity. Currently, water supply needs are met mostly from upland springs, rivers in the valley bottoms, and boreholes equipped with hand pumps. However, groundwater could play an important role, as it is a reliable water source, even in drought situations, and is generally of good quality compared to other water sources in the area. Water supply provision is complicated by the fact that settlement is concentrated on hill tops and extremely limited access exists to low lying areas, where a more assured water supply could be located. The extreme topography, however, would create static pumping heads of over 300 m; hence, groundwater exploration is predominantly restricted to the hill top regions.

The tillite has a very low permeability and forms a cover of up to 450 m thickness in the area, which prevents drilling through the formation into a more consistent aquifer. This fact is reflected in the very poor historical success rate in the area, with 84 % of the holes being dry.

These unfavourable hydraulic properties explain the relatively low yield of the aquifer. An average blow yield of 0.14 l/s can be expected in wet boreholes; however, this is not sustainable on a continuous basis since fractures in the area are seldom interconnected. Hence long-term sustainability is limited for all but very low pumping rates. The investigations suggest that high yielding boreholes can only be found at sites where several interconnected fractures exist to enlarge the general low permeability of the formation. The massive nature of the rock and the brittle calcite filled fractures suggest that the formation may be a candidate for hydrofracturing to increase yields and fracture connectivity.

The research study showed that successful groundwater exploration for the area is possible, but should be limited to establish hand pump schemes. In addition, the water quality of the Dwyka tillites is suitable for domestic consumption. An evaluation of the structural geology and the hydrogeological conditions of the area together with a suitable geophysical method for the environment pushed the drilling success rate up from a historical 12 % to 50 %. The unfavourable hydraulic properties of the tillite however, limit the yield of holes and median yields of successful holes could not be increased. Therefore, groundwater abstraction in the area will mostly be restricted to exploitation through hand pumps to support small communities. High yielding boreholes are seldom encountered and can only be found at major fault zones where interconnected fracture zones are present to distinctively enlarge the permeability of the subsurface. These are located at the margins of the Dwyka Group.

5. Natal Metamorphic Province

The Natal Metamorphic Province underlies 15% of all rural areas in KwaZulu-Natal and therefore underlies more of the rural areas than any other lithological province. It is also relatively densely settled. The research area is situated in the Mapumulo District of KwaZulu-Natal, about 30 km northwest of Stanger and 75 km north of Durban and extends over approximately 1300 km^2. The area is bounded by steep sandstone cliffs to the east and west, while the Tugela thrust belt forms the northern boundary.

Water in the study area is used for domestic purposes and partly for small-scale agricultural activity. Currently, water supply needs are mostly met from rivers and springs, with boreholes equipped with hand pumps playing a secondary role. However, groundwater could play an important role, as it is a reliable water source, even in drought situations and is generally of good quality compared to other water sources in the area. Settlement varies from dispersed and isolated kraals to dense settlements in communities.

The rocks of the Natal Metamorphic Province are characterised by negligible primary porosity and groundwater movement is primarily within hard rock aquifers and controlled by zones of deep weathering, faulting, fracturing and jointing. Accordingly, water strikes or seepage encountered in the exploration boreholes drilled during the investigations are either associated with the contact between weathered and solid bedrock, or deep-seated fracture zones of low permeability but high confining pressure. There is no evidence of any additional aquifers at contacts between different lithologies, suggesting that tectonic contacts are more relevant than lithological contacts. Lithological variations are more significant in terms of water quality, with poorer water quality having been recorded in schists and granites (King, 1997).

The area exhibits a poor historical success rate with about 46% of the holes being dry. Borehole yields are generally low with only 23% giving a yield greater than 1 l/s, however in this study greater than 75% of boreholes yielded more than 1 l/s. These reported borehole yields are mainly derived from blow tests and seldom from a long duration test. Therefore the percentage of boreholes with a sustainable yield exceeding 1 l/s is likely to be much lower. Dry boreholes as well as high yielding holes have been drilled into all lithologies and are not restricted to any specific rock type; poor and high yielding holes occur within the same lithology and give evidence that structures of tectonic origin are a major factor influencing groundwater occurrence.

During the Critical Intervention Programme, where only geophysical siting was used, 37% of 27 boreholes drilled in the study area were dry and only 2 had blow yields exceeding 1 l/s. The median yield of successful holes was 0.1 l/s. This study achieved an 89% success rate, with 7 of 9 boreholes exceeding 1 l/s and a median yield of between 1.8-3.3 l/s. This suggests that the aquifer can be reconsidered in terms of reticulated water supply if a scientifically appropriate exploration strategy is adhered to.

The research showed that successful groundwater exploration for the area is possible. An evaluation of the structural geology and the hydrogeological conditions of the area together with a suitable geophysical method for the environment pushed the drilling success rate up from a historical 54% (NGDB) and 63% (Critical Intervention Program) to 89%. Beside the improved success rates, the research did result in significantly improved yields. Whereas the median yield for the NGDB and CIP records is 0.1l/s, a median yield of 1.8l/s was achieved with the applied exploration method, which accordingly lowers water production costs considerably. The average yield of all boreholes was pushed up from a historical 0.96l/s to 2.55l/s.

6. Limpopo Mobile Belt

The research area is situated near the northern border of the Northern Province in the Limpopo River catchment and is underlain by rocks of the Limpopo Mobile Belt (LMB). This geological province is an E-W elongated low lying belt straddling eastern Botswana, southern Zimbabwe and the northern part of the Northern Province in South Africa. Two study areas were selected within the belt, one situated in the northern Bochum District west and southwest of Alldays (study area I), and the other (study area II) is located in Messina District east of Messina (Figure 6-1). Study area I is characteristic of the western part of the LMB, where a quaternary sand cover overlies the metamorphic basement rocks. Rock outcrops are few and the topography is level. Study area II represents the situation in the eastern part of the LMB, where the basement rocks are exposed at surface, with rare occurrences of quaternary cover.

The area exhibits a poor historical success rate with <40%of boreholes yielding water yielding more than 0.1 l/s. Borehole yields fall mainly in the category between 0.01 and 1 l/s (69% study area I and 45% study area II), with the median yield of successful boreholes being only 0.39 l/s. Only 13% of boreholes yield more than 2 l/s. Dry boreholes as well as high yielding boreholes have been drilled in all lithologies and are not restricted to any specific rock type.

The aquifers of the Limpopo Mobile Belt are predominantly structurally controlled and significant water movement is restricted to major fracture and fault zones, primarily related to recent (Post Karoo) geodynamics. These structures can be extremely high yielding and can generate blow yields in excess of 20 l/s. In many instances the distance to streams and rivers is indicative of a fault zone, since many rivers tend to follow structures when they deviate or dogleg from the northerly surface topographic gradient. The highest yielding boreholes are drilled into ENE striking features, the orientation considered as extensional in nature.

However, the scale of the feature shows a strong influence on the yield of the boreholes, with regional scale fault having a far better groundwater potential than local scale structures.

The results suggest that the Limpopo Mobile Belt is a poor aquifer due to marginal to poor water quality (class II-III) related to nitrate levels, low recharge and the extreme heterogeneity in targets. Low success rates exist concurrently with very high yielding features; however, these are restricted to mainly regional scale fault zones. Smaller fault zones and alluvial cover along the streams provide a more limited aquifer. Consequently, water abstraction will have to be reliant on regional abstraction systems from identified structures and reticulation to the point of need. Fortunately, the flat topography does not hinder reticulation.

7. Barberton Greenstone Belt

The study showed that an evaluation of the structural geology and the hydrogeological conditions of the area together with a suitable geophysical method for the environment pushed the drilling success rate up from a historical 50% (NGDB) to 89%. Beside the improved success rates, the proposed methodology resulted in significantly improved yields.

A substantial cut in costs in terms of water production expressed as R/l/s was achieved during this exploration programme. Historic success rates have resulted in an expenditure of approximately R24200 for the establishment of each successful borehole. In comparison, with an exploration budget of about R55000 for the proposed methodology, success rates of 89% can be expected and establishment costs would come down to about R18370 per successful borehole.

Median yields were increased from 0.4 l/s to up to 1.0 l/s, which brings down the costs of water production from 60500 R/l/s in case of random drilling to 18370 R/l/s in this project. The high median yield achieved during this project suggests that water supply systems in the area could involve reticulated systems.

Groundwater is an important resource in the study area, providing a clean, reliable, low cost water source. The geology of the area consists of impermeable granites and meta-basalts metamorphosed at a low-grade amphibolite schist to green schist facies. Fractures in the granites have been intruded by extensive quartz veining, which renders them relatively impermeable and makes them poor targets for groundwater exploration. The meta-basalts are the best targets for groundwater exploration, especially where fracture zones associated with faults and dykes are present.

Dip-slip and strike-slip faults were water bearing and are associated with the formation of deep open cavities that enhance the permeability of the greenstones. The geodynamic and strain analyses suggest that structures having a NNE – SSW strike direction are more likely to be under extension and therefore open, hence they are the primary hydrogeological targets. The E-W striking lineaments are more likely to be strike-slip faults and are also the hydrogeological targets if the target is not a shear zone where gouge material has reduced permeability. The N-S lineaments are expected to have high yielding holes as well, but only if the targeted lineament is a fault, however, this was not proven by drilling results.

8. Guidelines for Exploration in Complex Terrain

Potential hydrogeological targets are often selected based on a hydrocensus and/or a geological review of existing geological maps. Boreholes are subsequently sited using

ground-based geophysics, with the EM-34 and magnetometer being the most widely used methods. This approach has been widely used in the study areas investigated, and has been shown to be relatively unsuccessful and uneconomical when compared to the results that could be achieved by a more integrated and geologically focussed approach. However, using data from the Critical Intervention Programme in KwaZulu-Natal, where the above mentioned geophysical approach was adopted, the geophysical approach has been shown to be more economical than historical success rates, however, median yields were NOT increased. The major disadvantage of this method is that the nature of the hydrogeological targets is rarely understood, neither are the structural and geological stress conditions that control the orientation of structures, which in turn control the distribution of groundwater yield. Consequently, the method is commonly no more than 'anomaly hunting', with geophysical anomalies being attributed to potential weathering profiles, intrusive contacts, or potentially water bearing fracture zones that are assumed to be hydrogeological targets. Often little is known about variations in rock mineralogy, the presence of clay gouge in shears, or the existence of complex folding of the rock fabric, all of which could result in geophysical anomalies. These conditions result in geophysical anomalies over features that are not hydrogeologically significant or even water bearing. In addition, little is known about the regional extensiveness of potential targets or current structural stresses that determine whether the feature is hydrogeologically significant.

The addition of remote sensing to the exploration toolbox allows the regional extensiveness of targets to be identified. LANDSAT TM images or aerial photos assist with identifying potential geological lineaments that are regionally significant so that ground based geophysics can be more intelligently directed towards the location of specific targets. However, such lineaments are not always structurally significant, and the geological stresses responsible for the features are not understood, hence their ultimate water bearing potential is unknown.

A study of the tectonic history and the geodynamics of a region offers the advantage of providing a framework for identifying targets that are hydrogeologically significant based on the understanding of current stress conditions. Consequently, structurally significant lineaments can be identified and geophysical exploration restricted to targets considered to be of greatest potential.

Hydrocensus

Objective

The objective of a hydrocensus is to hydrogeologically characterise a region in terms of the physical and economic feasibility of meeting water demands through groundwater by quantifying:

- Expected borehole yields and their variability by geological domain
- Historic drilling success rates and probabilities of exceeding specific yields
- Proximity of boreholes to geological structures and their yield
- Depth to water strikes
- Static water levels
- Groundwater chemistry
- Potential hydrogeological targets

These investigations should attempt to determine the number of boreholes that will be required to meet water demands, the role of geological structures on yield, the depth to which boreholes should be drilled, and the suitability of water quality for the desired usage.

The location of high yielding boreholes may also assist in identifying targets that are potentially high yielding.

A hydrocensus should ideally also consider geological processes or mineralogies that may negatively impact on groundwater quality in the long term. Critical factors, such as the presence of volcanic massive sulphide deposits, hydrothermal alteration, carbonaceous shales, carbonatites etc., may be indicators of the presence of heavy metals, light metals and non-metals, heavy non-metals, halogens, alkaline earths, rare earths and noble metals that may pose a significant long term health hazard. These elements may be present in the rock but not observed in water samples from recently drilled boreholes; their mobility may be controlled by oxidation-reduction conditions that alter with time. A typical example is arsenic, which is prevalent in South Africa as arsenopyrites, but whose mobility is controlled by oxidation state. Consequently, its presence would only begin to appear in water samples after variations in drawdown due to pumping have introduced oxygen into the formation, resulting in oxidation and weathering.

Methodology

The hydrocensus is conducted by collecting data from the National Groundwater Data Base and previous hydrogeological investigations and subsequently overlaying the data onto existing geological maps using a GIS. The specific processes are:

- Inputting hydrocensus data into a GIS database, such as ARCVIEW, and creating layers for lithology, structures, yield, static water level, water strike depth and water quality
- Characterising domains by using domain boundary polygons to separate borehole data with similar hydrogeological attributes
- Determining the percentage of dry boreholes, and the variability in yield distribution of successful boreholes for each domain
- Determining the optimum drilling depth for each domain based on the depth below which few boreholes encounter water
- Identifying domains where poor water quality precludes water use by categorising median water quality
- Identifying geological indicators of potential geochemical hazards
- Performing a proximity analysis of yield versus distance from known structures to identify important structures and the importance of structures on borehole success.

Tectonics and Geodynamics

Objective

Geodynamic investigations require that the tectonic history of the target be unravelled so that mapped, identified or presumed structures and lineaments can be explained in terms of historic and present day geological strain. Depending on the age of the rocks and the structural complexity, this process may involve extensive literature review on the crustal evolution of the region. Since these processes are of a large scale, investigations often are much broader than the study area. For example, an understanding of the geodynamics of the Natal Metamorphic Province requires a comprehension of Archean craton movement and offshore transform faulting along the Aghulas Transform Fault during the break-up of Gondwanaland. The Limpopo Mobile Belt requires investigation into plate tectonics and craton collision during Archean times, and subsequent shearing during mobile belt emplacement.

Emphasis is given to tectonic events that resulted in brittle deformation, however, in many cases brittle deformation occurs along zones of existing weakness resulting from earlier ductile deformation, such as ENE faulting in the Natal Metamorphic Province along earlier ductile ENE shears.

Geodynamic investigations aim to develop a conceptual model of pre- post- and syntectonic geological evolution that describes historical extension, compression and shear orientations in geological time. The objective is to define a chronologically expected pattern to explain observed faulting by strain analysis using a strain ellipse. The potential rejuvenation of such structures by subsequent tectonic events can then be identified and the present strain on existing structures can be identified. Existing structures considered to be under extension present hydrogeological targets.

Strain analysis conducted during geodynamic investigations also permits an understanding or classification of observed lineaments and joint patterns in terms of their origin and present strain conditions, hence allowing the identification of preferred structures.

Methodology
The process involves investigations into:

- Identification of geological domains based on lithology, geochronology and structural setting
- Pre-depositional environment to identify aquifer boundaries and their nature (depositional-lithological versus post depositional or tectonic)
- Plate tectonics and its impact on geological strain in the region
- Metamorphism and ductile deformation episodes and their expression in the lithologies
- Intrusive and volcanic history
- Recent tectonic history and processes
- Mapping of faults and shears
- Application of strain analysis based on historic strain and stress to derive a pattern of faulting, folding, thrusting and shearing
- Verification of predicted faulting against observed fault pattern

Structural Analysis
Objective
A structural analysis attempts to identify strain conditions in rocks by identifying compressional and tensional orientations by mapping the strike and dip of joints and plotting the data on stereonets. The objective is to identify the orientation that is extensional, so that geological structures aligned perpendicular to extension can be identified. These targets are then assumed to be open and are targeted as preferential targets.

The risk of using this methodology is that in many cases rocks have been exposed to several tectonic events, perhaps with different stress orientations, hence jointing from several generations may be superimposed in joint patterns. Consequently, joints may be aligned in many orientations and the resulting structural analysis would be meaningless unless conducted on subsets related to a specific event. Identifying joint patterns from specific events requires a geodynamic analysis to identify stresses originating at various periods in time. A specific example can be observed in the Limpopo Mobile Belt, where joints are the result of late Archean shear, with post Karoo extension superimposed. For this reason, it is often necessary to conduct joint mapping in the most recent lithological formation present, even if outside the study area, to identify stresses originating from the most recent tectonic event. This process allows coarse dating of joint sets.

Methodology
The investigations conducted include:

- Identifying the age relationship of various formations present in the region

- Mapping of the strike and dip of joint sets in the various lithologies post-dating the study area, as identified at road cuttings and stream beds
- Plotting joint lineation and bedding data on stereonets
- Classification of joints by age relationship or by dip to categorise features by tectonic origin
- Derivation of compressional and extensional relationships by structural analysis

Remote Sensing
Objectives
The objective of using remote sensing methods is to identify structures that may be of hydrogeological significance and that are not noticeable in the field, or that have not already been mapped. These can be identified by satellite images using variations in surface reflectance, by aerial photos using variations in tone and contrast, or by airborne geophysics, which is based on variations in rock physical properties. Often digital filters are used to enhance features considered to be of interest, such as vegetation, structure, soil moisture, clay content, magnetic field etc.

Identified lineaments are presumed to have a hydrogeological significance, and are presumed to be related to lithological variations, faults, variations in saturation, topographical depressions are linear vegetation trends. However, field proofing is necessary to verify the nature of the identified lineament.

Unless a geodynamic analysis has been undertaken, it is usually not possible to identify the stress regime of a lineament or its structural significance. To some extent this is overcome by an analysis of lineament orientation and length so that the predominant regional scale features can be identified.

The usefulness of remote sensing is hindered where:
- disturbance of the land surface hinders lineament identification
- surface cover such as sands prevents identification of subsurface structures
- lineaments are related to non-structural features such as lithological variations of non-hydrogeological significance
- rock physical properties are not sufficiently distinct to permit geophysical delineation
- features are too narrow to be delineated at the scale of the image

Methodology
Remote sensing investigations ideally require the following steps:

- Selection of applicable digital features to highlight features of interest
- Identification of lineaments and overlaying onto topographic and geological maps using a GIS
- Preparation of strike-frequency rose diagrams to identify dominant orientations
- Preparation of strike-total length plots to identify regional orientations and trends
- Preparation of strike-maximum length plots to identify regional structures
- Identification of target lineament orientations based on geodynamics, structural analysis, and lineament strike analysis

Field Verification Investigations
Objective

Field proofing investigations are required to identify the nature of target lineaments to determine their nature and origin, and to pinpoint the lineaments in the field using observation or geophysics, with due consideration being given to constraints on siting. The objective is to identify drilling sites on structural features identified as being of hydrogeological significance

at locations where drilling and water abstraction are physically, economically, socially and legally acceptable.

A field survey is also required to evaluate the effect of constraints on target site selection. These constraints may include:

- topographic and access constraints affecting drilling rig mobilisation
- water demand location and topographical constraints on reticulation or distribution
- quantitative water demand and its impact on target location in terms of large regional structures versus smaller local structures
- access to properties and water rights
- contamination potential and vulnerability
- Acceptance of drilling site by stakeholders

These constraints impact on the point at which specific linear targets may be targeted and ultimately determine where the boreholes can be sited.

Methodology
Field investigations include:

- Observation of land use and geology to identify the nature of lineaments and ensure that they are structurally significant
- Observation and evaluation of constraints in terms of drilling rig accessibility, topographic constraints between source and demand location, distance from demand points, contamination
- Field geophysics to pinpoint the structure in the field at potential target points

9. Conclusions and Recommendations

The results obtained in the 4 selected study areas show that the methodology employed results in increased borehole success rates compared to previous drilling, as recorded in the National Groundwater Database and the Critical Intervention Programme, which utilised a geophysical approach:

Borehole Success Indicators

Geology	Success Rate			Median Yield		
	1	2	3	1	2	3
Dwyka Tillite	12%	27%	50%	0.16 l/s	0.1 l/s	0.1 l/s
NMP	50%	63%	89%	0.1 l/s	0.1 l/s	1.8 l/s
LMB	40%	38%	66%	0.39 l/s	0.1 l/s	3.9 l/s
BGB	50%		89%	0.4 l/s		1.0 l/s

Financial Indicators

Geology	R/successful borehole			R/l/s		
	1	2	3	1	2	3
Dwyka	99473	52100	28600	621706	521000	286000
NMP	22990	20710	18370	229900	207100	10206
LMB	30250	34855	24390	77564	348550	6254
BGB	24200		19875	60500		18370

The project indicates that groundwater exploration is significantly more cost effective when structural controls on groundwater occurrence are considered so that only potentially significant targets are considered for field investigation. However, groundwater exploration exhibits a significant economy of scale and unit costs per borehole decrease with the number of boreholes drilled. In the Dwyka Tillites exploration costs as a proportion of total borehole establishment costs were shown to drop from 27% for 3 boreholes to 14% for 20 boreholes to 12% for 50 boreholes. Consequently, such an approach is warranted only when the exploration costs can be distributed over several boreholes. Based on financial analyses for establishing 10 boreholes, the proposed methodology proved to be cost-effective in all the geological provinces investigated. Cost-effectiveness would subsequently increase with the number of boreholes required in each study area.

Consequently, cost effective groundwater exploration should:

- Have a regional focus and be based on identifying target features for a region rather than be locally demand driven, where boreholes are sited only for a few specific communities. This will minimise the exploration cost overhead per borehole due to the economy of scale principle. However, subsequent drilling of targets can be locally demand driven according to priorities.
- Consider the expertise required rather than the expertise locally available. Borehole siting is commonly undertaken by a local consultant using the tools and skills he has available. This often results in the repetition of poor practice and the use of instrumentation that cannot achieve the required results. This was seen to be the case in KwaZulu-Natal, where the EM-34 was consistently applied in spite of poor results resulting from its limited depth of penetration and a lack of understanding of the nature of structurally significant targets.
- In complex structural environments, exploration should be guided by a hydrogeologist with an understanding of the tectonic setting and geodynamics, together with the water bearing properties of identified targets, rather than be restricted to 'divining' using a variety for instrumentation.
- Consider the geological nature of targets prior to geophysical investigation. Some of the high yielding targets identified and drilled during this study did not exhibit any geophysical anomalies using magnetics or electromagnetics, yet were considered to be of structural significance and proved to be high yielding. Conversely, some geophysical anomalies yielded dry boreholes on targets that were drilled in spite of not being structurally relevant (compressional lineaments, compressional dykes, lithological variations etc.).
- Consider the nature of the geological environment, hence no fixed methodology is applicable. Not all the methodologies adopted proved to be successful in all areas. For example, a quaternary cover may limit the usefulness of remote sensing, or several generations of tectonic events super imposed on a lithology may limit structural analysis unless a younger formation is present.
- Groundwater exploration should be tendered on a per successful site or R/l's basis. *Define Outputs Rather than Inputs.* The current practice of sub-contracting borehole siting to geohydrological consultants purely on cost or a per borehole sited basis does not promote incentive to increase success rates. In fact, the opposite may be the case, with consultants' income increasing with the number of boreholes sited and the number of boreholes where drilling supervision is provided, regardless of success. The sub-contracting of borehole siting independent of drilling success also reduces the responsibility of the Implementing Agent, who carries the drilling budget. An incentive to increase success rates could be achieved by tendering groundwater exploration on a per successful site or a per R/l s basis, placing the onus for success on the tenderer. This approach would also encourage consultants to use the most appropriate methodology for exploration, as opposed to the current approach adopted

by DWAF where the approach is prescribed and standard rates are defined, as occurred during the Critical Intervention Programme as well as subsequent programmes such as BOTT.

The above-mentioned conclusions suggest that there is a significant need for a fundamental paradigm shift in groundwater exploration in South Africa. All of the above lessons can be considered as being opposed or contradictory to the current practice of groundwater exploration for rural water supply.

10. Recommendations for Future Research

The major shortcoming encountered during the project was that the current situation in South Africa has resulted in a fundamental split between geological mapping and groundwater exploration. Geological mapping has been lithologically and petrologically oriented, with little attention being paid to structures other than mapping the location of major faults. Little or no attention has been paid to joint mapping to permit a structural analysis. In addition, tectonic evolution, where it has been considered, has often ignored more recent post-deposition deformation. For example, resulting strain and stresses on Archean rocks resulting from the break-up of Gondwanaland is rarely described and the geological community has concentrated on Archean tectonics and unravelling the complexities related to the ages of metamorphic episodes. As a result, a hydrogeologist considering a structural analysis of target features must go through a mapping exercise. This project has shown that structural analysis usually requires 2 days to complete 4 1:50 000 sheets, however, a tectonic interpretation may require extensive literature review and the application of strain analyses to an observed fault set since the required information on recent tectonics is rarely available. This shortcoming requires that the scope of geological mapping be broadened if the results are to be of greater value to the hydrogeological community. A programme of structural mapping is urgently required if groundwater targets are to be regionally identified.

In contrast, the hydrogeological community has paid scant if any attention to the importance of geodynamics and structural analysis in groundwater exploration. Consequently, exploration has not been focussed and has been relegated to an exercise in anomaly hunting that adds little to the identification of future targets. A structural understanding of the aquifer is rarely built up and mistakes are commonly repeated. This shortcoming may reflect a lack of training in structural geology in South Africa, which is fundamental to groundwater exploration in fractured aquifers. This lack of awareness has resulted in minimal attention being given to structural models in hydrogeological investigations.

Urgent attention also needs to be given to cost-benefit analyses of past and current groundwater exploration strategies, as it is only by using the language of economics that the voice of hydrogeologists calling for a revision in exploration strategy will be heard.

Figure 1. Flow Chart of the Groundwater Exploration process

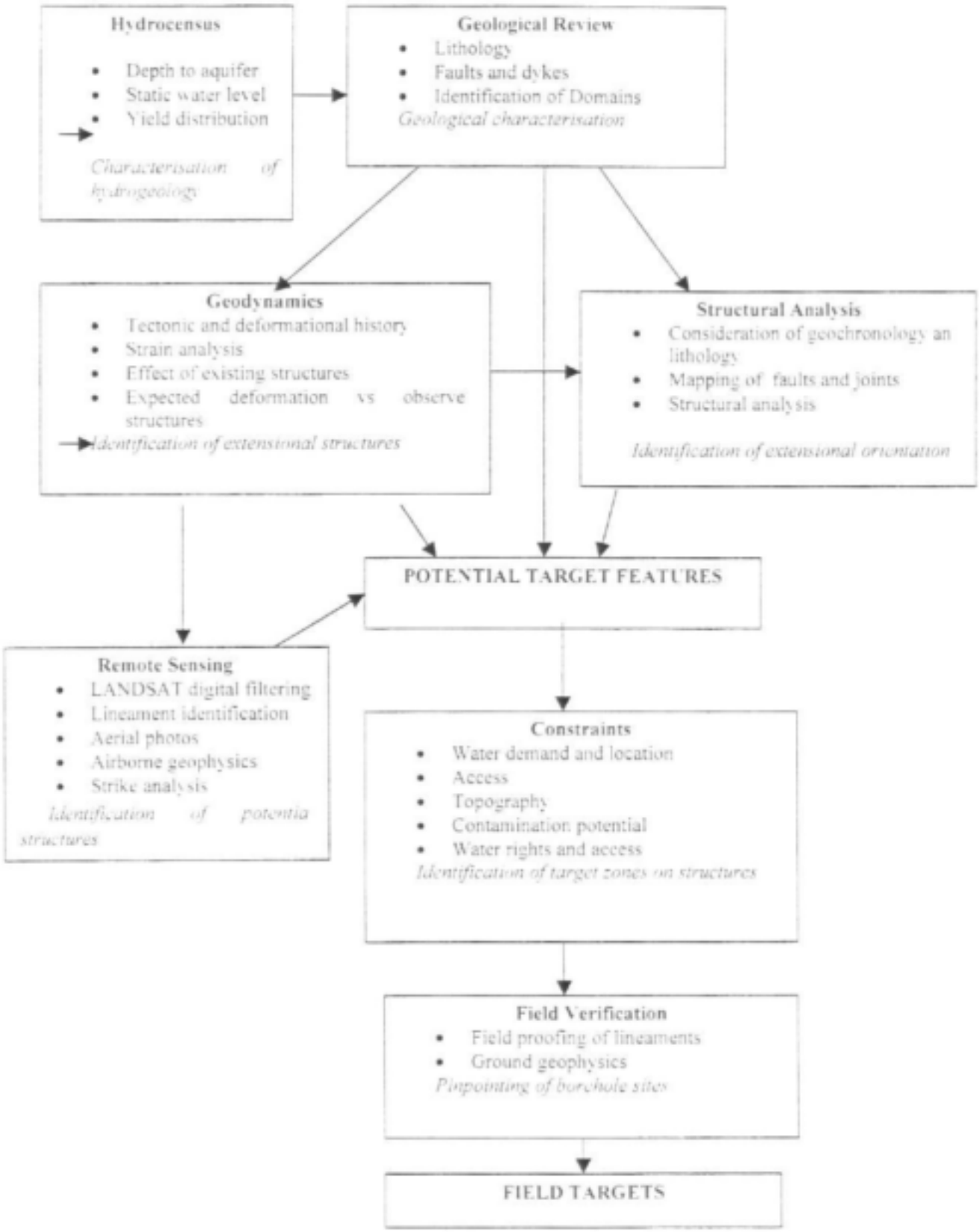

ACKNOWLEDGEMENTS

The research in this report emanated from a project funded by the Water Research Commission and the Department of Water Affairs and Forestry, and entitled:

Groundwater development for rural water supply in complex and problematic terrain: an assessment of geological controls, geophysical exploration methods and the quantification of exploitation potential

The Steering Committee responsible for this project, consisted of the following persons:

Mr. K. Pietersen	Water Research Commission (Chairperson)
Mr. H.M. du Plessis	Water Research Commission
Dr. J.H. de Beer	CSIR
Mr. R. Meyer	CSIR
Dr. E.H. Stettler	Council for Geoscience
Prof. M.K. Watkeys	University of Natal
Prof. J. Dunlevey	University of Durban Westville
Mr. E. van Wyk	Department of Water Affairs and Forestry
Prof. J. Van Bever Donker	University of the Western Cape
Ms. G.M. King	Department of Water Affairs and Forestry

The financing of the project and the contributions of the members of the Steering Commission are acknowledged gratefully.

The authors also express sincere thanks to Ms. G.M. King and Mr. W. du Toit, Assistant Directors of the Directorate Geohydrology, Department of Water Affairs and Forestry in Durban for their helpful guidance and for making personnel and equipment available for this project. Mr Eberhard Braune, Director, Geohydrology, and Messrs. Barry Venter and Lucas Smith of the Directorate Geohydrology are also gratefully acknowledged for the hydrofracturing of 4 boreholes at the Alldays test site.

TABLE OF CONTENTS

TABLE OF FIGURES

TABLE OF TABLES

1. DWYKA GROUP - KWAZULU-NATAL

1.1 General Setting

1.1.1 Site Locality

The area of investigation is situated immediately north of the Transkei border, about 12 km south-east of Harding in KwaZulu-Natal (Figure 1-1).

Figure 1-1 Locality map of the study area

The research area covers about 600 km^2. The four 1:50 000 topographical maps 3029 DB Harding, 3029 DD Bizana, 3030 CA St. Faith's and 3030 CC Izingolweni are covering the area, which extends over approximately 1200km^2. To the south the area extends to 31 00 latitude, whereas the north extends to 30 30 latitude. The east and west boundaries are represented by 30 15 and 29 45 longitude respectively.

The border between Kwazulu-Natal and the Eastern Cape is located in the south of the study area, where the Mtamvuna River marks the boundary. In the north of the study area, the border parallels the N2 highway. Two major access roads, the N2 Kokstad – Port Shepstone in the north and the R61 Kokstad – Port Edward in the south serve the region, from which a fair number of dirt roads diverge. The area is essentially rural with a high population density. Harding in the north and Bizana in the south are the two important villages in the area, containing schools, stores and hospitals.

1.1.2 Topography

The area is characterised by a highly undulating topography of rounded hills and deeply incised valleys. The steep topography varies in elevation between 130 m and 990 m and

defines the surface drainage pattern. The soft and easily eroded Dwyka Group rocks do not support large rock outcrops or the formation of rock cliffs in the study area.

1.1.3 Drainage

The most important watershed of the area runs from the NW to the SE dividing the area into two major drainage systems. To the north, surface water drains into the Mzimkhulwana, whereas in the south small streams drain into the Mtamvuna river. Both rivers running from the NW to the SE and draining into the Indian Ocean just south and north of Port Shepstone respectively (Figure 1-1). The rivers are perennial, whereas the numerous small streams in the area are most erratic due to the scarcity of flow regulating alluvium and the fact that rain falls mainly during thunderstorms (DWAF, 1995).

1.1.4 *Climate, Vegetation and Land Use*

The climate is characterised by the mean annual precipitation (MAP) of about 874 mm with precipitation occurring mainly in the summer months and much of it falls in heavy showers during thunderstorms. The data originates from the Computing Centre for Water Research (CCWR).

The climate accounts for a vegetation dominated by thorn scrub and grassland. Around Harding and Bizana natural vegetation is replaced by large-scale afforestation for commercial purposes. Besides that, agricultural activities in the area are limited to subsistence cattle and goat rearing, together with dry-land maize subsistence farming. Industrial activity within the rural is non-existent. Rural villages are mostly located on the hilltops, where basic infrastructure is available.

1.2 Regional Geology

1.2.1 Introduction

The research area is underlain by the Dwyka Group, which covers large tracts of ground in a belt stretching from the northeast of Ixopo, southwards to Inzingolweni and into the Eastern Cape. Here, the Dwyka Group comprises a 450 m thick succession westerly dipping of glacio-marine sedimentary rocks (Thomas et al., 1990). The Dwyka Group covers nearly 9% of all rural areas in KwaZulu-Natal, hence is of significance for rural water supply.
The basal sequence of the Dwyka rests unconformably on the Natal Group arenites, whereas the uppermost part of the Dwyka succession is succeeded abruptly by the Ecca Formation.

1.2.2 Geological History and Lithology of the Dwyka Group

During the Permo-Carboniferous South-Africa, within the Gondwana continental assemblage, migrated from E to W across high south-polar latitudes. Extensive ice caps developed on elevated regions in the southwestern Gondwana (Figure 1-2). The palaeo-topography primarily consists of a basin, which was bounded to the north by a highly dissected highland, termed the Cargonian highlands, that was open towards the west and extended eastwards into Antarctica, up to an elevated region located over the East Antarctic Plateau. A third highland is postulated to the south near the palaeo-pacific margin of Gondwana (Visser, 1989).

The present reconstruction of the palaeo-iceflow, based on striated pavements, fabric analyses, palaeo-valleys and lithofacies changes in the Dwyka Group, shows a complex pattern, that can be attributed to diachronous ice sheets entering the basin mainly from the north, but also from the east and south (Figure 1-2) (Visser, 1989).

The initial ice advance was grounded, as indicated by deformation of the bedrock. The basin floor was subsequently isostatically depressed by the weight of the ice and rising sea levels led to the decoupling of the ice sheet. This was the major depositional phase of the basin with sedimentation primarily by rainout from ice shelves and icebergs. During the final stages of glaciation a sharp rise in sea level led to a rapid break-up and eventual collapse of the ice-sheet (Visser, 1989).

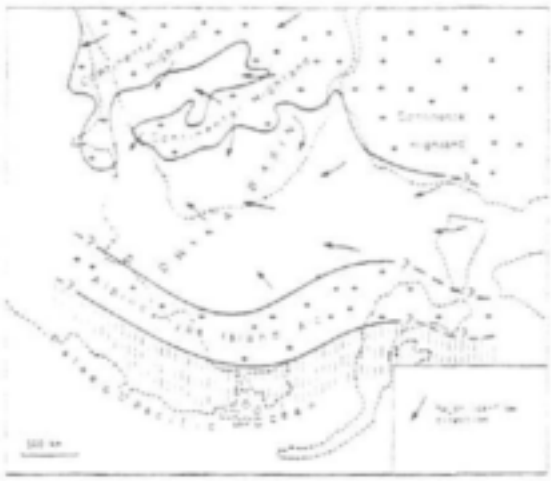

Figure 1-2 The late Carboniferous Dwyka Basin in southwestern Gondwana (source: Visser, 1989).

The Dwyka Group can be subdivided into two major facies (Figure 1-3) (Visser et al., 1990). The northern facies of the Dwyka Group predominantly represents valley and inlet fill deposits left on the dissected Cargonian highlands. The southern facies represents thick platform deposits of diamicton left by marine ice lobes entering the basin. This platform facies pinches out northwards against the palaeo-escarpment of the Cargonian highland, which formed the boundary between the valley and platform facies.

Figure 1-3 Distribution of the Dwyka Group in South Africa south of 25° S (after Visser et al. 1990).

The study area falls within the region of the platform deposits (Figure 1-4). In terms of its lithological character the glaciogenic facies in the area can be divided into three sedimentary lithofacies: the basal sequence, the middle and upper parts of the succession and the uppermost sequence.

In the basal sequence of the Dwyka, which rests unconformably on the Natal Group arenites, three sedimentary lithofacies are recognisable, namely 1) massive to crudely stratified diamictite, 2) shaley diamictite and 3) massive, horizontally and cross-laminated sandstone with rhythmitites. The units are from about 2 to > 20 m thick and occur in the lowermost 60 m of the Dwyka succession.

The dark-grey diamictite contains dispersed angular to subrounded clasts composed predominantly of granite, gneiss and quartzite. The diamictite originates from suspension settling of fine particles and release of clasts from a floating ice cover. The shaley diamictite consists of dark-grey to black distinctively fissile diamictite. This lithofacies is formed in a low energy environment by suspension settling of mud from meltwater plumes or fall-outs of debris from an ice cover. The sandstone units occur between 35 m and 60 m above the base of the Dwyka Group and consist of fine-grained, light-grey feldspathic sandstone and siltstone. This lithofacies is interpreted as the product of possible sub aqueous glaciogenic outwash and turbidity current sedimentation.

The middle and upper parts of the Dwyka succession is far more homogeneous with massive to crudely bedded, blue-black uniform diamictite. The facies contains pebble to cobble-sized clasts of granite, gneiss and quartzite. Rare lenses of fine-grained sandstone, up to 2 m thick interrupt the monotony of the sequence. The lithofacies is identical to the massive to crudely stratified diamictites in the basal 60 m of the Dwyka Group and may therefore have been deposited under similar conditions.

The uppermost part of the Dwyka succession, consisting of sandstone, siltstone and shale, is succeeded abruptly by the Ecca Formation. The thin upward-fining sequence observed above the massive diamictite is interpreted as the product of glacial retreat sedimentation during the closing stages of the Late Palaeozoic glaciation.

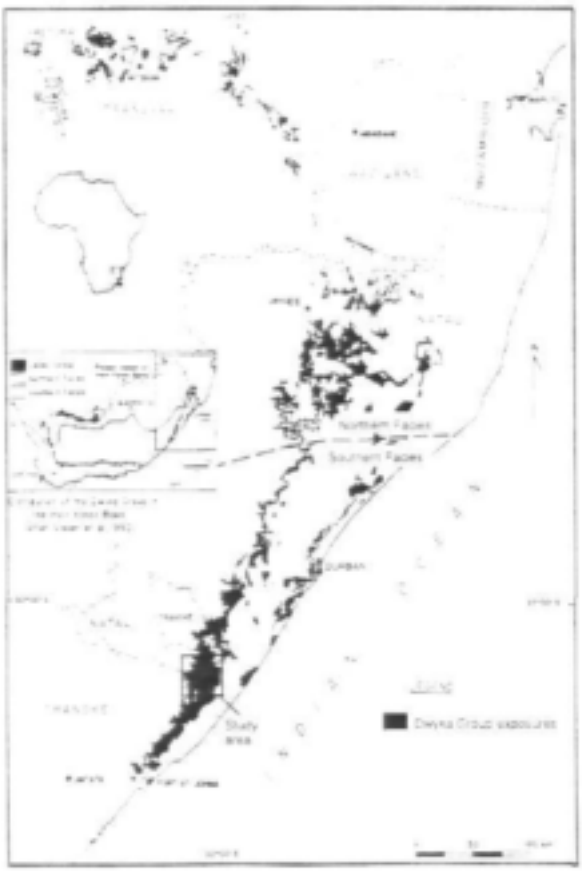

Figure 1-4 Locality map of the study area (source: von Brunn, 1994).

The glaciogenic deposits of the Dwyka Group underwent ongoing deposition that lead to burial resulting in diagenesis and consolidation. Subsequent tectonic events during the late Jurassic resulted in faulting and jointing. Consequently, the hydrodynamics of the system are no longer controlled only by different glaciogenic facies, but mainly fracture zones and weathered residual overburden are now of hydrogeological significance in the Dwyka rocks.

1.2.3 Structural Geology of the Study Area

An extensive and complex network of faults has been mapped in coastal KwaZulu-Natal (Maud, 1961). The faulting can be attributed to isostatic rebound after glaciation, but mainly to crustal warping following the break-up of Gondwana, which caused a SE oriented tension. This resulted in a complex pattern of block faulting associated with crustal normal to the continental margin, and/or strike slip movement parallel to the coastline along a fault known as the Agulhas Transform Fault. Faulting related to this tectonic event has been dated between 190-90Ma (Visser, 1989). The regional pattern consists of a series of arcuate faults trending from SW-NE to N-S and swinging E-W along the coast. In the study area these faults of regional scale are trending NNW to NNE (Figure 1-5), but are not widely recognised and occur mainly at the eastern geological contact to Natal Group Sandstones. These north-trending faults have produced graben structures to the east of the study area like the St. Faith's Graben and the Hell's Gate Fault. Here, thick accumulations of Dwyka sediments can be observed and are indicative of the progressive deepening and instability within the sedimentary repository.

Figure 1-5 Mapped structural features in the study area

In the southwest of the study area, the Dwyka succession is affected by regional scale faulting. Here the Bongwan Gas Fault forms the western fracture plane of a north-south trough in which Ecca Formation and dolerites have been thrown down about 550 m into the Dwyka (de Decker, 1981). The fault can be traced for quite some distance (du Toit, 1946). Movement on the fault was essentially vertical, and the fault has a dip of about 74 degrees. To

the north it extends into the Mzimkulu valley but the displacement decreases until the fault dies out. The fracture zone is marked by active release of CO_2 gas.

The tillite is normally well jointed vertically but most joints are infilled with calcite. Bedding is seldom visible.

1.3 Hydrocensus

Borehole locations in the study area are located primarily on the top of narrow ridges, small hilltops or wide valleys, for reasons of accessibility and population settlement pattern. Valley bottoms are generally inaccessible due to steep slopes. Consequently the majority of boreholes are drilled into topographically poor sites.

The hydrocensus shows that a total of 208 boreholes have been drilled into Dwyka tillite throughout the study area. About 84% of the holes in the area are dry (<0.01 l/s) (Figure 1-6 to Figure 1-9). Of the successful boreholes, 88 % give a yield between 0.01 and 1 l/s and only 11% of the holes have yields greater than 1 l/s (Figure 1-10 to Figure 1-12). The statistics of borehole yields are shown in Table 1-1.

In comparison with Dwyka covered areas further to the north, the success rates in the study area appear to be especially poor. This could be related to the lithological structure of the Dwyka succession. The lower part of the Dwyka could possibly contain groundwater in the shaley diamictites and sandstones layers. In the study area, boreholes are penetrating only the upper part of the Dwyka succession with its massive uniform diamictite where the potential to encounter water-bearing layers is far lower and could explain the high numbers of dry holes.

Three boreholes in the research area yielded greater than 2 l/s, none of which are situated at dolerite dyke contact zones. This suggests that suitable target features might exist.

To investigate the influence secondary features may have on borehole yields a comparison of yields and distance to LANDSAT lineaments was carried out. Boreholes were divided into five distance-to-feature classes and for every class a median yield was established for both the CIP data and the NGDB data set (Figure 1-13 and Figure 1-14).

Only for the CIP data set can a general trend of decreasing borehole yields with increasing distance from lineaments be observed. The NGDB data shows an opposite trend, however, borehole co-ordinates in the NGDB are notoriously poor. Both data sets have to be taken with caution due to the difficulty in measuring such small yield values. Due to the generally very low median yields, the increase in yield as shown in Figure 1-13 and Figure 1-14 is relatively minor with a maximum of 0.08l/s. This is regarded rather as a fluctuation between dry and very low yields than an actual trend to increasing or decreasing borehole yields in relation to the distance to LANDSAT lineaments.

The depth of the boreholes varies between 30 and 150 m with an average depth of 111 m. This reflects the great depth of water strikes in the area with approximately 75 % of the water strikes occurring below 60m (Figure 1-15).

The average water level in the area is 53 m below surface (Figure 1-16). The great depth of the water levels can be attributed to the location of the boreholes on the hilltops, where water levels are far below the surface.

Table 1-1 Statistics of borehole yields

Min	Max	Mean	Median	No. of records
0.02 l/s	4 l/s	0.5 l/s	0.1 l/s	208

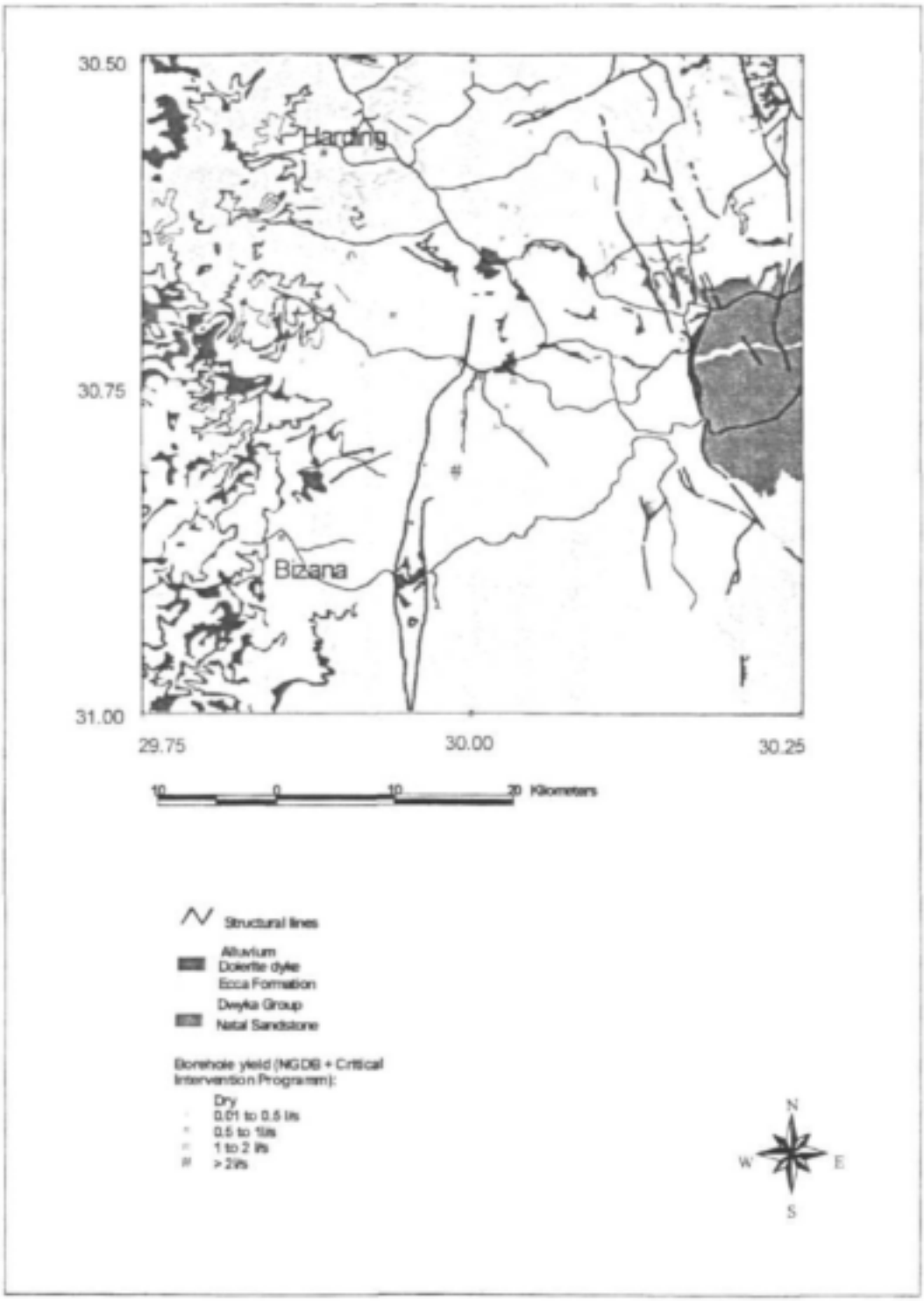

Figure 1-6 **Distribution and yield of boreholes registered in the NGDB and drilled during the Critical Intervention Program (CIP)**

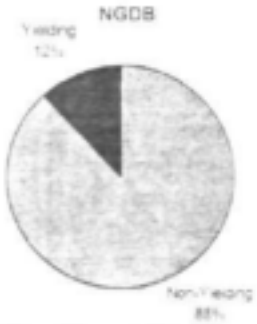

Figure 1-7 Success rate of boreholes registered in the NGDB

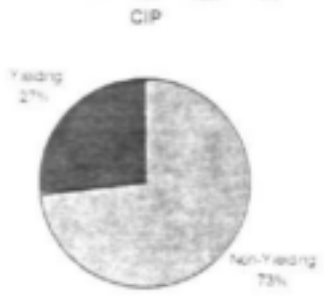

Figure 1-8 Success rate of boreholes drilled during the CIP of the middle 1990s

Figure 1-9 Success rate of all boreholes registered in the study area

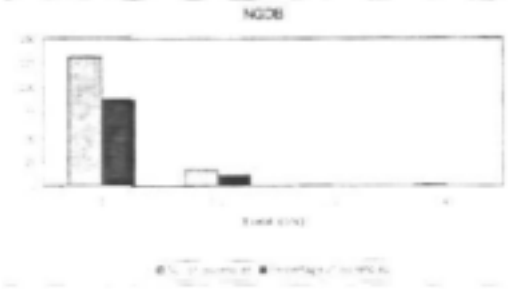

Figure 1-10 Distribution of borehole yield based on the NGDB data

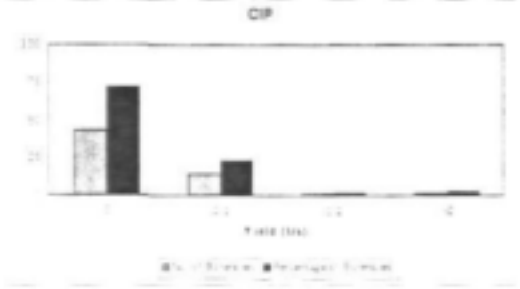

Figure 1-11 Distribution of borehole yield based on the CIP data

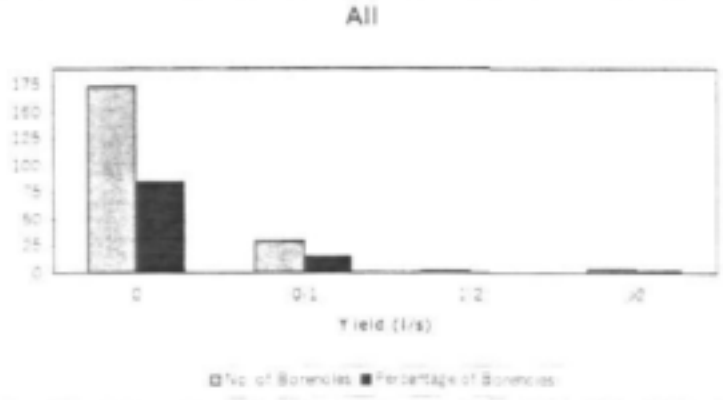

Figure 1-12 Distribution of borehole yield based on all available data for the study area

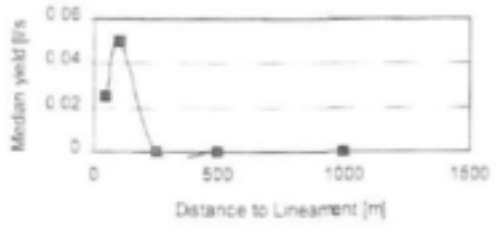

Figure 1-13 Borehole yield (CIP) in relation to the distance to LANDSAT lineaments

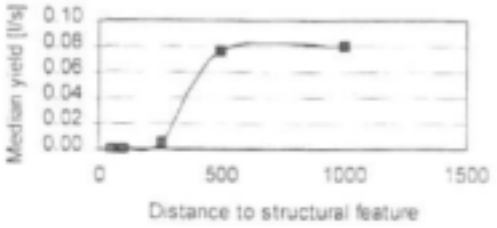

Figure 1-14 Borehole yield (NGDB) in relation to the distance to LANDSAT lineaments.

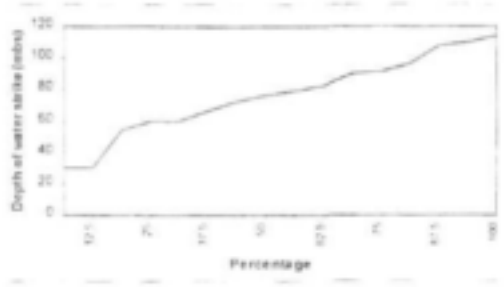

Figure 1-15 Depth of water strike in the study area

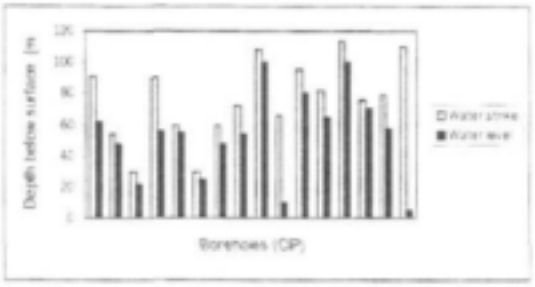

Figure 1-16 Depth of water level and water strike in the study area

Water quality data was available for the CIP data and revealed groundwater in the area to be of good to excellent quality. According to the DWAF classification system (DWAF, 1996), groundwater has been predominantly of class 0 and 1 for domestic consumption.

An investigation was also carried out into exploration methods, which were used by the consultants in the Dwyka tillite. The results show that the GEONICS EM-34 was used more than other instruments (Figure 1-17), in spite of the large number of unsuccessful boreholes (65%). Some of these boreholes intercepted dry or very low yielding fracture zones, while the majority of boreholes intercepted dry massive featureless tillite.

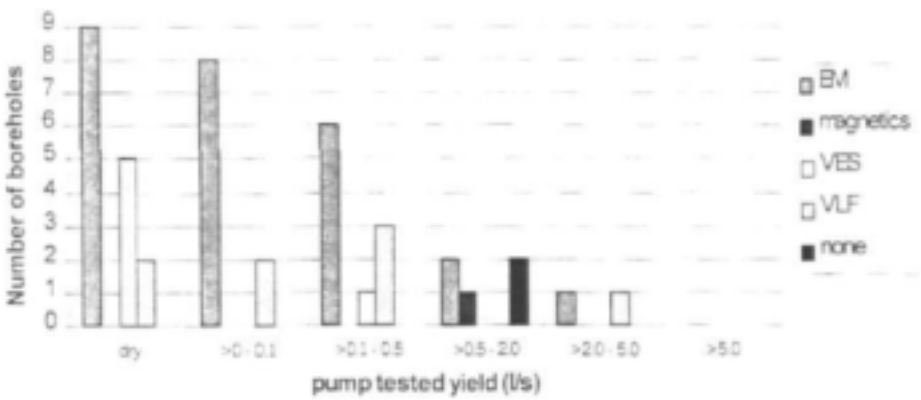

A)

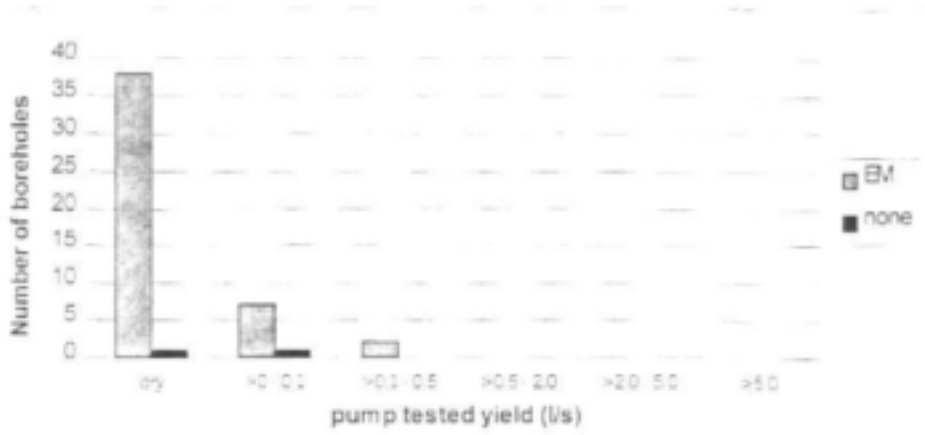

B)

Figure 1-17 Comparison of geophysical methods per yield range obtained during the CIP in for A) boreholes intersecting fracture zones and B) boreholes intersecting featureless tillite.

One main reason for the poor performance of the EM-34 in the study area is that the instrument was mostly used with 20 m coil spacing, giving a maximum depth of penetration of about 25 m in this lithology. In retrospect, the hydrocensus showed, that 75 % of the water bearing features are below 60 m (Figure 1-15). Hence the instrument tends not to penetrate to the depth required given the hydrogeological conditions. Also, the water strike is not necessarily related to weathered features and the indication of deep weathering using the EM-34 does not always imply a good target. Hence, it is unlikely that the use of the EM-34 contributed to the correct siting of successful boreholes.

1.4 LANDSAT imagery

The hydrocensus suggests that the occurrence and movement of groundwater in the study area is mainly controlled by the prevalence and orientation of secondary features, such as faults, joints and fracture zones. As such, the delineation and mapping of these lineaments and their extent has been an integral part of this groundwater exploration study. The interpretation of satellite imagery helps in the extraction of these specific features that possibly act as groundwater indicators.

The lineament map presented in Figure 1-18 is a composite image of all lineaments calculated from each of the images produced through different band combinations.

Lineaments were examined on the basis of their length, width, orientation and frequency (Figure 1-19 to Figure 1-22). The strike-frequency diagram exhibits a distinctive lineament set, which is dominated by three major strike directions. The NNW-SSE direction is the most prominent followed by SE-NW running features and NE-SW striking lineaments (Figure 1-19). The total length of lineaments in relation to their direction supports the dominance of the NNW-SSE direction (Figure 1-20). The majority of the examined features have a length less than to 2 km, with only 4 % being further (Figure 1-21). Looking at the distribution of the maximum lengths, a significant trend is observed (Figure 1-22). The ENE and ESE directions appear to be of greater regional significance.

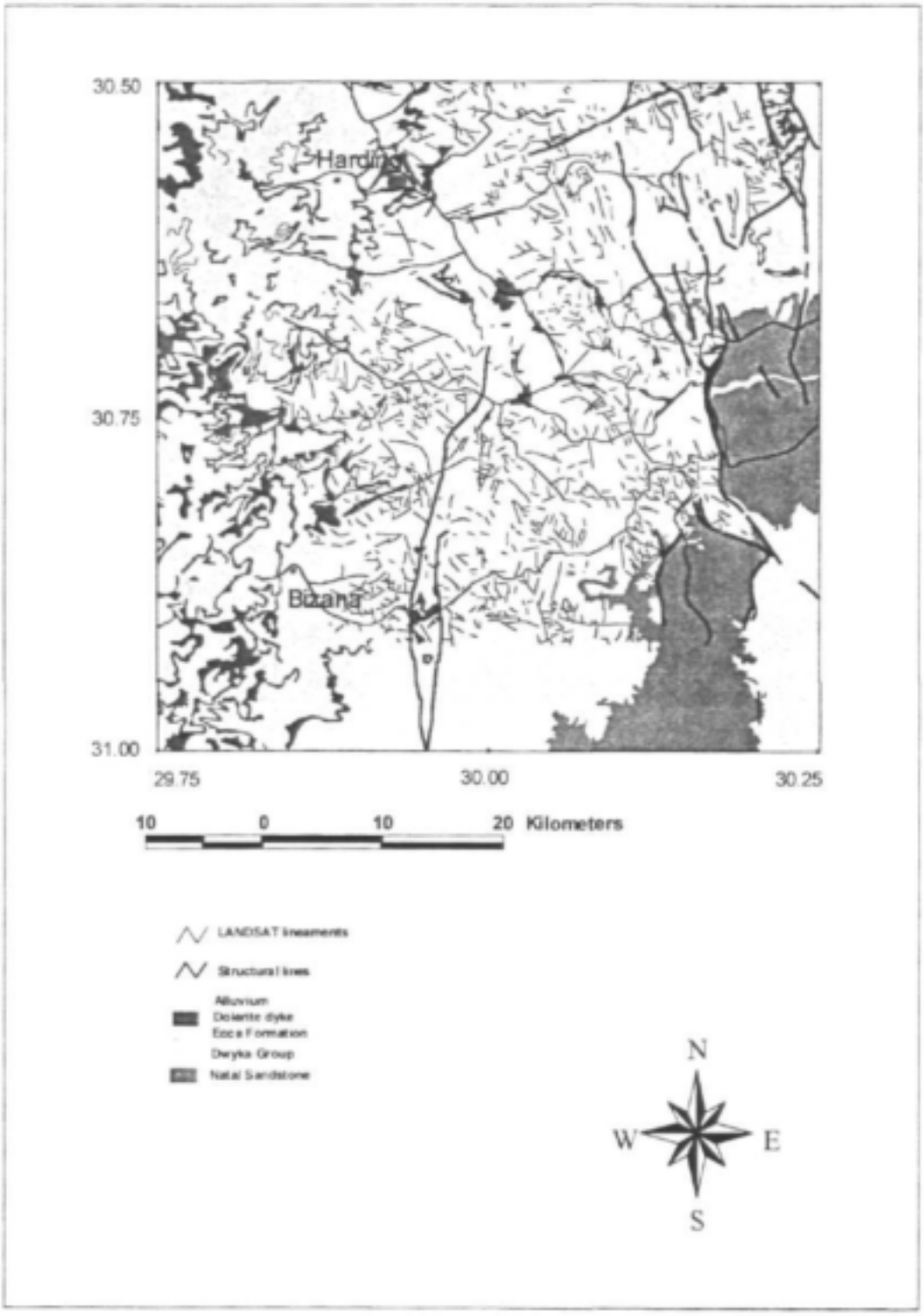

Figure 1-18 **Lineament map of the study area on the basis of LANDSAT data**

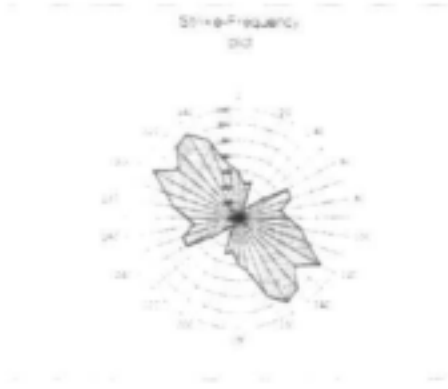

Figure 1-19 Strike-Frequency plot based on lineaments delineated through remote sensing

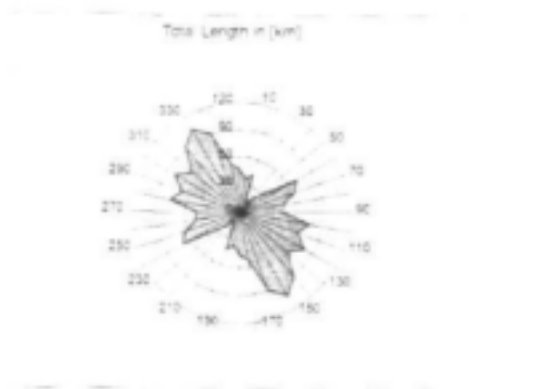

Figure 1-20 Strike-Total Length of lineaments delineated through remote sensing

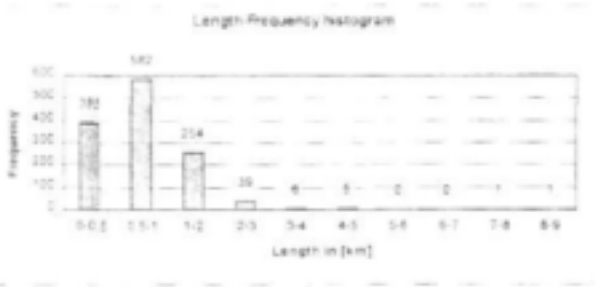

Figure 1-21 Length-Frequency histogram based on lineaments delineated through remote sensing

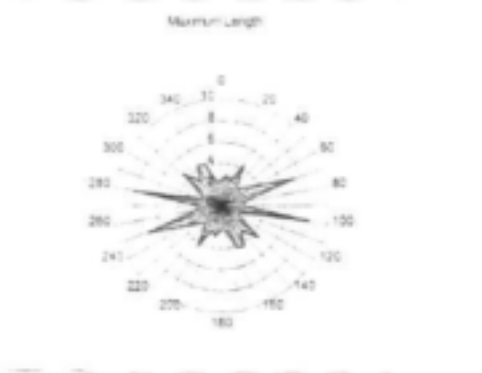

Figure 1-22 Strike-max. Length plot based on lineaments delineated through remote sensing

1.5 Structural Geology

Detailed field mapping in the study area was carried out to delineate preferential fracture or joint directions in the Dwyka Group. Unfortunately, the soft and easily eroded tillite does not support large outcrop areas or the formation of rock cliffs. Therefore outcrops in the area are very limited and the Dwyka Group is only exposed along roads blasted into hill slopes. Figure 1-24 shows the location of Dwyka outcrops visited in the study area.

1.5.1 Structural Features

Most structural features present are linear and comprise joint sets and normal faults. On joint surfaces, which are the most abundant, features such as scratches, grooves, gouge or brecciation are absent. Based on the angular relationship of cross-cutting sets joints can be classified as extensional or shear joints. Because no movement perpendicular or parallel to joint walls is obvious it is difficult to determine if the jointing is related to compressional or extensional forces. If vein minerals, or some of the above mentioned criteria, are present the nature of the force can be distinguished.

Joint systems where two or more joint sets that are thought to be genetically related are present. They maintain dihedral angles of about 5° to 60°. Non-systematic joints usually meet but do not cross. Individual sets may be short while master joints can ran for a long distance

and can influence geomorphology. Many lineaments observed in the area are related to the orientation of master joints and not faults. However, most joint patterns are unrelated to faults. Joints that form large-scale regionally consistent patterns are those that are of interest to geologists. The regularity of the joint system implies that they formed under stress states that showed some consistency both in orientation and magnitude of the principle stresses. The strains revealed by the joint system formation in the area are much less than 1%. They are unlikely to have formed during periods of high strain activity as faulting and veining occurs during major tectonic events.

Joints may develop adjacent to faults where they may take the form of sheeted zones parallel to the fault. At or near the fault such sheeting may become shearing or cleavage. They also may be diagonal to a fault and are referred to as feather or pinnate and may either be shear or extensional joints. Joints tend to be normal to bedding in steep or flat lying units as normality follows the least work principle. Sedimentary terrains most often possesses 2 or 3 joint sets although only one set may be present in many thick massive beds. The spacing of the joints is a function of bed thickness and jointing is more abundant in thin-bedded units. Irregular spacing is more prevalent in thick beds where zones of regularly and closely spaced joints may be alternate with wide zones of few or no jointing. A higher density of jointing requires a significant increase in strain.

Joints are mostly formed 1) soon after deposition and after long periods of down warping, burial and compaction and 2) later during uplift and unloading with or without considerable deformation. The uplift and denudation modify the pre-existing states of stress in three ways a) horizontal stretching through the geometry of uplift, b) expansion through the release of gravitational load and c) contraction through cooling.

After 2 or 3 joint sets form in a unit it becomes mechanically difficult to form additional ones. Joints in older rocks are gradually or periodically propagated into successively formed layers. Geometric classification of joints are 1) ORTHOGONAL JOINT SETS where they are perpendicular and 2) DIAGONAL JOINT SETS where the joints are not perpendicular.

1.5.2 The structural geology of the investigated area south of Harding

Structural features present in the Dwyka tillite are joints and faulting. Planar features (n=212) were measured at 26 stops along major roads where one and occasionally two crosscutting joint sets were present. Most of the joints interceptions are sub vertical with the joints trending NNE-SSW to N-S and NW-SE (Figure 1-25 to Figure 1-29). Only at one stop did secondary vein material occur in the vertical as well as sub horizontal joint planes. All of the planes were very even and smooth, with no grooves, gauge or brecciation present. No displacement was present at the intersections. At stop 14, 21 and 26 faults are present. At stop 14 the fault trends to the northeast (strike/dip: 032°/88°) while the joints are north and ENE respectively. At stop 21 sets of parallel joints (143°/73°) are present. Other planes present at this stop parallel the fault at stop 14 and one of the major joint directions. Stop 26 was inside the down faulted block of Ecca shales adjacent to the Gas fault. Most of the planes can easily be related to the three main joint directions in the tillite, which are the NNW-SSE, the NW-SE and the NE-SW to ENE-WSW directions (Figure 1-25). At stop 15 on the arenites of the Table Mountain Group only two joint sets were developed. The one parallels the ENE trend in the Dwyka, with the second trending WNW dividing the two other major sets in the tillite.

At all the stops the major joint sets intersections were vertical while inclined joints with a sub horizontal intersection were rather rare. The dips of these joint planes were much less than 35°. In many instances the trend of the joint planes were parallel.

The density of the various joint set directions is rather low with 1-3 joints per metre and a very moderate frequency. The length of the joints were determined by the size of the outcrop but was trace-able over the entire outcrop face, which at the most was in the order of 40 m. On an outcrop scale it is very difficult to identify major joints but the persistence of the joint directions indicate three major directions with one present at nearly all stops.

From the joint patterns and fault orientation, shown on the geological maps of the area, it is clear that the jointing and faulting are related to each other in origin. The prominent structural grain in the crystalline basement rocks of the Natal Metamorphic Province tends to be NE-SW striking and possible was transposed into the overlying Cape Supergroup and Dwyka tillite. The majority of joint sets probably developed with the down warping and subsequent unloading of the Karoo Supergroup while the North lineaments are related to the faulting and arching of the continental margin adjacent to the Agulhas Fracture Zone, during the transcurrent break-up of Gondwana. The fracture zone also indicates the contact between continental and oceanic crust.

Due to the absence of directional indicators and deformation in the joint sets the tectonic environment can be regarded as a pure shear system with $\sigma_1 < \sigma_2 < \sigma_3$. However it is not possible to distinguish between σ_1 and σ_3 on the outcrop scale. The NE and NW trending structures, dipping shallower than 65°, will tend to be the open joints. However, a majority of 82 % of joints and faults measured are steep to vertical dipping and tend to be either closed or filled with calcite (Figure 1-23).

A comparison with the LANDSAT data reveals that the structural measurements only coincide with joints and faults of NW orientation. The very prominent NNE-SSW trending structures seen on the outcrop scale seem to have no imprint on the morphology. However, an interesting correlation exists between Figure 1-19 and Figure 1-30. Joints dipping flatter than 65° exhibit a distinctive set of NW-SE and ENE-WSW orientations, which coincides well with the observed LANDSAT directions, especially those of regional extent (Figure 1-20). From the above, it can be concluded, that the NW-SE and NE-SW trending features might be open structures.

In conclusion, the implication is that the exploration needs to target the regional NNW, NW or NE lineaments, which are more likely to be tensional, open and sub vertical, which maximises the probability of encountering the joint set.

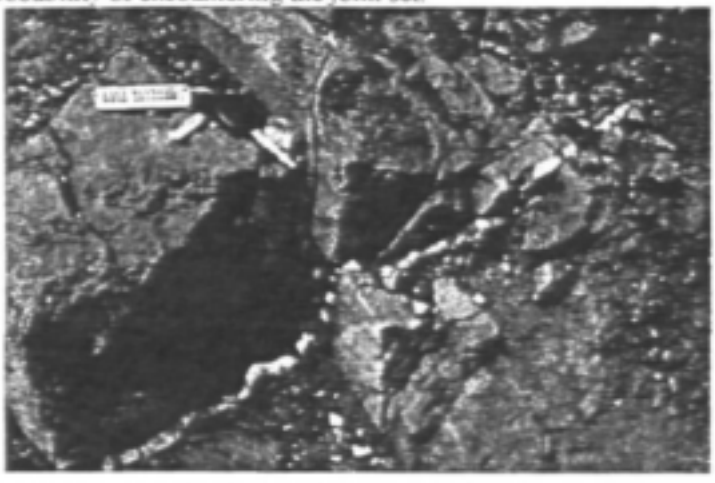

Figure 1-23 **Fracture zone in the tillite, filled with calcite**

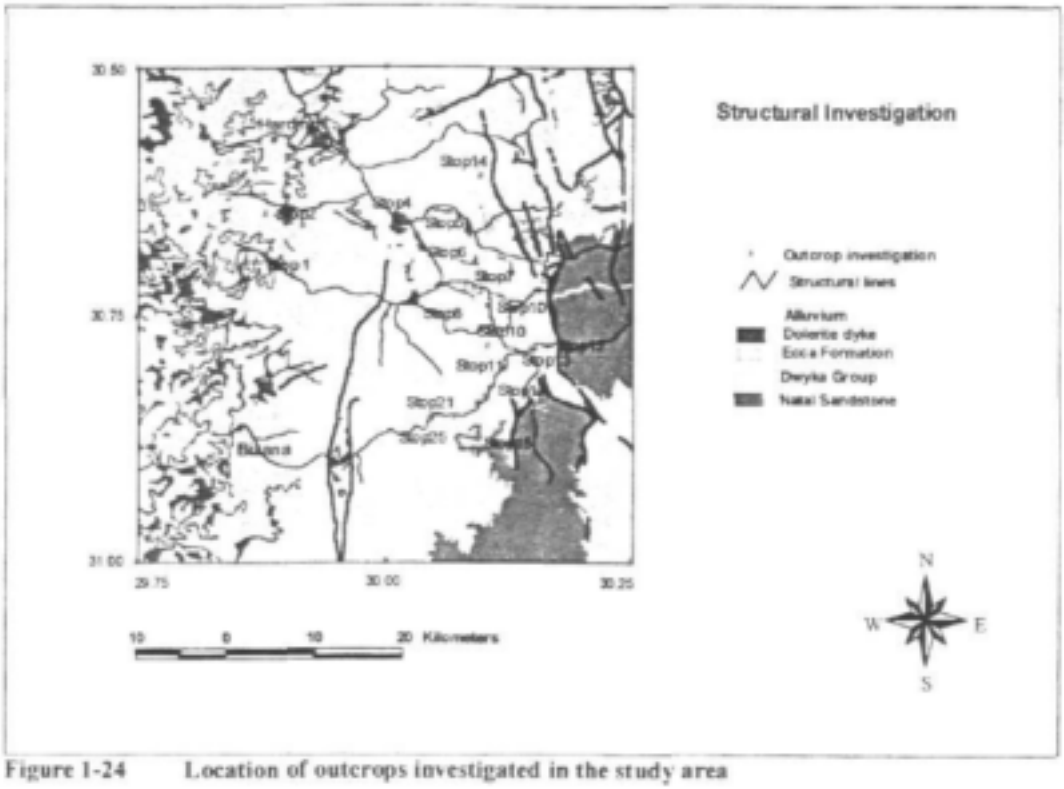

Figure 1-24 Location of outcrops investigated in the study area

Figure 1-25 Orientation of all joints and faults within the tillite

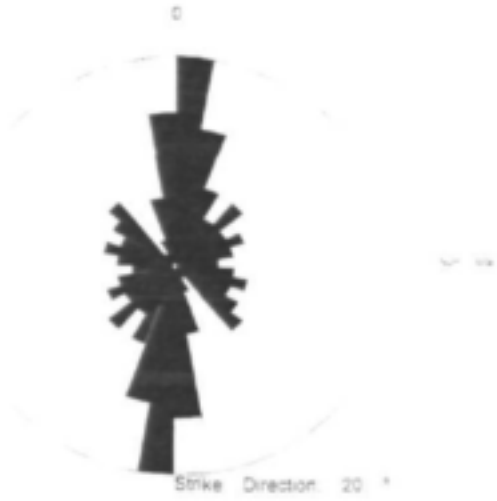

Figure 1-26 Orientations of joints with dips steeper than 80 °

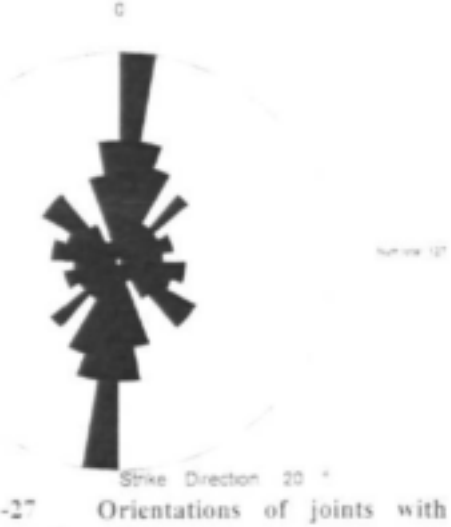

Figure 1-27 Orientations of joints with dips steeper than 75 °

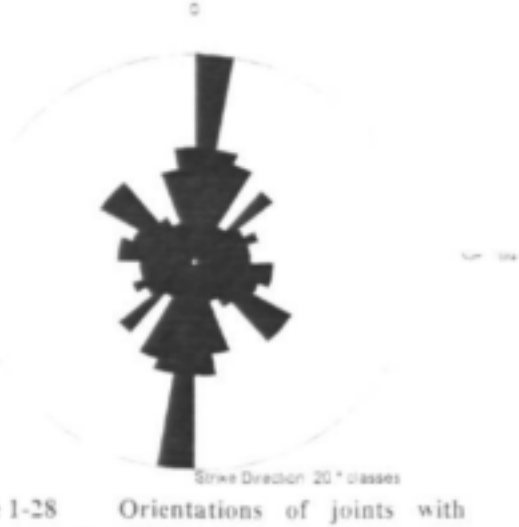

Figure 1-28 Orientations of joints with dips steeper than 70 °

Figure 1-29 Orientations of joints with dips steeper than 65 °

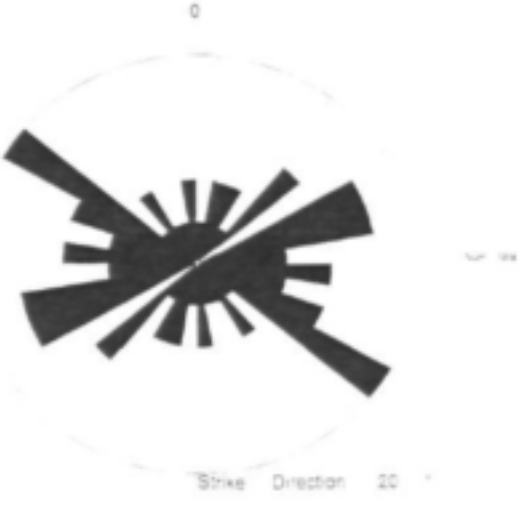

Figure 1-30 Orientations of joints with dips flatter than 65 °

1.6 Ground-based Geophysics

1.6.1 Introduction

To identify the appropriate geological features, the application of appropriate geophysical techniques is vital in the Dwyka deposits. As 75% of water strikes occur below 60m, the geophysical methods suitable for the Dwyka tillite need to generate information from the subsurface to a reasonable depth but remain within economical drilling limits, which are approximately 100m. Furthermore, the method must be suitable for locating relatively narrow conductive zones as it is assumed that groundwater in the glaciogenic Dwyka deposits occurs mostly in fracture zones. Therefore the electromagnetic technique chosen was the Max-Min (HLEM) technique, as it is suitable for locating fractured aquifers (Botha et al., 1992) as long as the conductivity thickness product of the conductive zone is larger than at the surface. Additionally, magnetics was applied.

A total of 23 electromagnetic and magnetic profiles were conducted in different parts of the study area. The recorded magnetic data and the conductivity responses for all traverses and stations are presented in Appendix 1-A. The location and number of each traverse is shown in Figure 1-31.

To investigate possible relationships between borehole sites and water bearing features in the subsurface, twelve traverses were carried out next to existing successful boreholes.

To prove a relationship between significant surface morphology and subsurface features, eleven magnetic and EM profiles were conducted over lineaments, which were pinpointed through the use of remote sensing, the careful study of aerial photographs and based on the outcome of the structural geology.

All profiles were carried out perpendicular to lineaments if present, otherwise perpendicular to one of the three major lineament directions in the study area.

The investigation suggested that yielding boreholes and prominent lineaments to be associated with three different geophysical response classes, which are believed to represent the following geological scenarios:

- The first geological scenario is the two-layered earth case, i.e. a weathered, conductive zone is underlain by unweathered fresh diamictite of higher resistivity. The overburden shows a distinct change in thickness generating a ramp, ridge or valley discontinuity in the electromagnetic results (Villegas-Garcia, 1979). The discontinuity itself could be associated with buried fracture zones.
- The second scenario, detected by the electromagnetic survey, shows a two-layered earth case, which has been interrupted by a thin dipping conductor.
- The third geological scenario is detected by magnetic anomalies and may represent buried dykes, sills or fault-steps.

Table 1-2 gives an overview of the feature investigated and their geophysical response obtained in accordance to the three geological scenarios described above.

Table 1-2 Geophysical surveys carried out in the research area

Site	BH drilled	Long	Lat	Feature	Geoph. used	Geoph. response	Traverse direction
D1		29.9500	30.7208	Yielding borehole (No. 12974)	Mag, MaxMin	No anom.[1]	S-N
D2		29.9933	30.7286	Yielding borehole (No. 920)	Mag, MaxMin	R/R/V-Disc.[2]	S-N
D3		29.9979	30.7476	Yielding borehole	Mag, MaxMin	No anom.[1]	S-N

D4	G45905	29.9925	30.7758	Yielding borehole, SE-NW running lineament	Mag, MaxMin	R.R.V-Disc [2]	SW-NE
D5	G45906 G45907	29.9951	30.7933	Yielding borehole, NW-SE running lineament	Mag, MaxMin	Cond. [3]	SW-NE
D6		29.9871	30.8036	Yielding borehole	Mag, MaxMin	No anom. [1]	S-N
D7		30.0000	30.8037	Yielding borehole, NNE-SSW running lineament	Mag, MaxMin	Mag. [4]	WNW-ESE
D8	G45908 G45909	29.9887	30.8208	Borehole, NW-SE running lineament	Mag, MaxMin	Mag. [4] R.R.V-Disc. [2]	SW-NE
D9		29.9603	30.8111	Yielding borehole	Mag, MaxMin	R.R.V-Disc. [2]	NNE-SSW
D10		29.9876	30.8150	Yielding borehole (No 907), SW-NE running lineament	Mag, MaxMin	Mag. [4]	SE-NW
D11		29.9924	30.7569	Yielding borehole	Mag, MaxMin	No anom. [1]	N-S
D12	G45912 G45913	29.9451	30.7125	SW-NE running lineament	Mag, MaxMin	R.R.V-Disc. [2]	SE-NW
D13		30.0916	30.7678	Yielding borehole (No 405-525)	Mag, MaxMin	R.R.V-Disc. [2]	NNW-SSE
D14		30.0483	30.8850	NNE-SSW running lineament	Mag, MaxMin	Mag. [4]	NW-SE
D15		30.0650	30.8933	E-W running lineament	Mag, MaxMin	R.R.V-Disc. [2]	SE-NW
D16		30.0453	30.5825	E-W running lineament	Mag, MaxMin	R.R.V-Disc. [2]	SSW-NNE
D17		30.0596	30.5543	SW-NE running lineament	Mag, MaxMin	Mag. [4] Cond. [3]	SSW-NNE
D18		30.0166	30.5300	N-S running lineament	Mag, MaxMin	R.R.V-Disc. [2]	E-W
D19		30.0416	30.5291	N-S running lineament	Mag, MaxMin	No anom. [1]	E-W
D20	G45910	29.9708	30.7861	N-S extension of Bongwan fault intersecting a E-W running lineament	MaxMin	No anom. [1]	E-W
D21	G45911	29.9699	30.7863	N-S extension of Bongwan fault intersecting a E-W running lineament	MaxMin	No anom. [1]	W-E
D22		30.0755	30.7641	N-S extension of Bongwan fault intersecting a E-W running lineament	MaxMin	No anom. [1]	N-S
D23	G45914	30.0755	30.7643	N-S running lineament	MaxMin	Disturb. [5]	NW-SE

No anom. [1] No geophysical anomaly
R.R.V-Disc. [2] Ramp, ridge or valley discontinuity
Cond. [3] Narrow conductor
Mag. [4] Magnetic anomaly
Disturb. [5] Disturbed by power lines

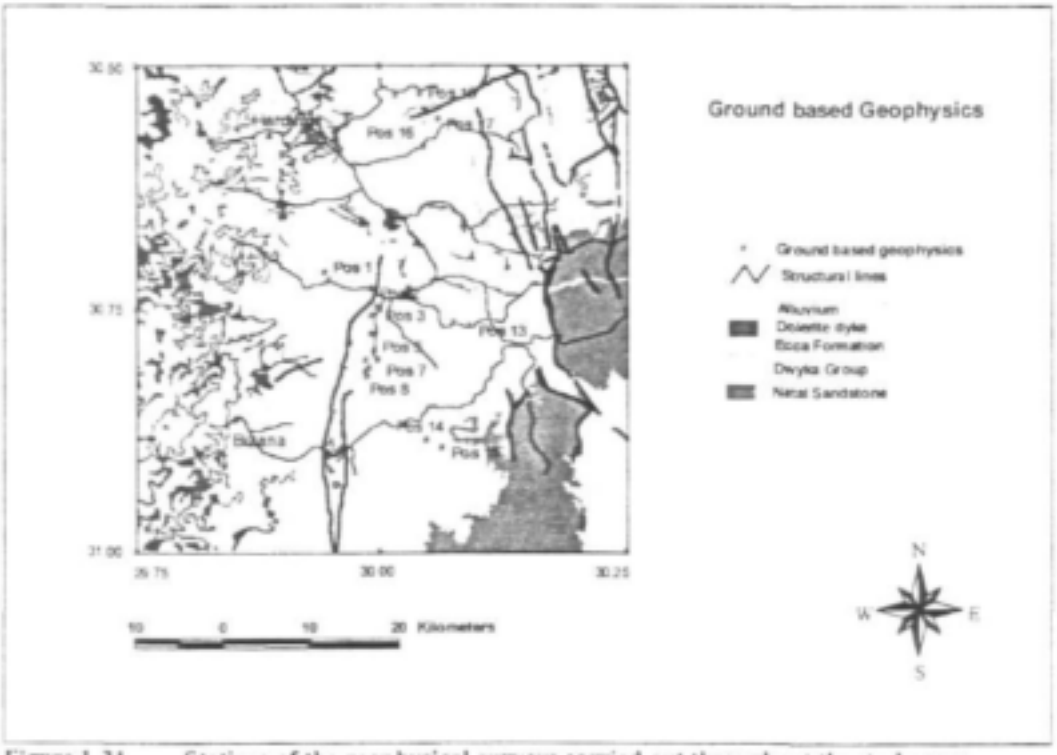

Figure 1-31 **Stations of the geophysical surveys carried out throughout the study area**

The results of the geophysical ground based surveys were grouped into three main categories: reflecting responses over inhomogeneous overburden, narrow conductors, or magnetic anomalies. Examples will be given below for each scenario.

1.6.2 Inhomogeneous overburden

A total of nine sites investigated exhibited a distinct change in overburden thickness generating a ridge, ramp or valley discontinuity on the EM response. Two sites will be discussed below to illustrate the response in relation to existing boreholes or lineaments.

D4 – SW-NW running lineament, yielding borehole

Site description

The traverse was carried out next to an equipped borehole. However, the borehole is not yielding, either because of a defective or the borehole running dry. The borehole is situated in a topographical depression, picked up by the LANDSAT image and the conducted profile is crossing the SE-NW running dip from the SW to the NE at a 90-degree angle (Figure 1-37).

The MAX-MIN was operated at 5 frequencies, ranging from 220 to 56320 Hz while the coil separation was set to 100 m. A station spacing of 10 m for the MaxMin as well as for the Magnetometer survey was selected. The results of the electromagnetic and magnetic data are shown in Figure 1-33 and Figure 1-34

Electromagnetic Survey

The electromagnetic data set shows a positive response of both the in-phase and the out-of phase components for the first 80 m. After that a decrease in in-phase and out-of phase values for all frequencies between station 8 and 10 marks an increase in the subsurface conductivity, due to a change in the thickness of the overburden. At this point borehole was drilled (G45905). The weathered tillite, overlaying the fresh diamictite, increases in its thickness and reaches its maximum towards the end of the traverse, generating a response similar to the anomaly seen over a ramp discontinuity (Villegas-Garcia & West 1983). The existing borehole is situated right at the contact between the relative thin and relative thick weathered overburden at locality 80m of the EM traverse.

Magnetic Survey

The magnetic data stays inconclusive, as the readings proofed to be very unstable for the first 120m of the traverse. The existing borehole is located at station 120m of the magnetic traverse, right at the change to magnetically more stable subsurface.

D12 – SW-NE running lineament

Site description

The traverse at site 12 crosses a well defined lineament running SW to NE, evident in the aerial photographs. It is visible in the morphology as a small depression of about 75 m width (Figure 1-32).

Figure 1-32 **Location of traverse no. 12**

The MAX-MIN was operated at 5 frequencies, ranging from 220 Hz to 56320 Hz while the coil separation was set to 100 m. A station spacing of 10 m was selected while the lineament was crossed from the SE to the NW. The results are shown in Figure 1-35 and Figure 1-36.

Electromagnetic Survey

Along the first 90 m of the traverse a constant response in the EM graph's gradient is recorded. This indicates a homogeneous two layered earth case consisting of a conductive overburden above the unweathered tillite. From 90 m to the end of the traverse, at 190 m, a broad anomaly in all frequencies is recorded. The trough-like response indicates a thickening of the conductive overburden from station 9 onwards. The respond is very similar to the anomaly seen over a ramp discontinuity (Villegas-Garcia & West 1983): the quadrature component is more affected by the discontinuity at low frequencies. This clearly shows the presence of the thickness change, while the in-phase component remains almost flat. At higher frequencies the quadrature response starts losing its characteristic shape and eventually becomes inverted for the highest frequency (small value of δ/t). An increase in the in-phase and out-of phase components at station 18 indicates a decrease in the thickness of the conductive overburden towards the end of the traverse. Two boreholes were drilled, one at an accessible site where the thickest overburden was predicted and the other at the margin of the zone of increasing overburden.

Magnetic Survey

Due to metal objects, the magnetic data shows an anomaly for the SE flank of the valley. Otherwise the magnetic response is stable and no anomalies are recognized.

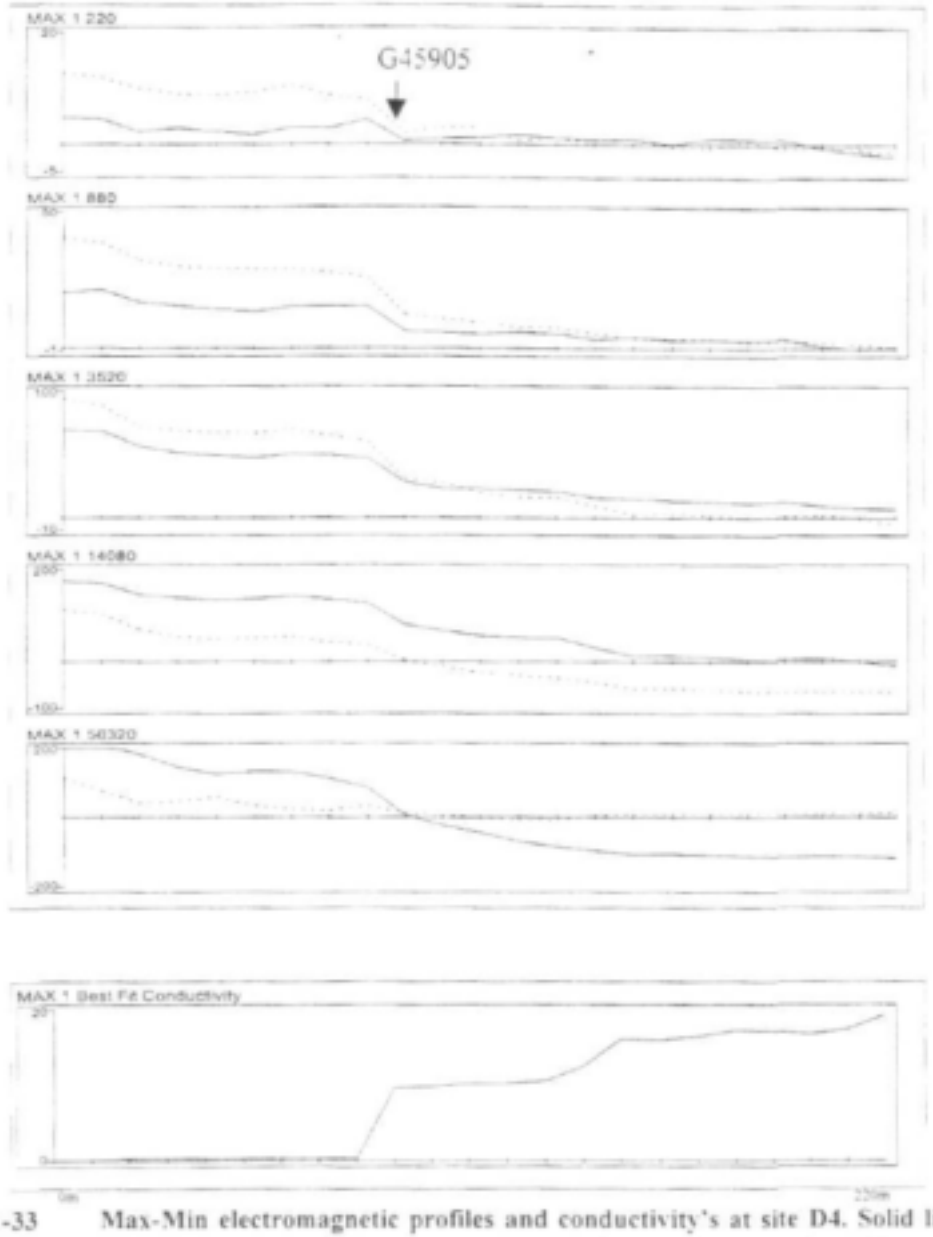

Figure 1-33 Max-Min electromagnetic profiles and conductivity's at site D4. Solid line: in-phase [%]; dotted line: out-of phase [%]; conductivity [mS/m]; coil separation 100 m, station spacing 10 m. Profile direction: SW-NE.

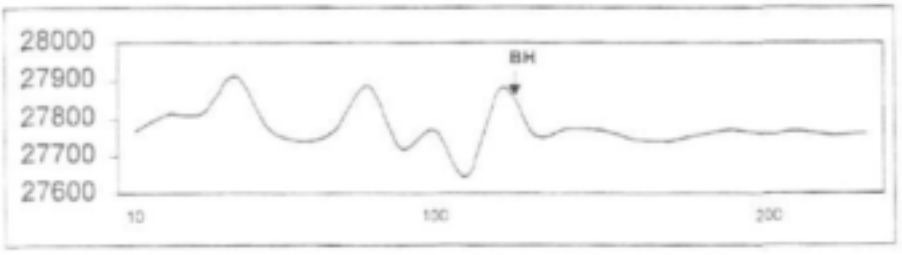

Figure 1-34 Magnetic profile in [nT] at site D4, station spacing 10 m. Profile direction: SW-NE

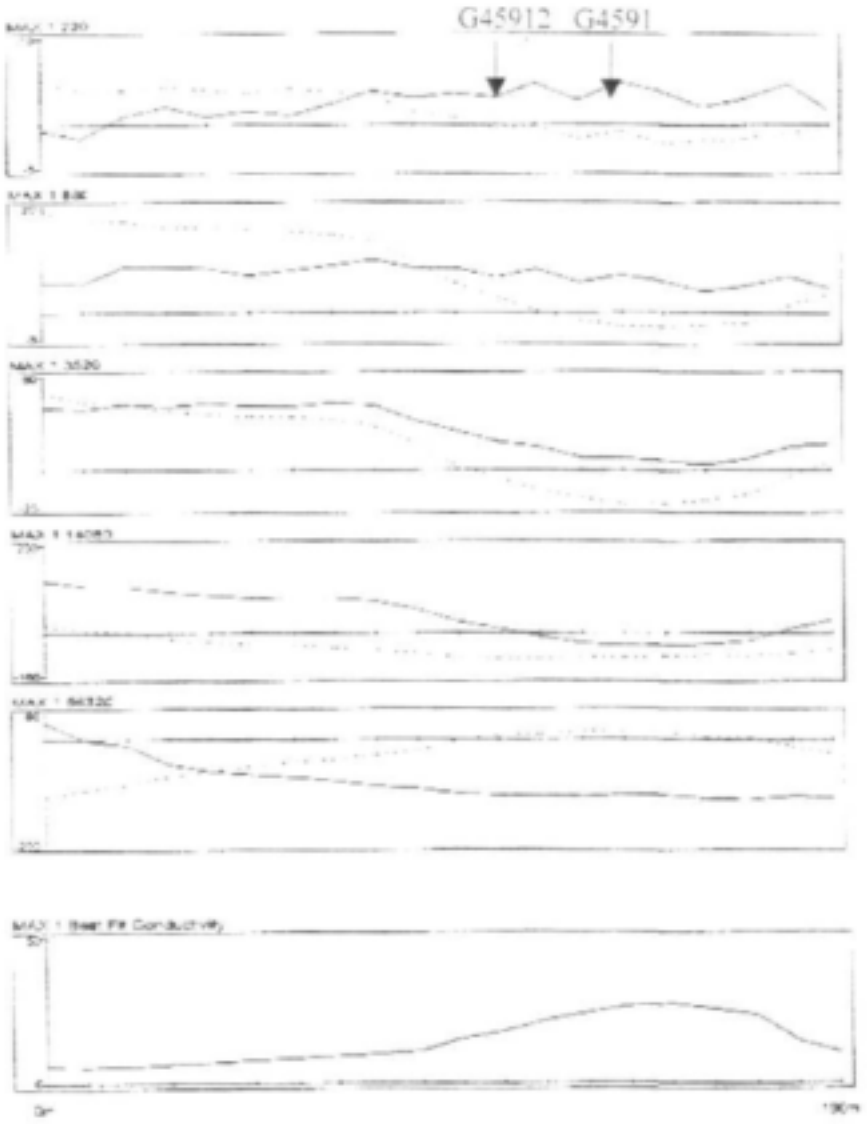

Figure 1-35 Max-Min electromagnetic profiles and conductivity's at site D12. Solid line: in-phase [%]: dotted line: out-of phase [%]; conductivity [mS/m]: coil separation 100 m, station spacing 10 m. Profile direction: SE-NW.

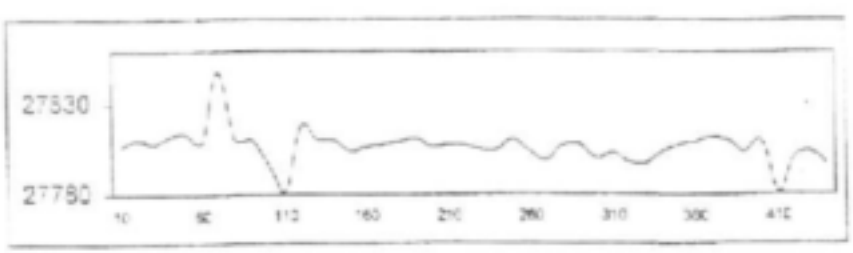

Figure 1-36 Magnetic profile in [nT] at site D12, station spacing 10 m. Profile direction: SE-NW

1.6.3 Narrow conductor

Two sites investigated exhibited a geophysical EM response indicating a buried narrow conductor in the subsurface. Both examples are given below to illustrate the geophysical response in relation to yielding boreholes and lineament direction.

D5 – NW-SE trending lineament and yielding borehole

Site description

The site of a existing borehole, which is not mentioned in the CIP or the NGDB, was investigated on the farm no.2 4666, near the Filippi Mission Station (Figure 1-37). The borehole is situated in a depression that is visible in the aerial photographs as part of a lineament, crossing from NW to SE and was pinpointed through the use of remote sensing. This is one of the open joint directions and is in the direction of long regional lineaments. The profile conducted was made perpendicular to the proposed lineament.

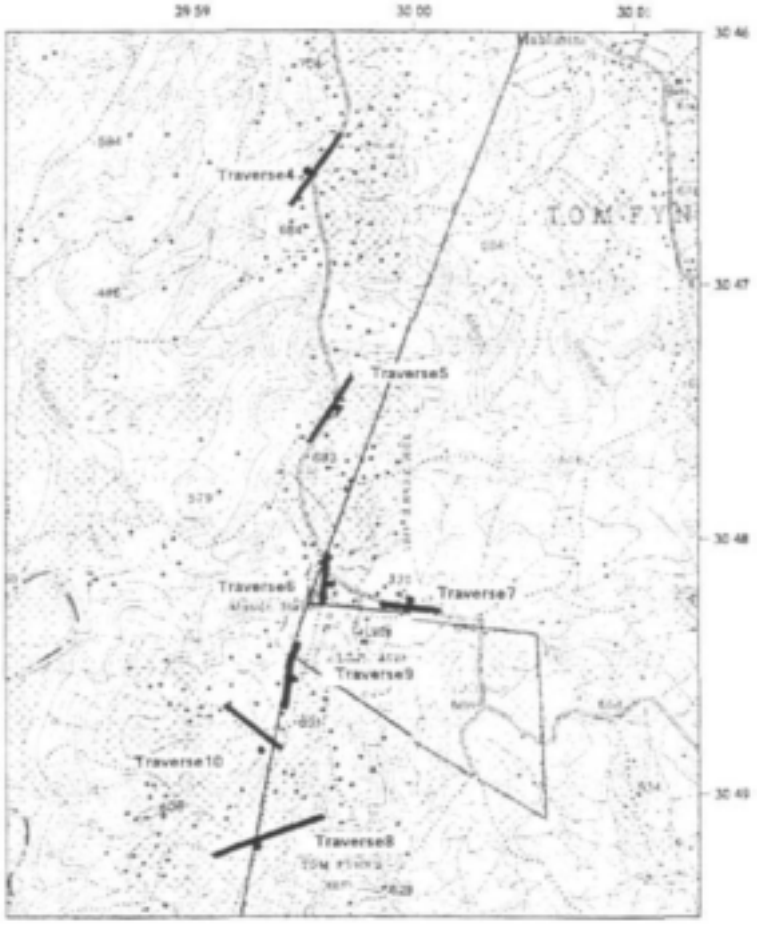

Figure 1-37 **Locality map for traverses D4 to D10.**

Electromagnetic Survey

The MAX-MIN was operated at 5 frequencies, ranging from 220 to 56320 Hz while the coil separation was set to 100 m. A station spacing for the magnetic and MaxMin survey was set to 10 m. Results are shown in Figure 1-39 and 1-40.

Up to station 10 only slightly varying in-phase and out-of phase values indicate a layered earth scenario throughout all frequencies. The second part of the traverse, from station 10 up to the end of the traverse, shows a response typical to a sheet-like conductor. A negative peak is flanked by two positive shoulders in both the in-phase and the out-of phase component. The distance between the zero points in frequency band 880 Hz to 14080 Hz is approximately 80 m, which is almost equal to the coil separation. The low amplitude ratios between in-phase and out-of phase indicate a weak conductor, which is dipping at a very steep angle towards the higher positive peak of the two shoulders, i.e. to the SW. This corresponds with the structural interpretation that NW structures are steeply dipping. One borhole was located near the presumed structure and the other to the SW in order to intersect the structure at greater depth. Borehole G45906 intersected the structure at about 71 m and obtained water, whereas borehole G45907 did not hit the structure by 120 m depth.

Magnetic Survey

The magnetic data did not identify the anomaly detected by using electromagnetics. Towards the end of the traverse, a fence line interfered with the results.

D 17 – SW-NE running lineament

Site description

A well-defined lineament, which was identified from the processing images and the aerial photographs, gave the site for an EM and magnetic traverse. The lineament is reflected through a dip running SW-NE in the morphology (Figure 138) but was not drilled.

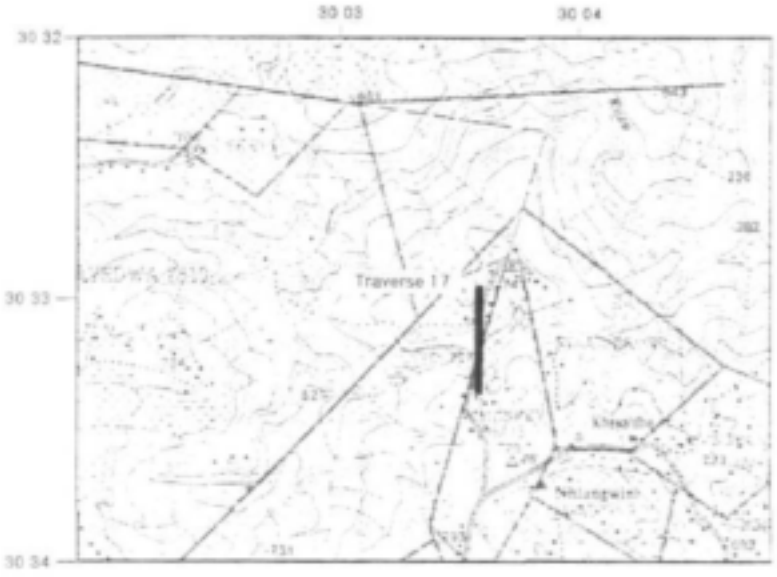

Figure 1-38 Locality map of traverse D17

Electromagnetic Survey

The MAX-MIN was operated at 5 frequencies, ranging from 220 Hz to 56320 Hz while the coil separation was set to 100 m. A station spacing of 25 m was selected for the MaxMin survey, while the magnetometer traverse was carried out with 10m station spacing. Results are shown in Figure 1-41 and 1-42.

Frequencies 3520 Hz and 14080 Hz showing a negative peak flanked by two positive shoulders in both, the in-phase and the out-of phase component for the centre of the valley. At lower frequencies the in-phase looses its significance while the quadrature component shows the anomaly furthermore clearly. The distance between the zero points in frequency 3520 Hz and 14080 Hz is approximately 80 m, which is almost equal to the coil separation. The response would suggest the presence of a sheet-like conductor.

Magnetic Survey

The magnetic data correspond very well to the EM data by showing a well-defined magnetic-low anomaly for the center of the valley. The magnetic fabric of the tillite has been disturbed slightly in the vicinity of the magnetic low, where the response amplitude is lower. This could indicate the presence of a fault. The fault zone itself is highly weathered and could be enriched with water-saturated clays, generating the EM anomaly.

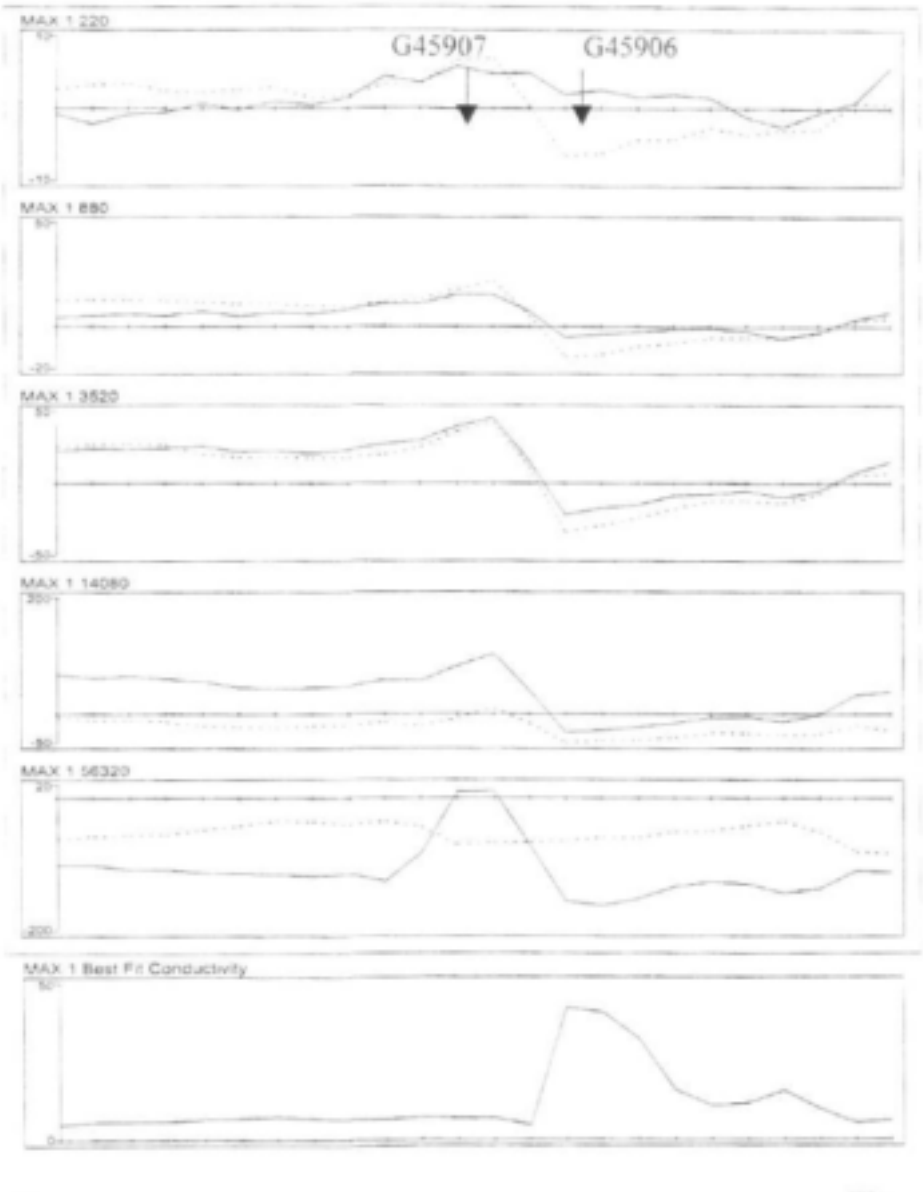

Figure 1-39 **Max-Min electromagnetic profiles and conductivity's at site D5. Solid line: in-phase [%]; dotted line: out-of phase [%]; conductivity [mS/m]; coil separation 100 m, station spacing 10 m. Traverse direction: SW-NE.**

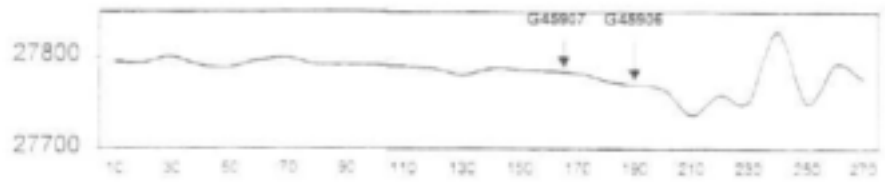

Figure 1-40 Magnetic profile in [nT] at site D5, station spacing 10 m. Traverse direction: SW-NE.

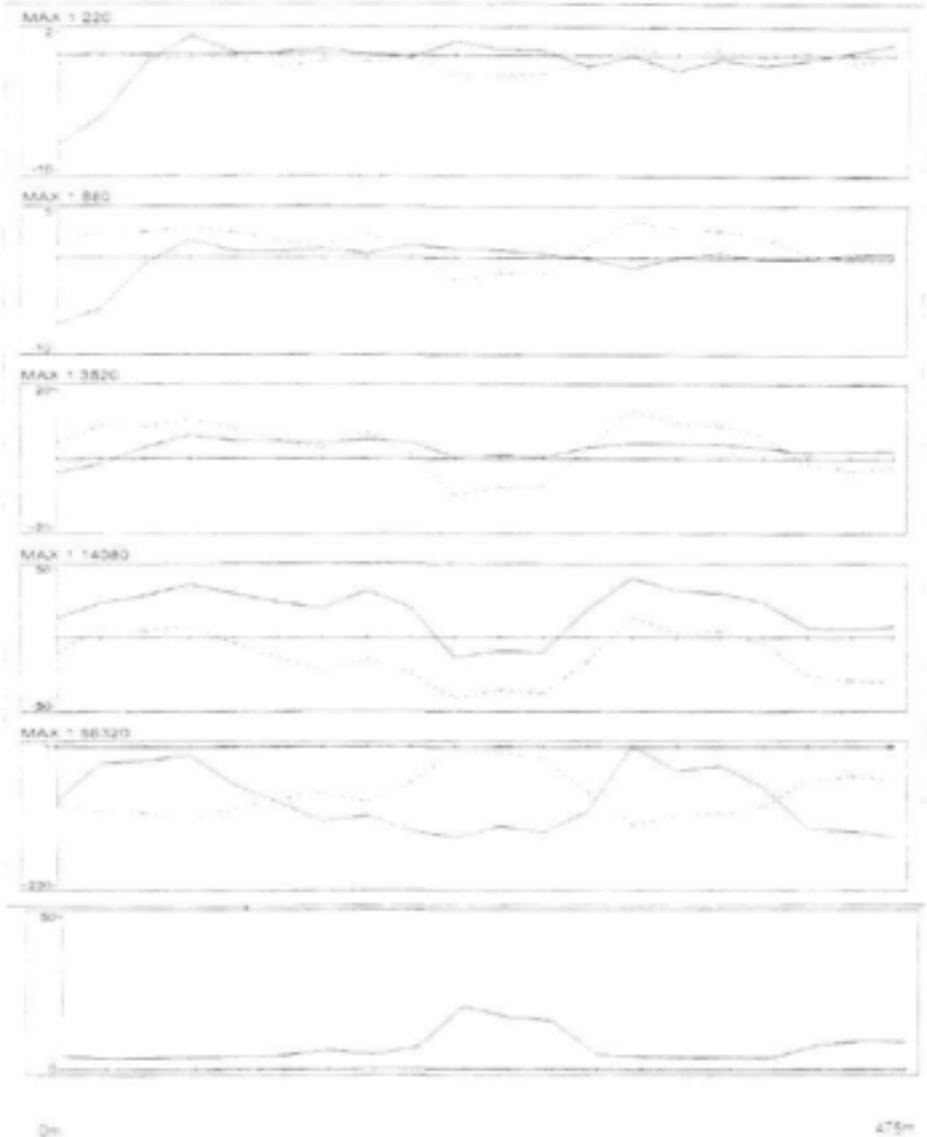

Figure 1-41 Max-Min electromagnetic profiles and conductivity's at site D17. Solid line: in-phase [%]: dotted line: out-of phase [%]: conductivity [mS/m]: coil separation 100 m, station spacing 25 m. Traverse direction: SSW-NNE.

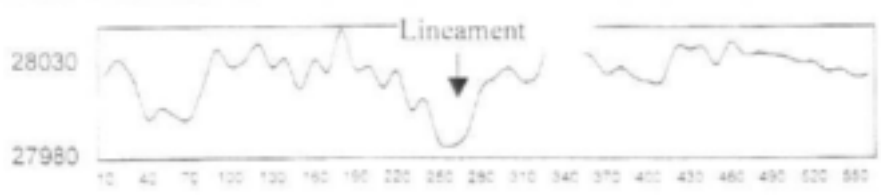

Figure 1-42 Magnetic profile in [nT] at site D17, station spacing 10 m. Traverse direction: SSW-NNE.

1.6.4 Magnetic structures

Five sites during the geophysical survey exhibited magnetic anomalies, which may represent dykes, sills or fault steps. Two examples are discussed below.

D8 – NW-SE running lineament and old borehole
Site description

Figure 1-37 shows the position of the traverse at site D8. A borehole with a broken pump is situated right next to a dirt road on the extension of a NW-SE running depression. The profile was conducted perpendicular to the dip direction and passes the borehole midpoint.

Electromagnetic Survey

The MAX-MIN was operated at 5 frequencies, ranging from 220 Hz to 56320 Hz while the coil separation was set to 100 m. A station spacing of 10 m was selected for both, the EM and magnetometer traverses. The results are shown in Figure 1-44 and Figure 1-45.

The EM response over the different frequencies shows a broad anomaly between station 6 and station 14: low in-phase and out-of phase values are flanked on both sides with positive shoulders. The quadrature component is largely affected by the discontinuity at lower frequencies. The presence of the anomaly is clearly shown while the in-phase component remains almost flat. With higher frequencies the out-of phase component looses its significance and eventually becomes inverted for the highest frequency. The response indicates a thickening of the conductive overburden, causing a clearly identifiable trough-like anomaly.

Magnetic Survey

Additionally, the magnetometer traverse generates a well-defined anomaly for the site. The shape of the anomaly could indicate a dyke structure, dipping to the NE. The total magnetic field intensity anomaly with a typical dipolar negative in the south and an increase in the north of the structure indicates a normal magnetization. However, the amplitude is very small and one could expect a more prominent response from a dyke-like structure in the tillite. Two boreholes were sited: one at the peak of the magnetic anomaly and the other to the NE to intersect the structure at depth. These sites also correspond to a thicker overburden in the electromagnetic profile.

D14 – NNE-SSW running lineament

Site description

The remote sensing data and the aerial photographs gave evidence of a prominent lineament, reflected through a depression running NNE-SSW in the morphology. Traverse 14 was conducted at a 90-degree angle across the lineament from the NW to the SE.

The MAX-MIN was operated at 5 frequencies, ranging from 220 Hz to 56320 Hz while the coil separation was set to 100 m. A station spacing of 20 m was selected. Results are shown in Figure 1-46 and Figure 1-47.

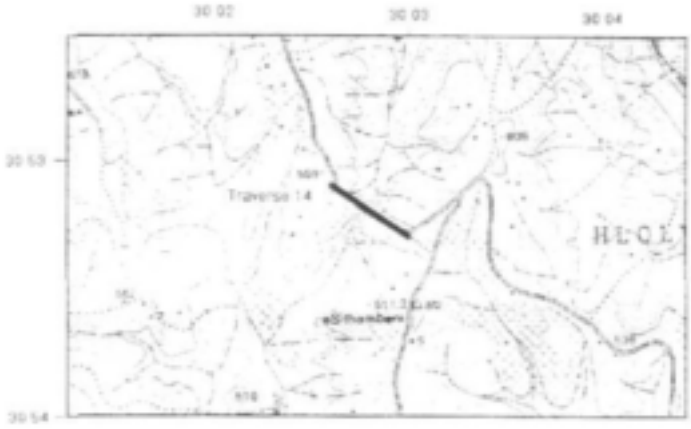

Figure 1-43 **Locality map of traverse D14**

Electromagnetic Survey

The in-phase and out-of phase components generate a very homogeneous picture throughout the traverse and no anomaly is detected.

Magnetic Survey

The magnetic data indicates an increase in the amplitude from the NW to the SE. The magnetic anomaly could represent a fault-step, at which a magnetic enriched layer within the tillite has been upthrown to the NW. A magnetic structure like a dyke is not likely, as the step in amplitude only is about 60 nT and the shape of the anomaly indicates a plate-like body.

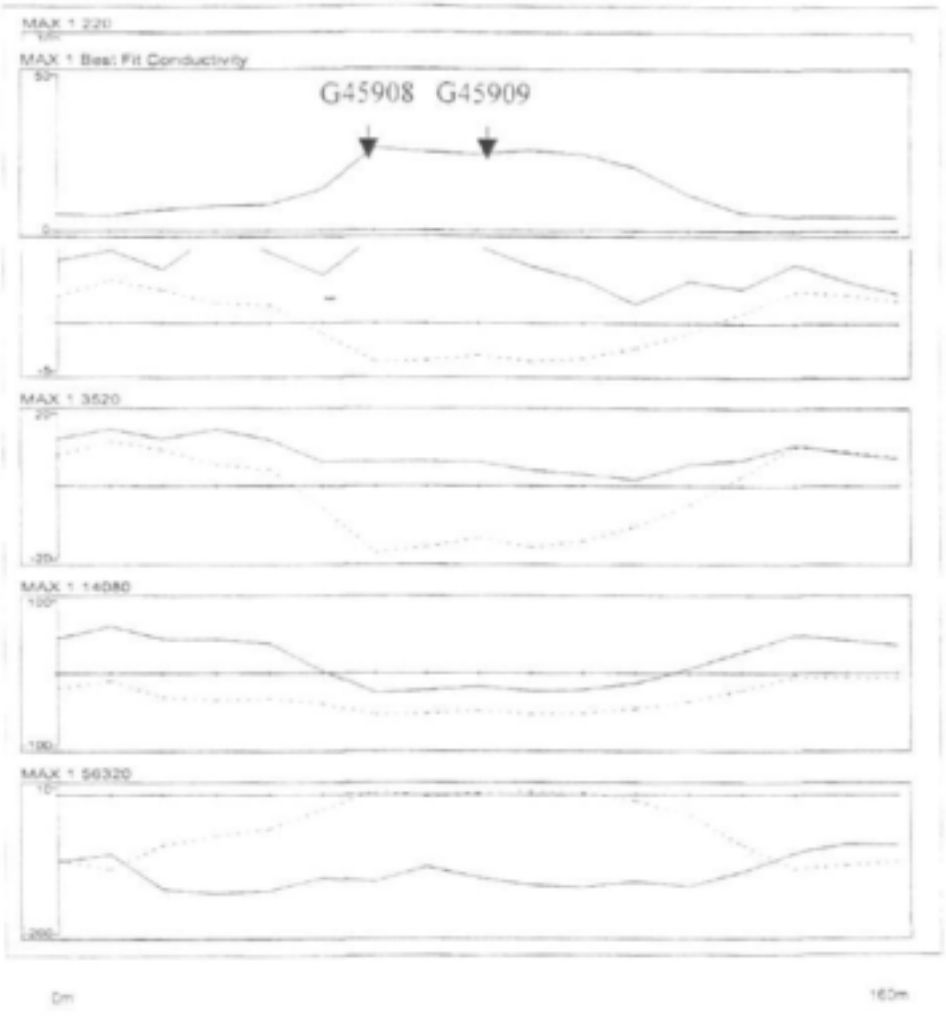

Figure 1-44 Max-Min electromagnetic profiles and conductivity's at site D8. Solid line: in-phase [%]; dotted line: out-of phase [%]; conductivity [mS/m]; coil separation 100 m, station spacing 10 m. Traverse direction: SW-NE.

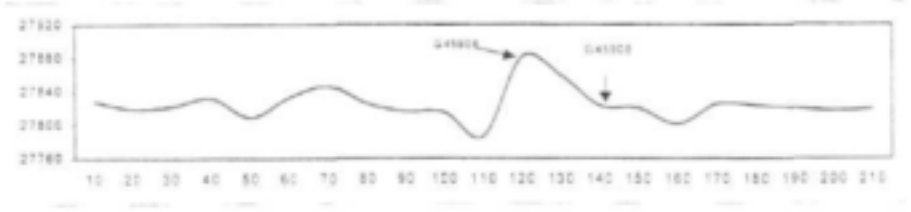

Figure 1-45 Magnetic profile in [nT] at site D8, station spacing 10 m. Traverse direction: SW-NE

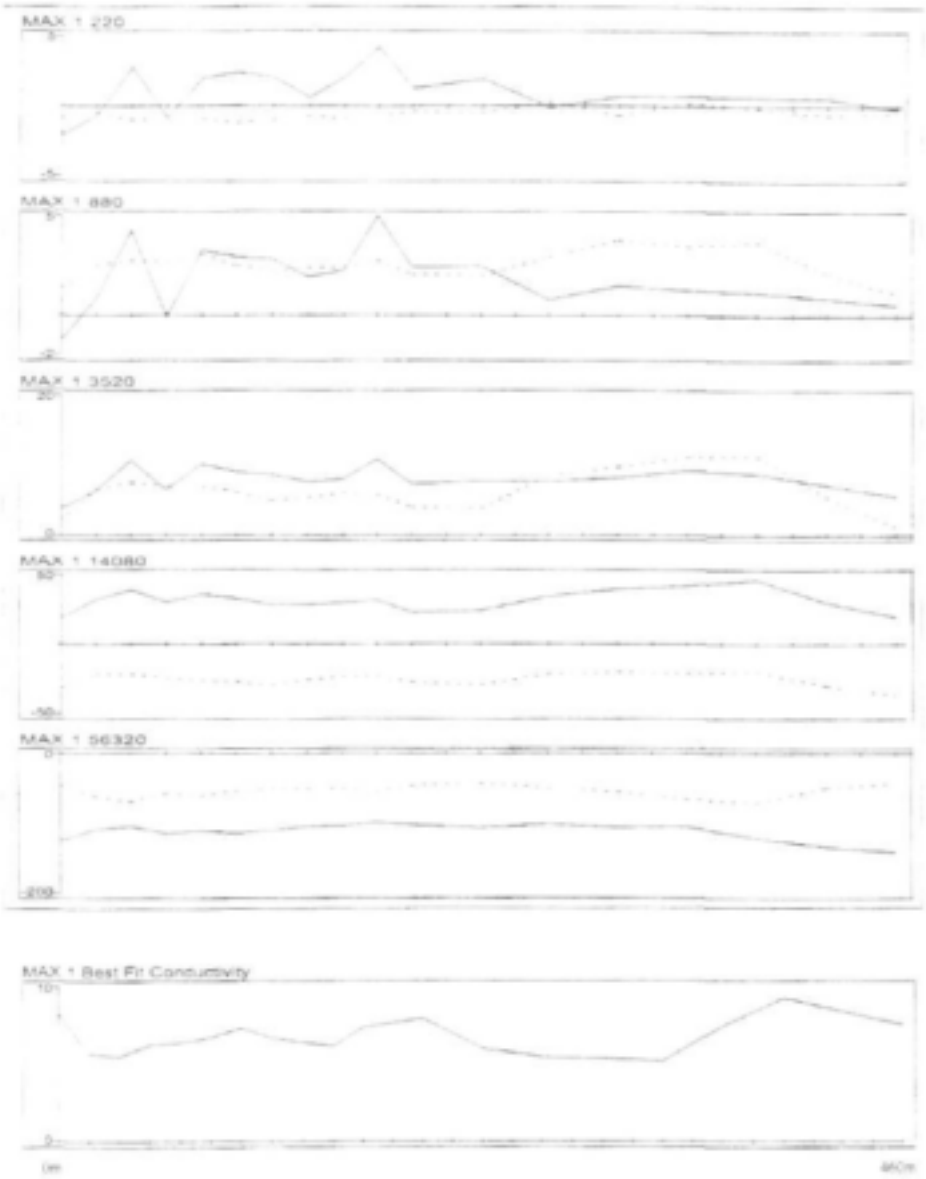

Figure 1-46 Max-Min electromagnetic profiles and conductivity's at site D14. Solid line: in-phase [%]: dotted line: out-of phase [%]: conductivity [mS/m]; coil separation 100 m, station spacing 10 m for stations 1-10, 20 m for stations 11-28. Traverse direction: NW-SE.

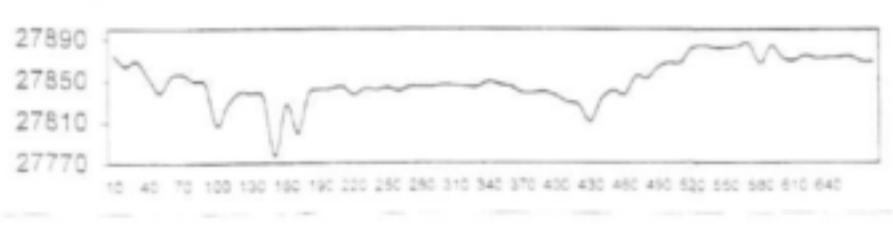

Figure 1-47 Magnetic profile in [nT] at site D14, station spacing 10 m. Traverse direction: NW-SE.

1.7 Drilling Results

To investigate the hydrological significance of the geophysical anomalies, 10 boreholes were drilled. Drilling was carried out by the Department of Water Affairs and Forestry using normal air percussion drilling.

The drilling sites covered all three geological scenarios represented by the different geophysical responses and all three major lineament directions. The geological logs and construction details, which are shown in Appendix 1-B are summarized below in terms of depth, construction, water strike, blow yield and structural feature investigated.

Table 1-3 Summary of Drilling Results

Borehole	Depth (m)	Water Strike (m)	Blow yield (l/s @ depth)	Feature investigated	Site ID of geophysical survey
G45905	120.00	N/A	Dry	• NW-SE running lineament; • Distinct change in weathered overburden thickness	D4
G45906	120.00	85.87	0.21 @ 83.9m 0.03 @ 120.00m	• NW-SE striking lineament. • Narrow conductor	D5
G45907	120.00	111.17	0.1 @ 112.00m	• NW-SE striking lineament. • Narrow conductor	D5
G45908	120.00	60.00	Seepage	• NW-SE running lineament • Deep weathered zone • Magnetic conductor	D8
G45909	120.00	55, 68, 73, 79-82	Seepage	• NW-SE running lineament • Deep weathered zone • Magnetic conductor	D8
G45910	72.00	42.00	0.07 @ 42m	• N-S extension of Bongwan gas fault, intersecting • E-W striking fault	D20
G45911	90	62.00	0.24 @ 66m	• N-S extension of Bongwan gas fault, intersecting • E-W striking fault	D20
G45912	120.00	N/A	Dry	• NE-SW running lineament • Distinct change in overburden thickness	D12
G45913	120.00	73 84	Seepage @ 76m 0.12 @ 84m	• NE-SW running lineament • Distinct change in overburden thickness	D12
G45914	120.00	N/A	Dry	• SSE-NNW running lineament	D23

Borehole G45905 on site D4

Borehole site

The site for borehole G 45905 was chosen on the basis of geophysical traverse no D4. The site is located in a NW-SE running depression intersecting a ridge. The traverse indicated a distinct change in the weathered overburden thickness from SW to NE (Figure 1-33). The hole was sited at locality 90m directly at the change of the thickness of the weathered tillite. The hole is located near the Fillipi Mission Station, on farm no. 4666 (Figure 1-48).

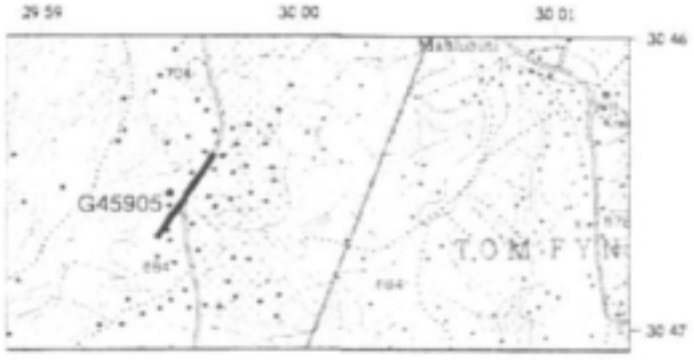

Figure 1-48 Location of borehole G45905

Geological description

The hole proved to be of very uniform lithology. The first 17 m consisted of light brown weathered tillite. From 17 to 120 m, the final depth, solid, fresh dark grey diamictite was penetrated. Very few drill cuttings showed the presence of narrow joints, and these were filled with calcite. No water strike was encountered and the hole was subsequently backfilled.

Borehole G45906 and G45907

Borehole site

Borehole G 45906 was drilled on traverse no. D5 (see section 4.6). The geophysical response was interpreted in terms of a NW-SE striking narrow conductor dipping steeply to the SW. The top of the conductor was interpreted at locality 175m of the EM profile (Figure 1-39). Borehole G45906 was selected at the EM negative peak response at station 150m to ensure the intersection of the fracture zone below the relatively deep static water level.

Figure 1-49 Location of boreholes G45906 and G45907

Geological description

After 11.70 m of soil and weathered tillite, solid rock was encountered consisting of partly fresh, partly fractured grey diamictite. The fractures were of 1-3 mm width and infilled with calcite. The predicted conductor was encountered at 71m depth together with a distinct change in lithology to a brown, clayey, highly fractured tillite. The fracture zone proved to be

16 m wide with an associated water strike at 83.9m and a blow yield of 0.2l/s. Drilling of the borehole continued to the final depth of 120m. The final blow yield measured as 0.23l/s.

The second borehole, G45907 was located on the same site, 25 m further to the SW in order to intersect the conductor a second time to calculate shape and extent of the fracture zone.

After 11 m of overburden and 100 m of solid to slightly fractured grey tillite, a fracture zone was hit at 111.2 m with an associated water strike of 0.1 l/s. In contrast to the feature penetrated in hole G45906 this fracture zone was not accompanied by a change in the lithology. This feature appeared to be much smaller and less weathered.

The different lithologies and widths of the fractures encountered in both holes suggest, that the EM anomaly does not originate from one single regular shaped conductor. It is more likely that the anomaly originates from a wider conductive zone containing several fractures of irregular shape and width that are not necessarily interconnected. However, the drilling results show that reliable interpretation of conductive zones and general dip directions can be obtained from the Max-Min survey.

Borehole G45908 and G45909

Borehole site

On the basis of traverse no. D8 (see section 1.6) two drilling sites were chosen in a NW-SE running depression zone along a ridge (Figure 1-50). The electromagnetic data suggests a wide trough of weathered tillite running from the NW to the SE, which may be associated with a fracture zone. Additionally, the magnetic data gave a distinct response suggesting the presence of a magnetic conductor. Borehole G45908 was selected at the EM negative peak response for the out-of phase component at locality 60m where the overburden is believed to undergo a change in thickness (Figure 1-44). This coincides with station 120m of the magnetic profile, on the SW flank of the anomaly.

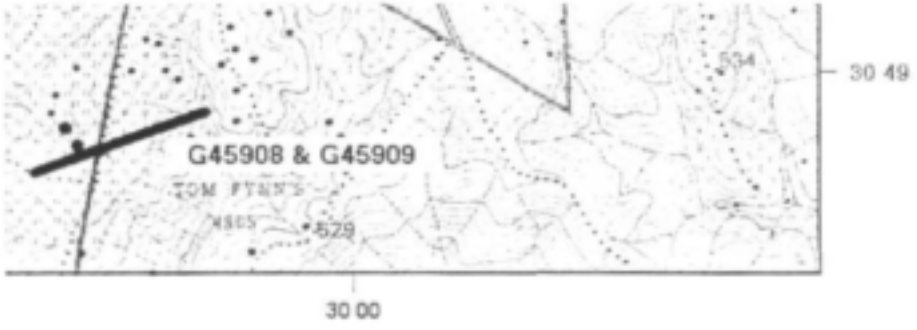

Figure 1-50 **Location of the boreholes G45908 and G45909**

Geological description

The first 22 meters of G45908 consist of a sequence of topsoil, clay, sand and highly weathered tillite. To a depth of 60 m the brownish tillite is highly fractured, with calcite, gypsum and ferricrete filling the joints indicating the partial presence of oxygen and water. At 60 m depth seepage occurred but due to the low flow rate the blow yield was not measurable. The lithology up to the final depth of 120 m remained constant with grey, slightly fractured tillite.

It was decided to drill a second borehole, G 45909 20 meters further towards the NW, but still situated at the edge of the thick overburden indicated by the EM anomaly. After penetrating through very thick soil, clay, sand and weathered tillite fresh but fractured tillite was hit at 18 m. The fractures are filled with calcite. Up to a depth of 41m gypsum and ferricrete occur. Gneiss clasts are scattered throughout the tillite. At 56m seepage was intersected but again due to the low flow rate, the blow yield was not measurable. Up to the final depth of 120 m the tillite contained calcite filled joints and gneiss clasts.

In conclusion, the drilling results reflect the predicted geology of the EM survey. The trough like anomaly between station 60m and 140m had its origin in the thick overburden encountered. Clay layers, highly weathered tillite and water-bearing minerals such as gypsum form a conductive zone identified by the Max-Min. This suggests that the Max-Min is capable of locating conductive zones very accurately, however they may not always be associated with a water bearing buried conductor. The magnetic anomaly is believed to have its origin in the ferricrete and the ferruginous tillite identified in the first upper meters.

Borehole G45910 and G45911

Borehole site

The next boreholes were selected on the basis of a distinct joint pattern identified from the aerial photographs and LANDSAT map in the valley bottom of the Mzinhlanga River. A N-S extension of the Bongwan gas fault, south of the study area intersects a W-E running lineament at a 90° angle at the site. The structures are imprinted into the morphology in the form of deeply incised valleys. The Mzinhlanga River has developed on this joint set and exhibits a right angle bend at the fault and lineament intersection. The steep topography made it impossible to fully traverse the large-scale fault zone during the geophysical survey; therefore, the EM data did not generate a consistent picture. As this site seemed to be most promising it was decided to site the boreholes according to observations on the structural geology. Both boreholes were established on the predicted line of the E-W running lineament near to a small river copying the gas fault orientation. The boreholes are 20 m apart.

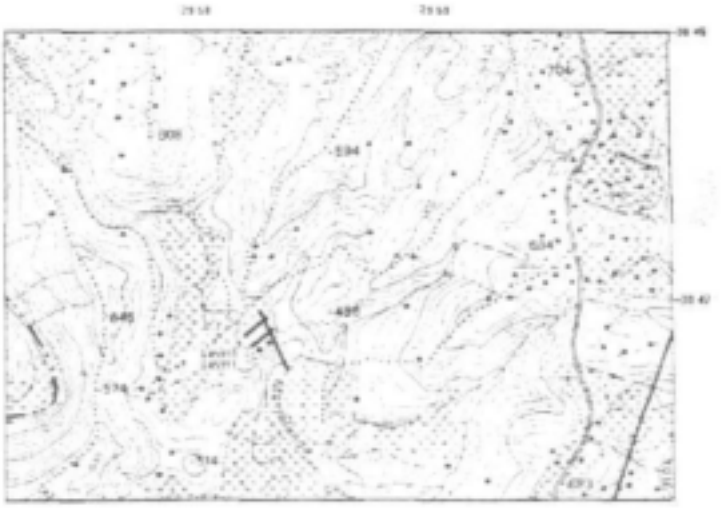

Figure 1-51 Location of the boreholes G45910 and G45911

Geological description

Borehole G 45910 intersected only a thin cover of soil and weathered tillite. Solid grey tillite with small fractures infilled with calcite and gneiss or sandstone clasts was encountered at a depth of up to 40 m. An increase in the density of fractures and their width announced the water bearing fracture zone hit at 42m with an associated blow yield of 0.07 l/s. Up to the final depth of 72 m grey, moderately fractured tillite with gneiss clasts was encountered. The final blow yield was measured to 0.05 l/s and the rest water level was 3.21 m below surface.

The second borehole, G45911, intersected similar geology. A 5-meter thick soil cover was followed by fractured tillite with gneiss clasts up to a depth of 61 m. The water strike occurred at 62m and is associated with a 1.5m white quartz layer reaching from 61.5 to 63m depth. The fracture yielded water in excess of 0.21 l/s. The hole was drilled up to a final depth of 90 m and intersected grey slightly fractured tillite with gneiss and sandstone clasts. The rest water level was measured to 3.63 m below the surface.

The drilling results of borehole G45910 and G45911 indicate that the most successful borehole sites are in the valley bottoms. Even though the yield of the holes do not exceed those drilled on the hilltops, the shallow water strike and the shallow water level make these sites more favourable in terms of drilling and pumping costs.

Borehole G45912 and G45913

Borehole site

Boreholes G45912 and G45913 were sited in a NE-SW running depression along a ridge, on the basis of the geophysical traverse 12 (see section 1.6) (Figure 1-52). The EM anomaly was interpreted as a valley discontinuity where the overburden thickens distinctively. This may be associated with a buried fracture zone. The positive peak ratio indicates the dip direction to be towards the NW. The deepest overburden or conductor is interpreted at station 140m and gives the drilling site for Borehole G45913. A second borehole, G 45912 was sited at station eleven on the down-dip site of a possible conductor to characterise shape and position of the feature.

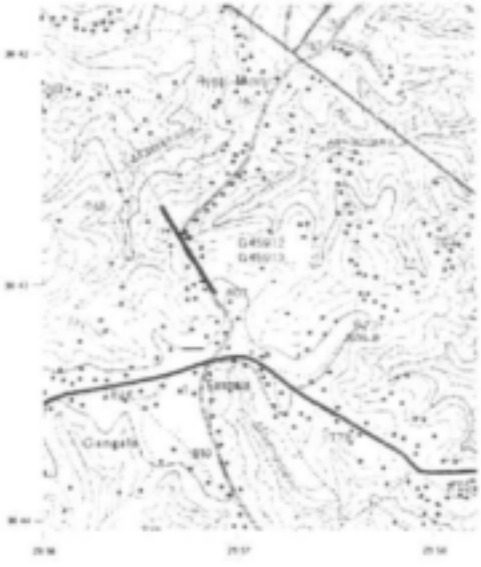

Figure 1-52 **Location of the boreholes G45912 and G45913**

Geological description

Borehole G 45913 intersected a deeply weathered zone predicted from the geophysical results until, at 27 m, solid rock was encountered. Fresh but slightly fractured grey tillite with gneiss clasts followed up to a depth of 76 m where seepage occurred. At 84 m a second water strike was intersected yielding water in the excess of 0.12 l/s. This water strike is associated with a fracture zone of about 3 m width infilled with weathered, residual tillite. To the final depth of 120 m the lithology remains unchanged with grey, slightly fractured tillite. The final blow yield was measured to 0.09 l/s and the rest water level was 70.4 m below the surface.

In borehole G 45912 weathered tillite occurs to a depth of about 27 m. To the final depth of 120 m the lithology consists of dark grey slightly fractured tillite. The conductor hit by the previous hole was not encountered.

In conclusion, the thick overburden indicated by the EM data is the result of a buried fracture zone, which was intersected by borehole G45913 at 76 m. Borehole G45912 missed this feature, probably due to the very steep dip of the fracture zone.

Borehole G45914

Borehole site

A last borehole was drilled near the Booker Bus Halt on the farm Ebenezer 784 (Figure 1-53). Both, aerial photographs and the remote sensing data indicated a prominent lineament running from the SSE to the NNW forming a steeply incised valley. The feature is well defined in the morphology by a steeply incised valley. The EM and magnetic survey was carried out perpendicular to the lineament. Unfortunately, the background noise is high due to power lines crossing the traverse. It was decided to site the borehole directly in the line of the valley representing the possible feature. But due to its steep morphology the site had to be removed by about 50 m towards the west of the linear feature due to accessibility problems.

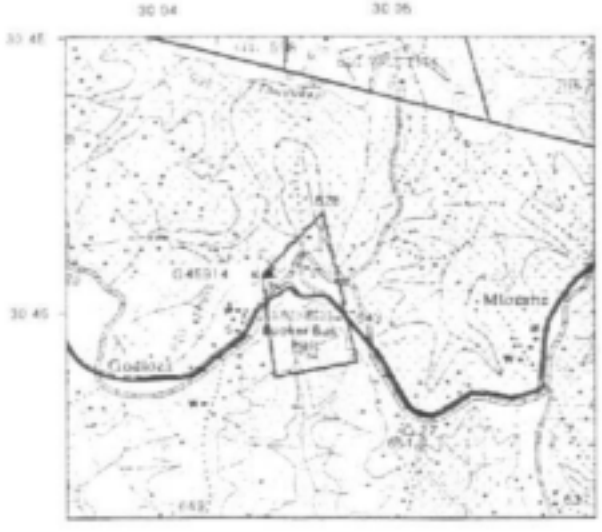

Figure 1-53 Location of the borehole G45914

After a 10 m thick cover of soil, solid grey tillite was encountered. The lithology stayed unchanged until the final depth of 120 m. No indication of a fracture zone was found.

The very homogeneous geological log suggests that a possible prominent feature was missed due to the accessibility problems with the rig. As conductors in the study area tend to dip very steeply, a site slightly off the geophysical or structural anomaly is likely to fail.

Conclusion

From the geological logs it is evident that the aquifers in the Dwyka tillites occur only within the fractured bedrock itself, as primary porosity is nearly absent. Thick weathered residual overburden is seldom encountered and does not constitute significantly to the groundwater occurrence in the area. Magnetic conductors that were not dolerite related proved not to be water bearing, which suggests that magnetic geophysical exploration may lead to false positives. Two boreholes (G45910 and G45911) were sited without any geophysics on presumed fault zones and these both proved successful, one of which was the highest yielding borehole drilled. These did not exhibit any electromagnetic or magnetic anomalies (Appendix 1-A). Two of 4 boreholes sited without geophysics during the CIP also proved successful and high yielding (>0.5 l/s) (Figure 1-17). This suggests that visual siting on structures may prove to be more successful in this terrane.

1.8 Test Pumping

On three of the newly drilled boreholes a constant discharge test was carried out in order to characterise hydraulic properties of the penetrated lithologies and to determine sustainable aquifer and borehole yields. Additionally, constant rate discharge and recovery data of borehole 405530, established during the Critical Intervention Program, is available. The test pumping and recovery data are presented in Appendix 1-C.

Transmissivity (T), storativity (S) were calculated by the Cooper-Jacob method. The sustainable yield of the single borehole was calculated according to a modification of the Cooper-Jacob equation known as the distance-to-boundary method (Sami & Murray 1998). This method incorporates T and S data together with a time value at which a hydraulic boundary is encountered. Common examples for recharge boundaries in the study area are water-bearing joints and faults. Examples for barrier boundaries are dolerite dykes or mineralised faults or fracture zones. The program calculates early transmissivity data for the time before a hydraulic boundary is encountered, known as fracture transmissivity (Tf), a late T value (Tm) for the period after the boundary is exceeded, representing the matrix conductivity and a T value from the recovery data. The program then calculates pumping rates that can be sustained over the long-term.

Borehole G45906 and G45907

The blow yield of G45906 was measured as 0.23 l/s and the rest water level to 73.8m. For the discharge test, the pump was inserted to a depth of 81.80m. For the first three hours of the pumping test, the hole was pumped at 0.075 l/s. Difficulties were encountered maintaining a constant discharge at such a low yield, hence water level fluctuations are evident. As the water level almost reached the pump intake after 3 hours, the pumping rate was lowered to 0.05l/s for the remaining 6 hours of the pump test.

The drawdown data for the first 2 h is negligible (<0.5 m) and remains relatively constant, suggesting flow primarily from a permeable fracture. However, after 2hours the rate of drawdown increases sharply, indicating that a closed boundary has been encountered. When the rate of pumping was reduced the borehole temporarily recovered until it once again exhibited closed boundary conditions.

The early and late time data transmissivity was calculated and is presented in Table 1-4. Due to the low trasnmissivity, minor variations in pumping rate resulted in significant drawdown variations (Appendix 1-C), hence transmissivity could not be calculated from pumping data. The recommended borehole yield is calculated on the basis of different methods and presented in Table 1-5. Due to closed boundary conditions, the sustainable yield appears to be only about 2.2 m^3/d.

Table 1-4 Transmissivity values for G45906

G45906	T_{early} (m^2/d)	T_{late} (m^2/d)	$T_{recovery}$ (m^2/d)
			0.17

Table 1-5 Recommended borehole yields for G45906

	Recommended borehole yields	hrs at max.
Method	m^3/d	pump.rate
Max. pumping rate (l/s)		0.2
Recovery	0.0	0.0
Late T	0.2	0.2
Drawdown to boundary	2.2	2.4
Distance to boundary	1.7	1.6
Flow characteristic 1	0.1	0.1
Maximum drawdown	2.5	3.0

Borehole G45907 was monitored while pumping G45906. Although, the drawdown curve reveals that both boreholes are in hydraulic contact, the observed drawdown in G45907 could be influenced by pumping from a nearby borehole equipped with a handpump and frequently used by the local inhabitants. Significant drawdown appears at 0.1 days, or after about 2.5 hours after the pumping test began. This borehole was used to calculate a transmissivity and storativity value using the Cooper-Jacob method and gave a T value of 0.23 m^2/d and an S value of 0.005,m which is similar to that calculated from G45906.

Borehole G45910 and G45911

The blow yield for borehole G45911 was measured as 0.2l/s and the rest water level was 20.98m below surface. For the discharge test the pump was lowered to 59.60m and the borehole was pumped for 12 hours at 0.1l/s. Borehole G45910 was monitored as an observation borehole.

The early time data of the log-log drawdown curve has a slope of about 0.25, which is indicative of linear flow through a fracture. After about 10 minutes (0.007 days) boundary conditions are encountered. The derivative curve shows a constant slope of greater than 0.5, indicating that radial flow conditions are never established. Flow can therefore be considered to be linear and predominantly through a single fracture system. An inflection point at 17 m of drawdown, or a water level of approximately 38 m, may indicate the water bearing fracture. Although the water strike was only picked up at 61 m, during drilling, the location of a water strike at 42 m in the adjacent borehole G45910, suggests that the water-bearing zone may be at 38 m. This may have been caused by compressor air pressure preventing water from entering the borehole hole or clogging of the small fracture by drill cuttings. After this point, the slope of the drawdown curve on the semi-log and log-log plots, as well as the derivative curve, increases sharply, providing further evidence that the water bearing fracture is at 38 m.

The calculated transmissivity is presented in Table 1-6. Radial flow conditions were never established, causing the application of the Cooper-Jacob method to be problematical. Transmissivities were calculated nevertheless using the period 0.006-0.03 days for early time and 0.3-0.5 for late time. On the basis of these parameters the safe yield of the borehole is presented in Table 1-7 and is probably about 5 m^3/d

Table 1-6 Transmissivity values for G45911

G45911	T_{early} (m^2/d)	T_{late} (m^2/d)	$T_{recovery}$ (m^2/d)
	0.45	0.02	0.09

Table 1-7 Recommended borehole yield for G45911

	Recommended borehole yields	hrs at max.
Method	m^3/d	pump.rate
Max. pumping rate (l/s)		0.2
Recovery		
Late T	0.6	0.8
Drawdown to boundary	5.4	7
Distance to boundary	2.4	3.1
Flow characteristic 1	0.4	0.6
Maximum drawdown	6	7.8

The water level in Borehole G45910 was observed during the discharge test of G45911. However, the water level in this borehole was gradually rising and rose about 0.5 m during the duration of the pumping test. This indicates that the linear fracture intersected by G45910 was not intercepted by G45911.

Borehole G45913

For the discharge test of borehole G45913 the pump was lowered to a depth of 85.80 m, pumping 12 hours with a rate of 0.07 l/s. The rest water level was measured to 70.54 m.

The results of the first 15min of the pumping test are unusable due to difficulties in adjusting the low flow rate. Thereafter the drawdown curve shows a steady decline, and the horizontal derivative curve indicates that radial flow conditions are approximated until about 240 minutes. Subsequently, the rate of drawdown increases substantially, indicating that closed boundary conditions are encountered. Towards the end of the test at 480 minutes the water level temporarily stabilises, indicating that a water bearing fracture may have been intercepted. Unfortunately, the test was discontinued and this cannot be validated.

The calculated transmissivity for G45913 is presented in Table 1-8. The recommended borehole yield is presented in Table 1-9. Early time transmissivity was calculated from the period 15-40 minutes, whereas late time transmissivity was calculated from the period after the boundary was encountered. The sustainable yield is probably about 1.4 m^3/d.

Table 1-8 Transmissivity values for G45913

G45913	T_{early} (m^2/d)	T_{late} (m^2/d)	$T_{recovery}$ (m^2/d)
	1.15	0.22	0.76

Table 1-9 Recommended borehole yields for G45913

	Recommended borehole yields	hrs at max.
Method	m^3/d	pump.rate
Max. pumping rate (l/s)		0.04
Recovery		
Late T	1.8	13.6
Drawdown to boundary	1.7	12.7
Distance to boundary	1.4	10.2
Flow characteristic 1	1.0	7.6
Maximum drawdown	2.5	18.4

Borehole 405530

Borehole 405530 is situated in the south of the study area on top of a ridge. It was established during the Critical Intervention Programme. The blow yield was measured as 2.5 l/s and was associated with a fracture zone at 90 m depth. The rest water level was measured as 55.56 m below surface, giving 45.4 m of available drawdown and the hole was pumped at a rate of 2 l/s. For the discharge test, the pump was inserted to a depth of 101, m. No geological data or geophysical data are available for the borehole' hence it can be presumed that the borehole was sited visually. The borehole could not be located in the field at the given co-ordinates. The local community also had no recollection of this borehole, in spite of the borehole having been drilled in 1995.

The drawdown curve of borehole 405530 behaves according to the double porosity concept known for fractured aquifers. The first 20 min of the drawdown curve reflects the flow contributed from the fractures. The flattening of the drawdown curve between 20 min and 3 h reflects a period during which leakage from the aquifer matrix occurs.

The transmissivity values are presented in Table 1-10. The recommended borehole yield is shown in Table 1-11. The sustainable yield is about 40 m^3/d.

Table 1-10 Transmissivity values for borehole 405530

405530	T_{early} (m^2/d)	T_{late} (m^2/d)	$T_{recovery}$ (m^2/d)
	2.38	1.7	2.5

Table 1-11 Recommended borehole yields for borehole 405530

	Recommended borehole yields	Hrs at max.
Method	m^3/d	pump.rate
Max. pumping rate (l/s)		2.7
Recovery	3.4	0.5
Late T	40.1	5.4
Drawdown to boundary	39.6	4.0
Distance to boundary	20.9	2.1
Flow characteristic 1	46.0	4.6
Maximum drawdown	55	5.6

The discharge test shows that the early time transmissivity of the tapped fracture is in the same order as the lower yielding boreholes discussed above. Hence, the high blow yield cannot be attributed to higher fracture permeabilities. The shallower water strike and the

larger available drawdown create a higher confining pressure, which leads to a relatively higher yield.

Conclusion

In conclusion, the discharge tests indicate that the aquifer consists mostly of single finite fractures of low permeability and low storativity, with a relatively impermeable rock matrix. The early time fracture transmissivity is about one order of magnitude higher than the late time transmissivity due to poor interconnection of fractures. This corresponds very well with the drilling results, which indicated that most fracture networks are calcite filled, resulting in poor interconnectivity.

Figure 1-54 shows the relationship between the blow yields, the sustainable yields and the transmissivities of the four boreholes tested. A linear relationship may exist between blow yield and sustainable yield, whereas the transmissivity proved not to be directly related to the yield of the boreholes, implying that yield may be related to available drawdown. That implies that storativity, fracture interconnection and the confining pressure in the tapped fractures are more important in regards to the yield of a borehole. However, Figure 1-54 is only based on four data points and the results have to be taken with caution.

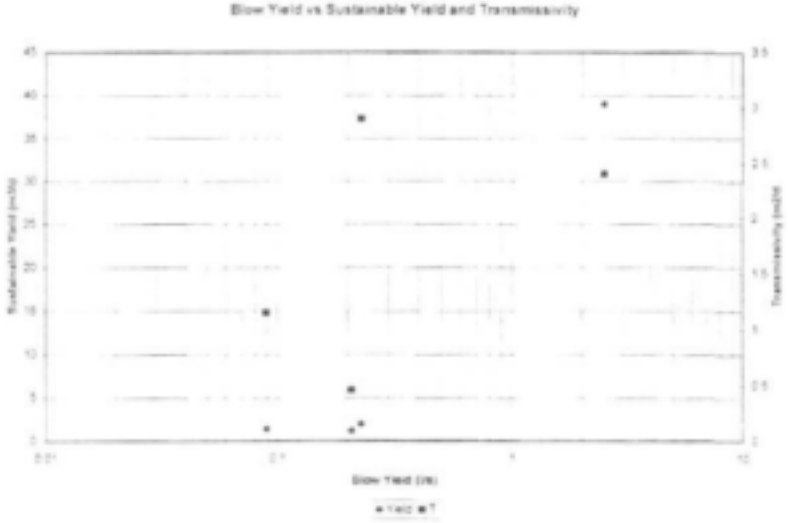

Figure 1-54 Relationship between sustainable yield, blow yield and transmissivity

1.9 Down-the-hole Geophysics

The newly drilled boreholes were logged using gamma and apparent resistivity logging to determine the formation composition in terms of lithology, permeability and conductivity. The data were obtained with the CHEMTRON R300 bore logger, which is with a portable bore hole logger that records the number of pulses detected per unit of time.

Gamma Logs

The gamma radiation intensity was measured for five of the newly drilled boreholes. The gamma logs for the respective boreholes are presented in Appendix 1-E.

In general all obtained gamma logs show a very uniform profile reflecting the very uniform character of the tillite formation. G45906, G45907 and G45913 are discussed together as they generate a very similar log. The weathered overburden is clearly identifiable with a lower

clay content compared to the tillite matrix since it has low radiation counts. A distinct increase in radiation intensity reflects the clay-enriched matrix of the tillite formation. At a depth of about 70m the radiation intensity changes again and less counts per second are obtained. This is believed to correlate with a lower clay content in the tillite matrix. Furthermore, the static water level at this depth backs the suggestion of a less permeable matrix above 70 m due to a higher clay content.

In boreholes *G45910* and *G45911* the weathered zone can be identified by a relatively low radiation intensity. After the first few meters the counts per second increase distinctively according to the change in lithology to clay enriched tillite. The tillite appears very homogeneous and no further differences in the radiation intensity are recorded.

Spontaneous Potential Logs (SP log)

The SP logs obtained from the yielding boreholes are shown in Appendix 1-E.

The logs generated a very homogenous picture, reflecting an unstructured tillite formation. Existing lithological changes seemed to be too insignificant to be picked up by the SP log.

Conclusion

In conclusion, it is not possible to gain any new information about the subsurface and its water-bearing features by using down-the-hole geophysics in the Dwyka tillite. The formation is too uniform and small changes in the lithology proved to be undetectable by gamma or SP logs.

1.10 Evaluation of climatic data

Rainfall data for the study area was obtained from the Computing Centre for Water Research (CCWR). Only one rainfall station exists in the vicinity of the study area and is at the Mehlomnyama police station, approximately 15 km east of the study area. The distribution of estimated mean annual precipitation (MAP) for the study area, based on the CCWR 1minute x1 minute rainfall grid is shown in Figure 1-55. The estimation of MAP at each grid point was determined using a regression surface in which MAP was regressed against factors such as altitude, latitude, longitude, continentality and aspect (Dent, Lynch & Schulze, 1989). Figure 1-55 suggests that MAP varies between 618.5 mm and 1204.5 mm in the area. Generally rainfall intensity increases with decreasing elevation towards the SE. Average mean annual rainfall for the study area is about 840 mm.

The monthly rainfall distribution in the area is characterised by intense summer rainfall and dry winter seasons and is presented in

Figure 1-58 for grid point 30.05 longitude and 30.75 latitude.

An estimation of rainfall distribution during wet and dry years is shown in Figure 1-56 and Figure 1-57, based on the rainfall that is likely to be exceeded in 20 % and 80 % of the years.
The mean monthly evapotranspiration data is presented in
Figure 1-59 for the grid point 30.0500 longitude and 30.7500 latitude. Mean annual S-pan evapotranspiration is 1570 mm.

The recharge for the area can be estimated on the basis of existing rainfall-recharge relationships. Several locally developed rainfall-recharge relationship formulae exist for South Africa (Bredenkamp et al., 1995). They give site-specific estimations of recharge values as a fraction of precipitation, although they ignore the complex nature of recharge

processes. Recharge for the study area can be calculated on the basis of a formula developed for Karoo aquifers (Sami & Murray 1998):

R = 1.5% of MAP [mm] (1)

According to equation (1) recharge in the study area is in the order of 12.6 mm/annum. This corresponds to values given by DWAF (1995) for the region, which are in the order of 10 to 20 mm/annum. A large proportion of recharge is discharged in high lying springs in the study area due to the low storage capacity of the rock, hence groundwater has a low residence time.

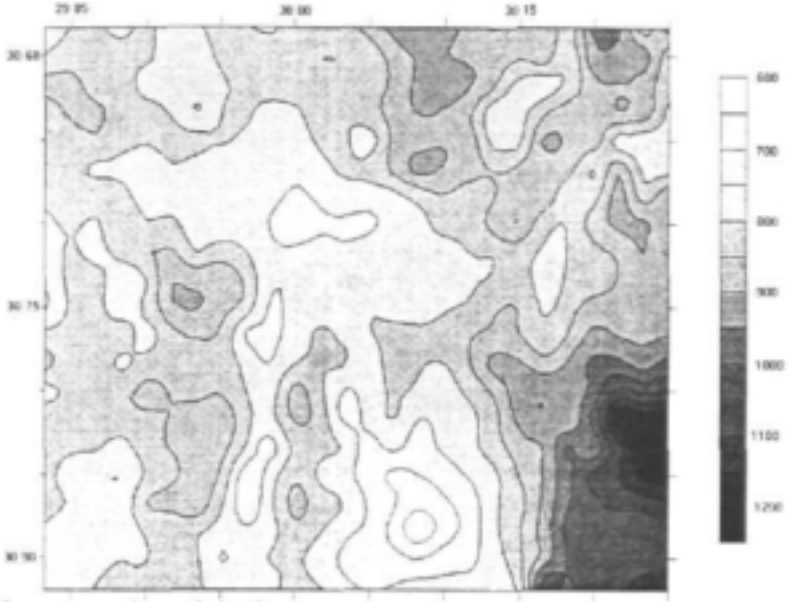

Figure 1-55 Mean annual precipitation

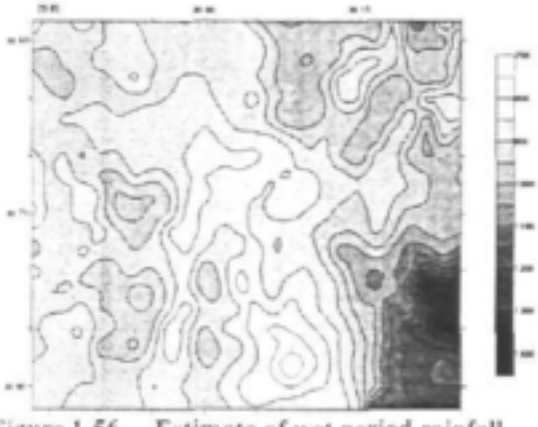

Figure 1-56 Estimate of wet period rainfall

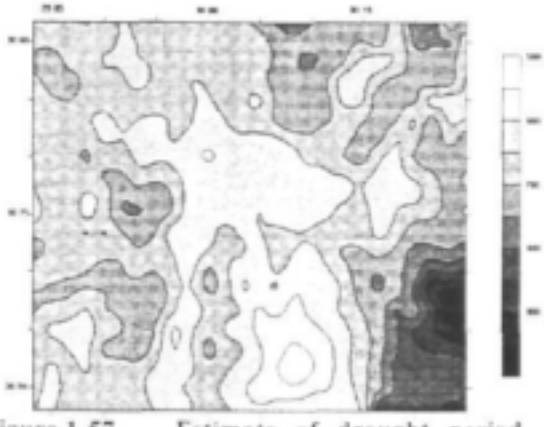

Figure 1-57 Estimate of drought period rainfall

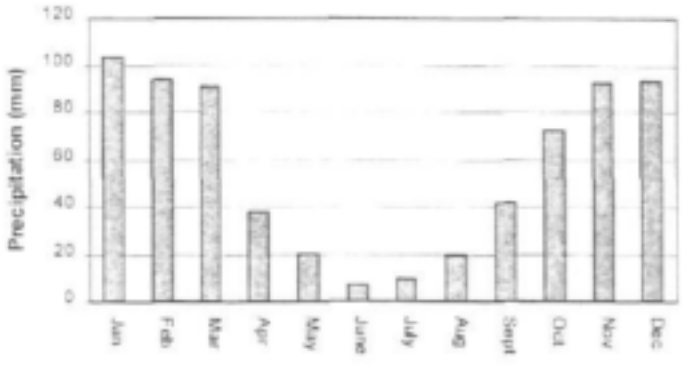

Figure 1-58 Mean monthly distribution of precipitation at grid point 30.0500 longitude and 30.7500 latitude

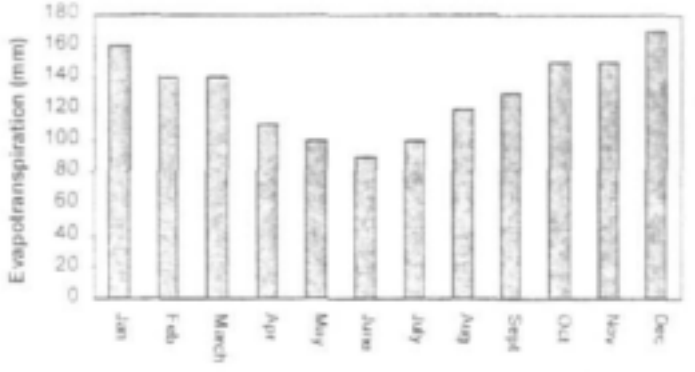

Figure 1-59 Mean monthly distribution of S-pan evapotranspiration at grid point 30.0500 longitude and 30.7500 latitude

1.11 Hydrogeological Evaluation

Water demand in the study area is primarily for domestic purposes and partly for small-scale agricultural activity. Currently, water supply needs are met mostly from upland springs, rivers in the valley bottoms, and boreholes equipped with hand pumps. However, groundwater could play an important role as it is a reliable water source, even in drought situations, and is generally of good quality compared to other water sources in the area. Water supply provision is complicated by the fact that settlement is concentrated on hill tops and extremely limited access exists to low lying areas, where a more assured water supply could be located. The extreme topography, however, would create static pumping heads of over 300 m. Hence, groundwater exploration is predominantly restricted to the hill top regions.

The tillite has a very low permeability and forms a cover of up to 450 m thickness in the area, which prevents drilling through the formation into a more consistent aquifer. The fine-grained tillite is generally an aquiclude, except where fractures are encountered. The drilling results and the pumping tests indicate that the very homogeneous sedimentary lithology lacks primary porosity. Porosities range between 0.0021-0.0076 (Brink, 1983). Secondary porosity has been reduced by numerous calcite veins. Clay minerals constitute an important part of the tillite matrix and affect the process of weathering, resulting in the formation of montmorillonite- illite-kaolinite. This fact is reflected in the very poor historical success rate in the area, with 84 % of the holes being dry.

Three of the boreholes drilled into fractured tillite during the critical intervention programme are thought to have intersected large faults and have yields of greater than 2.0 l/s. However, these faults occur at the contact of the Dwyka Group with other lithologies and were not investigated during this study as they were previously known structures and their occurrence is very limited. Hence, the project concentrated on alternative targets that are not currently considered. Smaller faults have been shown to yield generally less than the major faults. This could be attributed to the fact that the larger faults have created a greater spread of sympathetic faulting which increases connectivity and hence more groundwater collection occurs.

Drilling and the geophysical investigations in the area revealed that successful boreholes are associated with fracture zones only. They proved to be generally unconnected and, due to steep dip angles, and of very limited horizontal extent, even though all boreholes except for G45910 and G45911 were drilled on lineaments thought to be extensional features. The lack of regional extensional features is also highlighted by the LANDSAT TM lineament data set.

which indicates that the bulk of lineaments are of limited extent. Structures like dolerite dykes or sills are seldom found in the study area and hence do not play an important role. There is no indication that the highly weathered overburden material, with a thickness of up to 30m, act as an additional aquifer or that it provides a significant storage to replenish the underlying aquifer.

The discharge tests revealed that water abstraction from the Dwyka formation exhibits a strong time dependency. During early-time response groundwater flow to the borehole comes from storage in the permeable fractures. With progressive pumping boundary conditions quickly become evident, indicating a poor fracture connectivity. This can be attributed to the calcification of the existing fracture networks, which is evident to over 100 m depth. The calculated fracture transmissivities range in the order of 0.45 m^2/d to 2.8 m^2/d. The late time transmissivity ranges in the order of 0.02 m^2/d to 0.22 m^2/d.

These unfavourable hydraulic properties explain the relatively low yield of the aquifer. An average blow yield of 0.14 l/s can be expected in wet boreholes, however, this is not sustainable on a continuous basis since fractures in the area are seldom interconnected. Hence long-term sustainability is limited for all but very low pumping rates. The investigations suggest that high yielding boreholes can only be found at sites where several interconnected fractures exist to enlarge the general low permeability of the formation. The massive nature of the rock and the brittle calcite filled fractures suggest that the formation may be a candidate for hydrofracturing to increase yields and fracture connectivity.

Water strikes occur generally between 42m and 111m, depending on the topographical setting. The lower depth is found in valley bottoms, while the highlands generally exhibit water strikes of greater than 70 m in more than 50% of boreholes. Static water levels in the highland holes are also not significantly higher than the water strike depth (figure 1-16), limiting confining pressure and available drawdown. The only high yielding borehole evident had an available drawdown of 45 m, hence yield is topographically related and is dependent on the static water level. The static water level in the area is generally very deep, with an average depth of 53m. This is an expression of the distinct topography in the area and most boreholes being located on hilltops. In comparison, the water level in valley bottoms is located only a few meters below the surface, as boreholes G45910 and G45911 confirm.

The study revealed that topography is a significant factor affecting success rates. Two exploration boreholes drilled in a valley bottom had relatively shallow water strike between 40 to 60 m and shallow rest water levels between 3 and 4 m below the surface, although blow yields were similar to those achieved on hilltops. However, as a result of communities mainly living on hilltops, the aquifers in the valley bottom are not at the point of demand, yields are not sufficient to warrant pumping and pumping heads are prohibitive.

The water quality in the area was determined on the basis of water samples from 5 of the percussion drilled boreholes and is presented as Schoeller diagrams, tri-linear Piper diagrams, and Stiff diagrams (Appendix 1-D). An inspection of the graphs reveals that groundwater in the area has a similar chemical character, with sodium and magnesium being the dominant cations and bicarbonate (HCO_3) and chloride being the dominant anions. High pH values characterise the water as slightly alkaline. The water is primarily a result of carbonate-mineral dissolution.

The ambient water quality is considered to be good with most of the parameters generally meeting the recommended limits of the SABS 241 – 1999 specification for drinking water. Based on the water quality classification method developed by DWAF in 1996, the water samples fall mainly in category 0 and I, showing ideal drinking water quality (DWAF, 1996). Two exceptions in these regards exist for boreholes G45906 and G45913, which show

elevated calcium and chloride content respectively and therefore fall into category II of the DWAF classification system.

To assess the groundwater resources potential, the current groundwater abstraction in the study area was estimated. Since boreholes are equipped with hand pumps and static pumping heads are between 50-70 m, it can be assumed that discharges are about 150-250 l/h. Assuming a 60% usage rate over a 10 hour day, groundwater abstraction from each borehole would be about 0.9-1.5 m^3/day, which is within the sustainable yield of tested boreholes. At 15 litres per person per day, each borehole could supply about 60-100 people. Abstraction would be less than 548 m^3 annum for each borehole, which would equal the recharge from approximately 0.046 km^2.

The low permeability and the storage of the aquifer, as well as the low fracture connectivity, are significant factors restricting groundwater development. Groundwater supply using boreholes equipped with handpumps are obtainable and will be efficient for small communities.

1.12 Financial Analysis

The objective of this section is to evaluate the extent to which additional exploration is financially viable in terms of a reduction in overall borehole establishment costs based on experiences in the Dwyka tillites. Three different scenarios were considered to establish 11 successful boreholes: i) no structured exploration programme, or drilling randomly or by visual observation; ii) limited exploration based only on the frequently used method of limited EM-34 and magnetometer geophysical traverses and a desk study of existing maps; and *iii)* full exploration based on structural mapping, LANDSAT and aerial photo interpretation, and field geophysical exploration using the most appropriate system as defined by hydrogeological conditions.

Results for Scenario 1 are based on historic drilling records as recorded in the NGDB, which are assumed to represent random drilling or boreholes sited without modern exploration methods. In the study area 149 boreholes have been drilled, of which only 18 yield water. This success record was used to estimate the number of holes and associated costs required to establish 11 yielding boreholes.

Scenario 2 is based on success rates achieved during the Critical Intervention Programme, where 45 boreholes were sited using an EM-34 and magnetometer. Only 11 of these boreholes contained water.

Scenario 3 is based on the methodology adopted for this project, where a MAX-MIN EM system was used due to advantages of depth of penetration, and potential to collect data simultaneously in both the profiling and sounding modes. Traverses were conducted in order to site boreholes across lineaments identified from LANDSAT and aerial photo interpretation, field verification of lineaments, and the structural analysis of lineament orientations based on outcrop mapping. The investigation drilled 10 holes, of which 5 were successful. Costs were extrapolated in order to determine costs to achieve 11 yielding boreholes so that they could be compared to scenario 1 and 2.

Table 1-12 shows the assumptions made in terms of methodology and quantities to establish the exploration and drilling costs incurred to establish 11 successful holes:

Table 1-12 Approximate costs to establish 11 yielding boreholes according to scenarios 1, 2 and 3.

Item	Units	Rate	Scenario 1		Scenario 2		Scenario 3	
			Qty	Cost R	Qty	Cost R	Qty	Cost R
Desk Study[1]	Day	1600			1	1600	5	8000
Community liaison[2]	Hr	100	22	2200	22.5	2250	11	1100
EM 34 survey[3]	Day	1500			15	22500		
MAX-MIN survey[4]	Day	2500					11	27500
Accommodation	Day	150			15	2250	11	1650
Geophysical Interp.	Line	100			45	4500	22	2200
LANDSAT image[5]	Each	2500					1	2500
LANDSAT interp.	Day	1200					3	3600
Structural mapping[6]	Day	1350					3	4050
Drilling[8]	Hole	11000	91[7]	1001000	45[9]	495000	22[10]	242000
Drill supervision	Day	1000	91	91000	45[9]	45000	22[10]	22000
TOTAL				1094200		573100		314600
Per successful site	**R**			**99473**		**52100**		**28600**
Median yield[11]	L/s			0.16		0.1		0.1
R/l/s				**621706**		**521000**		**286000**

1: Review of topographical and geological maps and geological reports.
2: At 30 minutes per drilling site
3: At 1 technician and one labourer and 3 boreholes sited per day, including magnetometer surveys
4: At 2 technicians and 2 boreholes sited per day including magnetometer surveys
5: At 22% recovery per usage of R10 000 per 180 x 180 km image and R1200 in man-hours for co-ordinate registration.
6: Field mapping of outcrops and aerial photo interpretation
7: Assuming 12% success rate as determined from historic drilling records in the NGDB
8: Casing costs are not considered as it is assumed that only successful boreholes would be cased, which would result in similar casing costs for all scenarios.
9: Assuming 27% success rate as determined from the CIP records
10: According to the success rate of 50%, as achieved in this project.
11: Median yield based on the successful boreholes only.

Based on these costs, the total expenditure per each successful borehole was evaluated and compared to initial exploration costs in order to quantify the financial benefits that can arise from adequate exploration budgets. Figure 1-60 shows that historic success rates have resulted in an expenditure of approximately R100 000 for the establishment of each successful borehole. In comparison, a limited expenditure of about R33 000, or R735 per borehole drilled, would improve drilling success rates to 27% and would result in an expenditure of about R52000 per successful borehole. If exploration expenditure were increased to R50 000, success rates of 50% could be expected, hence the drilling budget could be greatly reduced. Expenditure would then be about R28600 per successful borehole.

As a result, an expenditure of R1094200 would result in the establishment of 11 boreholes if the budget were dedicated to drilling without scientific exploration. If only 6% of the budget were dedicated to exploration, 21 boreholes could have been established for the same expenditure. If exploration costs were 16% of the budget, 38 boreholes could have been established within the same project budget.

Exploration costs exhibit economies of scale as the larger the program the smaller is the proportion of the budget dedicated to exploration (Figure 1-61). For example, to establish 3 boreholes using the methodology of scenario 3, exploration would be 27% of the total project budget. If 50 boreholes were to be established exploration would only be 12% of project budget. Figure 1-61 suggests that exploration is most cost effective when more than 15 boreholes are to be established in a region.

This analysis suggests that a more comprehensive exploration program and a larger exploration budget could in the long-term result in significant cost savings, especially in large regional programs where the costs of regional geological exploration are spread over many boreholes. In such cases dedicating a larger proportion of the budget to exploration than is currently the case may result in more efficient drilling and a net reduction in establishment costs per site. For such an exploration program to be successful it must incorporate field geological mapping, remote sensing and appropriate geophysical exploration based on the identified hydrogeological regime.

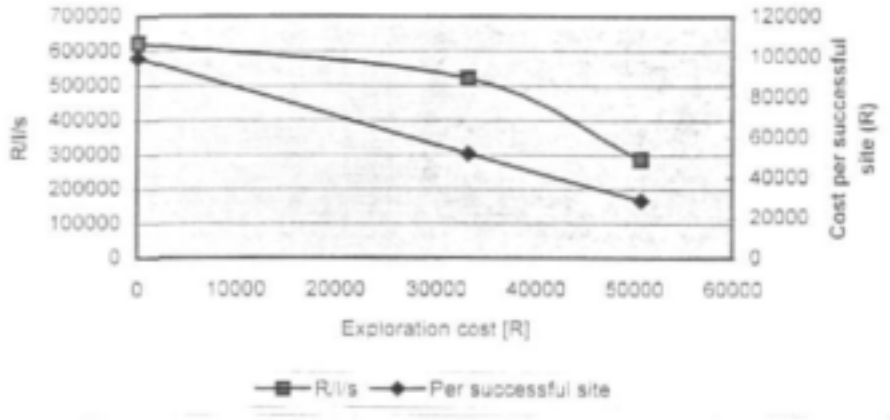

Figure 1-60 Exploration costs versus success rates

In some cases, such as reticulated systems where production rates are more important than the number of water points established, it may be beneficial to evaluate program efficiency in terms of costs per unit yield of water. In the Dwyka Group costs per unit yield are less relevant as the low yield of boreholes and the rugged topography constrain borehole schemes which supply several communities, hence the number of individual developed water sources is a more important indicator of success. Nevertheless, it is possible to measure the cost of water production in terms of R/l/s. Figure 1-60 suggests that drilling without prior scientific exploration results in a cost of R621706/l/s of water produced. Minimal exploration (scenario 2) results in costs of R521000/l/s of water produced. The data suggests that increased exploration results in reduced production costs of R286000/l/s. Median yields of successful boreholes of all three data sets are approximately 0.1 l/s, which suggests that exploration did not result in significantly improved yields as well as success rates. Only two boreholes of 149 in the region had yields exceeding 2 l/s and greater than 89 % had yields of less than 1 l/s. In the Critical Intervention Programme one borehole of 11 successful boreholes had a yield of 2.5 l/s, which introduces a significant statistical bias to the mean and cumulative yield achieved.

The low median yields encountered in successful boreholes and the low frequency of boreholes of yields greater than 2 l/s imply that water supply systems will be limited to hand-pump schemes. At pumping heads exceeding 70 m a Mono HP, which appears to be the most commonly used pump in the region, will deliver between 150-250 l/hour at 40-60 rpm. Assuming a 60% usage over a 10 h day, each pump can be expected to deliver between 900-1500 l/day, which is within the sustainable yield calculated for the established boreholes. This would be sufficient to supply between 60-100 people at 15 l/p/day. This implies that establishment of a water source would cost between R286-476 per person, or between R375-625 if casing and pump installation costs are included. Using similar usage assumptions the yield expected using hand pumps at 40 rpm with lower pumping heads is shown in Figure 1-62

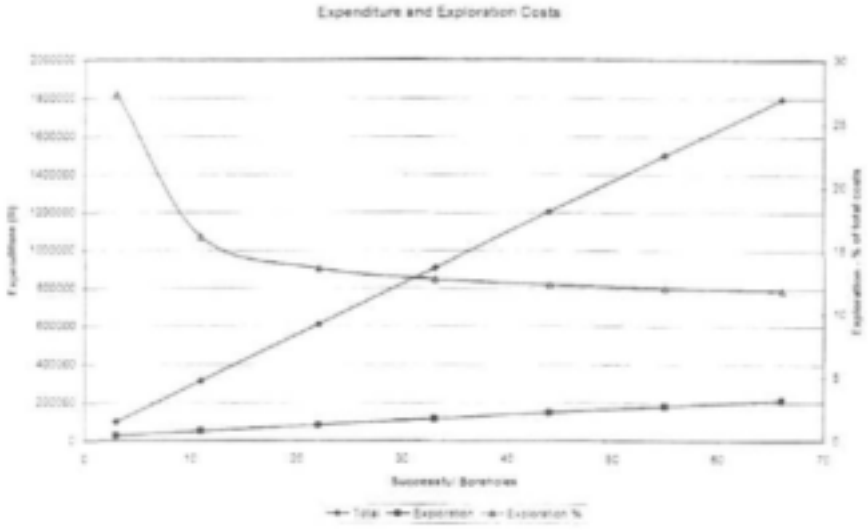

Figure 1-61 Expenditure and exploration costs

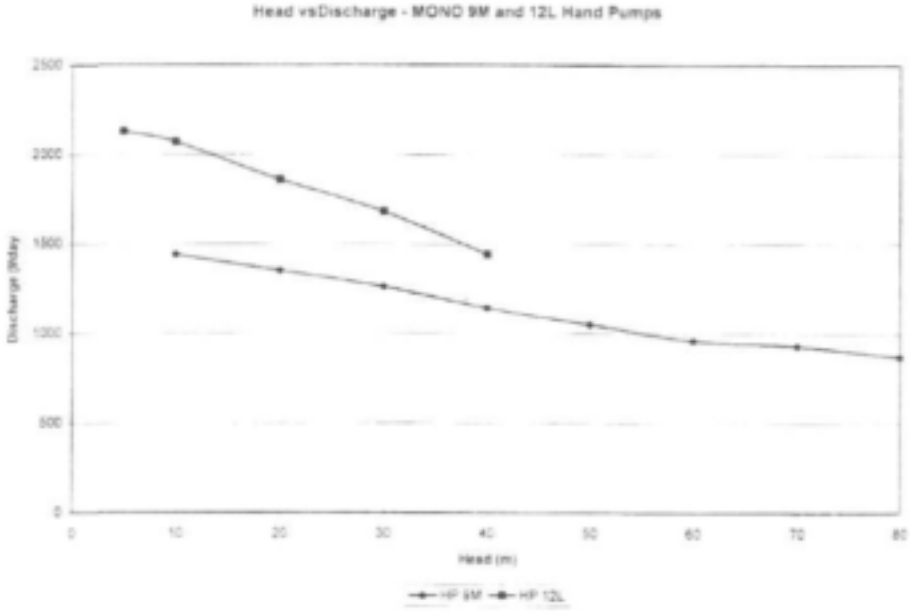

Figure 1-62 Head discharge relationship for Mono direct drive rotary hand pumps at 40 rpm and 6 hours per day operational time.

1.13 Conclusions and Recommendations

The following conclusions can be drawn from the research study:

Although of low potential, groundwater is an important resource in the study area, providing a clean and consistent water source. The geology in the area consists of low permeable tillite of the Dwyka Group, however it does not provide a productive aquifer. The low primary porosity of the tillite and extensive calcite veining restricts groundwater flow to poorly connected fracture zones. Successful groundwater exploration in the area has to delineate

fracture zones by taking the following geological, hydrogeological and geophysical considerations into account:

- Fractures follow a distinct joint set, with three dominant strike directions: NNE-SSW, N-S and SE-NW. This joint pattern is imprinted in the morphology of the area. Depressions along ridges, valleys and river beds are often the expression of a buried fracture zone and can be promising drill sites. Aerial photographs and LANDSAT imagery should therefore be used to pinpoint target areas before beginning the field exploration and visual borehole siting on these structures has been shown to be the most successful approach .

- Structures like dykes or sills are very seldom found and do not play an important role in the area. For this reason magnetic surveys are of limited value in the area.

- To delineate water-bearing features, the electromagnetic technique has not been a promising geophysical method to use in the study area. Water strikes are generally very deep, with 75% of the boreholes showing a water strike below 60m, and structures dip steeply. Therefore, only electromagnetic exploration techniques with a sufficient depth of penetration are suitable to delineate fracture zones, however, these structures are invariably thin, hence geophysical detection is masked by the overlying rock mass. The EM34 has proved to be inadequate in these hydrogeological conditions, especially when used with a 20m coil separation giving a penetration depth of about 25m. The APEX Max-Min electromagnetic system proved to be effective in locating buried narrow conductors, but geophysical anomalies were not always water bearing. With a coil separation of 100m, a depth of penetration of up to 50m or more can be obtained, depending on the lithology.

- The most promising electromagnetic response is where a dipping conductor is observed, exhibited as a trough in both the in-phase and out of phase signal. The distance where the borehole must be located relative to the centre of the trough depends on the depth of the static water level. As 82 % of the fractures in the area dipping steeper than 65°, a site of only a few meters off centre to the dipping side of the conductor is sufficient to hit the feature below the water table. However, steep dips indicate that boreholes must be accurately sited and based on a short station interval.

- Ramp, ridge or valley discontinuities in the conductive overburden layer are a common response in the study area. These can be an indication of a buried fracture zone and but did not prove to be promising drilling sites. If the discontinuity has its origin merely in a change of overburden thickness, the chances of hitting water are very low. These types of geophysical anomalies proved to be shallow features unrelated to water bearing features.

- Results obtained from the Max-Min survey indicate that the low frequencies of 220 Hz and 110 Hz often fail to produce a significant anomaly, even where water bearing features were subsequently detected. This can be attributed to the thin nature of deeper structures. The highest operating frequency of the Max-Min instrument, 56320 Hz is susceptible to background noise and variations in the shallow overburden. Therefore frequencies from 880 Hz up to 28160 Hz should be used.

- Fractures in the study area are seldom interconnected and are of limited thickness. Additionally, the horizontal extent of fracture zones is limited due to the generally steep dipping angle of the features and the steepness of the topography. Therefore, drilling sites should be carefully selected on a geophysical or structural anomaly in order not to miss the feature.

- The topography is a decisive factor controlling the availability of groundwater. At low altitude groundwater rest levels are generally shallower and the chances of hitting a fracture zone below the static water level are higher, resulting in more confining pressure, hence potentially higher yields. However, population distribution and poor access to valley bottoms limits the feasibility for boreholes at a low elevation. In addition, the low yields and high pumping heads from the valley bottoms to the high lying areas limit the economic feasibility of this option.

- A financial analysis suggests that a comprehensive exploration programme based on identifying key structures, with a correspondingly larger exploration budget, could in the long-term result in significant cost savings, especially in large regional programs where the costs of regional geological exploration are spread over many boreholes. In such cases dedicating a larger proportion of the budget to exploration than is currently the case may result in more efficient drilling and a net reduction in establishment costs per site. For such an exploration program to be successful it must incorporate field geological mapping, remote sensing and appropriate geophysical exploration based on the identified hydrogeological regime.

In conclusion, the research showed that successful groundwater exploration for the area is possible, but groundwater abstraction will be limited to hand pump schemes. An evaluation of the structural geology and the hydrogeological conditions of the area together with a suitable geophysical method for the environment pushed the drilling success rate up from a historical 12 % to 50 %. The unfavourable hydraulic properties of the tillite however, limit the yield of holes and median yields of successful holes could not be increased. Therefore, groundwater abstraction in the area will mostly be restricted to exploitation through hand pumps to support small communities. High yielding boreholes are seldom encountered and can only be found at major fault zones where interconnected fracture zones are present to distinctively enlarge the permeability of the subsurface. These are located at the margins of the Dwyka Group.

1.14 References

Bredenkamp, D.B. , Botha, L.J., van Tonder, G.J. and van Rensburg, H.J. (1995). Manual on quantitative estimation of recharge and aquifer storativity. WRC No. TT73/95. Pretoria. 363p.

de Decker, R.H. (1981). Geology of the Kokstad area. Explanation of sheet 3028. Geological Survey. Republic of South Africa. 22p.

Dent, Lynch & Schulze (1989): Mapping mean annual and other rainfall statistics over Southern Africa. Water Research Commission, Pretoria, South Africa, WRC Report 109/1/89.

Du Toit, A.L. (1946). The geology of parts of Pondoland, East Griqualand and Natal. Explanation of sheet 119, Geol. Surv. S.Afr.

DWAF (1995): Characterization and mapping of the groundwater resources. KwaZulu-Natal Province. Mapping unit 10. Dept. of Water Affairs and Forestry, 1995.

DWAF (1995): Characterization and mapping of the groundwater resources. KwaZulu-Natal Province. Mapping unit 4. Dept. of Water Affairs and Forestry, 1995.

DWAF (1996). A guideline for the health related assessment of the quality of water supplies. Pretoria. 1st Edition. 46p.

Maud, R.R. (1961). A preliminary review of the structure of coastal Natal. Trans. Geol. Soc. S.Afr., **64**, 247-256.

Sami, K. and Murray, E.C. (1998): Guidelines for the evaluation of water resources for rural development with an emphasis on groundwater. Water Research Commission Report. 677/1/98.. Pretoria, South Africa.

Thomas, R.J. (1988): The geology of the Port Shepstone area. Explanation to sheet 3030. Geological Surv. S.Afr. Pretoria. 136p.

Thomas, R.J., von Brunn, V., Marshall, C.G.A.(1990): A tectono-sedimentary model for the Dwyka Group in the southern Natal, South Africa. S.Afr. Journal of Geology, 93(5/6), 809-817.

Von Brunn, V. (1994): Glaciogenic deposits of the Permo-Carboniferous Dwyka Group in the eastern region of the Karoo basin. In: Deynoux, Miller, J.M.G. Domack, E.W. Eyles, N. Fairchild, I.J. and Young, G.M. (eds.): The Earth's Glacial Record. Cambridge University press, Cambridge, 60-69.

Villegas-Garcia, C.J. and West, G.F. (1983): Recognition of electromagnetic overburden anomalies with horizontal loop electromagnetic survey data. Geophysics, v.48, 42-51.

Visser, J.N.J. (1989): The Permo-Carboniferous Dwyka Fromation of Southern Africa: Deposition by a predominantly subpolar marine ice sheet, Paleogeography, Plaeoclimatology, Paleoecology, 70, 337-391.

Visser, J.N.J, Von Brunn, V. and Johnson, M.R. (1990): Dwyka Group. Catalogue of South African Lithostratigraphic Units. Geological Survey, Department of Mineral and Energy Affairs, Pretoria, 2-15 – 2-17.

APPENDIX 1-A
GEOPHYSICAL DATA

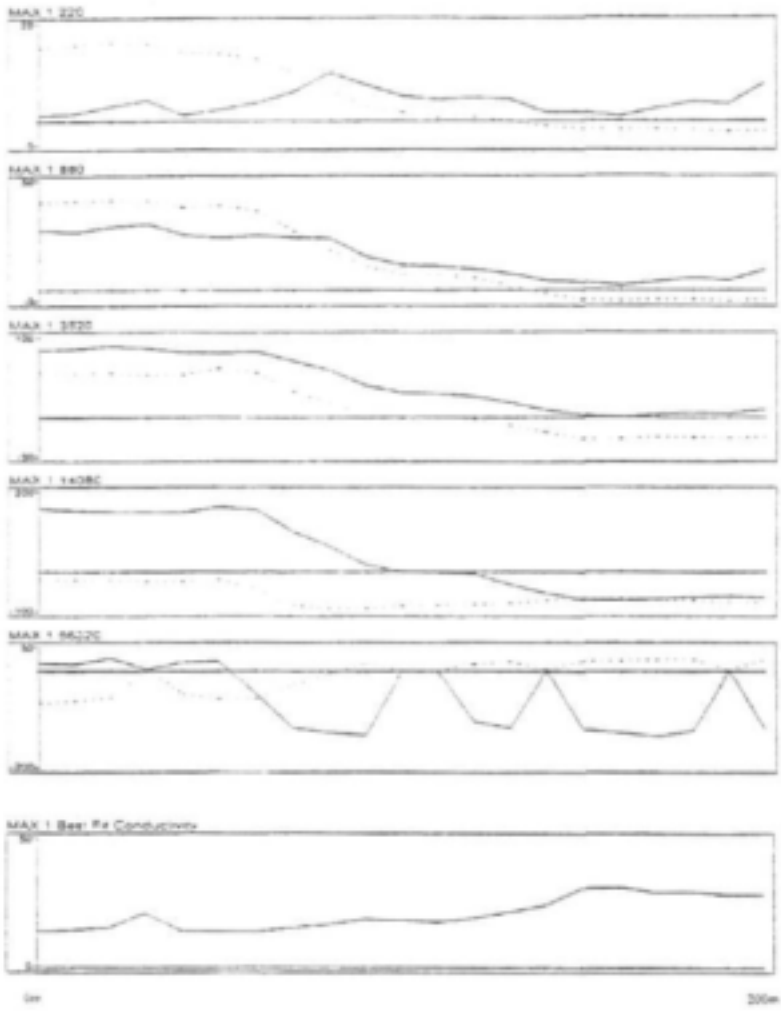

Max-Min electromagnetic profiles and conductivity's at site 13. Solid line: in-phase [%]; dotted line: out-of phase [%]; conductivity [mS m]; coil separation 100 m, station spacing 10 m. Traverse direction: NNW-SSE, borehole situated at station no. 10

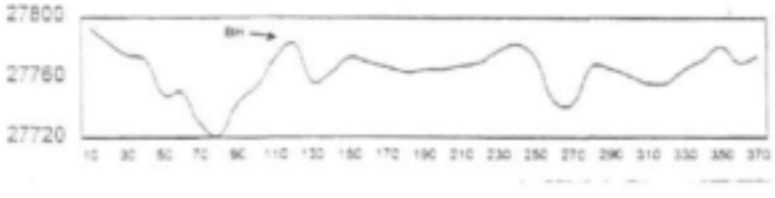

Magnetic profile in [nT] at site 13, station spacing 10 m. Traverse direction: NNW-SSE

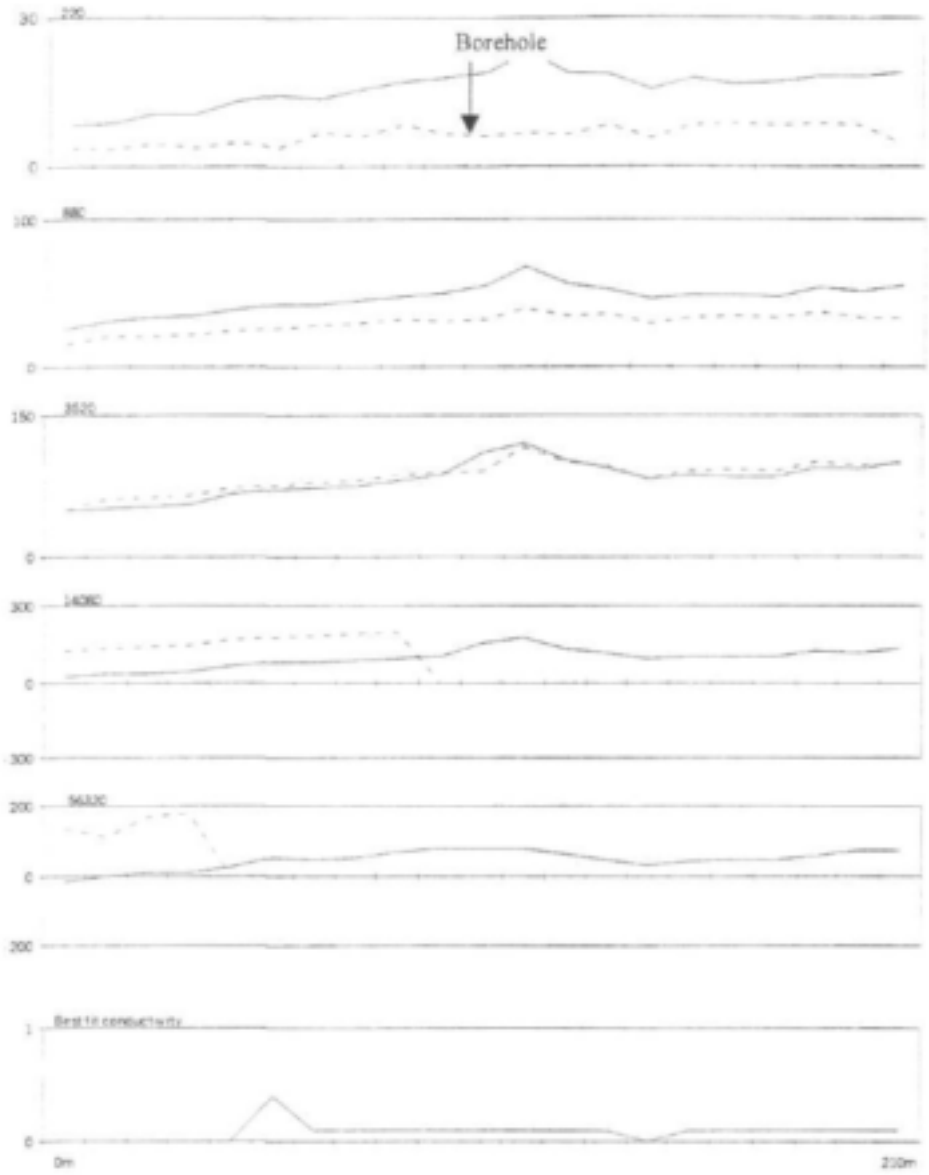

Max-Min electromagnetic profiles and conductivity's at site D1. Solid line: in-phase [%]; dotted line: out-of phase [%]; conductivity [mS/m]; coil separation 100 m, station spacing 10 m. Profile direction: S-N.

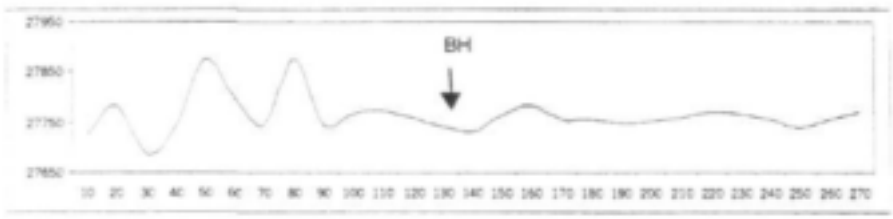

Magnetic profile in [nT] at site D1, station spacing 10 m. Profile direction: S-N

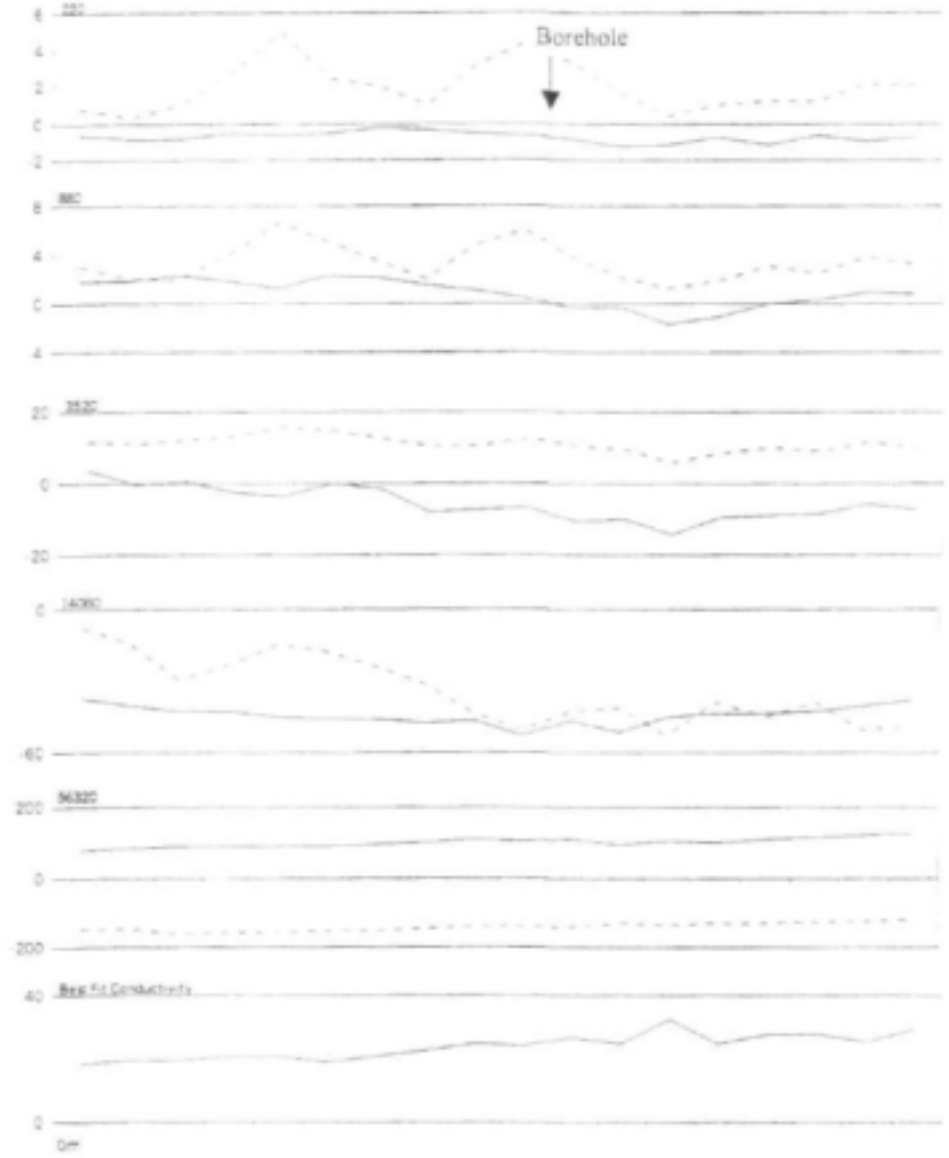

Max-Min electromagnetic profiles and conductivity's at site D3. Solid line: in-phase [%]; dotted line: out-of phase [%]; conductivity [mS/m]; coil separation 100 m, station spacing 10 m. Profile direction: N-S.

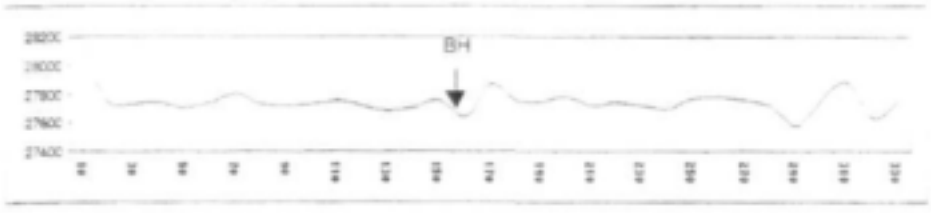

Magnetic profile in [nT] at site D3, station spacing 10 m. Profile direction: N-S

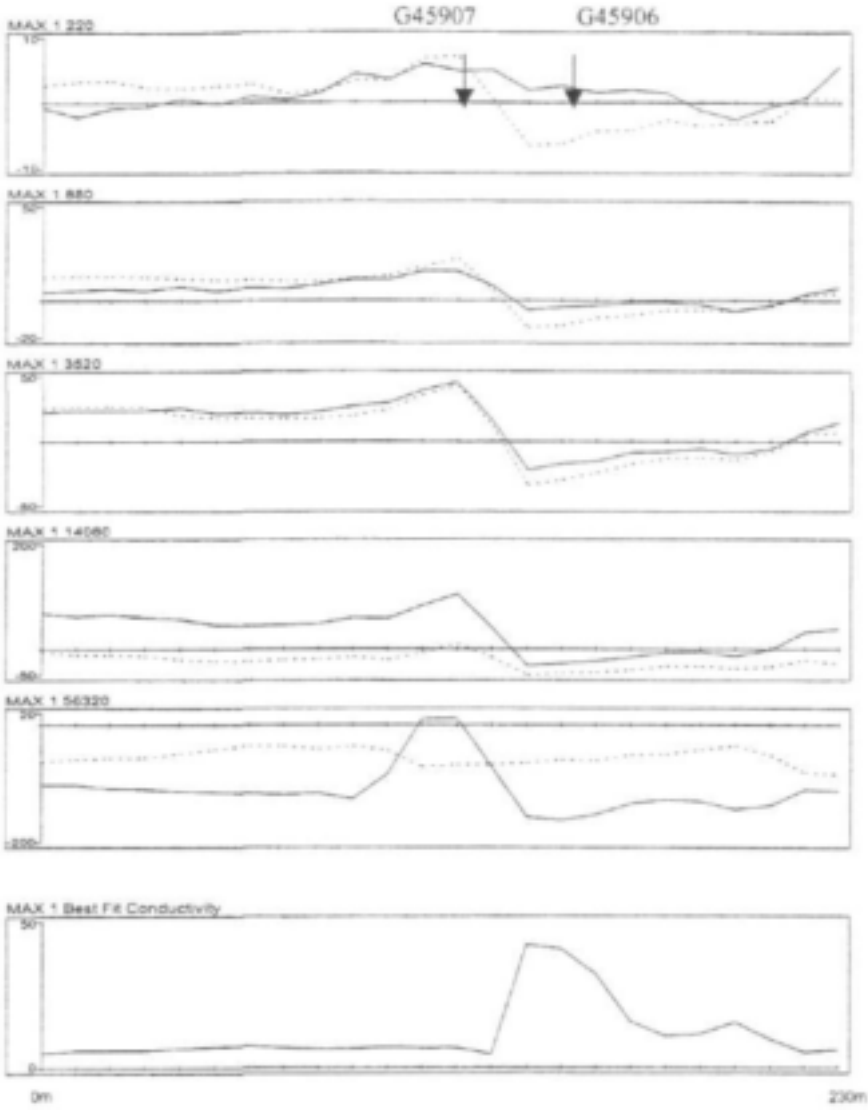

Max-Min electromagnetic profiles and conductivity's at site D5. Solid line: in-phase [%]; dotted line: out-of phase [%]; conductivity [mS/m]; coil separation 100 m, station spacing 10 m. Traverse direction: SW-NE.

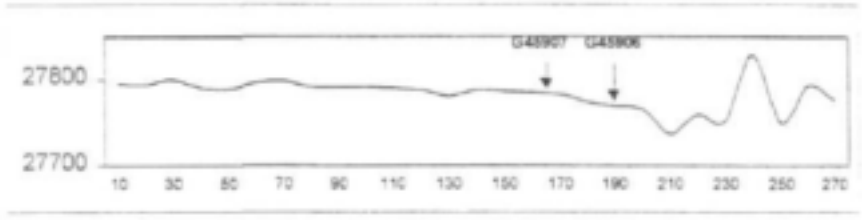

Magnetic profile in [nT] at site D5, station spacing 10 m. Traverse direction: SW-NE.

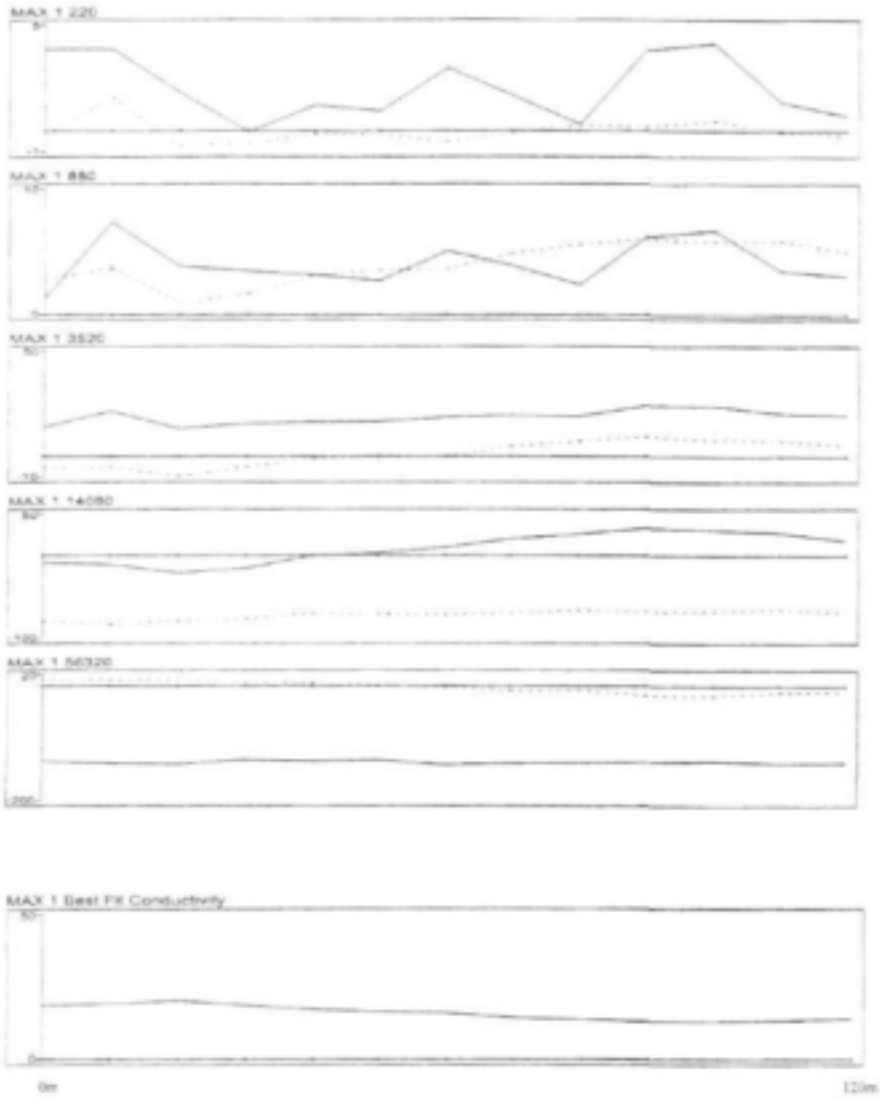

Max-Min electromagnetic profiles and conductivity's at site 7. Solid line: in-phase [%]: dotted line: out-of phase [%]: conductivity [mS/m]; coil separation 100 m, station spacing 10 m. Borehole located at station 6, traverse direction WNW-ESE.

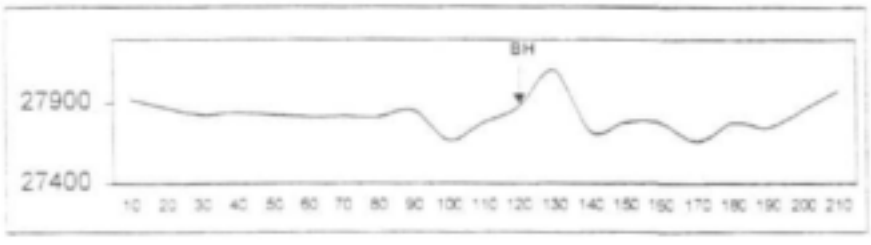

Magnetic profile in [nT] at site 7, station spacing 10 m. Traverse direction WNW-ESE

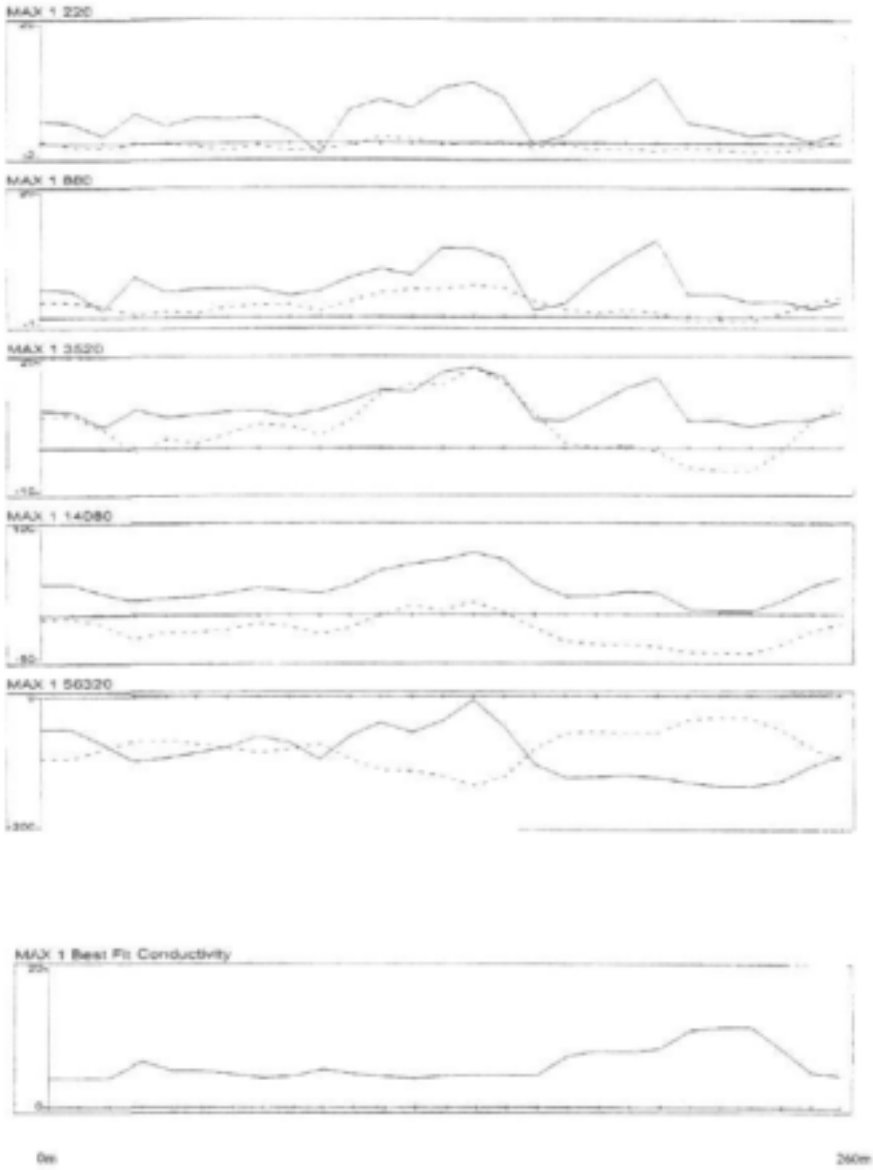

Max-Min electromagnetic profiles and conductivity's at site 9. Solid line: in-phase [%]; dotted line: out-of phase [%]; conductivity [mS/m]; coil separation 100 m, station spacing 10 m. The borehole is situated at station 16. Traverse direction: NNE-SSW.

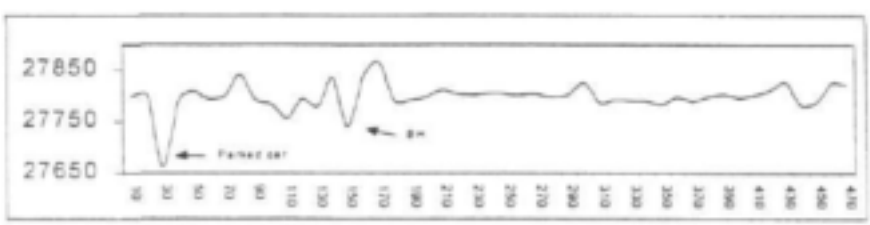

Magnetic profile in [nT] at site 9, station spacing 10 m. Traverse direction: NNE-SSW.

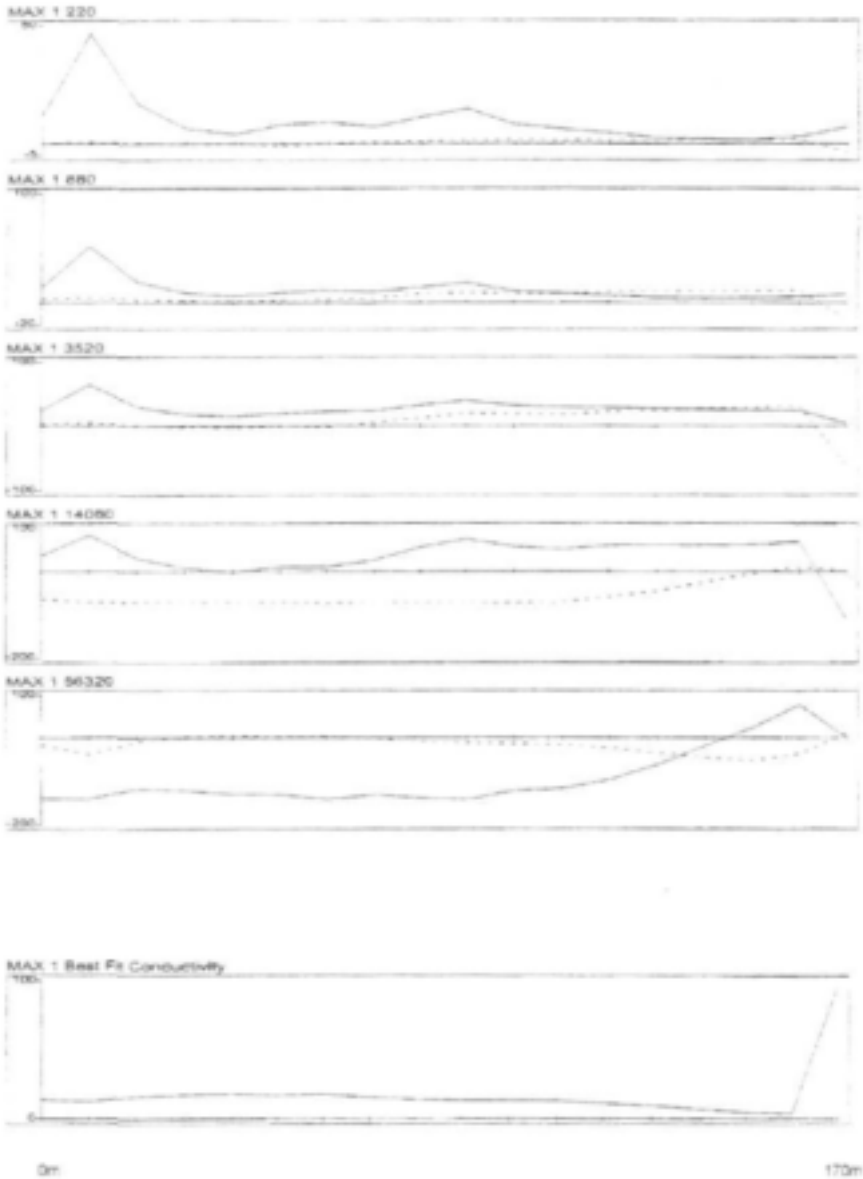

Max-Min electromagnetic profiles and conductivity's at site 11 Solid line: in-phase [%]; dotted line: out-of phase [%]; conductivity [mS/m]; coil separation 100 m, station spacing 10 m. The borehole is situated at station 10. Traverse direction: N-S.

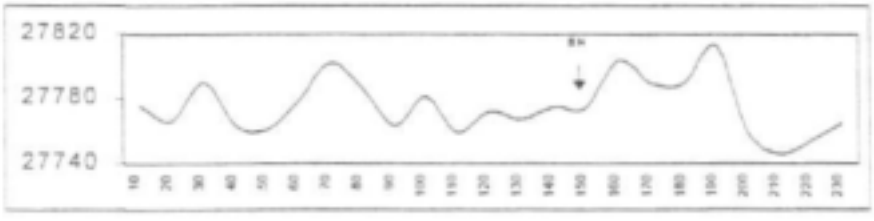

Magnetic profile in [nT] at site 11, station spacing 10 m. Traverse direction: N-S.

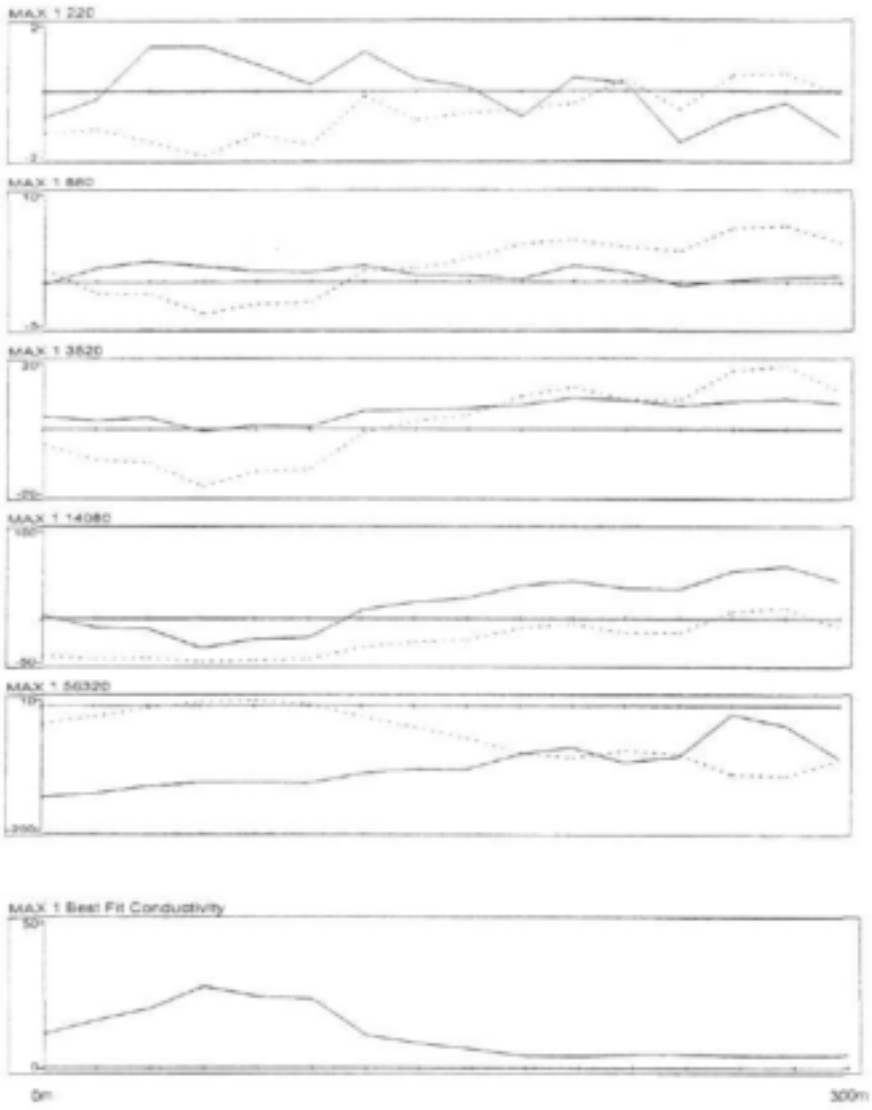

Max-Min electromagnetic profiles and conductivity's at site 15. Solid line: in-phase [%]; dotted line: out-of phase [%]: conductivity [mS/m]; coil separation 100 m, station spacing 20 m. Traverse direction: SE-NW.

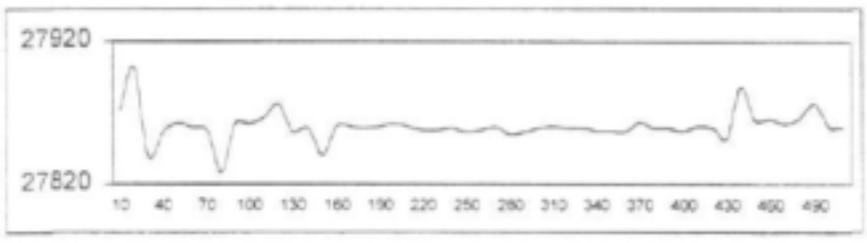

Magnetic profile in [nT] at site 15, station spacing 10 m. Traverse direction: SE-NW.

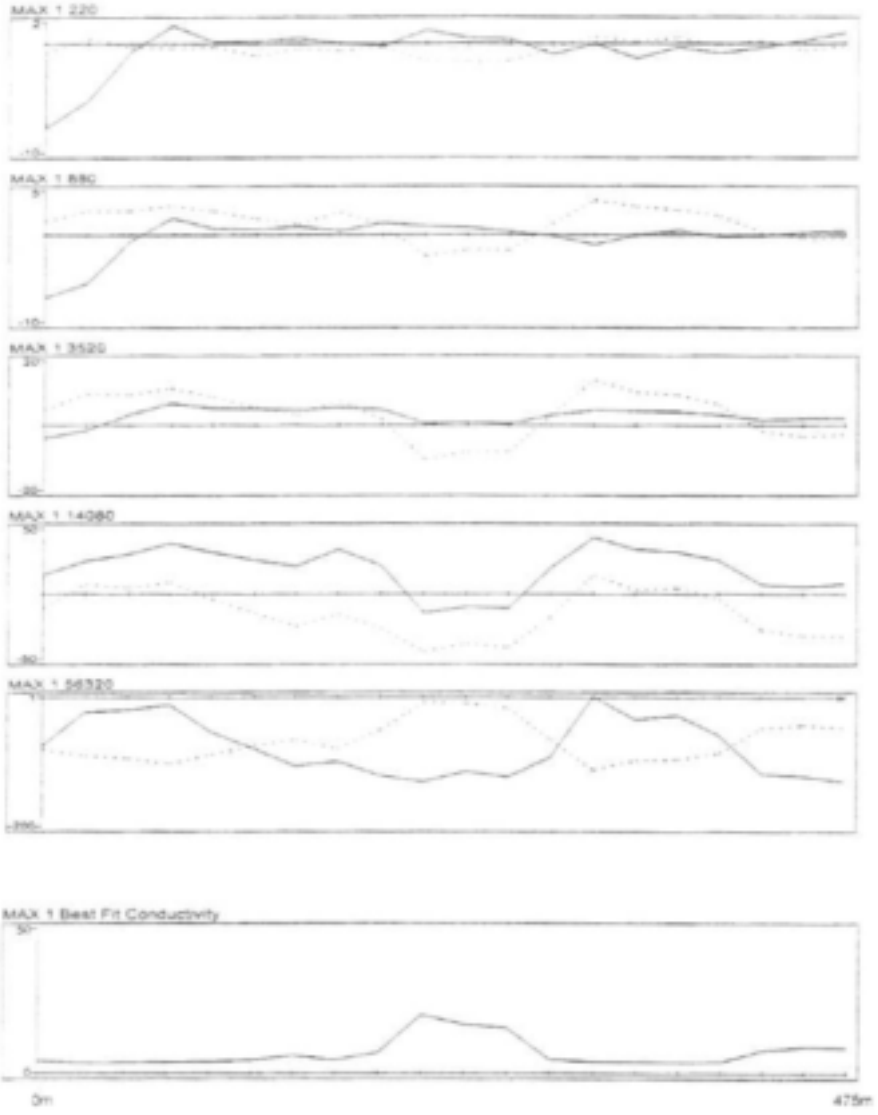

Max-Min electromagnetic profiles and conductivity's at site 17. Solid line: in-phase [%]; dotted line: out-of phase [%]; conductivity [mS/m]; coil separation 100 m, station spacing 25 m. Traverse direction: SSW-NNE.

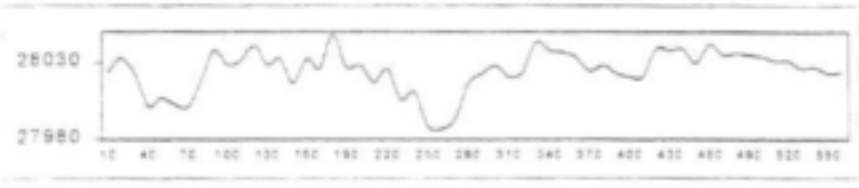

Magnetic profile in [nT] at site 17, station spacing 10 m. Traverse direction: SSW-NNE.

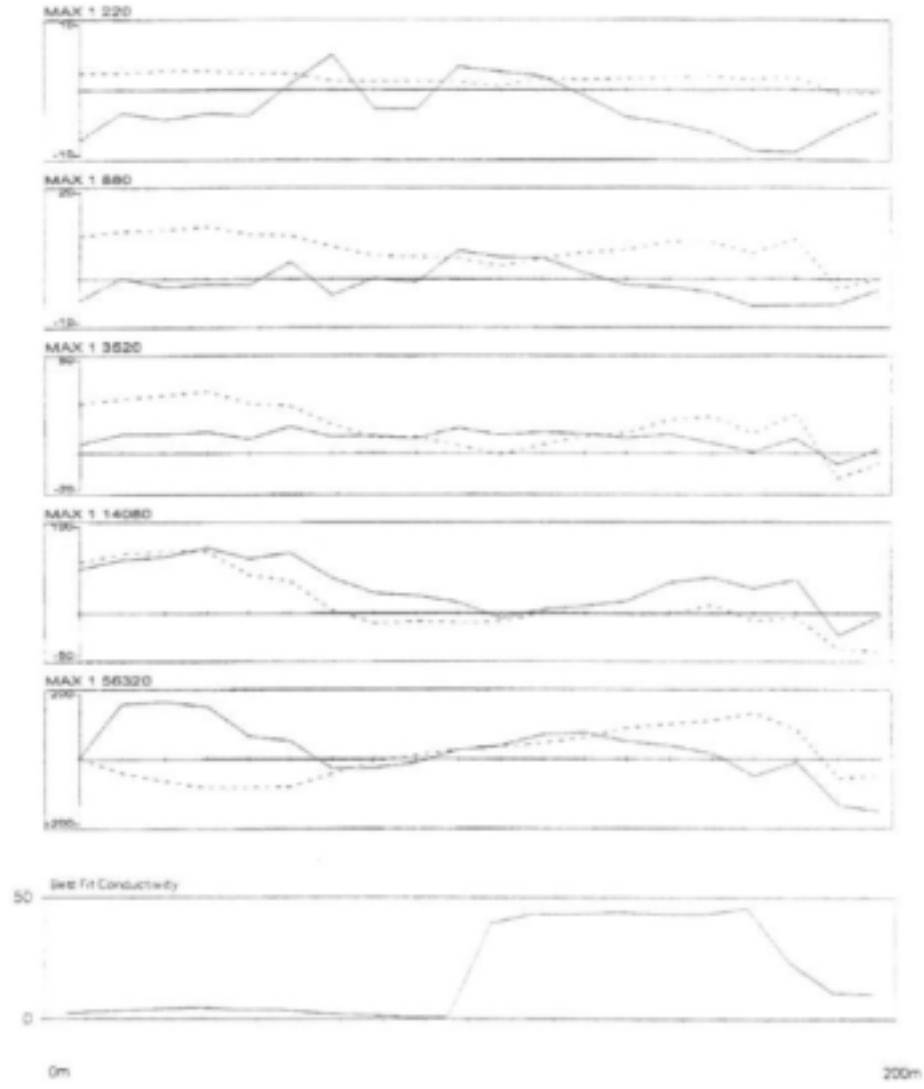

Max-Min electromagnetic profiles and conductivity's at site 19. Solid line: in-phase [%]; dotted line: out-of phase [%]; conductivity [mS/m]; coil separation 100 m, station spacing 20 m. Traverse direction: E-W.

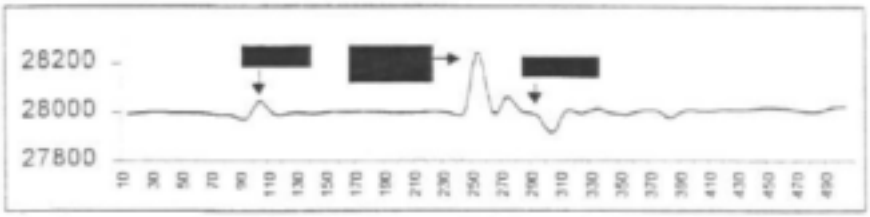

Magnetic profile in [nT] at site 19, station spacing 10 m. Traverse direction: E-W.

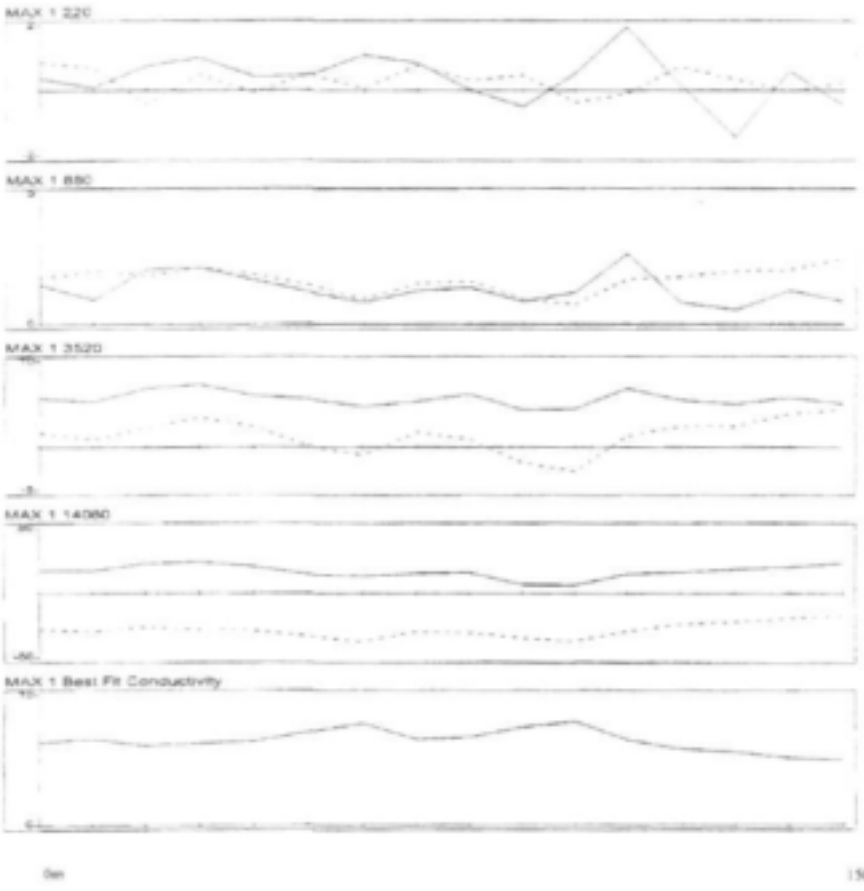

Max-Min electromagnetic profiles and conductivity's at site 21. Solid line: in-phase [%]; dotted line: out-of phase [%]: conductivity [mS/m]: coil separation 100 m, station spacing 10 m. Traverse direction: W-E.

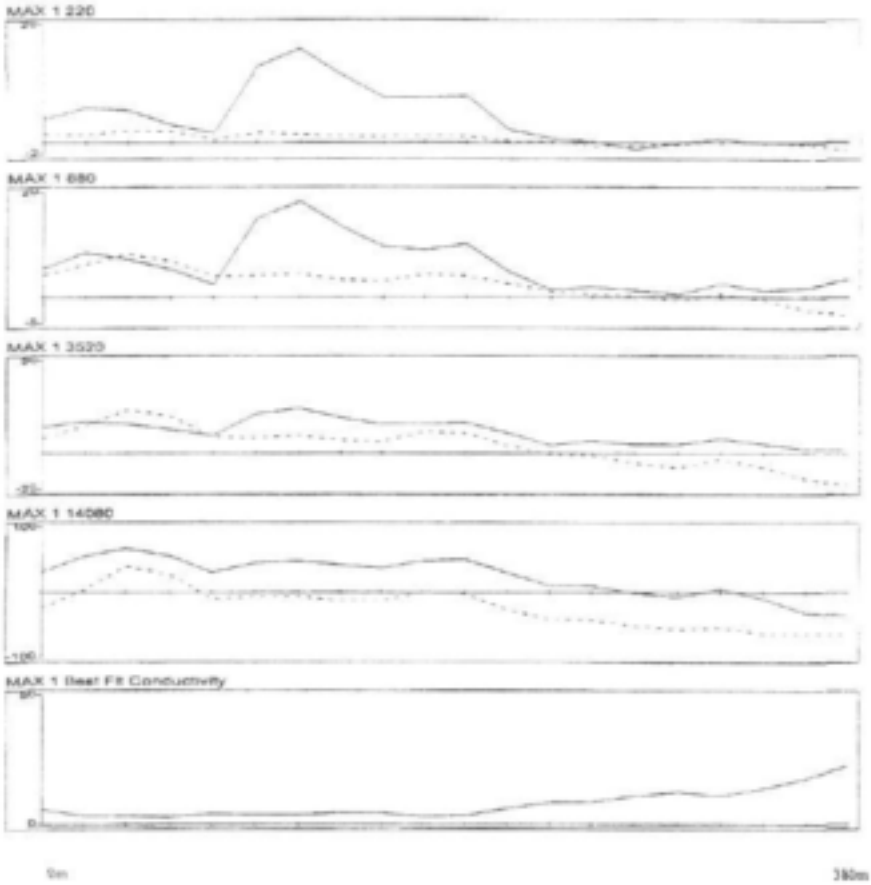

Max-Min electromagnetic profiles and conductivity's at site 22. Solid line: in-phase [%]; dotted line: out-of phase [%]; conductivity [mS/m]; coil separation 100 m, station spacing 20 m. Traverse direction: N-S.

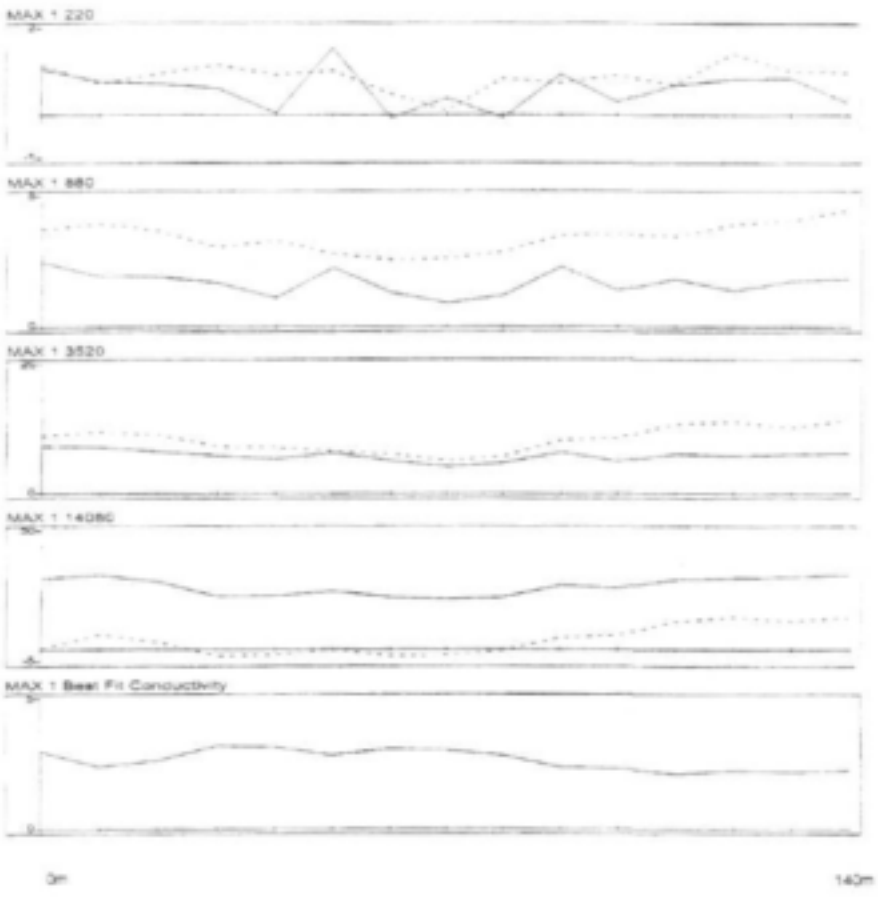

Max-Min electromagnetic profiles and conductivity's at site 20. Solid line: in-phase [%]; dotted line: out-of phase [%]: conductivity [mS/m]; coil separation 100 m, station spacing 10 m. Traverse direction: E-W.

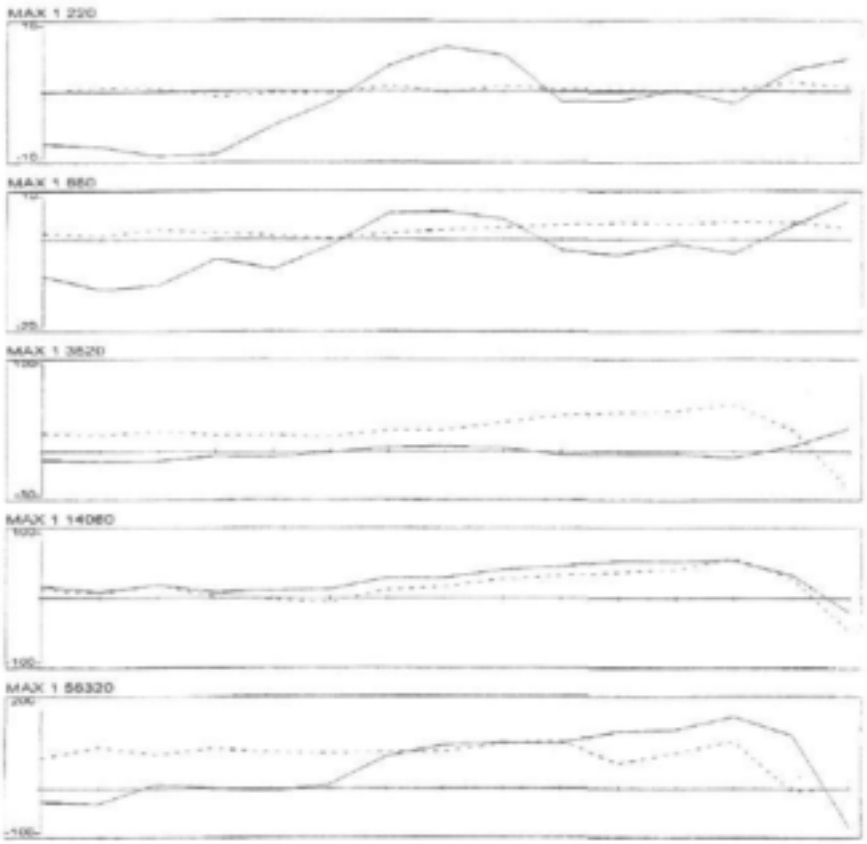

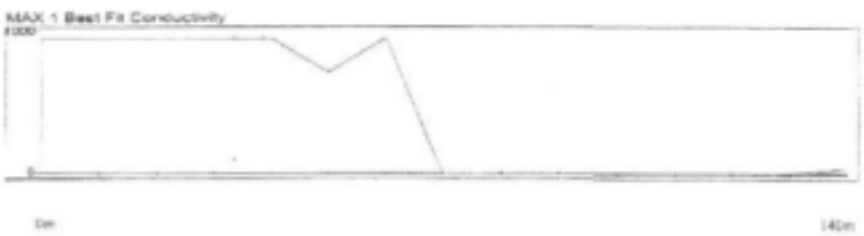

Max-Min electromagnetic profiles and conductivity's at site 18. Solid line: in-phase [%]; dotted line: out-of phase [%]; conductivity [mS/m]; coil separation 100 m, station spacing 25 m. Traverse direction: E-W.

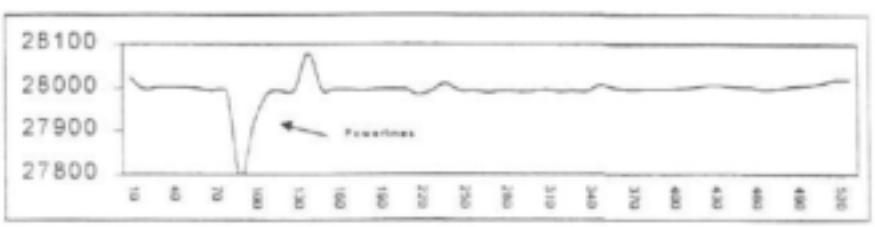

Magnetic profile in [nT] at site 18, station spacing 10 m. Traverse direction: E-W.

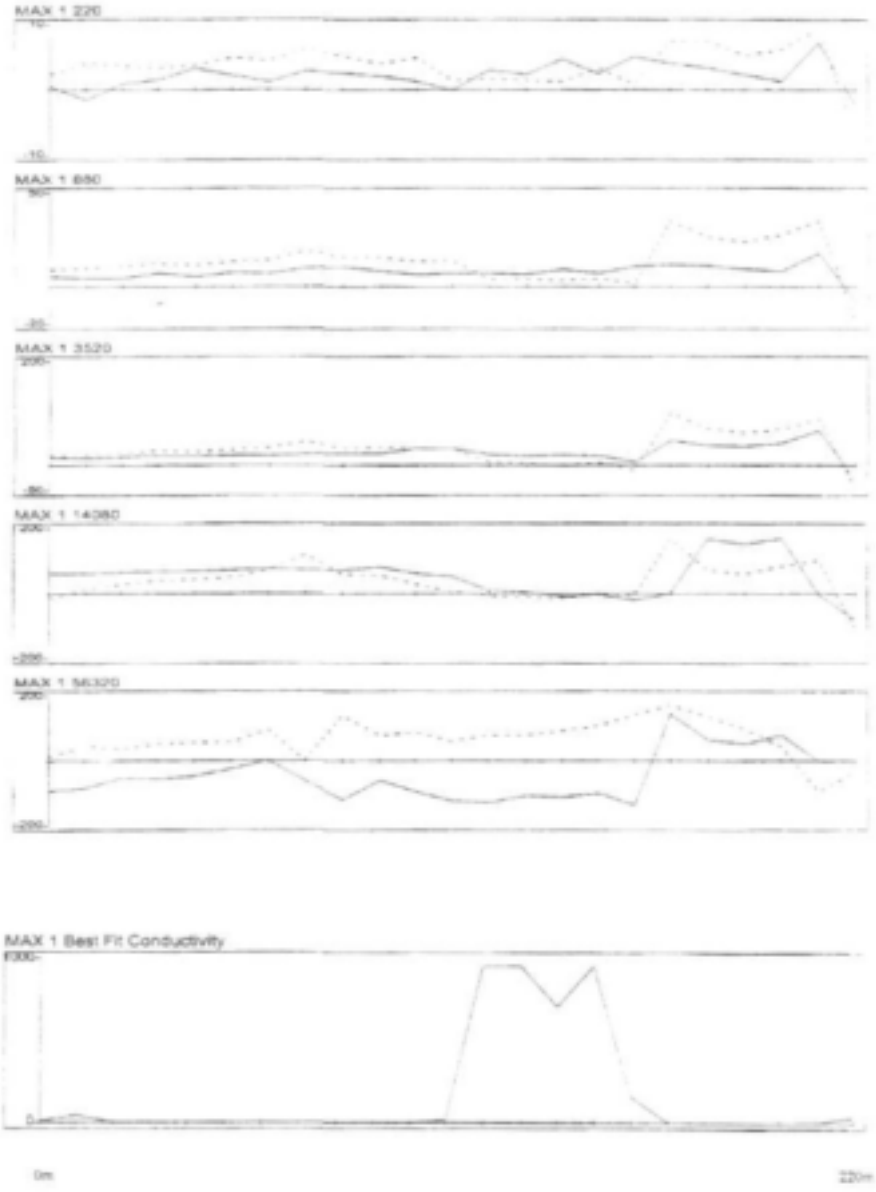

Max-Min electromagnetic profiles and conductivity's at site 16. Solid line: in-phase [%]; dotted line: out-of phase [%]; conductivity [mS/m]; coil separation 100 m, station spacing 10 m. Traverse direction: SSW-NNE.

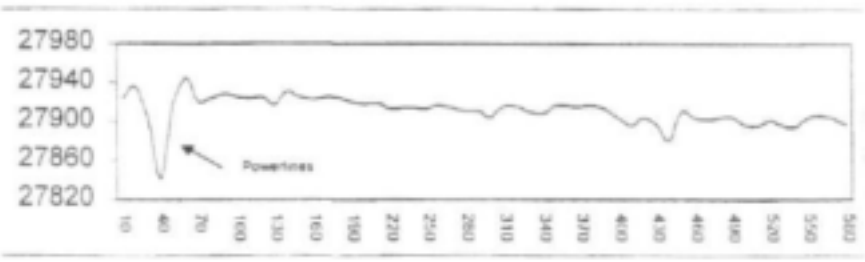

Magnetic profile in [nT] at site 16, station spacing 10 m. Traverse direction: SSW-NNE.

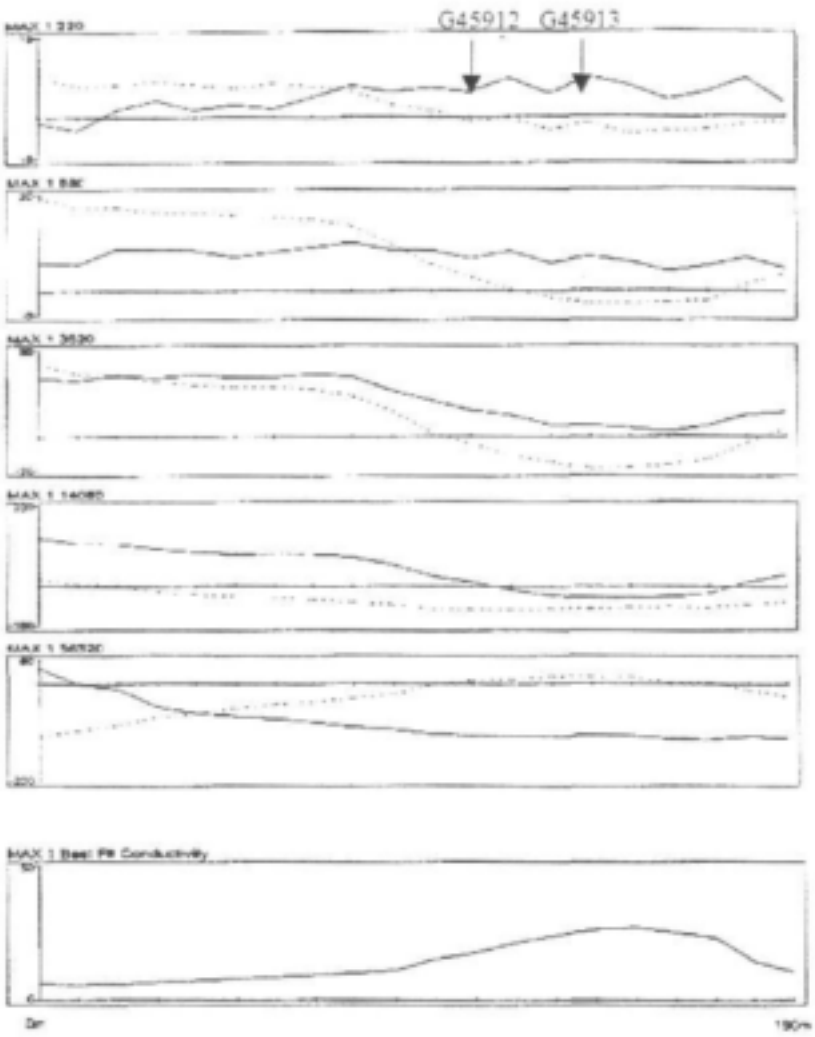

Max-Min electromagnetic profiles and conductivity's at site D12. Solid line: in-phase [%]; dotted line: out-of phase [%]; conductivity [mS/m]; coil separation 100 m, station spacing 10 m. Profile direction: SE-NW.

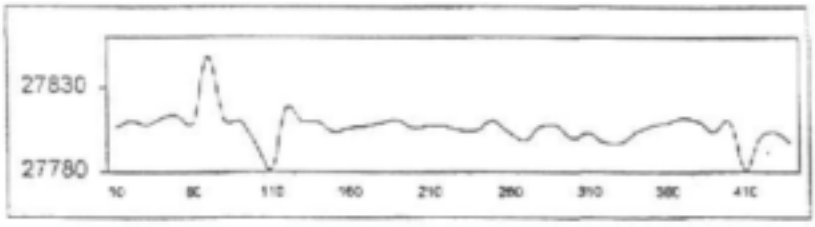

Magnetic profile in [nT] at site D12, station spacing 10 m. Profile direction: SE-NW

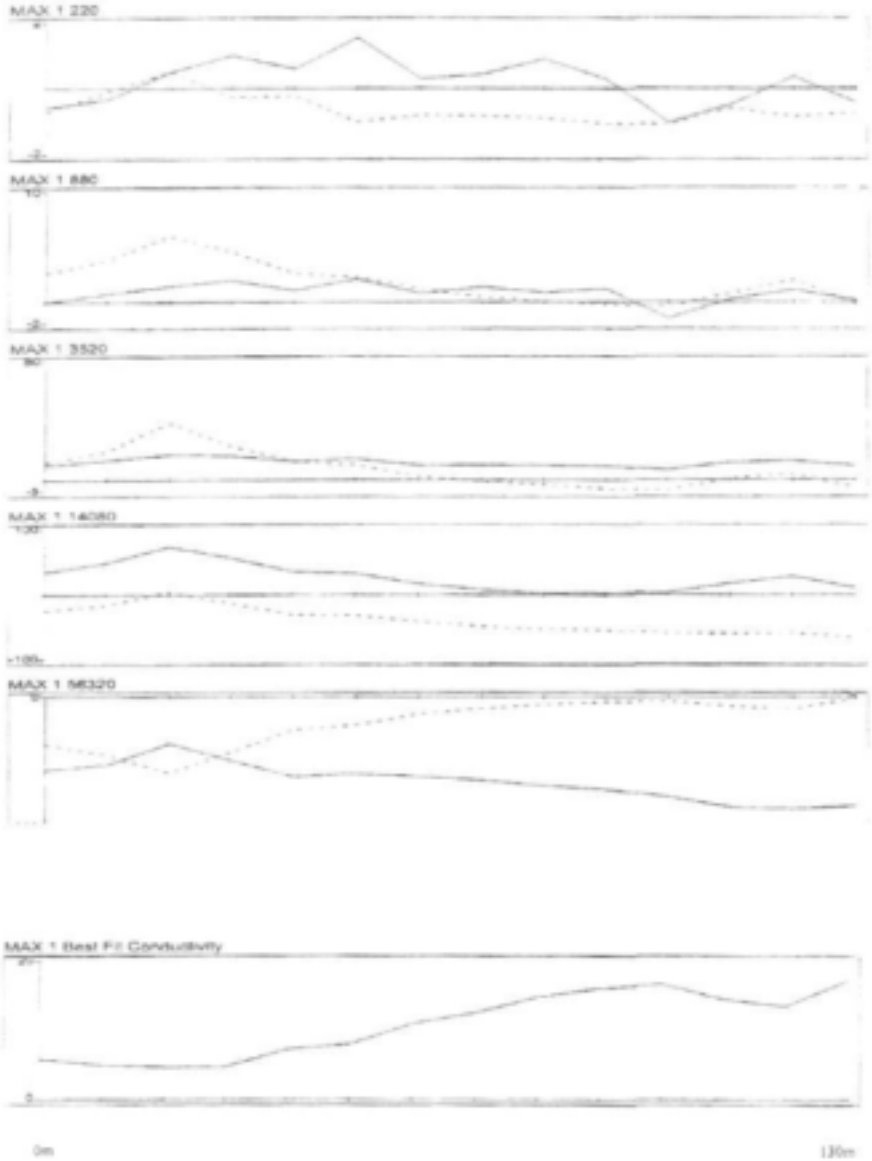

Max-Min electromagnetic profiles and conductivity's at site 10. Solid line: in-phase [%]; dotted line: out-of phase [%]; conductivity [mS/m]; coil separation 100 m, station spacing 10 m. Traverse direction: SE-NW. The borehole is situated at station 7.

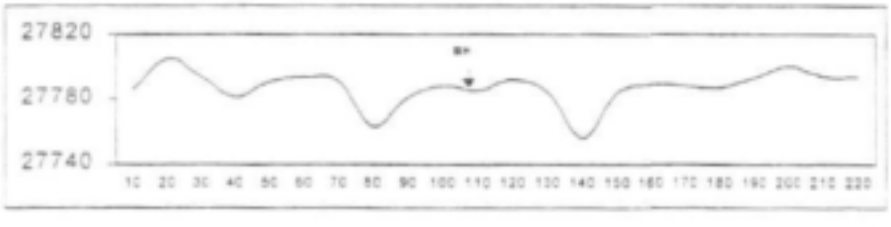

Magnetic profile in [nT] at site 10, station spacing 10 m. Traverse direction: SE-NW.

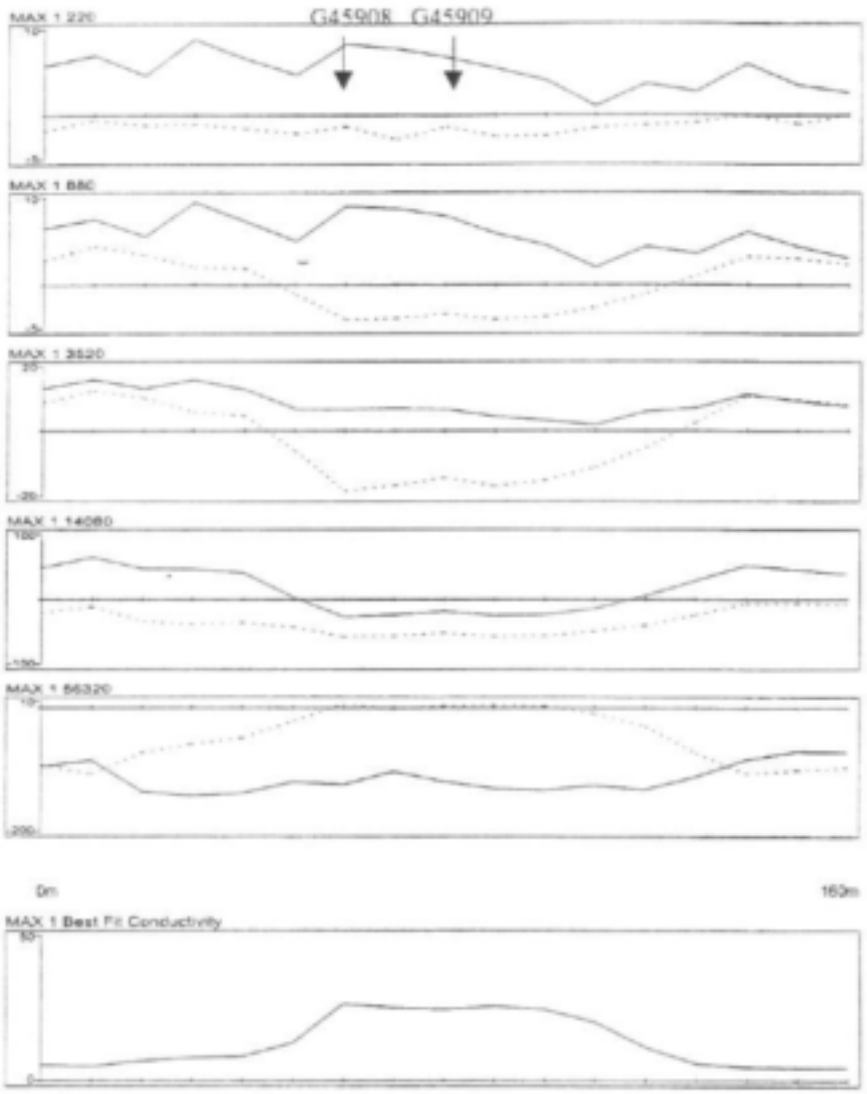

Max-Min electromagnetic profiles and conductivity's at site 8. Solid line: in-phase [%]; dotted line: out-of phase [%]; conductivity [mS/m]; coil separation 100 m, station spacing 10 m. Traverse direction: SW-NE.

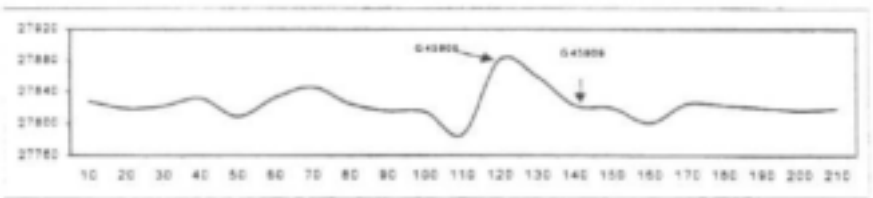

Magnetic profile in [nT] at site 8, station spacing 10 m. Traverse direction: SW-NE

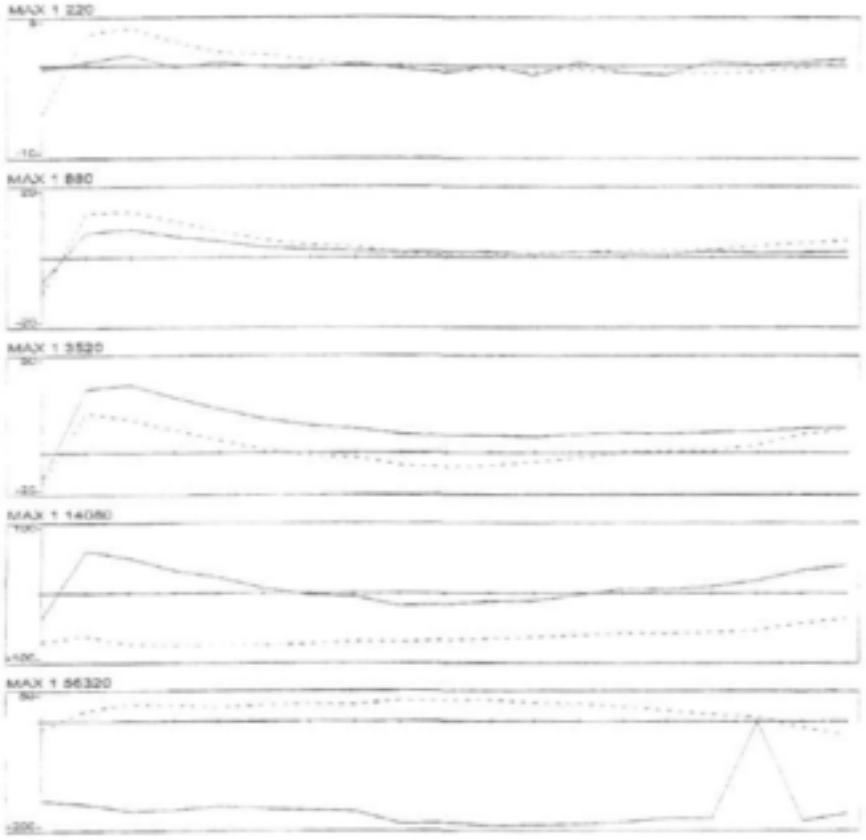

Max-Min electromagnetic profiles and conductivity's at site 6. Solid line: in-phase [%]; dotted line: out-of phase [%]; conductivity [mS/m]; coil separation 100 m, station spacing 10 m. The borehole is situated at station 9. Traverse direction: S-N.

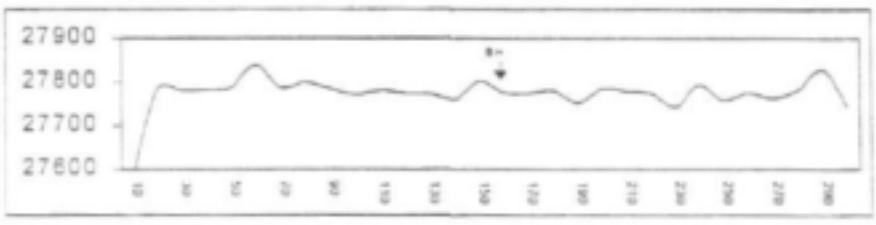

Magnetic profile in [nT] at site 6, station spacing 10 m. Traverse direction: S-N.

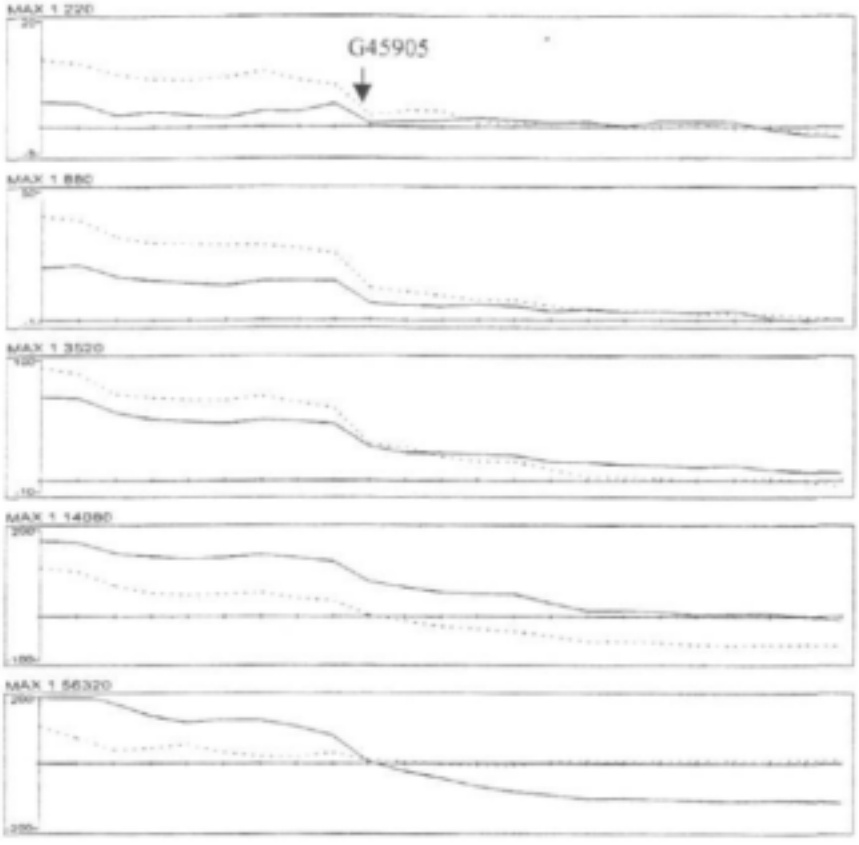

Max-Min electromagnetic profiles and conductivity's at site D4. Solid line: in-phase [%]; dotted line: out-of phase [%]; conductivity [mS/m]; coil separation 100 m, station spacing 10 m. Profile direction: SW-NE, borehole situated at station 10.

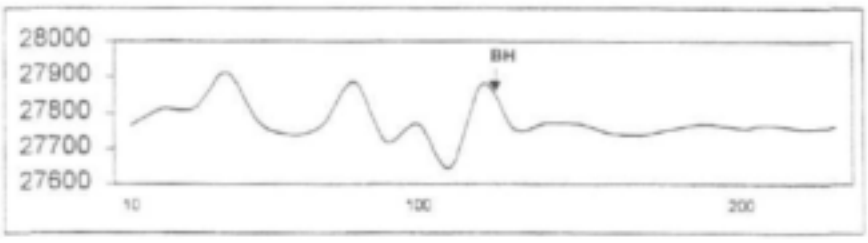

Magnetic profile in [nT] at site D4, station spacing 10 m. Profile direction: SW-NE

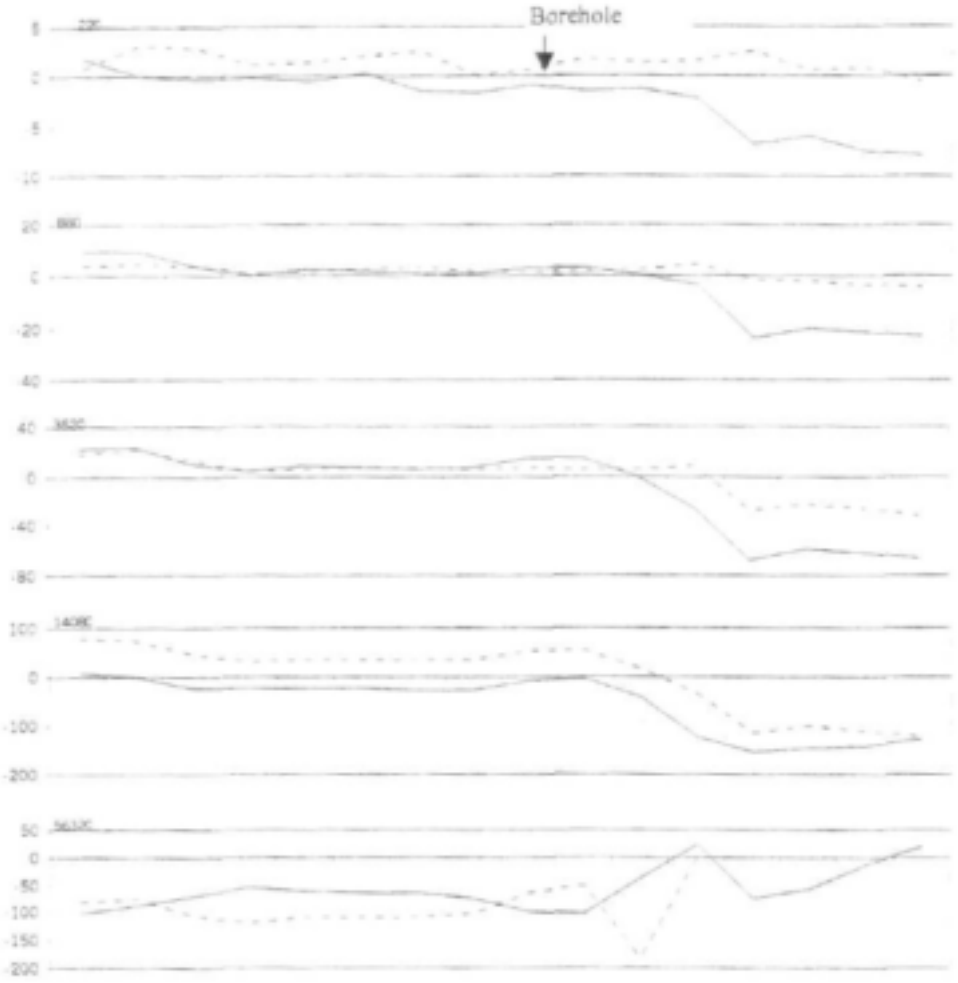

Max-Min electromagnetic profiles and conductivity's at site D2. Solid line: in-phase [%]; dotted line: out-of phase [%]: conductivity [mS/m]; coil separation 100 m, station spacing 10 m. Profile direction: S-N. Disturbance due to an electrical fence from station 2 onwards.

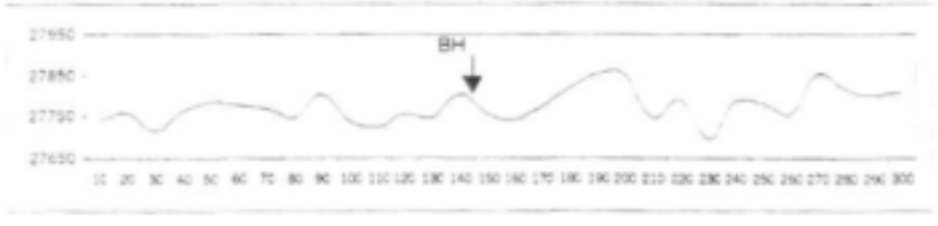

Magnetic profile in [nT] at site D2, station spacing 10 m. Profile direction: S-N

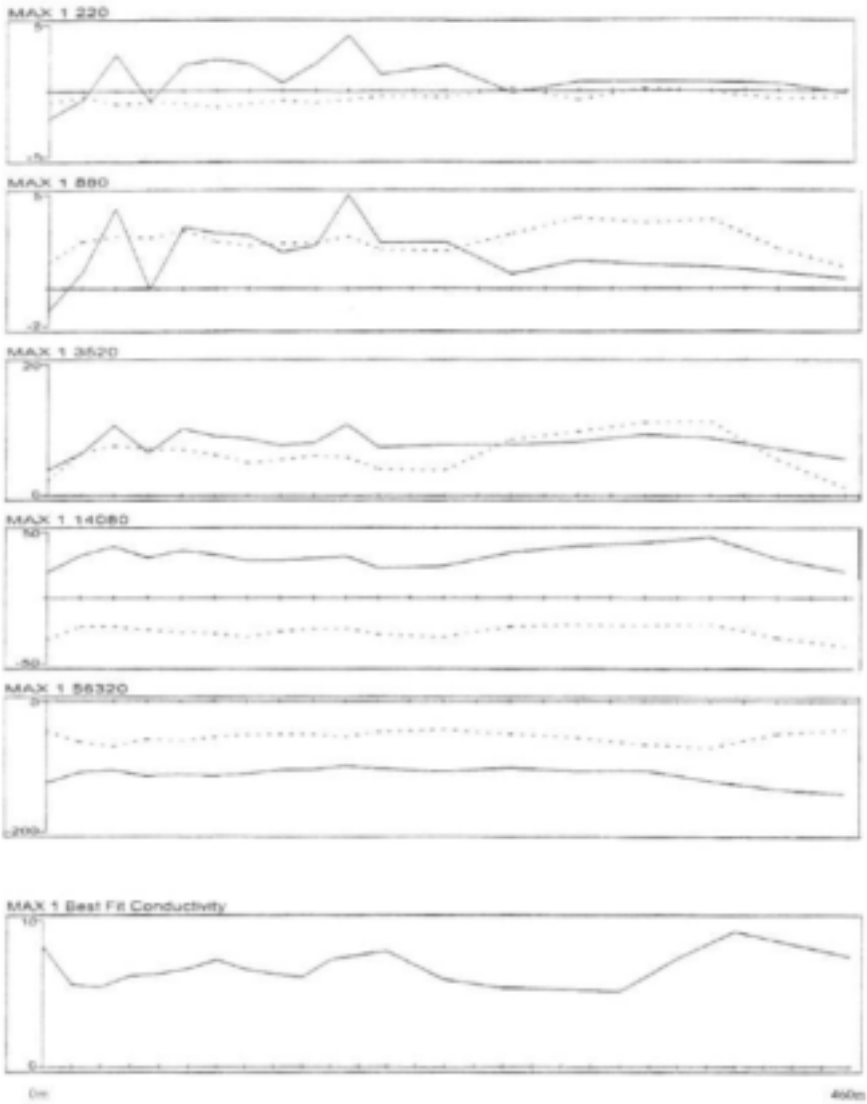

Max-Min electromagnetic profiles and conductivity's at site 14. Solid line: in-phase [%]; dotted line: out-of phase [%]: conductivity [mS/m]; coil separation 100 m, station spacing 10 m for stations 1-10, 20 m for stations 11-28. Traverse direction: NW-SE.

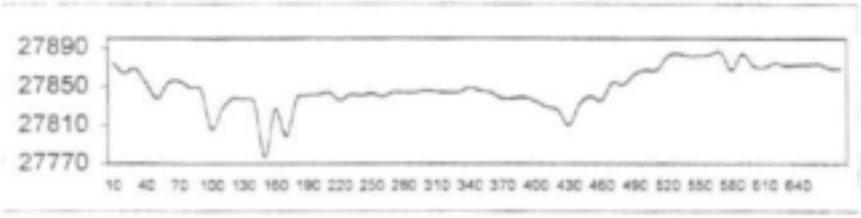

Magnetic profile in [nT] at site 14, station spacing 10 m. Traverse direction: NW-SE.

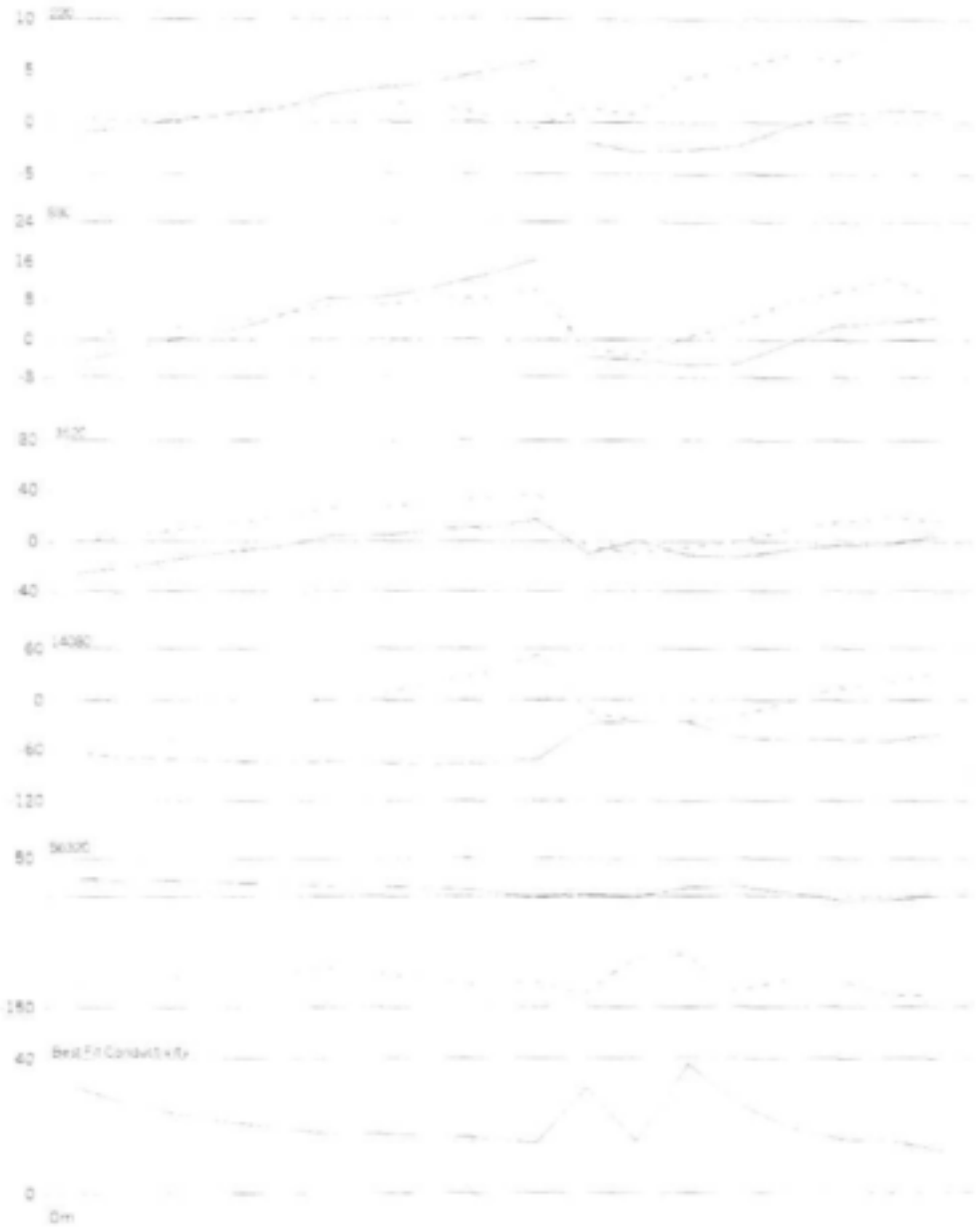

Max-Min electromagnetic profiles and conductivity's at site D23. Solid line: in-phase [%]; dotted line: out-of phase [%]; conductivity [mS m], coil separation 100 m, station spacing 10 m Traverse direction: NW-SE.

APPENDIX 1-B
GEOLOGICAL LOGS

COUNCIL FOR GEOSCIENCE

Private Bag X112
PRETORIA 0001
REPUBLIC OF SOUTH AFRICA

GROUNDWATER DEVELOPMENT IN COMPLEX TERRAIN

HOLE No: G45905
Sheet 1 of 2

PROJECT NUMBER: K5/966

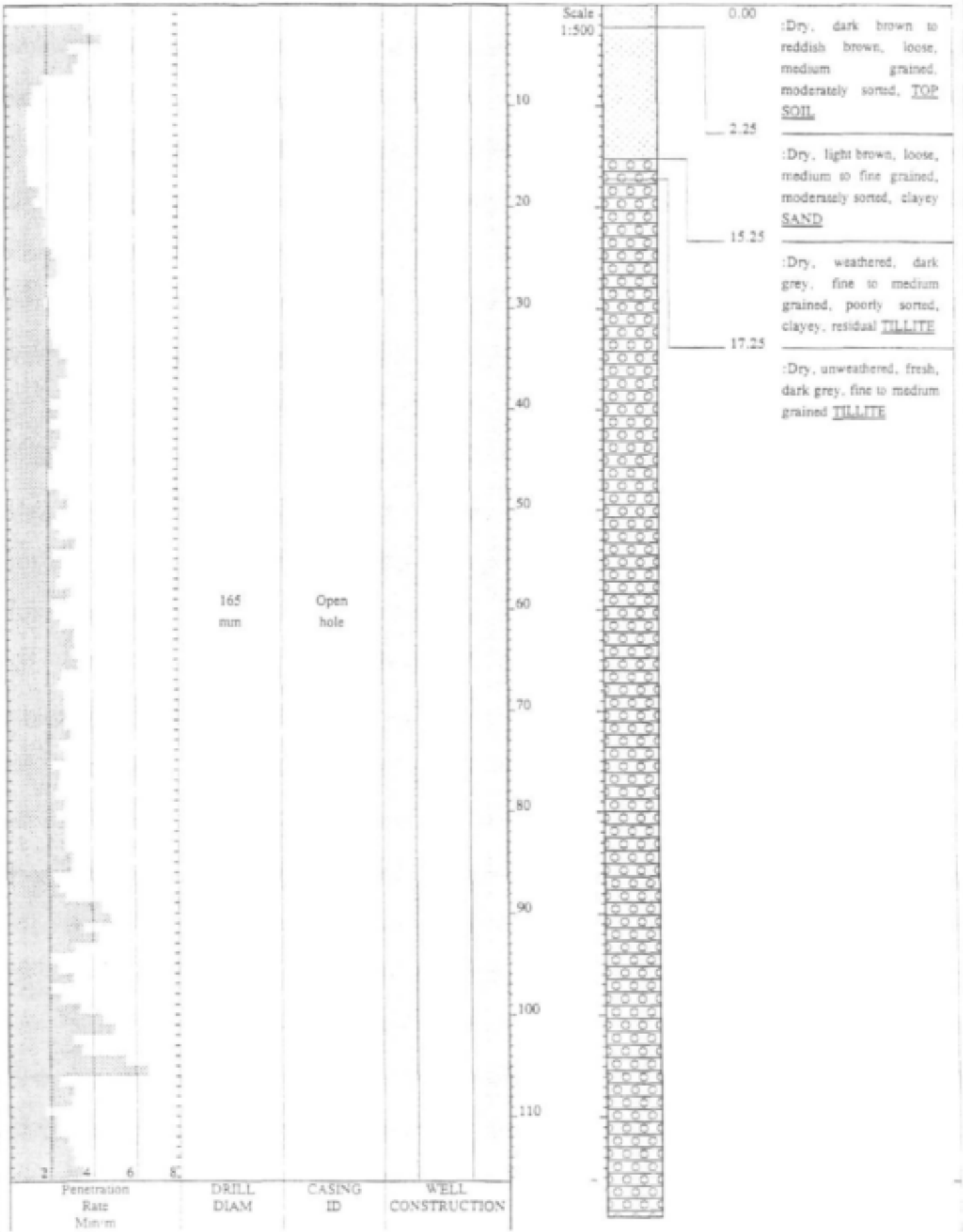

COUNCIL FOR GEOSCIENCE

Private Bag X112
PRETORIA 0001
REPUBLIC OF SOUTH AFRICA

GROUNDWATER DEVELOPMENT IN COMPLEX TERRAIN

HOLE No: G45906
Sheet 1 of 2

PROJECT NUMBER: K5/966

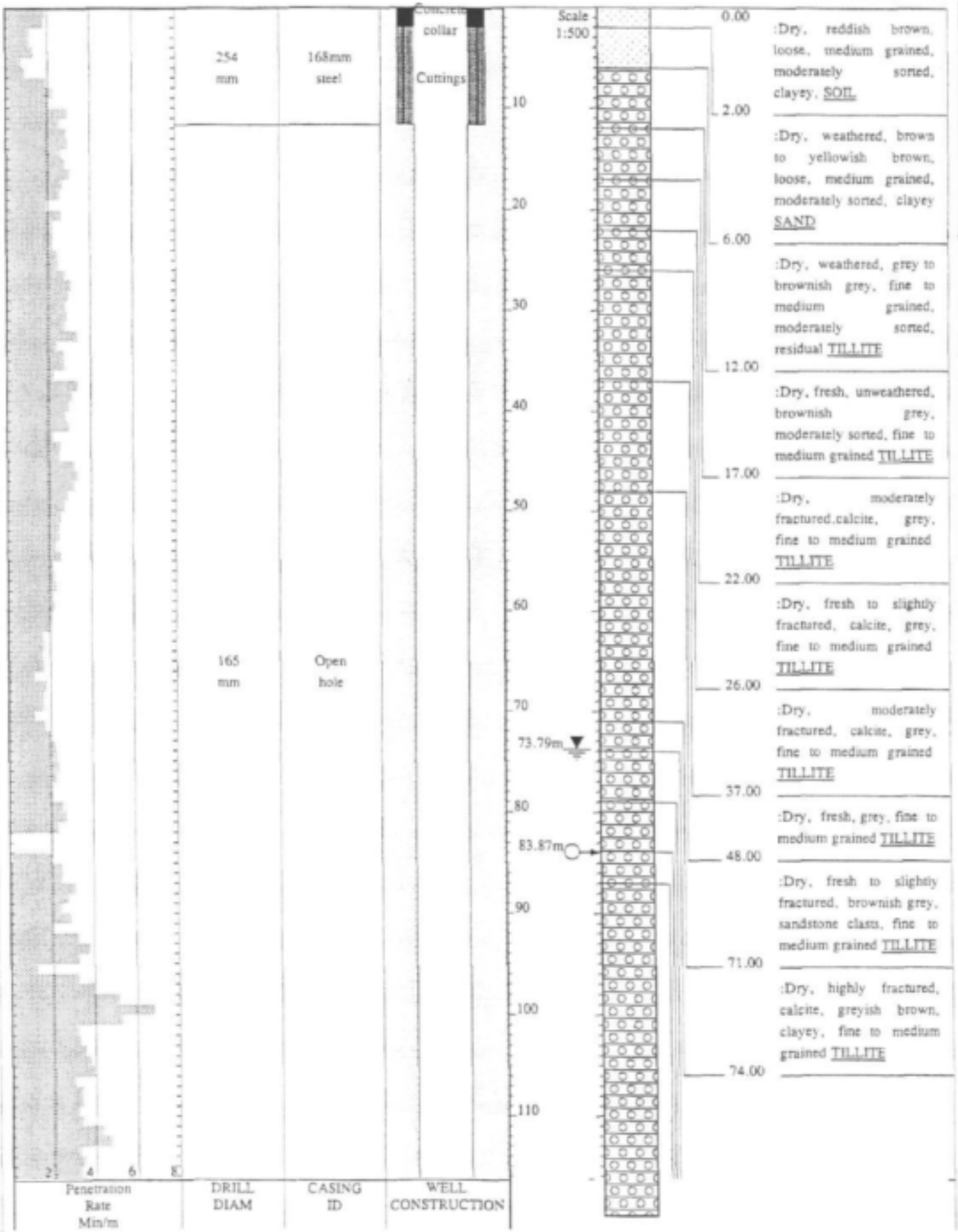

COUNCIL FOR GEOSCIENCE
Private Bag X112
PRETORIA 0001
REPUBLIC OF SOUTH AFRICA

GROUNDWATER DEVELOPMENT IN COMPLEX TERRAIN

HOLE No: G45907
Sheet 1 of 2

PROJECT NUMBER: K5/966

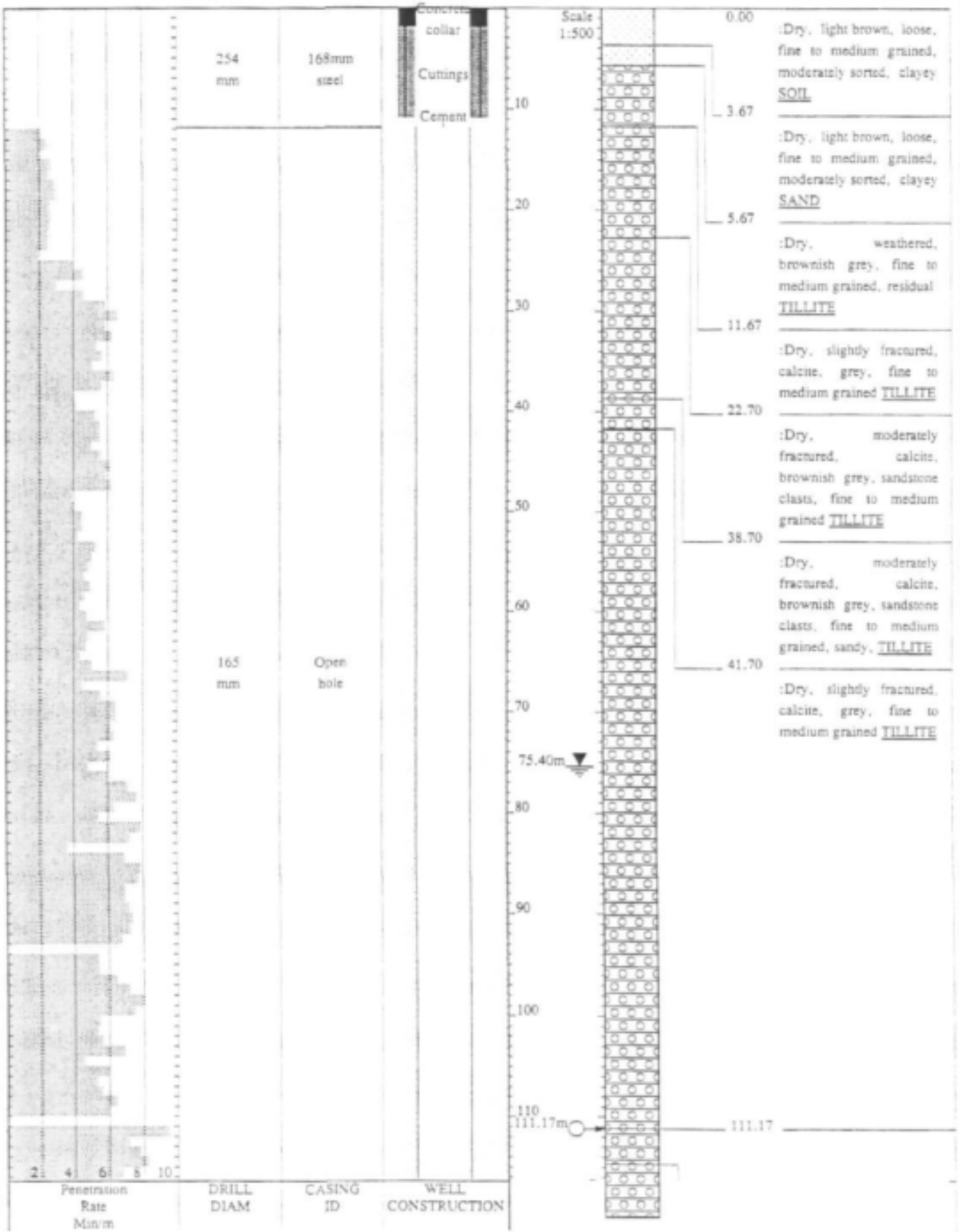

COUNCIL FOR GEOSCIENCE
Private Bag X112
PRETORIA 0001
REPUBLIC OF SOUTH AFRICA

GROUNDWATER DEVELOPMENT IN COMPLEX TERRAIN

HOLE No: G45908
Sheet 1 of 2

PROJECT NUMBER: K5/966

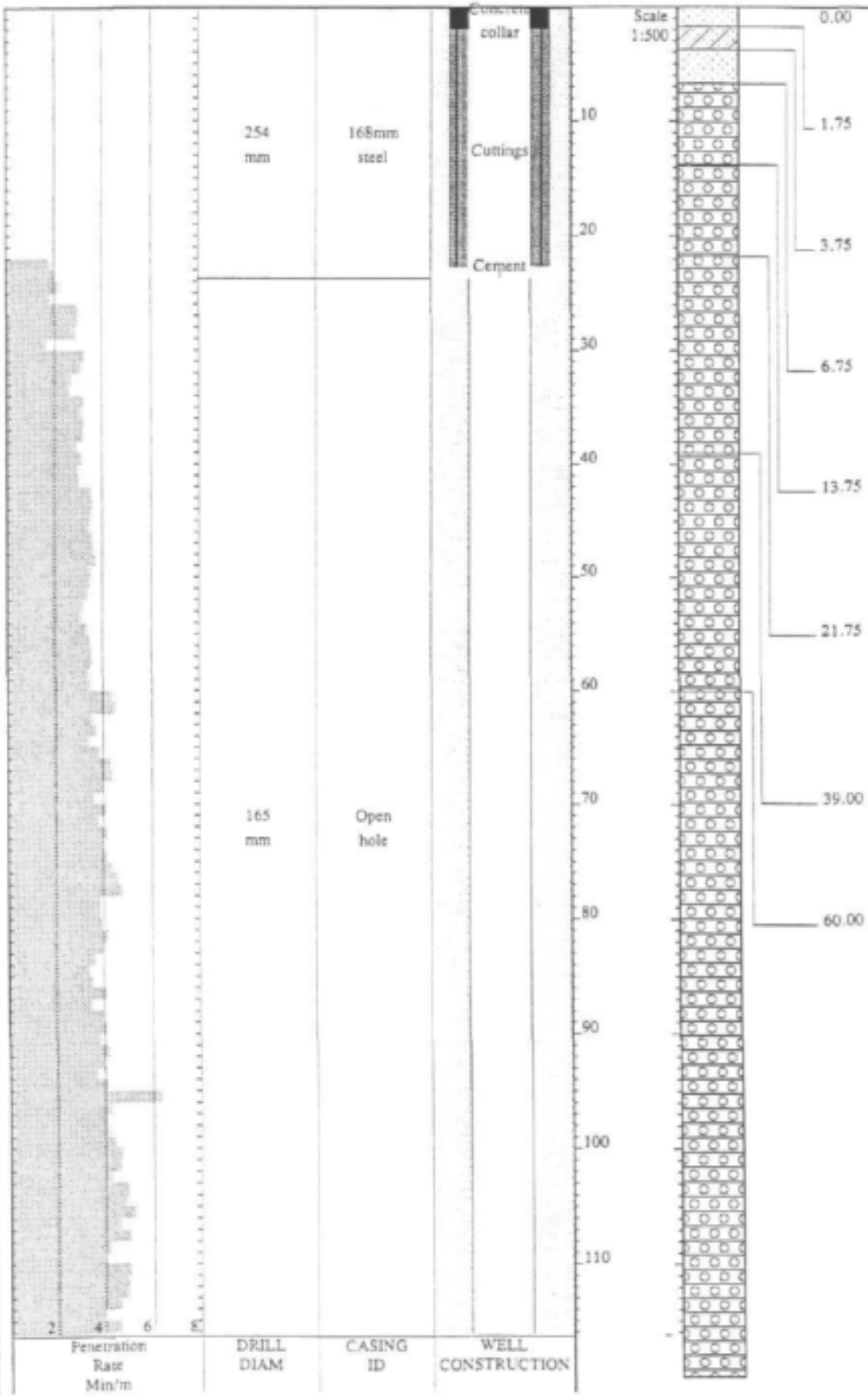

COUNCIL FOR GEOSCIENCE
Private Bag X112
PRETORIA 0001
REPUBLIC OF SOUTH AFRICA

GROUNDWATER DEVELOPMENT IN COMPLEX TERRAIN

HOLE No: G45909
Sheet 1 of 2

PROJECT NUMBER: K5/966

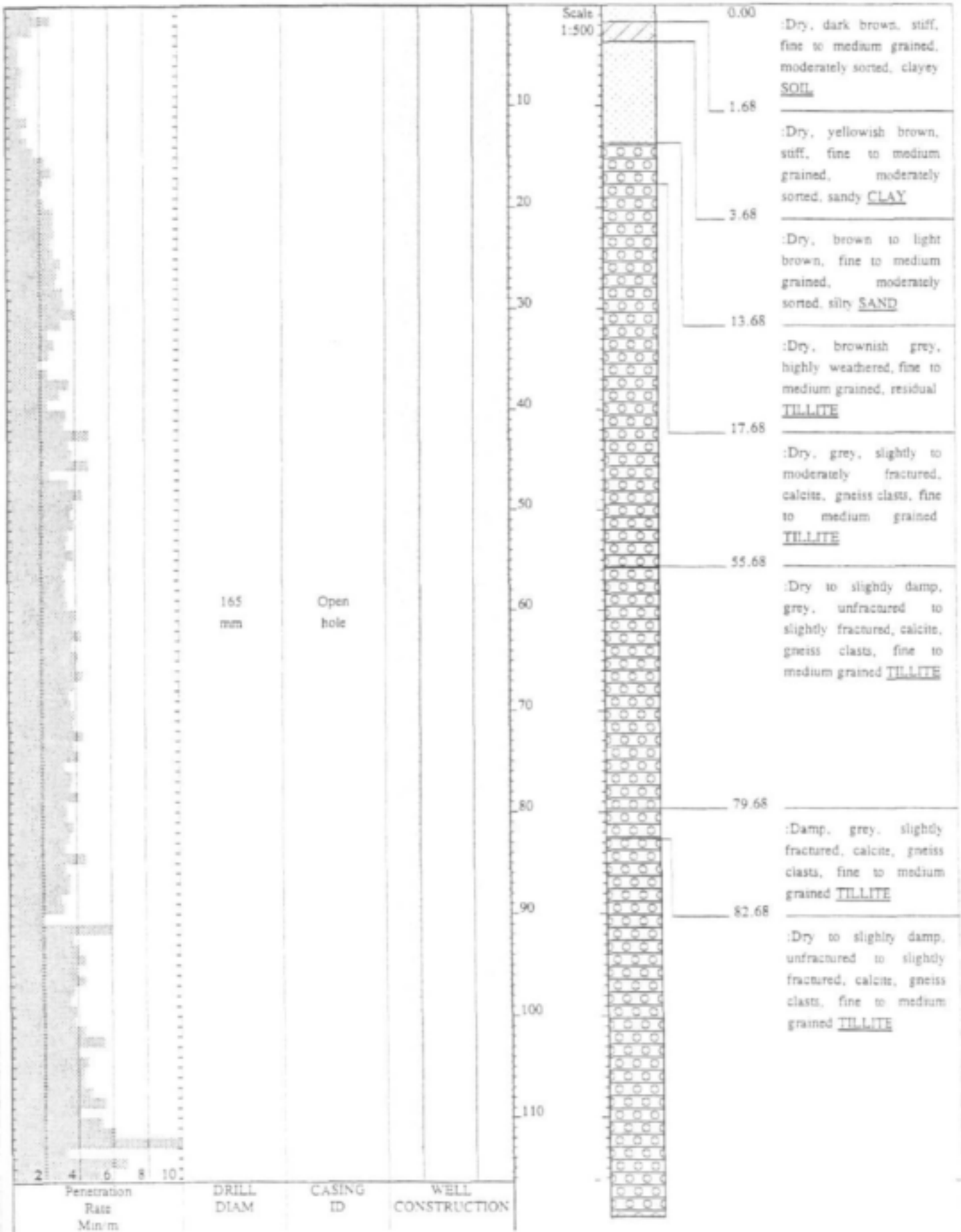

:Dry, dark brown, stiff, fine to medium grained, moderately sorted, clayey SOIL

:Dry, yellowish brown, stiff, fine to medium grained, moderately sorted, sandy CLAY

:Dry, brown to light brown, fine to medium grained, moderately sorted, silty SAND

:Dry, brownish grey, highly weathered, fine to medium grained, residual TILLITE

:Dry, grey, slightly to moderately fractured, calcite, gneiss clasts, fine to medium grained TILLITE

:Dry to slightly damp, grey, unfractured to slightly fractured, calcite, gneiss clasts, fine to medium grained TILLITE

:Damp, grey, slightly fractured, calcite, gneiss clasts, fine to medium grained TILLITE

:Dry to slighly damp, unfractured to slightly fractured, calcite, gneiss clasts, fine to medium grained TILLITE

COUNCIL FOR GEOSCIENCE

Private Bag X112
PRETORIA 0001
REPUBLIC OF SOUTH AFRICA

GROUNDWATER DEVELOPMENT IN COMPLEX TERRAIN

HOLE No: G45910
Sheet 1 of 2

PROJECT NUMBER: K5/966

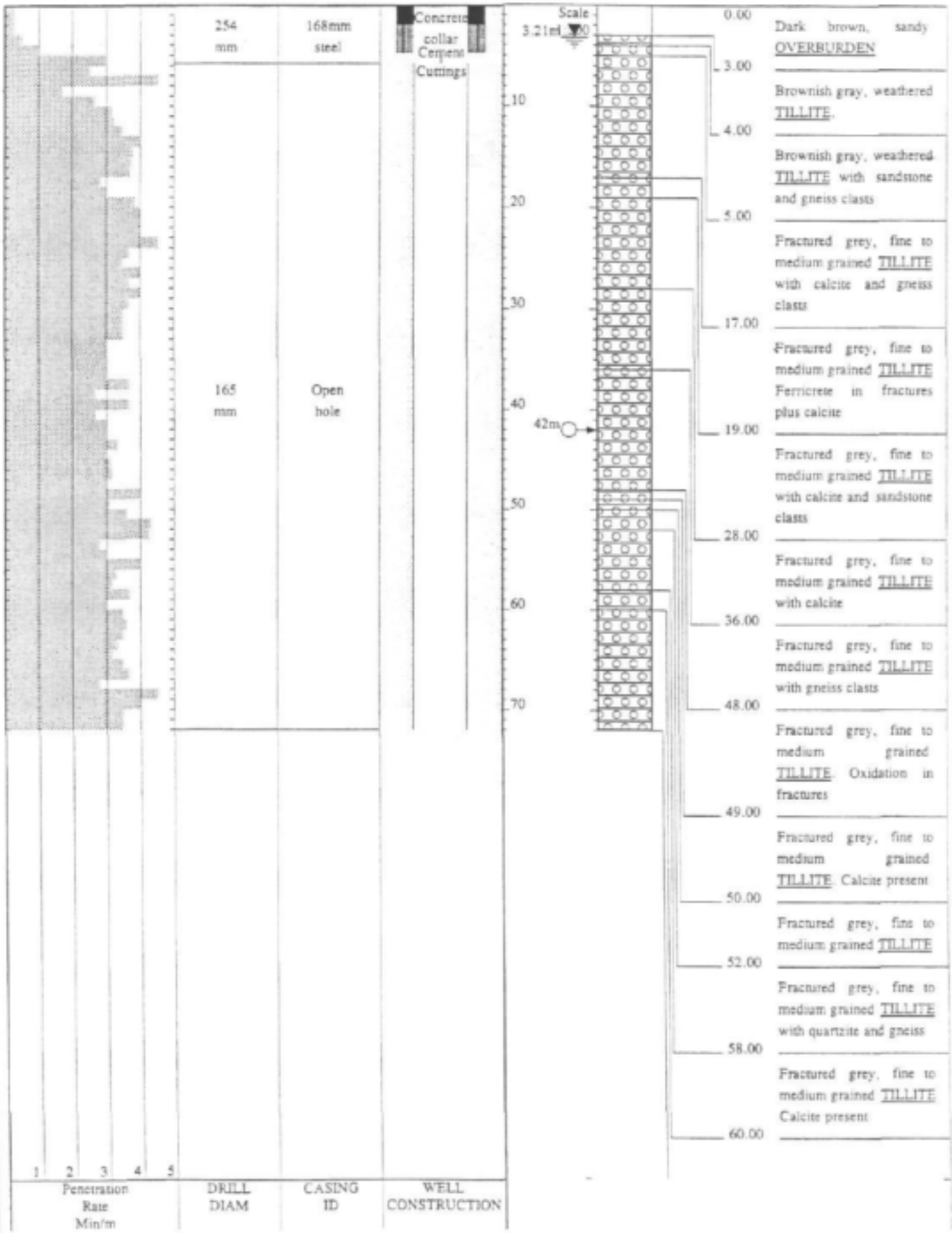

COUNCIL FOR GEOSCIENCE
Private Bag X112
PRETORIA 0001
REPUBLIC OF SOUTH AFRICA

GROUNDWATER DEVELOPMENT IN COMPLEX TERRAIN

HOLE No: G45911
Sheet 1 of 2

PROJECT NUMBER: K5/966

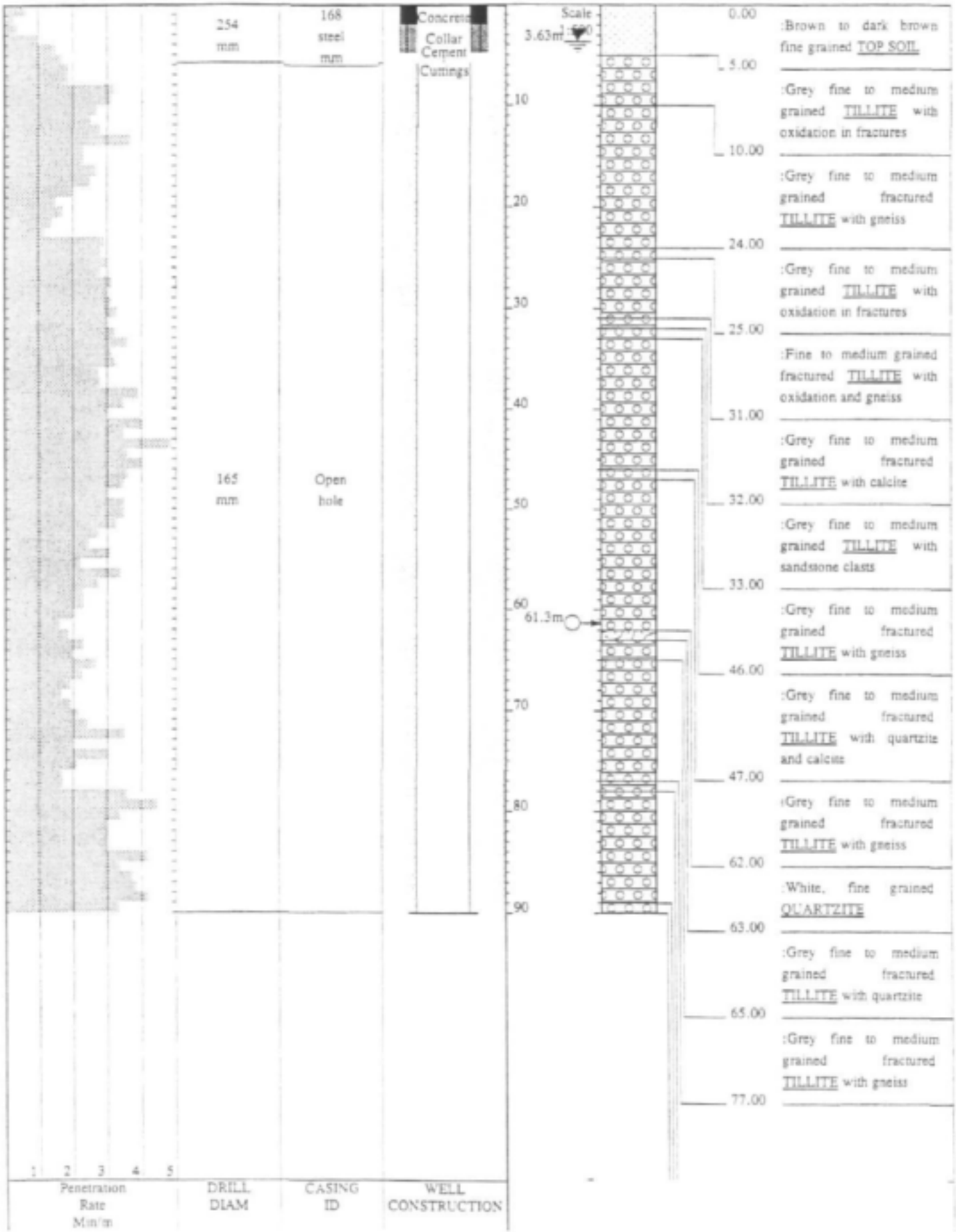

COUNCIL FOR GEOSCIENCE

Private Bag X112
PRETORIA 0001
REPUBLIC OF SOUTH AFRICA

GROUNDWATER DEVELOPMENT IN COMPLEX TERRAIN

HOLE No: G45912
Sheet 1 of 2

PROJECT NUMBER: K5/966

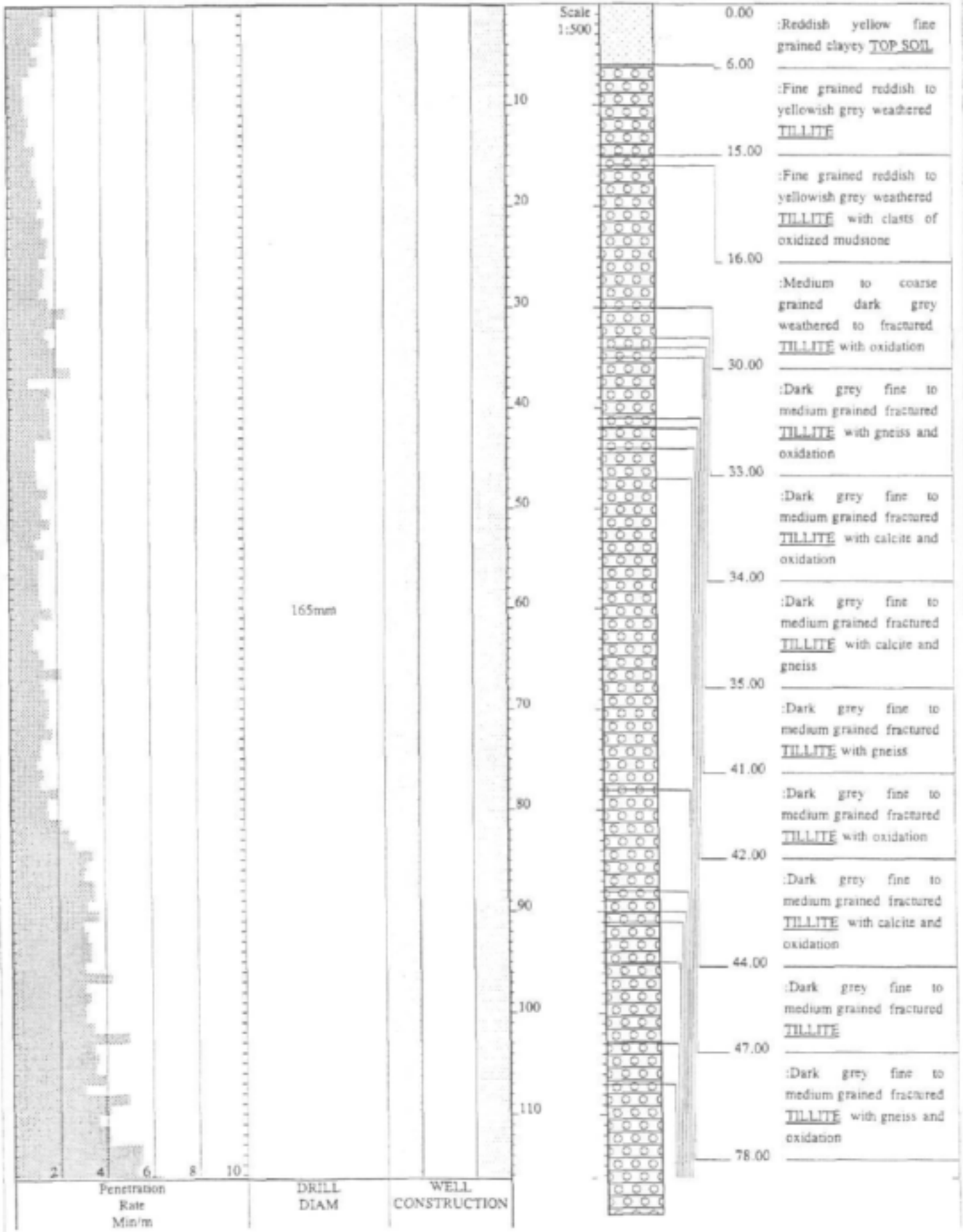

:Reddish yellow fine grained clayey TOP SOIL

:Fine grained reddish to yellowish grey weathered TILLITE

:Fine grained reddish to yellowish grey weathered TILLITE with clasts of oxidized mudstone

:Medium to coarse grained dark grey weathered to fractured TILLITE with oxidation

:Dark grey fine to medium grained fractured TILLITE with gneiss and oxidation

:Dark grey fine to medium grained fractured TILLITE with calcite and oxidation

:Dark grey fine to medium grained fractured TILLITE with calcite and gneiss

:Dark grey fine to medium grained fractured TILLITE with gneiss

:Dark grey fine to medium grained fractured TILLITE with oxidation

:Dark grey fine to medium grained fractured TILLITE with calcite and oxidation

:Dark grey fine to medium grained fractured TILLITE

:Dark grey fine to medium grained fractured TILLITE with gneiss and oxidation

COUNCIL FOR GEOSCIENCE
Private Bag X112
PRETORIA 0001
REPUBLIC OF SOUTH AFRICA

GROUNDWATER DEVELOPMENT IN COMPLEX TERRAIN

HOLE No: G45913
Sheet 1 of 2

PROJECT NUMBER: K5/966

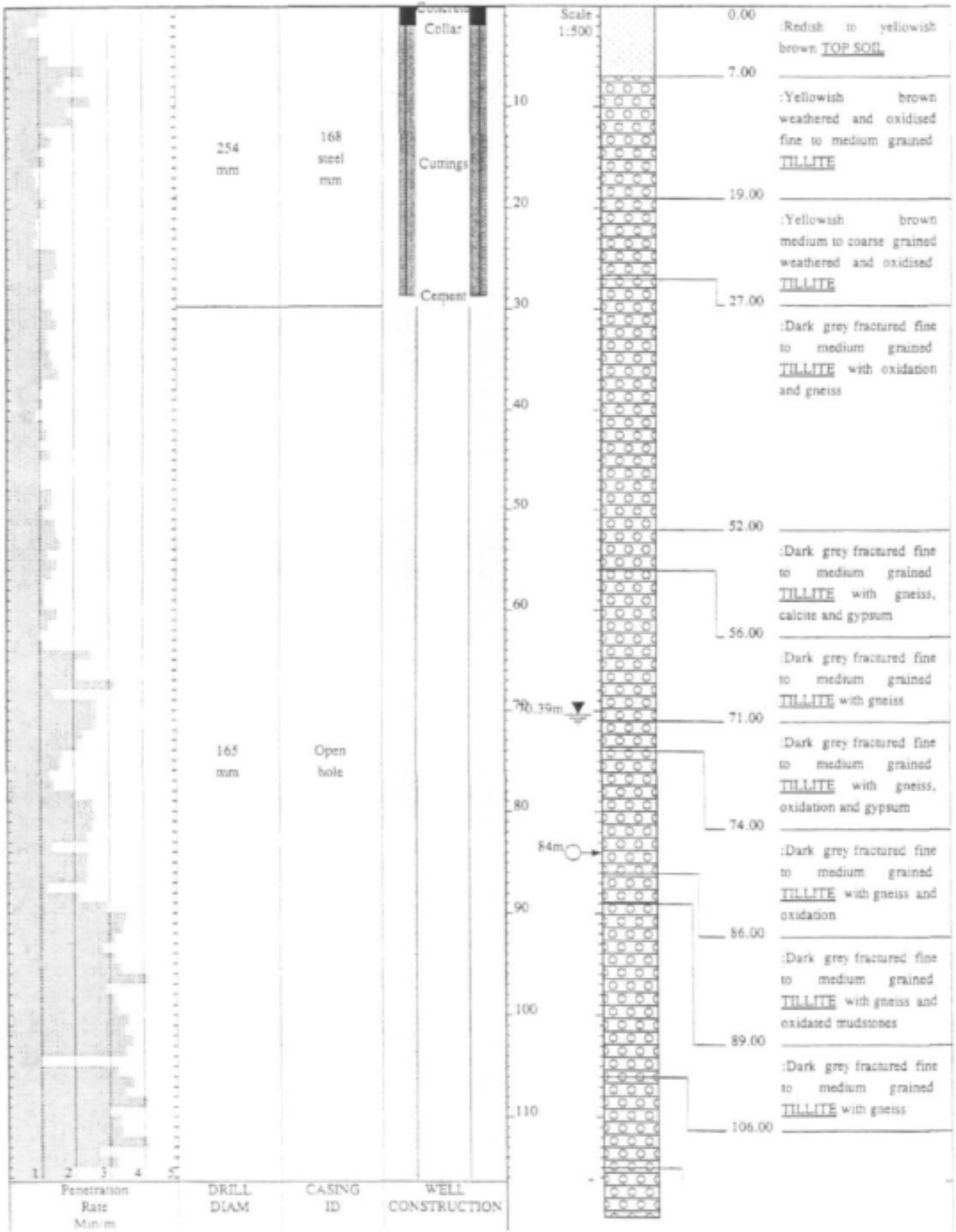

:Redish to yellowish brown TOP SOIL

:Yellowish brown weathered and oxidised fine to medium grained TILLITE

:Yellowish brown medium to coarse grained weathered and oxidised TILLITE

:Dark grey fractured fine to medium grained TILLITE with oxidation and gneiss

:Dark grey fractured fine to medium grained TILLITE with gneiss, calcite and gypsum

:Dark grey fractured fine to medium grained TILLITE with gneiss

:Dark grey fractured fine to medium grained TILLITE with gneiss, oxidation and gypsum

:Dark grey fractured fine to medium grained TILLITE with gneiss and oxidation

:Dark grey fractured fine to medium grained TILLITE with gneiss and oxidated mudstones

:Dark grey fractured fine to medium grained TILLITE with gneiss

COUNCIL FOR GEOSCIENCE
Private Bag X112
PRETORIA 0001
REPUBLIC OF SOUTH AFRICA

GROUNDWATER DEVELOPMENT IN COMPLEX TERRAIN

HOLE No: G45914
Sheet 1 of 2

PROJECT NUMBER: K5/966

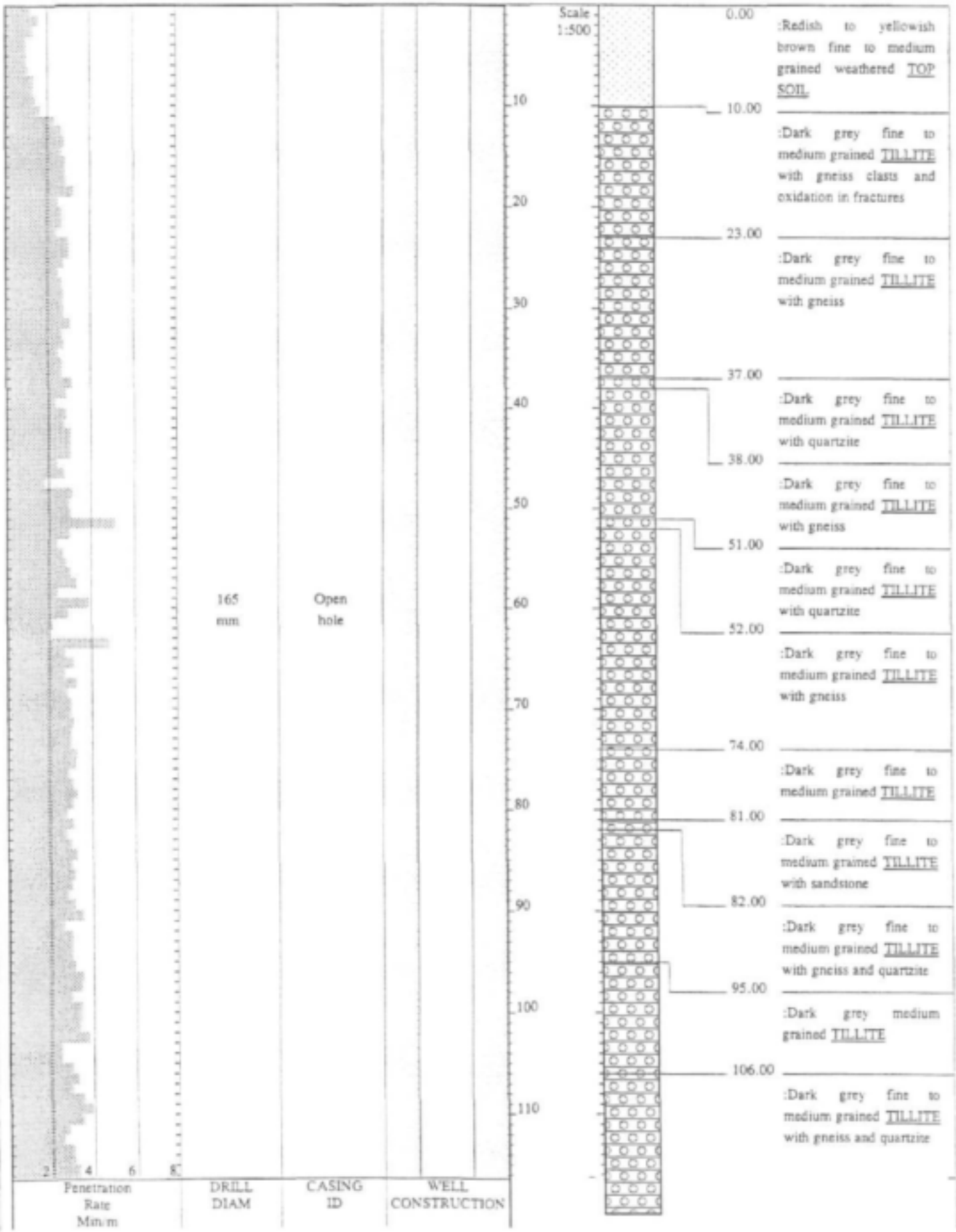

:Redish to yellowish brown fine to medium grained weathered TOP SOIL

:Dark grey fine to medium grained TILLITE with gneiss clasts and oxidation in fractures

:Dark grey fine to medium grained TILLITE with gneiss

:Dark grey fine to medium grained TILLITE with quartzite

:Dark grey fine to medium grained TILLITE with gneiss

:Dark grey fine to medium grained TILLITE with quartzite

:Dark grey fine to medium grained TILLITE with gneiss

:Dark grey fine to medium grained TILLITE

:Dark grey fine to medium grained TILLITE with sandstone

:Dark grey fine to medium grained TILLITE with gneiss and quartzite

:Dark grey medium grained TILLITE

:Dark grey fine to medium grained TILLITE with gneiss and quartzite

COUNCIL FOR GEOSCIENCE

Private Bag X112
PRETORIA 0001
REPUBLIC OF SOUTH AFRICA

GROUNDWATER DEVELOPMENT IN COMPLEX TERRAIN

HOLE No: G45905
Sheet 1 of 2

PROJECT NUMBER: K5/966

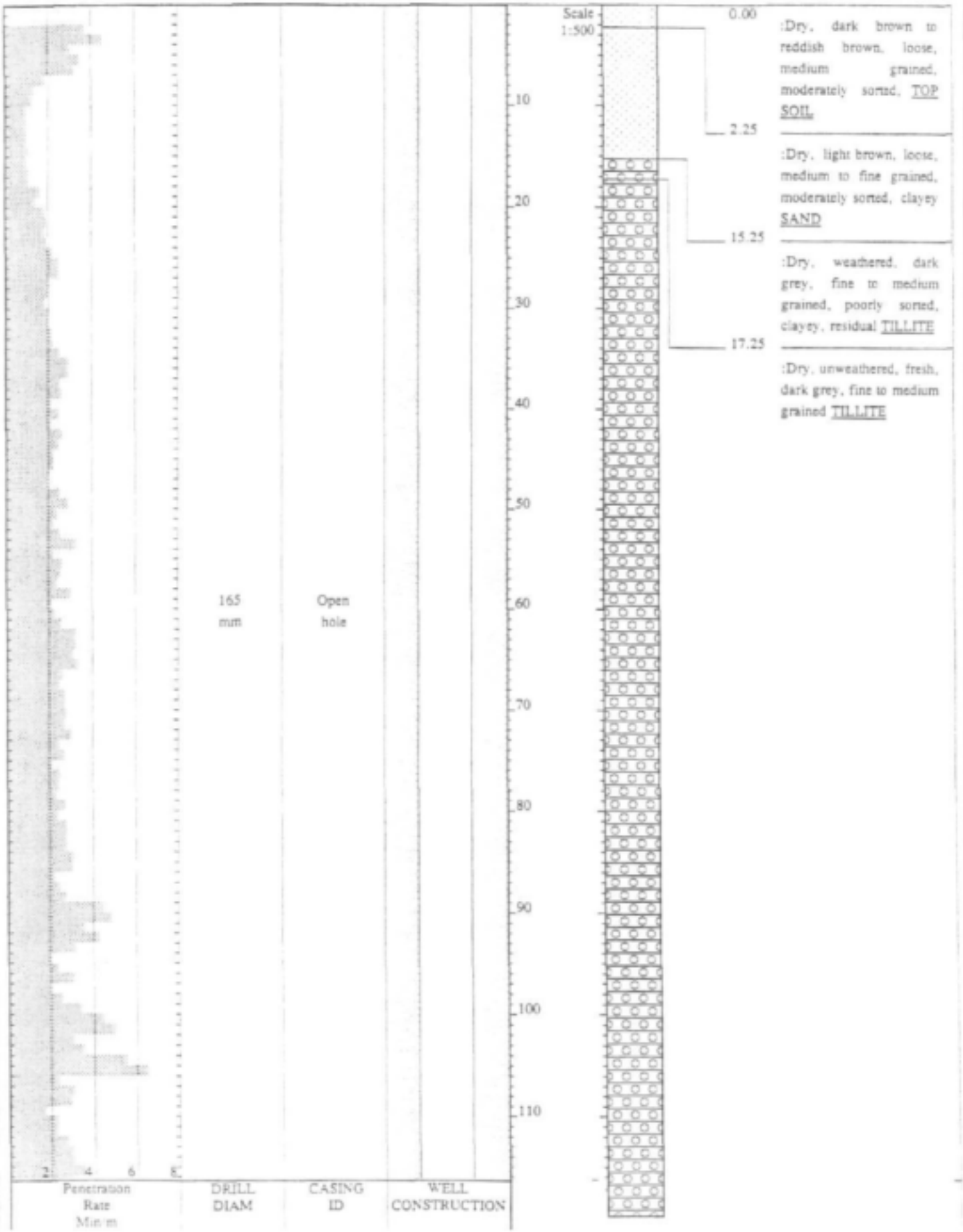

COUNCIL FOR GEOSCIENCE

Private Bag X112
PRETORIA 0001
REPUBLIC OF SOUTH AFRICA

GROUNDWATER DEVELOPMENT IN COMPLEX TERRAIN

HOLE No: G45906
Sheet 1 of 2

PROJECT NUMBER: K5/966

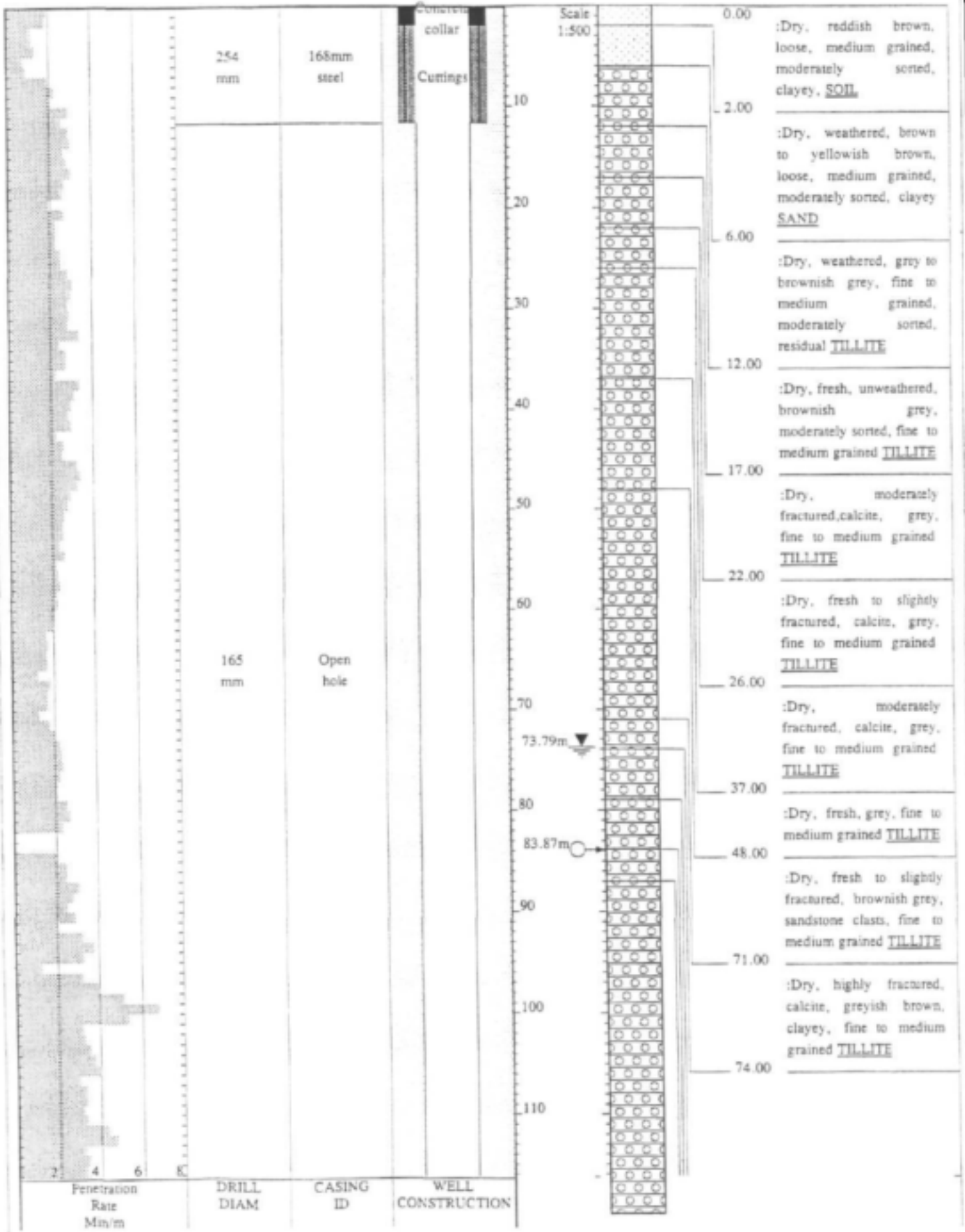

0.00	:Dry, reddish brown, loose, medium grained, moderately sorted, clayey, SOIL
2.00	:Dry, weathered, brown to yellowish brown, loose, medium grained, moderately sorted, clayey SAND
6.00	:Dry, weathered, grey to brownish grey, fine to medium grained, moderately sorted, residual TILLITE
12.00	:Dry, fresh, unweathered, brownish grey, moderately sorted, fine to medium grained TILLITE
17.00	:Dry, moderately fractured,calcite, grey, fine to medium grained TILLITE
22.00	:Dry, fresh to slightly fractured, calcite, grey, fine to medium grained TILLITE
26.00	:Dry, moderately fractured, calcite, grey, fine to medium grained TILLITE
37.00	:Dry, fresh, grey, fine to medium grained TILLITE
48.00	:Dry, fresh to slightly fractured, brownish grey, sandstone clasts, fine to medium grained TILLITE
71.00	:Dry, highly fractured, calcite, greyish brown, clayey, fine to medium grained TILLITE
74.00	

COUNCIL FOR GEOSCIENCE
Private Bag X112
PRETORIA 0001
REPUBLIC OF SOUTH AFRICA

GROUNDWATER DEVELOPMENT IN COMPLEX TERRAIN

HOLE No: G45907
Sheet 1 of 2

PROJECT NUMBER: K5/966

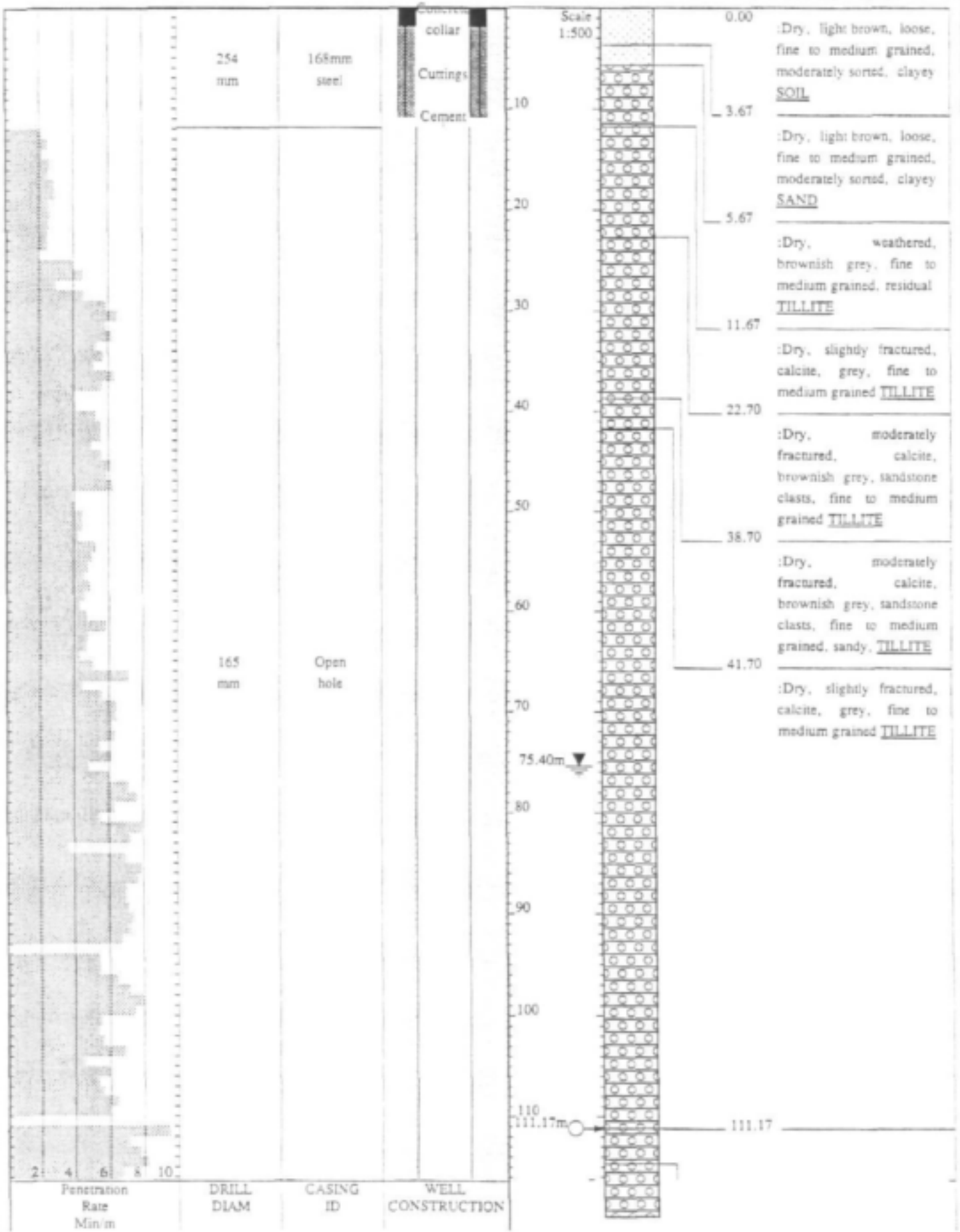

COUNCIL FOR GEOSCIENCE

Private Bag X112
PRETORIA 0001
REPUBLIC OF SOUTH AFRICA

GROUNDWATER DEVELOPMENT IN COMPLEX TERRAIN

HOLE No: G45908
Sheet 1 of 2

PROJECT NUMBER: K5/966

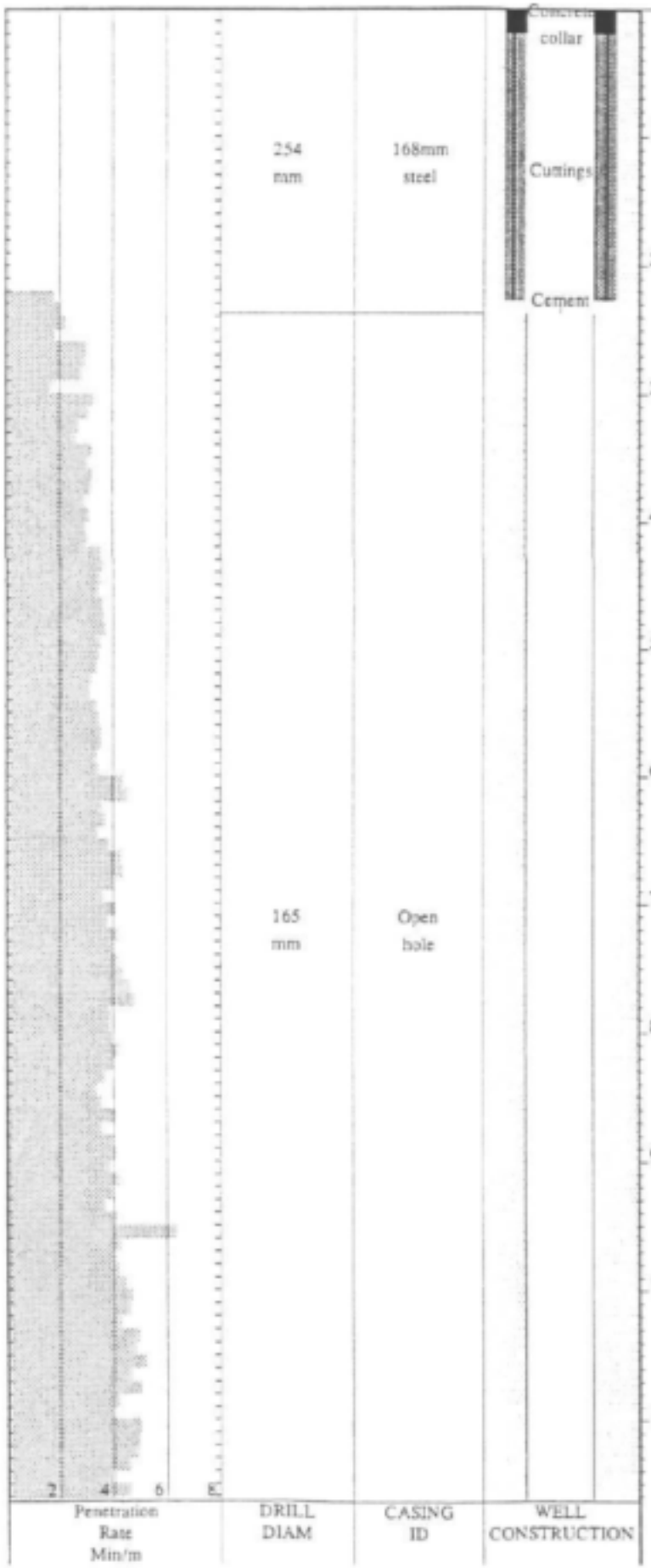

0.00 :Dry, dark brown, stiff, fine to medium grained, moderately sorted, clayey SOIL

1.75 :Dry, yellowish brown, stiff, fine to medium grained, moderately sorted, sandy CLAY

3.75 :Dry, light brown, loose to stiff, fine to medium grained, moderately sorted, clayey SAND

6.75 :Dry, light brown, highly weathered, fine to medium grained, residual TILLITE

13.75 :Dry, greyish brown, moderately to highly weathered, fine to medium grained, residual TILLITE

21.75 :Dry, grey to brownish grey, moderately to highly fractured, calcite, gypsum, ferruginous, fine to medium grained TILLITE

39.00 :Dry, grey, moderately to highly fractured, calcite, gneiss clasts, fine to medium grained TILLITE

60.00 :Dry to slightly damp, grey, slightly fractured, calcite, gneiss clasts, fine to medium grained TILLITE

COUNCIL FOR GEOSCIENCE
Private Bag X112
PRETORIA 0001
REPUBLIC OF SOUTH AFRICA

GROUNDWATER DEVELOPMENT IN COMPLEX TERRAIN

HOLE No: G45909
Sheet 1 of 2

PROJECT NUMBER: K5/966

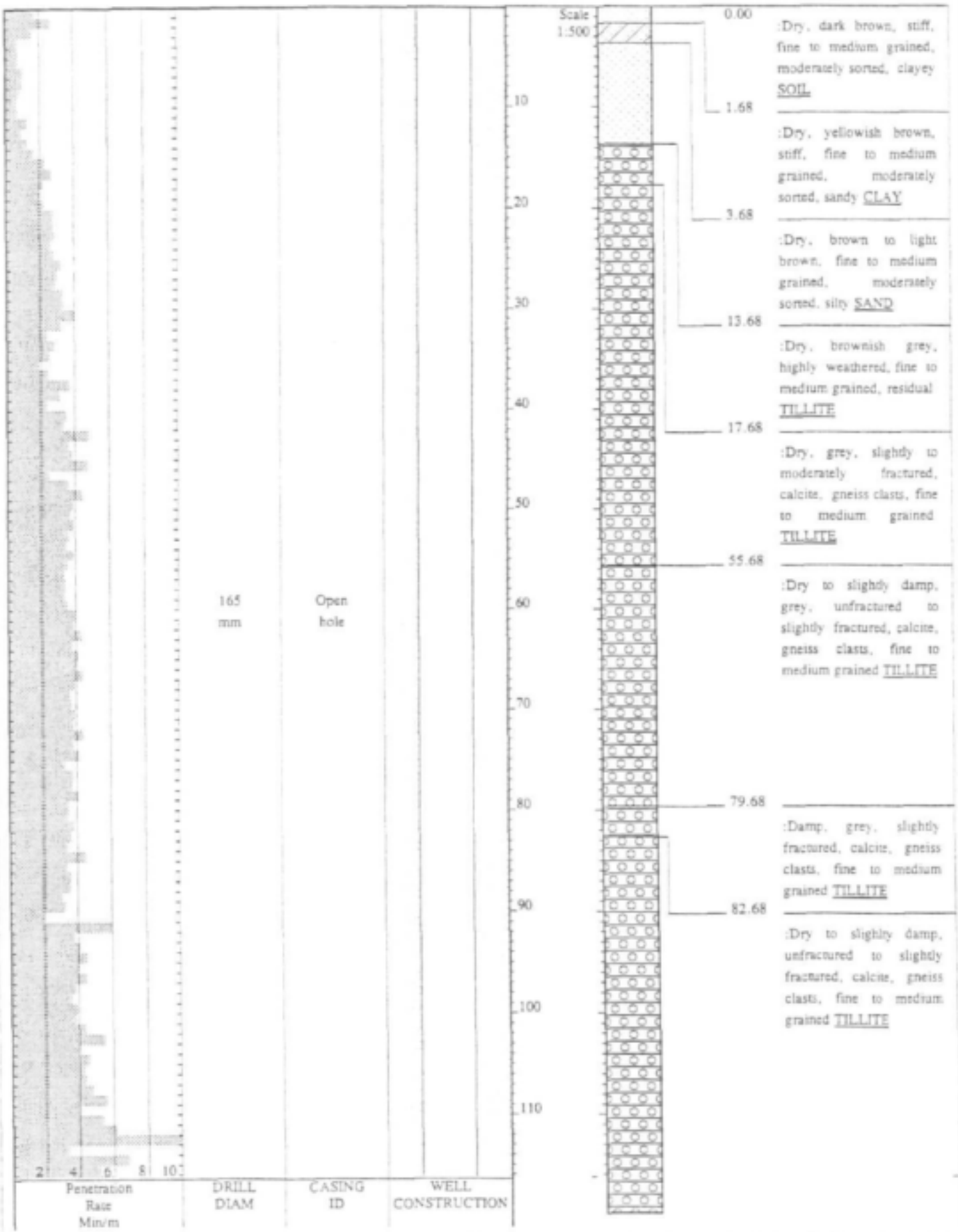

COUNCIL FOR GEOSCIENCE

Private Bag X112
PRETORIA 0001
REPUBLIC OF SOUTH AFRICA

GROUNDWATER DEVELOPMENT IN COMPLEX TERRAIN

HOLE No: G45910
Sheet 1 of 2

PROJECT NUMBER: K5/966

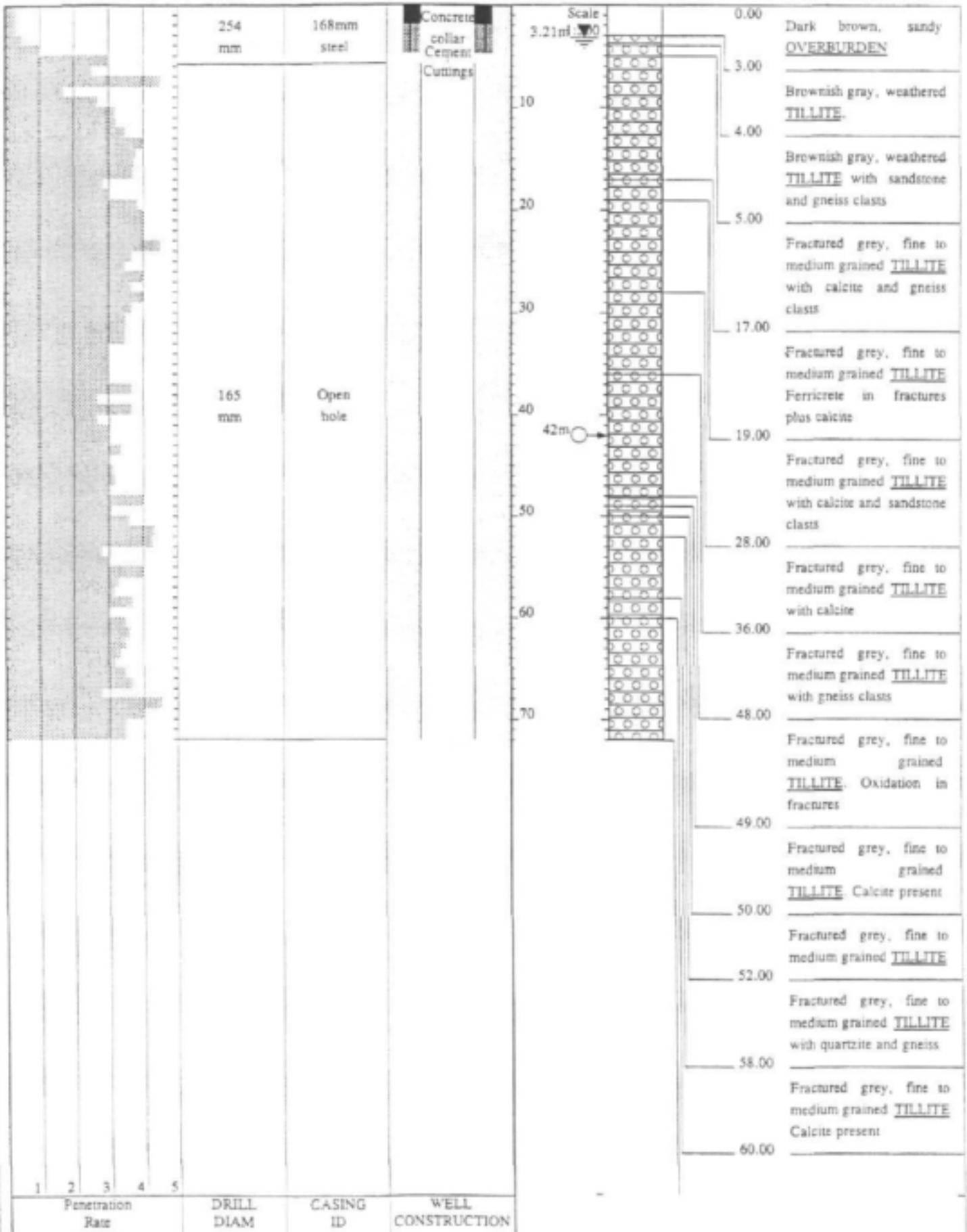

COUNCIL FOR GEOSCIENCE
Private Bag X112
PRETORIA 0001
REPUBLIC OF SOUTH AFRICA

GROUNDWATER DEVELOPMENT IN COMPLEX TERRAIN

HOLE No: G45911
Sheet 1 of 2

PROJECT NUMBER: K5/966

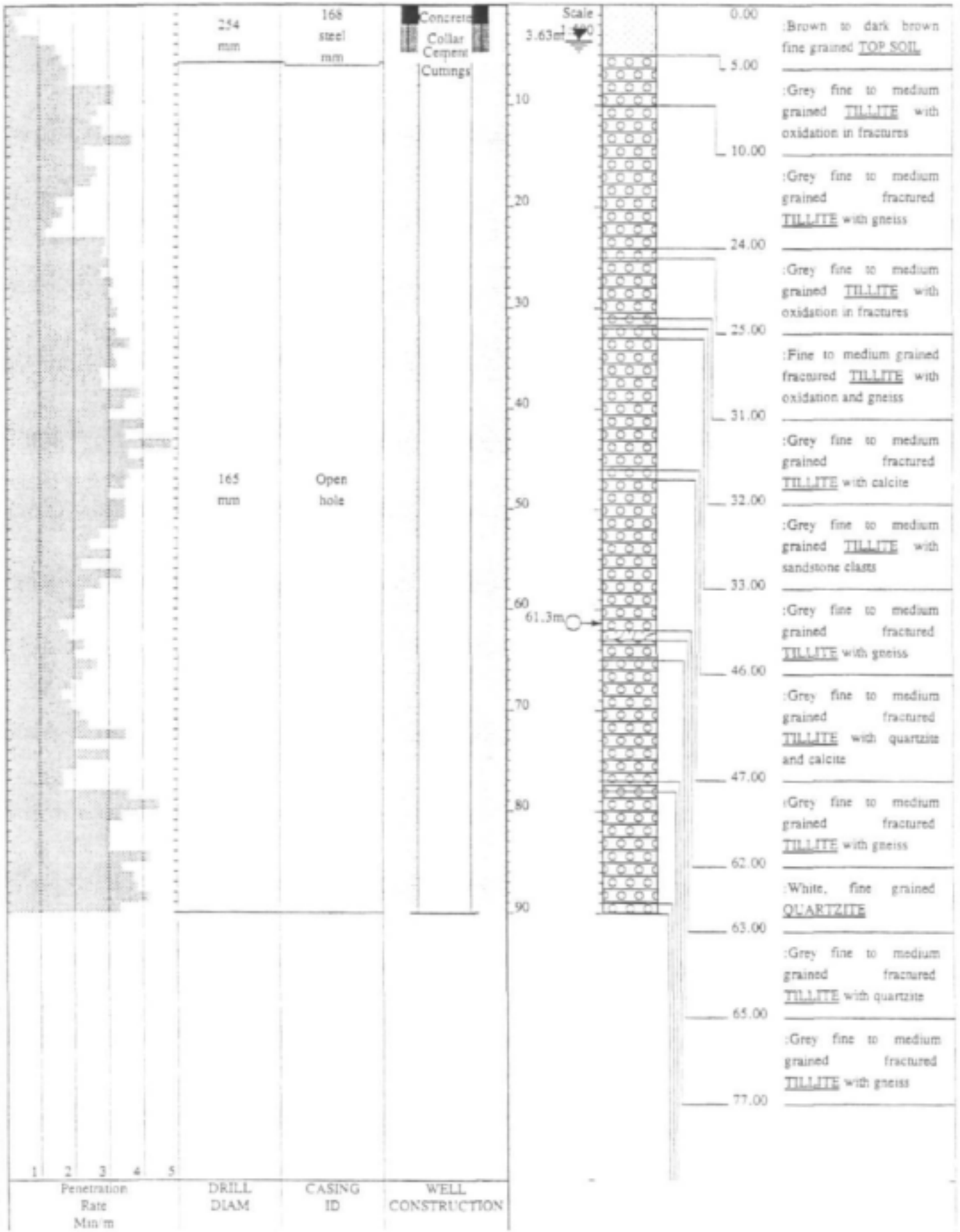

COUNCIL FOR GEOSCIENCE
Private Bag X112
PRETORIA 0001
REPUBLIC OF SOUTH AFRICA

GROUNDWATER DEVELOPMENT IN COMPLEX TERRAIN

HOLE No: G45912
Sheet 1 of 2

PROJECT NUMBER: K5/966

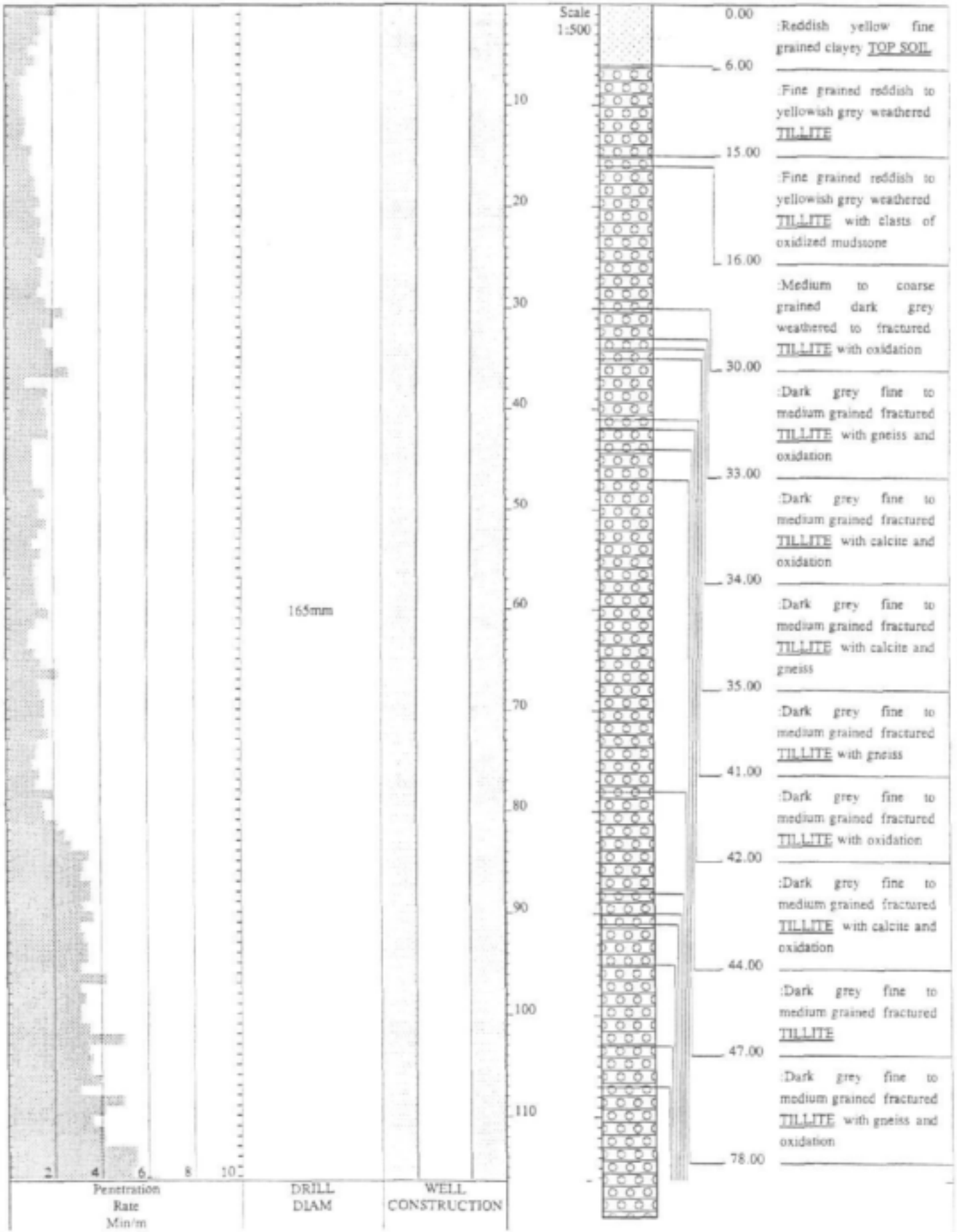

COUNCIL FOR GEOSCIENCE
Private Bag X112
PRETORIA 0001
REPUBLIC OF SOUTH AFRICA

GROUNDWATER DEVELOPMENT IN COMPLEX TERRAIN

HOLE No: G45913
Sheet 1 of 2

PROJECT NUMBER: K5/966

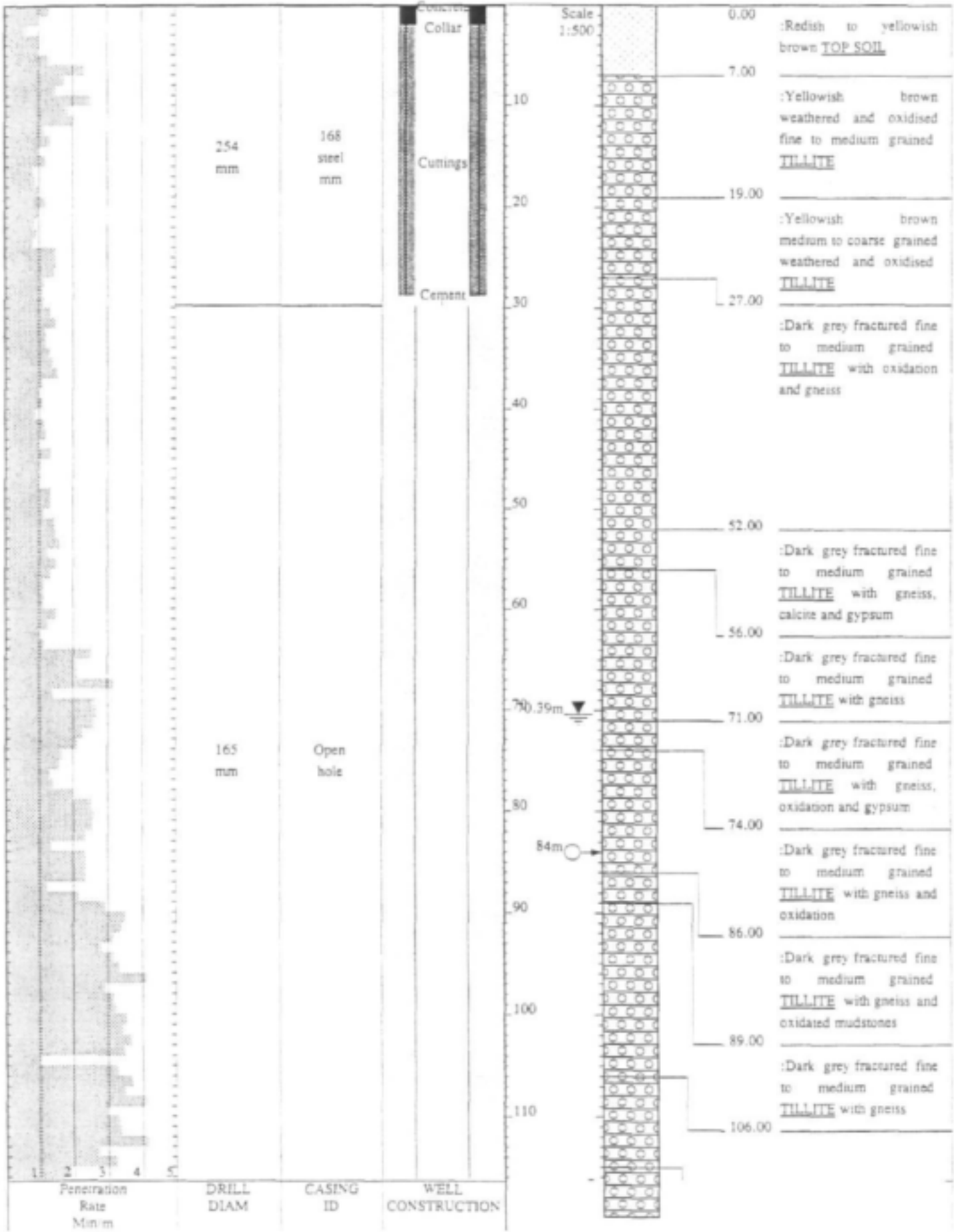

COUNCIL FOR GEOSCIENCE

Private Bag X112
PRETORIA 0001
REPUBLIC OF SOUTH AFRICA

GROUNDWATER DEVELOPMENT IN COMPLEX TERRAIN

HOLE No: G45914
Sheet 1 of 2

PROJECT NUMBER: K5/966

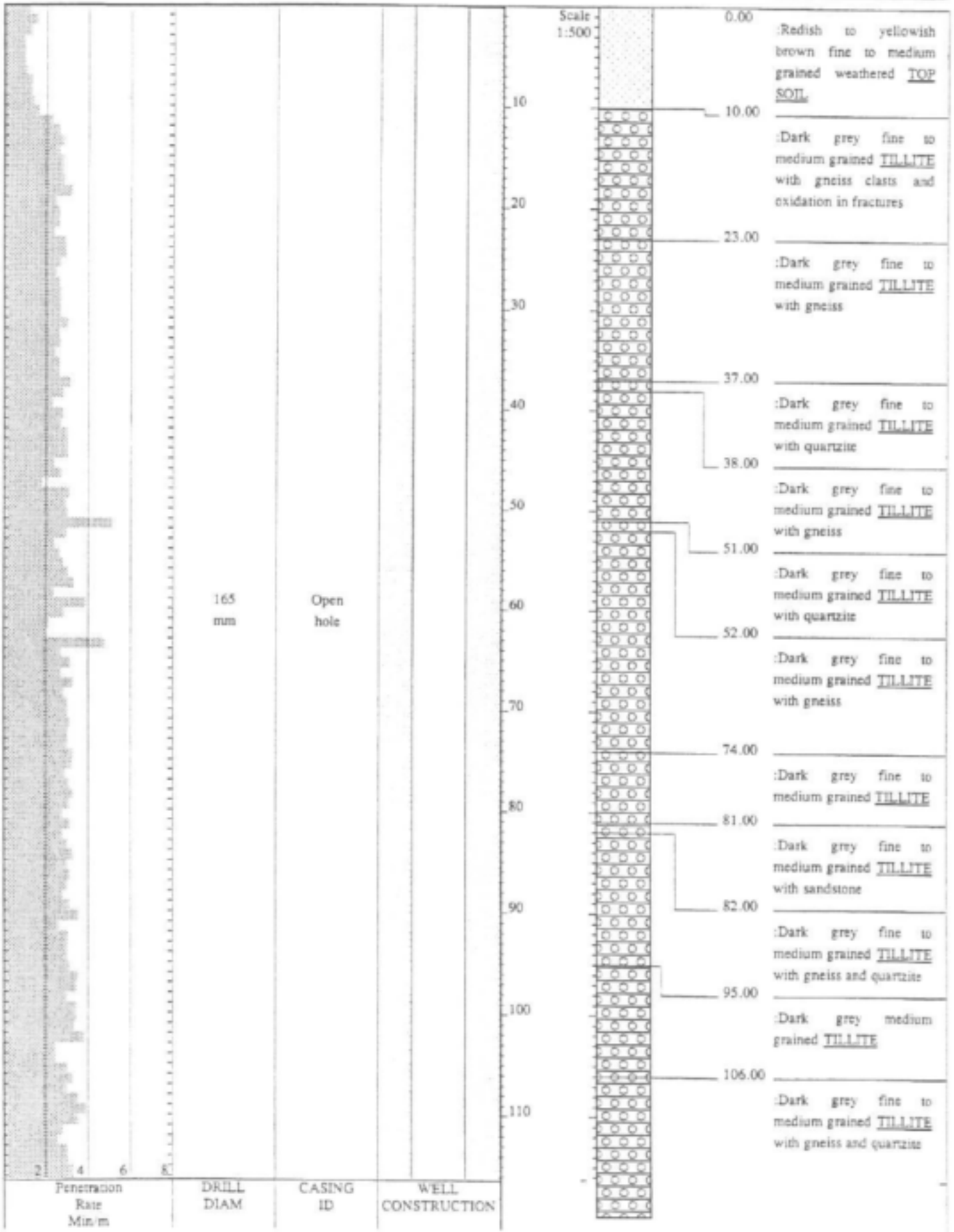

:Redish to yellowish brown fine to medium grained weathered TOP SOIL

:Dark grey fine to medium grained TILLITE with gneiss clasts and oxidation in fractures

:Dark grey fine to medium grained TILLITE with gneiss

:Dark grey fine to medium grained TILLITE with quartzite

:Dark grey fine to medium grained TILLITE with gneiss

:Dark grey fine to medium grained TILLITE with quartzite

:Dark grey fine to medium grained TILLITE with gneiss

:Dark grey fine to medium grained TILLITE

:Dark grey fine to medium grained TILLITE with sandstone

:Dark grey fine to medium grained TILLITE with gneiss and quartzite

:Dark grey medium grained TILLITE

:Dark grey fine to medium grained TILLITE with gneiss and quartzite

APPENDIX 1-C

TEST PUMP DATA

a)

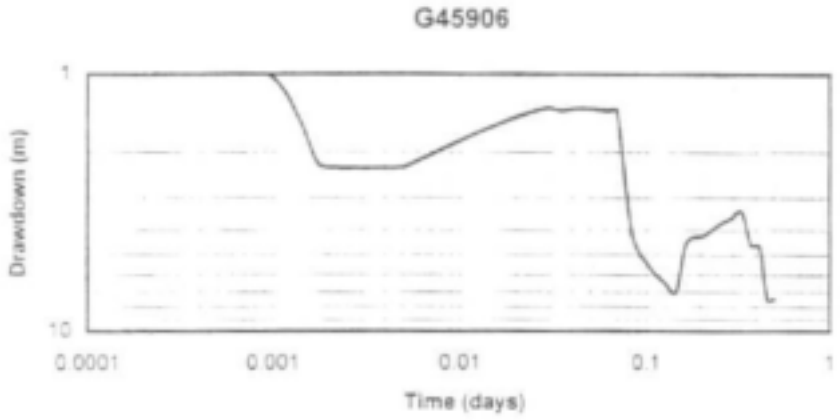

b)

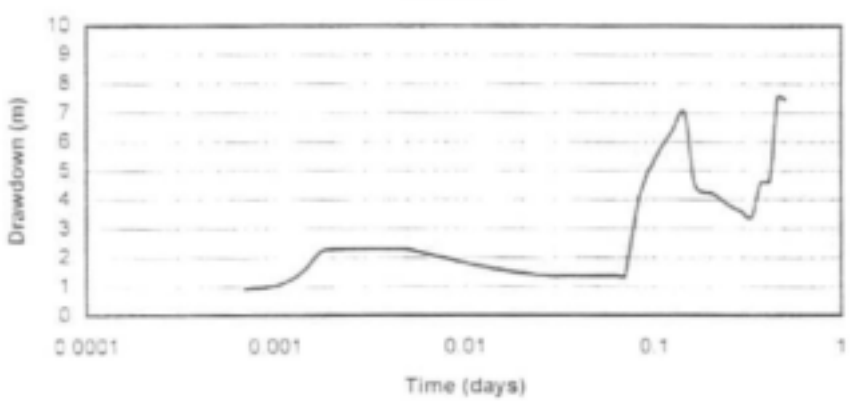

c)

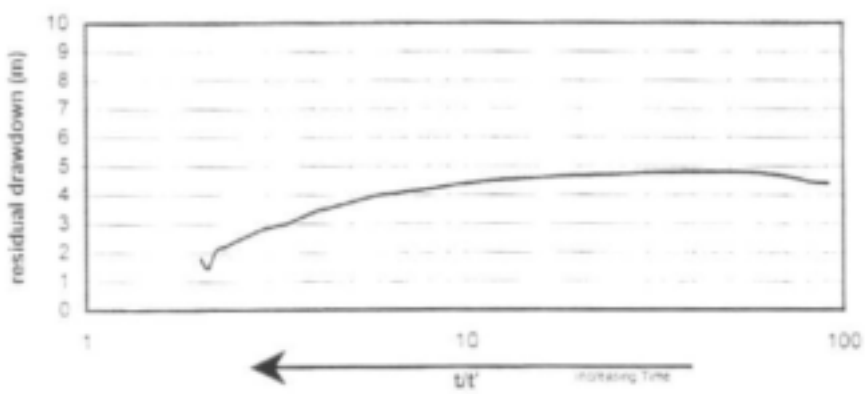

a) Drawdown data on a log/log scale
b) Drawdown data on a semi-log scale
c) Recovery data

a)

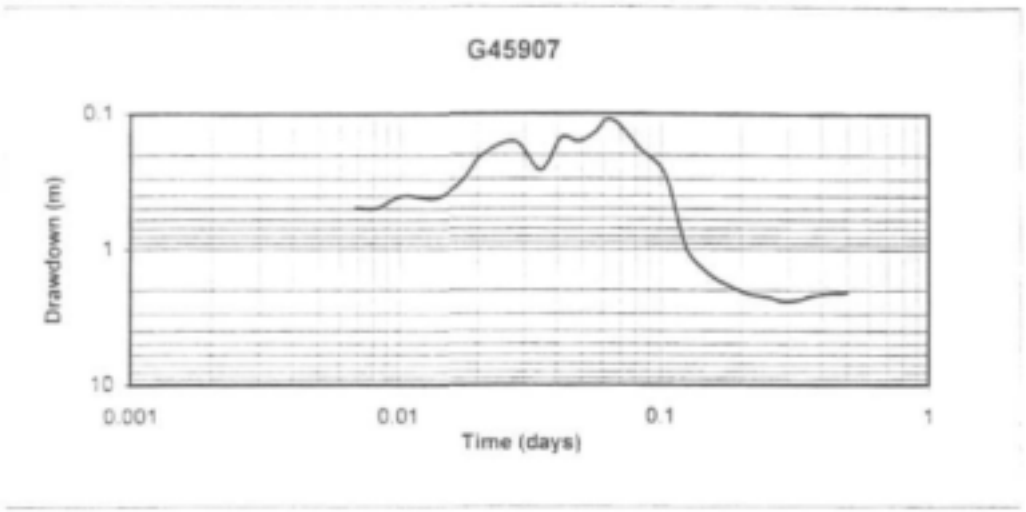

b)

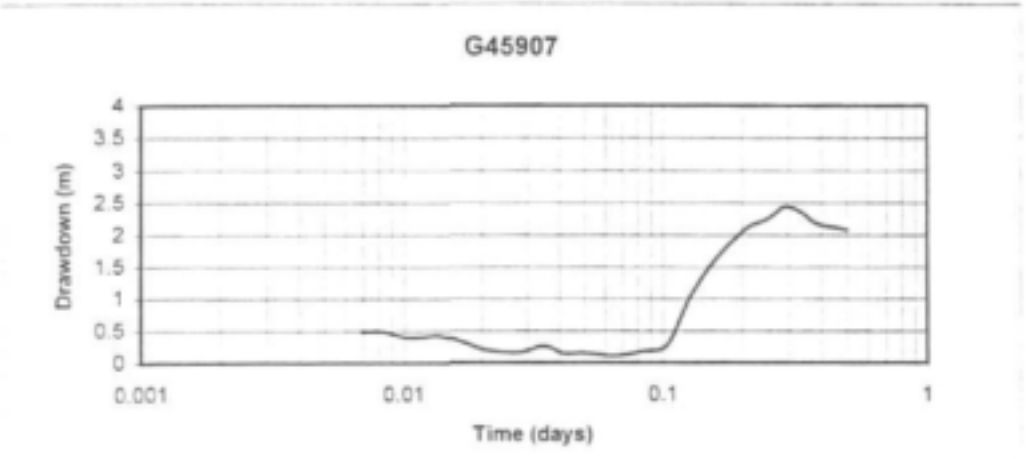

c)

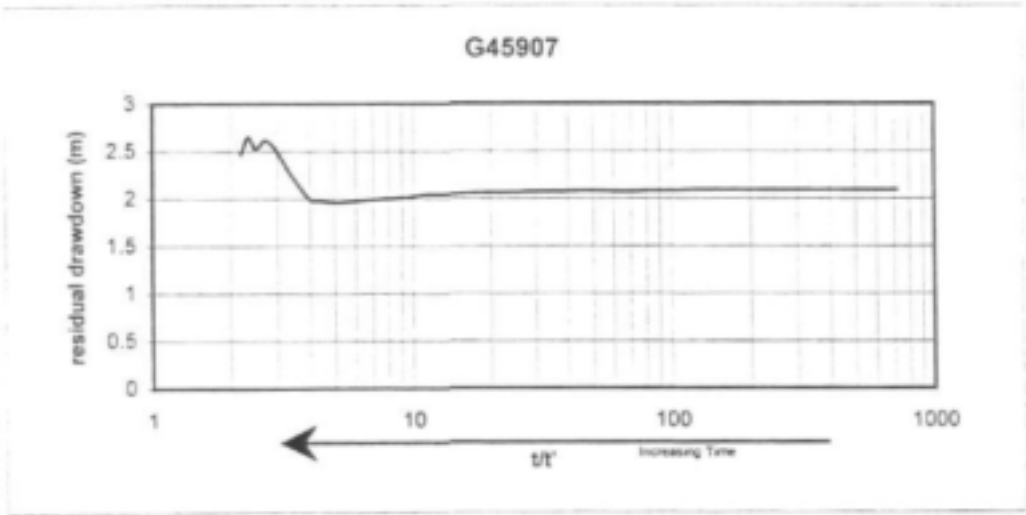

a) Drawdown data on a log/log scale
b) Drawdown data on a semi-log scale
c) Recovery data

a)

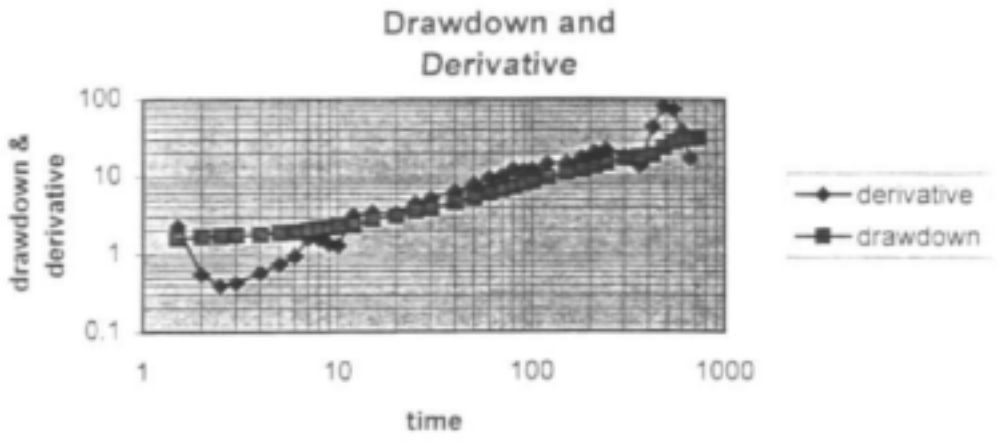

b)

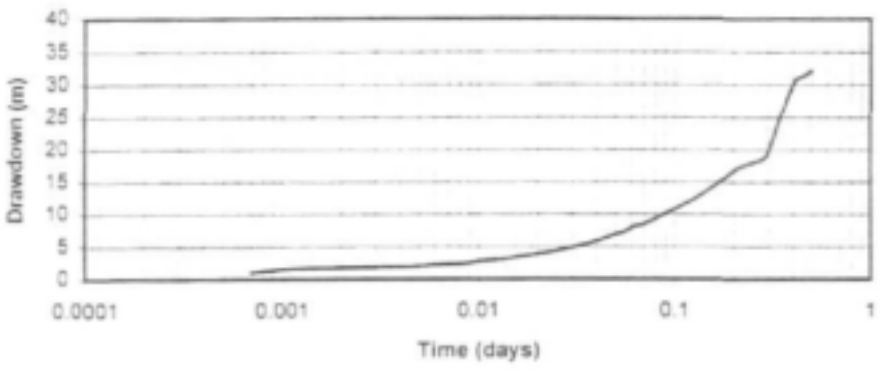

c)

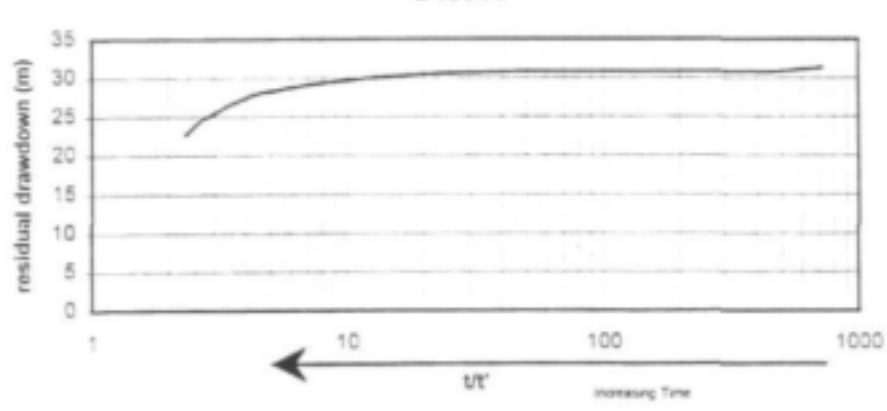

a) Drawdown data on a log/log scale
b) Drawdown data on a semi-log scale
c) Recovery data

a)

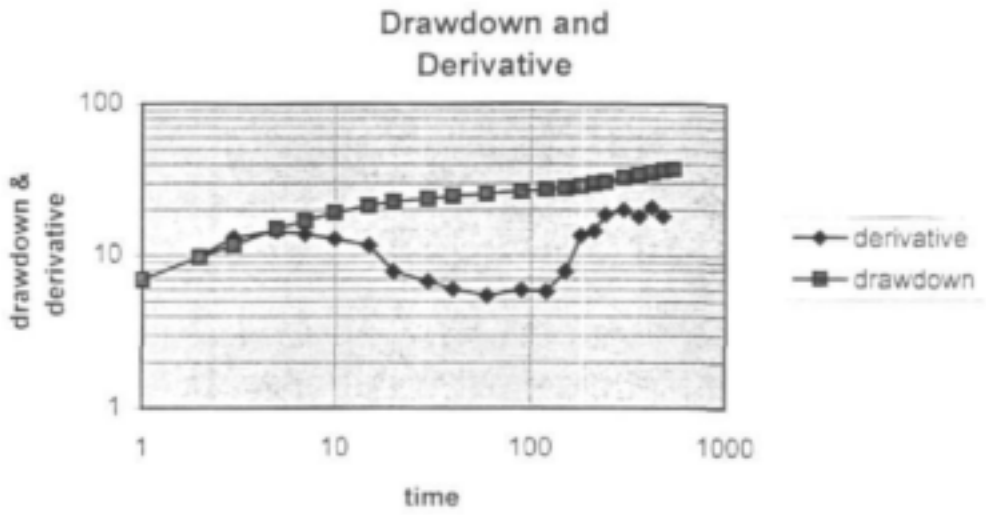

b)

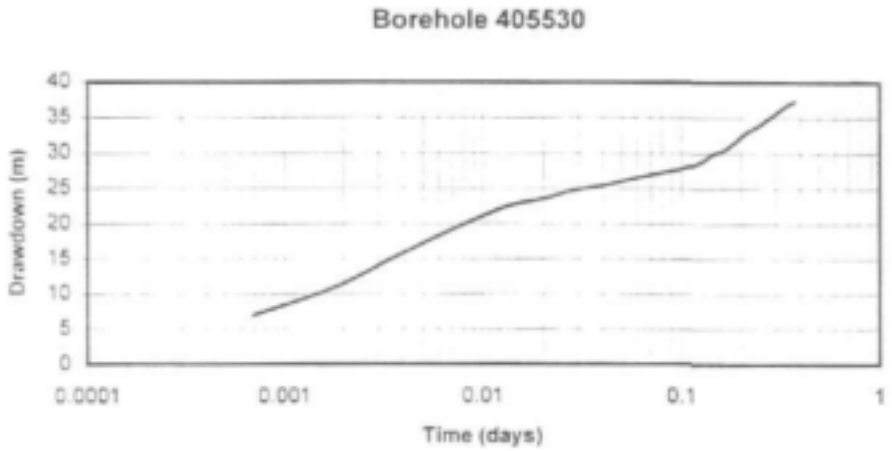

c)

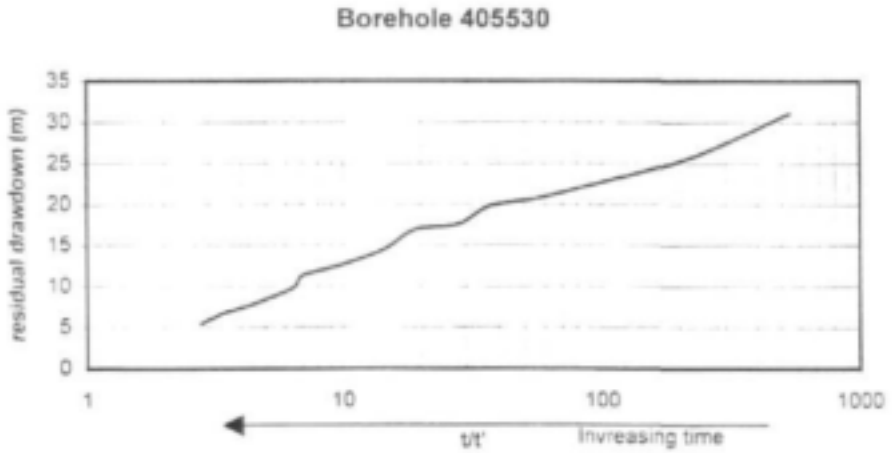

a) Drawdown data on a log/log scale
b) Drawdown data on a semi-log scale
c) Recovery data

APPENDIX 1-D

ANALYTICAL RESULTS OF THE WATER SAMPLES

Parameter	G45906	G45907	G45910	G45911	G45913
pH	8.10	8.05	8.12	8.9	7.33
pHs	7.44	7.86	7.8	8.52	7.58
EC (mS/m at 25°)	77	64	103	53	107.0
TDS (mg/l).	378.1	317.7	560.8	260.8	503.3
Total Alkalinity (mg/l)	250	158	320	80	115
Temp. Hardness (mg/l))	239	149	92	63	115
Perm. Hardness (mg/l)	0	0.0	0.0	10	190
Calcium (mg/l)	40.50	24	14.4	10.10	65.80
Magnesium (mg/l)	33.27	21.39	11.92	11.19	34.01
Sodium (mg/l)	58.20	61.90	193	60.9	64.30
Potassium (mg/l)	1.86	4.02	5.47	3.16	3.95
Sulfate (mg/l)	0.0	13.97	7.63	5.9	0.0
Phosphate (mg-l)	0.0	0.0	0.0	0.0	0.0
Chloride (mg/l)	88.40	64.2	120.53	106.22	247.39
Carbonate (mg/l)	0.0	0.0	0.0	10.5	0.0
Bicarbonate (mg/l)	305	192.15	390.4	76.25	140.3
Nitrate (mg/l)	3.28	27.6	3.68	14.63	17.67
Nitrite (mg/l)	0.0	3.8	7.29	0.0	0.0
Fluoride (mg/l)	0.0	0.7	1.19	0.0	0.0
Boron (mg/l)	0.05	0.07	0.46	0.07	0.05
Chemical Character	Mg $CaCO_3$	Na $CaCO_3$	Na $CaCO_3$	Na Cl	Ca Cl

Piper Diagram

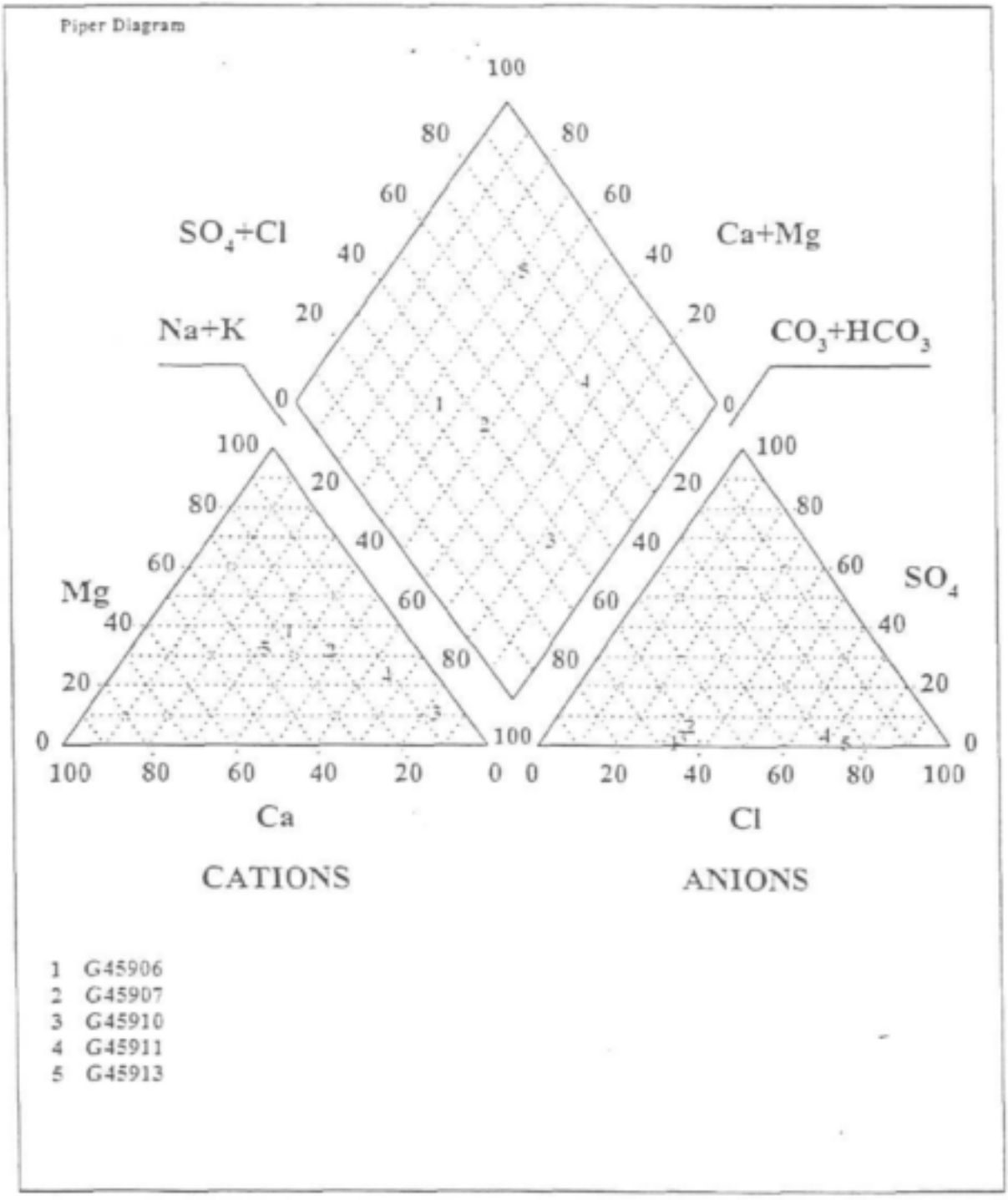

Well Ident
G45907

STIFF Diagram

Name	Type

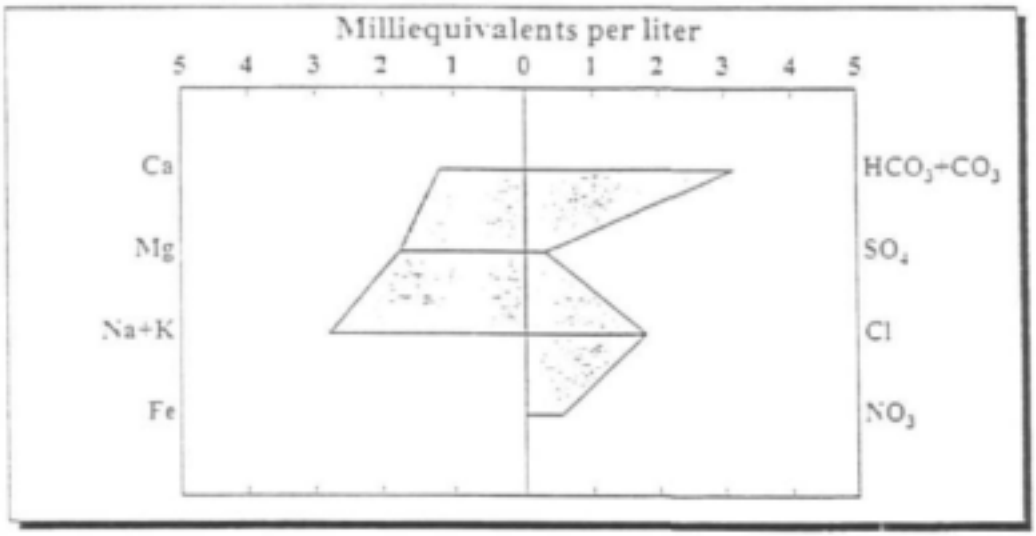

Cations

	Ca	*Mg*	*Na*	*K*	*Fe*
Milliequivalents per liter	1.20	1.76	2.69	0.10	
Milligrams per liter					

Anions

	HCO3	*CO3*	*SO4*	*Cl*	*NO3*
Milliequivalents per liter	3.15		0.29	1.81	0.53
Milligrams per liter					

BOD	COD	Dissolved Oxygen	F	B	SiO2
				0.02	

TDS	Hardness	Alkalinity	Conductivity	pH	SAR
317.70	2.98	3.15		8.05	2.2112

Water Type	*Sodium Bicarbonate*

Cations (epm)	Anions (epm)
5.75	5.80

Error Balance (%)
0.43

Aquifer

Well Ident
G45911

STIFF Diagram

Name	Type

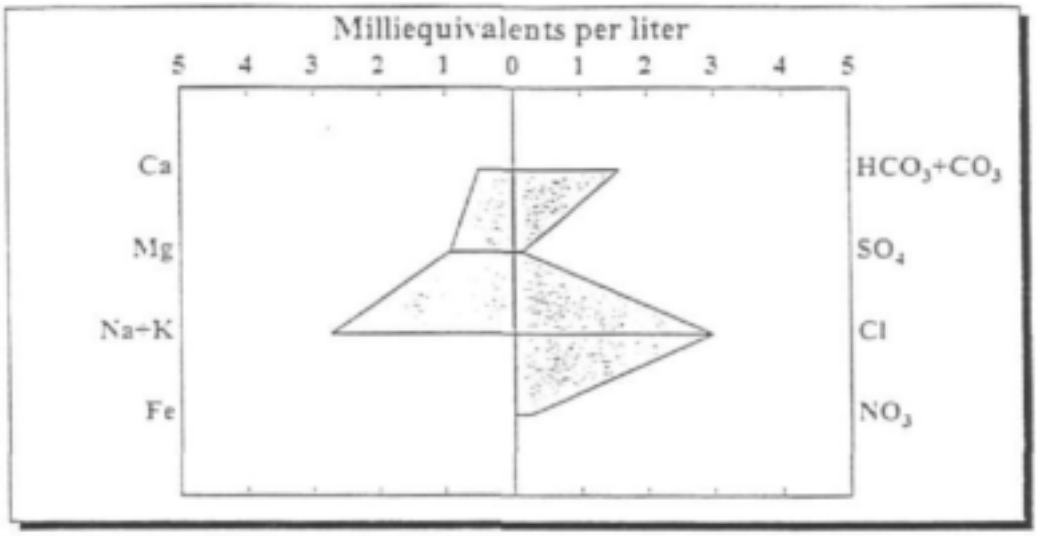

Cations

	Ca	*Mg*	*Na*	*K*	*Fe*
Milliequivalents per liter	0.51	0.92	2.65	0.08	
Milligrams per liter					

Anions

	HCO3	*CO3*	*SO4*	*Cl*	*NO3*
Milliequivalents per liter	1.60		0.12	2.99	0.24
Milligrams per liter					

BOD	COD	Dissolved Oxygen	F	B	SiO2
				0.02	

TDS	Hardness	Alkalinity	Conductivity	pH	SAR
260.80	1.45	1.60		8.90	3.1340

Water Type	*Sodium Chloride*

Cations (epm)	Anions (epm)
4.16	4.97

Error Balance (%)
8.87

Aquifer

a)

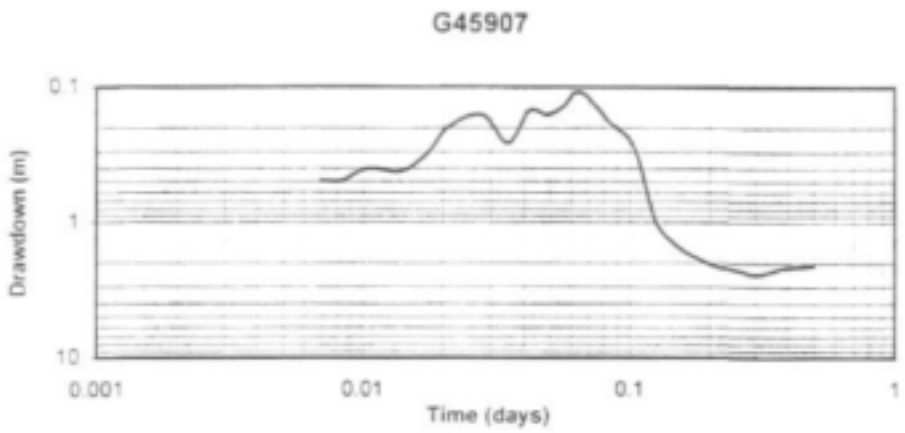

b)

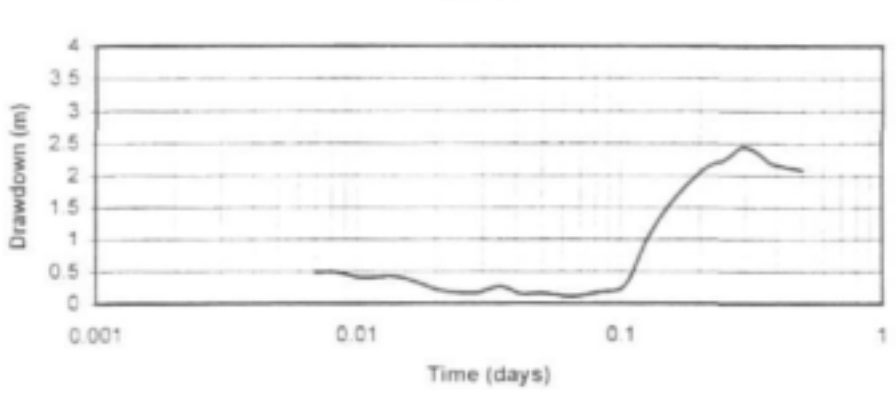

c)

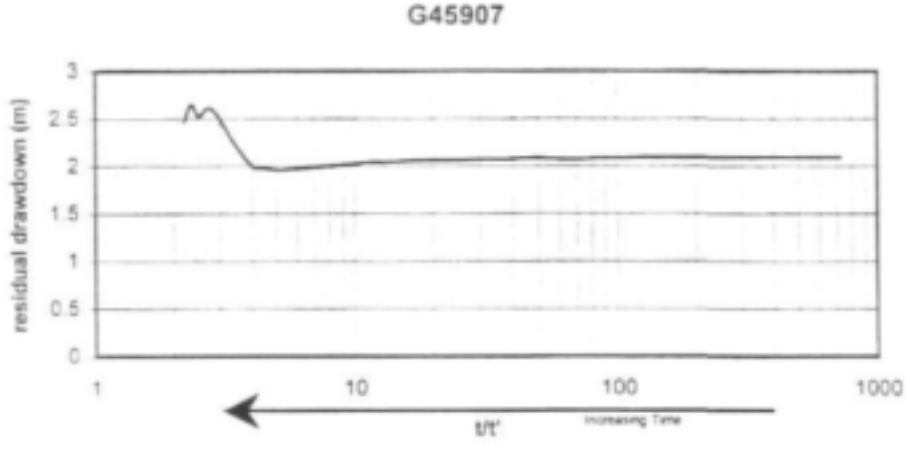

a) Drawdown data on a log/log scale
b) Drawdown data on a semi-log scale
c) Recovery data

a)

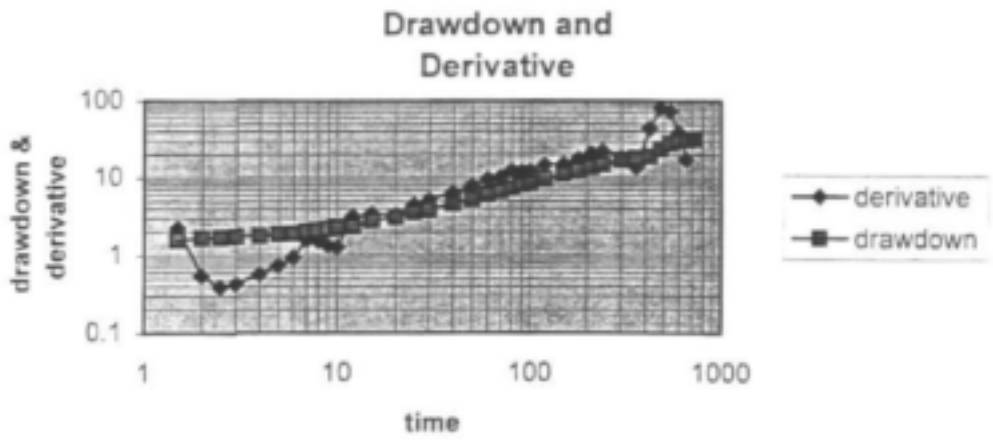

b)

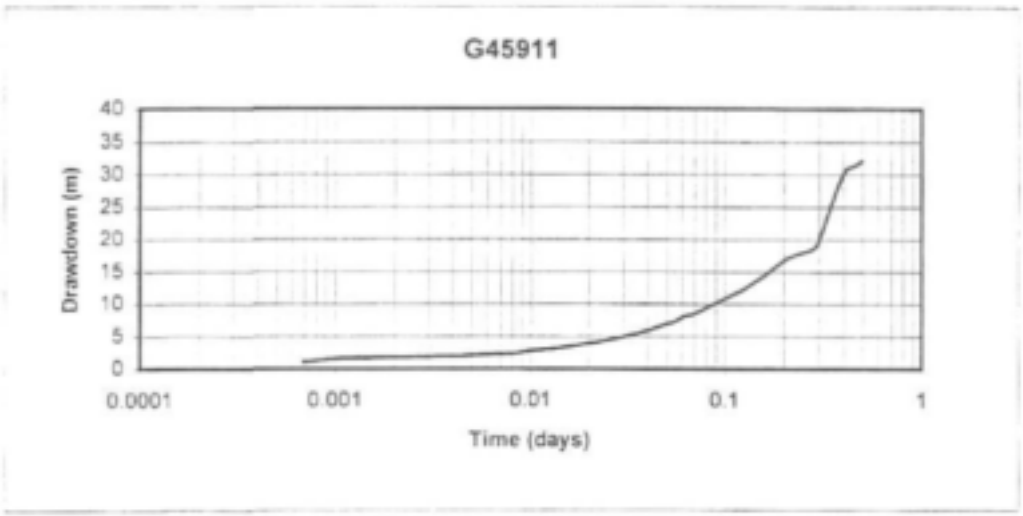

c)

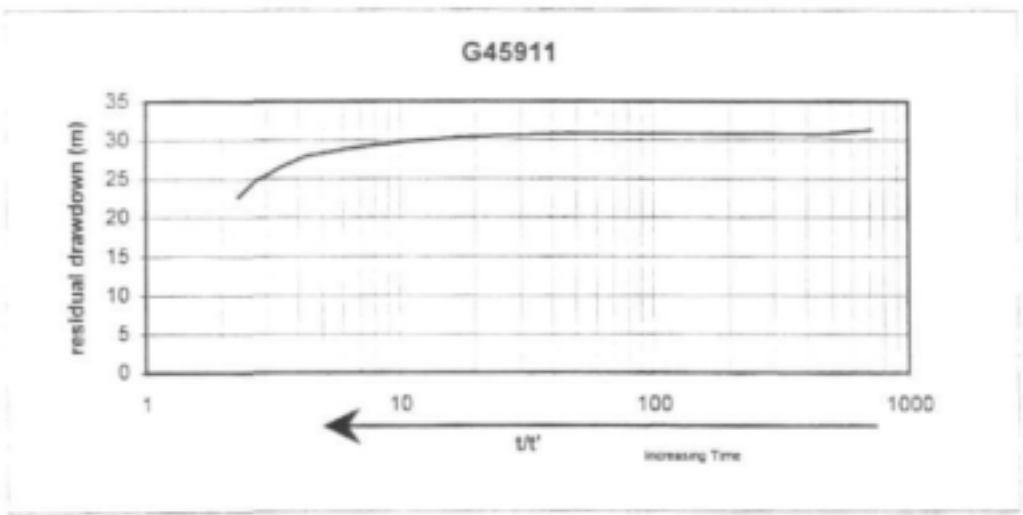

a) Drawdown data on a log/log scale
b) Drawdown data on a semi-log scale
c) Recovery data

a)

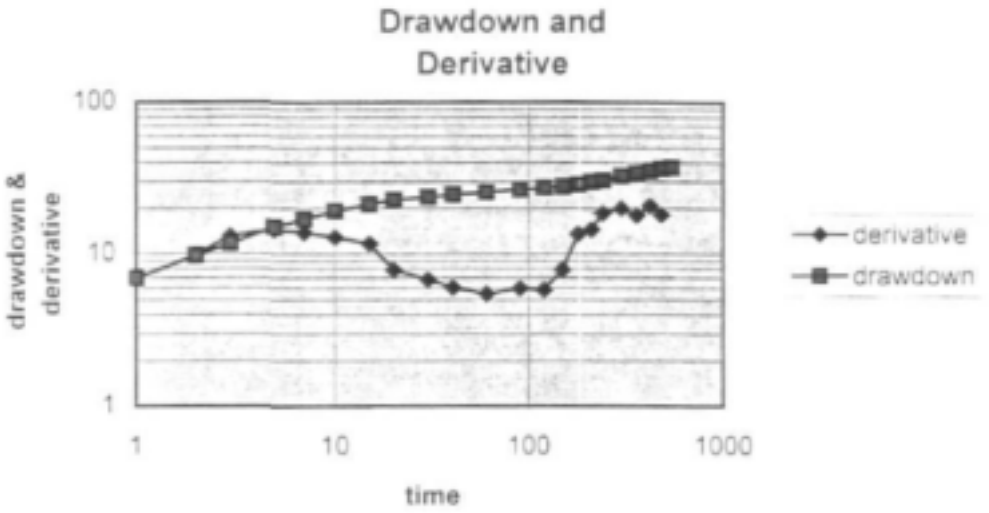

b)

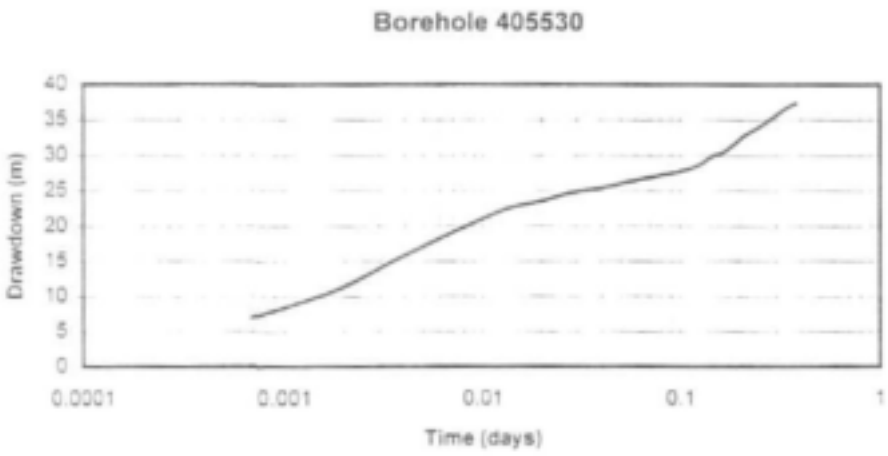

c)

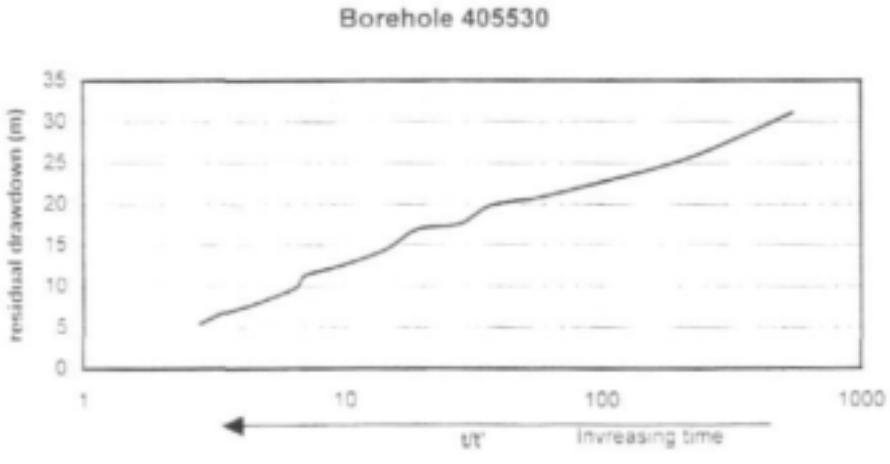

a) Drawdown data on a log/log scale
b) Drawdown data on a semi-log scale
c) Recovery data

APPENDIX 1-D

ANALYTICAL RESULTS OF THE WATER SAMPLES

Parameter	G45906	G45907	G45910	G45911	G45913
pH	8.10	8.05	8.12	8.9	7.33
pHs	7.44	7.86	7.8	8.52	7.58
EC (mS/m at 25°)	77	64	103	53	107.0
TDS (mg/l).	378.1	317.7	560.8	260.8	503.3
Total Alkalinity (mg/l)	250	158	320	80	115
Temp. Hardness (mg/l))	239	149	92	63	115
Perm. Hardness (mg/l)	0	0.0	0.0	10	190
Calcium (mg/l)	40.50	24	14.4	10.10	65.80
Magnesium (mg/l)	33.27	21.39	11.92	11.19	34.01
Sodium (mg/l)	58.20	61.90	193	60.9	64.30
Potassium (mg/l)	1.86	4.02	5.47	3.16	3.95
Sulfate (mg/l)	0.0	13.97	7.63	5.9	0.0
Phosphate (mg-l)	0.0	0.0	0.0	0.0	0.0
Chloride (mg/l)	88.40	64.2	120.53	106.22	247.39
Carbonate (mg/l)	0.0	0.0	0.0	10.5	0.0
Bicarbonate (mg/l)	305	192.15	390.4	76.25	140.3
Nitrate (mg/l)	3.28	27.6	3.68	14.63	17.67
Nitrite (mg/l)	0.0	3.8	7.29	0.0	0.0
Fluoride (mg/l)	0.0	0.7	1.19	0.0	0.0
Boron (mg/l)	0.05	0.07	0.46	0.07	0.05
Chemical Character	Mg $CaCO_3$	Na $CaCO_3$	Na $CaCO_3$	Na Cl	Ca Cl

Piper Diagram

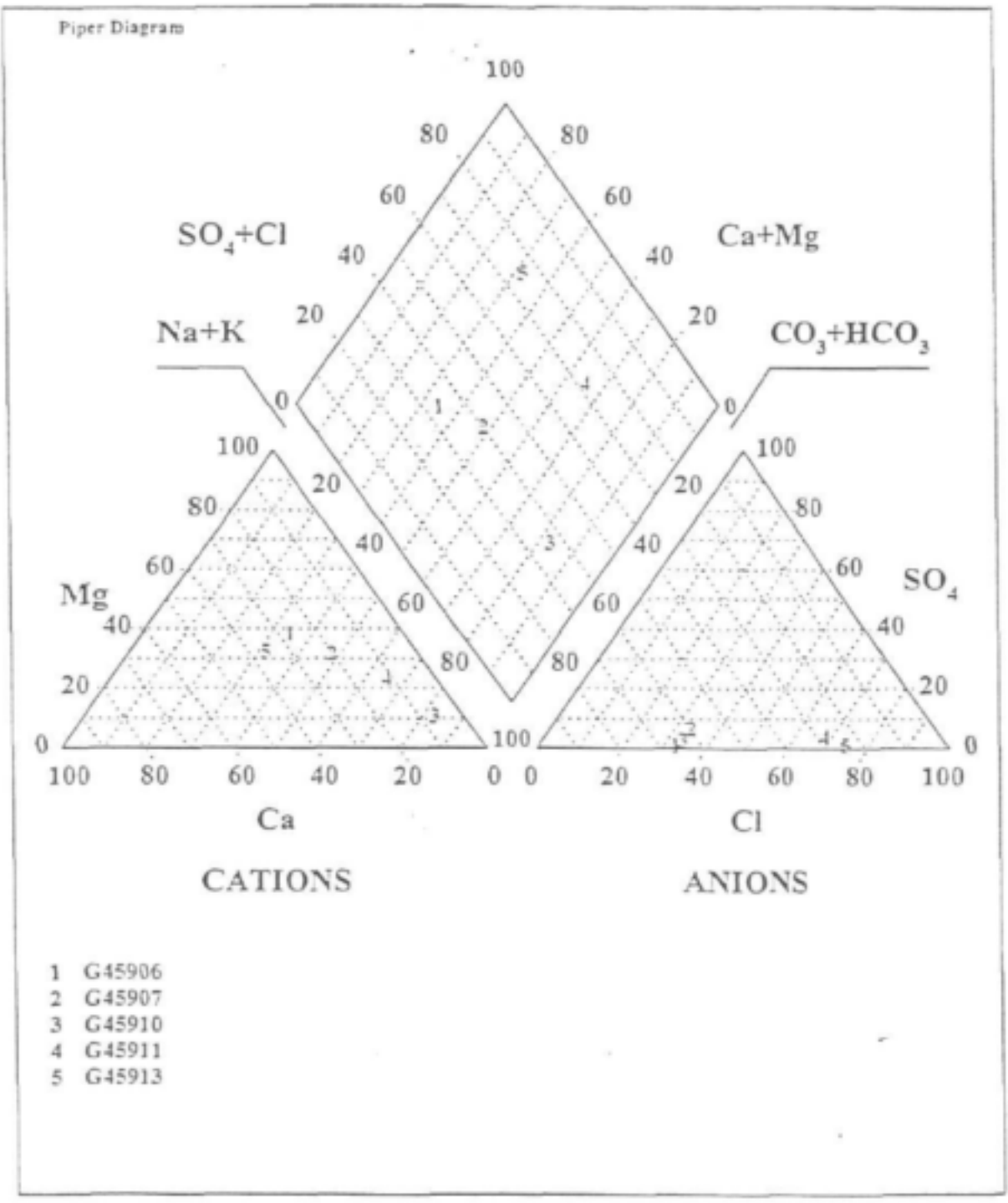

Well Ident
G45907

STIFF Diagram

Name	Type

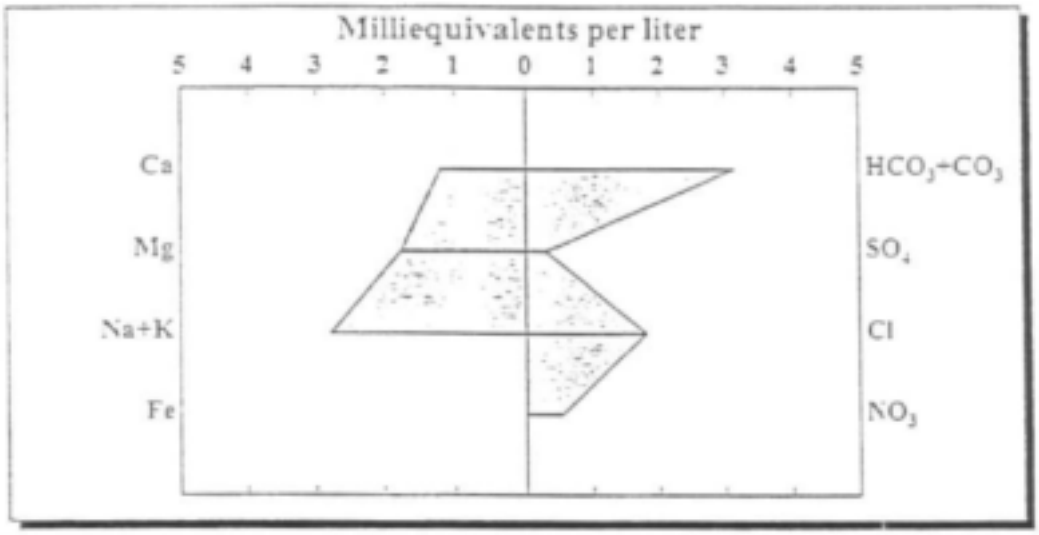

Cations

	Ca	*Mg*	*Na*	*K*	*Fe*
Milliequivalents per liter	1.20	1.76	2.69	0.10	
Milligrams per liter					

Anions

	HCO3	*CO3*	*SO4*	*Cl*	*NO3*
Milliequivalents per liter	3.15		0.29	1.81	0.53
Milligrams per liter					

BOD	COD	Dissolved Oxygen	F	B	SiO2
				0.02	

TDS	Hardness	Alkalinity	Conductivity	pH	SAR
317.70	2.98	3.15		8.05	2.2112

Water Type	*Sodium Bicarbonate*

Cations (epm)	Anions (epm)
5.75	5.80

Error Balance (%)
0.43

Aquifer

Well Ident
G45911

STIFF Diagram

Name	Type

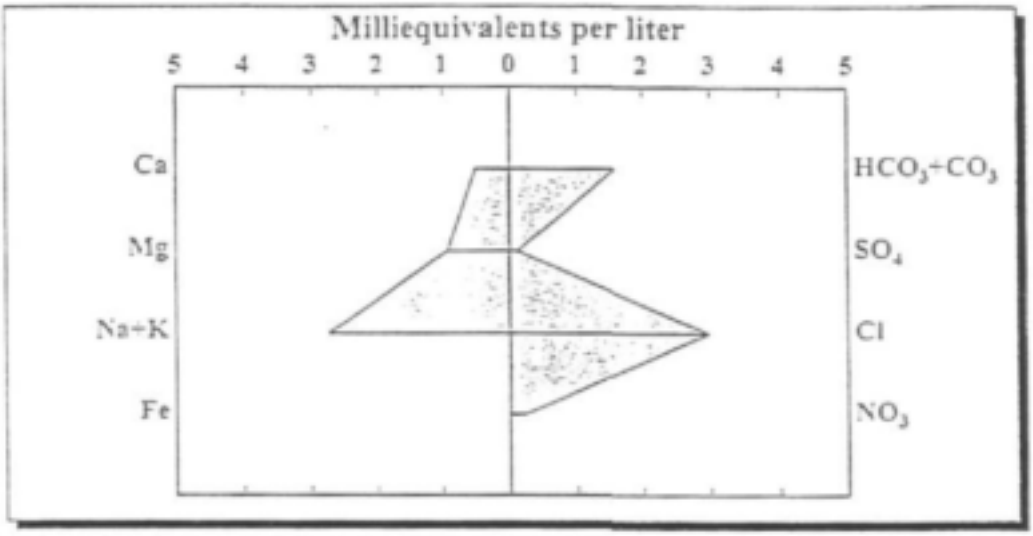

Cations					
	Ca	*Mg*	*Na*	*K*	*Fe*
Milliequivalents per liter	0.51	0.92	2.65	0.08	
Milligrams per liter					

Anions					
	HCO3	*CO3*	*SO4*	*Cl*	*NO3*
Milliequivalents per liter	1.60		0.12	2.99	0.24
Milligrams per liter					

BOD	COD	Dissolved Oxygen	F	B	SiO2
				0.02	
TDS	**Hardness**	**Alkalinity**	**Conductivity**	**pH**	**SAR**
260.80	1.45	1.60		8.90	3.1340

Water Type	*Sodium Chloride*

Cations (epm)	Anions (epm)
4.16	4.97

Error Balance (%)
8.87

Aquifer

APPENDIX 1-E

DOWN-THE-HOLE-GEOPHYSICS

G 45906

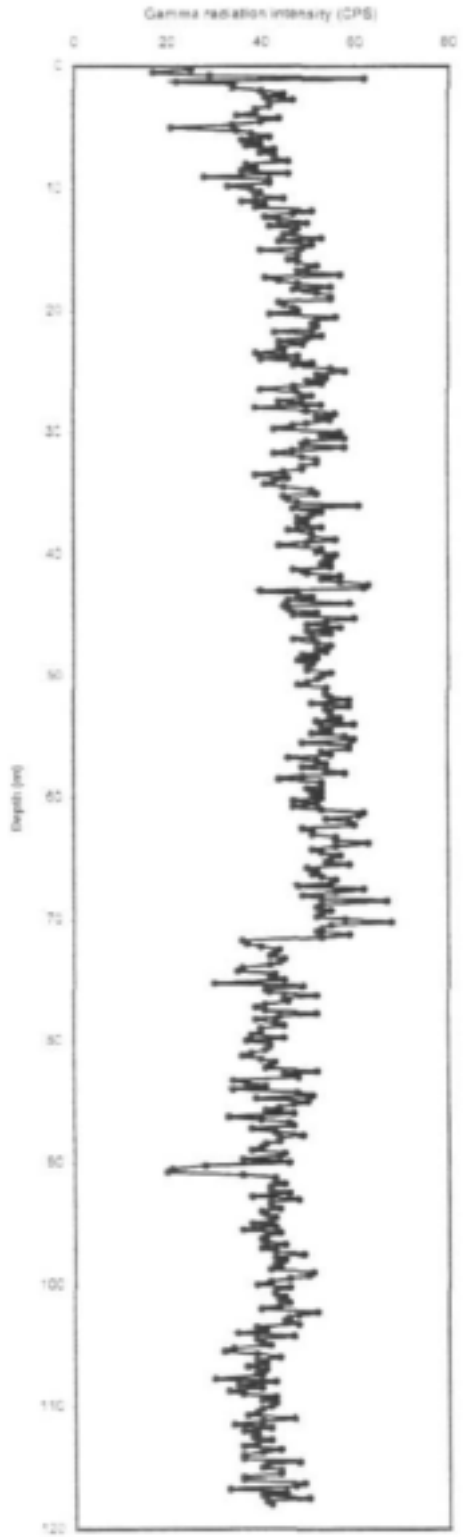

G45906

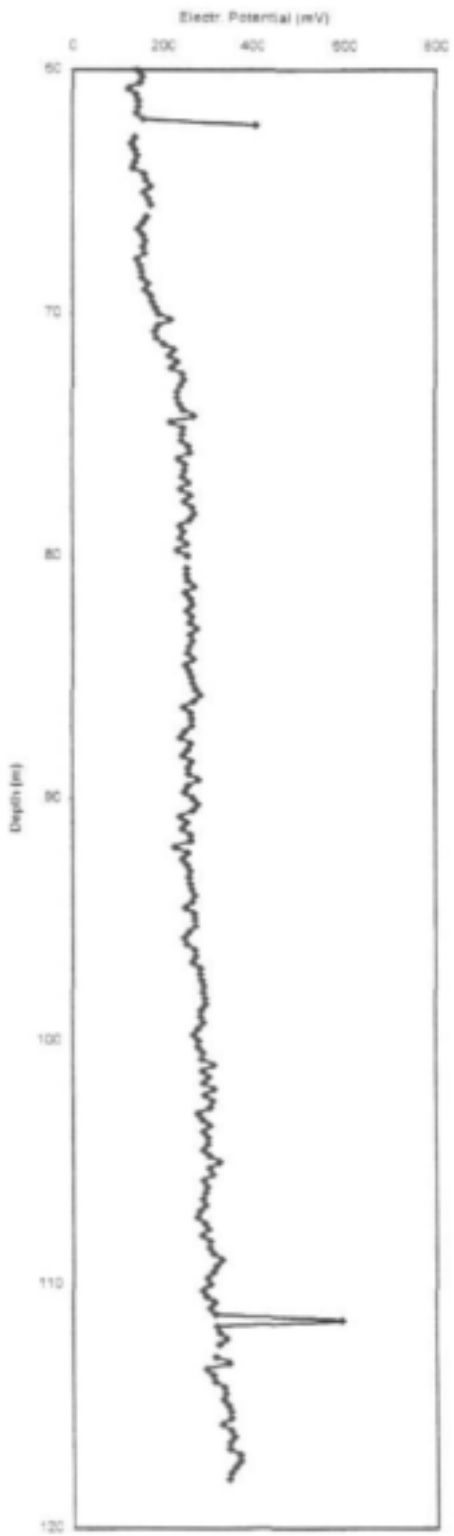

Natural gamma log and spontaneous potential log of borehole G 45906

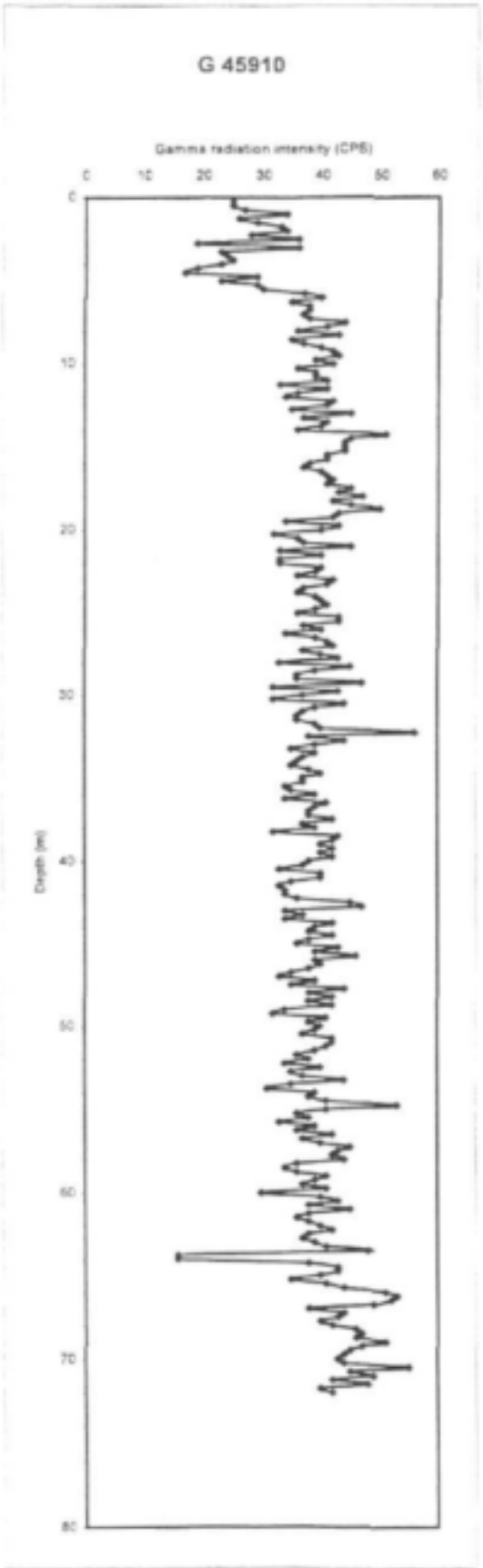

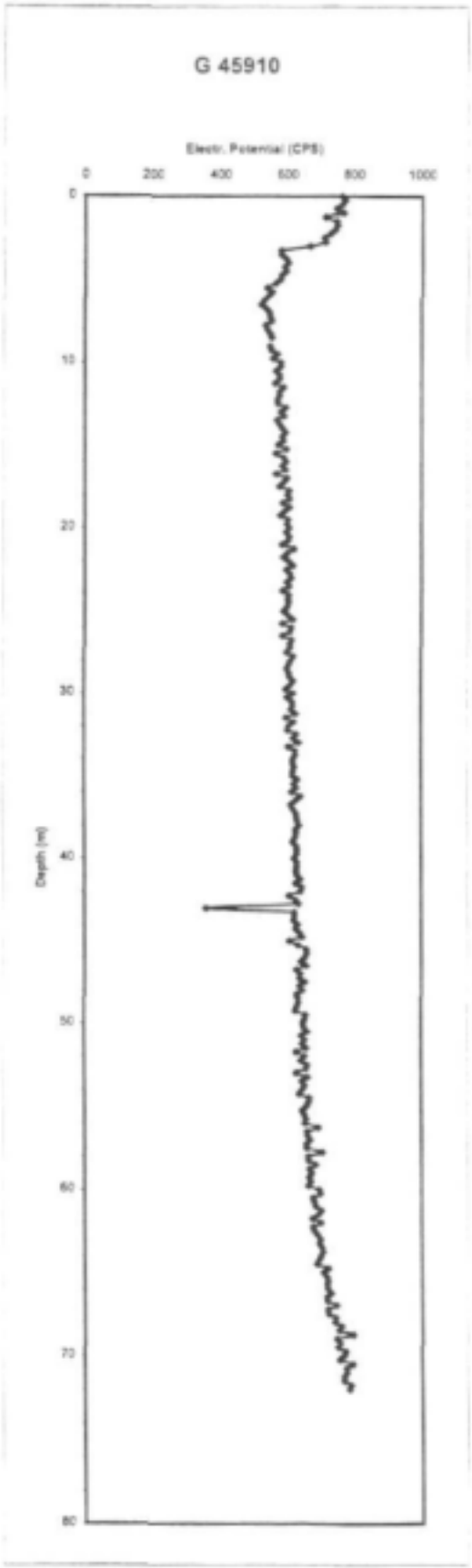

Natural gamma log and spontaneous potential log of borehole G 45910

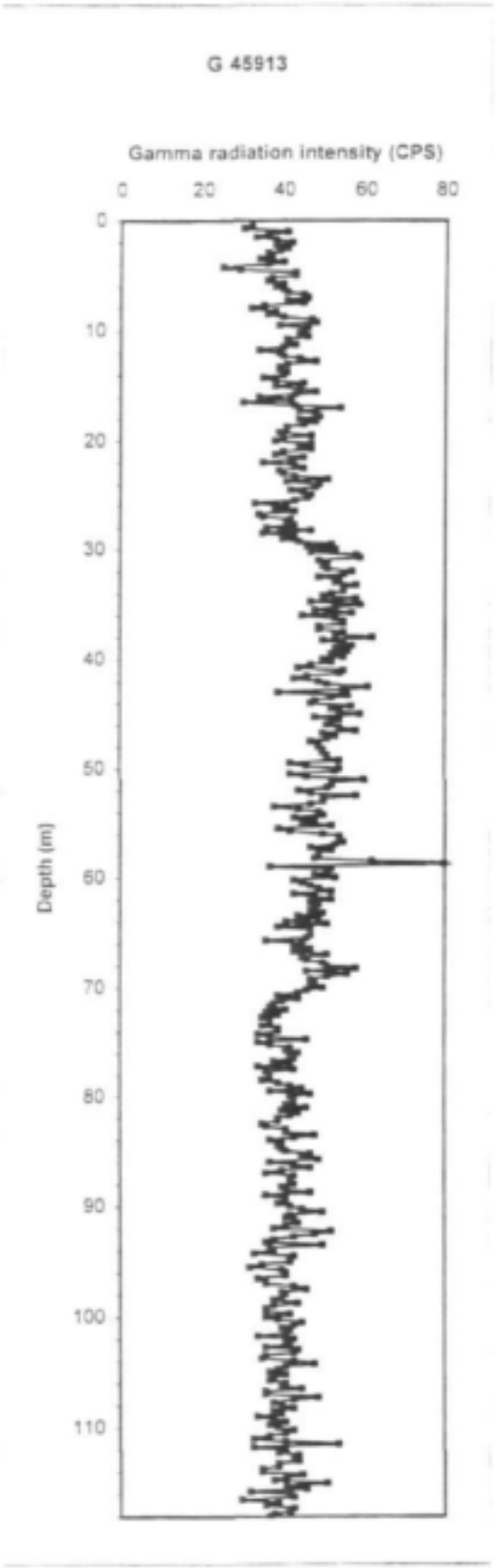

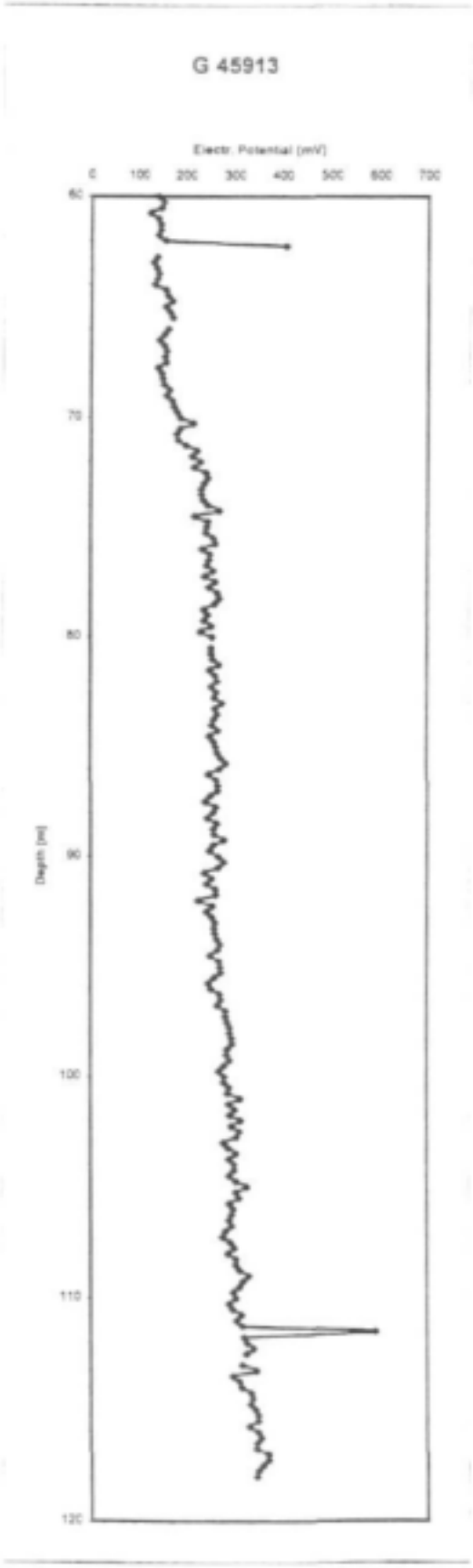

Natural gamma log and spontaneous potential log of borehole G 45913

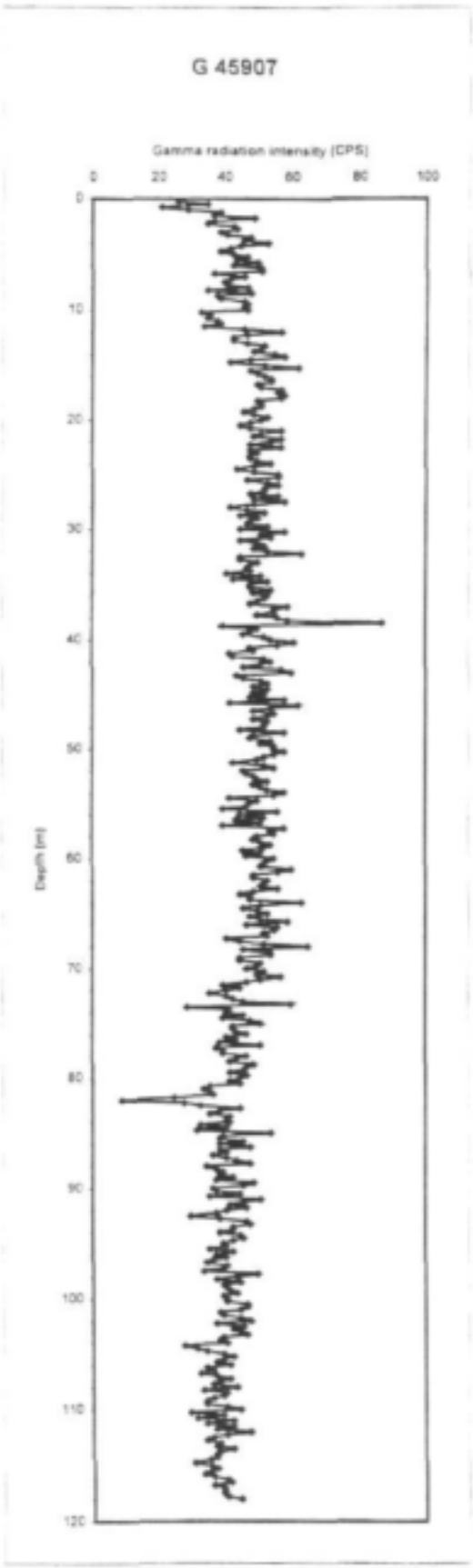

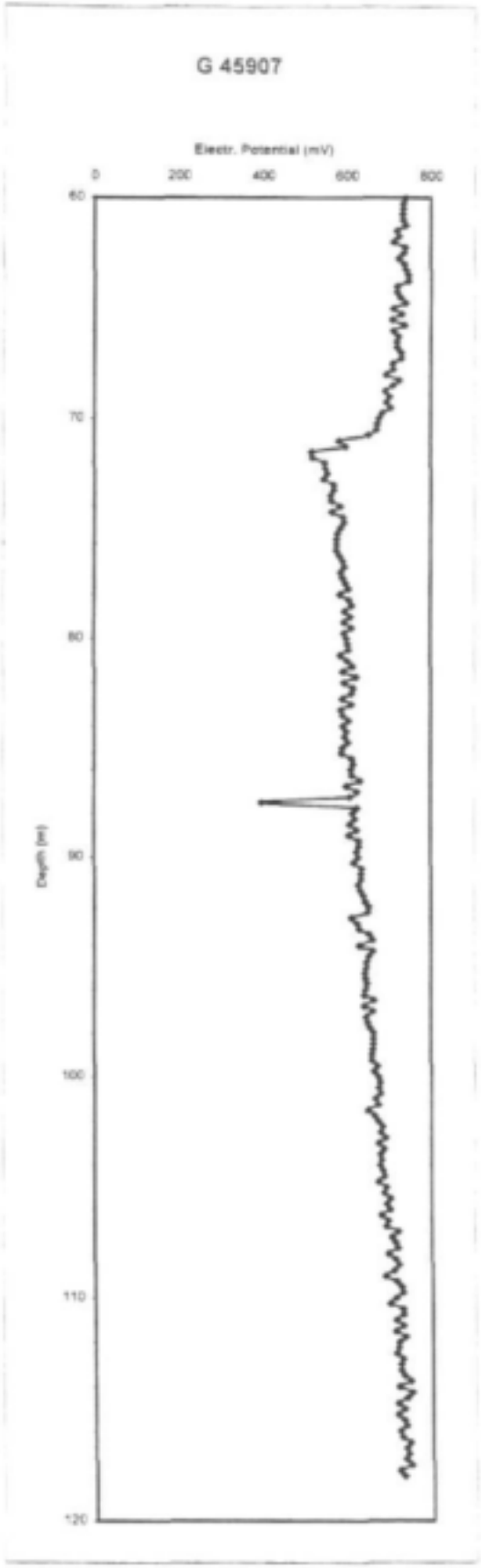

Natural gamma log and spontaneous potential log of borehole G45907

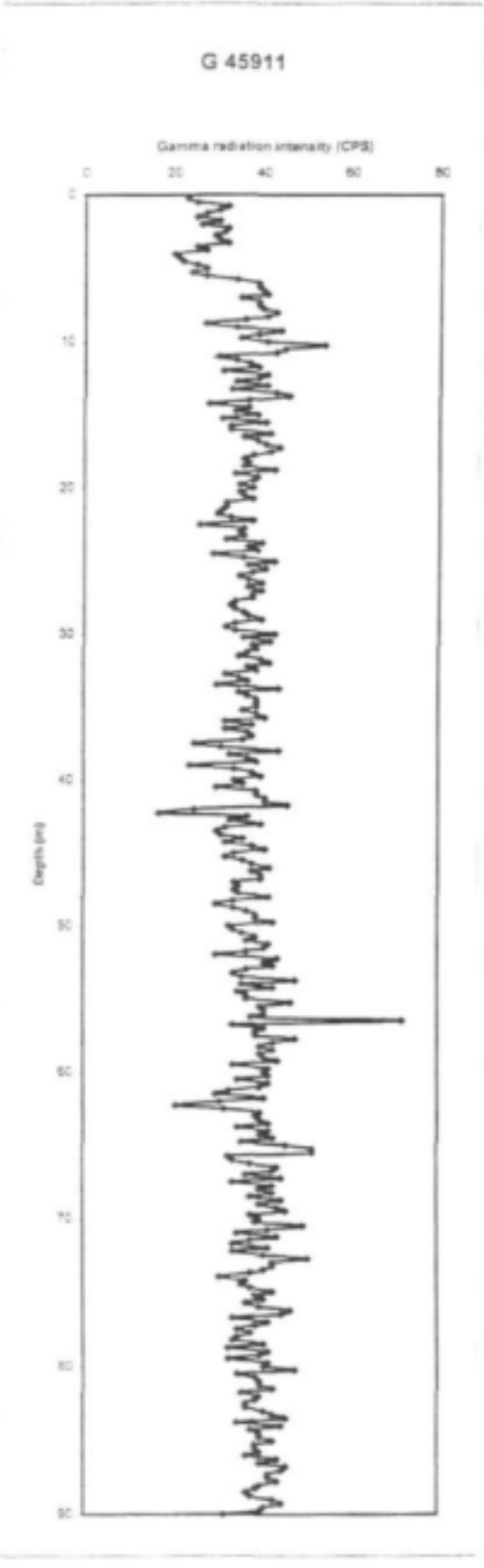

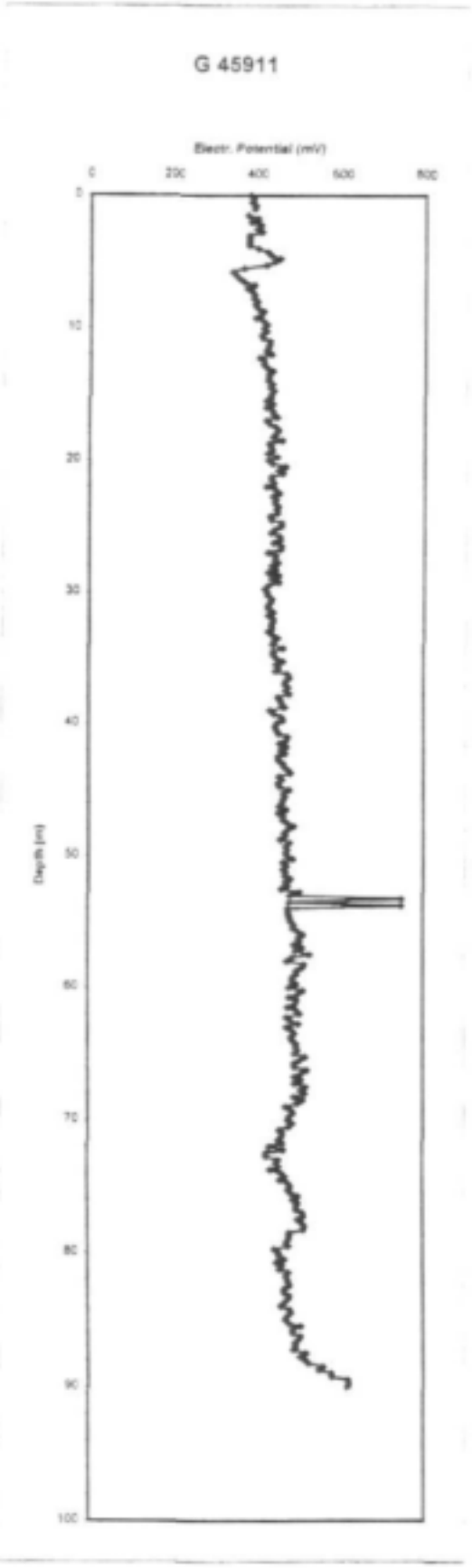

Natural gamma log and spontaneous potential log of borehole G 45911

2. NATAL METAMORPHIC PROVINCE

2.1 General Setting

The Natal Metamorphic Province (NMP) underlies 15% of all rural areas in KwaZulu-Natal and is therefore underlies more of the rural areas than any other lithological province. It is also relatively densely settled.

2.1.1 Site Locality

The research area is situated in the Mapumulo District of KwaZulu-Natal, about 30 km north-west of Stanger and 75 km north of Durban (Figure 2-1) and extends over approximately 1300 km^2. The area is bounded by steep sandstone cliffs to the east and west, while the Tugela thrust belt forms the northern boundary. To the south the area extends to 29 30 latitude. The study area is covered by four 1:50 000 map sheets: 2930 BB Ahrens, 2930 BD Noodsberg, 2931 AA Mapumulo and 2931 AC Shakaskraal.

Two major access roads, the R 75 Greytown - Stanger in the north and the 614 Dalton - Tongaat in the south serve the region, from which a fair number of dirt roads diverge. The area is essentially rural with a population density of < 100 persons per km^2 (DWAF 1995). Mapumulo is the most important village in the area with schools, stores and a hospital.

Figure 2-1 Site locality

2.1.2 Topography

Removal of the younger blanket of Cape and Karoo age sediments has resulted in the exposure of the NMP in a narrow elongated inlier that extends from the Valley of a Thousand Hills near Durban, northwards to the Nkandla area. The topography that developed on the well foliated and steeply dipping basement rocks is highly undulating, with rounded hills and

deeply incised valleys. The steep topography of the region varies between 1260m, where highlands are underlain by the Natal Group sandstones, to 40m in the valley occupied by the Tugela River (Figure 2-2).

The contact with the Natal Group rocks is demarcated by steep vertical cliffs. These are often tectonic fault contacts that form plateaux where the Natal Group exists as tilted uplifted fault blocks. These plateaux have subdued topography and often exhibit concordant summits across a single fault block. Ridges of Basement rock slope gently away from these cliffs. These sandstone cliffs form an escarpment capped by resistant orthoquartzite that extends North-South. The cliffs fade out in the highly faulted country in the vicinity of Otimati towards the east of the research area. The Basement rocks do not contain resistant bands and are deeply weathered. Washouts and dongas are common.

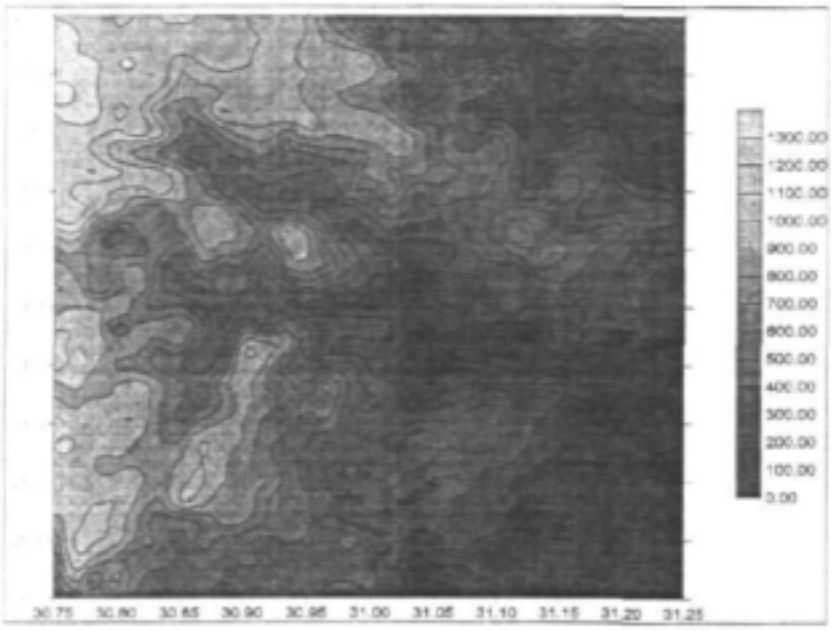

Figure 2-2 **Topography of the study area**

Three cycles of erosion and late Jurassic faulting have had a marked effect on topography. The first cycle resulted in the rolling undulating topography observed on the Natal Group sandstones and bevelled the underlying rocks of the NMP at about 650m, except for the orthoquartzite capped plateaux, resulting in a zone of deep weathering at this elevation. This early Cainozoic or 'African' erosion surface has resulted in flat-topped hills on the Natal Group sandstones, which slope regionally to the east at 2-2.5°. The underlying strata dip at 4-6°. The African surface is capped by massive laterites. These flat-topped hills and plateaux have been disturbed by faulting and stand at varying heights. The relief of the pre Cape surface decreases progressively southwards (Roberts 1971).

The second erosion surface resulted from Miocene up-doming. This erosion created rolling hills and infilled valleys on the Natal Group rocks and on Basement rocks of the southern part of the study area.

The third cycle began in the Quaternary due to the upheaval of southern Africa. This cycle is active to present and is exemplified by the deep dissection of the basement rocks due to the rejuvenation of rivers. This erosion cycle is responsible for the rugged topography observed

today. River terraces and riverbeds of protruding outcrop indicate that active down-cutting is still in progress.

2.1.3 Drainage

The area is drained mostly by the Tugela River and the Mvoti river systems, both perennial streams. Various tributaries of the Tugela and the Mvoti, such as the Hlimbitwa, the Otimati, the Mati, the Nsuze and the Pambela also dissect the study area. The major watershed between the Tugela in the north and the Mvoti in the south runs NW – SE and is approximated by the R74 highway.

The drainage texture is very fine, indicating that runoff is considerable and that subsurface storage of water and recharge are low. The underlying rocks have apparently exerted little structural control on the streams, except where wide zones of silicified fault breccia have caused major rivers to swing around in wide meanders. River terraces and riverbeds of protruding outcrop indicate that active down-cutting is still in progress.

The drainage pattern appears to be superimposed on the basement from the pre-existing Natal Group rocks, since the streams cut across the basement foliation at near right angles. Hence, rivers do not necessarily indicate zones of structural weakness. Drainage on the high lying Natal Group rocks flows down the eastward tilt of the fault blocks before crossing onto the basement rocks. Younger tributary streams, however, appear to be related to the foliation of the basement, especially the gneisses. On the more homogenous porphryoblastic gneiss in the south, drainage is dendritic.

2.1.4 Climate, Vegetation and Land Use

The climate in the study area is characterized by hot, humid and fairly wet summers and cool, dry winters. The wet season lasts approximately from October to April with rainfall mostly derived from heavy showers during thunderstorms.

The pattern of mean annual precipitation (MAP) is shown in Figure 2-88 and varies between 533mm and 1332mm throughout the area. The rainfall pattern reflects a general increase from west to east in sympathy with decreasing distance from the coast and altitude. A comparison between Figure 2-2 and Figure 2-88 reveals that rainfall is greatly affected by topography, with the higher lying areas underlain by the Natal Group rocks receiving higher precipitation.

The climate accounts for a vegetation dominated by thorn scrub and grassland. According to the Acocks Veld Types, the vegetation is classified as Coastal Tropical Forest, with Karoo and Karoid in the valley bottoms. To the east and west of the study area, natural vegetation on the Natal Group rocks has often replaced by sugar cane and to the west additionally by large-scale afforestation for commercial purposes. Other formal agricultural activity includes stock and poultry farming, whereas agricultural activity in the rural areas underlain by the basement rocks consists of subsistence cattle and dry-land maize farming.

2.2 Regional Geology

2.2.1 Introduction

The Natal Metamorphic Province is situated in the coastal belt of KwaZulu-Natal and outcrop is restricted to an erosional inlier that stretches N-S from the Tugela Valley to Port Edward. It consists of rocks varying in age from 1400 to 900 Ma. The rocks exhibit a general E-W strike and are characterised by polymetamorphism, with the degree of metamorphism increasing

from N to S (Matthews 1981). According to Thomas (1989), the Natal Metamorphic Province comprises three tectono-stratigraphic terranes separated by major southerly dipping thrust zones, where higher grade metamorphics are thrust over lower grade ones, and intrusive granitoids which post-date thrusting. These are from the North to the South the Tugela Terrane, the Mzumbe Terrane and the Margate Terrane (Figure 2-3).

The northern Tugela Terrane consists of layered amphibolites and subordinate quartzofeldspathic gneisses intruded by plagio-granites, mafic-ultramafic complexes and serpentinites (Matthews 1972). This zone has been interpreted as an ophiolite that was obducted northward onto the Kaapvaal Craton during the Kibaran Orogeny (Matthews 1972).

In the Margate and Mzumbe Terranes, the oldest rocks consist of supracrustal gneisses with subordinate paragneisses known as the Mapumulo Group. These were intruded about 1200 Ma by calc-alkalic orthogneisses, seen as the products of magmatism in mature volcanic arcs (Thomas & Eglington 1990). Later magmatic events in the Mzumbe and Margate Terranes resulted in the emplacement of granitoid and charnockite plutons. The study area is located within the Mzumbe Terrane.

The Mzumbe Terrane is bounded in the North by the ENE trending Lilani-Matigulu or Mapumulo Shear zone, which separates the Mzumbe from the thrust dominated Tugela Terrane. This sinistral shear zone immediately to the north of the study area is an important boundary between the older thrust dominated tectonics of the Tugela Terrane and the pervasive sinistral wrench tectonics of the Mzumbe Terrane.

Figure 2-3 Map of the tectono-stratigraphic terranes of the Natal Metamorphic Province (source: Thomas, 1989)

The Mzumbe Terrane is bounded in the south by the Melville Thrust, which separates the Mzumbe and Margate Terranes. It is made up of major ENE trending linear belts of highly deformed migmatitic rocks of the Mapumulo Group that usually dip steeply to the north. These belts vary in width from 2-15 km each and are separated by intervening belts of well foliated granite gneiss, porphyroblastic gneiss and augengneiss. The general strike of the rocks is NE-SW. The migmatites appear to be former pelitic sediments metamorphosed to grades ranging from an amphibolite to granulite facies. Lithological and structural relationships indicate that the belts of granitic intrusions represent anticlinal elements of a reconstituted crystalline basement, whereas the migmatic rocks of the Mapumulo Group represent infolded remnants of an original supracrustal sequence (Figure 2-4).

A marked unconformity exists between this Archean basement and the essentially flat lying Silurian age sedimentary Natal Group rocks that overly the Natal Metamorphic Province. This pre-deposition period terminated in the formation of a slightly undulating erosion plain known as the Pre-Cape surface. This surface has a relief varying between 20 to 60 m. Only in the immediate vicinity of the contact between the Natal Group and the Natal Metamorphic Province can weathering of the basement from this erosion surface be observed. Following the deposition of the Palaeozoic Cape and subsequent Karoo age rocks, a period of extensive faulting occurred. This tectonic event was related to the breakup of Gondwanaland and is the principal geological process controlling the hydrogeology of the region.

The study area forms a broad elongated belt running to the NE from the Valley of a Thousand Hills near Durban to the Tugela River and lies in between higher regions of sedimentary strata. The general strike of the rocks is NE-SW and the dip of foliation is usually steeply north. It is located in the Mzumbe Terrane, which is about 180 km wide. These belts of migmatic rocks are separated by intervening intrusive granitoids, some of which attain batholitic proportions.

2.2.2 Lithology of the Mzumbe Terrane

This Precambrian crystalline metamorphic complex forms part of the Namaqua-Natal mobile belt. It consists of porphyroblastic granite-gneiss separated by ENE trending belts of 1400 Ma Mapumulo Group rocks. The latter consist of belts of metamorphosed quartzofeldspathic and semi-pelitic lithotypes of a volcano-sedimentary origin. Granitoid gneisses and banded biotite or hornblende-biotite gneisses form the major proportion, with the remainder consisting of amphibolites, schists and granulites. Varying degrees of metamorphism and intense folding has obscured the succession of Basement Formations in the Mapumulo Group so that their chronostratigraphy has not established.

Metamorphism is related to increasing temperature and pressure resulting from Upper Proterozoic compression and folding as well as the intrusion of megacrsytic leucogranites. The resulting metasomatism of the Mapumulo Group rocks resulted in the formation of large pink porphryoblastic gneisses. Pegmatites and aplite veins also resulted due to the crystalisation of residual volatiles at the termination of orogenesis. These are common, especially in the highly migmatised zones where gneissic rocks of Mapumulo Group rocks have suffered plastic deformation.

Eight distinct lithostratigraphic units can be distinguished in the Mapumulo Group (Thomas 1988), seven of which have been named, however, the age relationships of these Formations is unclear. The 1:250 000 Durban geological map covering the area utilises an outdated classification, which distinguishes only four unnamed units classified according to lithology.

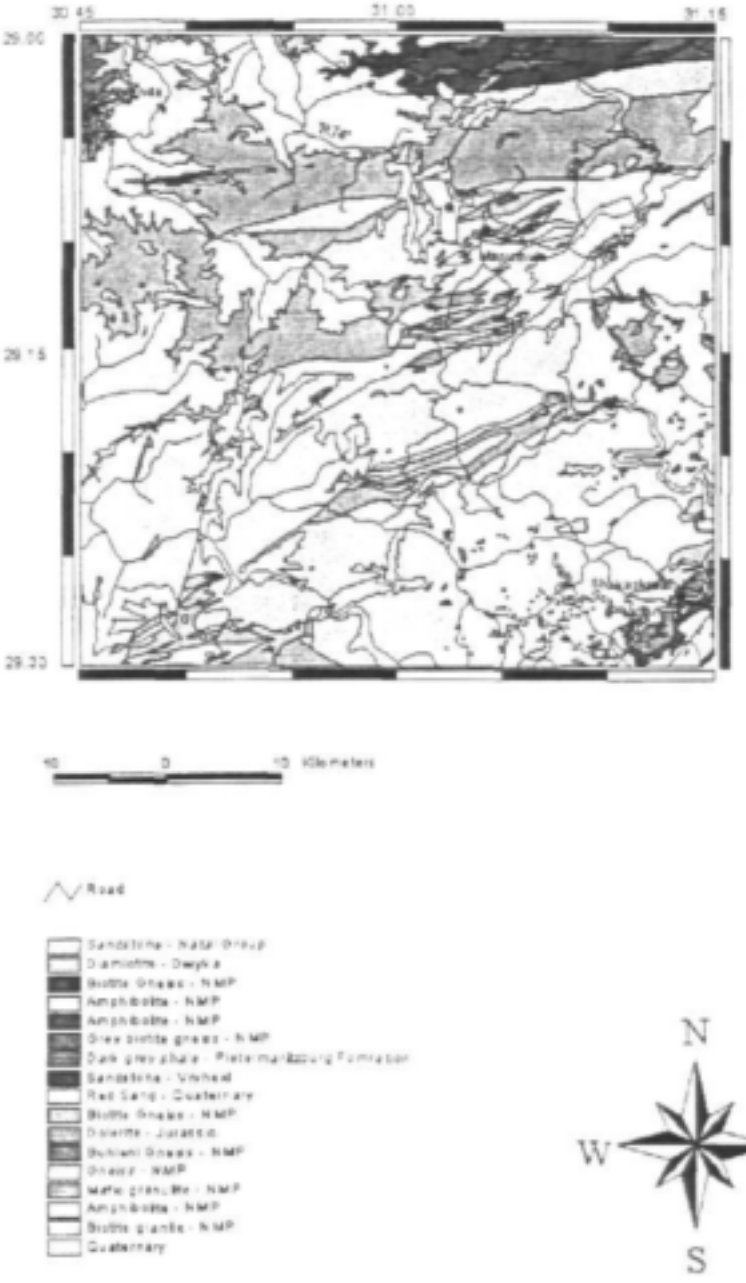

Figure 2-4 Geological map of the region

The succession is presumed to start with the carbonate rocks of the Marble Delta Formation, which outcrop only NW of Port Shepstone in the Margate Terrane. The lithological units identified in the study area consist of mafic granulites of the Mhlwazini Formation (Nm on map), amphibolites (Nh), a variety of pink leucocratic gneisses with subordinate quartzites (Nq), and pelitic and semipelitic biotite-hornblende gneisses with subordinate pelitic schists of the Quha Formation (Nbi), which is the most wide spread in terms of outcrop area.

MHLWAZINI FORMATION (Nm): This formation consists of poorly foliated, dark, fine to coarse grained mafic granulite characterised by feldspar primo-crysts that show rapakivi textures. While the granulite appears to be volcanic in origin, some researchers are of the opinion that it represents metamorphosed meta-sediments (Linstrom 1987).

MPAMBANYONI FORMATION (Nh): These amphibolites and banded hornblendes occur mainly as thin inter-layered discontinuous layers and lenses in the gneisses. They range from a homogenous black rock to one with leucocratic layers. The rocks are fine to medium grained and consist mostly of hornblende and plagioclase. Pegmatite veins occur in abundance.

PINK LEUCOCRATIC GNEISS (Nq): This unit contains a variety of pink, acid, medium to coarse grained, strongly foliated gneisses. These have a wide distribution and form a series of bands and discontinuous layers interbanded with the Quha Formation. The gneisses are uniform in mineralogy but heterogenous in appearance due to large differences in grain size, mineral proportions and deformation characteristics. Feldspar porphyroblasts of up to 25 mm as well as aggregates of dark red granet occur. Pegmatite veins of more than one generation cut the gneisses. Some layers of massive blue-grey quartzite are also noted.

THE QUHA FORMATION (Nbi): This Formation consists of pelitic and semi-pelitic gneiss (85%) consisting of biotite and biotite-hornblende gneiss/migmatites, with layers of amphibolite and calc-silicate gneiss. It has a grey to dark grey colour and is well foliated. Although pelitic schists and gneiss can occur over a large area, they constitute only a small percentage of the unit. They usually occur together with amphibolite and biotite-hornblende gneiss in irregular discontinuous layers.

Intrusions

The Mzumbe Terrane is intruded by a number of granitoids. Thomas (1988) divided the intrusive granitoids of the Natal Metamorphic Province into pre-tectonic, syntectonic and late to post-tectonic groups. The pre and syntectonic intrusives occur only in the Margate Terrane and the Amanzimtoti Shear Zones to the South. The intrusives found in the Mzumbe Terrane consist predominantly of megacrystic biotite granite and megacrystic charnockite of the batholithic Oribi Gorge Suite, with additional leucocratic granite and aplitic granite also present.

The Oribi Gorge intrusions are about 1000 Ma (Thomas 1988). They consist of very coarse-grained pink and grey porphyritic granite and dark green charnockite facies. Intrusions have outward dipping contacts and Thomas (1988) postulated that they may be mushroom shaped. The hot dry magmas produced localised contact metamorphism in the surrounding gneisses in up to 100-m wide contact zones. Many of the contacts between these intrusives and the Mapumulo Group rocks are tectonic, either related to subsequent Proterozoic ductile transcurrent shearing, which produced E-W belts of augengneiss, or to later post Karoo faults which now contain epidotite or mylonite. Intrusive granites occupy approximately 40% of the surface area of the Mzumbe and Margate Terranes and can be batholithic in size (up to 500 km^2).

2.2.3 Structure of the Natal Metamorphic Province

At the time of metamorphism, the rocks of the Basement Complex were folded on both a regional and local scale. Some faulting and shearing took place locally, producing mylonite zones. These rocks were later planed by erosion to form the pre-Cape surface. Closely following the period of Jurassic dolerite intrusion, when the rocks were intruded by thin dykes, came a period of extensive faulting, predominantly in NE-SW direction. Consequently, structures present in the rocks can be divided into those of Proterozoic and Post Karoo age.

2.2.3.1 Proterozoic Structures

The geological history of deformation during the Precambrian spans a period of 550 Ma of the upper Proterozoic, beginning at about 1200-1100 Ma. Structural observations show that early tectonic fabrics are consistent with NE directed thrusting and recumbent folding (Thomas 1989), during which the Natal Metamorphic Province Terranes were accreted onto the SE margin of the Kaapvaal Craton. Subsequently, the Mzumbe and Margate Terranes were extensively deformed by numerous NE to ESE trending sinistral, transcurrent ductile shear zones. Sinistral shearing occurred in response to the oblique orientation of the Kaapvaal Craton margin (E-W) with respect to the continuing NE oriented stress regime. Thomas (1989) suggested that the late post orogenic shearing was transtensional in nature, leading to a pull apart regime, which created space for the voluminous post-tectonic granitic intrusions.

At least four, and in places five, phases of deformation have been recognised during this tectonic event, as well as four related phases of metamorphism:

D1/M1 DEFORMATION (1100-1000 Ma): This phase was characterised by extreme compression, resulting in isoclinal folding and an associated axial-plane schistosity (S1) and lineation. These structures are seldom preserved due to subsequent deformation. Associated metamorphism of the original sedimentary and volcanic structure was at a granulite facies with high grade dehydration metamorphism (migmatisation), which aligned minerals with the regional tectonic fabric.

D2/M2 DEFORMATION (1000 Ma): This stage was caused by the intrusion and emplacement of megacrystic granites, which caused tightening and warping of D1 fold structures in the contact region. The D2 deformation is the most prevalent in terms of its expression and is exemplified by small and medium scale tight to isoclinal folds plunging to the southwest as well as low angle shearing. It has resulted in pervasive south dipping S2 foliation and lineation in the rocks sub parallel to the earlier S1 foliation.

D3/M3 DEFORMATION (1000-850 Ma): This phase is expressed by medium to large scale open, upright folds plunging to the west-southwest. The intrusion of late to post orogenic granites, such as the Oribi Gorge Suite, resulted in local tightening of the folds adjacent to forcefully intruded batholiths. There is limited associated schistosity or lineation. It can be considered a retrograde metamorphic event caused by re-equilibration under waning temperatures and pressures during uplift of the basement complex subsequent to the M1 and M2 metamorphic events.

D4/M4 DEFORMATION (850 Ma): This phase is characterised by widespread ENE ductile shearing and has given rise to dome and basin structures by interference with major F3 folds. Metamorphism continued as a retrograde metamorphic episode.

D5/M5 DEFORMATION: This is exemplified by a second generation of small shears and open F5 folds, manifested in the gentle warping of the F4 fold axes.

2.2.3.2 Metamorphic Structures

Foliation: The parallel alignment of mafic minerals has given rise to a well developed foliation, which coincides with the stratification of the original sediments. Foliation trends ENE-WSW and the rocks dip mainly to the NNW and SSE at between 60-80 degrees (Roberts 1971).

Lineations: These are generally inconspicuous and are related to the parallel elongation of minerals on foliation planes. The direction of plunge is shallowly (20-25 degrees) ENE-WSW.

Joints: Joints are well developed, especially in the foliated leucogranites. The majority are vertical to sub-vertical fractures having little or no displacement. Two trends are evident: in NE and WNW joint planes. Jointing could have been caused by contraction during cooling of the basement rocks, or as a result of the folding, shearing and loading which the rocks underwent.

Faults: These are of rare occurrence and only a few Precambrian breccia and mylonitic zones have been observed, which appear to strike roughly E-W. Two distinct ages of faults can be distinguished. The earliest is preserved as mylonite zones that grade into surrounding gneisses and amphibolites, and as regional anomalies in the trend of foliation. This phase appears to be of similar age to the rocks and displacement is difficult to measure due to poor outcrop and deep weathering. The younger phase of faulting is evidenced by zones of brecciation approximately 20 cm wide transgressing foliation and mylonite zones. Large zones of brecciation are relatively rare.

Folds: Several anticlinal and synclinal axes can be deduced from opposing dips, some of which are fairly extensive (Leith 1966). Fold axes trend ENE.

2.2.3.3 Post Karoo Faulting

An extensive and complex network of faults has been mapped in coastal Natal (Maud 1961) in a tectonic region known as the Natal Arch or the Natal Monocline (Figure 2-5). Faulting on the Natal Arch is related to the break-up of Gondwanaland and was caused by a SE oriented tensional regime. This process resulted in a complex pattern of faulting associated with crustal extension normal to the continental margin (SE oriented tension), and/or strain along rotational couples resulting in strike slip movement parallel to the coastline along a transform fault known as the Agulhas Transform Fault. Faulting related to this tectonic event has been dated between 190-90Ma (Visser 1989).

The Agulhas Transform Fault is a dextral (right lateral) transform margin with a 1200-km offset that formed during the movement of the Falkland Plateau past South Africa. Faulting began about 150 Ma during the break-up of Gondwanaland. It stretches from the southern face of the Tugela Cone (offshore from the Tugela Mouth), where an E-W rifted margin exists, and runs to the SW. Strike-slip movement began about 122-127 Ma. Near Port Shepstone the Agulhas Transform Fault is oriented about N35E and at its termination at the Tugela Cone it is oriented at N25E. The most important tectonic features evident in the coastal regions of Natal are related to this movement and on-shore faults are about 110-90 Ma.

Strain resulting from movement on the Aghulas Transform Fault has resulted in faulting on land between 28 30 and 31 S and 30-32 E. The regional pattern consists of a series of fault arcs trending from SW-NE to N-S and swinging E-W along the coast. A second band of en echelon curved faults of similar orientation occurs along the coast. In the study area these

faults have been mapped by Maud (1961), Guy (1974), Leith, 1966), Roberts (1971), Rhodes (1967), and Robinson (1969) (Figure 2-6). Faults on the Natal Arch are arcuate in geometry and at least 4 arcuate fault systems have been identified (Maud 1961):

1) From west of Port Shepstone to south of Durban a NNW trending arc of faults extends towards Highflats, then swings NE and E towards Durban. This sequence exhibits several series of N and NE oriented en echelon faults, diverging and converging faults, and splays of faults emanating from curved sections of master faults. On some of the faults the downthrow reverses from E to W along the strike, indicating that tilting of fault blocks has occurred.

2) From the mid Ilovo area 50 km SE of Pietermaritzburg to the south-eastern side of the Ngoye Horst a second arc stretches NNW then bends towards the NE in the study area, before continuing towards the N-E trending Ngoye Horst. This belt is also known as the North Coast Arc. Maud (1961) considers the area to the east of this arc to represent a single block dipping to the east, exhibiting tilted block faulting. Von Veh and Anderson (1990) believe that the arc consists of listric fault structures developed by hanging wall collapse (Figure 2-7).

3) From approximately 10km northeast of Pietermaritzburg to east of Greytown, faults extend NE towards the ENE trending Nkwaleni Graben, bending towards the east on their northern extremities.

4) A single fault on the north-west side of the Nkwaleni Graben exhibits an inverted 'S' shape and forms the northern margin of the Nkwaleni Graben.

The Tugela Fault is not related to these belts as it is an E-W oriented post Karoo fault that parallels a Precambrian thrust zone (Matthews 1959). Its origin is probably related to the relaxation of NE thrusting.

Folds have not been widely recognised but are reported around Port Shepstone (Gevers 1941), Durban (Du Toit 1954) and Umhloti (Kent 1938). Drag folds associated with motion on fault planes have been recognised (Von Veh & Anderson 1990), indicating dip-slip activity.

Extensional structures, including normal faults with down-dip lineations, breccias, open space fillings, tension gashes and dolerite dykes are abundant. Most faults are widely spaced single fractures with only one or two associated subsidiary faults and are of the normal type. Faulting is associated with silicified breccias and voids partially infilled with quartz encrustations. The rocks adjacent to faults are often transected by numerous quartz and calcite filled tension gashes that strike parallel or perpendicular to the faults and confirm a south-easterly extension direction (Von Veh & Andersen 1990). Re-orientation of bedding by drag folding occurs along several faults, with strata on the downthrow side usually dragged into a mesoscopic monocline, or rotated downwards and dipping towards the fault in a roll-over monocline, indicative of listric normal faulting.

The fault in belt 4 has a downthrow to the SE while the others have downthrows on their convex (western) side and the strata inside the arcs tilted towards the coast (eastward). Displacement ranges from a few metres to more than 1000 m and increases towards the extremities of the arcs (Maud 1961), suggesting that block tilting has occurred. The displacement is in places reversed towards the ends of the arcuate faults. The faults of the first 3 systems are en echelon or reveal divergence and convergence, zig-zag and splay patterns. Most of the faults strike NE, parallel to the coastline and often curve eastward towards the coast at their northern extremities. In the north-east ENE and NNW faults intersect.

suggesting that faults have various ages since active faults do not intersect (Wernicke & Burchfield 1982).

The study area lies in the third belt that extends NE from approximately 10km NE of Pietermaritzburg to east of Greytown. At the Nkwaleni Graben north of the study area the eastern upthrow side raises the base of the Natal Group to its greatest elevation (1200 m).

Figure 2-5 **Faulting on the coast of KwaZulu-Natal (Martin, 1983).**

2.2.3.4 Review of faulting

Theories about the origin of the arcuate fault system are still highly controversial and Maud (1961) summarised earlier theories. To explain the general eastward to south-eastward tilting of strata on the concave side of arcuate faults, Maud proposed tension acting at right angles to the present coastline (SE oriented tension). This explanation is pre-plate tectonics theory, consequently it does not explain how such tectonic forces could have arisen based on what is currently known about the break-up of Gondwanaland.

De Swardt and Bennett (1974) compared tectonic features of KwaZulu-Natal with the East African Rift system, where downward movement of graben floors was accompanied by strong uplift of the flanks on rift faults due to isostatic rebound and erosion following unloading. They speculated that the Natal Arch formed as the fault scarp retreated inland due to erosion, forming graben structures. Faulting on the Natal Arch is explained as contemporaneous with monoclinal arching and was the result of stresses that could not be accommodated by flexure

alone. This model is not entirely consistent with modern rift valley systems since most of the movement on the Natal Arch seems to have taken place very early prior to significant erosion and furthermore, there is no indication that faulting has migrated landwards, as in the East African rift valley system.

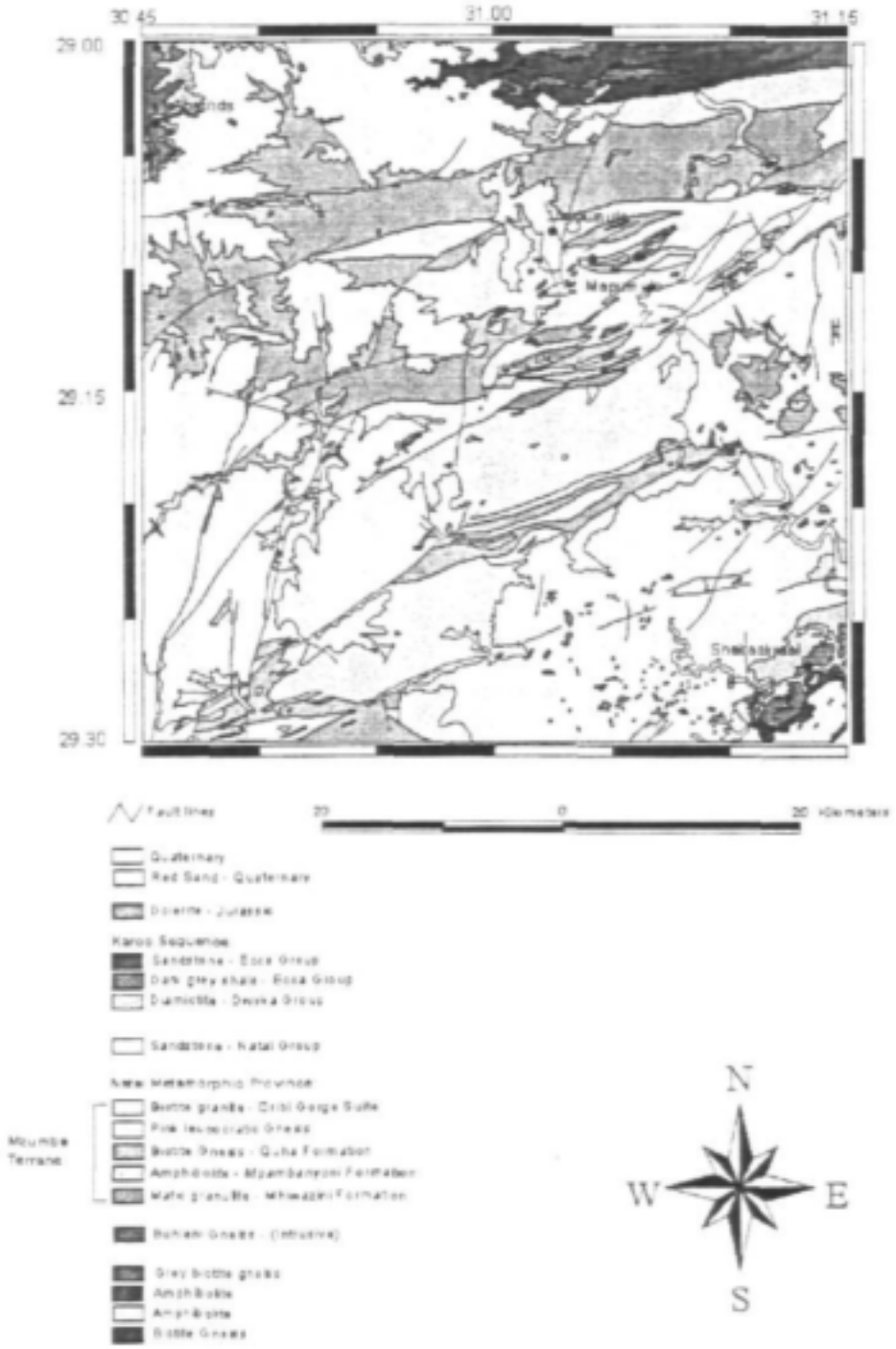

Figure 2-6 **Fault lines in the study area**

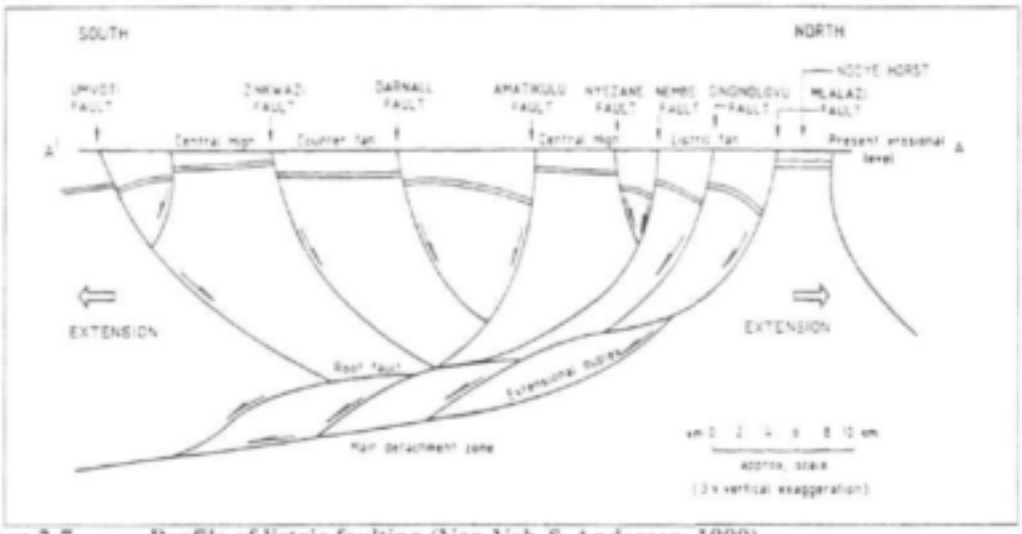

Figure 2-7 Profile of listric faulting (Von Veh & Andersen, 1990)

Martin (1984) invoked wrench tectonics theory (Wilcox et al., 1973) to explain faulting in relation to dextral strike-slip movement on the Agulhas Transform Fault. Martin argued that the prevalence of transcurrent faults offshore, the onshore en echelon, curved, splayed and anastamosing fault pattern, the reversal of throw along strike, pull apart grabens and other features are consistent with tectonic strain resulting from dextral strike-slip motion along the Agulhas Transform Fault. The dominant strain resulting from strike-slip motion on a transform fault should be manifested along rotational couples rather than SE tensional forces as suggested by Maud (1961). According to wrench tectonics theory, synthetic strike-slip fractures should be oriented sub-parallel to the orientation of wrench strike structures such as the Agulhas fault (figure 2-8). In Natal, therefore, we would expect NE oriented synthetic faults, connected by ENE trending normal faults at low angle to the wrench strike and perpendicular to the direction of tension (Figure 2-9). In Natal thrusts or reverse faults would be NNW-N oriented, with E-ENE oriented antithetic faults (figure 2-9). The total lack of reported thrusts is, however, a problem with this model, as is the rarity of other observed structures related to compressional tectonics such as reverse faults and folds, and upthrown or upwarped fault blocks.

Von Veh and Andersen (1990), based on a study of a portion of the North Coast Arc coastal region between Umvoti Mouth and Port Durnford, subdivided faults on the Zululand north shore into two main groups: earlier arcuate faults and later NNE trending coastal-parallel faults. The former set has a southerly downthrow in their northern parts and vice versa in the south. The arcuate trends, the presence of roll-over folds on hanging walls and the increase in downthrow towards the points of maximum arcuation were seen as evidence of the structures having listric profiles at depth, coalescing into a basal decollement. They suggested the faults formed by hanging wall collapse (dip-slip), whereby a new normal fault breaks off the hanging wall of an older one due to extensional forces. They concluded that the fault patterns are consistent with extensional stresses perpendicular to the coastline as proposed by Maud.

Watkeys & Sokoutis (1998) argued that the fault pattern is related to both strike-slip movement on the Agulhas Fracture Zone and SE extensional stretching operating in tandem. This has caused a reactivation of pre-existing Proterozoic shear structures, resulting in southerly transtensional stretching which has developed in 5 stages. The first stage (180-175 Ma.) was marked by faulting and rifting along the Lebombo monocline stretching from Empangeni into Mozambique. This was followed (175-155 Ma.) by dextral strike-slip movement along the Agulhas Transform fault.

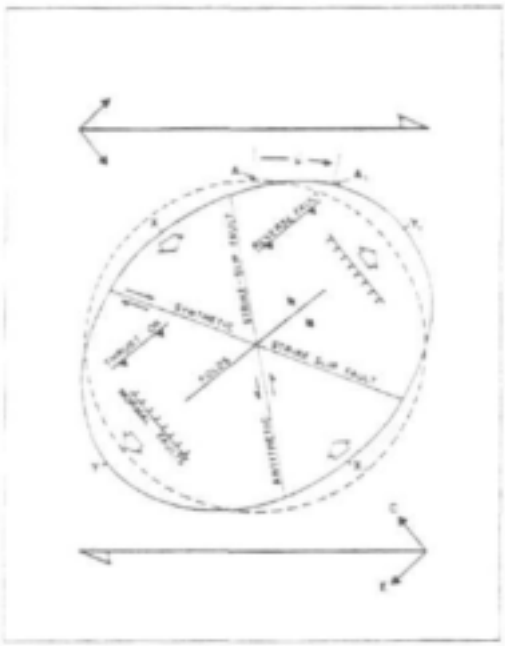

a)

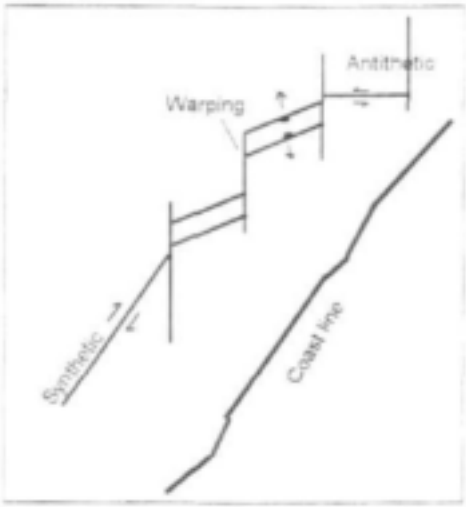

b)

Figure 2-8 a) **Strain ellipse and fault pattern resulting from wrench faulting (Martin, 1983).**
Figure 2-9 b) **Conceptual Model of faulting in KwaZulu-Natal according to wrench tectonics theory.**

2.2.3.5 Discussion

The interpretation of the fault pattern is hampered by poor exposure due to sub-tropical weathering, which preferentially affects fault zones except where they contain silicified breccia (Thomas 1988). Nevertheless, several observations can be made regarding faulting in coastal Natal:

- Faults are en echelon (e.g. coastal zone from Port Shepstone to North of Umhloti)
- Large arcuate structures exhibit an inverse S shape (e.g. NE of Greytown)
- Several faults show a reversal of vertical separation along strike caused by anastamosing of faults (e.g. SE and E of Greytown)
- Faults are curved, dog-legged or braided and form an interconnecting grid enclosing downsagged or upthrust wedges (e.g. Bongwan Gas Fault)
- The beds in fault blocks between en echelon faults dip to the east
- Where faults terminate a series of subsidiary faults splay outwards (e.g. SE of Greytown)
- Divergence of faults has resulted in N-S oriented tension, resulting in ENE or NE oriented graben structures (e.g. Ngoye Graben)
- Side stepping faults leading to N-S transtension has caused pull apart basins (e.g. Egosa fault)

In the coastal zone the en echelon fault planes are steep and give an overall appearance of listric normal faults convex towards the coast. Faults often dip inland to the west, with the downthrown block to the north or west, while the beds dip to the east. This confirms an extensional model of tilted fault blocks with fault planes dipping inland (Figure 2-10), as suggested by Von Veh and Andersen (1990).

In areas underlain by the Mzumbe Terrane, ENE fault segments tend to have horizontal slickenlines, indicating an oblique sinistral strike-slip movement to the ENE. These faults also have dip-slip slickenlines indicating transtension to the SE-S, hence movement may have been related to more than one event, as suggested by Watkeys & Sotoukis (1998). In contrast the N-S segments display only dip-slip slickenlines, indicating they are normal faults.

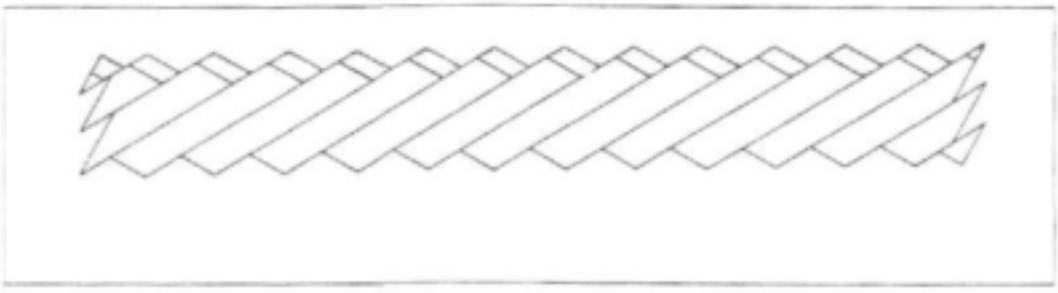

Figure 2-10 Fault plane of extensional normal faults, W-E cross section.

This pattern indicates that two predominant extensional orientations are responsible. Discrete blocks are pulling apart to the east along N-S normal faults and shearing in a transtensile manner, resulting in ENE oriented transtensile faults (figure 2-11 and 2-9). These latter faults parallel the orientation of Precambrian shearing, faulting and foliation in the supracrustal basement rocks, utilising such zones of weakness. As the blocks move to the ENE extension is accommodated behind the blocks through normal faulting, resulting in approximately N-S grabens inland. As the sides of the moving blocks are not parallel but tend to diverge eastward, extension occurs at approximately right angles to block movement, resulting in normal faults along block margins. On the coastal ENE segments shear transtension to the SE is accomodated by dip-slip faulting, resulting in ENE oriented grabens along the coast.

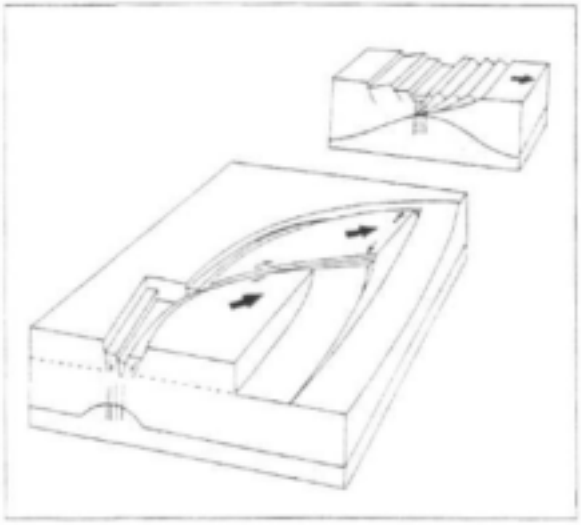

Figure 2-11 Conceptual model of transtensional faulting (Watkeys & Sokoutis, 1998)

A tectonic analysis of faulting in terms of the potential of faults and their related joint systems to be water bearing requires that the orientation of tensional, compressional and shear couples be understood. On the Natal coast, this requires an understanding of tectonic processes at work on the Aghulas Transform Fault and the resulting onshore fault and fracture system.

Transform faults are strike-slip faults where plates move laterally past each other in response to horizontal shear couples within the earth's crust. A simple dextral parallel strike-slip fault where crustal blocks move parallel with the fault results in a characteristic strain ellipse (Figure 2-8).

Point A on an undeformed circle would move to point A^1, defining the shear angle ι. The maximum compression and tension are parallel with the major and minor axes (X,X^1 and Y, Y^1 respectively). Rocks may initially deform plastically, leading to en echelon folds oriented at 90 degrees to the maximum compression over a finite distance from the fault trace. Anticlines would plunge away from the fault perpendicular to maximum compression. As deformation proceeds two intersecting sets of vertical fractures would also form. One set would form at low angles to the wrench trend (10-30 degrees), termed the synthetic set (and which would be oriented NNE-NE in Natal since wrenching is to the NNE), and the second would be at high angles to the wrench trend (70-90 degrees), termed the antithetic set (and oriented ENE-E in Natal). Both of these conjugate strike-slip fault sets would form en echelon. The main through-going fault then develops, mainly along the synthetic faults, connecting to the antithetic faults by NE normal faults or by N-NNW trending thrusts, resulting in a series of inter-connected dog-legged faults. Through continued motion faults are rotated, particularly the antithetic ones, hence they tend to be oriented at even higher angles to the wrench-strike. The rotation would hence imparts characteristic reverse S shape in the case of dextral movement. The NW-N orientation would be compressional, with warping, thrusting or reverse faulting expected.

Oblique or divergent movement on transform faults, leading to transtension, may be caused by non-parallel movement of crustal blocks or by changes in orientation of the master fault. The increasingly SW trend of the Aghulas Transform Fault indicates that such rotational forces indeed occur and results in divergent movement. Divergent movement or wrenching away from the fault leads to a combination of transcurrent and tensional faulting and is termed transtensile. In a transtensile regime, extensional forces lead to extensive block faulting, producing grabens oriented perpendicular to the axis of tension, such as the NE trending grabens visible in coastal Natal. Oblique shear motion is often taken up by the high angle antithetic faults, which are oriented ENE in Natal. These faults should exhibit negligible lateral displacement and develop into high angle normal faults with oblique slip, resulting in both horizontal and dip-slip slickenlines, as observed in ENE faults in Natal. Consequently, faulting in Natal can be explained by divergent wrenching on the Aghulas Fault, in which case the maximum extensional force would be directed perpendicular to normal faults (to the SE). In this case, ENE transtensile normal faults are expected to have the maximum SE oriented transtensional strain, while North trending faults are likely to be extensional normal faults. Northeast trending faults are likely to be synthetic and in shear.

Because the main faults visible in Natal have developed along NE trending synthetic faults at low angles to the wrench trend, they tend to dog-leg onto ENE antithetic faults. The side – stepping of faults to the ENE leads to transtension or pull apart zones on antithetic faults where the synthethic fault dies out (Figures 2-11 and 2-12). Where NE shearing cannot be continued on a parallel fault transtension may lead to ENE graben formation (Figure 2-13). The end of fault structures leading to transtension are related to the Tugela Cone, which ends the Aghulas Transform Fault along a N-S spreading margin (Goodlad, et al. 1982, Watkeys & Sotoukis, 1998). Consequently, a SE-SSE oriented tensional regime is expected from the Tugela Mouth to Greytown. The resulting ENE transtensile zones are often zones of preferential basic dyke intrusion, hence the ENE oriented dolerite dykes in the region provide additional confirmation of a SE oriented transtension. This interpretation suggests that E-W or ENE segments of faults may be transtensional, hence groundwater targets.

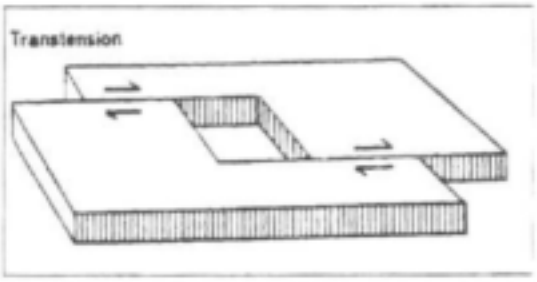

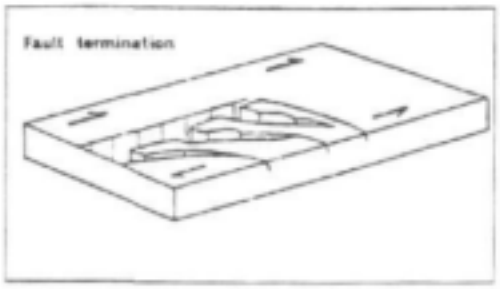

a) b)

Figure 2-12 **The creation of transtension (a)**
Figure 2-13 **Arcurate transtension at end of fault structures (b)**

The offsetting of faults results in a great variation in throw and reversals of displacement along the wrench strike. Characteristically, strike-slip systems result in subsidiary faults splaying off long straight master faults where the master fault develops a curve. Splays may continue in a new direction or rejoin the master fault forming a wedge. Alternatively, splays may form where a master form dies out (Figure 2-13). In complex terrains braided or anastamosing fault systems with complex patterns of uplifted and down sagged wedges along strike can result (Figure 2-14). Variations and reversals of throw on faults also result from fault convergence. Where curving faults converge, compression ensues, while tension exists in areas of divergence. The leading edge of the compressed wedge is uplifted while the trailing edge subsides with divergence, leading to tilted fault blocks and potentially a reversal of throw, as observed in Natal. This process would suggest that the northern or NE extremity of faults splays in Natal where downthrow is greatest are tensional, hence good groundwater targets, whereas the convergence of splays and zones where fault blocks are tilted upwards are compressional.

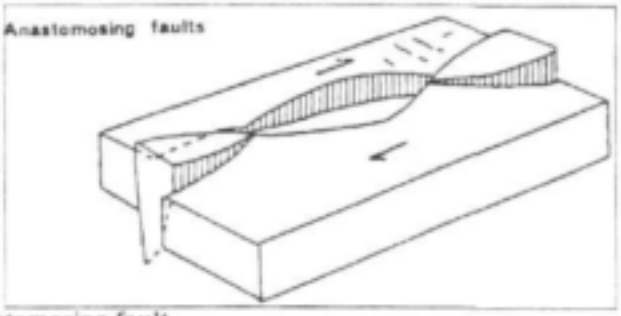

Figure 2-14 **Anastomosing fault**

2.2.3.6 Neotectonics

The region can be considered as one of tectonic inversion or reactivation, where pre-existing structures related to older geological stress environments have been reactivated. In this case older compressional thrust related structures have undergone reactivation by extension due to the break up of Gondwanaland. This process of reactivation is selective; not all structures are reactivated and reactivation is dependent on their orientation, length and attitude.

Present day tectonic stresses can be evaluated from an analysis of the orientation of seismicity and the general forces acting on the lithosphere (Zobak et al. 1989). The most widely used method for obtaining stress orientation data is from earthquake focal mechanisms. In

KwaZulu-Natal, two stress fields are evident. South of Richard's Bay principal horizontal extensional stresses appear to be oriented NNW (Zoback 1992, Andreoli et al., 1996), resulting in extension on ENE trending structures.

2.3 Hydrocensus

The research area is a densely populated rural region where potable water demands are met by surface water, springs and boreholes. Communities rely mainly on water from the Tugela River, the Mvoti River, and their tributaries. Springs are a further water source in the area, especially near the Natal Sandstone escarpment, where field surveys identified springs as being associated primarily with the geological contact of rocks of the Natal Metamorphic Province (NMP) and the overlaying Natal Sandstone Formation. However, these traditional sources often produce water of poor quality and fail in drought situations. Borehole water would be a preferred water option in the area because of its generally availability, even in drought situations, and its relatively good quality.

The hydrocensus showed that a total of 163 boreholes have been drilled into the Natal Metamorphic Province throughout the research area. The majority, 120 records, are held on the NGDB. The borehole positions have co-ordinate accuracies varying between 10m to 10km with the vast majority having an accuracy poorer than 1000m. Additional information was obtained from the CIP and from Geomeasure and Drennan, Maud & Partners (Table 2-1). For investigations into the relationship between yield and structural features only boreholes with an accuracy of at least 100m were used.

Table 2-1 Borehole statistics available from various sources

	NGDB	CIP	Geomeasure	Drennan, Maud & Partners
No. of records in the study area (only NMP)	120	27	9	7

Figures 2-15 and 2-16 show the distribution of yield of boreholes drilled into the Natal Metamorphic Province in the research area. About 26 % of all registered boreholes in the area are recorded as being dry (Figure 2-15), whereas 28% of records on the NGDB lack information about the yield of the boreholes. It may be speculated that these holes are unsuccessful. However, to gain an overall figure of drilling success rate in the research area, the assumption was made that 50% of the boreholes with no yield specification were successful. This leads to a success rate of 60% for the research area.

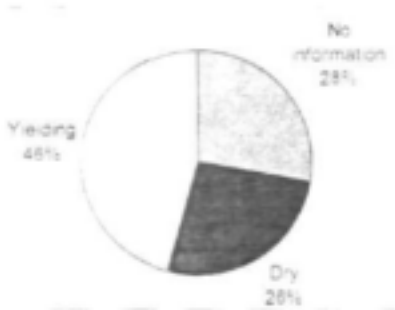

Figure 2-15 Success rates for all registered boreholes in the study area drilled into the NMP (sources: NDGB, CIP, Geomeasure, Drennan, Maud & Partners).

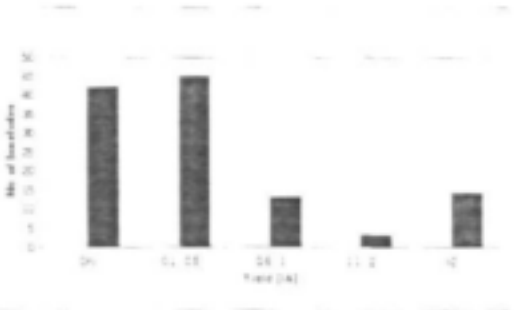

Figure 2-16 Distribution of borehole yield based on boreholes drilled in the study area into the NMP.

Of the successful boreholes, 77 % have a yield between 0.1 and 1 l/s and only 23 % of the holes have yields greater than 1 l/s (Figure 2-15). However, these borehole yield figures have to be used with caution and are rather an overestimate of long term yield, as they are probably derived from recorded airlift yields rather than proven pump-out yields. The statistics of borehole yields are shown in Table 2-2.

Table 2-2 Statistics of borehole yields

	Min. yield	Max. yield	Mean	Median
All boreholes	n.a.	n.a.	0.96 l/s	0.1 l/s
Successful boreholes	0.05 l/s	20 l/s	1.5 l/s	0.27 l/s

Figure 2-21 indicates that dry boreholes are drilled into all lithologies and do not occur only in specific lithologies. Poor and relatively high yielding boreholes occur within the same lithology, suggesting that secondary features like fracture zones, lineaments and dykes are the major control on groundwater occurrence in the study area.

To investigate the influence of major structural features on borehole yields and success rates a proximity analysis of yields and distance to mapped faults and LANDSAT lineaments was carried out. Boreholes were divided into five distance-to-feature classes and for every class a success rate and a median yield was established (Figure 2-17 and Figure 2-18).

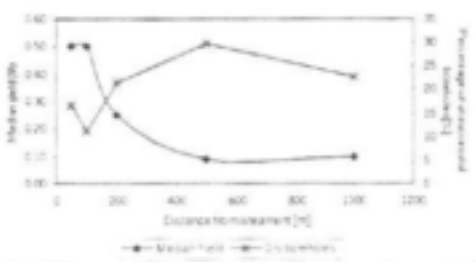

Figure 2-17 Borehole yield and drilling success rate in relation to the distance to LANDSAT lineaments. Distance class <50m: n=6; Distance class<100m: n=9; Distance class<200m: n=14; Distance class<500m: n=47; Distance class<1000m: n=75.

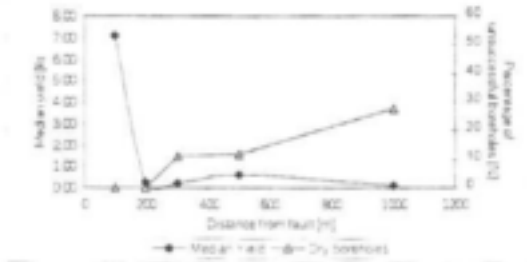

Figure 2-18 Borehole yield and drilling success rate in relation to the distance to faults. Distance class <100m: n=1; Distance class<200m: n=6; Distance class<300m: n=9; Distance class<500m: n=17; Distance class<1000m: n=106

A general trend of decreasing borehole yields and success rate with increasing distance from structural features can be observed, highlighting the importance of secondary features on drilling success and borehole yield. However, the high median yield of 7 l/s for boreholes within 100m to a fault has to be taken with caution as it is only based on 1 record (Figure 2-18). This borehole is located in the vicinity of an ENE running fault, a fault direction that proved to be of extensional nature, which may explain the relatively high yield.

The depth of boreholes varies between 24m and 183m, with a median depth of 105m. This reflects the depth of water strikes in the area, with approximately 50 % of water strikes occurring below 70m (Figure 2-19). Due to the large variation in relief in the research area, the static water level is extremely variable and ranges from 2 to 75mbs (Figure 2-20), with a median water level of 46m below surface.

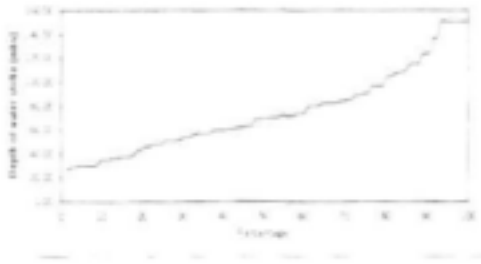

Figure 2-19 Depth of water strike

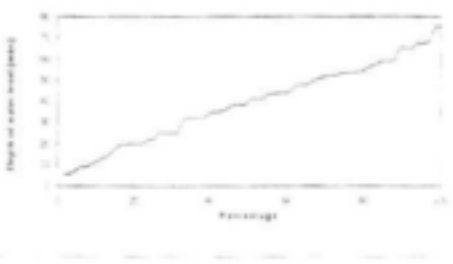

Figure 2-20 Depth of water level

The overall groundwater quality of the Natal Metamorphic Province appears to be suitable for domestic consumption. Based on the water quality classification method developed by DWAF in 1996, the water falls mainly in category 0 and I, showing ideal drinking water quality. However, water extracted from schists exhibits noticeably poorer quality and falls in category II of the DWAF qualification system. Table 2-3 shows the mean values of the major-ion chemistry of water from the different lithologies in the Natal Metamorphic Province, as well as the resulting classification using the DWAF system.

Table 2-3 Statistics of major-ion chemistry in the Natal Metamorphic Province (in mg/l) (after King, 1997) (M=Mean value, C=Class of the DWAF classification system)

	Fractured Amph. [1]		Fractured Diorite [2]		FRACTURED Migm. [3]		Fractured Schist [4]		Fractured Gneiss [5]		Sec. Por. Gneiss [6]		Featurel. Gneiss [7]		Gneiss/ Schist [8]		Fractured Granite [9]		Sec. Po. Gran.. [10]	
	M	C	M	C	M	C	M	C	M	C	M	C	M	C	M	C	M	C	M	C
PH	7.8	0	7.9	0	8.3	0	8.1	0	7.8	0	8.1	0	8.3	0	8.0	0	7.9	0	7.2	0
EC *	68.3	0	88	1	63	0	192	II	98.0	1	111.8	1	76	1	223	II	130.7	1	39.8	0
TDS	526	I	674	I	488	I	1301	II	662	I	757	I	504	I	1268	II	811.5	I	271.7	0
Mg	23.6	0	28.7	0	29	0	84.9	II	35.4	I	46	I	28	0	27	0	31.9	I	11.4	0
Na	77.8	0	105.2	I	58	0	182	I	106	I	88.7	0	71	0	321	II	190.0	I	42.5	0
K	4.6	0	5.1	0	5	0	11.5	0	9.5	0	7.5	0	-	-	4.1	0	8	0	5.8	0
Cl	62.2	0	136	I	48	0	267	II	126.4	I	131	I	95	0	366	II	309.7	II	52.7	0
SO4	15.1	0	14.4	0	19	0	154.6	0	64.4	0	76	0	51	0	226	I	55.5	0	13.5	0
NO3	4	0	9	I	2.9	0	16.8	II	2.4	0	18.5	II	12.4	II	7.5	0	2.7	0	2.5	0
F	0.8	0	0.7	0	0.4	0	2.2	II	1.0	II	0.5	0	0.2	0	2.0	II	0.9	0	0.5	0
Result		I		I		I		II		I		II		II		II		II		0

* mS/m

1 Fractured Amphibolite, 27 records
2 Fractured Diorite, 5 records
3 Fractured Migmatite, 1 record
4 Fractured Schist, 10 records
5 Fractured Gneiss, 42 records
6 Secondary Porous Gneiss, 3 records
7 Featureless Gneiss, 1 record
8 Gneiss/Schist contact, 1 record
9 Fractured Granite, 38 records
10 Secondary Poros Granite, 7 records

An investigation into the exploration methods used by the consultants in the research area during the CIP programme revealed that the majority of boreholes, 23 from the available 25 records, were sited with the GEONICS EM-34 in conjunction with the Magnetometer. The EM-34 penetrates to about 30m in this lithology using a 20m coil separation. In retrospect, the hydrocensus showed that 50% of the water bearing features occur below 70m. Hence, the instrument does not always penetrate to the required depth under the given hydrogeological conditions and it is suspected that the high failure rate of boreholes may be attributed to the limited depth of penetration of the instrument, together with an incomplete understanding of the controls on fractured aquifer occurrence.

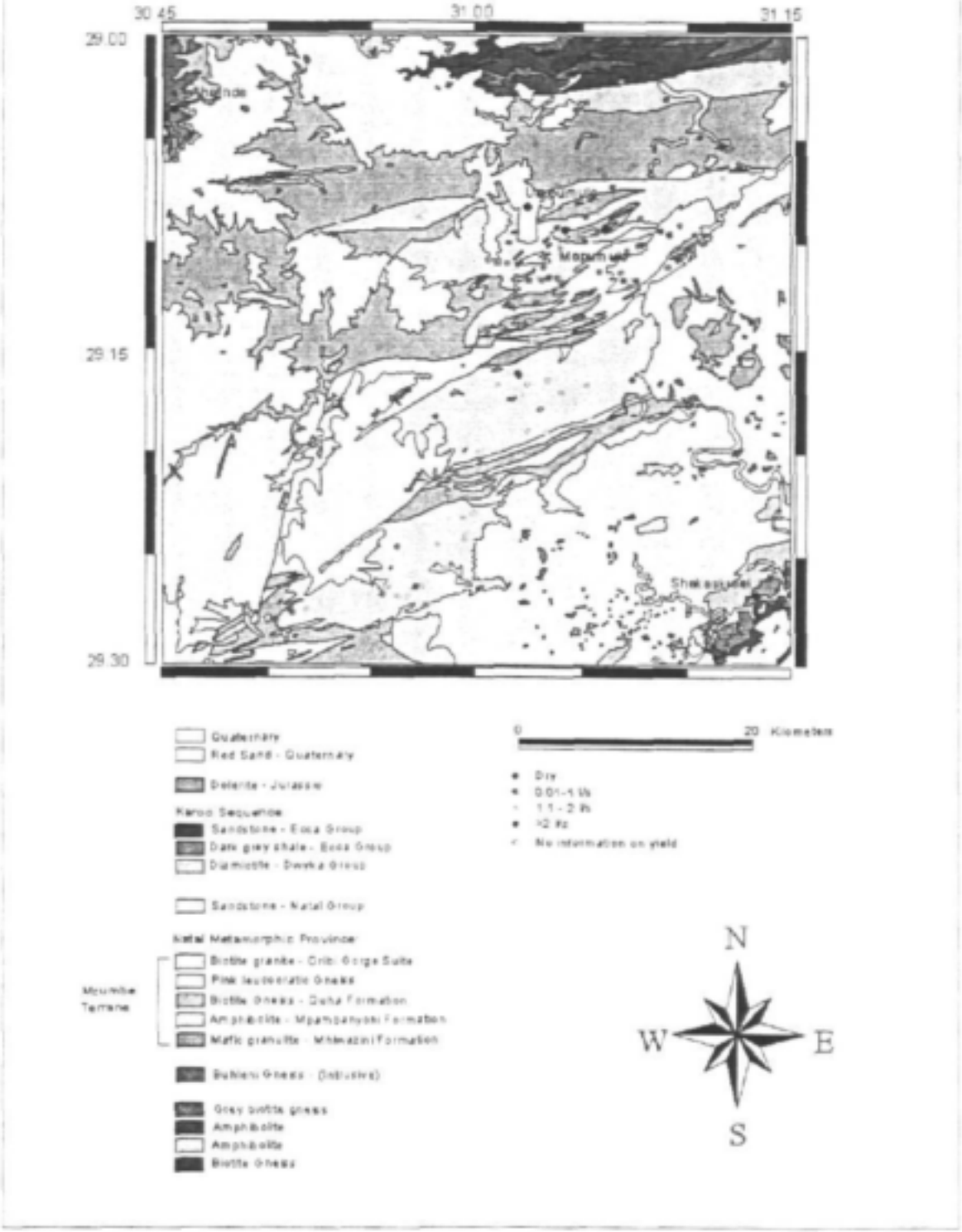

Figure 2-21 **Distribution of borehole yields throughout the study area**

2.4 LANDSAT Imagery

The hydrocensus suggests that the occurrence and movement of groundwater in the study area is primarily controlled by the prevalence and orientation of secondary features, such as faults, fractures zones and dykes. Accordingly, the delineation and mapping of these lineaments, and their thickness and extent has been an integral part of this groundwater exploration study. The interpretation of satellite imagery assists in the extraction of structural features that possibly act as groundwater indicators.

The lineament map presented in Figure 2-30 is a composite image of all lineaments identified from each of the images produced through the various enhancement techniques. Lineaments were examined on the basis of their length, width, orientation and frequency.

The strike-frequency plot presented in Figure 2-22 exhibits a distinctive lineament set, which is dominated by three major strike directions, the N-S to NNW-SSE, ENE-WSW and NW-SE direction. The total length of lineaments (Figure 2-23) suggests that ENE-WSW striking features are the most regionally extensive. These could be associated with lithological contacts associated with Proterozoic shears. The maximum length plot (Figure 2-24) is dominated by a single lineament of 14km length associated with a mapped NE-SW running fault line. Despite that, the NW-SE and ENE-WSW features appear to be of greater regional significance, whereas the lineaments striking N-S proved to be of only local importance.

Figure 2-22 Strike – frequency plot based on LANDSAT lineaments. (Scale of frequency: major unit: 10, min.: 0, max.: 50)

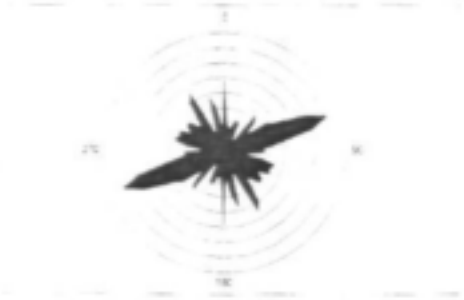

Figure 2-23 Strike-Total Length of LANDSAT lineaments (Scale of total length: 0-80km).

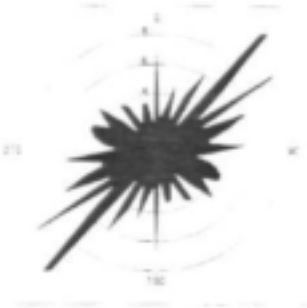

Figure 2-24 Strike-max. Length plot based on LANDSAT lineaments

To highlight the correlation between lineament length and strike direction, strike-frequency plots based on lineaments of different length were generated (Figure 2-25 to Figure 2-29). Short lineaments exhibit a predominant of NW-SE, WNW and N-S strikes. As the scale becomes more regional these strike directions fade in the favour of ENE striking lineaments. These lineaments coincide with lithological boundaries in the study area, which are often of tectonic origin and mirror fault or shear zones.

Figure 2-25 Strike-Frequency plot based on lineaments under 0.5 km length

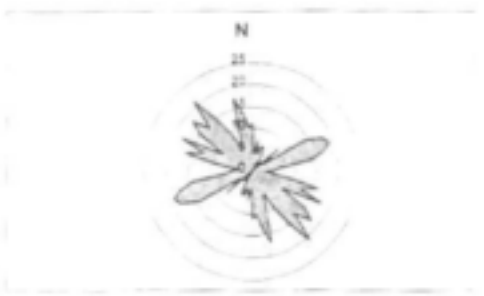

Figure 2-26 Strike-Frequency plot based on lineaments of 0.5 km to 1 km length.

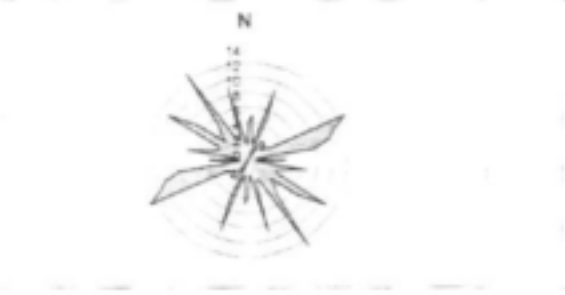

Figure 2-27 Strike-Frequency plot based on lineaments of 1km to 1.5 km length.

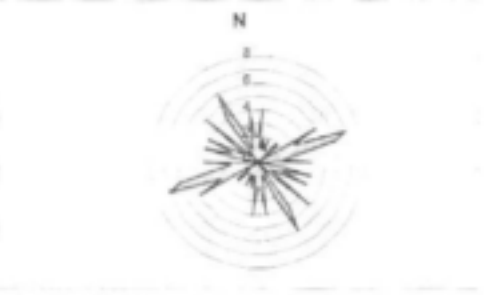

Figure 2-28 Strike-Frequency plot based on lineaments of 1.5 km to 2 km length.

Figure 2-29 Strike-Frequency plot based on lineaments over 2 km length.

Figure 2-31 shows the areal distribution of lineaments of different strike directions in the study area. The regional NE-SW (25°-65°NE) lineaments coincide with the boundaries of the various lithologies in the study area, whereas the approximately E-W (70°-110°E) striking lineaments become very prominent towards the north of the study area as a morphological expression of the Tugela thrust belt. N-S (340°-20°N) and NW-SE (115°-155°SE) striking features are distributed evenly over the entire geological lithologies in the research area.

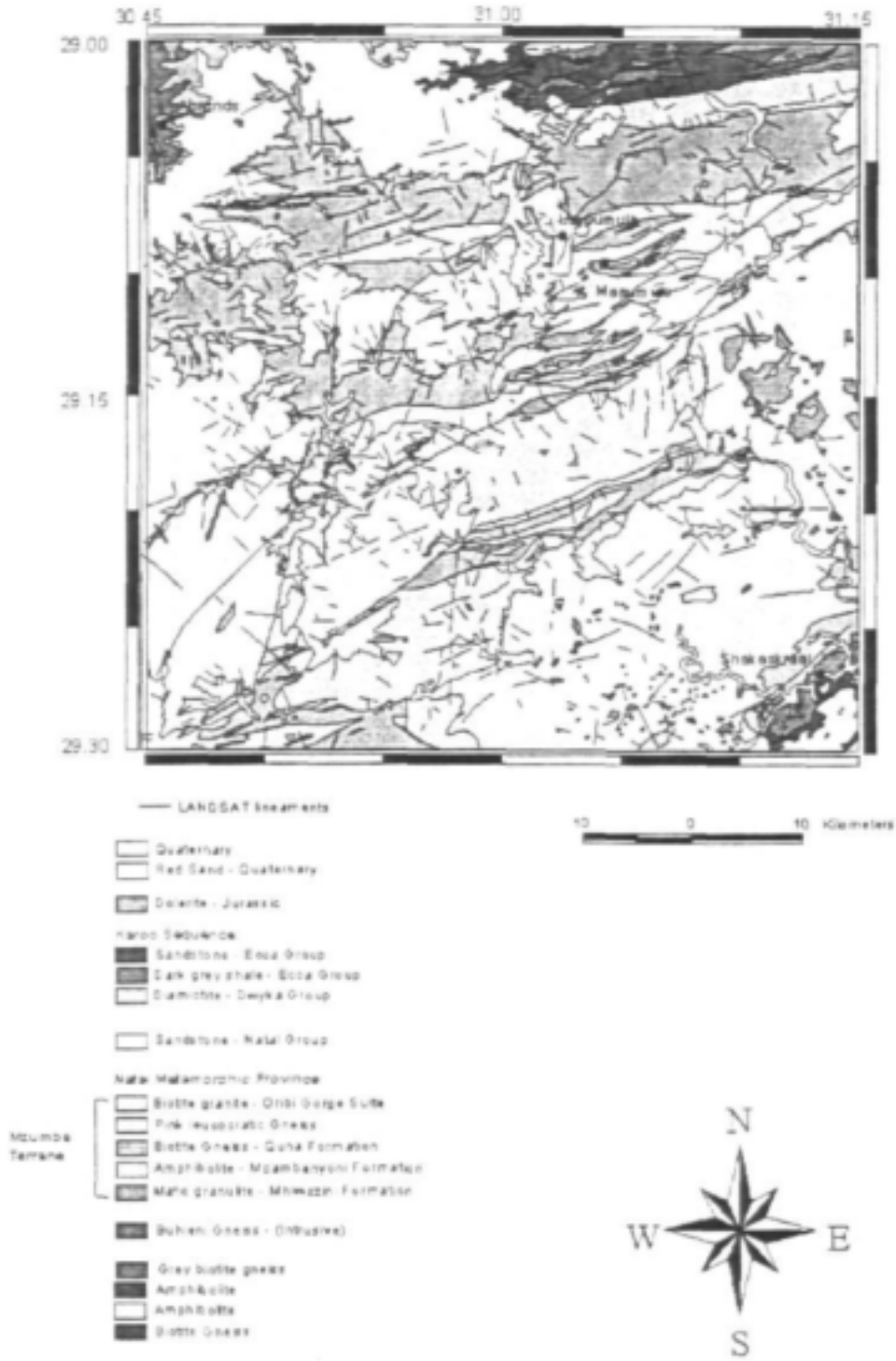

Figure 2-30 **Lineament map of the study area based on the LANDSAT ™ data**

Figure 2-31 NE-SW (25°-65°), E-W (70°-110°), N-S (340°-20°) and NW-SE (115°-155°) striking lineaments

2.5 Structural geology

2.5.1 Structural features in the research area

A total of 66 outcrops were investigated in the research area (Figure 2-32), obtaining 584 measurements of bedding, schistosity, fault and joint planes in different lithologies.

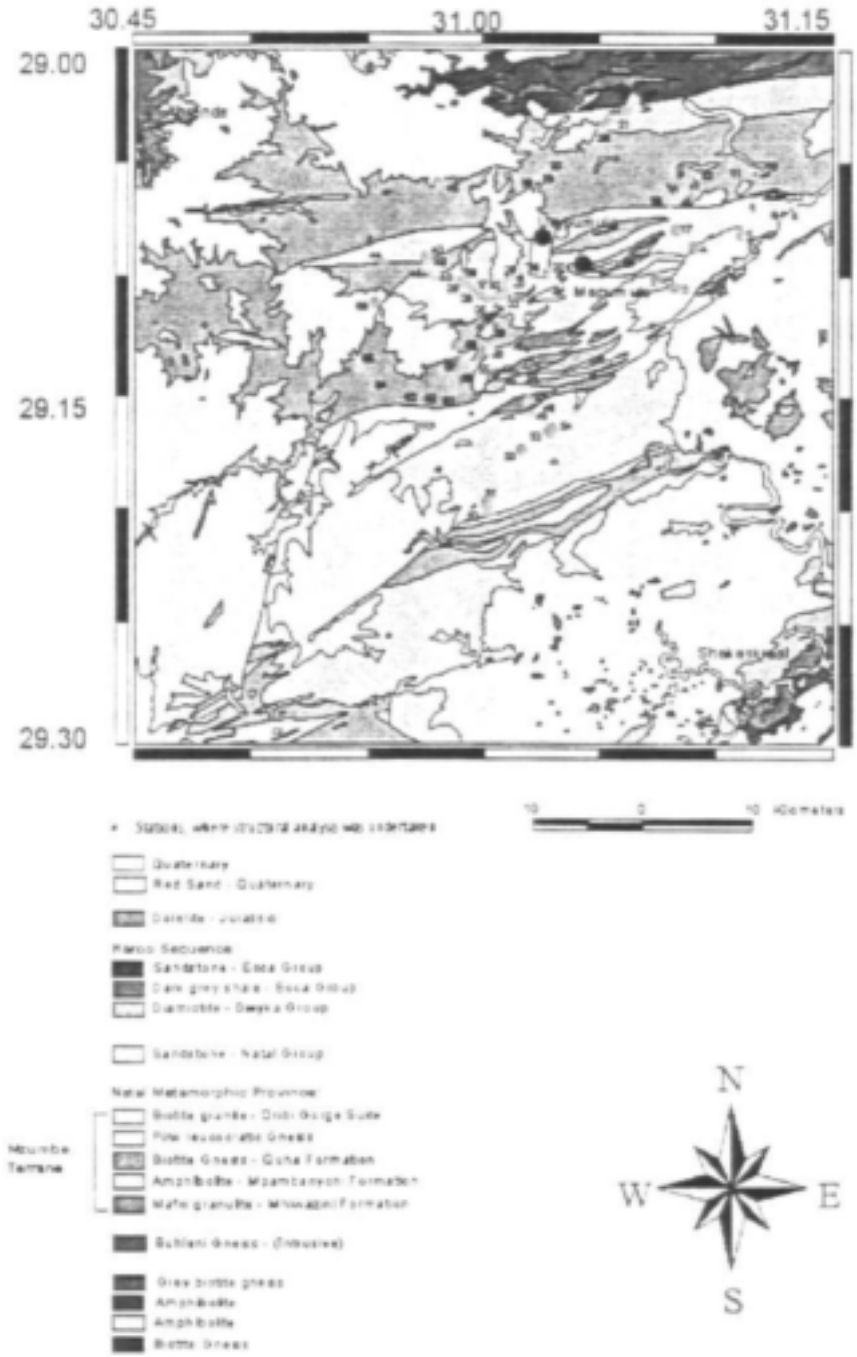

Figure 2-32 **66 outcrops investigated in the research area**

From the discussions on regional development of the terrane (2.2), it is evident that transcurrent forces were involved in the evolution of the structural features in the study area. The brittle structures in the area under investigation cut across all the rock units, irrespective of composition, with a limited deviation in trend and fracture spacing. All the structures observed were typically pure shear phenomena and were treated as such.

2.5.1.1 Primary bedding

Primary bedding was only recognizable in the Natal Group sedimentary rocks and in most cases was sub horizontal or slightly tilted up to 7° dipping towards or away from the relevant faults.

2.5.1.2 Fault zones

Fault zones were not easy to find in the metamorphic rocks due to the lack of marker beds and the homogenous nature of the gneisses. Displacements were best observed along the contact with the tabletop erosional remnants of the Natal Group. The faults observed in the metamorphic rocks are all of Kibaran age. The younger faults are mostly thin breccia zones with minimal displacement.

2.5.1.3 Joints

The most obvious features present in the research area are sub vertical joints dipping steeper than 80° (Figure 2-33). These joints are traceable from the undeformed Natal Group arkoses into the underlying gneisses. Two main orientations, almost perpendicular to each other, were distinguished. The first direction tends to be parallel with the trend of the tectonometamorphic fabric in the Kibaran age gneiss, while the second set cuts across the grain of the gneisses.

a)

b)

Figure 2-33 a) Oribi Gorge porphyritic granite (Stop 49), with two near vertical dip-slip, Mode 1 joint sets.

Figure 2-34 b) Oribi Gorge porphyritic granite (Stop 39) in a river exposure displaying two sets of sub vertical Mode 1 joints. The one set is prominent and densely spaced, while the second set is nearly perpendicular to it and much wider spaced. The intersecting line is near vertical. The two directions are parallel to the approximate N-S and E-W faulting.

Joints and conjugated joints were found in most of the outcrops and four sets were distinguished:

- Two of the sets are vertical and nearly perpendicular to each other, trending ENE and NNE respectively. The vertical conjugated sets are parallel to the regional N-S and E-W planes of faulting and have associated vertical joints (Mode 1 joints), bisecting their acute intersection angle (Figure 2-34). The intersecting lines of the three joints are all sub-horizontal and strike either in a northerly or easterly direction. In the easterly trending set the conjugated joints were influenced by the steepness of the

fabric in the gneiss. Where the dip is very steep, the conjugated joints crosscut the fabric at small angles and the Mode1 plane developed parallel to the fabric.

Where the foliation dips at angles of 70°-50° the one joint set develops along the fabric and the other cuts across it (Figure 2-35). The Mode 1 plane may bisect the intersection or the faulting may occur parallel to the tectonometamorphic fabric. Where the conjugated and Mode 1 fractures are nearly perpendicular to the tectonometamorphic fabric, the gneiss reacts as an isotropic medium with no modification to the joint plane orientations. The conjugated joint orientation and intersecting lines illustrate that the steep sets are related to two dip-slip fault sets, which were oriented nearly perpendicular to each other.

Another vertical set, very scarce, trends to the north with the Mode 1 plane bisecting the conjugated joints. In this case the intersecting line is sub vertical and linked to strike-slip faulting.

- The third joint set is sub horizontal and is related to unburdening.

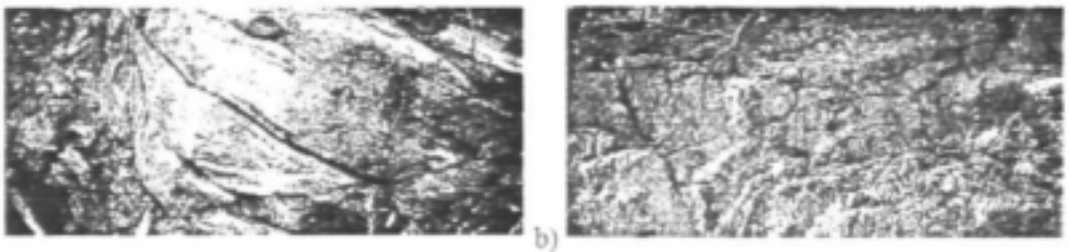

a) b)

Figure 2-35 a) Quartz-hornblende gneiss of the Quha Formation (Stop 10) with vertical Mode 1 joint sets. The one set forms the vertical face to the left of the photograph while the second forms the face of the rock to the right. The lens cap lies on a diagonal fracture.

Figure 2-36 b) Highly weathered Oribi Gorge porphyritic granite (Stop 51). Thrust-slip setting is expressed by a conjugated set of joints, with additional Mode 1 fractures bisecting the acute angle. The main compressive force is not completely horizontal but plunges slightly to the Northeast.

- The fourth conjugated joint set is not as prominent as the vertical joint systems, but occurs in almost all the granite and gneiss outcrops. In these conjugated sets the acute angle is parallel to a sub horizontal axis with Mode 1 tension joints bisecting the acute conjugate angle. The intersecting lines of these planes are horizontal and strike to the east and to the north and are linked to thrust-slip (Figure 2-36).

2.5.1.4 Appearance of structural features

Most of the joints observed in the study area are open by 1-2 mm. Occasional secondary precipitation occurs on the surface. Displacement along fractures is rare, and only found at some Kibaran age thrusts. On only a few occasions do striations occur on the fault planes. Spacing of the joints depends on the proximity to a fault zone. If close to the fault zone the Mode 1 joints are closely spaced (up to 5 cm apart) otherwise they may be several meters apart (Figure 2-37).

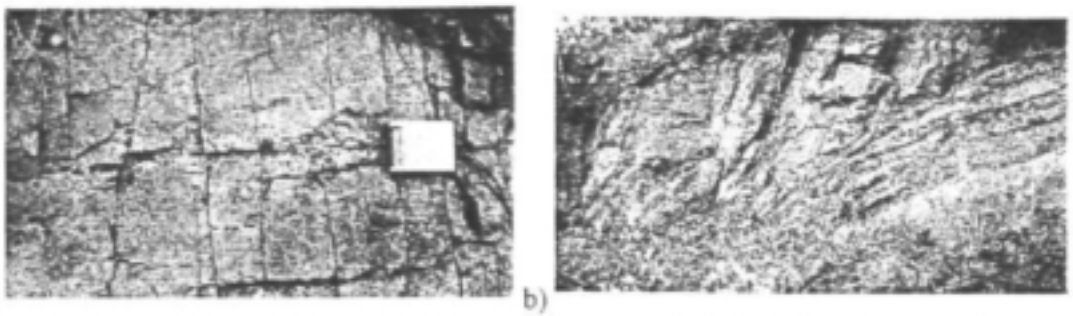

a) b)

Figure 2-37 **At stop 13 the cliff face parallels the schistosity in the (Quha Formation) and the east trending faulting. A second parallel vertical fracture set, with occasional conjugated joints, is perpendicular to the schistosity and represents the north trending faulting. Both the vertical fractures are Mode 1 joints of dip-slip faulting. A third joint set, sub horizontal with better-developed conjugated joints, show the presence of thrust-slip conditions.**

Figure 2-38 **The Oribi Gorge granite exposure at stop 47 shows a top zone of weathered granite with prominent vertical joints, a middle fault zone with penetrative brittle flaser fabric, and a lower zone of poorly jointed and fractured, fresh porphyritic granite.**

In the porphyritic granite-gneiss the hanging wall sometimes is well-fractured displaying typical dip-slip conditions while the fault zone separates the hanging wall from the relative undeformed footwall (Figure 2-38)

The field appearance of the planar structures indicates that the Mode 1 joints are the most abundant and prominent features varying from a joint of a few millimetres to a brittle zone of a few meters.

2.5.2 Analysis of structural features in the research area

The systematic relationships, which exist between planar features, provide a basis for interpreting palaeo-stress directions in rocks deformed millions of years ago. This involves the separation of the surfaces of the various joint sets and plotting them on stereonets as an aid to deal with the three-dimensional geometries of the stress fields.

A total of 486 joint planes were measured in the study area and are displayed in Figure 2-39. On the basis of these planes density contours could be drawn and are presented Figure 2-40. Two density poles at 2/87 and 181/87 display a dominant N-S strike at a plunge around 87° to the east and west. Two minor density poles show a strike of joints towards the west dipping steeply to the north and a strike of joints towards the northeast with a dip steeply to the south. The clustering in the centre relates to sub horizontal joint fractures.

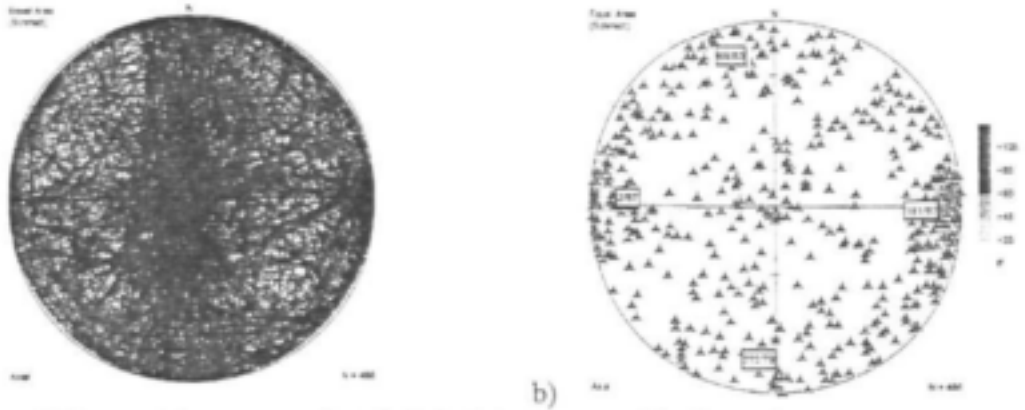

a) b)

Figure 2-39 **a) A stereonet plot of all the joints measured in the study area.**

Figure 2-40 **b) Stereonet plot and density distribution of all poles of the fracture planes measured in the study area.**

From the structural plots alone it is impossible to distinguish between the different stress fields. Therefore a detailed analyses of data at various outcrops (Appendix 2-E) had to be carried out to separate the various orientations of the joint sets present in the study area. Therefore data from every outcrop was plotted on a stereonet. By applying the orientations of the dip-slip, thrust-slip and strike-slip systems, according to figures 3.1 and 3.2, it was possible to determine the orientation of the stress-fields active at each site. Examples of stereonets from nine outcrops, which cover the entire variety of structural features occurring in the study area are given in Appendix 2-E.

The plotted data sets from the various stops, shown and not shown, highlight the three-dimensional fractures along an N-S strike as well as an E-W trend, the N-S oriented strike-slip faulting and in most cases slightly tilted thrust-slip fracturing. Since the thrust-slip Mode 1 plane mostly dips less than 15° the deflection may be linked to the orientation of the tectono-metamorphic fabric. With these conclusions in mind the poles of all measured planes were divided into sets dipping :

- 90°-80°
- 80°-61°
- 90°-75°
- 60°-46°
- 45°-16°
- < 15°

These were plotted on stereo nets and contoured showing the planes, the poles and the orientation of the planes linked to the clusters. These "cluster-planes" again were plotted to determine the orientation of the stress-field causing the joint-set. Where the fracture patterns are due to three-dimensional faulting the mean orientation for the relating sets can be determined.

Planes dipping 90°-80°

The fractures dipping steeper than 80° are considered to be dip-slip Mode 1 joints (Figure 2-41). The clustering of the poles of the measured fracture planes around the 90° and 270° positions indicate that the best developed fracture set is oriented N-S. A second clustering, close to 180° with its opposing cluster setting at ±345°, emphasizes the E to ENE trend of the second dip-slip stress field. Some minor clusters appear in the SW-quadrant showing modes trending to the southeast.

Planes dipping between 80° and 60°

The fractures dipping between 80° and 60° are considered to be linked to dip-slip stress environments (Figure 2-42). The clustering of the poles of the planes are at a plunge of ±70° with the fractures displaying a strong conjugated N-S trending joint set. Smaller and subordinate clusters identifying a well-developed SW-NE trend of three-dimensional fractures show several conjugated joint sets.

Planes dipping between 90° and 75°

In Figure 2-43 all planes dipping steeper than 75° were combined and display a N-S as well as a WSW-ENE trend. Obvious in this combination is the NW-SE fracture with the three-dimensional fractures towards the southwest.

Planes dipping between 60° and 45°

Eight well-defined clusters of planes dipping between 60° and 45° can be seen in Figure 2-44. These planes can belong to either dip-slip or thrust-slip stress settings. If the opposing clusters are grouped as a conjugated joint set, the N-S trending fracture has the strongest cluster at position 265°/35° and a similar cluster at 156°/34° showing the northeasterly trend. A very well defined conjugated fracture set has a NW-SE trend. The fourth conjugated set is a SW-NE fracture set with planes with a strike and dip of 206°/45° and 49°/53°, which is indicative of the thrust-slip stress setting.

Planes dipping between 45° and 16°

The orientations of the thrust-slip fractures are shown in Figure 2-45 where two slightly tilted conjugated joint sets are indicated. In both these sets the steeper planes dip at nearly 36° and the shallower planes at 21°. The fractures of one thrust set trends ESE and the second, almost perpendicular to it, trends towards the NNE.

Planes dipping between15° and 0°

The density distribution of the cluster of poles from the planes dipping between 15° and 0°allowes no grouping and shows that the Mode 1 fractures to the thrust-slip stress setting are just sub horizontal (Figure 2-46). It may be that some of the sub horizontal fractures are linked to erosional pressure release. However, field evidence argues for a compressional origin, as the Mode 1 plane may form a narrow deformation zone along with occasional displacement in the field. It seems that all of these sub horizontal joint fractures are open features.

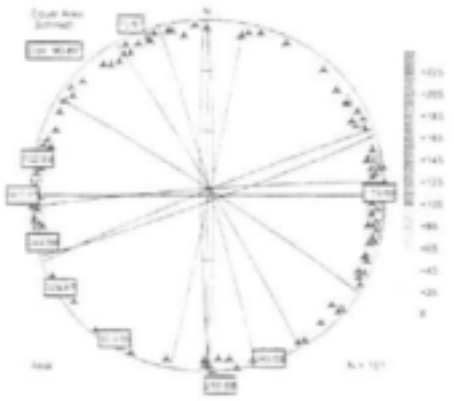

a)

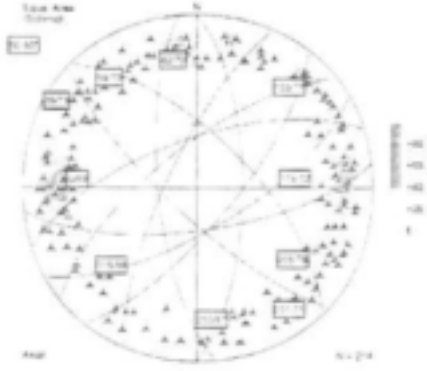

b)

Figure 2-41 a) Stereonet plot of all fractures dipping steeper than 80°.
Figure 2-42 b) Stereonet plot of all fractures dipping between 80° and 60°.

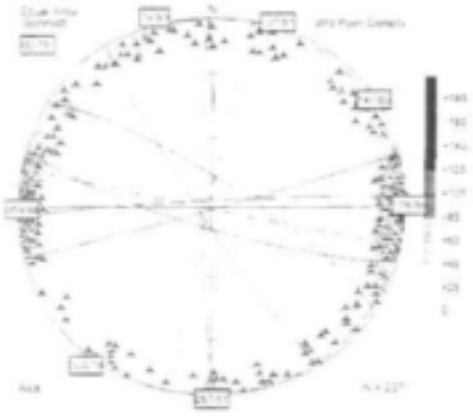

a)

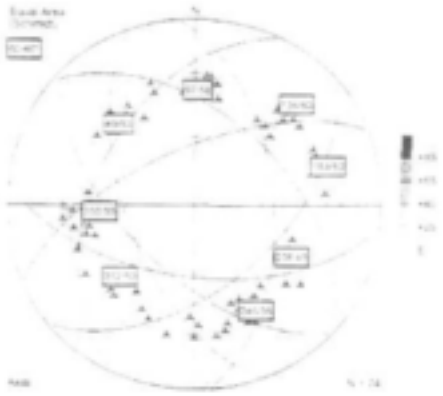

b)

Figure 2-43 a) Stereonet of all planes dipping between 90° and 75°
Figure 2-44 b) Stereonet plot of all joints dipping between 60° and 45°.

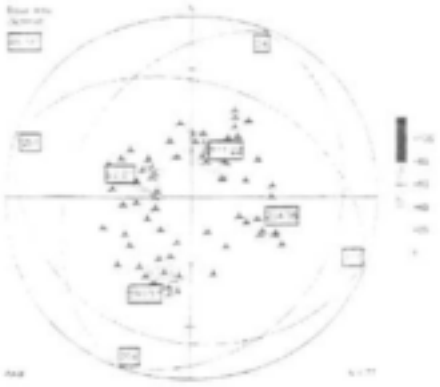

a)

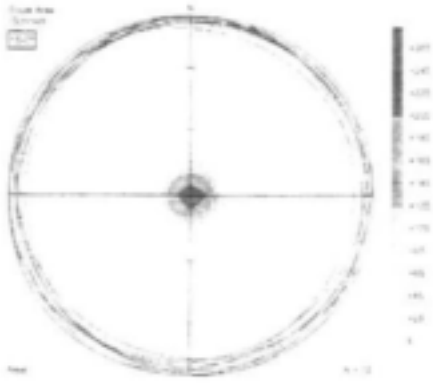

b)

Figure 2-45 a) Stereonet of all data dipping between 45° and 16°
Figure 2-46 b) Stereonet plot of all the fractures dipping less than 15°

To determine the orientation of the strain ellipsoid for the area under investigation the principle axis for the fracture sets distinguished from the above described plots (Figure 2-41-46) ere calculated and are listed in Table 2-4.

Table 2-4 The orientation of the strain ellipsoid axis as determined from the data obtained in Figure 2-41 to Figure 2-46

	Setting	Orientation strike/dip	σ1 Compression	σ2 Neutral	σ3 Extension
90°-80°	Dip-slip (conj)	360°/87° 179°/86°	356°/82°	180°/08°	90°/01°
	dip-slip (conj)	70°/88° 248°/88°	65°/82°	249°/08°	159°/01°
	dip-slip	266°/88°	90°/90°	86°/00°	356°/00°
	dip-slip	329°/87°	329°/90°	149°/00°	59°/00°
	dip-slip	344°/86°	347°/82°	163°/08°	253°/11°
	dip-slip	12°/89°	176°/86°	12°/04°	282°/01°
	dip-slip	303°/86°	33°/90°	123°/00°	213°/01°
80°-60°	dip-slip (conj)	000°/89° 174°/72°	00°/81°	177°/08°	267°/02°
	dip-slip (conj)	135°/90° 315°/66°	16°/84°	134°/03°	224°/06°
	dip-slip (conj)	250°/87°	20°/84°	256°/03°	166°/05°

		82°/70°			
	dip-slip (conj)	059°/70° 231°/71°	58°/79°	235°/11°	325°/01°
	dip-slip (conj)	39°/73° 205°/76°	35°/66°	211°/24°	302°/02°
	dip-slip (3D)	39°/73° 59°/70° 82°/70° 250°/67° 231°/71° 205°/76°	54°/54°	234°/36°	324°/00°
Dip	**Setting**	**Orientation strike/dip**	**σ1 Compression**	**σ2 Neutral**	**σ3 Extension**
90°-75°	dip-slip	178°/87°	268°/87°	178°/03°	88°/03°
	dip-slip	74°/89°	254°/89°	74°/01°	344°/01°
	dip-slip	267°/87°	357°/87°	267°/03°	177°/03°
	dip-slip (3D)	303°/78°	33°/78°	303°/13°	213°/13°
	dip-slip (3D)	303°/78° 147°/86° 107°/81°	78°/86°	215°/04°	306°/04°
60°-45°	thrust or dip-slip (conj)	134°/60° 312°/50°	47°/81° or 224°/09°	314°/01°	224°/09° or 47°/81°
	dip-slip (conj)	159°/60° 355°/55°	358°/77°	166°/12°	257°/03°
	thrust or dip-slip (conj)	49°/53° 206°/45°	21°/77° or 128°/04°	219°/13°	128°/04° or 21°/77°
	dip-slip (conj)	97°/58° 246°/56°	79°/68°	262°/22°	172°/01°
45°-16°	thrust-slip (conj)	22°/21° 204°/35°	293°/07°	23°/00°	117°/83°
	thrust-slip (conj)	111°/22° 290°/37°	20°/08°	290°/00°	198°/82°
	Strike-slip (conj)	348°/84° 189°/82°	189°/37°	2°/53°	96°/03°

Orientation of the strain ellipsoid

Dip-slip setting

Figure 2-47 shows the stereonet plot of the direction of maximum extension (σ3) for the dip-slip strain ellipsoid based on the data from Table 2-4. Major extension occurred along an E-W as well as a nearly N-S axis producing the major faulting directions. Minor concentrations indicate extension in a SW-NE direction (218°) as well as two sub-extensions in the NW-SE direction (304° and 325°) causing the subordinate normal fault sets.

Thrust-slip setting

The calculated σ1 (compressional) values for the thrust-slip settings in Table 2-4 are shown in Figure 2-48 and are clearly along a SE (128°) and a SW (224°) axis.

Strike-slip setting

The σ1(compressional) value of 189°/37° as well as the intersection lineation (σ2 = 2°/53°) for the strike-slip setting (Figure 2-49) indicates that the movement was not sub horizontal but inclined towards the south with some extension to the east.

For the dip-slip setting the strain ellipsoid has two orientations causing normal faulting parallel to the Mode 1 surfaces (the $\sigma1/\sigma2$ plane) and with $\sigma3$, the direction of maximum extension perpendicular to the $\sigma1/\sigma2$ plane, causing the N-S and E-W faults to be open structures. In the thrust-slip setting however, the open structures tend to be the sub horizontal fractures, which do not appear on surface and cannot be detected by geophysical methods. The subordinate dip-slip settings have the axis of maximum extension parallel to the axis of maximum compression of the thrust-slip strain ellipsoid implying that the normal faulting of the diagonal oriented strain field caused the thrust-slip strain environment. This means that although the diagonal Mode 1 fractures are supposed to be open structures, the compressional environment present may cause a lot of them to be closed up and not necessarily be good water conductors. Note worthy is the fact that all the observed strike-slip fracture sets are parallel to the prominent N-S fractures and are indicative of right-lateral displacement. If the strike-slip fractures are not clearly identified, they can easily be misinterpreted as dip-slip joints.

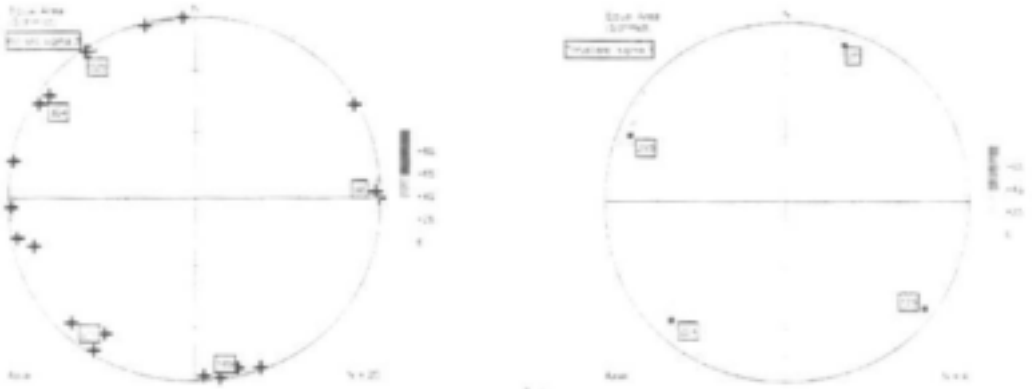

a) b)

Figure 2-47 **a) Stereonet plot of the direction of maximum extension ($\sigma3$) for the dip-slip strain ellipsoid**

Figure 2-48 **b) Stereonet plot of the direction of maximum compression ($\sigma1$) for the thrust-slip strain ellipsoids.**

Figure 2-49 **Stereonet plot of the orientation of the strain ellipsoid for the strike-slip faulting**

The structural development for the terrain

At about 150 Ma to about 110 Ma ago an east-west spreading ridge, now aborted and situated east of Somalia, caused East Gondwana (India/Madagascar/Antarctica) to move southward along the north-south, right-lateral Davie Fracture Ridge which extended into the South

Falkland Fault Zone causing transpression in the adjacent crust. In the Tanzania/Mozambique sector the displacement is parallel to the tectonometamorphic fabric of the high-grade gneisses. However along the eastward extension of the Natal Metamorphic Province the prominent schistosity and shear zones of the underlying Kibaran metamorphic rocks were at an acute angle (15-20°) to the antithetic fractures linked to the N-S displacement along the Falkland Fracture Zone. The inheritance of these planes causes the N-S shearing to be replaced by the south-southwest fracture system of the Agulhas Fracture Zone, which resulted in the breakup of Africa and South America. This behaviour is following the findings of Handin (1969) who concluded that it is unlikely that a new fracture pattern will develop if one pattern already exists at an acute angle to the applied stress field. During this transcurrent movement simple shear conditions prevail leading to arching in the adjacent terrane due to fault-bounded uplift. Although the fracture zone and doming were initiated by simple shear (rotational), all the internal structure development was controlled by pure shear (flattening).

The theoretical fracture patterns, which developed in a dextral shear zone, are accompanied by second order fractures whose orientations are shown schematically in Figure 2-50. These fractures consist of tension gashes (T), shear zones (P) and shear fractures (R). When the external conditions cause dilation of the fault zone the P, X, T system is activated preferentially. Under compression the R/R' system is predominant.

When the observed fracture pattern is compared with the fault, it is noticeable that the fault-bounded uplift of the terrane occurred parallel to the synthetic P faults, which trend in a SSW direction making an acute angle to the present coastline. The related antithetic structures (X), oriented nearly perpendicular to the coastline, are the best developed close to the coast or occur as short minor fractures further west. The tension gashes (T) would trend ENE and make an angle of approximately 45° to the coast. Such faults appear abundant and well developed in the coastal region.

Where the ENE (T) structures intersects the SW to SSW synthetic (P) structures, the gashes are mostly truncated and the dip-slip faulting along the gash fracture causes strike-slip faulting to occur in the synthetic (P) fault plane. Differential faulting along the (X) and (T) structures produced a sinuous terrain in which basement and cover sedimentary successions alternately are exposed from north to south. The simultaneous normal faulting along the synthetic (P) and (T) fractures causes south and eastward directed slumping leading to an interference of the two dip-slip strain ellipsoids. The gravity slumping produces diagonal normal faults (mostly parallel to the R plane) and WNW-ESE compression (parallel to R') in the distal areas in which the thrust-slip conjugated fractures developed. As the NNE-SSW compression is perpendicular to the trend of the Agulhas Fracture Zone it is directly related to the transpression occurring with the transform fault system. Comparing the fracture pattern in Figure 2-50 with the stereographic plots of Figure 2-41 and Figure 2-46, the main directions follow the (P), (X) and (T) fractures while the R and R' are subordinate and present in Figure 2-45 and Figure 2-46.

The most obvious features distinguished in the study are the NNE (P) and ENE (T) trending fault sets with subordinate NE (R) and NW (X) trending faults. The intersection of the (P), the R and the (T) fractures creates the illusional arcuate form, with an eastward slumping, of many of the faults.

From the above investigation the best structures for water are the major N to NNE and ENE fractures, as they seem to be the open ones. The subordinate NW and NE fractures which are dipping steeper than ±60° may also be good water carriers but the fractures dipping less than 45° are closed due to the presence of a thrusting component. The sub horizontal fractures may also be open but are difficult to detect by geophysical methods.

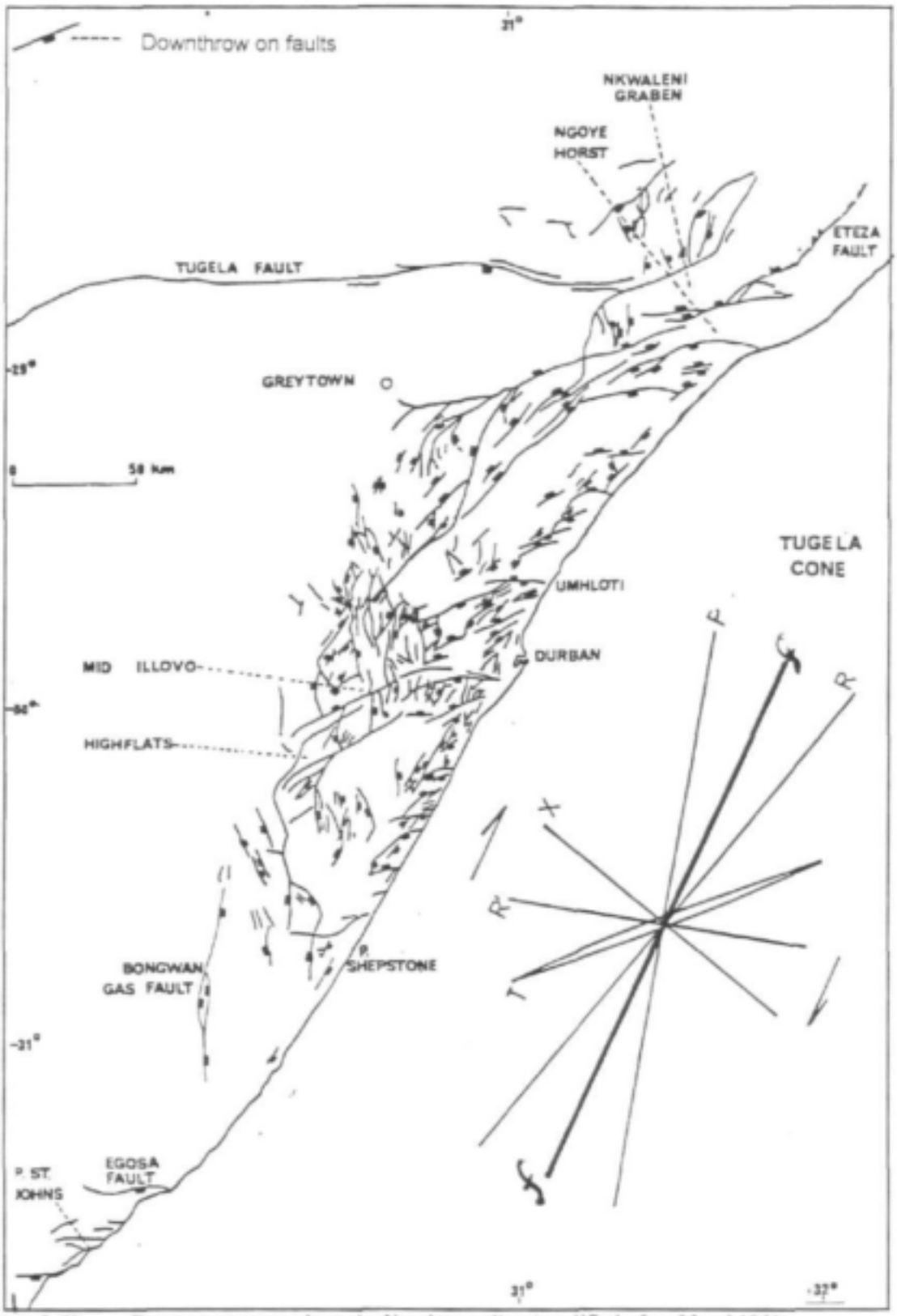

Figure 2-50 Fracture pattern along the Natal coast line (modified after Maud 1961)

2.6 Ground-based Geophysics

2.6.1 Introduction

Since water strikes are relatively deep, applicable geophysical methods for the area need to provide information about the subsurface conditions to approximately 100m. Furthermore, they need to be able to locate relatively narrow conductive zones associated with sub vertical structures. The electromagnetic instrument chosen was the Max-Min (HLEM), since its multiple frequencies allow soundings to various depths and its depth penetration is greater than the EM-34 (Botha et al. 1992). Electrical resistivity soundings were also conducted to determine the depth of weathering or fracturing of the bedrock in order to identify potential bedrock contact aquifers. Additionally, magnetic traverses were used to possibly identify lithological contacts and the location of intrusive dykes or sills.

Geophysical investigations were undertaken at structural features presumed to be under various conditions of tensional or compressional strain, as determined from the tectonic interpretation, strain analysis of field outcrop mapping, and specific structures were identified by aerial photo and LANDSAT imagery interpretation. Target features included lineaments in all four major stress directions at geological structures such as fault lines, mylonite zones, dykes, lithological contacts of dipping strata and undifferentiated lineaments. The geophysical data is summarised in Table 2-5 in terms of the geological feature investigated.

A total of 26 electromagnetic traverses, 29 magnetic profiles and 13 resistivity sounding were carried out throughout the study area. The location and number of each traverse is shown in Figure 2-51. The surveys covered a total distance of 15120 m.

The recorded magnetic data, sounding data and the conductivity responses for all traverses and stations are presented in Appendix 2-A.

The results of the geophysical ground based surveys were grouped into three main categories, reflecting responses over fault zones, lineaments and dyke structures. Examples are given below for each scenario.

Table 2-5 Geophysical surveys carried out in the research area

Name	Boreh. Drilled	Lat	Long	Feature	Geophysics	Traverse direction
NMP1		29 14 44	31 00 06	SW-NE striking fault (Leith 1966)	Mag,MaxMin	W-E
NMP2		29 13 39	31 05 02	Dolerite dyke and NNE-SSW striking lineament	Mag,MaxMin,Resistivity	SE-NW
NMP3		29 12 08	31 05 15	SW-NE striking lineament	Mag, MaxMin	NNW-SSE
NMP4	G47157	29 08 08	31 11 15	NW-SE striking fault crosses a SW-NE running fault	Mag,MaxMin,Resistivity	SW-NE
NMP5	G47158	29 06 55	31 11 41	NE-SW striking lineament	Mag,MaxMin,Resistivity	SSW-NNE
NMP6		29 05 10	31 10 07	NW-SE striking lineament	Mag,MaxMin	NE-SW
NMP7		29 06 11	31 08 43	NW-SE striking lineament	Mag, MaxMin	NE-SW
NMP8		29 13 39	30 54 54	E-W striking lineament	Mag,MaxMin,Resistivity	SSW-NNE
NMP9	G47154 5	29 13 15	30 55 00	E-W striking lineament	Mag,MaxMin,Resistivity	S-N
NMP10		29 14 20	30 55 26	NNE-SSW striking fault	Mag,MaxMin,Resistivity	E-W
NMP11		29 14 16	30 51 00	SW-NE striking lineament	Mag, MaxMin	NW-SE
NMP12		29 14 08	30 47 30	N-S striking lineament	Mag, MaxMin	W-E
NMP13		29 08 00	31 13 55	NE-SW striking fault, separating Natal sandstone and NMP	Mag, MaxMin	N-S
NMP14		29 06 05	31 08 46	E-W striking lineament	Mag,MaxMin,Resistivity	S-N
NMP15	G47159	29 06 47	31 08 19	W-E striking fault	Mag,MaxMin,Resistivity	SW-NE
NMP16		29 08 19	31 08 30	Three dolerite dykes	Mag	N-S
NMP17		29 02 30	31 06 36	NNW-SSE striking lineament	Mag, MaxMin	NE-SW
NMP18		29 04 27	31 03 18	WSW-ENE striking fault, separating Natal sandstone and NMP	Mag, MaxMin	NE-SW

NMP19		29 26 18	30 50 49	Two lineaments crossing (NW-SE and NE-SW)	Mag, MaxMin	NE-SW
NMP20		29 26 15	30 57 58	N-S striking lineament	Mag, MaxMin	W-E
NMP21		29 27 19	30 56 23	Dyke	Mag	WNW-ESE
NMP22		29 19 36	30 59 24	Two lineaments crossing (NW-SE and NE-SW)	Mag, MaxMin	W-E
NMP23		29 19 36	30 59 24	Two lineaments crossing (NW-SE and NE-SW)	Mag, MaxMin	SW-NE
NMP24	G47153	29 19 30	31 00 48	N-S striking lineament	Mag,MaxMin,Resistivity	ENE-WSW
NMP25		29 10 18	30 59 41	N-S striking lineament	Mag, MaxMin	ESE-WNW
NMP26		29 09 36	31 01 41	NNE-SSW striking lineament	Mag, MaxMin	E-W
NMP27	G47151 2	29 16 16	31 01 51	NE-SW striking brecciated zone	Mag,MaxMin,Resistivity	S-N
NMP28		29 10 11	31 03 24	N-S striking lineament	Mag, MaxMin	WNW-ESE
NMP29		29 06 32	31 08 24	NW-SE striking lineament	Resistivity	
NMP30	G47156	29 12 15	31 00 20	E-W striking wide weathered zone	Resistivity, Mag	NW-SE

2.6.2 Fault lines

A total of six fault zones were investigated on the basis of geophysical surveys. All faults were either mapped on the 1:250000 Durban geological map, or by MSc. theses carried out in the research area.

NMP4 – NW-SE striking fault line

Site description

Magnetic and Max-Min surveys were carried out over a fault line mapped on the Durban 1: 250000 geological map (Figure 2-52). The fault strikes NW-SE and the 380m survey were conducted perpendicular to the feature from the SW to the NE. A distinct change in the morphology indicates the fault line in the field. Here, solid bedrock gives way abruptly to a wide weathered zone.

Electromagnetic survey

The Max-Min was operated at 4 frequencies, ranging from 220 to 14080 Hz with the coil separation set at 100m. A station spacing of 20m was selected. The results of the electromagnetic data are shown in Figure 2-56.

The electromagnetic data set shows a broad anomaly for the first 200m in all frequencies. The trough-like response indicates a thickening of the conductive overburden, with the thickest zone corresponding to the peak in conductivity at 100m. This is assumed to be the approximate position of the fault line. At this point a borehole was sited to evaluate this presumed compressional fault, which was unsuccessful. An increase in the in-phase and out-of phase components at 200m indicates a decrease in the thickness of the conductive overburden towards the end of the traverse.

Magnetic survey

Using a 20m station spacing, a magnetic survey was carried out over the fault zone from the SW to the NE. The data is shown in Figure 2-56.

The magnetic data supports the Max-Min results and identifies a change from solid gneiss bedrock to weathered bedrock between 60 and 80m with a decrease in amplitude of about 150nT.

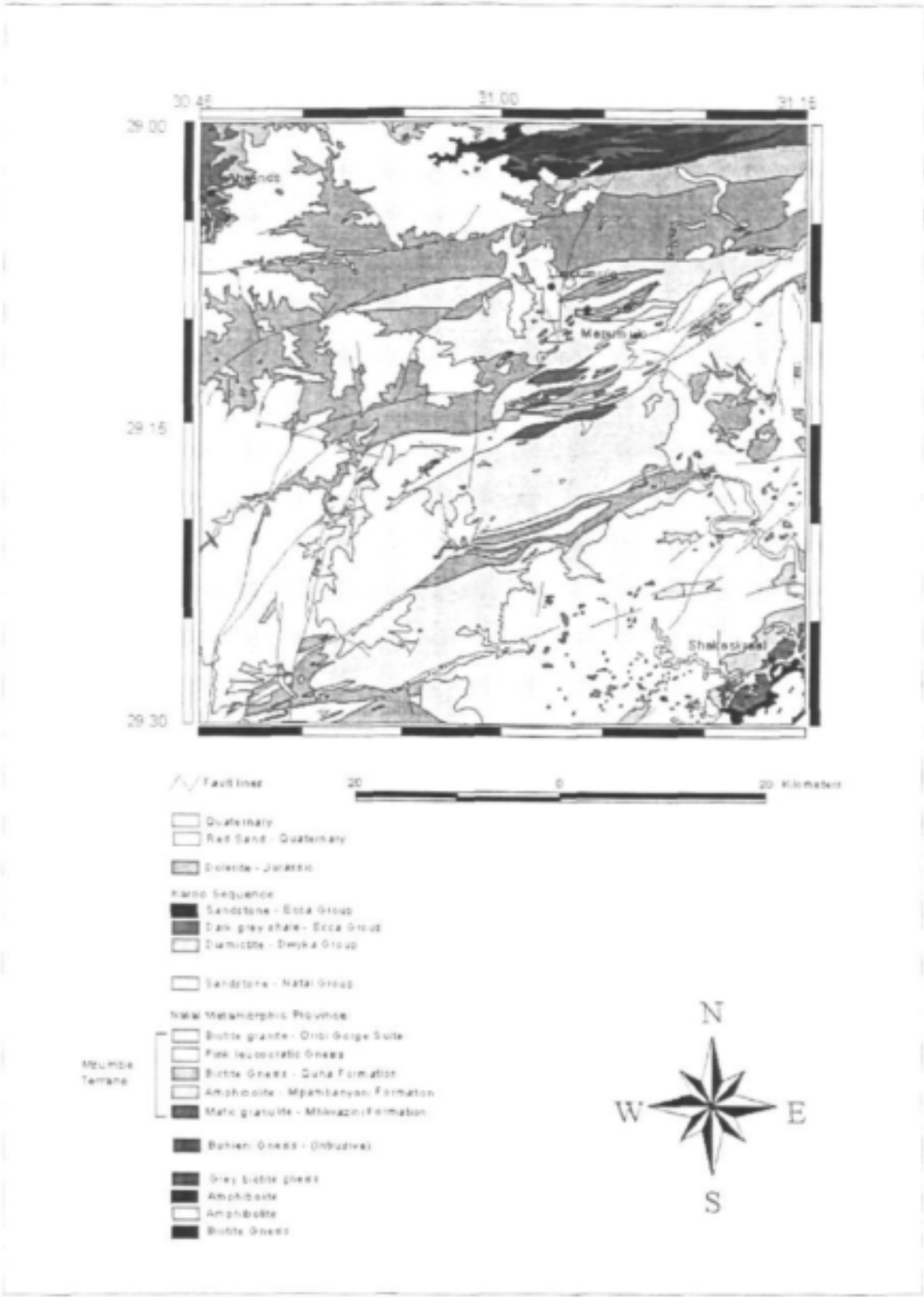

Figure 2-51 **Stations of the geophysical surveys carried out throughout the study area**

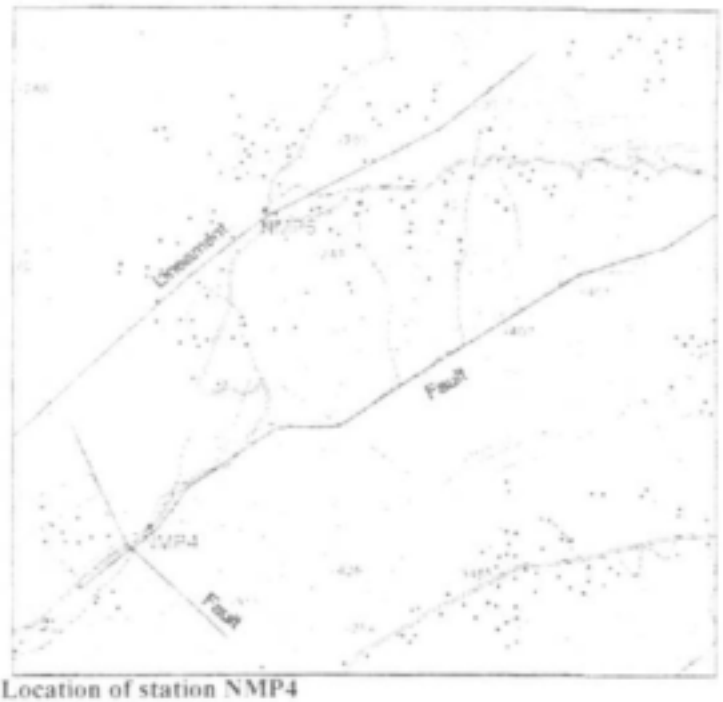

Figure 2-52 Location of station NMP4

Resistivity sounding

An electrical sounding was carried out at the 100m locality of the electromagnetic traverse, perpendicular to the suspected fault line to try and determine the overburden thickness (Figure 2-57). Visual analysis of the sounding curve indicates that it is a three layer curve with $\rho1<\rho2<\rho3$ and, therefore, an A-type curve. The constant ρ values at short AB spacings indicate a resistivity of 300 Ωm for the first layer, which has a thickness of about 10m. As the spacing is increased the effect of the second layer becomes progressively more dominant. By curve matching the following values for the three layers are determined (master curve A15):

Layer	Thickness (m)	Resistivity (Ωm)
Layer1	10m	300
Layer2	65m	1200
Layer3	∞	resistive bedrock

The high resistivity values indicate a poor water bearing potential.

NMP15 – E-W striking fault zone mapped on the Durban 1:250000 geological map

Site description

An E-W striking fault zone mapped on the 1:250 000 Durban geological map was the target of traverse NMP15 (Figure 2-53). The fault zone is of regional scale, starting in the far north-eastern corner of the study area, where it forms a tectonic contact between Natal Sandstone and rocks of the Natal Metamorphic Province. The fault zone then bends from a NE-SW strike direction into an E-W direction and runs out just to the west of the Mati River. An electromagnetic and magnetic survey was carried out at the site, crossing the feature from the SW to the NE.

Electromagnetic survey
The Max-Min was operated at 4 frequencies, ranging from 220 to 14080Hz while the coil separation was set to 100m. A station spacing of 20m was selected. The results of the electromagnetic and magnetic data are shown in figure 2-58.

No anomaly in the electromagnetic data could be detected, although the borehole sited on this traverse proved to be the highest yielding borehole drilled (Table 2-6). A steady increase in response amplitude for the in-phase and out-of phase from the SW to the NE is recorded. The first 160m of the electromagnetic traverse are characterised by a negative out-of phase component and a low response amplitude in the in-phase throughout all frequencies, indicating a conductive weathered zone. From 160m onwards, the in-phase and the quadrature component increase in response amplitude testifying a decrease in the subsurface conductivity.

The borehole was sited at 160 m, at the edge of the conductive weathered zone, where the fault was suspected to be based on geological observations.

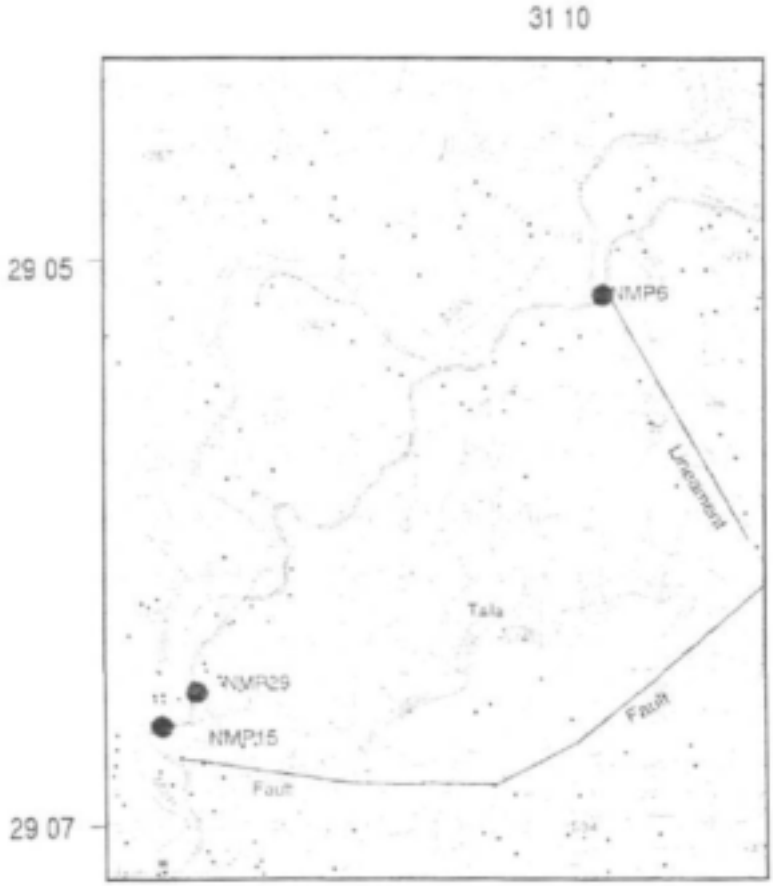

Figure 2-53 **Locality of site NMP15**

Magnetic survey
The magnetic data is inconclusive for the entire traverse.

Resistivity survey
A resistivity sounding was carried out at 160m on the geophysical traverses, at the contact between the higher and lower conductive zones. The data is presented in Figure 2-57.

Visual analysis of the sounding curve indicates that it is a three layer curve of the A-type with $\rho 1<\rho 2<\rho 3$. A three layer master curve (A6) was fitted to the field curve and the following values for the three layers were determined:

	Thickness (m)	Resistivity (Ωm)
Layer 1	2.7	380
Layer2	17.55	950
Layer3	∞	6175

NMP18 – WSW-ENE striking fault line, separating Natal Sandstone and Natal Metamorphic Province

Site description

A fault line forming a tectonic contact between the Natal Sandstone from the Natal Metamorphic Province was investigated with an electromagnetic and magnetic survey (Figure 2-54). The fault strikes WSW-ENE and the contact of the two lithologies is expressed in the topography. The more erodable gneisses and granites of the Natal Metamorphic Province form a red coloured soil and are further expressed as a low in the topography. An abrupt change in the colour of the soil to a light yellow indicates the change in lithology to Natal sandstone as the less erodable unit forms a topographical high. Traverses were conducted at a 90° angle to the fault line.

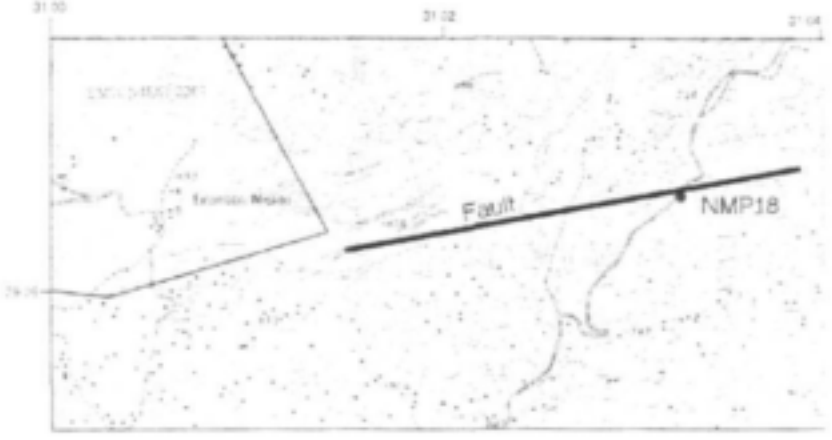

Figure 2-54 Location of station NMP18

Electromagnetic survey

The Max-Min was operated at 4 frequencies, ranging from 220 Hz to 14080 Hz while the coil separation was set at 100m. A station spacing of 20m was selected. Results for the electromagnetic and magnetic survey are shown in Figure 2-59.

The electromagnetic response is typical to that obtained over the edge of a ramp discontinuity in the overburden. A positive peak response in both the in-phase and out-of phase components are obtained in the first 110m of the traverse, indicating a conductive host, the Natal sandstone. After that a decrease in response amplitude predominantly in the in-phase component for all frequencies characterises the change in lithology by an increase in the subsurface conductivity. This can be attributed to an increase of the overburden thickness over the gneisses and granites of the Natal Metamorphic Province. A second positive peak normally found over steeply dipping conductors, like fracture zones, is absent, hence the structure was not considered water bearing and was not drilled.

Magnetic survey
The magnetic data with amplitude changes of only 40 nT remains inconclusive.

NMP27 – NE-SW striking mylonite zone
Site description
An electromagnetic and magnetic survey plus a resistivity sounding were carried out at station NMP27 to investigate the geophysical response of a suspected fault zone striking NE-SW (Figure 2-55). Williams-Jones (1968) mapped the feature as a mylonite zone of 3.5km length and 40m width. An abrupt change from solid bedrock into a wide-open weathered zone marks the feature in the field.

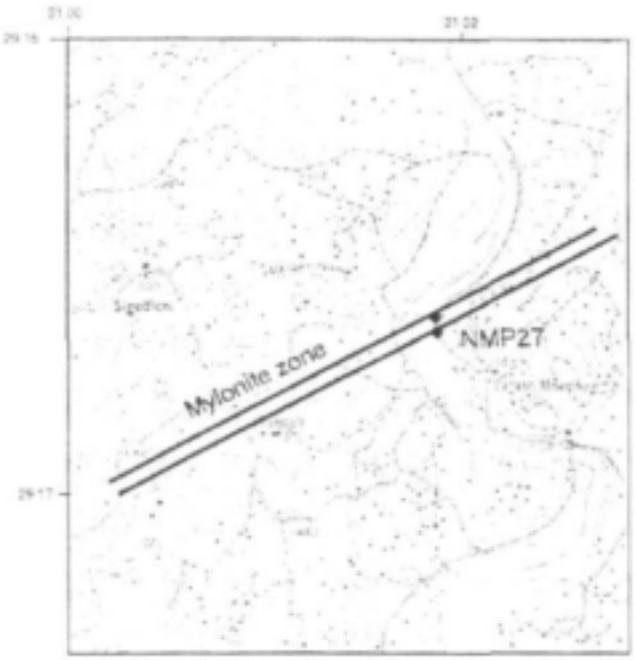

Figure 2-55 **Location of station NMP27.**

Electromagnetic survey
The Max-Min was operated at 4 frequencies, ranging from 220 to 14080 Hz while the coil separation was set to 100m. A station spacing of 20m was selected. The results of the electromagnetic data are shown in figure 2-60.

The response of the Max-Min out-of-phase component over the contact zone between weathered zone and solid bedrock changes from negative to a positive response in all frequencies, indicating a decrease in conductivity from the mylonite zone towards the solid bedrock. The in-phase response is inconclusive. Boreholes were sited at 100 m and 140 m based on geological observation on the mylonite zone.

Magnetic survey
The magnetic survey was conducted over the mylonite zone from the S to the N using a station spacing of 20m. The magnetic data are shown in figure 2-60.

The magnetic data also reflects the lithological change between 190m and 210m with a distinct change in response amplitude. The total field intensity increases by about 200nT from 28450 to 28640nT.

Resistivity sounding

Two resistivity soundings were carried out along the traverse to determine the depth to bedrock. At 100m, within the mylonite zone, the first sounding was conducted with the direction of AB expansion being N-S. The sounding curve is shown in Figure 2-61.

A comparison with theoretical sounding curves suggest a three-layered earth case with $\rho1>\rho2<\rho3$. This H-type curve was fitted to H50 master curve and the following resistivity values were determined:

	Thickness (m)	Resistivity (Ωm)
Layer 1	19	360
Layer2	1.9	3.6
Layer3	∞	resistive bedrock

A second sounding was carried out further towards the contact zone between solid bedrock and the mylonite zone at 150m of the traverse (Figure 2-61). The direction of AB expansion remained N-S. The sounding curve represents a three layered earth case with $\rho1>\rho2<\rho3$, indicating a more conductive overburden for the first 6.5m over solid bedrock. By fitting the master curve H25 to the field curve the following values were determined:

	Thickness (m)	Resistivity (Ωm)
Layer 1	1.3	210
Layer2	5.2	21
Layer3	∞	resistive bedrock

Conclusion

In conclusion, the magnetic and the Max-Min systems did not always effectively locate fault lines and geological observation was necessary. If the fault line separates two different lithologies, the detectability depends on the differences in conductivity and weathering of the different units. The electromagnetic response over the fault line is typical to that obtained over the edge of a horizontal conductor or ramp discontinuity, where the positive peak is located over the resistive host and the negative peak is obtained over the conductor.

If the investigated feature represents a downthrow, upthrow or transversal fault within the same geological unit, then only the fault zone itself is detectable, if it differs in conductivity from the host rock. A weathered fault zone or a fault breccia will act as a narrow, dipping conductor and the electromagnetic response over the fault will therefore be typical to that obtained over a thin sheet-like conductor – a negative peak flanked by two positive shoulders. The centre of the negative anomaly will be located over the top of the fault zone.

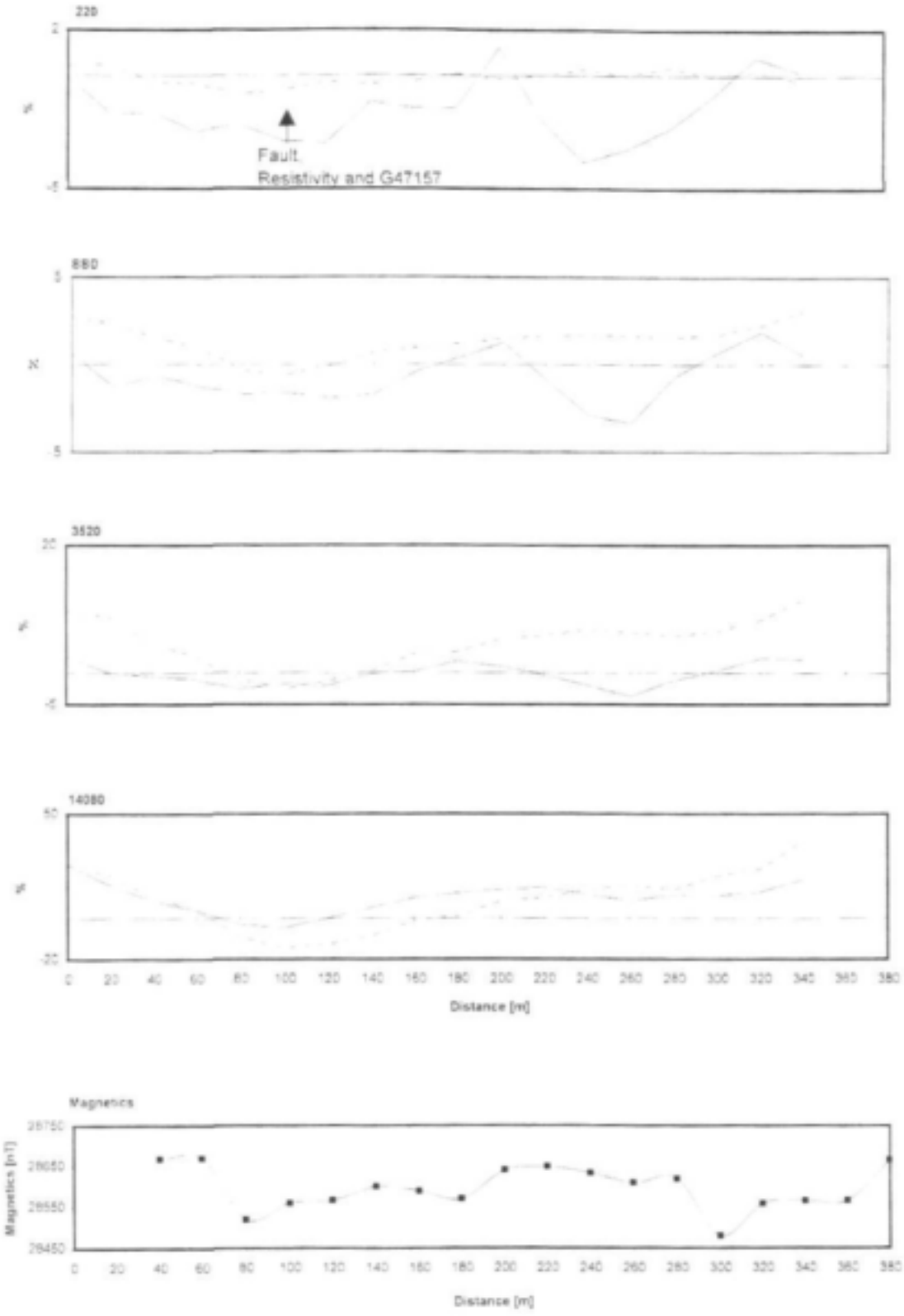

Figure 2-56 MAX-MIN electromagnetic and magnetic profiles at site NMP4. Solid line: in-phase [%]; dotted line: out-of phase [%]; coil separation 100m, station spacing 20m. Traverse direction: SW-NE.

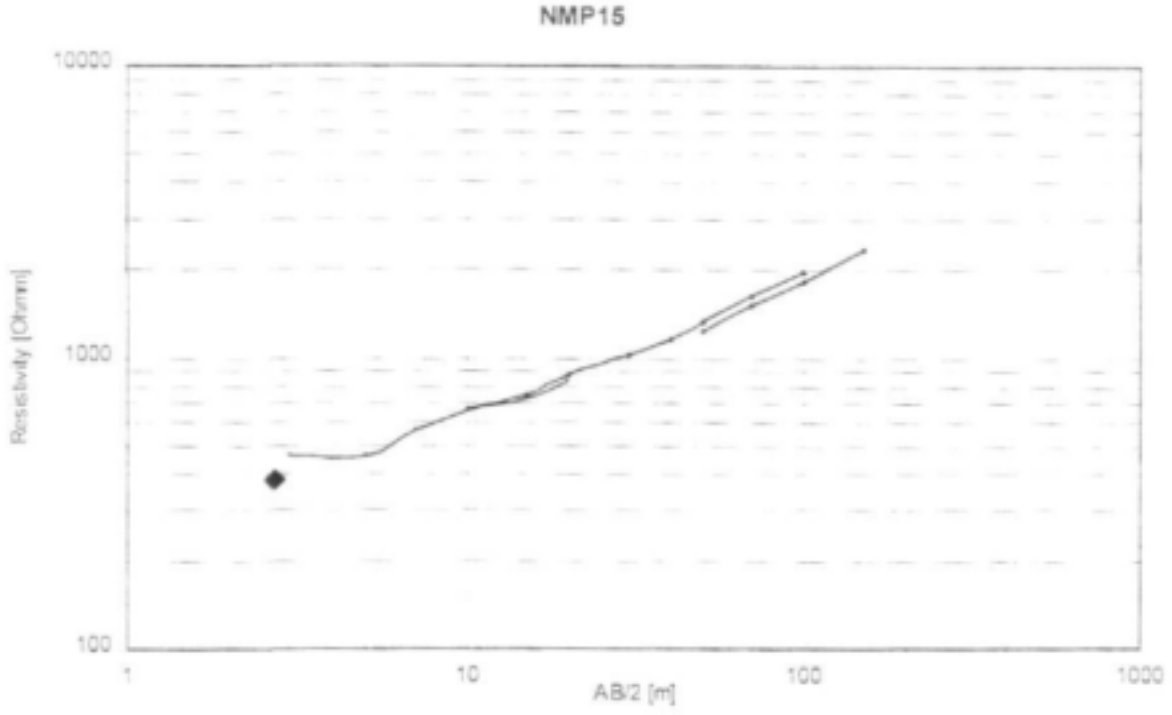
NMP15
10000
1000
100
Resistivity [Ohmm]
1
10
100
1000
AB/2 [m]

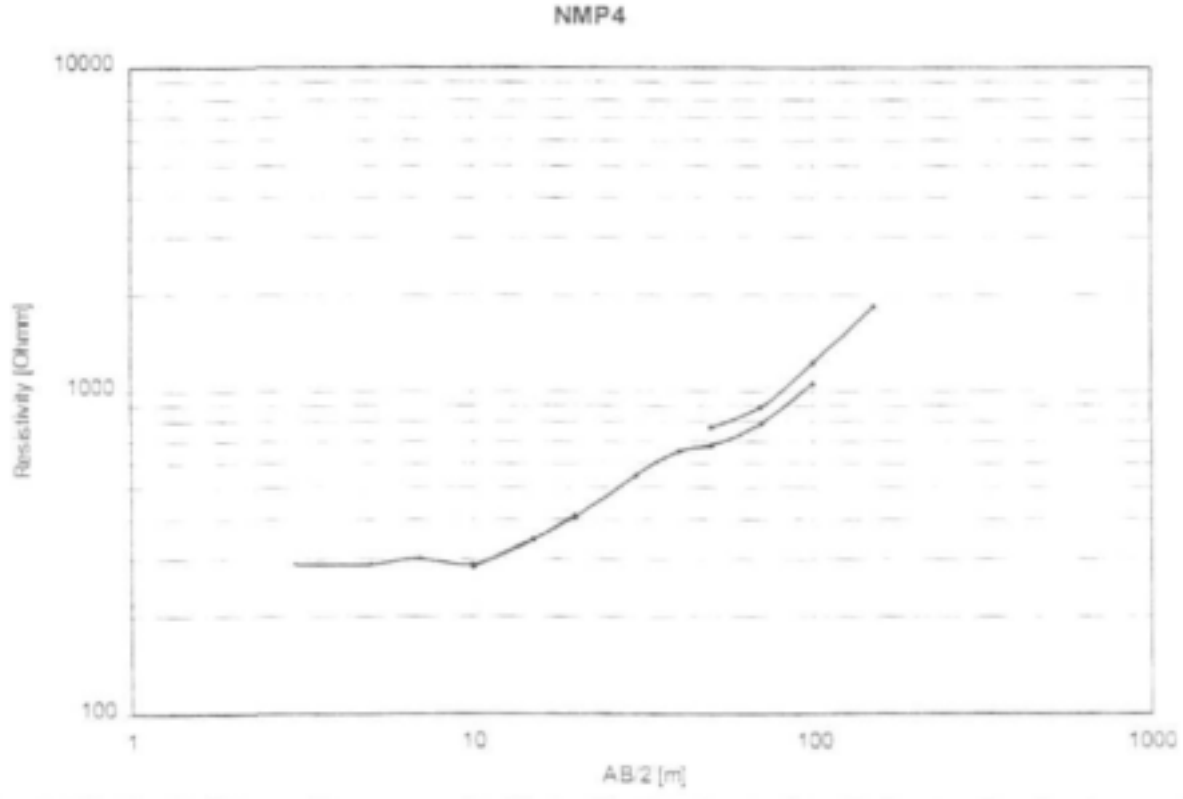
NMP4
10000
1000
100
Resistivity [Ohmm]
1
10
100
1000
AB/2 [m]

Fi
ct

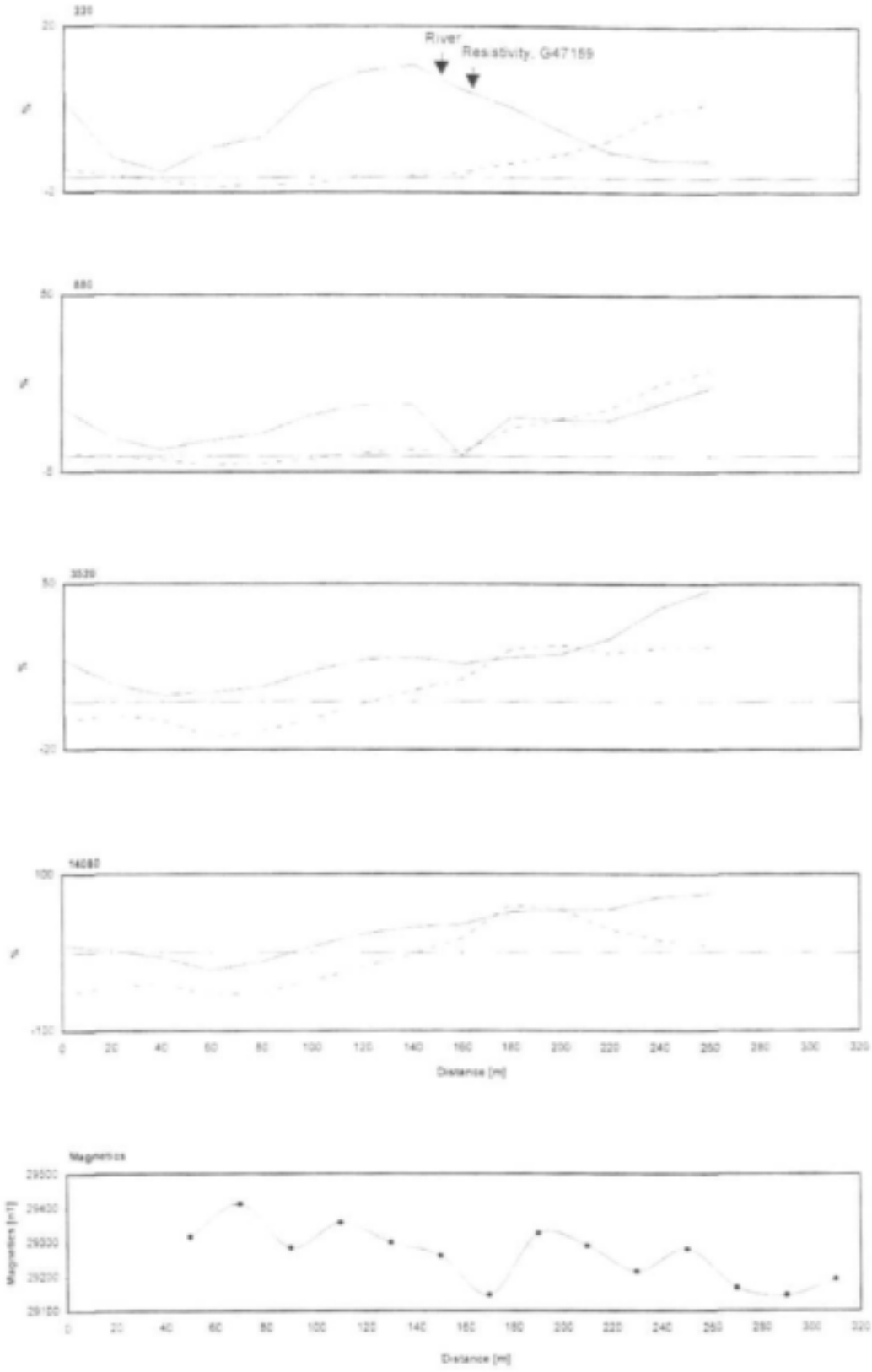

Figure 2-58 MAX-MIN electromagnetic and magnetic profiles at site NMP15. Solid line: in-phase [%]; dotted line: out-of phase [%]; coil separation 100m, station spacing 20m. Traverse direction: SW-NE

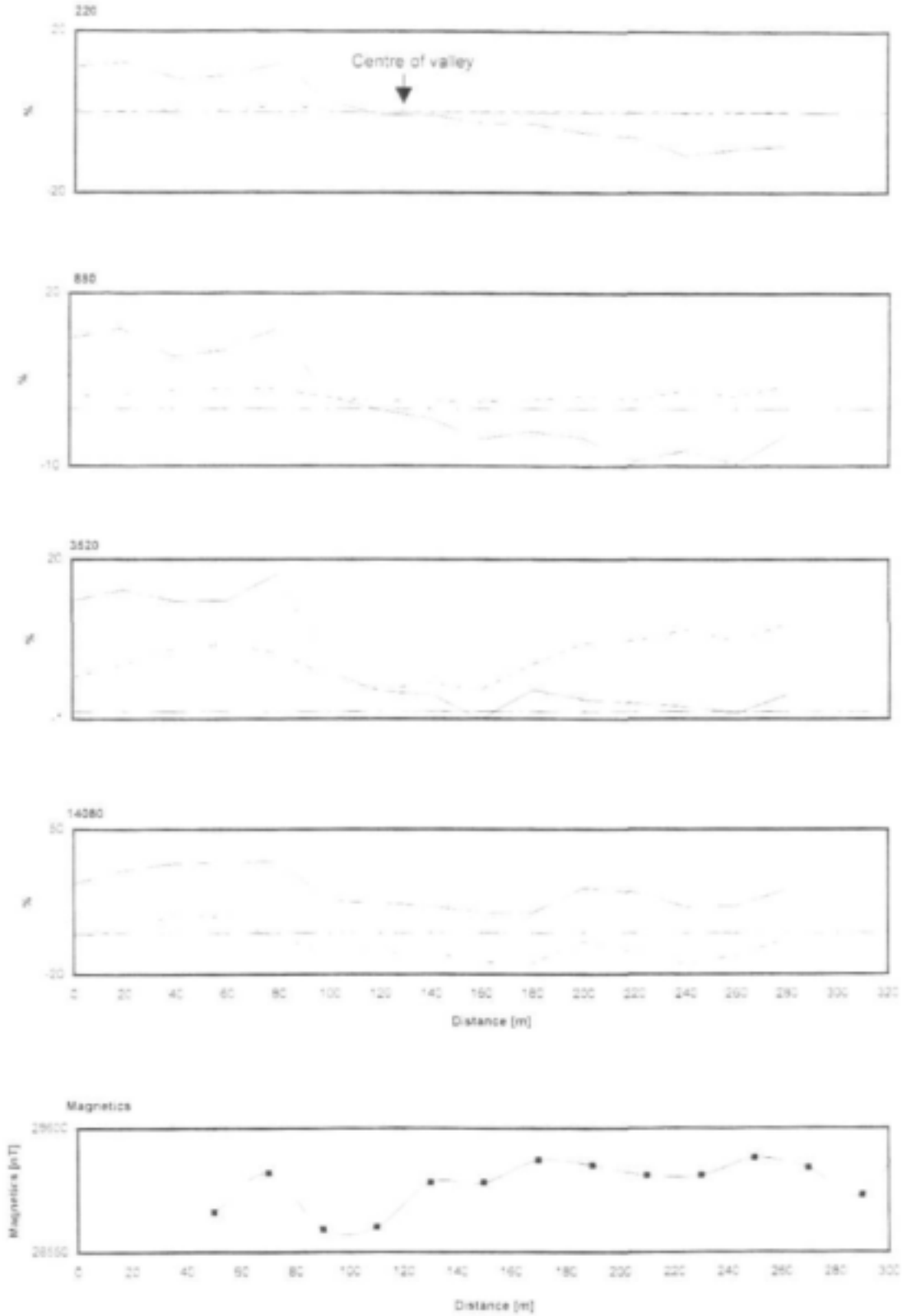

Figure 2-59 MAX-MIN electromagnetic and magnetic profiles at site NMP18. Solid line: in-phase [%]: dotted line: out-of phase [%]: coil separation 100m, station spacing 20m. Traverse direction: NE-SW

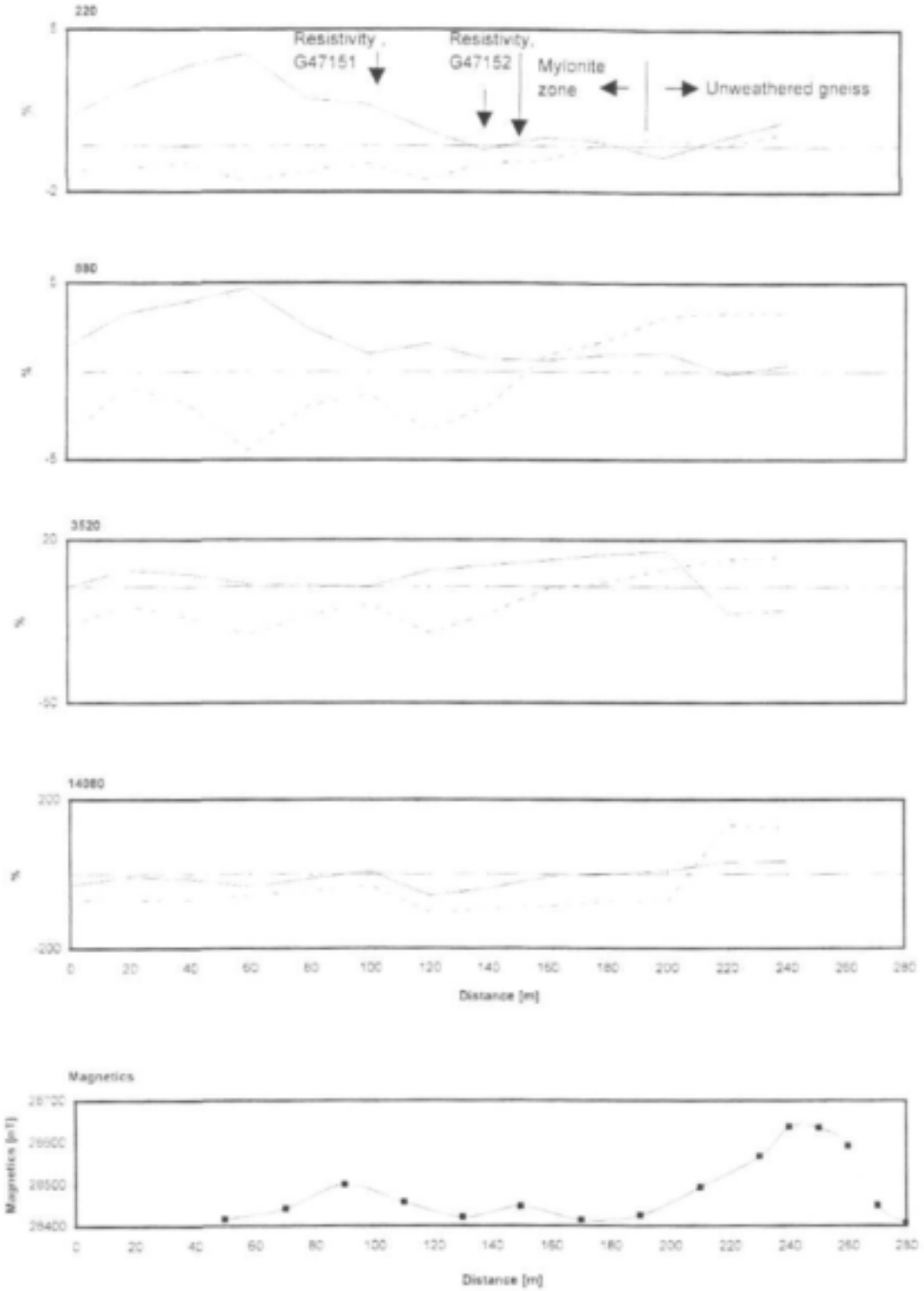

Figure 2-60 MAX-MIN electromagnetic and magnetic profiles at site NMP27. Solid line: in-phase [%]; dotted line: out-of phase [%]; coil separation 100m, station spacing 20m. Traverse direction: S-N

NMP27(1)

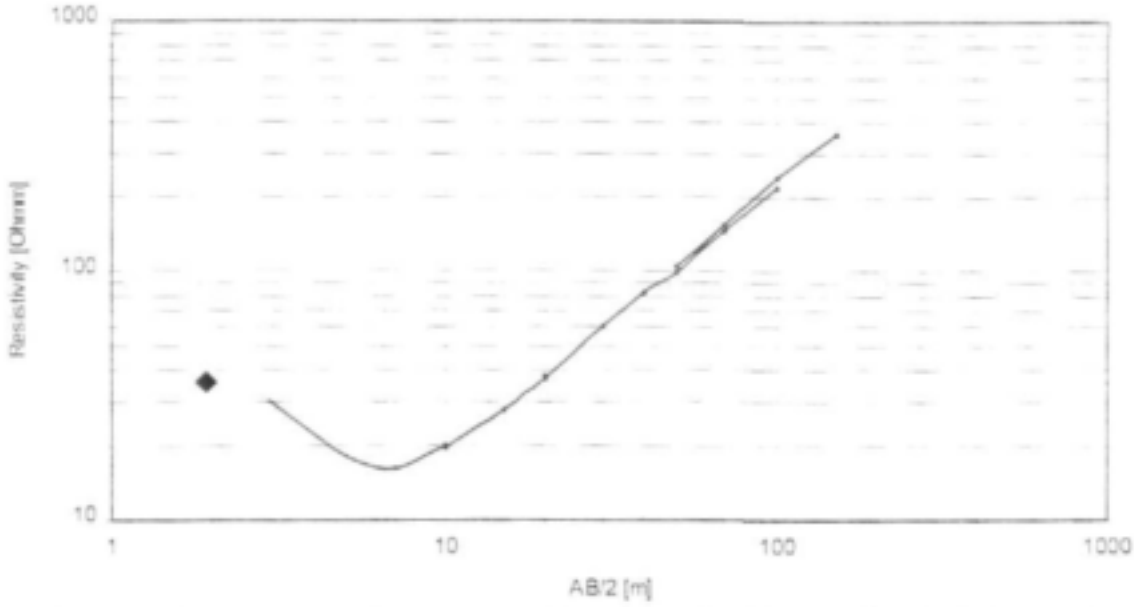

NMP27(2)

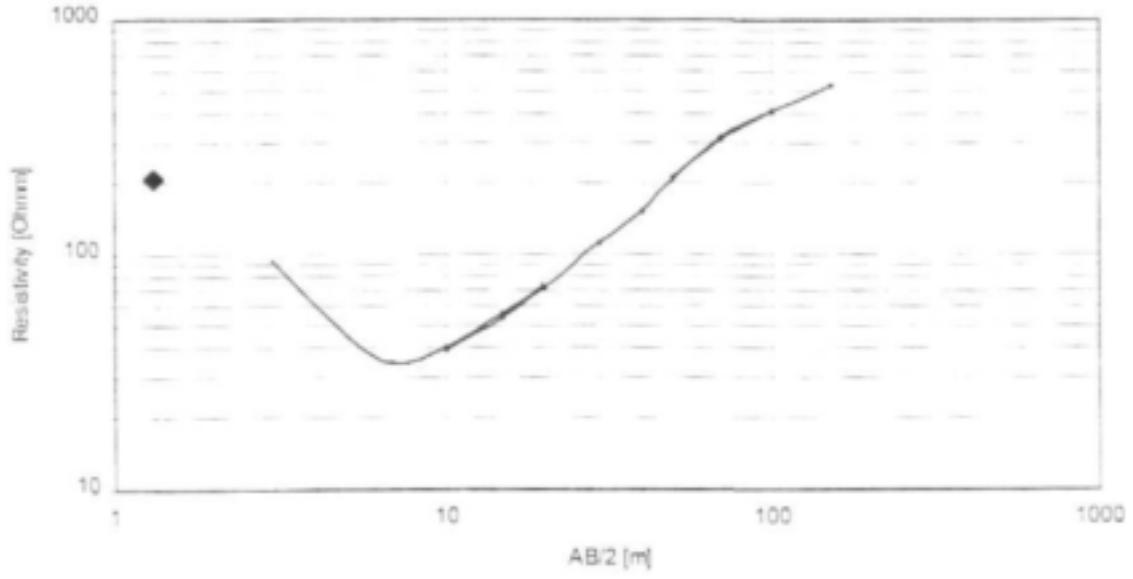

2.6.3 Lineaments

A total of 21 lineaments were investigated covering all major stress directions as distinguished from structural analyses. Lineaments were identified through the enhancement of satellite and aerial photography images.

NMP 2 – NNE-SSW striking lineament

Site description

A NNE-SSW running lineament delineated on aerial photographs and a nearby dyke structure were investigated with magnetic and electromagnetic surveys. To try and determine the depth to bedrock a resistivity sounding was carried out. The lineament is characterised in the field by a depression in the topography and forms part of a riverbed, whereas the dyke is outcropping at several locations to the north of the depression (Figure 2-62). The surveys were carried out perpendicular to the feature from the SE to the NW.

Electromagnetic survey

The Max-Min was operated at 4 frequencies, ranging from 220 Hz to 14080 Hz while the coil separation was set to 100m. A station spacing of 10m was selected. The magnetic and electromagnetic data are shown in figure 2-66.

The electromagnetic data generates a typical trough-like discontinuity over the traverse. This broad negative anomaly is recorded in the in-phase and out-of phase for all frequencies and suggests a thickening of the conductive overburden. An increase in the in-phase and out-of phase components from 150m onwards indicates a decrease in the thickness of the weathered zone overlying unweathered bedrock.

Magnetic survey

The magnetic profile conducted over the lineament and a nearby dolerite dyke shows a steady decrease in the total magnetic field intensity from south to north for the first 150m of the traverse, indicating a gradual lithological change from amphibolites outcropping in the south of the traverse to gneisses in the north. At 150m, where the electromagnetic response shows a distinct change in the weathered overburden thickness, an increase in the total magnetic field intensity of 270nT suggests a further change in the lithology, however, the magnetic data for the following 180m of the traverse is inconclusive. No magnetic response is obtained over the dyke structure at 230m of the traverse, suggesting that the gneissic host rock and the dyke itself do not differ greatly in their magnetic signature.

Resistivity sounding

A resistivity sounding was carried out at the locality of 85m of the geophysical traverses with the direction of AB expansion perpendicular to the strike of the lineament, due to topographical constraints. The results of the resistivity sounding are shown in Figure 2-67. Visual analysis of the sounding curve indicates that it is a three layer H-type curve with $\rho 1 > \rho 2 < \rho 3$. By curve matching using the master curve H15, the following values for the three layers are determined:

	Thickness (m)	Resistivity (Ωm)
Layer 1	3.4	240
Layer 2	5.44	60
Layer 3	∞	resistive bedrock

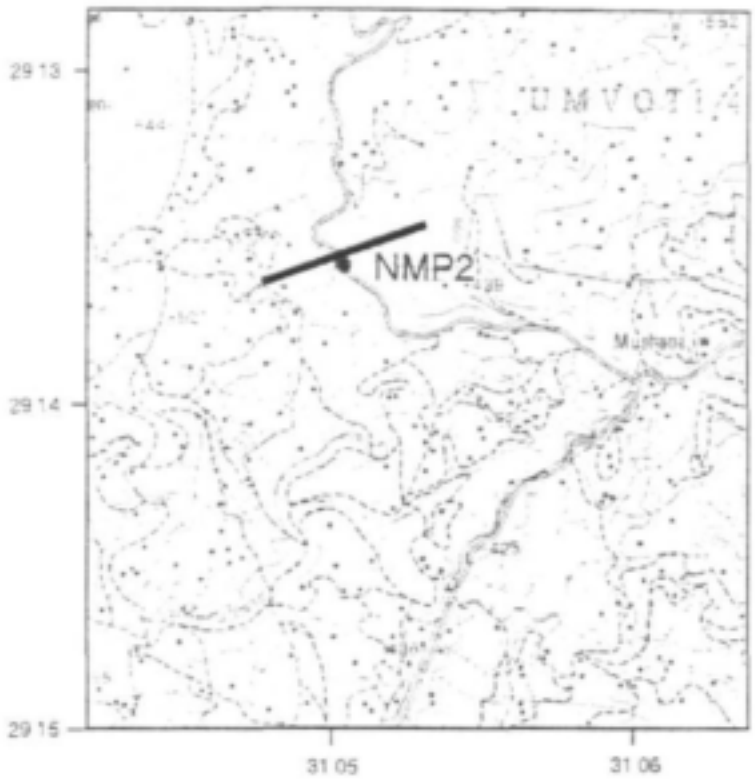

Figure 2-62 **Position of site NMP2**

NMP5 – Prominent NE-SW striking lineament of regional scale

Site description

An electromagnetic and magnetic survey was carried out to investigate a prominent NE-SW striking lineament, delineated by LANDSAT TM and aerial photographs. The lineament is of 10.5 km length and is expressed topographically as a long linear valley stretching from the Tugela River in the NE to the Natal Sandstone escarpment in the SW. The electromagnetic and magnetic traverses were conducted over the feature from the south to the north.

Electromagnetic survey

The Max-Min was operated at 4 frequencies, ranging from 220Hz to 14080Hz while the coil separation was set to 100m. A station spacing of 20m was selected. The electromagnetic data is shown in Figure 2-68.

The electromagnetic data depicts a 110m wide anomaly located from 180m to 290m along the traverse. Two positive shoulders flank negative in-phase and out-of phase components and this trough-like anomaly indicate a thickening of the weathered overburden. A borehole was sited at 280 m, in the zone of the thickened overburden, which proved to be a successful weathered zone aquifer (4 l/s).

Magnetic survey

A magnetic survey was conducted over the lineament from the SSW to the NNE with a station spacing of 10m. The data is shown in Figure 2-68.

The magnetic data indicates an increase in the total magnetic field intensity over the electromagnetic anomaly.

Resistivity sounding

A resistivity sounding was carried out at distance 280m of the electromagnetic and magnetic traverse, at the northern edge of the trough-like electromagnetic anomaly. The direction of AB expansion paralleled the geophysical traverses. The sounding curve is shown in Figure 2-67.

The sounding curve represents a three layered earth case of the A-type with $\rho 1 < \rho 2 < \rho 3$. By fitting the field curve to the master curve A5 the following values for the three layers could be determined:

	Thickness (m)	Resistivity (Ωm)
Layer 1	2	27
Layer 2	32	43.2
Layer 3	∞	resistive bedrock

The sounding data shows a thick weathered overburden of 34m for the site, whereas the low resistivity suggests a weathered zone aquifer of high conductivity. The borehole drilled on the site confirmed this by yielding 4 /s at 18-23 m, with a total dissolved solids content of 1600 mg/l.

NMP8 – E-W striking lineament

Site description

A roughly E-W striking lineament identified on aerial photographs and LANDSAT imagery was investigated with an electromagnetic and magnetic survey and a resistivity sounding (Figure 2-63). The surveys were conducted in a 90° angle to the feature from south to north.

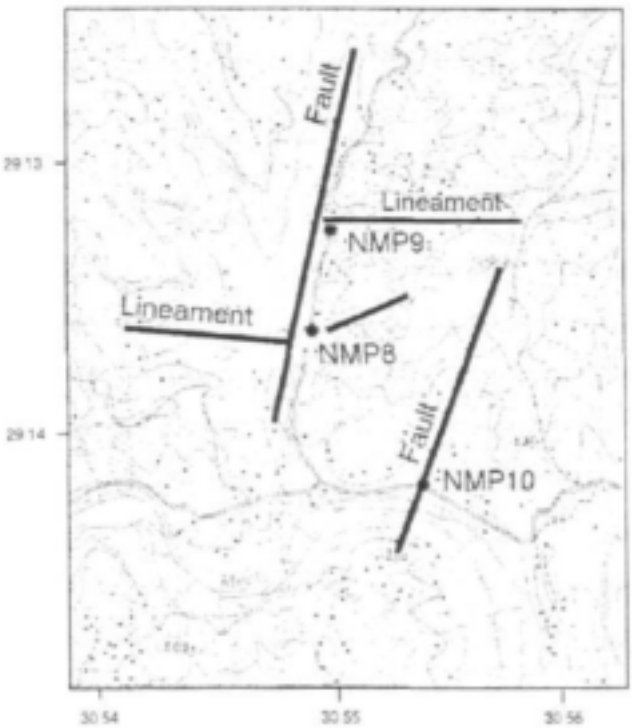

Figure 2-63 Position of site NMP8, NMP9 and NMP10

The Max-Min was operated at 4 frequencies, ranging from 220 Hz to 14080 Hz while the coil separation was set to 100m. A station spacing of 10m was selected. The magnetic and electromagnetic data are shown in Figure 2-69.

Electromagnetic survey
The electromagnetic response reflects a combination of the response of two ramp discontinuities in the overburden. The data for frequencies 880 Hz and higher are characterised by two minima in both the in-phase and out-of phase, bounding a central maximum in both phases from 120 to 250m, indicating a resistive zone of about 100m. At depth, the 220Hz frequency generates a single ramp discontinuity reflecting a distinct change in conductivity from 190m onwards to the NNE.

Magnetic survey
The magnetic data supports the Max-Min results, producing an anomaly at 190m of the traverse with a distinct increase in the total magnetic field intensity of about 150nT from south to north. The magnetic signature is characteristic of either a fault where a magnetic layer has been upthrown, or of a thick dyke-like or plate like feature, where a magnetic body intersects the host rock. The shape of the magnetic anomaly with a low in the south and a high towards the north of the structure indicates a normal magnetisation with the plate-like body extending towards the north.

Resistivity sounding
In addition, a resistivity sounding was carried out at the 100m locality of the traverse with the direction of AB expansion being N-S to try and determine the depth to bedrock. The data obtained is shown in Figure 2-70. The resistivity curve obtained describes a three layered earth case with $\rho 1 > \rho 2 < \rho 3$. The second layer represents a weathered overburden of about 10m thickness and a resistivity of approximately 75Ωm overlying resistive bedrock.

NMP9 – E-W striking lineament , intersecting a N-S striking fault zone
Site description
A geophysical survey was conducted over an E-W striking lineament, which intersects a N-S running fault zone (Figure 2-63). The lineament was identified on aerial photographs and LANDSAT imagery and is characterised in the field as a distinct depression in the topography. An electromagnetic and magnetic survey was conducted perpendicular to the feature from the south to the north. Additionally a resistivity survey was carried out to determine the depth to bedrock.

Electromagnetic survey
The Max-Min was operated at 4 frequencies, ranging from 220Hz to 14080Hz while the coil separation was set to 100m. A station spacing of 10m was selected. The electromagnetic data are shown Figure 2-71.

The electromagnetic data shows a broad anomaly for the first 100m of the traverse. The trough-like response indicates a thickening of the conductive overburden. A Borehole was sited in this zone at 80 m. From 100m onwards a constant response in the EM's graph is recorded, generating a homogeneous picture of the subsurface lithology for about 100m. This is followed by a sharp increase in the response amplitude indicating a further decrease in the subsurface conductivity towards the end of the traverse. A second borehole was sited at 190 m in this second trough, which also proved successful.

Magnetic survey
A magnetic survey was carried out over the lineament with a station spacing of 10m. The data is shown in Figure 2-71.

The magnetic data stays inconclusive for the first 170m of the traverse. Thereafter a distinct rise in response amplitude at the 190m locality indicates a change in the subsurface lithology, supporting the electromagnetic data.

Resistivity sounding
A resistivity sounding was carried out at 80m along the profile, at the southern flank of the trough-like anomaly of the electromagnetic traverse. Visual analysis of the sounding curve (Figure 2-70) indicates that it is a four layer curve H-A type curve with $\rho 1 > \rho 2 < \rho 3 < \rho 4$. Constant ρ values at short AB spacings indicate a resistivity of < 100 Ωm for the first three layers. Below 10m resistive bedrock is encountered, indicating a shallow overburden.

NMP 24 – N-S striking lineament
Site description
The site represents a N-S striking lineament that was observed on LANDSAT imagery as well as on aerial photographs (Figure 2-64). Magnetic and electromagnetic surveys were conducted perpendicular to the feature from the ENE to the WSW.

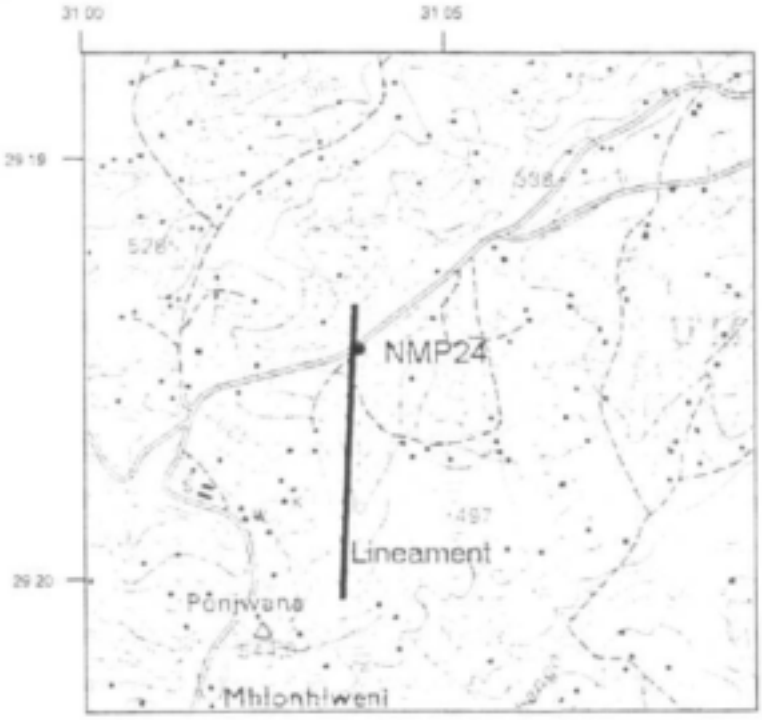

Figure 2-64 **Position of site NMP24**

Electromagnetic survey
The Max-Min response was recorded at 4 frequencies, ranging from 220 Hz to 14080 Hz while the coil separation was set to 100m. A station spacing of 20m was selected. Results are shown in Figure 2-72.

For all frequencies a trough-like anomaly is recorded, flanked by two positive shoulders, predominantly in the out-of phase component for the centre of the valley. At 14080 Hz the quadrature component looses its significance while the in-phase shows the anomaly more

clearly. The anomaly is about 90 m wide, which is almost equal to the coil separation. The response suggests a thickening of the conductive overburden between 140m and 240m of the traverse. A borehole was sited at 150 m, at the southern edge of the conductive zone.

Magnetic survey
Apart from an artificial magnetic anomaly caused by a bridge, no other anomalies exist indicating a magnetically homogeneous subsurface.

Resistivity sounding
An electrical sounding was carried out at station 15 at the northern edge of the electromagnetic anomaly with the direction of AB expansion being ENE-WSW. The results are shown in Figure 2-73. With $\rho1>\rho2<\rho3$ the subsurface can be described as a three layered earth case. By fitting the field curve to the master curve H35, the following values for the three layers were determined:

	Thickness (m)	Resistivity (Ωm)
Layer1	3.4	94
Layer2	2.2	3.76
Layer3	∞	resistive bedrock

NMP30 – Deeply incised wide valley striking form E to W
Site description
Site NMP30 is located within a deeply incised valley striking from E to W (Figure 2-65). Surrounding mountains drain from the north, east and south into the valley, which slopes gently from 600m in the west to 320m in the east, where it joins with the Hlimbitwe river valley. The topographical setting suggests a deep weathered profile for this site, which was investigated by a magnetic survey and a resistivity sounding. The magnetic survey crossed the valley from the NW to the SE, whereas the resistivity sounding was conducted in the centre of the valley with the direction of the AB expansion being NW-SE. The geophysical data is shown in Figure 2-73 and Figure 2-74.

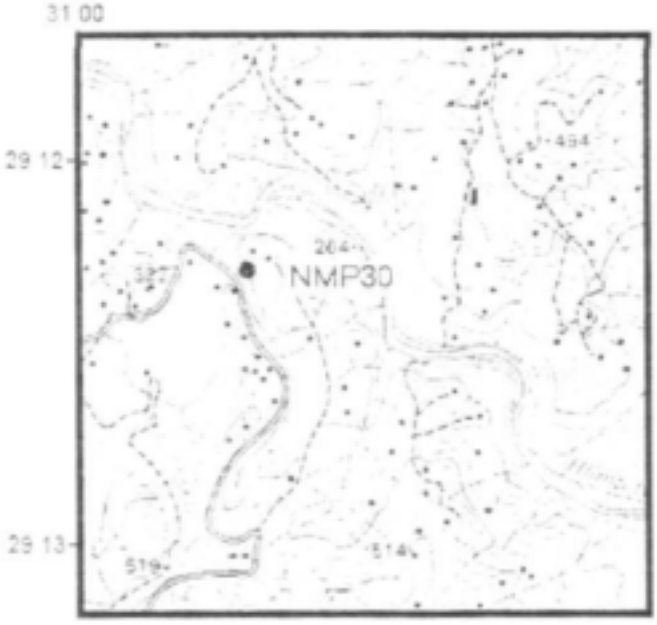

Figure 2-65 Position of site NMP30

Magnetic survey

To the north and south of the valley high magnetic field intensity values of around 28570nT are recorded bounding a magnetic low for the full extent of the valley. The magnetic response could reflect the weathering profile in the valley. Unweathered solid bedrock to the south and north are bounding the highly weathered valley centre, reflected by a low magnetic field intensity due to leaching of magnetic minerals following the weathering process.

Although no target feature could be detected geophysically, a borehole was sited by geological observation of the lineament orientation, which yielded 1.2 l/s.

Resistivity sounding

A resistivity sounding was carried out at the locality 170m of the magnetic traverse in the centre of the valley. Due to weather conditions (heavy rain) the data turns out to be partially noisy and could not be adequately interpreted.

Conclusion

The investigations carried out over 21 lineaments in the study area revealed that these features are often linked to zones of more deeply weathered overburden. The electromagnetic responses obtained are mainly ramp discontinuities or trough-like anomalies, where the positive peak is obtained over the resistive host and the negative peak over the conductive overburden. The magnetic data supports the electromagnetic profiles clearly showing different magnetic field amplitudes for the host rock and the weathered zones.

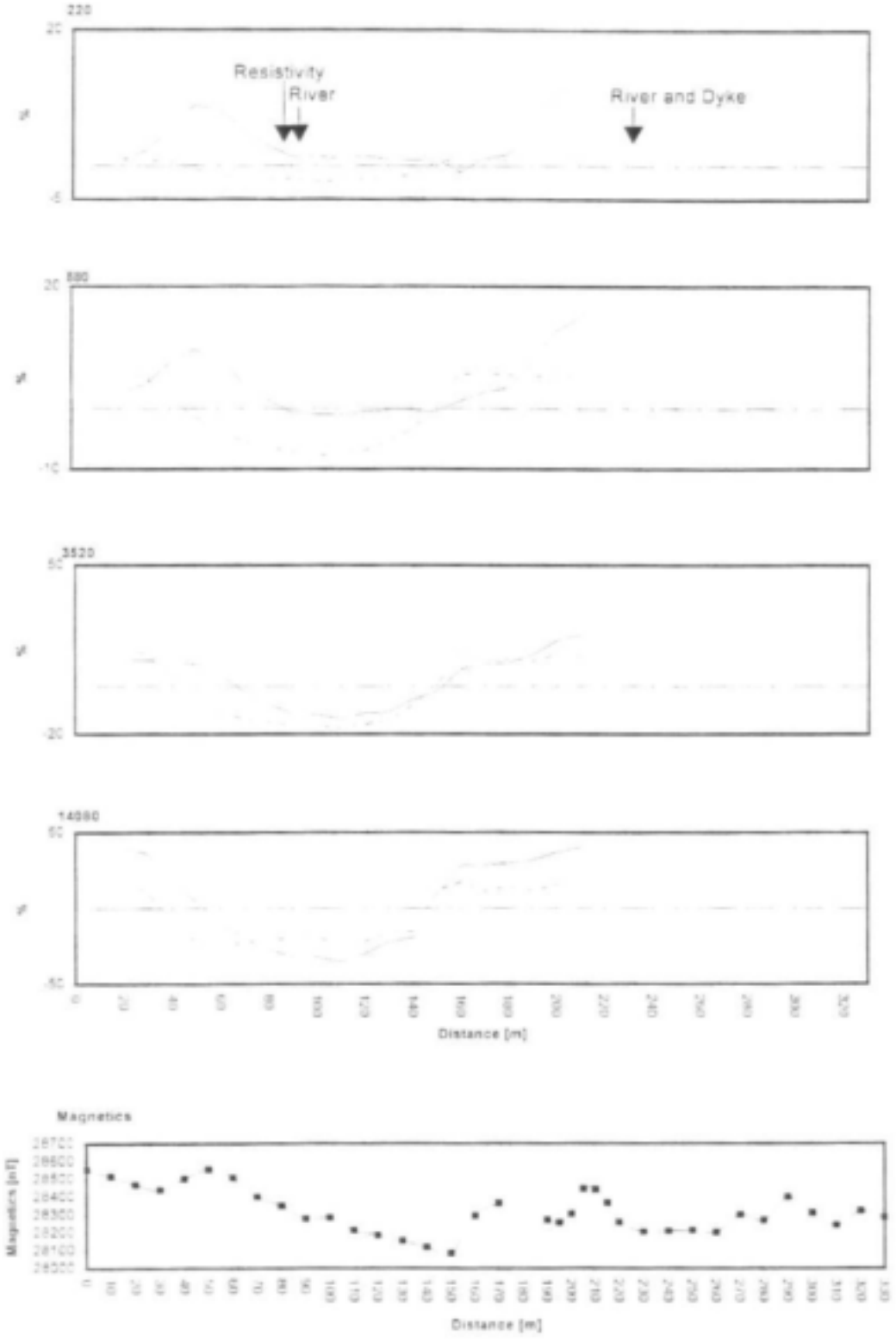

Figure 2-66 MAX-MIN electromagnetic and magnetic profiles at site NMP 2. Solid line: in-phase [%]; dotted line: out-of phase [%]; coil separation 100m, station spacing 10m. Traverse direction: SE-NW

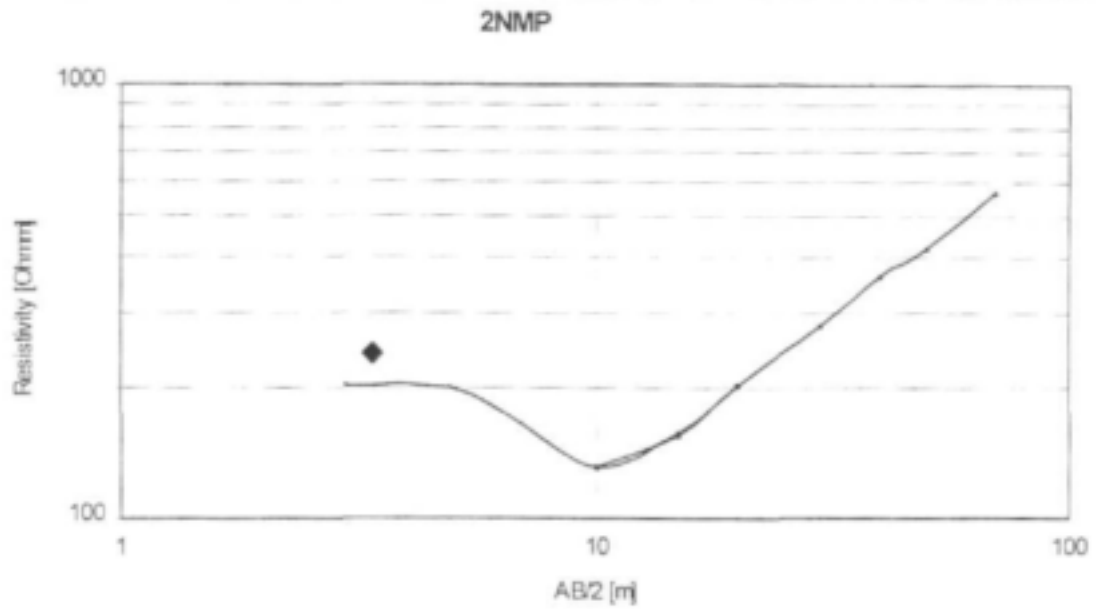
2NMP
1000
100
Resistivity [Ohmm]
1
10
100
AB/2 [m]

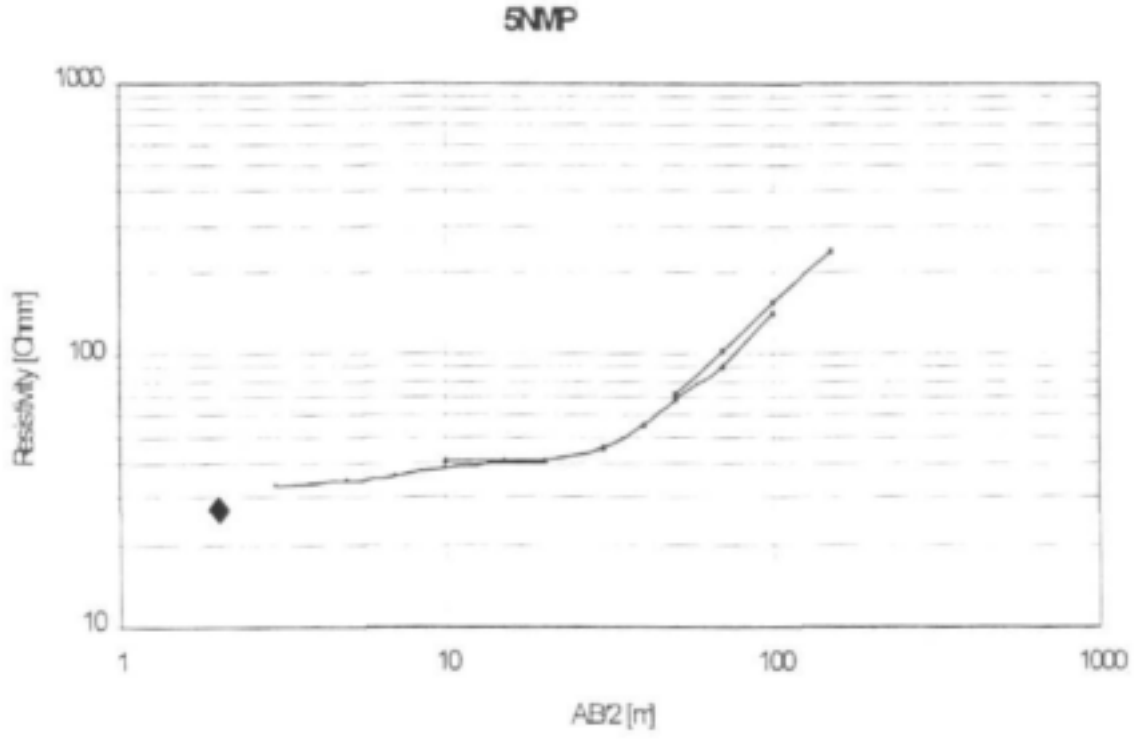
5NMP
1000
100
10
Resistivity [Ohmm]
1
10
100
1000
AB/2 [m]

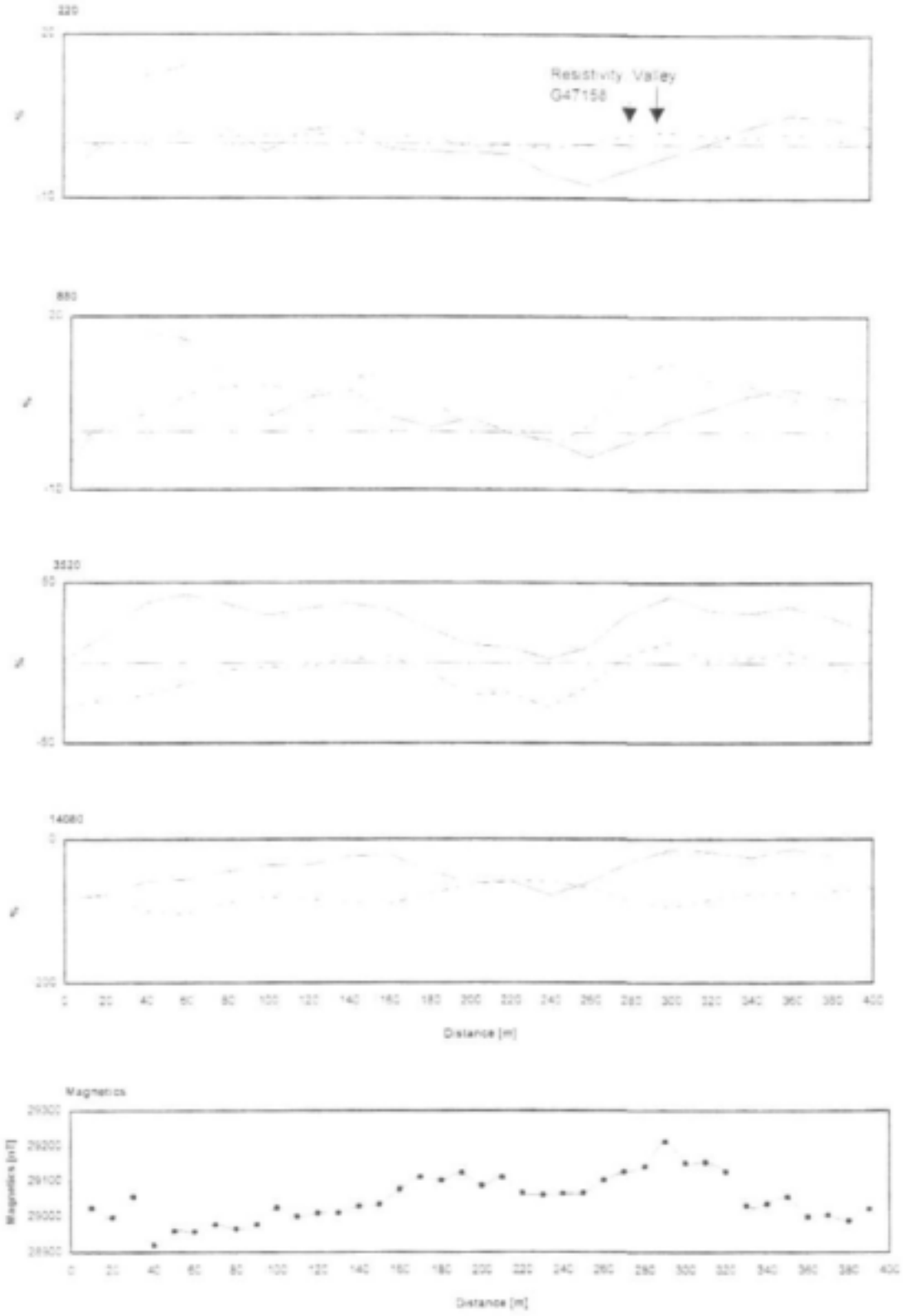

Figure 2-68 MAX-MIN electromagnetic profiles at site NMP 5. Solid line: in-phase [%]: dotted line: out-of phase [%]; coil separation 100m, station spacing 20m (Max-Min), 10m (Magnetometer). Traverse direction: SSW-NNE.

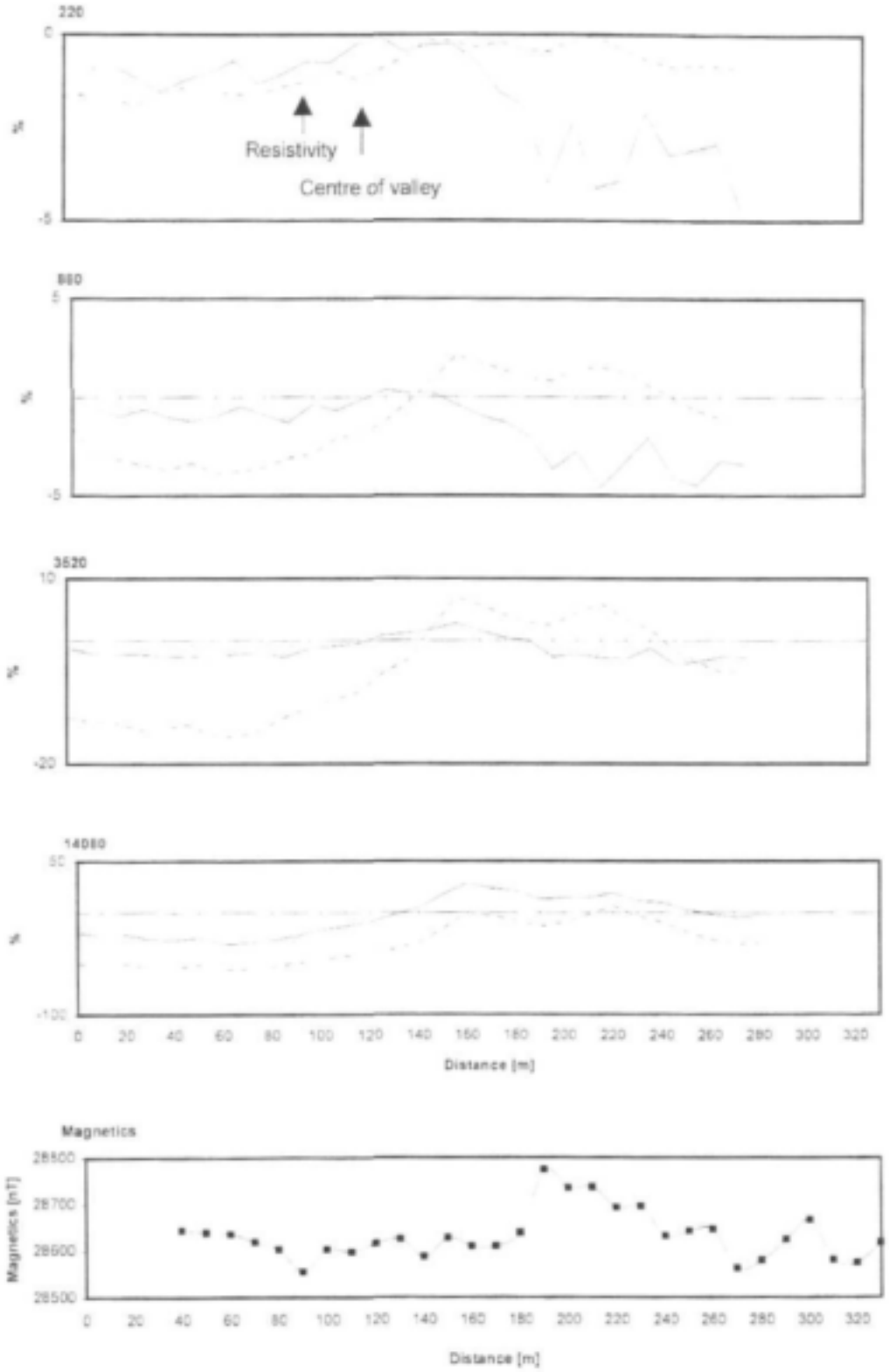

Figure 2-69 MAX-MIN electromagnetic and magnetic profiles at site NMP 8. Solid line: in-phase [%]; dotted line: out-of phase [%]; coil separation 100m, station spacing 20m. Traverse direction: SSW-NNE

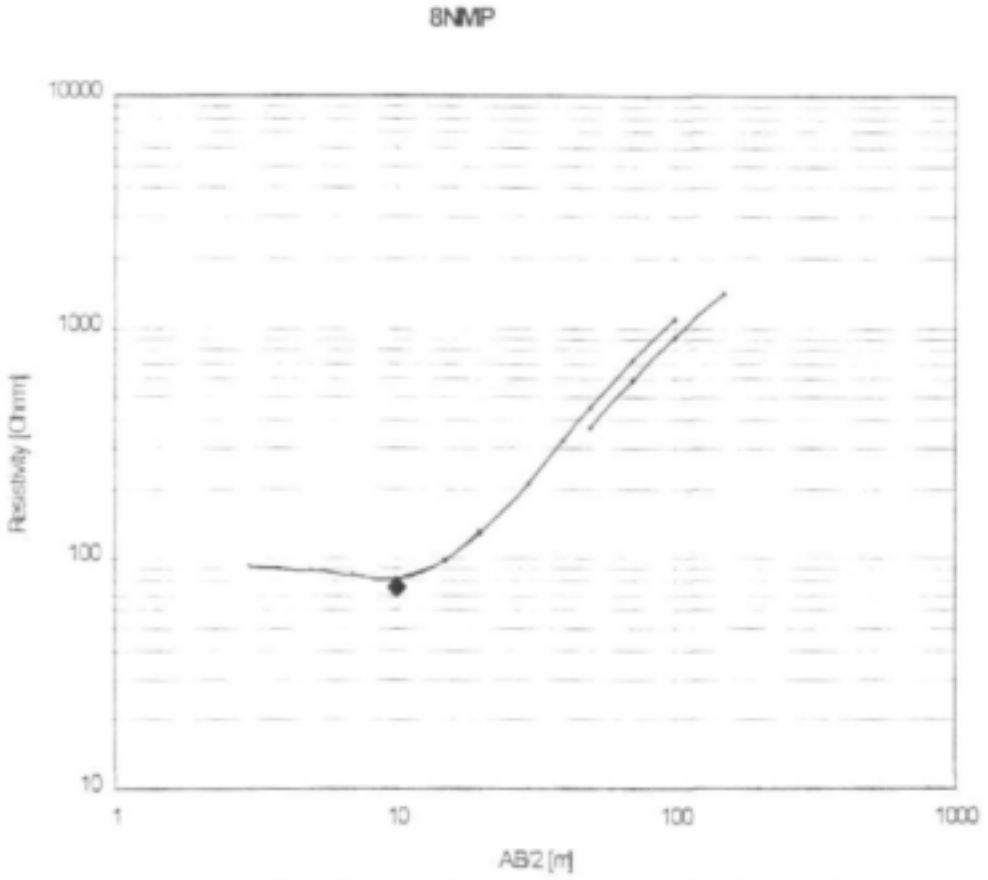

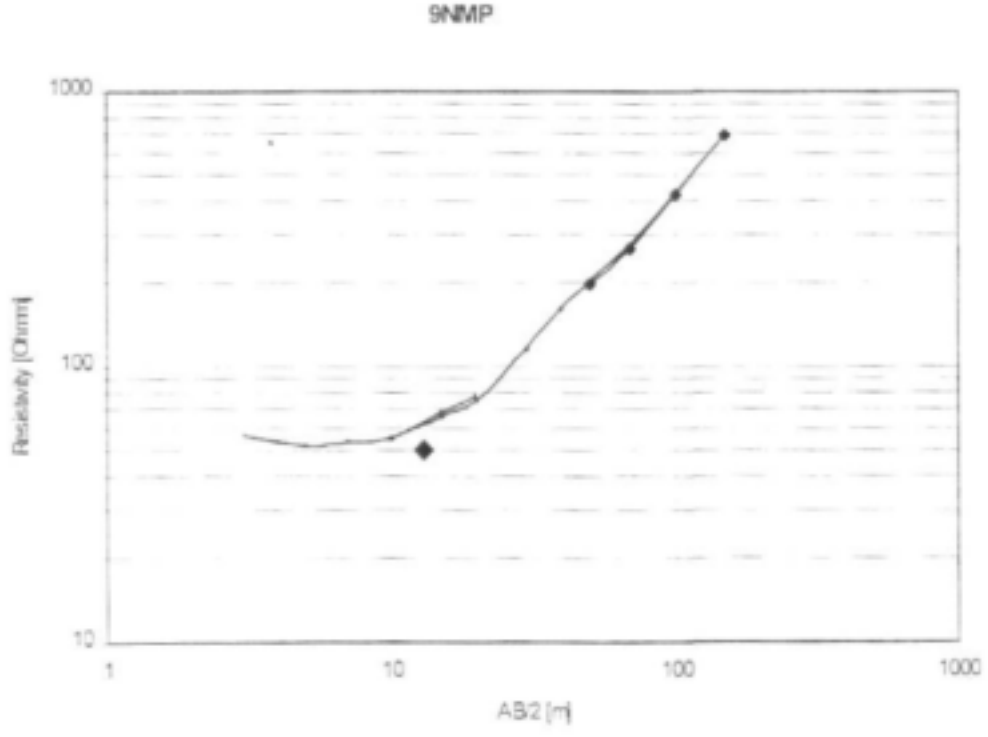

Figure 2-70 Resistivity data for station NMP8 and station NMP9. Black cross for master curve fitting.

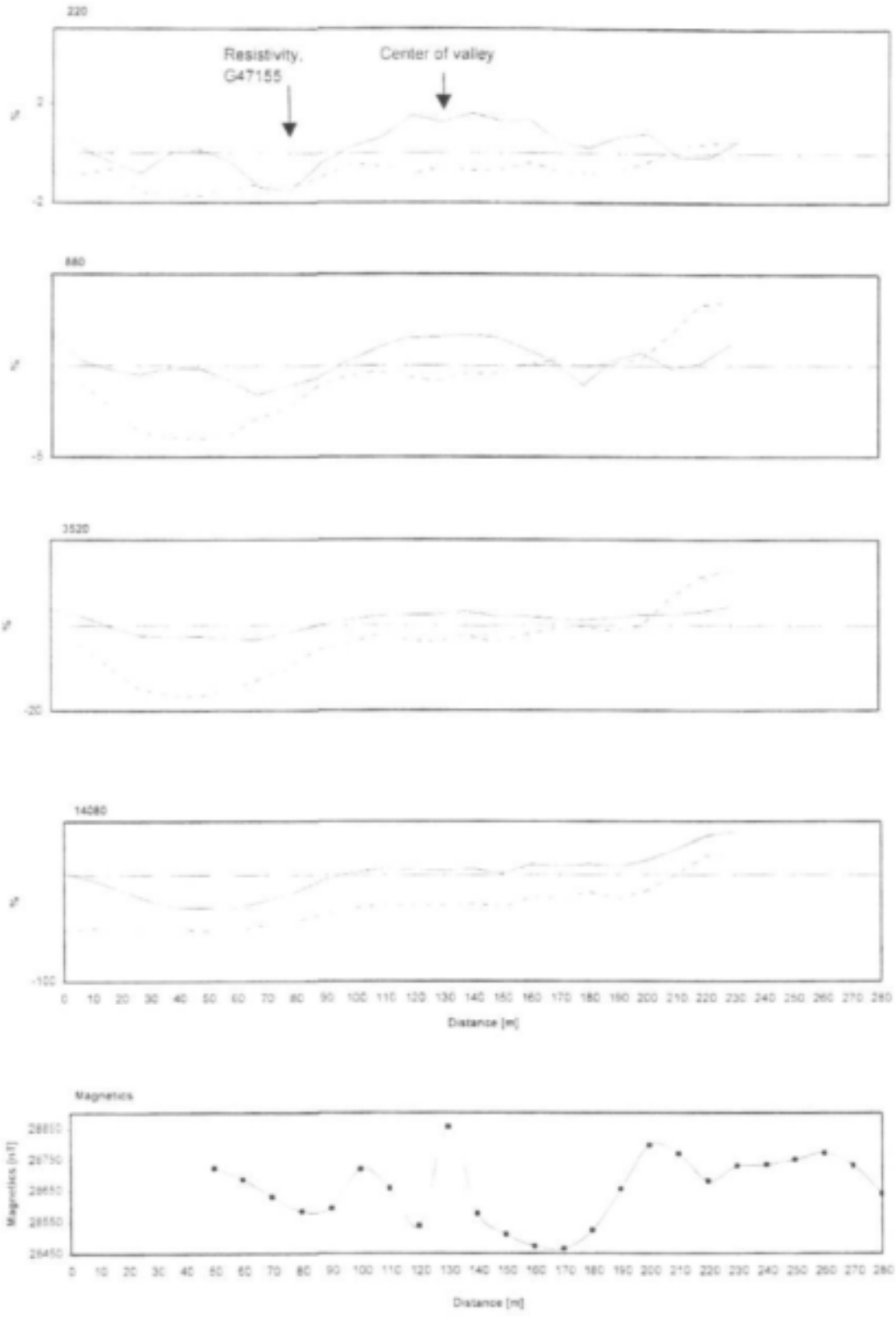

Figure 2-71 Max-Min electromagnetic and magnetic profiles at site NMP9. Solid line: in-phase [%]; dotted line: out-of phase [%]; coil separation 100m, station spacing 10m. Traverse direction: S-N

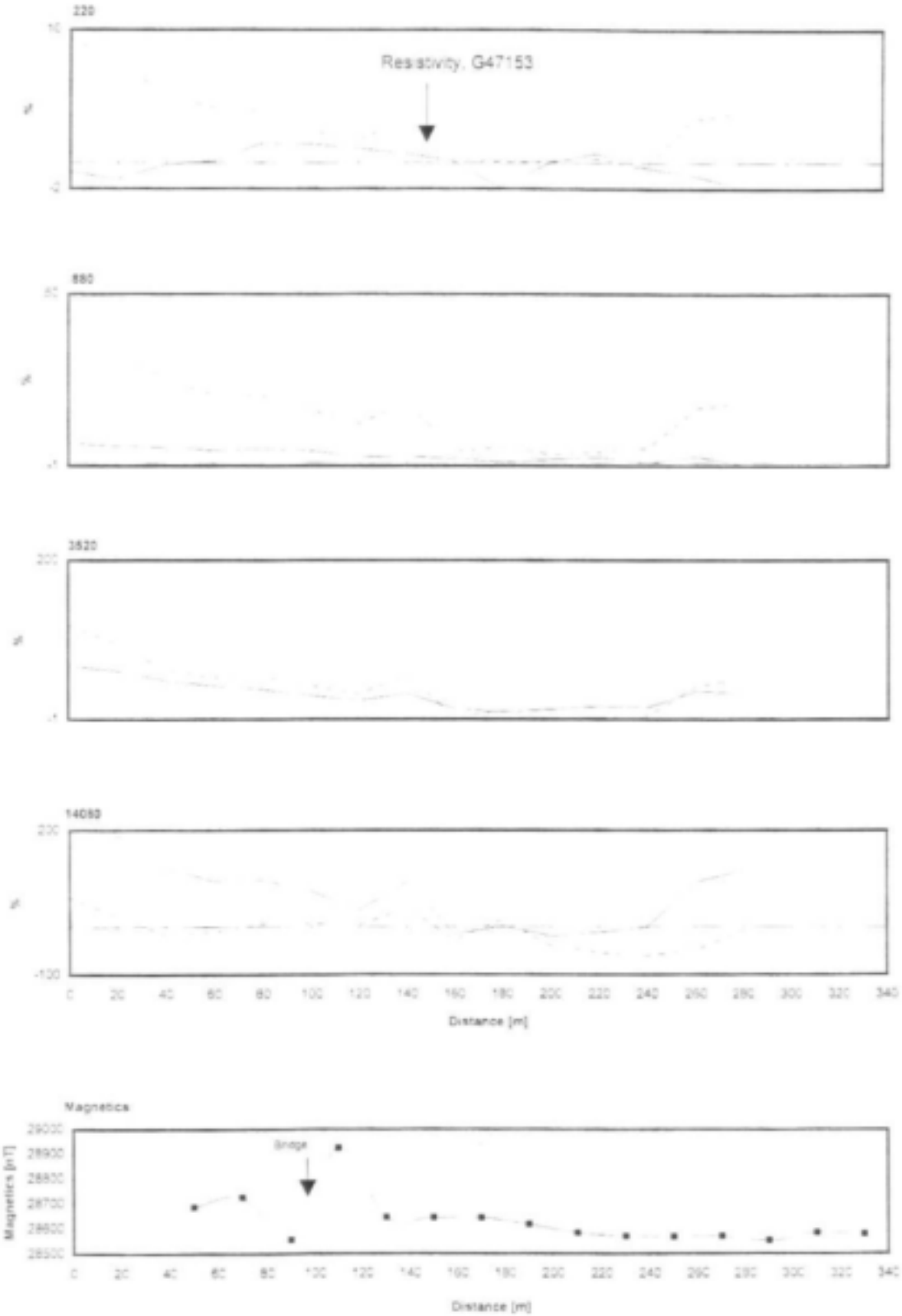

Figure 2-72 MAX-MIN electromagnetic and magnetic profiles at site NMP 24. Solid line: in-phase [%]; dotted line: out-of phase [%]: coil separation 100m, station spacing 20m. Traverse direction: ENE-WSW

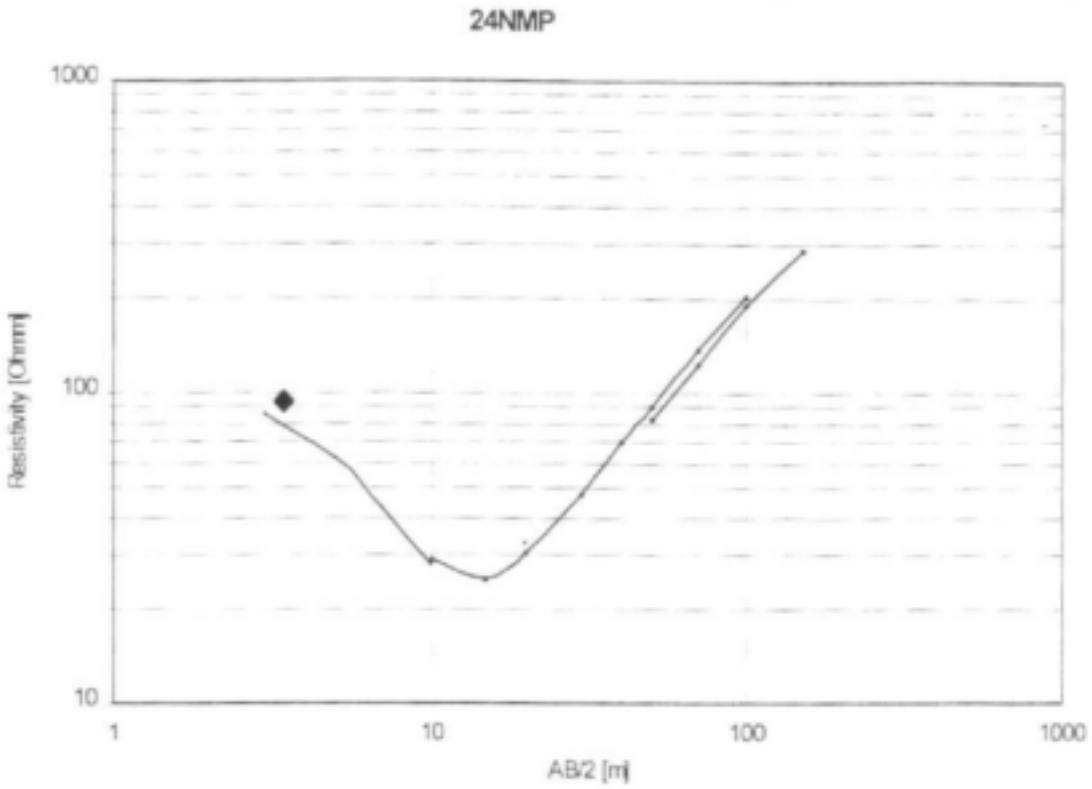

Figure 2-73 Resistivity data at station NMP24. Black cross for master curve fitting.

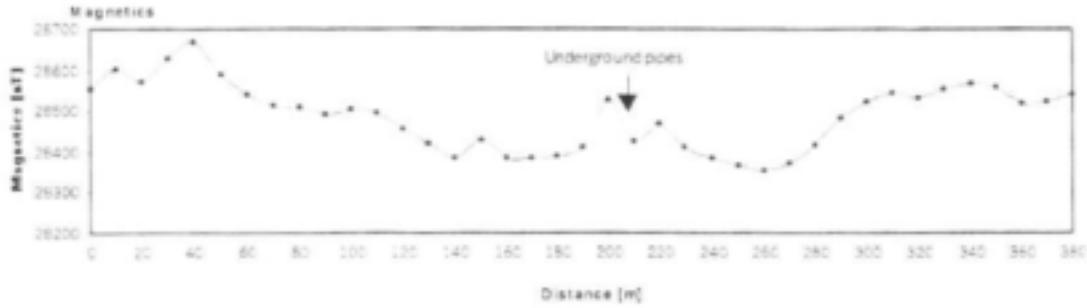

Figure 2-74 Magnetic data at site NMP30. Station spacing: 10m. Traverse direction: NW-SE

2.6.4 Dykes

Five magnetic and electromagnetic traverses were carried out over dyke structures. Dykes in the research area are generally thin: a few metres thick at most and compared with their occurrence in the Natal Sandstone, quite rare (Figure 2-80). None of the dyke structures investigated are identified on the Durban 1:250 000 geological map and all were detected during the field survey. These were not subsequently drilled as the water bearing properties of dolerite dykes is already well known. Geophysical traverses to characterise their geophysical signature

NMP6 – NE dipping dyke like structure and NW-SE striking lineament
Site description
A geophysical survey was conducted over a NW-SE striking lineament (Figure 2-75). The magnetic and Max-Min survey was carried out perpendicular to the feature from the NE to the SW.

Figure 2-75 Location of station NMP6, NMP15 and NMP29

Electromagnetic survey
The Max-Min was operated at 4 frequencies, ranging from 220Hz to 14080Hz while the coil separation was set to 100m. A station spacing of 20m and 10m for the Max-Min survey and the magnetic survey was selected respectively. The results are shown in Figure 2-78.

For the first 120 m, only slight variations of the in-phase and out-of phase components are recorded, indicating a homogeneous two layered earth case consisting of a conductive overburden over unweathered bedrock. From 240m to 360m a broad anomaly is recorded for frequencies 3520 and 14080Hz. The trough-like response indicates a thickening of the

conductive overburden. From 360m onwards a general increase in the in-phase and out-of phase components indicates a decrease in the thickness of the conductive overburden.

Magnetic survey

The magnetic data generates a well-defined anomaly NE of the Max-Min anomaly, which was not detected by the Max-Min. The shape of the anomaly indicates a dyke-like structure, dipping at about 30° to the NE. The total magnetic field intensity anomaly with a typical dipolar negative in the south and an increase in the north of the structure indicates a normal magnetization.

NMP19 – NE dipping dyke like structure

Site description

The intersection of a NW-SE and a NE-SW striking lineament was investigated at site NMP19 with an electromagnetic and magnetic survey (Figure 2-76). The surveys were carried out from the NE to the SW.

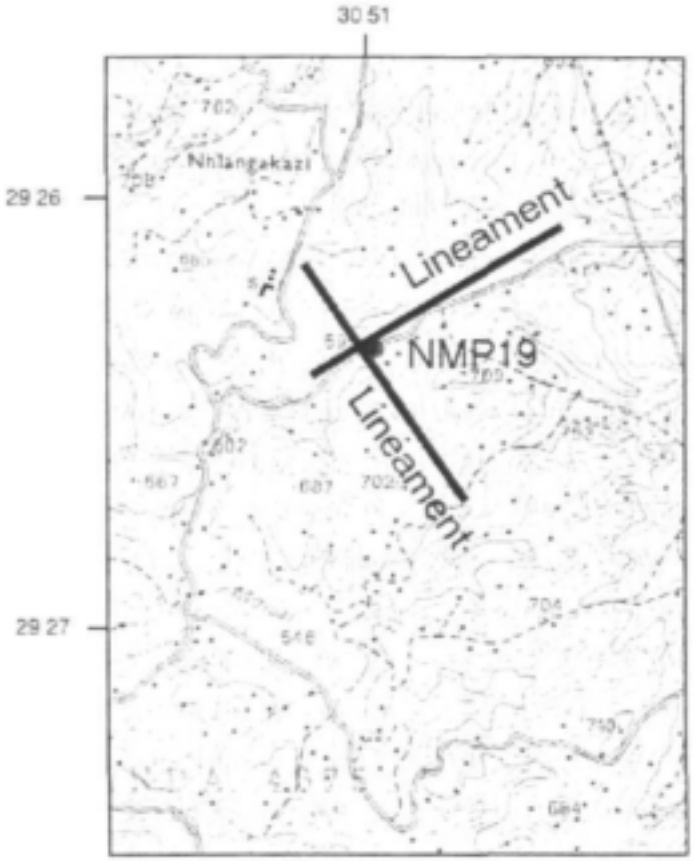

Figure 2-76 Position of site NMP19

Electromagnetic survey

The Max-Min was operated at 4 frequencies, ranging from 220Hz to 14080Hz while the coil separation was set to 100m. A station spacing of 10m for the Max-Min survey and the magnetic survey was selected. The results are shown in Figure 2-79.

The electromagnetic response depicts three peaks in the in-phase with the centre peak also repeated on the out-of-phase. However, the anomalies are of small scale and two of the three cases represent only one-point anomalies and may not be related to significant structural features.

Magnetic survey

The magnetic data produces a well-defined anomaly between 25m and 50m. The shape of the anomaly could indicate a dyke like structure, dipping at about 40° to the NE. The response amplitude is 380nT.

Conclusion

Dyke structures were located by magnetics but were proved to be of limited extent, with maximum thicknesses of only a few meters (Figure 2-77). Dyke structures were detectable only by magnetics and left no impact on the electromagnetic profile of the subsurface. Suprisingly, the lack of electromagnetic signature would indicate a low water bearing potential. This is confirmed by boreholes G47151 and G47152, both of which intersected and drilled through dolerite below the regional water level without intersecting water. This may be due to the NW orientation of the dykes, an orientation presumed to be compressional.

Figure 2-77 Dolerite dyke intruded into gneiss

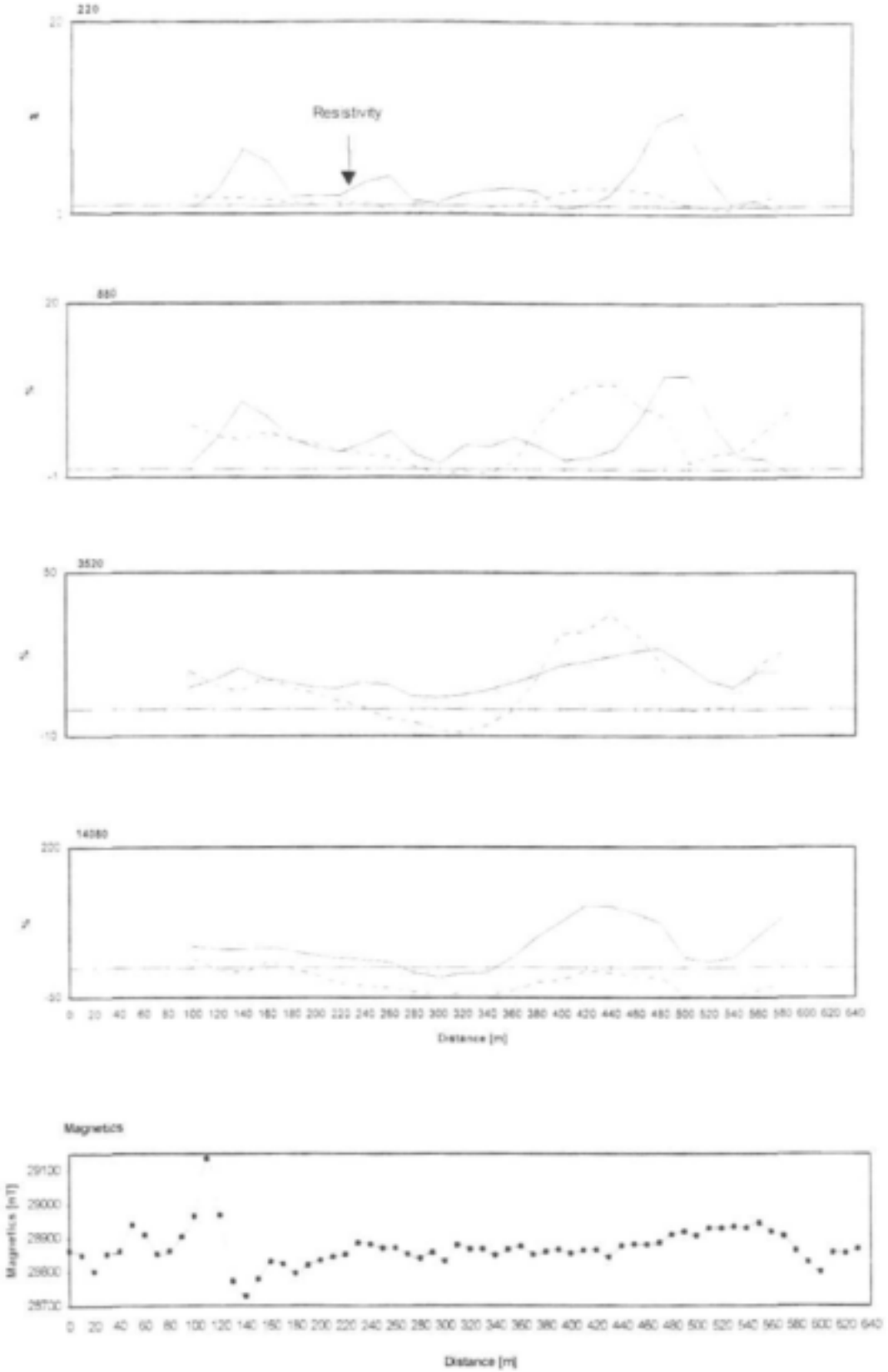

Figure 2-78 MAX-MIN electromagnetic and magnetic profiles at site NMP 6. Solid line: in-phase [%]; dotted line: out-of phase [%]; coil separation 100m, station spacing 20m. Traverse direction: NE-SW

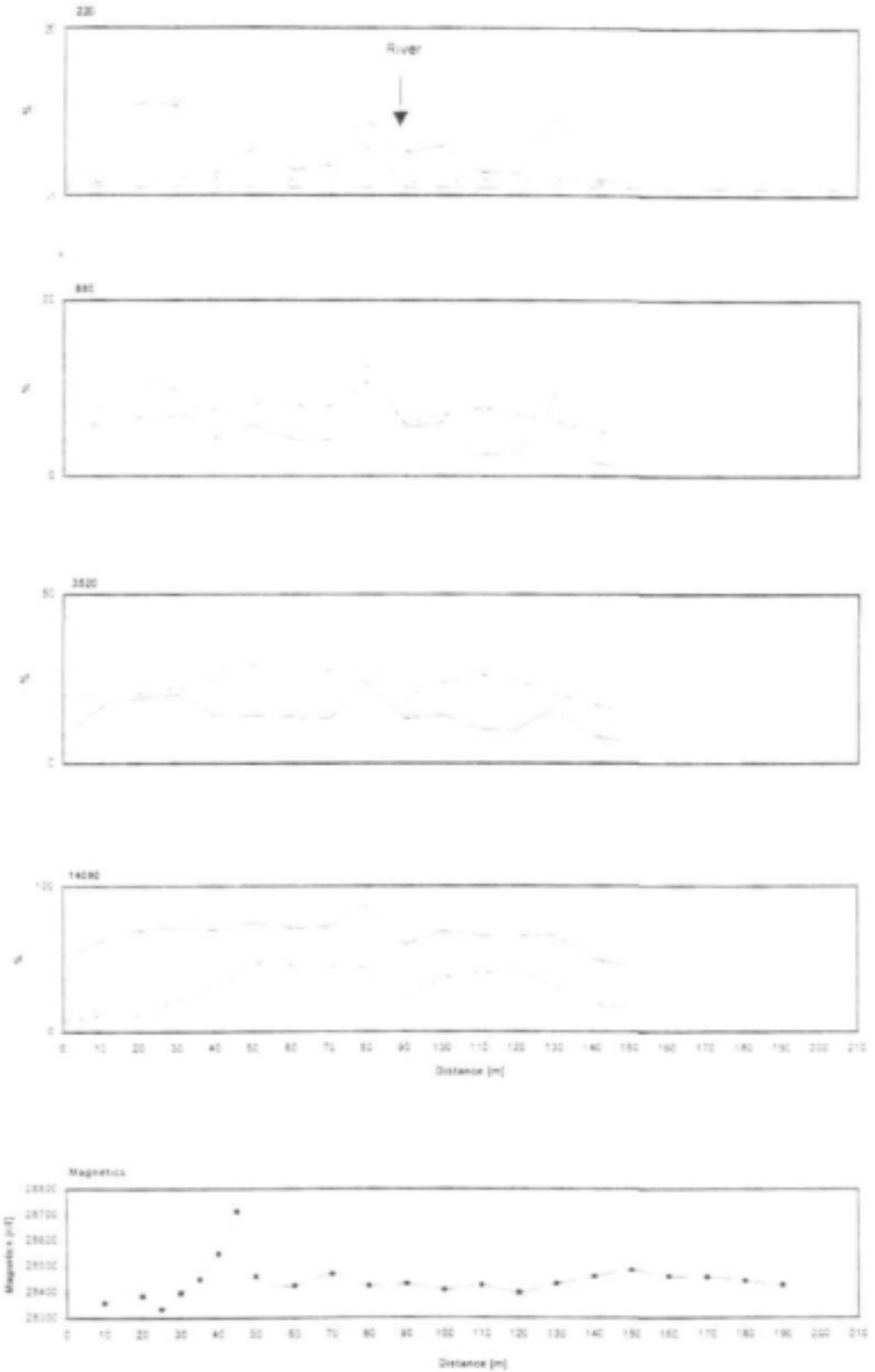

Figure 2-79 MAX-MIN electromagnetic profiles at site NMP 19. Solid line: in-phase [%]: dotted line: out-of phase [%]: coil separation 100m, station spacing 10m. Traverse direction: NE-SW

Figure 2-80 **Distribution of dykes in the study area**

2.7 Drilling Results

To investigate geological and structural features in the study area, nine boreholes were drilled in the research area. Drilling was carried out by the Department of Water Affairs and Forestry using normal air percussion drilling. Due to sidewall stability problems, ODEX was required on two of the nine boreholes.

The drilling sites were chosen to cover fault zones and all four major joint orientations, as delineated through the structural analyses. The geological logs and construction details, which are shown in Appendix 2-B, are summarised below in terms of depth, water strike, blow yield and geological feature investigated.

Table 2-6 Summary of Drilling Results

Borehole	Depth (m)	Water Strike (m)	Blow Yield (l/s @ depth)	Feature	Site ID of geophysical survey
G47151	82	35.5, 76	0.5 @ 35.5 0.37 @ 76	NE-SW striking mylonite zone	NMP27
G47152	102	59, 64, 92.2	0.2 @ 59, 0.1 @ 64, 3.7 @ 92.2	NE-SW striking mylonite zone	NMP27
G47153	84	60.8, 73.4	1.1 @ 60.8, 0.69 @ 73.4	N-S running lineament	NMP24
G47154	84	51	3.3 @ 51	E-W striking lineament and N-S running fault	NMP9
G47155	96	64.2, 72.5	0.83 @ 64.2, 0.17 @ 72.5	E-W striking lineament and N-S running fault	NMP9
G47156	102	9.8, 30.7, 73.2	0.54 @ 9.8 0.2 @ 30.7 0.7 @ 73.2	E-W striking wide weathered zone	NMP30
G47157	102		Dry	SW-SE running fault crosses a SW-NE running fault	NMP4
G47158	84	17.9 - 20.6	4.0 @ 17.9-20.6	NE-SW striking lineament	NMP5
G47159	82	62.4	6.6 @ 62.4	E-W running fault	NMP15

Borehole G47151 and G47152 on site NMP27

Borehole site

Borehole G47151 and borehole G47152 were drilled to investigate the hydrogeological significance of a wide mylonite zone striking from NE to SW (Figure 2-81). Whereas G47151 was drilled at locality 100m on the electromagnetic and magnetic traverse NMP27 within the mylonite zone, G47152 was drilled close to the contact of the mylonite zone and the unweathered gneiss, at 140m of the geophysical traverses.

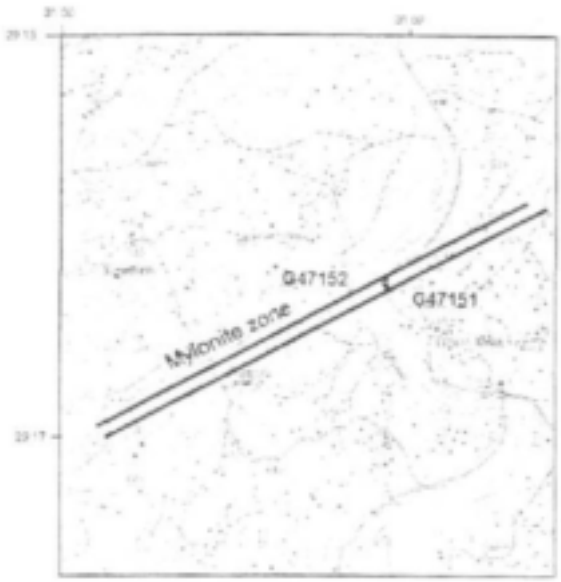

Figure 2-81 Position of borehole G47151 and G47152 on site NMP27

Geological description

Borehole G47151 was drilled into the Oribi Gorge Granite. From 0 to 10m, weathered overburden was encountered, consisting of clay, sand and weathered granite. Subsequently the borehole was cased to 11.62m using 165 x 4.5mm steel casing. A 5m thick transition zone between granite and gneiss followed. Reddish-black partly fractured gneiss continued down to 56m, with penetration rates varying between 2.5 and 5min/m. At 35.5m the first water strike was encountered, producing a yield of 0.5l/s. With a sharp increase in penetration rates, a black dolerite intrusion was encountered at 56m. The contact is only slightly weathered, and no water strike was encountered. From 64m to the final depth of the hole the geology consists of partly fractured gneiss. A small fracture zone at 76m resulted in a second water strike of 0.37l/s, bringing the total yield of the borehole to 0.87l/s. The borehole was developed for 30min by airlift.

The penetration of gneiss below the granite suggests that the intrusion is a mushroom shaped diapir, an interpretation further confirmed by the presence of augen gneiss nearby (Thomas, 1988). The presence of mylonitic augen gneiss confirms that the boreholes tap a post emplacement ductile shear zone.

The first 13m of borehole G47152 consists of weathered granite and gneiss and consequently, the borehole was cased to a depth of 17.70m using 4.5mm steel casing. Fresh gneiss followed to 36m. A 2.5m zone of weathered gneiss preceded a weathered dolerite intrusion of 7.8m thickness encountered at 38.5m depth. A cross-section between borehole G47151 and G47152 indicates that the dolerite intrusion dips with 22° to the south. However, as in borehole G47151, no water strike occurred at the upper or lower contact of the intrusion, despite the fact that the intrusion is situated below the rest water level. From 46.3 to the final depth of the hole at 102m, gneiss bedrock was encountered, with occasional calcite filled fractures. These fractures were the source of the first two minor water strikes at 59 and 64m depth. A third water strike was encountered when a large fracture zone was penetrated at 92 m. This strike yielded 3.7l/s bringing the total blow yield of the borehole to 4l/s. The borehole was developed for 30 min by airlift.

Borehole G47153 on site NMP24

Borehole site

Borehole G47153 was drilled on a N-S running lineament delineated from LANDSAT imagery and aerial photographs (Figure 2-82). A trough-like electromagnetic anomaly indicates a 90m wide zone of deep weathering. On the basis of the electromagnetic data borehole G47153 was drilled at 150m of the traverse at the northern edge of the conductive zone.

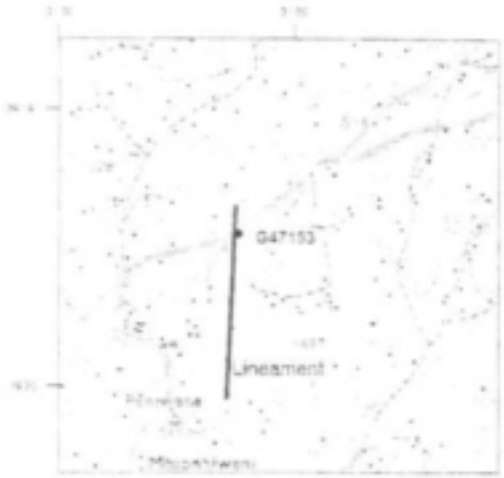

Figure 2-82 Location of borehole G47153 on site NMP24

Geological description

Borehole G47153 was drilled into the Oribi Gorge Granite. It was characterised by a deep weathered zone. Up to a depth of 33m weathered gneiss and amphibolite were encountered. Subsequently the borehole was cased to a depth of 35.46m using 4.5mm steel casing. Solid bedrock was encountered at 33m and consisted of reddish black amphibolite until the final depth of the borehole at 84m. Between 60.6 and 66m and 72 and 75m depth calcite filled fractures were encountered. These fracture zones produced the two water strikes at 60.8m and 73.4m with a yield of 1.1 and 0.69l/s respectively. The final blow yield of borehole G47153 was measured as 1.8l/s. The borehole was developed for 30min by airlift.

Borehole G47154 on site NMP9

Borehole site

Borehole G47154 was drilled to investigate a prominent N-S running fault, mapped on the Durban 1:250000 geological map (Figure 2-83). A deeply incised valley indicates the fault in the field. Because of accessibility problems no geophysical traverses could be conducted over the selected drilling site, where the fault was postulated based on geological observations. However, electromagnetic and magnetic profiles were carried out on traverse NMP9 25m away, parallel to the fault zone. The borehole was sited parallel to the 190m locality on these traverses, where a distinct increase in the magnetic field intensity indicates a change in the subsurface lithology. However, as the traverse does not intersect the fault zone, the geophysical data has to be taken with caution as it might differ from conditions at the borehole site itself.

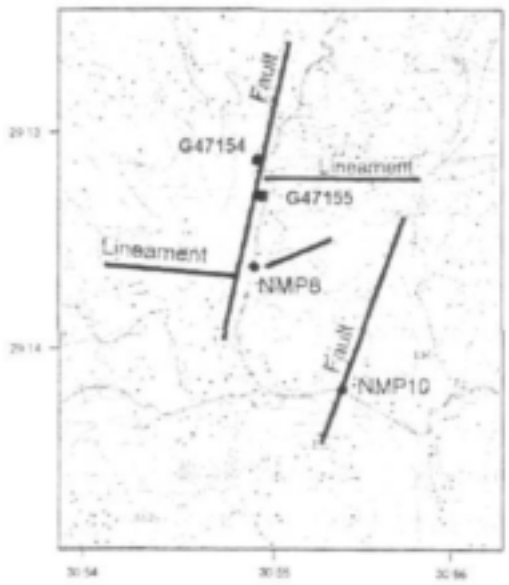

Figure 2-83 **Location of borehole G47154 and G47155 on site NMP9**

Geological description

Borehole G47154 was drilled into the Quha Formation. Deeply weathered bedrock was encountered. The geology consists of highly weathered gneiss interlayering with weathered amphibolites to a depth of 49m. At the contact between the weathered and unweathered bedrock a water strike with a yield of 3.3l/s was encountered. Interlayered bedding of gneisses and amphibolites were encountered up to the final depth of the borehole of 84m. Varying penetration rates characterise the amphibolite as the slightly softer and the gneisses as the harder rock type. No water strikes were encountered at these lithological contacts.

Borehole G47155 on site NMP9

Borehole site

Borehole G47155 was drilled to investigate an E-W striking lineament, which intersects the N-S running fault described above (Figure 2-83). The lineament is characterised in the field by a distinct depression in the topography. Borehole G47155 was drilled at the 80m locality of the electromagnetic traverse, at the southern flank of a trough-like anomaly, which is indicating the thickening of the conductive overburden.

Geological description

Borehole G47155 was drilled into the Quha Formation (Nbi) and showed a deep weathering profile similar to borehole G47154. Alternating weathered gneiss, granite and amphibolites were penetrated up to 61m, consequently the borehole had to be cased down to a depth of 59.4m using 4.5mm steel casing. A water strike was encountered at 64.2m, at the contact between the weathered and unweathered bedrock, producing a yield of 0.8l/s. Until the end of the borehole at 96m, interlayered bedding of gneiss, granite and amphibolite was encountered. A small scale fracture zone produced a second water strike at 72.5m with a yield of 0.17l/s, giving a final blow yield for borehole G47155 of 1.0l/s. The borehole was developed for 30min by airlift. As observed in borehole G47154 lithological contacts did not produce any

water strikes, and groundwater is associated only with fracture zones and contacts between weathered and unweathered bedrock.

Borehole G47156 on site NMP30

Borehole site

Borehole G47156 was drilled to investigate the hydrogeological significance of a deeply weathered profile along an E-W striking valley (Figure 2-84). The borehole was drilled at 170m of the magnetic traverse on the basis of the magnetic data and the resistivity sounding, which confirm a deeply weathered profile for the centre of the valley.

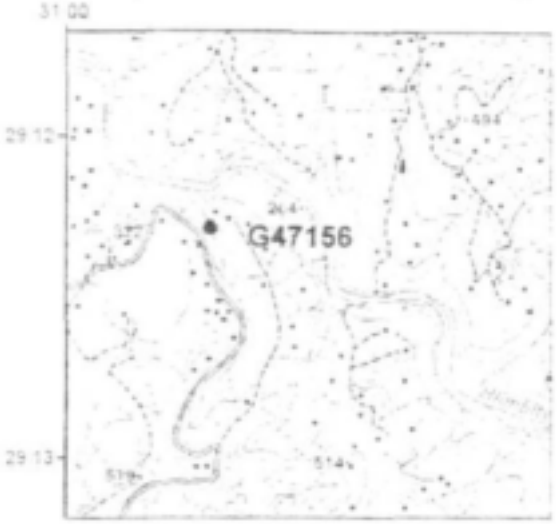

Figure 2-84 Position of borehole G47156 on site NMP30

Geological description

Borehole G47156 is situated within the Quha Formation (Nbi). The hole penetrated weathered overburden down to a depth of 11m and conditions were such that ODEX equipment had to be used down to a depth of 11.5m. The first water strike occurred within the weathered overburden at 9.8m, yielding 0.5l/s. Unweathered solid bedrock was encountered at 15m depth. Until the end of the borehole at 102m, partly fractured granite was encountered. Pyrite and biotite content vary throughout the profile. Small fracture zones at 30.7m and 73.2m yielded water in excess of 0.2l/s and 0.7l/s respectively resulting in a final blow yield of the borehole of 1.44l/s. The borehole was developed for 30 minutes by airlift.

Borehole G47157 on site NMP4

Borehole site

Borehole G47157 was drilled to investigate a NW-SE striking fault zone, mapped on the 1:250 000 geological map Durban within the Oribi Gorge granites (Figure 2-85). The site was investigated with a magnetic and electromagnetic survey and a resistivity sounding and a detailed discussion of the results is given in chapter 5.6, page 5-44. Borehole G47157 was sited at 100m of the electromagnetic and magnetic traverse, where the geophysical data indicates a distinct change in the subsurface lithology from solid bedrock to a wide weathered zone.

Geological description

Borehole G47157 penetrates through 9m of weathered overburden until, with a sharp increase in penetration rate, solid bedrock was encountered, confirming the resistivity sounding data. Until the final depth of 102m the borehole penetrates through partly fractured gneiss rock with varying contents of pyrite. At a depth of 50m, the penetration rate increases considerably and it may be suspected that a fracture zone or a fault was encountered. Either because of the high altitude of borehole G47157 or because of the fact that the NW-SE orientation is not extensional in nature, no water strike was encountered. The borehole was backfilled.

Borehole G47158 on site NMP5

Borehole site

A prominent large-scale NE-SW striking lineament was the target for borehole G47158 (Figure 2-85). Electromagnetic and resistivity data indicated a thick weathered overburden at the site. The borehole was drilled at 280m locality on the geophysical traverses on the basis of the electromagnetic and resistivity data.

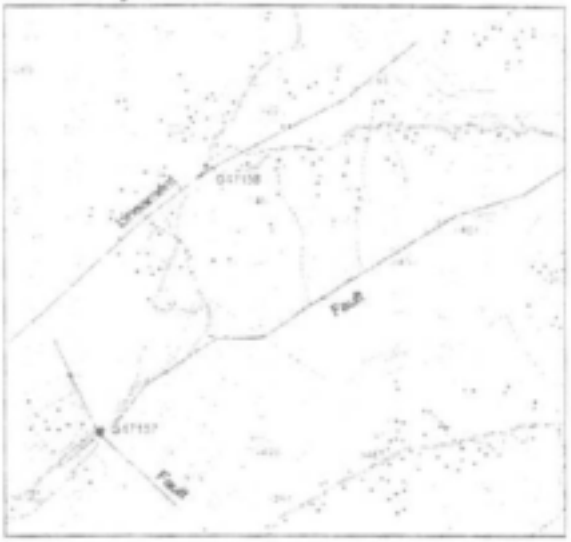

Figure 2-85 Position of borehole G47157 and G47158 on site NMP4 and NMP5 respectively

Geological description

According to the Durban 1:250000 geological map, borehole G47158 is drilled into the Oribi Gorge granites. However, the log shows a weathered gneiss profile reaching down to 24m. At 17.9m, within the weathered zone, the first water strike occurred. The yield increased steadily up to a depth of 20.6m and the final blow yield of G47158 was measured as 4l/s. The borehole was cased to a depth of 23.46m using 4.5mm steel casing, with the bottom 7m being slotted.

At 24m the lithology changes from weathered gneiss to unweathered amphibolite bedrock and a sharp increase in penetration rate is observed. At 52m the borehole penetrates through gneiss characterised by slightly faster penetration. From a depth of 64 to the final depth of 84m solid amphibolite was encountered. No further water strikes were observed at the lithological contacts between gneiss and amphibolite.

Borehole G47159 on site NMP15

Borehole site

An E-W striking fault zone mapped on the 1:250 000 geological map Durban was the target of borehole G47159 (Figure 2-86). Borehole G47159 was drilled at 160m on the electromagnetic traverse, at the contact between a higher and lower conductive zone.

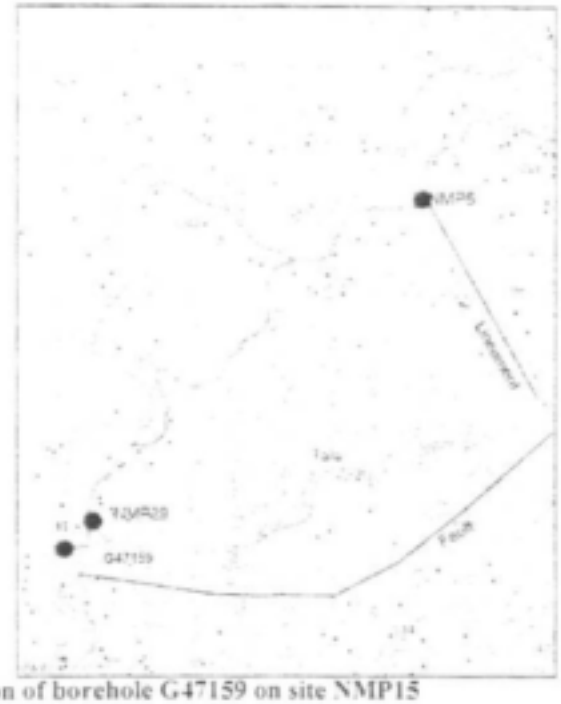

Figure 2-86 Position of borehole G47159 on site NMP15

Geological description

The first 5.52m of borehole G47159 were drilled with ODEX equipment as the highly weathered overburden consisting of residual dolerite, gneiss and granite threatened to collapse. Thereafter, slightly weathered gneiss was encountered and normal air percussion drilling could be used. At 25m unweathered bedrock is encountered, confirming the resistivity data, and at 30m depth a lithological change from gneiss to amphibolite occurs. Thereafter an inter-layered sequence of gneiss and amphibolite is observed. At 62.4m water is encountered associated in a large feldspar rich fracture zone. The blow yield was measured as 6.6l/s.

Conclusion

The geological logs suggest that Natal Metamorphic Province aquifers occur both within the thick weathered residual overburden and within the fractured bedrock itself. Hence the aquifer can be considered as being fractured and weathered. Lithological contacts do not appear to be water bearing. The contacts between dyke structures and the host rock also did not prove to be water bearing. In general, higher yields occur in the fractured portion of the aquifer due to greater confining pressure, however, borehole G47158 encountered 4 l/s within the weathered zone.

A correlation between lineament or fault azimuth and yield shows that successful boreholes are associated with N-S, E-W and NE-SW running structural features, orientations of extensional nature. The only unsuccessful borehole was drilled into a NW-SE fault, the orientation regarded as compressional in nature. However, results may not be conclusive as they are based on nine boreholes only. The wide range of azimuth trends related to successful boreholes may also indicate a pervasive influence such as erosional unloading is operating on

all existing fracture systems. The four highest yielding boreholes are associated entirely with regional scale structural features, which suggests that a strong correlation exists between yield and lineament or fault length.

In conclusion, the drilling results suggest that the highest yielding boreholes in the Natal Metamorphic Province are associated with extensional structural features of regional scale, which are often associated with particularly deep weathering profiles. However, the structural control of groundwater occurrence can be overwritten by the local morphology. At high altitude boreholes can prove to be unsuccessful even though drilled into a favourable structural feature, if the hole intersects the feature above the local static water level.

2.8 Test Pumping

A constant discharge test was carried out on all of the newly drilled boreholes in order to characterise hydraulic properties of the penetrated lithologies, to assist with developing a conceptual model of aquifers, and to determine sustainable borehole yields. The test pumping and recovery data are presented in Appendix 2-C.

Pump test G47151

Borehole G47151 had two water strikes at a depth of 35.5m (0.5l/s) and at a depth of 76m (0.37l/s). The final blow yield was measured as 0.9l/s and the rest water level of the hole is 12.27m below surface, giving an available drawdown of 23 m. The pump was set at 78m below surface during the test. Borehole G47151 was then pumped at a rate of 1l/s for 12h.

The drawdown curve shows a linear decline on the semi-log drawdown curve and an approximately horizontal line on the derivative curve throughout the 12h-discharge test, reflecting radial flow conditions. At 12.5-15, 17-18m and 19-22m steps in the semi-log drawdown and humps in the derivative curve indicate a dewatering of small fracture networks, yet the derivative curve indicates that no boundaries are encountered. This suggests that the aquifer consists of a network or hierarchy of fractures. Since drawdown continues at a line of equal slope after each step, the fracture networks are of relatively uniform permeability. After about 8 h of pumping drawdown intercepts the main fracture zone at a depth of 35m. For the remaining 4h of the discharge test, the water level stabilises as dewatering occurs. However, as drawdown has reached already the main water strike, it can be expected that boundary conditions would be encountered if pumping continues. Consequently, the boundary conditions are taken as the point of dewatering of the first water bearing fracture and this point is considered equivalent to a single barrier boundary.

The recovery of borehole G47151 was monitored for 12h. The data shows that after 180min since pumping was stopped, the recovering of the water level slows down, probably due to the rewatering of microfractures. After 12h, where the recovery time for the borehole is equal to the preceding pumping time, the water level has recovered to within 1.57m below the original rest water level. The incomplete recovery indicates a limited storage or extent of the aquifer. No evidence of leakage from an overlying weathered zone is noted, hence storage is limited. For this reason, a hydrogeologist must be conservative when recommending a yield for this hole.

Calculated transmissivity values are presented in Table 2-7. The transmissivity, calculated on the basis of the early time data represents a mean fracture transmissivity (Tf), valid for the period before the main water strike is dewatered. A late transmissivity value cannot be measured as no barrier boundary is encountered within the pumping time of 12h. However, as the two water strikes are approximately equal, it was assumed that each water strike has a T value of approximately 1 m^2/d. Hence late T is estimated at 1 m^2/d.

Borehole G47152, 30 m away, was monitored while pumping G47151. Drawdown was observed after 8min and reached 0.5m within 12h of pumping. This drawdown curve gives a T value of 7 m^2/d and an S value of 0.000475, which is taken to be as a representative S value for fractured gneiss.

The sustainable yield calculated on the basis of the various methods is shown in Table 2-8. The various parameters for each of these methods are listed in Table 2-9.

Table 2-7 Transmissivity values for G47151

G47151	$T_{(early)}$ [m^2/d]	$T_{(recovery)}$ [m^2/d]
	1.9	2.2

Table 2-8 Recommended borehole yields for G47151

Method	m^3/d
Late T	15
Recovery	29
Drawdown to boundary	27
Distance to boundary	7
Flow characteristic	25
Max. drawdown	40

Table 2-9 Critical parameters for sustainable yield estimation

	G47151	G47152	G47153	G47154	G47155	G47156	G47158	G47159
T_{early}	1.9	3.9	4.6	3.7	0.9	4.3	11.1	26.3
T_{late}	1	-	1.4	-	-	0.3	11.1	-
$S_{fracture}$	0.000475	0.000475	0.000475	0.005	0.005	0.0005	0.005	0.0005
S_{matrix}	0.000475	0.000475	0.000475	0.01	0.01	0.01	0.01	0.0005
Boundary (m)	23	48	12	43	46	10	11.8	-
Boundary (d)	0.5	-	0.049	-		0.29	0.146	-
Lithology	Gneiss	Gneiss	Amphibolite	Weathered Gneiss	Weathered granite/gneiss	Weathered Granite	Weathered Gneiss	Amphibolite
F2	2	2	2.7	0.5	0.5	5	1.5	
Yield (m^3/d)	25-30	115-130	35	110-115	30	26	110	~300
Conceptual Model	Network of uniform fractures	Network of uniform fractures	Dipping Plane	Leaky confined bedrock contact	Leaky confined bedrock contact	Leaky Vertical fracture	Leaky Horizontal fractures	Leaky Horizontal fracture

The sustainable borehole yield varies from 7-40 m^3/d for the different methods. The drawdown-to-boundary method estimate of 27 m^3/d is considered to be the best approximation since all the parameters are measured. The recovery method is based on an estimated recovery at $t/t' = 1.5$, which assumes that the rate of recovery would have increased once fracture networks are rewatered. This assumption is based on the recovery behaviour of the observation borehole, which displayed a characteristic S curve that steepens after the last measurement. On the basis of the results from the different methods the recommended borehole yield for borehole G47151 is proposed to be 25-30m^3/d.

Pump test G47152

The final blow yield of borehole G47152, which is only 30 m from G47151, was measured as 4l/s. The main water strike occurred within a large fracture zone at 92.2m below surface and yielded 3.7l/s. Two minor water strikes were encountered at 59m and 64m, yielding 0.2l/s and 0.1l/s respectively. The pump was lowered to 60m. The rest water level was measured to 11.31m below surface, giving an available drawdown of 81 m. The borehole was pumped for 12h at the maximum rate of 1.5l/s of the submersible pump.

At 8 m of drawdown a dip is seen in the semi-log plot and the derivative curve. This can be attributed to the water level reaching the bottom of the casing, which results in the dewatering of the weathered zone, where a temporary water bearing horizon was created by upwelling water when the confining hard rock layers were penetrated by the borehole. Thereafter, the aquifer exhibits similar characteristics as G47151, namely a series of steps in the semi-log drawdown or humps on the derivative curve. Consequently, the drawdown data reflects the drainage of a homogenous network of fractures.

For the duration of the pumping test no effects of low permeability boundaries can be noted, however, the aquifer was only tested to a drawdown of 20 m. Consequently, it was assumed that boundary effects would only occur at 48 m, the drawdown at which the first water strike is encountered. This assumption is based on the previous pumping test, where no boundary condition was encountered until the water strike. This assumption may result in the underestimation of sustainable yield since this first water strike is only a minor one.

The recovery of the borehole was monitored for 12h. The semi-log time-residual drawdown curve follows a straight line indicating a constant recovery of the water table. At 12 h of recovery, t/t' = 2, a residual drawdown of 1.65m remains. The low storativity of the fracture networks, the lack of observed leakage from an overlying weathered aquifer and the incomplete recovery suggests that yield estimates should be conservative.

Calculated transmissivity values are presented in Table 2-10. The transmissivity was calculated on the basis of the entire drawdown curve, hence it represents a mean fracture transmissivity. A late transmissivity value cannot be obtained as no barrier boundary is encountered within the pumping time of 12h. The sustainable yield calculated on the basis of the various methods is shown in Table 2-11. The various parameters for each of these methods are listed in Table 2-9.

Table 2-10 Transmissivity values for G47152

G47152	$T_{(early)}$ [m^2/d]	$T_{(recovery)}$ [m^2/d]
	3.9	4.4

Table 2-11 Recommended borehole yields for G47152

Method	m^3/d
Flow characteristic	132
Recovery	17
Drawdown to boundary	114
Max. Drawdown	135

The discharge test shows that the transmissivities of the high yielding borehole G47142 are in the same order as G47151. Hence, the high blow yield cannot be explained by higher fracture permeability. It is more likely that the tapped fracture networks are under more confining pressure, due to the significantly deeper water strike at 92.2 m.

The sustainable yields for borehole G47152 is probably 115-130 m^3/d. The recovery method gives a low yield since t/t' extrapolation is only 1.15 and it may be affected by the rewatering of the weathered zone by upwelling water. The FC method predicts 132 m^3/d, which may be too high since no late T value could be established.

Pump test G47153

Borehole G47153 showed two water strikes at 60.8m (1.11l/s) and 73.4m depth (0.69l/s). The final blow yield was measured as 1.8l/s. The rest water level is at 30.7 m, giving an available

drawdown of 30 m. The pump was lowered to 78m and the borehole was pumped for 24h at the maximum rate of the submersible pump of 1.5l/s.

The semi-log plot of the time-drawdown curve exhibits an exponentially increasing curve while the derivative curve has a continuous positive slope of 0.25. This indicates that flow is linear instead of radial. Hence the aquifer can be conceptualised as a strongly anisotropic finite dipping plane, such as a narrow fault zone. No significant boundary conditions can be noted. After 24h the water level is approximately at the main water strike and boundary conditions are imminent. Continued pumping would result in fracture de-watering. The inflection point at which the rate of drawdown increases (12m) and no longer fits the best-fit line from which the early T was established is considered to represent a boundary condition. This point is represented on the derivative curve as a localised steep increase in slope. This point can probably be conceptualised as the time at which the transition to purely linear flow occurs.

The recovery of borehole G47153 was monitored for 24h. For the first 19h the recovery rate was low, with a water table rising only 0.8m. This is expected if only a single vertical fracture is replenishing the borehole in a linear manner. In the last 5h, after the fracture has been recharged, the water level rising more rapidly but the borehole has not fully recovered. A residual drawdown of 2.52 m remains at t/t'=2. However, the rate of recovery is increasing, suggesting that the aquifer is of significant extent.

The calculated early and late time transmissivity values for borehole G47153 are presented in Table 2-12. Recommended borehole yields by the various methods are in Table 2-13.

Table 2-12 Transmissivity values for G47153

G47153	$T_{(early)}$ [m^2/d]	$T_{(late)}$ [m^2/d]
	4.8	1.4

Table 2-13 Recommended borehole yields for G47153

Method	m^3/d
Late T	28
Recovery	49
Drawdown to boundary	33
Distance to boundary	45
Flow characteristic	21
Max. Drawdown	50

Recommended borehole yields for borehole G47153 range from 21-50m^3/d. The recovery method provides a qualitative indication that recovery is not yet complete. The high yield estimated suggests that the hydrogeologist need not be unduly conservative when considering this borehole. The FC method appears overly conservative, however, its application was problematical as no defined boundaries can be identified in the derivative curve, making the determination of F2 difficult. If boundaries are assumed at 12 m (early time inflection) and at 30 m of drawdown (water strike), an F2 of 2.7 can be calculated. The drawdown-to-boundary method is the most applicable and has given accurate estimates in similar aquifer types (Sami & Murray, 1998), hence a figure of approximately 35 m^3/d can be accepted.

Borehole G47154

Borehole G47154 is characterised by a very deep weathering profile with a shallow rest water level of 7.9m below surface. The water strike occurred at 51m at the contact of the weathered overburden and the solid bedrock, giving an available drawdown of 43 m. The blow yield was measured as 3.33l/s. The pump was lowered to 59m and the discharge test was carried out for 5h, when pseudo-steady state conditions occurred.

The semi-log drawdown and derivative curves indicate that radial flow towards the borehole occurred in the first 12 min of the test. Subsequently, leakage from the overlying weathered confining layer occurs and the rate of drawdown decreases. By 40-min pseudo steady state conditions begin to appear and are characterised by the derivative curve having a slope of –1. Drawdown stabilises at 12.1 m towards the end of the test. These two inflection points correspond to a depth of water level of 16.9 and 18.9m respectively. The geological log of borehole G47154 indicates that these inflection points correspond to lithological changes in the bedrock. At 16m (approximately 9 m of drawdown) the gneiss becomes highly weathered, therefore, the storativity is expected to be higher. Once the water level drops to this level this zone begins to dewater and a transition in hydraulic behaviour occurs. The response of the water level to the release of water from storage is no longer controlled by the confined storativity but by the unconfined specific yield related to the dewatering of the pore volume. This results in the release of a greater volume of water per unit drop in water level and a decline in the rate of drawdown. At 19m depth the gneiss changes into highly weathered amphibolite, which is expected to have an even higher specific yield, hence the rate of drawdown declines further. The rate of drawdown would increase once these weathered horizons have been dewatered. For this reason, it can be expected that boundary conditions would occur at 51 m (44 m of drawdown), the point at which the water level drops below the overlying weathered zone.

The recovery data for borehole G47154 indicates that leakage occurred from overlying formations while the borehole recovered. At t/t' = 2.4 the water level had recovered to its original pre-pumping level.

The transmissivities given in Table 2-14 are calculated on the basis of the recovery data and the early time drawdown data, before the effects of leakage were encountered. The recommended borehole yields calculated on the various methods are listed in Table 2-15.

Table 2-14 Transmissivity values for G47154

G47154	$T_{(early)}$ [m^2/d]	$T_{(recovery)}$ [m^2/d]
	3.7	5.5

Table 2-15 Recommended borehole yields for G47154

Method	m^3/d
Late T	116
Recovery	76
Drawdown to boundary	110
Flow characteristic	233
Max. Drawdown	140

The recommended borehole yield varies from 76-233m^3/d. The 110 m^3/d estimate from the drawdown to boundary method is considered to be conservative as it is based only on transmissivity and a presumed boundary effect while ignoring the effects of leakage. The flow characteristic method estimates a sustainable yield of 233 m^3/d, which is too high since it is based on an F2 value of 0.5 due to the leakage from the weathered zone. In this case it does not consider the extent of storage. If leakage is ignored and a single barrier boundary is assumed, giving an F2 of 2, the FC method would generate a yield of 91 m^3/d.

Pump test G47155

Borehole G47155 is characterised by a 64m deep weathered overburden. At the contact between the weathered overburden and bedrock the main water strike of 0.83 l/s is encountered. A second water strike is encountered at a depth of 72.5m, where fractured gneiss

changes into fresh solid gneiss bedrock. The final blow yield of borehole G47155 was measured as 1l/s. The rest water level is at 17.95 m, giving an available drawdown of 46 m. A pumping test was carried out at 1.5l/s for 6h until pseudo steady-state conditions were reached.

This borehole behaves in a manner similar to borehole G47154 and can also be visualised as a leaky bedrock contact aquifer, with leakage occurring from an overlying high storage low permeability weathered zone. For the first 12 min of pumping the semi-log drawdown curve follows a straight line while the derivative curve is horizontal, indicating radial flow from fractures towards the borehole. After 12 min leakage commences and by 20 min the derivative plot has a slope of –1. After 2.5h the borehole reaches pseudo steady-state conditions at about 36 m of drawdown, with the water table dropping only 0.17m in the last 3.5h of the discharge test. Now, leakage from the weathered overburden nearly equals the rate of abstraction and the cone of depression enlarges more slowly. These inflection points are not related to any lithological variations. Hence boundary conditions are assumed to occur at 46 m, after the water strike is reached.

The recovery test shows that by 60min (t/t' =7) the water level had fully recovered, testifying that a significant volume of leakage from the weathered overburden is contributing to the aquifer.

The transmissivities were calculated on the basis of the recovery data and the early time pump test data and presented in Table 2-16. The recommended borehole yield was calculated on the various methods and the results are shown in Table 2-17.

Table 2-16 Transmissivities for borehole G47155

G47155	$T_{(early)}$ [m^2/d]	$T_{(recovery)}$ [m^2/d]
	0.9	1.0

Table 2-17 Recommended borehole yields for G47155

Method	m^3/d
Late T	32
Recovery	111
Drawdown to boundary	31
Flow characteristic	71
Max. Drawdown	70

The recommended borehole yield varies from 32-111m^3/d. The 31 m^3/d estimate from the drawdown to boundary method is considered to be conservative as it is based only on transmissivity and a presumed boundary effect while ignoring the effects of leakage. The recovery method provides a high estimate as it considers only the rate of recovery and does not consider the extent of storage. The Flow Characteristic method estimates a sustainable yield of 70 m^3/d, which is too high since it is based on an F2 value of 0.5 due to the leakage from the weathered zone. In this case it does not consider the extent of storage. If leakage is ignored and a single barrier boundary is assumed, giving an F2 of 2, the FC method would generate a yield of 25 m^3/d.

Pump test G47156

The first water strike was encountered at the contact between weathered overburden and solid bedrock at 9.8m (0.54l/s) but it was cased off. A second minor water strike was encountered in solid granite at 30.7m (0.2l/s), while the main water strike of 0.7l/s was struck in granite at 73.2m below surface. The final blow yield was measured as 1.4l/s. The static water level is at

5.15m below surface, giving an available drawdown of 68m. The pump was lowered down to 78m and the borehole pumped at a rate of 1.3l/s for 12h. It recovered within 2 hours.

The first water strike is cased off and drill cutting provide the annular fill. Flow to the borehole consists of downward leakage from the weathered zone into the underlying less weathered granite, from where it can subsequently enter the hole. For this reason, the early time data reflects the transmissivity not of the water bearing horizon but of the underlying granite and the rate at which water can leak into this horizon. The result is a flat semi-log drawdown curve characteristic of leakage. As the weathered aquifer in the immediate vicinity of the borehole begins to dewater, the rate of drawdown increases. At about 6.8 m of drawdown the water level is below the water strike and the weathered quartzite and granite horizon, and a transition to unconfined conditions begins. The dewatering of this upper aquifer results in a flattening of the drawdown curve. It is also marked by a small peak in the derivative curve when the water strike is encountered, followed by a subsequent trough. Once this zone is dewatered, the water level drops immediately to 10m and the rate of drawdown increases sharply. This suggests that the main aquifer is the weathered granite zone shown on the drilling log, which extends from 5.15 m to about 15m depth, and that water bearing fractures are steeply dipping and collect water from the overlying saturated weathered zone. Once the weathered zone above the intercepted fracture network is dewatered the upper aquifer ceases to contribute water and a dramatic decline in yield is experienced. The dewatering of the upper aquifer can be considered as a closed boundary effect, hence an F2 value of 5 was selected. The subsequent data reflects the hydraulic properties of the less permeable deeper water strikes. The thickness of the weathered aquifer (10m) therefore denotes the drawdown depth of the onset of boundary conditions.

The residual drawdown-time relationship of recovery is not log-linear, reflecting a slow recovery of the water bearing fracture zone for the first few minutes. This can be attributed to the slow lateral recharge of the fractured zone, which occurs before vertical recharge of fractures from the dewatered weathered zone. Thereafter, once the weathered zone recovers, vertical leakage from the weathered overburden increases the rate of recovery of the borehole. The rate of recovery decreases once more when the water level reaches about 5 m of residual drawdown. This can be attributed to a change in storativity conditions due to the rewatering of the more porous weathered zone. The rest water level is reached within 2h-recovery time, at t/t' = 7, confirming that significant vertical recharge of the water-bearing horizon has occurred.

The transmissivities for borehole G47156 are calculated on the basis of the early and late time drawdown curve and on the recovery data and are presented in Table 2-18. The borehole yields estimated from the various methods and are shown in Table 2-19.

Table 2-18 Recommended borehole yield for G47156

G47156	$T_{(early)}$ [m²/d]	$T_{(late)}$ [m²/d]	$T_{(recovery)}$ [m²/d]
	4.3	0.3	1.2

Table 2-19 Recommended borehole yields for G47156

Method	m³/d
Late T	15
Recovery	96
Drawdown to boundary	26
Distance-to-boundary	26
Flow characteristic	17
Max. Drawdown	42

The calculated sustainable yields fall within a range of 15-96m³/d. The late T and Flow Characteristic methods appear overly conservative since they are directly related to the low

transmissivity value calculated from late time data. They ignore leakage from the weathered zone that would occur if the borehole were pumped at a rate less than the ability of this zone to contribute water. These estimates also do not consider the rapid recovery due to leakage from the upper weathered aquifer. The drawdown-to-boundary and distance-to-boundary methods estimate a yield of 26 m^3/d, which is about 0.3 l/s and less than the yield from the upper water strike. They can therefore be considered as acceptable estimates. Although these methods do not consider the extent of storage, the rapid recovery suggests that the yield assessment need not be overly conservative.

Pump test G47158

Borehole G47158 was pump tested for 5h at the highest rate of 1.5l/s of the submersible pump. The first water strike occurred at 17.9m below surface, at the contact between weathered and slightly weathered gneiss. Between 17.9 and 20.6m, where sapprolite grades into unweathered gneiss, the rate of inflow steadily increased until at 20.6m the final blow yield of 4l/s was observed. The rest water level was measured as 6.04m below surface, giving an available drawdown of 11.8 m. The pump was set at 56m.

The semi-log drawdown curve is linear for the first 15 min indicating radial flow through the weathered overburden. Subsequently the rate of drawdown increasingly declines, indicating that leakage from the overlying weathered gneiss is occurring. The onset of leakage is characterised on the derivative curve as a dip where the derivative value declines. With increasing leakage at 120 min the derivative declines further. At 20, 50, 90 and 210-min boundary conditions are indicated on the derivative curve due to declines in the rate of leakage. These may result from the dewatering of localised networks of vertical fractures. They are unlikely to represent low permeability boundary conditions since leakage continues after the boundary effects are encountered. Consequently, boundary conditions would probably not be encountered until a drawdown of 11.8 m, when the main water bearing fractures are encountered. The steadily increasing inflow over 3 m of slightly weathered gneiss suggests that the main water bearing fractures are sub-horizontal. This horizontal nature limits the ability of the saturated overburden to provide leakage to recharge the fractures, hence the slow rate of leakage and the dewatering of pockets of vertical fractures.

After the pump test was terminated, borehole G47158 was monitored for 80min until the water level fully recovered. The data reveals that the borehole experiences a fair amount of leakage from the weathered overburden, which results in a 't/t' intercept value of 10.

The transmissivities, calculated on the basis of the recovery data and the early time drawdown data are given in Table 2-20. The recommended borehole yields calculated by the various methods are presented in Table 2-21.

Table 2-20 Transmissivities for borehole G47158

G47158	$T_{(early)}$ [m^2/d]	$T_{(recovery)}$ [m^2/d]
	11.1	11.6

Table 2-21 Recommended borehole yields for G47158

Method	m^3/d
Recovery	117
Drawdown to boundary	84
Distance to boundary	127
Flow characteristic	110
Max. Drawdown	120

The transmissivity value of borehole G47158 is significantly higher than those from the previously examined boreholes. This is due to the fact that the aquifer consists of a 3m thick fracture zone that responds in a radial manner.

The drawdown-to-boundary method calculates a sustainable yield of $84m^3/d$, which is regarded as being too conservative since it ignores the effects of leakage. The recovery method generates a recommended borehole yield of $117m^3/d$, which suggests that the yield estimate need not be overly conservative. The Flow Characteristic methods were applied by assuming a late T value equivalent to the early T, hence assuming no permeability boundary conditions until the borehole would fail due to dewatering of the water bearing fracture zone. An F2 of 1.5 was applied in order to account for the dewatering effects encountered during leakage.

Pump test G47159

Borehole G47159 had a water strike at 62.4m with an associated blow yield of 6.6 l/s. Consequently, it is potentially the highest yielding borehole in the region. The rest water level was measured at 6.38m below surface, giving an available drawdown of 56 m. The pump was lowered to 70m and the borehole was tested at 1.5l/s. Due to technical problems the discharge test had to be terminated after 2.5h. Within this short period, the semi-log drawdown curve is log-linear reflecting radial flow to the borehole. No barrier boundary was encountered during the limited duration of the test, however, the derivative curve suggests that some leakage may be occurring in the first few minutes of the test and towards the end of the test. Since the rest water level is in only slightly weathered rock, leakage must be conceptualised as a network of small vertical fractures feeding a main sub-horizontal water bearing fracture.

The recovery was monitored for 50min, a t/t' of 4. At that stage the water level had recovered to 0.03 m below the water level prior to pumping. This confirms that vertical leakage to the fracture has occurred.

The transmissivities calculated from the recovery and early drawdown data are presented in Table 2-22. No estimates of sustainable yield can be made due to the short duration of the test. However, if it is assumed that boundary conditions would be encountered at 19m of drawdown, where the water level reaches unweathered gneiss, the drawdown-to-boundary method would calculate a yield of $277m^3/d$, which ignores the effects of leakage. By assuming an F2 of 6, implying closed boundary conditions within 100 m of the borehole and ignoring leakage, the flow characteristic method would estimate 326 m^3/d. This discharge rate is approximately 56% of the blow yield. Hence it can be assumed that the sustainable yield must be in the vicinity of 300 m^3/d.

Table 2-22 Transmissivities for borehole G47159

G47159	$T_{(early)}$ [m^2/d]	$T_{(recovery)}$ [m^2/d]
	26.3	21.0

Conclusion

Table 2-23 summarises the results of the eight discharge tests in terms of calculated transmissivities, blow yield, sustainable yield and pressure head.

The discharge tests indicate that at least 4 types of aquifers occur: networks of uniform fractures, sub-vertical fractures with or without leaky weathered overburdens, bedrock contacts with a leaky overburden, and leaky deep seated horizontal fractures. All these aquifer types can have high sustainable yields (>2 l/s for 12 h/d), except for the vertical fracture type. The latter, whether associated with a leaky confining layer or not, is limited in terms of

exploitation potential due to the fractures being finite and presence of low permeability boundaries, which were encountered early during the pumping test. The highest transmissivities are associated with horizontal fracture aquifers.

Table 2-23 Results of the eight discharge tests

	$T_{(early)}/T_{(recovery)}$ (m2/d)	Sustainable Yield (m3/d)	Blow Yield (l/s)	Sustainable Yield (% blow yield)	Pressure head (m)
G47151	1.9 / 2.2	25-30	0.9	32-39	63.73
G47152	3.9 / 4.4	115-130	4	33-38	80.9
G47153	4.8 / 1.4	35	1.8	23	30.1
G47154	3.7 / 5.5	110-115	3.33	38-40	43.1
G47155	0.9 / 1.0	30	1	35	46.25
G47156	4.3 / 1.2	26	1.4	21	68.05
G47158	11.1 / 11.6	110	4	32	14.56
G47159	26.3 / 21.0	~300	6.66	53	56.02

All the aquifer types are confined in character and respond to abstraction in a discontinuous fashion due to the finite nature of the fractures or, where a thick weathered overburden is encountered, due to leakage that leads to partly steady-state conditions during pumping. High yields are generally derived from aquifers overlain by a thick weathered overburden, or from large fault zones, as experienced in borehole G47152 and G47159. Only G47152 had a high sustainable yield without an overlying leaky weathered zone. In this case the high sustainable yield is attributed to the large available drawdown, which compensates for the low storativity of the fractured gneiss and granite aquifer. Where the saturated thick weathered overburden is too thin and fault zones are missing yields are generally low.

Figure 2-87 shows the relationship between the blow yield and sustainable yield and transmissivity. The sustainable yield of borehole G47159 is not included because it could not be adequately assessed. A linear relationship exists between sustainable yield and blow yield, whereas transmissivity and blow yield do not seem to be strongly correlated. The latter can be attributed to the influence of confining pressure on blow yield.

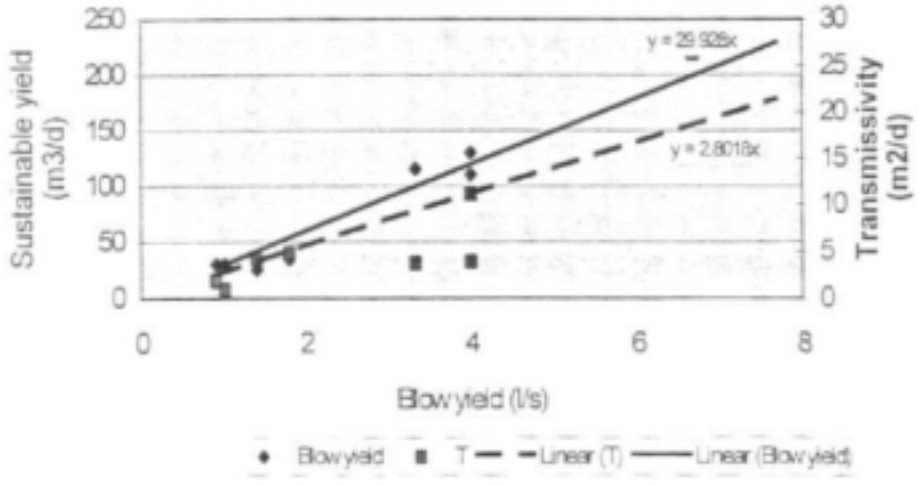

Figure 2-87 Relationship between blow yield, sustainable yield and transmissivity

2.9 Down-the-hole Geophysics

Five of the nine newly drilled boreholes were logged using apparent resisitivity and self-potential probes to determine the formation composition in terms of lithology, permeability and electrical conductivity.

G47151

The resistivity log for borehole G47151 indicates an average apparent resistivity of 350-360Ωm for the gneiss bedrock. This high resistivity interval indicates that the rock has nearly no porosity, or at least no connected porosity. Fracture zones can be identified at depths of 24m, 28-31m and 35 to 38m and are characterised by low resistivity values. These correspond to the fracture zones identified by the test pumping analysis. The latter zone (35-38m) equates to the first water strike with a 0.5l/s yield. The dolerite intrusion is reflected in the log by generally lower resistivity values between a depth of 56 to 64m. Even lower values are recorded for the weathered gneiss above the dolerite, probably due to an increase in the clay content.

G47152

The first 18m of the electrical log of borehole G47152 are influenced by the casing. The water level at 11.3m is clearly detectable due to the very poor electrical conductivity of the dry formation above 11.3m and the reduction in resistivity with saturation of the formation below 11.3m. The average apparent resistivity for the gneiss bedrock varies between 305 and 320 Ωm. This high resistivity interval indicates, that the rock formation is neither altered nor fractured. Slight reductions in resistivity can be observed from 20-22m, 34m-40m, 46m-53m and 73m-78m, and are most likely zones of fracturing and/or weathering with an associated increase in clays with bound water. A faster drilling penetration is recorded in these zones, which would support this assumption. The zones from 34-40m and 46-53m reflect weathered gneiss rock at the lower and upper contact of the dolerite intrusion. The dolerite intrusion itself is characterised by slow penetration and slightly lower resistivity, but as the dolerite rock has a composition cognate to gneiss, the log responses are similar. However, the resistivity log indicates that the resistivity of fracture zones is only slightly lower than that of the host rock, implying that the fractures are small and probably not interconnected.

A large anomaly can be observed between 91m and 94m, with a decrease in resistivity of about 100Ωm, indicating a wide open fracture zone. This forms the major water strike of borehole G47152 with a yield of 3.7l/s.

The SP log adds little to the interpretation as the formation has little shale or clay and therefore a baseline does not occur on the log.

G47153

The SP and resistivity logs for borehole G47153 are disturbed in the first 35.5m due to casing. The water level is clearly detectable with an increase in conductivity at 30.7m where the formation becomes saturated. Until 38m depth, the resistivity log indicates conductive rocks, probably due to the deep weathering profile associated with clays with bound water. Up to a depth of 65m, the average resistivity of the amphibolite bedrock is 365Ωm. Three distinct conductivity peaks are observed at 42-45m, 51-54m and 61-65m. The latter zone shows the most prominent conductivity peak and is associated with a fracture zone and the major water strike of the borehole. The SP log correlates with the resistivity curve, which shows deflections towards higher electrical potentials, indicating the presence of water bearing horizons. All three zones are expressed as slight bumps in the derivative of drawdown, which are indicative of small water bearing zones.

Over the last quarter of the borehole, higher resistivity values and lower electrical potentials are recorded, indicating an average apparent resistivity of 380Ωm for the solid amphibolite bedrock. The distinct shift is either associated with less fracturing of the bedrock or alteration in the conductive mineral content, such as pyrite or magnetite, within the amphibolite.

G47154

Up to the depth of 49m, the casing in borehole G47154 influences the electrical logs. The remaining part of the resistivity log is characterised by resistivity changes, correlating well with lithological changes in the bedrock. Portions of relatively high resistivity correspond to gneiss bedrock, whereas an increase in conductivity is observed for amphibolite layers. The difference in conductivity can be explained by either a higher degree of weathering/fracturing or a higher content of magnetite as a conductive mineral in the amphibolites compared to the gneiss bedrock. As the penetration rate does not vary significantly between gneiss and amphibolite layers, the latter assumption is more likely. Additionally, the resistivity is generally very high, indicating that the metamorphic bedrock is not altered or fractured or only to a very slight degree.

G47156

The first 12m of the electrical logs of borehole G47156 are disturbed by casing, but the water level at 5.1m is clearly detectable with a sharp increase in conductivity. From 14m to 18m the resistivity of the bedrock is relatively low, with two main peaks of conductive rock at 14m and 17m. This correlates with steps in the derivative of drawdown curve at about 9 and 12 m of drawdown, indicating water bearing horizons and subsequent boundary conditions once the water bearing horizons are dewatered. Below 18m solid bedrock is encountered and a high average apparent resistivity of 400Ωm reflects solid granitic bedrock, which has not been altered or fractured. Slightly lower resistivities are observed between 24m and 36m, 28m and 31m and at 73m, reflecting fractured bedrock zones. Only the latter two equate to identifiable water bearing horizons.

A small zone between 53m and 56m exhibits a high content of biotite, which lowers the resistivity due to its conductive properties. A further increase in conductivity can be observed from 82m until 100m, accompanied by faster penetration. This leads to the assumption that a zone of weaker, more fractured bedrock is encountered. Additionally, variations in pyrite content are observed throughout the borehole, influencing the distribution of conductive peaks.

In conclusion, the resistivity logs show that water strikes in the area are associated either with the contact zone between weathered and unweathered bedrock or fracture zones. The size of the anomaly on the resistivity log is directly related to the yield associated with the fracture zone and reflects if fractures are open or closed, connected or interconnected and their potential size. Resistivity anomalies also agree and validate fracture zones identified during test pumping. Changes in the lithology are mostly reflected in the resistivity profile, even though gneiss has a composition similar to granite and therefore the responses can be quite similar. In general, the SP logs add little to the interpretation in this area, as the formations contain little shale or clay and therefore a baseline does not occur on the log.

2.10 Evaluation of Climatic and Runoff data

Rainfall data for the study area was obtained from the Computing Centre for Water Research (CCWR). Data for the following rainfall stations are available between 30 45 – 31 15 E and 29 00 – 29 30 S (Table 2-24).

Table 2-24 Available data from rainfall stations in the study area

Station number		Station Name	Elev.	Start	End	Years	Lat	Long	MAP
270481	A	WALDECKE, HERMANNSBU	1140	1976	1991	12	2901	3047	781.8
270721	W	SALEM	1060	1932	1947	12	2901	3055	708.8
270722	W	GLEN ELAND	1050	1932	1997	57	2902	3056	953.8
270753	W	ELANDSKOP	1066	1919	1944	11	2903	3056	1058
270544	W	BOSCOMBE	1140	1928	1998	49	2904	3049	1092.3
270694	W	ELANDSVLEI	1050	1925	1953	25	2905	3055	893.1
271815	W	NYONI (POL)	58	1967	1967	16	2905	3128	1040.2
271038	S	MAPUMULO	716	1977	1998	20	2908	3102	1073.7
271099	W	MAPUMULO (TNK)	533	1923	1998	53	2910	3104	1083.2
271252	A	MAYFIELD, STANGER	660	1948	1991	41	2912	3109	1251
271402	S	DOORNKOP	442	1934	1997	61	2912	3114	1070
271283	S	DOORNKOP(SPRINZ)	545	1957	1998	38	2913	3110	1204.5
271315	W	MOUNT ALBERT	457	1919	1922	2	2915	3111	1568.1
271435	S	COLERINE ESTATE	390	1955	1970	10	2915	3115	959.9
271347	S	SPROWSTON	305	1957	1970	11	2917	3112	1144.7
271198	S	GLENDALE	129	1966	1998	32	2918	3107	844.4
271408	S	KEARSNEY	277	1929	1998	41	2918	3114	1102.8
271438	S	KEARSNEY	317	1920	1932	12	2918	3115	1060.4
271409	P	BALCOMB WT UMHLALI	274	1931	1983	51	2919	3114	1078.7
271170	W	GLENDALE (POL)	450	1967	1974	3	2920	3107	644.4
270472	A	HONEY GROVE, DALTON	940	1961	1989	23	2922	3046	842.7
270472	S	GORDONS OVERSTONE	944	1985	1998	13	2922	3046	776.5
271232	S	CHAKA KRAAL(FERNEY)	368	1929	1998	40	2922	3108	1003.1
270563	S	GORDONS	960	1971	1985	13	2923	3049	767
270772	W	NSUZE (POL)	564	1967	1997	22	2923	3057	860.4
271383	S	GROUTVILLE	122	1934	1998	41	2923	3113	908.8
270505	S	GLENSIDE	997	1974	1998	22	2925	3047	908.1
271085	P	COLLINS RM UPPER TONGA	457	1942	1982	20	2925	3103	1152.5
271085	S	UPPER TONGAAT	457	1957	1998	41	2925	3103	1097.4
271357	S	CHAKAS KRAAL (EXPT.FARM)	50	1957	1998	41	2927	3112	987.8
271448	P	ARMSTRONG RSR UMHLALI	91	1930	1983	23	2928	3115	1078.3
270449	W	UMHUME-WATTLE ESTATE	670	1932	1939	3	2929	3045	1193.7
271149	S	SINEMBE	237	1945	1998	41	2929	3105	1033.2
271330	S	COMPENSATION	24	1933	1972	38	2930	3111	1054
271420	W	UMHLALI BEACH	50	1973	1998	15	2930	3114	1064.2

Generally the precipitation increases from north to south and from west to east in the 2640km^2 area. However, since a large portion of rainfall occurs as convective summer storms, whose total rainfall can vary significantly over small distances, gauge elevation and aspect also influences the MAP in the research area. Figure 2-88 presents the distribution of the mean annual precipitation on the basis of the CCWR 1 minute by 1 minute median monthly rainfall grid over the study area. The estimate of MAP at each point was determined using a regression surface in which MAP was regressed against factors such as altitude, latitude, longitude, continentality and aspect (Dent, Lynch & Schulze, 1989). This grid suggests that MAP varies in a broad range between 533mm and 1332mm with an average figure of 921mm. The map shows that low lying areas appear to have a lower MAP.

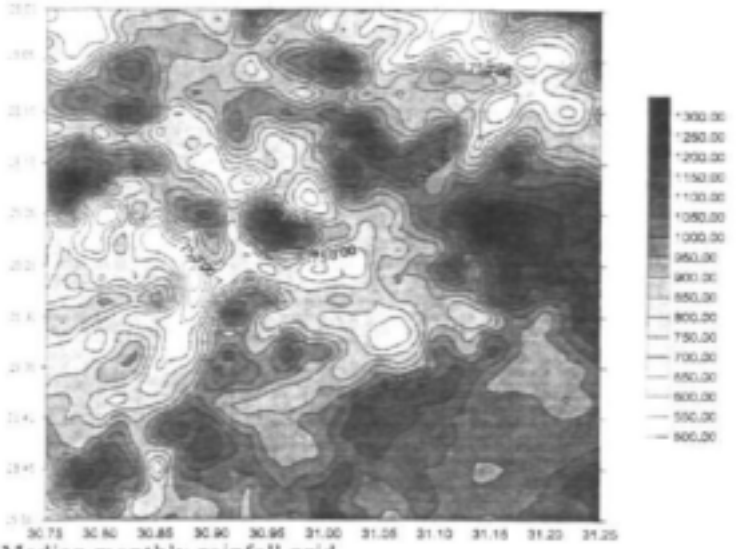

Figure 2-88 **Median monthly rainfall grid**

In general data from 34 rainfall stations are available in the area (Table). However, a minimum record of 30 years is required to provide a statistically meaningful mean average precipitation (MAP). 15 stations provide over 30 years of complete data in the research area, which gives a gauge density of one gauge per 176km^2. However, only one rain gauge with a record over 30 years exists in the rural area itself within the Natal Metamorphic Province. Mapumulo (TNK) station has a record of 53 years and provides a MAP figure of 1083.2mm at an altitude of 533m.

The inter-annual distribution of rainfall for Mapumulo (TNK) is shown in Figure 2-90. The mean monthly distribution of rainfall in the area is characterised by intense summer rainfall and dry winter seasons and is presented in Figure 2-89.

An estimation of rainfall during wet seasons and drought periods is shown in Figure 2-92 and Figure 2-93 on the basis of the rainfall that is likely to be exceeded in 20% and 80% of the years.

Symons Pan evaporation data is available for the Mapumulo station and is presented in Figure 2-91. An annual pan evapotranspiration value of 1338mm (S-pan data) can be estimated for the study area.

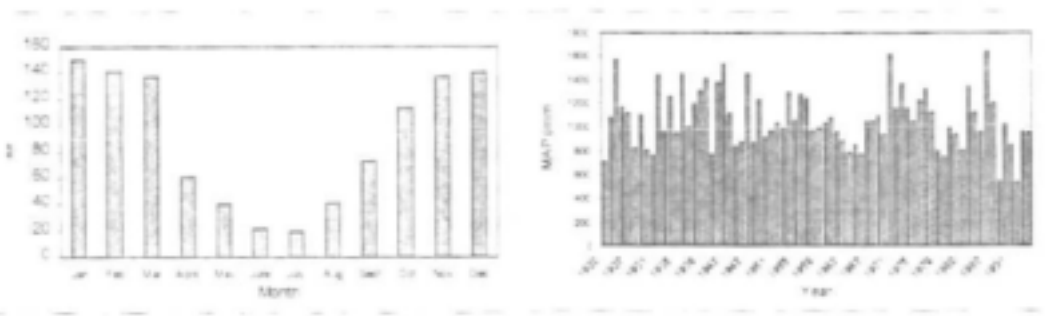

(a) (b)

Figure 2-89 **Mean monthly distribution of rainfall at Mapumulo (TNK) station (a)**

Figure 2-90 **Inter-annual distribution of rainfall at Mapumulo (TNK) (b)**

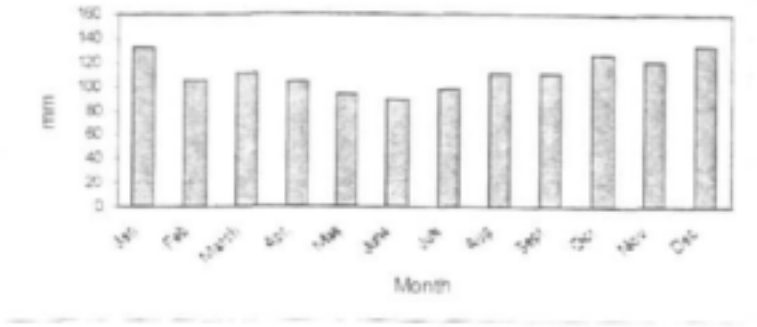

Figure 2-91 **Mean monthly distribution of evapotranspiration at Mapumulo station**

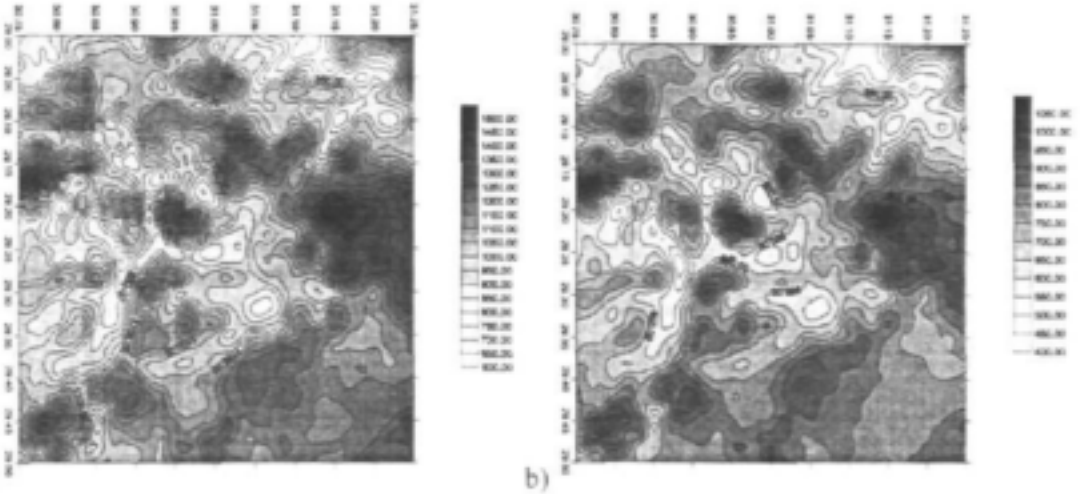

Figure 2-92 **Estimate of wet period rainfall (rainfall is likely to be exceeded in 20%of the years) (a)**
Figure 2-93 **Estimate of drought period rainfall (rainfall is likely to be exceeded in 80% of the years) (b)**

To study the rainfall-runoff characteristics and groundwater controlled baseflow response, runoff data was obtained from DWAF. However, the data is sparse with only three gauges located in the vicinity of the study area (Table 2-25).

Table 2-25 **Available runoff data for the study area**

Number	River	Locality	Catchment area (km^2)	Lat	Long	Record
V5H002	Tugela	Mandini	28920	29 08 26	31 23 31	1962-1986
V6H002	Tugela	Tugela Ferry	12862	28 45 00	30 26 34	1978-1990
U3H001	Tongati	Riet Kuile	236	29 32 00	31 05 22	1966-1986

None of the gauges fall within the Natal Metamorphic Province, with gauge V5H002 and U3H001 situated on the Natal Sandstone and V6H002 on the Ecca shales. Additionally, the catchment area for two of the three gauges are very large, hence it was decided to estimate recharge using rainfall-recharge relationship formulae rather than hydrograph separation based on the gauges listed in Table 2-25.

Several locally developed rainfall-recharge formulae exist for South Africa (Bredenkamp et al. 1995). They give site specific estimations of recharge values as a fraction of precipitation.

Recharge in the study area was estimated according to five different methods based on an average MAP figure of 921mm. The results are presented in Table 2-26.

Table 2-26 Recharge estimation for the study area

Method	Formulae	Recharge (mm)	Description
	R = a*MAP, with a=5%	46mm	The simplest empirical formula. It takes recharge (R) as a proportion (a) of MAP
Kirchner et al 1991, thin soil cover	R = 0.06 (MAP–120)	48mm	Kirchner et al (1991) produced this formulae which take the soil thickness into account
Granitic aquifers	R=MAP² 20000	42mm	Variation of the DWAF method (R=(MAP)2/10000), for granitic aquifers
Enslin		97mm	Enslin produced the first rainfall-recharge relationship for the entire county. The values are derived from water balance estimates and lowflow discharges from small river catchments.
NGM		25-37mm	Based on the national scale recharge map, referred to as the National Groundwater Map (NGM)

Four of the five methods listed in Table 2-26 give a recharge from rainfall in the range of 2.7%-5.2%. This corresponds very well to values given by DWAF (1995) for the region, which are in the order of 2.7% to 6.8%. The Enslin method calculates a recharge value of 10.5% of MAP and seems to be an overestimate. An overall figure of 37mm/annum or 4% recharge from rainfall can be accepted for the study area. However, this must be considered as a rough estimate, as the steep topography in the area together with varying soil thickness influences recharge locally. Additionally, a large proportion of recharge is lost to springs in the area.

2.11 Hydrogeological Evaluation

Water in the study area is used for domestic purposes and partly for small scale agricultural activity. Currently, water supply needs are mostly met from rivers and springs, with boreholes equipped with hand pumps playing a secondary role. However, groundwater could play an important role as it is a reliable water source, even in drought situations and is generally of good quality compared to other water sources in the area. Settlement varies from dispersed and isolated kraals to dense settlements in communities.

The rocks of the Natal Metamorphic Province are characterised by negligible primary porosity and groundwater movement is primarily within hard rock aquifers and controlled by zones of deep weathering, faulting, fracturing and jointing. Accordingly, water strikes or seepage encountered in the exploration boreholes drilled during the investigations are either associated with the contact between weathered and solid bedrock, or deep seated fracture zones of low permeability but high confining pressure. There is no evidence of any additional aquifers at contacts between different lithologies, suggesting that tectonic contacts are more relevant than lithological contacts. Lithological variations are more significant in terms of water quality, with poorer water quality having been recorded in schists and granites (King, 1997).

Topography has a marked effect on the development of groundwater resources in the area. Where steep slopes encourage surface runoff, weathering products have been entirely removed and groundwater is exclusively controlled by faults and fracture zones. Lower lying areas or areas of a more gentle relief experience a significantly reduced surface runoff and aquifers can develop in both the weathered profile and the underlying fracture zones of the

basement rocks. The weathered overburden material provides a significant storage to replenish the underlying fractured aquifer.

The area exhibits a poor historical success rate with about 46% of the holes being dry. Borehole yields are generally low with only 23% giving a yield greater than 1l/s, however in this study greater than 75% of boreholes yielded more than 1 l/s. These reported borehole yields are mainly derived from blow tests and seldom from a long duration test. Therefore the percentage of boreholes with a sustainable yield exceeding 1l/s is likely to be much lower. Dry boreholes as well as high yielding holes have been drilled into all lithologies and are not restricted to any specific rock type; poor and high yielding holes occur within the same lithology and give evidence that structures of tectonic origin are a major factor influencing groundwater occurrence.

During the Critical Intervention Programme, where geophysical siting was used, 37% of 27 boreholes drilled in the study area were dry and only 2 had blow yields exceeding 1 l/s. The median yield of successful holes was 0.1 l/s. The present study achieved an 89% success rate, with 7 of 9 boreholes exceeding 1 l/s and a median yield of between 1.8-3.3 l/s. This suggests that the aquifer can be reconsidered in terms of reticulated water supply if a scientifically appropriate exploration strategy is adhered to.

The water table in the area is extremely variable due to the rugged topography. The static water level ranges from 2 to 75m with an average depth of 46m below surface. In general, the depth of water level increases with rising altitude. As the water strikes in the drilled boreholes occur much deeper, the aquifers are considered to be of a confined nature.

Discharge tests carried out on eight exploration boreholes indicate that at least 4 types of aquifers occur: networks of uniform fractures, sub-vertical fractures with or without leaky weathered overburdens, bedrock contacts with a leaky overburden, and leaky deep seated horizontal fractures. Sustainable yield vary between $26m^3/d$ and $300m^3/d$. All aquifers are confined in character and respond to abstraction in a discontinuous fashion, due to limited extent of fractures or, where a thick weathered overburden is encountered, due to leakage that leads to partly steady-state conditions during pumping. High yields are generally derived from aquifers overlain by thick weathered overburden, or large fault zones. Where these are absent or the saturated overburden too thin, small scale fracture zones represent the main target. Transmissivities vary mostly between 1 and $23m^2/d$.

A correlation between lineament or fault azimuth and yield shows that successful boreholes are associated with N-S, E-W and NE-SW running structural features, orientations of extensional nature. The only unsuccessful borehole was drilled into a NW-SE fault, the orientation regarded as compressional in nature. However, results have to be taken with caution, as they are based on nine boreholes only. In general, the wide range of azimuth trends related to successful boreholes suggests that a pervasive influence such as erosional unloading is operating on all existing fracture systems.

The yield data set based on the nine boreholes drilled during this investigation shows also a clear correlation between borehole yield and lineament or fault length, indicating, that regional scale features have a far better groundwater potential than local scale structures.

Appendix 2-D presents the summarized results of the laboratory analyses for all sampling points and the DWAF specifications for drinking water and the water quality criteria after the SABS 241-1999, respectively. The water samples from all the successful boreholes are graphed as Schoeller diagrams, tri-linear Piper diagrams and Stiff diagrams (Appendix 2-E). The ambient water quality ranges from ideal to marginal, falling within the DWAF class 0-2

due to the total dissolved solids content, however, some of the samples fall within class 3 in terms of their fluoride concentrations. Electrical conductivities, as a guide to the overall potability of the groundwater, plot between 47 and 266mS/m.

The samples obtained from borehole G47154, G47155, G47156 reflect the water quality from aquifers in the weathered overburden and have water of class 0-1. As HCO_3 is the dominant anion, the groundwater from these boreholes is of a recent origin, and indicating the influence of rainfall recharge. Boreholes G47154 and G47155 are drilled into the same fault structure and have similar water qualities of $CaMgHCO_3$ type water, except that G47155 has a higher total dissolved solids content. This can be attributed to the lower transmissivity of this borehole. G47155 probably missed the main permeable flowpath, hence water has a longer residence time, resulting in class 1 water.

Borehole G47156 was drilled into granite, although it location was mapped as Mapumulo Group gneisses. It has a slightly different geochemical signature and can be characterised as an $NaHCO_3$ type water. It also has a significantly higher fluoride content and hence is classified as type 2. This enrichment by fluoride and apparent enrichment of Na relative to Ca and Mg can be attributed to mixing with deeper water due to a water strike in unweathered red granite, which has a longer residence time. The presence of calcite in the deeper fractures of G47156 (Appendix 2-B) and a higher pH suggests that Ca and Mg may be precipitating out of solution, resulting in Na becoming more dominant even though the borehole is not enriched in Na relative to G47155.

Boreholes G47151, G47152, G47153 and G47159, tap deep seated fracture zones and can be considered to represent water of longer residence time. These boreholes are characterised by NaCl type water and are generally of class 1-2, except for fluoride contents, which give rise to class 3 water for some boreholes.

Although boreholes G47151 and G47152 are located 30 m apart, are hydraulically connected, and have similar lithologies and total dissolved solid contents, they exhibit different geochemical signatures in terms of the Piper Plot. This can only be explained in terms of the impact of the dolerite dyke. Borehole G47152 taps most of its water from below the dolerite dyke, whereas G47151 taps water both below and above the dyke. Water below the sub-horizontal dyke can be considered to have a longer residence time, hence it has elevated fluoride contents (class 3) and is enriched in sodium relative to G47151 due to the precipitation of calcite. Ca, Mg and bicarbonate ions are significantly depleted in G47152 and pH is elevated, confirming that the borehole has a geochemical signature indicative of calcite precipitation.

Borehole G47159 and G47153 are similar to G47151, however, they have a lower fluoride content. This can be attributed to their amphibolite provenance, which has a meta-greywacke-volcanic origin, which also causes some magnesium enrichment.

Borehole G47158 in the Tugela Valley, although having its main water strike in the weathered overburden, has a geochemical signature representative of older water, suggesting that the aquifer lies in an upwelling zone. It has a geochemical signature similar to G47151 and G47153, however, sodium and chloride are considerably enriched. This may also be due to lower rainfall recharge in the lower lying Tugela Valley. The high fluoride content, however, suggests that the water originates from deep seated fracture zones, in spite of the shallow water strike.

2.12 Financial Analysis

The objective of this section is to evaluate the extent to which additional exploration is financially viable in terms of a reduction in overall borehole establishment costs based on experiences in the Natal Metamorphic Province. Three different scenarios were considered to establish *10* successful boreholes: *i)* no structured exploration programme, or drilling randomly or by visual observation; ii) limited exploration based only on the frequently used method of limited EM-34 and magnetometer geophysical traverses and a desk study of existing maps; and iii) full exploration based on structural mapping, LANDSAT and aerial photo interpretation, and field geophysical exploration using the most appropriate system as defined by hydrogeological conditions.

Results for Scenario 1 are based on historic drilling records as recorded in the NGDB, which are assumed to represent random drilling or boreholes sited without modern exploration methods. In the study area 120 boreholes have been drilled, of which 46% yielded water. This success record was used to estimate the number of holes and associated costs required to establish 10 yielding boreholes.

Scenario 2 is based on success rates achieved during the Critical Intervention Programme, where 27 boreholes were sited using an EM-34 and magnetometer. Only 17 of these boreholes contained water.

Scenario 3 is based on the methodology adopted for this project, where a MAX-MIN EM system was used due to advantages of depth of penetration, and potential to collect data simultaneously in both the profiling and sounding modes. Traverses were conducted in order to site boreholes across lineaments identified from LANDSAT and aerial photo interpretation, field verification of lineaments, and the structural analysis of lineament orientations based on outcrop mapping. The investigation drilled 9 holes, of which 8 were successful. Costs were extrapolated in order to determine costs to achieve 10 yielding boreholes so that they could be compared to scenario 1 and 2.

The estimated costs for all three scenarios are shown in Table 2-27. The costs are based on the Council for Geoscience rates and man-hours expected during the investigation.

Table 2-27 Approx. costs to establish 10 yielding boreholes according to scenarios 1,2 and 3

ITEM		Units	Rate	Scenario1		Scenario2		Scenario3	
				Qty	Cost	Qty	Cost	Qty	Cost
Desk Study[1]	EXPLORATION	Day	1600			1	1600	5	8000
EM34 survey[2]		Day	1500			5.3	7950		
Max Min survey[3]		Day	2500					5.5	13750
Resistivity survey[3]		Day	2500					5.5	13750
Geophysical interp.		Line	100			32	3200	33	3300
Accommodation		Day	150			5	750	11	1650
Landsat image[4]		Each	2500					1	2500
Landsat interp.		Day	1200					3	3600
Structural mapping		Day	1350					3	4050
Sub total - Exploration					0		13500		50600
Community liaison[5]		Hr	100	19[9]	1900	16[10]	1600	11[11]	1100
Drilling[6]		Hole	11000	19	209000	16	176000	11	121000
Drill supervision		Day	1000	19	19000	16	16000	11	11000
TOTAL					229900		207100		183700

Per successful site			22990	20710	18370
Median yield	L/s		0.1	0.1	1.8
R/l/s	R/l/s		229900	207100	10206

1: Review of topographical and geological maps and geological reports
2: At 1h per drilling site
3: At 1 technician and one labourer and 3 boreholes sited per day, including magnetometer surveys
4: At 2 technicians and 2 boreholes sited per day including magnetometer surveys
5: At 2 technicians and 2 boreholes sited per day
6: At 22% recovery per usage of R10000 per 180 x 180 km image and R1200 in man-hours for co-ordinate registration
7: Field mapping of outcrops and aerial photo interpretation
8: Casing costs are not considered as it is assumed that only successful boreholes would be cased, which would result in similar casing costs for all scenarios
9: According to the success rate of 54% as determined from the drilling records in the NGDB
10: According to the success rate of 63% as determined from the drilling records in the CIP
11: According to the success rate of 89% achieved during this investigation

The results from Table 2-27 are illustrated graphically in Figure 2-94.

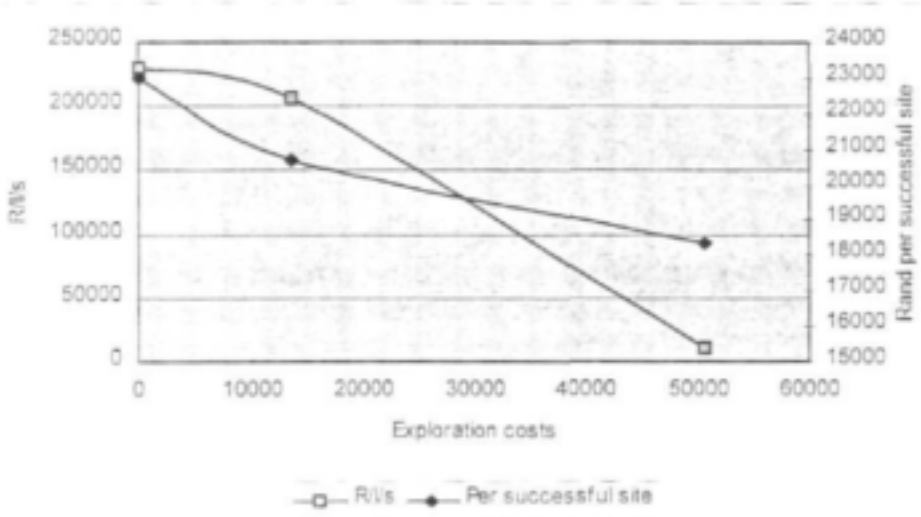

Figure 2-94 Exploration costs versus success rate

Figure 2-94 shows that with a larger budget for exploration a substantial cut in costs per successful borehole site or in terms of water production in R/l/s can be achieved. Historic success rates have resulted in an expenditure of approximately R23000 for the establishment of each successful borehole. In comparison, an increase in the exploration budget of R13500 would improve drilling success rates and result in expenditure of about R20700 per successful borehole. If exploration expenditure is increased further to about R50600, then success rates of 89% can be expected and establishment costs would come down to about R18370 per successful borehole.

Exploration costs exhibit economies of scale, hence the larger the program the smaller is the proportion of the budget dedicated to exploration. A more comprehensive exploration program and a larger exploration budget could in the long-term result in significant cost savings, especially in large regional programs where the costs of regional geological exploration are spread over many boreholes. In such cases dedicating a larger proportion of the budget to exploration than is currently the case may result in more efficient drilling and a net reduction in establishment costs per site. For such an exploration program to be successful

it must incorporate field geological mapping, remote sensing and appropriate geophysical exploration based on the identified hydrogeological regime.

In some cases, such as reticulated systems where production rates are more important than the number of water points established, it may be beneficial to evaluate program efficiency in terms of costs per unit yield of water. For the Natal Metamorphic Province, costs of water production in terms of R/l/s are shown in Figure 2.94. These suggest that drilling without prior scientific exploration results in a cost of R229900/l/s of water produced. Minimal exploration (scenario 2) results in costs of R207100/l/s of water produced. The data suggests that increased exploration results in reduced production costs of R10206/l/s, or 5% of those achieved during the CIP. This saving can be attributed to the high median yield achieved during this study.

2.13 Conclusions and Recommendations

Groundwater is an important resource in the study area, providing a clean and consistent water source. The geology in the area consists mainly of gneisses, granites and amphibolites of the Natal Metamorphic Province. The low primary porosity of this hard rock aquifer restricts groundwater flow to fracture zones or deeply weathered profiles, where successful boreholes can be established. Successful groundwater exploration in the area has to delineate these features by taking the following geological, hydrogeological and geophysical considerations into account:

- A tectonic analysis of faulting in terms of the potential of faults and their related joint systems to be water bearing requires that the orientation of tensional, compressional and shear couples be understood. On the Natal coast, this requires an understanding of tectonic processes at work on the Agulhas Transform Fault and the resulting onshore fault and fracture system. It is most probable that the faulting in Natal is related to divergent wrenching on the Agulhas Transform Fault, in which case the maximum extensional force would be directed perpendicular to normal faults. In this case, ENE transtensile normal faults are expected to have the maximum tensional strain, while NE trending faults are likely to be synthetic strike-slip faults and in shear. E-W faults are likely to be antithetic and in shear, while north trending faults can be interpreted as high-angle faults connecting synthetic fault trends.

- Field structural measurements and consequent strain analysis suggest that the most prominent features are the NNE and ENE trending fault sets, with subordinate NE and NW trending faults. The structures to favour for groundwater exploration are the major N to NNE and ENE fractures as they seem to be the open structures. The subordinate NW and NE fractures that dip steeper than +/- 60° may also be good water carriers, but the fractures dipping less than 45° are closed due to the presence of a thrusting component.

- Lineaments in the study area follow a distinct joint set, which is dominated by three major strike directions: N-S to NNW-SSE, ENE-WSW and NW-SE. The ENE-WSW and NW-SE features appear to be of greater regional significance, whereas the lineaments striking N-S proved to be of only local importance.

- Discharge tests carried out indicate that at least 4 types of aquifers occur in the research area: networks of uniform fractures, sub-vertical fractures with or without leaky weathered overburdens, bedrock contacts with a leaky overburden, and leaky deep seated horizontal fractures. High yields are generally derived from aquifers overlain by a thick weathered overburden, or from large fault zones.

- To delineate water-bearing fracture-zones, the electromagnetic technique can be a promising geophysical method to use in the study area where shallow weathered aquifers exist. However, water strikes are generally deep, with 50% of water strikes occurring below 70m. These targets were only detected using the 220 and 880 Hz frequencies (figs. 5-58 and 5-71). Therefore, only electromagnetic techniques with a sufficient penetration depth are suitable to delineate fracture zones. The EM34 has proved to be inadequate under the given hydrogeological conditions, especially when used with a 20m coil separation giving a penetration depth of about 25m in this lithology. The APEX Max-Min electromagnetic system proved to be effective in locating buried narrow conductors. With a coil separation of 100m reliable information from the subsurface of up to 50m and more, depending on the lithology, can be obtained.

- Resistivity sounding proved to be helpful in locating deep weathered profiles, which could be an indication of buried fracture zones. Consequently, resistivity profiling would be the most effective means of geophysical exploration. Furthermore, changes in lithology can be detected. Whereas thick weathered overburden is a promising groundwater target in the area, no evidence of any additional aquifer at contacts between different lithologies could be found.

- The magnetometer helps in delineating faults or fracture zones if the features are either broad so that weathering is significant and hence alters the magnetic properties of the fault or fracture zone compared to the unweathered bedrock, or if the fault or fracture zone separates different lithologies.

- Besides fracture zones, the most important water-bearing features in the study area are deep weathered profiles. The occurrence of deeply weathered zones is strongly linked to the geomorphology of the area. Where steep slopes encourage surface runoff, weathering has been entirely removed and groundwater is exclusively controlled by faults and fracture zones. Lower lying area or areas of a more gentle relief experience a significantly reduced surface runoff and aquifers can develop in both the weathered profile and the fracture zones of the basement rock. Additionally, the weathered overburden can increase significantly in depth over fault or fracture zones providing an additional shallow aquifer. The weathered material provides significant storage, replenishes the underlying aquifer.

- To delineate deeply weathered profiles all three geophysical methods, the Max-Min profiling and sounding, resistivity sounding and magnetometer profiles were beneficial. The electromagnetic technique indicates changes in the thickness or conductivity of the weathered overburden with ramp, ridge or valley discontinuities. To determine the thickness of the weathered overburden, resistivity soundings are necessary.

- Structures like dykes or sills are relatively rare and do not play an important role as groundwater targets in the area. Furthermore, they are difficult to detect by magnetics as the intrusions exhibits similar magnetic properties as the host rock.

- A correlation between lineament or fault azimuth and yield shows that successful boreholes are associated with N-S, E-W and NE-SW trending structural features, orientations of extensional nature. The only unsuccessful borehole was drilled into a NW-SE fault, the orientation regarded as compressional in nature. However, results have to be taken with caution, as they are based on nine boreholes only. In general, the wide range of azimuth trends related to successful boreholes suggests that a pervasive influence such as erosional unloading is operating on all existing fracture systems.

- The yield data set shows a strong correlation with lineament or fault length. The four highest yielding boreholes are associated entirely with regional scale structural features, whereas local features have a poorer groundwater potential.

- The topography is a decisive factor controlling the availability of groundwater in the study area. Besides the fact that geomorphology has a strong effect on the development of weathered profiles, it also influences the depth of the static water level. At low altitude static water levels are generally shallower and occur in the weathered profile, which serve as a storage horizon.
- The financial analysis suggests that a more comprehensive exploration programme and a larger exploration budget could in the long-term result in significant cost savings, especially in large regional programs where costs of regional geological and structural exploration are spread over many boreholes. In such cases dedicating a larger proportion of the budget to exploration than is currently the case may result in more efficient drilling and a net reduction in establishment costs per site. For such an exploration program to be successful it must incorporate field geological mapping, remote sensing and appropriate geophysical exploration based on the identified hydrogeological regime.

In conclusion, the research study showed that successful groundwater exploration for the area is possible. An evaluation of the structural geology and the hydrogeological conditions of the area together with a suitable geophysical method for the environment pushed the drilling success rate up from a historical 54% (NGDB) and 63% (Critical Intervention Program) to 89%. Beside the improved success rates, the research did result in significantly improved yields. Whereas the median yield for the NGDB and CIP records is 0.1l/s, a median yield of 1.8l/s was achieved with the applied exploration method, which accordingly lowers water production costs considerably. The average yield of all boreholes was pushed up from a historical 0.96l/s to 2.55l/s.

2.14 References

Andreoli, M.A.G., Doucoure, M., Van Bever Donker, J., Brandt, D., Andersen, N.J.B. (1996): Neotectonics of southern Africa – a review. Africa Geoscience Review, Vol. 3, No. 1, pp. 1-16.

Botha, W.J., Wiegmans, F.E., van der Walt, J.J. and Fourie, C.J.S. (1992): Evaluation of electromagnetic exploration techniques in groundwater exploration. WRC Report No. 212/1/92. 214 p.

Bredenkamp, D.B., Botha, L.J., van Tonder, G.J., van Rensburg, H.J. (1995): Manual on quantitative estimation of recharge and aquifer storativity. WRC No. TT73/95. Pretoria. 363p.

De Swardt, A.M., Bennett, G. (1974): Structural and physiographic development of Natal since the Late Jurassic. Trans. Geol. S. Afr. 77, 309-322.

Dent, Lynch, Schulze (1989): Mapping mean annual and other rainfall statistics over Southern Africa. Water Research Commission, Pretoria, South Africa, WRC Report 109/1/89.

Du Toit, A.L. (1954): Geology of South Africa, third Edition. Oliver and Boyd, Edinburgh.

DWAF (1995): Characterization and mapping of the groundwater resources, KwaZulu-Natal Province, mapping Unit 2. Dept. of Water Affairs and Forestry, South Africa.

DWAF (1996). A guideline for the health related assessment of the quality of water supplies. Pretoria. 1st Edition. 46p.

Enslin, J.F., Bredenkamp, D.B. (1963): The value of pumping tests for the assessment of ground-water supplies in secondary aquifers in South Africa. Technical Report No 30. Division of Hydrological Research, Dept. of water Affairs and Forestry, South Africa.

Gevers, T.W. (1941): Carbon dioxide springs and exhalations in North Pondoland and Alfred County, Natal. Trans. Geol. Soc. S. Afr. **44**, p. 233-301.

Goodlad, S.W., Martin, A.K., Hartnady, C.J.H. (1982): Mesozoic magnetic anomalies in the southern Natal Valley. Nature **295**, p. 686-688.

Guy, J.E. (1974): The geology of an area to the North-West of Mandini, Zululand. Thesis (MSc), University of Natal, Durban, South Africa.

Kent, L.E. (1938): The geology of a portion of Victoria County, Natal. Trans. Geol. Soc. S. Afr. **41**, p. 1-36.

King, G. (1997): The development potential of KwaZulu-Natal aquifers for rural water supply. Thesis (MSc), Rhodes University, South Africa.

King, L.C. (1972): The Natal Monocline: explaining the origin and scenery of Natal, South Africa. Univ. of Natal, Durban, South Africa.

Leith, M.J. (1966): The geology of an area to the south of Mapumulo, Natal. Thesis (MSc), University of Natal, Durban, South Africa.

Linstroem, W. (1987): Die geologie van die gebied Durban. Explanation to sheet 2930. Geological Surv. S. Afr. Pretoria.

Martin, A.K. (1983): Fault pattern of coastal Natal – a result of strike-slip motion during Gondwanaland Break-up. . Joint Geological Survey/University of Cape Town, marine geol. Prog. Techn. Rept. **14**, p. 194-214.

Martin, A.K. (1984): Plate tectonic status and sedimentary basin in-fill of the Natal valley (S.W. Indian ocean).Joint Geological Survey/University of Cape Town, marine Geoscience Unit, Bulletin No. **14**, South Africa.

Matthews, P.E. (1959): The metamorphism and tectonics of the pre-Cape formations in the post-Ntingwe Thrust-Belt, S.W. Zululand, Natal. Trans. Geol. Soc. S. Afr., **62**, p. 257-324.

Matthews, P.E. (1972): Possible Precambrian obduction and plate tectonics in Southeast Africa. Nature **240**, p. 37-39.

Matthews, P.E. (1981): A new tectonic model for the northern region of the Namaqua-Natal Mobile Belt in Natal (Natal Belt). In: Abstr. of papers: South African Geodynamics Symposium, Geocongress 1981, geol. Ver. S. Afr., p. 150-151.

Maud, R.R. (1961): A preliminary review of the structure of coastal Natal. Trans. Geol. Soc. S.Afr., **64**, 247-256.

APPENDIX 2-A

GEOPHYSICAL DATA

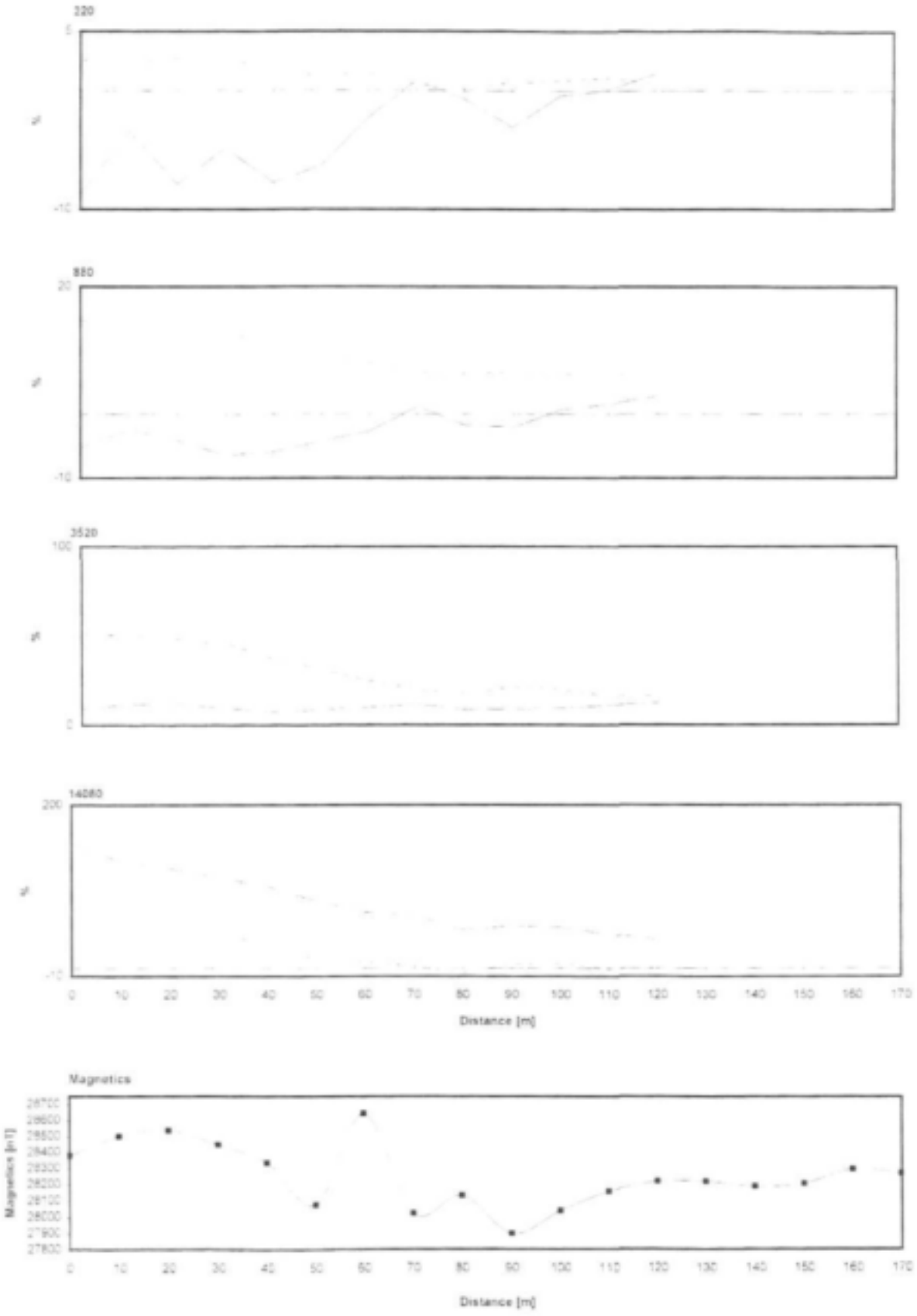

Magnetic data and Max-Min electromagnetic profiles at site NMP1. Solid line:in-phase [%]; dotted line: out-of phase [%]; coil separation 100m, station spacing 10m. Traverse direction: W-E

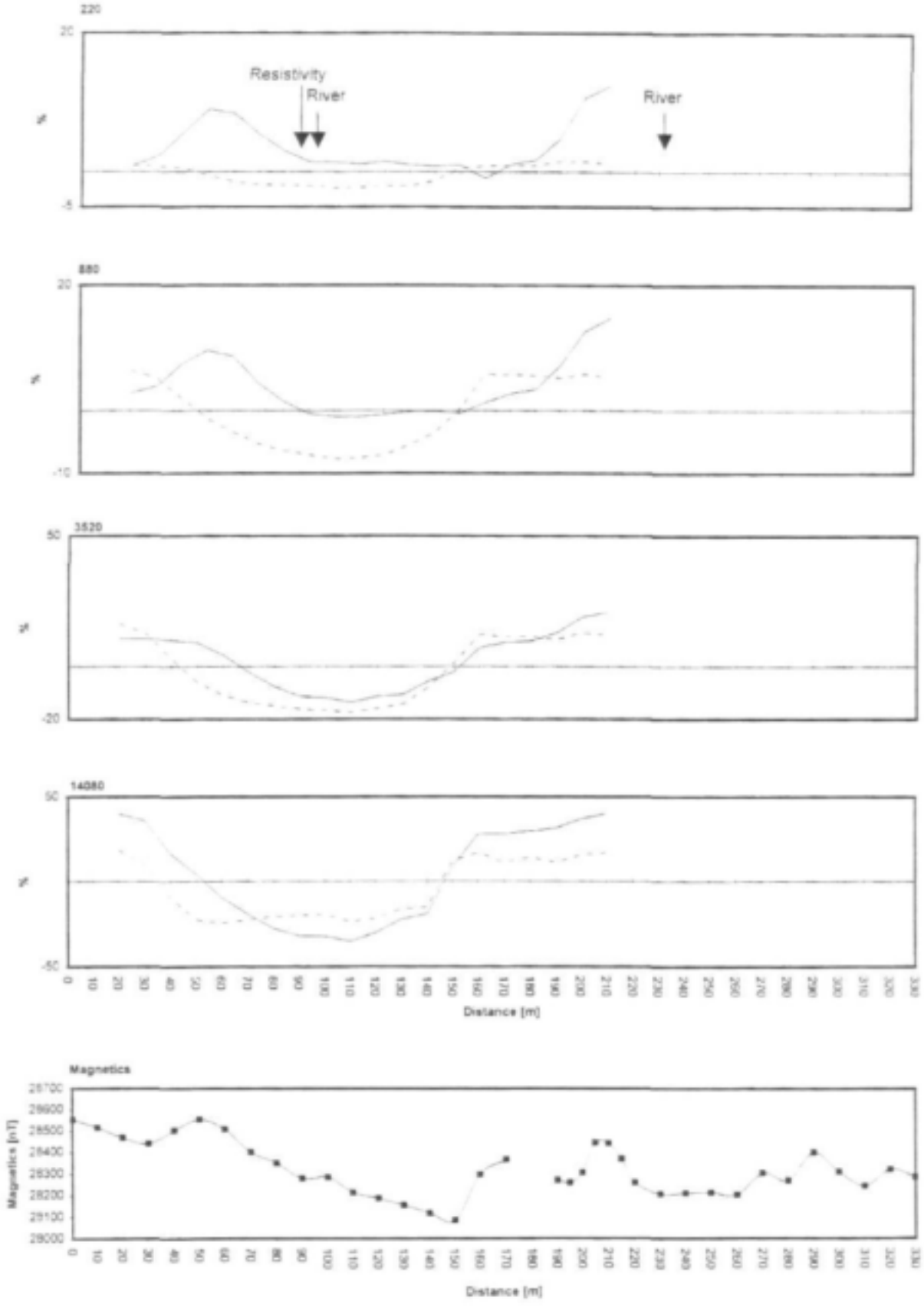

Magnetic data and Max-Min electromagnetic profiles at site NMP2. Solid line:in-phase [%]; dotted line: out-of phase [%]; coil separation 100m, station spacing 10m. Traverse direction: SE-NW

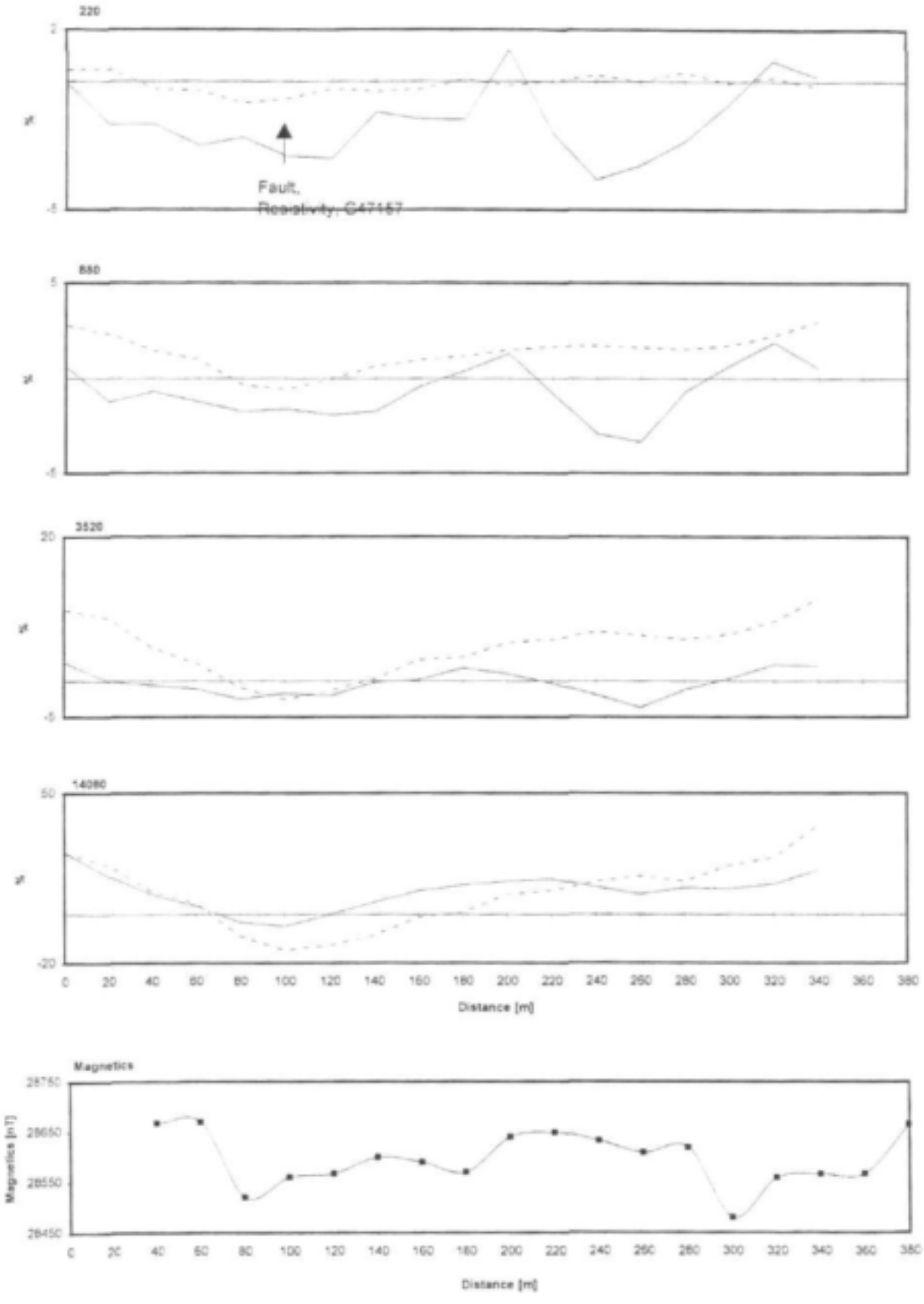

Magnetic data and Max-Min electromagnetic profiles at site NMP4. Solid line:in-phase [%]; dotted line: out-of phase [%]; coil separation 100m, station spacing 20m. Traverse direction: SW-NE

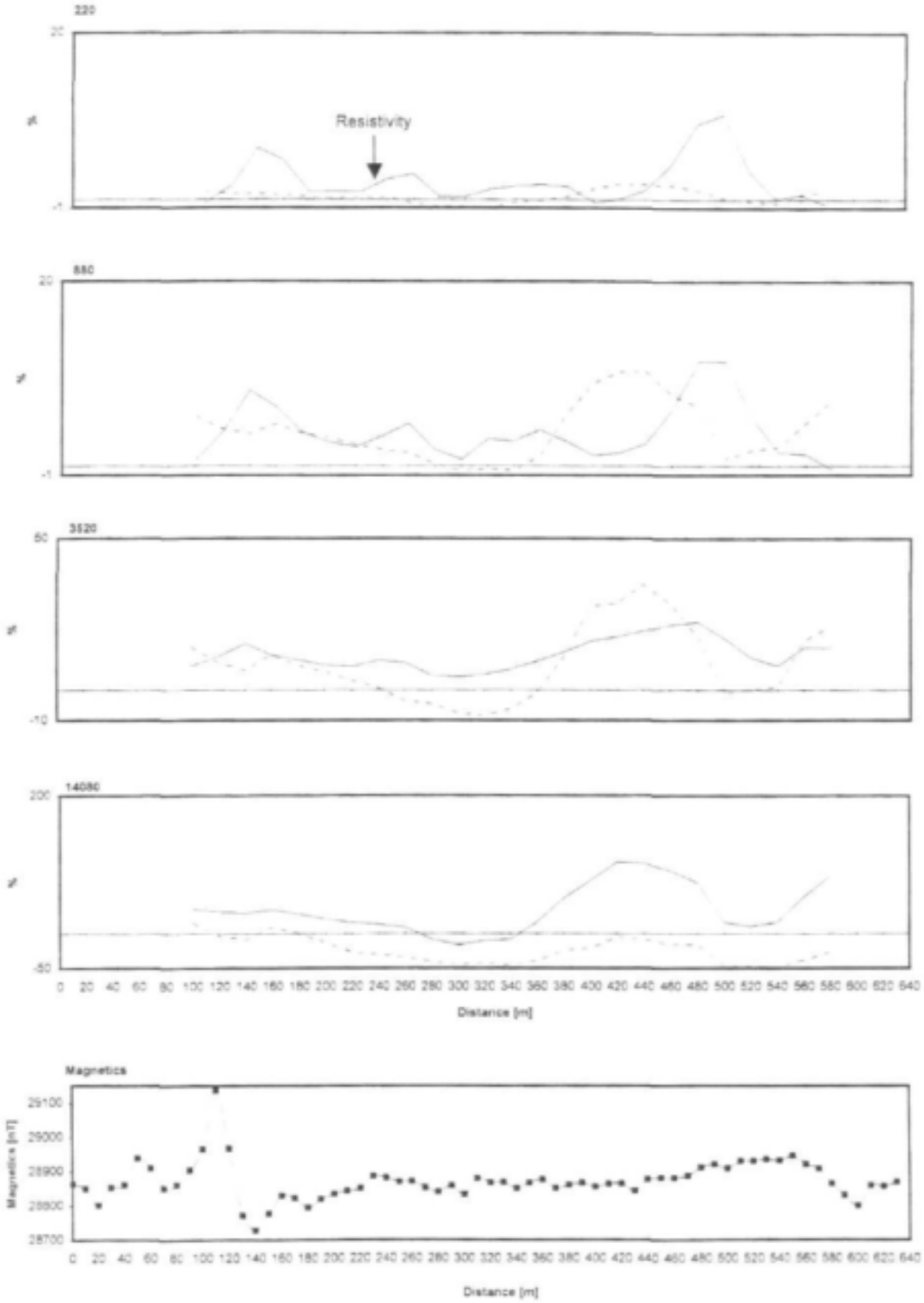

Magnetic data and Max-Min electromagnetic profiles at site NMP6. Solid line:in-phase [%]; dotted line: out-of phase [%]; coil separation 100m, station spacing 20m. Traverse direction: NE-SW

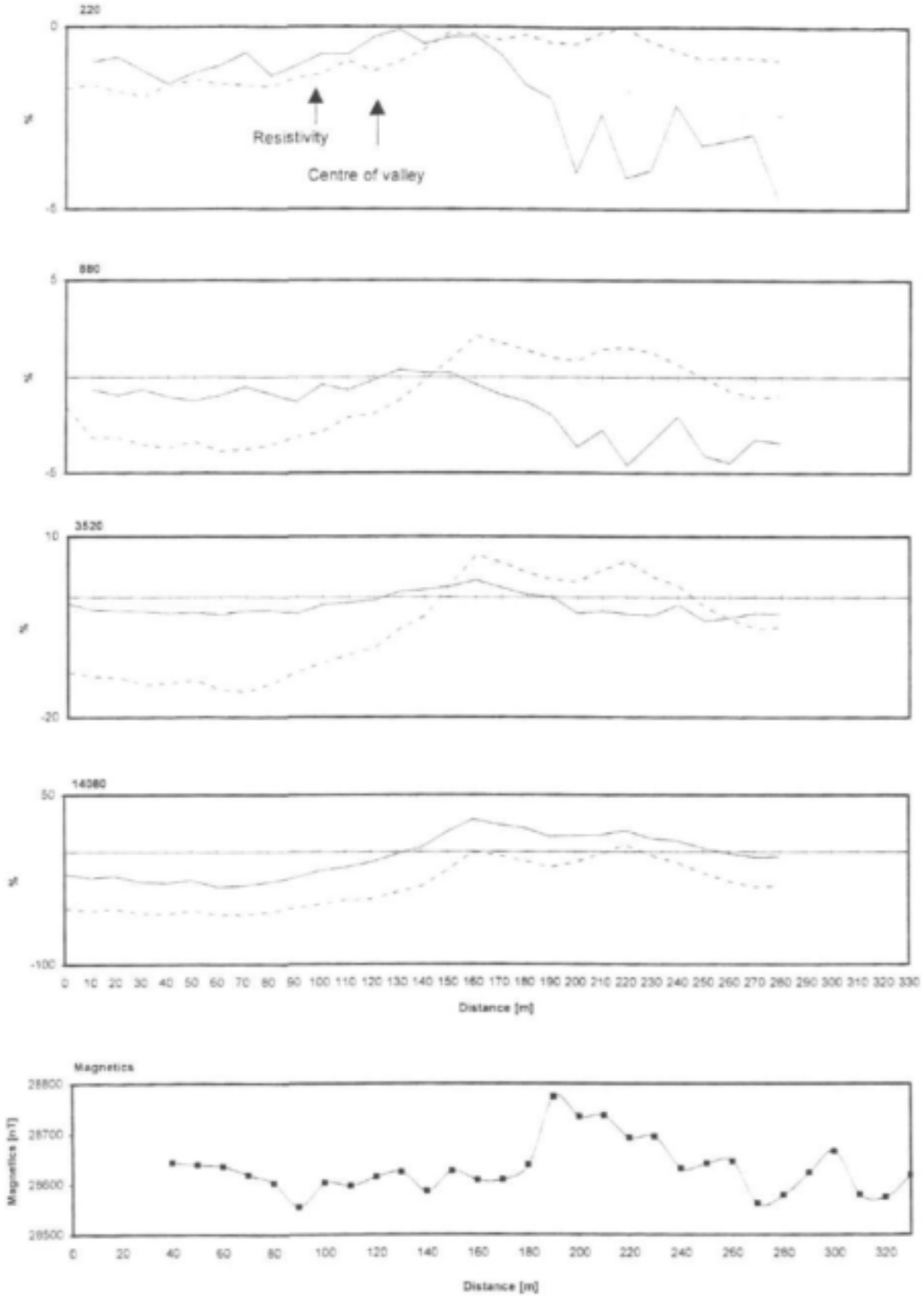

Magnetic data and Max-Min electromagnetic profiles at site NMP8. Solid line:in-phase [%]; dotted line: out-of phase [%]; coil separation 100m, station spacing 10m. Traverse direction: SSW-NNE

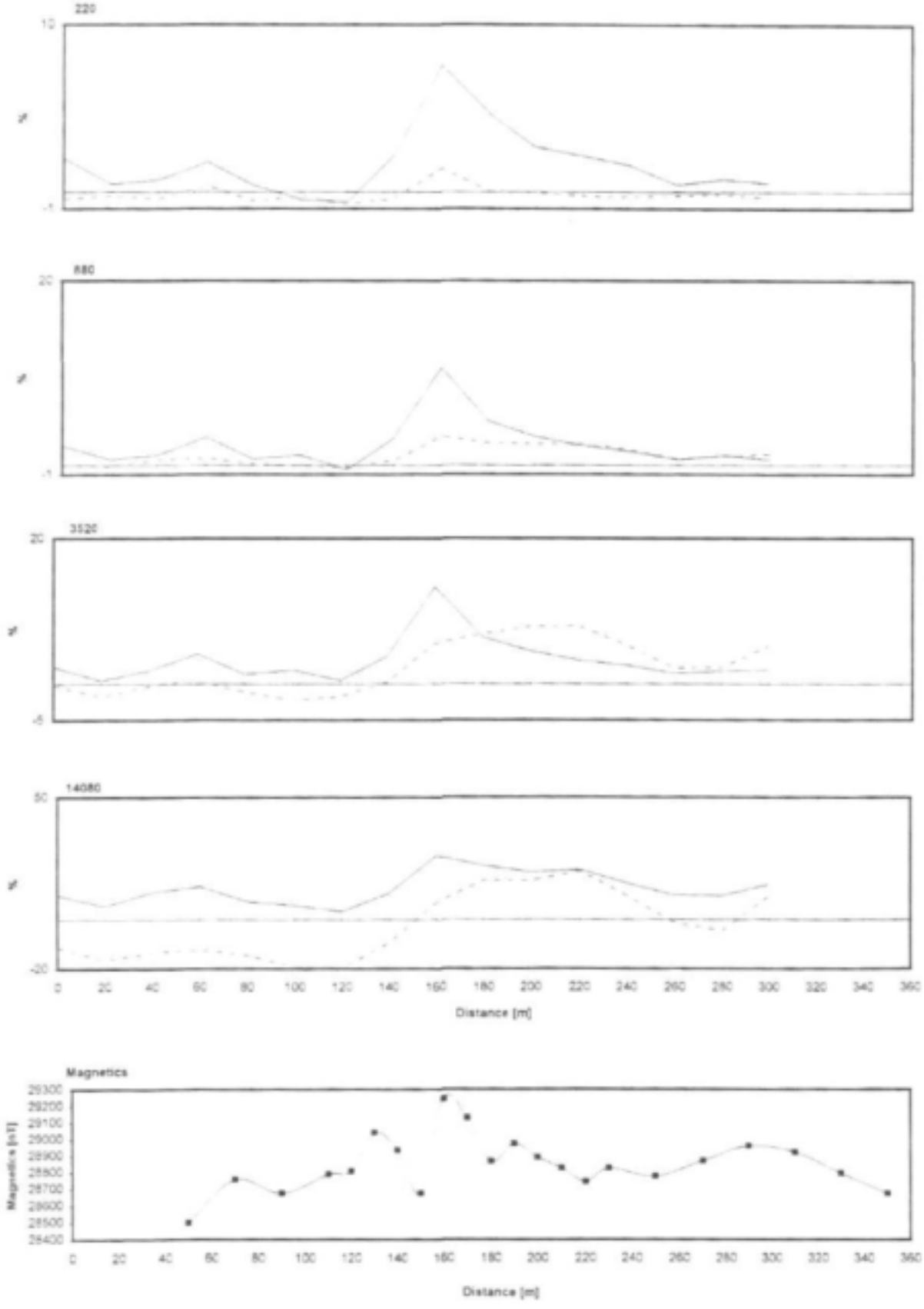

Magnetic data and Max-Min electromagnetic profiles at site NMP10. Solid line:in-phase [%]; dotted line: out-of phase [%]; coil separation 100m; station spacing 20m. Traverse direction: E-W

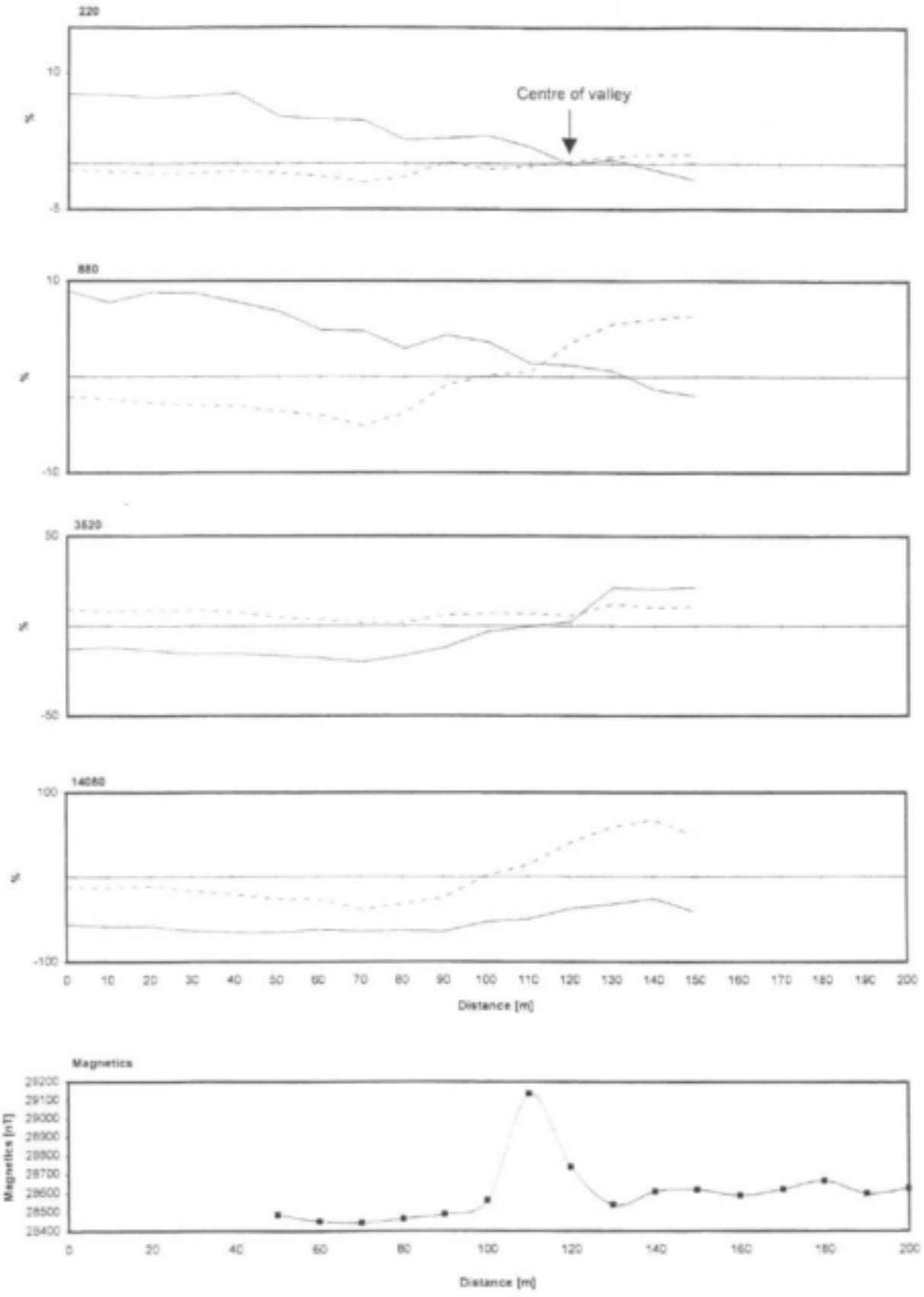

Magnetic data and Max-Min electromagnetic profiles at site NMP12. Solid line:in-phase [%]; dotted line: out-of phase [%]; coil separation 100m, station spacing 10m. Traverse direction: W-E

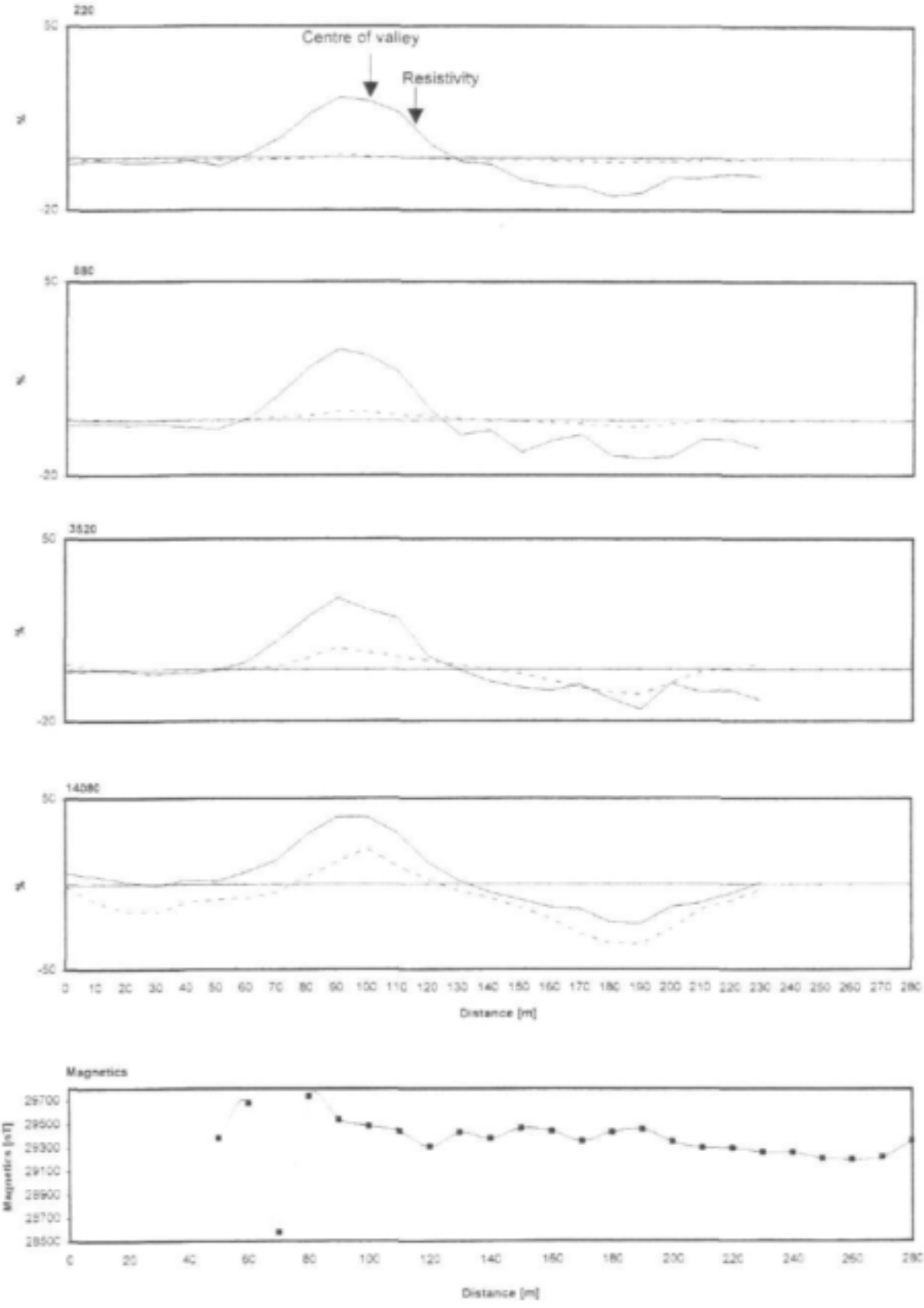

Magnetic data and Max-Min electromagnetic profiles at site NMP14. Solid line:in-phase [%]; dotted line: out-of phase [%]; coil separation 100m; station spacing 10m. Traverse direction: S-N

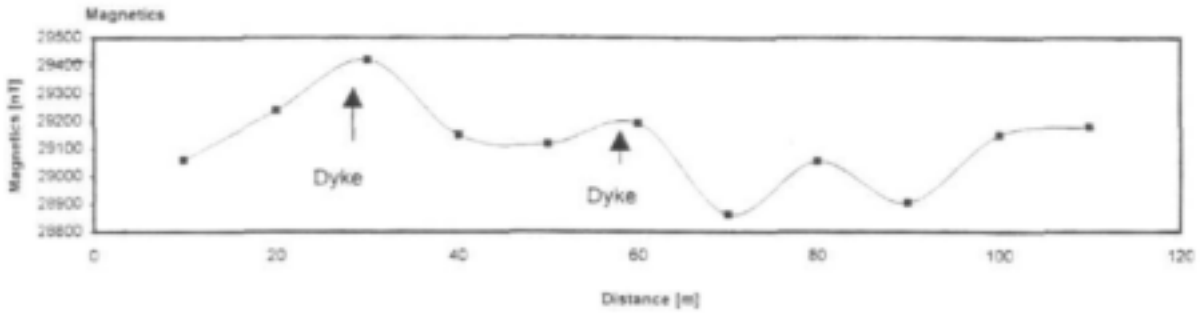

Magnetic profile at site NMP16. Station spacing: 10m, traverse direction: N-S

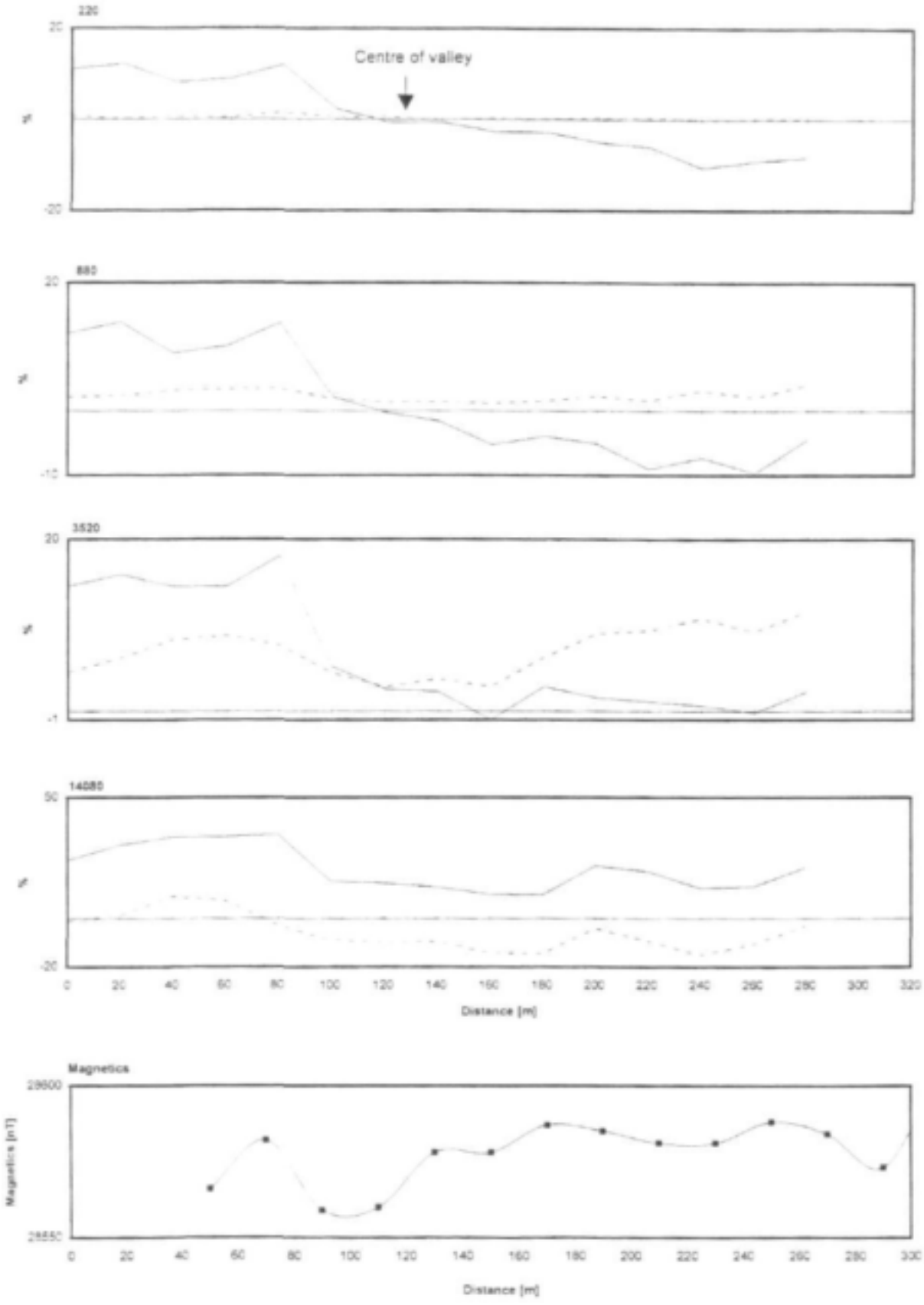

Magnetic data and Max-Min electromagnetic profiles at site NMP18. Solid line:in-phase [%]; dotted line: out-of phase [%]; coil separation 100m; station spacing 20m. Traverse direction: NE-SW

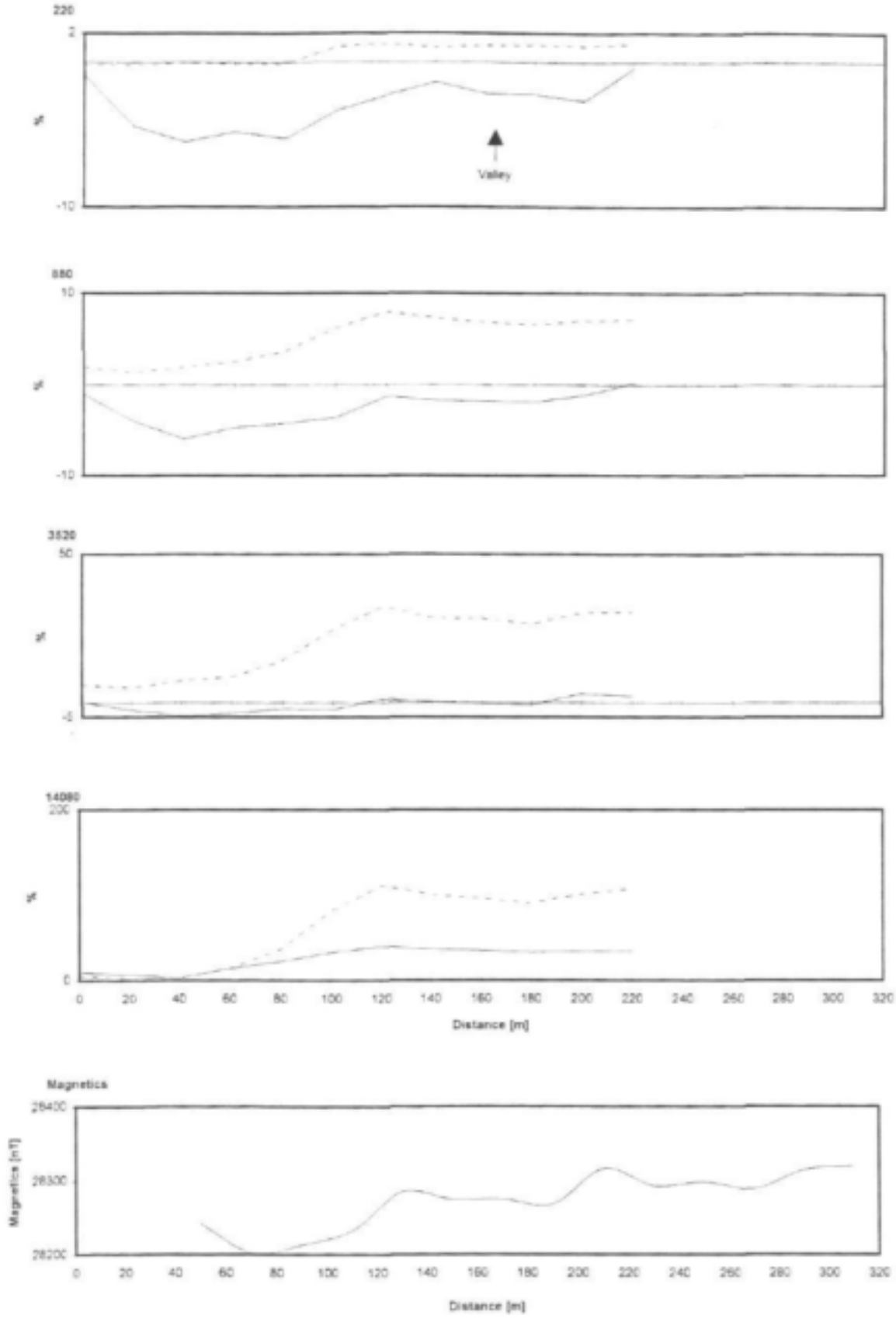

Magnetic data and Max-Min electromagnetic profiles at site NMP20. Solid line:in-phase [%]; dotted line: out-of phase [%]; coil separation 100m; station spacing 20m. Traverse direction: W-E

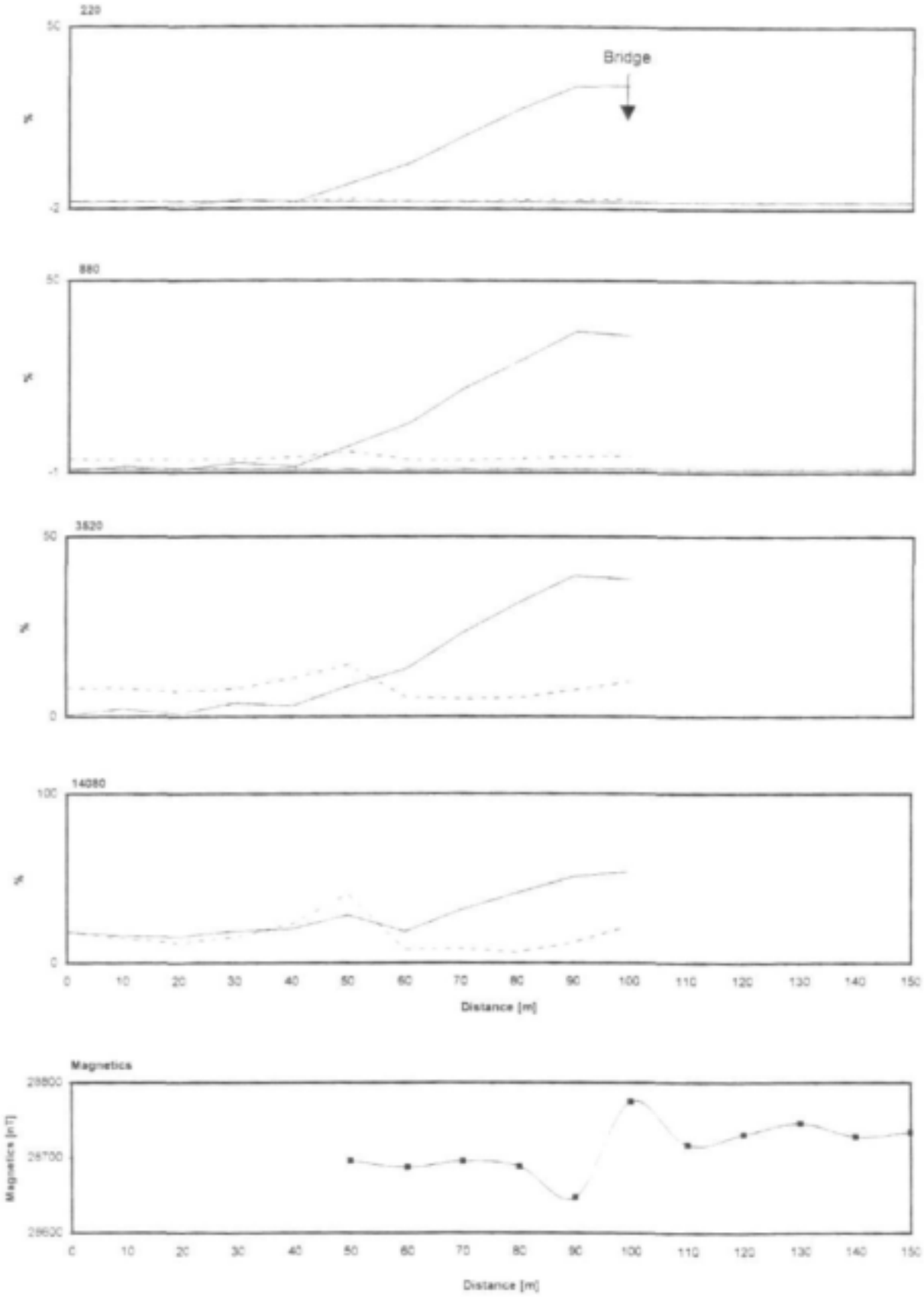

Magnetic data and Max-Min electromagnetic profiles at site NMP22. Solid line in-phase [%]; dotted line: out-of phase [%]; coil separation 100m, station spacing 10m. Traverse direction: W-E

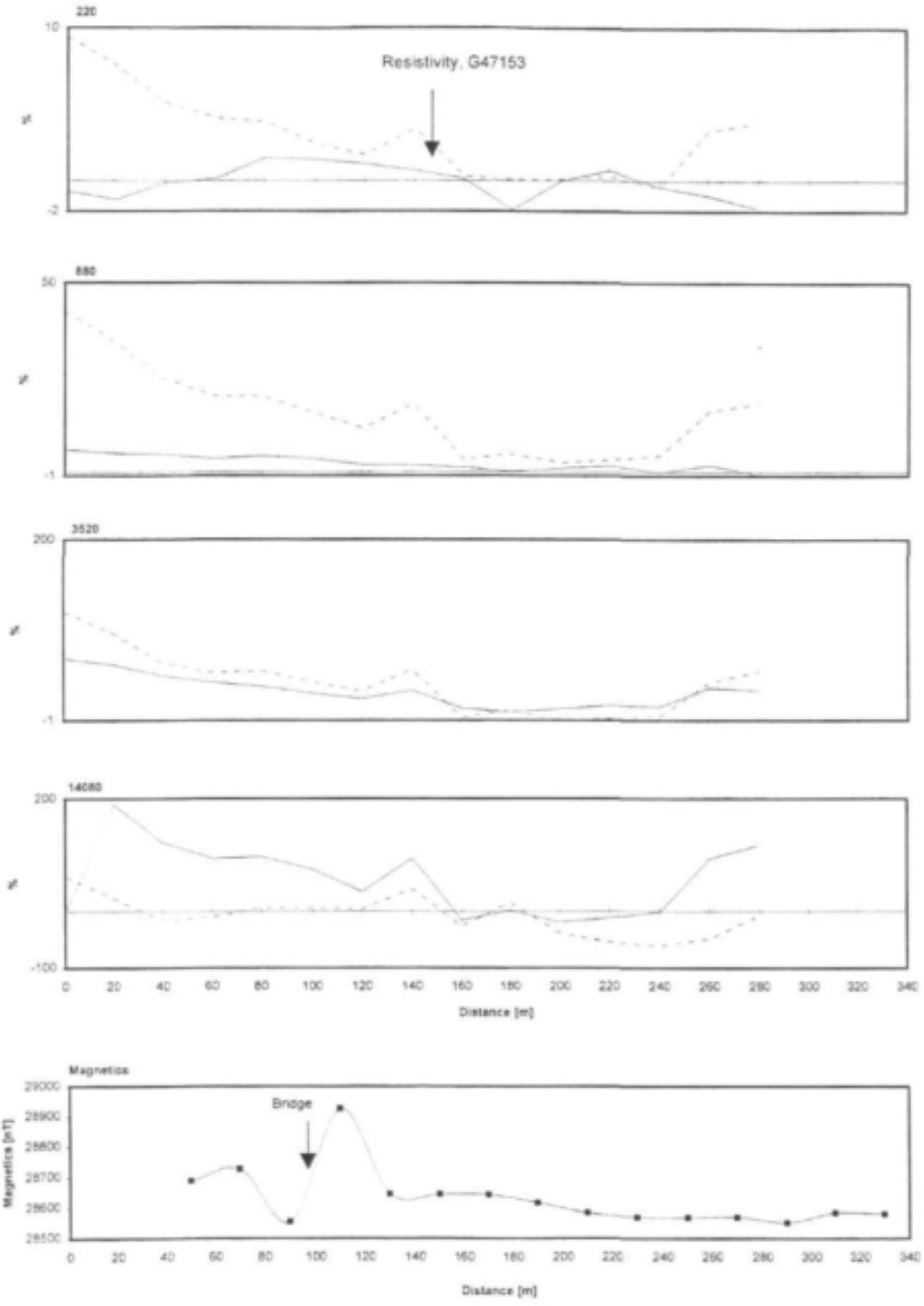

Magnetic data and Max-Min electromagnetic profiles at site NMP24. Solid line:in-phase [%]; dotted line: out-of phase [%]; coil separation 100m, station spacing 20m. Traverse direction: ENE-WSW

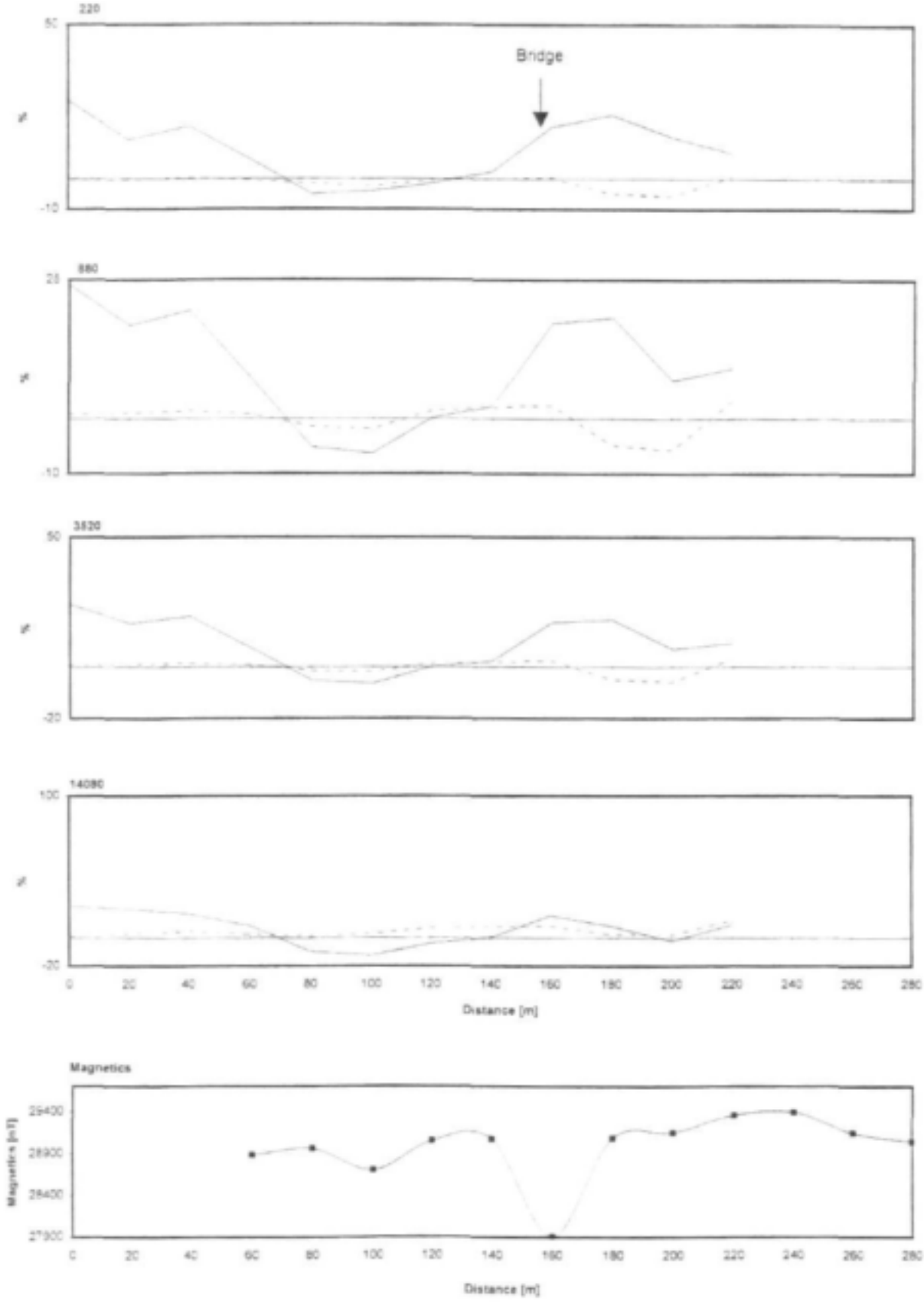

Magnetic data and Max-Min electromagnetic profiles at site NMP26. Solid line:in-phase [%]; dotted line: out-of phase [%]; coil separation 100m; station spacing 20m. Traverse direction: E-W

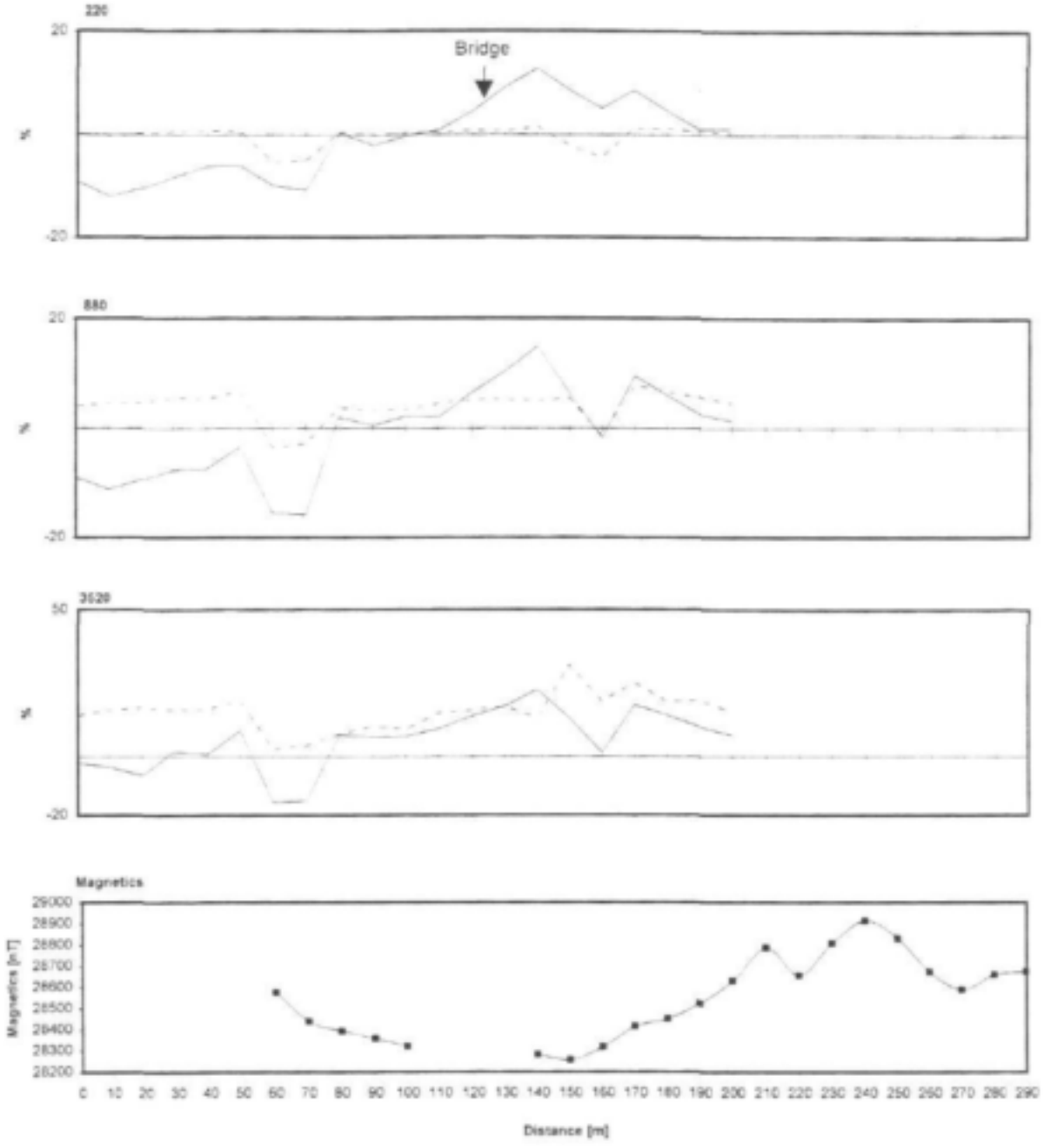

Magnetic data and Max-Min electromagnetic profiles at site NMP28. Solid line: in-phase [%]; dotted line: out-of phase [%]; coil separation 100m, station spacing 10m. Traverse direction: WNW-ESE

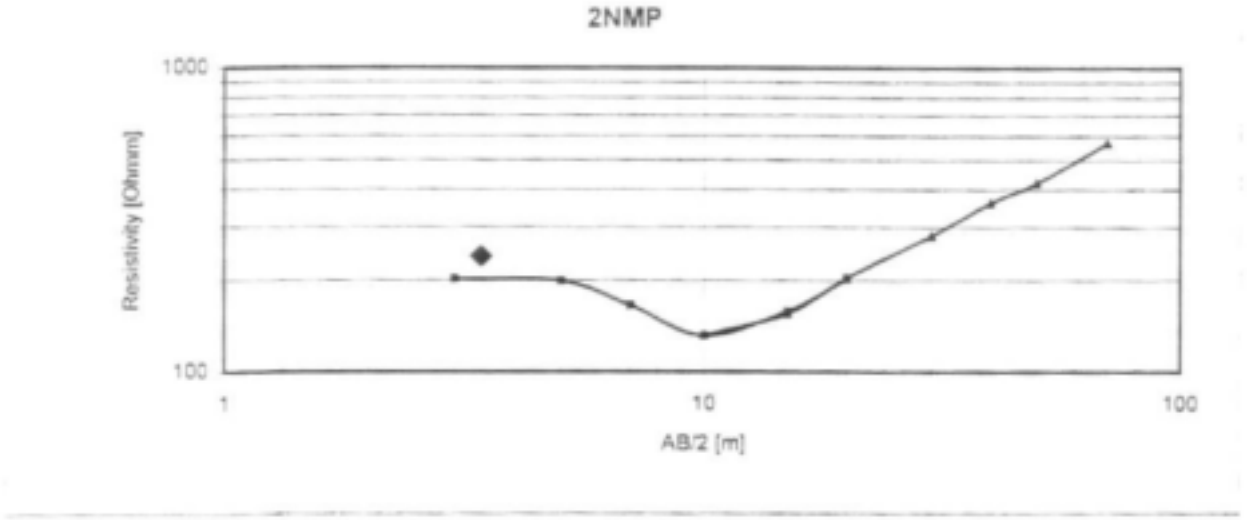
2NMP
1000
100
Resistivity [Ohmm]
1
10
100
AB/2 [m]

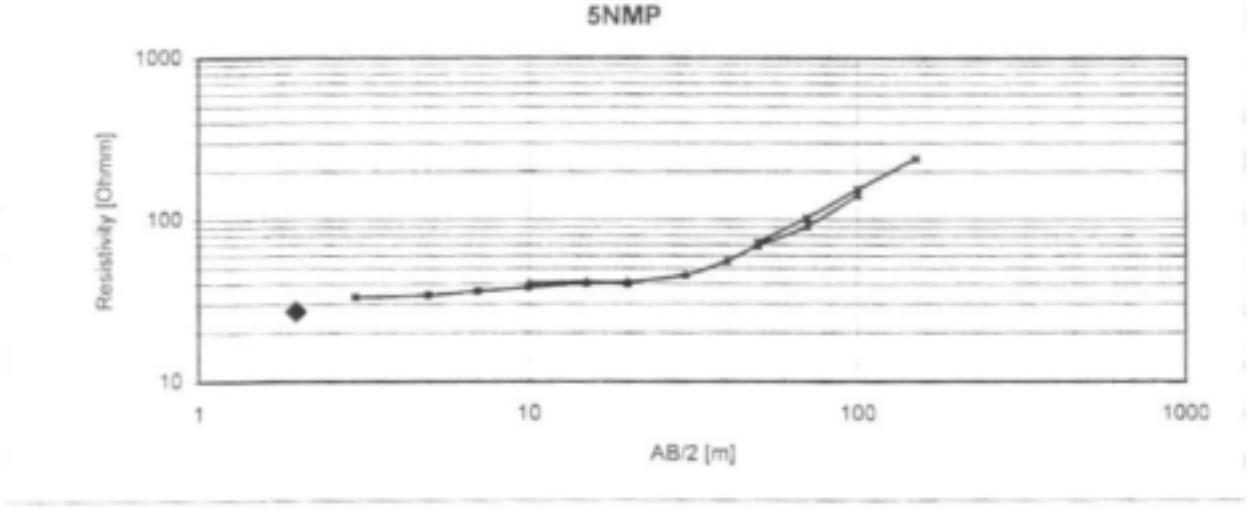
5NMP
1000
100
10
Resistivity [Ohmm]
1
10
100
1000
AB/2 [m]

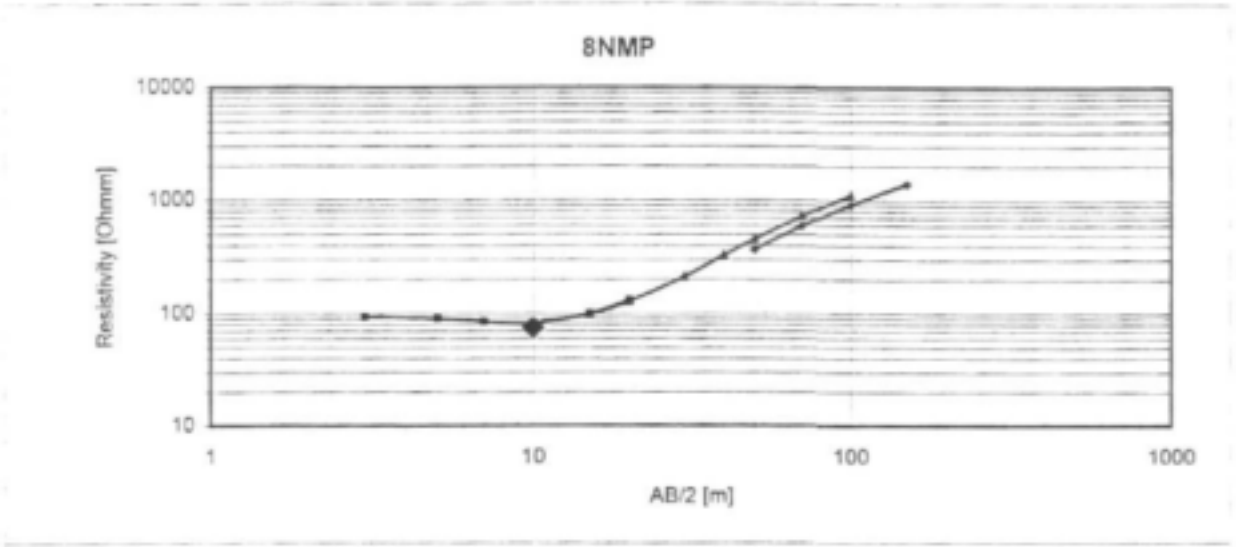
8NMP
10000
1000
100
10
Resistivity [Ohmm]
1
10
100
1000
AB/2 [m]

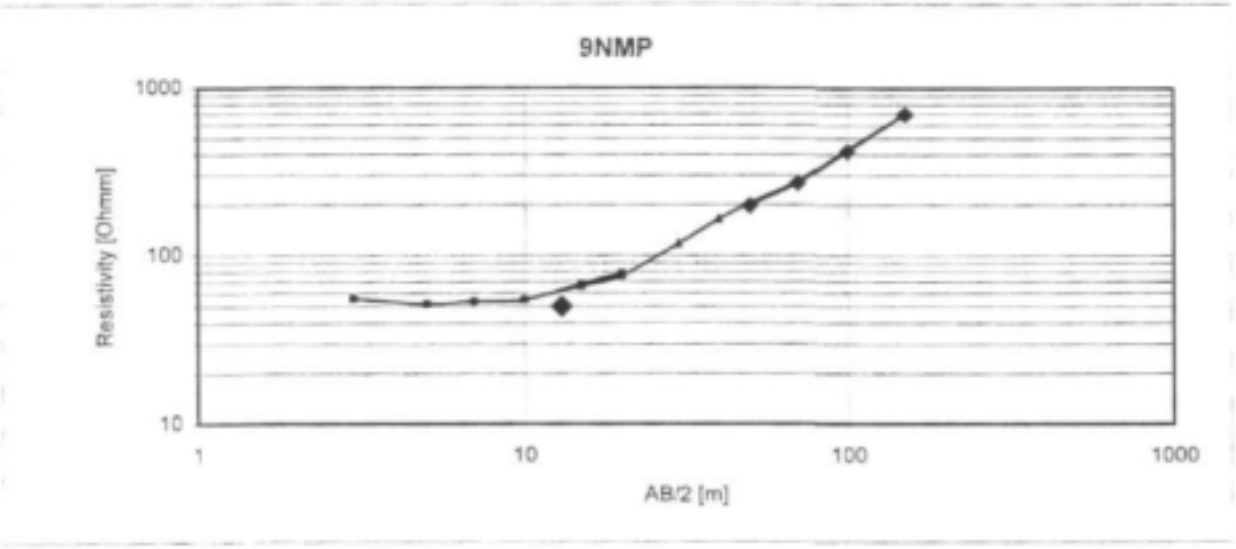
9NMP
1000
100
10
Resistivity [Ohmm]
1
10
100
1000
AB/2 [m]

NMP15

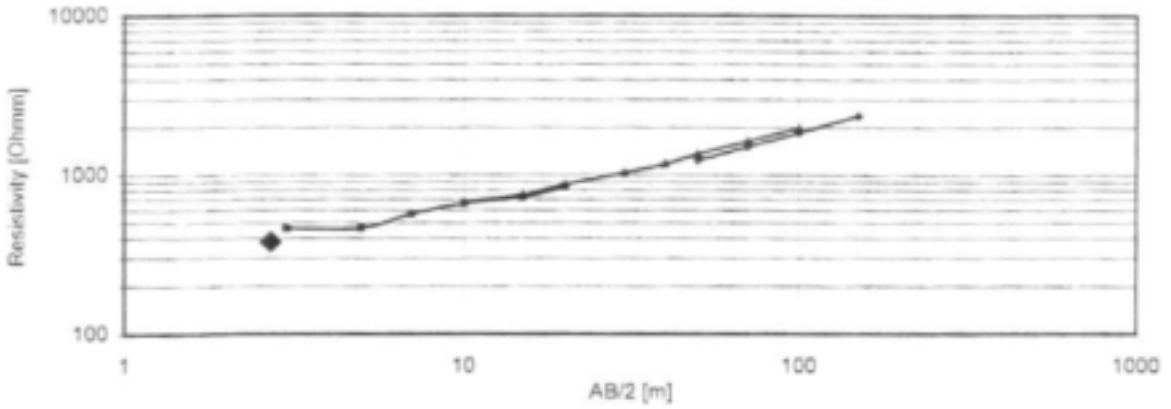
10000
1000
100
Resistivity [Ohmm]
1
10
100
1000
AB/2 [m]

NMP4

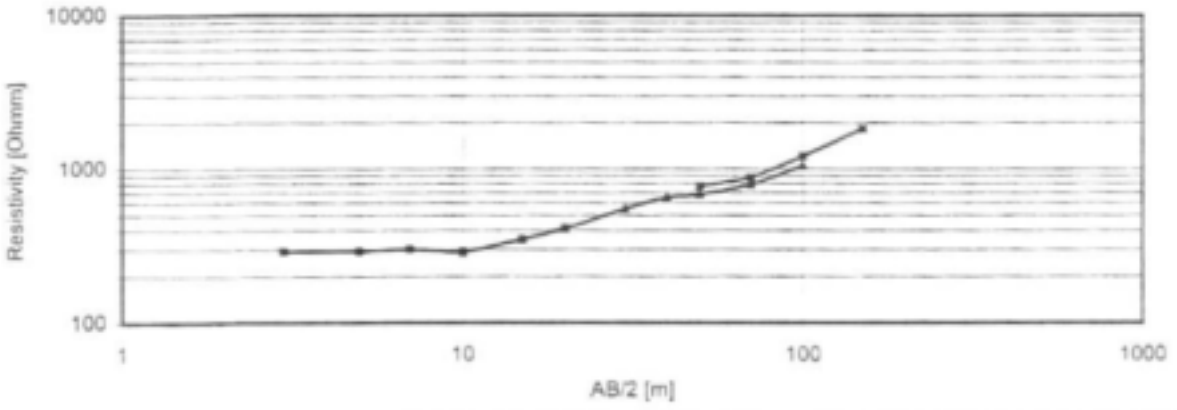
10000
1000
100
Resistivity [Ohmm]
1
10
100
1000
AB/2 [m]

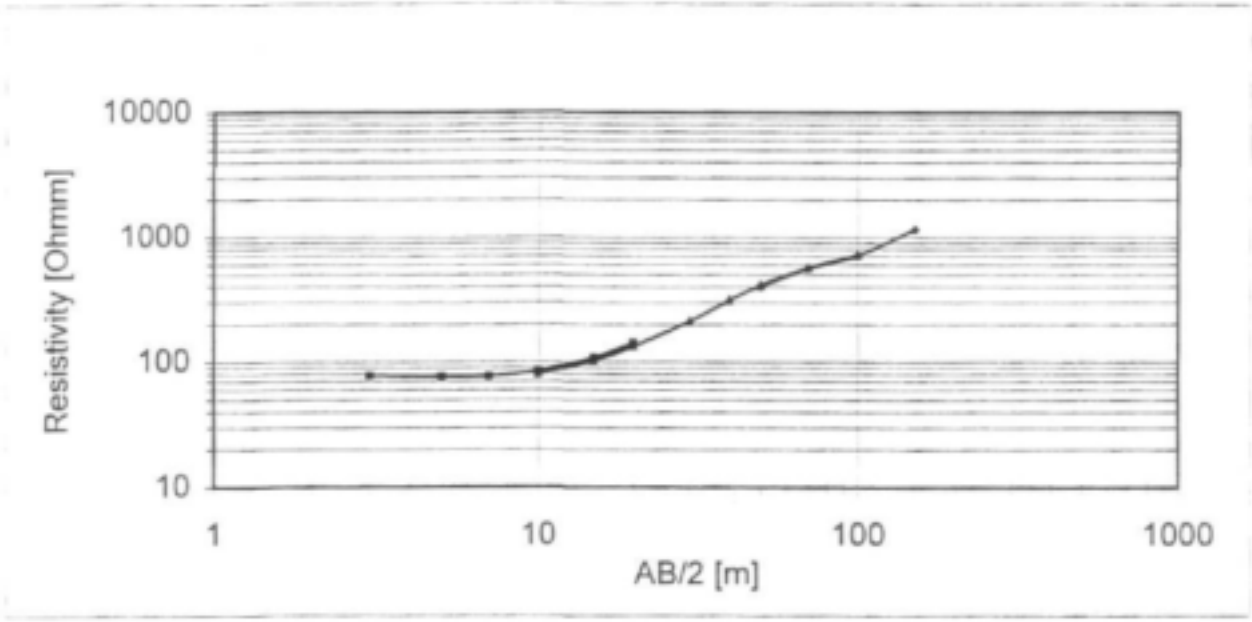

Resistivity data for site NMP10

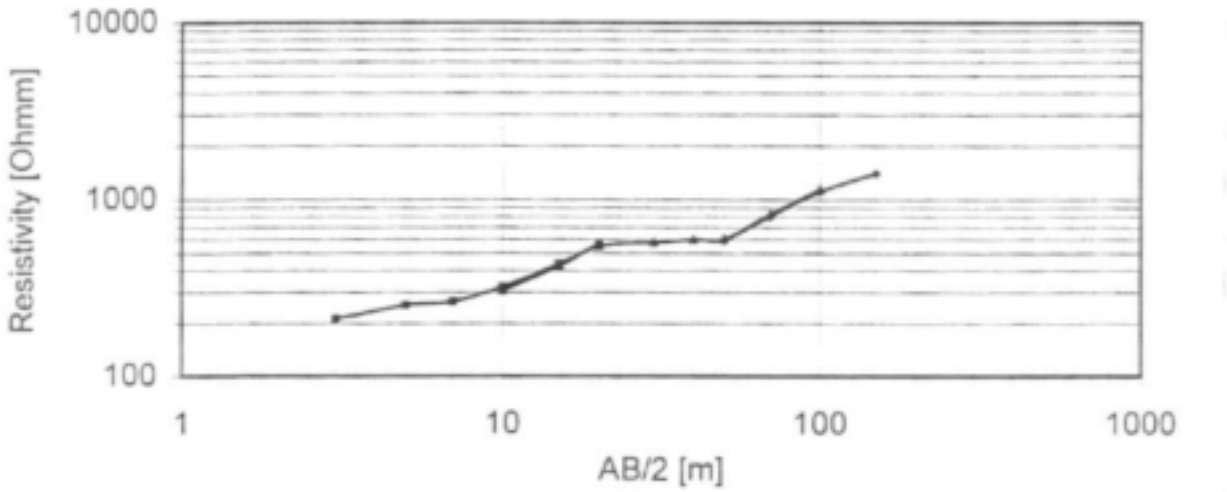

Resistivity data at site NMP14

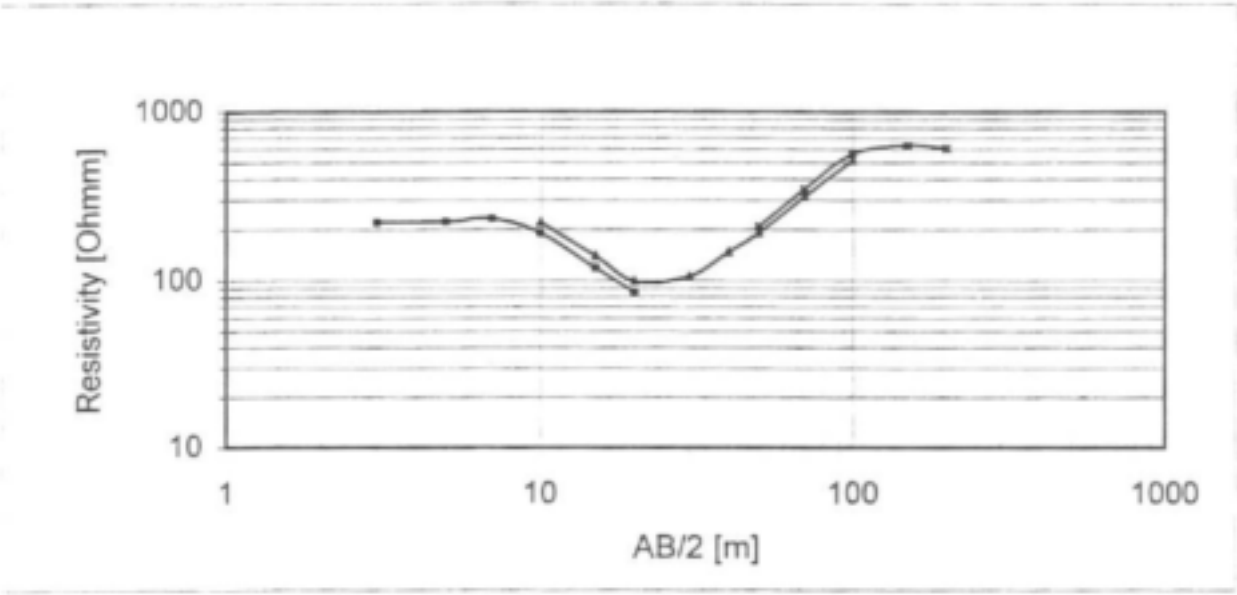

Resitivity data at site NMP6

NMP27(1)

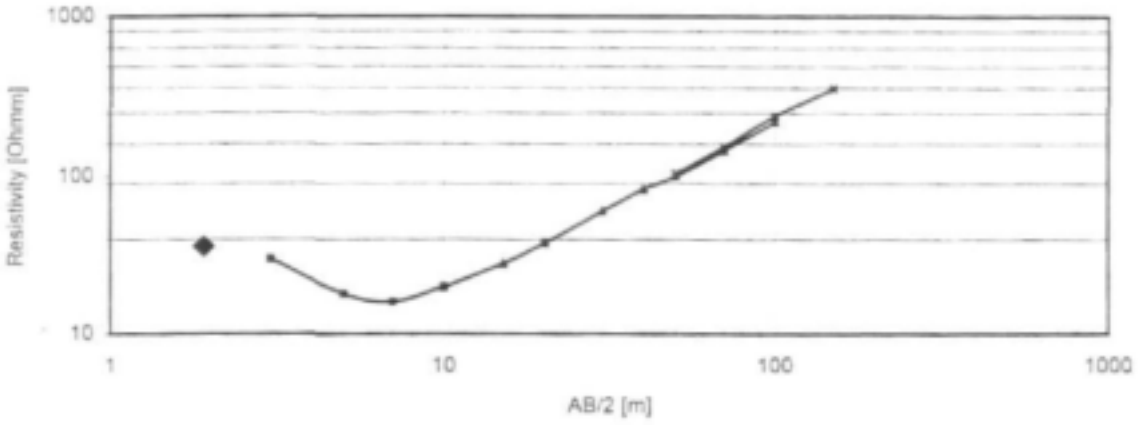

NMP27(2)

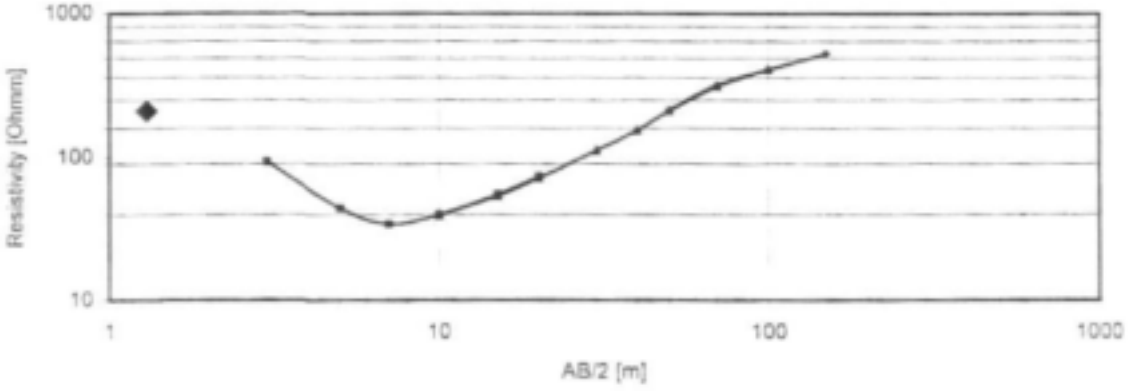

Resistivity data for site NMP27

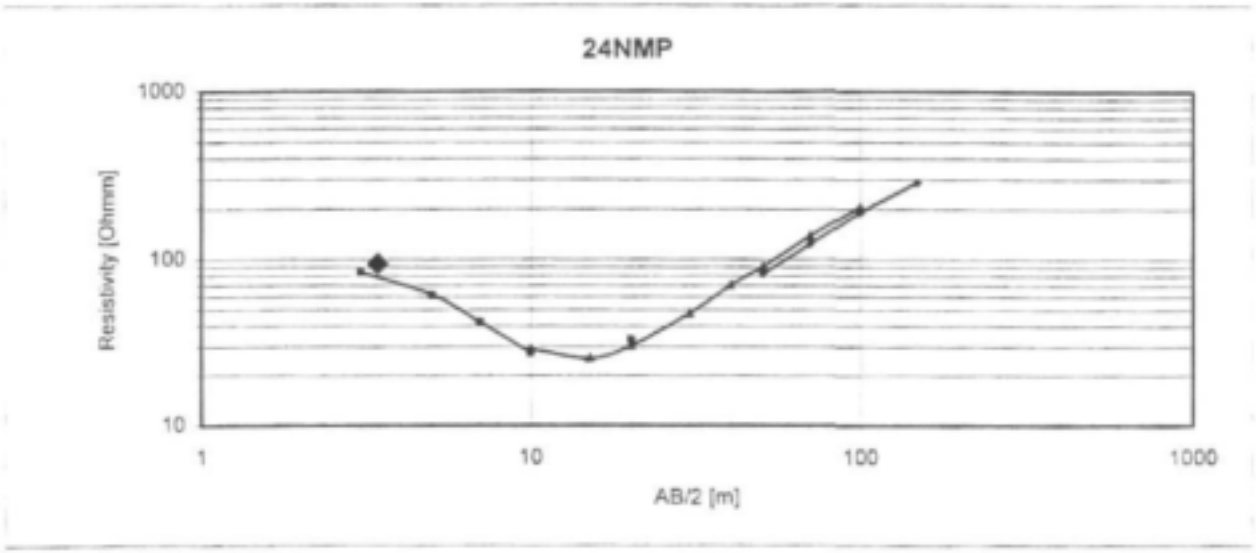
24NMP
1000
100
10
Resistivity [Ohmm]
1
10
100
1000
AB/2 [m]

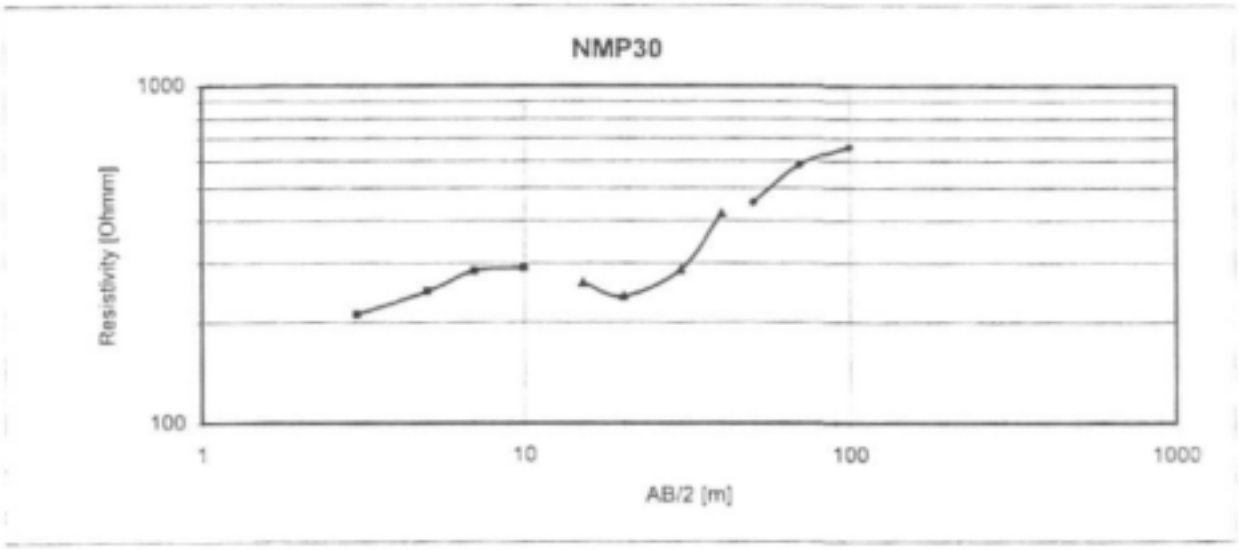
NMP30
1000
100
Resistivity [Ohmm]
1
10
100
1000
AB/2 [m]

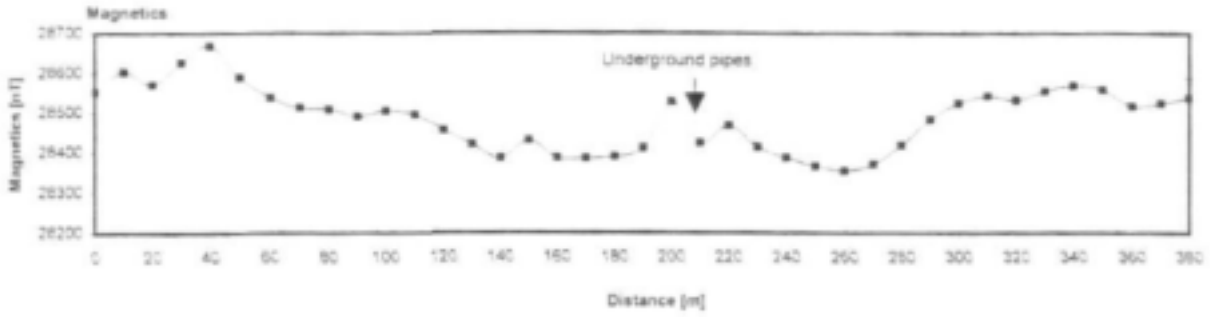

Magnetic profile at site NMP30. Station spacing: 10m, traverse direction: NW-SE.

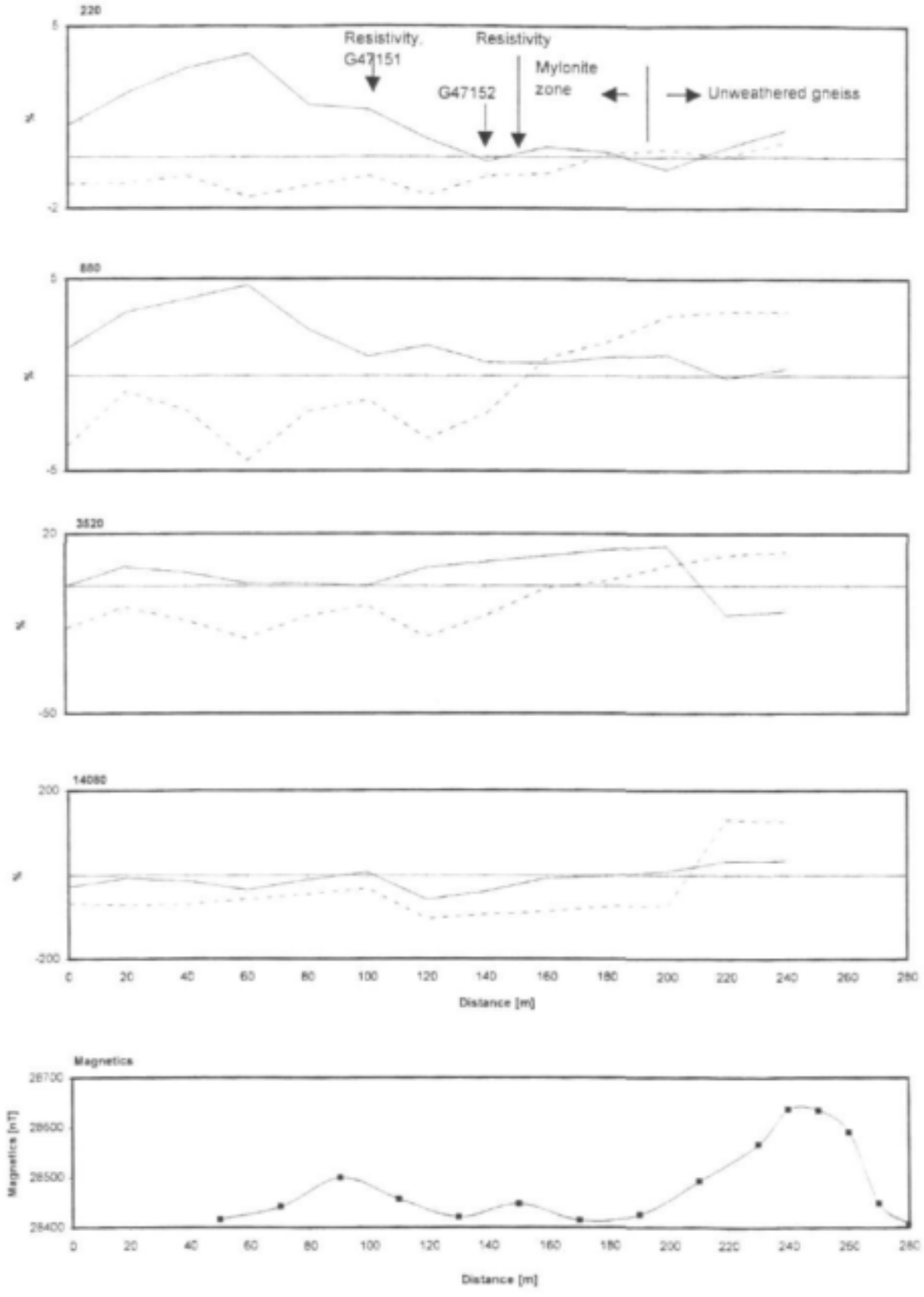

Magnetic data and Max-Min electromagnetic profiles at site NMP27. Solid line:in-phase [%]; dotted line: out-of phase [%]; coil separation 100m, station spacing 20m. Traverse direction: S-N

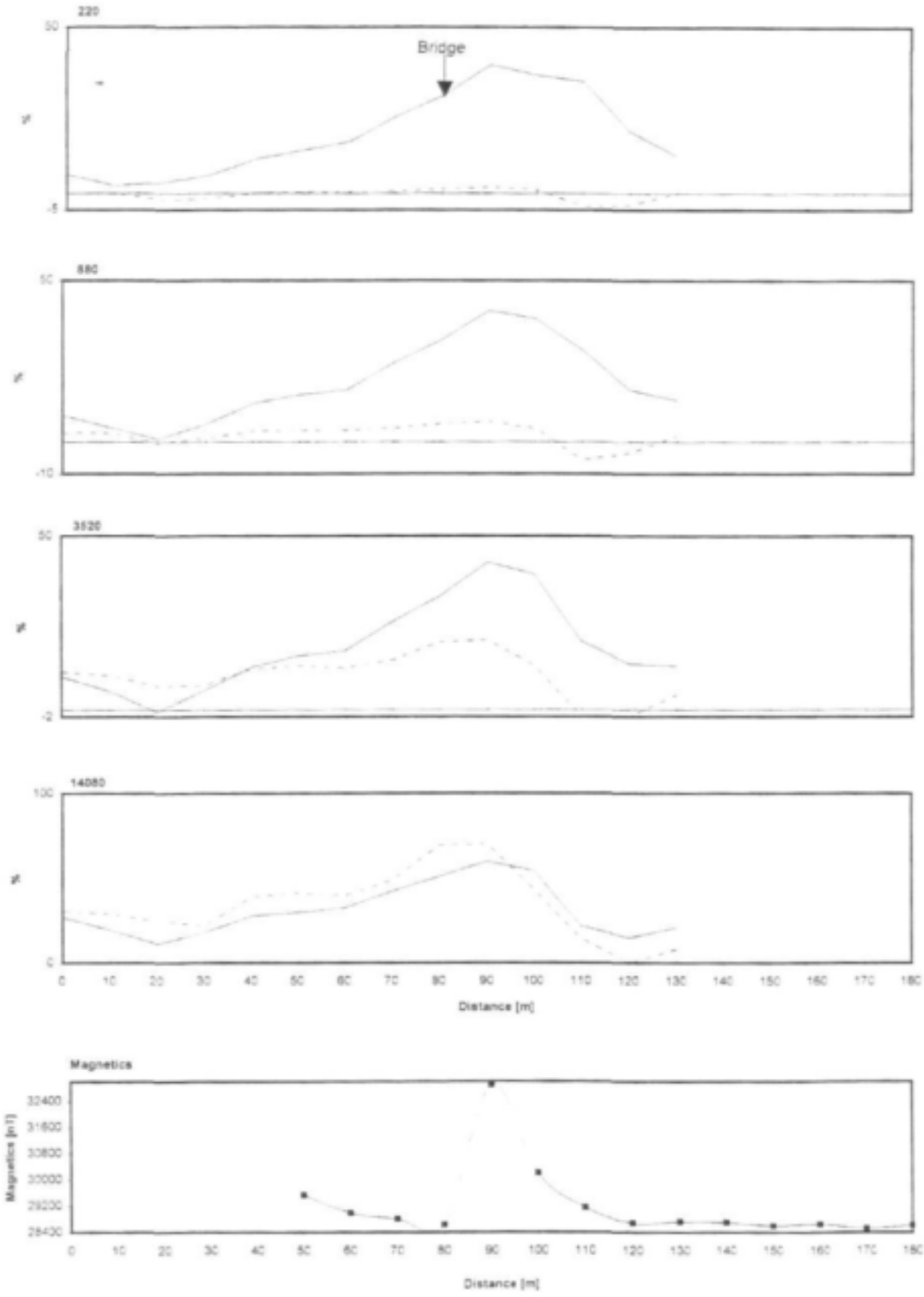

Magnetic data and Max-Min electromagnetic profiles at site NMP25. Solid line in-phase [%]; dotted line: out-of phase [%]; coil separation 100m, station spacing 10m. Traverse direction: ESE-WNW

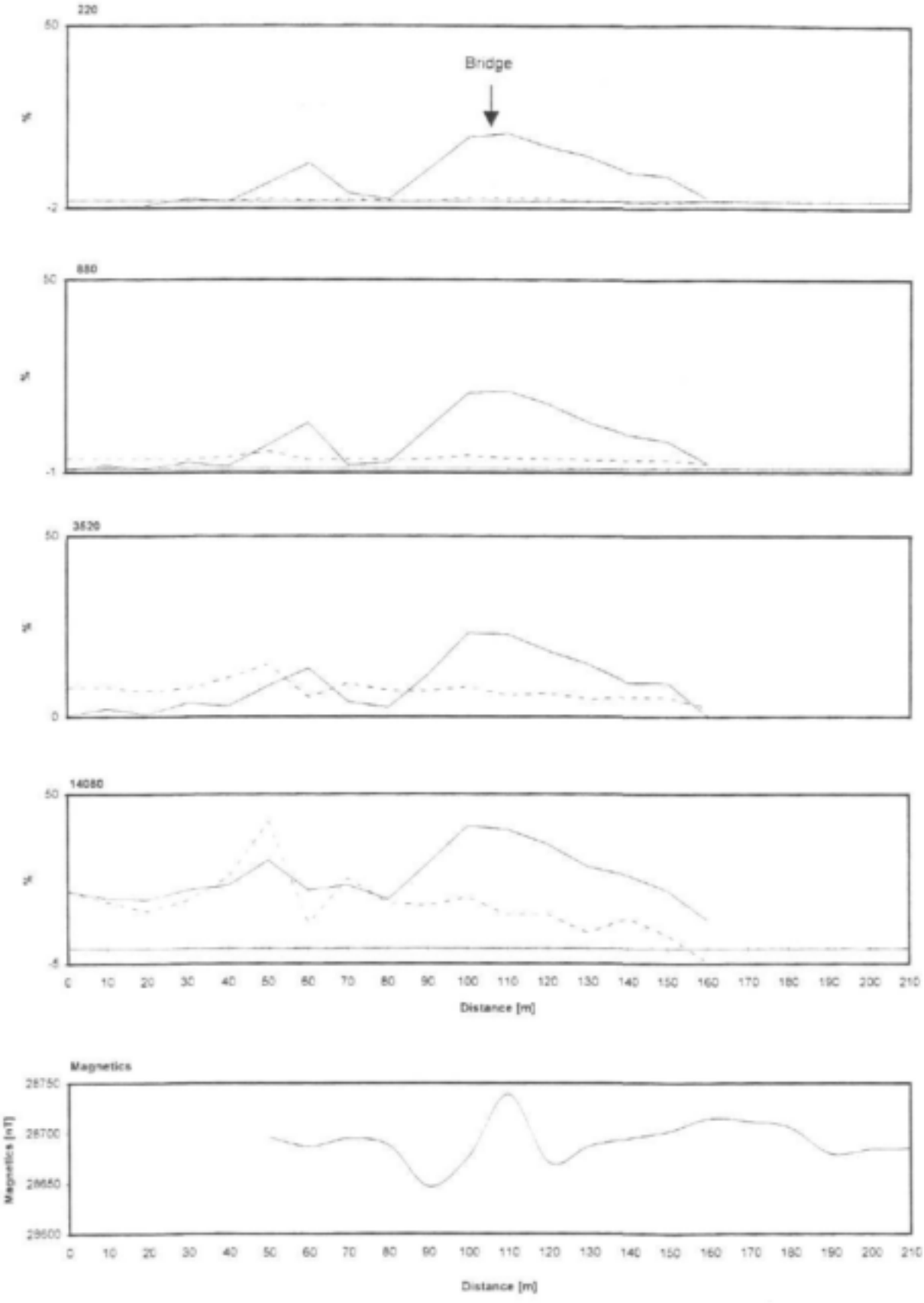

Magnetic data and Max-Min electromagnetic profiles at site NMP23. Solid line:in-phase [%]; dotted line: out-of phase [%]; coil separation 100m, station spacing 10m. Traverse direction:SW-NE

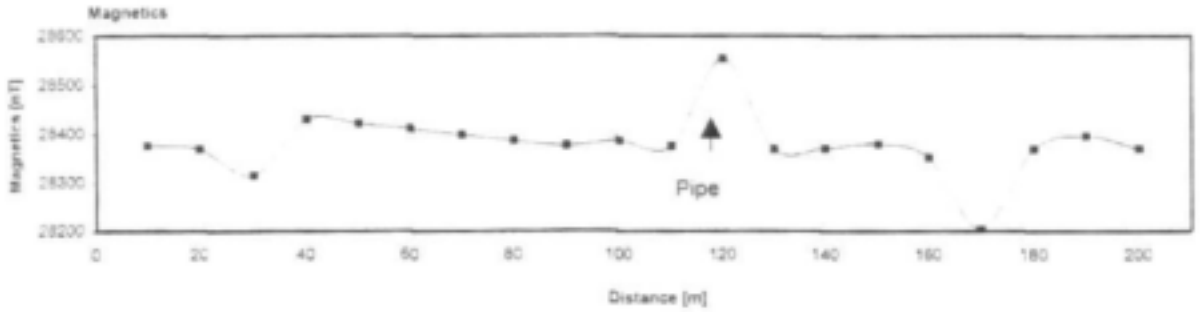

Magnetic profile at site NMP21. Station spacing: 10m. traverse direction: WNW-ESE

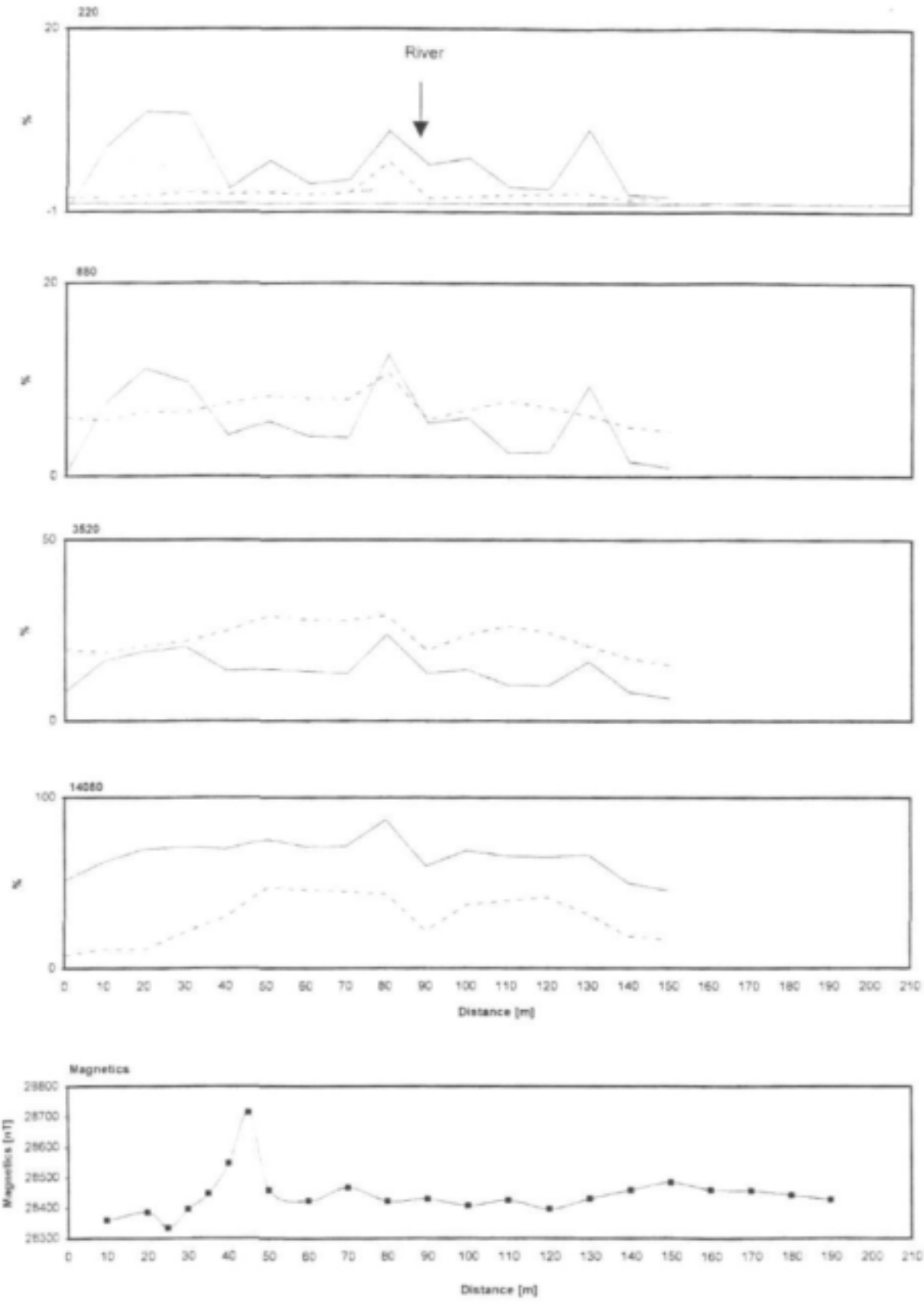

Magnetic data and Max-Min electromagnetic profiles at site NMP19. Solid line:in-phase [%]; dotted line: out-of phase [%]; coil separation 100m, station spacing 10m. Traverse direction: NE-SW

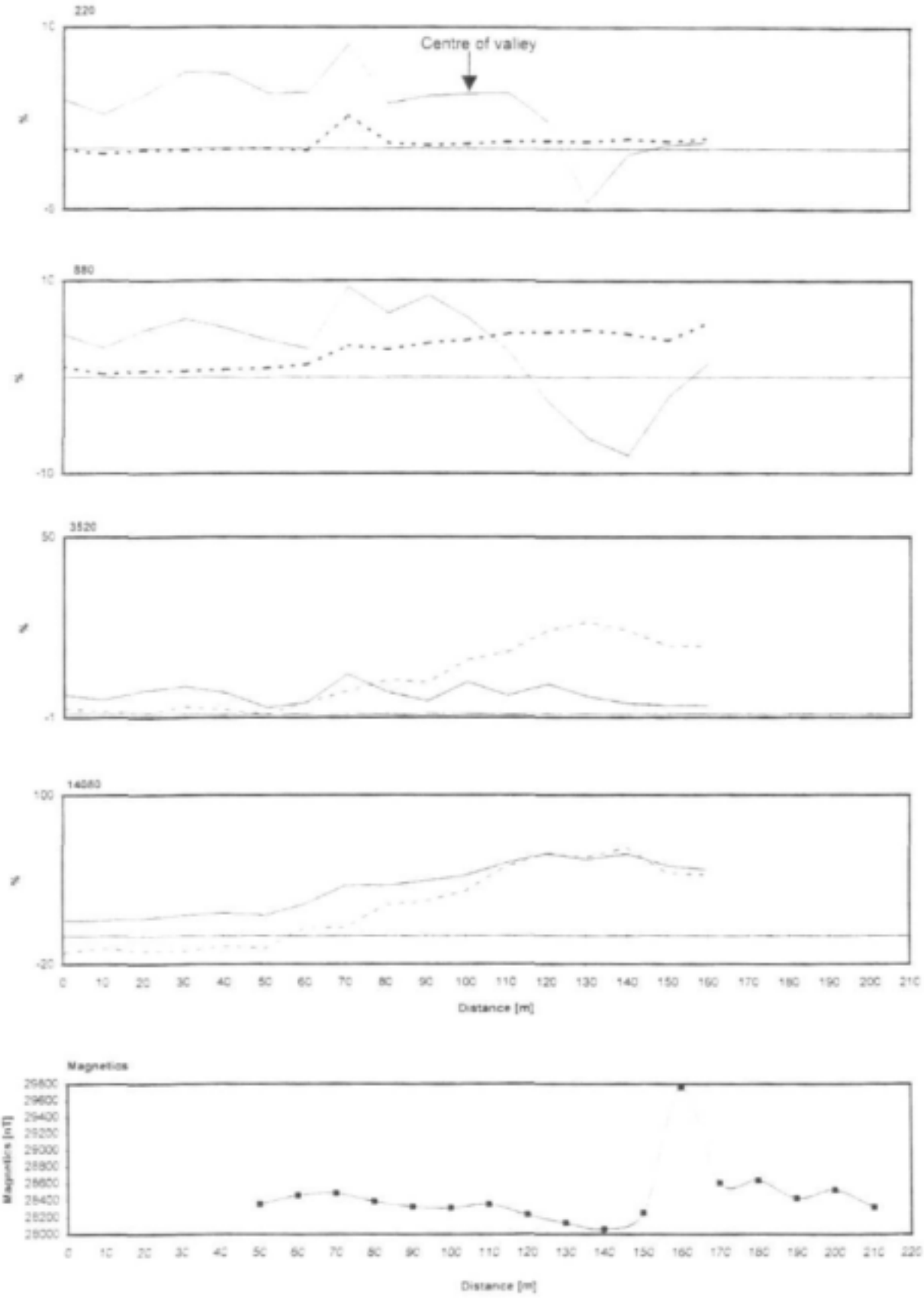

Magnetic data and Max-Min electromagnetic profiles at site NMP17. Solid line: in-phase [%]; dotted line: out-of phase [%]; coil separation 100m, station spacing 10m. Traverse direction: NE-SW

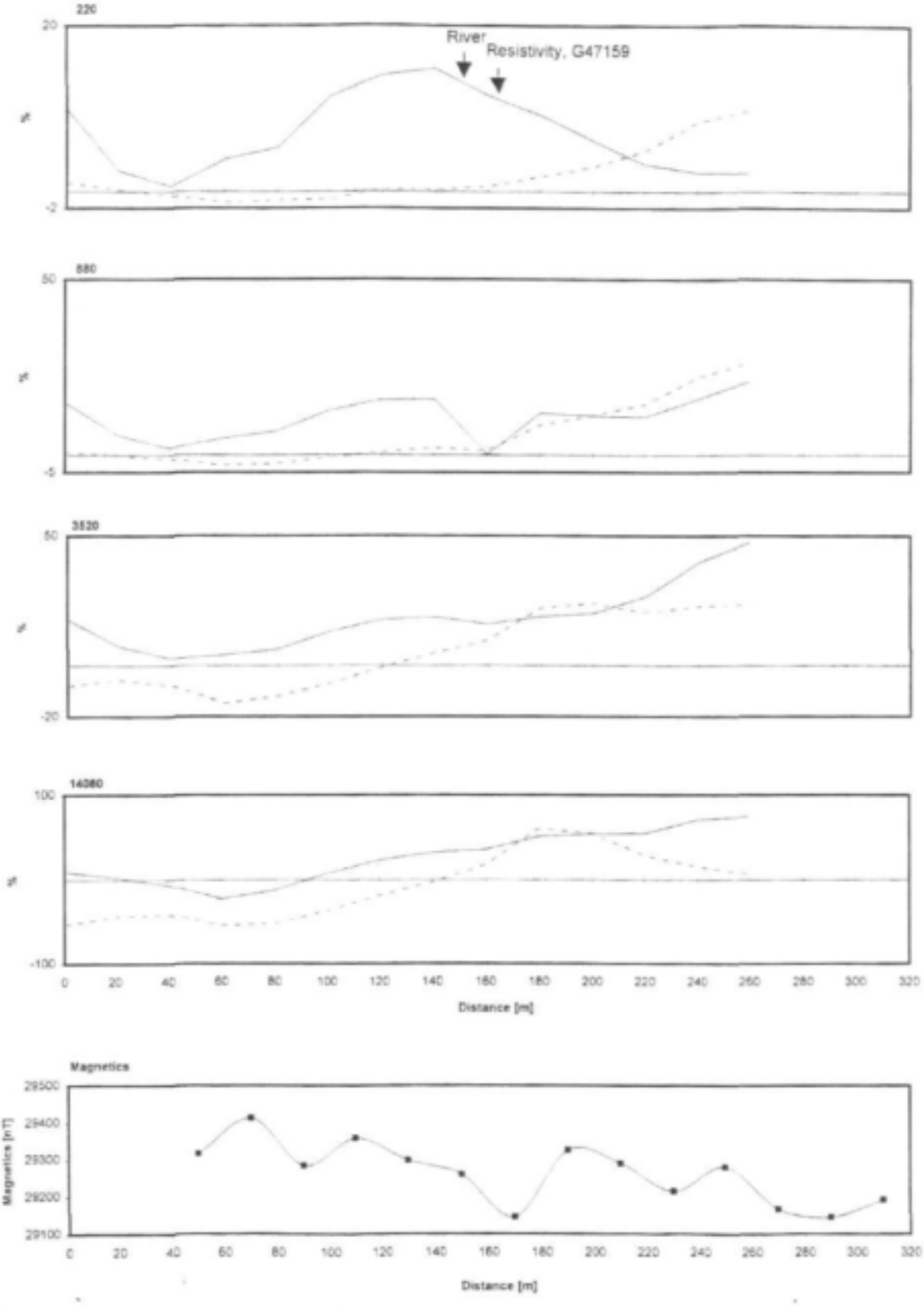

- Magnetic data and Max-Min electromagnetic profiles at site NMP15. Solid line:in-phase [%]; dotted line: out-of phase [%]; coil separation 100m, station spacing 20m. Traverse direction:S W-NE

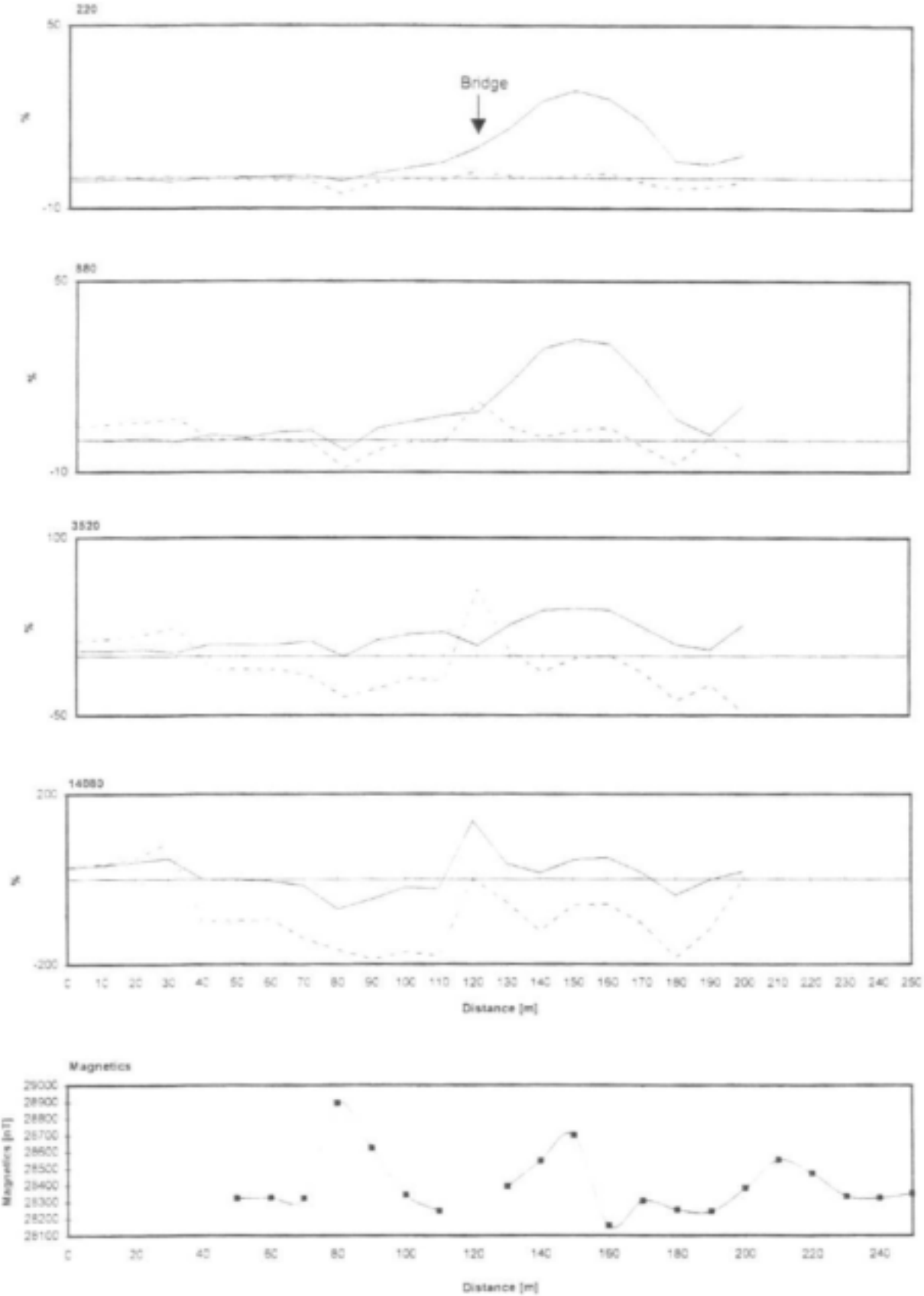

Magnetic data and Max-Min electromagnetic profiles at site NMP13. Solid line in-phase [%]; dotted line: out-of phase [%]; coil separation 100m, station spacing 10m. Traverse direction: N-S

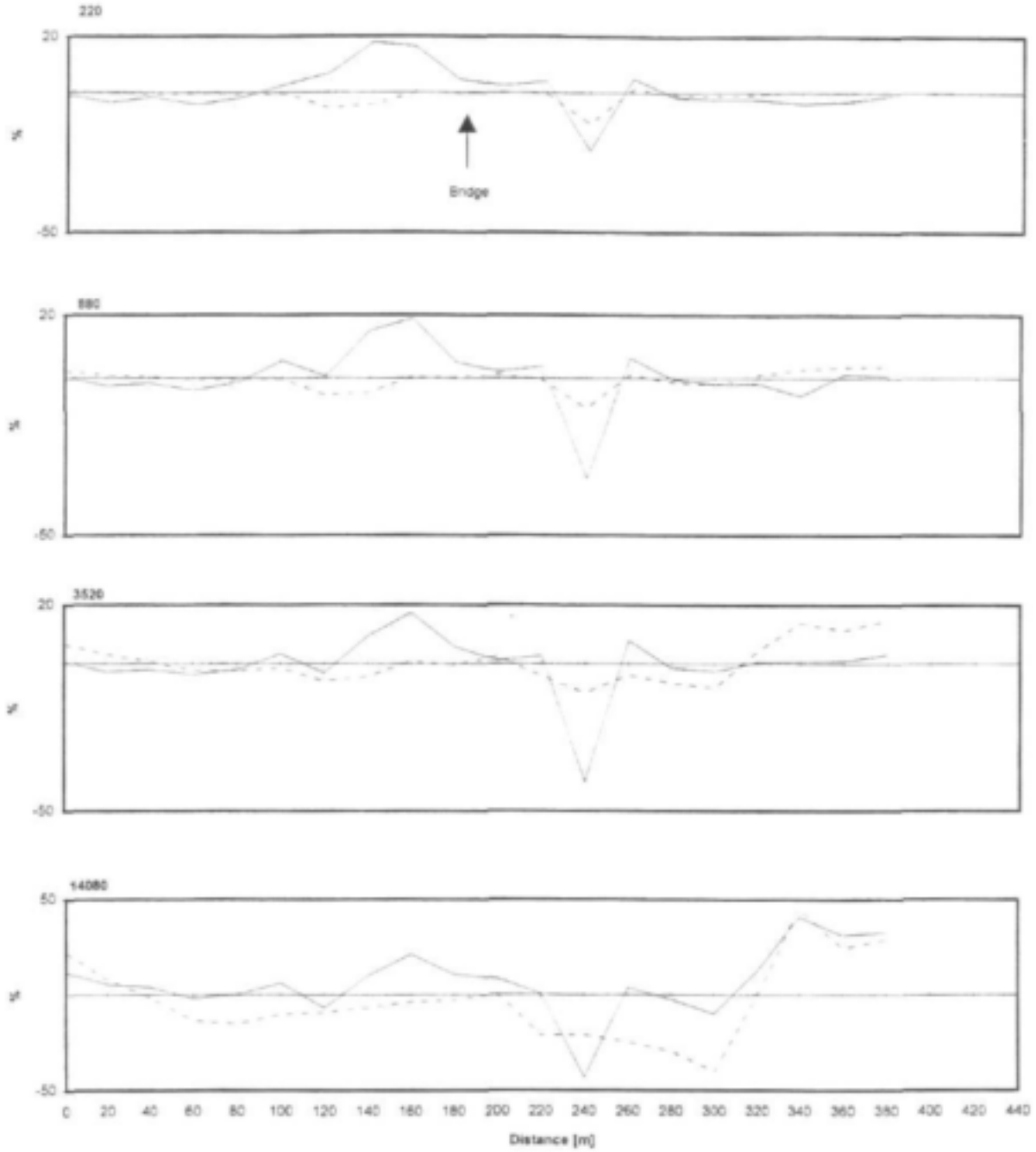

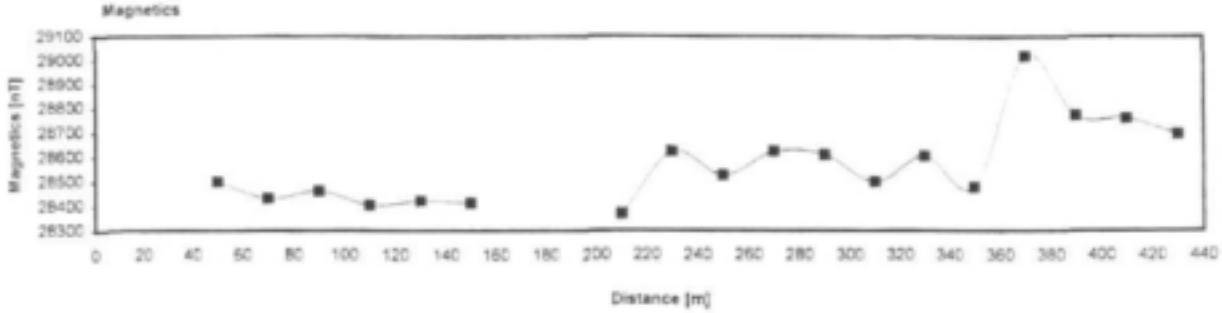

Magnetic data and Max-Min electromagnetic profiles at site NMP11. Solid line: in-phase [%]; dotted line: out-of phase [%]; coil separation 100m, station spacing 20m. Traverse direction: NW-SE

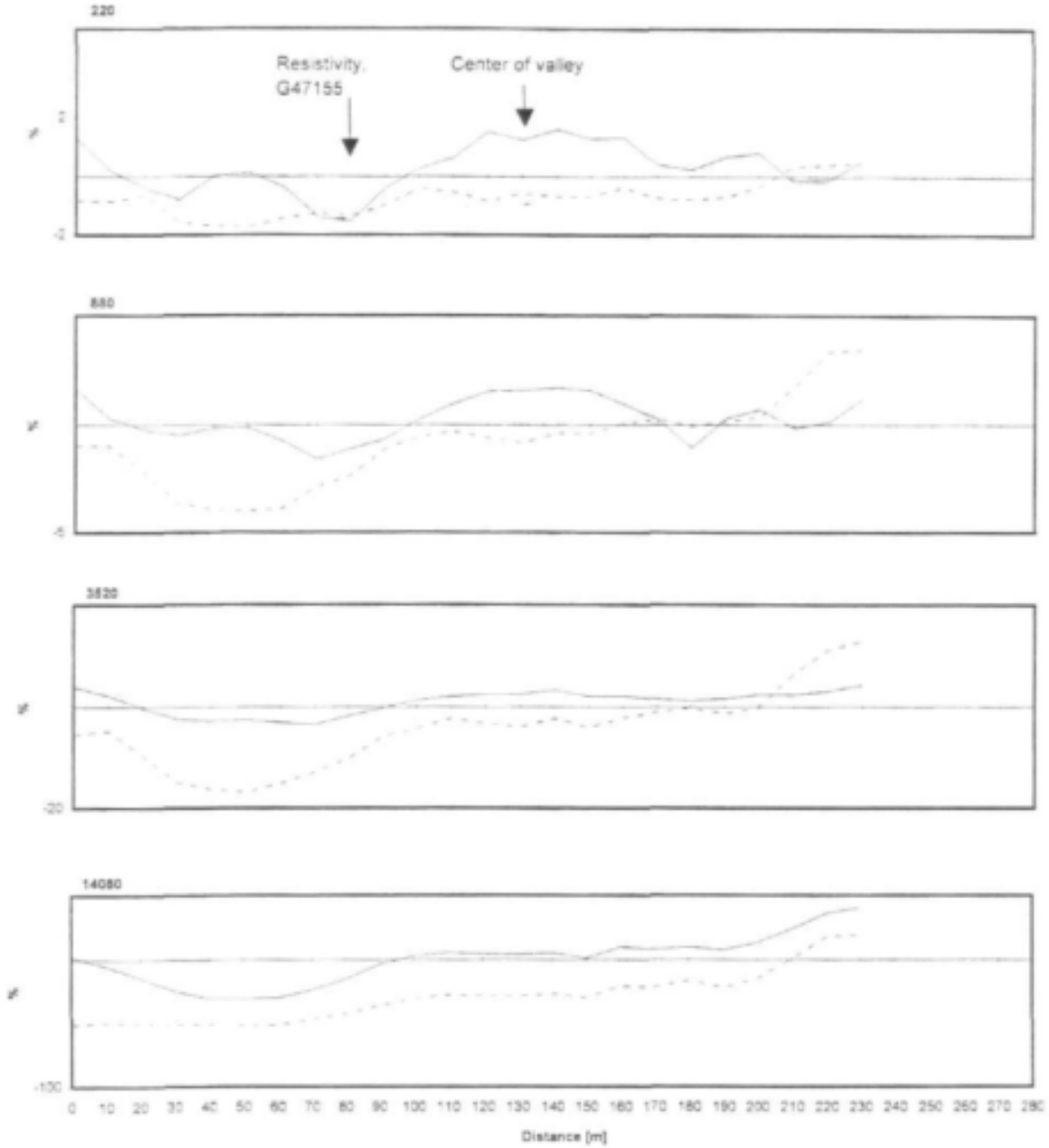

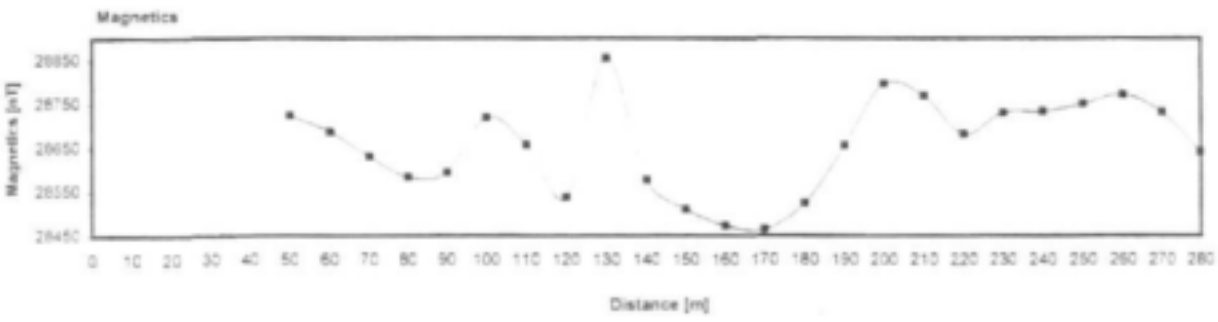

Magnetic data and Max-Min electromagnetic profiles at site NMP9. Solid line:in-phase [%]; dotted line: out-of phase [%]; coil separation 100m, station spacing 10m. Traverse direction: S-N

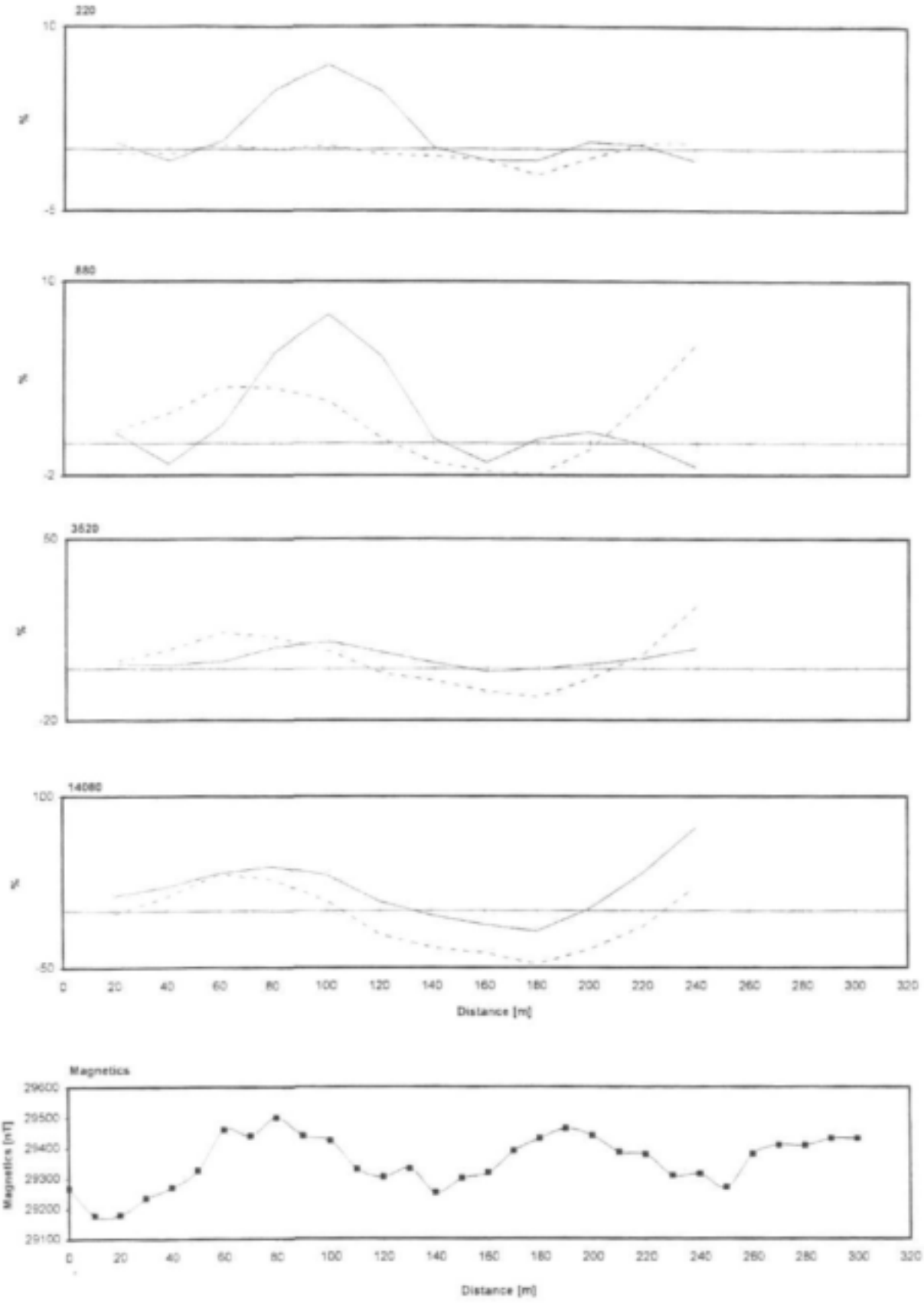

Magnetic data and Max-Min electromagnetic profiles at site NMP7. Solid line:in-phase [%]; dotted line: out-of phase [%]; coil separation 100m, station spacing 20m (Max-Min), 10m (Magnetometer). Traverse direction:NE-SW

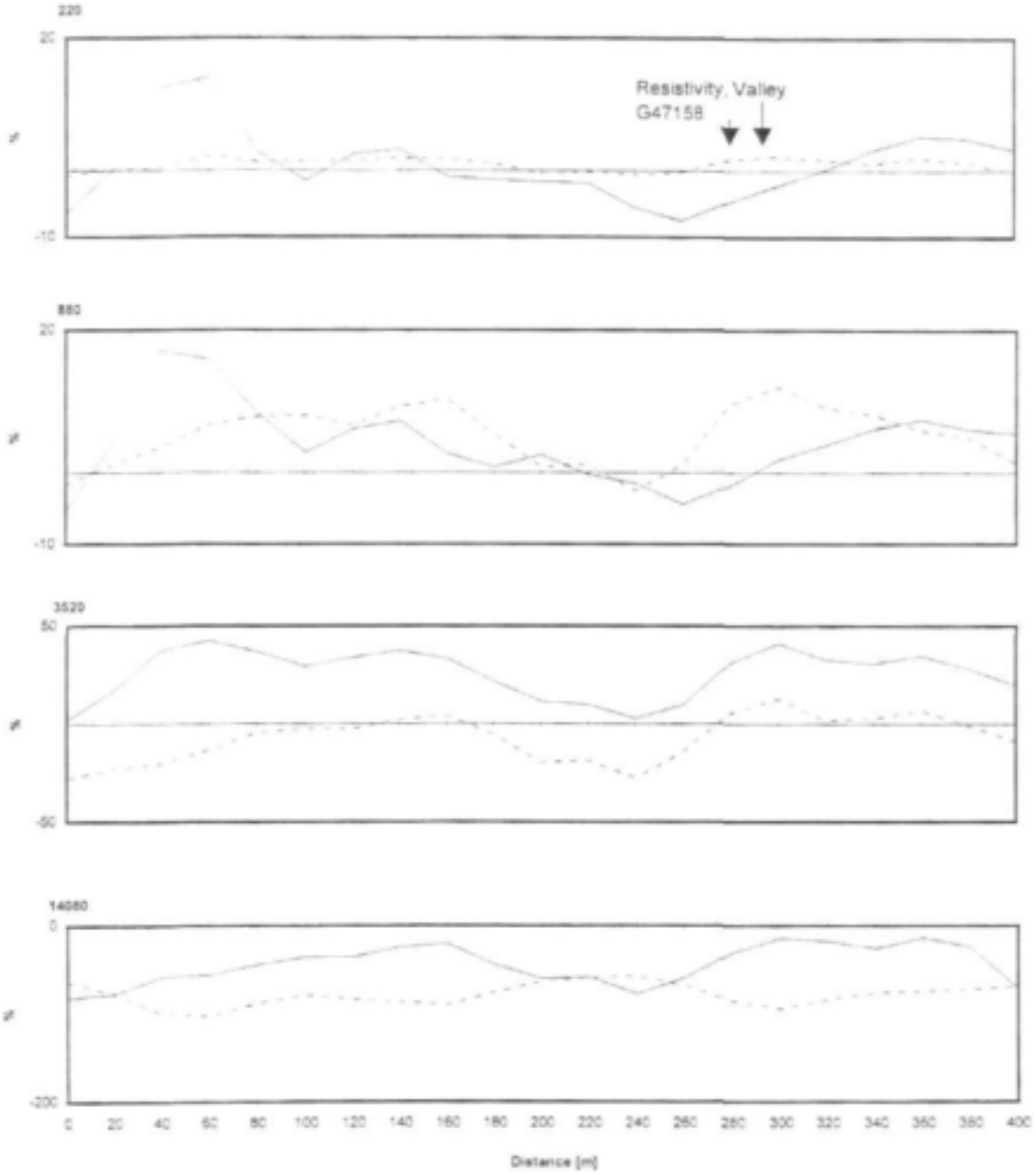

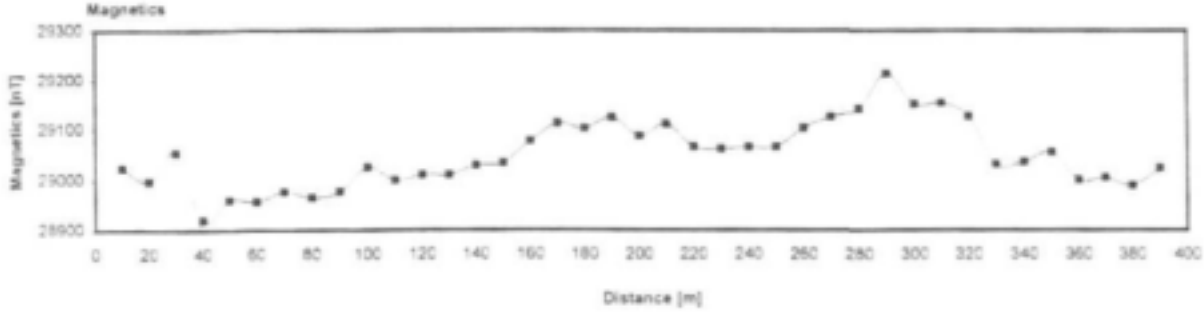

Magnetic data and Max-Min electromagnetic profiles at site NMP5. Solid line:in-phase [%]; dotted line: out-of phase [%]; coil separation 100m, station spacing 20m (Max-Min), 10m (Magnetometer). Traverse direction:SSW-NNE

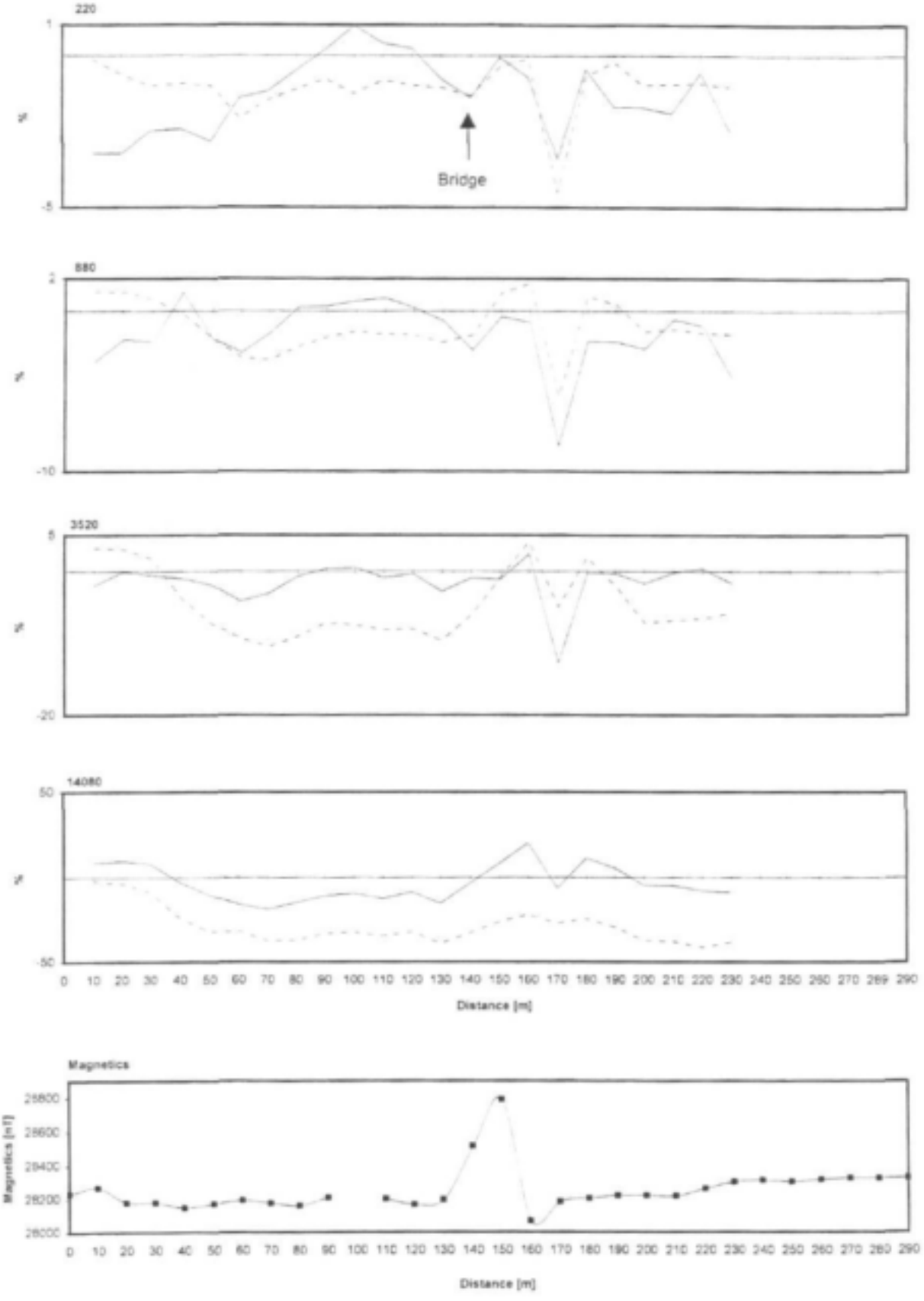

Magnetic data and Max-Min electromagnetic profiles at site NMP3. Solid line:in-phase [%]; dotted line: out-of phase [%]; coil separation 100m, station spacing 10m. Traverse direction: NNW-SSE

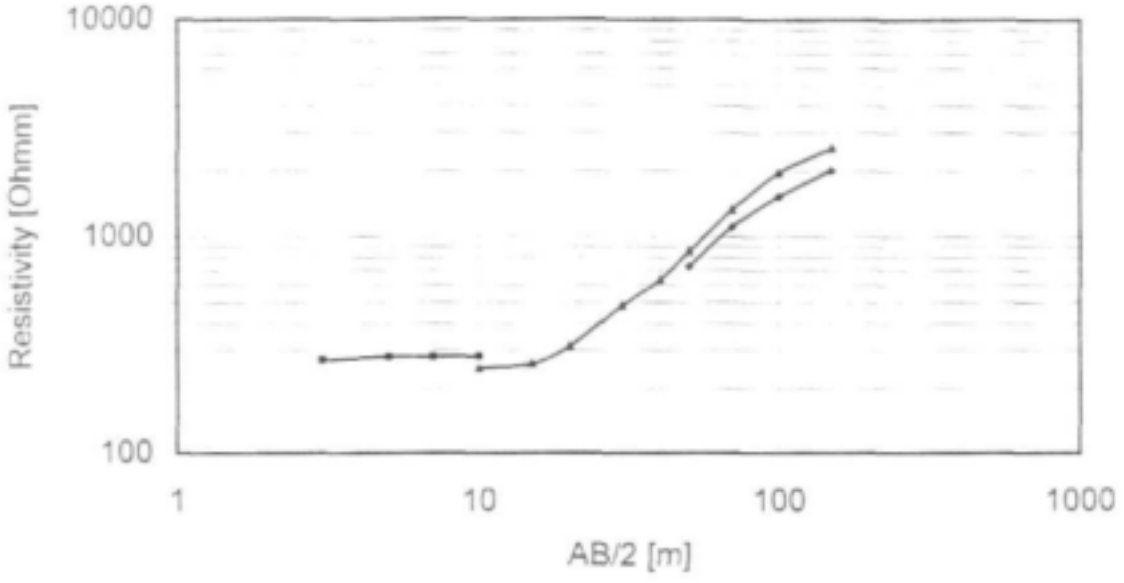

Resistivity data at site NMP29

APPENDIX 2-B

GEOLOGICAL LOGS

GROUNDWATER DEVELOPMENT IN COMPLEX TERRAIN

HOLE No: G47151
Sheet 1 of 1

PROJECT NUMBER: K5/966

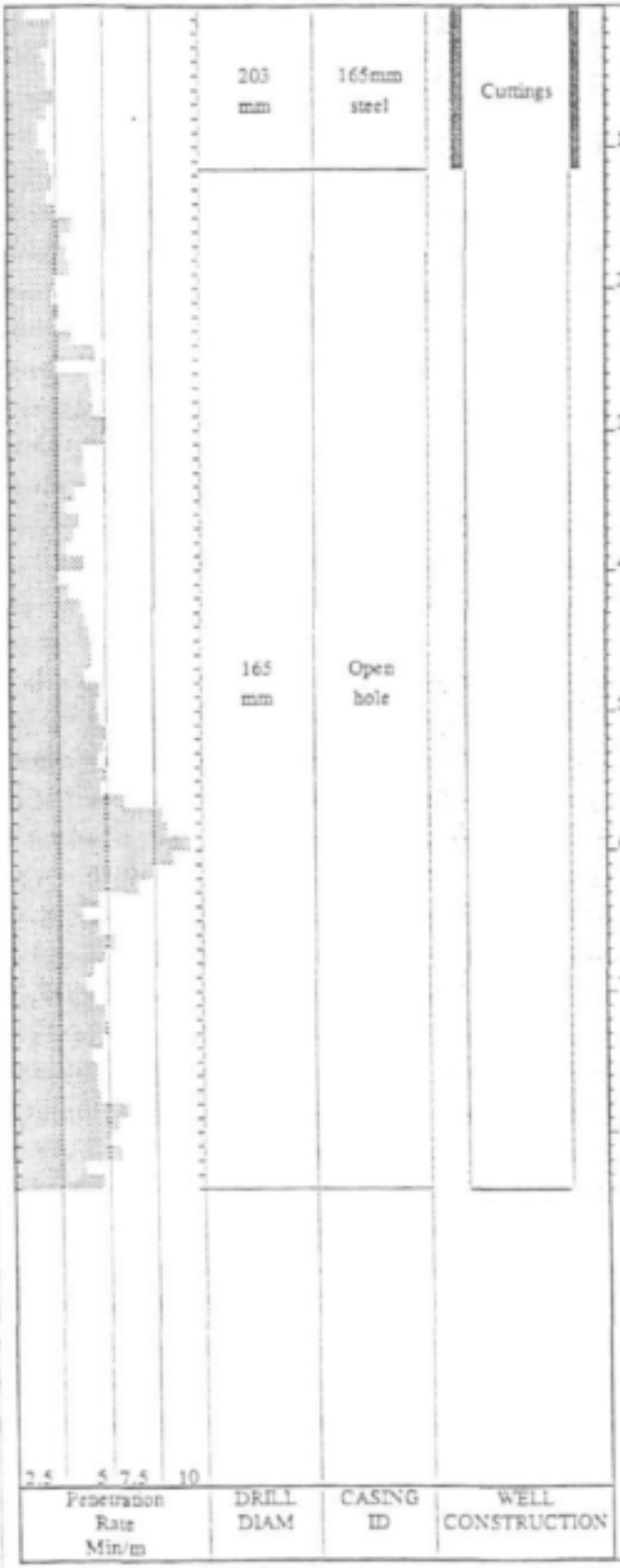

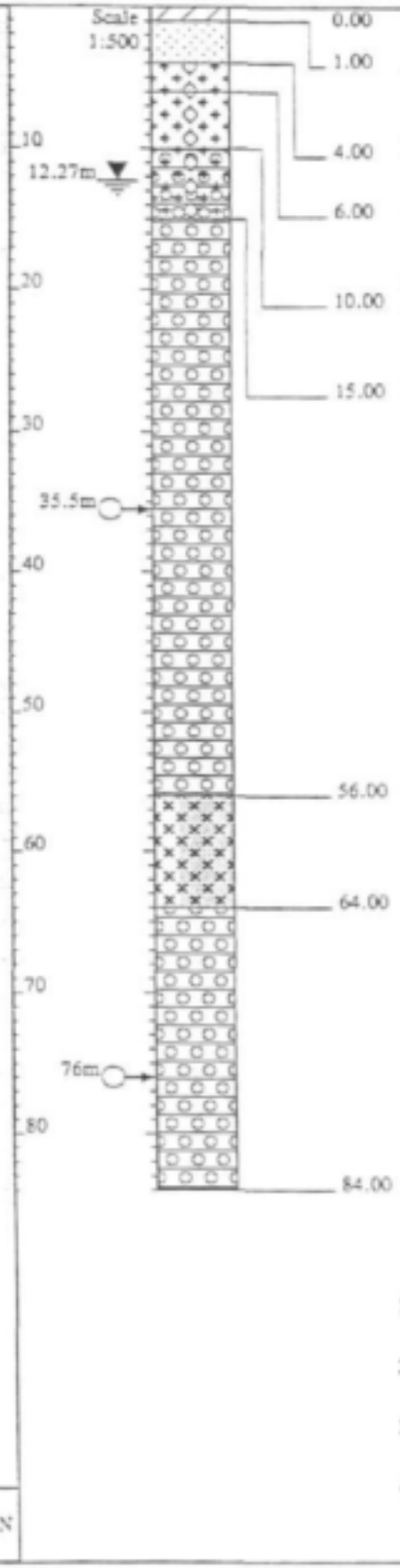

0.00	:Brown-grey sandy CLAY
1.00	:Brown, medium to coarse grained SAND
4.00	:Reddish brown, weathered GRANITE
6.00	:Reddish, fine grained weathered GRANITE
10.00	:Reddish, fine grained GRANITE/ GNEISS
15.00	:Reddish black GNEISS: red feldspar, hornblende, calcite, epidote
56.00	:Black DOLERITE
64.00	:Reddish GNEISS: pale pink feldspar, hornblende, epidote, calcite, quartz
84.00	

NOTES -

1) First water strike at 35.5m (0.5 l/s)

2) Second water strike at 76m (0.37 l/s)

3) Rest water level at 12.27m

4) Developed for 30 min by airlift

CONTRACTOR : DWAF
DRILLED BY : B. PIETERSE
DRILL METHOD : DTH HAMMER
SAMPLING : BLOWN CUTTINGS

INCLINATION : Vertical
DIAMETER : 165 mm
DRILL DATE : 19 OCTOBER 1999
CASING TYPE : 4,5 mm steel

ELEVATION : 210m
COLLAR HEIGHT : 0.38 m
BLOW YIELD : 0.87 l/s

LOGGED BY : I. NEUMANN
SETUP FILE : STANDARD.SET

DATE : 17/03/00 13:32
TEXT : C:\DOTPLOT\DATA\NMP1.TXT

HOLE No: G47151
CANAAN MISSION

dot PLOT 3022 - 14 Bit Inc

GROUNDWATER DEVELOPMENT IN COMPLEX TERRAIN

HOLE No: G47153
Sheet 1 of 1

PROJECT NUMBER: K5/966

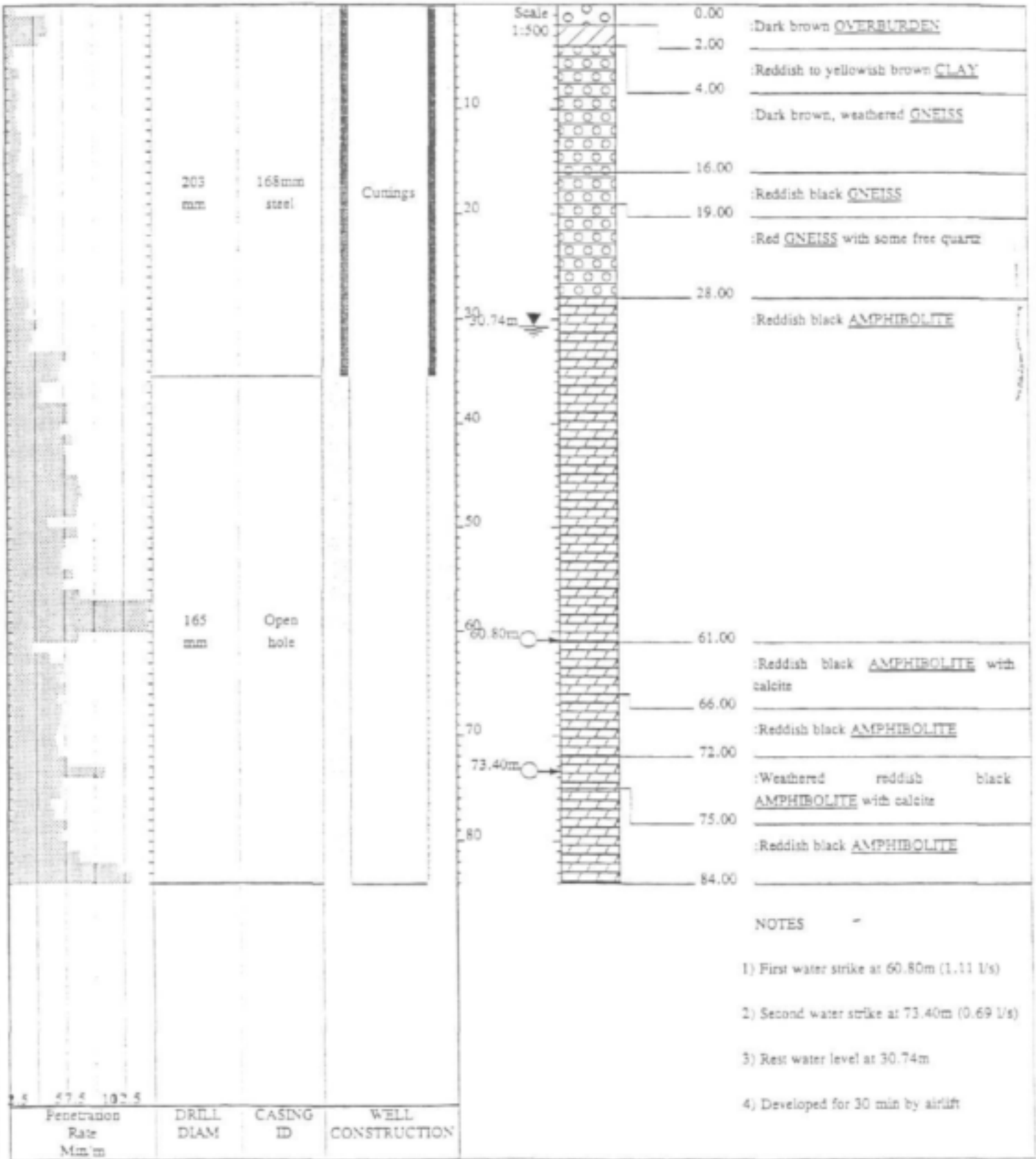

CONTRACTOR : DWAF
DRILLED BY : B. PIETERSE
DRILL METHOD : DTH HAMMER
SAMPLING : BLOWN CUTTINGS

INCLINATION : Vertical
DIAMETER : 165 mm
DRILL DATE : 26 OCTOBER 1999
CASING TYPE : 4,5 mm steel

ELEVATION : 370m
COLLAR HEIGHT : 0.54 m
BLOW YIELD : 1.8 l/s

LOGGED BY : M. PRINSLOO
SETUP FILE : STANDARD.SET

DATE : 17/03/00 14:46
TEXT : C:\DOTPLOT\DATA\NMP2.TXT

HOLE No: G47153
PONTWANA, MVOTI 4667

dot.PLOT 3027 J&W Inc

GROUNDWATER DEVELOPMENT IN COMPLEX TERRAIN

HOLE No: G47155
Sheet 1 of 1

PROJECT NUMBER: K5/966

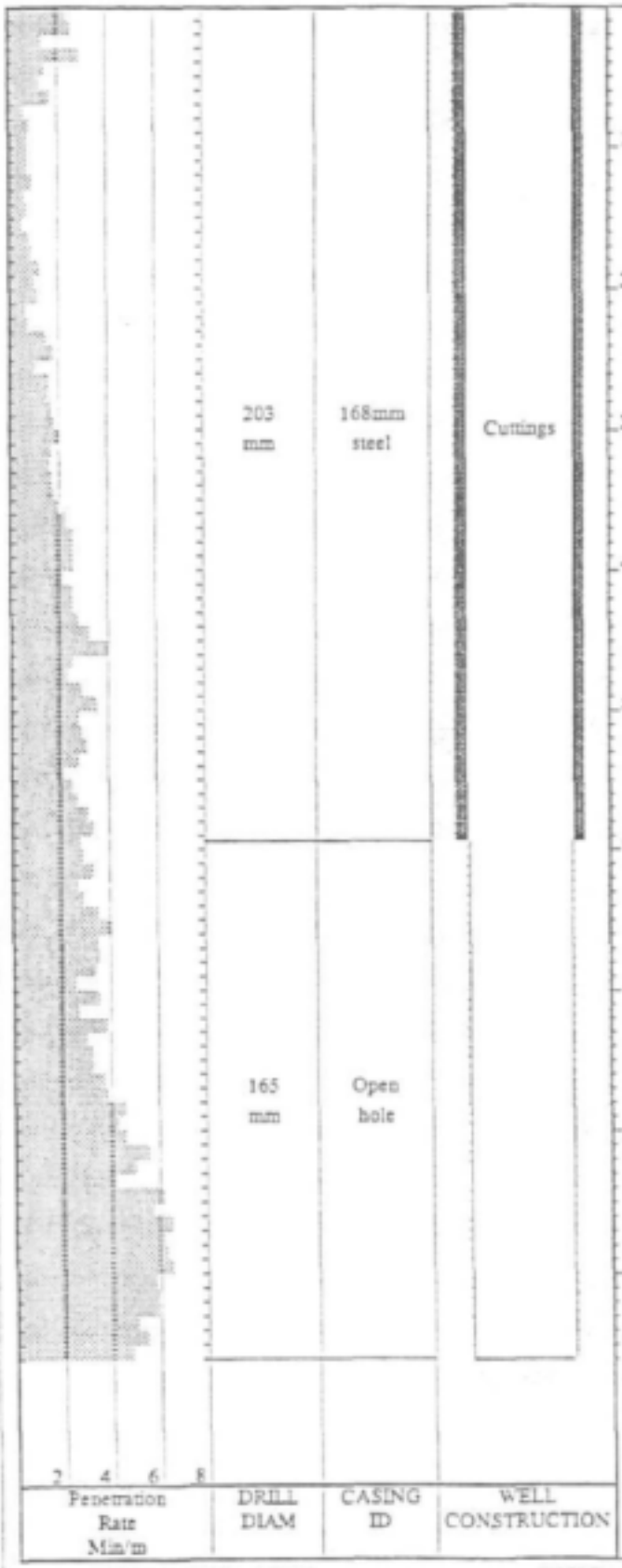

0.00	:Reddish-brown, clayey OVERBURDEN
1.00	:Unweathered quartzite boulders
5.00	:Weathered GRANITE, showing quartz, quartzite and some feldspar
8.00	:Clayey, weathered GRANITE
10.00	:Weathered AMPHIBOLITE with biotite and free quartz
15.00	:Weathered GNEISS with biotite and some free quartz
27.00	:Grey weathered AMPHIBOLITE with biotite, but less feldspar and free quartz
34.00	:Weathered, clayey brownish GNEISS with biotite and free quartz
61.00	:Weathered GRANITE/ GNEISS with free quartz
64.00	:Fine grained GRANITE
66.00	:Dark weathered GRANITE/ SCHIST
68.00	:Oxidized GNEISS zone with biotite and free quartz present in large quantities
72.00	:Unweathered GNEISS with biotite and calcite
79.00	:Grey- black AMPHIBOLITE with free quartz, biotite and some pink feldspar
96.00	

NOTES

1) First water strike at 64.20m (0.83 l/s)

2) Second water strike at 72.50m (0.17 l/s)

3) Rest water level at 17.95m

4) Developed for 30 min by airlift

CONTRACTOR : DWAF
DRILLED BY : B. PIETERSE
DRILL METHOD : DTH HAMMER
SAMPLING : BLOWN CUTTINGS

INCLINATION : Vertical
DIAMETER : 165 mm
DRILL DATE : 09 NOVEMBER 1999
CASING TYPE : 4,5 mm steel

ELEVATION : 445m
COLLAR HEIGHT : 0.61 m
BLOW YIELD : 1.00 l/s

LOGGED BY : M. PRINSLOO
SETUP FILE : STANDARD.SET

DATE : 17/03/00 14:29
TEXT : C:\DOTPLOT\DATA\NMP3B.TXT

HOLE No: G47155
ST JOAN OF ARC MISSION STAT

GROUNDWATER DEVELOPMENT IN COMPLEX TERRAIN

HOLE No: G47156
Sheet 2 of 2

PROJECT NUMBER: K5/966

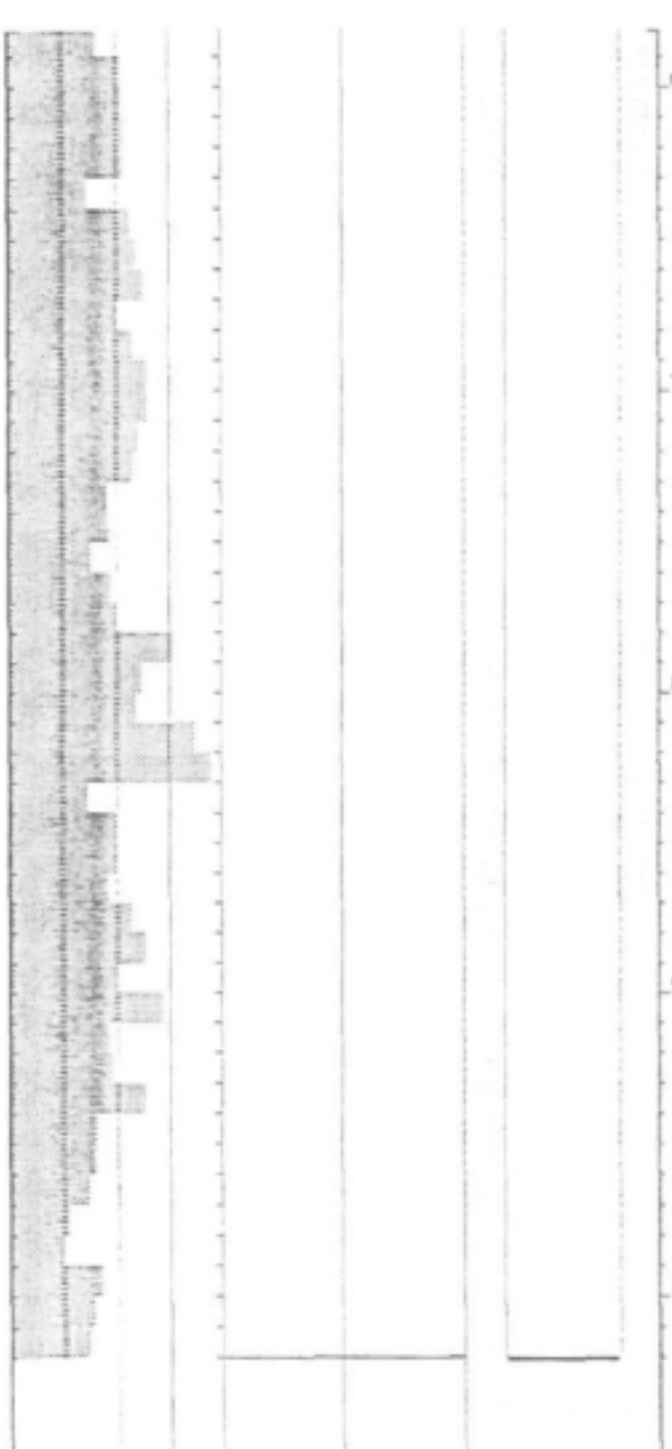

60

:Unweathered pink GRANITE with auxiliary pyrite, calcite and biotite

70

73.20m — 73.00

:Unweathered red GRANITE with auxiliary pyrite, calcite and biotite

80

90

92.00

:Unweathered reddish to pink GRANITE showing some pyrite, calcite and biotite

100

102.00

NOTES

1) First water strike at 9.80m (0.54 l/s)

2) Second water strike at 30.70m (0.20 l/s)

3) Third water strike at 73.20m (0.70 l/s)

4) Rest water level at 5.15m

CONTRACTOR : DWAF
DRILLED BY : B. PIETERSE
DRILL METHOD : DTH HAMMER
SAMPLING : BLOWN CUTTINGS

LOGGED BY : M. PRINSLOO
SETUP FILE : STANDARD.SET

INCLINATION : Vertical
DIAMETER : 165 mm
DRILL DATE : 11 NOVEMBER 1999
CASING TYPE : 6 mm steel ODEX

DATE : 17/03/00 14:48
TEXT : C:\DOTPLOT\DATA\NMP4.TXT

ELEVATION : 280m
COLLAR HEIGHT : 0.46 m
BLOW YIELD : 1.44 l/s

HOLE No: G47156
STTUNDU, UMVOTI 4667

GROUNDWATER DEVELOPMENT IN COMPLEX TERRAIN

HOLE No: G47158
Sheet 1 of 1

PROJECT NUMBER: K5/966

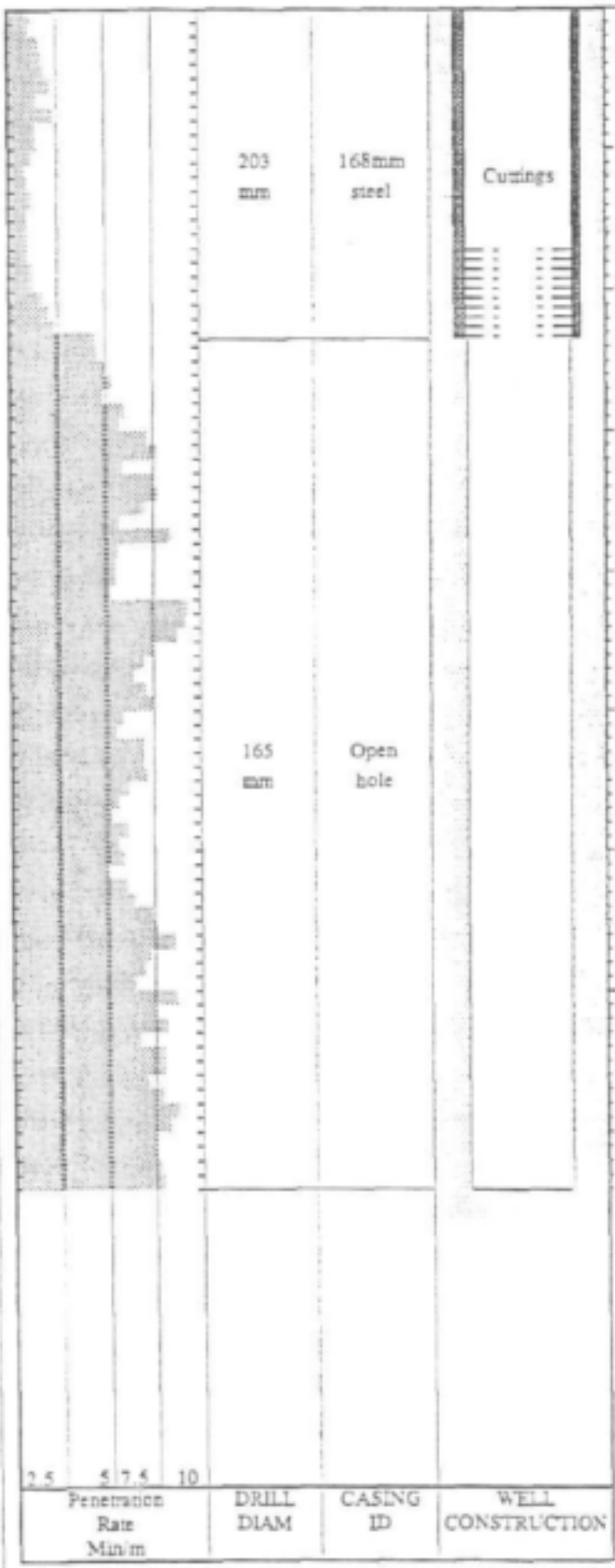

:Weathered, brown sandy GNEISS

:Weathered light to dark brown GNEISS with occasional pyrite and biotite

:Slightly weathered dark GNEISS with abundant amphibole and biotite

:Unweathered AMPHIBOLITE with a high biotite content and occasional pyrite and calcite

:Unweathered reddish GNEISS with little biotite

:Unweathered black to red GNEISS with abundant amphibole and biotite

:Reddish, unweathered GNEISS with biotite

:Unweathered black AMPHIBOLITE with abundant biotite

NOTES

1) Water strike at 17.90m. Increasing water to 20.60m (4 l/s)

2) Rest water level at 6.04m

3) Developed for 30 min by airlift

CONTRACTOR : DWAF
DRILLED BY : B. PIETERSE
DRILL METHOD : DTH HAMMER
SAMPLING : BLOWN CUTTINGS

LOGGED BY : M. PRINSLOO
SETUP FILE : STANDARD.SET

INCLINATION : Vertical
DIAMETER : 165 mm
DRILL DATE : 16 NOVEMBER 1999
CASING TYPE : 4.5 mm steel

DATE : 17/03/00 14:46
TEXT : C:\DOTPLOT\DATA\NMP6.TXT

ELEVATION : 150m
COLLAR HEIGHT : 0.54 m
BLOW YIELD : 4.0 l/s

HOLE No: G47158
EMABHOBHANE DRIFT

GROUNDWATER DEVELOPMENT IN COMPLEX TERRAIN

HOLE No: G47159
Sheet 1 of 1

PROJECT NUMBER: K5/966

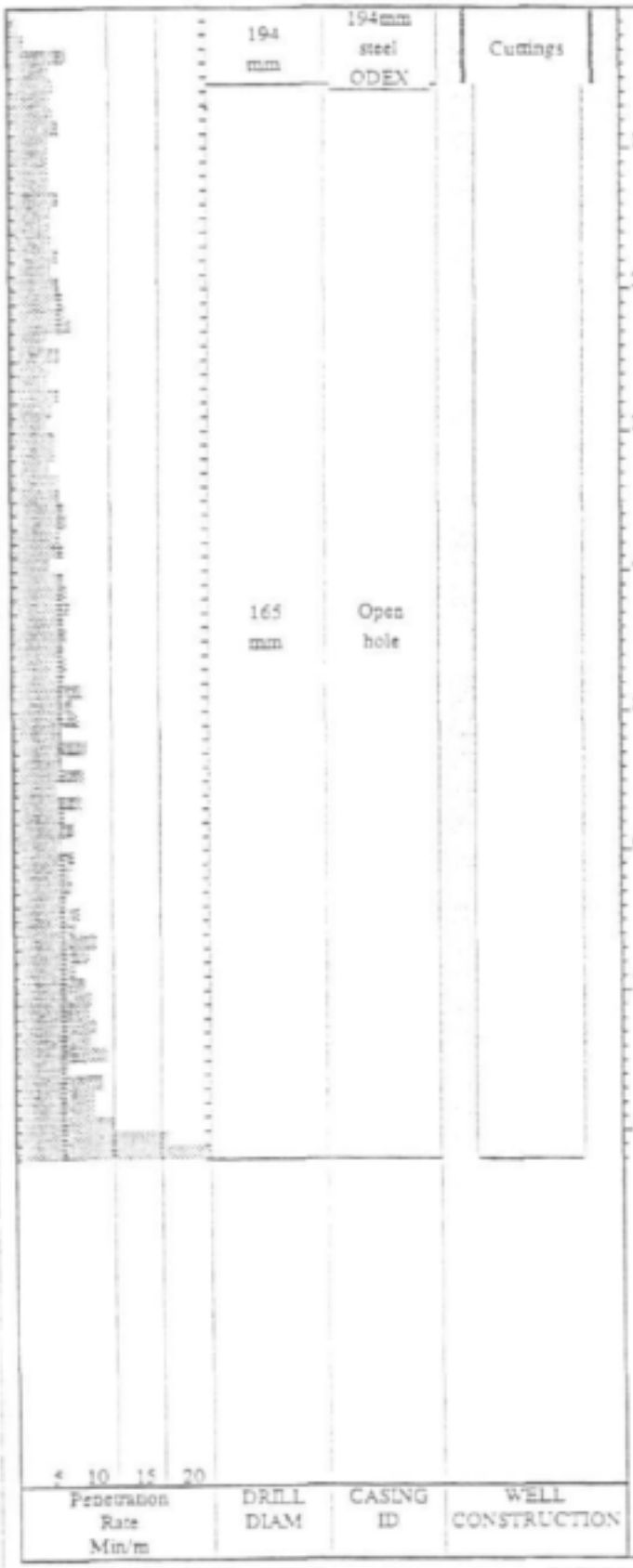

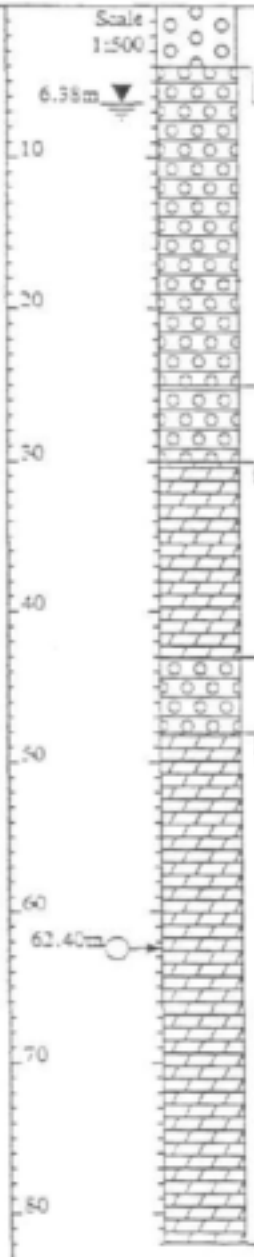

0.00 :Loose rocks of dolerite, gneiss and granite as OVERBURDEN

4.00 :Reddish black slightly weathered GNEISS with occasional calcite and pyrite

25.00 :Dark unweathered GNEISS. Transition from gneiss to amphibolite

30.00 :Black unweathered AMPHIBOLITE with abundant biotite

43.00 :Pink to grey unweathered GNEISS with increasing amphibole from 46m

48.00 :Black, unweathered AMPHIBOLITE with feldspar rich zones between 51-56m, 61-70m and 76-82m

82.00

NOTES

1) Water strike at 62.40m

2) Rest water level at 6.38m

3) Developed for 30 mm by airlift

CONTRACTOR : DWAF
DRILLED BY : B. PIETERSE
DRILL METHOD : DTH HAMMER
SAMPLING : BLOWN CUTTINGS

INCLINATION : Vertical
DIAMETER : 165 mm
DRILL DATE : 18 NOVEMBER 1999
CASING TYPE : 6 mm steel ODEX

ELEVATION : 205m
COLLAR HEIGHT : 0.48 m
BLOW YIELD : 6.67 l/s

LOGGED BY : M. PRINSLOO
SETUP FILE : STANDARD.SET

DATE : 17/03/00 14:16
TEXT : C:\DOTPLOT\DATA\NMP7.TXT

HOLE No: G47159
MBULWINI, UMVOTI 4667

GROUNDWATER DEVELOPMENT IN COMPLEX TERRAIN

HOLE No: G47157
Sheet 1 of 1

PROJECT NUMBER: K5/966

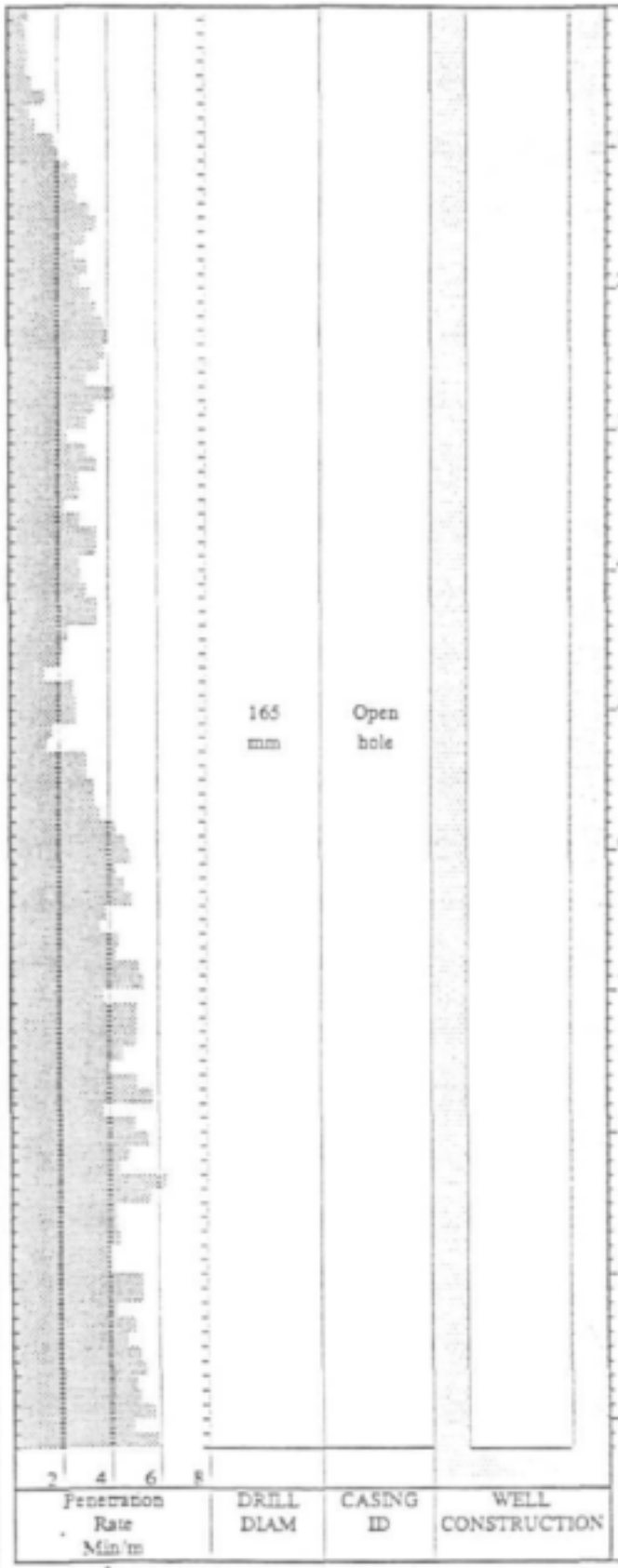

0.00 :Dark reddish brown weathered material showing red feldspar, quartz and amphibole

9.00 :Unweathered dark red GNEISS with occasional calcite and pyrite

67.00 :Weathered dark red GNEISS

68.00 :Unweathered dark red GNEISS with occasional calcite and pyrite

90.00 :Unweathered red GNEISS / GRANITE

93.00 :Unweathered dark red GNEISS with occasional calcite and pyrite

102.00

NOTES

1) No water strike

CONTRACTOR : DWAF
DRILLED BY : B. PIETERSE
DRILL METHOD : DTH HAMMER
SAMPLING : BLOWN CUTTINGS

INCLINATION : Vertical
DIAMETER : 165 mm
DRILL DATE : 15 NOVEMBER 1999
CASING TYPE : 4,5 mm steel

ELEVATION : 490m
COLLAR HEIGHT : 0.0 m
BLOW YIELD : 0.00 l/s

LOGGED BY : M. PRINSLOO
SETUP FILE : STANDARD.SET

DATE : 17/03/00 14:47
TEXT : C:\DOTPLOT\DATA\NMP5.TXT

HOLE No: G47157
OQAQENI, UMVOTI 4667

GROUNDWATER DEVELOPMENT IN COMPLEX TERRAIN

HOLE No: G47156
Sheet 1 of 2

PROJECT NUMBER: K5/966

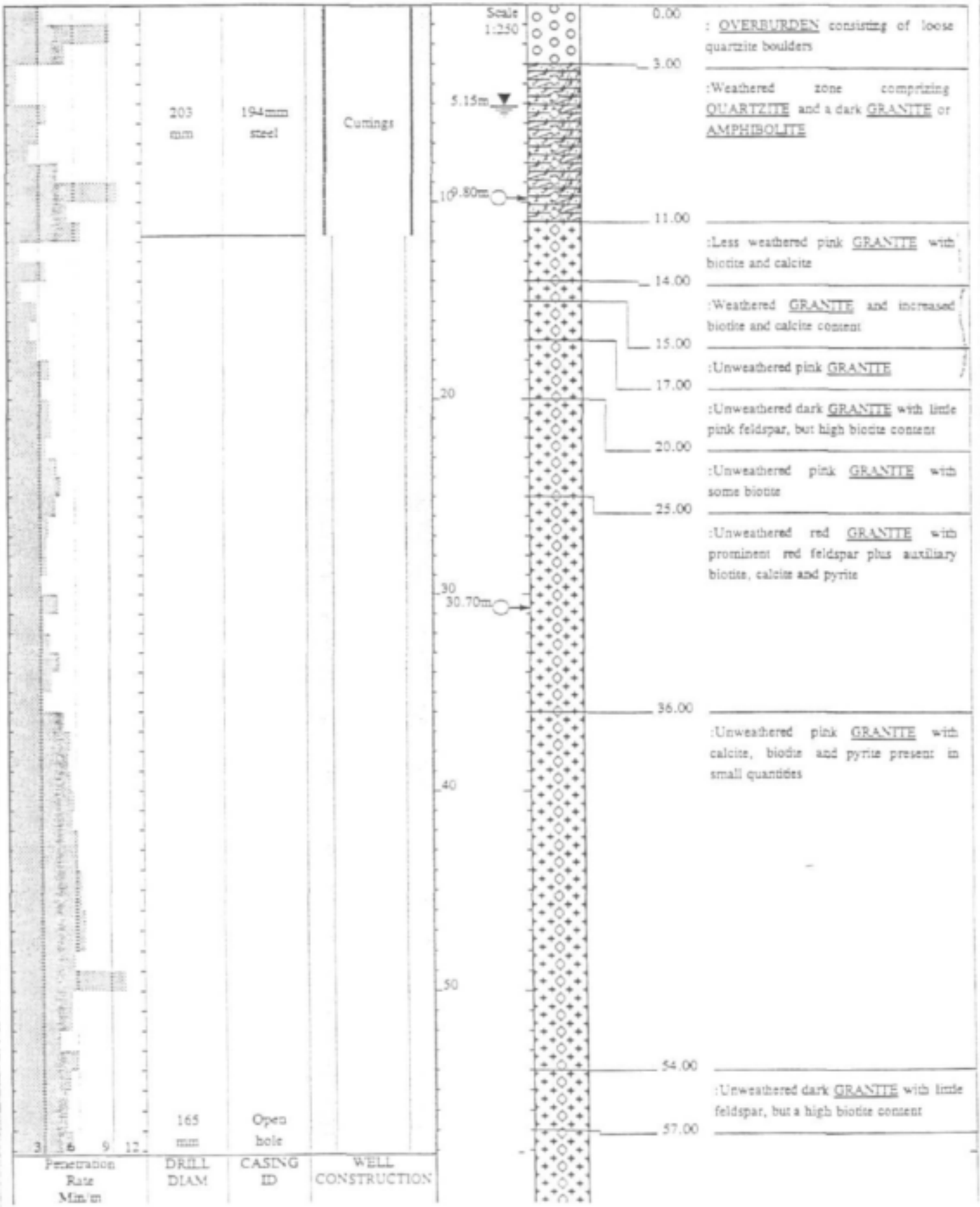

GROUNDWATER DEVELOPMENT IN COMPLEX TERRAIN

HOLE No: G47154
Sheet 1 of 1

PROJECT NUMBER: K5/966

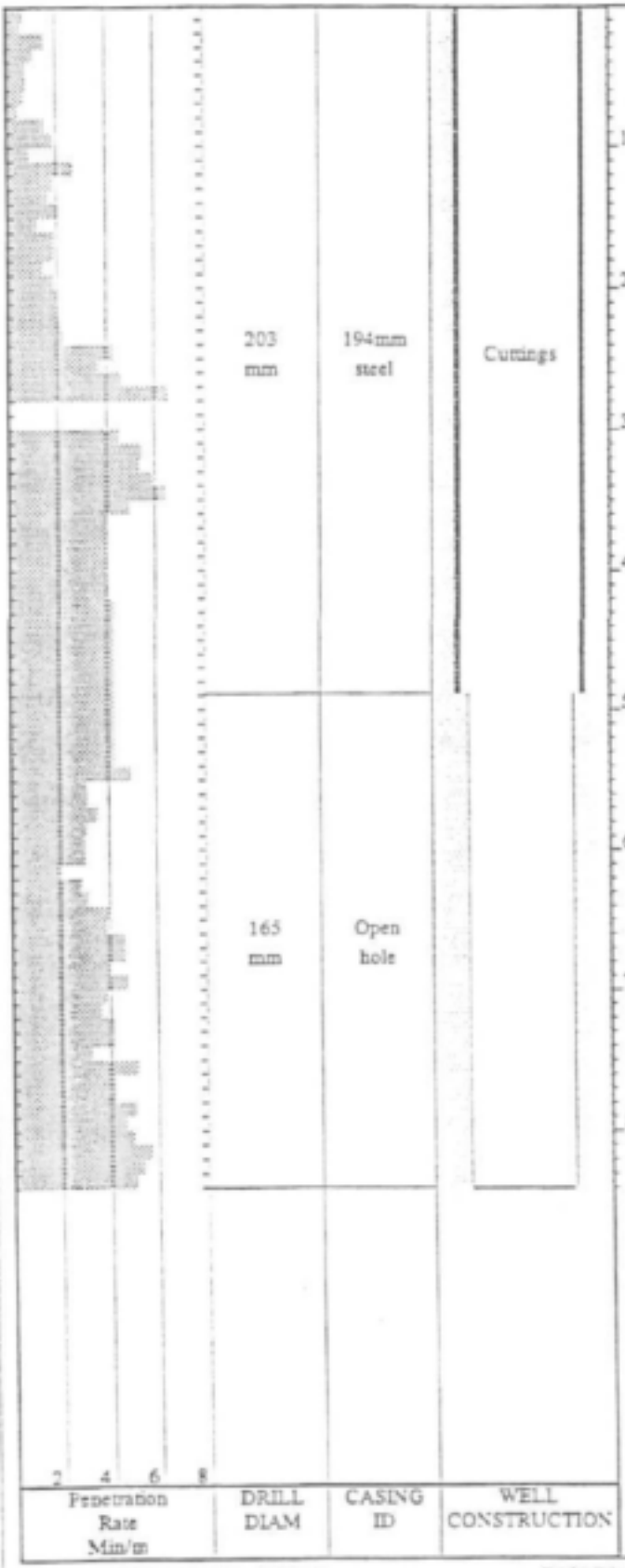

0.00	:Reddish brown overburden of loose rocks. GNEISS QUARTZITE
3.00	:Weathered GNEISS. Feldspar, quartz visible
10.00	:Weathered GNEISS with calcretion
16.00	:Highly weathered GNEISS as a reddish brown mud. 2-3mm quartz and 20mm quartzite crystals present
19.00	:Highly weathered AMPHIBOLITE as a greyish brown mud. Quartz and quartzite crystals as above
36.00	:Weathered reddish brown GNEISS with biotite
54.00	:Unweathered black AMPHIBOLITE with little pink feldspar, but rich in biotite
66.00	:Pale AMPHIBOLITE with lesser biotite and more pink feldspar
71.00	:Black to pinkish AMPHIBOLITE with varying percentages of both biotite and pink feldspar
76.00	:Pink GNEISS with some biotite
84.00	

NOTES

1) Water strike at 51m (3.33 l/s)

2) Rest water level at 7.90m

3) Developed for 30 min by airlift

CONTRACTOR : DWAF
DRILLED BY : B. PIETERSE
DRILL METHOD : DTH HAMMER
SAMPLING : BLOWN CUTTINGS

INCLINATION : Vertical
DIAMETER : 165 mm
DRILL DATE : 28 OCTOBER 1999
CASING TYPE : 6 mm steel ODEX

ELEVATION : 430m
COLLAR HEIGHT : 0.4 m
BLOW YIELD : 3.33 l/s

LOGGED BY : M. PRINSLOO
SETUP FILE : STANDARD.SET

DATE : 17/03/00 14:23
TEXT : C:\DOTPLOT\DATA\NMP3A.TXT

HOLE No: G47154
ST. JOAN OF ARC MISSION STA

dot.PLOT 3027 J&W

GROUNDWATER DEVELOPMENT IN COMPLEX TERRAIN

HOLE No: G47152
Sheet 1 of 1

PROJECT NUMBER: K5/966

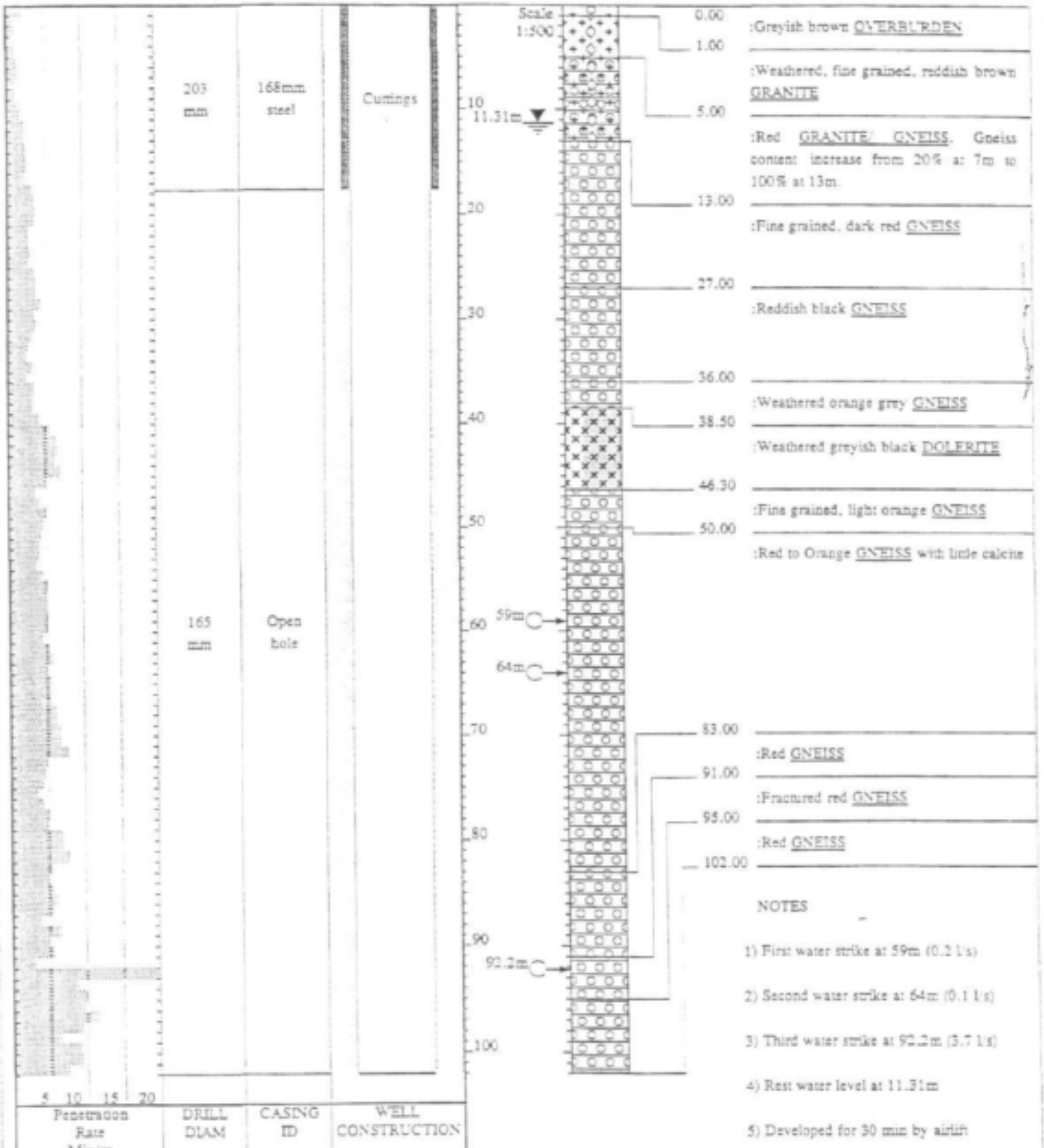

NOTES

1) First water strike at 59m (0.2 l/s)

2) Second water strike at 64m (0.1 l/s)

3) Third water strike at 92.2m (3.7 l/s)

4) Rest water level at 11.31m

5) Developed for 30 min by airlift

CONTRACTOR : DWAF
DRILLED BY : B. PIETERSE
DRILL METHOD : DTH HAMMER
SAMPLING : BLOWN CUTTINGS

INCLINATION : Vertical
DIAMETER : 165 mm
DRILL DATE : 21 OCTOBER 1999
CASING TYPE : 4.5 mm steel

ELEVATION : 210m
COLLAR HEIGHT : 0.3 m
BLOW YIELD : 4 l/s

LOGGED BY : M. PRINSLOO
SETUP FILE : STANDARD.SET

DATE : 17/03/00 14:22
TEXT : C:\DOTPLOT\DATA\NMP1B.TXT

HOLE No: G47152
CANAAN MISSION

dot PLOT 3027 (A3) Inc

APPENDIX 2-C

TEST PUMP DATA

Borehole G47151

Time vs drawdown

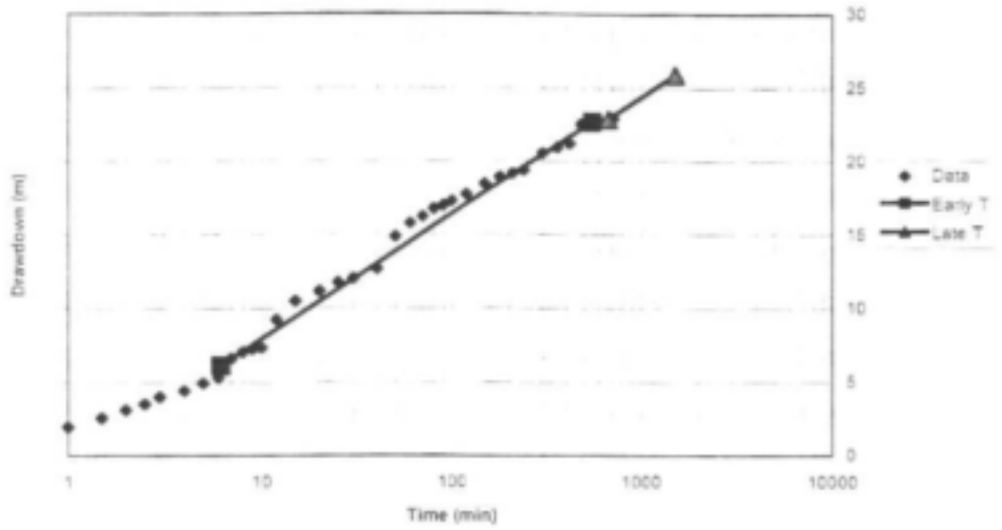

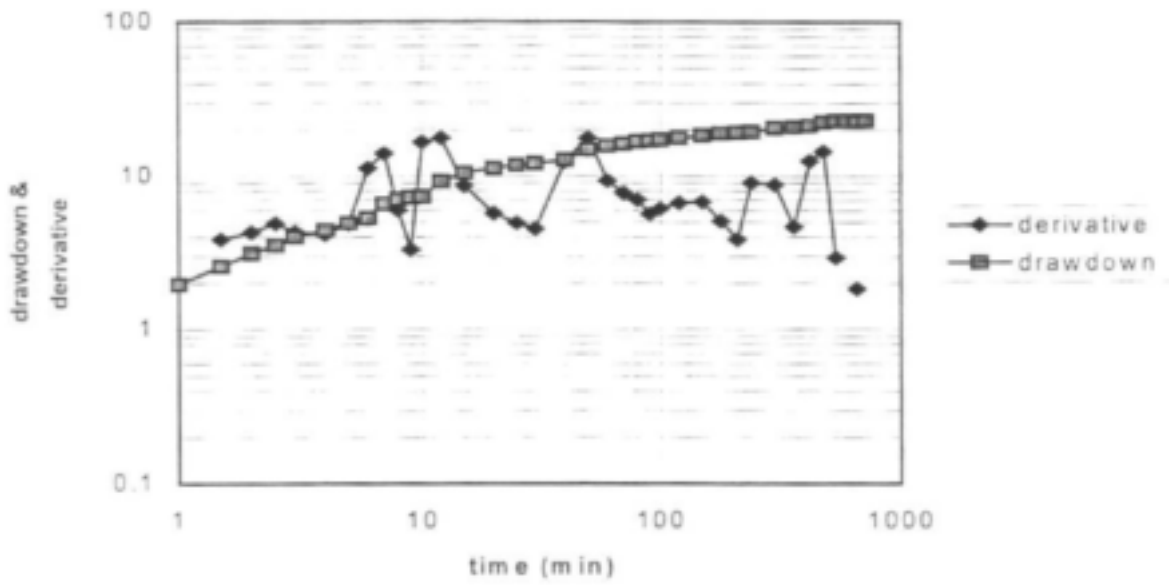

t/t' vs residual drawdown

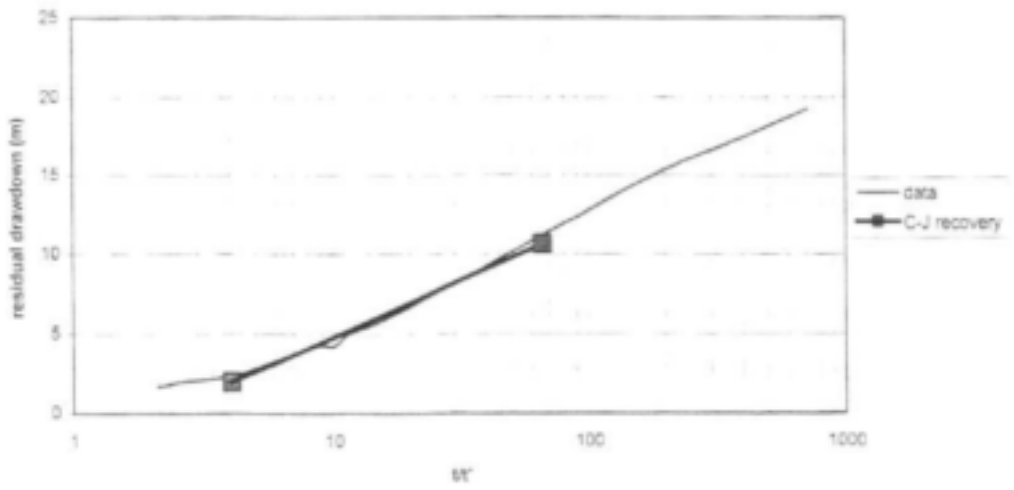

G14752 Obervation

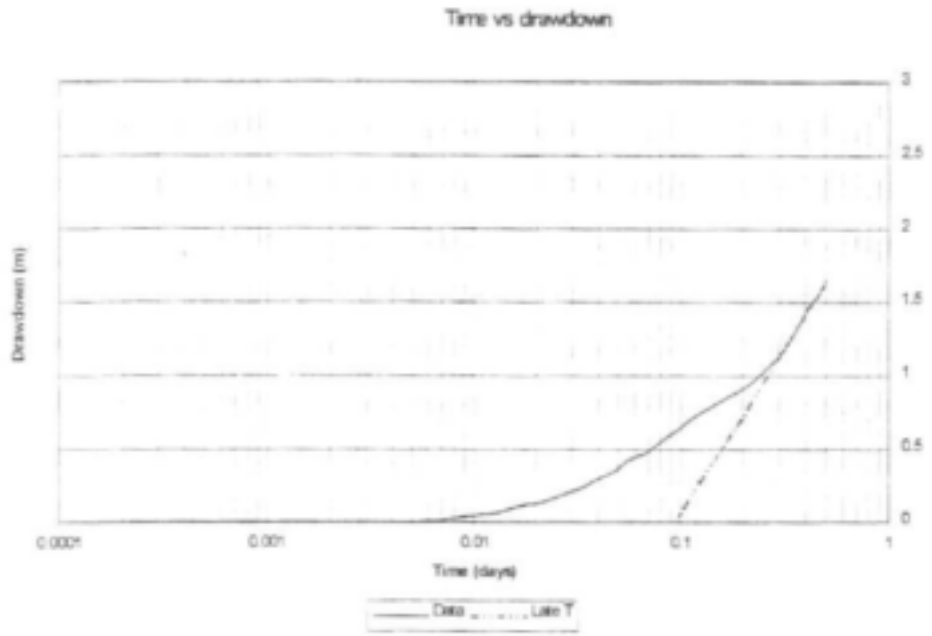

G47153

Time vs drawdown

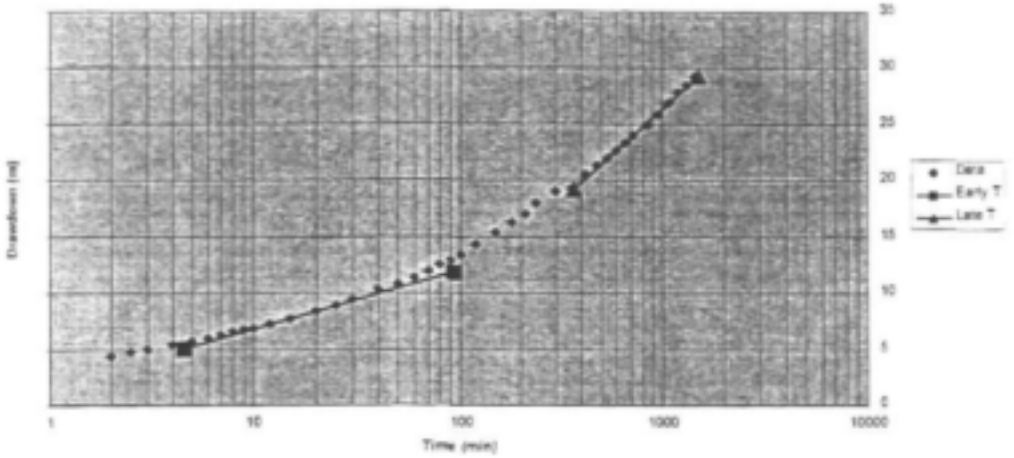

Drawdown and Derivative

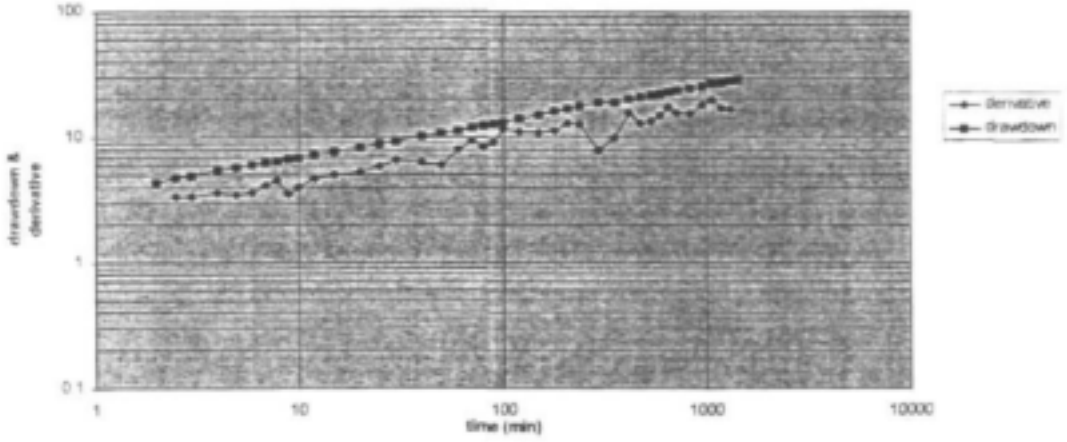

t/t' vs residual drawdown

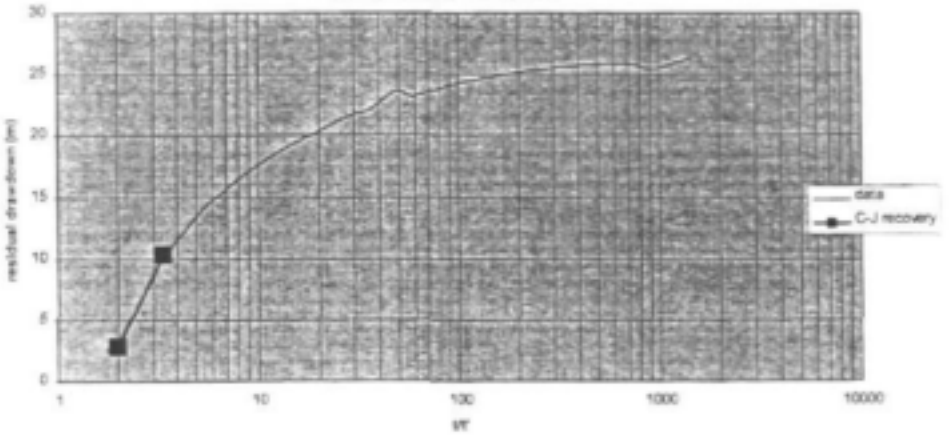

G47155

Time vs drawdown

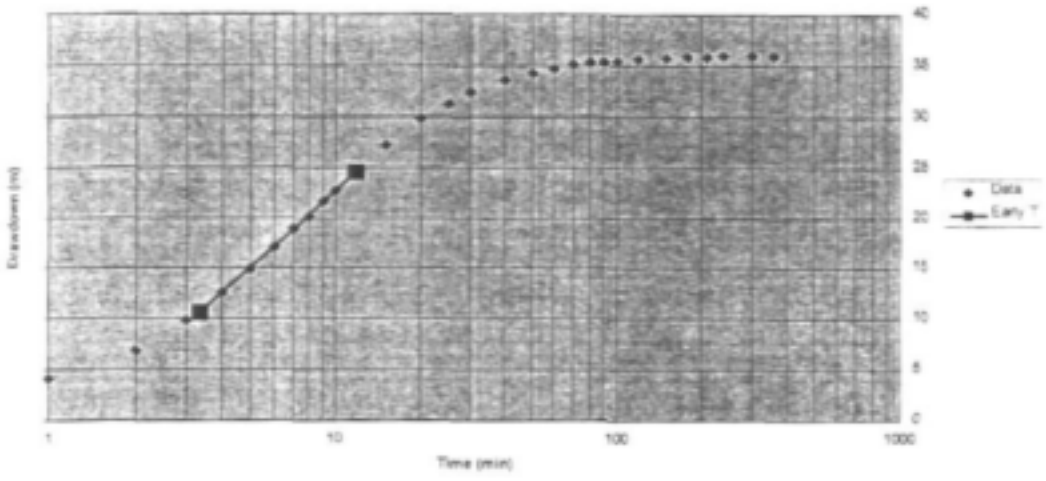

Drawdown and Derivative

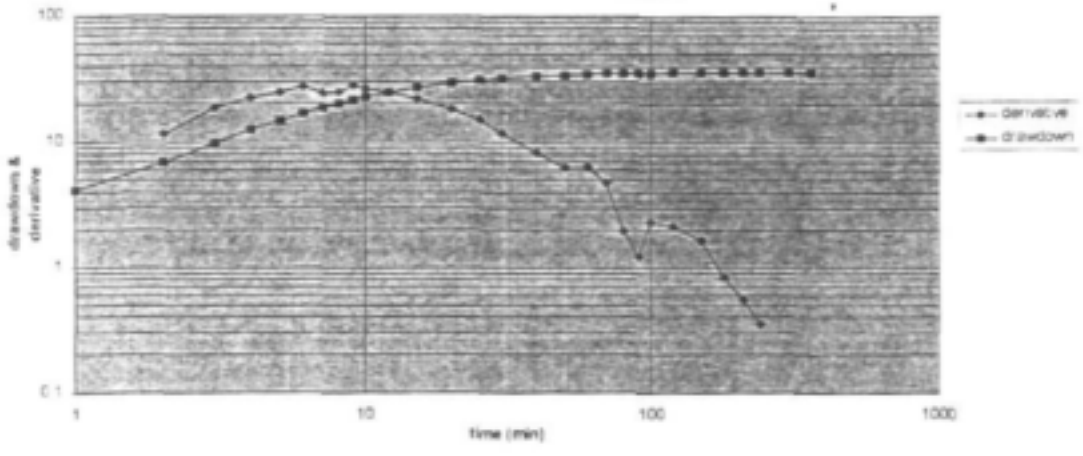

t/t' vs residual drawdown

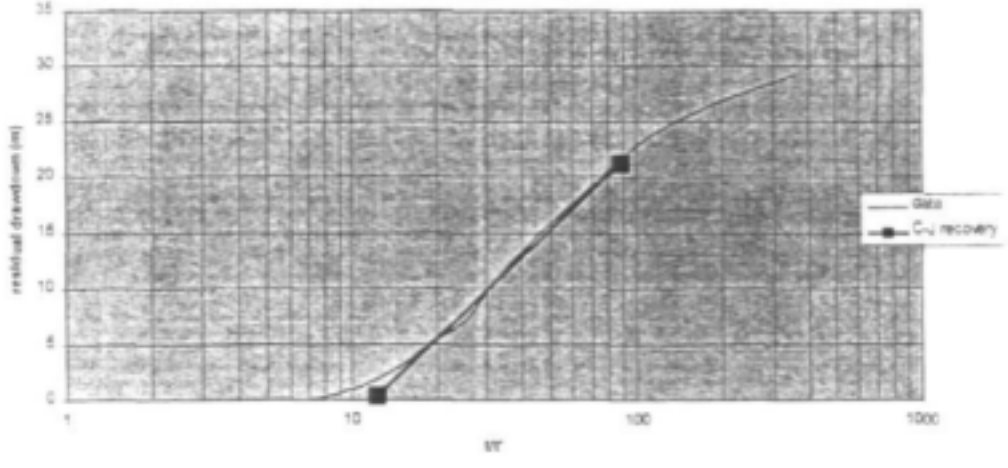

G47158

Time vs drawdown

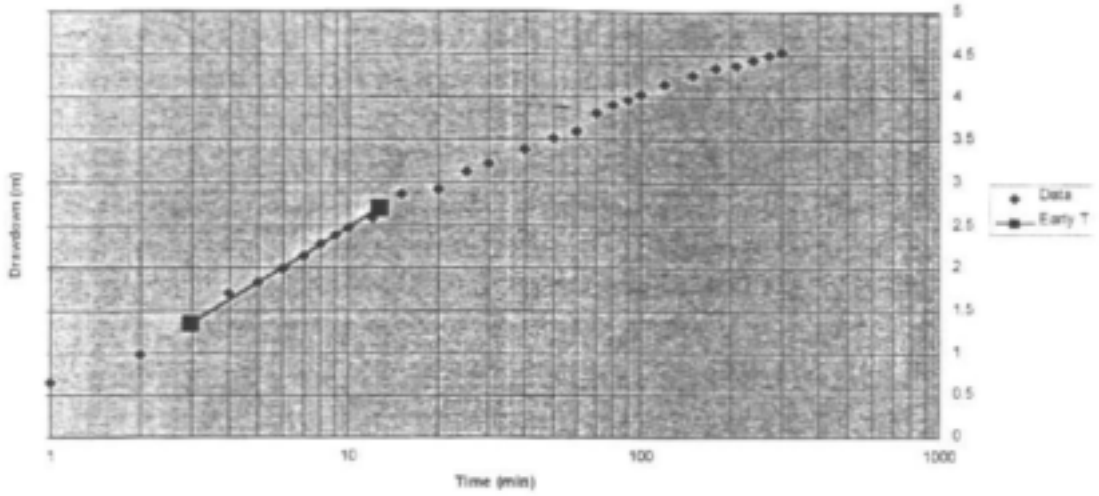

Drawdown and Derivative

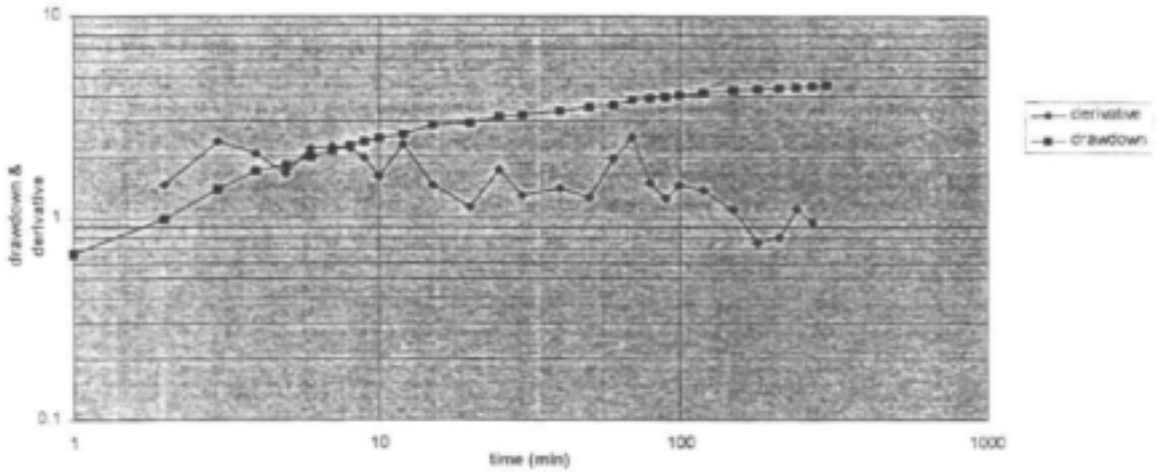

t/t' vs residual drawdown

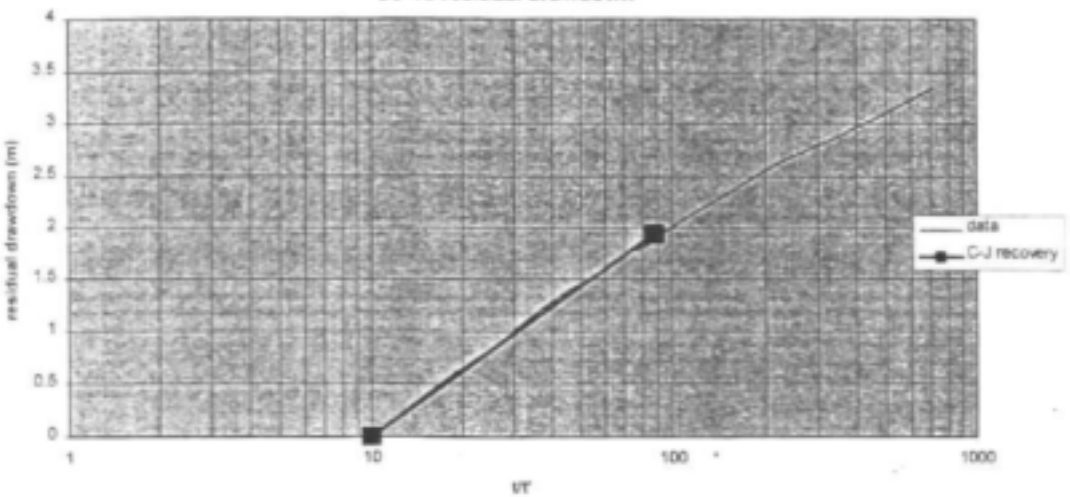

Time vs drawdown

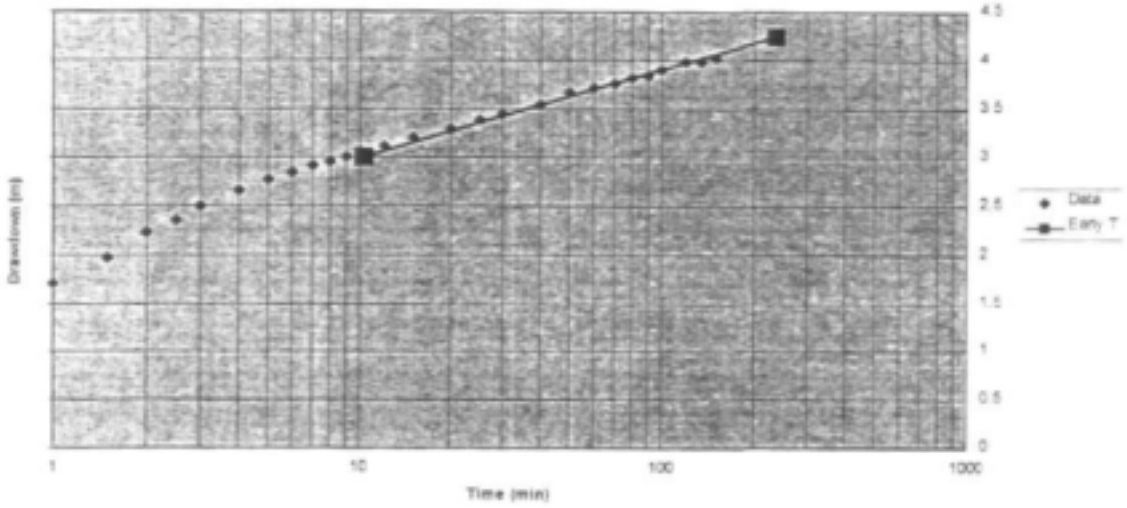

Drawdown and Derivative

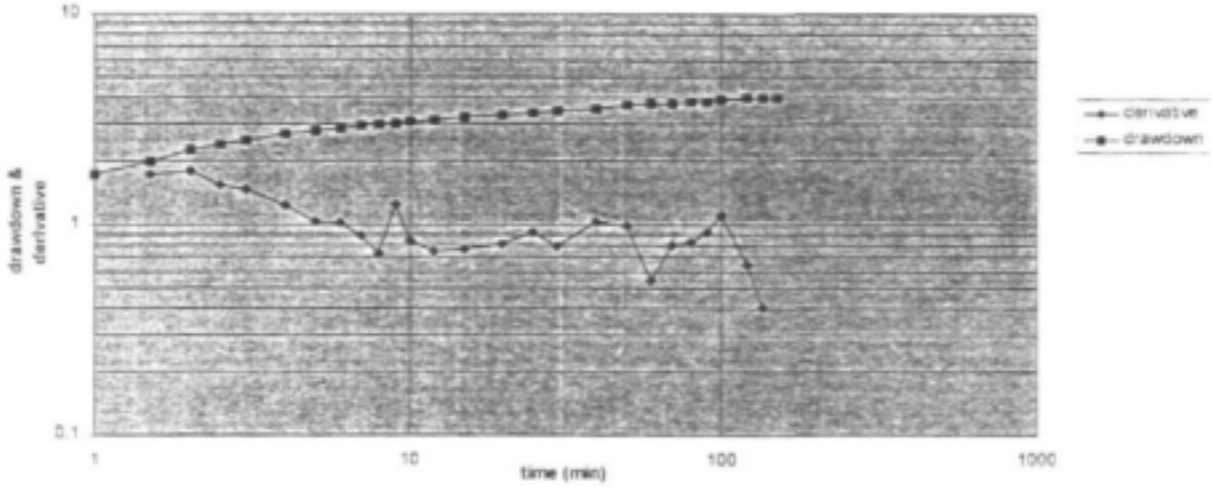

t/t' vs residual drawdown

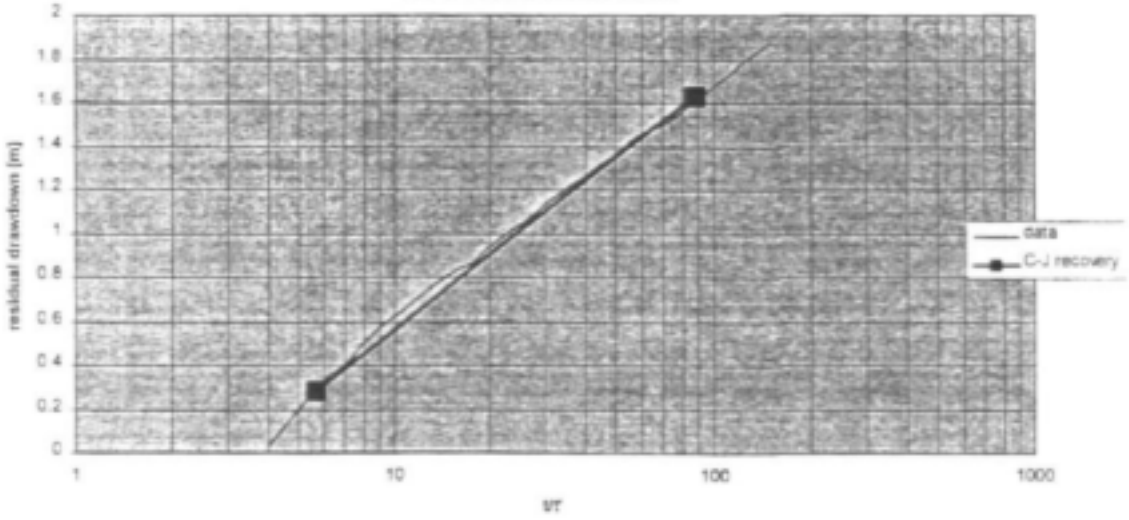

G47156

Time vs drawdown

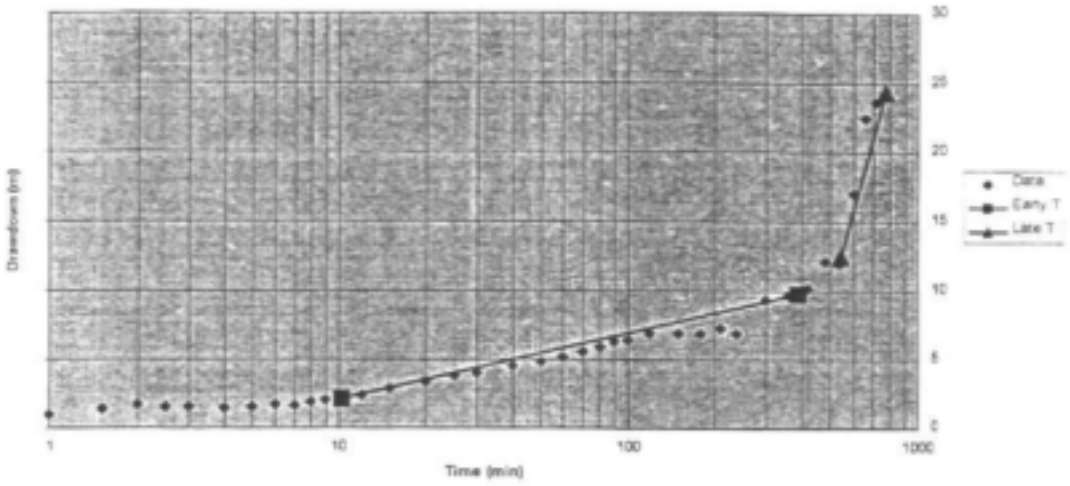

Drawdown and Derivative

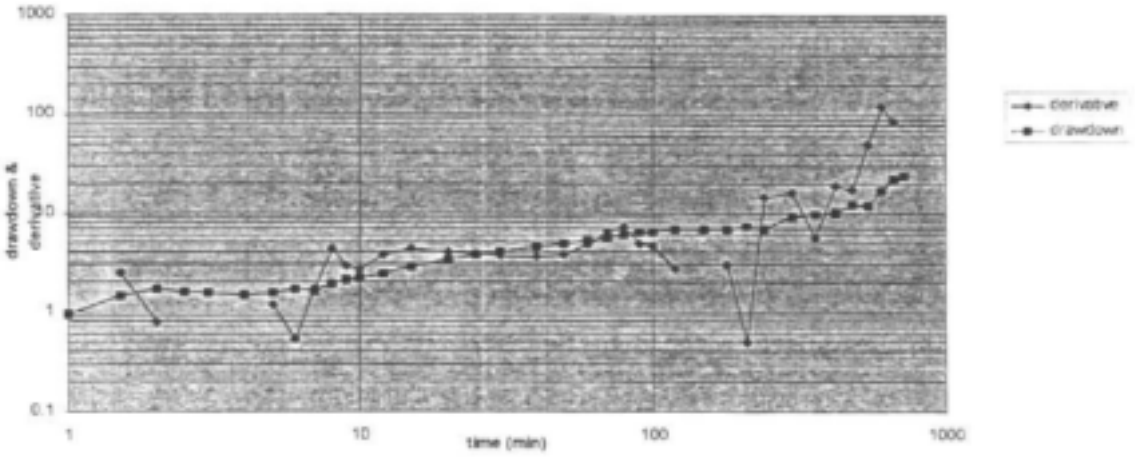

t/t' vs residual drawdown

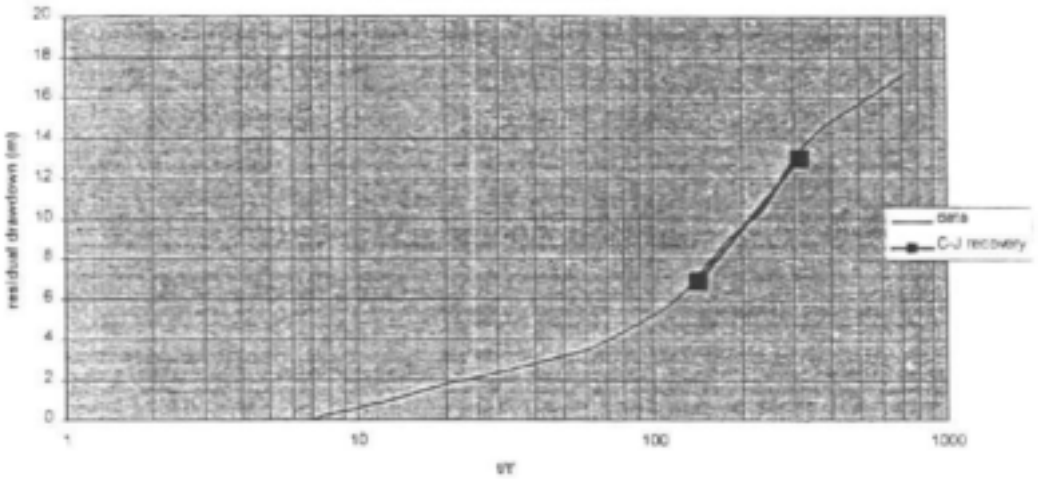

G47154

Time vs drawdown

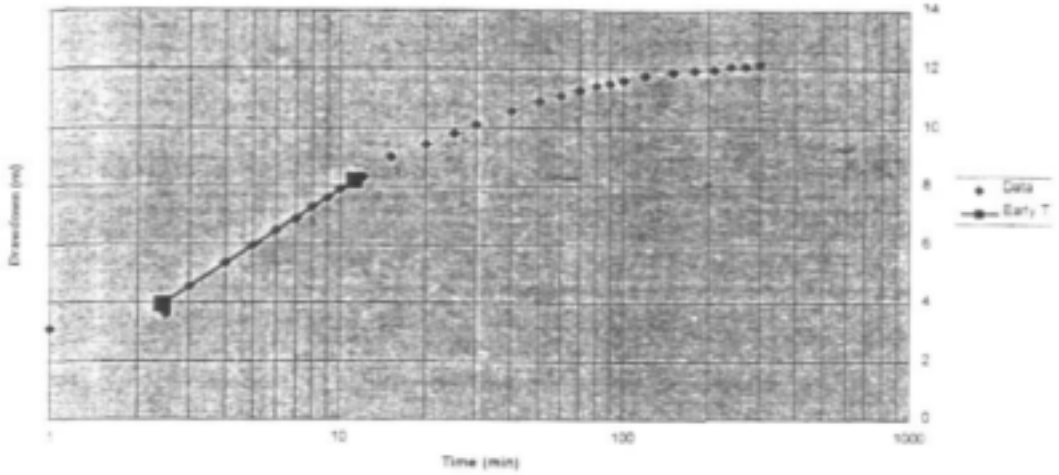

Drawdown and Derivative

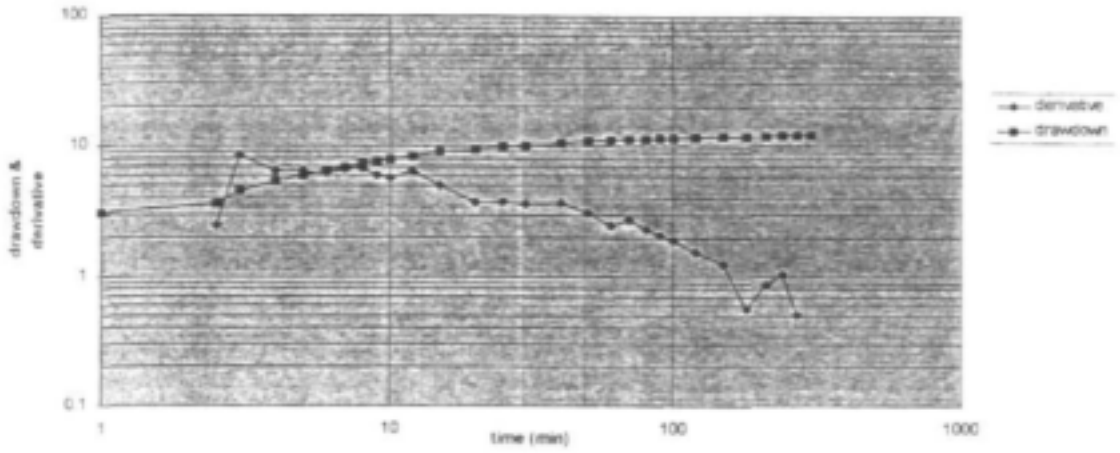

t/t' vs residual drawdown

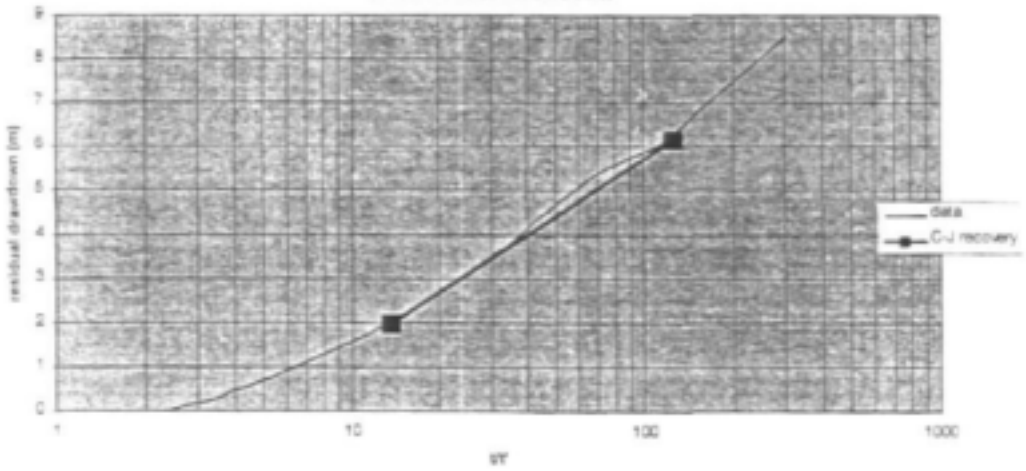

G47152

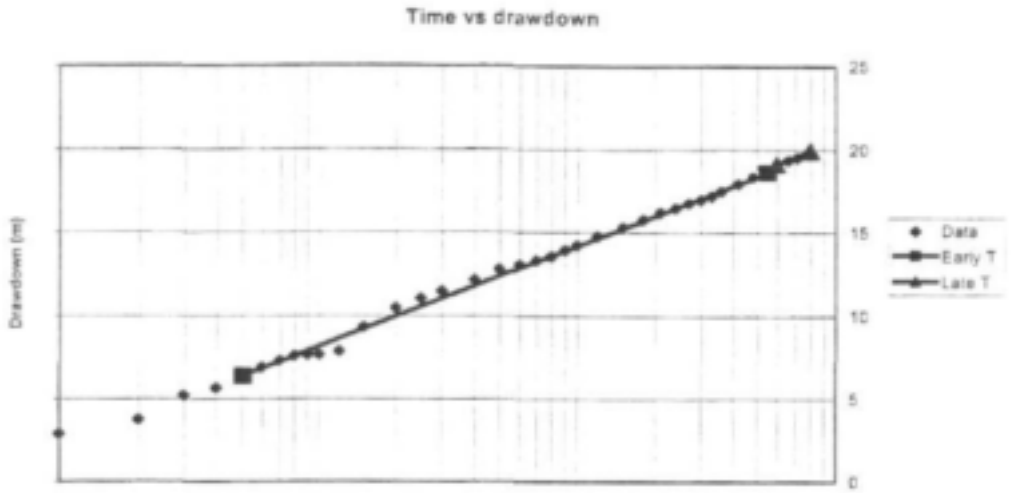
Time vs drawdown
Drawdown (m)
0
5
10
15
20
25
Data
Early T
Late T

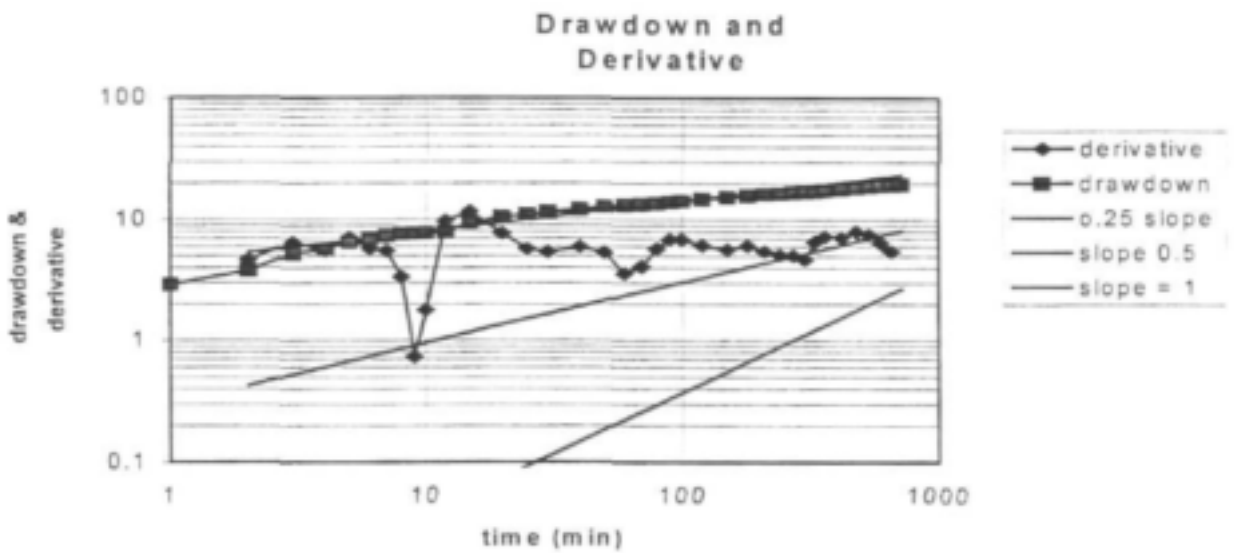
Drawdown and Derivative
drawdown & derivative
100
10
1
0.1
1
10
100
1000
time (min)
derivative
drawdown
0.25 slope
slope 0.5
slope = 1

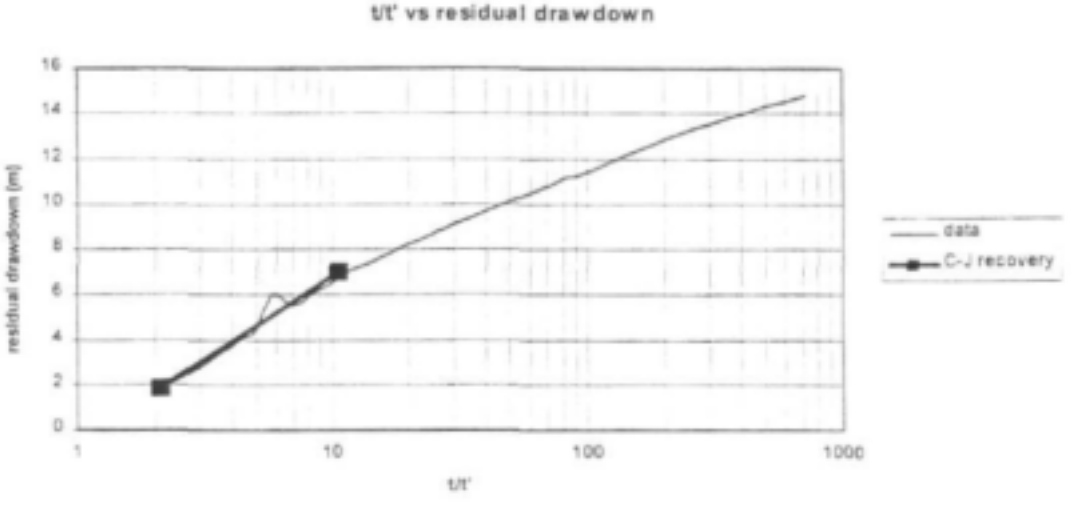
t/t' vs residual drawdown
residual drawdown (m)
0
2
4
6
8
10
12
14
16
1
10
100
1000
t/t'
data
C-J recovery

APPENDIX 2-D

ANALYTICAL RESULTS OF THE WATER SAMPLES

	G47151	G47152	G47153	G47154	G47155	G47156	G47158	G47159
pH	7.47	8.1	7.77	6.94	6.9	7.24	7.01	7.53
EC (mS/m at 25°)	156	144	125	47	81	67	266	100
TDS (mg/l).	967.2	869	734	267.2	477.7	376	1687.6	618.40
COD	n.a.	n.a.	n.a	n.a	n.a.	n.a.	n.a	n.a
Total Alkalinity (mg/l)	280	90	260	125	238	198	540	160
Calcium (mg/l)	82.2	36.1	59.3	26.5	50.8	33.5	117	50.90
Magnesium (mg/l)	40.02	8.19	42.38	19.42	29.91	14.86	86.9	28.42
Sodium (mg/l)	194	252	142	34.7	76.3	89.1	378	116
Potassium (mg/l)	1.3	1.6	3.4	2.1	2	2.1	3.1	3.9
Sulfate (mg/l)	81.55	123.47	32.33	16.6	27.57	12.59	117.44	142.04
Chloride (mg/l)	350.49	388.82	282.89	40.95	116.74	101.96	651.8	178.58
Bicarbonate (mg/l)	341.6	109.8	317.2	152.5	289.75	240.95	658.8	195.2
Nitrate plus nitrite as N (mg/l)	2.2	0.0	2.6	11.2	6.4	0.0	0.0	0.0
Fluoride (mg/l)	1.93	3.68	1.01	0.23	0.5	1.39	3.58	0.83
Boron (mg/l)	0.14	0.23	0.09	0.07	0.06	0.11	0.29	0.12
Chemical Character	NaCl	NaCl	NaCl	MgCaCo3	NaCaCo3	NaCaCo3	NaCl	NaCl

SABS (1984) specification for water for domestic supplies (max. allowable limit):

EC (mS/m)	300
PH	5.5-9.5
Fluoride (mg/l)	1.5
Nitrate + Nitrite (mg/l N)	10
Faecal coliforms (counts/100 ml)	0

Proposed water quality criteria of the Department of National Health and Population development (Auscamp and Visser, 1990):
Maximum limit for no risk

Boron (mg/l)	0.5	Potassium (mg/l)	200
Calcium (mg/l)	150	Sodium (mg/l)	100
Chloride (mg/l)	250	Sulphates (mg/l)	200
Iron (mg/l)	0.1		
Magnesium (mg/l)	70		

Classification for the assessment of the suitability of borehole water for potable use (DWAF, 1996).

CONSTITUENT	CLASS 0	CLASS I	CLASS II	CLASS III
TDS (mg/l)	0 - 450	450 - 1000	1000 - 2450	> 2450
Electrical Conductivity (mS/m)	0 - 70	70 - 150	150 - 370	> 370
Nitrate – Nitrite as N (mg/l)	0 - 6	6 - 10	10 - 20	> 20
Fluoride (mg/l)	0 - 1.0	1.0 - 1.5	1.5 - 3.5	> 3.5
Sulphate (mg/l)	0 - 200	200 - 400	400 - 600	> 600
Magnesium (mg/l)	0 - 30	30 - 70	70 - 100	> 100
Calcium (mg/l)	0 - 32	32	32 - 80	> 80
Potassium (mg/l)	0 - 50	50 - 100	100 - 400	> 400
Sodium (mg/l)	0 - 100	100 - 200	200 - 400	> 400
Chloride (mg/l)	0 - 100	100 - 200	200 - 600	> 600
pH (pH units)	6.0 - 9.0	5.0 - 9.5	4 - 5 or 9.5 - 10	< 4 or > 10
Iron (mg/l)	0 - 0.1	0.1 - 0.2	0.2 - 2.0	> 2.0
faecal coliforms (counts/100ml)	0	0 - 1	1 - 10	> 10

Class 0 water is classed as ideal drinking water, suitable for life time use.
Class I water is still safe for life time use.
Class II water is allowable for limited short term use.
Class III water can cause serious health effects. Particularly in infants and elderly people.

Well Ident

G47158

STIFF Diagram

Name	Type

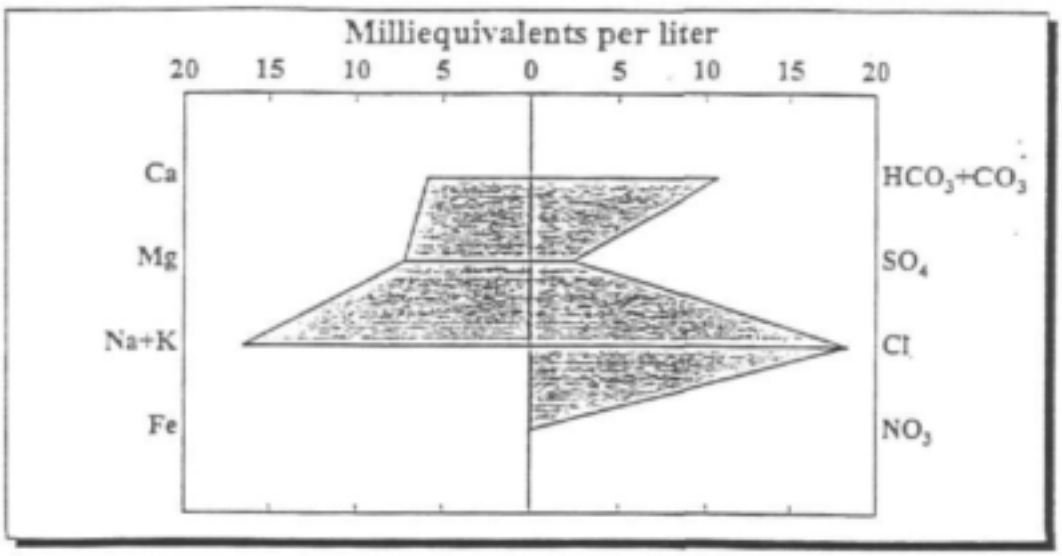

Well Ident

G47159

STIFF Diagram

Name	Type

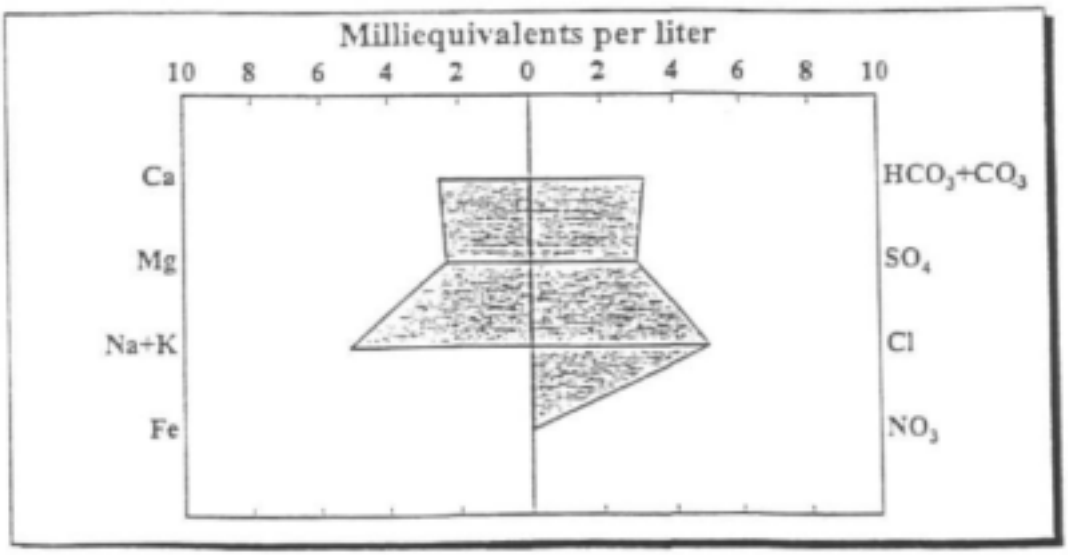

Well Ident

G47153

STIFF Diagram

Name	Type

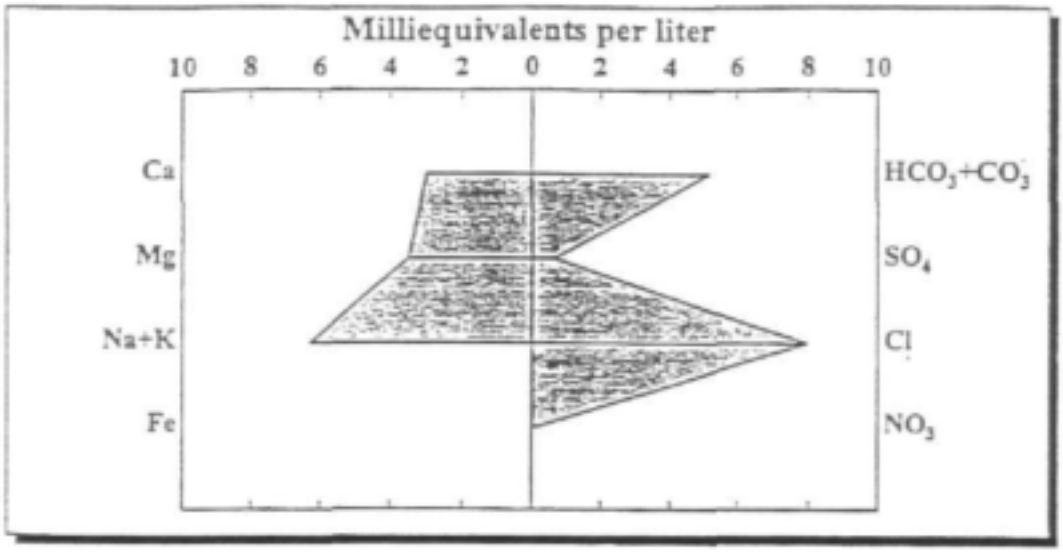

Well Ident

G47154

STIFF Diagram

Name	Type

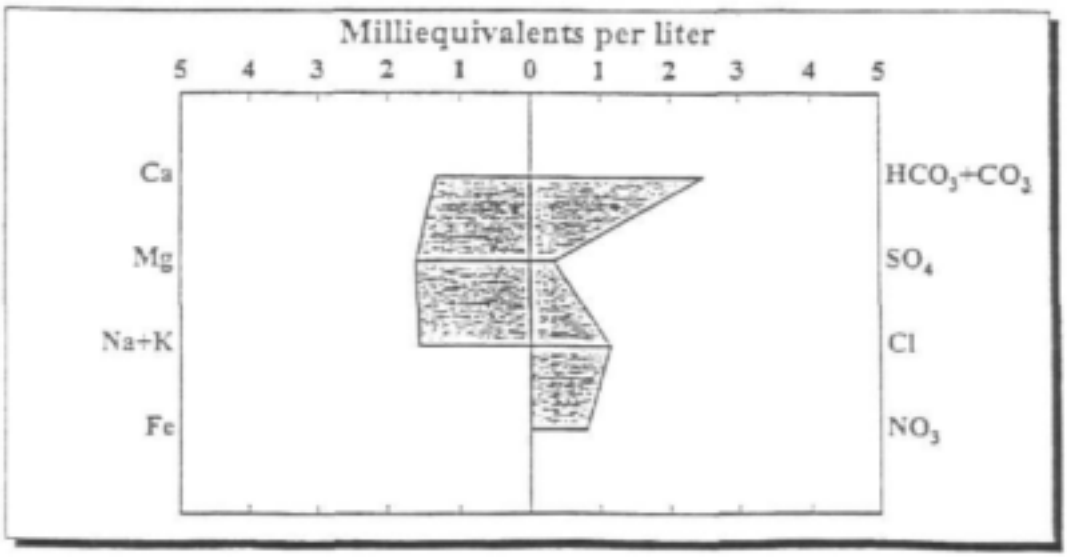

Piper Diagram

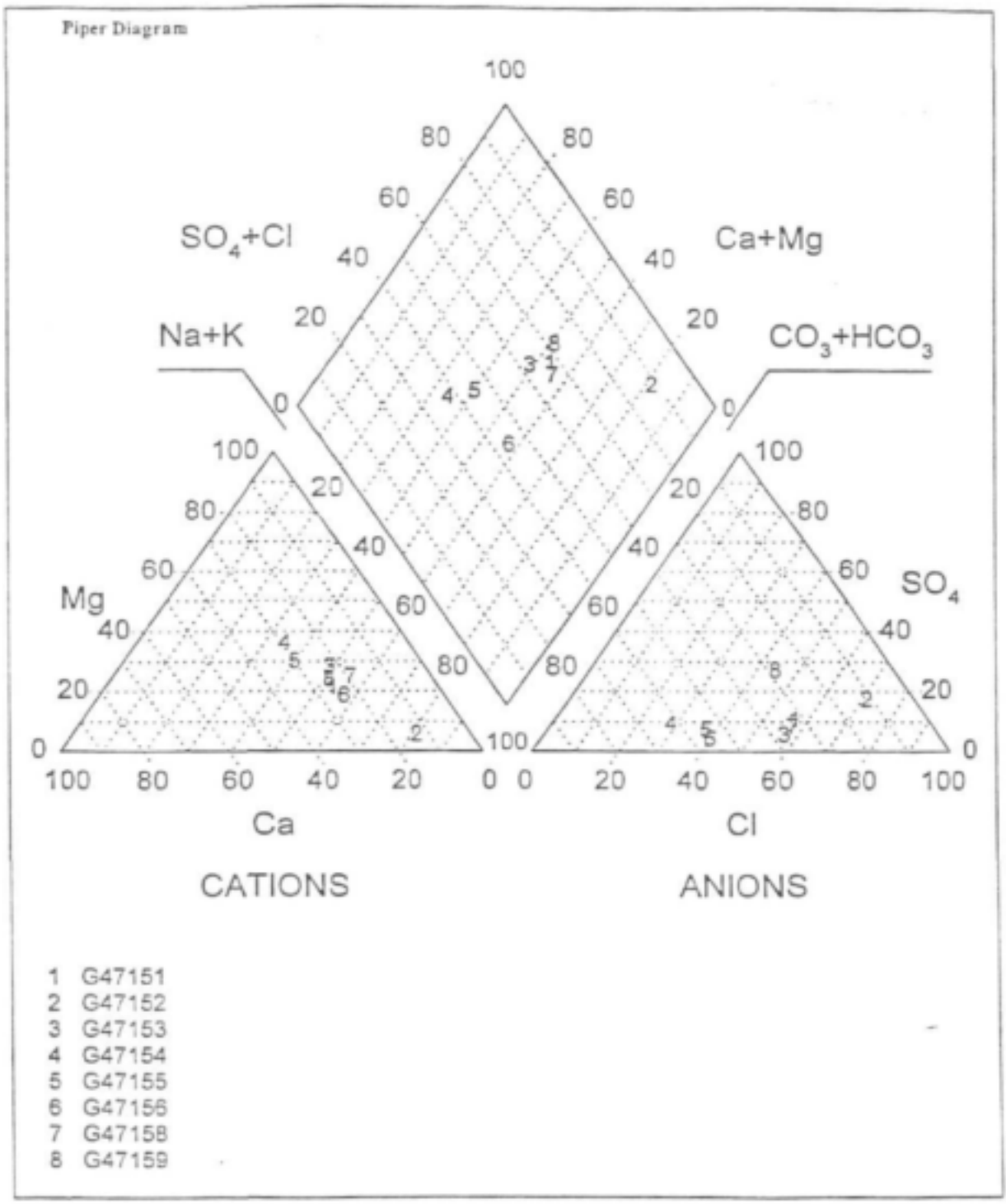

Schoeller Diagram

Schoeller Diagram

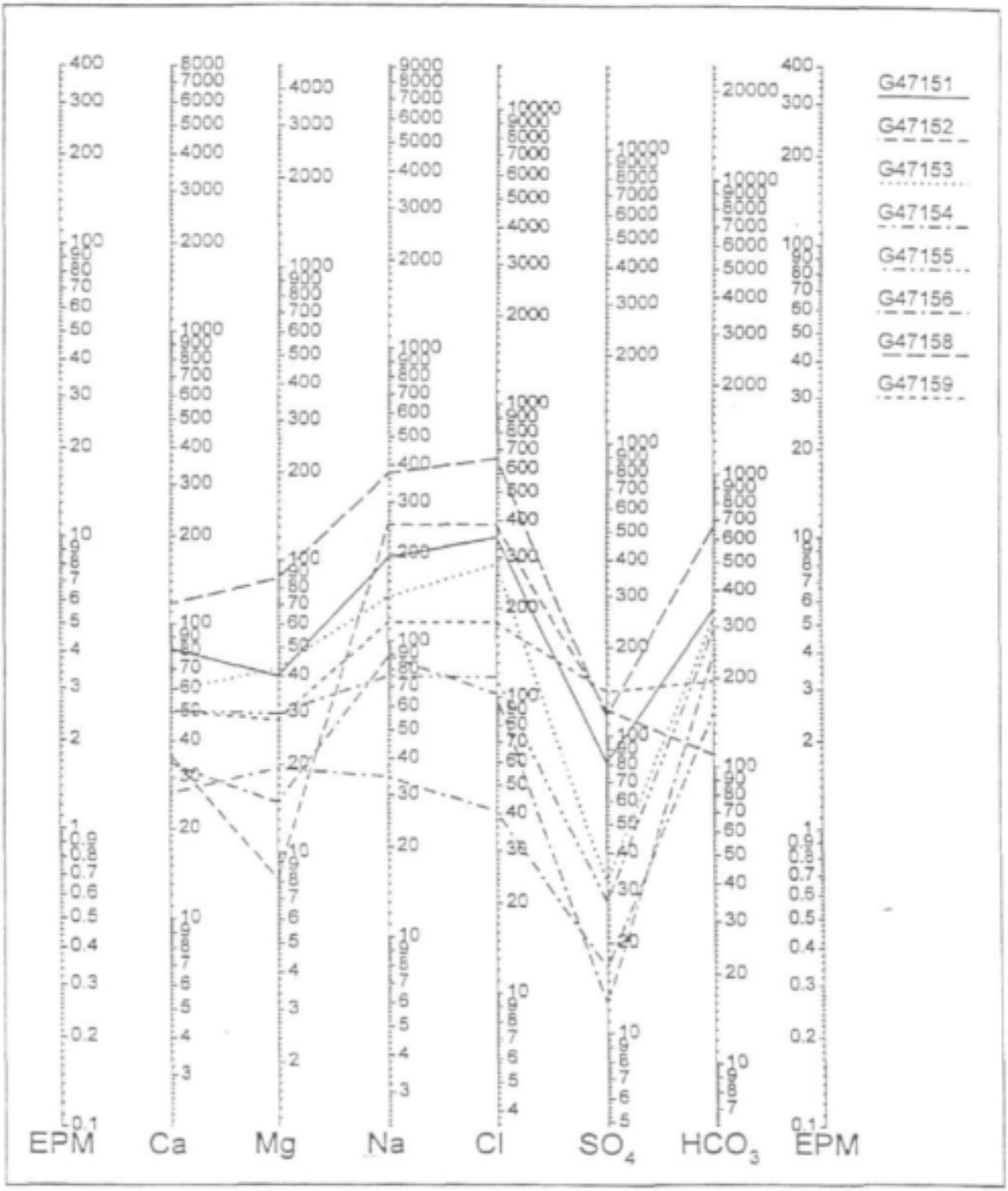

Well Ident

G47151

STIFF Diagram

Name	Type

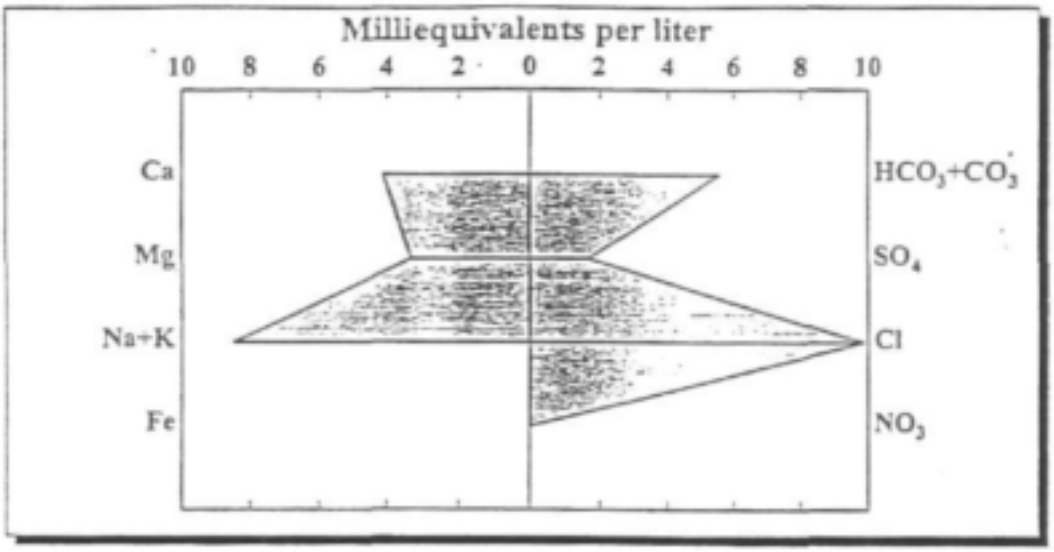

Well Ident

G47152

STIFF Diagram

Name	Type

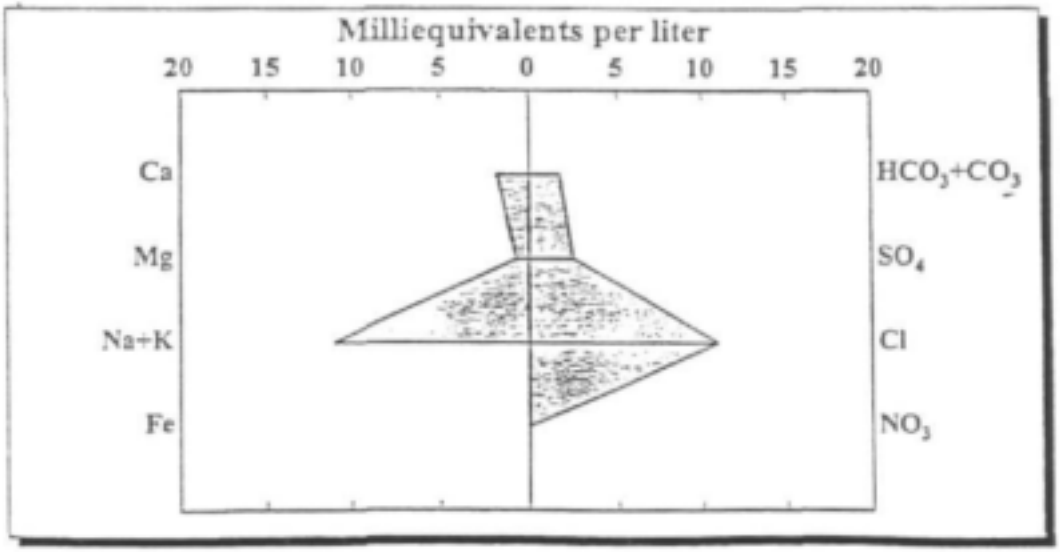

Well Ident

G47155

STIFF Diagram

Name	Type

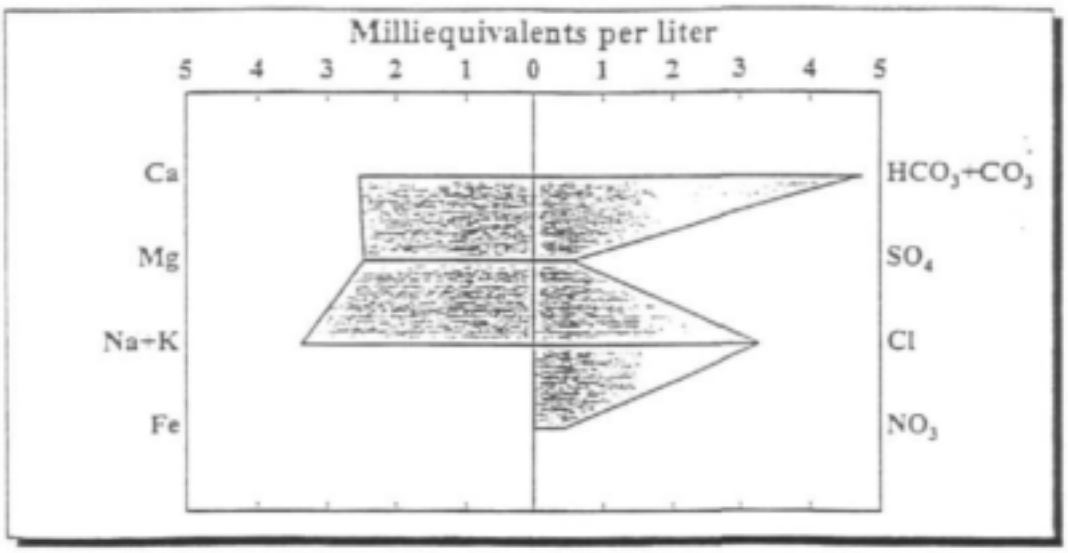

Well Ident

G47156

STIFF Diagram

Name	Type

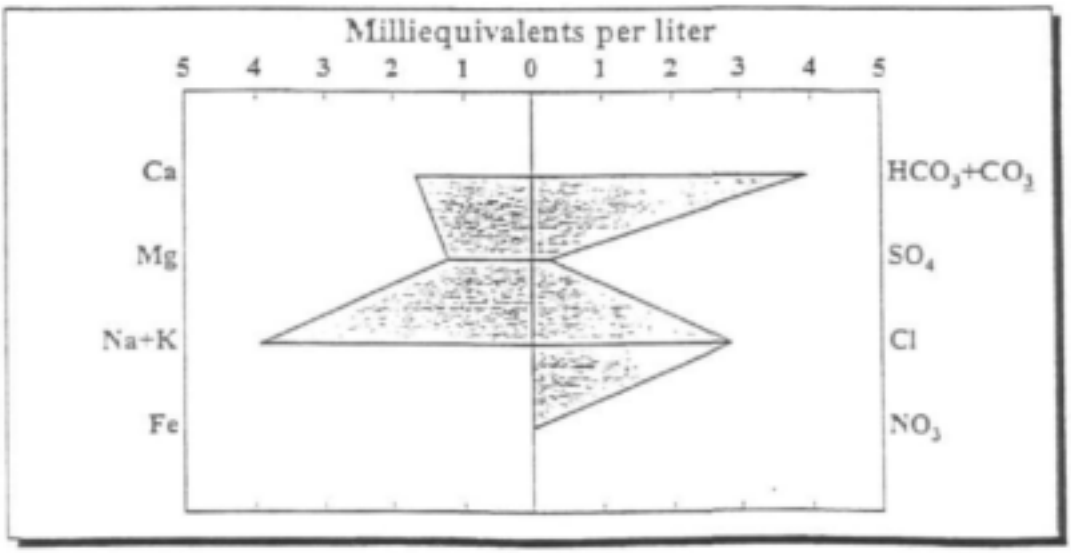

APPENDIX 2-E

DOWN-THE-HOLE-GEOPHYSICS

G47151

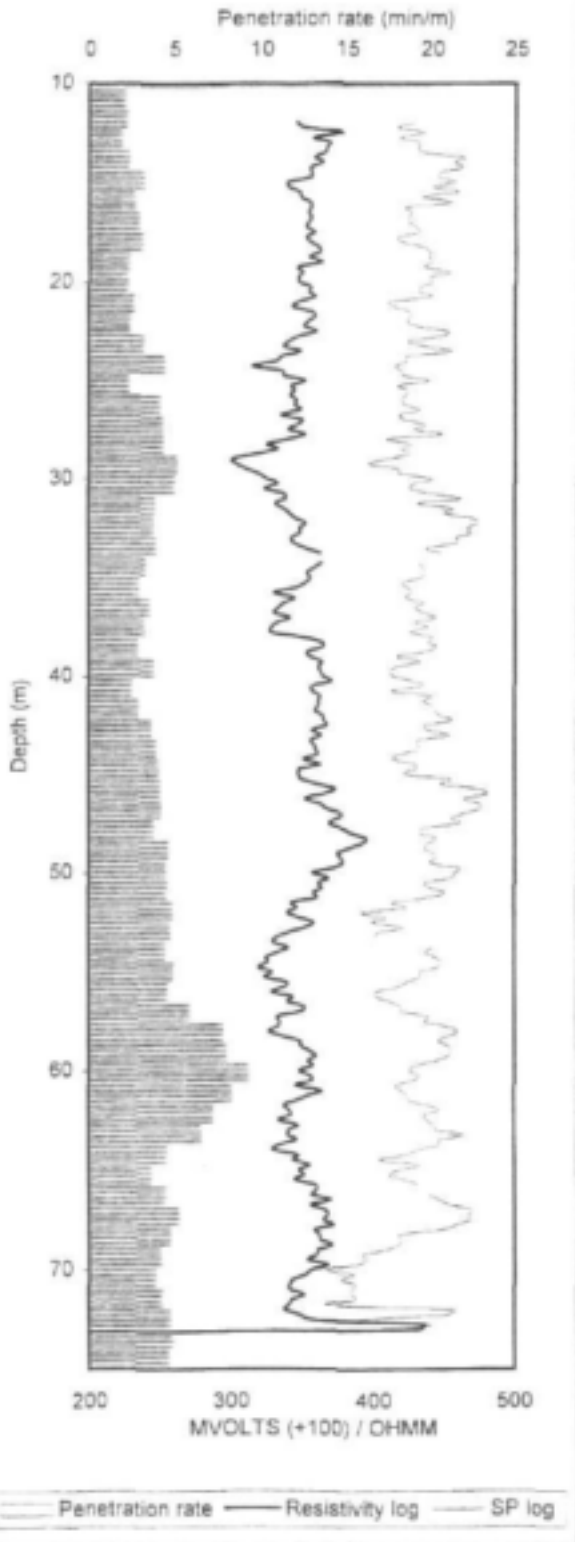

G47151

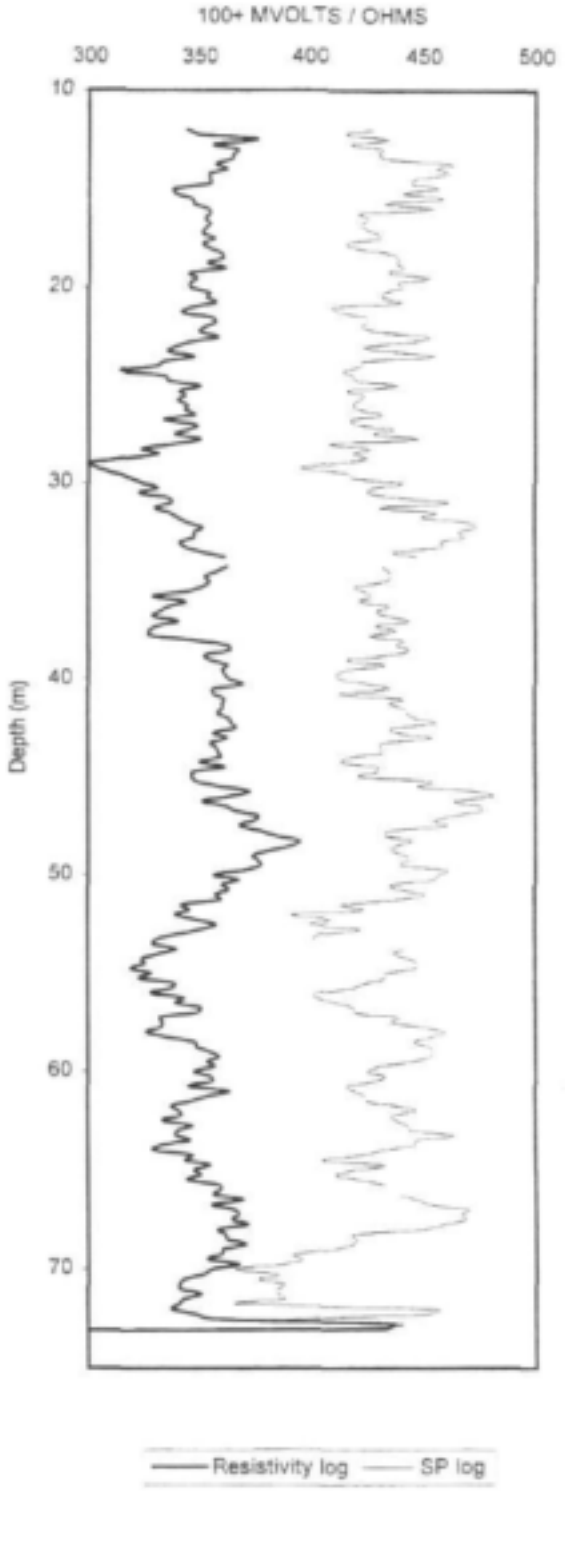

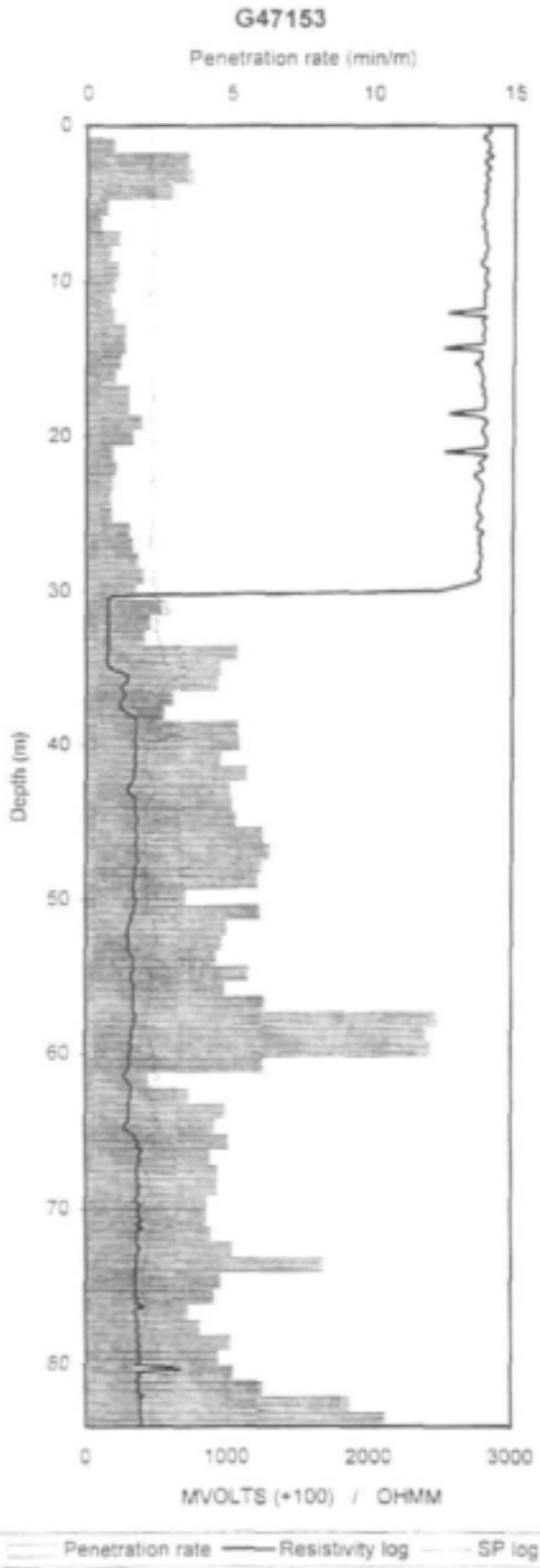
G47153
Penetration rate (min/m)
0
5
10
15
Depth (m)
0
10
20
30
40
50
60
70
80
0
1000
2000
3000
MVOLTS (+100) / OHMM
Penetration rate
Resistivity log
SP log

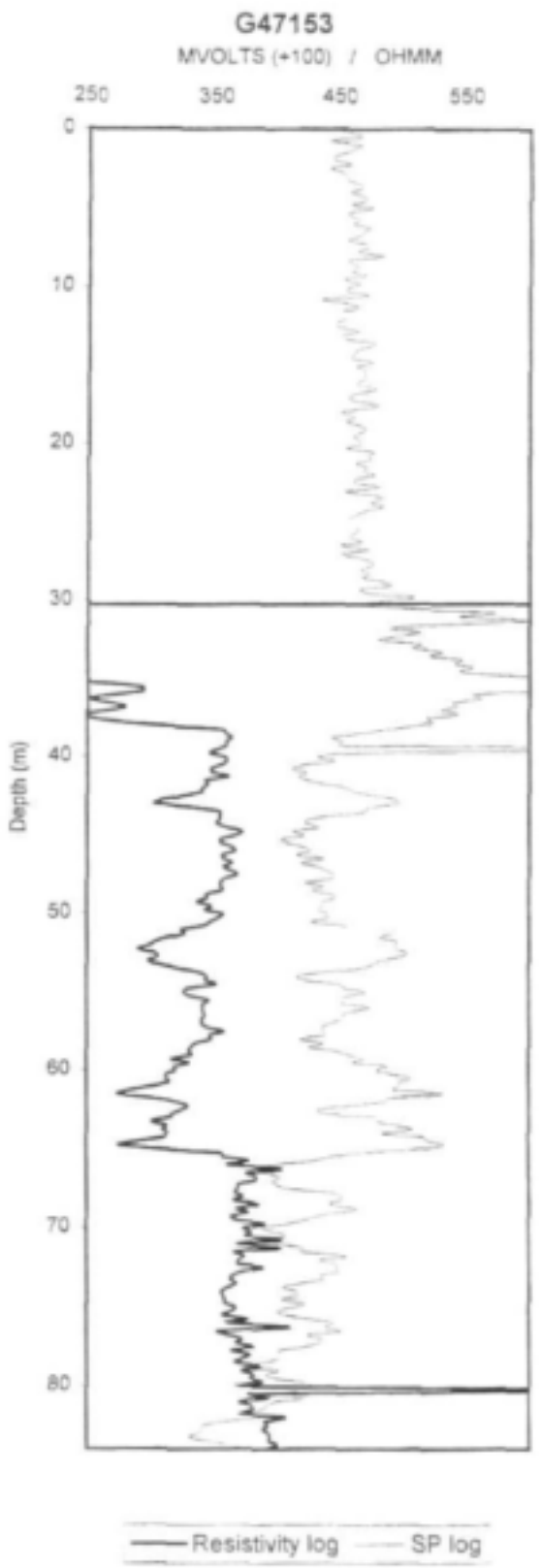
G47153
MVOLTS (+100) / OHMM
250
350
450
550
Depth (m)
0
10
20
30
40
50
60
70
80
Resistivity log
SP log

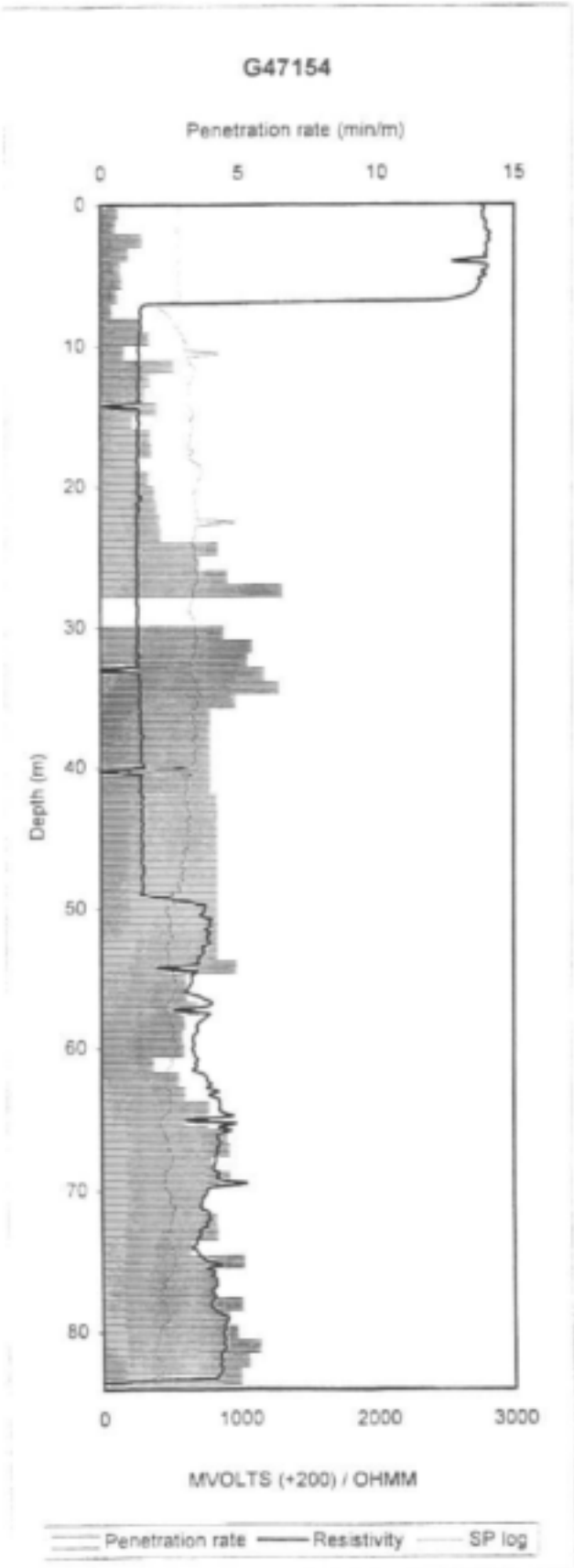
G47154
Penetration rate (min/m)
0
5
10
15
0
10
20
30
40
50
60
70
80
Depth (m)
0
1000
2000
3000
MVOLTS (+200) / OHMM
Penetration rate
Resistivity
SP log

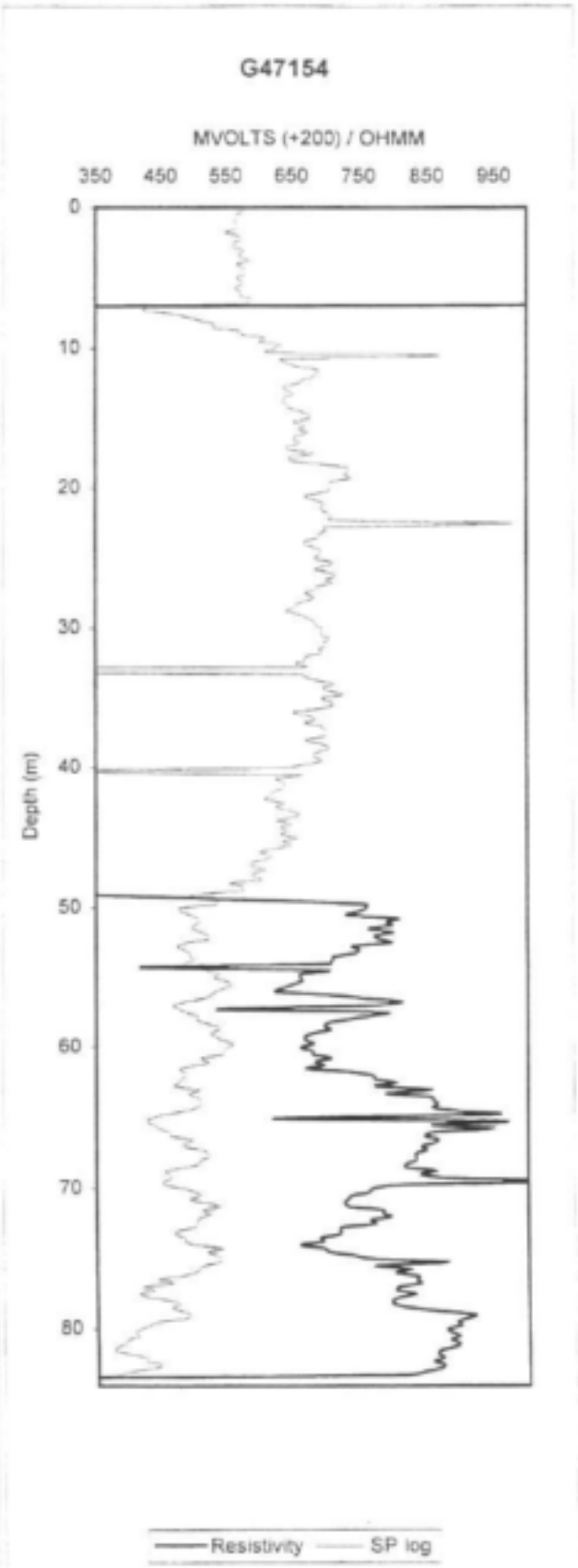
G47154
MVOLTS (+200) / OHMM
350
450
550
650
750
850
950
0
10
20
30
40
50
60
70
80
Depth (m)
Resistivity
SP log

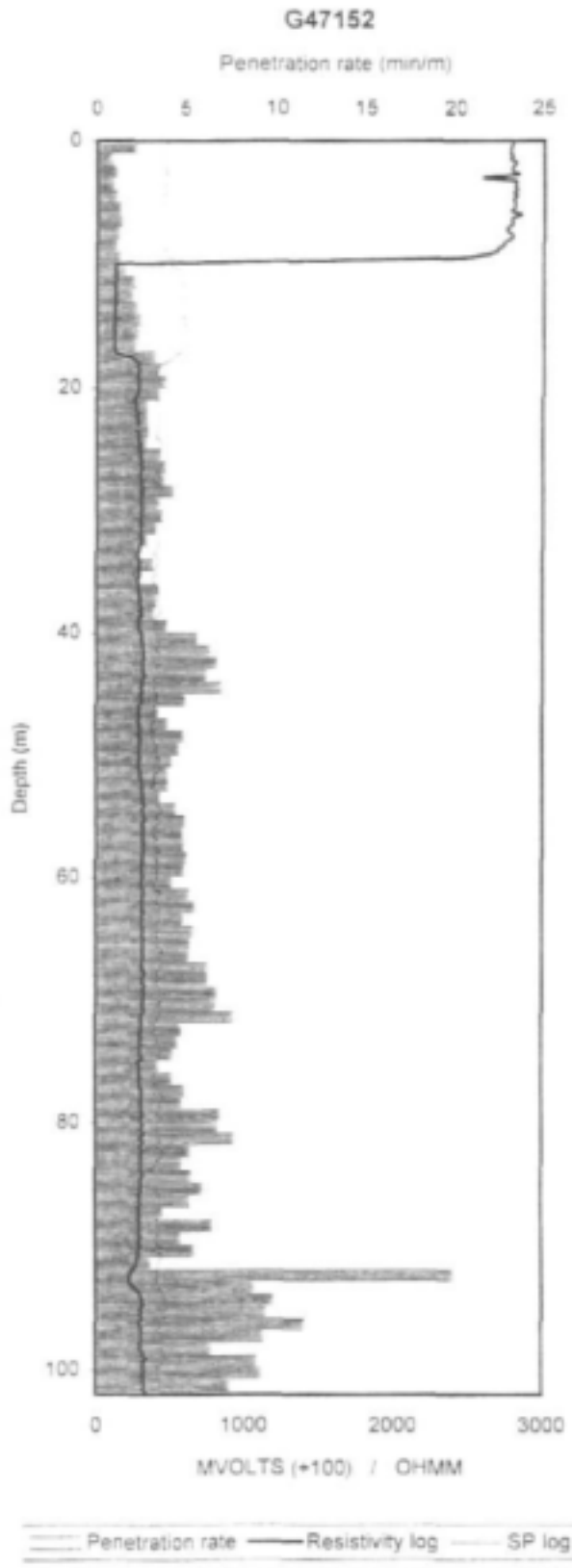
G47152
Penetration rate (min/m)
0
5
10
15
20
25
0
20
40
60
80
100
Depth (m)
0
1000
2000
3000
MVOLTS (+100) / OHMM
Penetration rate
Resistivity log
SP log

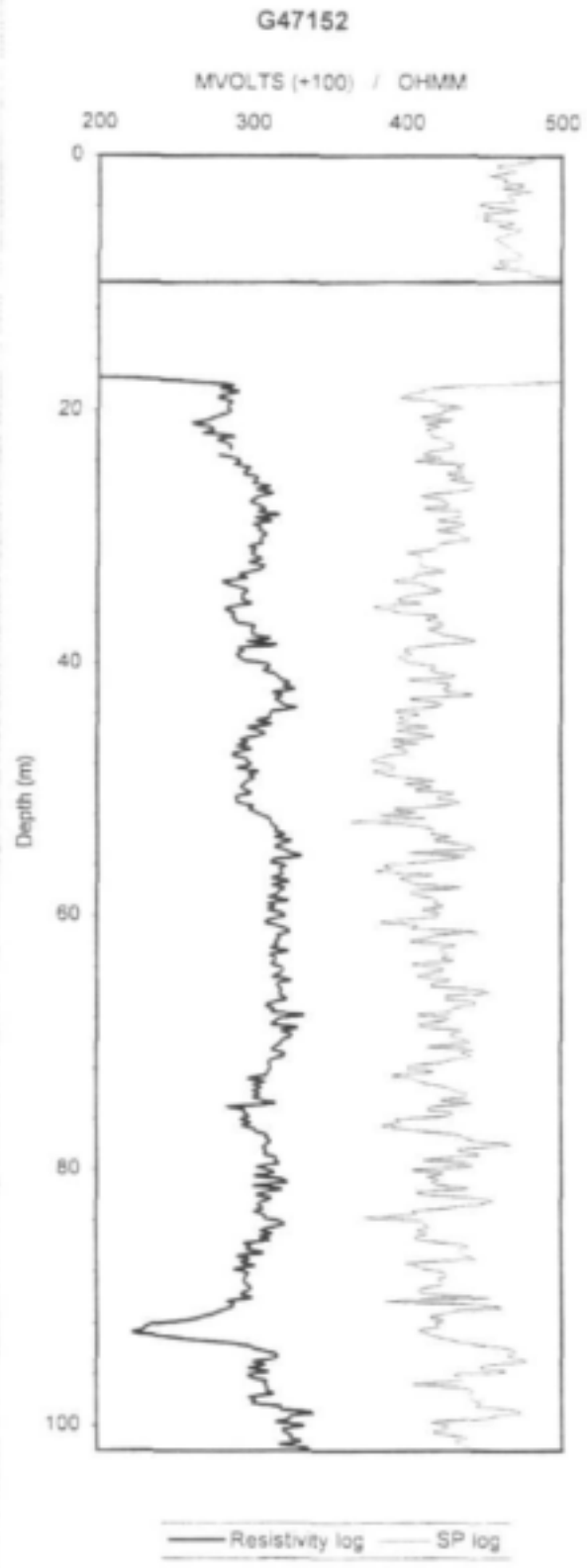
G47152
MVOLTS (+100) / OHMM
200
300
400
500
0
20
40
60
80
100
Depth (m)
Resistivity log
SP log

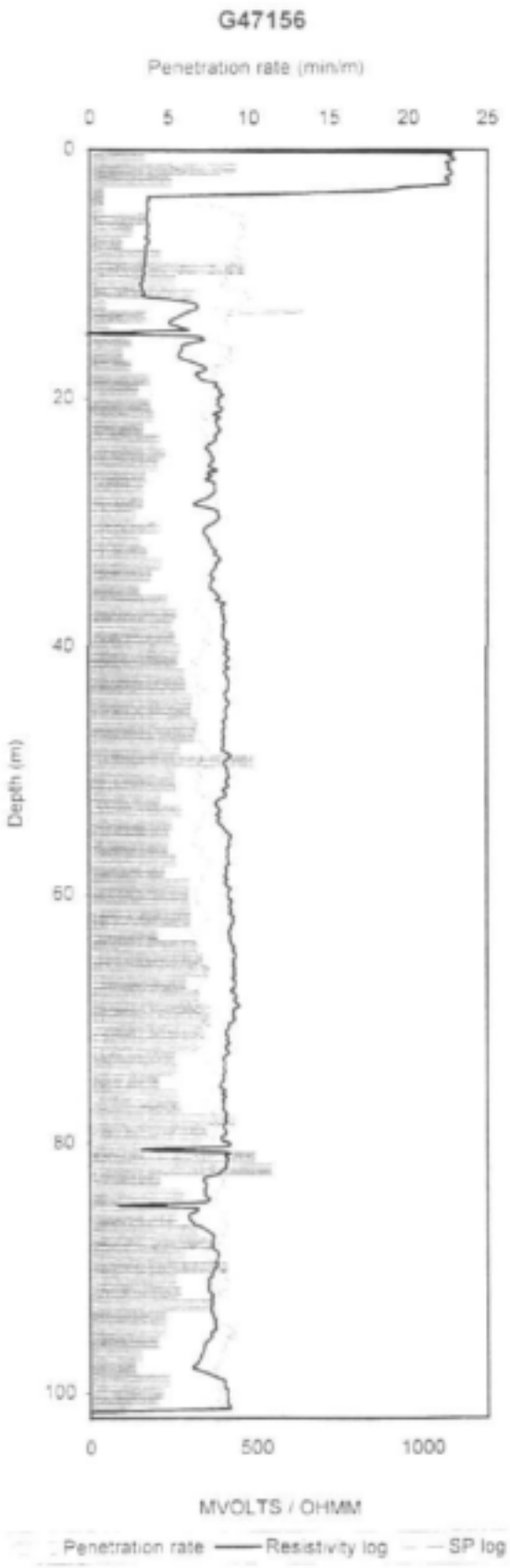
G47156
Penetration rate (min/m)
0
5
10
15
20
25
0
20
40
60
80
100
Depth (m)
0
500
1000
MVOLTS / OHMM
Penetration rate
Resistivity log
SP log

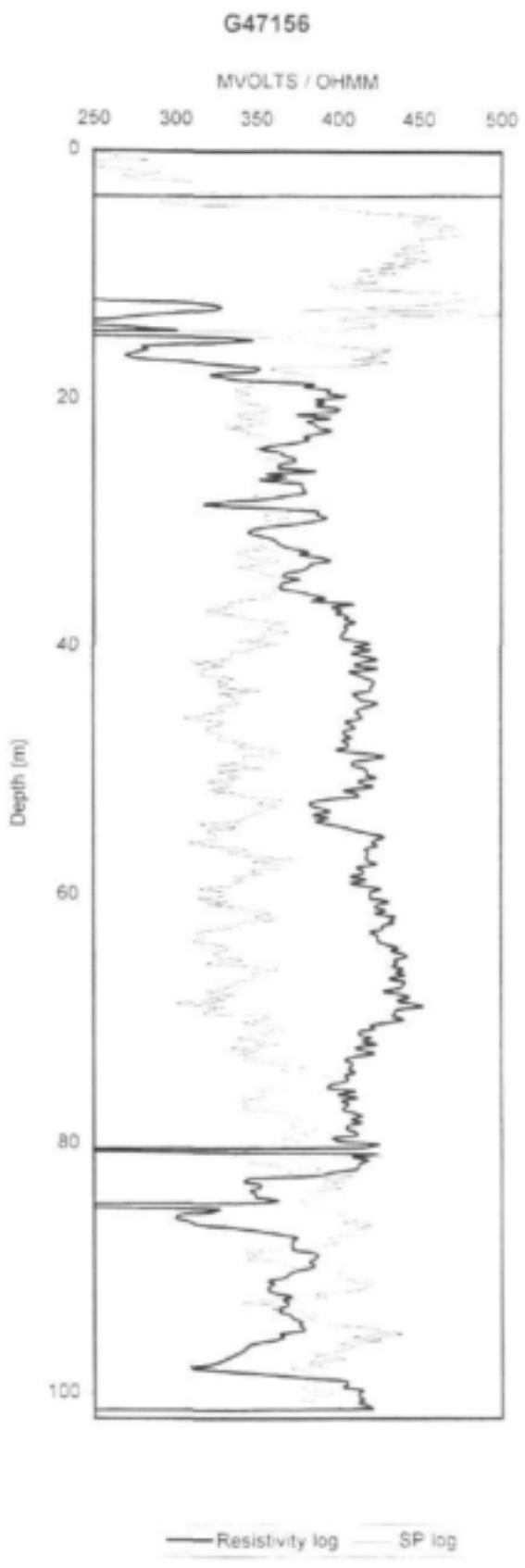
G47156
MVOLTS / OHMM
250
300
350
400
450
500
0
20
40
60
80
100
Depth (m)
Resistivity log
SP log

APPENDIX 2-F

STRUCTURAL GEOLOGY

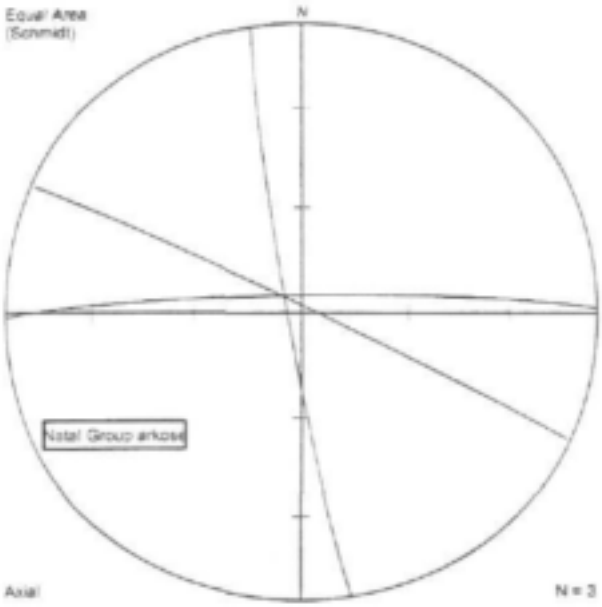

Stereonet plot on the very steep major fractures occurring in the Natal Group arkose striking northerly, easterly and northwesterly.

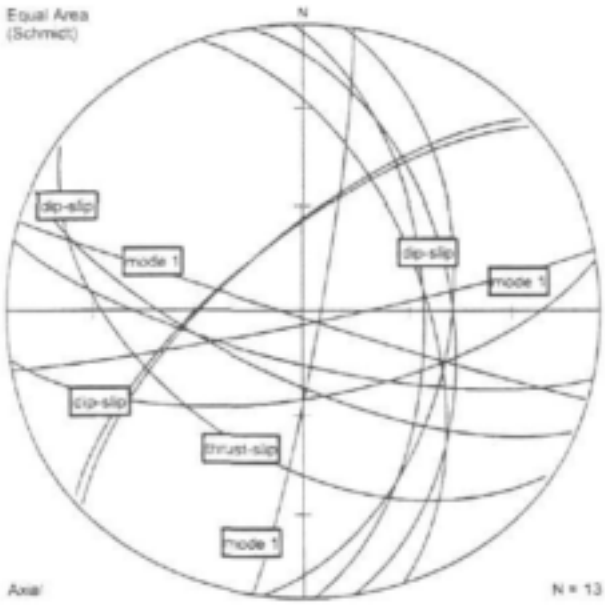

Stereonet plot of the data from stop 5 indicating N-S and E-W dip-slip jointing and Mode 1 fracturing. Intermediate dipping planes to the southeast may be due to thrust-slip fracturing. A conjugated joint set strikes ENE.

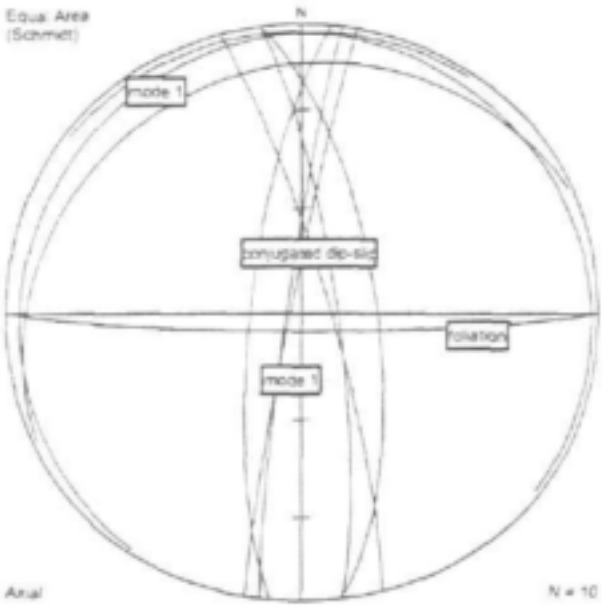

Data from stop 19 show N-S strike-slip conjugated and Mode 1 fractures as well as a E-W dip-slip mode 1 and some subhorizontal thrust-slip Mode 1 fractures.

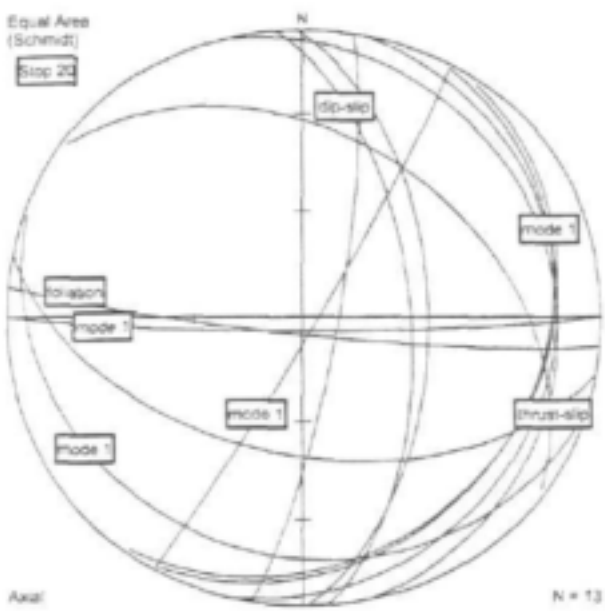

Stop 20 provided information on N-S and E-W dip-slip jointing as well as SE oriented conjugated thrust-slip fracturing with several Mode 1 planes.

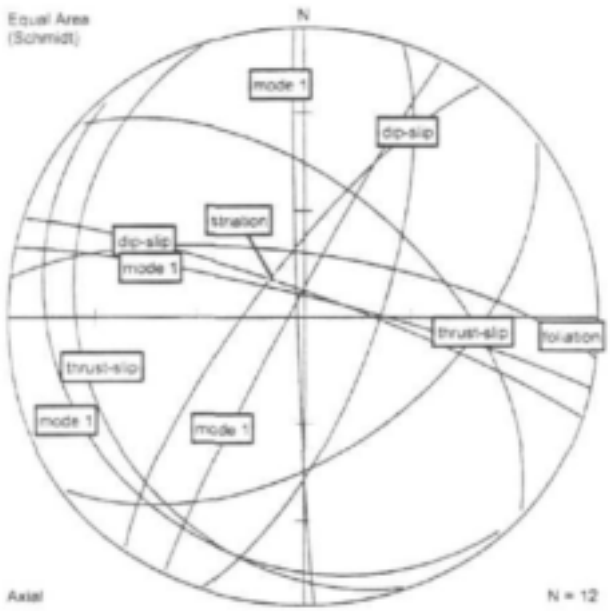

The stereonet plot of data from stop 21 illustrates the effects of N-, NE-, and W-trending joints and Mode 1 fracture sets of a dip-slip component as well as an east trending conjugated thrust-slip, with subhorizontal Mode 1 fracture set. The striation indicates westward dip-slip (323°/76°) on the NE conjugated dip-slip set. The parallelism between the tectonic fabric and the E-W dip-slip fractures is very obvious.

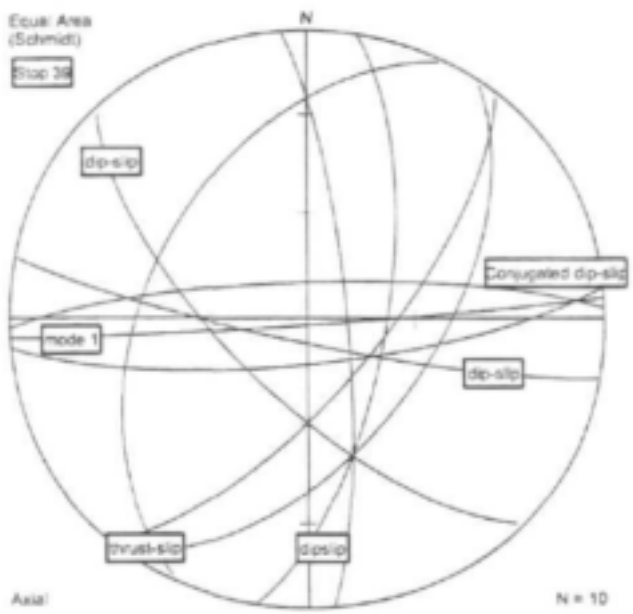

The stereonet plot of stop 39 show the N-S Mode 1 fracture sets and the conjugated EW dip-slip sets with a Mode 1 fracture.

Stereonet plot of stop 6 data displaying a NW conjugated fracture set with a Mode 1 joint as well as WSW trending Mode 1 fracture.

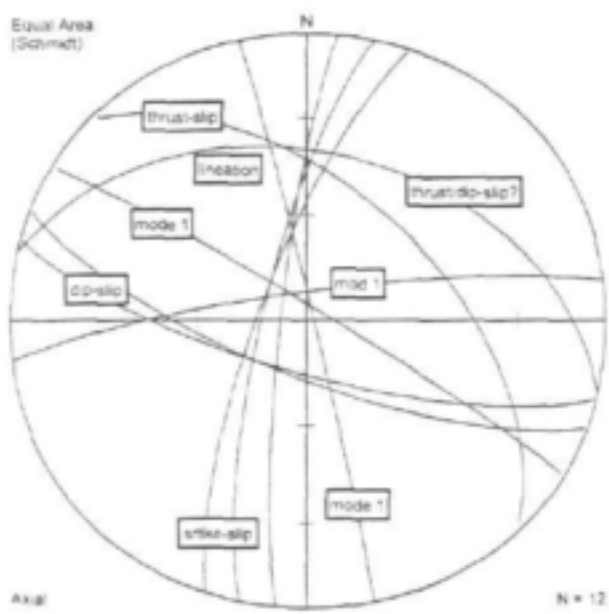

The data from stop 14 display dip-slip, thrust-slip and Mode 1 fractures on the stereonet diagram. The thrust-slip fractures dip to the NE.

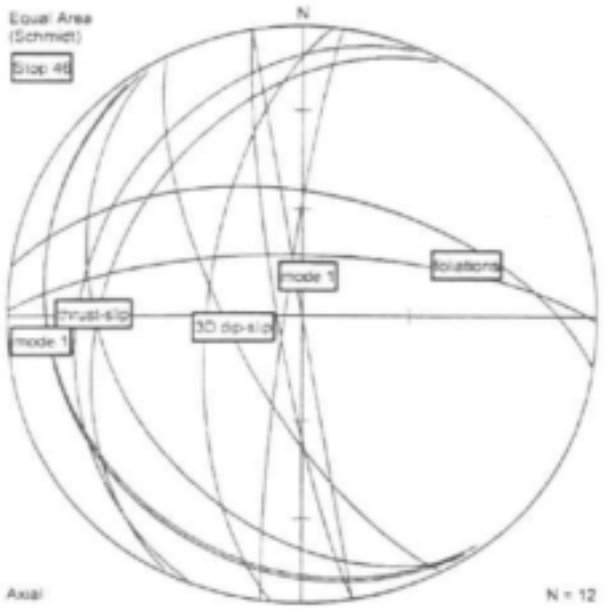

Stereonet plot of three-dimensional fractures with accompanying Mode 1 planes at stop46. Note worthy is the shallow dipping thrust-slip set on the same N-S orientation indicating a dip-slip and a thrust-slip component with exactly the same σ 2 axis.

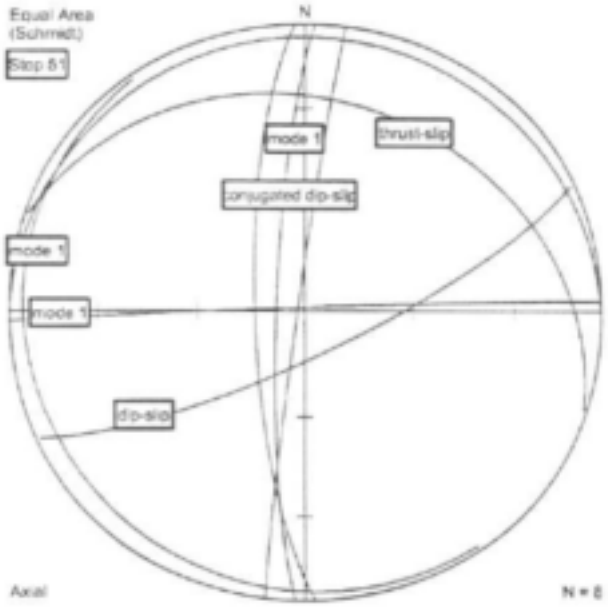

Data from stop 51 illustrates two dip-slip fracture sets with vertical Mode 1 planes oriented N-S, ESE and E as well as a NW trending thrust-slip fracture with subhorizontal Mode 1 planes.

3 LIMPOPO MOBILE BELT

3.1 General Setting

3.1.1 Site Locality

The research area is situated near the northern border of the Northern Province in the Limpopo River catchment and is underlain by rocks of the Limpopo Mobile Belt (LMB). This geological province is an E-W elongated low lying belt straddling eastern Botswana, southern Zimbabwe and the northern part of the Northern Province in South Africa. The belt is lenticular in shape and is about 375 km long by 60 km at its widest point. Two study areas were selected within the belt, one situated in the northern Bochum District west and southwest of Alldays (study area I), and the other (study area II) is located in Messina District east of Messina (*Figure 3-1*). Study area I is characteristic of the western part of the LMB, where a quaternary sand cover overlies the metamorphic basement rocks. Rock outcrops are few and the topography is level. Study area II represents the situation in the eastern part of the LMB, where the basement rocks are exposed at surface, with rare occurrences of quaternary cover.

Study area I:
Study area I is approximately 1200km^2 and is located within the Bochum District and Soutpansberg Districts. Its southern boundary is formed by several ENE-WSW running faults, separating the Karoo Supergroup in the South from the metamorphics of the Limpopo Mobile Belt (LMB) in the North. The northern boundary is formed by the approximately E-W running Limpopo River. The area is covered by four 1:50 000 map sheets: 2228 DD Raditshaba, 2228 DB Gregory, 2228 DA Usutu and the 2228 DC Tonash.

The major access road is the R 572 from Alldays to Swartwater, from which a fair number of dirt roads diverge. The area is essentially rural, with private game farms occupying the northern part of the area within the Soutpansberg District and rural African communities occupying the southern part, which falls mainly within the Bochum District. Here, Raditshaba, Eldorado and Taaiboschgroet are the important villages in the area with schools, stores and one hospital.

Study area II:
Study area II is approximately 1000 km^2 and is covered by the following 1: 50 000 maps: 2230 CB Gaandrik, 2230 AD Esmefour, 2230 AC Messina and 2230 CA Tshipise. The southern boundary is formed by ENE-WSW running faults separating the Karoo Clarens and Letaba Formations in the South from the metamorphics of the Limpopo Mobile Belt (LMB) in the North. The northern boundary is formed by the Limpopo River.

The area is accessed by the R525 from Louis Trichardt to Tshipise and the R508 from Tshipise to Messina. From these, only a few dirt roads diverge into the area. The region is rural and consists of a number of small villages and communities, game farms, irrigated produce in the Limpopo Valley, and some stock farming. Population density is low and important centres are Messina in the Northwest and Tshipise in the South. Copper and diamond mining also takes place.

Except for the larger rivers, which are used for irrigation, domestic water supply is met from groundwater.

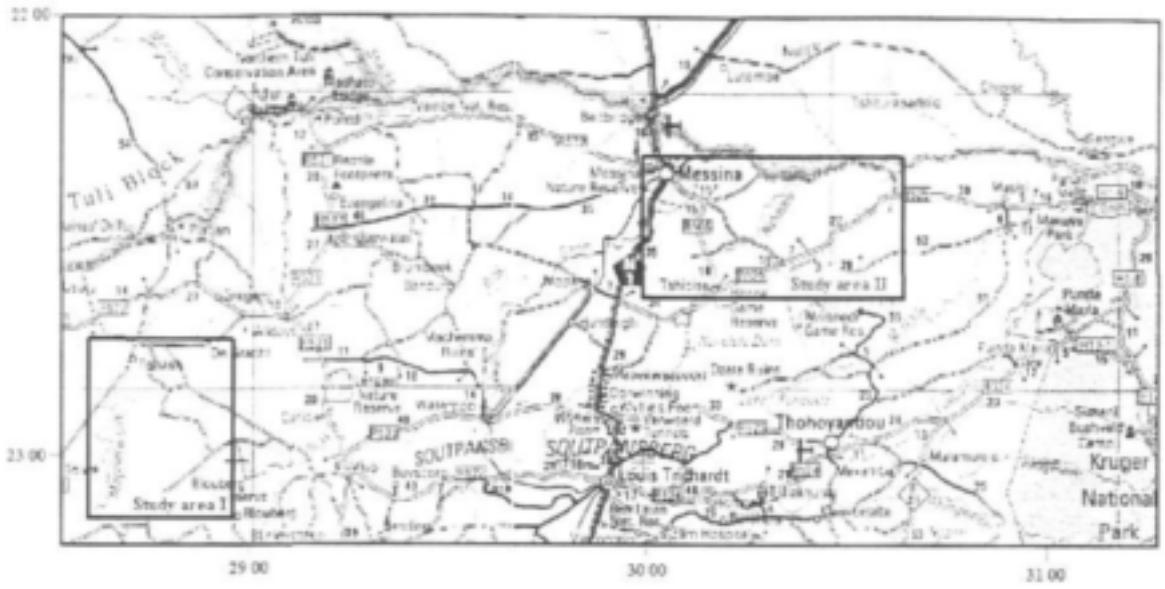

Figure 3-1 Locality of study area I and II

3.1.2 Topography

The basement topography is developed on well-foliated and mainly steeply dipping basement rocks of the LMB. Several resistant lithologies are recognized in the study area, which are expressed as prominent local topographical highs. These are primarily quartzite bands, which occur primarily in the Beit Bridge Complex, and pegmatite veins, which can be several meters thick. Additionally, diabase intrusions are common throughout the region and give rise to high, narrow ridges in the basement rocks. The contact with the Karoo Sequence to the South is demarcated by either steep sandstone cliffs or by uniformly flat terrain where the Karoo age Letaba Formation is encountered, consisting of mainly basaltic lava.

The region forms part of the Lowveld and is characterized by rolling hills and ridges of moderate height. Study area I has a relatively low relief and the gently undulating bush clad land slopes gradually upward to the south. Variations in bedrock topography are levelled out by overlying deposits of Quaternary age, which consist of alluvium, sand and gravel. Occasional broken hills of metaquartzite and magnetite quartzite break through the quaternary cover as broken isolated hills. Large, fairly thick alluvial deposits are found along the Nzhelele and the Mogalakwena Rivers. Towards the western part of the LMB (study area I), quaternary deposits cover the entire basement rocks and outcrop is limited. Here, the terrain is flat lying with only few narrow ridges of resistant lithologies being present (Figure Figure 3-2). Occasional ridges consisting of LMB rock outcrop through the quaternary cover.

Area II exhibits a somewhat steeper topography, with altitudes varying between 350m along the Limpopo River up to 1250m in the Karoo covered South (Figure 3-3).

3.1.3 Drainage

The entire South African portion of the LMB is drained by the approximately E-W running Limpopo River in the North. Several smaller watercourses dissect the LMB, running approximately S-N and draining into the Limpopo. In the study area I this is the Mogalakwena, whereas in the study area II the Sand River and the Nzhelele drain the region. Runoff is approximately 4-5 mm/a in area I and under 4 mm in area II. In area I runoff is generally restricted between October-April, corresponding to the rainfall period, indicating

that recharge is very limited. Area II has perennial runoff due to runoff generation from the Soutpansberg, however, no baseflow is generated within the LMB during the dry season.

The underlying basement rocks seem to have exerted structural control of the streams, with the Mogalakwena and the Nzhelele bending in 90° angles to run for a short while parallel to the Tshipise and Boskop fault respectively. Various resistant lithologies seem to cause these rivers to swing around in wide meanders (Figure 3-4).

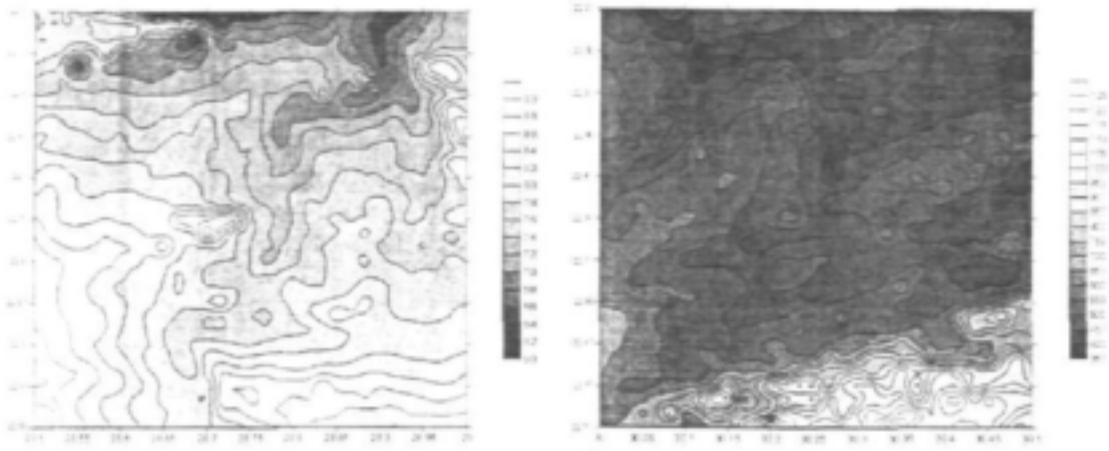

a) b)

Figure Figure 3-2 **a) Topography of research area I**
FigureFigure 3-3 **b) Topography of research area II**

3.1.4 Climate, Vegetation and Land Use

The study area is characterized by hot and humid summers and cool, dry winters. The wet season lasts approximately from October to April with rainfall occurring mostly as heavy thunderstorms.

The pattern of the mean annual precipitation (MAP) is shown in Figure 3-60 and Figure 3-61 for area I and II respectively. Whereas study area I exhibits a homogeneous rainfall pattern with values varying between 320 and 480mm, area II shows values increasing from 150mm in the north along the Limpopo
river up to 950mm in the SE corner of the study area where the area is underlain by the Soutpansberg. The area underlain by the LMB generally has a rainfall of between 300-400 mm. In comparison, S-pan evaporation is between 2000-2200 mm/a in area I and between 1800-2000 mm/a in area II.

The semi-arid subtropical climate accounts for a vegetation dominated by thorn scrub and grassland, which is classified as tropical Bush and Savannah under the Simplified Acocks Veld Types. The area is used mainly for game farming. Additionally formal agricultural activity includes potato and tomato farming, where irrigation from the larger rivers. The agricultural activity in the rural black areas consists of subsistence cattle and dry-land maize farming.

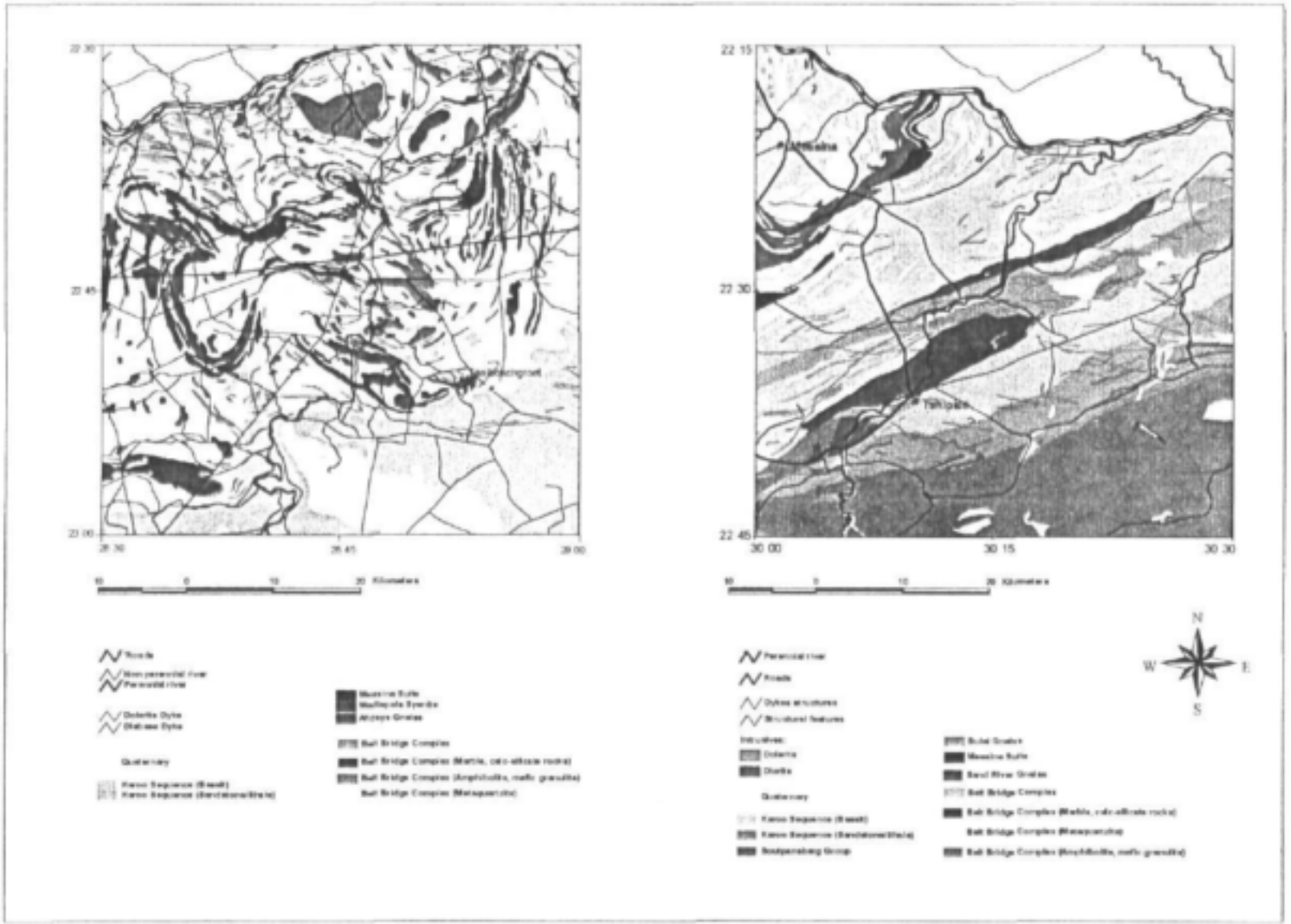

Figure 3-4 **Rivers and major roads in study area I and II**

3.2 Regional Geology

3.2.1 Introduction

The ca. 2.7 Ga highly deformed polymetamorphic Limpopo Belt is situated between the two lower-grade granite-greenstone cratons, the Kaapvaal Craton in the south and the Zimbabwe Craton in the north (van Reenen et al. 1992). The belt emerges from beneath Kalahari Sands in the west, extending for over 700km in length and up to 250km in width before disappearing under Proterozoic and Phanerozoic cover at the eastern end. Further east any possible extension has been over printed by the Pan-African Mozambique Belt, whilst at the western termination, the belt seems to expire a short distance into the Kalahari Basin (Watkeys, 1983). The Limpopo Belt can be subdivided into a northern and southern marginal zones and a central zone, each with a distinctive geological signature and separated from each other, and from adjacent cratons, by well defined shear zones (Watkeys., 1983, van Reenen et. al. 1992) of up to 10 km width. The present shape of the belt is a function of late Archean-Early Proterozoic deformation, rather than representing the shape of the original Archean sedimentary basin.

The Northern Marginal Zone, which occurs only in Zimbabwe, is composed of granite-greenstone material metamorphosed to granulite grade and is separated from the Zimbabwe Craton by a southerly-dipping shear zone. To the south, the southerly dipping Tuli-Sabi shear zone separates the Northern Marginal Zone from the shelf-type supracrustal sequence of the Central Zone, in which the study areas are located (Figure 3-5). The Marginal Zones contain rocks that are the high-grade equivalents of a granite-greenstone terrain and display ENE trending structures. The Central Zone has north trending structures and a completely different stratigraphic sequence, representing equally high grade metamorphic phases but of a more shelf like sedimentary origin sequence.

The Central Zone consists of supracrustal metaquartzites, magnetite quartzite, meatpelites, granulites, leucogneiss, calc-silicates, marble and intrusive gneisses, meat-anorthosite, metagabbros, serpentinite and metapyroxenite. The supracrustals represent an early Proterozic cover sequence that as infolded and metamorphosed with the basement rocks to a granulite facies of high grade, high temperature regional metamorphism. Metamorphic grade decreases to the west-southwest, until the granulite grades give way to amphibolite facies in Botswana. The Palala Shear Zone forms the boundary between the Central and the Southern Marginal Zone, which has a composition similar to the Northern Marginal Zone.

The Southern Marginal Zone occurs south of the Soutpansberg and is bounded in the north by the Palala Shear Zone and in the south by Hout River Shear Zone. It is separated from the Central Zone by the Soutpansberg Trough. This zone contains numerous highly deformed disconnected slivers of pelitic and mafic gneisses together with minor ultramafics and magnetite quartzite enveloped by tonalitic gneisses (3200 Ma). The origins of these rocks are Archean metavolcanics and intercalated meta-sediments. During the Limpopo Orogeny these rocks were metamorphosed to a granulite grade, but have been retrogressed to amphibolite grade within a narrow zone north of the Hout River Shear Zone. The boundary between the Limpopo Belt and the Kaapvaal Craton is formed by the Hout River Shear Zone, a northwards dipping ductile shear zone.

6.2.2 Lithology of the Central Zone

The central Zone consists predominantly of a sequence of supracrustal gneisses of the Beit Bridge Complex (>3230 Ma) (Figure 3-4). These were subjected to several intrusive episodes. All of these lithologies have been subjected to granulite grade metamorphism.

Anatexis is widespread and the structures observed record a polyphase tectonic evolution (Fripp, 1983; Watkeys, 1983).

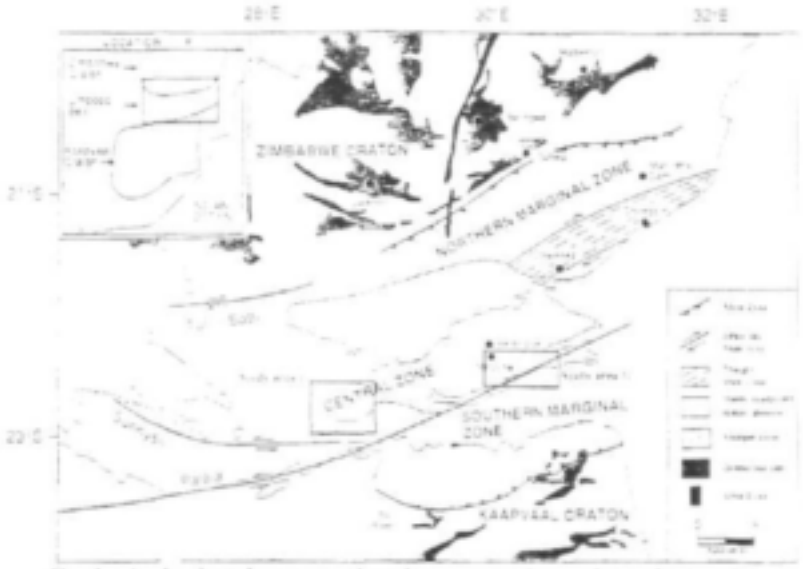

Figure 3-5 Geological sketch map showing tectonic units of the Limpopo Belt with bounding shear zones and adjacent Archean cratons (after Kroener et al., 1998).

Sand River Gneisses

The oldest rock units of the Central Zone are grey tonalitic, migmatitic, quartz dioritic or granodioritic in composition and referred to as Sand River Gneisses. The Sand River Gneiss outcrops as a small NE trending belt SE of Messina. The gneisses range in colour from dark to light grey, have varying content of feldspars, quartz, biotite and hornblende, and display evidence for polyphase deformation (Kroener et al., 1998). The gneisses are thought to be of sedimentary origin and a minimum age of 3780 Ma is postulated (Brandl, 1981). The gneiss has been intruded by mafic amphibolite dykes, which were subsequently folded and metamorphosed.

These rocks have been considered, on structural grounds, to represent a tectonic or depositional basement to the Beit Bridge Complex (Horrocks, 1983; Brandl, 1981; Watkeys, 1983), whereas others question this "basement-cover" relationship (van Reenen et al., 1992). Kroener et al. (1998) gives an age of 3 260 Ma suggesting an intrusive relationship with the Beit Bridge Complex rocks.

Both the Sand River Gneiss and the Beit Bridge Complex were intruded by two groups of basic dykes with ages of 3643 ± 102 and 3128 ± 81 Ma respectively (Barton et al., 1983), now altered to amphibolite.

Beit Bridge Complex

The high-grade supracrustal succession of the Beit Bridge Complex consists mainly of quartzo-feldspathic gneisses, metaquartzite and marble (Brandl, 1981). Brandl (1981) subdivided the Beit Bridge Complex into 3 groups:

The Mount Dowe Group consists of greyish, white, coarse grained, massive metaquartzites, magnetite quartzite and subordinate leucocratic gneiss (Metaquartzite on Figure 3-4). Biotite, garnet or pyroxene, whose origin is related to impurities in the original sandstone, have imparted a banded appearance in places. In the vicinity of tight folds these bands have been recrystallised to resemble vein quartz. The presence of laminated black magnetite quartzite has given rise to sharp crested hills.

The Malala Drift Group consists of leucocratic quartzofeldspathic gneiss with minor intercalated garnetiferous biotite and or hornblende bearing gneiss, interbedded quartzite and calc-silicates. This group covers extensive areas of the Central Zone.

The Gumbu Group consists of calc-silicates containing plagioclase, microcline, quartz, clinopyroxene, hornblende, calcite and lenticular intercalations of white and pink marble (Marble, calc-silicates on Figure 3-4). Individual bands stand out as narrow sharp ridges. The Group is well developed north of Tshipise and further to the northeast.

The Beit Bridge Complex also contains minor amounts of amphibolite, metapelites (Amphibolite, mafic granulite on Figure 3-4) and granitoid gneiss (Singele Gneiss) intercalated with the above Groups.

Whether this succession represents a conformable sequence is still uncertain. According to Brandl (1981), the complex represents a group of metasediments deposited in a shallow basin as arkose, sandstone, calcareous shale, limestone, dolomite and volcanic material. Eriksson et al. (1988) interpreted the sedimentary association as a cratonic shelf sequence.

Intruded into the Beit Bridge Complex are the Messina Suite, the Bulai Gneiss and the Singelele Gneiss.

Messina Suite
Mafic and ultramafic complexes consisting of anorthositic to leucogabbroic rocks, metapyroxenites serpentinites and hornblendites of the Messina Suite have been emplaced into the supracrustal Beit Bridge Complex as intrusive layers or lenses present as concordant sills. The mafic rocks are mostly associated with the metaquartzites of the Mount Dowe Group and have an age of 3270 +105 -112 Ma (Pb-Pb) (Barton et al., 1979). The ultramafic rocks have been disrupted by subsequent deformation so that they outcrop as isolated boudins, mostly in the eastern half of the Central Zone (study area I).

Bulai Gneiss
The gneiss (~2690 Ma) (Barton et al., 1979) is a greyish coarse grained rock with large porphyroblasts of microcline in a matrix of plagioclase, microcline, quartz and biotite (Brandl, 1981). The Bulai Gneiss forms a prominent batholith northwest of Messina.

Radiometric dating suggests an age of 2700 Ma (Barton et al., 1979), suggesting that the Bulai Gneiss intruded syntectonically with the deposition of the Beit Bridge Complex. It is believed that these gneisses intruded as an anatectic melt originating from remobilised basement rocks. Watkeys (1984) suggests that the Bulai Gneiss intruded syntectonically into rocks at high grade metamorphism as a crystallising pseudo-plastic body, which after solidifying, moved as a solid diapir into the supracrustal gneisses, hence contact metamorphsim is not expected.

Singelele Gneiss
Interlayered with the Beit Bridge Complex and Sand River Gneisses are the Singelele Gneisses, a light orange to almost white quartzo-feldspathic gneiss in the vicinity of Messina. They are granitic in composition and contain minor amounts of garnet (Hofmann et al., 1998).

Alldays Gneiss
The intrusive Alldays Gneiss occurs throughout the Central Zone as discrete elliptical bodies or as concordant sheets up to 1km wide (Brandl, 1990). The Gneiss is a greyish, in places pinkish grey medium-grained rock of tonalitic composition, which is well foliated and often migmatised or banded. Until now, no reliable radiometric age is available for the Alldays

Gneiss, though field relations indicate that it is older than the Messina Suite (Barton et. al, 1979).

Intrusions
Deformed mafic dykes with granulite facies metamorphism are present in the Sand River Gneiss and can be attributed to a pre-3000 Ma event (Barton et al., 1990). At least 9 generations of intrusive mafic dykes have been identified (Watkeys et al., 1983), ranging from 3550-180 Ma.

E-NE and W-NW striking diabase and dolerite intrusions are common throughout study areas I and II and occur as sills and dykes. Typically the diabase is a medium- to coarse-grained, dark-gray rock, composed mainly of calcic plagioclase and clinopyroxene (Brandl, 1981).

3.2.3 Geological History of the Limpopo Belt

The basement rocks of the Central Zone have undergone several major tectonic events causing complex interference fold patterns. During the last 25 years, numerous models have been proposed to explain the tectonic evolution of the Limpopo Belt (Coward et al. 1973, 1976 a,b, Coward 1976, Barton and Key, 1981, Watkeys, 1983, Horrocks, 1983, Fripp 1983, Barton 1983, McCourt and Vearncombe, 1992 Van Reenen et al. 1987, 1992, 1995, Roering et al. 1992). All the tectonic models postulated assume that plate tectonics was active during the Archean, and that the Limpopo Mobile Belt is an intracratonic feature that developed when a belt of high heat flow developed at the site (~3.2 Ga), at a time when the Zimbabwe and Kaapvaal Cratons were united. They attribute the formation and subsequent uplift of the granulite facies exposed in the Limpopo Belt to a collision between the Kaapvaal and Zimbabwe Cratons or exotic terranes, which resulted in crustal thickening. The theories differ with respect to the mechanics of the collision, with some viewing the interaction between cratons as a predominantly strike-slip event rather than a continental collision.

In the earlier models, it was postulated that the epicontinental rocks found within the Central Zone represented sediments deposited during an early rift phase between the Kaapvaal and the Zimbabwe Craton, which were assumed to be united before 3200 Ma. Rifting permitted the deposition of the Beit Bridge Complex sediments and their subsequent burial and metamorphism (Robertson & Du Toit, 1981).

Later work by Roering et al. (1992), however, suggests that the Central Zone could either be an independent crustal fragment caught up in the collision of the Kaapvaal and Zimbabwean Cratons, or that it might have been already been attached to the Kaapvaal Craton by an earlier tectonic event.

According to Watkeys (1984), major horizontal tectonics involving overthrusting and subduction from the north-northwest subsequently commenced and brought the Zimbabwe Craton and the Central Zone together. From about 2 Ga, the Limpopo Belt attained rigidity and changed from a zone of mobility to one of shears and rifts, which were reactivated to a lesser extent throughout the later history of the belt.

Another model tries to explain the LMB as an assemblage of discrete terranes with different geological histories prior to approx. 2.6 Ga. The Kaapvaal Craton is postulated to act as a stable continental block against which accretionary, northerly growth took place (Rollinson, 1993).

McCourt and Vearncombe (1992) suggest that the Central Zone was emplaced from NE to SW, suggesting that thrusting was arcuate around the Central Zone, hence N-S cratonic collision did not take place; rather, a NE-SW collision occurred, oblique to the craton collision direction, between the Central Zone and the Kaapvaal craton, outwardly thrusting up

the adjacent marginal zones onto the cratons. This model implies the Central Zone is a thrust sheet that can be considered the over-riding plate of a continental collision. McCourt & Vearncombe (1987) suggest that the Palala Shear acted as a lateral ramp during the emplacement of the Central Zone (~2.7 Ga). Van Reenen et al. (1987) interpret lateral motion on the Palala Shear as being of later age (~2050 Ma).

Craton collision models imply that northerly directed thrusting emplaced the continental shelf deposits of the Central Zone onto the Zimbabwe craton due to collision between the cratons between 2.9-2.7 Ga, leading to a crustal thickening and burial metamorphism at a granulite facies. Later, southerly directed backthrusting and east-west transcurrent shearing along wrench faults resulted due to transpression during the Limpopo Orogeny ~ 2.7 Ga. This resulted in considerable shear zone development in the form of south verging thrusts and ENE trending strike slip faults (Figure 3-6).

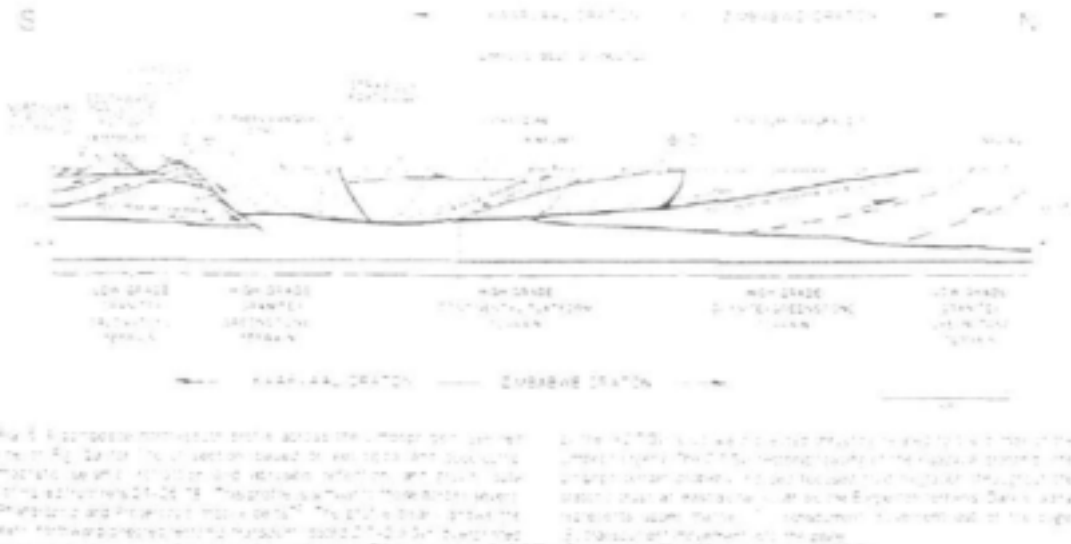

Figure 3-6 North-South profile across LMB (Source: De Wit et al., 1992)

The rocks exposed at the surface today were originally buried to depth of up to 35km. This uplift was due to the formation of a tectonic 'pop-up' structure between ductile shear zones (Roering et al., 1992) related to compression. Uplift could also have been assisted by erosion of the overlying rock, tectonic erosion due to normal faulting, and the generation of anatectic melt, which increased buoyancies (Roering et al., 1992). At about 2.0 Ga, subsequent regional uplift and the reactivation of shear zones when a 110 km westward displacement of the Central Zone took place along wrench faults, such as the Palala Shear (Roering et al., 1992).

In the Central Zone several periods of deformation and metamorphism, with at least one high grade metamorphic episode, have been recognised. Barton et al. (1979) identify four main tectonic events leading to the Limpopo Orogeny (2.7 Ga):

The first event (D1M1) starting about 3270 Ma resulted in the large scale duplication of the supracrustal rocks and the intrusive Messina Suite by ductile recumbent isoclinal folding about nearly flat lying axial surfaces oriented N-S, with fold hinges plunging gently to the west. According to Watkeys (1984), this was accompanied by high pressure granulite metamorphism and the development of a heterogenous schistosity. Heating occurred due to tectonic loading caused by crustal thickening during the carton collision. Northerly thrusting and nappe formation may have led to the emplacement of the Messina Suite at different stratigraphic levels at about 3150 Ma.

The second event (D2M2) started at about 2900 Ma with the initiation of decompression and uplift, but can be seen as a continuous pressure-temperature loop from the M1 event. It involved the isoclinal folding and shearing of the rocks about a more upright axial surface oriented NE-SW, with approximately horizontal fold hinges. This led to the repetition of rock units from the NE to the SW and the development of wide spread schistosity and foliation. Watkeys (1984) states that this episode consists of two phases of co-planar folding separated by the intrusion of the Bulai Gneiss accompanied by high pressure granulite metamorphism. Metamorphism was considered to have decreased rapidly from a high pressure granulite facies to a low pressure granulite facies with uplift.

The third event (D3M3) is characterised by the introduction of water through shear zones and decompression to an amphibolite facies. It is marked by a ductile-brittle refolding of the succession co-planar to the second event but with fold hinges diverging from the parallel. This resulted in a tightening of existing structures, and the attenuation of some folds so that minor anticlines occur adjacent to each other with the corresponding syncline between them being obliterated. Watkeys (1984) suggests that this event was separated from the D2M2 event by anatexis and the diapiric uprise of the Bulai Gneiss , which was accompanied by low pressure amphibolite facies metamorphism.

The fourth event (D4 M4) at ± 2670 Ma involved the refolding of the entire succession about an E-W axial surfaces and resulted in shearing, mainly south directed thrusts and the formation of mylonite and flaser gneiss.

Following the cessation of major tectono-thermal activity at about 2000 Ma, small peridotite and pyroxenite plugs and pegmatite dykes intruded the LMB. This was followed by the deposition of volcanic and sedimentary rocks of the Waterberg Group in bounded basins between 1900-1600 Ma. Following renewed activity along existing faults (D5) during the Waterberg deposition with predominantly vertical movement, numerous basic dykes and sills associated with volcanic activity related to the deposition of the Waterberg intruded into the major fracture trends of the LMB to dissect the LMB and Waterberg rocks.

The Karoo Supergroup was also deposited on an even floor of crystalline rocks and on Waterberg strata between 300-180 Ma. Most Karoo deposits are fault bounded on the north side and were deposited in yoked basins controlled by pre-Karoo structures. Karoo deposition occurred concurrent with faulting and fracturing along the ENE trend (D6). Karoo and Post-Karoo dykes, sills and sheets follow the major WNW and ENE fracture trends and many faults were wholly or partially filled by dolerites. A subsequent intrusive episode from ±190-182 Ma, resulted in the intrusion of ring dykes, sheets and related dykes. These consist of granites, gabbros and syenites, and the development of radial and concentric faults and fractures.

The presence of thermal springs in the Soutpansberg area and sporadic seismic activity suggest weak tectonic activity has continued to the present day.

3.2.4 Structural Features of the Central Zone

The Palala Shear Zone at the southern margin of the study areas represents a northerly and steeply dipping zone of intense ductile deformation of up to 10 km wide, with an exposed strike length of about 30 km. It trends NE in the east near study area I and bends through a ENE to E strike near study area II. Its origin is thought to be related to the initiation of mobile belt activity during the D2 deformation when the Central Zone of the LMB moved westerly between the adjacent cratons. It is characterised as a strong magnetic anomaly. It represents a transpression zone along which left-lateral strike-slip movement took place. Transpression was caused by the oblique convergence of the Central Zone with the Kaapvaal Craton.

Ductile shear movement ceased about 1970 Ma. (Brandl & Reimold, 1990). Post-Waterberg and post-Karoo movement along faults in the shear zone has been predominantly normal, with downthrown blocks to the south.

Four domains can be recognised on the basis of structural and lithological differences. The northern domain is about 2 km wide and contains hornblende granites and dark grey to black mylonite. The ~ km wide central zone is divided into a zone of granulite grade Beit Bridge Complex rocks that are invariably mylonitised and where prominent quartz extension lineations are evident; and a south central domain containing mainly gabbroic Bushveld rocks. The fourth southern domain rhyolites, and granites are present. Deformation is rather weak and mylonite is not present in the fault zones.

The Central Zone of the Palala shear is dominated by series of major ENE trending faults and shears, and a major fracture trend to the WNW. Many of these fracture zones are filled with basic dykes of post-Waterberg and post-Karoo age. Most of the major faults display evidence of transcurrent and vertical movements, indicating that repeated rejuvenation has occurred with changing tectonic stress regimes. Vertical post-Karoo normal faulting that has resulted in Karoo age rocks abutting against LMB rocks can be considered the most recent phase.

To arrive at a conceptual model of recent tectonic evolution and its expression in existing structures, the following pertinent aspects can be summarised:

- The D2 deformation resulting from N-S compression during cratonic collision resulted in crustal thickening, severe folding, together with associated syntectonic intrusions (Bulai Gneiss). Uplift during the Limpopo Orogeny could have resulted in vertical shears developing due to variations in crustal thickness and uplift (Stage 1 Figure 3-7). This vertical movement would have been oriented E-W, perpendicular to the direction of compression.
- With the development of uplift as a compressional 'pop-up' structure and transpression during the Limpopo Orogeny that brought deeply buried granulites to the surface (Figure 3-8a), tensional stresses would have been generated oriented N-S by extrusion to the north and south along thrusts with strike slip movement (Figure 3-8b) on parallel to the dominant ENE-WSW shear.
- Continued uplift due to erosion of the overlying rock, tectonic erosion due to normal faulting, and the generation of anatectic melt would have rejuvenated the ENE thrusts and shears (Figure 3-7 Stage 2), resulting in extensive normal faulting. Diabase dykes could subsequently intrude into these tensional faults.
- NE-SW wrenching of the Central Zone at ~2.7 Ga, as suggested by McCourt and Vearncombe (1992), or at ~ 2.0 Ga as suggested by Van Reenen et al. (1987), would imply that ENE structures, such as the Palala Shear are synthetic strike-slip faults, as confirmed by the extensive lateral movement on this structure. However, such a model would suggest complementary NNW antithetic faults, NNE extension, NW trending normal faults and north trending compressional structures in LMB lithologies (Figure 2-8a). These trends cannot be observed in mapped structures (Figure 3-4) or the LANDSAT lineaments (3.4). However, joint mapping (3.5.4) suggests that joints and faults in the pre-Karoo lithologies have dominantly steep dips >70° suggesting that compressional or contractional structures are absent (Figure 3-36) and that the structures are predominantly extensional in origin. The structures in area I in the pre-Karoo lithologies have strikes which show concentrations towards ~N, NW and WNW, which are consistent with Pre-Waterberg NE-SW wrenching. Such a model would also imply N-S extension, which is consistent with the development of subsequent Waterberg and Karoo Age easterly normal faulting. Since the northerly and northwesterly structures are not recorded in Karoo lithologies

(3.5.4), post Karoo tectonics geodynamics has been primarily related to N-S extension.

- Regional uplift at about 2.0 Ga combined with continuous N-S oriented tension has resulted in sub-vertical dip slip movement on the ENE faults, resulting in half grabens or troughs bounded by normal faults into which the Waterberg and Karoo Sediments were deposited (Figure 3-7 Stage 3).
- ENE trending normal faults and the deposition of Waterberg and Karoo sediments in an ENE trending half-graben suggest continuous extension to the NNW (Figure 2.8a).
- The intrusion of ENE dolerite Karoo dykes (Figure 3-31) confirms continued extension.
- The vertical faulting has resulted in tectonic contacts between older and younger rocks along lithological contacts, such as contact between the Clarens Formation sandstones against basalts of the Karoo Supergroup and LMB rocks. Consequently, many E-W lithological contacts are tectonic in nature.
- A conjugate system of synthetic and antithetic faulting related to NNW extension would suggest NE synthetic strike-slip faulting and WNW trending antithetic faulting (Figure 2.8a). This is confirmed by the strike of mapped faults in study area II (Figure 3-32). The Kalahari cover over large parts of study area I precludes the identification of all but major faults.
- Post Karoo isostatic readjustment led to the formation of subparallel E-W grabens between post-Karoo normal faults.
- Continued northerly extension has led to the development of post Karoo ENE normal faulting (Figure 3-4).

In terms of implications for groundwater investigations, rejuvenated structures, such as the ENE trending Bosbokpoort and Tshipise faults in study area II and the Tshipise fault in study area I, have been under N-S extension since at least Waterberg times, making them groundwater target features. NW and NE striking features have been reactivated by shear and may also be good targets depending on lithology.

3.3 Hydrocensus

Research area I is a rural region where potable water demands are met by river water, boreholes and recently by piped water schemes originating from the Karoo basalt aquifer to the south. Whereas the water supply from rivers might be of poor quality and fails in drought situations, groundwater piped from the Karoo aquifer rocks to the south is currently the preferred water option in the area because of its generally availability. The LMB rocks have up to now been considered a poor aquifer due to low success rates and low yields. However, the economic sustainability of the piped water scheme can be questioned, since it involves piping water for 30 km to dispersed settlements with a low population density, hence costs are substantial while ability to pay is low. Groundwater located closer to the demand location is a more cost-effective solution.

Research area II is mainly covered by private game farms, or fruit and vegetable farms where irrigation is possible from the major rivers, and the rural areas meet their potable water demands from borehole water.

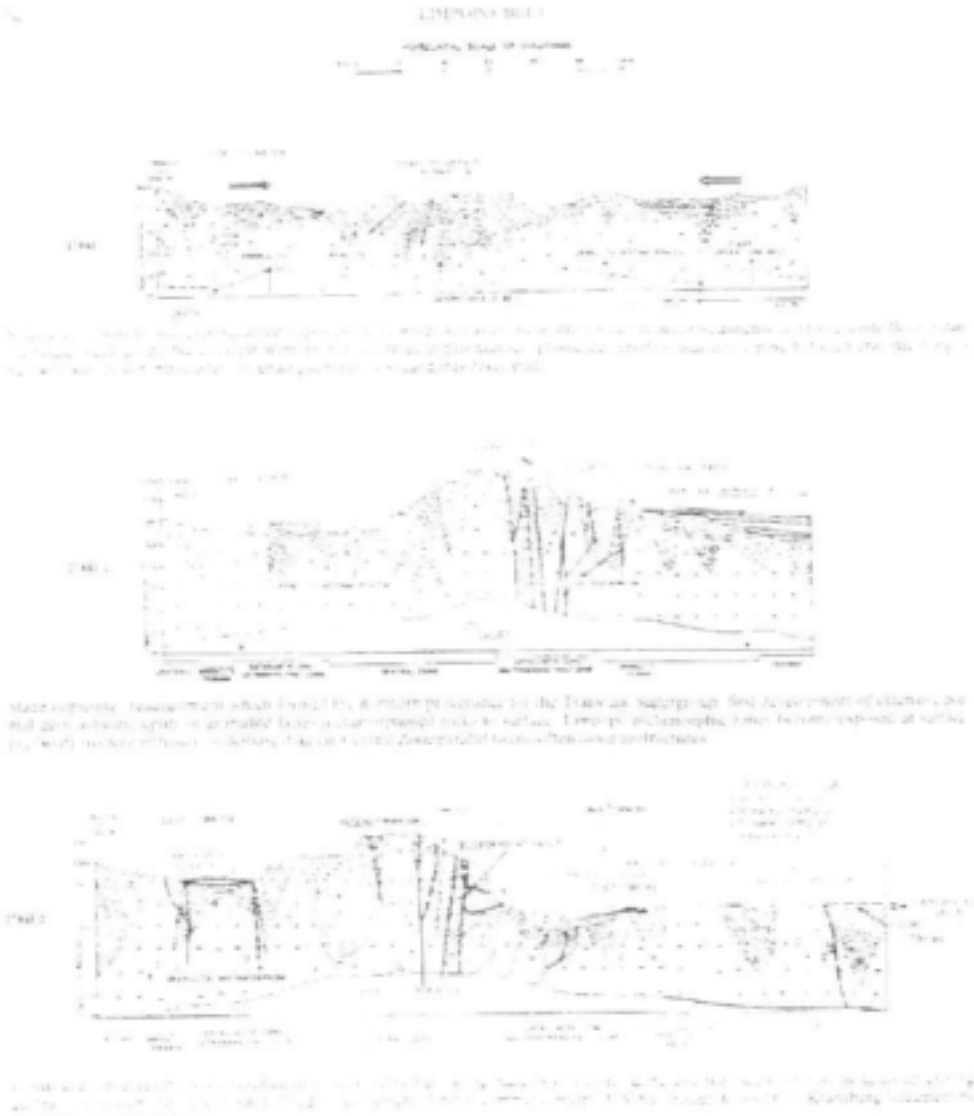

Figure 3-7 Sequential model for the structural development of the LMB (source: Barker, 1983)

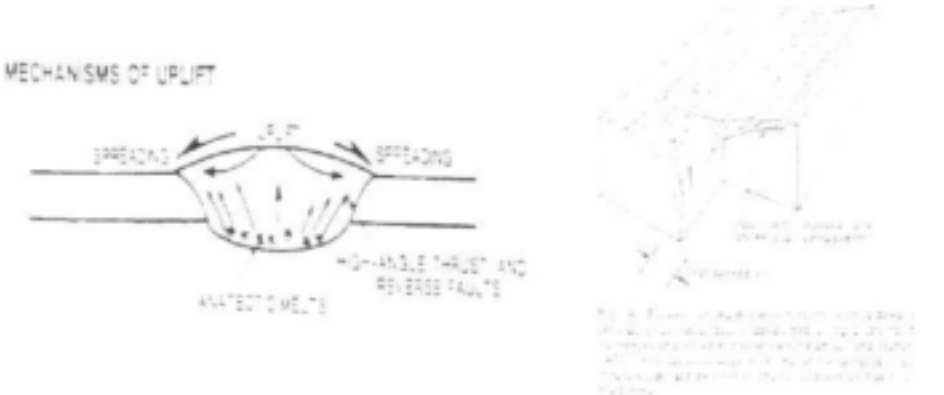

Figure 3-8 a&b Models of the development of a compressional pop up structure and associated extensional stress (Source: Anhaeusser, 1992 & Van Reenen et al., 1987)

The NGDB hydrocensus showed that a total of 2061 boreholes have been drilled into study areas I and II. These records were examined in terms of the drilling success rate achieved, borehole yield distribution and the relationship between borehole yield and distance to structural features. Figure 3-8 and Figure 3-9 demonstrate the success rates in study areas I and II. 29% of all registered boreholes in area I are recorded as being successful (>0.01 l/s), whereas 42% in area II are yielding. However, 57% (area I) and 29% (area II) of the registered boreholes do not have a reported a yield, hence an accurate success rate can only be estimated. Assuming, that 50% of the boreholes without yield specification are dry, success rates of 58% for area I and 56% for area II are estimated, however, this is probably an overestimate. The Map of the Groundwater Resources of the Republic of South Africa suggests that less than 40% of all boreholes in the region are successful (>0.1 l/s), and that 20-30% of these have yields of greater than 2 l/s.

A survey by Vegter (2001) found that only 9 out of 24 boreholes sited using electromagnetics proved successful (38%), and of these, at least 3 sites had other boreholes drilled short distances away from the anomaly which also proved successful. This suggests that boreholes could have been sited just as effectively without the geophysical data.

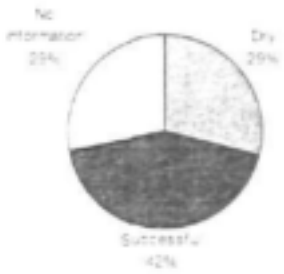

a) b)

Figure 3-8 **a) Success rates for all registered boreholes in the study area I**
Figure 3-9 **b) Success rates for all registered boreholes in the study area II**

Figure 3-10 and Figure 3-11 depict the distribution of the yield in both study areas. Of the boreholes with yield data available, 32% of boreholes are dry in study area I, and 30% in study area II. 56% (study area I) and 30% (study area II) of the recorded boreholes yield between 0.01 and 0.5 l/s, whereas 13% (area I) and 20% (area II) do yield more than 2 l/s. Hence, high yielding targets do exist in the LMB. However, these records are primarily derived from recorded airlift yields rather than from proven pump-out yields and long term sustainable yields may be significantly lower due to the arid nature of the region. The statistics of borehole yields in both areas are shown in Table 3-1.

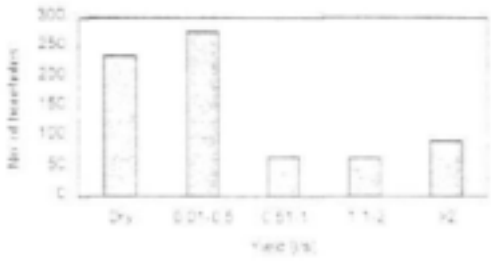

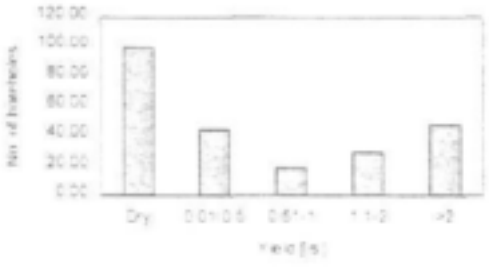

a) b)

Figure 3-10 **a) Distribution of borehole yield in study area I**
Figure 3-11 **b) Distribution of borehole yield in study area II**
Table 3-1 **Hydrocensus data for research area I and II**

	Min yield	Max. yield	Median yield	Average Yield	Average Water level	Average Water strike
Area I	0.01	18.17	0.39*	1.32*	24.26	44.42
Area II	0.02	10.1	1.19*	1.8*	18.04	50.35

* Calculated on the basis of only successful boreholes

Figure 3-4 indicates that unsuccessful boreholes occur in all lithologies and are not restricted to any specific rock type. Poor and relatively high yielding boreholes occur within the same lithology, suggesting that topography and or secondary features like fracture zones, lineaments and dykes are the major control on groundwater occurrence in the Limpopo belt rocks. However, Bush (1989) found that diabase and dolerite dyke contact zones had lower yields than boreholes drilled away from dykes.

To investigate the influence of secondary features and topography on borehole yields and success rates, comparisons of yields versus altitude and distance to structural features were carried out (Figure 3-12, Figure 3-13, Figure 3-14 and Figure 3-15).

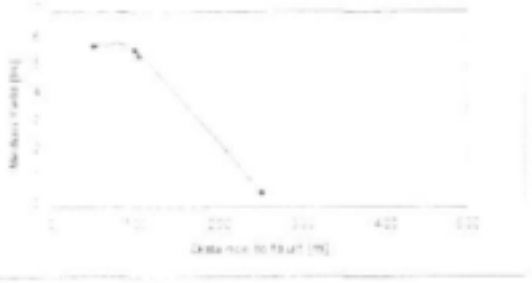

a)

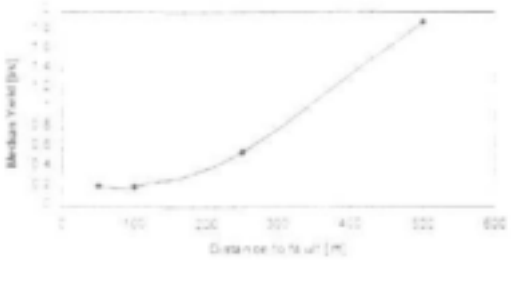

b)

Figure 3-12 a) Borehole yield in relation to the distance to mapped faults (area I). N values: 0-50m=4, 50-100m=1, 100-250m=3, 250-500m=0

Figure 3-13 b) Borehole yield in relation to the distance to mapped faults (area II). N values: 0-50m=5, 50-100m=5, 100-250m=9, 250-500m=2

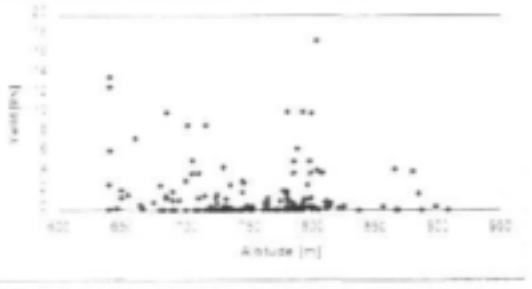

a)

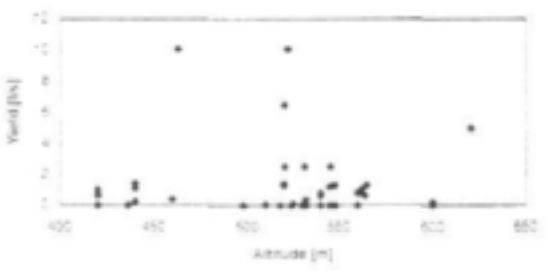

b)

Figure 3-14 a) Borehole yield in relation to topographical height (area I).

Figure 3-15 b) Borehole yield in relation to topographical height (area II).

Study area I appears to exhibit a strong relationship between borehole yield and distance to faults, however, the sample size is small (N=8). Whereas median yields of boreholes close to a fault are recorded to be in the order of 5-6l/s, the yield decreases considerably with increasing distance to structural features (Figure 3-12). In contrast, study area II exhibits an opposite trend, with borehole yields increasing with distance to faults. One reason for this may be that of all the boreholes drilled into the Tshipise and Bosbokpoort fault, the major fault systems in study area II, none have recorded yields. Secondly, high yielding boreholes are recorded along the Nzhelele and Limpopo river (Figure 3-17); their recorded high yields are believed to be a function of the alluvium cover and the shallow water strike and water level along riverbeds, rather than on the distance to structural features. In addition, the low N value suggests that these results are not statistically valid.

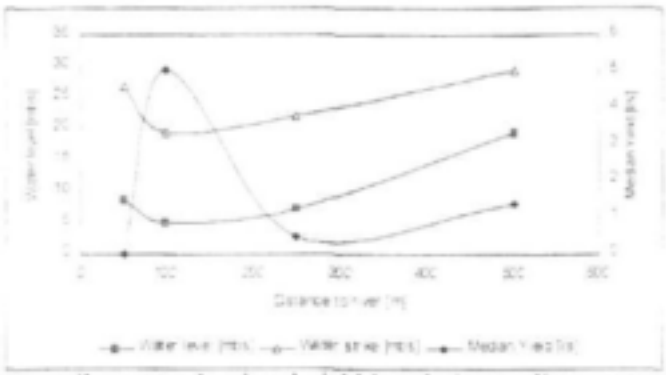

Figure 3-16 **Water strike, water level and yield in relation to distance to rivers in study area II. Record no.: 0-50m: n=2, 50-100: n=2, 100-250m: n=7, 250-500m: n=7**

No relationship can be observed between the altitude of the borehole site and the yield (Figure 3-14 and Figure 3-15). This is probably due to the fact that both study areas exhibit a gentle relief and no major topographical height differences are present.

The average borehole depth is between 56 and 66m in both areas but varies widely, with shallow holes of not more than 11m being recorded in alluvial sands next to rivers and deeper boreholes being drilled into the LMB rocks, where water strikes are deeper. Accordingly, the depth of water strikes varies widely in accordance to the borehole position and its distance to rivers. 50% of water strikes occur below 36m (area I) and 34m (area II), whereas the median water strike is at a depth of 44m (area I) and 50m (area II). Water levels are generally shallow with a median depth of 24m in study area I and 18m in study area II (Figure 3-17, Figure 3-18, Figure 3-19 and Figure 3-20).

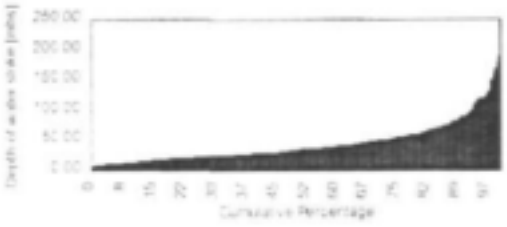

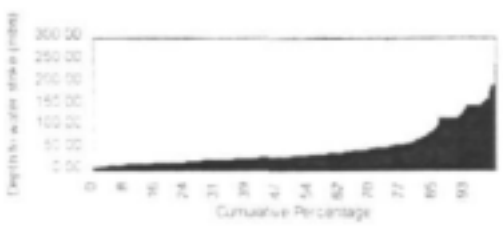

a) b)

Figure 3-17 **a) Depth of water strike (study area I)**
Figure 3-18 **b) Depth of water strike (study area II)**

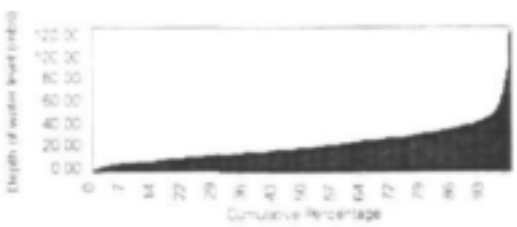

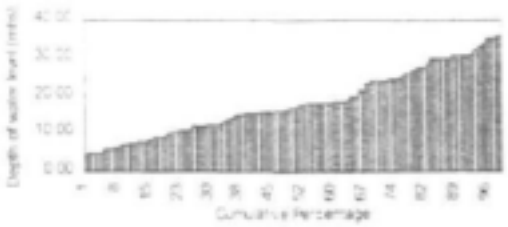

a) b)

Figure 3-19 **a) Depth of water level (study area I)**
Figure 3-20 **b) Depth of water level (study area II)**

The overall groundwater quality of the LMB rocks appears to be good. Based on the water quality classification method developed by DWAF (1996), the median water quality falls mainly in category 0 and 1. Table 2 and Table 3 shows the minimum, maximum, average and mean values of the major-ion chemistry of water from the study area I and study area II

respectively, as well as the resulting classification using the DWAF system. The table is based on 63 records available for the LMB lithologies in study area II and on 211 records available for study area.

Table 3-2 Statistics of major-ion chemistry in LMB covered research area I (in mg/l)

	min	max	average	median	Class
PH	6.20	8.80	7.93	7.94	0
EC	2.60	1570.00	206.73	133.00	I
Na	15.90	2410.60	240.93	135.40	I
Mg	0.00	1025.30	88.48	60.50	I
Cl	6.80	5403.30	354.75	141.45	I
So4	4.00	1649.30	168.85	30.15	0
No3	0.00	239.40	17.55	9.99	I
F	0.04	7.46	1.17	0.70	0
K	0.34	54.18	8.30	7.79	0
Ca	10.40	652.30	100.34	73.30	II

Table 3-3 Statistics of major-ion chemistry in LMB covered research area II (in mg/l)

	min	max	average	median	Class
PH	5.75	8.30	7.75	7.90	0
EC	7.30	1460.00	230.62	139.50	I
Mg	8.90	290.70	92.71	89.00	II
Na	29.60	847.40	157.28	91.50	0
K	0.98	15.66	5.06	4.40	0
Cl	34.00	1218.00	238.66	177.25	I
SO4	13.80	400.90	117.94	103.75	0
NO3	0.00	104.97	10.97	8.65	I
F	0.00	0.07	0.02	0.00	0

3.4 LANDSAT Imagery

The hydrocensus suggests that the occurrence and movement of groundwater in the study area is mainly controlled by the prevalence and orientation of secondary features, such as faults, joints and fracture zones, and by the distance to rivers where sand and gravel alluvial aquifers exist. As such, the delineation and mapping of these structural features was attempted from satellite imagery.

The lineament map shown in Figure 3-33 is a composite image of all lineaments identified by the different enhancement techniques described in chapter 3.2. The recorded lineaments were categorised according to their orientation, frequency and length. In both areas, lineaments are primarily orientated in an ENE-WSW direction (Figure 3-23), or E-W (Figure 3-28), which corresponds to the orientation of major shears believed to be extensional normal faults under the post-Precambrian stress regime. These lineaments appear to be regional extensive (Figures 3-24 & 3-29). Their presence in the Soutpansberg and Karoo basalts (Figure 3-33) confirms that these structures have been affected by post-Karoo tectonic events.

When examining the maximum lineament length orientations (Figures 3-25 & 3-30), complementary WNW-ESE and NW-SE trends become apparent. These represent part of a conjugate system of antithetic faulting related to NNW extension, however, corresponding NE synthetic strike-slip strain seems to be taken up on the ENE structures since NE structures are not readily visible. Consequently, the regional scale observed lineaments correspond well with expected fault patterns expected from a N-S oriented extensional regime.

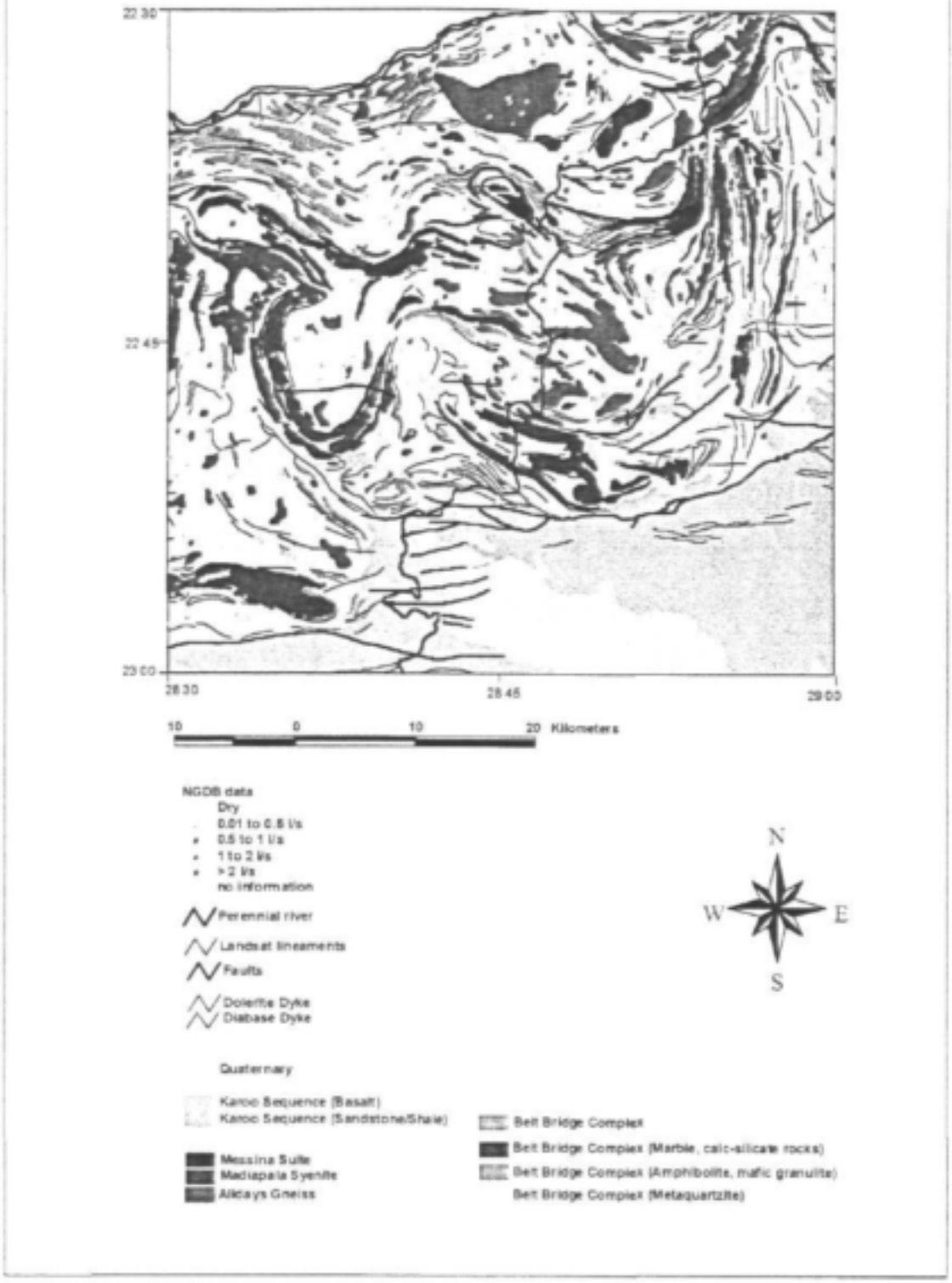

Figure 3-21 **Distribution of borehole yields in study area 1 (NGDB records)**

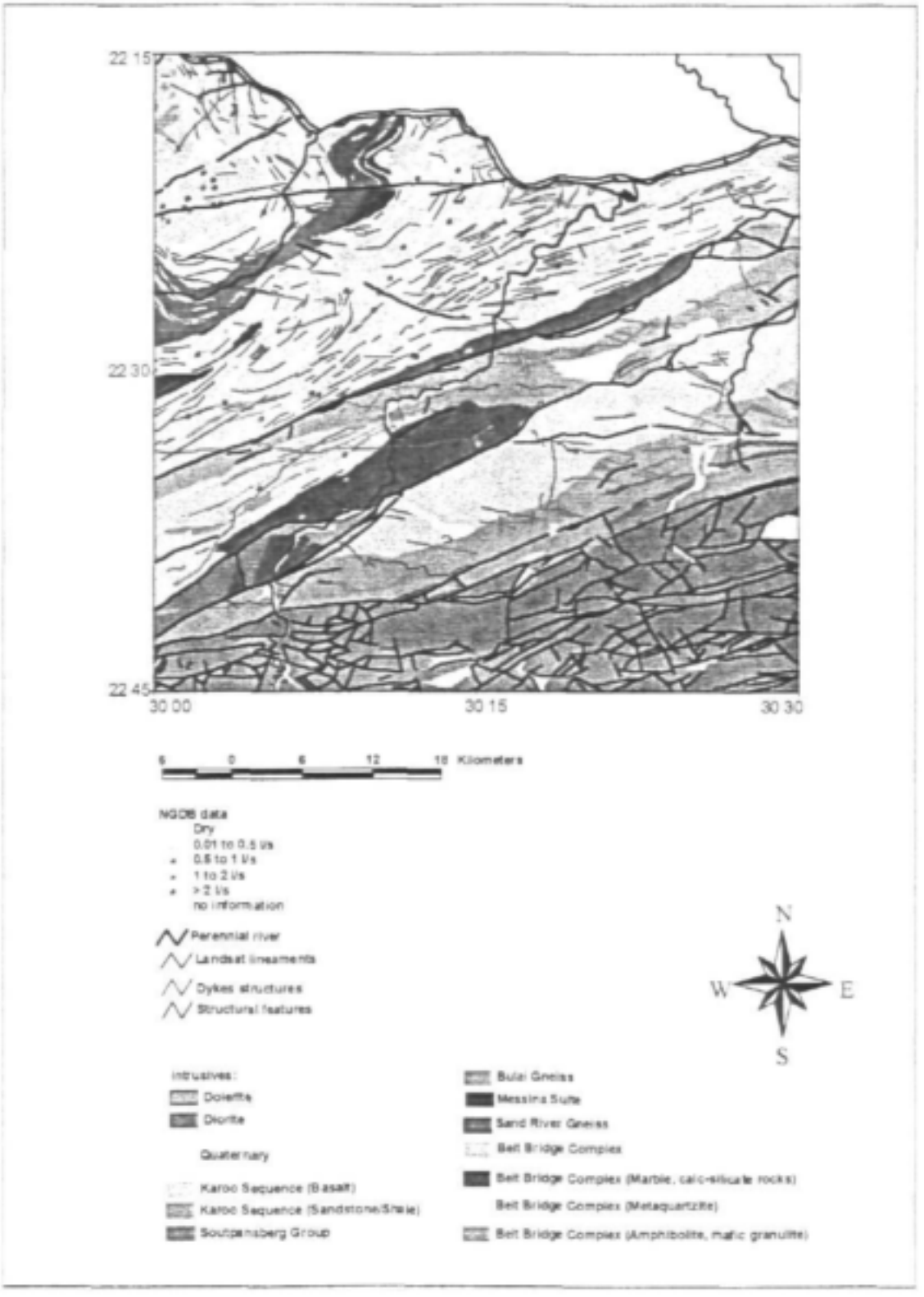

Figure 3-22 Distribution of borehole yields in study area II (NGDB records)

When analysing mapped faults only (Figures 3-26 & 3-31), a similar pattern is observed; a prominent E-W trend and ENE-WSW trend in areas I and II suggest that the lineament trend is related to faults. Secondary NE and WNW trends represent expected anti and synthetic faulting. Mapped dykes (Figures 3-27 & 3-32) have a similar trend and provide further evidence that the ENE orientation is the primary extensional orientation.

A comparison between the geological map of the study area and the lineament orientation reveals that many lineaments correspond to lithological boundaries (Figure 3-33). However, many of these contacts are tectonic in origin, hence are structurally significant. Faults have been mapped along ENE contacts between LMB rocks and Karoo rocks, and between Karoo basalts and sandstones, hence these lineaments are hydrogeologically significant. ENE trending faults and lineaments are also observed within the Soutpansberg Group. In the LMB, however, many ENE lineaments do not correspond to mapped faults (Figure 3-33). This can be attributed to the Quaternary cover, which has restricted the mapping of faults, and the fact that if these lineaments represent normal faulting it is possible that the contact would be gneiss against gneiss, hence vertical movement would be difficult to detect. Alternatively, lineaments could represent tension fracturing parallel to major ENE normal faults. It is likely that the extensional nature of strain has resulted a series of parallel faults with the same ENE orientation.

Other observed lineaments represent lithological contacts between LMB lithologies (Figure 3-33). As these contacts are the result of folding and deformation that occurred in a ductile manner, these lithological contacts do not necessarily represent groundwater targets unless subsequent faulting occurred. Consequently, great care is required when interpreting lineaments; many are likely not to be hydrogeologically significant.

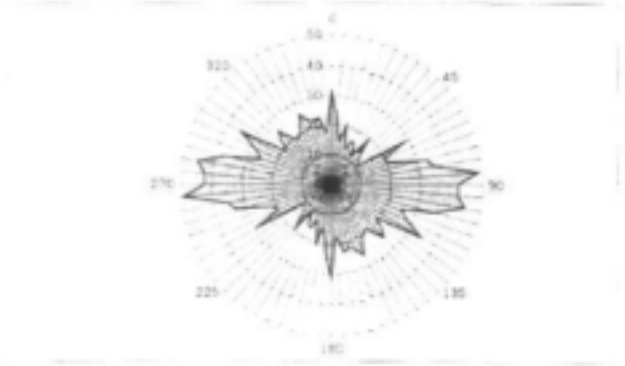

Figure 3-23 **Lineament strike-frequency plot in study area I**

a) b)

Figure 3-24 **a) Lineament length-frequency plot for study area I**
Figure 3-25 **b) Max. lineament length-frequency plot for study area I**

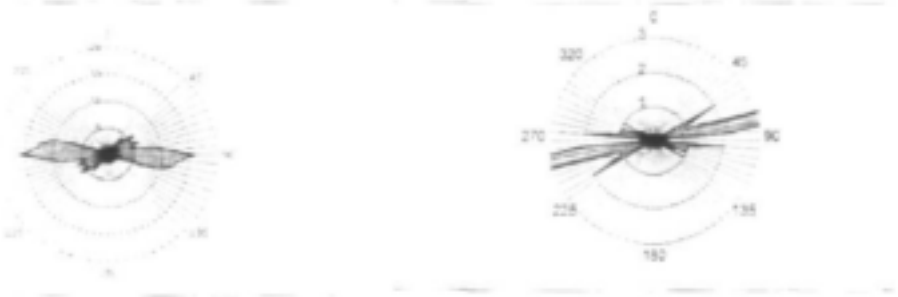

a) b)

Figure 3-26 a) Strike-frequency plot of faults in study area I
Figure 3-27 b) Strike-frequency plot of dykes in study area I

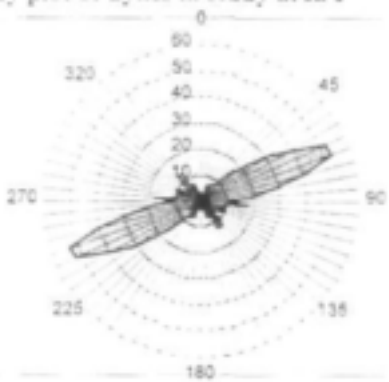

Figure 3-28 Lineament strike-frequency plot (Study area II)

a) b)

Figure 3-29 a) Lineament length-frequency plot (study area II)
Figure 3-30 b) Max. Lineament length-frequency plot (study area II)

a) b)

Figure 3-31 a) Strike-frequency plot of mapped faults in study area II
Figure 3-32 b) Strike-frequency plot of mapped dykes in study area II

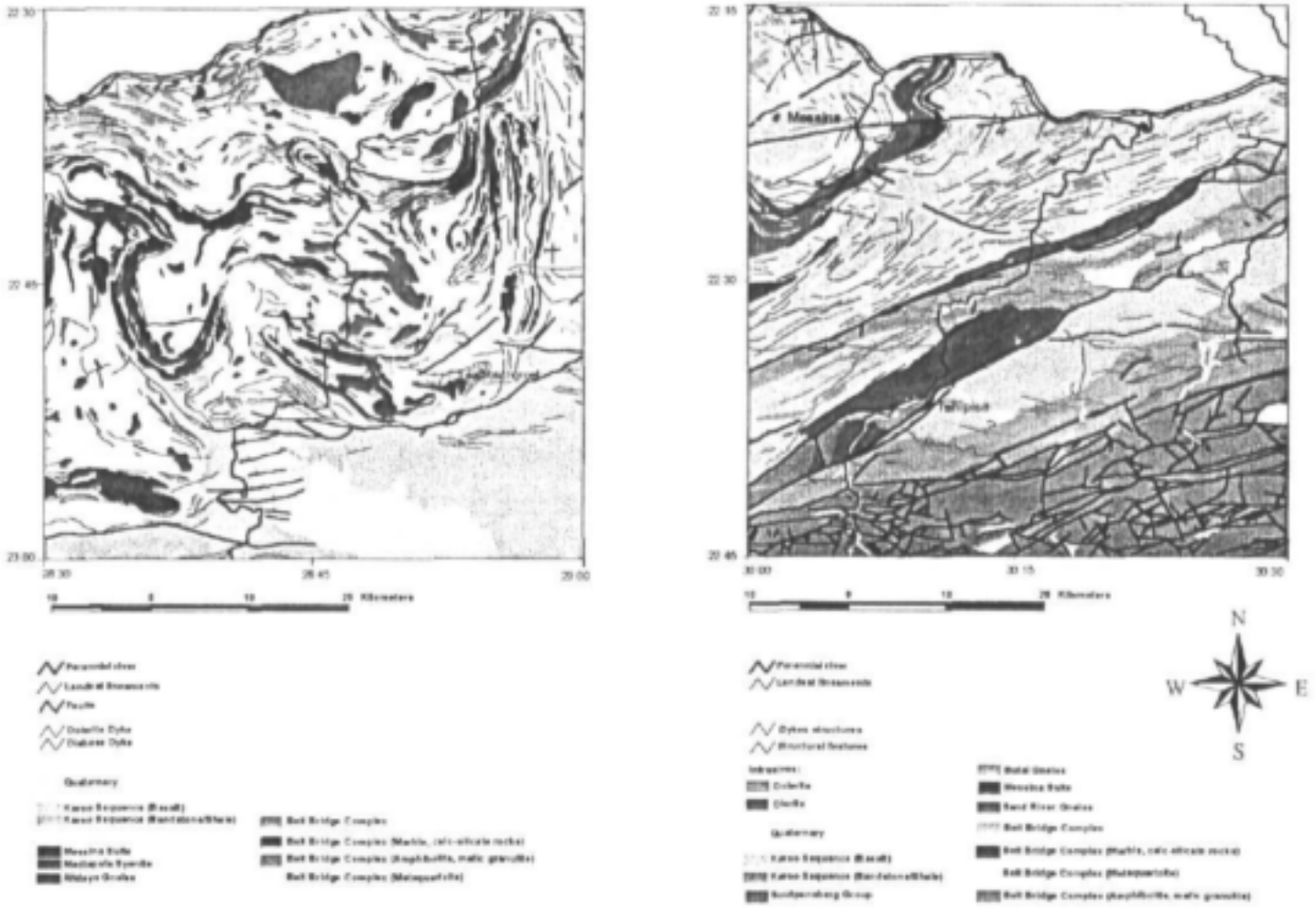

Figure 3-33 LANDSAT lineaments for study area I and II

3.5 Structural Geology

3.5.1 Introduction

The two research areas were traversed on a reconnaissance basis using public access roads only (i.e. no farms were accessed) for the purpose of mapping structural features observed on outcrops. The study focussed on brittle structures (i.e. Joints and faults) and dykes as potentially good groundwater targets. A total of 75 localities were visited at which 408 joint, fault and dyke orientation measurements were made. The joint measurements form the bulk of these data (Figures 3-35 & 3-36).

3.5.2 Previous work in the study areas

Numerous studies have concentrated on the tectonothermal evolution of the Limpopo Metamorphic Province (see chapter 3.2.3). These studies mostly paid attention to the late Archaean to early Proterozoic ductile evolution of the Limpopo Metamorphic Province with little attention being paid to the subsequent brittle evolution of the area. Studies which include some information on the brittle structures of this area are those by Jansen (1975), Barker (1976), Barker (1979), Watkeys (1983) and Andersen and Ainslie (1994).

3.5.3 Geological history of the areas sampled

The rocks in both areas have crystallisation/deposition ages ranging from the late Archaean, represented by the dominantly granitoid gneisses and related rocks of the Limpopo Metamorphic Province, to the Jurassic age Karoo basaltic lavas and related dolerite dykes and the Clarens Formation sedimentary rocks which underlie the basalts. The structural framework of both areas is broadly similar in that both are underlain to the northwest by rocks of the Limpopo Metamorphic Province separated, by ENE striking faults, from the rocks to the southeast which comprise basalts and sedimentary rocks of Karoo age (Figure 3-4) and Soutpansberg Group rocks in study area II. These faults are post-Karoo in age because they affect the Karoo-age rocks.

The first period of brittle deformation in the area is recorded in the Limpopo Metamorphic Province lithologies and the cratonic platform sedimentary sequence of the Soutpansberg Group which is exposed approximately 10-20kms to the south of study area II and >30-40km to the south of study area I.

The age of the Soutpansberg Group is uncertain. Rb/Sr data suggest an age of ~1750Ma (Barton, 1979). In addition, to the south of area I Waterberg Group sedimentary rocks, which are considered to be time equivalents of the Soutpansberg Group, overly the ~2050Ma old Bushveld Complex unconformably. The Soutpansberg Group comprises intercalated coarse to medium grained siliciclastic sedimentary rocks and basic to intermediate volcanic rocks. These rocks do not record the effects of the high-grade metamorphism and ductile deformation preserved in the Limpopo Metamorphic Province lithologies.

They were deposited unconformably on the Limpopo Metamorphic Province lithologies after those rocks had been exhumed to surface by uplift and erosion. The Soutpansberg Group rocks are deformed and weakly metamorphosed but still preserve primary sedimentary structures and textures. The Soutpansberg Group is extensively faulted with three generations of faulting recognised (Jansen 1975) with reactivation of older faults during later deformation. The earliest phase of faulting included both syn-depositional dip-slip normal faulting and sinistral strike slip faulting (Jansen, 1975). Jansen (1975) also indicated the depositional trough and associated deformation die out westward towards Botswana. Jansen (1975) also reported pre- and post Karoo faults in the Soutpansberg Group with all three fault phases

having similar ENE strike orientations. Although the Soutpansberg Group rocks are not represented in the study area, their close geographic proximity to the study areas implies that the deformation recorded in them also affected the study areas to varying degrees. In particular, the proximity of the Soutpansberg Group to study area II implies that the deformation recorded in the Soutpansberg Group is likely to have affected that area to a greater degree in comparison to study area I which is located to much further west, in which direction Jansen (1975) suggests deposition and deformation were not as extensive. Barker (1983) recognised four tectonic trends namely a dominant ENE trend and subordinate N-S Lebombo trends, and a conjugate NNE-NNW post-Transvaal dyke trend. Barker (1983) also indicates that reactivation of the pre-Karoo dip-slip and strike-slip structures have been reactivated during the extensional Karoo and post-Karoo deformation, and that post Karoo uplift is evident by the presence of high level unconsolidated river gravels.

Figure 3-34 Geological map of study area I showing the localities where joint measurements were made (black clusters of strike & dip symbols).

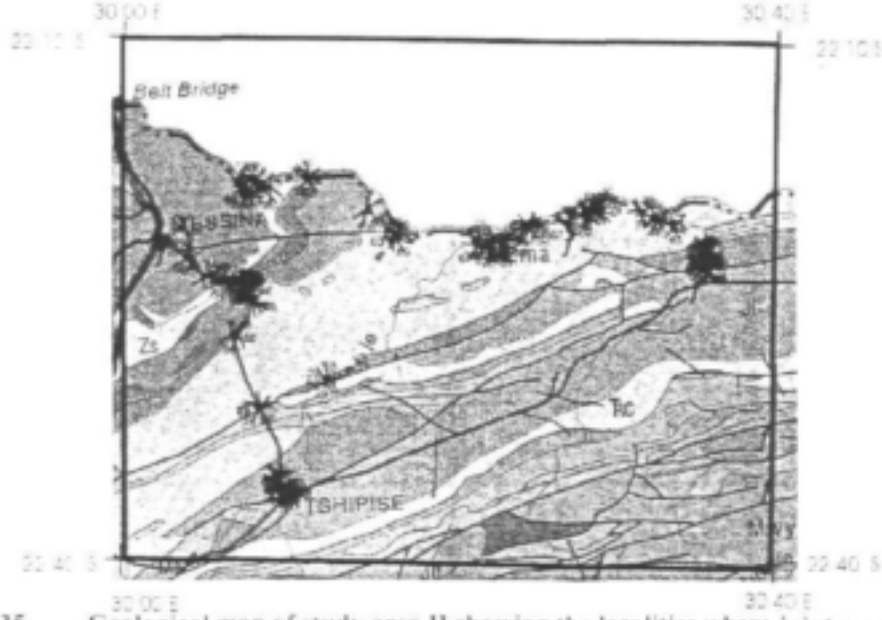

Figure 3-35 Geological map of study area II showing the localities where joint measurements were made (black clusters of strike & dip symbols).

3.5.4 Structures recorded in Pre-Karoo lithologies in the study areas

Rock types included in this group are dominated by granitic orthogneisses with subordinate proportions of quartz veins and supracrustal, banded gneisses of mafic and quartzofeldspathic composition and marbles and calc-silicates. Joints are best developed in the more siliceous, homogeneous lithologies (granitic orthogneisses and quartz veins) in contrast to the more heterogeneous banded supracrustal lithologies. Fractures developed in these rocks are likely to vary in age from the oldest brittle structures developed during the deposition and early deformation recorded in the Soutpansberg Group to the youngest structures developed during Gondwana fragmentation during Karoo times as well as those structures (if any) developed during post Karoo uplift.

The stereonets and rose diagrams for the structures recorded in the pre-Karoo lithologies in study area I and II are shown in Figure 3-36, Figure 3-37, Figure 3-38 and Figure 3-39. The joints and faults in the pre-Karoo lithologies in area II dip steeply (Figure 3-37) and strike mostly NW to N, with lesser groups striking NE and ENE. In addition a significant number of structures with dips <60° were recorded although most dip at >60°. The development of structures with dips <60° is likely to have been related to a contractional or compressional environment. Such a setting could conceivably have prevailed during the sinistral strike-slip transpressional faulting (NE to SW) reported by Jansen (1975) and Barker (1983) that occurred at ~ 1.7 Ga.

The joints and faults in area I have dominantly steep dips >70° suggesting that compressional or contractional structures are absent (Figure 3-36) and that the structures are dominantly extensional in origin. The structures in area I in the pre-Karoo lithologies have strikes which show concentrations towards ~N, NW and WNW, the first two directions being similar to those in area II (Figure 3-38).

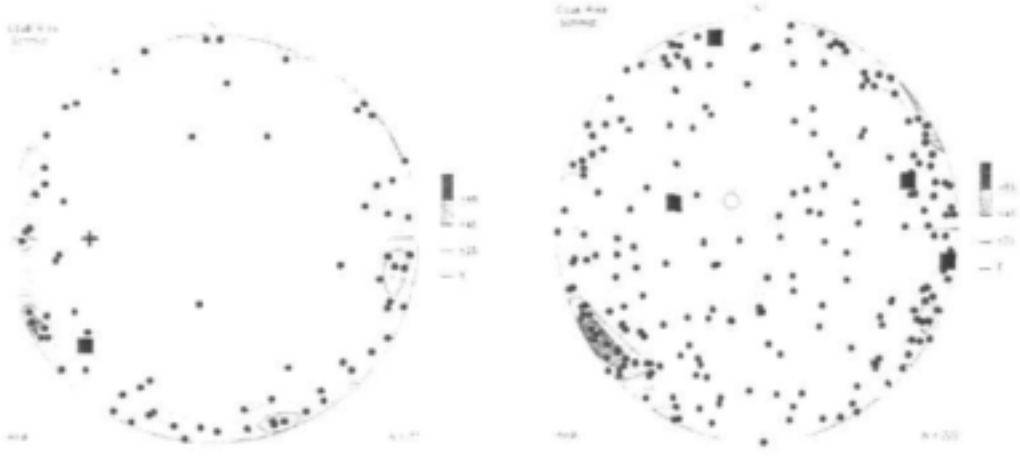

Figure 3-36 a) Contoured stereographic projection of poles to joints (points), faults (squares) and dykes (plus symbol) measured in the Limpopo Metamorphic Province lithologies from area I
Figure 3-37 b) Contoured stereographic projection of poles to joints (points), faults (squares) and dykes (plus symbol) measured in the Limpopo Metamorphic Province lithologies from area II.

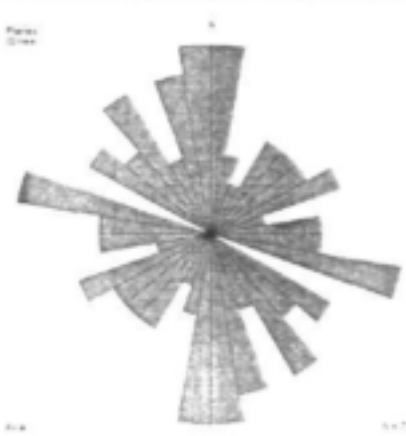

a)

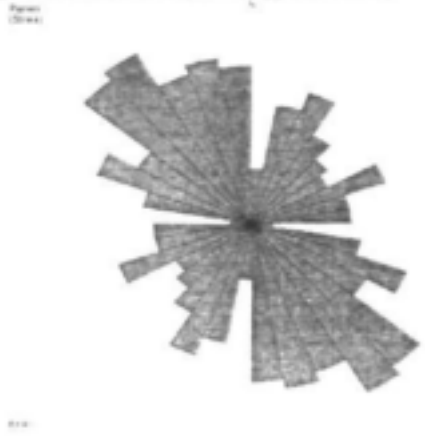

b)

Figure 3-38 **a) Rose diagram showing the frequency of strike directions for joints and faults in the pre Karoo lithologies in study area I**

Figure 3-39 **b) Rose diagram showing the frequency of strike directions for joints and faults in the pre Karoo lithologies in study area II**

3.5.5 Structures recorded in Karoo-age lithologies

Rock types included in the group are the Clarens Formation sandstones, siltstones and mudrocks and Karoo basalts and dolerite dykes. Joints are best and most frequently developed in the basalts and dolerites and to lesser degrees in the sandstones and mudrocks respectively. These lithologies are the youngest lithologies in the study areas and consequently record the orientations of the most recent structural events in the areas

The stereonet for the structures recorded in the Karoo-age lithologies in area II shows that the joints and dolerite dykes dip steeply almost exclusively >60° (Figure 3-40) and strike ENE to E, with subordinate NNE orientations (Figure 3-42). The ENE to E joint and dyke orientations are consistent with the extensional regime that prevailed during Gondwana fragmentation. A subordinate NNW direction is also present ,suggesting ENE extension. This direction is similar to the Karoo-age Lebombo trend described by Saggerson and Logan (1970) and is consistent with the two-stage Gondwana fragmentation described by Cox (1992) and Grantham (1996).

Barker (1983) presented a rose diagram of 3190 measurements of joints, dykes and faults from all lithologies over a large area, which included both of the areas, sampled in this study and found that the dominant structural trend is ENE. Unfortunately he made no attempt to analyse the fractures in the various lithological units separately however the dominant ENE direction he determined would suggest that the Karoo-age fractures dominate the fracture systems in the areas studied.

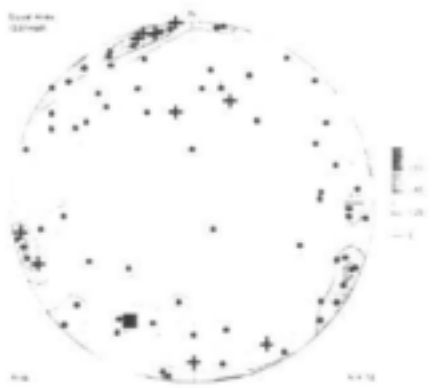

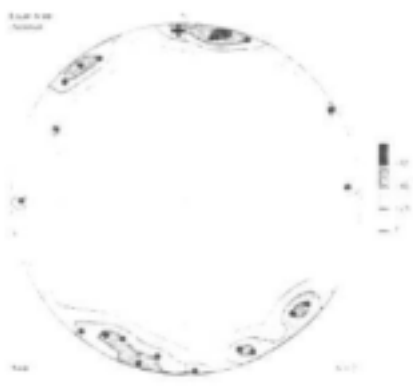

a) b)

Figure 3-40 a) Contoured stereographic projection of poles to joints (points), faults (squares) and dykes (plus symbol) measured in the Karoo-age lithologies from area II

Figure 3-41 b) Contoured stereographic projection of poles to joints (dots), dykes (plus symbols) and faults (square) in the Karoo-age lithologies from area I

The stereonet for the structures recorded in the Karoo-age lithologies from area I shows the joints dip steeply (>70°) (Figure 3-41) and have two dominant strike directions namely WNW and NE (Figure 3-43).

It is interesting to compare these data from area I with the study of Andersen and Ainslie (1994), which was located in the same area. The orientations of the structures measured in this study coincides with, and is consistent with, the orientations related to Karoo-age Gondwana extension. No concentration of structures with orientations NNW and ~WNW, similar to their proposed neotectonic-extension structures, were recognised in the cover rocks in study area I, however, N and WNW orientations are common in the Limpopo Metamorphic Province lithologies (Figure 3-39). This suggests that the neotectonic-extension structures proposed by Andersen and Ainslie (1994) are actually pre-Karoo in origin. Andersen and Ainslie (1994) concluded from a study of known successful borehole location and structure orientation that the NNE and NNW structures were most successful in area I with regard to ground water exploration.

3.5.6 Conclusions

The joint orientations in the Limpopo Metamorphic Province in both areas are distinctly different from these in the Karoo-age cover and intrusive lithologies. The joints in the Limpopo Metamorphic Province mostly dip steeply and are oriented NW to N suggesting E-W to NE/SW extension. The subordinate shallow dipping joints that only occur in the basement rocks in area II may be related to the strike-slip fault regime proposed by Jansen (1975) and possibly was prevalent during the Soutpansberg depositional phase. The joints in the Karoo-age sedimentary rocks, basalts and intrusives all dip steeply and are oriented E to ENE in area II and ESE and NE in area I suggesting N-S extension. This confirms the results obtained from the geodynmanic analysis (6.2.4). Recognising the difference in joint patterns between the pre-Karoo-age lithologies and the Karoo and younger lithologies, suggests that the more recent fractures have orientations similar to those preserved in the Karoo-age lithologies. Consequently it is fractures with orientations similar to those preserved in the Karoo-age lithologies which are likely to be more open and which therefore represent the best structures for ground water exploration.

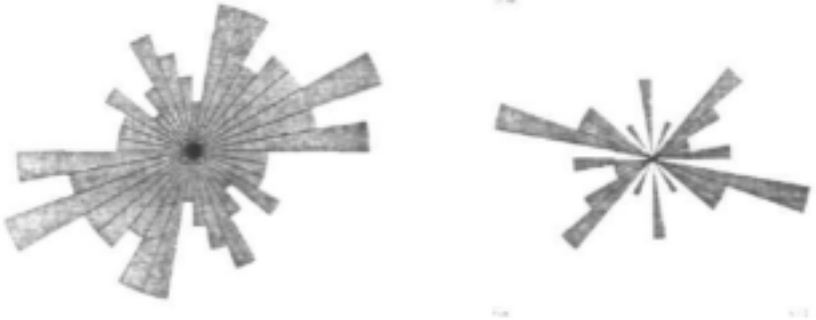

a) b)

Figure 3-42 a) Rose diagram showing the dominant strike orientations of joints in the Karoo-age lithologies in area II

Figure 3-43 b) Rose diagram showing the dominant strike orientations of joints in the Karoo-age lithologies in area I

3.6 Ground Based Geophysics

3.6.1 Introduction

Traget features for geophysical investigations included lineaments, geological features such as fault lines, dykes or sills and lithological contacts of dipping strata. The geophysical data is summarized in Table 3-4 in terms of the geological feature investigated.

A total of 21 electromagnetic traverses, 27 magnetic traverses and 10 resistivity soundings were carried out in research areas I and II. The location and number of each traverse is shown in Figure 3-44. The data for all traverses and stations are presented in Appendix 3-A.

Table 3-4 Geophysical surveys carried out in the research area

Name	Boreh. drilled	Lat	Long	Feature	Geophysics	Traverse direction
LMB1		22.6640	28.7937	NW-SE running dyke	Mag, Max Min	S-N
LMB2		22.6648	28.7937	NW-SE running dyke	Mag, Max Min	S-N
LMB3		22.6473	28.7878	WNW-ESE striking fault	Mag, Max Min	N-S
LMB4		22.6833	28.7970	E-W dyke	Mag, Max Min	S-N
LMB5	H26-0426	22.8641	28.8791	Geological contact between Karoo Sandstone and LMB rocks	Mag, Max Min Resistivity	SSE-NNW
LMB6	H26-0428	22.8268	28.8186	NNE-SSW running Lineament	Mag, Max Min	S-N
LMB7		22.8165	28.8740	NE-SW striking fault	Mag, Max Min	SSE-NNW
LMB8		22.7849	28.8592	NE-SW striking fault	Mag	SSE-NNW
LMB9	H26-0432	22.7849	28.8592	ESE-WNW running dyke	Mag, Max Min	SSE-NNW
LMB10	H26-0429 H26-0430	22.7435	28.7911	NE-SW striking fault	Mag, Max Min Resistivity	NNW-SSE
LMB11		22.7554	28.7934	E-W running dyke	Mag, Max Min Resistivity	S-N
LMB12		22.8737	28.7582	Tshipise fault, E-W striking	Mag, Max Min Resistivity	N-S
LMB13	H26-0427 H26-0434	22.8813	28.7787	Tshipise fault, E-W striking	Mag, Max Min	N-S
LMB14		22.8011	28.9217	WNW-ESE running fault	Mag, Max Min	S-N
LMB15	H26-0433	22.7814	28.9203	NE-SW striking fault	Mag	S-N
LMB16		22.3331	30.5423	Massive dyke structure	Mag	S-N
LMB17		22.3852	30.5951	Tried to locate Tshipise fault, but missed the feature	Mag	N-S
LMB18		22.3852	30.5951	Tshipise fault, ENE-WSW striking	Mag, Max Min Resistivity	SSE-NNW
LMB19		22.3379	30.4511	Massive pegmatite vein	Mag, Max Min Resistivity	E-W
LMB20		22.3594	30.3586	SE-NW running fault	Mag, Max Min Resistivity	WSW-ENE
LMB21		22.3504	30.2681	ENE-WSW striking fault	Mag, Resistivity	NW-SE
LMB22		22.4111	30.1372	NW-SE running fault	Mag, Max Min Resistivity	ESE-WNW
LMB23		22.4284	30.1544	ENE-WSW striking fault	Mag	NW-SE
LMB24		22.4967	30.2132	Tshipise fault, WSW-ENE striking	Mag, Max Min Resistivity	SSE-NNW
LMB25		22.3509	30.2632	ENE-WSW running fault	Mag, Max Min	SW-NE
LMB26		22.3587	30.3553		Mag, Max Min	W-E
LMB27		22.3236	30.4867	Several small scale faults o outcrop scale	Mag	W-E
LMB28	H26-0431	22.7988	28.7828	Alluvium		

The results of the geophysical ground based surveys were grouped into four main categories, reflecting responses over fault zones, lineaments, magnetic structures and other targets of possible hydrogeological significance. Examples from each category are described below.

3.6.2 Fault Zones

A total of 16 faults were investigated using ground-based geophysics in study areas I and II. Four traverses were carried out to investigate the Tshipise and Bosbokpoort fault respectively. Locations were chosen at contacts between LMB rocks and Karoo basalts, as well as LMB

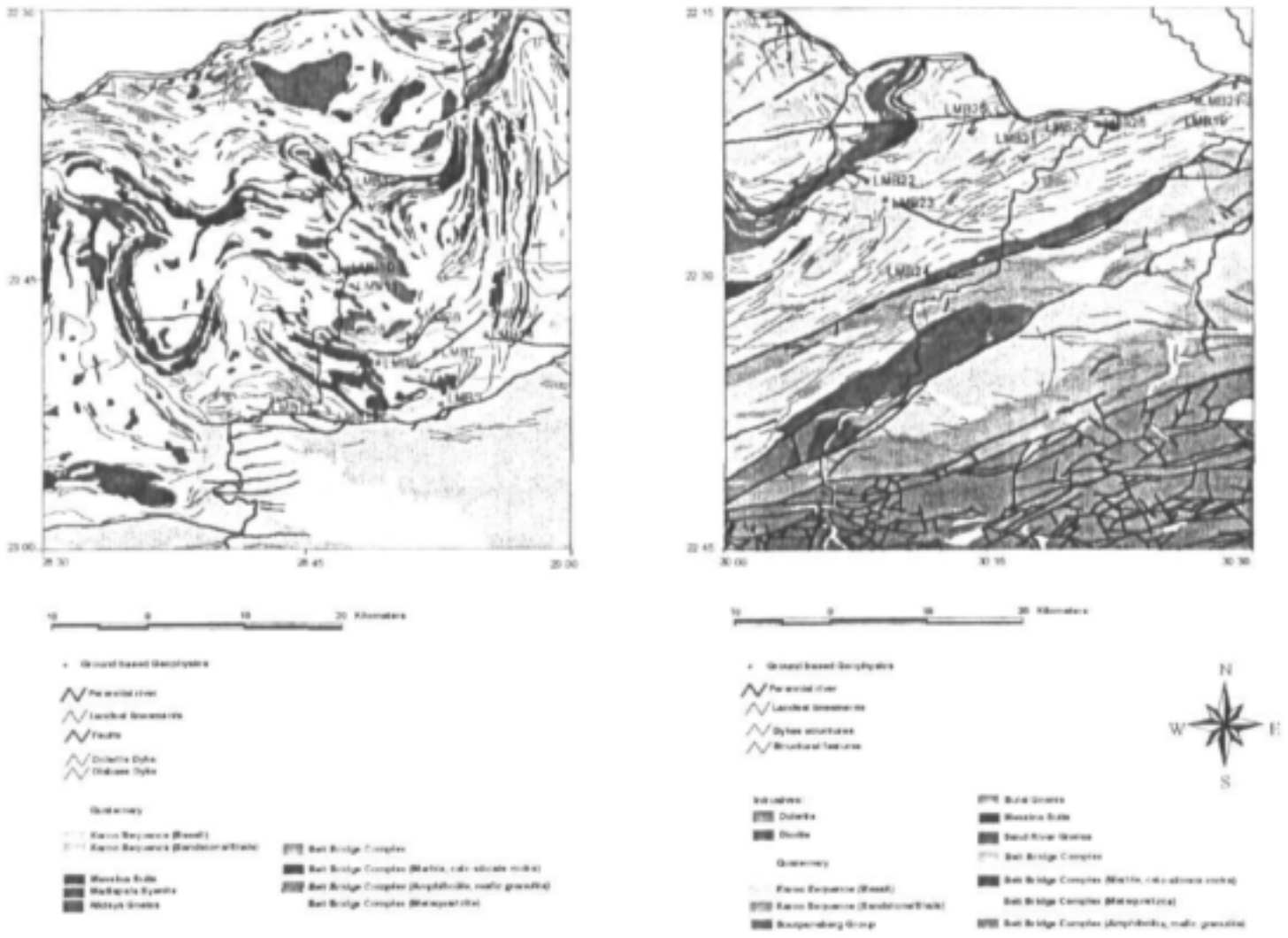

Figure 3-44 **Stations of geophysical surveys carried out throughout the study area**

rocks in tectonic contact with Karoo Clarens Formation sandstones. Minor faults striking WNW-ESE to NW-SE and ENE-WSW to SE-NW were also traversed. Examples for geophysical responses over these fault zones are given below.

LMB13 – Tshipise fault separating Karoo basalts and Limpopo mobile belt rocks
Site description
A regional scale fault, striking ENE-WSW to E-W, separates the Limpopo Mobile Belt rocks in the North from basalts of the Karoo Supergroup in the South. In several localities in the study areas, where the fault separates Karoo basalts from LMB rocks, it is well marked in the field as a topographical down throw from resistive LMB rocks in the north to the easier erodable basalts in the South. The feature is mapped on the 1:250000 geological map Alldays and Messina and is named the Tshipise and Bosbokpoort fault respectively.

The transect was located at the contact between LMB rocks and Karoo basalt, at the northern contact of what appears to be a half-graben structure (Figure 3-46). This fault is parallel to the Palala Shear, which occurs at the contact with Waterberg strata further south.

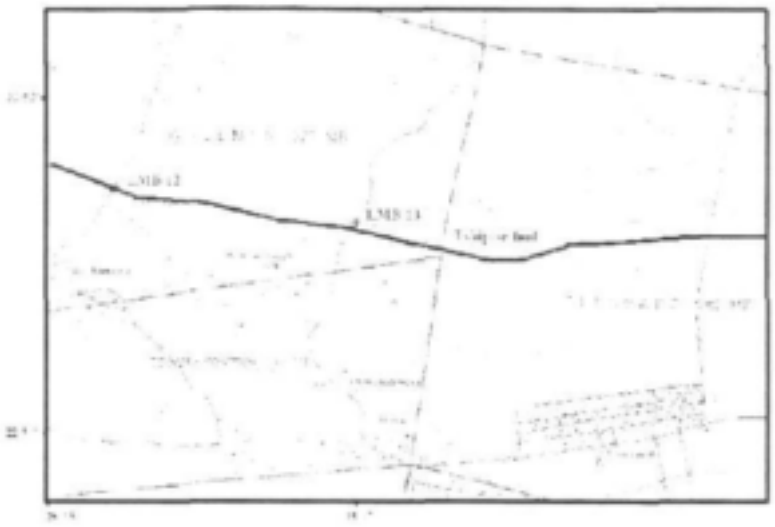

Figure 3-45 Location of LMB13

Electromagnetic Survey
The Max-Min was operated at 4 frequencies, ranging from 220 to 14080 Hz, while the coil separation was set to 100m. A station spacing of 10m was selected. The results of the electromagnetic data are shown in Figure 3-50.

The electromagnetic response is typical to that obtained over a valley discontinuity in the overburden. A negative response in both the in-phase and out-of-phase is flanked by two positive shoulders, indicating a conductive host, interpreted as the Tshipise Fault zone. The high shoulder to the SSW shown in frequency 220 to 3520 Hz indicates the fault to be southerly dipping, as expected due to southerly directed extension (Figure 3-8).

Magnetic Survey
The magnetic survey was conducted from the N to the S over the fault zone with a station spacing of 10m. The results of the magnetic data are shown in Figure 3-50.

The magnetic data shows a stable response for the first 140m, reflecting the gneisses and quartzites of the Limpopo Belt. At 150m a distinct drop in the magnetic intensity of 350nT indicates a change in the subsurface lithology. This signature represents a flat lying magnetic geological body, believed to represent Karoo basalts. It has an approximate width of ca. 60m.

At 210m a second magnetic low indicates the other contact of the basalt with Karoo sandstone.

A borehole was drilled at 150m, south of at the fault zone that represents the contact between the LMB and Karoo basalt in order to intercept the fault at depth (H26-0427). Another borehole was drilled at 210 m in order to intercept the contact with Clarens Formation rocks (H26-0434), however, this borehole had similar lithology and intercepted Karoo basalt and LMB quartzite (Appendix 3-B).

LMB10 – NE-SW running fault zone

Site description

The site covers a mapped ca. 2.5km long fault zone through Alldays Gneiss striking NE to SW (Figure 3-47). The fault is mapped on the 1:250000 geological map Alldays, but leaves no imprint on the morphology at the site itself.

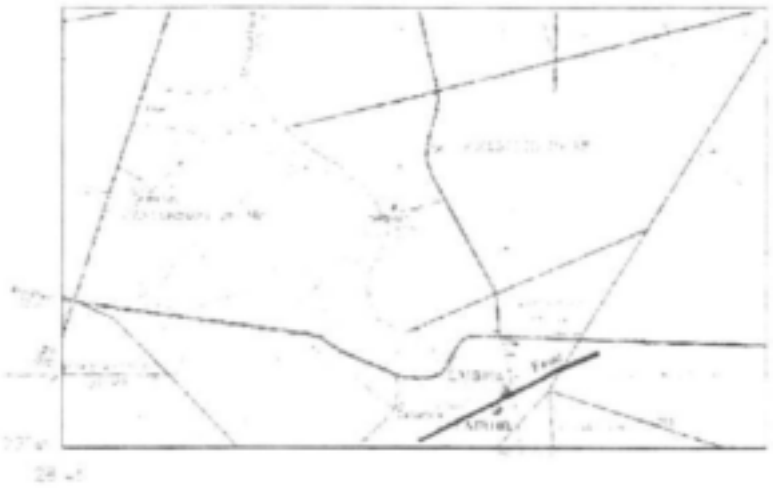

Figure 3-46 Location of LMB10

Electromagnetic survey

The Max-Min was operated at 4 frequencies, ranging from 220 to 14080 Hz while the coil separation was set to 100m. A station spacing of 10m was selected. The results of the electromagnetic data are shown in Figure 3-51.

The electromagnetic response at LMB10 indicates a shallow conductive host from 190m to 290m, flanked by two positive response shoulders reflecting more resistive rocks to the north and south, however, the response is not very pronounced. This valley discontinuity is most pronounced in the out-of phase and in the frequencies 14080 to 3520 Hz, indicating a shallow depth. This may suggest that the fault is not the tectonic contact between differing lithologies, but may represent synthethic strike-slip movement, which has subsequently resulted in a deeper weathered profile. The relatively higher response shoulder to the North indicates the conductor to dip to the South. A second negative peak is recorded towards the end of the traverse and could indicate a second conductive zone from station 400m onwards.

Magnetic Survey

The magnetic data shows a steady decrease in magnetic intensity from the north to the south, until at 230m a sudden drop followed by a magnetic high indicates a change in the subsurface lithology. No anomaly was detected at this point by the Max-Min profile. This magnetic anomaly is believed to indicate the fault zone. Thereafter, the magnetic intensity remains stable with values around 29150 nT.

A borehole (H26-0429) was drilled on the magnetic anomaly but a fault was not observed. The presence of mafic minerals may explain the magnetic anomaly. A shallow weathered zone aquifer was detected at the bedrock contact (27m), explaining the shallow electromagnetic anomaly.

A second borehole (H26-0430) was drilled at 480 m to investigate the second electromagnetic anomaly. This borehole also intercepted a shallow bedrock contact aquifer.

Resistivity Sounding

A resistivity sounding was carried out at distance 235m of the electromagnetic traverse and magnetic traverse, at the northern edge of the trough like electromagnetic anomaly. The direction of AB extension paralleled the geophysical traverses. The sounding curve is shown in Figure 3-56.

The sounding curve represents a three layered earth case of a A-type curve with $\rho1<\rho2<\rho3$. The sounding data indicates a thick weathered/fractured overburden of ca. 50m for the site. By fitting the field curve to the master curve A9 the following values for the three layers could be determined:

	Thickness (m)	Resistivity (Ωm)
Layer 1	2	420
Layer2	50	600
Layer3	∞	resistive bedrock

A 27 m thick weathered zone was confirmed by drilling.

LMB15 – NE-SW running fault zone

Site description

A fault zone mapped on the 1:250000 geological map Alldays was the target of geophysical traverse LMB15 (Figure 3-48) using magnetic only. The feature is mapped as being of 9.5km extent, but has no reflection in the morphology. The site is flat and quaternary covered with no outcrops of the underlying Limpopo host rock being present.

Magnetic Survey

The magnetic profile was from the South to the North with a station spacing of 10m. The data is shown in figure 3-48.

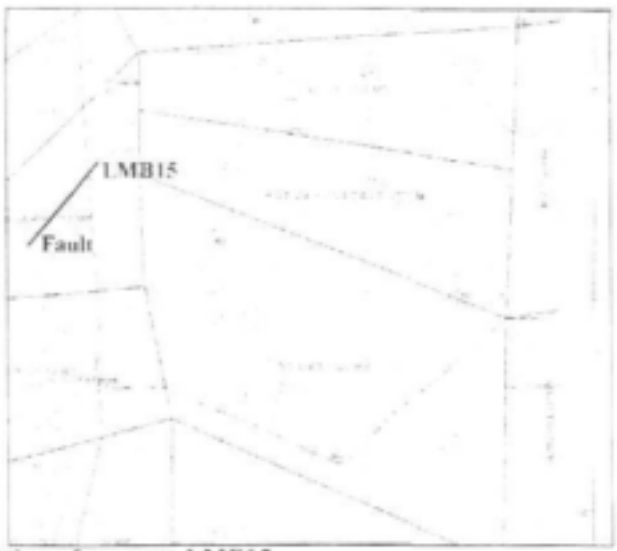

Figure 3-47 Location of traverse LMB15

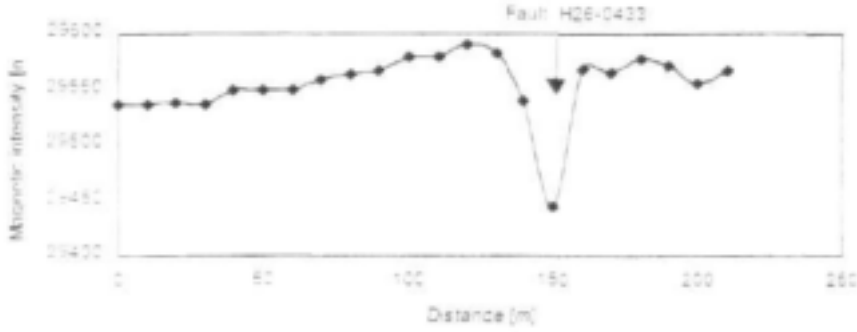

Figure 3-48 Magnetic data for site LMB6. Station spacing 10m, traverse direction: S-N

The magnetic data generates a well-defined anomaly from station 135m to 155m. The anomaly could indicate the edge of a magnetically enriched layer, which may be attributed to amphibolite bands. The magnetic intensity increases from north to south, hence a remnant magnetization has to be assumed.

A borehole (H26-0433) was drilled on the magnetic anomaly but proved to be dry.

3.6.3 Lineaments

A comparison between the geological map in the study areas and the generated LANDSAT lineament map revealed that the vast majority of lineaments were identified along lithological boundaries. These often represent contacts related to Precambrian ductile deformation, hence may not be of hydrogeological significance if no subsequent brittle deformation took place.

LMB6 – N-S running lineament

Site description

A N-S running lineament was detected through the study of aerial photographs. The lineament had no morphological expression in the field. The area is covered by quaternary deposits and is flat (Figure 3-49).

Electromagnetic survey

The Max-Min was operated at 4 frequencies, ranging from 220 to 14080 Hz while the coil separation was set to 100m. A station spacing of 10m was selected. The results of the electromagnetic data are shown in Figure 3-52.

The electromagnetic response over the lineament is largely inconclusive. A positive peak in the in-phase and out-of phase at station 150m might indicate a local change in the subsurface conductivity, however, no pronounced anomaly is observed.

Magnetic Survey

The magnetic data indicates a steady decline in the magnetic intensity from south to north. No anomaly is recorded and the changes in response amplitude are believed to reflect different magnetic properties in the host rock (Figure 3-52).

Figure 3-49 Location of traverse LMB6

A borehole (H26-0428) was drilled at 150 m on the electromagnetic anomaly, which proved to be dry. This highlights the problem of reliance on remotely sensed lineaments in this area.

3.6.4 Magnetic Structures

Magnetic intrusions mapped by airborne geophysics are very common in study areas I and II and occur as sills and dykes. The preferred orientations of the dykes are NE-SW to ESE-WNW, corresponding to the orientation of maximum tensional strain. A total of five magnetic structures were investigated in the study area and one example of their geophysical response is given below.

LMB9 – Sill like structure

Site description

A sill-like structure mapped on the 1:250000 geological map Alldays was the target of traverse LMB9. The feature runs from ESE to WNW and was traversed in an approx. 90° angle. The site itself is quaternary covered and no outcrop is present. The area is flat except for a very gentle dip centred on the feature (Figure 3-49).

Electromagnetic Survey

The Max-Min was operated at 4 frequencies, ranging from 220 to 14080, Hz while the coil separation was set to 100m. A station spacing of 10m was selected. The results of the electromagnetic data are shown in Figure 3-53.

The conductivity data for LMB9 produced no pronounced anomaly. However, at 340m a distinct ramp discontinuity can be observed in the in-phase and out-of phase throughout all frequencies. This coincides with the edge of the sill like structure.

Magnetic Survey
The magnetic survey was conducted from the SSE to the NNW over the feature, applying a 10m station spacing.

For the first 340m, the magnetic intensity is stable, indicating a homogeneous subsurface lithology, with values varying around 29000nT. The sill is encountered at 350m, where an increase in the total field intensity occurs. Values increase for about 100m before the field intensity drops to constant levels around 29600nT. The shape of the anomaly indicates a sill like structure, dipping gently to the NNW. The total magnetic field intensity anomaly, with a typical dipolar negative in the south and an increase in the north of the structure, indicates a normal magnetization. The step in amplitude is nearly 1000nT.

A borehole was drilled at 350 m (H26-0432), which proved to be dry. The magnetic anomaly can be attributed to the presence of bands of mafic minerals. This highlights the problem of the interpretation of magnetic and electromagnetic anomalies. In many cases, lithological variations, or variations in overburden thickness generate geophysical anomalies that are not hydrogeologically significant.

3.6.5 Other structures

A few other targets of possible hydrogeological significance were investigated in both study areas. In study area II massive pegmatite veins occur and possibly form a groundwater target. In addition, the hydrocensus indicated that in both study areas that streams with their alluvial cover might be groundwater targets and could in some areas be a preferred option compared to drilling into the low permeability host rock of the LMB.

LMB19 – Pegmatite vein
Site description
An observed pegmatite vein approximately 10m thick was the target of traverses LMB19. The vein consists mainly of quartzite and feldspar crystals of several cm in size. The contact with the gneissic host rock is marked by a 1 m thick weathered zone. The vein forms a small topographical height in the otherwise flat surrounding.

Electromagnetic Survey
The Max-Min was operated at 4 frequencies, ranging from 220 to 14080 Hz while the coil separation was set to 100m. A station spacing of 10m was selected. The results of the electromagnetic data are shown in Figure 3-54.

The electromagnetic response is typical to that obtained over the edge of a ramp discontinuity in the overburden. A positive peak response predominantly in the out-of phase component is observed on the first 90m of the traverse, indicating a resistive host of gneisses of the Limpopo Mobile Belt. Subsequently, a decrease in response amplitude characterises the change in lithology due to the pegmatite vein.

Although this anomaly was promising, it was not drilled since it was not located in Bochum, hence was outside the constraint related to restricting drilling to rural areas.

Magnetic survey
The magnetic data generates a homogeneous response over the entire traverse. The magnetic intensity decreases slightly from E to W, but no anomaly is observed (Figure 3-55).

Resistivity sounding
The resistivity sounding on site LMB19 was carried out at position 240m of the electromagnetic traverse on the eastern contact between the pegmatite vein and the host rock.

The direction of the AB expansion paralleled the geophysical traverses. The sounding curve is shown in Figure 3-57.
The sounding curve indicates that it is a three layer H-type curve with $\rho1>\rho2<\rho3$. By curve matching using the master curve H25, the following values for the three layers are determined:

	Thickness (m)	Resistivity (Ωm)
Layer1	2	180
Layer2	20	18
Layer 3	resistive bedrock	

This indicates the presence of a potential shallow weathered zone aquifer (<22m depth), however, it was not drilled as this was considered too shallow to be indicative of a major structure.

LMB5 – Contact between the Karoo Sandstones and Limpopo Belt gneisses

Site description

Traverse LMB5 targeted the ENE trending contact between the Karoo sandstones and the Limpopo Mobile Belt rocks. At this site the contact is covered by a seemingly thick quaternary overburden. The contact of both lithologies is discontinuous due to faulting, however, at the site no fault zone has been mapped, probably due to the contact being under Quaternary cover. The Tshipise fault, which is the contact with Karoo basalt, only occurs further to the south of the site. The geophysical traverse was conducted from the SSE to the NNW, starting on sandstone rocks of the Clarens Formation, and continuing onto a 100m wide zone of quaternary cover overlying the gneisses of the Limpopo Belt.

Electromagnetic Survey

The Max-Min was operated at 4 frequencies, ranging from 220 to 14080 Hz, while the coil separation was set to 100m. A station spacing of 10m was selected. The results of the electromagnetic data are shown in Figure 3-55.

The electromagnetic data is characterised by two minima in both the in-phase and out-of phase, located on either side of a ridge, where both phases reach a response maximum. The ridge discontinuity is more pronounced at 200 m and is likely to represent a fault with a shallow dip to the north. On either side of this ridge discontinuity are troughs of lower conductivity material. The less conductive trough to the north is probably related to the dry low conductivity Quaternary overburden. The decreasing conductivity with distance to the north probably indicates an increasing thickness of quaternary cover. The fact that this trough is increasingly prominent with increasing frequency indicates that it is a shallow lying feature, hence it is probably related to the Quaternary overburden.

Magnetic Survey

The magnetic traverse was conducted from the SSE to the NNW over the geological boundary using a station spacing of 10m.

The magnetic response is characterised by a magnetic high over the Karoo sandstones and the gneisses of the Limpopo Belt. Both flank a magnetic low of about 100m. The response reflects the anomaly over two plate like bodies, believed to be the Karoo Sandstone in the South and the LMB rocks towards the North.

A borehole (H26-0426) was drilled at 280 m to intersect the shallow dipping structure. A 3 m thick clay was intercepted between highly weathered gneiss and weathered gneiss. This was underlain by quartzite veins, however, no water was encountered. This suggests that the

structure is most likely a Pre-Karoo shear. A water strike (0.4 l/s) was obtained at a dolerite dyke contact in amphibolite. Hence, the magnetic anomaly can be characterised as a northerly dipping dolerite structure.

Resistivity Sounding

A resistivity sounding was carried out at the locality 280m of the magnetic and electromagnetic traverse at the southern edge of a trough-like EM anomaly where quaternary overburden is encountered (Figure 6-59). The subsurface can be described as a six layer earth case, with a thin soil cover over more resistive rock. From about 15 to 40m a more conductive weathered fractured zone is encountered before solid bedrock is reached.

LMB28 – Alluvium at the Mogalakwena River

The hydrogeological significance of alluvial cover in the LMB was only examined by drilling since it was presumed to be shallow feature. No geophysical surveys were undertaken.

Conclusions

Regional scale fault lines were identified as valley discontinuities with the Max-Min system. However, these can be identified by field observation. These structures are more prominent using magnetics, however, magnetics frequently generated anomalies related to bands of mafic minerals unrelated to faults or water bearing structures. Smaller scale faults, especially those covered by quaternary deposits, often have no magnetic nor EM signature, hence it was not possible to locate the feature in the field without extrapolating the structure from observed outcrops. This implies that geophysics in isolation, without structural evidence of a fault, is problematical and would be inconclusive in identification of target features.

Caution needs to be applied in terms of interpreting the geological origin of magnetic anomalies, as besides dolerite and diabasee sills and dykes, amphibolites do occur in the LMB lithologies and could generate similar magnetic response. Magnetic responses can also be attributed to mineralogical variations as a result of granulite facies metamorphism. The magnetic structures seldom left an imprint on the EM profiles, implying that there might be no weathered conductive zone accompanying these structures, which would impact negatively on their hydrogeological significance.

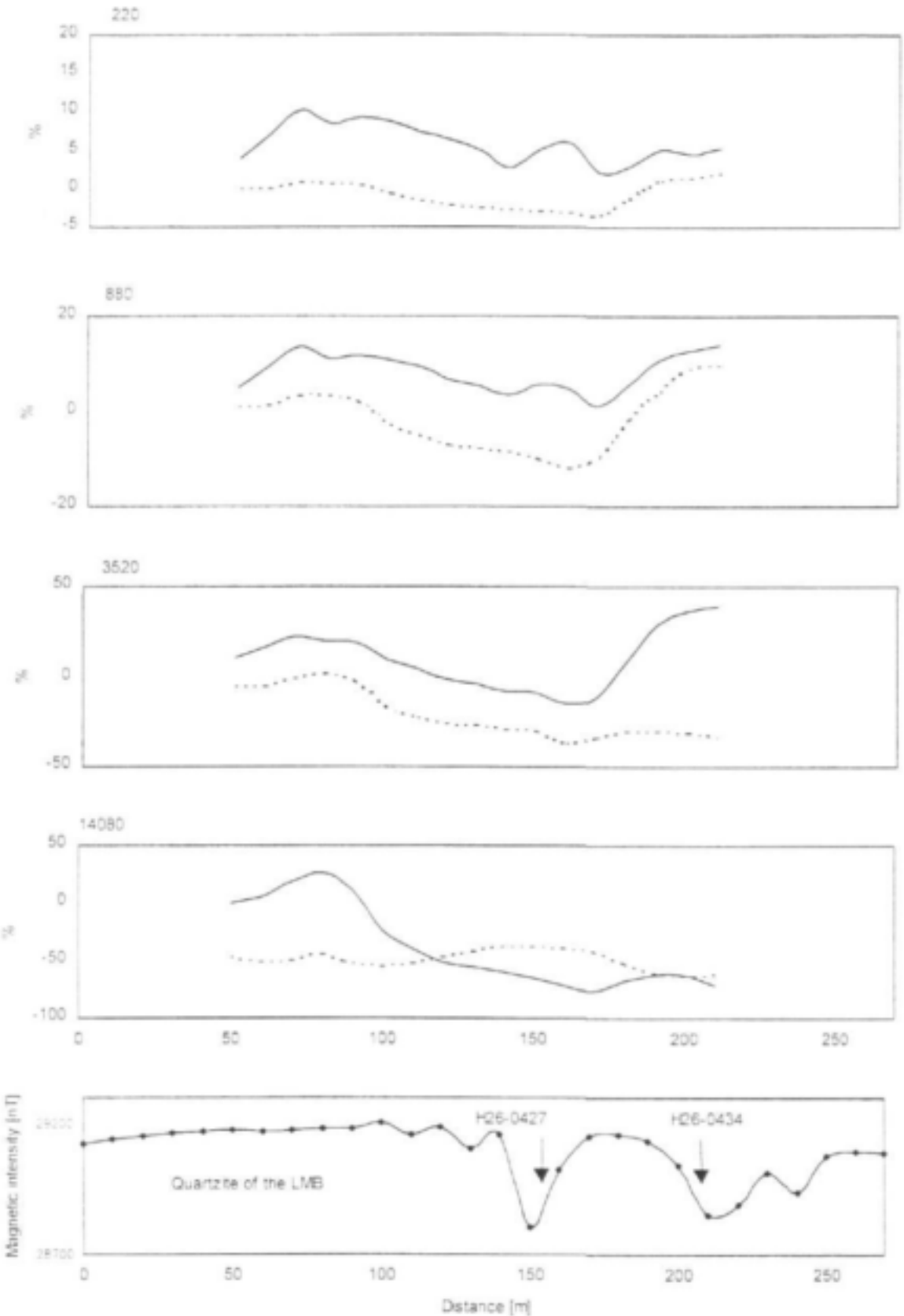

Figure 3-50 MAX-MIN electromagnetic and magnetic profiles at site LMB13. Solid line: in-phase [%]; dotted line: out-of phase [%]; coil separation 100m, station spacing 10m. Traverse direction: N-S

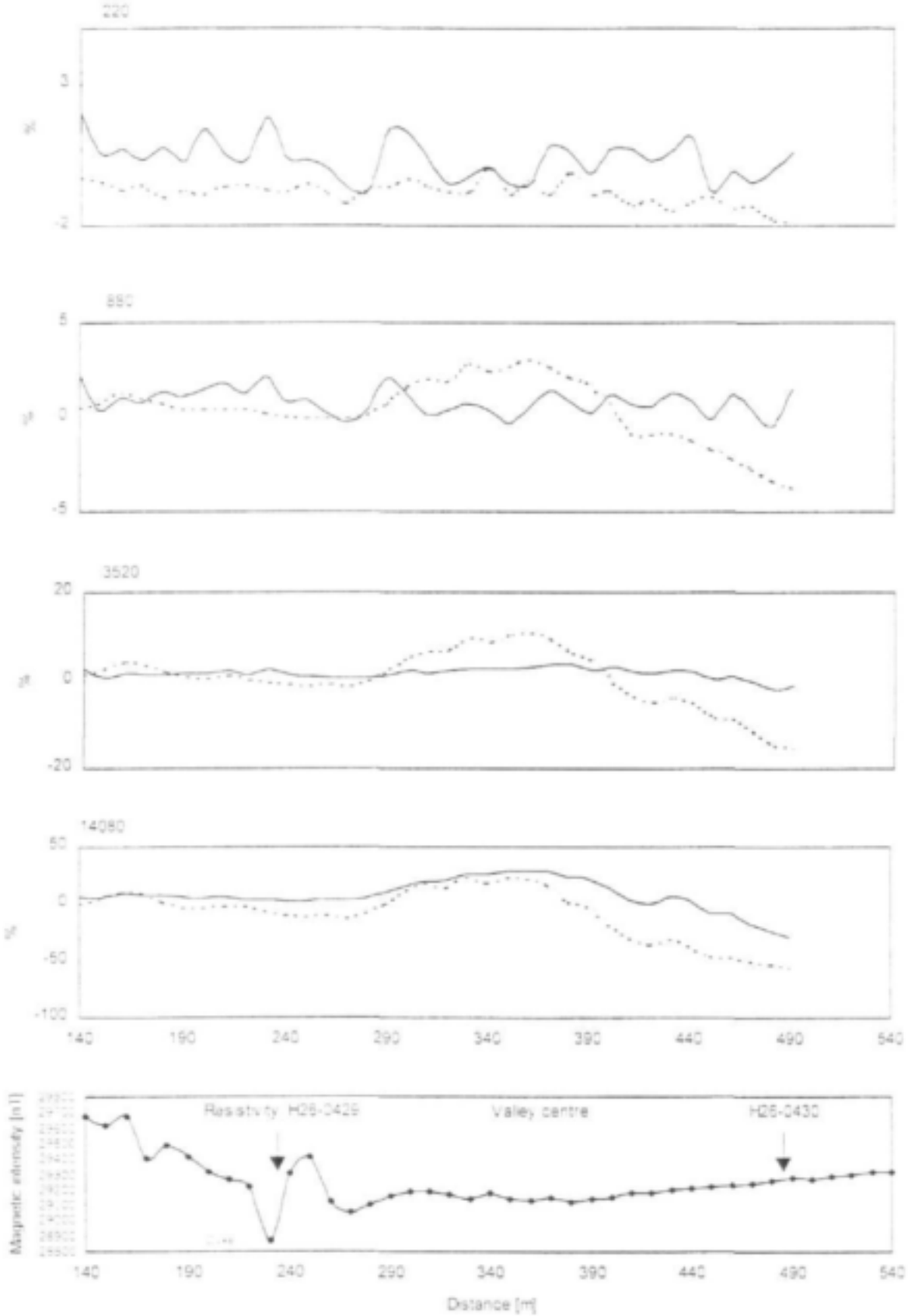

Figure 3-51 MAX-MIN electromagnetic and magnetic profiles at site LMB10. Solid line: in-phase [%]; dotted line: out-of phase [%]; coil separation 100m, station spacing 10m. Traverse direction: NNW-SSE

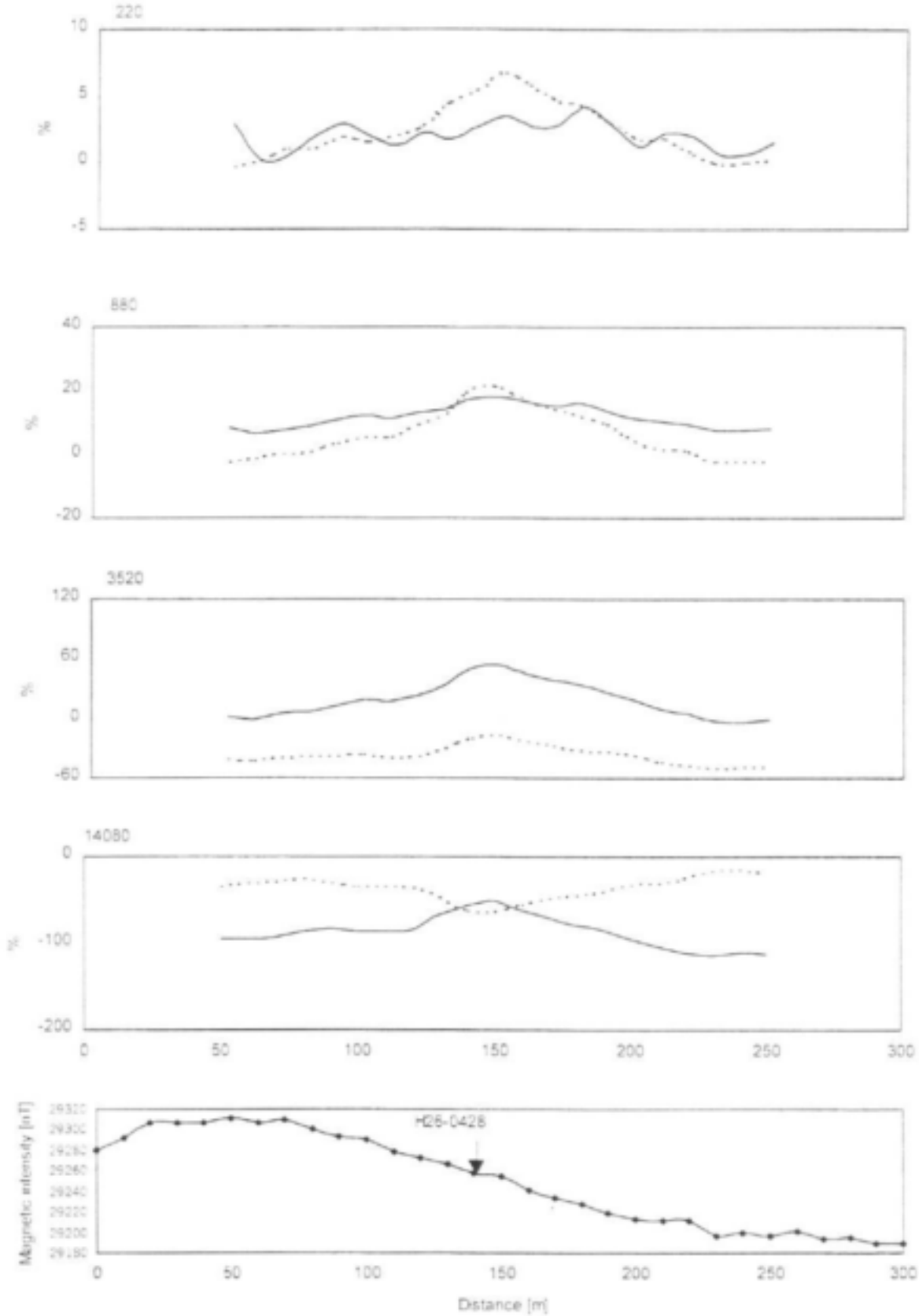

Figure 3-52 MAX-MIN electromagnetic and magnetic profiles at site LMB6. Solid line: in-phase [%]; dotted line: out-of phase [%]; coil separation 100m, station spacing 10m. Traverse direction: S-N

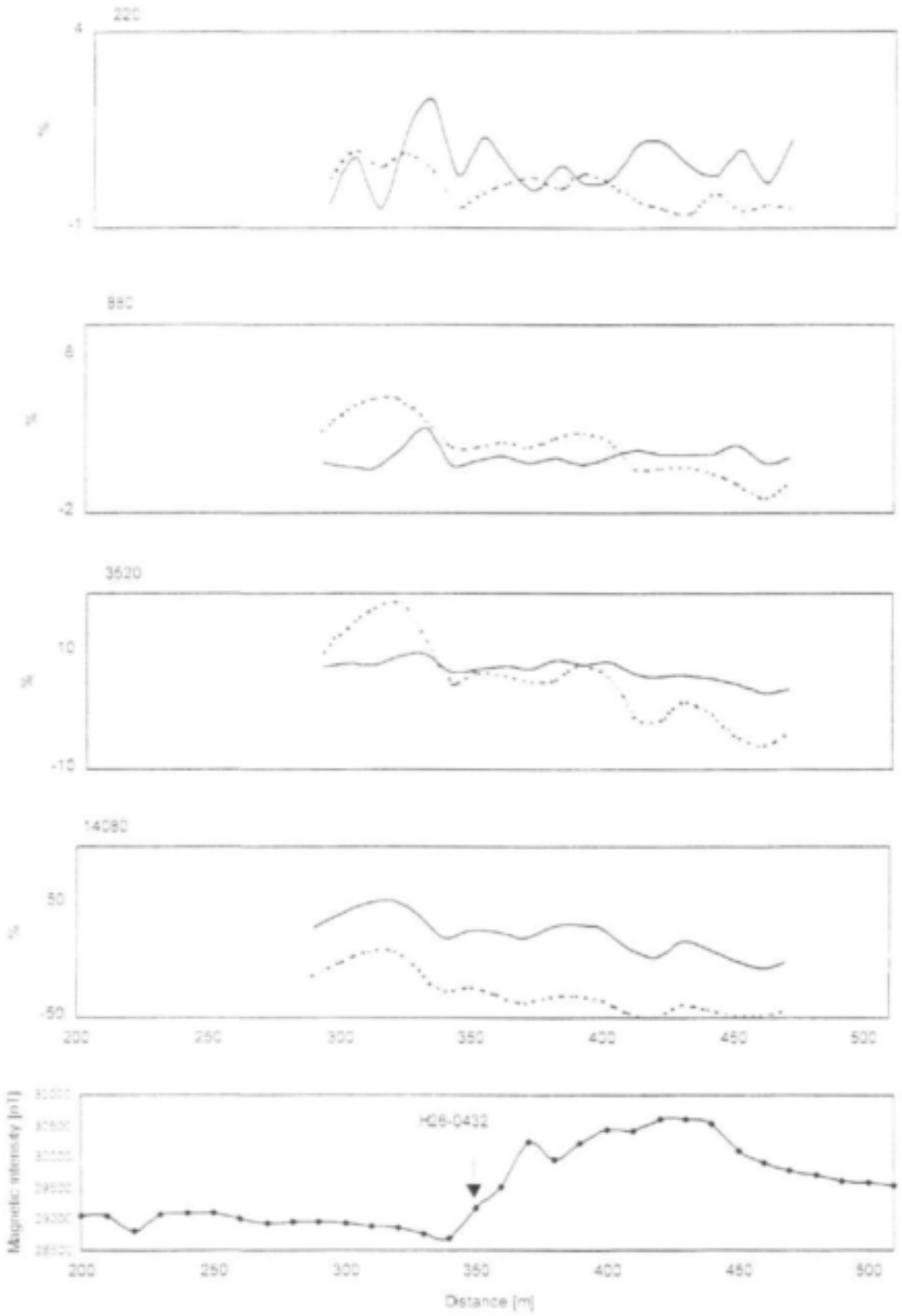

Figure 3-53 MAX-MIN electromagnetic and magnetic profiles at site LMB9. Solid line: in-phase [%]; dotted line: out-of phase [%]; coil separation 100m, station spacing 10m. Traverse direction: SSE-NNW

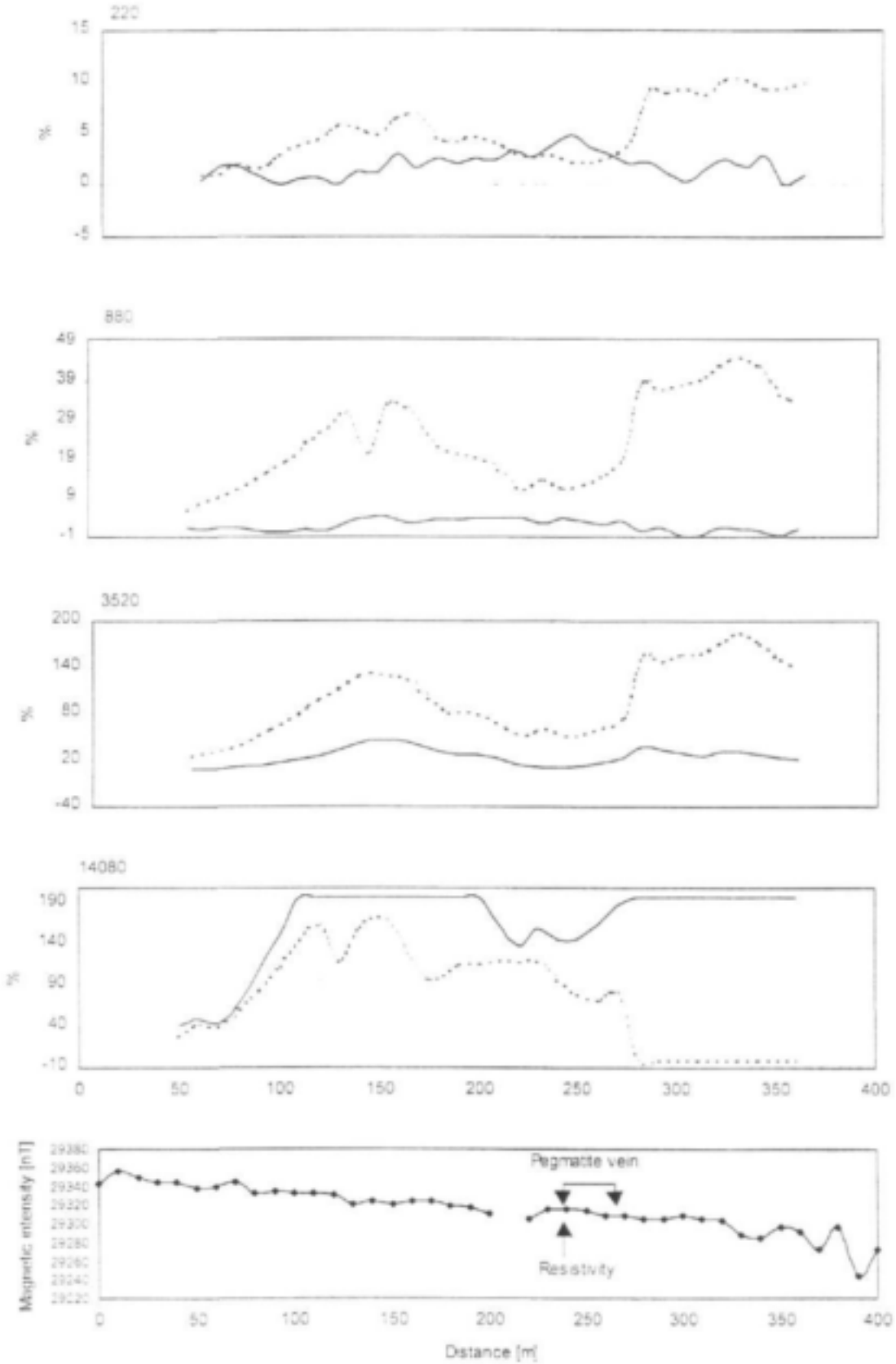

Figure 3-54 MAX-MIN electromagnetic and magnetic profiles at site LMB19. Solid line: in-phase [%]; dotted line: out-of phase [%]; coil separation 100m, station spacing 10m. Traverse direction: E-W

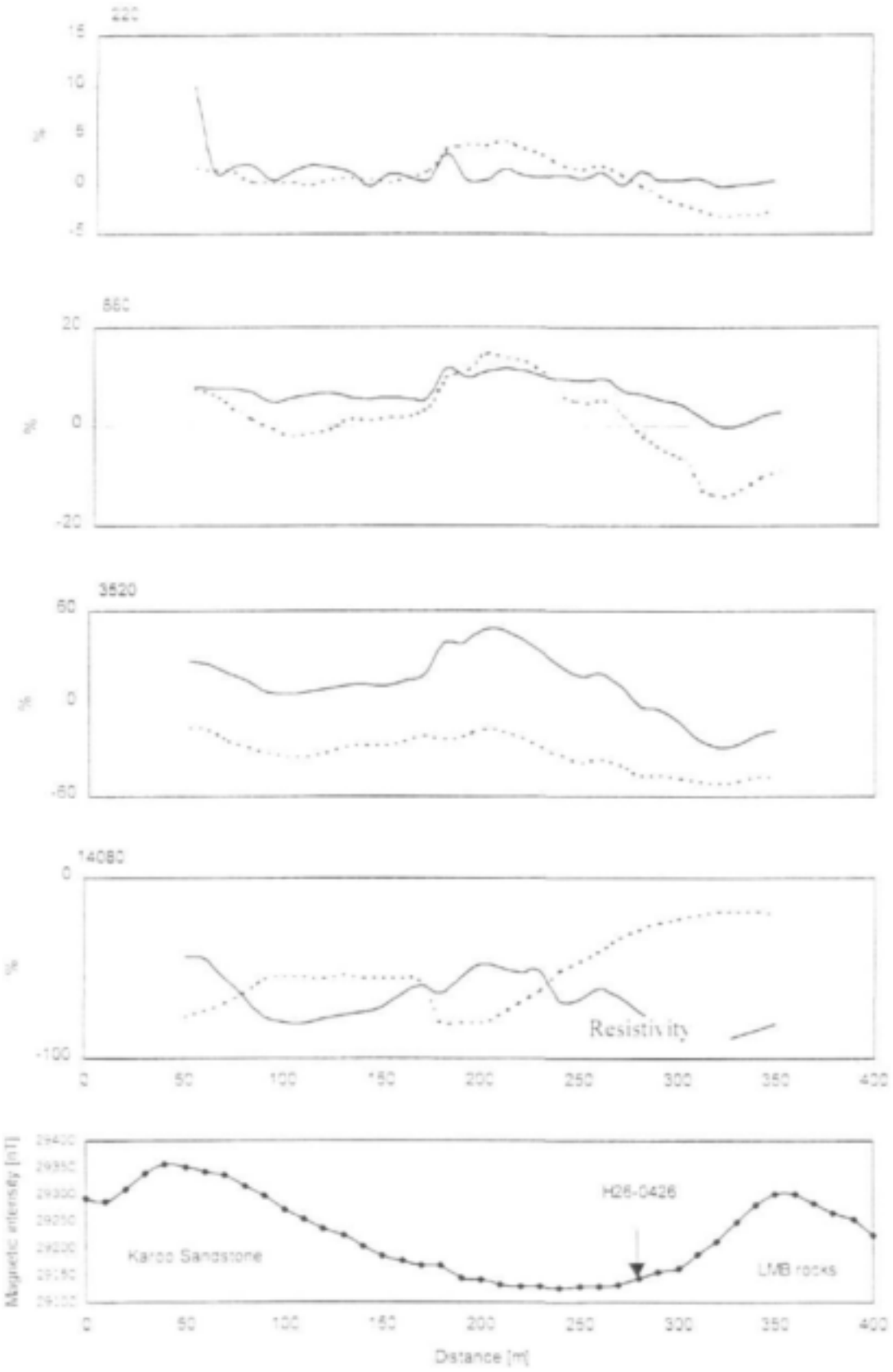

Figure 3-55 MAX-MIN electromagnetic and magnetic profiles at site LMB5. Solid line: in-phase [%]; dotted line: out-of phase [%]; coil separation 100m, station spacing 10m. Traverse direction: SSE-NNW

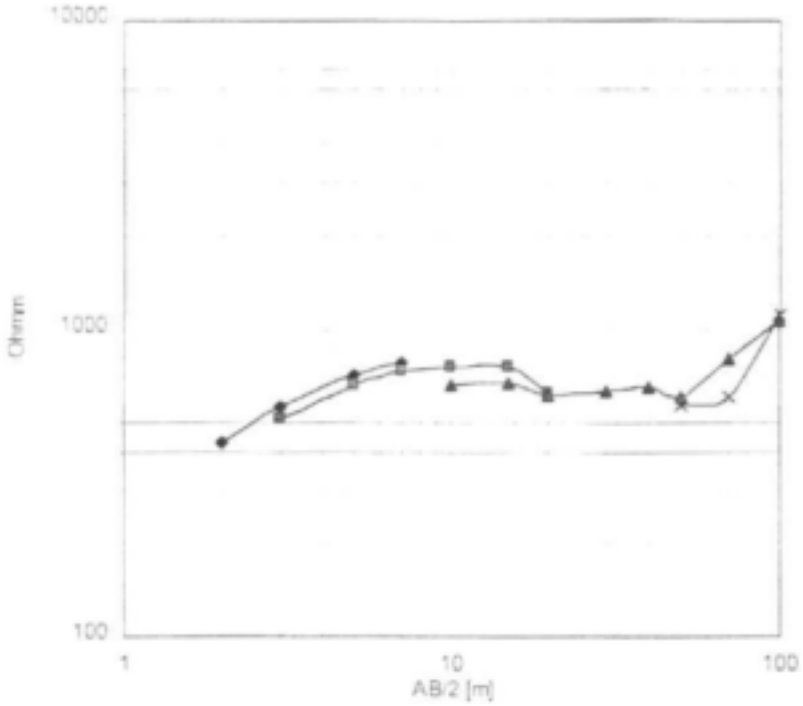

Figure 3-56 Resistivity data at station LMB10

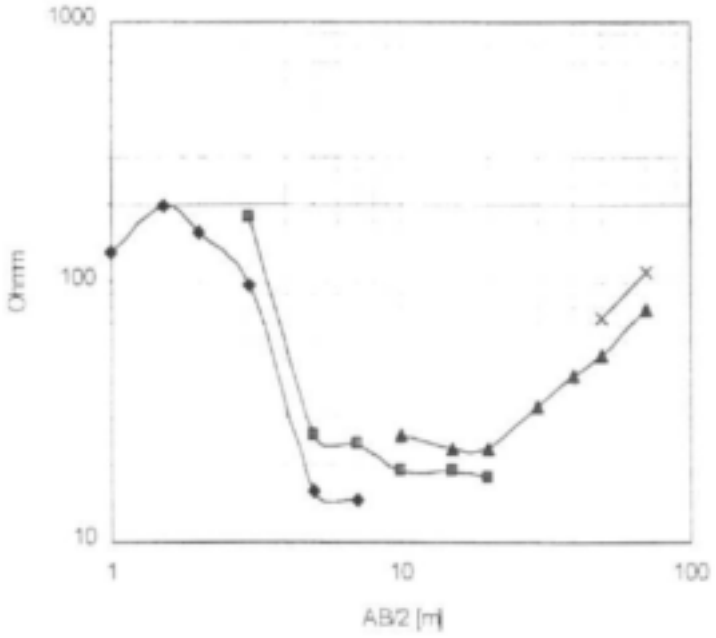

Figure 3-57 Resistivity data at station LMB19

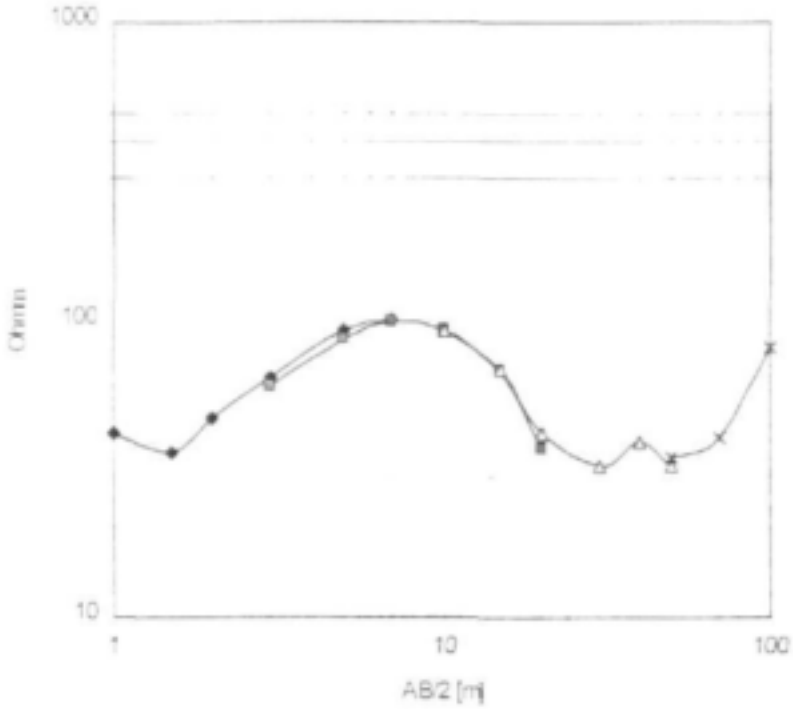

Figure 3-58 Resistivity data at station LMB5

Electromagnetic exploration is based on the assumption that anomalies representing water-bearing fracture zones are distinguishable from other conductors in the weathered zone. The significant depth of weathering (down to 43 mbgl) found in boreholes (Appendix 3-A) suggests that near surface contrasts resulting from variations in degree of weathering may be the cause of anomalies.

Lineaments identified by remote sensing can identify lithological features with little or no hydrogeological significance due to banded nature of the lithologies, hence field proofing of their structural significance is necessary.

3.7 Drilling Results

To investigate identified geological and structural features in the Limpopo Mobile Belt, nine boreholes were drilled. Drilling was restricted to the portion of research area I occupied by the Bochum District so that the boreholes could be utilised by rural black communities. Drilling was undertaken by the Department of Water Affairs and Forestry using air percussion.

The drilling sites were chosen to characterise fault zones, lineaments, magnetic features and alluvial deposits, as delineated by the structural and geophysical investigations. The geological logs and construction details, which are shown in Appendix 3-B are summarised in Table 3-5 in terms of depth, water strike, blow yield and geological feature investigated.

Table 3-5 Summary of Drilling Results

Borehole	Depth [m]	Water strike [m]	Blow Yield [l/s @ depth]	Feature	Site ID of geophysical survey
H26-0426	90	42m	0.4 l/s @ 42.5 m	Tectonic contact	LMB5
H26-0427	92	Seepage 18.5m Water strike 56m	4.0 l/s @ 56-92 m	ENE Tshipise Fault	LMB13
H26-0428	108	Dry	-	N-S running lineament	LMB6

H26-0429	90	Seepage: 19m. Water strike: 27m	2.1l/s @ 27m	NE-SW striking fault	LMB10
H26-0430	96	Seepage: 12m Water strike: 19m	3.9 l/s @ 19/21 m	NE-SW striking fault	LMB10
H26-0431	66	6m	1 l/s @ 6m	Alluvium	LMB28
H26-0432	96	Dry		ESE-WSW running Dyke	LMB9
H26-0433	90	Dry		NE-SW running fault	LMB15
H26-0434	66	Seepage: 11m, 18m. Water strike: 55m	1.7l/s @ 55m	Tshipise fault	LMB13

Borehole H26-0426 on site LMB5

Borehole site

Borehole H26-0426 was drilled to investigate the presumed extensional ENE trending lithological contact between the Clarens Formation and gneisses of the Limpopo Belt, which is discordant, but no fault zone is mapped due to quaternary cover. The contact was believed to be tectonic in nature and was presumed to be a normal fault (3.2.4). The geological boundary separates sandstones outcropping in the south from gneisses exposed in the north. In between is an approximately 100m wide zone where the depth of weathering increases and a thick soil cover is developed. Borehole H26-0426 is drilled on the geophysical traverse LMB5 on position 285m into the Limpopo rocks.

Geological description

Borehole H26-0426 is characterised by rapidly changing lithologies. After penetrating a 1m thick soil cover, a 27 m thick weathered zone was encountered. Down to a depth of 17m, weathered gneiss with varying contents of red feldspar, black hornblende and green epidotite is encountered leading to a rapid change of colours. After 17m the degree of weathering increases and weathered clayey gneiss gives way to a 5m zone of brown clay. This could represent a steeply dipping fault zone in the Beit Bridge Complex. From 23 to 28m a red to dark brown weathered gneiss is encountered., with a solid 2m thick quartzite vein at 28 m. From 30 to 44m lithologies change rapidly form reddish-brown gneisses with a high content of feldspar, to black and white gneisses where feldspar is nearly absent and black amphibolites. The presence of amphibolite in the gneiss sequence could be indicative of a metamorphosed intrusive dyke. The amphibolite facies suggests an M3 to M4 origin for the dyke, hence its association with the Limpopo orogeny and suggests that the dyke could have intruded into a normal fault zone. The last two meters are strongly fractured and form the upper weathered contact for a two meter thick black dolerite dyke. The presence of dolerite at the amphibolite contact suggests that the dolerite intruded into a rejuvenated fault zone. Water was hit within the fractured amphibolite at the upper contact of the dolerite dyke at 42.5m and the blow yield was measured to be 0.4 l/s. From 43m down to the final depth of the hole, interlayered bedding of black amphibolite and gneisses with varying contents of red to pinkish feldspar, black hornblende, green epidotite and quartzite was encountered. Fracturing occurs at several depths intervals, all infilled with calcite. Calcite veins up to one meter thickness were observed.

The presence of gneiss below the fault zone instead of sandstone suggests that the borehole missed the suspected fault between the gneiss and sandstones. The borehole should preferably have been drilled further south at 170 m on the geophysical transect (Figure 6-56).

The borehole was cased off down to 29m using solid steel casing. The final blow yield was measured to be 0.4 l/s and the hole was developed for 30min by airlift. The static water level is at 26.54 mbgl.

Borehole H26-0427 and H26-0434 on site LMB13

Borehole site

An ENE to E trending regional scale fault zone, separating the LMB rocks in the north from Karoo basaltic lava in the south, was the target of boreholes H26-0427 and H26-0434. This fault, known as the Tshipise fault zone, is mapped on the 1:250 000 geological map Alldays and has been shown to be an extensional normal fault in nature (3.2.4). The boreholes were sited on position 155m and 210m of the geophysical traverse.

Geological description

Borehole H26-0427

A 2m thick soil cover overlays a thick overburden sequence containing greenish quartzite rocks of the LMB and basalt of the Karoo SuperGroup. From 12m onwards, basalt is penetrated. The profile is highly weathered up to a depth of 39m. Seepage occurred at 18.5m within the weathered zone. Solid basalt is encountered up to a depth of 53m. From 53 to 55m a highly weathered layer of basalt preceded a highly fractured fault zone, consisting of light brown pure quartzite, which confirms a southerly dipping fault. The water strike was encountered at 56m and yield exceeded 20 l/s. Yield increased steadily until the final depth of the hole of 72m. Further penetration was hindered by water inflows and drilling had to be stopped at 72m due to the highly fractured nature of the fault zone, which produced cuttings of up to 8cm in size.

The borehole was cased down to 41m using solid steel casing. The final blow yield is higher than 23 l/s and estimated to be around 40 l/s, which confirms the extensional orientation of ENE structures. The hole was developed for 30min by airlift.

Borehole H26-0434

A second pronounced anomaly further south on the magnetic traverse was the site for borehole H26-0434.

The lithology penetrated proved to be similar to H26-0427. After penetrating 5m of overburden, highly weathered basalt is encountered. Seepage occurred at 11 and 18m within this weathered zone. Fractured basalt follows from 30 to 55m, where the highly fractured fault zone consisting of pure LMB quartzite is encountered. The water strike at 55m yields water in excess of 17 l/s. Drilling had to be terminated due to nature of the highly fractured zone, which produced cuttings of several cm in diameter.

The borehole was cased off with solid steel casing from 0 to 17m and slotted casing from 17 to 30m. The borehole was developed by airlift for 30min.

Borehole H26-0428 on site LMB6

Borehole site

An N-S trending lineament identified on the aerial photographs forms the site for borehole H26-0428. Such structures are presumed to be compressional in nature. The borehole is sited at position 140m on traverse LMB6.

Geological discussion

Borehole H26-0428 was drilled into Karoo rock covering LMB rocks. The hole penetrated weathered Karoo sandstone for the first 43m. Colours vary between red, brown and greyish brown and the consistency of the weathered lithology is slightly clayey to clayey. From 43m until 65m a solid dark greyish gneiss was penetrated, indicating that a southerly dipping fault zone has been encountered. However, no associated fracturing is evident and the underlying gneiss is only slightly weathered. This confirms that northerly structures are compressional in nature. From 66m onwards the feldspar, epidotite and mafic mineral content changes frequently, and subsequently inter-layering of greenish, greyish and pinkish gneisses are encountered. With a decrease in the penetration rate at 90m depth, a quartzite is encountered.

High contents of epidotite results in the rock a whitish-greenish appearance. The lithology remains consistent until the final depth of the hole, 108m. No water was encountered and subsequently the hole was backfilled.

Borehole H26-0429 and H26-0430 on site LMB10

Borehole site

A SW-NE running fault zone mapped on the 1:250000 geological map Alldays formed the site for borehole H26-0429 and H26-0430. These structures are postulated as being synthetic strike slip shears (6.2.4). The boreholes were sited on station no. 235m and 490m on the geophysical traverse LMB10, where the electromagnetic data indicates a thickening of the conductive overburden.

Geological description

Borehole H26-0429

Borehole H26-0429 was drilled into Alldays Gneiss. The first 28m of the hole constitute of weathered, greyish, sometimes pinkish gneiss, which is in very weathered patches slightly clayey. Seepage was encountered at 19m, still within the weathered zone. The main water strike was encountered at 27m, the contact between the weathered and solid bedrock. The yield was measured to be 2.1l/s. From 29m, solid gneiss was encountered. A dark, greyish-black gneiss was penetrated changing at 37m into a greyish-pinkish gneiss and the hole stayed within the same lithology until the final depth of 90m.

The weathered zone was cased off with solid steel casing up to 11m depth and slotted casing being installed from 11 to 29m. The final blow yield of the borehole was 1.9l/s and the hole was developed for 30min using airlift. The static water level is at 10.91 m, and is probably affected b the slotted casing below, which encourages water loss from the borehole into the formation. Consequently, the true piezometric surface is probably higher.

Borehole H26-0430

A 3 m thick soil cover overlays weathered red gneiss until 22m. A first water strike was encountered at 12m, with a yield of 0.1l/s. The main water strike was hit at 19m at the bottom end of the weathered zone. The yield was measured at 3.9l/s at 23 m. From 22m until the final depth of the hole at 96m the lithology stayed unchanged, penetrating red solid gneiss. However, from 67m onwards the quartz content of the rock is decreasing, while the red feldspar component increases until the gneiss is nearly entirely made up by red feldspar and hornblende.

Solid steel casing was installed from 0 to 13.5m, while slotted screen from 13.5 to 23m was installed. The final blow yield after casing the hole was measured to be 0.5 l/s. The decline in yield after installation of the casing implies that the slotted casing and backfilled drill cuttings sealed of the water strike. The hole was developed for 40min using airlift. The static water level is 6.75 m.

Borehole H26-0431 on site LMB28

Borehole site

Possible groundwater targets in the area are shallow aquifers in the alluvial cover along streams and rivers on a stretch where the river is northerly flowing. Therefore borehole H26-0431 was drilled next to the Mogalakwena River into the alluvium.

Geological description

Borehole H26-0431 penetrated a thin alluvial cover of 4m, before encountering highly weathered and fractured amphibolite. Water was hit at 6m, at the amphibolite/gneiss contact with a blow yield of 1l/s. Up to the final depth of the hole solid gneiss was encountered with varying content of feldspar and mafic minerals. The shallow nature of the amphibolite

suggests a shallow dipping sub-horizontal layered intrusion lying over intrusive Alldays Gneiss.

Solid steel casing was installed from 0 to 5m followed by slotted casing down to 11m depth. The final blow yield was measured to be 11/s. The hole was developed for 30min by airlift. The static water level was 2.84 m.

Borehole H26-0432 on site LMB9

Borehole site

An ESE-WNW trending magnetic structure forms the site for borehole H26-0432 and the borehole was sited to investigate a magnetic anomaly. The geophysical data suggests a gently dipping sill to the North. Borehole H26-0432 is sited on position 350m on the magnetic traverse, at the contact between the sill and the host rock.

Geological description

Borehole H26-0432 penetrated a thick overburden layer of 10m, overlying gneiss. The gneiss was fractured until 24 m, however, fractures were infilled with calcite. Below 24 m the lithology proves to be fairly homogeneous until the end of the hole at 96m. Only occasional varying content of mafic minerals changes the appearance of the gneiss, which could be the cause of the magnetic anomaly.

No water was encountered and subsequently the hole was backfilled.

Borehole H26-0433 on site LMB15

Borehole site

A fault zone, running from the SW to the NE forms the site for borehole H26-0433. The fault is mapped on the 1:250000 map Alldays but has no imprint on the morphology at the site. This fault is postulated to be of a strike slip nature (6.2.4). Borehole H26-0433 was sited at position 150m on geophysical traverse LMB15.

Geological description

After 15m of overburden a sequence of gneisses and amphibolites is encountered. Fine grained, grey to light grey gneisses are interlayered with black, medium to coarse grained amphibolites. From 66 to 76m the rock profile is fractured with calcite infilling, but no water is encountered. These fractures represent an old fracture zone associated with an amphibolised mafic dyke. The fracturing is probably related to post intrusive strike slip movement.

As no water was encountered, the borehole was backfilled.

Conclusions

A host of apparent lineaments, structures and geophysical anomalies are present as potential hydrogeological targets. Based on the limited drilling data, the following can be tentatively concluded:

- Magnetic features may not be targets as they may be associated with lithological features related to mafic mineral content, or dykes of Pre-Waterberg age metamorphosed to amphibolite. Since these dykes intruded in a ductile manner, their contact zones are not associated with brittle deformation. Magnetic features may be a target when associated with ENE trending Karoo age dolerite dykes (such as at H26-0426) or faults. Hence field mapping of the intended target is essential.
- High yields from boreholes H26-0427 and H26-0434 confirm that ENE trending structures are highly fractured, open and concurrent with post-Karoo normal faulting.
- Two NE trending faults investigated were shown to yield limited quantities of water.

- A N-S trending lineament representing a tectonic contact between Karroo sandstone and LMB rocks proved to be dry, suggesting N-S lineaments are under present day compression.
- Fractured amphibolites yielded some water at various targets, however, fracturing is believed to be associated with Post-Waterberg tectonic activity, hence amphibolites may be target when oriented E-W and associated with subsequent Karoo intrusions.
- Mapped lithological contacts in LMB rocks are not a target as they represent Archean to early Proterozoic ductile deformation, hence are welded or transitional in nature. Unless sheared or faulted they are not water bearing.

The drilling of structural targets in the research area should therefore be restricted to ENE structures that have been active since Waterberg times. Where lower yields are sufficient, NE trending strike-slip faults may be considered.

3.8 Test Pumping

A constant discharge test was carried out on all of the newly drilled boreholes in order to characterise hydraulic properties of the penetrated lithologies, to assist with developing a conceptual model of aquifers, and to determine sustainable borehole yields. The test pumping and recovery data are presented in Appendix 3-C.

Pump test H26-0426

Borehole H26-0426 had a water strike at a depth of 42.5m (0.4l/s). The static water level of the hole is 26.54 m below surface, giving an available drawdown of 16 m. The pump was set at 41m below surface during the test. The borehole was then pumped at a rate of 0.48 l/s for 30 min, after which the water level reached the pump inlet.

The drawdown curve shows an exponential increase on the semi-log drawdown curve and a linear increase of slope 0.5 on the derivative curve, which suggests linear flow through a thin dyke or a long fracture. Radial flow conditions are never encountered, making it difficult to establish a transmissivity value. The aquifer is a thin near vertical structure related to the weathered amphibolite at the dolerite contact zone. No boundaries are encountered before the water level reached the pump inlet in the vicinity of the water strike at 13.8 m of drawdown.

The recovery of the borehole was monitored for 100 minutes. The data shows that after 100min since pumping was stopped, the recovering of the water level slows down, suggesting that some residual drawdown will remain, indicating a limited storage or extent of the aquifer. No evidence of leakage from an overlying weathered zone is noted, hence storage is limited and is limited to fractures. For this reason, a hydrogeologist must be conservative when recommending a yield for this hole.

Calculated transmissivity values are presented in Table 3.6. The transmissivity calculated on the basis of the early time and late time data does not have a physical meaning, as radial flow conditions have not been established. These values are calculated for the purpose of obtaining a sustainable yield only.

The sustainable yield calculated on the basis of the various methods is shown in Table 3.7. The various parameters for each of these methods are listed in Table 3.8.

Table 3-6 Transmissivity values for H26-0426

H26-0426	$T_{(early)}$ [m²/d]	$T_{(late)}$ [m²/d]	$T_{(recovery)}$ [m²/d]
	2.5	0.7	0.8

Table 3-7 Recommended borehole yields for H26-0426

Method	m^3/d
Late T	7.5
Recovery	9.6
Drawdown to boundary	12.5
Distance to boundary	5.5
Flow characteristic	5.8
Max. drawdown	14

Table 3-8 Critical parameters for sustainable yield estimation

	H26-0426	H26-0429	H26-0427	H26-0430	H26-0431
T_{early}	2.5	18.4	865		8.0
T_{late}	0.7	9.0	253		-
$S_{fracture}$	0.0005	0.000475	0.0003		0.01
S_{matrix}	0.0005	0.000475	0.003		0.01
Boundary (m)	8	8.5	2.09		3.4
Boundary (d)	0.0035	-	2.04		
Lithology	Amphibolite	Gneiss	Quartzite	Weathered Fractured Gneiss	Weathered Gneiss
F2	2	1.6	5		0.5
Yield (m^3/d)	6-12	120	751-2500	~200	50-60
Conceptual Model	Single uniform fracture or dyke	Weathered bedrock contact	Fault zone at tectonic contact	Weathered gneiss Bedrock contract	Leaky confined bedrock contact

The sustainable borehole yield varies from 6-12 m^3/d for the different methods. The recovery method is based on an estimated recovery at $t/t' = 1.3$. The drawdown-to-boundary method estimate of 12 m^3/d is considered to be the best approximation since all the parameters for the method can be defined.

Pump test H026-0427

The final blow yield of H26-0427, which is 50 m from H26-0434, was measured as in excess of 23 l/s and was estimated at about 50 l/s. Seepage occurred at 18.5 m and the main water strike occurred within a large fracture zone at 56 m, and inflows appeared to continue until 72 m, at which point water pressure and the size of the rock cuttings prevent further penetration. The pump was lowered to 60 m. The casing height is 0.28 m and the rest water level was measured to 12.18m below surface, giving an available drawdown of 44 m. The borehole was pumped for 3 days at 23.4 l/s, the maximum rate of abstraction due to the diameter of the borehole. Only 2.35 m of drawdown could be achieved, which is considered insufficient.

For the first 540 min the semi-log drawdown and derivative curves indicate that flow is radial, since the derivative curve is approximately horizontal. Thereafter, the rate of drawdown has a slope of almost 1 on the derivative curve, indicating that closed boundary conditions are encountered. This condition is expected in a fault zone, where flow is expected to be extremely anisotropic. Consequently, the drawdown data suggests that flow is primarily linear and oriented along the fault zone. No significant boundary conditions are noted since insufficient drawdown was achieved to stress the borehole and to drop water levels to the vicinity of the water strike. Consequently, sustainable yield estimation is overly conservative and is likely to be higher than estimated.

The recovery of the borehole was monitored for 2220 min. The semi-log time-residual drawdown curve indicates that the rate of recovery is increasing towards the end of the test, since at early times recovery is purely due to linear flow. At $t/t' = 2.95$, a residual drawdown

of 0.68 m remains. An extrapolation of recovery suggests that the borehole will not fully recover by t/t'=1, hence dewatering seems to have taken place.
A step drawdown test was also conducted at discharges of 6.7, 13.25 and 25.0 l/s. The resulting drawdowns were 0.31, 0.62 and 1.15 m respectively. These results indicate that the B parameter is 0.00053 d/m^2 and that C is 5^{-11} d^2/m^5. These parameters suggest that the borehole is very efficient and that efficiencies exceed 99% at the tested discharges (Appendix 3-C).

Borehole H26-0434 was used as an observation borehole for the pumping test in order to obtain a storativity value. Fracture storativity was calculated as 0.0003. The low storativity of the fracture networks, the lack of observed leakage from an overlying weathered aquifer and the incomplete recovery suggests that yield estimates should be conservative.

Calculated transmissivity values are presented in Table 3-9. The early time transmissivity was calculated on the basis of the drawdown curve from 10-170 min, a period when the derivative curve indicates radial flow conditions. The late time transmissivity was calculated from the period after 2880 min, after a suspected boundary was encountered. The sustainable yield calculated on the basis of the various methods is shown in Table 3-10. The various parameters for each of these methods are listed in Table 3-8.

Table 3-9 Transmissivity values for H26-0427

H26-0427	$T_{(early)}$ [m^2/d]	$T_{(late)}$ [m^2/d]	$T_{(recovery)}$ [m^2/d]
H26-0427	865	253	594
H26-0434 Observation	1061	293	293

Table 3-10 Recommended borehole yields for H26-0427

Method	M^3/d
Flow characteristic	2515
Late T	6045
Distance to boundary	755
Drawdown to boundary	851
Max. Drawdown	1500

The sustainable yields for borehole H26-0427 is probably 750-850 m^3/d, which is nearly 10 l/s, however, this value is considered very conservative as the pumping rate was too low to evaluate boundary conditions. The FC method predicts 2515 m^3/d, even though an F2 value of 5 was used.

Pump test H046-0429

The borehole encounter seepage at 19 m and a water strike of 2.1 l/s at 27 m. The bedrock interface is at 29 m. The final blow yield was measured as 1.9l/s. The rest water level is at 10.61m, giving an available drawdown of 16 m. The pump was lowered to 29m and the borehole was pumped for 12h at the maximum rate of the submersible pump of 2.2 l/s.

The semi-log plot of the time-drawdown curve exhibits a straight line, while the derivative curve has generally horizontal trend. This indicates that flow is radial, which can be expected since the aquifer occurs in the weathered zone above the bedrock contact. The many and regular dips in the derivative curve every half meter of drawdown may be attributed to the location of slots in the casing and zones where water rising up through the casing has migrated into the weathered gneiss, to re-enter the borehole during pumping. The aquifer can be conceptualised as a confined weathered bedrock contact aquifer. No significant boundary conditions were encountered, however, it can be assumed that the water level can safely be dropped to 19 m (8.5 m of drawdown), the level where saturation or seepage was encountered (3.7), since this would minimise water loss from the formation into the overlying dry weathered gneiss.

The recovery of borehole H26-0429 was monitored for 100 minutes (t/t'=8.2) and the water level recovered to within 0.5 m of the original static water level. Full recovery is extrapolated at t/t'=2.7, indicating an extensive aquifer and no significant dewatering during the test. This suggests that the sustainable yield estimation need not be conservative.

The calculated early and late time transmissivity values for borehole H26-0429 are presented in Table 3-11. Recommended borehole yields by the various methods are in Table 3-12.

Table 3-11 Transmissivity values for H26-0429

H46-0429	$T_{(early)}$ [m²/d]	$T_{(late)}$ [m²/d]	$T_{(recovery)}$ [m²/d]
	18.4	9.0	7.7

Table 3-12 Recommended borehole yields for H26-0429

Method	m³/d
Late T	98
Recovery	121
Drawdown to boundary	101
Distance to boundary	73
Flow characteristic	119
Max. Drawdown	120

Recommended borehole yields for the borehole range from 73-121m³/d. The recovery method provides a qualitative indication that an overly conservative approach need not be adopted. The FC method and drawdown to boundary method were problematical to apply since no defined boundaries can be identified in the derivative or drawdown curves. A boundary was assumed at 8.5 m (the end of the test), the point where seepage occurred and the top of the saturated horizon, early time inflection) and at 30 m of drawdown (water strike), and an F2 of 1.6 was used for the FC method. An S value of 0.01 was adopted since the aquifer ranges from weathered to highly weathered in nature. The sustainable yield is estimated at approximately 120 m³/d.

Borehole H26-0430

Borehole H26-0430 is a weathered bedrock contact aquifer and had seepage at 12 m and inflow were encountered between 19-21 m (3.9 l/s). The bedrock interface is at 21 m. The static water level of the hole is at 6.75 m below surface, giving an available drawdown of 12 m. The pump was set at 19 m below surface during the test. The borehole was then pumped at a rate of 0.46 l/s for 30 min, after which the water level reached the pump inlet. The low yield can be attributed to the casing off of the water strike.

The drawdown curve shows an exponential increase on the semi-log drawdown curve and a linear increase of slope 0.25 on the log-log drawdown curve, which suggests linear flow through a horizontal fracture. However, the more likely explanation is that skin effects have resulted in inefficiencies that increase with drawdown. Radial flow conditions are never encountered, also making it difficult to establish a transmissivity value. No boundaries are encountered before the water level reached the pump inlet in the vicinity of the water strike at 11.9 m of drawdown.

The recovery of the borehole was monitored for 30 minutes, after which only 0.16 m of residual drawdown remained. However, the data also shows that after 30 min since pumping was stopped, the recovering of the water level slows down, which can be attributed to skin effects resulting from the drill cuttings sealing of the water bearing horizon. It is expected that the aquifer would have recovered much earlier due to its high permeability. No evidence of leakage from an overlying weathered zone is noted, even though wet weathered gneiss was

encountered from 3 m depth. However, this may not be the case as skin effects may have resulted in insignificant drawdown in the adjacent formation.

Transmissivity values and sustainable yields could not be calculated due to poor borehole construction. If it is assumed that the sustainable yield has a similar relationship to the blow yield as the adjacent H26-0429, then a yield of approximately 200 m^3/d can be calculated (60% of blow yield)

Pump test H26-0431

The borehole is characterised by an 11m deep overburden consisting of 4 m of alluvium, followed by 1 m of dry weathered and fractured amphibolite, then by wet weathered gneiss. The main water strike occurred at 6m, near the amphibolite/gneiss interface and is about 1 l/s. The rest water level is at 2.61 m, giving an available drawdown of about 3.4 m. A pumping test was carried out at 1.0 l/s for 600 min., when pseudo steady-state conditions were reached.

This borehole can also be conceptualised as a leaky bedrock contact aquifer, with leakage occurring from an overlying alluvium and fractured and weathered amphibolite. Since the aquifer is located in weathered gneiss of relatively high permeability, it can be considered confined by the low permeability highly weathered amphibolite. Only for the first 3-5 min of pumping does the semi-log drawdown curve follows a straight line, while the derivative curve is horizontal, indicating radial flow towards the borehole. After 3 min., leakage commences and by 5 min the derivative plot has a slope of –1, indicating significant leakage. After 100 min. the borehole reaches pseudo steady-state conditions at about 2.95 m of drawdown.

The recovery test shows that after 90 min. (t/t' =7.7), only 0.12 m of drawdown remain. The rate of recovery appears to be declining, however, once drawdown is less than 1.5 m it can be assumed that upwelling water is seeping out the slotted casing into the overlying alluvial deposits, hence recovery rates observed are less than the actual formation recovery. For this reason, recovery was extrapolated from the recovery data until residual drawdown reached 1.2 m.

The transmissivities were calculated on the basis of the recovery data and the early time pump test data and presented in Table 3-13. The recommended borehole yield was calculated on the various methods and the results are shown in Table 3-14.

Table 3-13 Transmissivities for borehole H26-0431

H46-0430	$T_{(early)}$ [m^2/d]	$T_{(recovery)}$ [m^2/d]
	8.0	5.3

Table 3-14 Recommended borehole yields for H26-0431

Method	m^3/d
Late T	19
Recovery	85
Drawdown to boundary	19
Flow characteristic	42
Max. Drawdown	25

The recommended borehole yield varies from 19-85m^3/d. The drawdown to boundary method, maximum drawdown method and late T method are considered to be too conservative as they based only on transmissivity and a presumed boundary effect, while ignoring the effects of leakage. The recovery method may be too high as it is based on the extrapolation of early recovery, generating a t/t' intercept of 160. The Flow Characteristic method estimates a sustainable yield of 42 m^3/d, which is likely to be too conservative given the extent of leakage from the overburden. The sustainable yield is probably between 50-60 m^3/d.

3.1.1.1 Conclusion

Table 3-15 summarises the results of the discharge tests in terms of calculated transmissivities, blow yield, sustainable yield and pressure head.

Table 3-15 Results of the discharge tests

	T_{early}; $T_{recovery}$ (m2 d)	Sustainable Yield (m3 d)	Blow Yield (l/s)	Sustainable Yield (% blow yield)	Pressure head (m)
H26-0426	2.5 0.8	12	0.4	35	16
H26-0427	865 594	750-850	~50	~20	44
H26-0429	18.4 7.7	120	2.1	66	16
H26-0430		202	3.9	60	12
H26-0431	8.0 5.3	50-60	1.0	58-69	3.4

3.9 Hydrofracturing

Boreholes H26-0426, H26-0429, H26-0430 and H26-0431 were hydrofractured by DWAF Geohydrology in order to verify whether hydrofracturing is viable in this environment (Appendix 3E). Specific capacities before and after hydrofracturing are given below:

	Yield (l/s)	Pre Test (l/s/m)	Post test (l/s/m)	Improvement (%)
H26-0426	1.05	0.016	0.017	6.2
H26-0429	1.33	0.235	0.248	5.4
H26-0430	1.33	0.024	0.032	34.8
H26-0431	1.33	0.037	0.059	59.4

Increased specific capacities suggest that hydrofracturing was apparently successful in H26-0430 and 0431; however, the hydrofracturing curves indicate that increased specific capacities cannot be attributed to fracturing since no sudden break in the water pressure curve is observed. The water pressure in 0430 could not be built up sufficiently due to the permeability of the fracture being too high. Consequently, improved specific capacity can be attributed to a development affect. In borehole 0431 no evidence of fracturing is evident (sudden break in the water pressure curve), hence improved specific capacity can also be attributed to development.

3.10 Evaluation of climatic and runoff data

Rainfall data for the study area I is available for stations 0763 675 De Gracht, and 0763 743 Stolzenfels. These data were obtained from the Computing Center for Water Research (CCWR) and show an MAP of 380 and 343 mm/a respectively. The mean monthly distribution of rainfall for the Messina station is shown in Figure 3-59. The climate is characterised by intense summer rainfall and dry winter periods.

Additionally, the distribution of the median annual precipitation on the basis of the CCWR 1 x1 minute median monthly rainfall grid over study area I and II is available. The estimate of the MAP for this grid was regressed against factors such as altitude, latitude, longitude, continentality and aspect (Dent, Lynch & Schulze, 1989). The distribution of rainfall in areas I and II show different distribution patterns. The rainfall increases form the Limpopo river towards the South, indicating, that low-lying areas appear to have a lower MAP (Figure and Figure 3-61). In area I rainfall varies only in a small range between 320 and 480mm (Figure 3-60), with the higher figure towards the south where the orographic effects of the Blouberg range is felt. In contrast, the grid for area II suggests that MAP varies in a broad range between 150mm and 950mm (Figure 3-61), primarily due to orographic effects related to the Soutpansberg in the south, however, the area underlain by LMB rocks receives less than 350 mm.

An estimation of the rainfall pattern in both areas during wet and dry years is shown in Figure 3-62, Figure 3-63, Figure 3-64 and Figure 3-65), on the basis of the rainfall which is likely to be exceeded in 20% and 80% of the years.

The evaporation data shown in Figure 3-66 and Figure 3-67 for area I and II respectively is based on the CCWR 1 x 1 minute S-pan evaporation grid for grid point Lat 22 30 / Long 30 15 for area II and Lat 22 45/ Long 28 45 for area I.

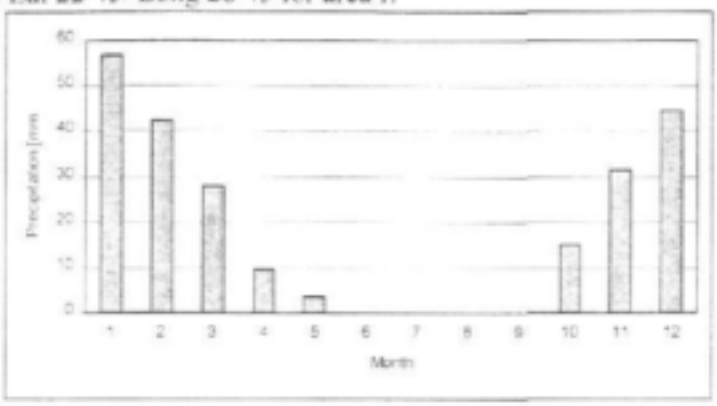

Figure 3-59 **Mean monthly distribution of rainfall**

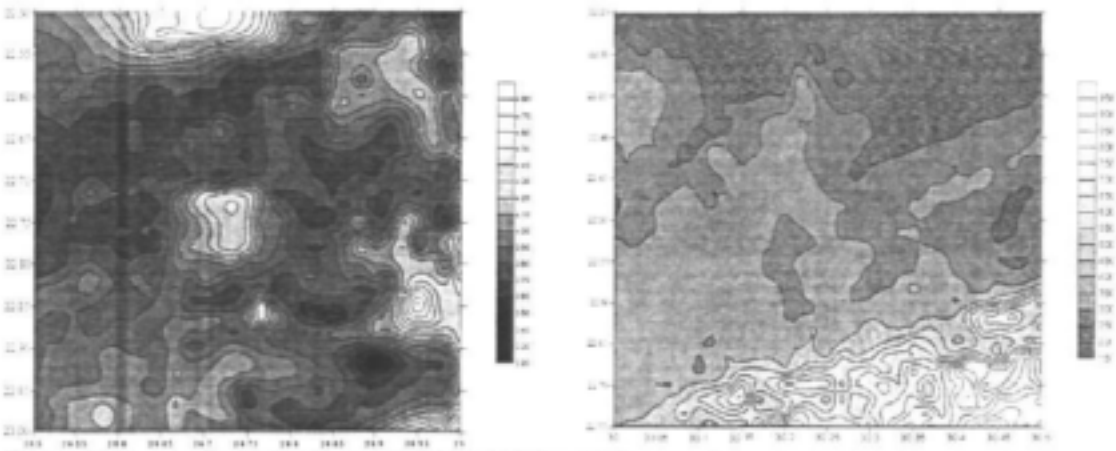

Figure 3-60 **(Left) Median monthly rainfall grid for area I**

Figure 3-61 **(Right) Median monthly rainfall grid for area II**

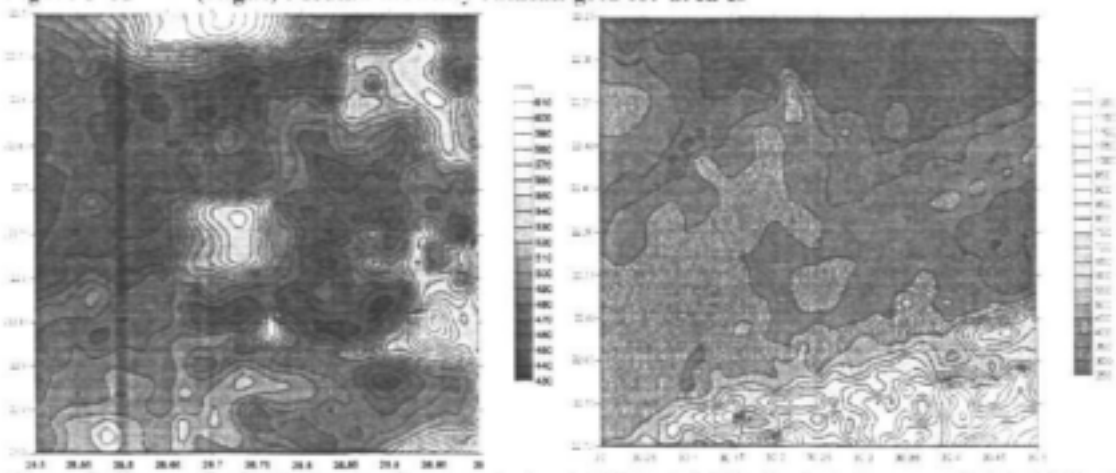

Figure 3-62 **(Left) Estimate of wet period rainfall (rainfall is likely to be exceeded in 20% of the years) – area I**

Figure 3-63 **(Right) Estimate of wet period rainfall (rainfall is likely to be exceeded in 20% of the years) – area II**

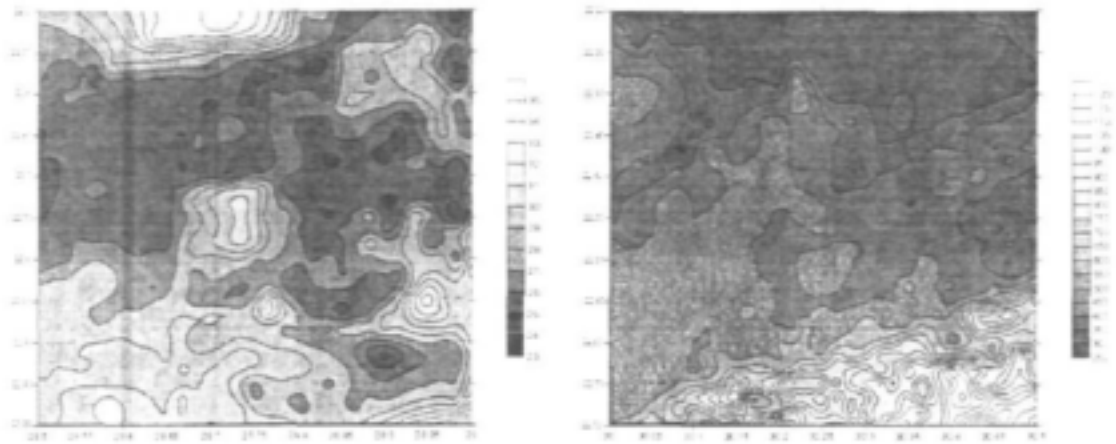

Figure 3-64 (Left) Estimate of drought period rainfall (rainfall is likely to be exceeded in 80% of the years) – area I

Figure 3-65 (Right) Estimate of drought period rainfall (rainfall is likely to be exceeded in 80% of the years) – area II

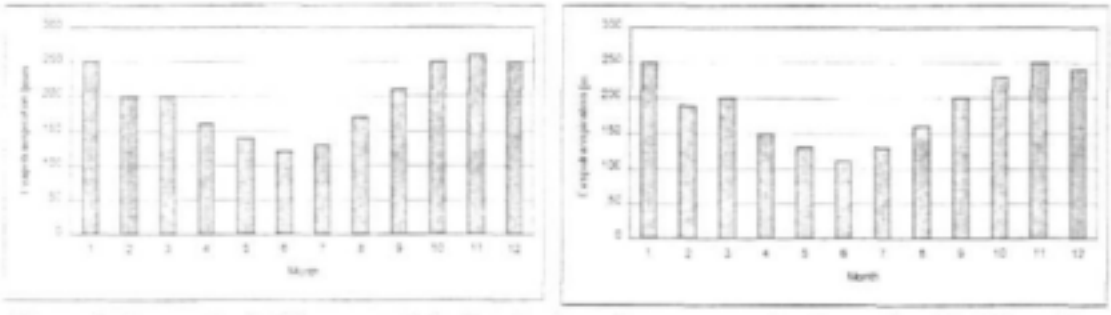

Figure 3-66 (Left) Mean monthly distribution of evapotranspiration at Lat 22 45° and Long 28 45°

Figure 3-67 (Right) Mean monthly distribution of evapotranspiration at Lat 22 30° and Long 30 15°

3.11 Hydrogeological Evaluation

The area exhibits a poor historical success rate with <40%of boreholes yielding water yielding more than 0.1 l/s. Borehole yields fall mainly in the category between 0.01 and 1 l/s (69% study area I and 45% study area II), with the median yield of successful boreholes being only 0.39 l/s. Only 13% of boreholes yield more than 2 l/s. Dry boreholes as well as high yielding boreholes have been drilled in all lithologies and are not restricted to any specific rock type.

The aquifers of the Limpopo Mobile Belt are predominantly structurally controlled and significant water movement is restricted to major fracture and fault zones, primarily related to recent (Post Karoo) geodynamics. These structures can be extremely high yielding and can generate blow yields in excess of 20 l/s. In many instances the distance to streams and rivers is indicative of a fault zone, since many rivers tend to follow structures when they deviate or dog-leg from the northerly surface topographic gradient. The highest yielding boreholes are drilled into ENE striking features, the orientation considered as extensional in nature. However, the scale of the feature shows a strong influence on the yield of the boreholes, with regional scale fault having a far better groundwater potential than local scale structures.

In some localities significant weathered zone bedrock contact aquifers also exist where deep weathering is present. The recovery of these aquifers after pumping suggests that they are extensive in nature and that flow is radial. However, leakage from the overlying saturated

weathered zone appears to be restricted to zones where an overlying alluvial aquifer exists. The exploitation potential of such aquifers will therefore be ultimately controlled by recharge.

There is no evidence of any aquifers at the contact between different lithological units of the LMB as these contacts have been deformed and metamorphosed in a ductile manner. Lithological contacts between LMB rocks and Karoo or Waterberg/Soutpansberg rocks are tectonic in nature and have been subjected to extensive post deposition brittle deformation by normal faulting. This faulting appears to be associated with a dense fracture network on a macro scale and parallel secondary faulting characteristic of tensional block faulting. Consequently, these targets provide the best groundwater potential in the region. Other studies have suggested these targets could yield up to 1 million m^3 per annum per kilometre (Fayazi & Orpen, 1989), however, Verhagen and Butler (2000) estimate the exploitation potential as an order of magnitude less.

The water table in the area is relatively shallow with an average of 24 m in area 1. Water strikes are generally within 20 m of the water level. Water table as well as water strike depth vary over a wide range, with very shallow strikes and static water tables being present along the Limpopo and other streams dissecting the area. In the solid bedrock fault structures water strikes and levels appear to be deeper. In general, the water strikes occur deeper than the recorded static water level and the aquifers are considered to be of confined nature. 50% of water strikes occur within 36 m, which suggests that historically water strikes in the shallow weathered aquifers may be the cause of low yields. Deeper water strikes are encountered in the high yielding tectonic structures, both due to extensive fracturing and confining pressure.

After Enslin's regional rainfall/recharge relationship for summer rainfall regions in South Africa (Bredenkamp et al. 1995), the study area experiences recharge in the order of 2.5% of MAP, or 8 mm. Recharge was also estimated by the relationship developed by DWAF and modified by Sami & Murray (1998) for granitic aquifers:

$$R = (MAP)^2 / 20000 \text{ [mm]}$$

This formula yields a recharge estimate of 5.3 mm for both research areas. Based on isotopic studies in the Taaibosch fault, Verhagen and Butler (2000), estimated recharge to be 4-6.4 mm, however, this estimate was derived from an area with extensive Karoo sandstone outcrop, hence recharge may be higher than in the area underlain by Quaternary sands over LMB rocks.

Large variations in Cl concentrations (41-2825 mg/l) suggest that recharge is highly variable. The lowest chloride values appear in the high yielding ENE structure (H26-0434), indicating that the fault zone receives the most recharge due to the presence of Karoo sandstone outcrop along its length. Assuming a rainfall Cl concentration of 0.6 mg/l, the lower figure suggests that recharge is about 5 mm/a for the aquifer feeding the ENE trending fault zone (H26-0426). Cl values of 110-308 mg/l from the weathered zone aquifer suggest recharge of 1-2 mm/a.

Based on the above, recharge to the Quaternary covered LMB aquifer is considerably less than 5 mm/a, with up to 5 mm/a for the southern region supplying the fault zone. This suggests that regional exploitation potential is probably less than 2500 $m^3/a/km^2$.

Appendix 3-D presents the summarized results of the laboratory analyses for all sampling points. The water samples from all successful boreholes are graphed in so called Schoeller diagrams, tri-linear Piper diagrams and Stiff diagrams. The ambient water quality is generally of the Mg/Ca-HCO3 type. Enriched Mg and HCO3-Cl indicate recently recharged water in a low recharge environment where base exchange in the weathered mafic overburden has resulted in elevated magnesium levels at the expense of other cations.

Borehole H26-0426 has an anomalous geochemistry due to elevated chloride levels, which implies the aquifer located in the dolerite dyke contact zone receives little recharge. By implication, all other constituents are elevated due to the reduced dilution of ions.

Nitrate levels vary from 88-428 mg/l NO3, with the lowest value being in the high yielding ENE fault zone (H26-0434). To convert these figures to NO3-N the values need to be divided by 4.5. Elevated Nitrates result in all boreholes being classified as type III water, with the exception of H26-0434, which is class II. Elevated nitrate levels are a regional problem and can be attributed to:

- Low density vegetation cover of thornveld with little ground cover, hence nitrogen fixation in vegetation is inhibited
- Low organic content limits substantial nitrate accumulation in the soil, hence leaching of nitrates is facilitated
- Low rainfall limits plant cover and results in episodic plant die offs, thus plant cover fluctuates. Large summer rainfall subsequently leaches nitrates released by plant die off
- High temperatures ensures rapid biological nitrification
- Low carbon to nitrogen ratios result in nitrogen being freely available for nitrifying bacteria as well as low clay content in the quaternary cover
- Absence of surface runoff
- Variations in recharge result in variations in nitrate by dilution

Boreholes H26-0429 and H26-0434 were also submitted for ICP-MS analysis at the Council for Geoscience due to suspected hydrothermal activity in the region, which may have resulted in mineralistion in quartz veins. These boreholes represent the high yielding fault zone and the weathered aquifer. The results for 71 elements show that no elements exceed International Standards. High levels of strontium are recorded (0.8 and 0.6 mg/l), however, this is within the 20 mg/l drinking water equivalent standard set by the US EPA, and within their 4 mg/l life time standard.

3.12 Financial Analysis

Three scenarios were investigated to establish the costs of establishing 10 successful boreholes:

1 *No structured exploration, or drilling randomly or by visual observation*
This scenario is based on historic drilling records obtained form the NGDB. A total of 2061 records are available for the study area I and II, of which 1083 (53%) holes have no information on yield and 31% are reported to be successful. It was assumed that 40% of the boreholes with no yield specification were unsuccessful, as listed by Vegter (1995). This rate was used to estimate the number of holes and associated costs required to establish 10 yielding boreholes.

2 *Exploration based on geophysical surveys based on the use of GENIE SE-88 electromagnetic profiling (Bush, 1989).*
This scenario is based on success rates shown in Vegter (2001), where 9 of 24 boreholes were successful (38%) (>0.025 l/s). This investigation also contained supporting magnetic, VLF, resistivity and seismic refraction profiling. Hence it can be assumed that it represents the highest success rates that can be achieved using a geophysical approach.

3 *Full exploration based on structural mapping, LANDSAT and aerial photo interpretation, geophysical exploration using the most appropriate method under the given hydrogeological conditions.*

This scenario is based on the methods used for this project, where a MAX-MIN system was used due to advantages of depth of penetration in conjunction with the resistivity sounding method and the magnetometer. Boreholes were sited on structural features, such as lineaments, faults and brecciated zones and on deeply weathered rock profiles identified in the field. Nine holes were drilled of which 6 were successful. Costs were extrapolated in order to determine the costs to establish 10 yielding boreholes in order to compare the results to scenario 1.

The estimated costs for all two scenarios are shown in Table 3-16. The costs are based on the Council for Geoscience rates and man-hours expected during the investigation.

Table 3-16 Approx. costs to establish 10 yielding boreholes according to scenarios 1 and 2

ITEM		Units	Rate	Scenario 1		Scenario2		Scenario3	
						Qty	Cost	Qty	Cost
Desk Study[1]	EXPLORATION	Day	1600			1	1600	5	8000
EM34 survey[3]		Day	1500			9	13500		
Max Min survey[4]		Day	2500					7.5	18750
Resistivity survey[5]		Day	2500					7.5	18750
Geophysical interp.		Line	100			54	5400	48	4500
Accommodation		Day	150			9	1350	15	2250
LANDSAT image[6]		Each	2500					1	2500
LANDSAT interp.		Day	1200					3	3600
Structural mapping[7]		Day	1350					3	4050
Sub total - Exploration					0		21850		62400
Community liaison[2]		Hr	100	25	2500	27	2700	15[10]	1500
Drilling[8]		Hole	11000	25	275000	27	297000	15	165000
Drill supervision		Day	1000	25	25000	25	27000	15	15000
TOTAL					302500		348550		243900
Per successful site					30250		34855		24390
Median yield		L/s			0.39		0.1		3.9
R/l/s per site					77564		348550		6254

1: Review of topographical and geological maps and geological reports
2: At 1h per drilling site
3: At 1 technician and one labourer and 3 boreholes sited per day, including magnetometer surveys
4: At 2 technicians and 2 boreholes sited per day including magnetometer surveys
5: At 2 technicians and 2 boreholes sited per day
6: At 22% recovery per usage of R10000 per 180 x 180 km image and R1200 in man-hours for co-ordinate registration
7: Field mapping of outcrops and aerial photo interpretation
8: Casing costs are not considered as it is assumed that only successful boreholes would be cased, which would result in similar casing costs for all scenarios
9: According to the success rate of 40%
10: According to the success rate of 67% achieved during this investigation

Table 3-16 shows that with a larger budget for exploration the costs per successful site will be about R5500 less than without any exploration. This can be attributed that the fact that the success rate was not dramatically increased.

A substantial cut in costs in terms of water production expressed as R/l/s can be achieved by an exploration programme. Historic success rates have resulted in an expenditure of approximately R30250 for the establishment of each successful borehole. In comparison, an exploration budget of R62400 could result in an increase of median yield from 0.4 l/s to up to

3.9 l/s, which brings down the costs for the water production from 77564 R/l/s in case of random drilling to 6254 R/l/s. However, a lower median yield would be achieved if known existing high yielding faults are not included.

Geophysical surveying resulted in significantly higher costs per successful site and for water production due to the low success rates and median yields achieved. This can be attributed to anomalies being drilled that did not reflect water bearing features.

This analysis suggests that improved exploration results in significantly improved yields and success rates, which considerably lower water production costs. The relatively high median yield achieved under this project suggests that water supply systems in the area could involve hand pump and wind pump schemes as well as reticulated systems, however, the low recharge rate suggests that reticulated schemes require careful monitoring.

3.13 Conclusions and Recommendations

The following conclusions can be drawn from the research area:

- Field structural analysis shows that the joint orientations in the Limpopo Mobile Belt lithologies are distinctly different from these in the Karoo-age cover and intrusive lithologies due to Pre-Karoo geodynamics. The joints in the Limpopo Mobile Belt mostly dip steeply and are oriented NW to N, suggesting E-W to NE/SW extension, or E-W shearing. The regional geodynamics (6.2.3) suggest that extensive ENE shearing occurred prior to Waterberg times (2.0 Ga.), hence pre-Waterberg shearing associated with the emplacement of the Central Zone of the Mobile Belt is the responsible mechanism.
- Subsequent or more recent tectonic events are superimposed in the Limpopo Mobile Belt structural geology, but are difficult to define due to the various ages of joint structures. The joints in the Karoo-age sedimentary rocks and basalts only record tectonic events that occurred in post-Karoo times, hence they provide information on structures in the Limpopo Mobile Belt that are of interest as hydrogeological targets. These all dip steeply and are oriented E to ENE in area II and ESE and NE in area I, suggesting N-S extension, and are associated with uplift and block faulting. Consequently it is fractures with orientations similar to those preserved in the Karoo-age lithologies that are likely to be more open and which therefore represent the best structures for ground water exploration.
- Lineaments in both study areas are primarily orientated in an ENE-WSW direction and are associated with normal faults related to block faulting. These targets are the most favourable hydrogeological feature in the region and yields of up to 50 l/s can be obtained from regional structures. A second complementary antithetic WNW-ESE trend is apparent, however, these are strike-slip structures and have a lower potential.
- A comparison between the geological map of the study area and the lineament orientation reveals that the majority of lineaments were picked along boundaries of different geological formations. As lithological boundaries within the Limpopo rocks itself are not particularly be considered a groundwater target, lineaments have to be taken with caution and examined in the field for their hydrogeological significance.
- Discharge tests carried out in the research area I indicates that a significant weathered zone aquifer exists, with yields of up to 4 l/s. Test pumping recovery suggests that this aquifer is extensive in nature. Deep seated fractures are only an aquifer when part of a regional fault structure.
- Regional scale fault lines can be picked up effectively with the magnetic and the Max-Min systems. However, smaller scale faults cannot be easily located by magnetic or electromagnetic methods where significant quaternary cover exists.
- Lineaments, which do not simply reflect geological contacts of different lithologies are scarce scares in both areas. Target identification requires differentiating between

lithological and tectonic contacts. Lithological contacts investigated left no impact on none of the geophysical methods applied, unless associated with faulting.

- Magnetic structures are commonly found in both study areas and are easily detectable with the magnetic method. Caution has to be taken in terms of the geological origin of magnetic anomalies, as anomalies can result from dolerite and diorite sills and dykes, amphibolites, and variations in mafic content in LMB lithologies. The magnetic structures seldom had an associated anomaly on the EM profiles, implying that there might be no weathered zone accompanying these structures, which would impact on their hydrogeological importance.
- Electromagnetic borehole siting has been shown to be ineffective in the region, since success rates are similar to those obtained by random drilling (Vegter, 2001). Anomalies can be attributed to variations in weathering in the deeply weathered profiles. This proved to be the case in spite of supporting resistivity, VLF, magnetic, and seismic refraction profiling.
- From the exploration drilling it is evident, that regional scale dip-slip normal faults are the most important water-bearing features in the study area, with the most important of these being rejuvenated shear systems. Small-scale faults can be successful, but have a poorer groundwater potential. An additional aquifer is found within the alluvial deposits accompanying streams, which can be tapped through the underlying fault system. Consequently, regions where streams dog-leg in an easterly orientation are the most promising points. Lithological contacts as well as dyke or sill structures were found to be either not water-bearing or yielded only small amounts of water. The contact between overlying Karoo Sandstone and LMB rocks, which is a significant unconformity, appears to be dry, unless encountered at an ENE tectonic contact. Deeply weathered overburden acts as an additional aquifer where deep weathering has resulted or NE or NW faults.
- The financial analysis suggests that improved exploration results in significantly improved yields and considerably lower water production costs. The relatively high median yield achieved under this project suggests that water supply systems in the area could involve hand pump and low density reticulated systems.

The results suggest that the Limpopo Mobile Belt is a poor aquifer due to marginal to poor water quality (class II-III) related to nitrate levels, low recharge and the extreme heterogeneity in targets. Low success rates exist concurrently with very high yielding features, however, these are restricted to mainly regional scale fault zones. Smaller fault zones and alluvial cover along the streams provide a more limited aquifer. Consequently, water abstraction will have to be reliant on regional abstraction systems from identified structures and reticulation to the point of need. Fortunately, the flat topography does not hinder reticulation.

3.14 References

AnHaeusser, C.R. (1992): Structures in granitoid gneisses and associated migmatites close to the granulite boundary of the Limpopo Belt, South Africa, Precambrian Research, 55, 81-92.

Andersen, N.J.B & Ainslie, L.C. (1994): Neotectonic reactivation – an aid to the location of ground water. African Geoscience Review, Vol. 1, No1, pp. 1-10.

Barker, O.B. (1976) The Soutpansberg Trough - An Aulacogen. . Discussion Transactions of the Geological Society of South Africa. 79, 146.

Barker, O.B. (1979) A contribution to the Geology of the Soutpansberg Group, Waterberg Supergroup, Northern Transvaal. Unpublished MSc Thesis, University of the Witwatersrand, pp116.

Barker, O.B. (1983) A proposed geotectonic model for the Soutpansberg Group within the Limpopo Mobile Belt, South Africa. Special Publication of the Geological Society of South Africa, 8, 181-190.

Barton J.M. (1979) The chemical compositions, Rb-Sr isotope systematics and tectonic setting of certain post-kinematic mafic igneous rocks, Limpopo Mobile Belt, southern Africa. Precambrian Research, 9, 57-80.

Barton, J.M., Fripp, R.E.P., Horrocks, P. & McLean, N. (1979): Of the Messina Layered Intrusion, Limpopo Mobile Belt, Southern Africa. Am. Journal of Science, 279(10), pp. 1108-1134.

Barton, J.M. & Key, R.M. (1981): The tectonic development of the Limpopo Mobile Belt and the evolution of the Archean Cratos of southern Africa. In: Precambrian plate tectonics (Kroener, A. ed.). Elsevier, Amsterdam, 185-212.

Barton, J.M., Ryan, B. & Fripp, R.E.P. (1983): Rb-Sr and U-Th-Pb isotopic studies of the Sand River Gneisses, Central Zone, Limpopo Mobile Belt: Special publication, Geological Society of South Africa, 8, pp. 9-18.

Barton, J.M., Van Reenen, D.D. & Roering, C. (1990): The significance of 3000 Ma granulite facies mafic dykes in the Central Zone of the Limpopo Belt, southern Africa. Precambrian Research, 48, 299-308.

Brandl, G. (1981): The Geology of the Messina Area. Explanation of sheet 2230, scale 1:250 000. Geological Survey South Africa, Pretoria.

Brandl, G. (1990): Geological setting, petrography and geochemistry of the Alldays Gneiss and associated mafic dykes, Limpopo Belt, South Africa. In: The Limpopo Belt, a field workshop on granulites and deep crustal tectonics (Barton J.M. ed.). Extended abstracts Volume, Rand Afrikaans University, pp. 95-99.

Brandl, G. & Reimold, W.U. (1990): The structural setting and deformation associated with pseudo-tachylite occurrences in the Palala Shear Belt and Sand river Gneiss, Northern Transvaal Tectonophysics, 171, 201-220.

Bush, R.A. (1989): A geohydrological assessment of the Swartwater and Beauty areas, NW Transvaal. Gh. report 3577, Dir. Geohydrology, DWAF, Pretoria.

Coward, M.P., Graham, R.H., James, p.R. & Wakefield J. (1973): A structural interpretation of the northern margin of the Limpopo orogenic belt, southern Africa. Philosophical Transactions of the Royal Society of London, A 273, 487-491.

Coward, M.P., James, P.R. & Wright, L. (1976): Northern Margin of the Limpopo Belt, southern Africa. Geological Society of America Bulletin, 87, 601-611.

Cox, K.G. (1992) Karoo igneous activity, and the early stages of the break-up of Gondwanaland. In Magmatism and the causes of continental Breakup. Storey, B.C., Alabaster, A. and Pankhurst, R.J (eds). Geological Society of London Special Publication

De Wit, MJ., Van Reenen, D.D. & Roering, C. (1992): Geological observations across a tectono-metamorphic boundary in the Babangu area, Giyani greenstone belt, South Africa. Precambrain Research, 55, 111-122.

Eriksson, K.A., Kidd, W.S.f. & Krapez, B. (1988): Basin analysis in regionally metamorphosed and deformed early Archean terrains: examples from Southern Africa and Western Australia. In: New perspectives in basin analysis (Kleinspehn K.L. & Paola C. (eds.). Springer – Verlag, New York, pp 371-404.

Fayazi, M & Orpen, W.R.G. (1989): Development of a water supply for Alldays from groundwater resources associated with the Taaibos fault. Techn. Rep. GH 3664, DWAF, Pretoria.

Fripp, R.E.P. (1983) The Precambrian Geology of the area around the Sand River near Messina, Central Zone, Limpopo Mobile Belt. Special Publication of the Geological Society of South Africa, 8, 89-102.

Grantham, G.H (1996) Aspects of Jurassic Magmatism and Faulting in western Dronning Maud Land, Antarctica: Implications for Gondwana breakup. pp63-71 in Weddell Sea Tectonics and Gondwana Break-up. Storey, B.C., King, E.C. and Livermore, R.A. (Eds). Geological Society Special Publication No. 108.

Hofmann, A., Kroener, A. & Brandl, G. (1998): Field relationships of mid- to late Archaean high-grade gneisses of igneous and sedimentary parentage in the Sand River, Central Zone of the Limpopo Belt, South Africa. S. Afr. J. Geol. 101(3), pp. 185-200.

Horrocks, P.C. (1983): The Precambrian geology of an area between Messina and Tshipise, Limpopo Mobile Belt: Special publication, Geological Society of South Africa, 8, pp. 81-88.

Jansen H. (1975) The Soutpansberg Trough - An Aulacogen. Transactions of the Geological Society of South Africa, 78, 129-136.

Kroener, A., Jaeckel, P. Hofmann, A., Nemchin, A.A. & Brandl, G. (1998): Field relationships and age of supracrustal Beit Bridge Complex and associated granitoid gneisses in the Central Zone of the Limpopo Belt, South Africa. S. Afr. J. Geol., 101 (3), 201-213.

Key, R.M. & Hutton, S.M. (1976): The tectonic generation of the Limpopo Mobile Belt, and a definition of its western extremity. Precambrian Research 3, pp. 79-90.

Mason, R. (1973): The Limpopo mobile belt – southern Africa. Phil. Trans. R. Soc. Lond. A. 273, pp. 463-485.

McCourt, S. & Vearncombe, J.R. (1987): Shear Zones bounding the central zone of the Limpopo Mobile Belt, Southern Africa, J. Structural Geol., 9, 127-137.

McCourt, S. & Vearncombe, J.R. (1992): Shear zones of the Limpopo Belt and adjacent granitoid-greenstone terranes: implications for late Archaean collision tectonics in southern Africa. Precambrian Research 55, pp 553-570.

Robertson, I.D.M. & Du Toit M.C. (1981): The Limpopo Belt. In: The Precambrian of the southern hemisphere, (hunter D.R. ed.), Elsevier, Amsterdam, 641-671.

Roering, C., van Reenen, C.A., Barton, J.M., de Beer, J.H., de Wit, M.J., Stettler, E.H., van Schalkwyk, J.F., Stevens, G. & Pretorius, S. (1992): Tectonic model for the evolution of the Limpopo Belt. Precambrian Research 55, pp. 539-552.

Rollinson, H.R. (1993): A terrane interpretation of the Archean Limpopo Belt, Geological Magazine, 130, 755-765.

Saggerson E.P. and Logan C.T. (1970) Distribution and controls of layered and differentiated mafic intrusions in the Lebombo volcanic province. Spec. Publ. Geol. Soc. S. Afr., 1. 721-733.

Van Reenen, D.D., Barton, J.M., Roering, C., Smith, C.A. & van Schalkwyk, J.F. (1987): Deep crustal response to continental collision: The Limpopo Belt of southern Africa. Geology, Volume 15, pp. 11-14.

Van Reenen, D.D., McCourt, S., Smit, C.A. (1995): Are the Southern and Northern Marginal Zones of the Limpopo Belt related to a single continental collisional event ?. S. Afr. J. Geol. 98(4), pp. 498-504.

Van Reenen, D.D., Roering, C., Ashwal, L.D., de Wit, M.J. (1992): Regional geological setting of the Limpopo Belt. Precambrian Research, 55, pp. 1-5.

Vegter, J.R. (2001): Region 3: Limpopo granulite-gneiss belt. Water Research Commission Report TT 136/00, Pretoria.

Verhagen, B. T., Butler, M.J., Levin, M. & Van Wyk, E. (2000). Environmental isotope studies as part of a rural water supply development: Taaibosch Fault Zone, Northern Bochum district, Northern Province, South Africa. Rep to coord. Meting on IAEA regional model project RAF/8/029, Kampala, Uganda.

Watkeys, M.K. (1983): Brief explanatory notes on the provisional geological map of the Limpopo Belt and environs. Spec. Publ. Geol. Soc. S. Afr., 8, pp 5-8.

Watkeys, M.K. (1984): The Precambrain geology of the Limpopo Belt north and west of Messina. Ph.D. thesis, Witswatersrand University, Johannesburg, 349 pp.

Watkeys, M.K., Light, M.P.R. & Broderick, T.J. (1983): A retrospective view of the central zone of the Limpopo Belt, Zimbabwe. In: The Limpopo Belt (Van Biljon W.J. & Legg, J.H. (eds.). Special Publication 8, geological Society 65-80.

Wilson, J.F. (1990): A craton and its cracks: some of the behaviour of the Zimbabwe block from the Late Archaean to the Mesozoic in response to horizontal movements, and the significance of some of its mafic dyke fracture patterns. J. of African Earth Sciences, Vol. 10, No.3, pp. 483-501.

APPENDIX 3-A

GEOPHYSICAL DATA

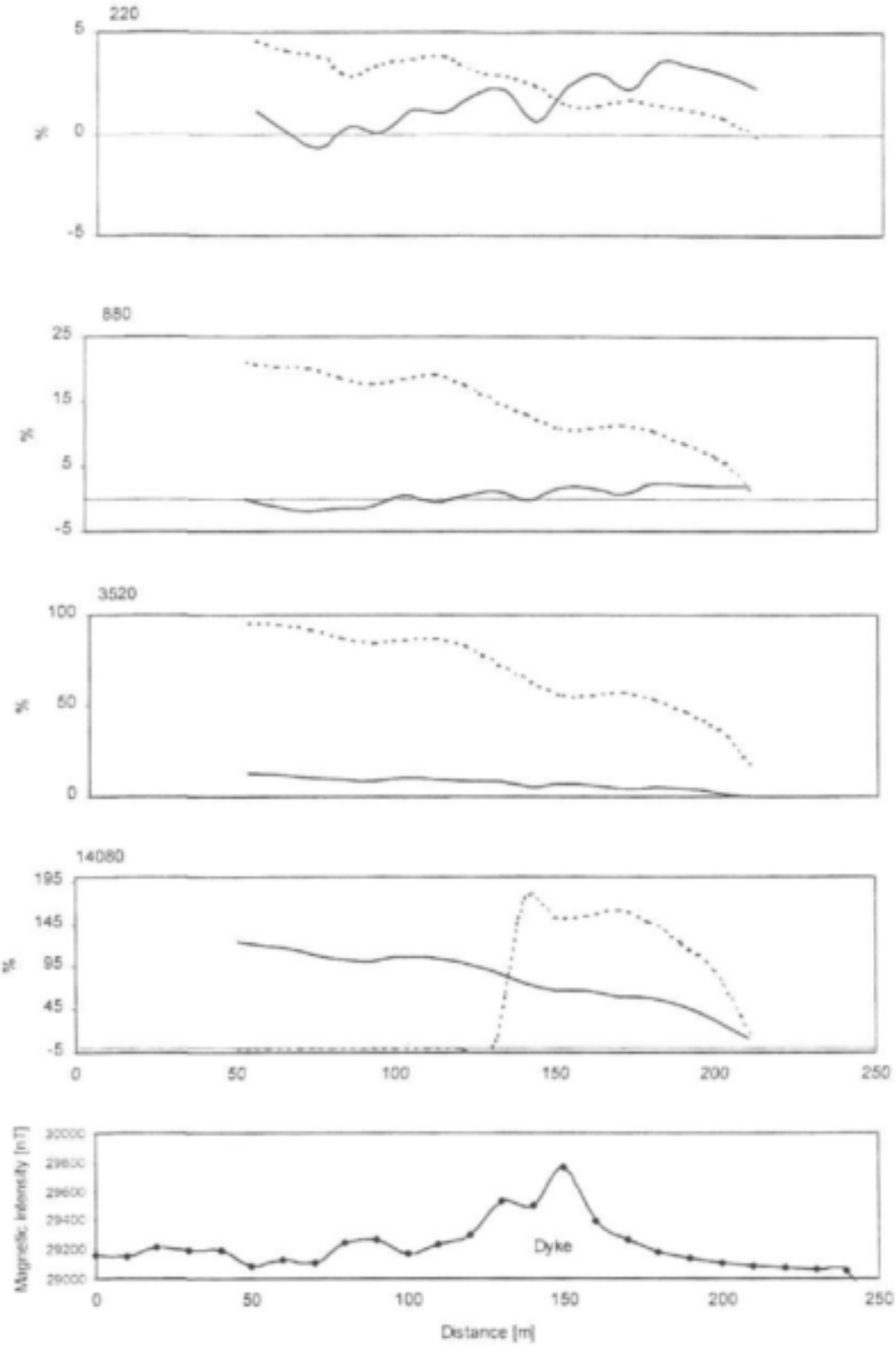

MAX-MIN electromagnetic and magnetic profiles at site LMB1. Solid line: in-phase [%]; dotted line: out-of phase [%]; coil separation 100m, station spacing 10m. Traverse direction: S-N

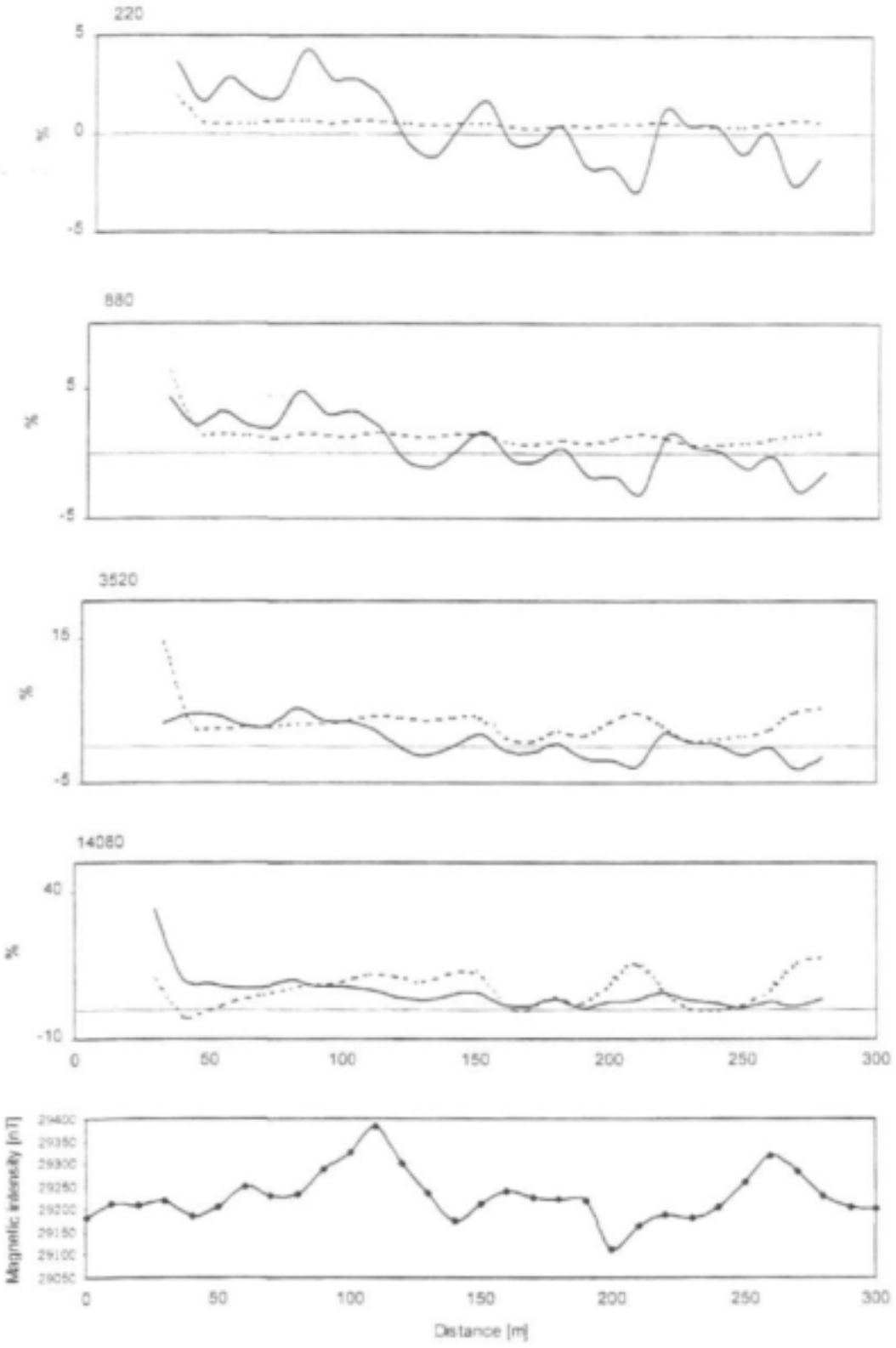

MAX-MIN electromagnetic and magnetic profiles at site LMB3. Solid line: in-phase [%]; dotted line: out-of phase [%]; coil separation 50m, station spacing 10m. Traverse direction: N-S

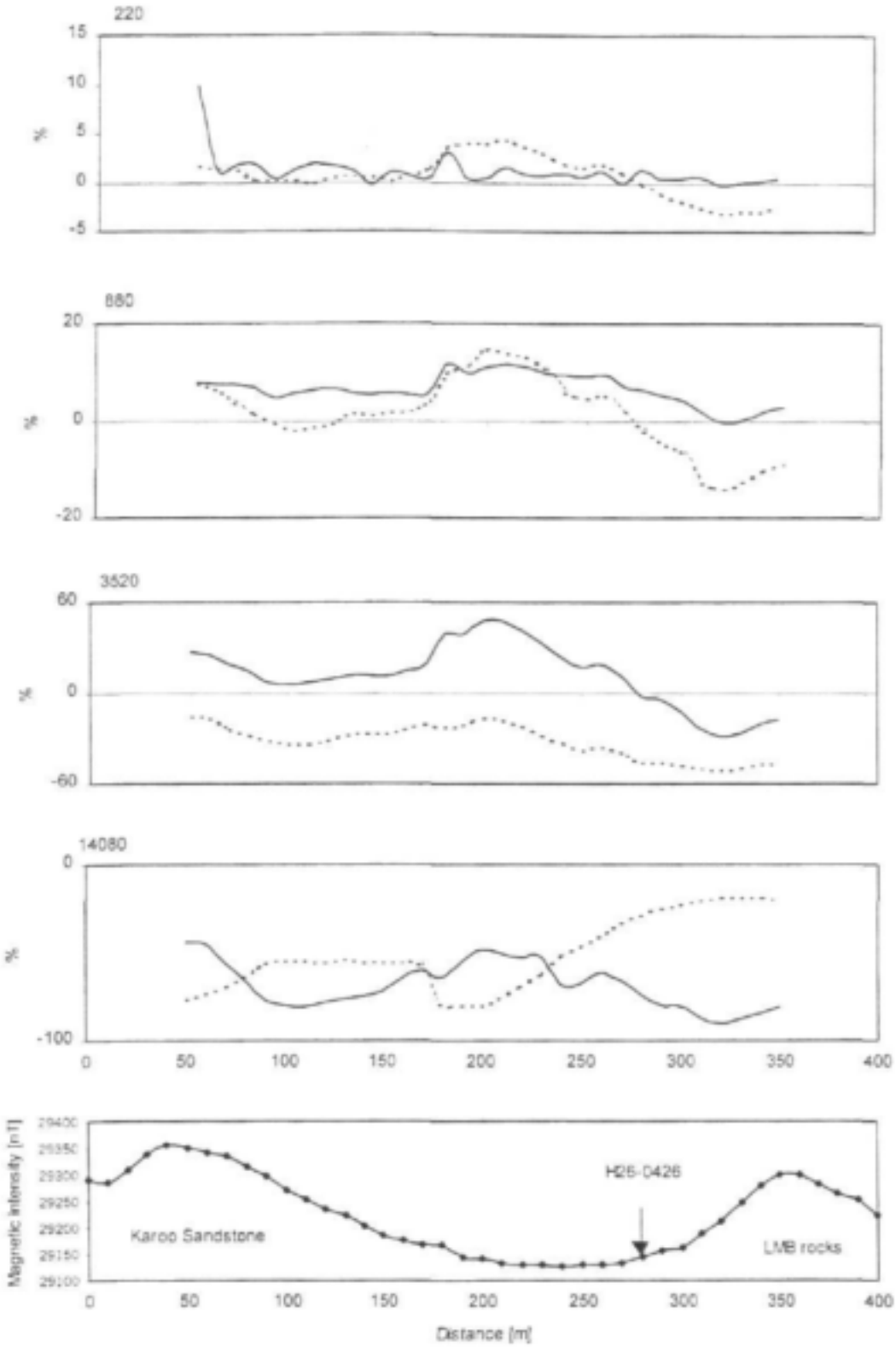

MAX-MIN electromagnetic and magnetic profiles at site LMB5. Solid line: in-phase [%]; dotted line: out-of phase [%]; coil separation 100m, station spacing 10m. Traverse direction: SSE-NNW

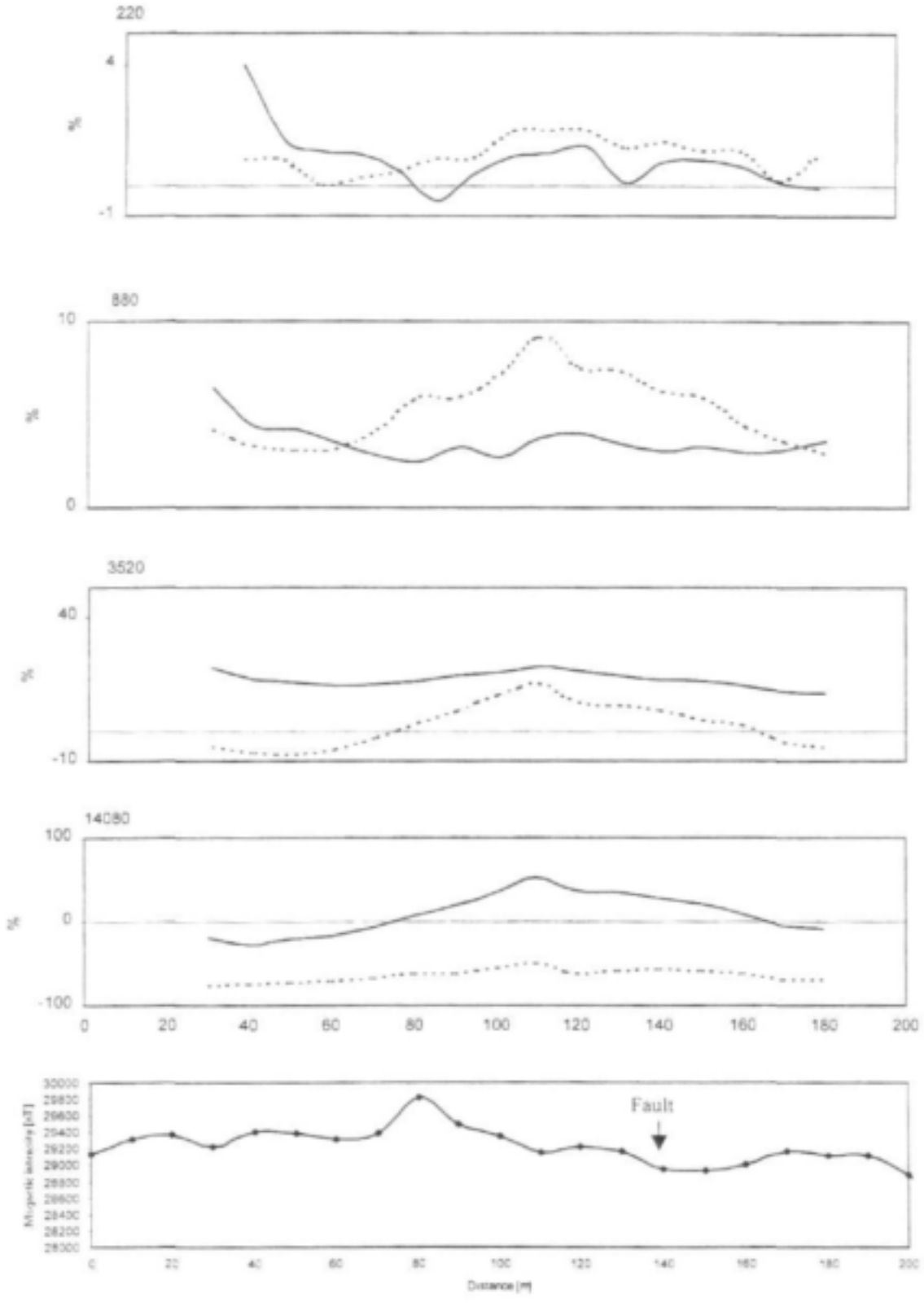

MAX-MIN electromagnetic and magnetic profiles at site LMB7. Solid line: in-phase [%]; dotted line: out-of phase [%]; coil separation 100m, station spacing 10m. Traverse direction: SSE-NNW

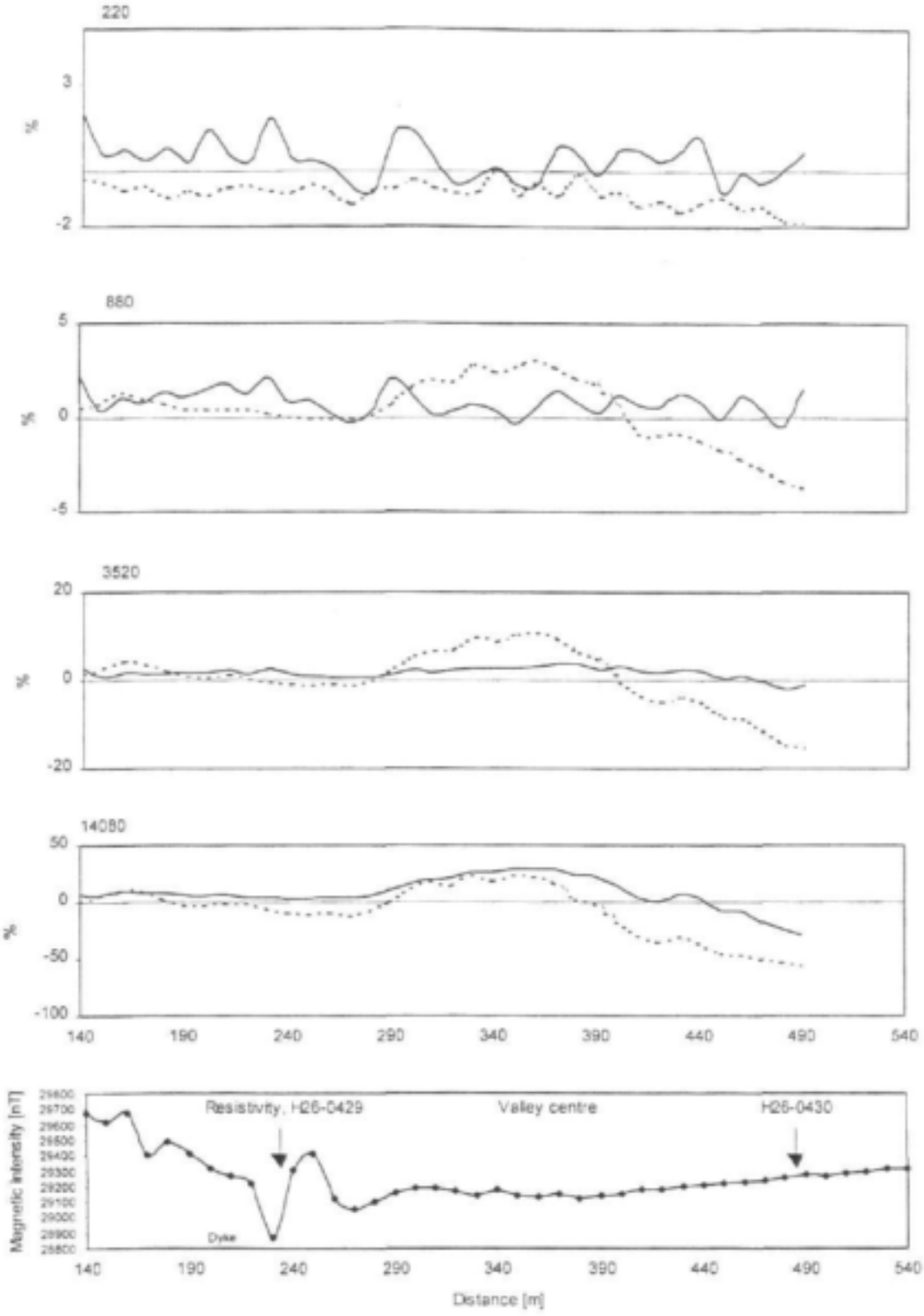

MAX-MIN electromagnetic and magnetic profiles at site LMB10. Solid line: in-phase [%]; dotted line: out-of phase [%]; coil separation 100m, station spacing 10m. Traverse direction: NNW-SSE

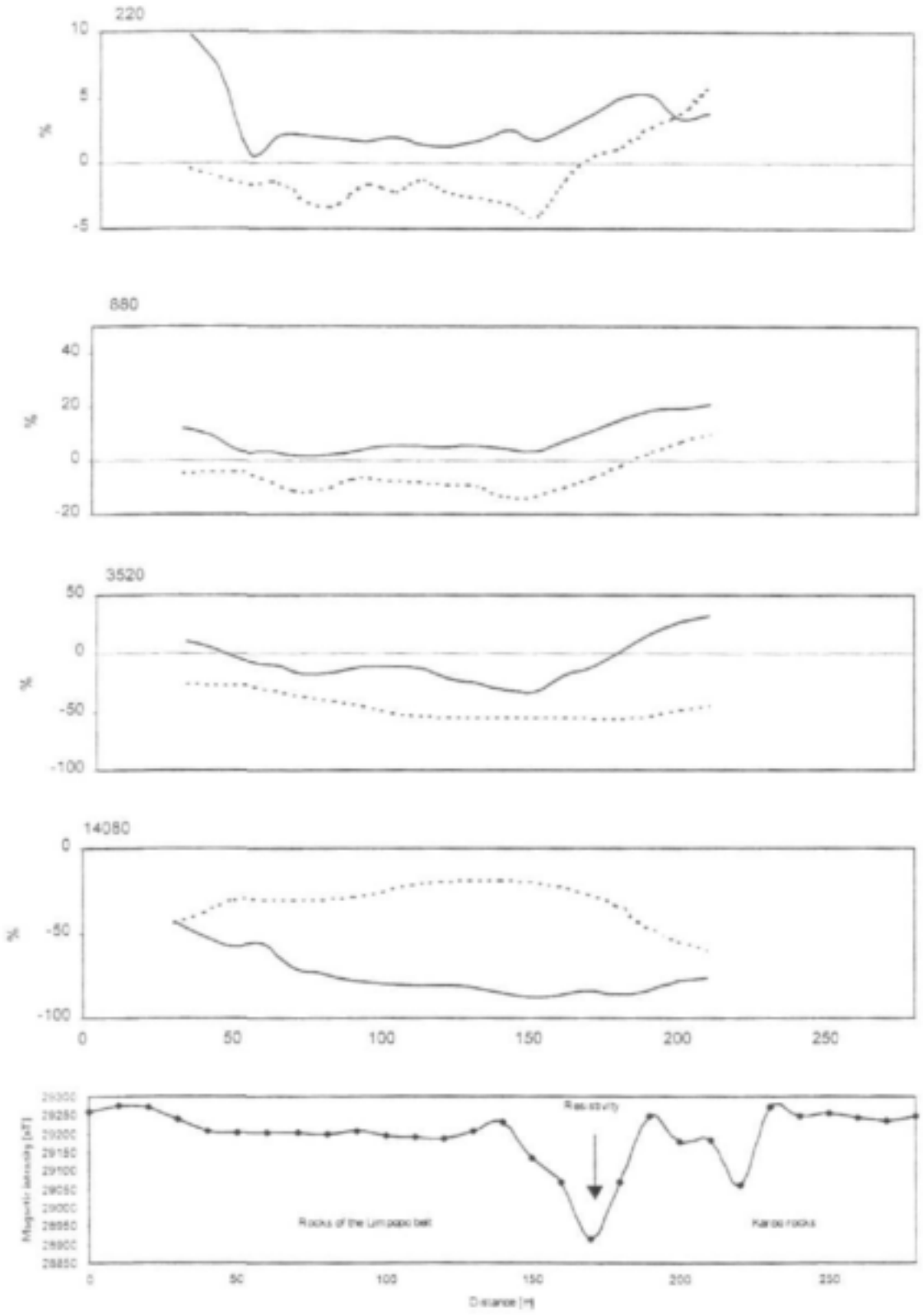

MAX-MIN electromagnetic and magnetic profiles at site LMB12. Solid line: in-phase [%]; dotted line: out-of phase [%]; coil separation 100m, station spacing 10m. Traverse direction: N-S

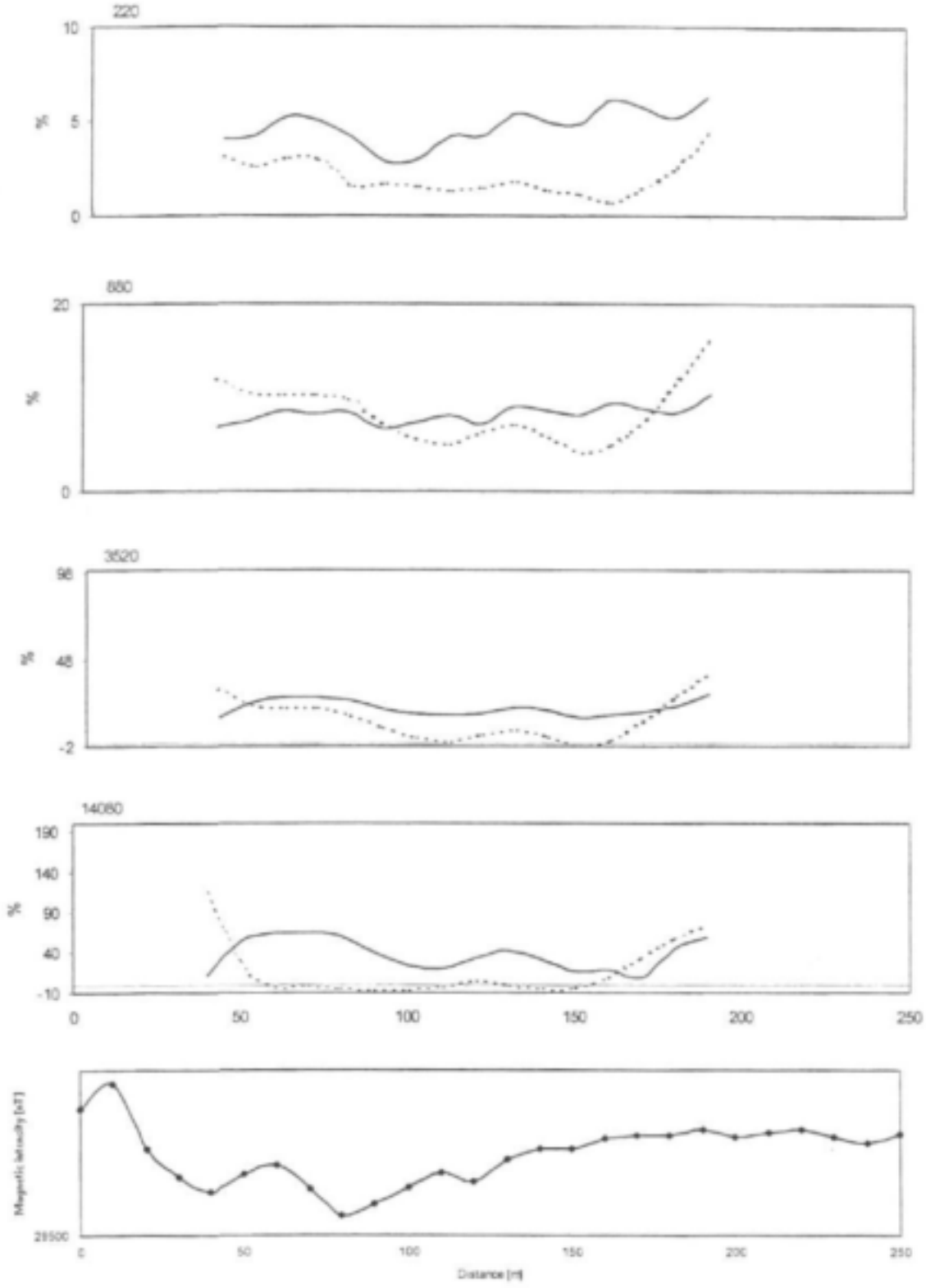

MAX-MIN electromagnetic and magnetic profiles at site LMB14. Solid line: in-phase [%]; dotted line: out-of phase [%]; coil separation 100m, station spacing 10m. Traverse direction: S-N

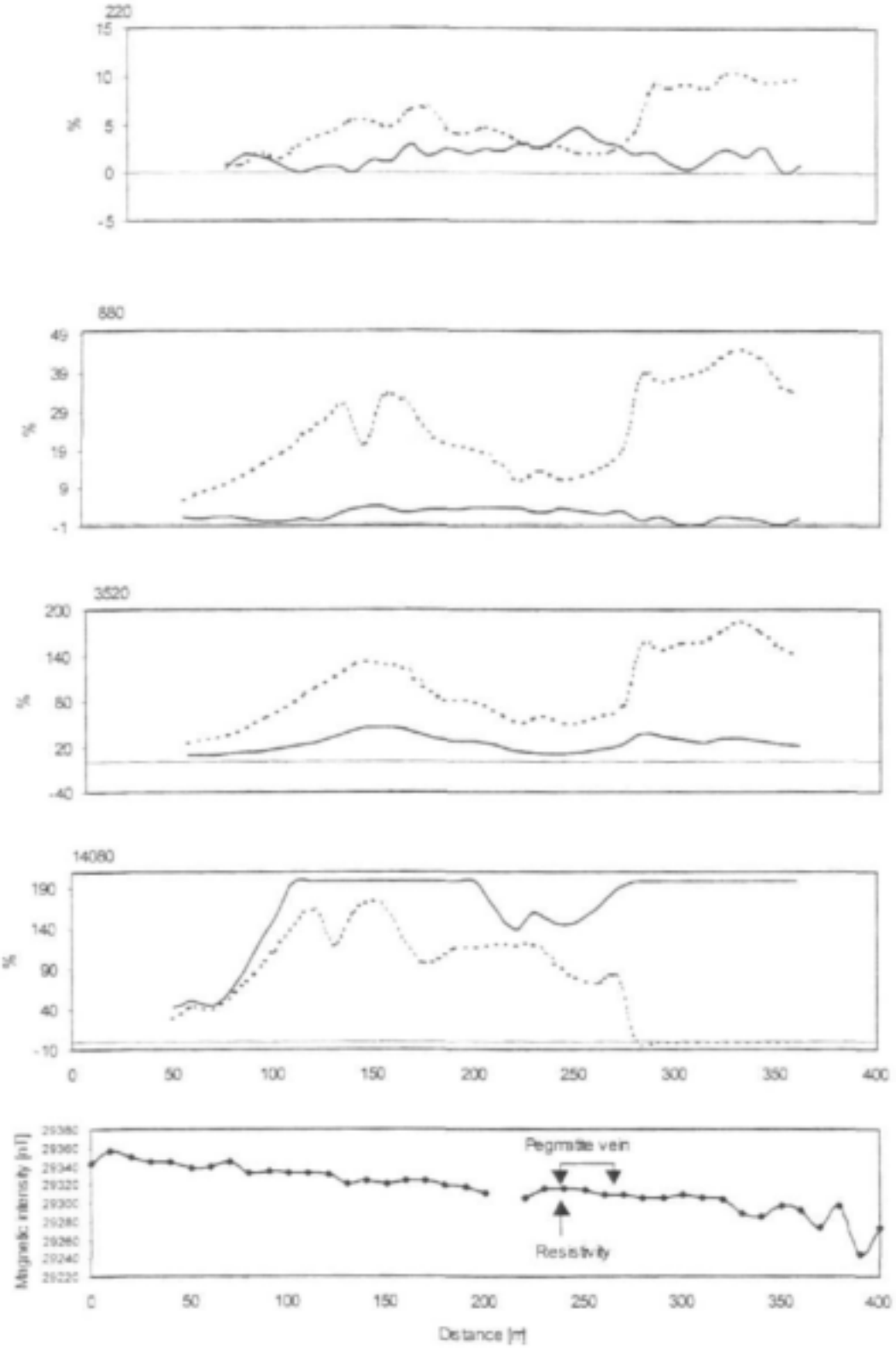

MAX-MIN electromagnetic and magnetic profiles at site LMB19. Solid line: in-phase [%]; dotted line: out-of phase [%]; coil separation 100m, station spacing 10m. Traverse direction: E-W

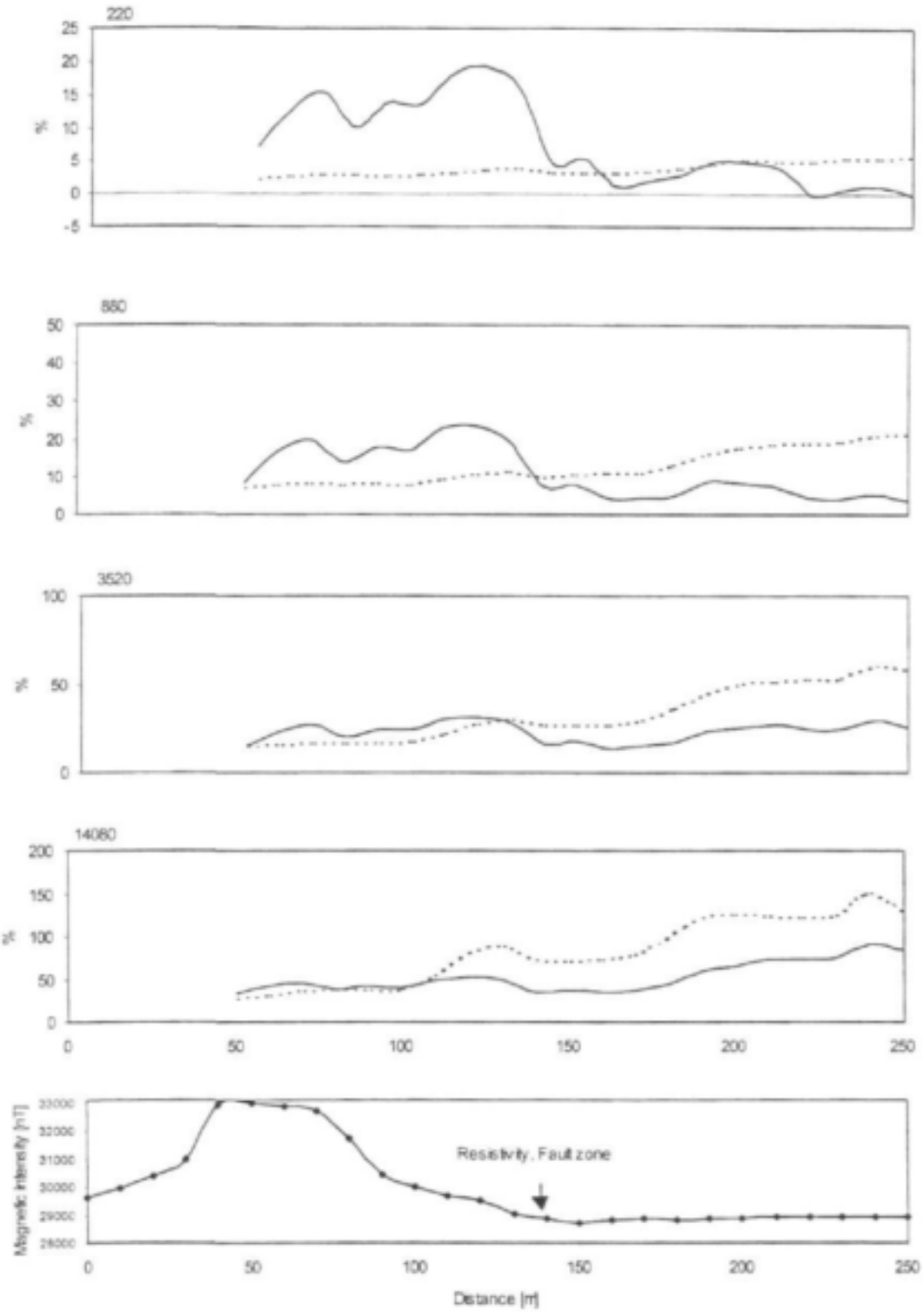

MAX-MIN electromagnetic and magnetic profiles at site LMB22. Solid line: in-phase [%]; dotted line: out-of phase [%]; coil separation 50m, station spacing 10m. Traverse direction: ESE-WNW

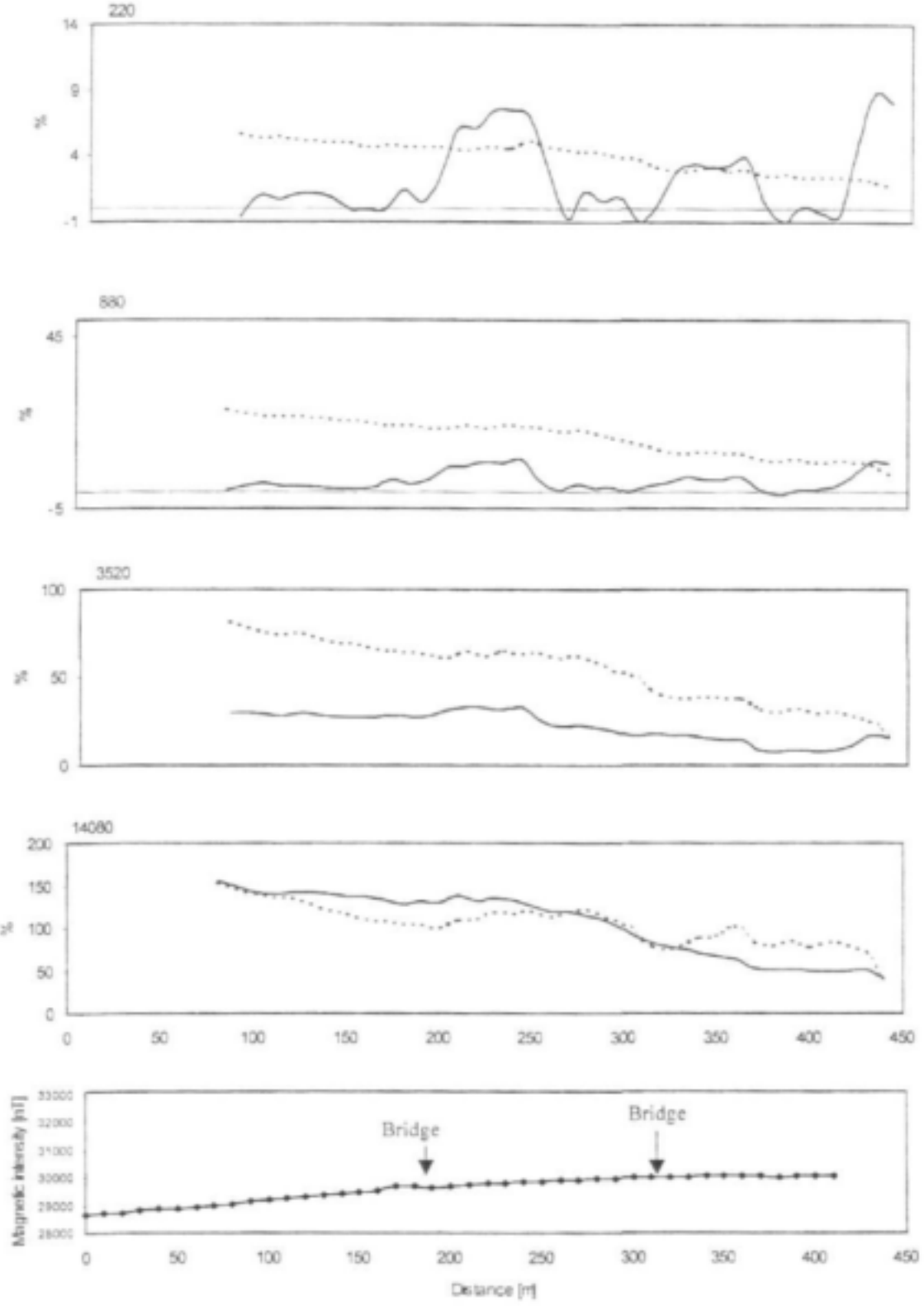

MAX-MIN electromagnetic and magnetic profiles at site LMB25. Solid line: in-phase [%]; dotted line: out-of phase [%]; coil separation 50m, station spacing 10m. Traverse direction: SW-NE

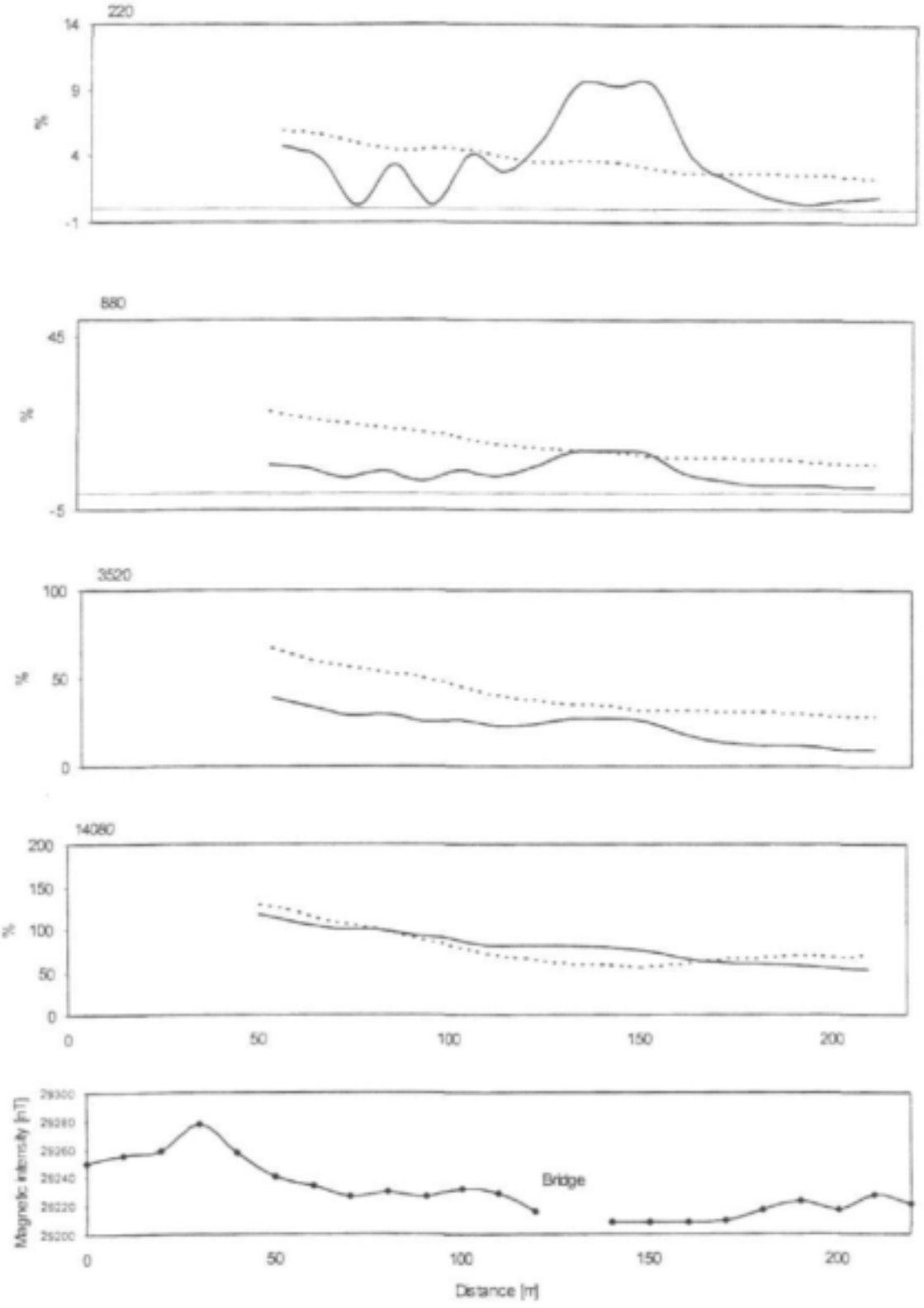

MAX-MIN electromagnetic and magnetic profiles at site LMB26. Solid line: in-phase [%]; dotted line: out-of phase [%]; coil separation 50m, station spacing 10m. Traverse direction: W-E

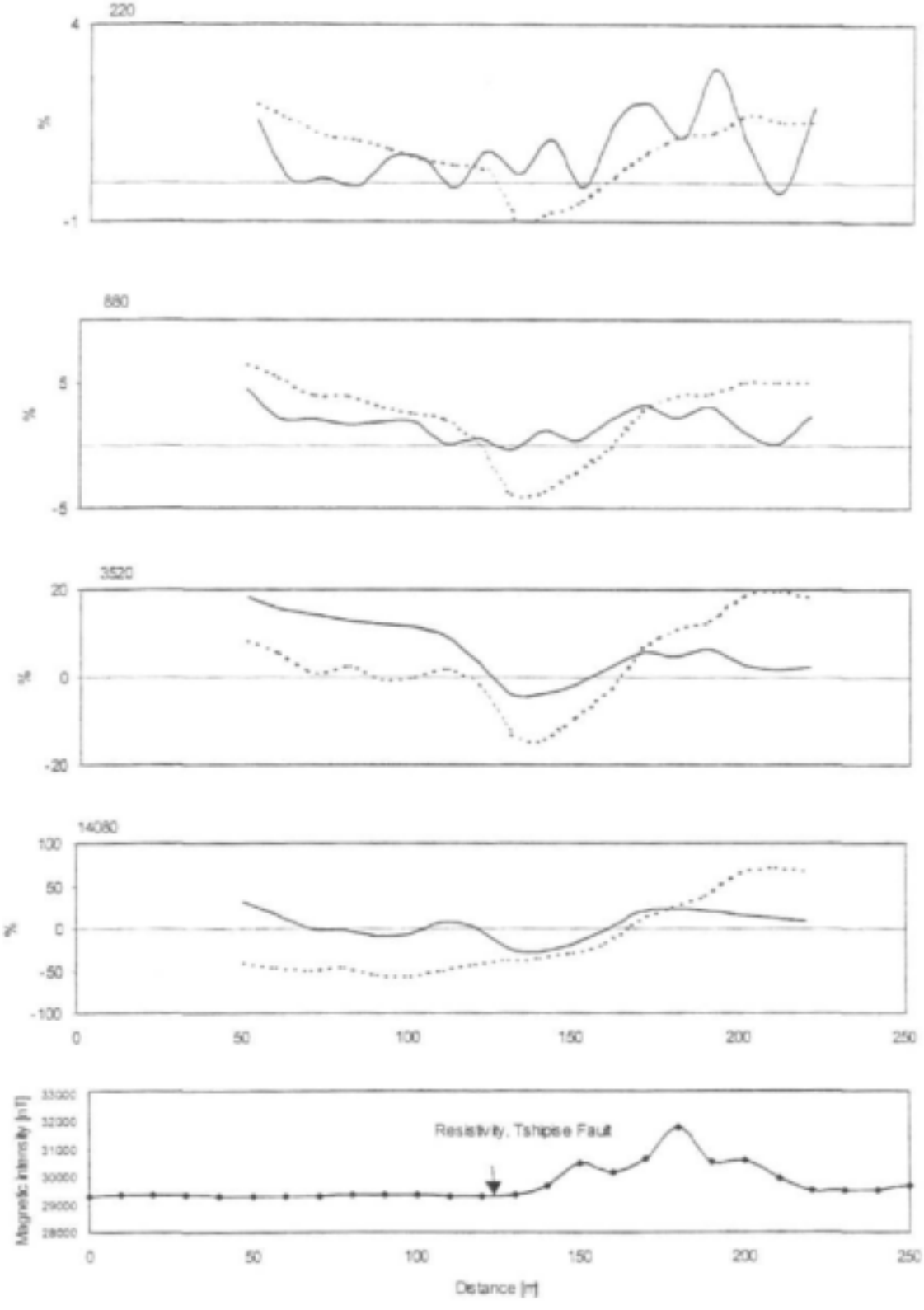

MAX-MIN electromagnetic and magnetic profiles at site LMB24. Solid line: in-phase [%]; dotted line: out-of phase [%]; coil separation 50m, station spacing 10m. Traverse direction: SSE-NNW

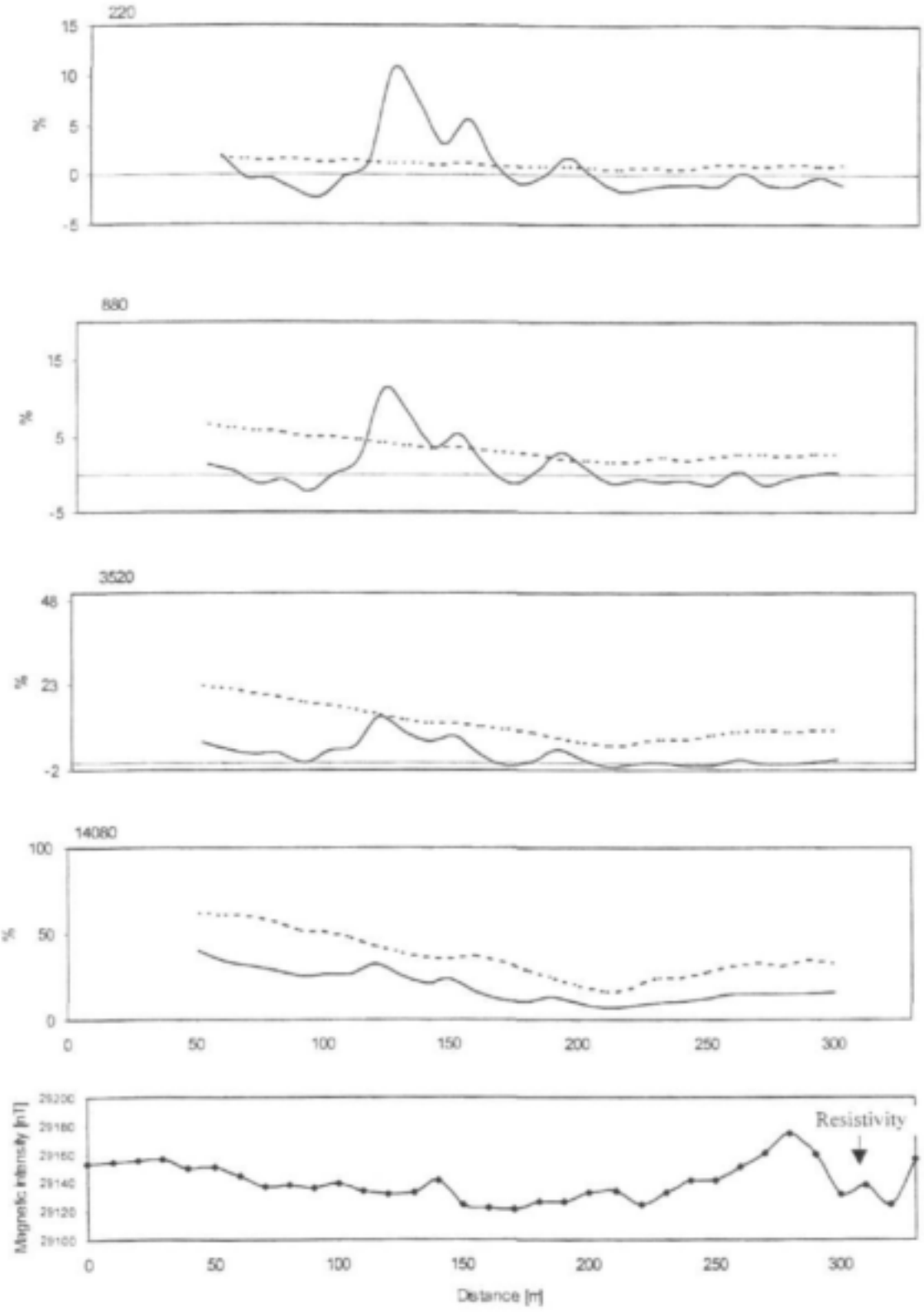

MAX-MIN electromagnetic and magnetic profiles at site LMB20. Solid line: in-phase [%]; dotted line: out-of phase [%]; coil separation 50m, station spacing 10m. Traverse direction: WSW-ENE

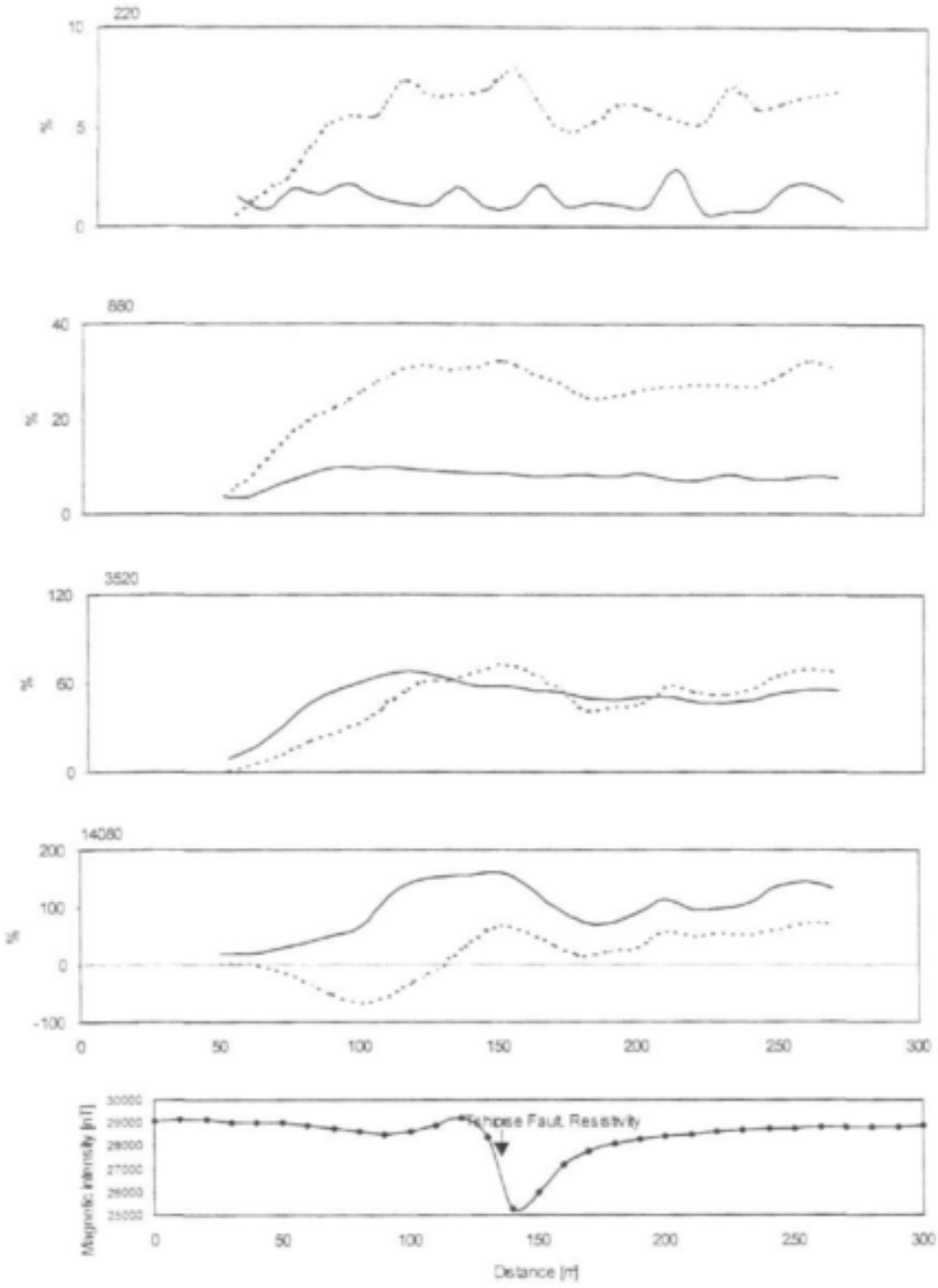

MAX-MIN electromagnetic and magnetic profiles at site LMB18. Solid line: in-phase [%]; dotted line: out-of phase [%]; coil separation 100m, station spacing 10m. Traverse direction: SSE-NNW

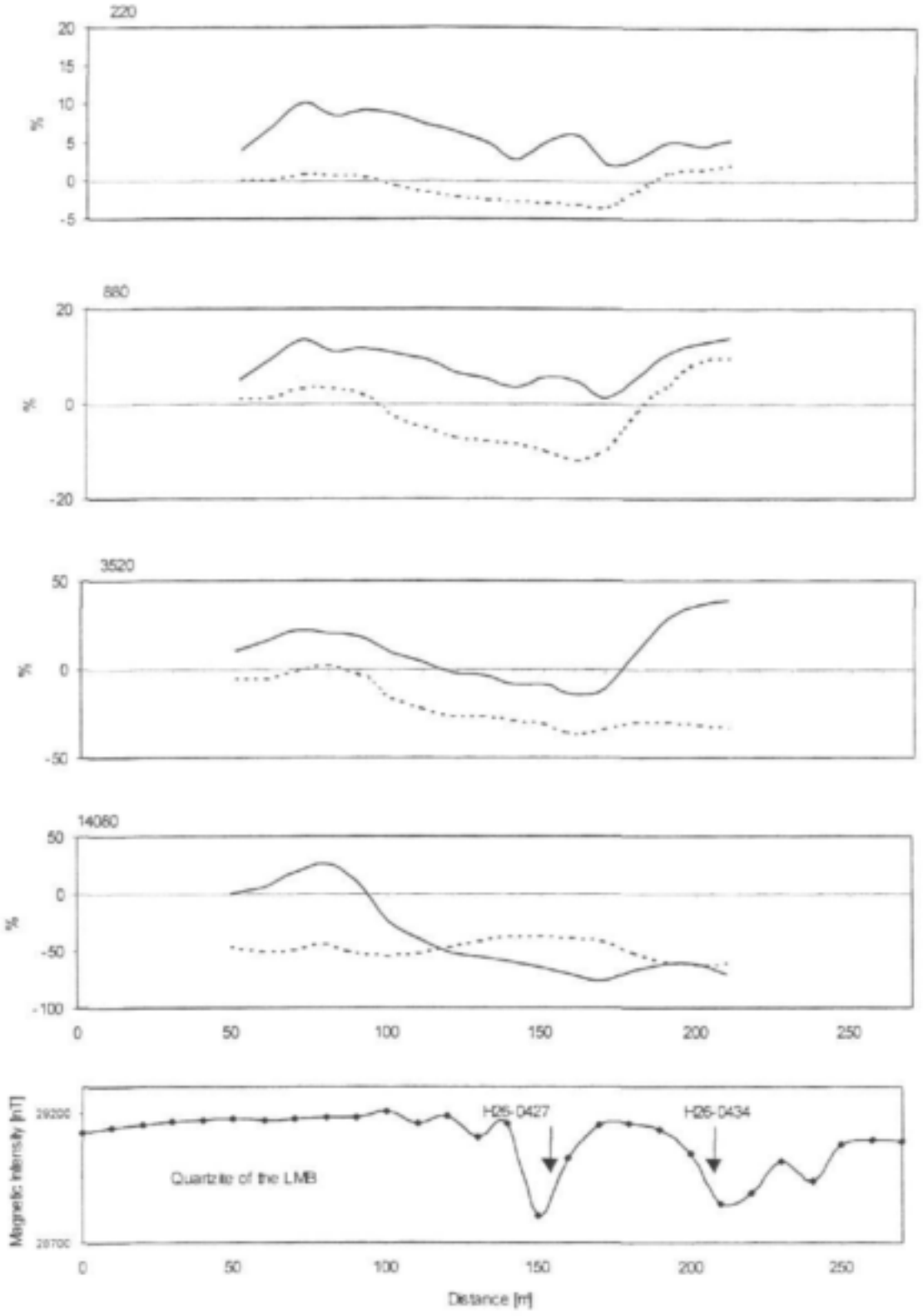

MAX-MIN electromagnetic and magnetic profiles at site LMB13. Solid line: in-phase [%]; dotted line: out-of phase [%]; coil separation 100m, station spacing 10m. Traverse direction: N-S

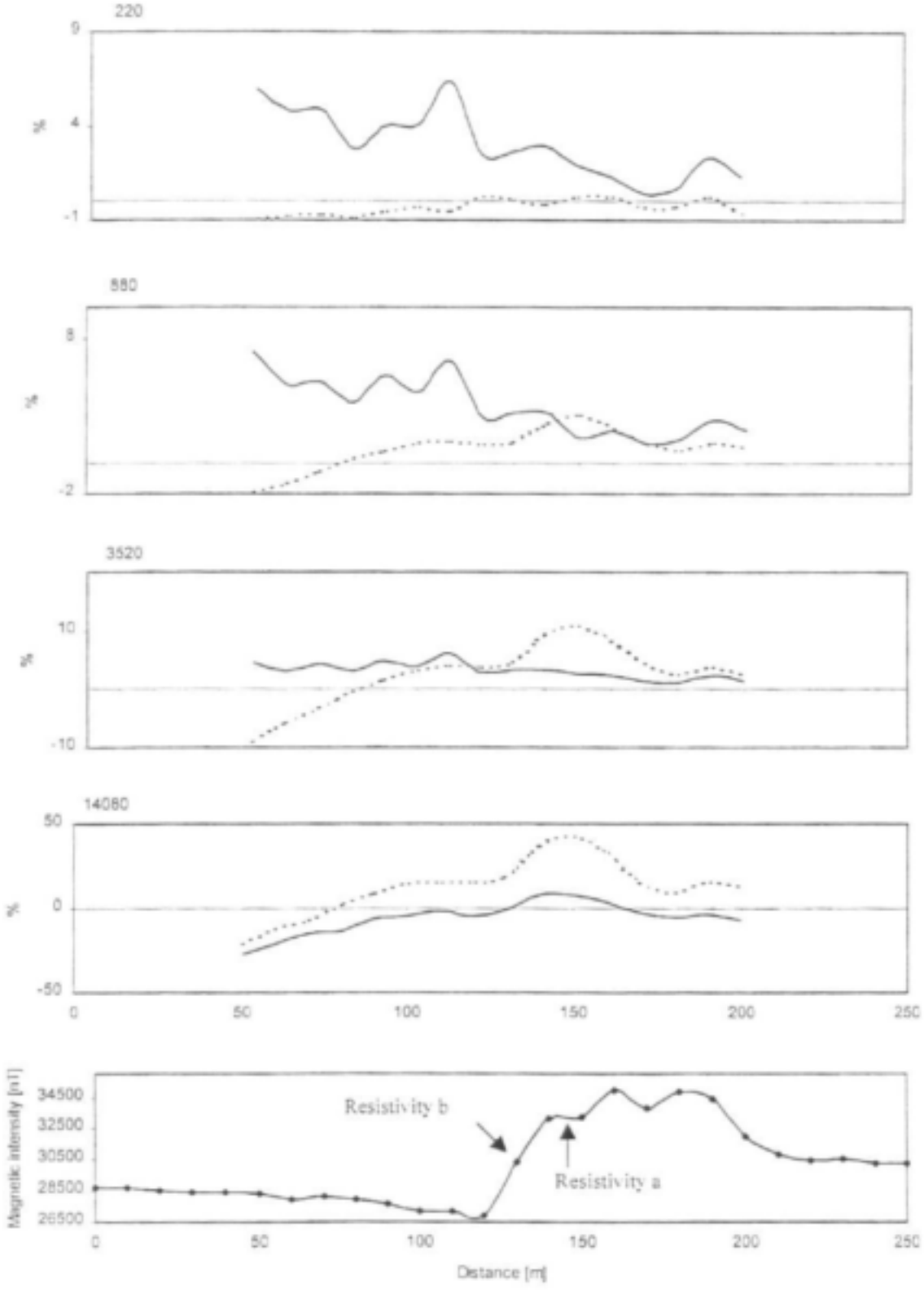

MAX-MIN electromagnetic and magnetic profiles at site LMB11. Solid line: in-phase [%]; dotted line: out-of phase [%]: coil separation 100m, station spacing 10m. Traverse direction: S-N

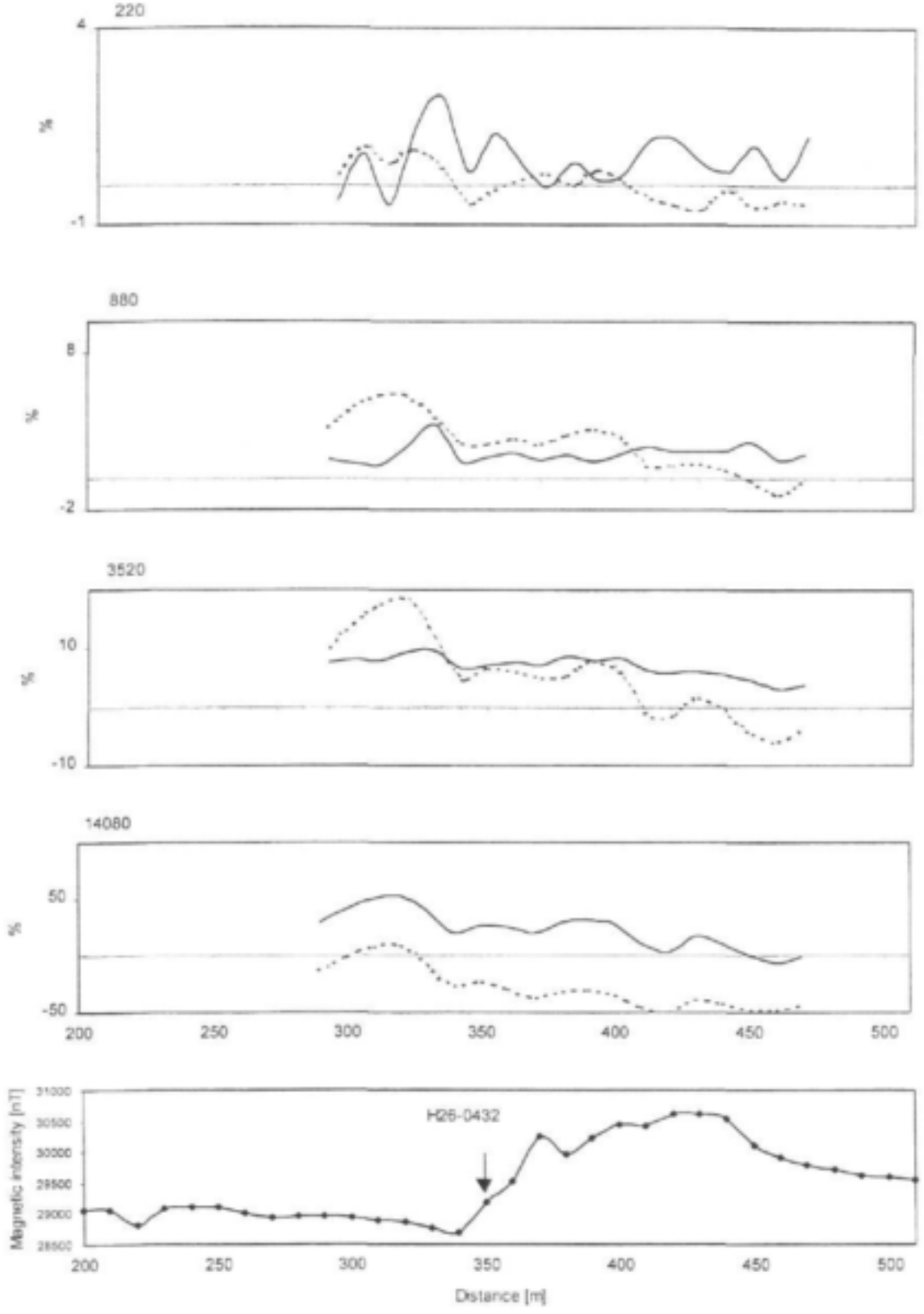

MAX-MIN electromagnetic and magnetic profiles at site LMB9. Solid line: in-phase [%]; dotted line: out-of phase [%]; coil separation 100m, station spacing 10m. Traverse direction: SSE-NNW

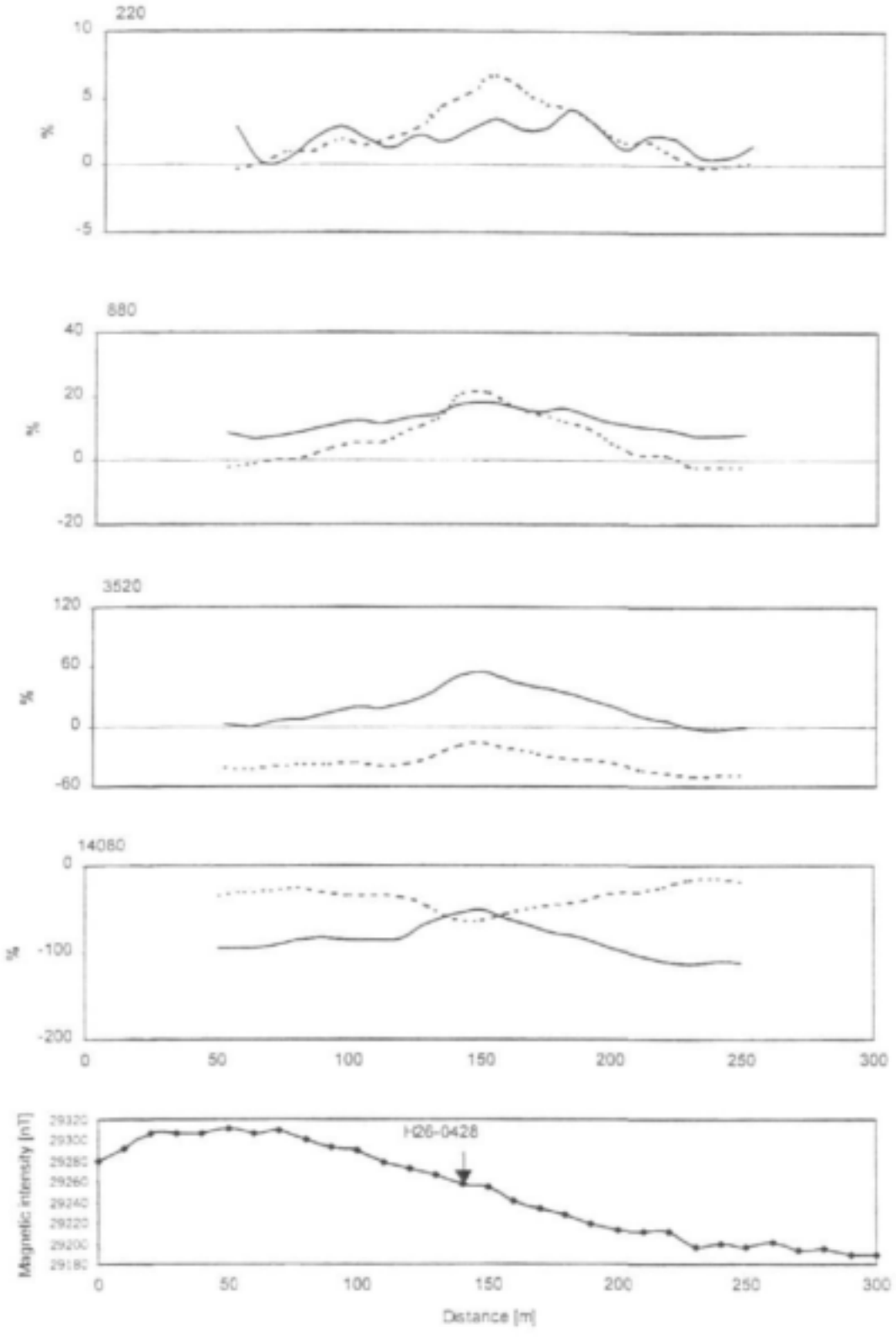

MAX-MIN electromagnetic and magnetic profiles at site LMB6. Solid line: in-phase [%]; dotted line: out-of phase [%]; coil separation 100m, station spacing 10m. Traverse direction: NW-SE

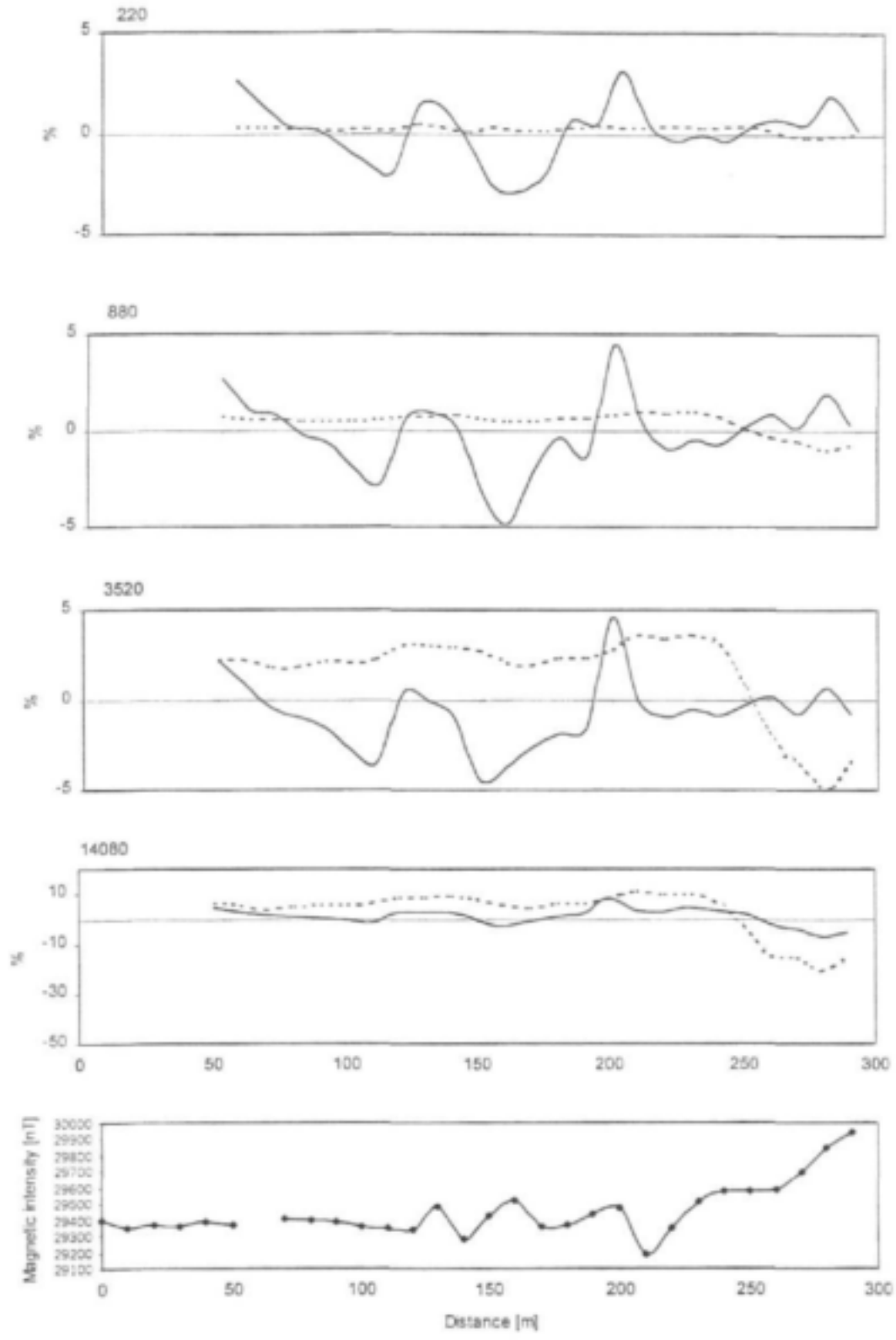

MAX-MIN electromagnetic and magnetic profiles at site LMB4. Solid line: in-phase [%]; dotted line: out-of phase [%]; coil separation 50m, station spacing 10m. Traverse direction: S-N

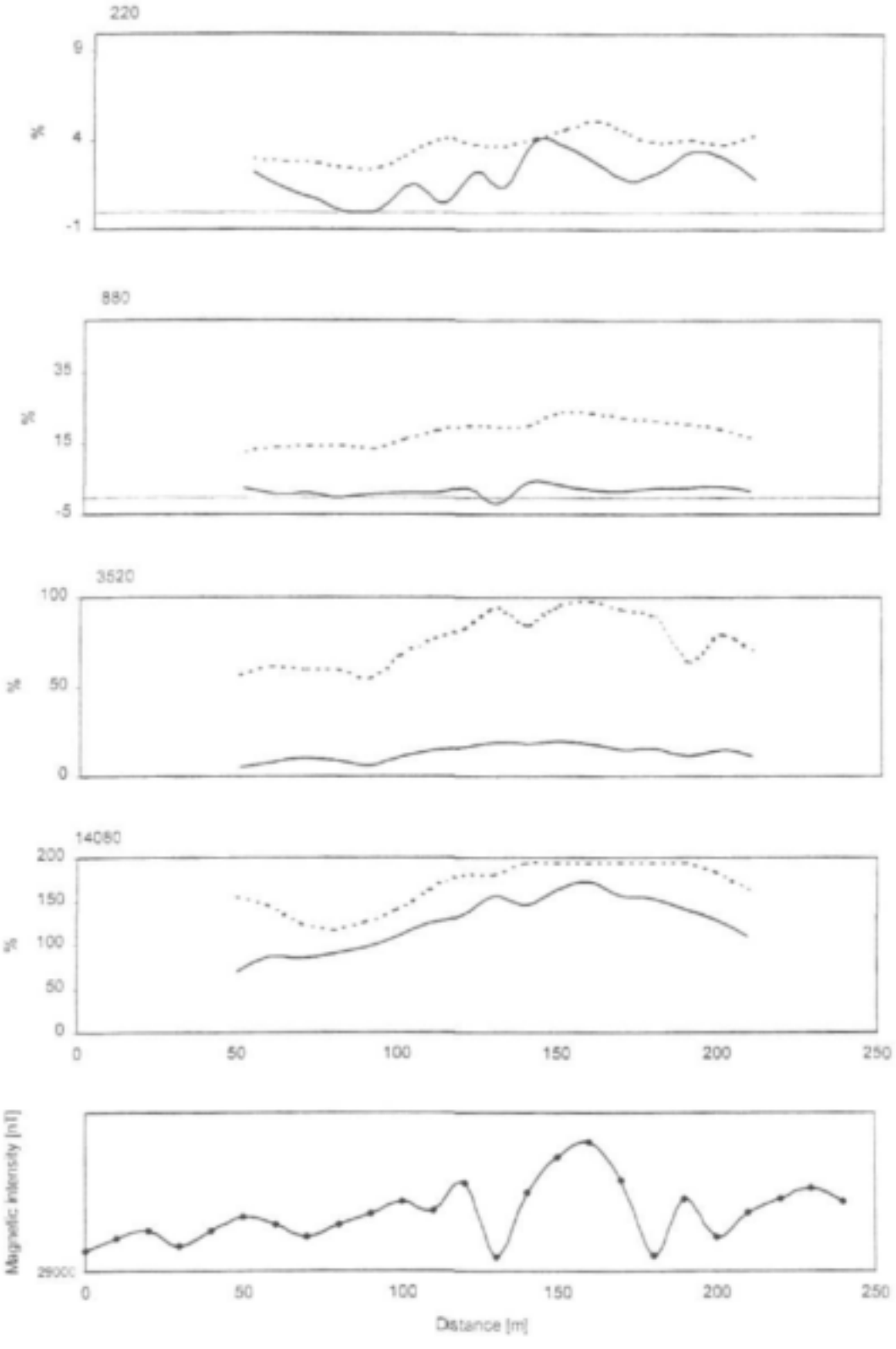

MAX-MIN electromagnetic and magnetic profiles at site LMB2. Solid line: in-phase [%]; dotted line: out-of phase [%]: coil separation 100m, station spacing 10m. Traverse direction: S-N

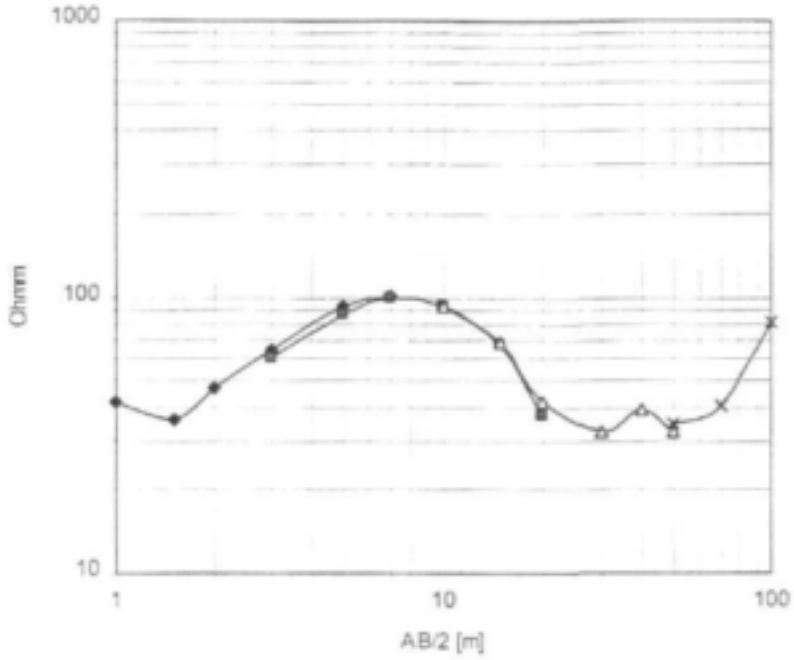

Resistivity data for site LMB5

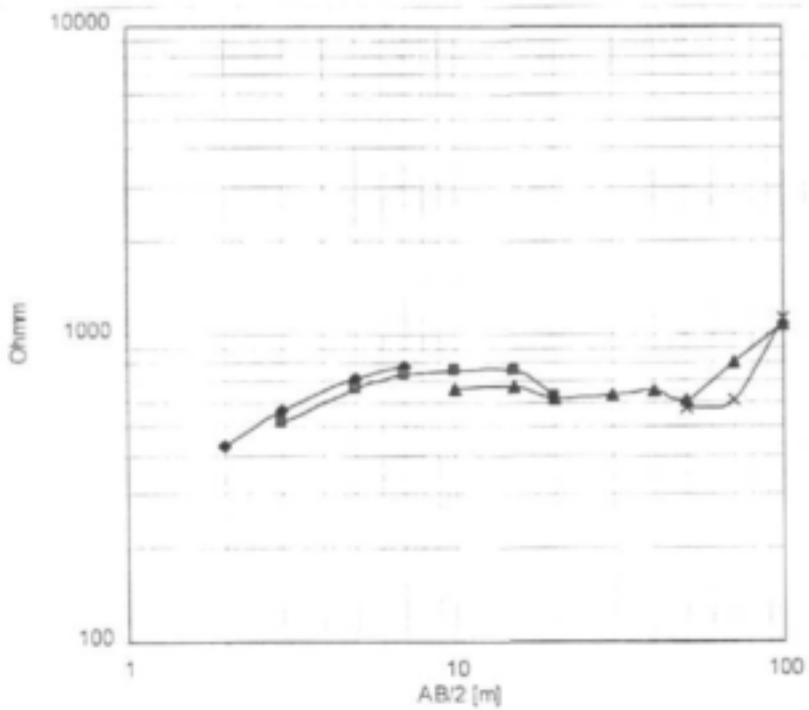

Resistivity data for site LMB10

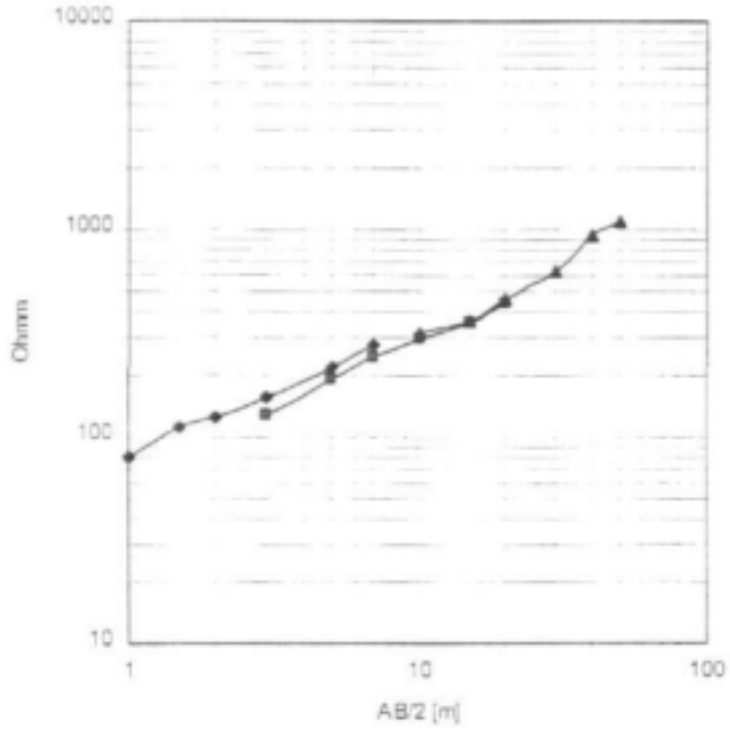

Resistivity data for site LMB11a

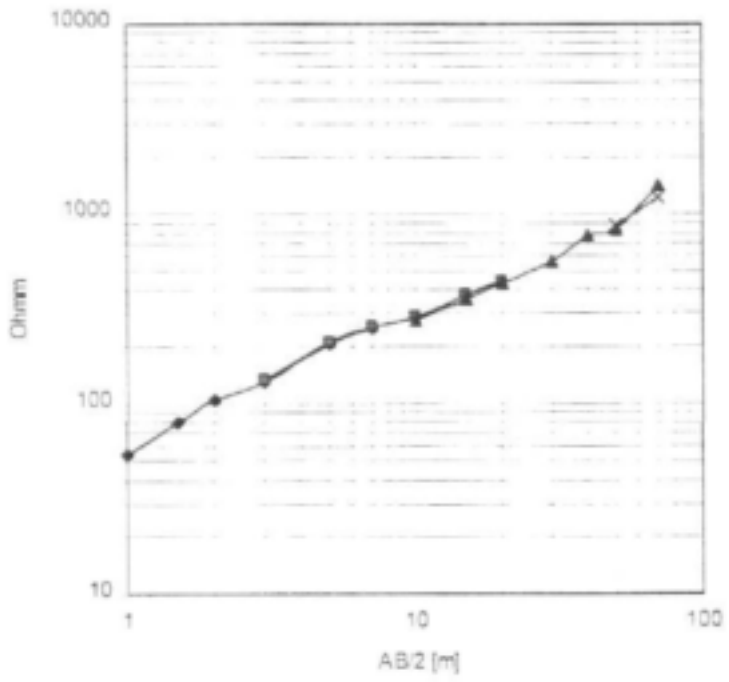

Resistivity data for at site LMB11b

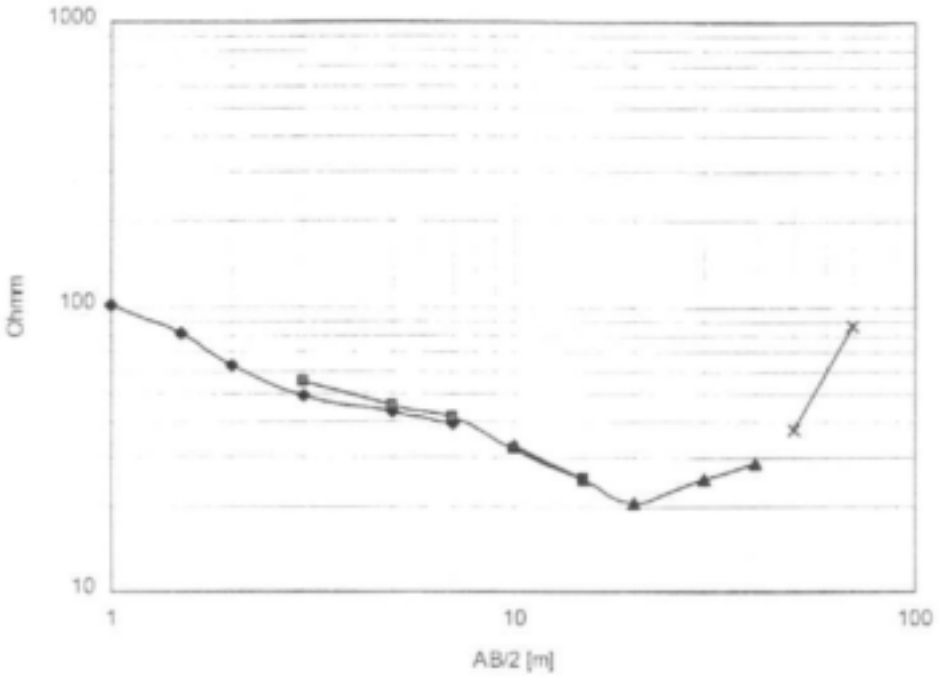

Resistivity data for site LMB12

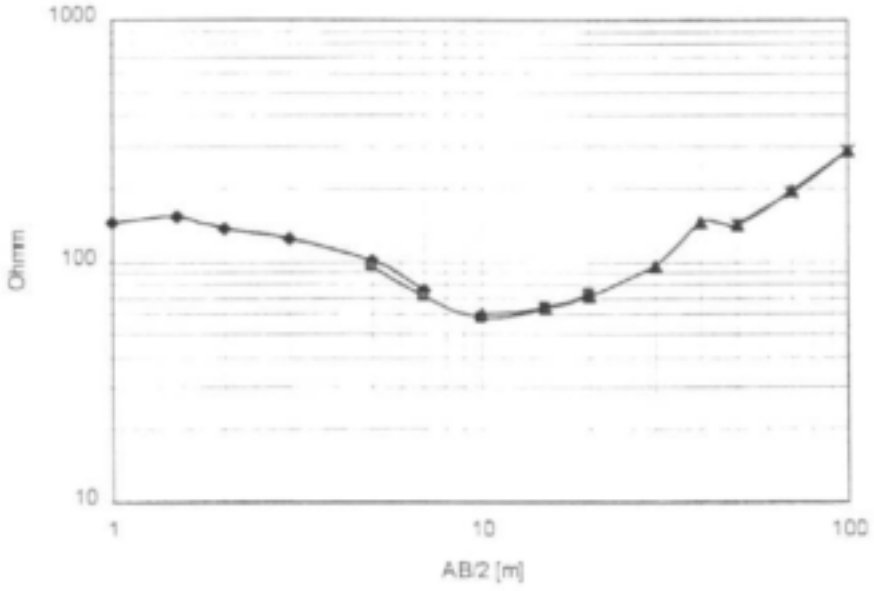

Resistivity data for site LMB18

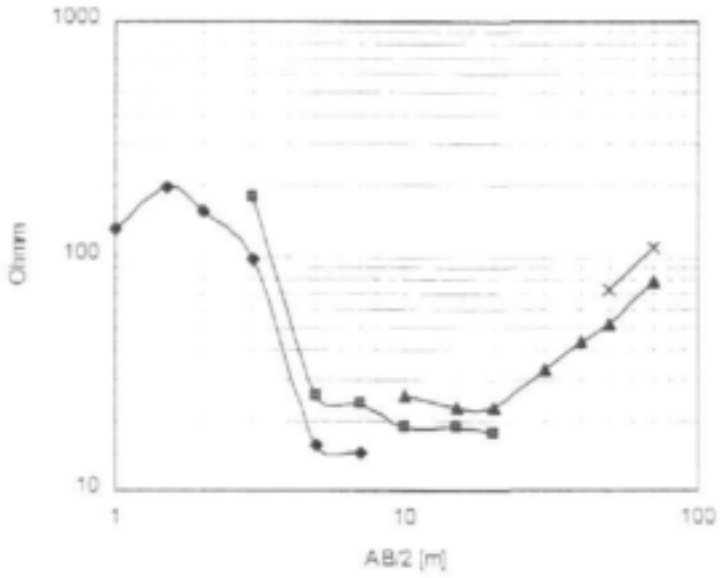

Resistivity data for site LMB19

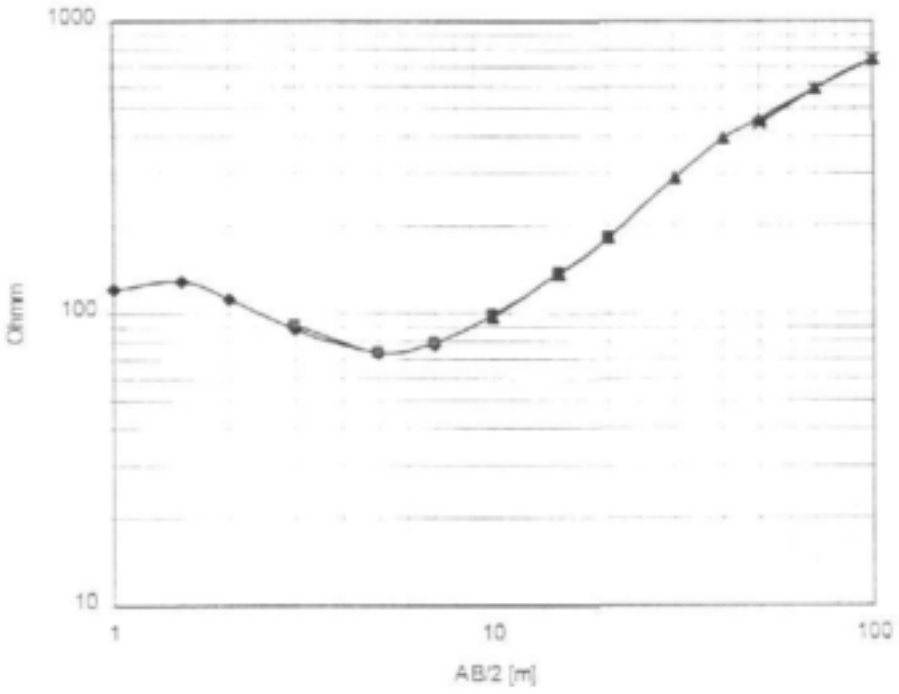

Resistivity data for site LMB20

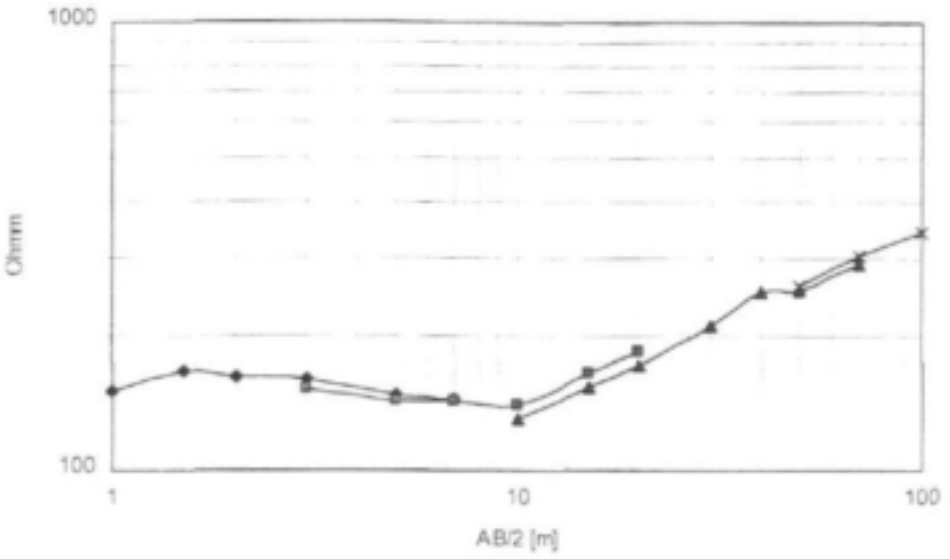

Resistivity data for site LMB21

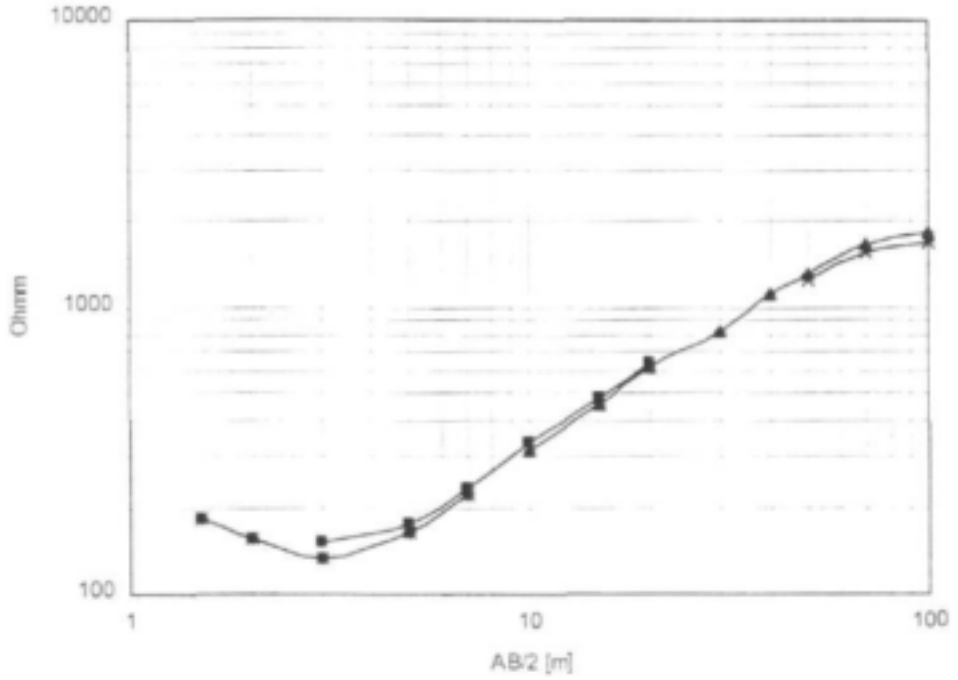

Resistivity data for site LMB22a

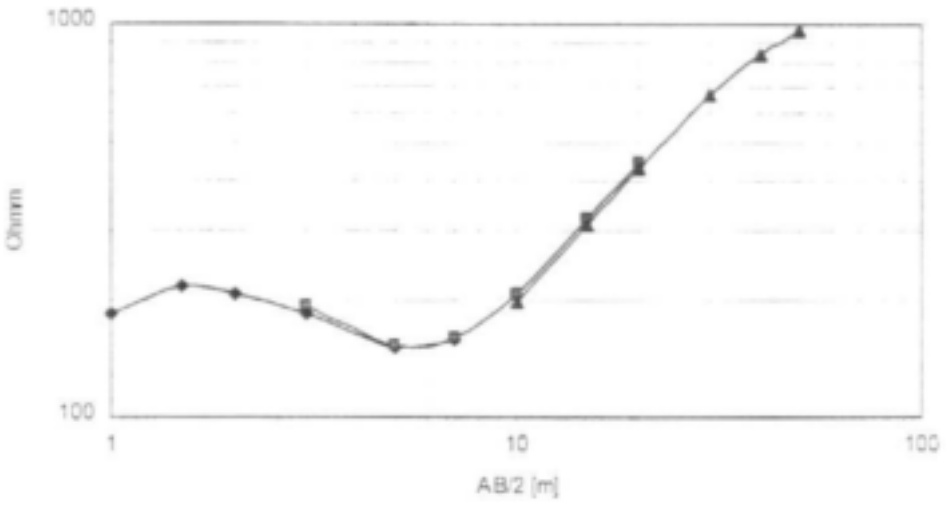

Resistivity data for at site LMB22b

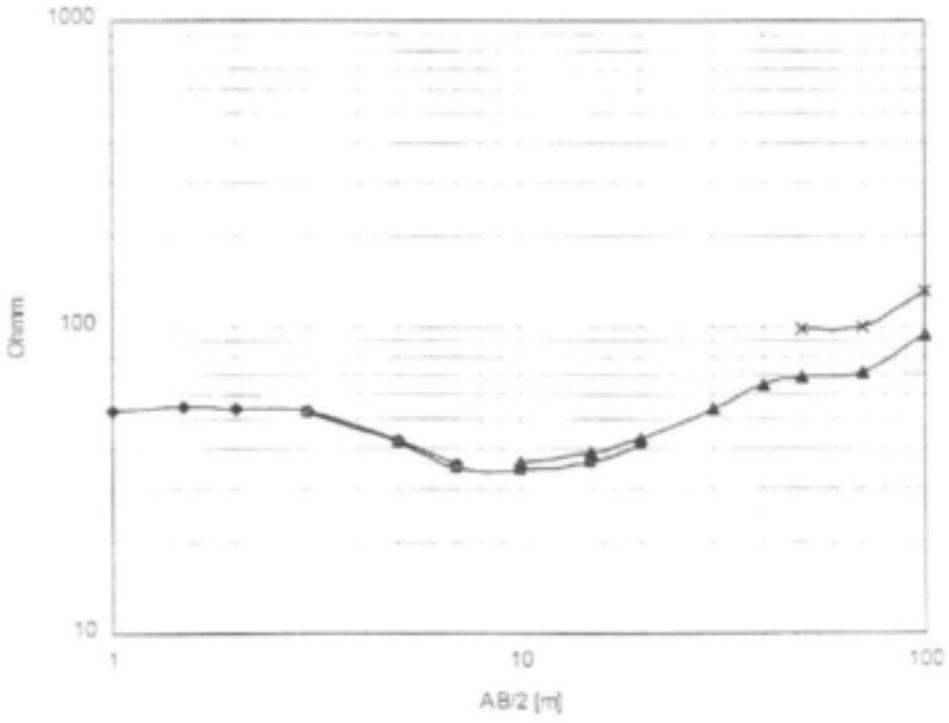

Resistivity data for at site LMB24

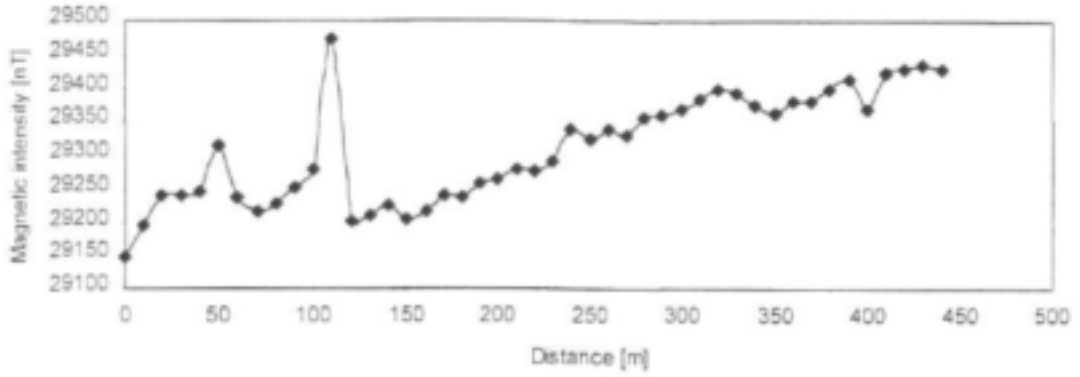

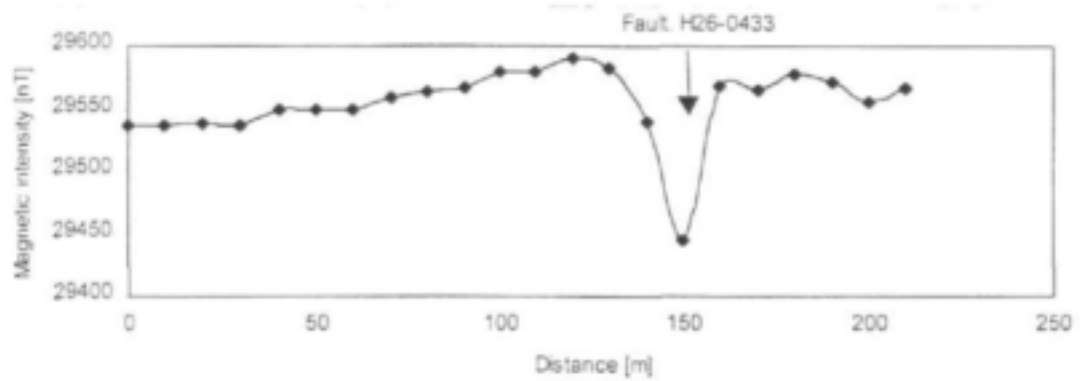

Magnetic data on site NMP15. Traverse direction: S-N, station spacing: 10m

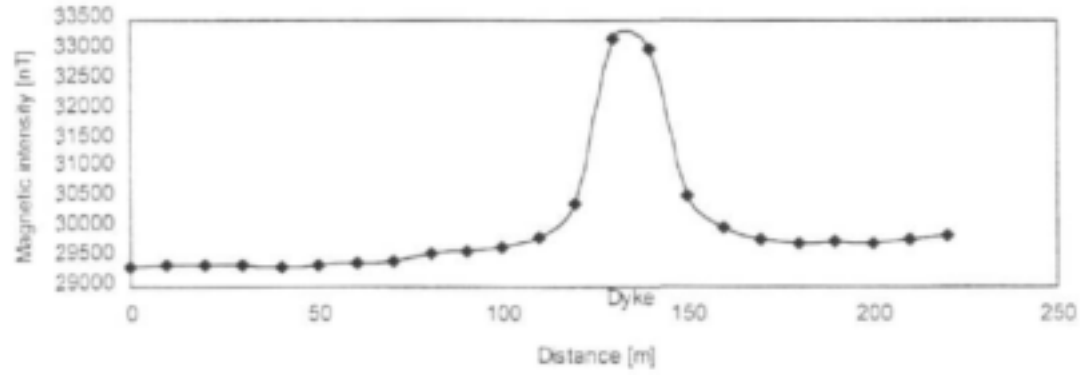

Magnetic data on site NMP16. Traverse direction: S-N, station spacing: 10m

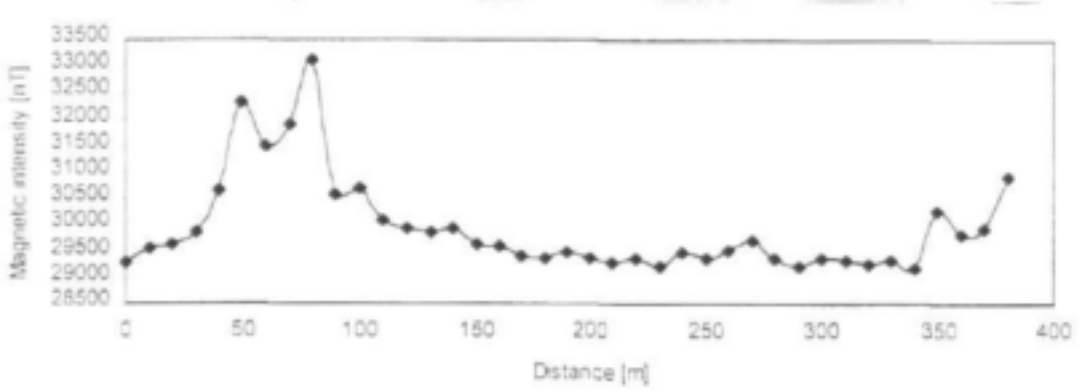

Magnetic data on site NMP17. Traverse direction: N-S, station spacing: 10m

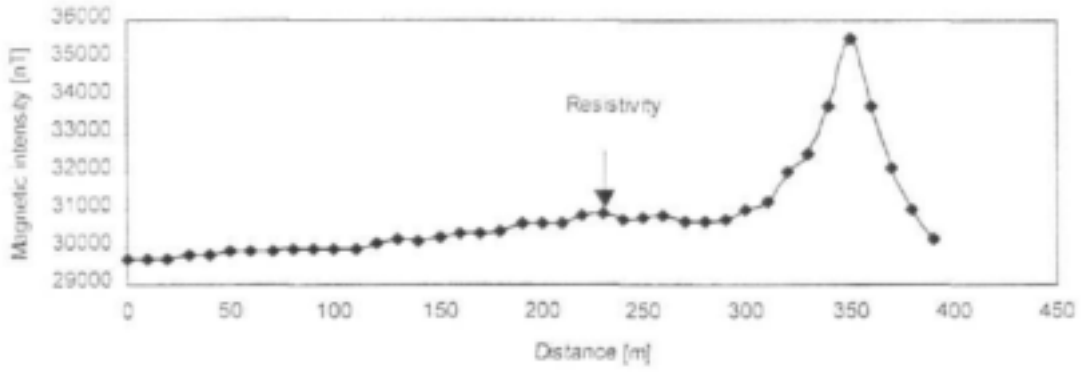

Magnetic data on site NMP21. Traverse direction: NW-SE, station spacing: 10m

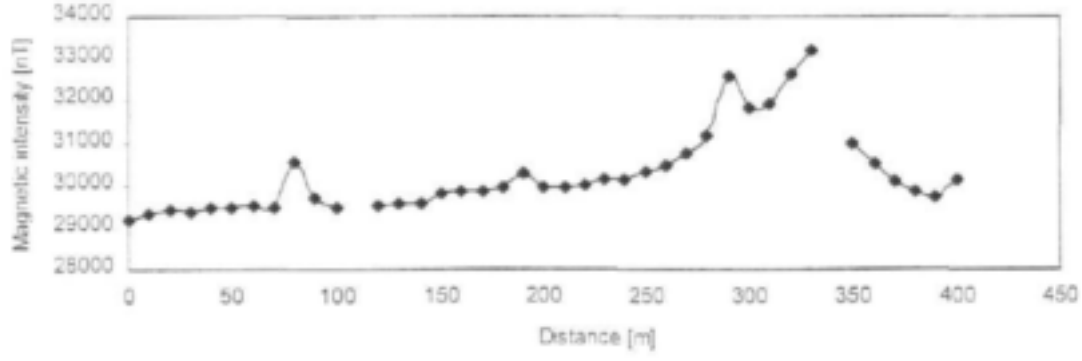

Magnetic data on site NMP23. Traverse direction: NW-SE, station spacing: 10m

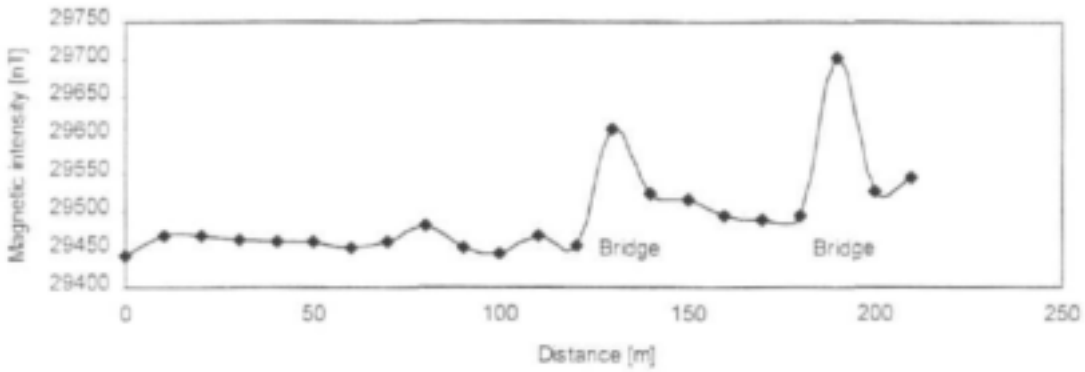

Magnetic data on site NMP27. Traverse direction: W-E, station spacing: 10m

APPENDIX 3-B

GEOLOGICAL LOGS

COUNCIL FOR GEOSCIENCE
Private Bag X112
PRETORIA 0001
REPUBLIC OF SOUTH AFRICA

GROUNDWATER DEVELOPMENT IN COMPLEX TERRAIN

HOLE No: H26-0426
Sheet 1 of 2

PROJECT NUMBER: K5/966

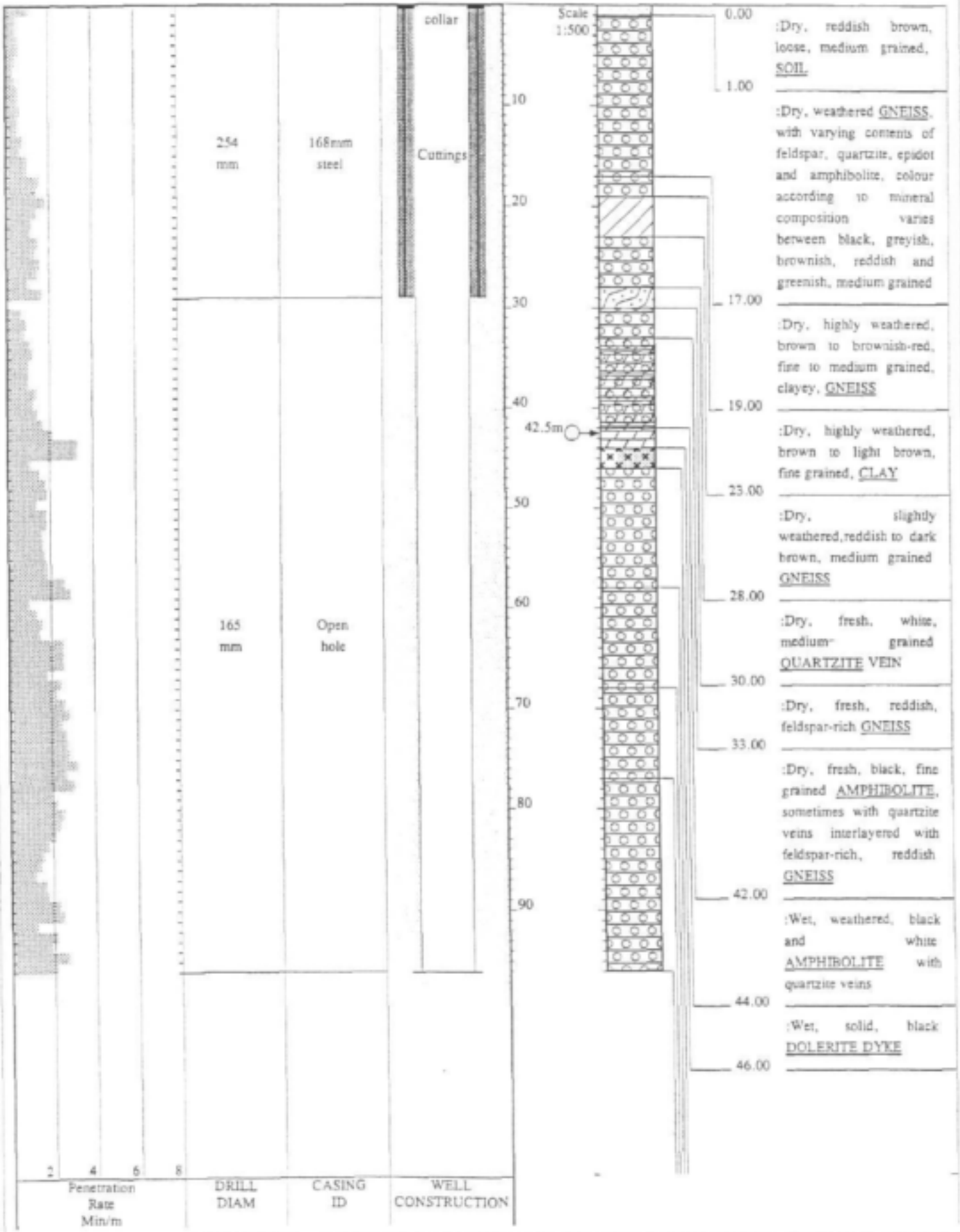

COUNCIL FOR GEOSCIENCE
Private Bag X112
PRETORIA 0001
REPUBLIC OF SOUTH AFRICA

GROUNDWATER DEVELOPMENT IN COMPLEX TERRAIN

HOLE No: H26-0427
Sheet 1 of 1

PROJECT NUMBER: K5/966

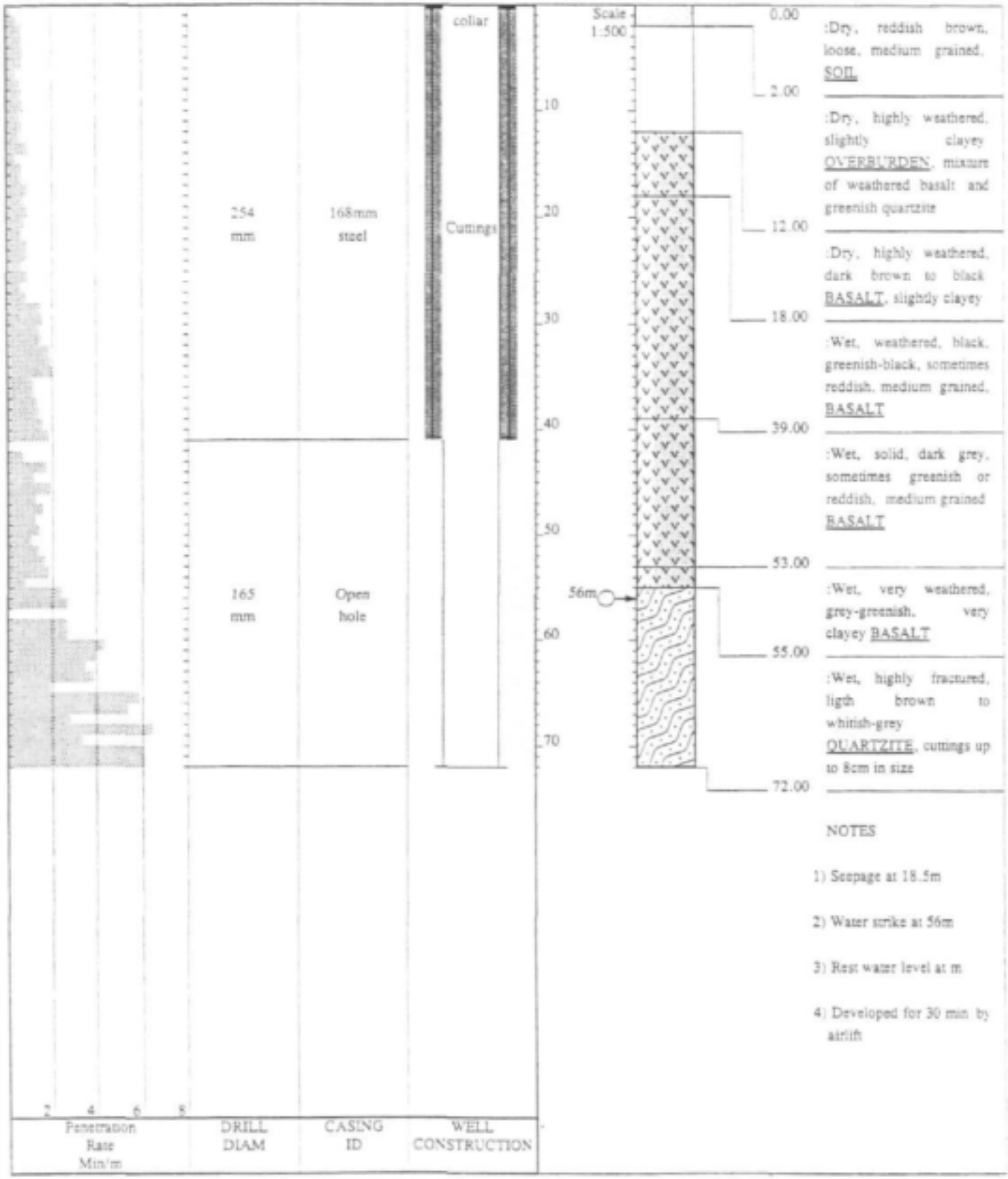

:Dry, reddish brown, loose, medium grained, SOIL

:Dry, highly weathered, slightly clayey OVERBURDEN, mixture of weathered basalt and greenish quartzite

:Dry, highly weathered, dark brown to black BASALT, slightly clayey

:Wet, weathered, black, greenish-black, sometimes reddish, medium grained, BASALT

:Wet, solid, dark grey, sometimes greenish or reddish, medium grained BASALT

:Wet, very weathered, grey-greenish, very clayey BASALT

:Wet, highly fractured, ligth brown to whitish-grey QUARTZITE, cuttings up to 8cm in size

NOTES

1) Seepage at 18.5m

2) Water strike at 56m

3) Rest water level at m

4) Developed for 30 min by airlift

CONTRACTOR : DWAF
DRILLED BY : Mr. Mabasa
DRILL METHOD : DTH HAMMER
SAMPLING : BLOWN CUTTINGS

LOGGED BY : I. NEUMANN
SETUP FILE : STANDARD.SET

INCLINATION : Vertical
DIAMETER : 165 mm
DRILL DATE : 23 October 2000
CASING TYPE : 4,5 mm steel

DATE : 26/01/01 10:07
TEXT : C:\DOTPLOT\DATA\H26-0427.TXT

ELEVATION : 776m
COLLAR HEIGHT : 0.28 m
BLOW YIELD : > 23 l/s

HOLE No: H26-0427
Goudmyn 327MR

COUNCIL FOR GEOSCIENCE
Private Bag X112
PRETORIA 0001
REPUBLIC OF SOUTH AFRICA

GROUNDWATER DEVELOPMENT IN COMPLEX TERRAIN

HOLE No: H26-0428
Sheet 2 of 2

PROJECT NUMBER: K5/966

108.00

NOTES

1) Borehole is dry

2) Borehole is backfilled

2 4 6 8

Penetration Rate Min/m	DRILL DIAM	CASING ID	WELL CONSTRUCTION : Concrete collar : Cuttings :

CONTRACTOR : DWAF
DRILLED BY : Mr. Mahasa
DRILL METHOD : DTH HAMMER
SAMPLING : BLOWN CUTTINGS

INCLINATION : Vertical
DIAMETER : 165 mm
DRILL DATE : 24 October 2000
CASING TYPE : 4,5 mm steel

ELEVATION : 780m
COLLAR HEIGHT :
BLOW YIELD : Dry

LOGGED BY : I. NEUMANN
SETUP FILE : STANDARD.SET

DATE : 17/01/01 13:58
TEXT : C:\DOTPLOT\DATA\H26-0428.TXT

HOLE No: H26-0428
Raditshatu

COUNCIL FOR GEOSCIENCE
Private Bag X112
PRETORIA 0001
REPUBLIC OF SOUTH AFRICA

GROUNDWATER DEVELOPMENT IN COMPLEX TERRAIN

HOLE No: H26-0429
Sheet 2 of 2

PROJECT NUMBER: K5/966

NOTES

1) Seepage at 19m

2) Water strike at 27m

3) Borehole developed for 30min by airlift

2 4 6 8 Penetration Rate Min/m	DRILL DIAM	CASING ID	WELL CONSTRUCTION

CONTRACTOR : DWAF
DRILLED BY : Mr. Mahasa
DRILL METHOD : DTH HAMMER
SAMPLING : BLOWN CUTTINGS

INCLINATION : Vertical
DIAMETER : 165 mm
DRILL DATE : 25 October 2000
CASING TYPE : 4.5 mm steel

ELEVATION : 736m
COLLAR HEIGHT :
BLOW YIELD : 1.9 l/s

LOGGED BY : I. NEUMANN
SETUP FILE : STANDARD.SET

DATE : 17/01/01 13:58
TEXT : C:\DOTPLOT\DATA\H26-0429.TXT

HOLE No: H26-0429
Simson

COUNCIL FOR GEOSCIENCE

Private Bag X112
PRETORIA 0001
REPUBLIC OF SOUTH AFRICA

GROUNDWATER DEVELOPMENT IN COMPLEX TERRAIN

HOLE No: H26-0431
Sheet 1 of 1

PROJECT NUMBER: K5/966

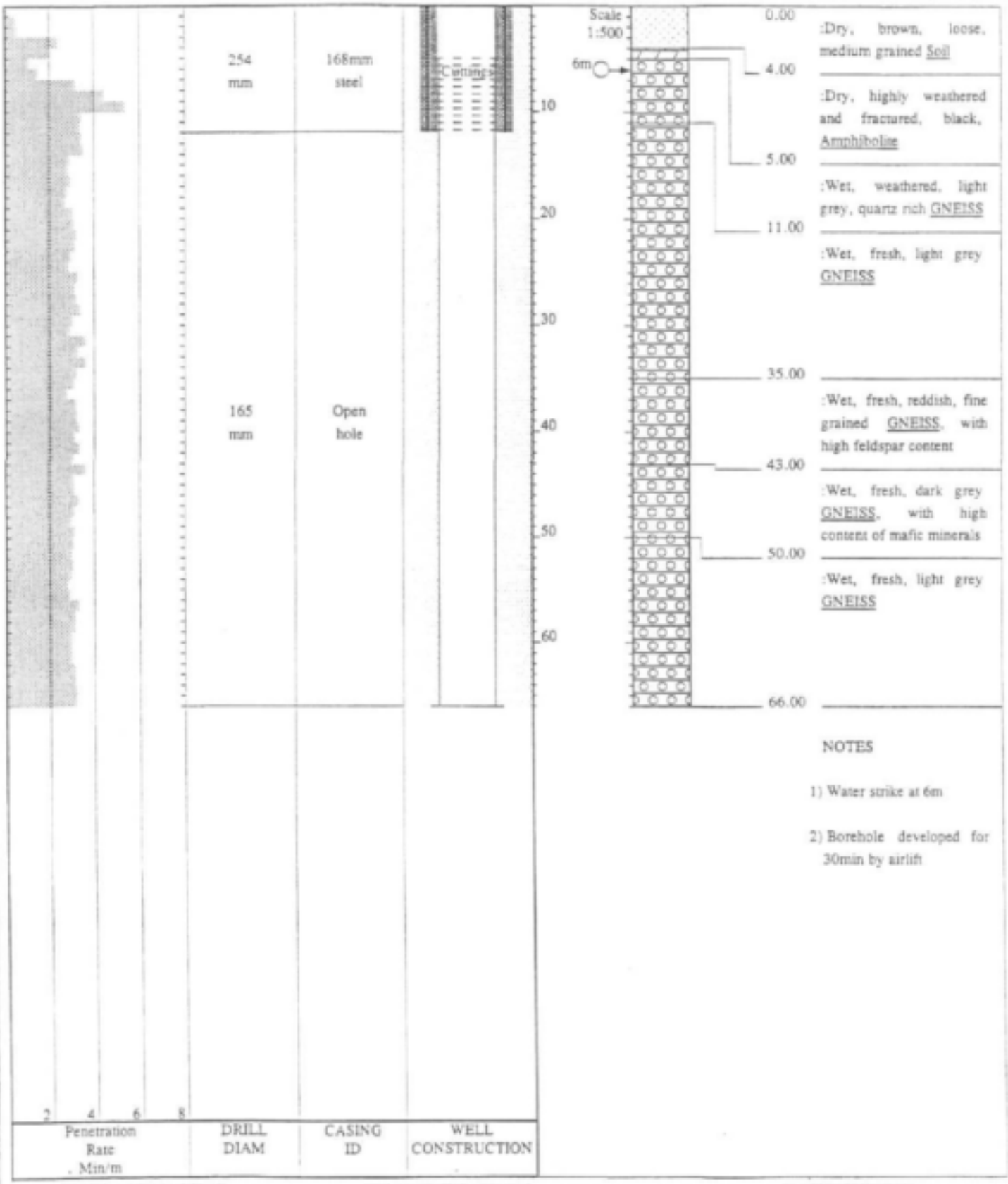

NOTES

1) Water strike at 6m

2) Borehole developed for 30min by airlift

CONTRACTOR : DWAF
DRILLED BY : Mr. Mabasa
DRILL METHOD : DTH HAMMER
SAMPLING : BLOWN CUTTINGS

INCLINATION : Vertical
DIAMETER : 165 mm
DRILL DATE : 30 October 2000
CASING TYPE : 4,5 mm steel

ELEVATION : 740m
COLLAR HEIGHT :
BLOW YIELD : 1 l/s

LOGGED BY : I. NEUMANN
SETUP FILE : STANDARD.SET

DATE : 26/01/01 10:10
TEXT : C:\DOTPLOT\DATA\H26-0431.TXT

HOLE No: H26-0431
Arrie

COUNCIL FOR GEOSCIENCE
Private Bag X112
PRETORIA 0001
REPUBLIC OF SOUTH AFRICA

GROUNDWATER DEVELOPMENT IN COMPLEX TERRAIN

HOLE No: H26-0433
Sheet 1 of 2

PROJECT NUMBER: K5/966

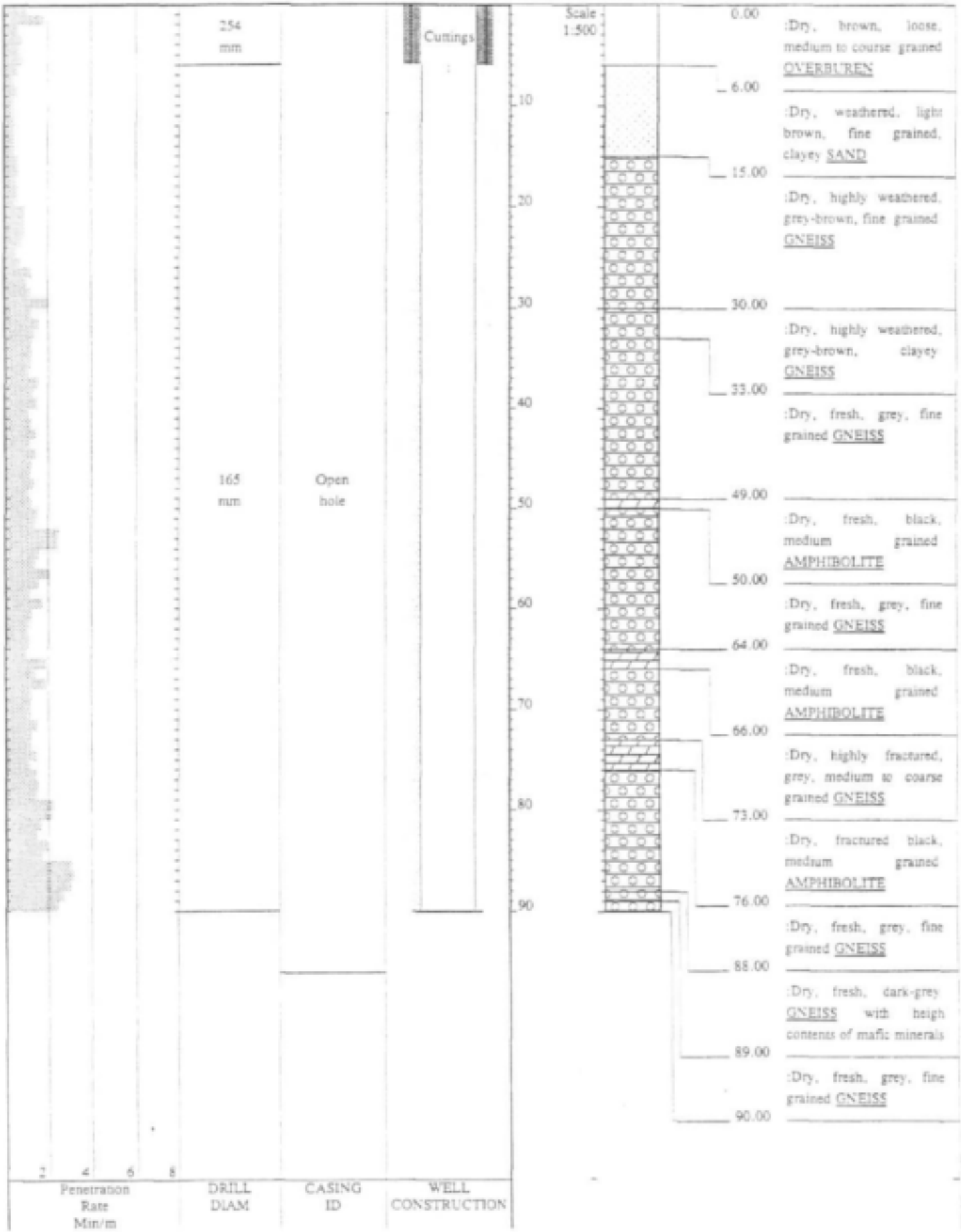

COUNCIL FOR GEOSCIENCE

Private Bag X112
PRETORIA 0001
REPUBLIC OF SOUTH AFRICA

GROUNDWATER DEVELOPMENT
IN COMPLEX TERRAIN

HOLE No: H26-0433
Sheet 2 of 2

PROJECT NUMBER: K5/966

NOTES

1) No water strike encountered

2) Borehole is backfilled

2 4 6 8

Penetration Rate Min/m	DRILL DIAM	CASING ID	WELL CONSTRUCTION

CONTRACTOR : DWAF
DRILLED BY : Mr. Mabasa
DRILL METHOD : DTH HAMMER
SAMPLING : BLOWN CUTTINGS

INCLINATION : Vertical
DIAMETER : 165 mm
DRILL DATE : 01 November 2000
CASING TYPE : 4,5 mm steel

ELEVATION : 790m
COLLAR HEIGHT :
BLOW YIELD : Dry

LOGGED BY : I. NEUMANN
SETUP FILE : STANDARD.SET

DATE : 26/01/01 10:11
TEXT : C:\DOTPLOT\DATA\H26-0433.TXT

HOLE No: H26-0433
Holmwood 315 MR

COUNCIL FOR GEOSCIENCE
Private Bag X112
PRETORIA 0001
REPUBLIC OF SOUTH AFRICA

GROUNDWATER DEVELOPMENT IN COMPLEX TERRAIN

HOLE No: H26-0432
Sheet 1 of 1

PROJECT NUMBER: K5/966

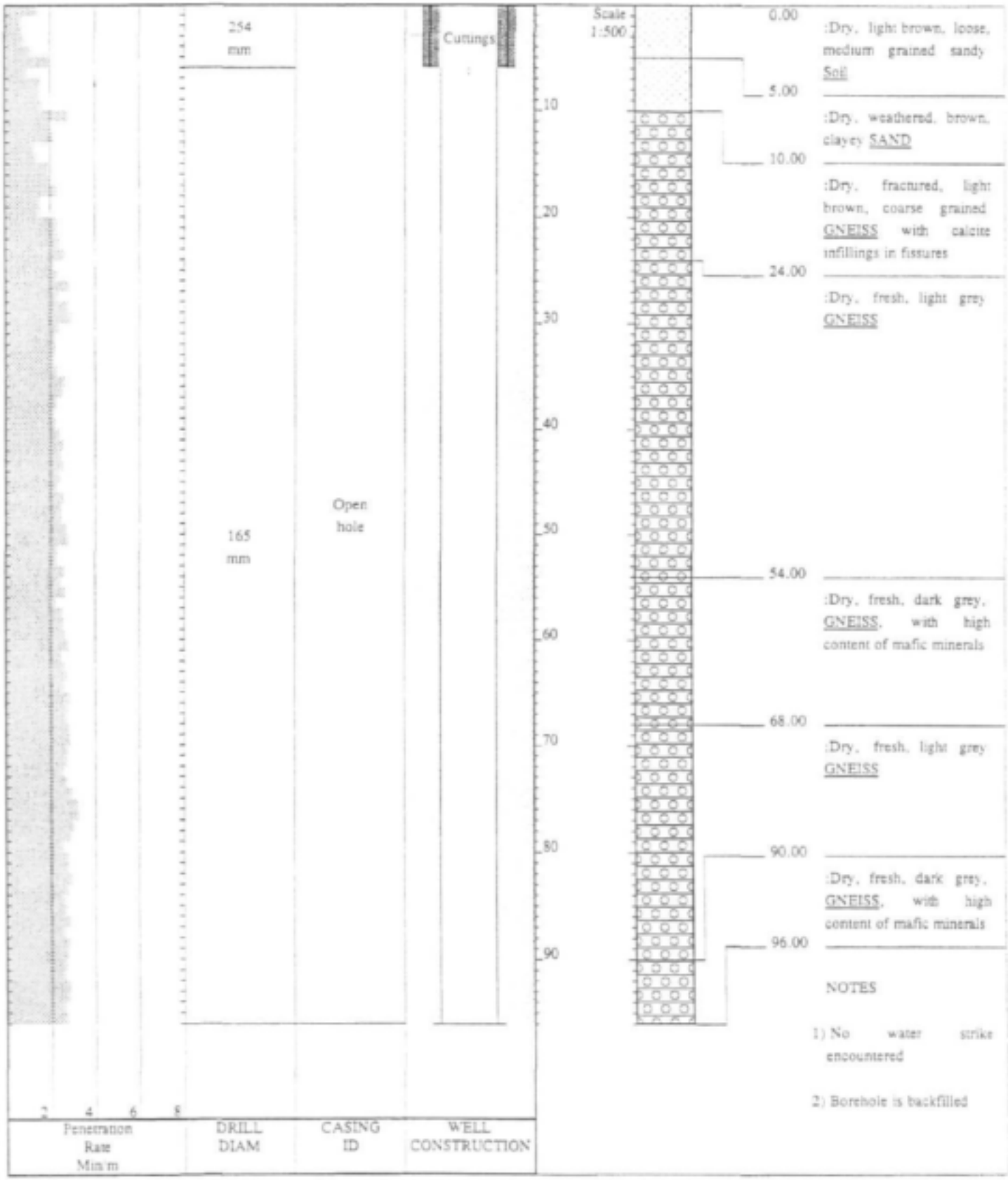

CONTRACTOR : DWAF
DRILLED BY : Mr. Mabasa
DRILL METHOD : DTH HAMMER
SAMPLING : BLOWN CUTTINGS

INCLINATION : Vertical
DIAMETER : 165 mm
DRILL DATE : 31 October 2000
CASING TYPE : 4.5 mm steel

ELEVATION : 795m
COLLAR HEIGHT :
BLOW YIELD : Dry

LOGGED BY : I. NEUMANN
SETUP FILE : STANDARD.SET

DATE : 26/01/01 10:11
TEXT : C:\DOTPLOT\DATA\H26-0432.TXT

HOLE No: H26-0432
Groepan 311 MR

COUNCIL FOR GEOSCIENCE

Private Bag X112
PRETORIA 0001
REPUBLIC OF SOUTH AFRICA

GROUNDWATER DEVELOPMENT IN COMPLEX TERRAIN

HOLE No: H26-0430
Sheet 1 of 1

PROJECT NUMBER: K5/966

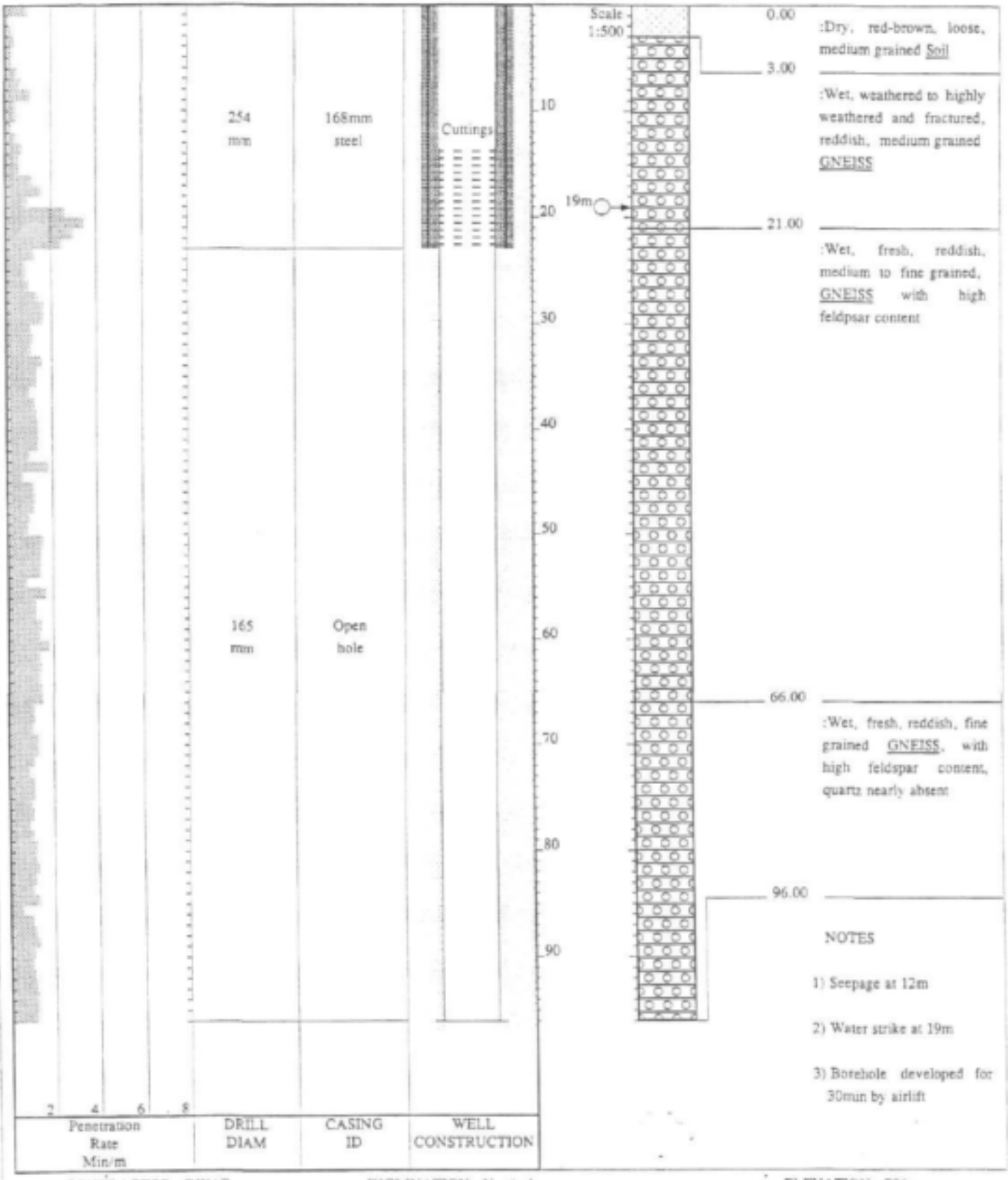

:Dry, red-brown, loose, medium grained Soil

:Wet, weathered to highly weathered and fractured, reddish, medium grained GNEISS

:Wet, fresh, reddish, medium to fine grained, GNEISS with high feldpsar content

:Wet, fresh, reddish, fine grained GNEISS, with high feldspar content, quartz nearly absent

NOTES

1) Seepage at 12m

2) Water strike at 19m

3) Borehole developed for 30mun by airlift

CONTRACTOR : DWAF
DRILLED BY : Mr. Mabasa
DRILL METHOD : DTH HAMMER
SAMPLING : BLOWN CUTTINGS

INCLINATION : Vertical
DIAMETER : 165 mm
DRILL DATE : 27 October 2000
CASING TYPE : 4.5 mm steel

ELEVATION : 736m
COLLAR HEIGHT :
BLOW YIELD : 0.5 l/s

LOGGED BY : I. NEUMANN
SETUP FILE : STANDARD.SET

DATE : 17/01/01 13:59
TEXT : C:\DOTPLOT\DATA\H26-0430.TXT

HOLE No: H26-0430
Simson

COUNCIL FOR GEOSCIENCE

Private Bag X112
PRETORIA 0001
REPUBLIC OF SOUTH AFRICA

GROUNDWATER DEVELOPMENT IN COMPLEX TERRAIN

HOLE No: H26-0429
Sheet 1 of 2

PROJECT NUMBER: K5/966

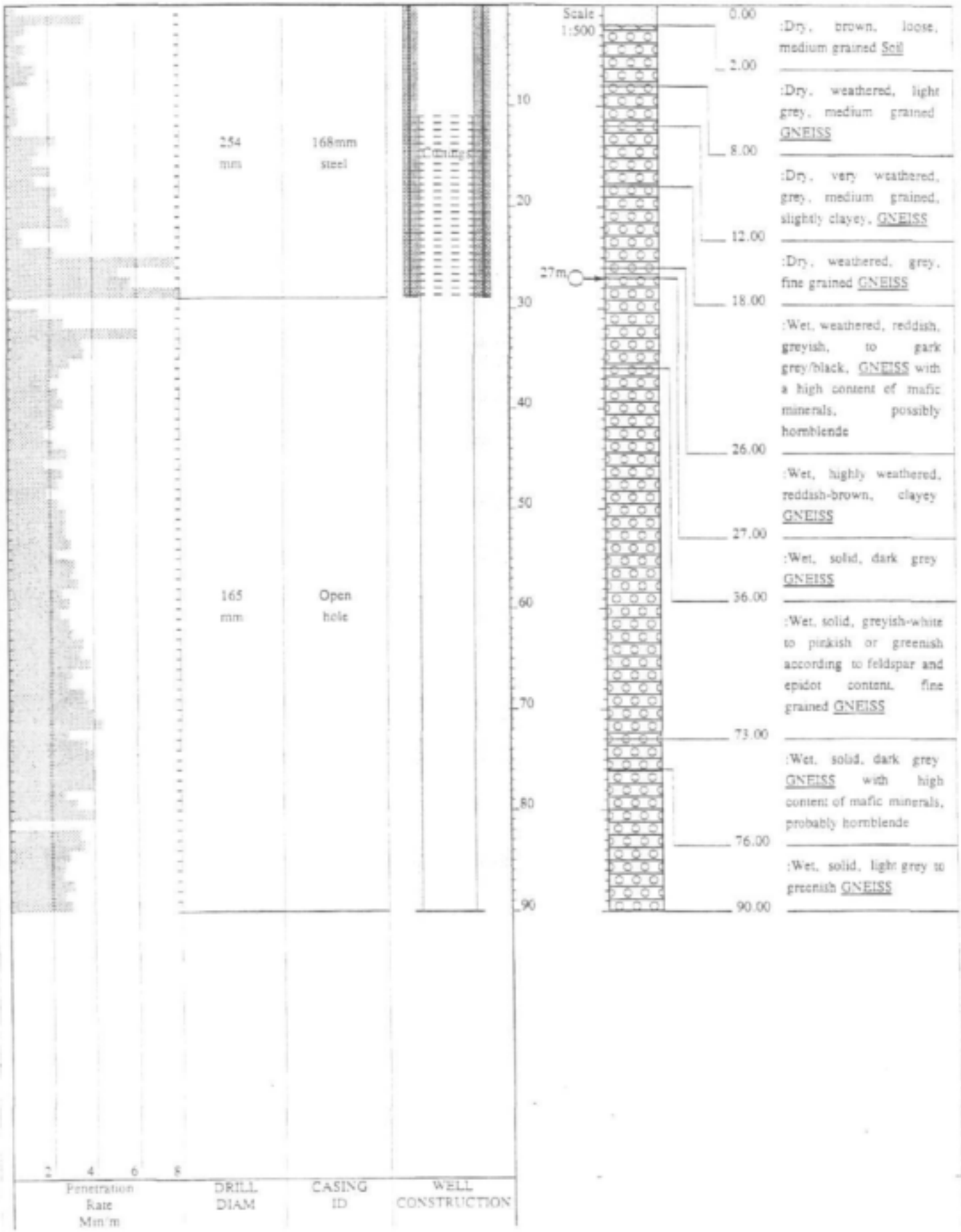

COUNCIL FOR GEOSCIENCE

Private Bag X112
PRETORIA 0001
REPUBLIC OF SOUTH AFRICA

GROUNDWATER DEVELOPMENT IN COMPLEX TERRAIN

HOLE No: H26-0428
Sheet 1 of 2

PROJECT NUMBER: K5/966

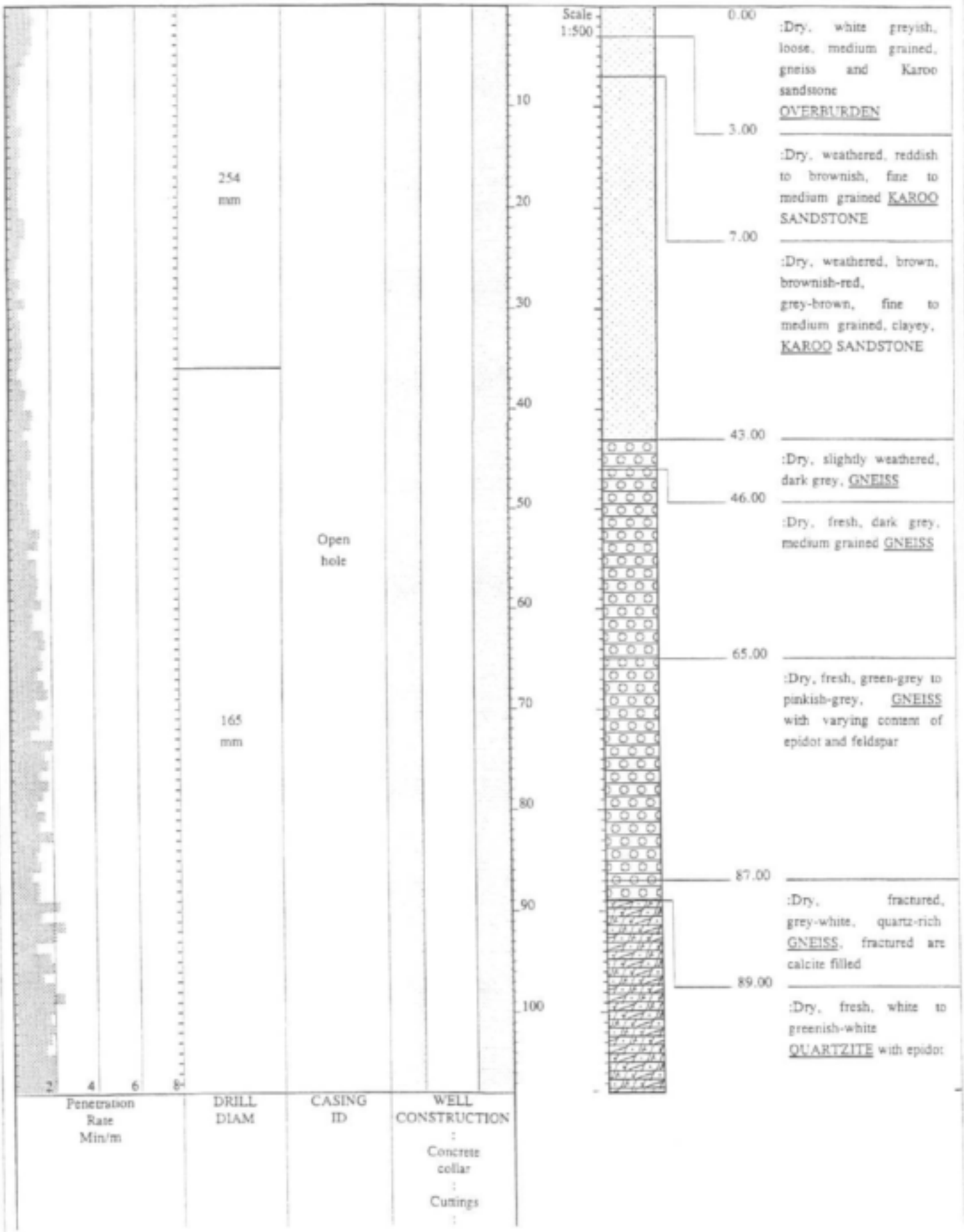

COUNCIL FOR GEOSCIENCE
Private Bag X112
PRETORIA 0001
REPUBLIC OF SOUTH AFRICA

GROUNDWATER DEVELOPMENT IN COMPLEX TERRAIN

HOLE No: H26-0426
Sheet 2 of 2

PROJECT NUMBER: K5/966

	:Wet, fresh, white to greenish-white, GNEISS with varying content of epidot, amphibolite, muscovite, Calcite veins
58.00	
	:Wet, fresh, greenish-black, GNEISS with varying content of epidot, amphibolite, fine grained
68.00	
	:Wet, fresh, pinkish-grey to dark grey, fine grained GNEISS
77.00	
	:Wet, fresh, greenish-black, fine grained GNEISS
96.00	

NOTES

1) Water strike at 42.5m

2) Rest water level at m

3) Developed for 30 min by airlift

2 4 6 8

Penetration Rate Min/m	DRILL DIAM	CASING ID	WELL CONSTRUCTION

CONTRACTOR : DWAF
DRILLED BY : Mr. Mabasa
DRILL METHOD : DTH HAMMER
SAMPLING : BLOWN CUTTINGS

INCLINATION : Vertical
DIAMETER : 165 mm
DRILL DATE : 20 October 2000
CASING TYPE : 4,5 mm steel

ELEVATION : 820m
COLLAR HEIGHT :
BLOW YIELD : 0.4 l/s

LOGGED BY : I. NEUMANN
SETUP FILE : STANDARD.SET

DATE : 17/01/01 13:57
TEXT : C:\DOTPLOT\DATA\H26-0426.TXT

HOLE No: H26-0426
Ga-Rakwele

COUNCIL FOR GEOSCIENCE

Private Bag X112
PRETORIA 0001
REPUBLIC OF SOUTH AFRICA

GROUNDWATER DEVELOPMENT IN COMPLEX TERRAIN

HOLE No: H26-0434
Sheet 1 of 1

PROJECT NUMBER: K5/966

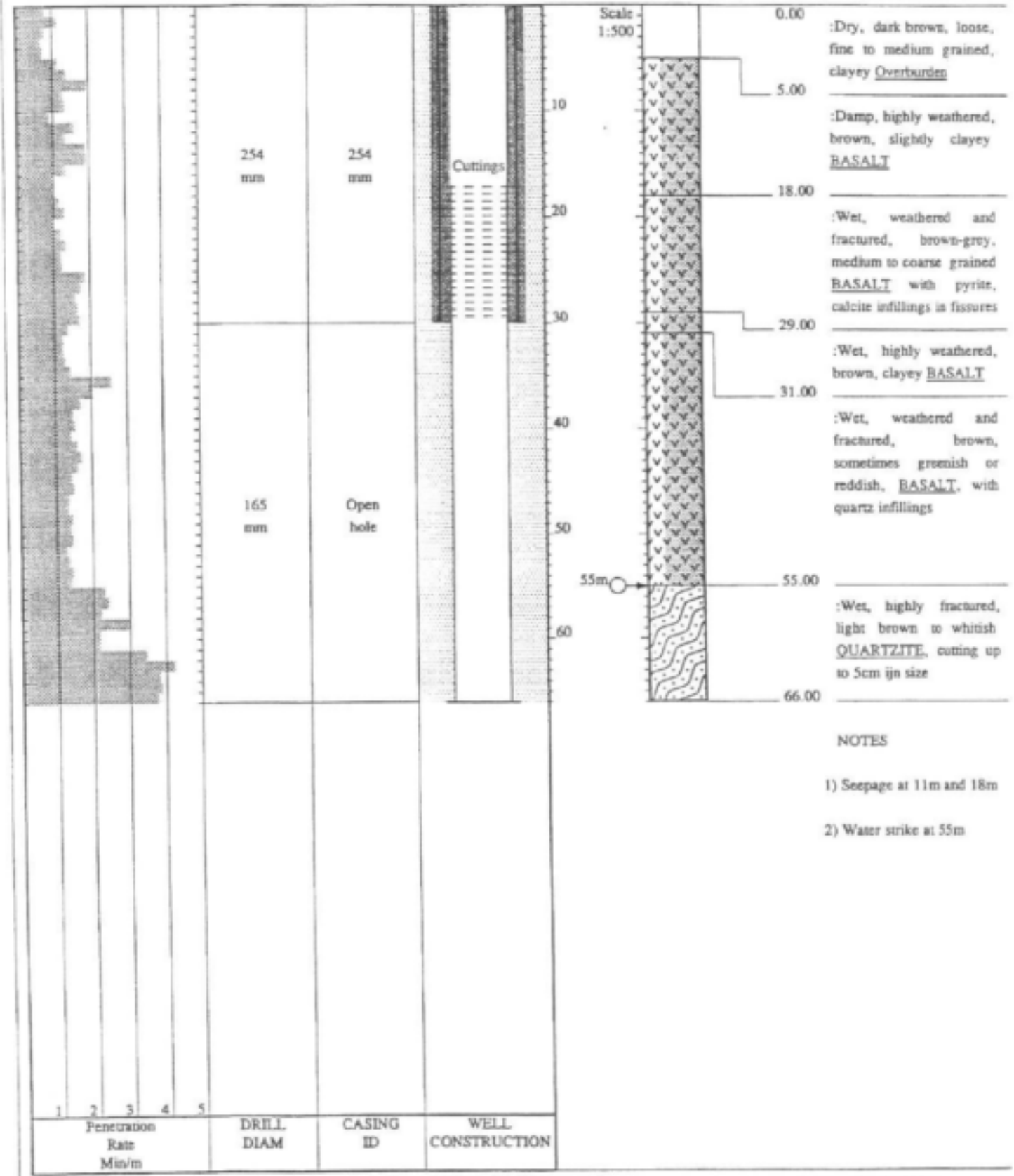

:Dry, dark brown, loose, fine to medium grained, clayey Overburden

:Damp, highly weathered, brown, slightly clayey BASALT

:Wet, weathered and fractured, brown-grey, medium to coarse grained BASALT with pyrite, calcite infillings in fissures

:Wet, highly weathered, brown, clayey BASALT

:Wet, weathered and fractured, brown, sometimes greenish or reddish, BASALT, with quartz infillings

:Wet, highly fractured, light brown to whitish QUARTZITE, cutting up to 5cm in size

NOTES

1) Seepage at 11m and 18m

2) Water strike at 55m

CONTRACTOR : DWAF
DRILLED BY : Mr. Mabasa
DRILL METHOD : DTH HAMMER
SAMPLING : BLOWN CUTTINGS

LOGGED BY : I. NEUMANN
SETUP FILE : STANDARD.SET

INCLINATION : Vertical
DIAMETER : 165 mm
DRILL DATE : 2 October 2000
CASING TYPE : 4,5 mm steel

DATE : 26/01/01 10:11
TEXT : C:\DOTPLOT\DATA\H26-0434.TXT

ELEVATION : 777m
COLLAR HEIGHT :
BLOW YIELD : 17 l/s

HOLE No: H26-0434
Grootpan 311 MR

APPENDIX 3-C

TEST PUMP DATA

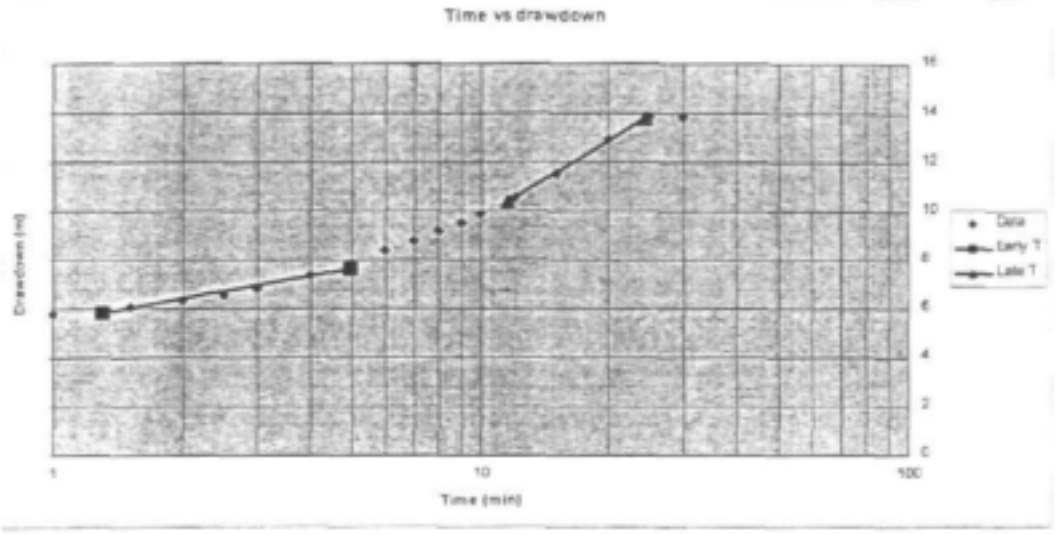
Time vs drawdown
Drawdown (m)
Time (min)
Data
Early T
Late T

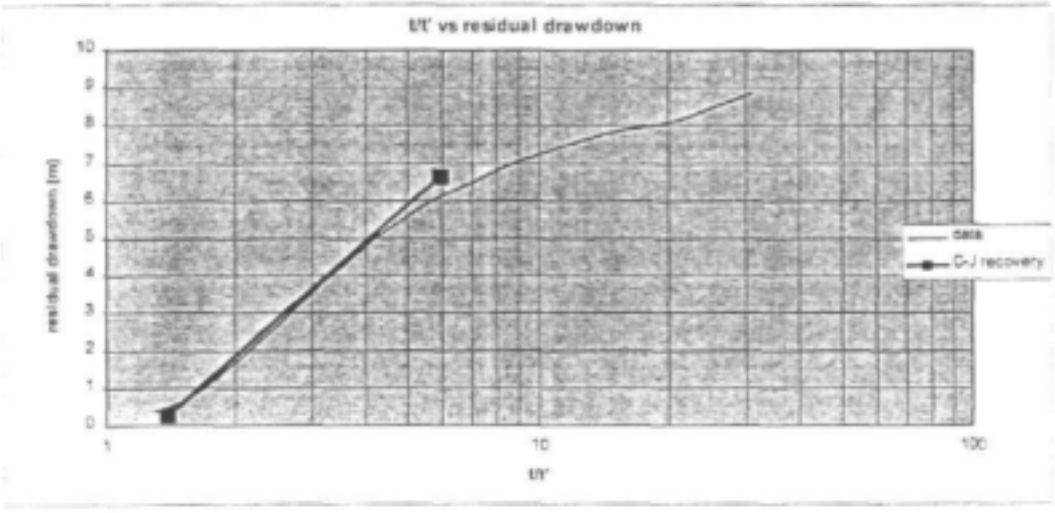
t/t' vs residual drawdown
residual drawdown (m)
t/t'
data
C-J recovery

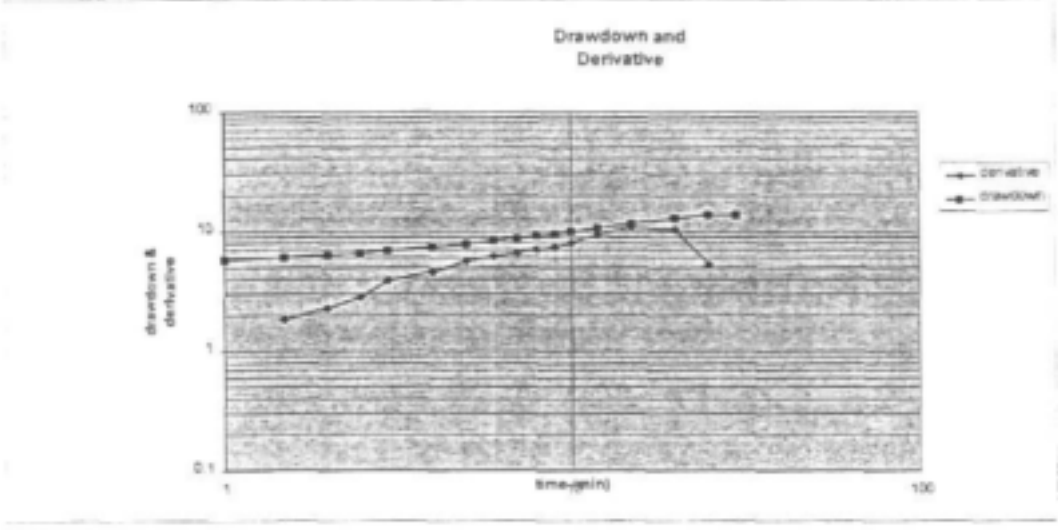
Drawdown and
Derivative
drawdown & derivative
time (min)
derivative
drawdown

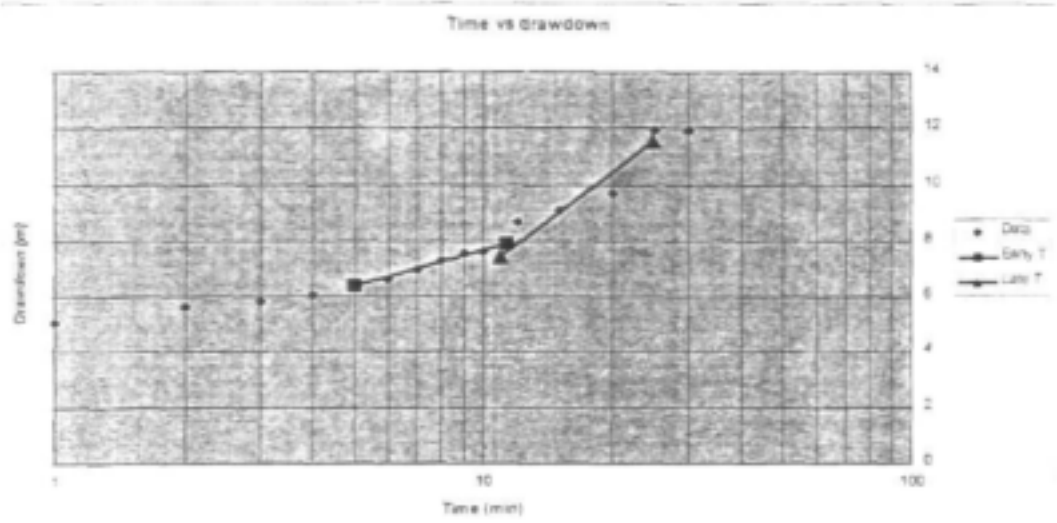
Time vs drawdown
Drawdown (m)
Time (min)
Data
Early T
Late T

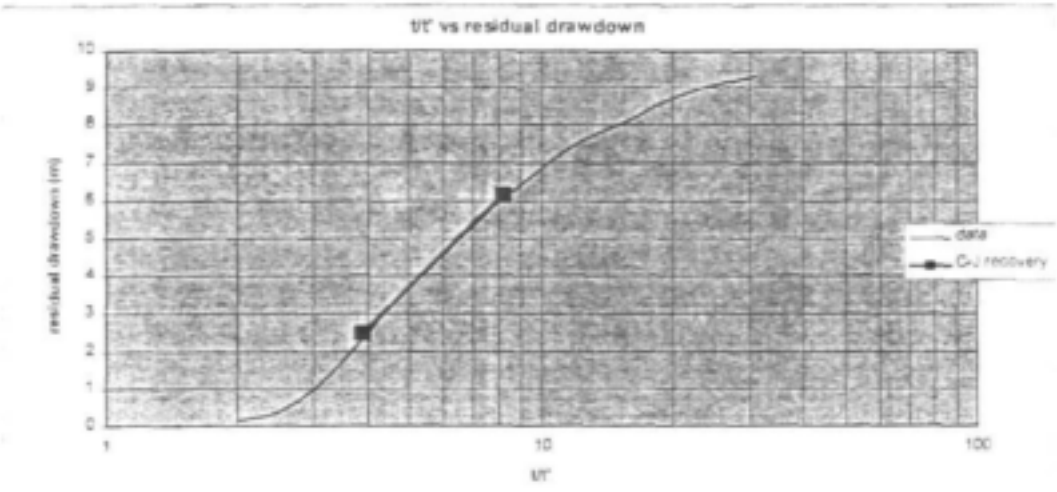
t/t' vs residual drawdown
residual drawdown (m)
t/t'
data
C-J recovery

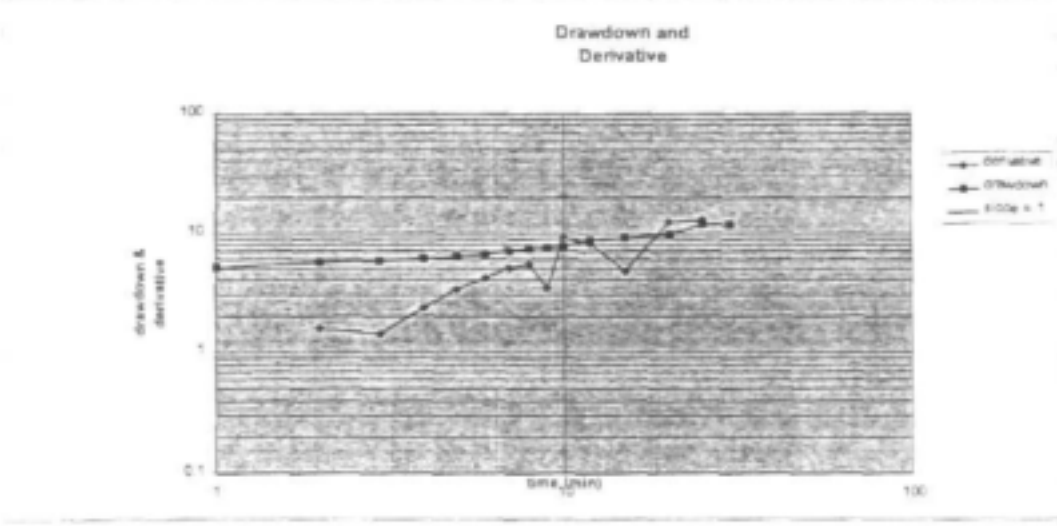
Drawdown and
Derivative
drawdown &
derivative
time (min)

H026-0434 Obervation for H026-0427

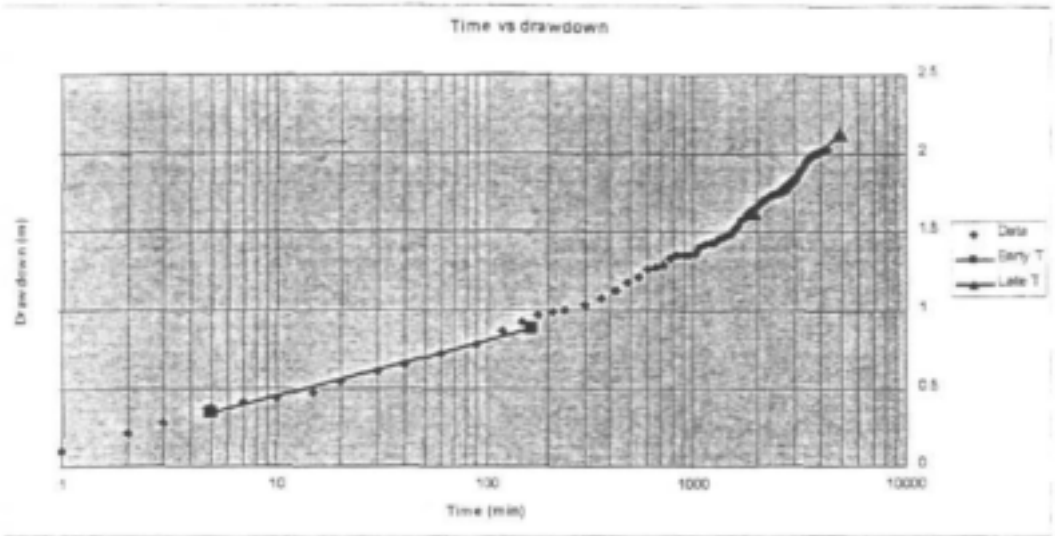

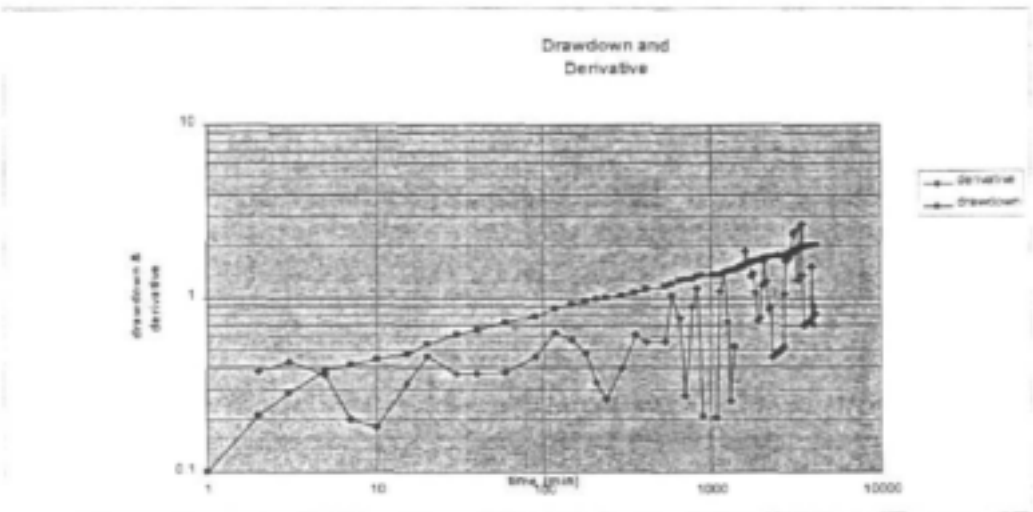

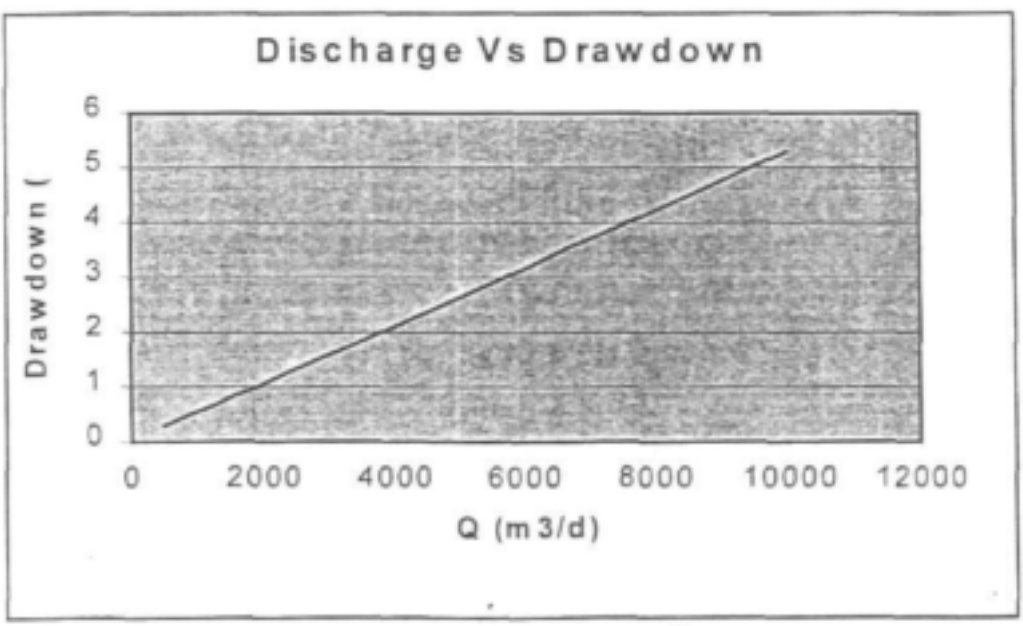

Time vs drawdown

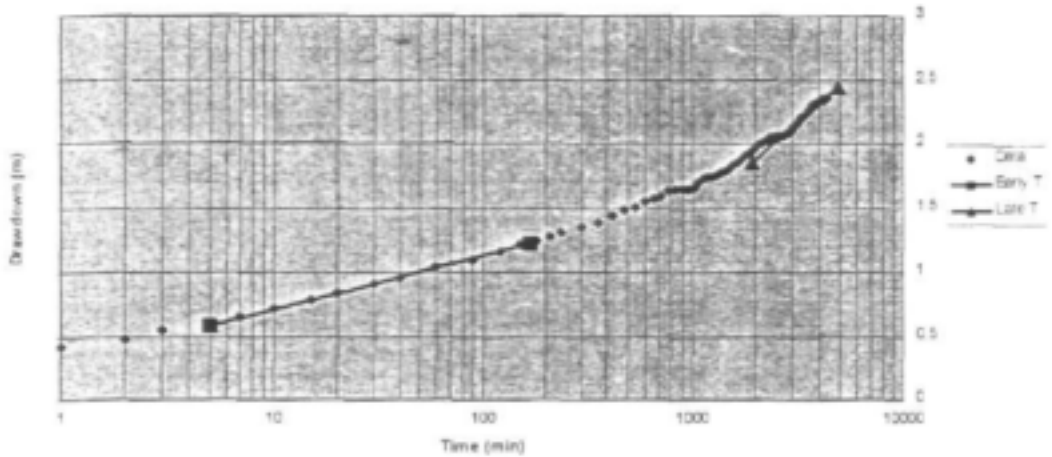

t/t' vs residual drawdown

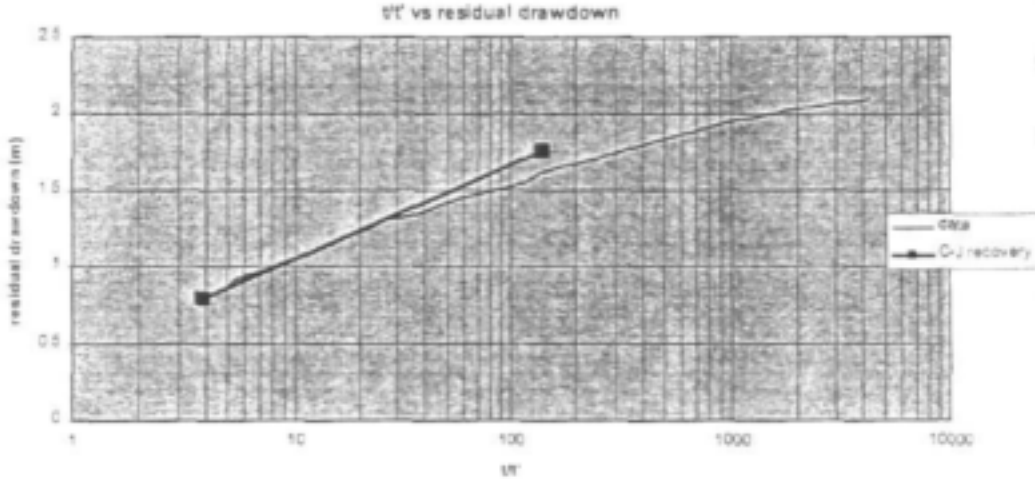

Drawdown and Derivative

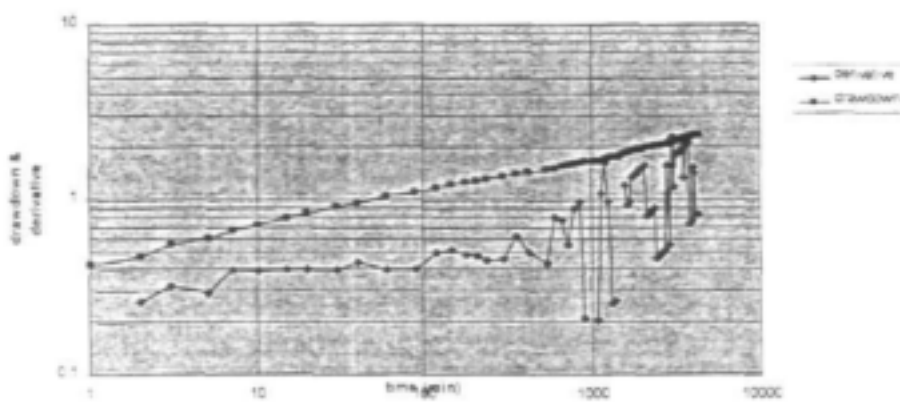

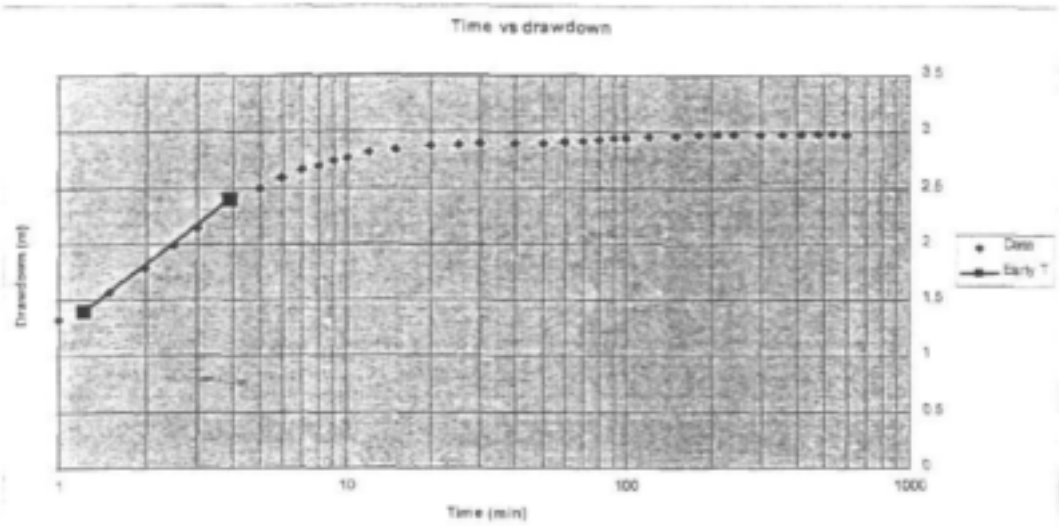
Time vs drawdown
Drawdown (m)
Time (min)
Data
Barty T

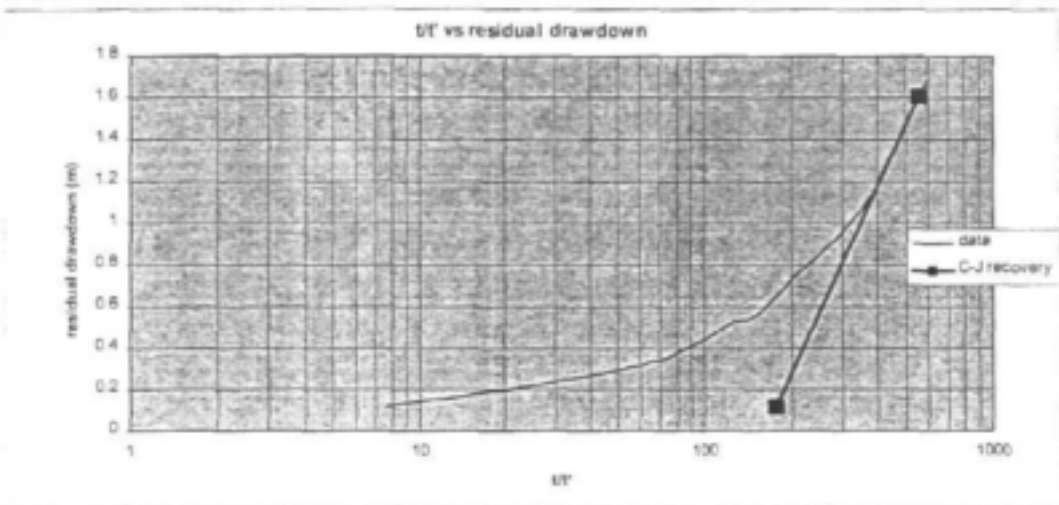
t/t' vs residual drawdown
residual drawdown (m)
t/t'
data
C-J recovery

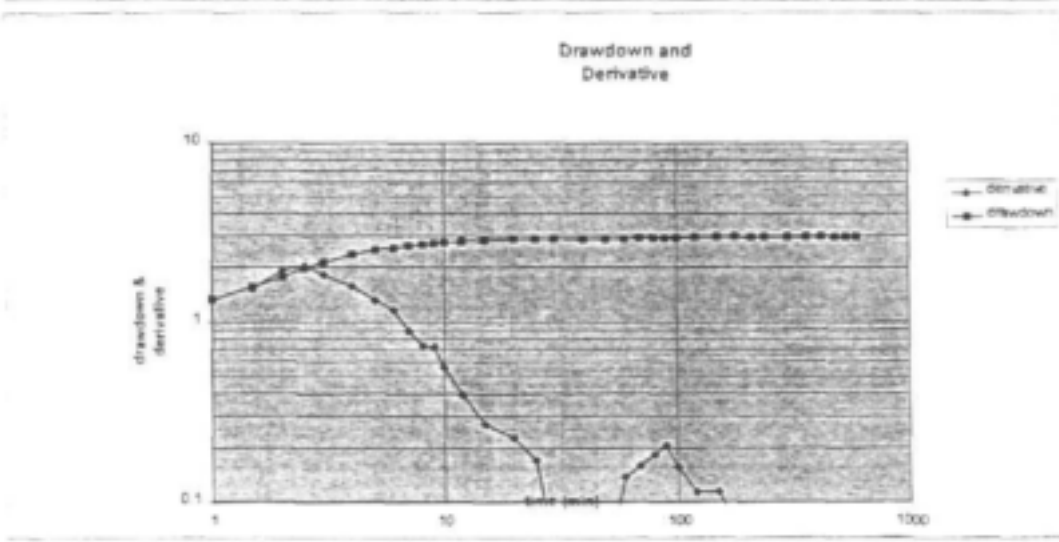
Drawdown and
Derivative
drawdown &
derivative
Time (min)

Time vs drawdown

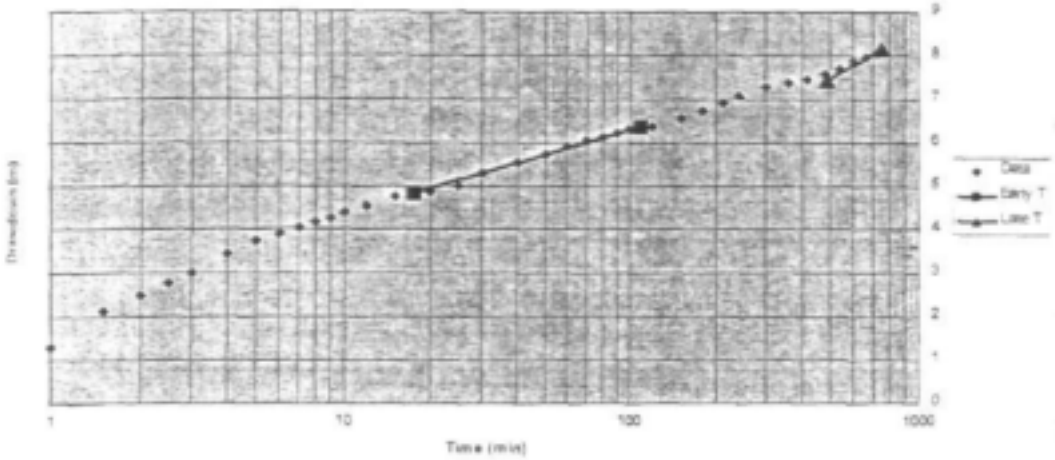

t/t' vs residual drawdown

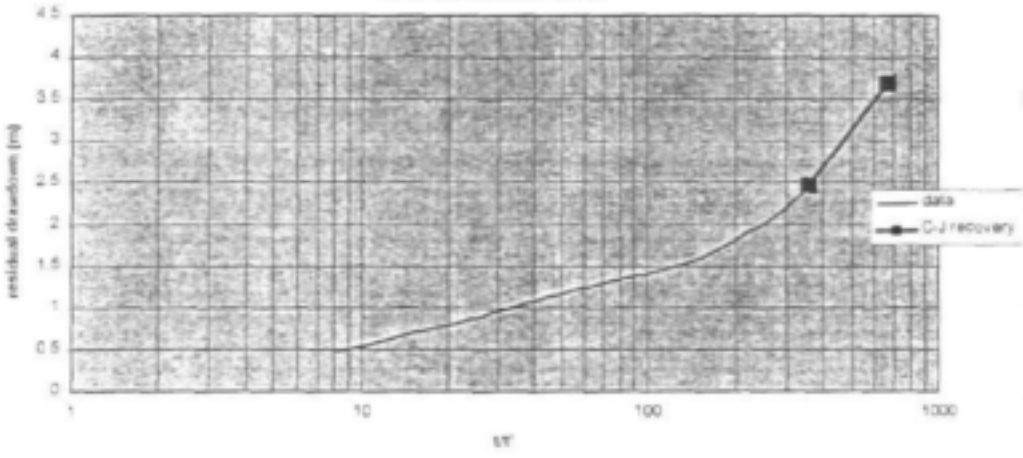

Drawdown and Derivative

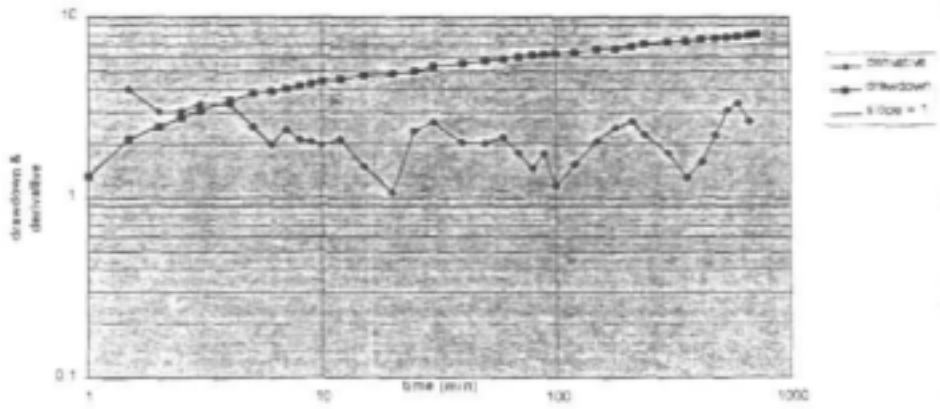

APPENDIX 3-D

ANALYTICAL RESULTS OF THE WATER SAMPLES

Schoeller Diagram

Schoeller Diagram

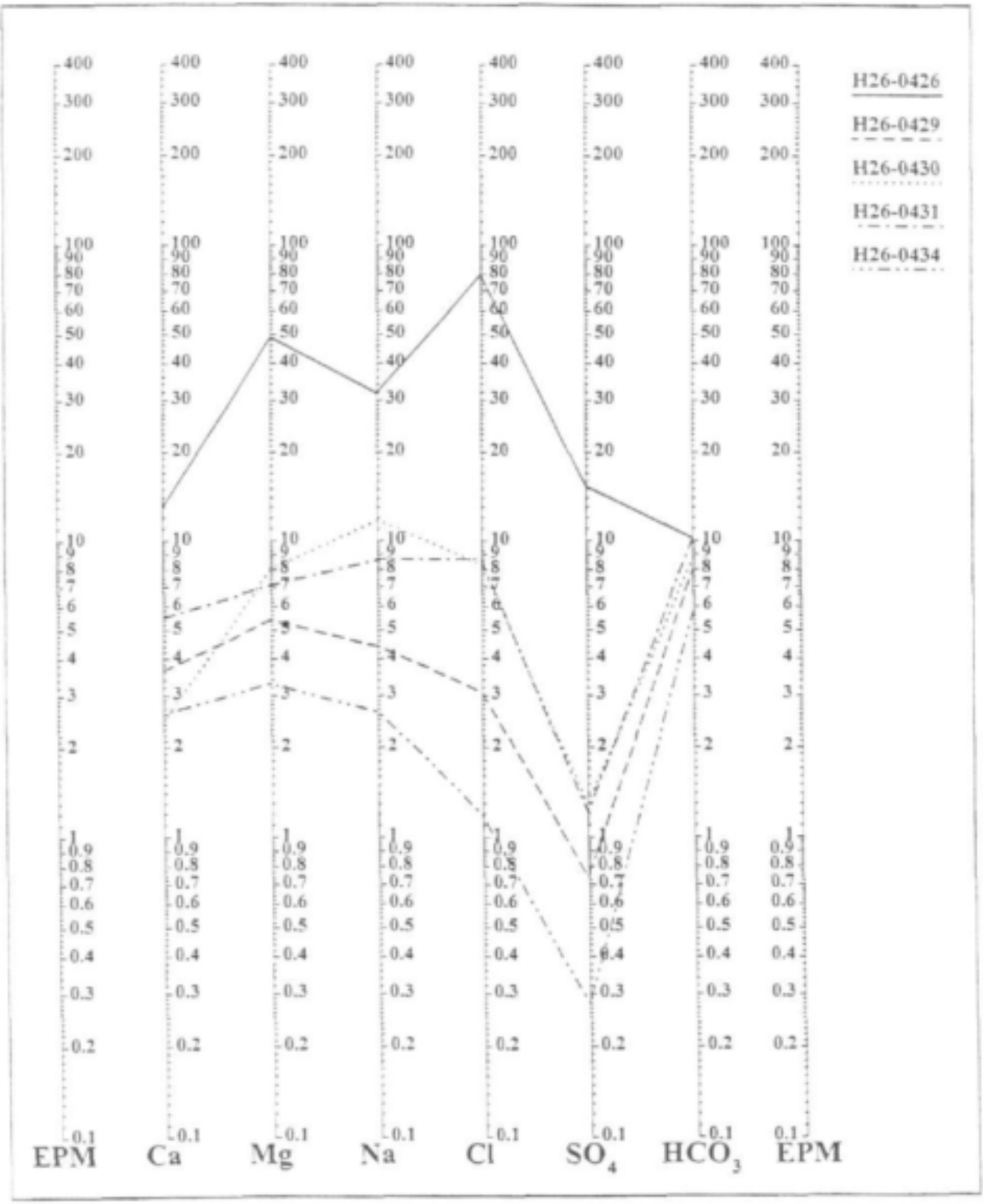

Well Ident
H26-0429

STIFF Diagram

Name	Type
H26-0429	

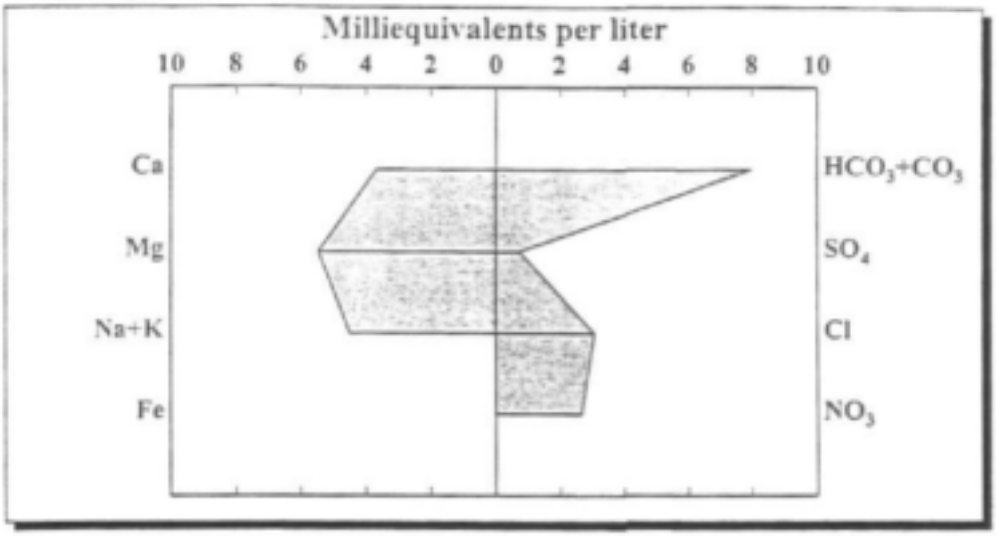

Cations

	Ca	*Mg*	*Na*	*K*	*Fe*
Milliequivalents per liter	3.65	5.43	4.43	0.05	
Milligrams per liter					

Anions

	HCO3	*CO3*	*SO4*	*Cl*	*NO3*
Milliequivalents per liter	8.00		0.74	3.09	2.67
Milligrams per liter					

BOD	COD	Dissolved Oxygen	F	B	SiO2
TDS	Hardness	Alkalinity	Conductivity	pH	SAR
800.00	1.22	8.00	128.00	7.69	2.0791

Water Type	*Magnesium Bicarbonate*

Cations (epm)	Anions (epm)
13.56	14.50

Error Balance (%)
3.35

Aquifer
Gneiss

Well Ident
H26-0431

STIFF Diagram

Name	Type
H26-0431	

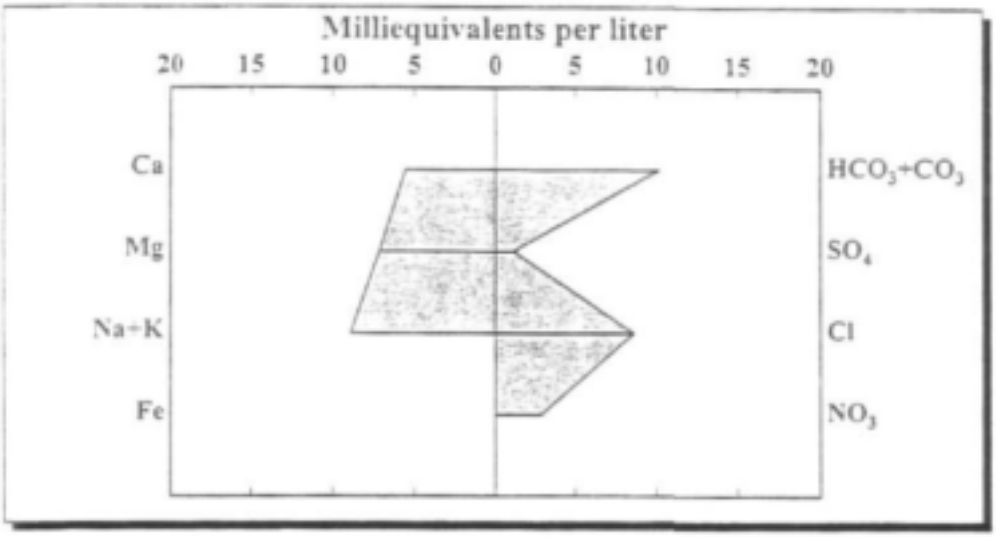

Cations

	Ca	*Mg*	*Na*	*K*	*Fe*
Milliequivalents per liter	5.50	7.11	8.70	0.16	
Milligrams per liter					

Anions

	HCO3	*CO3*	*SO4*	*Cl*	*NO3*
Milliequivalents per liter	10.20		1.21	8.69	2.94
Milligrams per liter					

BOD	COD	Dissolved Oxygen	F	B	SiO2

TDS	Hardness	Alkalinity	Conductivity	pH	SAR
1264.00	2.53	10.20	185.00	7.54	3.4648

Water Type	Cations (epm)	Anions (epm)
Sodium Bicarbonate	21.47	23.04

Error Balance (%)
3.53

Aquifer
Gneiss

Mnr L Neumann

Raad vir Geowetenskap

P/Bag X112 Pretoria
0001
Tel : 012 8411458
Fax/Faks: 012 8411221

ARC • LNR

ARC: INSTITUTE FOR SOIL, CLIMATE AND WATER
LNR: INSTITUUT VIR GROND, KLIMAAT EN WATER
Private Bag X79, PRETORIA, 0001
Tel: (012) 310 2500
Fax: (012) 310 2500

Date / Datum: 02/01/2001

REPORT NO:
VERSLAG NR: WATER 200001 2276

Sender ID: H26-0426 Lab. No: W 2041

pH	pHS	SAR	Electric Conductivity
7.22	6.36	5.73	839.00 mS/m at 25 °C

ANIONS	mg/l	mmol(c)/l
Fluoride (1.5)	0.00	0.00
Nitrite (4.0)	0.00	0.00
Nitrate (44.0)	428.59	6.91
Chloride (250)	2825.24	79.58
Sulphate (500)	735.27	15.32
Phosphate	47.98	1.02
Carbonate (20.0)	0.00	0.00
Bicarbonate	622.20	10.20
Subtotal	4659.28	113.04

CATIONS	mg/l	mmol(c)/l
Sodium (400)	733.00	31.87
Potassium (400)	32.74	0.84
Calcium (200)	260.00	13.00
Magnesium (100)	595.00	48.93
Boron (1.5)	0.99	0.27
Subtotal	1621.73	94.91

Sodium Carbonate	0.00	0.00
Sodium Bicarbonate	0.00	0.00
Alkalinity	510.00	10.20
Temp. Hardness	510.00	10.20
Perm. Hardness	2600.28	52.01

Total	6281.00
Less (*)	311.10
Total disolved Solids	5969.90

* Correction for any volatile substances, HCO3/2 or .... HCL + HNO3 + HF + ...
() Figures in brackets are the recommended maximum values for human use in mg/l.

Raad vir Geowetenskap

P/Bag X112 Pretoria
0001
Tel : 012 8411458
Fax/Faks: 012 8411221

ARC • LNR

Private Bag X79, PRETORIA, 0001
Tel: (012) 310 2500
Fax:: (012) 310 2500

Date / Datum: 02/01/2001

REPORT NO:
VERSLAG NR: WATER 200001 2276

Sender ID: H26-0430 Lab. No: W 2040

pH	pHS	SAR	Electric Conductivity
7.66	7.16	5.15	199.00 mS/m at 25 °C

ANIONS	mg/l	mmol(c)/l
Fluoride (1.5)	2.21	0.12
Nitrite (4.0)	0.00	0.00
Nitrate (44.0)	369.22	5.96
Chloride (250)	296.20	8.34
Sulphate (500)	61.77	1.29
Phosphate	5.05	0.11
Carbonate (20.0)	0.00	0.00
Bicarbonate	530.70	8.70
Subtotal	1265.15	24.51

CATIONS	mg/l	mmol(c)/l
Sodium (400)	271.00	11.78
Potassium (400)	1.98	0.05
Calcium (200)	49.20	2.46
Magnesium (100)	97.50	8.02
Boron (1.5)	0.73	0.20
Subtotal	420.41	22.51

Sodium Carbonate	0.00	0.00
Sodium Bicarbonate	0.00	0.00
Alkalinity	435.00	8.70
Temp. Hardness	435.00	8.70
Perm. Hardness	99.03	1.98

Total	1685.00
Less (*)	265.35
Total disolved Solids	1419.65

* Correction for any volatile substances. HCO3/2 or .... HCL + HNO3 + HF + ...
() Figures in brackets are the recommended maximum values for human use in mg/l.

ND: No analysis was done for microbiological pathogenes, organic compounds and insecticides.

Mnr I. Neumann

Raad vir Geowetenskap

P/Bag X112 Pretoria
0001
Tel : 012 8411458
Fax/Faks: 012 8411221

ARC • LNR

ARC: INSTITUTE FOR SOIL, CLIMATE AND WATER
LNR: INSTITUUT VIR GROND, KLIMAAT EN WATER
Private Bag X79, PRETORIA, 0001
Tel: (012) 310 2500
Fax: (012) 310 2500

Date / Datum: 02/01/2001

REPORT NO:
VERSLAG NR: WATER 200001 2276

Sender ID: H26-0431 Lab. No: W2042

pH	pHS	SAR	Electric Conductivity
7.54	6.74	3.46	185.00 mS/m at 25 °C

ANIONS	mg/l	mmol(c)/l
Fluoride (1.5)	0.81	0.04
Nitrite (4.0)	0.00	0.00
Nitrate (44.0)	182.47	2.94
Chloride (250)	308.41	8.69
Sulphate (500)	58.07	1.21
Phosphate	1.58	0.03
Carbonate (20.0)	0.00	0.00
Bicarbonate	622.20	10.20
Subtotal	1173.54	23.12

CATIONS	mg/l	mmol(c)/l
Sodium (400)	200.00	8.70
Potassium (400)	6.17	0.16
Calcium (200)	110.00	5.50
Magnesium (100)	86.50	7.11
Boron (1.5)	0.42	0.12
Subtotal	403.09	21.58

Sodium Carbonate	0.00	0.00
Sodium Bicarbonate	0.00	0.00
Alkalinity	510.00	10.20
Temp. Hardness	510.00	10.20
Perm. Hardness	126.50	2.53

Total	1576.00
Less (*)	311.10
Total disolved Solids	1264.90

* Correction for any volatile substances, HCO3/2 or .... HCL + HNO3 + HF + ...
() Figures in brackets are the recommended maximum values for human use in mg/l.

SENDER:
I. Neumann
Raad vir Geowetenskap
P/Sak X112
Pretoria

INSTITUUT VIR GROND, KLIMAAT EN WATER
Privaatsak X79
PRETORIA
0001

DATUM: 20/11/00

B E S O N D E R H E D E V A N W A T E R M O N S T E R

KENMERKE VAN HOUER: H26-0429 LAB NOMMER: W02001 2000/01

RESULTATE:	me/l	ppm		me/l	ppm
Fluoried (1.5)	0.11	2.02	Natrium (400)	4.43	102.00
Nitriet (4.0)	0.00	0.00	Kalium (400)	0.05	1.9
Nitraat (44.0)	2.67	165.52	Kalsium (200)	3.65	73.00
Chloried (250)	3.09	109.75	Magnesium (100)	5.43	66.00
Sulfaat (500)	0.74	35.44	Boor (1.5)	0.14	0.49
Fosfaat	0.00	0.00			
Karbonaat (20.0)	0.00	0.00			
Bikarbonaat	8.00	488.00			
Subtotaal	14.61	800.73	Subtotaal	13.70	243.36
			Totaal		1044.10
			Min (*)		244.00 *
			Totale Opgeloste Stowwe		800.10
Na Karbonaat	0.00	0	Tyd Hardheid	8.00	400
Na Bikarbonaat	0.00	0	Perm Hardheid	1.22	61
Alkaliteit	8.00	400			

* Korreksie vir enige vlugtige stowwe, HCO3/2 of.. HCl+HNO3+HF+..
() Aanbeveelde maksimum waarde vir mense in ppm.

pH (> 6.5 en < 8.6)	pHS	NAV	Elektriese Geleidingsvermoe
7.69	7.01	2.08	126.0 mS/m By 25 grade C

Aanbeveling:

	Mens	Dier	Besproeing
Nie geskik			
Geskik			

NB Ontledings is nie vir mikrobiologiese patogene, organiese verbindings en plaagbeheermiddels gedoen nie.

Well Ident
H26-0434

STIFF Diagram

Name	Type
H26-0434	

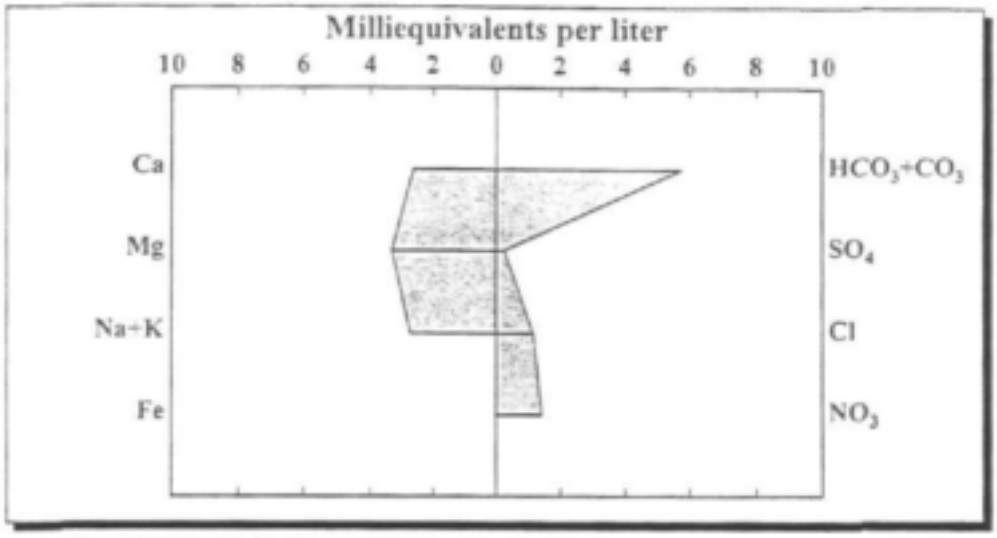

Cations

	Ca	*Mg*	*Na*	*K*	*Fe*
Milliequivalents per liter	2.61	3.30	2.65	0.05	
Milligrams per liter					

Anions

	HCO3	*CO3*	*SO4*	*Cl*	*NO3*
Milliequivalents per liter	5.80		0.28	1.18	1.43
Milligrams per liter					

BOD	COD	Dissolved Oxygen	F	B	SiO2

TDS	Hardness	Alkalinity	Conductivity	pH	SAR
476.00	0.24	5.80	80.00	7.80	1.5416

Water Type	*Magnesium Bicarbonate*

Cations (epm)	Anions (epm)
8.61	8.69

Error Balance (%)
0.46

Aquifer
Quartzite

Well Ident
H26-0430

STIFF Diagram

Name	Type
H26-0430	

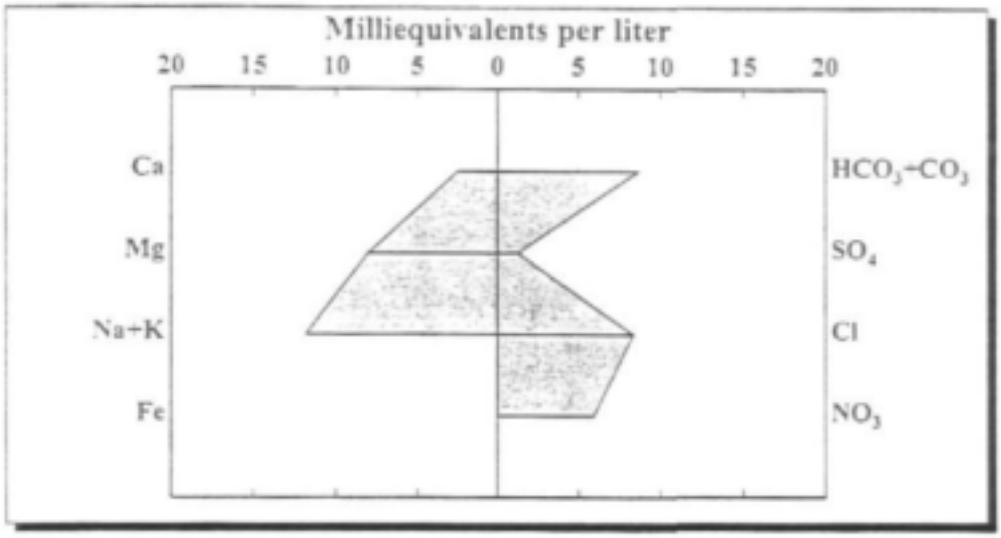

Cations

	Ca	*Mg*	*Na*	*K*	*Fe*
Milliequivalents per liter	2.46	8.02	11.78	0.05	
Milligrams per liter					

Anions

	HCO3	*CO3*	*SO4*	*Cl*	*NO3*
Milliequivalents per liter	8.70		1.29	8.34	5.96
Milligrams per liter					

BOD	COD	Dissolved Oxygen	F	B	SiO2

TDS	Hardness	Alkalinity	Conductivity	pH	SAR
1419.00	1.98	8.70	199.00	7.66	5.1461

Water Type	Cations (epm)	Anions (epm)
Sodium Bicarbonate	22.31	24.29

Error Balance (%)
4.25

Aquifer
Gneiss

Well Ident
H26-0426

STIFF Diagram

Name	Type
H26-0426	Bh

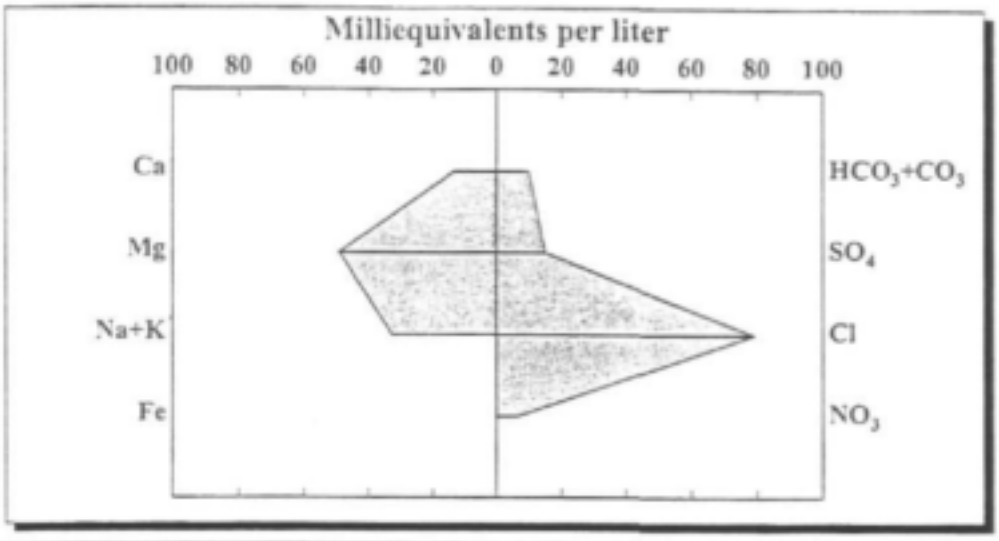

Cations

	Ca	Mg	Na	K	Fe
Milliequivalents per liter	13.00	48.93	31.87	0.84	
Milligrams per liter					

Anions

	HCO3	CO3	SO4	Cl	NO3
Milliequivalents per liter	10.20		15.32	79.58	6.91
Milligrams per liter					

BOD	COD	Dissolved Oxygen	F	B	SiO2

TDS	Hardness	Alkalinity	Conductivity	pH	SAR
5969.00	52.01	10.20	839.00	7.20	5.7273

Water Type	*Magnesium Chloride*

Cations (epm)	Anions (epm)
94.64	112.01

Error Balance (%)
8.41

Aquifer	*Amphibolite*

LANDBOUNAVORSINGSRAAD

SENDER:
I. Neumann
Raad vir Geowetenskap
P/Sak X112
Pretoria

INSTITUUT VIR GROND, KLIMAAT EN WATER
Privaatsak X79
PRETORIA
0001

DATUM: 20/11/00

B E S O N D E R H E D E V A N W A T E R M O N S T E R

KENMERKE VAN HOUER: H26-0434 LAB NOMMER: WC2002 2000/01

RESULTATE:	me/l	dpm		me/l	dpm
Fluoried (1.5)	0.01	0.10	Natrium (400)	2.65	60.90
Nitriet (4.0)	0.00	0.00	Kalium (400)	0.05	2.0
Nitraat (44.0)	1.43	88.69	Kalsium (200)	2.61	52.20
Chloried (250)	1.18	41.74	Magnesium (100)	3.30	40.14
Sulfaat (500)	0.28	13.42	Boor (1.5)	0.13	0.47
Fosfaat	0.00	0.00			
Karbonaat (20.0)	0.00	0.00			
Bikarbonaat	5.80	353.80			
Subtotaal	8.70	497.75	Subtotaal	8.74	155.67
			Totaal		653.40
			Min (*)		176.90 *
			Totale Opgeloste Stowwe		476.50
Na Karbonaat	0.00	0	Tyd Hardheid	5.80	290
Na Bikarbonaat	0.00	0	Perm Hardheid	0.24	12
Alkaliteit	5.80	290			

* Korreksie vir enige vlugtige stowwe, HCO3/2 of.. HCl+HNO3+HF+..
() Aanbeveelde maksimum waarde vir mense in dpm.

pH (> 6.5 en < 8.6)	pHS	NAV	Elektriese Geleidingsvermoe
7.79	7.27	1.54	80.0 mS/m By 25 grade C

Aanbeveling:

	Mens	Dier	Besproeing
Nie geskik			
Geskik			

NB Ontledings is nie vir mikrobiologiese patogene, organiese verbindings en plaagbeheermiddels gedoen nie.

APPENDIX 3-E

HYDROFRACTURE

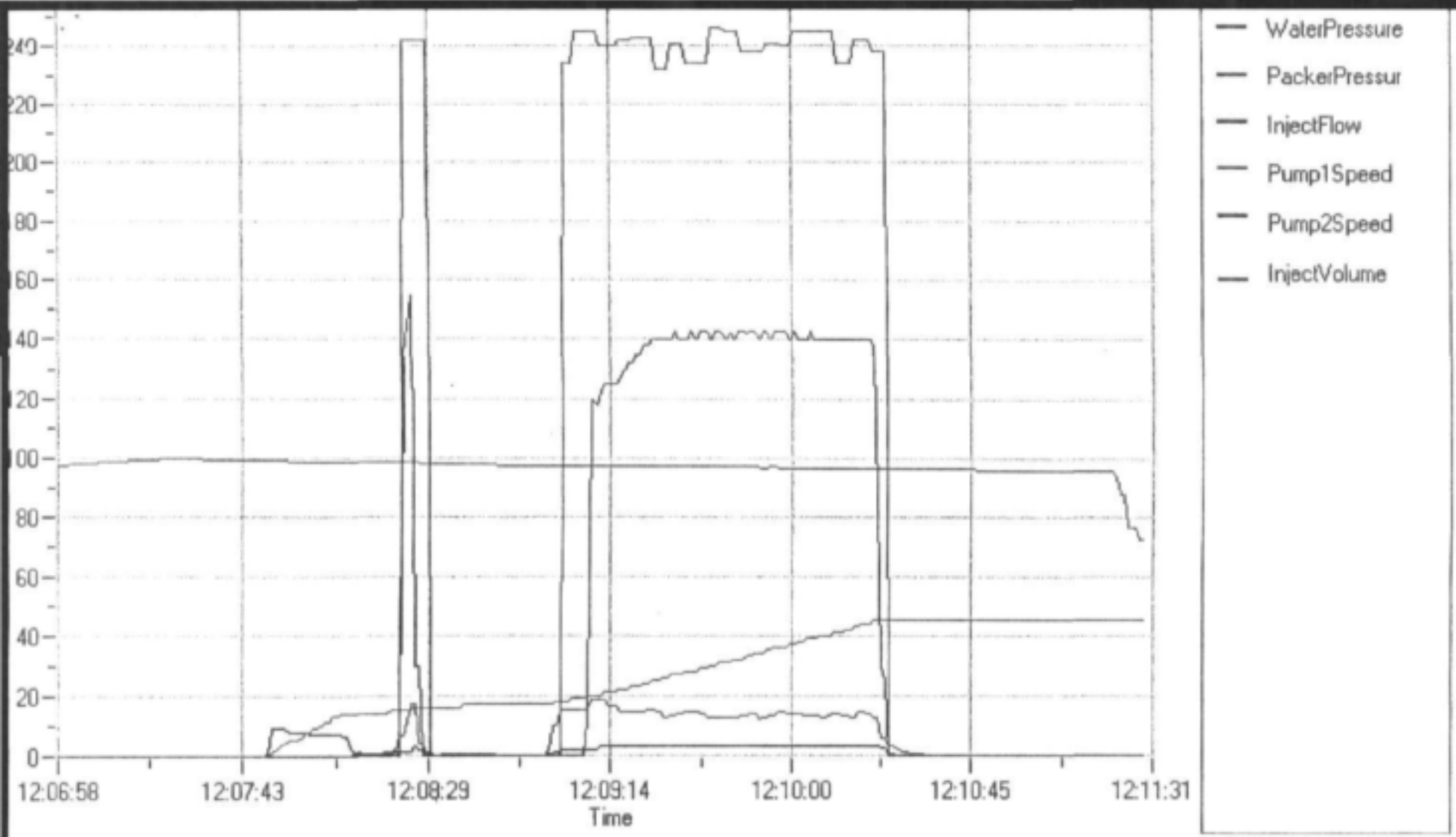

DWAF -- Geohydrology

Locality: Lappidood - Alldays

Borehole no: H26 - 0430

Date: 16/02/2001

Packer Setting: stradle packers - target 17,5m to 20,5m

Waterlevel: 7,60m

Borehole Depth: 96,0m

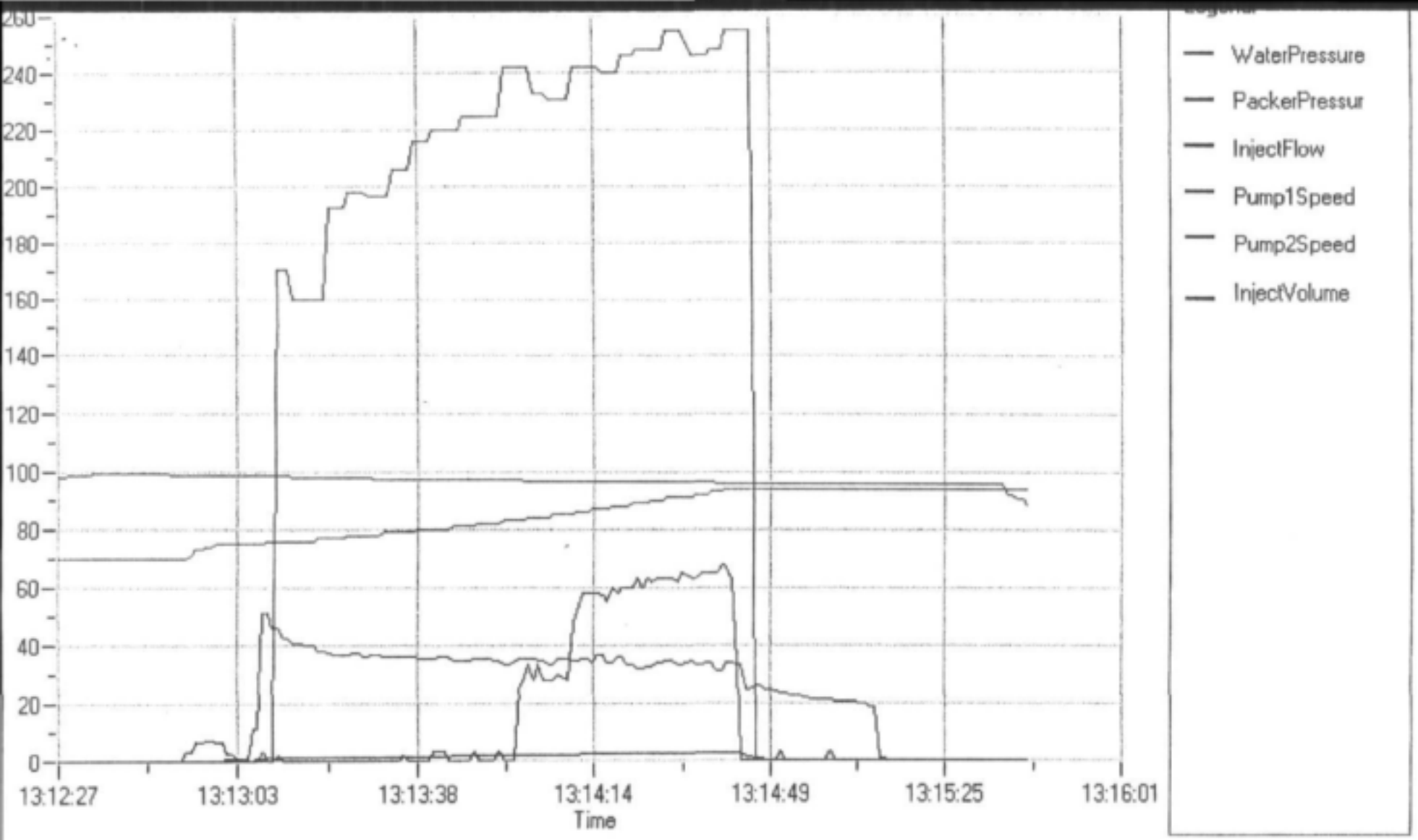

DWAF -- Geohydrology

Locality: Lappidood - Alldays

Borehole no: H26 - 0430

Date: 16/02/2001

Packer Setting: stradle packers - target 32,5m to 35,5m

Waterlevel: 7,60m

Borehole Depth: 96,0m

H26 - 0430 Lappidood
Drawdown and Recovery Test

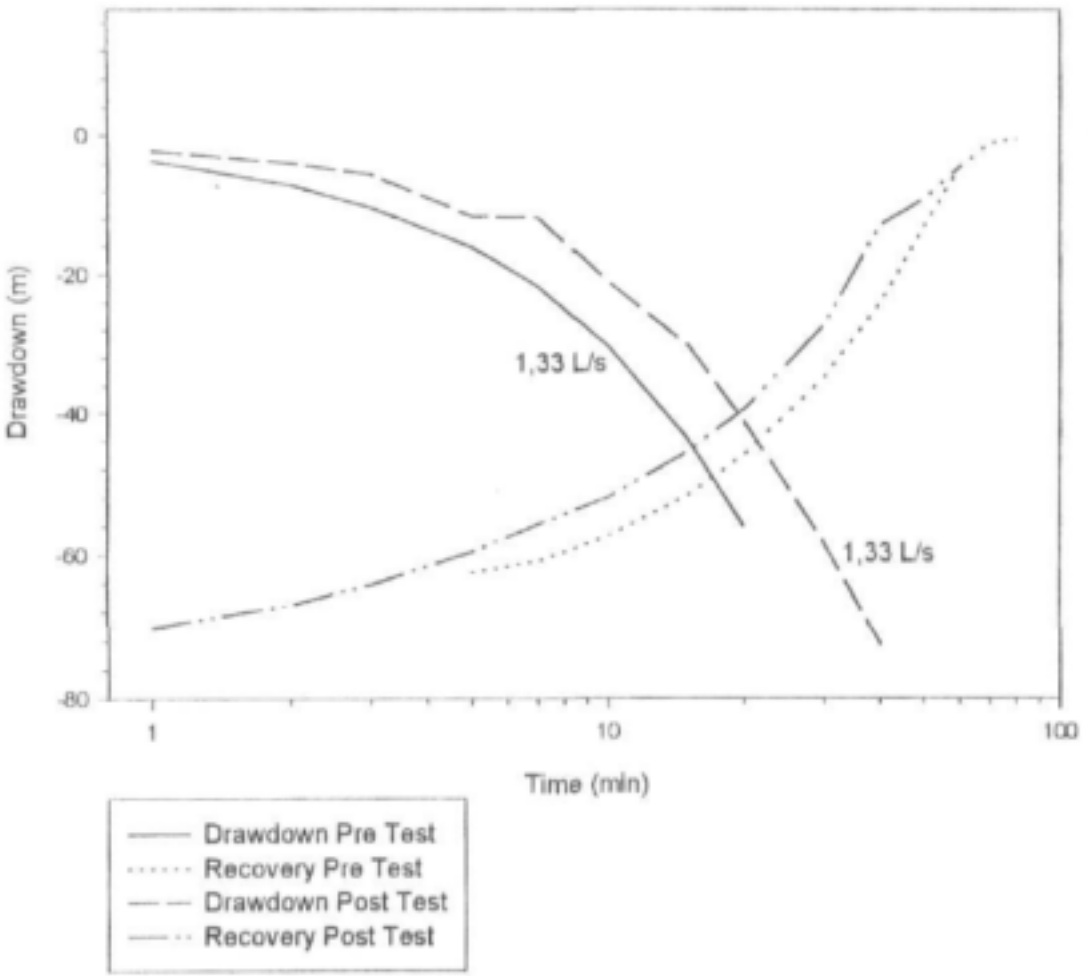

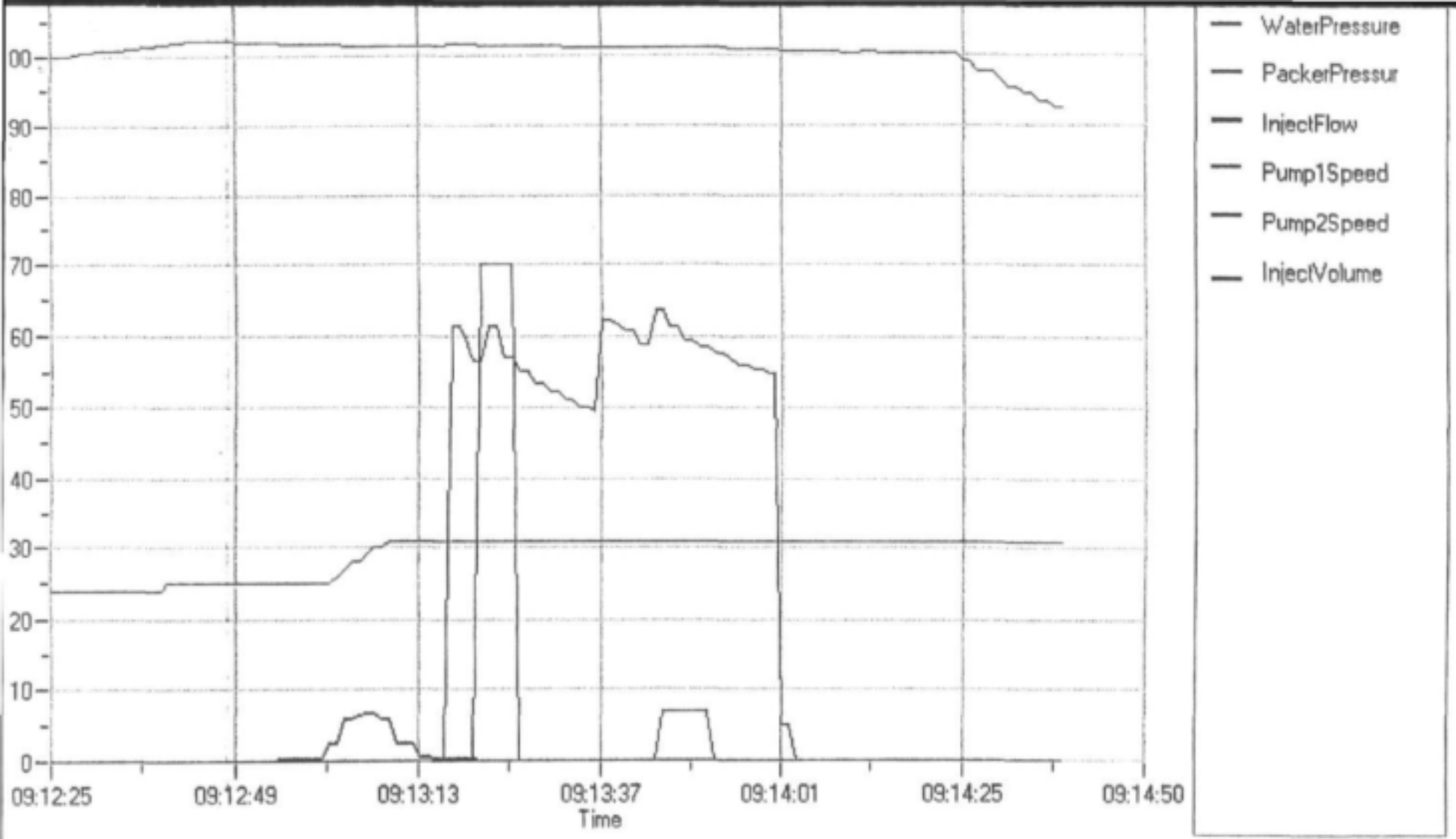

DWAF -- Geohydrology

Locality: Weg van My - Alldays

Borehole no: H26 - 0431

Date: 20/02/2001

Packer Setting: stradle packers - target 35,5m to 38,5m

Waterlevel: 3,32m

Borehole Depth: 66,0m

H26 - 0431 Weg van My
2 hour Constant Drawdown and Recovery Test

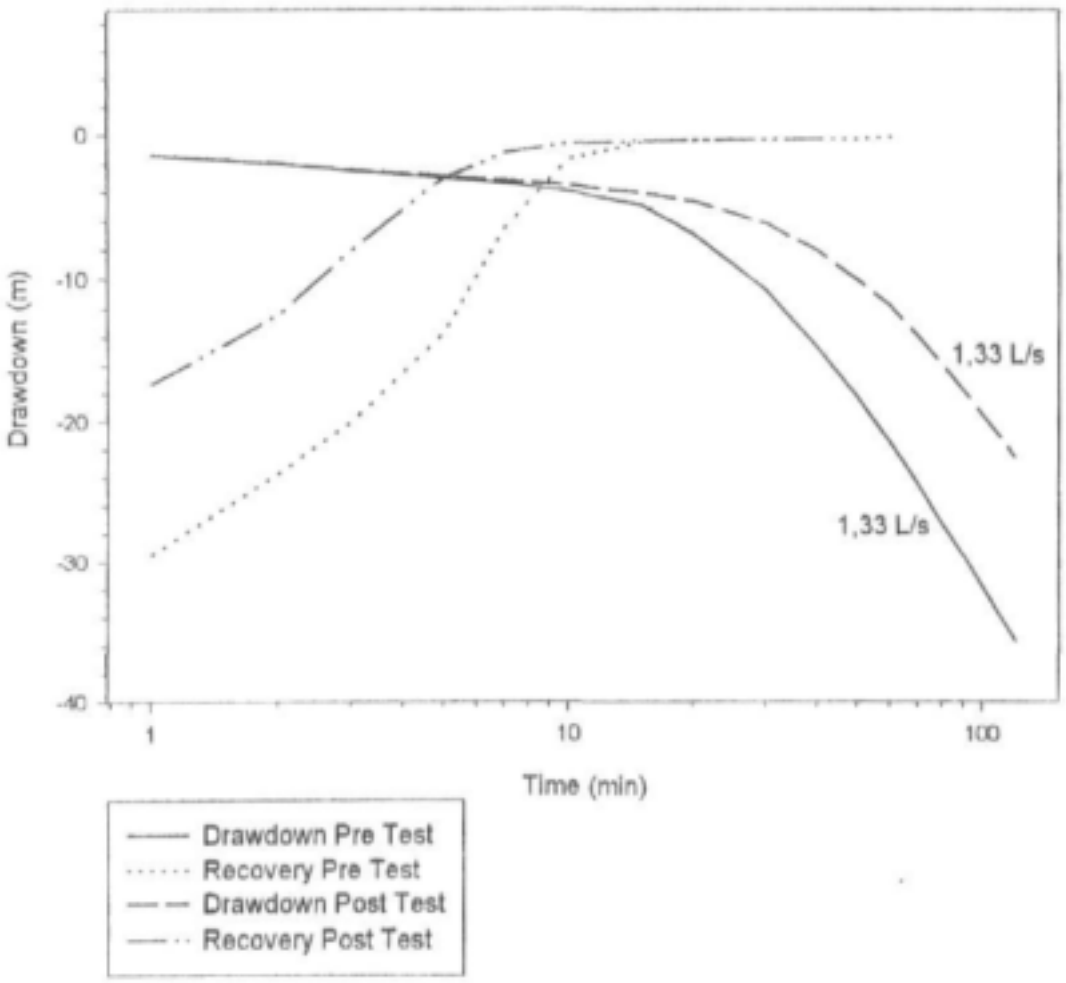

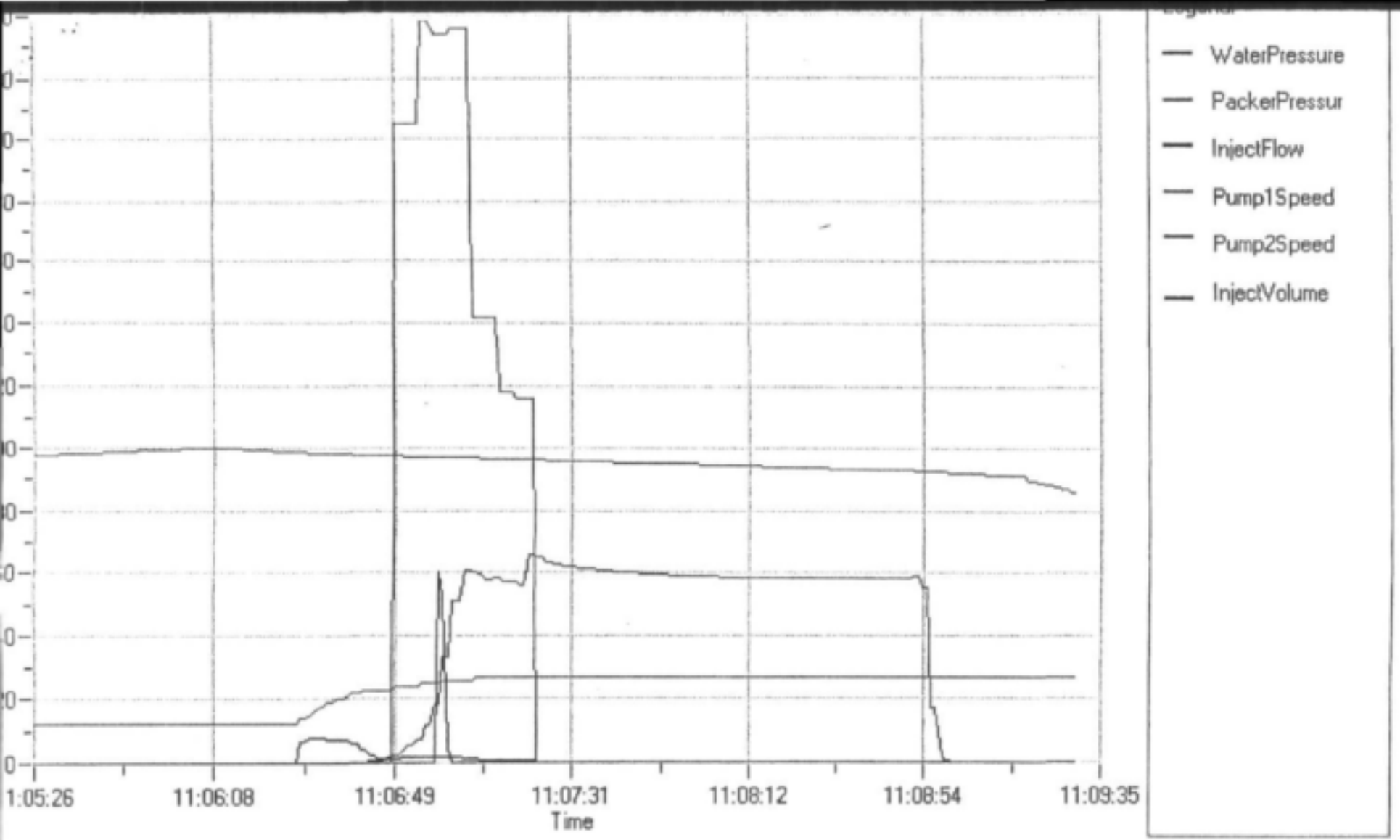

DWAF -- Geohydrology

Locality: Lappidood - Alldays

Borehole no: H26 - 0429

Date: 15/02/2001

Packer Setting: stradle packers - target 65,5m to 68,5m

Waterlevel: 12,72m

Borehole Depth: 90,0m

H26 - 0429 Lappidood
2 hour Constant Drawdown and Recovery Test

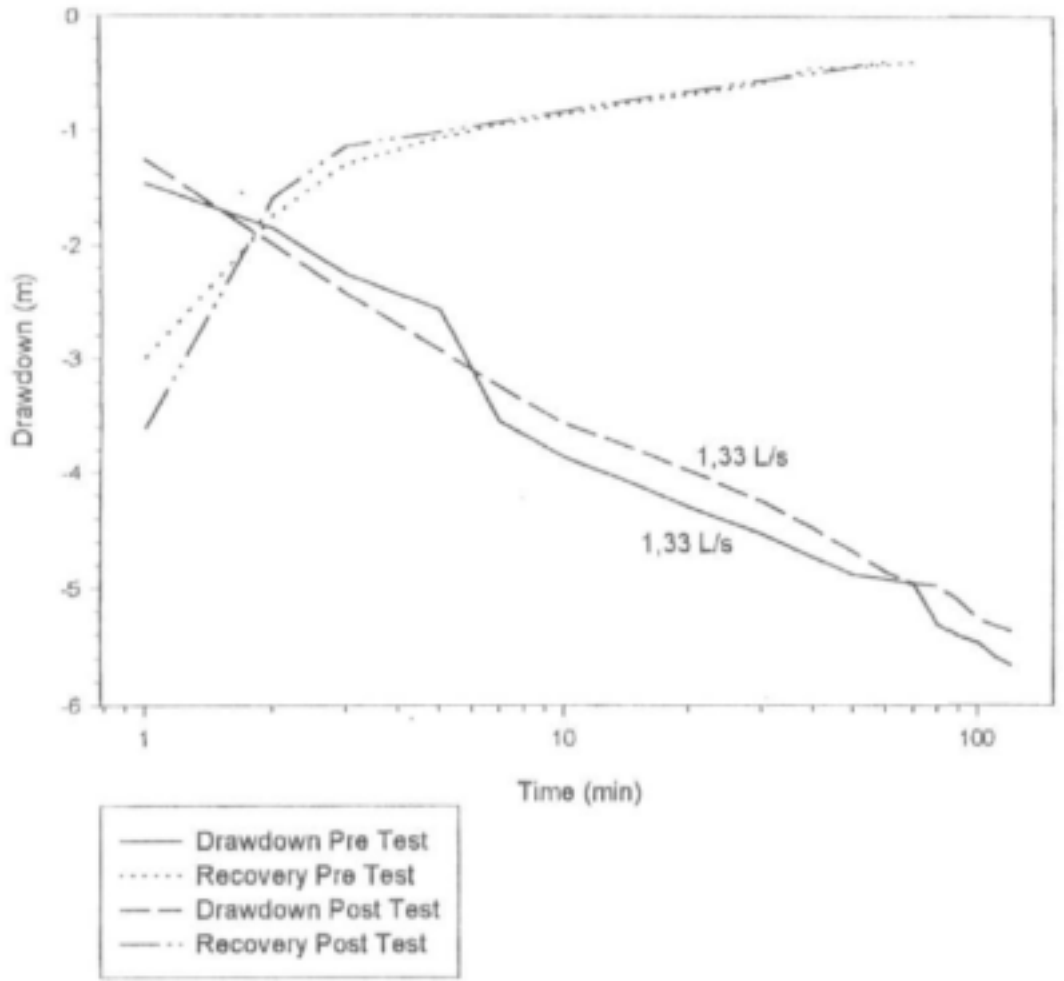

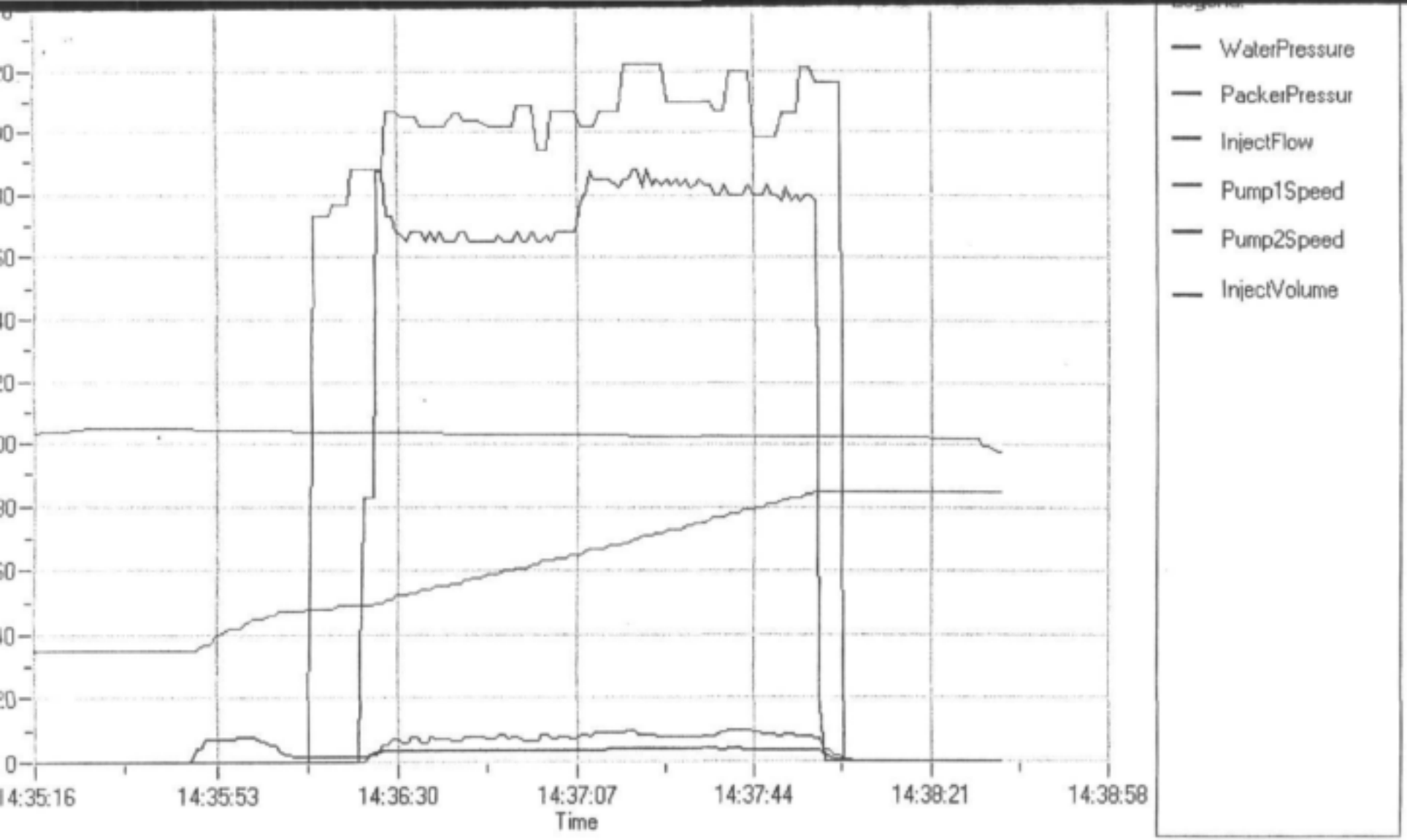

DWAF -- Geohydrology

Locality: Juniorsloop - Alldays

Borehole no: H26 - 0426

Date: 21/02/2001

Packer Setting: stradle packers - target 41,5m to 44,5m

Waterlevel: 26,13m

Borehole Depth: 96,0m

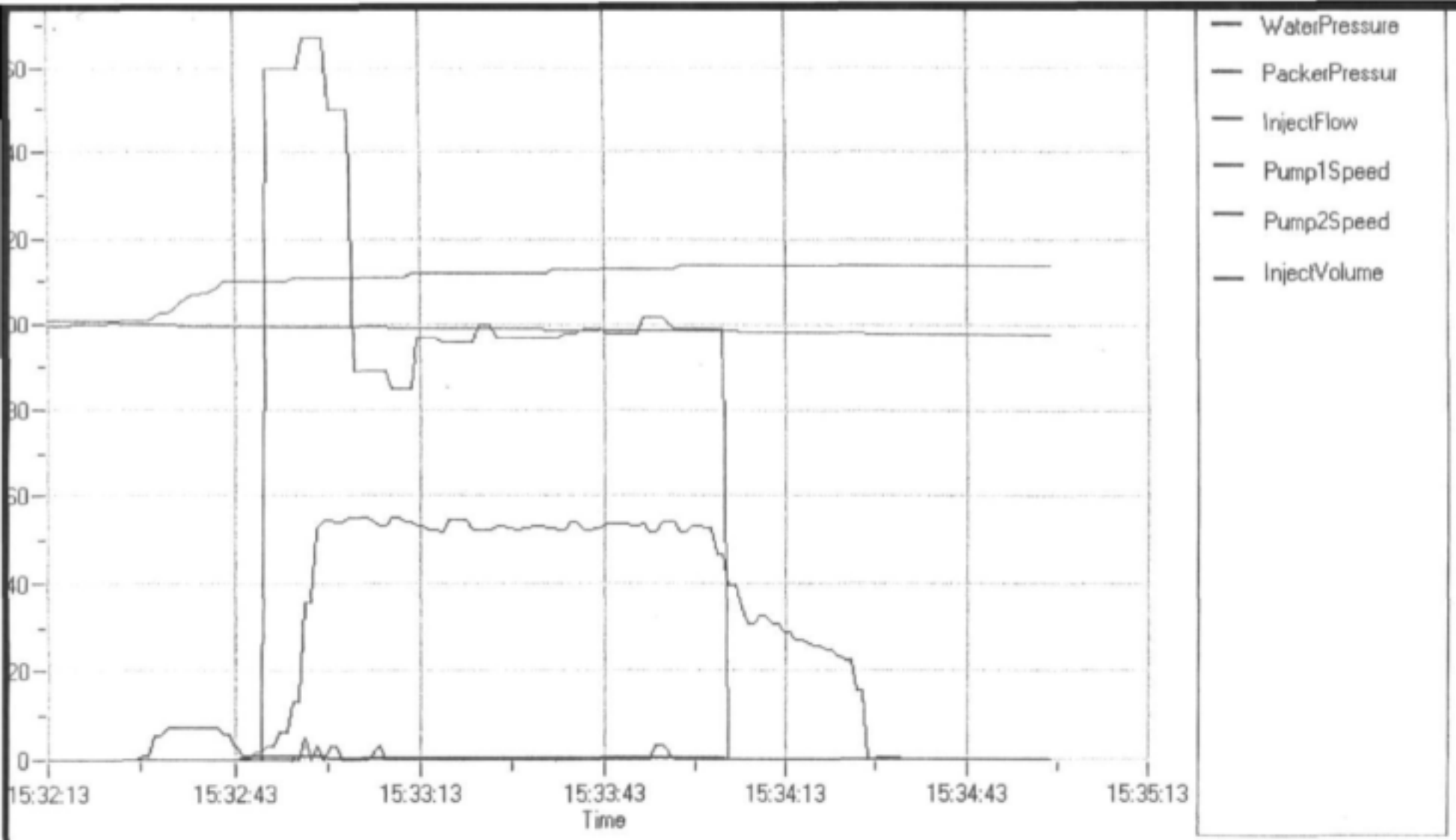

DWAF -- Geohydrology

Locality: Juniorsloop - Alldays

Borehole no: H26 - 0426

Date: 21/02/2001

Packer Setting: stradle packers - target 59,5m to 62,5m

Waterlevel: 26,13m

Borehole Depth: 96,0m

H26 - 0426 Juniorsloop
Drawdown and Recovery Test

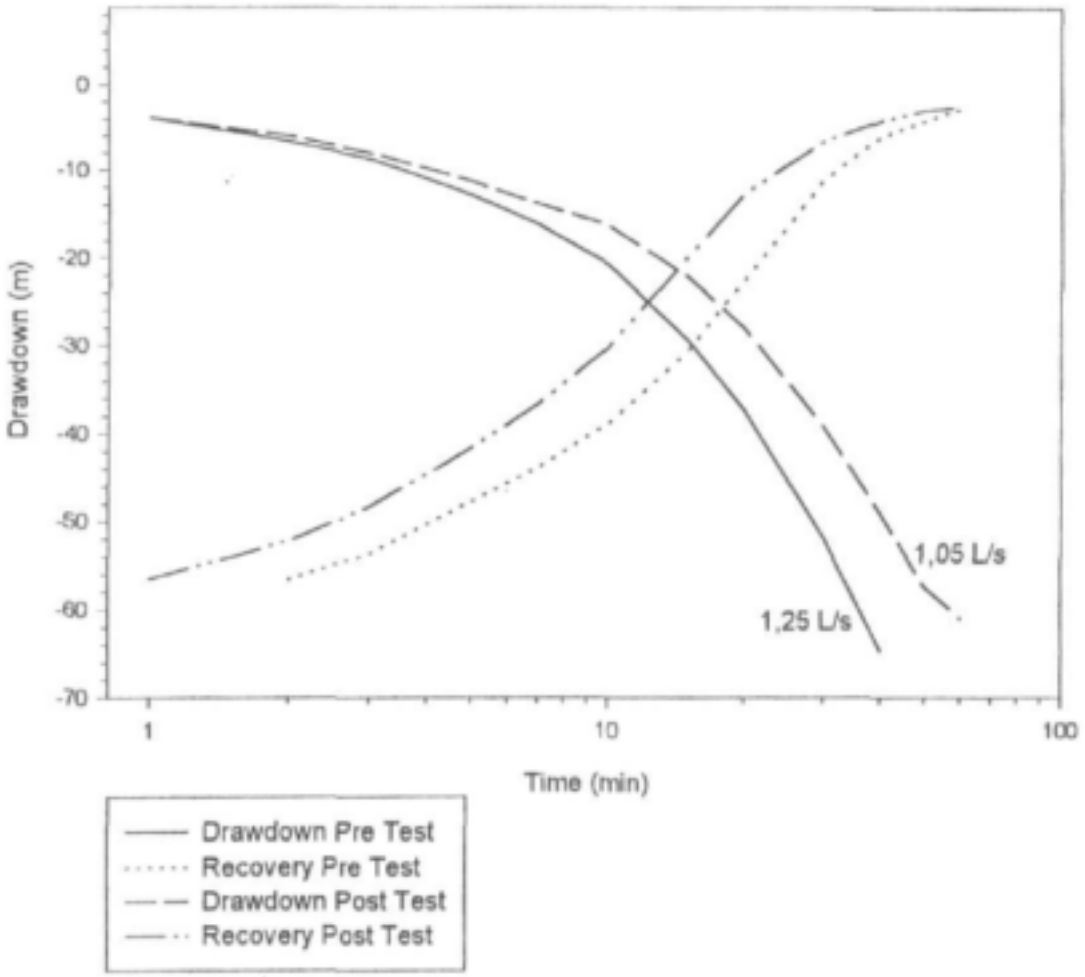

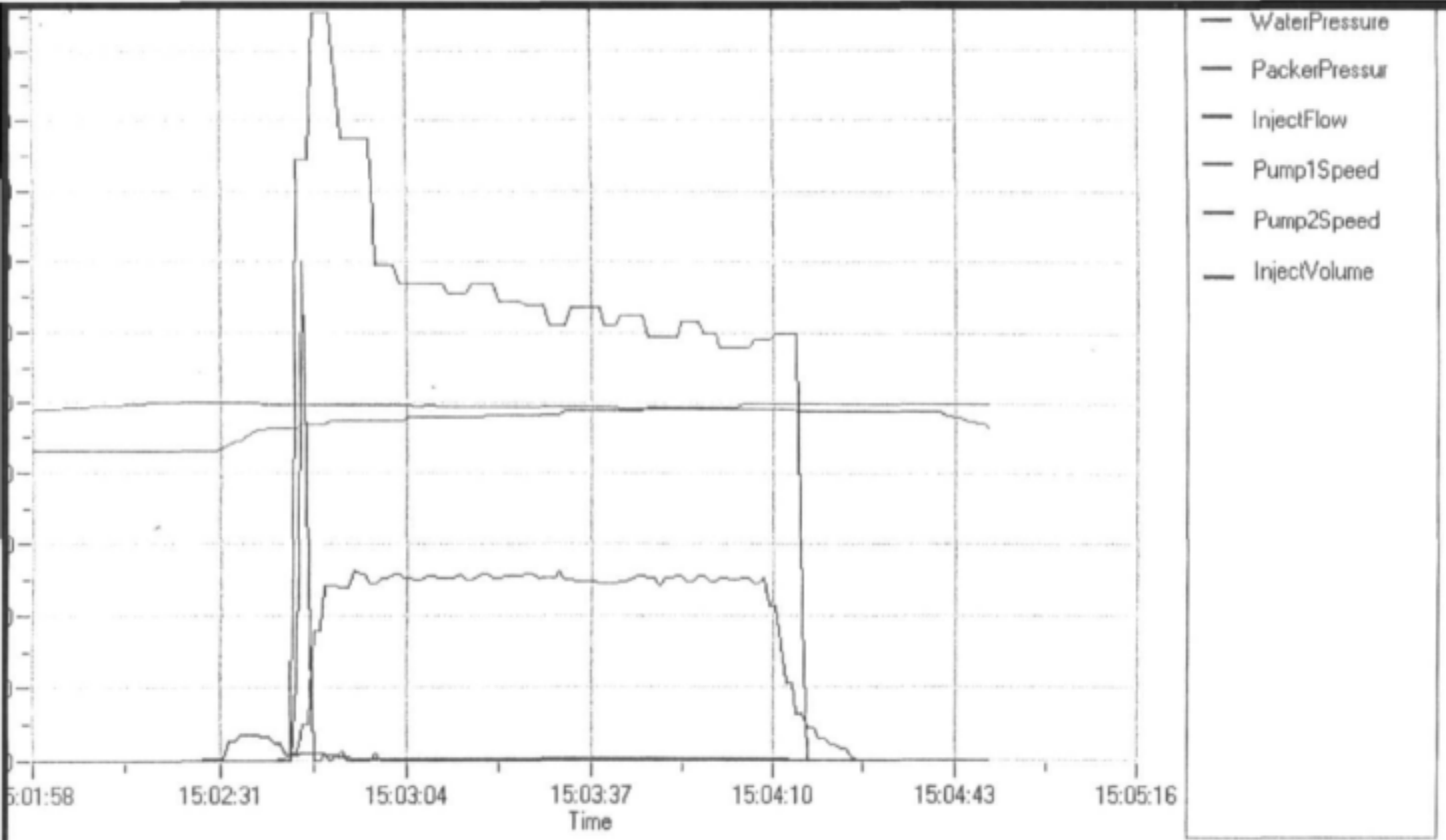

DWAF -- Geohydrology

Locality: Juniorsloop - Alldays

Borehole no: H26 - 0426

Date: 21/02/2001

Packer Setting: stradle packers - target 47,5m to 50,5m

Waterlevel: 26,13m

Borehole Depth: 96,0m

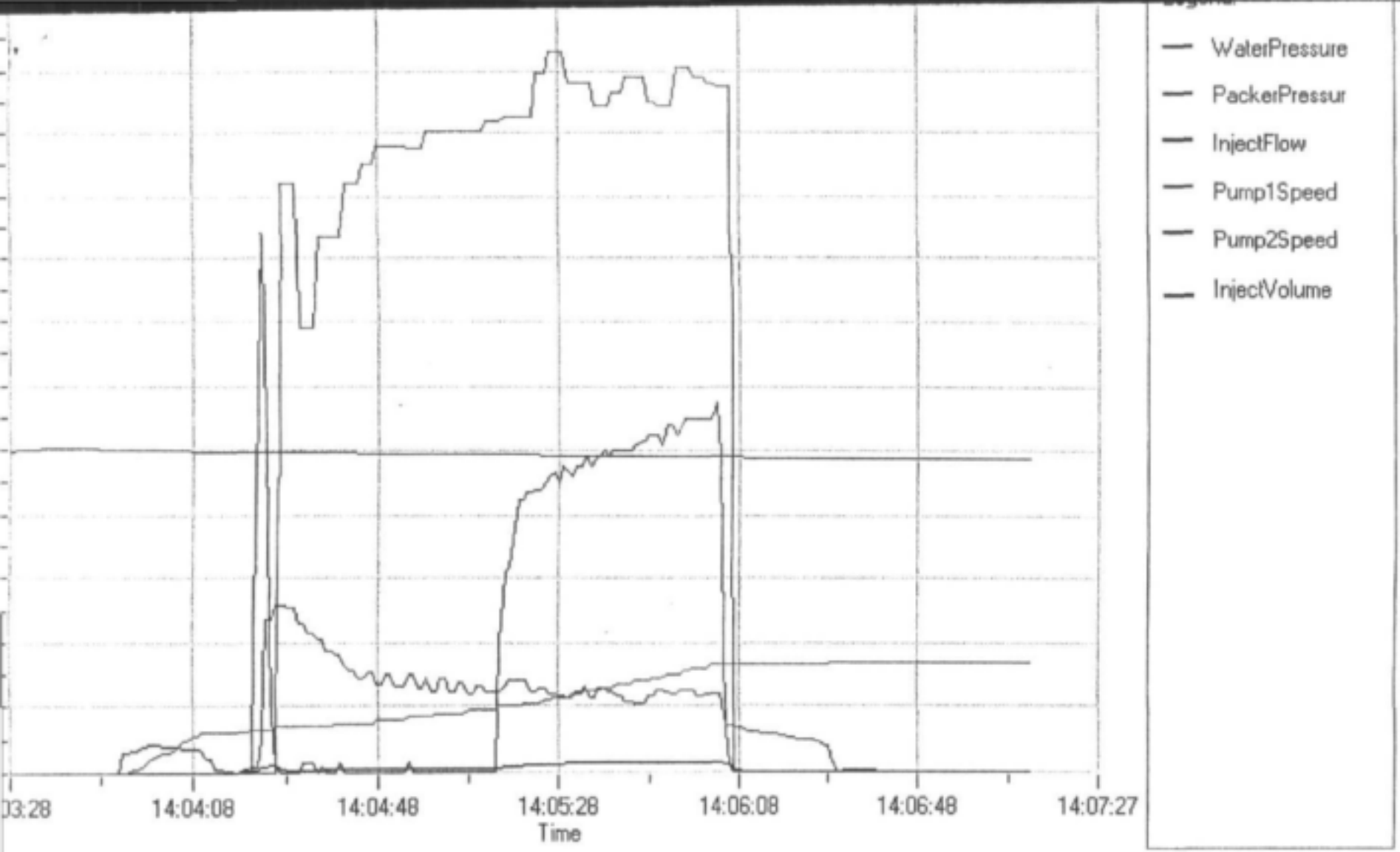

DWAF -- Geohydrology

Locality: Juniorsloop - Alldays

Borehole no: H26 - 0426

Date: 21/02/2001

Packer Setting: stradle packers - target 35,5m to 38,5m

Waterlevel: 26,13m

Borehole Depth: 96,0m

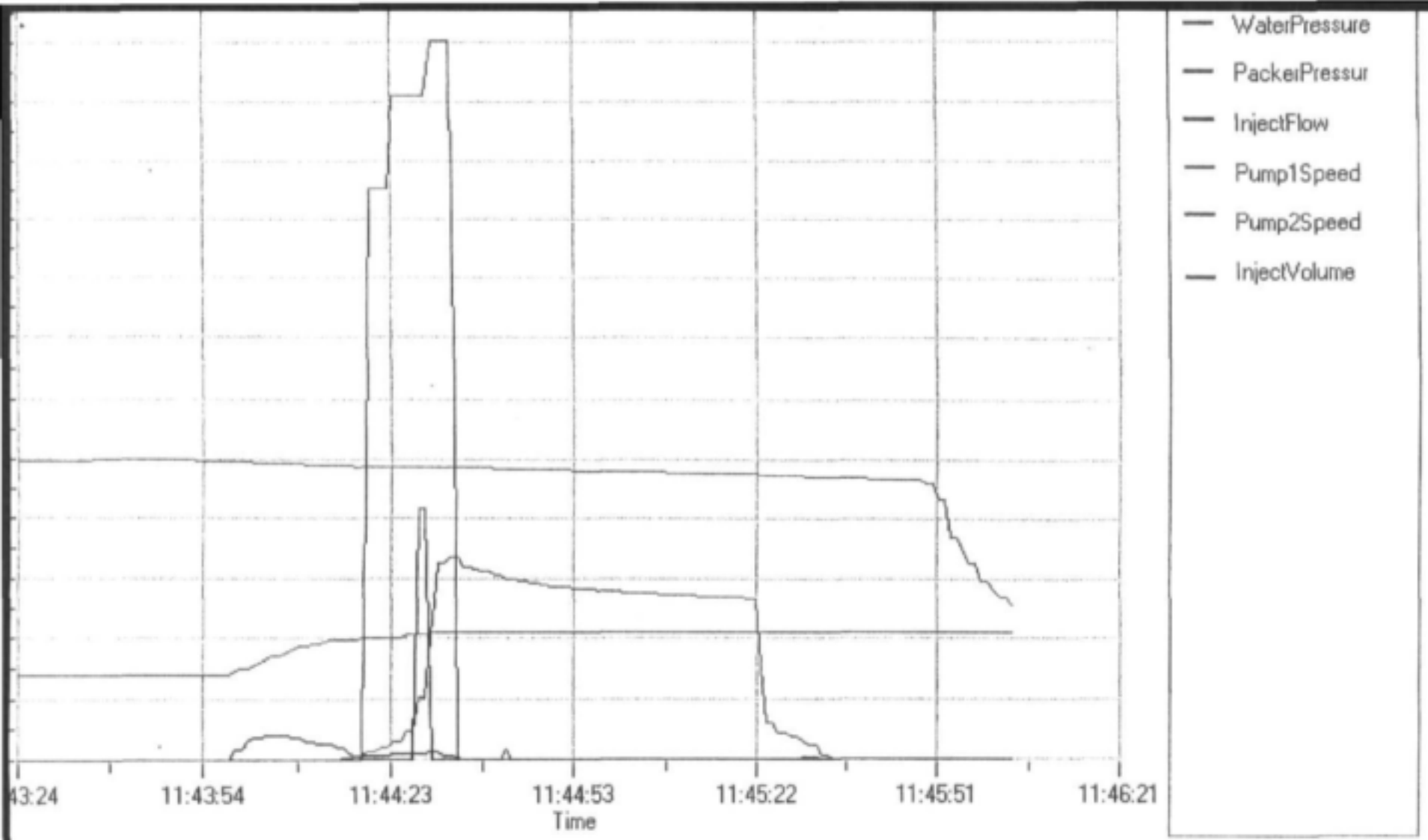

DWAF -- Geohydrology

Locality: Lappidood - Alldays

Borehole no: H26 - 0429

Date: 15/02/2001

Packer Setting: stradle packers - target 74,5m to 77,5m

Waterlevel: 12,72m

Borehole Depth: 90,0m

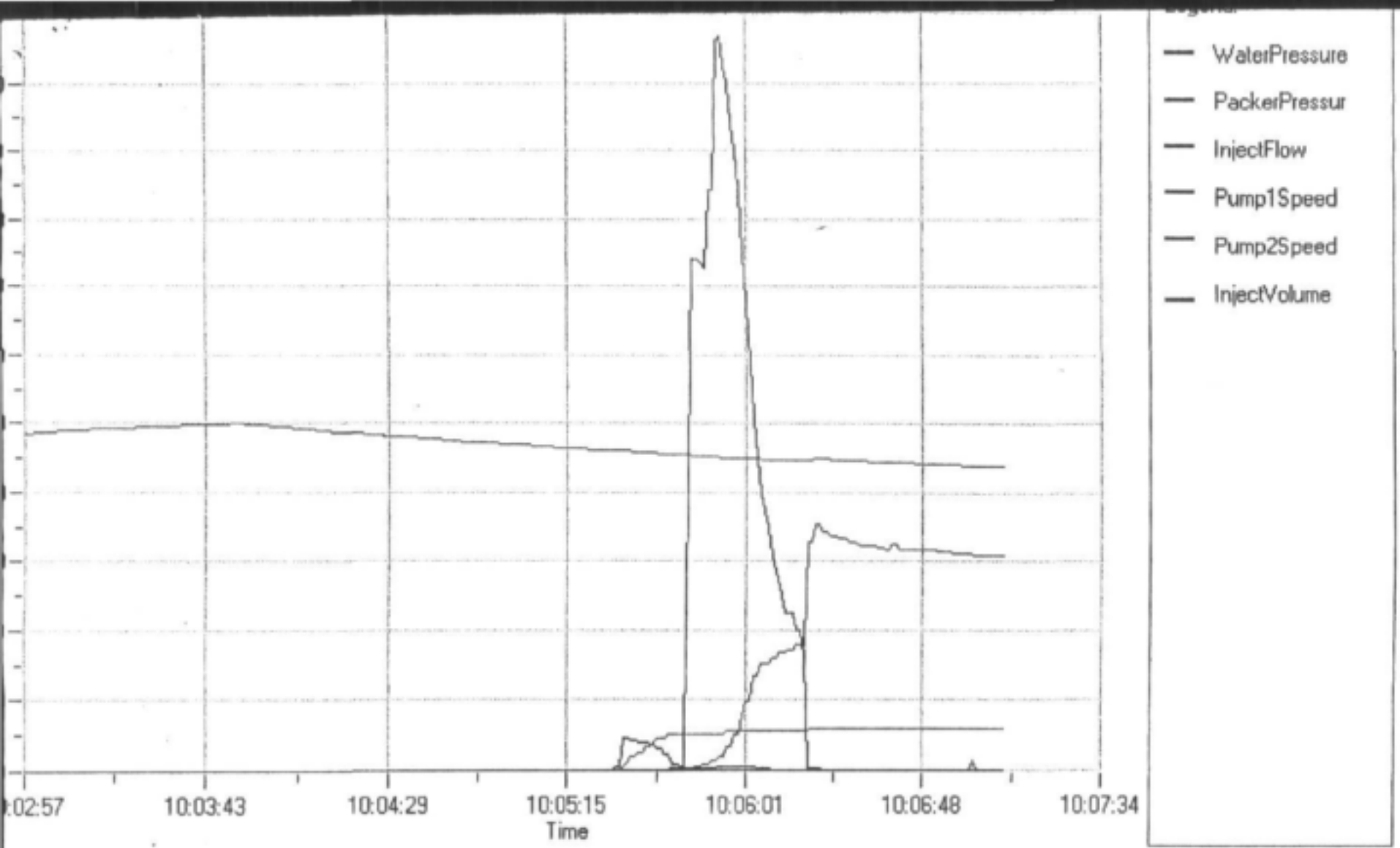

DWAF -- Geohydrology

Locality: Lappidood - Alldays

Borehole no: H26 - 0429

Date: 15/02/2001

Packer Setting: stradle packers - target 44,5m to 47,5m

Waterlevel: 12,72m

Borehole Depth: 90,0m

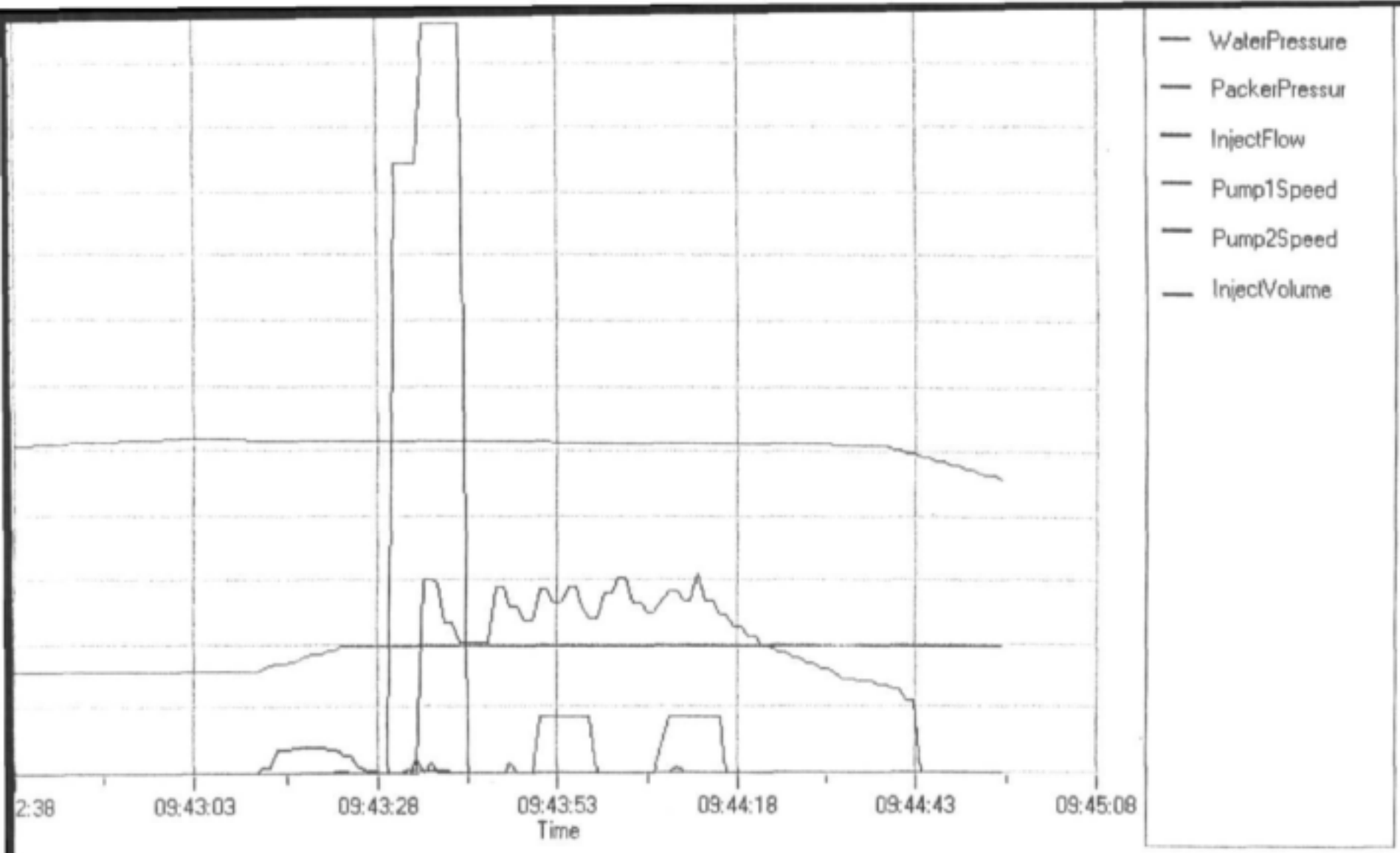

DWAF -- Geohydrology

Locality: Weg van My - Alldays

Borehole no: H26 - 0431

Date: 20/02/2001

Packer Setting: straddle packers - target 47,5m to 50,5m

Waterlevel: 3,32m

Borehole Depth: 66,0m

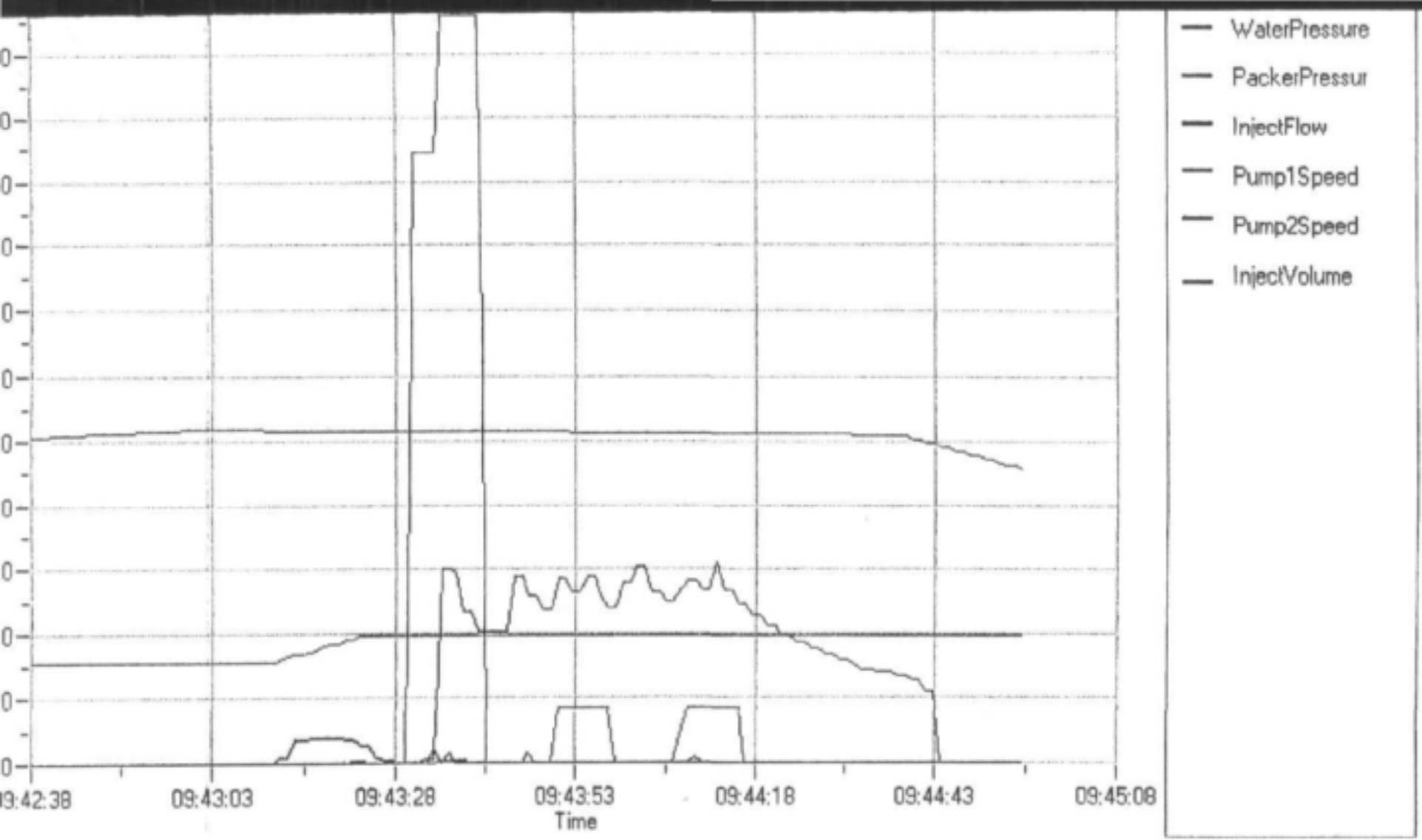

DWAF -- Geohydrology

Locality: Weg van My - Alldays

Borehole no: H26 - 0431

Date: 20/02/2001

Packer Setting: stradle packers - target 47,5m to 50,5m

Waterlevel: 3,32m

Borehole Depth: 66,0m

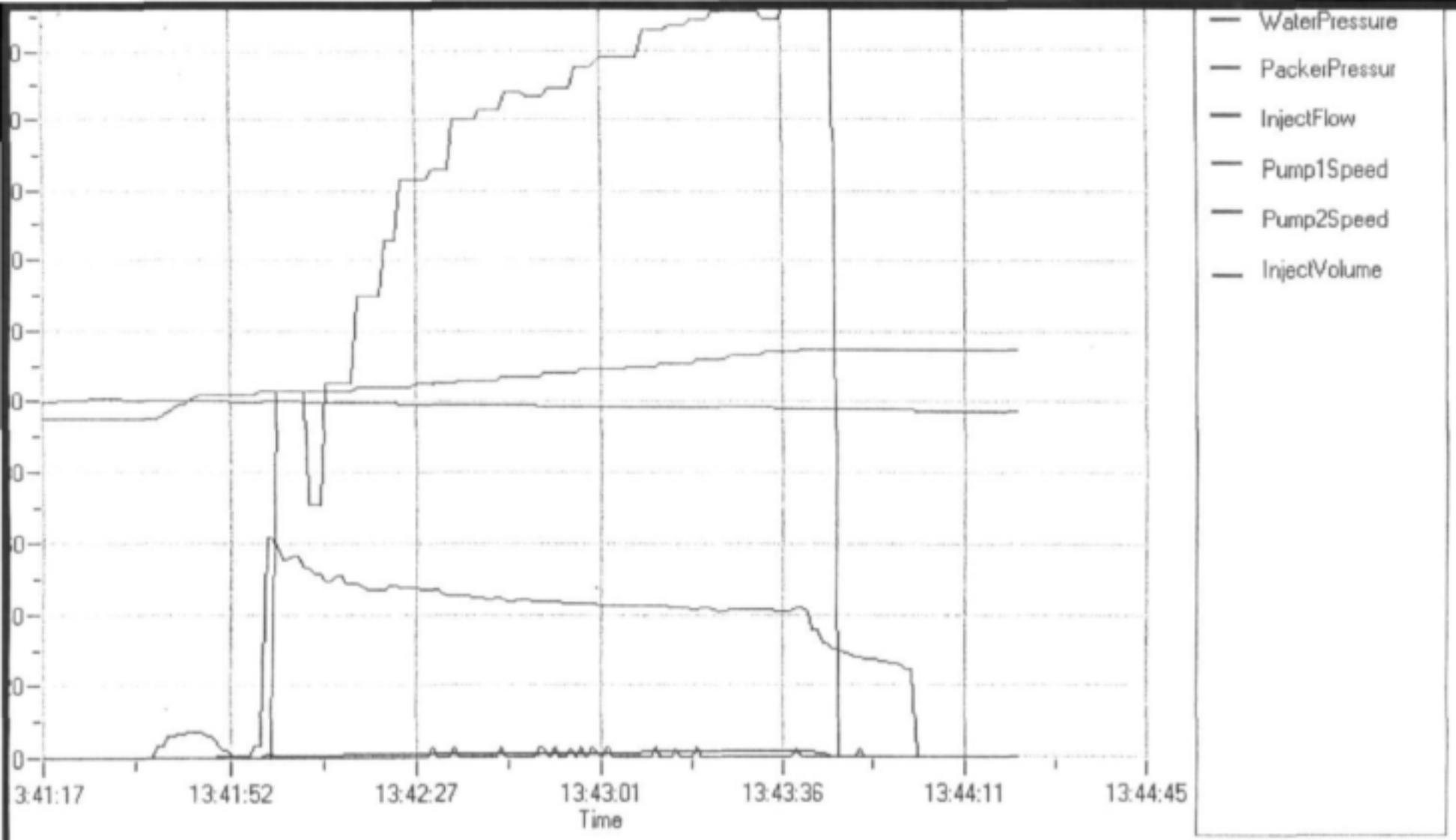

DWAF -- Geohydrology

Locality: Lappidood - Alldays

Borehole no: H26 - 0430

Date: 16/02/2001

Packer Setting: stradle packers - target 44,5m to 47,5m

Waterlevel: 7,60m

Borehole Depth: 96,0m

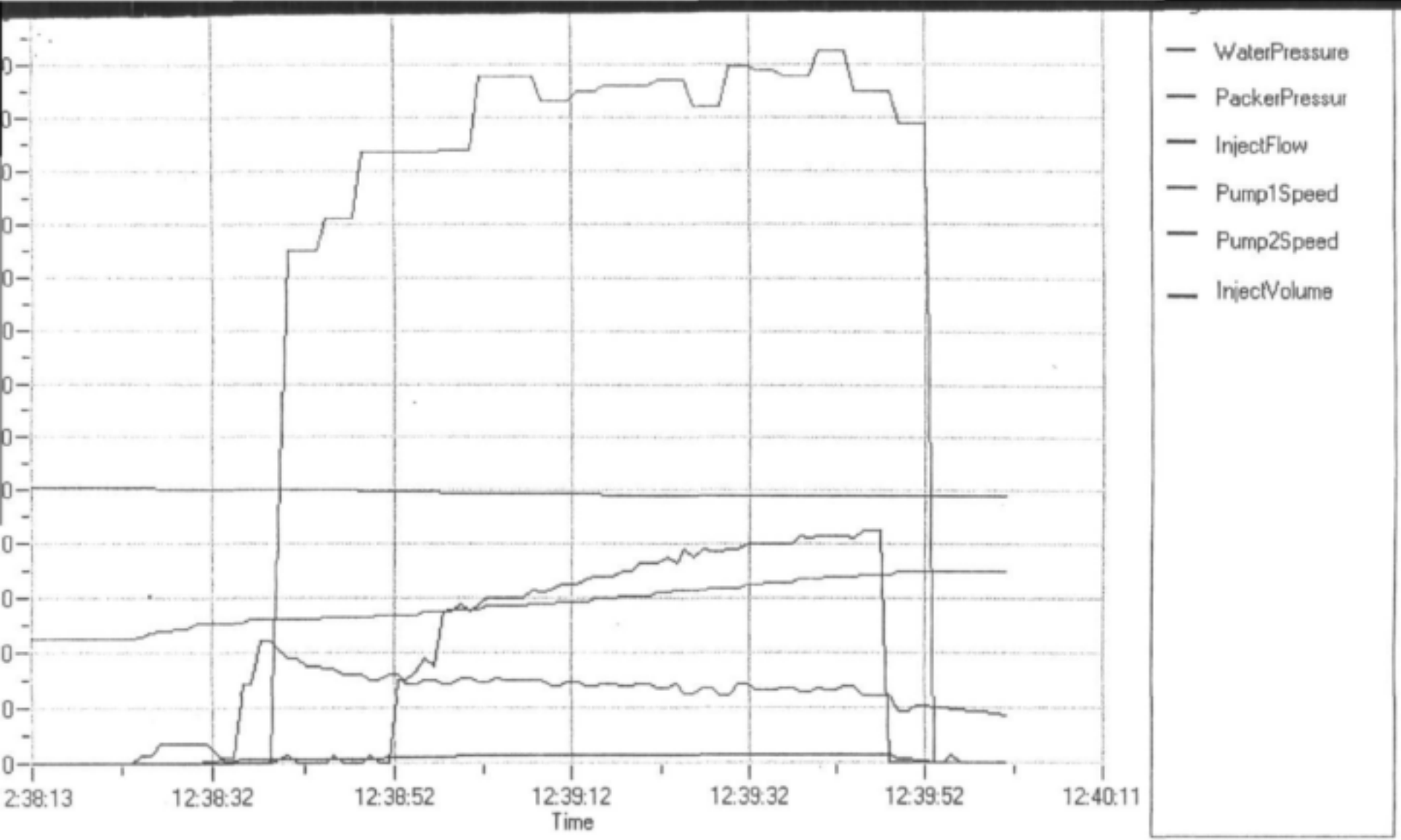

DWAF -- Geohydrology

Locality: Lappidood - Alldays

Borehole no: H26 - 0430

Date: 16/02/2001

Packer Setting: stradle packers - target 26,5m to 29,5m

Waterlevel: 7,60m

Borehole Depth: 96,0m

4 BARBERTON GREENSTONE BELT

4.1 General Setting

4.1.1 Site Locality

The study focussed on the Tjakastad Subgroup of the Onverwacht Group, since this is the geological unit that is most densely settled by rural communities in the of the Barberton Greenstone Belt. This area consists of Archean greenstones and associated granitic plutons. It is located near the eastern edge of the Kaapvaal craton in the Province of Mpumalanga. The study area is situated south east of Barberton about 15 km north west of Swaziland border in the districts of Tjakastad and Steynsdorp (Figure 4.1).

Figure 4-1 **Locality map of the study area.**

The area of investigation covers about 2760km^2 and is bounded by 25°95', 26° 25' latitudes and 30° 75', 31° 10' longitudes. Four topographical maps: 2530 DD, 2531 CC, 2630 BB, 2631 AA, cover the area. The major access road is the main road to Swaziland that goes through Badplaas (R541) to the Tjakastad and Stynsdorp Districts. The area is predominantly rural, with high population density in the Township areas, which are relatively fast growing. Tjakastad, Ntlazatshe, Ekulindeni, Nhlaba and Stynsdorp are the main settlement townships in the study area.

4.1.2 Topography

The Barberton Greenstone Belt can be divided into the Barberton Mountain Land, which is characterised by highly complex, rugged topography, and the Lowveld region, which is generally rugged with ridge and valley morphology. This morphology can be attributed to differential erosion within a volcano-sedimentary greenstone terrain, where quartzite forms prominent ridges separated by deep valleys underlain by basic schists (Lageat & Robb, 1984). Lageat & Robb (1984) observed that variations in composition, mineralogy and texture of rocks influence erosion and denudation of the Barberton terrain. The geomorphology of the Barberton Greenstone Belt is the result of several major cycles of erosional degradation, planation and isostatic uplift of the region since marginal rifting initiated the Atlantic and Indian oceans (Ward, 1999).

Mount Emlembe is the highest peak in the area, some 1838 m above mean sea level (m.a.s.l). The Barberton Mountain Land is generally greater than 1500 m a.m.s.l and the Lowveld is commonly less than 1500 m a.m.s.l. An intermediate bench is located along the escarpment in the Sabie – Elandshoogte area and further south (Ward, 1999).

4.1.3 Drainage

The Komati River forms the major drainage system in the study area. It is one of the main tributaries of the greater Limpopo. The Limpopo tributaries arise along the greater escarpment known as the Drakensberg escarpment (Lageat and Robb, 1984).

4.1.4 Climate, Vegetation and land-use

The climate of the Lowveld region is characterised by the mean annual precipitation of 836 mm, which is calculated over an 80-year period from the rain gauge situated at Badplaas (Midgley et. al., 1990). Much of the rainfall occurs as heavy showers during the summer season and occasional results into floods, which have devastating effects on the infrastructure of the region, thus damaging the roads, bridges etc. The S-pan evaporation ranges from 1300 in the Mountain Land to 1650 mm in the Lowveld (Midgley et.al., 1990).

The vegetation of the Barberton Greenstone Belt is classified as Savannah Biome, which is sub-classified into the Sour Lowveld Bushveld and the Northeastern Mountain Grassland (Low and Rabelo, 1996). The Sour Lowveld Bushveld covers the mountainous areas of the Barberton Greenstone Belt and it consists of open trees (e.g. Silver Cluster Leaf), shrubs (e.g. Sickle Bush) and a tall, tufted and relatively dense grass constituent (e.g. Yellow Thatching Grass). The Northeastern Mountain Grassland covers areas south of the Barberton Mountainland including Swaziland and Northern Natal. The Northeastern Mountain Land and consists mainly of grassland species e.g. Giant Speargrass, *Trachypogon Spictatus* etc. (Low and Rabelo, 1996). The land is predominantly used for subsistence agricultural purposes that include crop production and cattle farming. The region is historically known for gold, antimony, asbestos mining.

4.2 Regional Geology

4.2.1 Introduction

The Barberton Greenstone Belt is one of the few regions on earth where relatively pristine Mid-Archean rocks had been preserved. It is the largest and the most widely known greenstone belt terrain in the world. The belt represents a 3570 to 3080 Ma xenolithic remnant of an Archean fold and thrust belt located in the Kaapvaal Craton (Cornel et.al.,

1994). The Kaapvaal craton represents the crust of the earliest continental margins and consists predominantly of a variable mixture of plutonic rocks with calc-alkaline chemistry, and supra-crustal rocks of sedimentary origin that are often green in colour (Kirsters and Anhaeusser, 1994). The plutonic rocks are traditionally classified as tonalitic-trontjemite granodiorites (TTG) and granites, and the supracrustal rocks are referred to as 'greenstones' by virtue of their green appearance (Lowe and Nochitha, 1999). This combination of rocks makes up the "granite-greenstone" terrains of Archean Cratons. The broad structure of the Barberton Belt is that of a synform with pronounced NNE to ENE trend (Cornel et.al., 1994). The surface geology of the Barberton Greenstone Belt is preserved in this synformal structure (Figure 4.2).

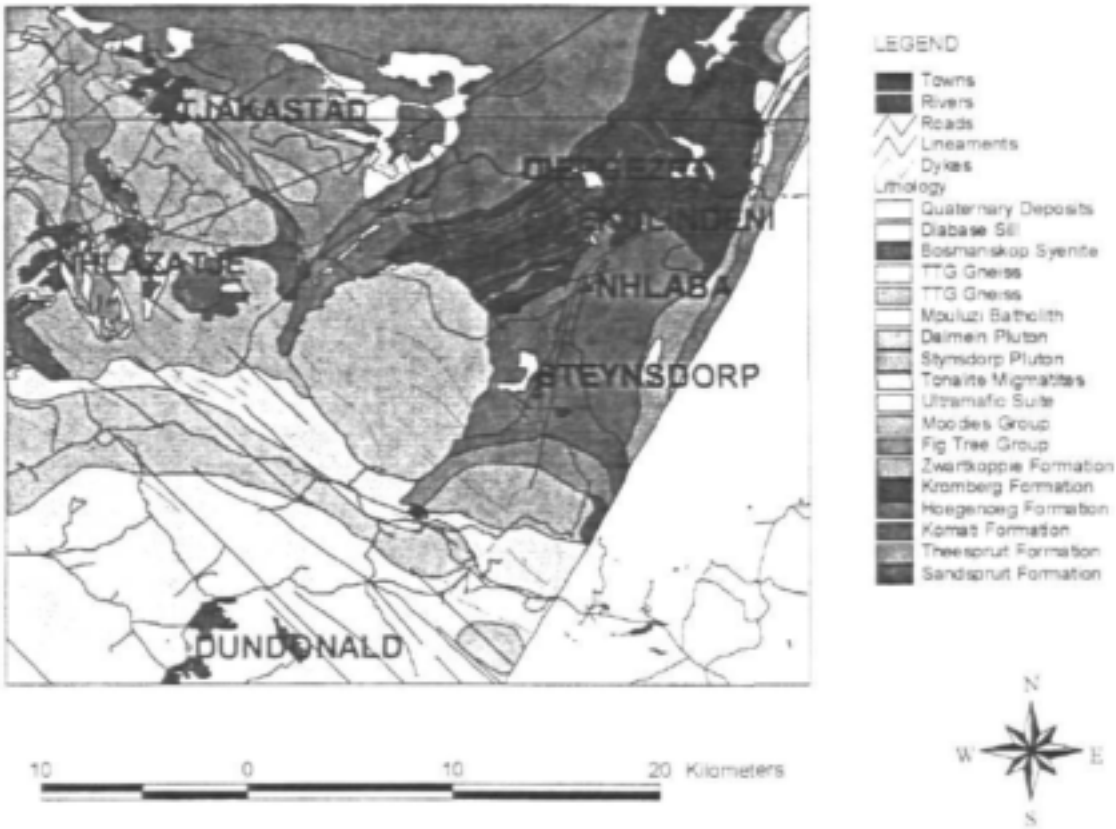

Figure 4-2 Geological Map of the Barberton Greenstone Belt.

4.2.2 The stratigraphy and lithology of the Barberton Greenstone Belt

The Barberton Greenstone Belt contains the most complete stratigraphy of all the greenstone belts. Its basal unit is the Onverwacht Group. The Onverwacht Group represents a geochemical transition from ultramafic units at its base to mafic and felsic units at the top of the Group (Table 4.1). This unit is sub-divided into the Tjakastad and Geluk Subgroups by a persistent sedimentary horizon termed the Middle Chert Marker (SACS, 1980).

The Tjakastad Subgroup consists of three formations; the Sandspruit, Theespruit and the Komati Formations. These Formations consist of subaqueous lava flows, and metaperidotite, meta-basalt and meta-tholeite dominate the ultramafic assemblage. Most settlements are

situated in areas covered by the rocks of the Tjakastad Subgroup and TTG granites, hence it has been the focus of this investigation.

The Sandspruit Formation occurs only as xenoliths of metamorphosed komatiitic and basaltic rocks within the TTG intrusive units along the southern margin of the Barberton Greenstone Belt. The Theespruit Formation consists of metamorphosed and sheared basalts, felsic tuffs and breccias, and cherty sediments south of the Komati fault.

Table 4-1 The stratigraphy of the Barberton Greenstone Belt

Group		Formation	Lithological Description	Thickness (m)	Age (Ma)
Moodies		Baviaanskop	Sandstone, grits, conglomerates, shales, Subgraywackes, quartzite, phyllites.	685	
		Joe's Luck	Shales, subgraywackes, sandstones, quartzites, phyllites, ferruginous shales. Basaltic lava.	740	
		Clutha	Shales, quartzites, conglomerates, jaspalites.	1600	
Fig Tree			Trachytic tuffs, agglomerates, lavas, tuffaceous graywackes and graywacke conglomerates.	- 550	3460
		Belvue Road	Siltstone, shales and subordinates graywacke with banded ferruginous cherts and trachytic tuff.	600	
		Sheba	Graywackes with some shales and interlayers of chert and ferruginous chert.	1000	2980 +/- 20
Onverwacht	Geluk	Zwaartkoppie	Felsic volcanics and intelayered chert.	900 – 915	+/- 3360
		Kromberg	Mafic and felsic lavas, pyroclastics and agglomerates, banded cherts and carbonate rocks, mainly metamorphosed.	1900 – 1920	3290 +/- 45
		Hoogenoeg	Mafic and felsite and pyroclastics. Banded cherts. Mainly metamorphosed.	4850	3355+/- 70
	Tjakastad	Komati	Mafic and ultramafic (Komatiites) lavas, chert, metamorphosed.		3350 +/- 70
		Theespruit	Mafic and subordinate ultramafic lavas and felsic tuffs, schists, carbonaceous cherts, mainly metamorphosed.	1890 – 1900	
		Sandspruit	Ultramafic and subordinate mafic lavas, mainly metamorphosed.	2100 – 2130	

The Komati Formation consists of metamorphosed peridotitic and basaltic komatiites and underlies tholeiitic volcanic rocks of the Hoogenoeg Formation. The type locality is the spinefex stream in the valley of the Komati River on the west limb of the Onverwacht anticline, where the formation reaches 3500 m thick.

The Middle maker separates the Hoegenoeg Formation from the underlying Komati Formation. The Hoegenoeg Formation consists of a thick sequence of tholeiitic basalts, komatiites, felsic igneous rocks and thin cherty units. These are silicified volcano-clastic turbidites. The Kromberg Formation overlies the Hoegenoeg Formation and it consists of massive extrusive ultramafic rocks at the base. This Formation includes about 1700 m of volcanic and sedimentary rocks representing three principal lithofacies, namely: massive and pillowed basalt, mafic lapilli tuff and lapillistone and black-banded chert (Ward, 1999). The overlying Zwartkoppie Formation forms the top of the Geluk subgroup and consists of sheared intermediate to felsic volcanics and inter-layered cherts.

The Fig Tree Group consists of inter-stratified terrigenous clastic units and dacitic volcaniclastic and volcanic rocks (Lowe and Nocitha, 1999). Three Formations make up the Fig Tree Group. The Sheba Formation consists principally of greywackes. It is the oldest known low-grade metamorphosed turbidite in the world (Lowe and Nocitha, 1999). The overlying Belvua Road Formation consists predominantly of shales and is characterised by banded ferruginous cherts. The Schoongezicht Formation that overlies the Belvua Road Formation comprises mainly volcanic rocks. The Schoongezicht Formation includes 1500 to 2000m of dacitic tuff, coarse volcaniclastic sandstone, conglomerate and breccia and minor chert-clast conglomerate.

The Moodies Group consists of the youngest rocks in the Barberton Greenstone Belt. This Group includes feldspathic and quartzose sandstone, chert-clast conglomerate and siltstone. The strata have a maximum thickness of 2600 m. The Moodies group is made up of three Formations, which consists of repeated cycles of arenaceous and argillaceous rocks that accumulated in diverse alluvial and marginal marine and deltaic environments (Heubeck and Lowe, 1999). These are the Clutha, Joe's Luck and Baviaanskop Formations. The wide development of chert-clast conglomerate at the base of the Moodies, resting with angular unconformity on the rocks of the Onverwacht Group, suggests that the base of the Moodies Group is an unconformity over much of the Barberton Greenstone Belt (Heubeck and Lowe, 1999).

4.2.3 Intrusions

A prominent swarm of NNE trending dykes has intruded the rocks of the Barberton Greenstone Belt. According to Ward (2001), some of these dykes are of post-Karoo age and can be distinguished from the older diabases by their fresh mineralogy and relatively strong aeromagnetic signature. The majority of dykes are steeply dipping to the west (Cox, 1970). These dykes may therefore be genetically associated with the formation of the Lebombo monocline (Cox, 1970). They can be readily observed in the field but have not been mapped on the 1:250 000 Barberton geological map. The majority of post-Karoo dolerite dykes strike east of north whereas older diabase dykes follow many different trends of which another important strike direction is NW, indicating a change in tectonic stress conditions over geological time. The N-S orientation of major dyke swarms in the Barberton Greenstone Belt indicates an E-W extensional palaeo-stress field during post-Karoo times. Sills of the same age as the dykes are found through out the area.

4.2.4 Geological History of the Barberton Greenstone Belt

Archean Deformation

The Barberton Greenstone Belt represents complexly deformed rock assemblages, juxtaposed during collisional orogenesis of the Kaapvaal and Zimbabwean cratons (Lowe et. al., 1999).

The broad structure is that of a synform with a pronounced NNE-ENE trend. Within this synform a number of tight synclinal often overturned folds with steeply dipping limbs are present. They are separated by major thrust faults resulting in ENE trending segments. Many of these ENE thrusts have been subsequently reactivated as transcurrent faults.

De Ronde and de Wit (1994) acknowledged that structural geometry (i.e. kinematics) and evolution of greenstone belts represent one of the most complicated problems in structural geology. Many studies of the stratigraphy of the Barberton Greenstone Belt have incorrectly assumed that thick successions of meta-sedimentary and meta-volcanic rocks occur without structural repetitions and that they have undergone relatively small amounts of deformation. According to de Wit et al. (1992), the variations in strata thickness in greenstones are associated with thrust faulting and recumbent folding, which are responsible for the overall distribution of rock types in the greenstone belts.

The structural development of the Barberton greenstone belt is quite variable, but it typically shows some or all of the following elements:

- Well developed thrusting and folding
- Limited early extensional faulting,
- Polyphase tectonic history (de Ronde and de Wit, 1994).

The Barberton greenstone belt sustained polyphase deformation during Archean times. De Wit et al. (1992) recognised an early deformation phase associated with the intrusions of granitic plutons that caused numerous folds with steep plunge and an associated cleavage. This is the earliest recognisable phase of compressional deformation (D1) and has been dated between 3445 and 3430 Ma (Pb –Pb dating). It is best preserved in the southern and central parts of the belt. D1 deformation included the formation of the recumbent nappes and downward facing sequences. The zones that were weakened by earlier extensional tectonism prior to D1 deformation were reactivated during D1, producing transcurrent faults, drag and disharmonic folds and numerous second and higher order faults, fractures and joints (de Ronde & de Wit, 1994).

According to de Ronde and De Wit (1994), the second deformation phase (D2) can be dated at about +/- 3229 Ma and was responsible for the tightening of folds. The D2 deformation resulted in the widespread development of slaty cleavage and schistosity. According to de Wit et al. (1992), large-scale steeply plunging folds were formed during D2 deformation, which took place contemporaneously with the emplacement of the porphyritic granite of the Nelspruit suite. The evidence of D2 deformation is observed in some rock outcrops at Stynsdorp where the foliation wraps around the Stynsdorp pluton. This suggests that the foliation is post-tectonic to the Stynsdorp D1 diapiric event.

The third deformational phase (D3) is thought to be a continuation of D2 deformation, since folds related to D3 are coaxial to D2 folds (de Wit et. al., 1992). D3 deformation is approximately 3226 Ma old and is observed as shear zones associated with gold mineralisation, thus a link between D3 deformation and gold mineralisation was established in the Barberton Greenstone Belt (Anhaeusser, 1986). It is conceivable, therefore, that a change in tectonic regime allowed a large scale, rapid release of deep crustal auriferous fluids as hydrothermal veins.

According to de Ronde and de Wit (1994), the three phases of deformation suggest that the compressive strain was more prevalent and was induced by granitic diapirism of the later intruded plutons. The differential compression of the greenstone successions induced by granitic diapirism caused isoclinal folding, pebble and pillow flattening and mineral orientation.

The forth deformation phase (D4) was an extensional collapse stage (de Wit et. al., 1992). This phase is dated at approximately 3100 Ma and suggests extensional processes and re-folds of the earlier folds locally associated with the reactivation of thrusts as strike-slip faults oriented at high angle to D3 shear zones (de Wit et. al., 1992). According to de Ronde and de Wit (1994), the approximate onset of regional extensional tectonics within the Kaapvaal craton can be estimated to be 3070 Ma, which is contemporaneous with D4 deformation.

The NW trending diabase dyke swarms are of different ages, some are pre-Transvaal and others are post-Transvaal Supergroup. According to Ward (2001), the dykes are commonly vertical and therefore exhibit linear outcrops that range from 10 to 15m in thickness. These two generations of dykes intruded through Archean joints that were tectonically reactivated during the Proterozoic times. The incursion of the post-Transvaal dyke phase may either be associated with the Bushveld complex as precursor intrusions, or associated with the subsidence of the Transvaal basin as an early magmatic response (Ward, 1999). The stresses that inherently formed the NE-SW synformal shape of the Barberton Greenstone Belt resulted into Archean joints with a NW trend direction (Ward, 1999). Such Archean fractures were reactivated during Proterozoic and the diabase dykes intruded as dyke swarms of different ages. The stress field that persisted during the Archean times can be represented diagrammatically by applying a strain ellipse (Figure 4.4).

The pre and post-Transvaal mafic diabase dykes that formed NW dyke swarms subsequently intruded in the direction of maximum extension.

The response of the rocks to NW directed Archean compressional stresses could be summarised as follows:

- NW-SE structures would be tensional
- NNW structures would be antithetic strike slip faults
- ESE to E trending structures would be synthetic shears or strike slip faults
- N-S structures: would antithetic faults
- NE-SW structures would be thrusts of fold axes

Gondwana Age Deformation

The Barberton Greenstone Belt was subjected to primarily compressional stresses during Archean times. During the Proterozoic era, the region was subjected to cycles of uplift and erosion, thus resulting in a period of crustal instability (Tankard et. al., 1982).

During Jurassic times, the southeastern regions of Africa were subjected to extensional stresses of the crust associated with Gondwana break-up (Cox, 1970). The distribution of stress zones is presented in Figure 4.3. The extensional stresses manifest themselves in the earth's crust as either structures related to crustal thinning (zones A, E and F) or dyke swarms (Zones B, D and C).

The key feature that marks the tensional stress regime in the south east of the African continent is the Lebombo Monocline. This is a large flexure of post-Karoo age with a S-N trend, extending from southern Zimbabwe to KwaZulu-Natal and stretching about 700 km (Cleverly, 1977). The structural features of the Lebombo are interpreted as having formed in an E-W tensional stress regime related to the rupture of Gondwanaland (Cleverly, 1977). Cox (1970) reported that the stretching mechanism of the crust had sufficient strength to transmit stresses laterally over long distances, hence tensional stresses influenced the tectonism of the Barberton Greenstone Belt. The period of maximum deformation of the Lebombo monocline is dated as early Jurassic, thus 180 Ma. The region of maximum monoclinal flexuring near the

Lebombo is most likely related to a zone of greater crustal thinning. A large swarm of Karoo dolerite dykes (the Rooirand dyke swarm) that occur in Mpumalanga and Swaziland can also be related to the tectonic stresses associated with monoclinal warping.

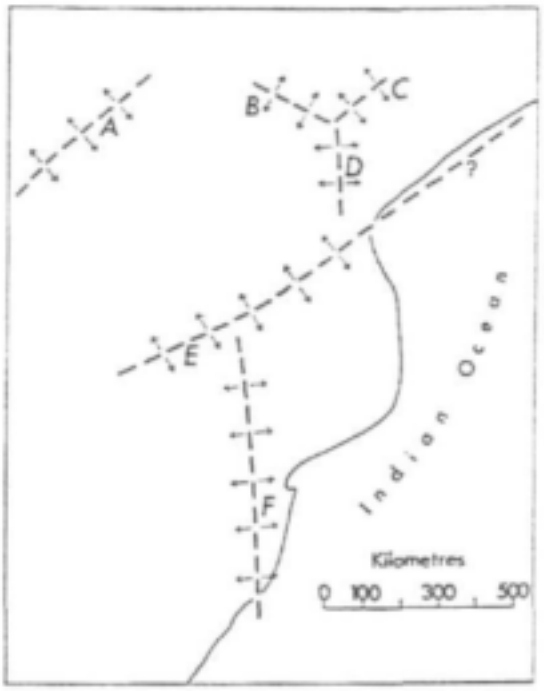

Figure 4-3 **Zones of crustal extension in southeastern Africa (after Cox, 1970).**

The structures associated with this tensional stress field are expected to mimic the N-S direction, which is the trend of the axis of the monocline. Such structures include joint sets and normal faults orientated in the N-S direction. As such, N-S normal faults in Barberton region can be assumed to be of tensional structures of Karoo age. A widespread occurrence of minor block and trough normal faulting is also related with the formation of the monocline.

According to Cleverly (1977), the jointing in the Barberton greenstone belt can be divided into groups:

- Archean age jointing related to the intrusion of granite basement plutons,
- Post-Karoo age joints associated with monoclinal flexuring,
- Post-monoclinal joints related with post-Karoo tectonic activities.

It is expected that monoclinal flexuring would produce the following joint sets in the vicinity of the monocline axis:

- N-S tensional joints and faults parallel to the monoclinal axis and along the convex portion of the fold. These have often been infilled by dolerite dykes.
- E-W joints perpendicular to the monoclinal axis in the concave part of the monocline. These have been observed in the Jozini Rhyolites on the concave flexure of the monocline in Mozambique (Sami, 1998).
- Conjugate shear fractures oriented NW and NE. Sami (1998).

In the distal regions like the Barberton Greenstone Belt, it is expected that the tensional joint sets would be predominantly parallel to the monocline axis; oriented north-south.

Figure 4-4 Representation of stress field.

The post-Karoo dolerite dyke swarms represents another tectonic scenario, which can be represented by 90° rotation of tectonic stresses in the anticlockwise direction during Lebombo times when the region was subjected to an E-W tensional stress. This resulted in:

- The development of N-S tensional joints and faults into which dolerite dykes were later emplaced through them.
- Previous easterly trending shears coming under compressional stress
- The NW-SE dykes and strike-slip faults coming under shear strain
- The NNE to ENE trending thrust structures being rejuvenated as synthetic shears

4.3 Hydrocensus

A hydrocensus was carried out on the basis of data from the National Groundwater Database (NGDB). Data for 219 borehole records were available for the area in relevant strata, most of these being located in the granitic plutons. Success rates have been historically low and yields only marginal. Figure 4.5(a) demonstrates the distribution of borehole yields in these strata. The statistics of borehole yields are shown in Table 4.2.

About 50% of boreholes with a recorded discharge are dry. About 1/3 of successful boreholes with a recorded discharge rate have a yield greater than 1l/s, of which half yield more than 2l/s. More than 50% of successful boreholes have only a marginal yield lower than 0.5l/s and the median yield is 0.4 l/s. However, as these discharge rates derive from reported airlift yields rather than proven pump-out yields. Over all, these statistics are based on only 64 records, as 71% of borehole records fail to report a discharge rate (Figure 4.5(b)).

a) b)

Figure 4-5 Distribution of borehole yields in the study area (a) and success rates for all registered boreholes in the study area (b).

Table 4-2 Statistics of borehole yield in the study area

Min yield	Max yield	Median yield	Average yield
0.08l/s	10l/s	0.4 l/s*	1.3l/s*

* calculated on the basis of successful boreholes only

To investigate the relationship between geological structures and borehole yield and success rates, a proximity analysis between LANDSAT lineaments and yields were carried out. Boreholes were divided into three distance-to-feature classes and for every class a success rate and a median yield was established (Figure 4.6). No investigation into the relationship between distance to fault and borehole yield was carried out, as the data set proved insufficient for statistical purposes.

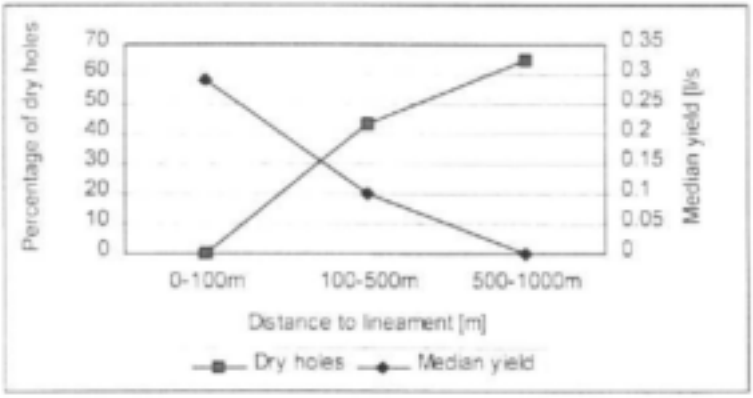

Figure 4-6 Borehole yield and success rate in relation to the distance to mapped lineaments. (1-100 m, N= ; 100-500 m, N= ; 500-1000 m, N=).

Figure 4.6 shows a distinct relationship between borehole yield and distance to lineaments: the further the borehole is drilled from a lineament, the lower the median yield. A similar relationship exists between success rates and distance to lineaments, with an increasing percentage of dry boreholes being encountered with increasing distances to lineaments.

A concentration of high yielding boreholes was also observed in the very south of the study area. However, this cluster exhibits distances to lineaments which are greater than 1km and hence, their high yields cannot be explained by proximity to observed features.

A comparison between yield and depth of water strike suggests that the highest yields are associated with shallow water strikes (figure 4-7). The statistics of depth of boreholes, water strikes and water levels are shown in Table 4.3. Approximately 50% of water strikes in the area occur above 25m (Figure 4.8(b)) and only about 25% of boreholes strike water below 60 m. This indicates the presence of a widespread shallow weathered zone aquifer. However, since 50% of boreholes are less than 60 m deep, the presence of a deeper seated fracture zones cannot be ruled out (Table 4.3). Indications are that the deeper fracture systems are of low permeability since yields are low despite high confining heads. Water levels are generally shallow with an average depth below surface of 13m (Figure 4.8(a)).

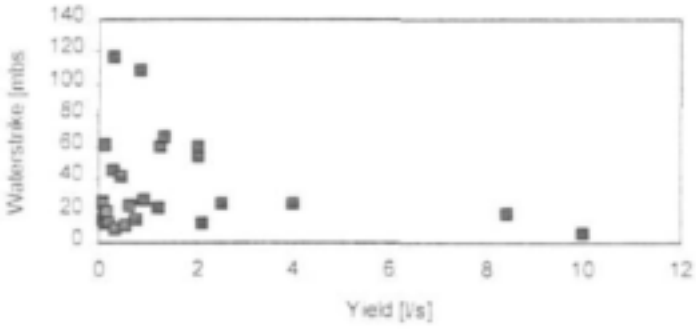

Figure 4-7 Borehole yield in relationship to depth of water strike.

Table 4-3 Statistics of depth of boreholes water level and water strike

Water level				Water strike				Depth of Borehole			
Min	Max	Median	Avg	Min	Max	Median	Avg	Min	Max	Median	Avg
1m	65m	11m	13m	3m	140m	25m	47m	1m	141m	60m	64m

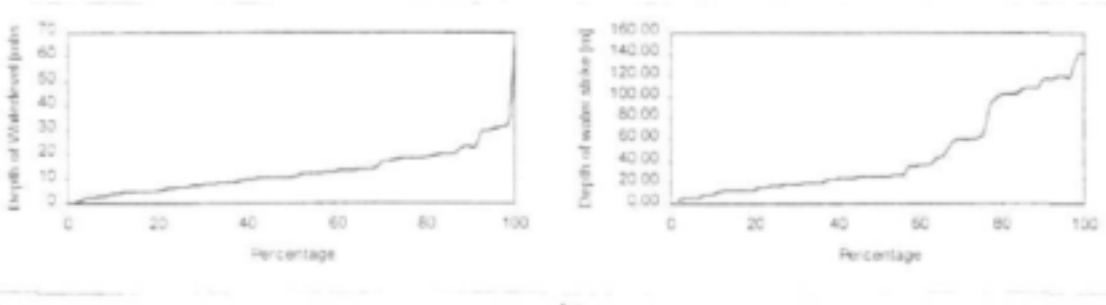

a) b)

Figure 4-8 Depth of water level in meters below surface (a) and depth of water strike in metres below surface.

4.4 LANDSAT Imagery

The occurrence and movement of groundwater in the study area has been shown to be related to lineaments associated with secondary features, such as faults, fracture zones and dykes. As such, the delineation and mapping of these lineaments has been an integral part of this groundwater exploration study.

The lineament map presented in Figure 4.9 is a composite image of all lineaments identified from each of the images produced through the various enhancement techniques described in Volume 1. Lineaments were examined on the basis of their length, orientation and frequency.

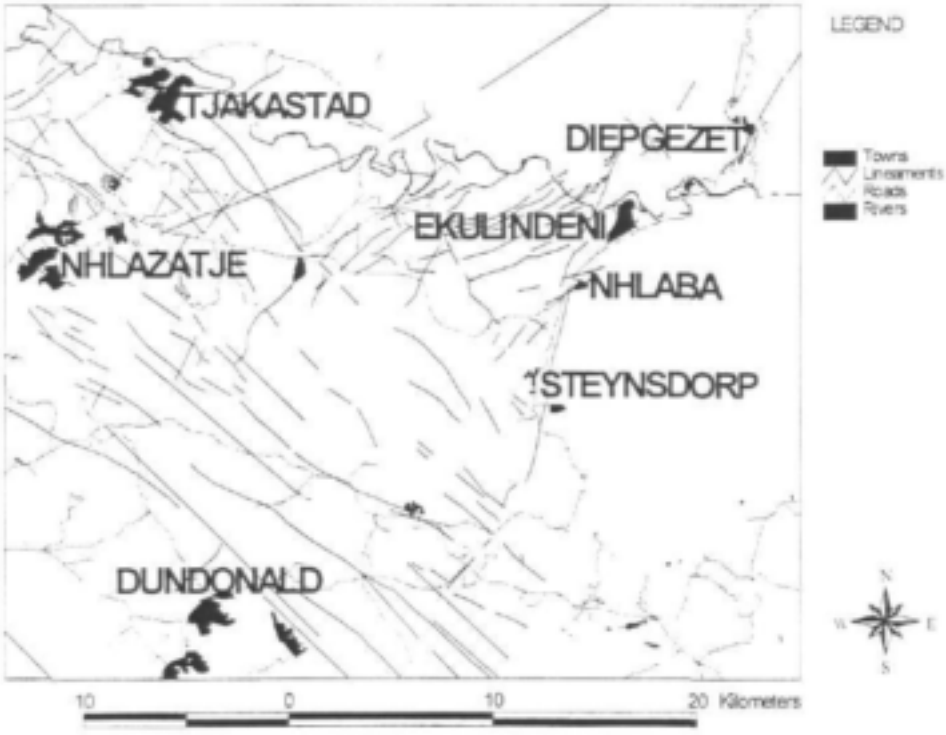

Figure 4-9 Lineament map of the study area generated by analysis of LANDSAT data.

The LANDSAT lineament data plotted on the rosenets (Figure 4.10) indicate the strike frequency and the strike-length occurrence of the lineaments, respectively.

The strike frequency plot exhibits three trends, which are the NW-SE, NE-SW and nearly E-W trends. These are orientations associated with Archean and Proterozoic structures. The NW-SE is the dominant lineament frequency, however, these are relatively short, indicating they are not regional in extent. This prominent lineament direction is associated with the direction of the pre and post Transvaal dyke swarms, which are under present day shear and not likely to be groundwater targets. The longer but less frequent NNW structures would be Archean strike-slip faults. The long NE trending structures oriented at greater than 45 degrees are associated with Archean thrusts, hence they are regionally extensive but are less numerous in frequency. These are under present day shear and are also unlikely to be groundwater targets. The shorter NE striking features are associated with post-Karoo dykes, the orientation of post Karoo extension. The E-W and ESE trends are associated with Archean shear zones

under present day compression. The absence of the N-S trending lineaments suggests that expected tensional structures and Karoo age N-S dykes cannot be observed on the LANDSAT image. Since structures with this orientation are expected to be of the greatest significance to groundwater exploration, the ability of LANDSAT imagery to identify target features is limited.

Figure 4-10 Rose diagrams of LANDSAT lineament data.

4.5 *Structural Geology*

A total number of 468 planar structures were measured at 49 stops in the lower units of the Barberton Greenstone Belt (Figure 4.11) in areas where outcrops are best exposed, such as road cuttings and riverbeds.

These planar features include joint surfaces, foliation and hydrothermal quartz veins. All of the planes were even and smooth, with no grooves, fault gauge or brecciation present. At stop 6 (Figure 4.11), a normal micro dip-slip fault with a 2-cm displacement towards the SE direction was observed. This is an indication of tensional stress that prevailed in the NW-SE directions, resulting in extensional NE oriented structures. Boudins of amphibolite schist were observed at stop 15 with principal axis orientation of 47° that indicates a NW – SE extension. This is again evidence of extensional stresses in the NW – SE direction, which consequently results to the NE – SW trending joint sets.

4.5.1 Linear Structures

The main structural features in the Onverwacht Group are the folds, thrust faults, faults and joints. Most shear zones that are shown on the 1:250 000 geological map have a NW-SE orientation. The folds and NE oriented thrust faults are Archean in age and are of less interest from the hydrogeological point of view. Post-Karoo extensional structures are the targets of primary interest.

The mapped joint sets do not show any movement parallel or perpendicular to joint walls and as such, compressional or extensional forces can only be determined from strain analysis using stereonets. Due to the great abundance of quartz veins in most outcrops that were visited, the origin of most joints can be associated with extensional stresses. The NW – SE trend of the mapped joints coincides with the orientation of diabase dykes, hence it can be associated with the predicted tensional orientation during Proterozoic times.

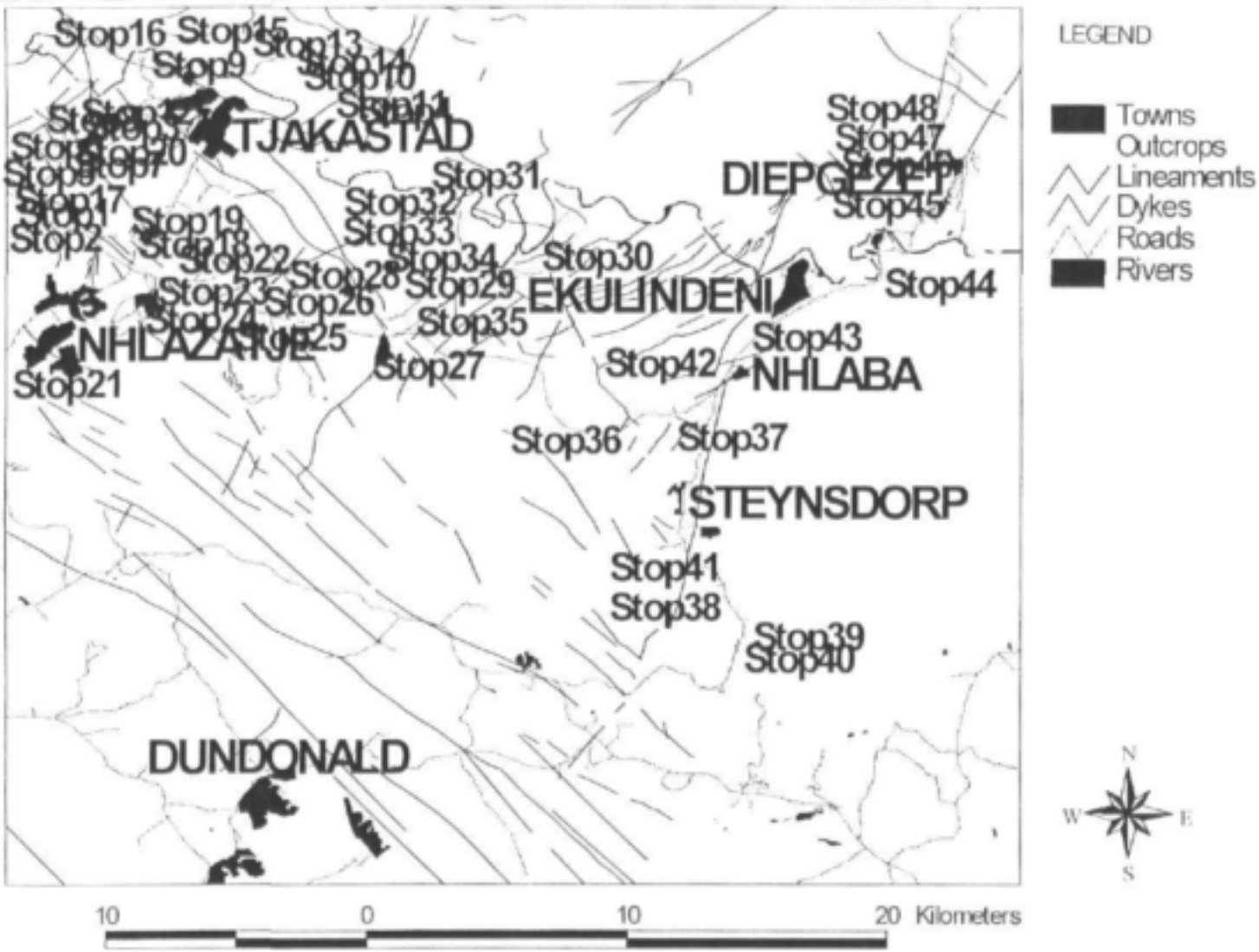

Figure 4-11 **Locality map of rock outcrops**

4.5.2 Structural Geology of the investigated area

Figure 4.12 (a) is a stereonet density plot of all joint data. Several density contour centres are observed in widely distributed poles to the measured planes, which suggests that joints are related to several structural origins and that the structural setting is complex. Figure 4.12 (b) is a rosenet that displays the orientation of all joint data. It can be observed that there is a greater concentration of joint planes orientated N-S. It can be observed in Figure 4.12(a) that dips are highly variable, but that the majority of joint planes dip from vertical to sub-vertical. The majority of steeply dipping joints have poles that plot in the N to E and W to S quadrants, which suggests a dominant NW joint orientation.

The joint set data can be grouped according to the angles of dip in order to determine the tectonic settings, which are expected to fall in any one of the following categories:

- dip-slip vertical tensional joints and inclined conjugate joint planes,
- shallow inclined thrust-slip joint planes,
- intermediate planes that may be dip-slip or thrust-slip tectonic settings.

Figure 4.12(c) is a contoured stereo-plot of all planes dipping steeper than 80°. The planes in the density plot also show four major tension joint sets trending towards N-S, NE-SW, E-W and NW-SE. The rosenet diagram (Figure 4.12 (d)) conforms to the observed density planes of the stereonet diagram (Figure 4.12 (c)). The most prominent joint set direction is the E-W direction followed by the NW direction. The two minor trend directions are the NE-SW and N-S. Both the NE-SW and N-S trending joints intersect at steep angles, which suggests a *three-dimensional dip-slip setting or strike-slip tectonism*.

Figures 4.12 (e) and 4.12 (f) are the stereonet and rosenet plots that represent the conjugate joints of the dip-slip tectonic setting. It can be observed in the stereonet (Figure 4.12 (e)) that each inclined plane has an opposite dipping plane, indicating a dip-slip tectonic setting. Strike-slip faulting is therefore unlikely. It can be observed that the N-S direction is prominent, but that the NW-SE three-dimensional trend is the best developed. Both Figures 4.12 e and e indicate that the NE-SW trend is less pronounced but that it represents a well developed three-dimensional dip-slip setting.

Figures 4.12 (g) and 4.12 (h) are the stereonet and rosenet plots, respectively, of joint set with planes dipping less than 30°. These are joints that formed under the compressional environment of thrust-slip tectonic settings. Three conjugate sets can be distinguished from the pole density contouring (Figure 4.12 (g)), indicating a sub-horizontal intersection of planes along the N-S, NE-SW and NW-SE directions. The rosenet (Figure 4.12(h)) also shows a pronounced N-S trend direction.

A large proportion of joint planes in the study area dip between 60° and 30° and represent either a dip-slip or a thrust-slip tectonic setting. It can be observed in Figure 4.12 (i) that the NW-SE trend seems to be one-dimensional while the N-S and NE-SW trends have a wider distribution of the opposite conjugate planes suggesting a three-dimensional deformation along these trends. If the thrust-slip trends of Figure 4.12 (h) are compared with the trends of Figure 4.12 (j), it can be observed that some of the trends seem to be similar but do not overlie exactly on top of each other. The rosenet plot of Figures 4.12 (d) and 4.12 (f) are similar to that of the thrust-slip joints, even though a better fit occurs for the three-dimensional joint sets with N-S and NE-SW trends. The mono-dimensional E-W dip-slip joints of Figures 4.12 (f) and 4.12 (j) are the least compatible, with 6° offset in the clockwise

direction. It therefore appears as if most of the joints, except some of the NE-SW trending ones, dipping between 30° and 59° represent dip-slip and not thrust-slip features.

4.5.3 Conclusions

The occurrence of joints in the Archean Barberton Greenstone Belt can be associated with several events since its cratonisation, some 3 100 million years ago. This terrain was uplifted and subsided during depositional and erosional events, and intruded by various dyke sets during tensional episodes.

In both the stereonet and rosenet plots of the joint planes, the dip-slip fault setting occurred in four major directions. These are the N-S trending three-dimensional faulting, three-dimensional faulting in the NE-SW direction and one-dimensional normal faulting trending NW-SE as well as E-W. The lower angle joint planes show trends in the N-S, NW-SE and ENE-WSW directions, indicating that these are thrust-slip joint trends.

The N-S trending three-dimensional jointing is related to flexuring of the crust during the development of the Lebombo monocline, suggesting east-west extension and supports a tectonic model of N-S structures being extensional in nature (4.2.5). The conjugate appearance of the joints, however, indicates a strong possibility of a lateral N-S wrenching parallel to the transform margin adjacent to the aborted oceanic crust. If so the direction of maximum extension is to the SE and the joint set to the east of north is the more open feature, while the joint set trending to the north represents the synthetic direction and is in shear. The one –dimensional NW direction would be under compression. If the deformation is due only to E-W extensional three-dimensional deformation then the NE and NW conjugate sets are in shear and the N-S direction is open.

The conjugate NNE-SW and ENE joint sets (figure 4-12 (f)) support extension to the SE resulting from N-S wrenching. If so, all the joints between these directions will be open features, with maximum extension in NE directed joints.

The E-W trending one – dimensional fracture set is parallel to the spreading axis of the aborted oceanic crust, indicating shearing from N-S wrenching. This direction fits the antithetic shear of rotational extension and probably developed with the onset of N-S wrenching prior to the development of the transform margin.

The NW-SE trending joint set is parallel to the pre-Transvaal dyke set and may be an inherited feature resulting from NW directed compressional stresses during Archean times. It also resembles the synthetic conjugate shear direction of a right lateral rotational wrench system that could have occurred during E-W shearing.

The thrust-slip fractures parallel to the three major joint set directions indicate compressional conditions oriented to the NW, N-S and NE-SW, none of which are oriented parallel to the regional strike of the Barberton volcano-sedimentary strata.. It is possible that some of these low angle joints are of Archean origin as the Barberton terrain was established by the accretion of several tectonic terrains by convergence. The NE direction can be attributed to NW directed compression during Archean times, with the NW-SE and N-S orientations being conjugate sets. Since no post-Karoo faulting occurred in this region, more recent compressional stress fields are not due to simultaneous faulting along different strike directions but can be associated to compression due to the minimal flexuring along the N-S axis of the Lebombo monocline and the clockwise rotation of the Kaapvaal craton caused by the intrusion of the Botswana dyke swarm. These low angle joints represent compressional features that are closed and are poor water carriers.

It is clear that the Barberton Greenstone Belt was subjected to extension and shear, which resulted in fracturing of the rocks of the area. Thus, the steep dipping joint structures in the Barberton Greenstone Belt that seem to be open and good targets for groundwater exploitation are:

i) the N to NE trending conjugate set with a greater possibility on the NE trending joints

ii) the E-W trend, resulting from N-S wrenching of the crust, linked to the now-aborted spreading ridge in the northern Natal valley.

The field observations therefore fit the conceptual model on the basis of identifying the N-S to and NE-SW trending joint sets as open features. These are associated with tensional stress field that prevailed during post-Karoo times.

Fig 4.12 (a)

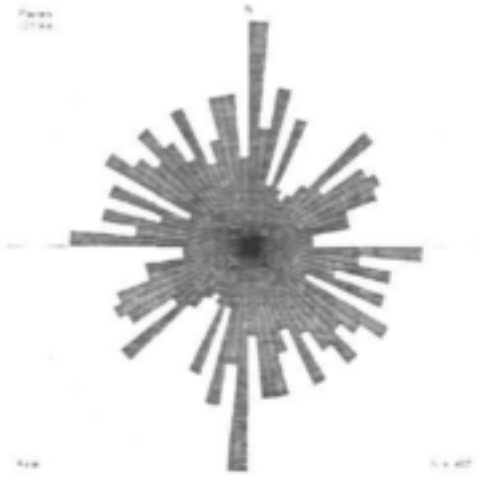

Fig 4.12 (b)

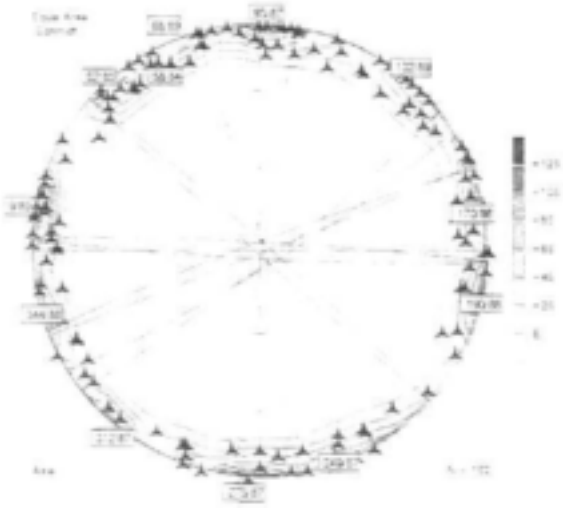

Fig4.12(c)

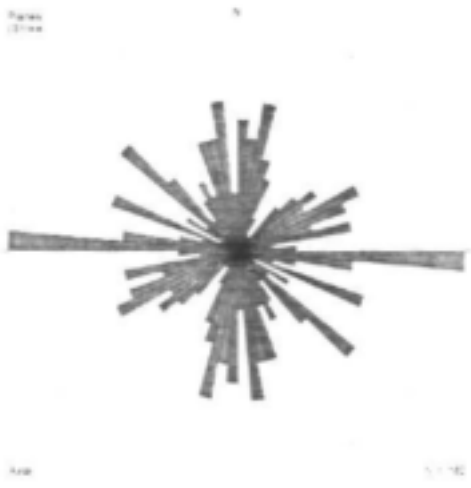

Fig 4.12 (d)

Fig. 4.12 (e)

Fig. 4. 12 (f)

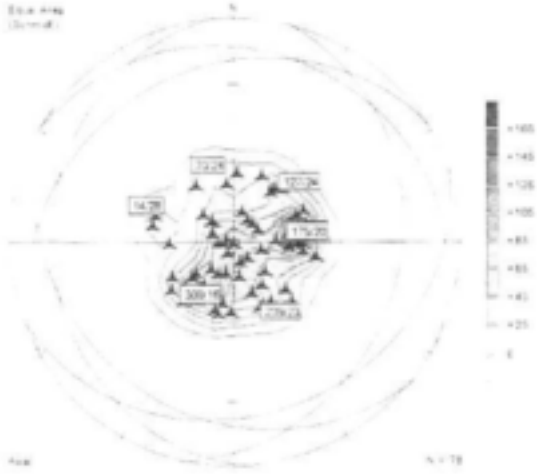

Fig. 4.12(g)

Fig. 4.12(h)

Fig. 4.12(i)

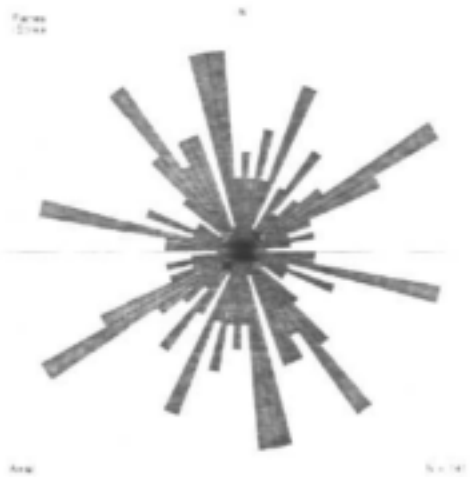

Fig 4.12(j)

Figure 4-12 Stereonet and rosenet plots of all structural data (a and b), dips greater than 80° (c and d), dip slip conjugate sets with dips > 80° (e and f), dips < 30° (g and h), and dips from 30-60° (I and j).

4.6 Ground Based Geophysics

4.6.1 Introduction

Since it was assumed that groundwater occurs in steeply dipping fractured zones in meta-volcanic terrains like the Onverwacht Group, or at dyke contact zones, the geophysical methods chosen were the:

- Electromagnetic, Max-Min (HLEM) technique,
- Resistivity, electrical sounding method and
- Magnetic method.

A total of 27 HLEM and magnetic traverses were conducted. The recorded magnetic, resistivity and conductivity responses from all traverses are presented in Appendix 4-A. The location and the number of traverses are shown in Figure 4.13 and table 4.4.

These traverses were selected to investigate various structural orientations and were identified from LANDSAT lineaments and aerial photographs. All HLEM and magnetic surveys were carried perpendicular to the lineaments. Vertical electrical soundings were undertaken with the Schlumberger electrode array, extended parallel to lineament features.

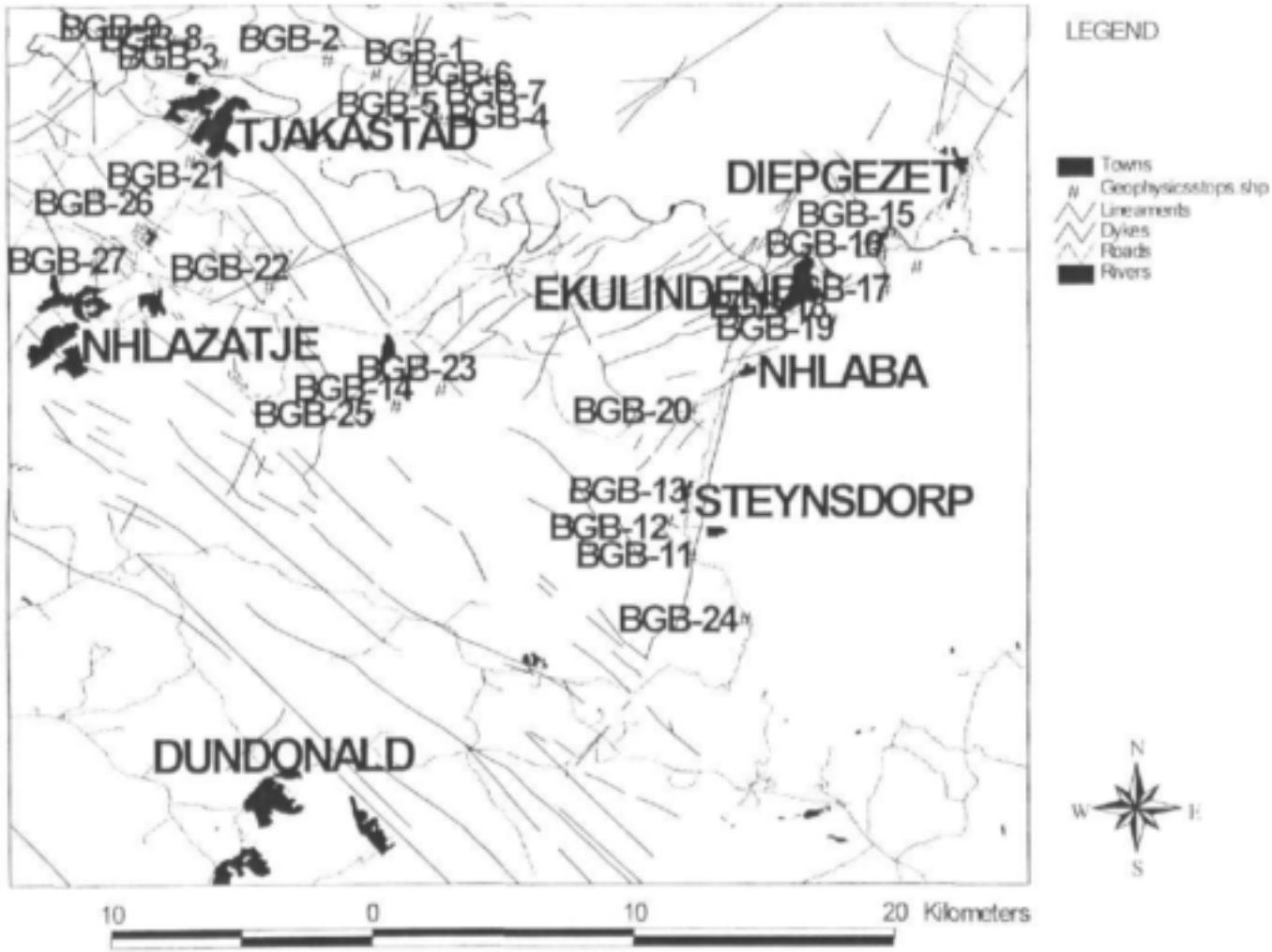

Figure 4-13 Stations for geophysical surveys carried throughout the study area

The geophysical responses were expected to identify the following geological scenarios:

- Broad, deep highly conductive sources, detected by HLEM survey, thus typically of deep weathered zones (a valley discontinuity profile).
- Narrow, shallow poorly conductive source, detected by HLEM survey i.e. dolerite dykes (a ridge discontinuity profile).
- Two layered earth case, i.e. an unweathered fresh greenstone of higher resistivity underlain by weathered conductive zone, detected by electrical sounding survey.
- Buried dykes or sills or fault steps detected by magnetic survey (a ramp discontinuity profile).

Table 4-4 Geophysical Survey carried out in the research area

Name	BH Drilled	Long	Lat.	Feature	Geophys. Used	Traverse Direction
BGB-1		30.8767	25.9731	NE-SW trending fault	Mag. Max-Min	SE-NW
BGB-2	XT2-03	30.8597	25.9681	Borehole, NW-SE Trending fault	Mag. Max-Min, E-S	NE-SW
BGB-3	XT2-04	30.8233	25.9692	Borehole, E-W trending lineament	Mag. Max-Min	S-N
BGB-4	XT2-01	30.8989	25.9897	Borehole, NE-SW Striking lineament	Mag. Max-Min, E-S	SE-NW
BGB-5		30.8961	25.9867	Long NE-SW striking Dyke	Mag. Max-Min	SE-NW
BGB-6	XT2-02	30.8933	25.9839	Borehole, E-W Striking shear zone	Mag. Max-Min, E-S	S-N
BGB-7		30.8889	25.9797	NE-SW trending fault	Mag. Max-Min	SE-NW
BGB-8		30.8056	25.9617	N-S trending lineament	Mag. Max-Min	E-W
BGB-9		30.8114	25.9628	N-S trending fault	Mag,Max-Min	E-W
BGB-10						
BGB-11		30.9844	26.1381	NW-SE trending lineament	Mag,Max-Min	S-N
BGB-12		30.9764	26.1256	NW-SE trending lineament	Mag,Max-Min	SW-NE
BGB-13	XT2-08	30.9830	26.1153	Borehole, NE-SW Striking lineament	Mag,Max-Min, E-S	S-N
BGB-14	XT2-05	30.8736	26.0894	Borehole, E-W striking fault	Mag. Max-Min	SW – NE
BGB-15		31.0536	26.0283	NW-SE trending lineament		E-W
BGB-16		31.0622	26.0397	NW-SE trending lineament	Mag,Max-Min	S-N
BGB-17		31.0503	26.0356	NE-SW trending lineament	Mag,Max-Min	NE-SW
BGB-18		31.0511	26.0469	N-S trending lineament	Mag,Max-Min	N-S
BGB-19		31.0525	26.05**2	NW-SE trending lineament	Mag,Max-Min	E-W
BGB-20		30.9842	26.08**2	NW-SE trending fault	Mag,Max-Min	E-W
BGB-21		30.8122	26.0033	N-S striking dyke	Mag,Max-Min	S-N
BGB-22		30.8394	26.0458	Long NE-SW trending lineament	Mag,Max-Min	SW-NE
BGB-23		30.8975	26.0808	N-S trending lineament	Mag,Max-Min	S-N
BGB-24	XT2-09	31.0025	26.1592	Borehole, NNE-SSW Striking lineament	Mag, E-S	NW-SE
BGB-25		30.8825	26.0861	NE-SW trending lineament	Mag,Max-Min	W-E
BGB-26	XT2-06	30.7803	26.0133	Borehole, N-S Striking dyke	Mag. Max-Min, E-S	S-N
BGB-27	XT2-07	30.7672	26.0419	Borehole, N – S Striking lineament	Mag,Max-Min, E-S	SE-NW

The results of the ground-based geophysics were grouped on the basis of geophysical responses reflected by fault zones, lineaments, shear zones and dyke structures. The results for the sites that were drilled are discussed below.

4.6.2 Lineaments

Three lineament sites were identified for drilling exploration in the study area.

BGB 4 ENE striking lineament

This location of this lineament is shown in Figure 7.14. The lineament cuts across the meta-basalts of the Komati Formation in the NNE direction. It is not evident from field observation weather it is a fault or a dyke, but it is inferred from the LANDSAT image as a well defined linear feature. It is not easy to delineate a fault in a mono-lithotype geological environment like the meta-basalts of the Komati Formation, where displacement of one unit cannot be clearly defined. A 250m HLEM and magnetic survey was carried out perpendicular to the linear feature in an effort to delineate it on the ground. The direction of the geophysical traverses is from SE to NW.

Figure 4-14 Location of Traverse BGB4

Electromagnetic survey

The Max – Min was operated at 4 frequencies, namely 220, 880, 3520 and 14080 Hz, with coil separation set at 100 m and a station spacing of 10 m. The results are shown in Figure 4.15. The data show a trough like response from a 120 to 210 m points of the traverse in all

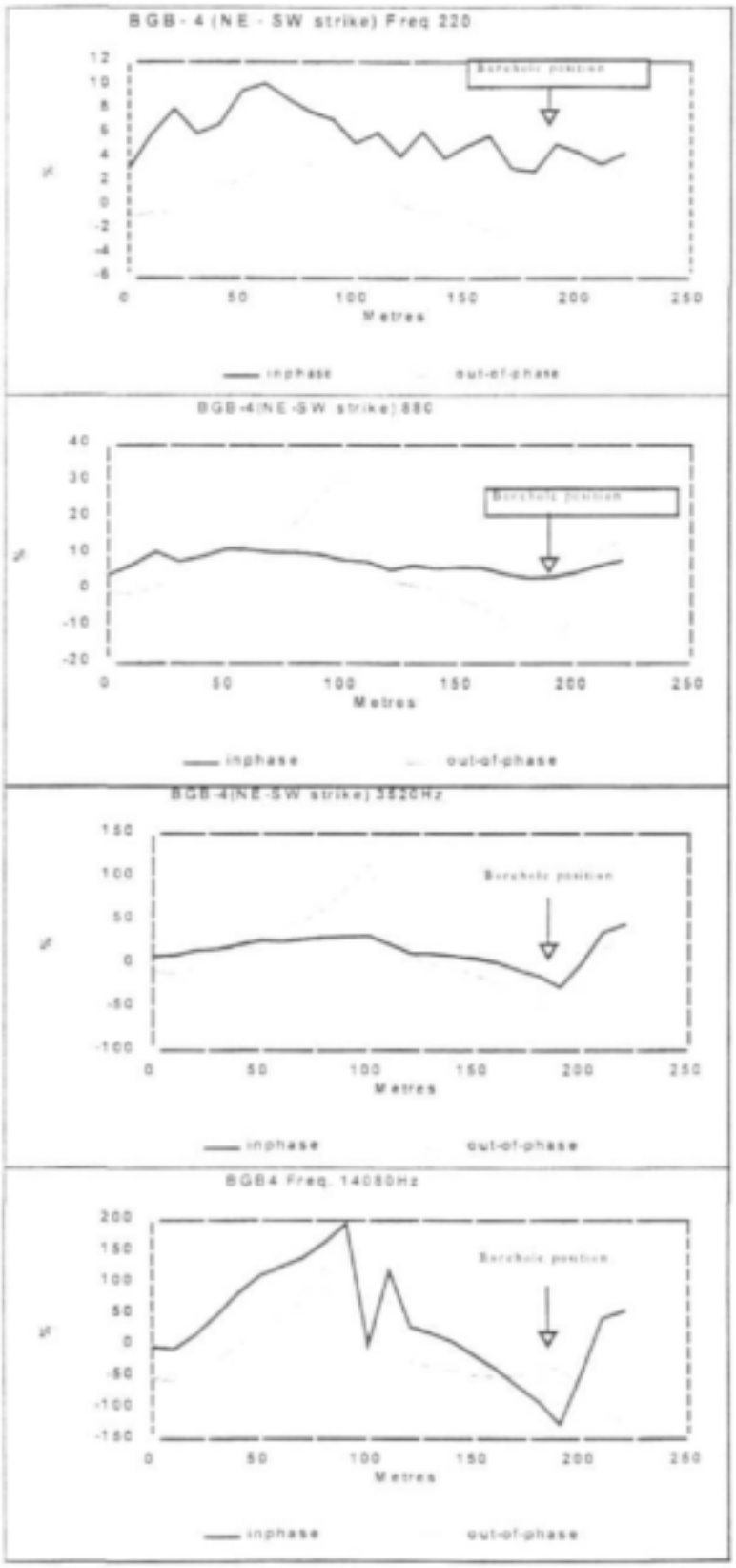
BGB - 4 (NE - SW strike) Freq 220
Borehole position
12
10
8
6
4
2
0
-2
-4
-6
%
0
50
100
150
200
250
Metres
inphase
out-of-phase
BGB-4(NE-SW strike) 880
Borehole position
40
30
20
10
0
-10
-20
%
0
50
100
150
200
250
Metres
inphase
out-of-phase
BGB-4(NE-SW strike) 3520Hz
Borehole position
150
100
50
0
-50
-100
%
0
50
100
150
200
250
Metres
inphase
out-of-phase
BGB4 Freq. 14080Hz
Borehole position
200
150
100
50
0
-50
-100
-150
%
0
50
100
150
200
250
Metres
inphase
out-of-phase

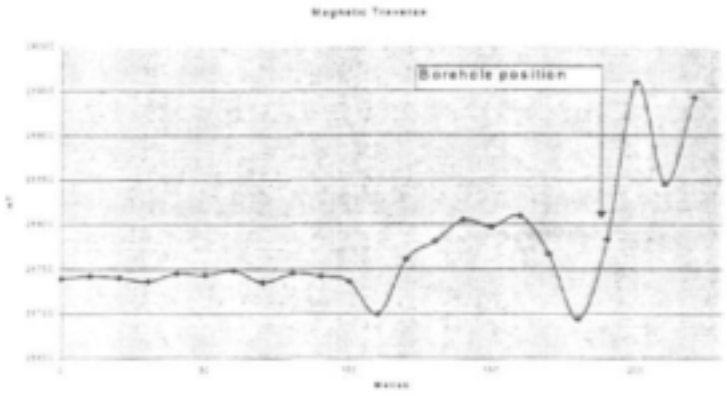

Figure 4-15 Geophysical profiles (HLEM and Magnetics) of traverse BGB4 (Traverse direction: NE→SW).

frequencies. It can be observed that the ratio of the in-phase to out-of-phase is relatively high in lower frequencies. This suggests a shallow, high conductive source. The asymmetrical form of the trough in the profile is an indication that the conductive body is dipping. The profile shows a valley overburden response, which may be associated with a deeper overburden over a sub-vertical fault, or a thin dyke.

Magnetic Survey

The magnetic survey was carried out over the lineament from the NE to the SW, using a 10 m spacing. Figure 4.15 shows the magnetic profile generated from this survey. The magnetic survey shows an increase in amplitude of about 175 nT at 180 m, suggesting a sub vertical. SE dipping fault, on which a borehole yielding 10 l/s (X12-01) was sited.

Electrical sounding Survey

An electrical sounding was conducted at 190m position of the HLEM survey, parallel to the lineament to try to ascertain the extent of deep weathering at this position (Appendix 4-A). The sounding curve shows a three layer curve, based on visual analysis, with $\rho_1 < \rho_2 < \rho_3$ and therefore an A-type curve. The following values of the three layer curve profile are determined:

Layers	Thickness (m)	Resistivity (Ωm)
Layer1	8	29
Layer2	20	40
Layer3	∞	resistive bedrock

BGB 14 - NW – SE striking lineament

An HLEM survey was carried over the lineament. This lineament was identified by image processing of the LANDSAT product. The lineament strikes at NW – SE direction and the HLEM traverse of 180 m was carried perpendicular to the lineament orientation. The locality of this site is shown in Figure 4.16.

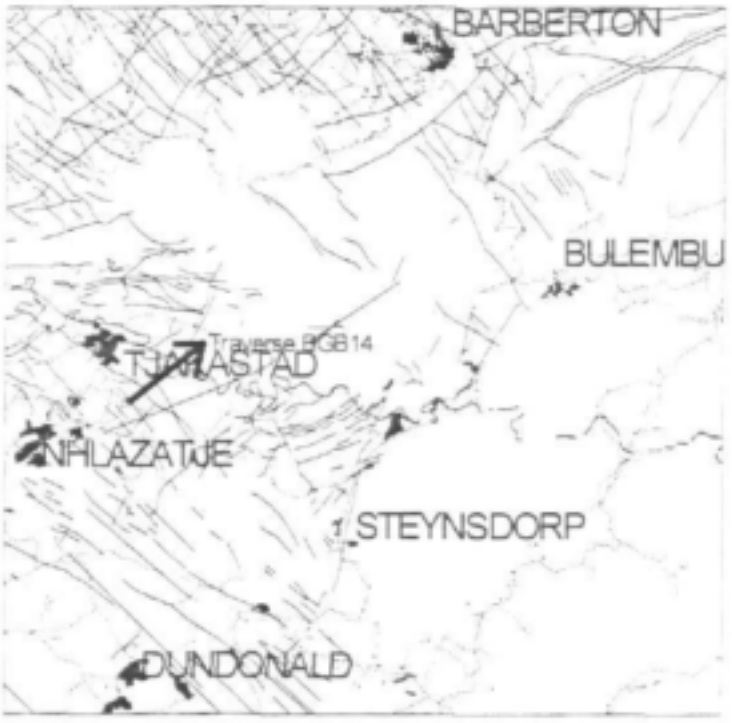

Figure 4-16 Location of traverse BGB-14

Electromagnetic survey

The Max – Min was operated at 4 frequencies that range from 220 to 14080 Hz with 100 m coil separation and 10 m station spacing. The results are presented in Figure 4.17. A broad conductive zone is observed from 90 to 160 m. This was suspected as being a possible fault zone where geological unit of different conductivity are separated by a fault line at 90 m point of the HLEM traverse where a borehole was sited. However, the conductive zone was a zone of deeply weathered schist and meta-basalt, and a low yielding borehole (X12-05) provided 0.1 l/s.

4.6.3 Faults

BGB 2 NW – SE trending fault

HLEM and magnetic surveys were carried over a strike-slip fault with left lateral displacement that was identified from field mapping. The surface impression of this fault resulted into a gorge in the hills of Hoggenoeg in Tjakastad. The fault was observed to cut across through the Hoggenoeg and Komati Formations. Thus the main lithological units in area of the geophysical traverse are the meta-basalts of the Komati Formation and the dolerite sill that occur at a distance of about 50m north of the fault line. A 120m HLEM and magnetic survey were conducted perpendicular across the fault line from the NE to SW direction. Figure 4.18 is illustrates the position of the Traverse BGB 2.

Electromagnetic survey

The Max – Min was operated at 4 frequencies, ranging from 220 to 14080 Hz, while the coil separation was set to 100m and a station spacing of 10m was selected. The results are shown

in Figure 4-19. A ridge discontinuity response is observed with a steady decrease in conductivity from 80m and onwards, where a borehole yielding 0.3 l/s (X12-03) was sited.

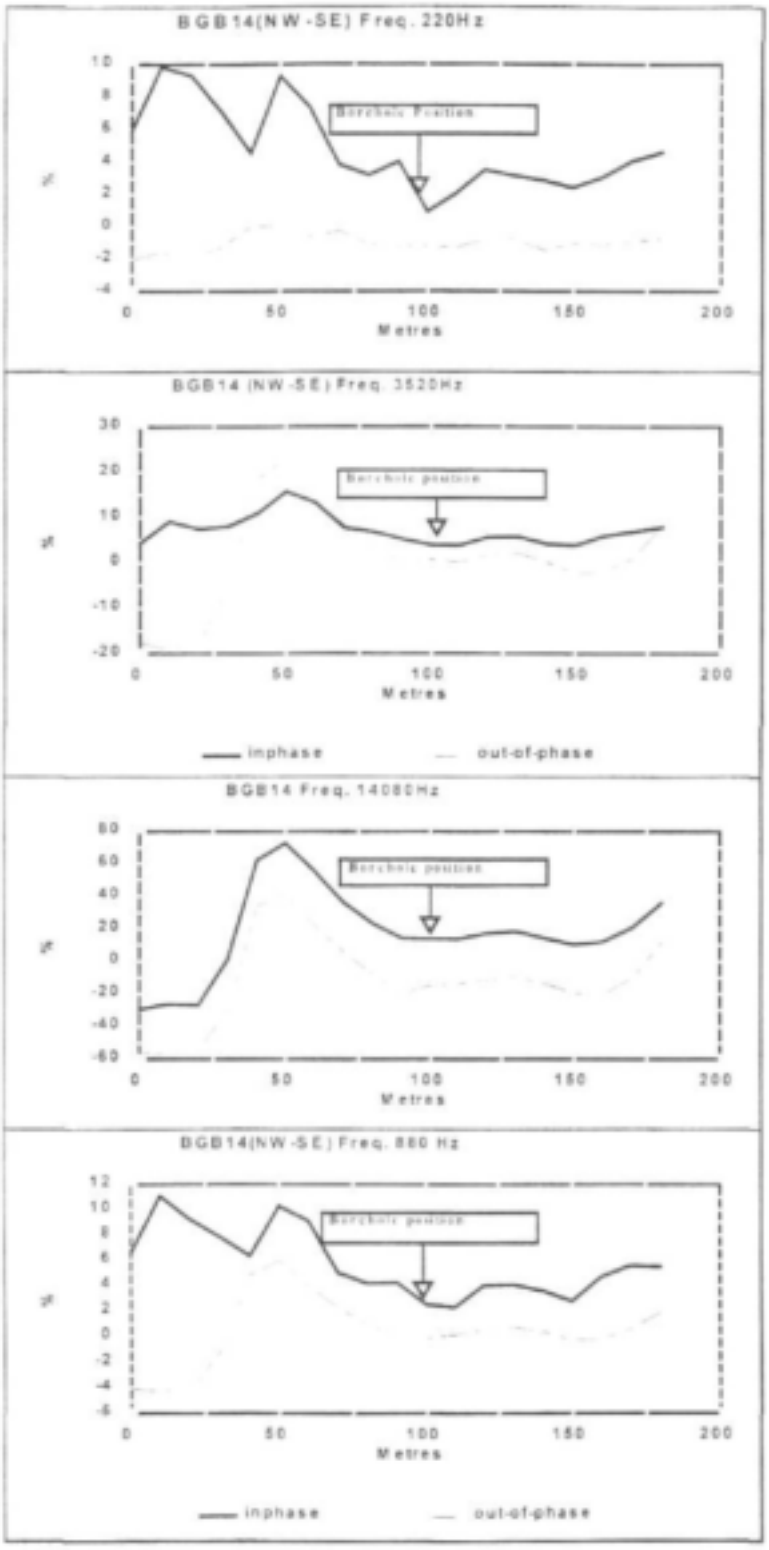

Figure 4-17 Geophysical profiles (E-M) of traverse BGB14 (Traverse direction: SW→NE).

Figure 4-18 **Locality map of traverse BGB 2**

Magnetic survey

The magnetic method was not appropriate to delineate the fault line because of the presence of a dolerite sill in the fault vicinity. However, a survey was carried out in the NE-SW direction and an anomaly was observed in the approximate vicinity of the fault line (Figure 4.19). The magnetic profile suggests that the fault dips steeply in the NE direction.

Electrical sounding Survey

An electrical sounding was carried out at the 100m point of the HLEM traverse, parallel to the fault line. The sounding data is plotted as BGB2 in Appendix 4-A. The sounding curve shows a three layer curve with $\rho_1 < \rho_2 < \rho_3$, thus an A-type curve. The following resistivity and thickness values for the three-layer curve profile are calculated:

Layers	Thickness (m)	Resistivity (Ωm)
Layer1	10	32
Layer2	50	93
Layer3	∞	resistive bedrock

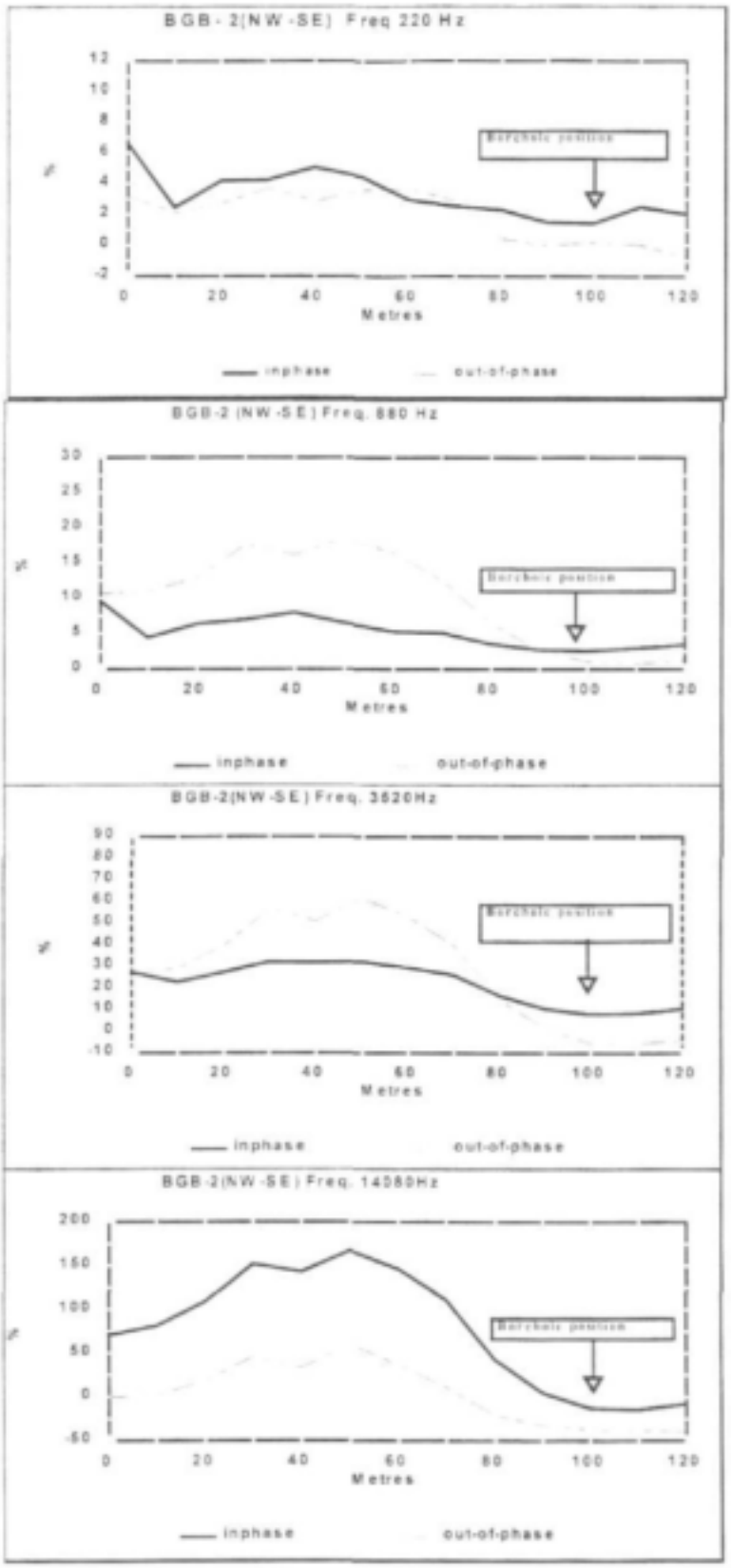
BGB - 2(NW -SE) Freq 220 Hz
12
10
8
6
4
2
0
-2
%
Barchaic position
0
20
40
60
80
100
120
Metres
inphase
out-of-phase
BGB-2 (NW -SE) Freq. 880 Hz
30
25
20
15
10
5
0
%
Barchaic position
0
20
40
60
80
100
120
Metres
inphase
out-of-phase
BGB-2(NW -SE) Freq. 3520Hz
90
80
70
60
50
40
30
20
10
0
-10
%
Barchaic position
0
20
40
60
80
100
120
Metres
inphase
out-of-phase
BGB-2(NW -SE) Freq. 14080Hz
200
150
100
50
0
-50
%
Barchaic position
0
20
40
60
80
100
120
Metres
inphase
out-of-phase

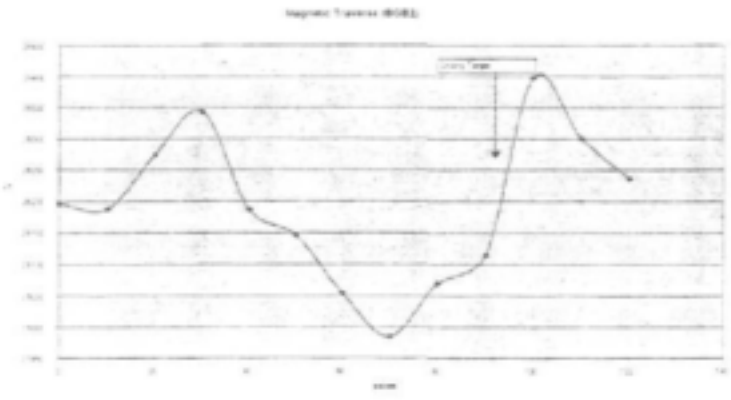

Figure 4-19 Geophysical profiles (E-M and Magnetics) of traverse BGB2 (Traverse direction: NE→SW).

BGB 3 E – W fault

This fault is mapped on the 1:100 000 metallogenic map (Ward, 1999) and is observable in the field by an almost 1m thick secondary quartz veins which can be traced for about 100m along the E-W strike direction. The fault is a strike slip fault as there is a shear zone related to this fault that runs through the meta-basalts and phyllite schists of the Theespruit Formation. There are two parallel dykes of about 10m in thickness that bound this fault line and are about 200m apart. The fault line runs almost in the centre of the dykes. HLEM and magnetic surveys of 150m were carried across the fault and in the N-S direction. Figure 4.20 is the locality map of the traverse line BGB 3.

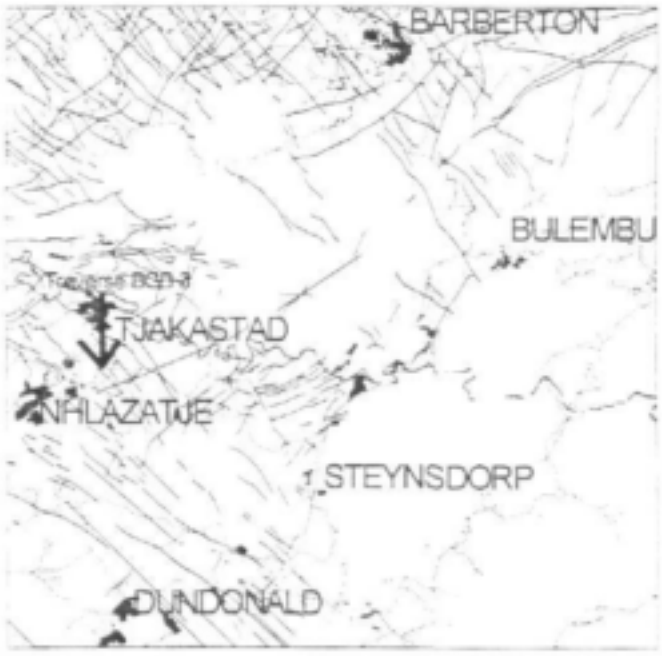

Figure 4-20 Locality map of traverse BGB3

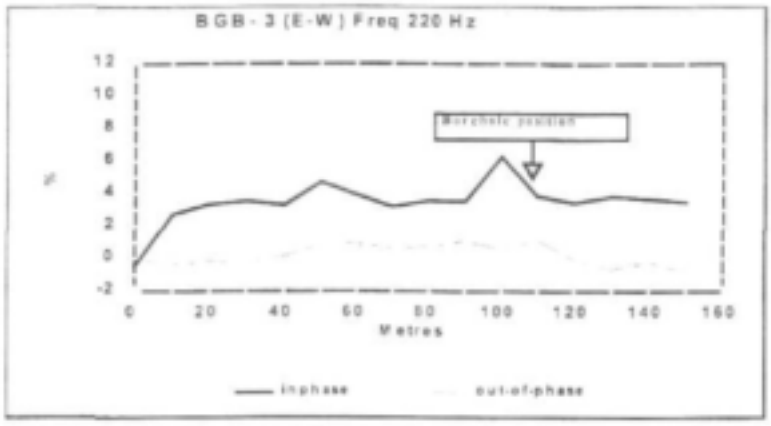
BGB - 3 (E-W) Freq 220 Hz
Borehole position
%
Metres
inphase
out-of-phase

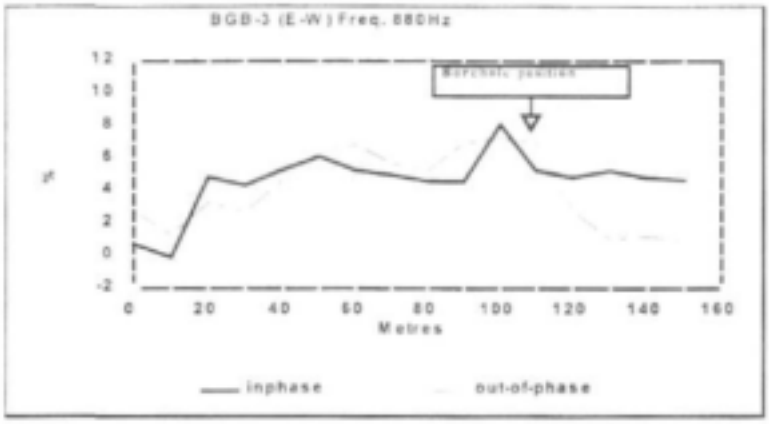
BGB-3 (E-W) Freq. 880Hz
Borehole position
%
Metres
inphase
out-of-phase

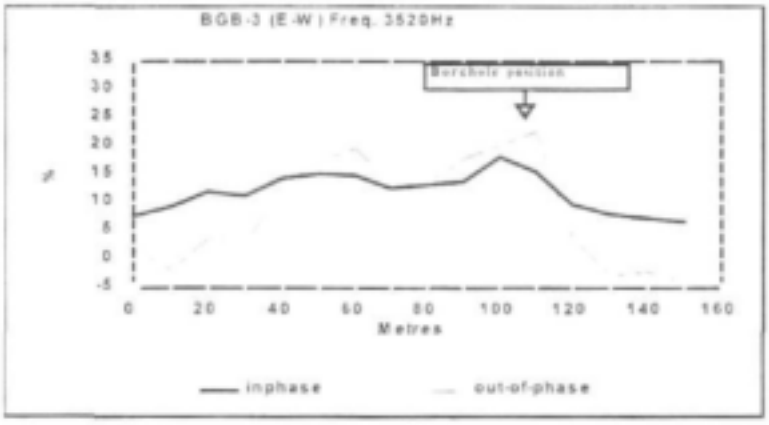
BGB-3 (E-W) Freq. 3520Hz
Borehole position
%
Metres
inphase
out-of-phase

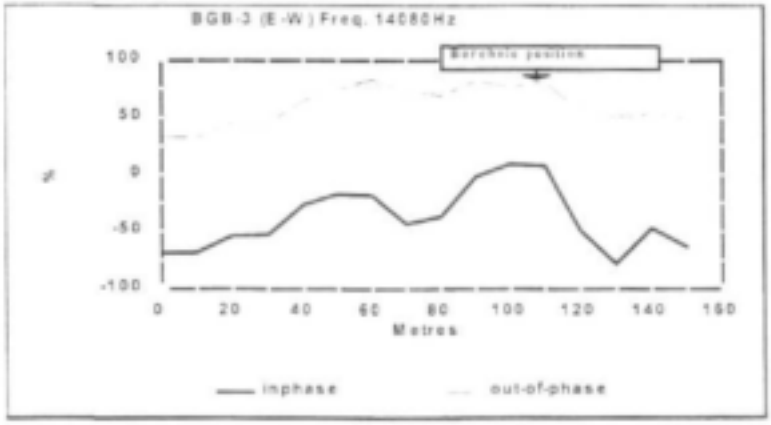
BGB-3 (E-W) Freq. 14080Hz
Borehole position
%
Metres
inphase
out-of-phase

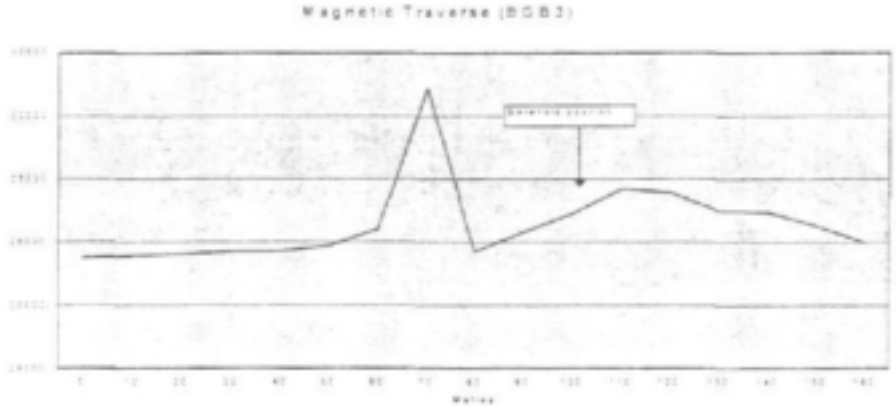

Figure 4-21 **The geophysical profiles of traverse BGB3 (Traverse direction: N→S).**

Electromagnetic survey

The Max-Min was operated at 4 frequencies that range from 220 to 14080 Hz with 100m coil separation and 10m station spacing. The results of the HLEM survey are presented in Figure 4.21. The high ratio of in-phase and out-of-phase suggests a good conductor occurs at depth. The ridge continuity response can be observed at almost 120 m on the 3520 Hz profile, which is almost the position of the fault line. At this point a borehole yielding 1.2 l/s was sited (X12-04).

Magnetic survey

The results of the magnetic survey did not show any significant magnetic changes across the fault line. A sharp peak can be observed at the 70m point of the survey line and is suspected to be the magnetic interference noise.

4.6.4 Shear Zones

BGB 6 E – W striking shear

This shear zone was identified in the field. There is great abundance of quartz veins, which seem to have been hydrothermally deposited in this zone of weakness. The meta-basalt of the Komati Formation in this zone is low grade metamorphosed to form a phyllite-chlorite schist, which deforms in a ductile manner. There is great abundance of clay minerals in the shear zone.

The observed shear zone in this study area is striking in the E – W direction and the HLEM, magnetic and electrical sounding surveys were carried in the N-S direction to observe the geophysical response of this structural feature. Figure 4.22 is the locality map of the geophysical traverse.

Figure 4-22 **The locality map of traverse BGB6.**

Electromagnetic survey

The Max-Min was operated at 4 frequencies, ranging from 220 to 14080 Hz. The traverse was of 180m length with a 100m coil separation and a 10m spacing. The HLEM profile suggests a shallow, conductive source (Figure 4.23). A zone of higher conductivity is observed at 100m on the lower frequency profiles of 220 and 880 Hz, which almost coincides with the locality of the shear zone. Here a borehole (X12-02) was sited yielding 1 l/s. The 14080 Hz frequency profile shows a zone that can be interpreted as a wide, shallow, poorly conductive geological feature. This zone is observed at 20 to 150m of the traverse profile.

Magnetic survey

The magnetic data is inconclusive for the entire traverse, though a sharp peak occurs at the beginning of the traverse, which is interpreted as noise.

Electrical sounding survey

The electrical sounding survey was carried out at 100m on the traverse. The results of the electrical sounding survey are presented as profile BGB6 in Appendix 4-A. The sounding curve displays a three layer A-type curve. A cusp caused by resistive lateral heterogeneity, probable a gravel body, can be observed at 15m depth. The following values are determined in this three layer sounding curve:

Layers	Thickness (m)	Resistivity (Ωm)
Layer1	5	40
Layer2	25	75
Layer3	∞	resistive bedrock

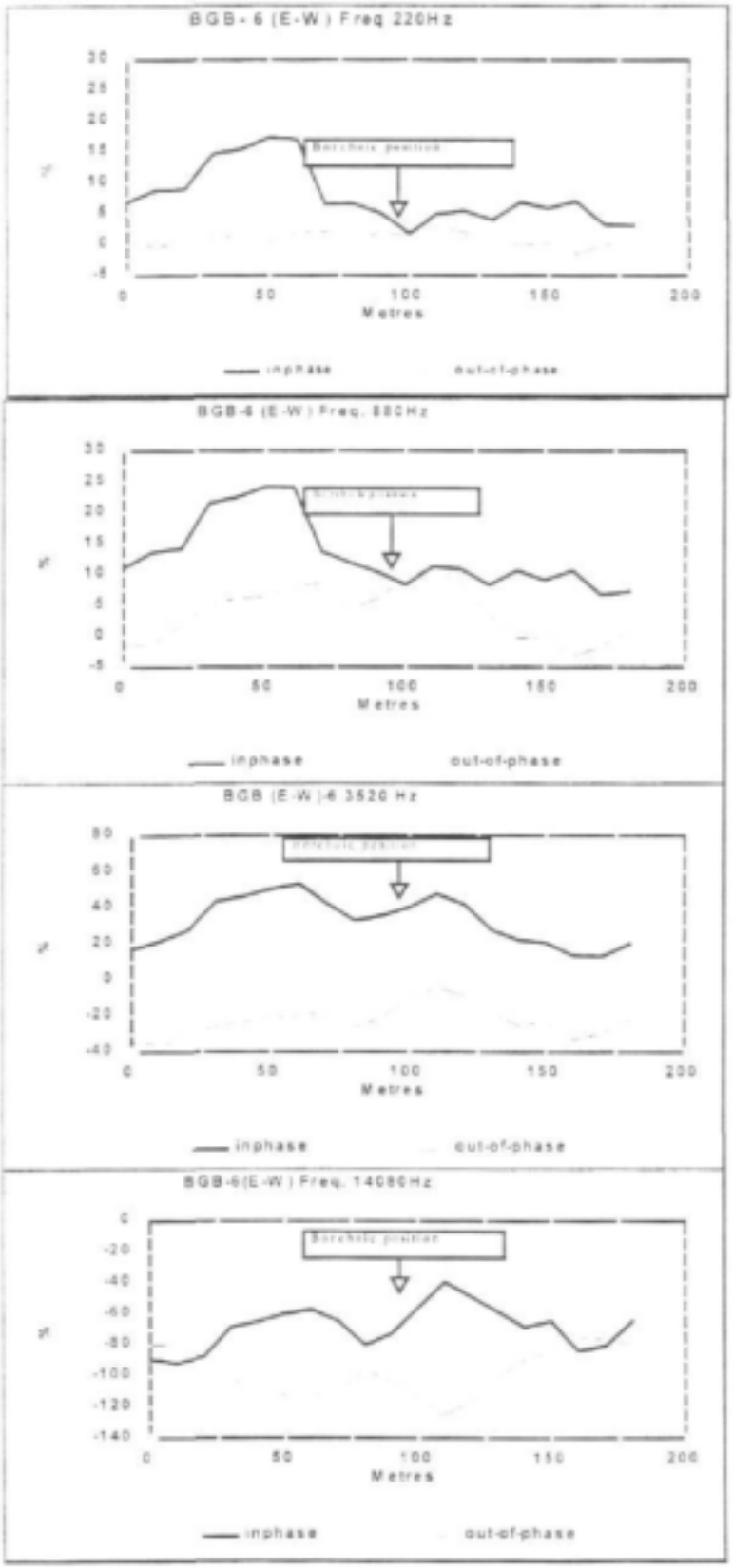
BGB - 6 (E-W) Freq 220Hz
30
25
20
15
10
5
0
-5
%
Borehole position
0
50
100
150
200
Metres
inphase
out-of-phase
BGB-6 (E-W) Freq. 880Hz
30
25
20
15
10
5
0
-5
%
Borehole position
0
50
100
150
200
Metres
inphase
out-of-phase
BGB (E-W)-6 3520 Hz
80
60
40
20
0
-20
-40
%
Borehole position
0
50
100
150
200
Metres
inphase
out-of-phase
BGB-6(E-W) Freq. 14080Hz
0
-20
-40
-60
-80
-100
-120
-140
%
Borehole position
0
50
100
150
200
Metres
inphase
out-of-phase

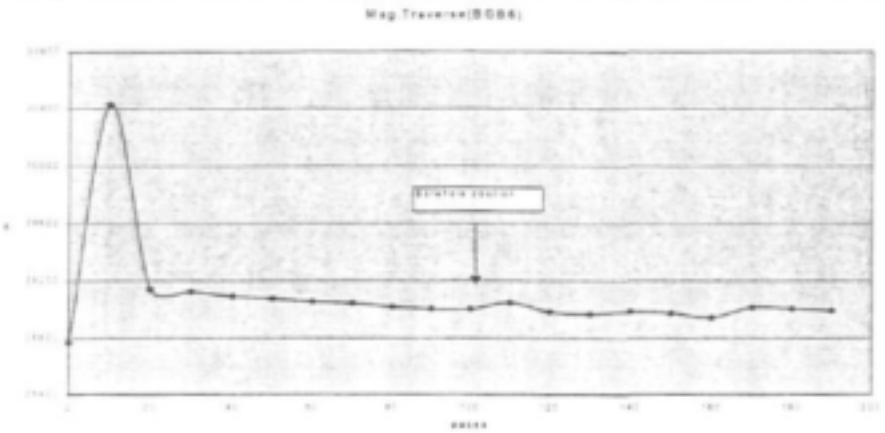

Figure 4-23 Geophysical profiles (E-M and Magnetics) of BGB6 (Traverse direction: N→S).

4.6.5 Dolerite Dykes

BGB13 NE – SW Striking dyke

Dolerite dykes of probable Karoo age were considered for groundwater investigation. BGB 13 was carried out across a dyke identified from the LANDSAT processed data as a lineament. It was also readily observed in the field with NE – SW strike orientation. The dyke intrudes the greenschists of the Theespruit Formation. The E-M, magnetic and electrical soundings were carried in the SE-NW direction. Figure 4.24 is the locality map of traverse BGB 13.

Electromagnetic survey

There is no significant anomaly in the E-M profile, but the 220 Hz profile depicts a deep conductive source at 70m, which coincides with the dyke position and where a 2 l/s borehole was sited (X12-08). It is suspected that the interference noise from the nearby power lines may have affected the Max-Min data (Figure 4.25).

Magnetic survey

A wide magnetic anomaly of 300nT is observed in the magnetic data (Figure 4.25). This suggests a shallow wide sub-vertical to vertical magnetic feature that is associated with the dolerite dyke.

Electrical sounding survey

An electrical sounding survey was conducted at 70m position of the HLEM traverse. The resistivity data is shown in Appendix 4-A, as profile BGB13. The data display a three layer curve with $\rho_1 < \rho_2 < \rho_3$, which is an A-type curve. The following values were determined in this three layer curve profile:

Layers	Thickness (m)	Resistivity (Ωm)
Layer1	8	28
Layer2	45	55
Layer3	∞	resistive bedrock

Figure 4-24 **The locality map of traverse BGB 13.**

BGB 26 N – S dyke

The dyke was identified in the 1:250 000 geological map of Barberton. This dyke intrudes a granitic pluton known as the Stolzburg gneiss. A xenolith of Theespruit Formation occurs in the vicinity of the dolerite dyke. The traverse was undertaken across the granite gneiss contact with the dolerite dyke. The HLEM, magnetic and electrical sounding surveys were carried perpendicular in the case of the HLEM and magnetics and parallel to the dyke in the case of the electrical soundings. The dyke strikes in the N-S direction and the locality map of the geophysical traverse is shown in Figure 4.26.

Electromagnetic survey

The Max-Min was operated at 220, 880, 3520 and 14080 Hz. A traverse of 170m was carried out with a coil separation of 100m and a station spacing of 10m (Figure 4.27). A zone of high conductivity can be observed at 90m on the traverse. The high frequency profiles show an asymmetrical ridge at the 90m point, which suggest a shallow conductive source. This is the expected zone of the of granite and dolerite contact. A borehole was sited here (X12-06), but yielded only 0.1 l/s.

Magnetic Survey

The magnetic data (figure 4.27) display the granite-dyke contact at 100m point of the traverse. The magnetic anomaly is a step discontinuity that resembles that of a dolerite sill.

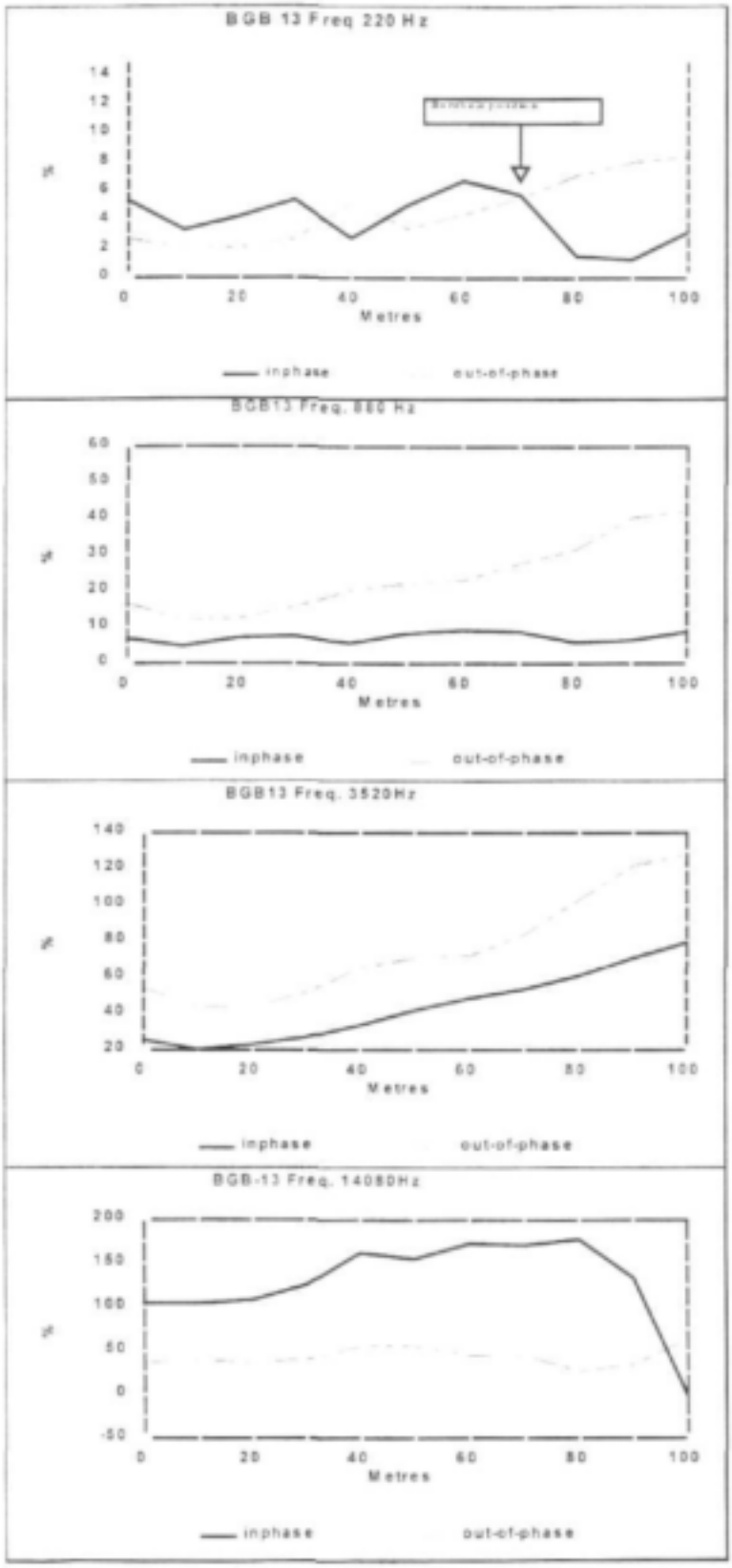
BGB 13 Freq 220 Hz
14
12
10
8
6
4
2
0
%
0
20
40
60
80
100
Metres
inphase
out-of-phase
BGB13 Freq. 880 Hz
60
50
40
30
20
10
0
%
0
20
40
60
80
100
Metres
inphase
out-of-phase
BGB13 Freq. 3520Hz
140
120
100
80
60
40
20
%
0
20
40
60
80
100
Metres
inphase
out-of-phase
BGB-13 Freq. 14080Hz
200
150
100
50
0
-50
%
0
20
40
60
80
100
Metres
inphase
out-of-phase

Figure 4-25 Geophysical profiles (E-M, Magnetic) of traverse BGB13 (traverse direction SE-NW).

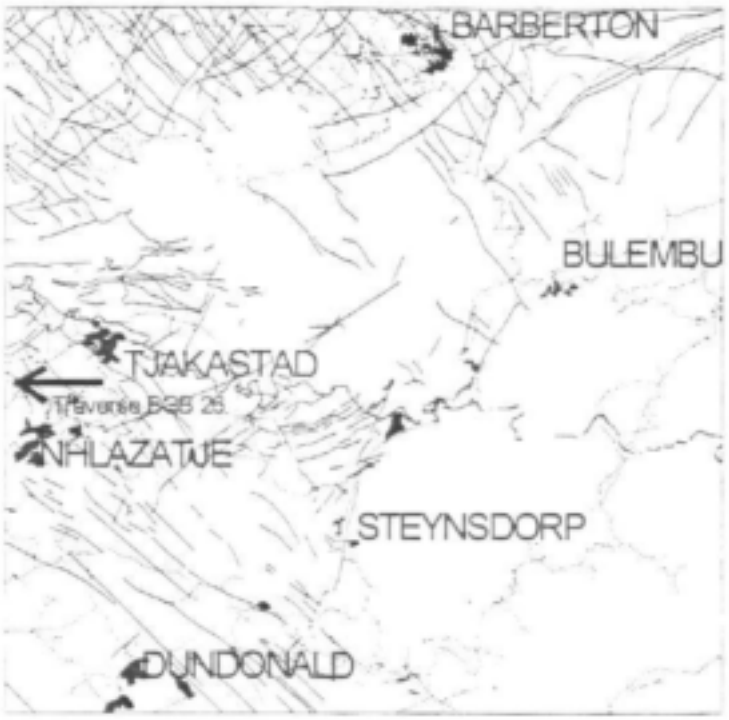

Figure 4-26 Locality map of traverse BGB26.

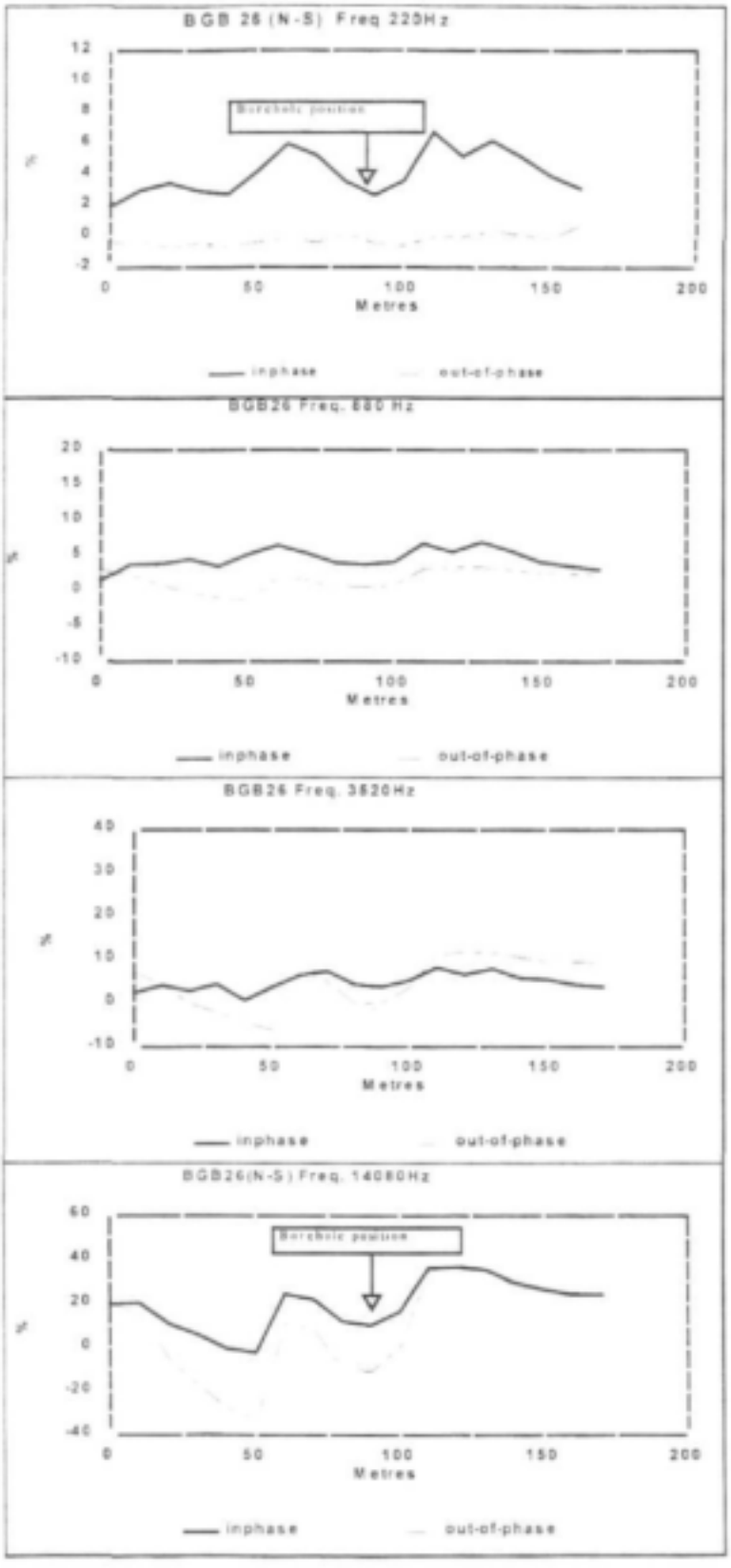
BGB 26 (N-S) Freq 220Hz
Borehole position
Metres
inphase
out-of-phase
BGB26 Freq. 880 Hz
Metres
inphase
out-of-phase
BGB26 Freq. 3520Hz
Metres
inphase
out-of-phase
BGB26(N-S) Freq. 14080Hz
Borehole position
Metres
inphase
out-of-phase

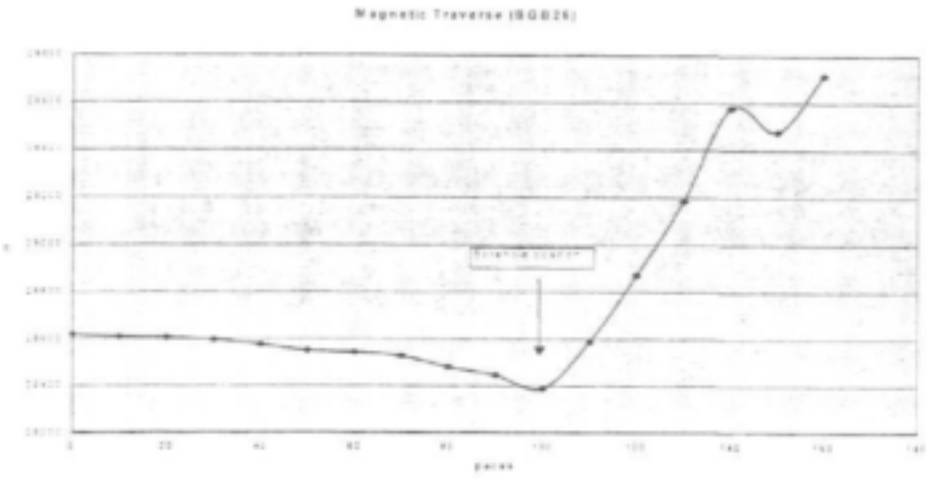

Figure 4-27 Geophysical profile (E-M and Magnetic) of traverse BGB26 (traverse direction: E-W)

Electrical sounding survey

The sounding survey was conducted at the 90m position of the HLEM survey line, parallel to the assumed dyke contact. The results of the electrical sounding survey are presented as profile BGB26 in Appendix 4-A. The survey was very short because the instrument was malfunctioning. Therefore, the resistivity data is inconclusive for this traverse.

4.7 Drilling Results

A total of 9 boreholes were drilled by the Department of Water Affairs and Forestry operation with an air percussion rig to investigate the hydrogeological significance of the selected structures.

The drilling sites were selected to investigate the major structural orientations identified, which are N – S, NW – SE and NE – SW. The geological logs and construction details of boreholes are presented in Appendix 4-B. Table 4.5 is a summary of drilling results in terms of borehole depth, water strikes, blow yield and structural features targeted. Figure 4.28 shows the position of the drilled boreholes.

Table 4-5 **Summary of Drilling Results**

Borehole	Depth (m)	Water Strike (m)	Blow yield (l/s @ Depth m)	Feature investigated	Site ID of geophysical survey
X12-01	120.0	15,24,36,81	0.5 @ 15 0.5 @ 24 5.0 @ 36 4.0 @ 81	NE-SW running lineament	BGB-4
X12-02	102.0	24,66	0.2 @ 24 0.8 @ 66	E-W striking shear zone	BGB-6
X12-03	120.0	20,97	0.1 @ 20 0.2 @ 97	NW-SE striking fault	BGB-2
X12-04	120.0	19,62	0.3 @ 19 0.9 @ 62	E-W striking fault	BGB-3
X12-05	120.0	18,32,66	Seepage @ 18 Seepage @ 32 0.1 @ 66	E-W striking shear zone	BGB-14

X12-06	74	27.42	Seepage @ 27 0.1 @ 42	N-S striking dyke	BGB-26
X12-07	47	37	Seepage @ 37	N-S striking lineament	BGB-27
X12-08	120	19.53	0.5 @ 14 1.5 @ 36	NE-SW striking lineament	BGB-13
X12-09	120	12.40	0.2 @ 12 1.0 @ 40	NNE-SSW striking Lineament	BGB-24

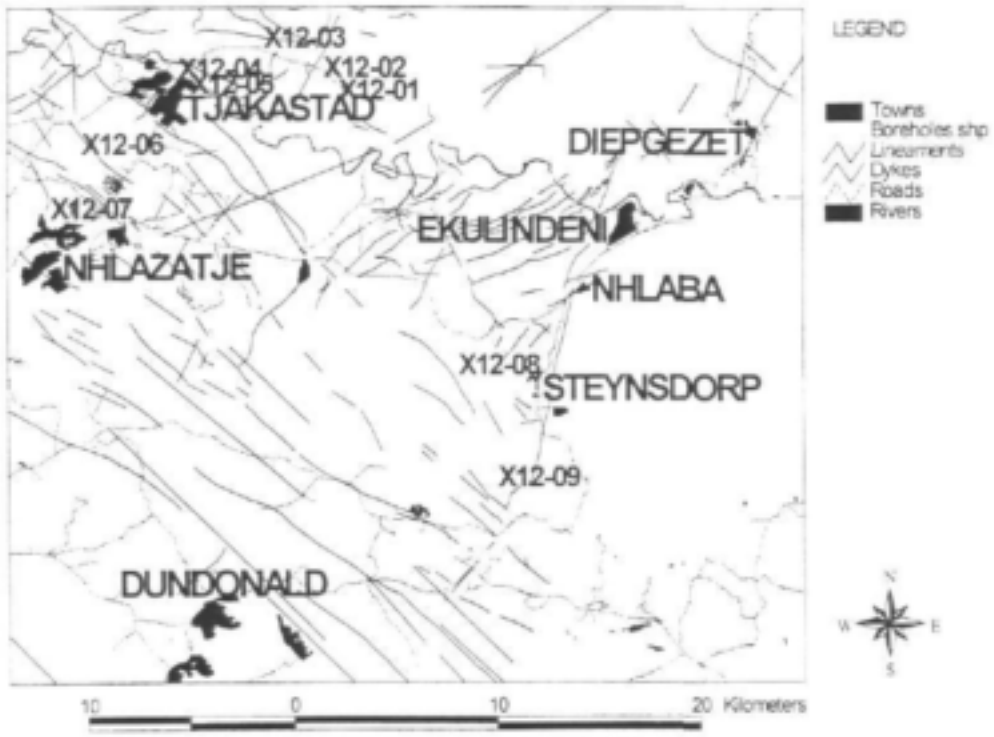

Figure 4-28 **Locality map showing the position of the drilled boreholes.**

Borehole X12-01 on site BGB4

Borehole site

Borehole X12-01 was drilled into a NEE lineament (Figure 4.14), which is believed to represent an extensional structure. The site is located on a footslope below a rugged hillock sloping towards the Mbhejeka stream. The borehole was sited based on the HLEM and magnetic surveys BGB4. The traverse indicated a more conductive zone and a magnetic step

over the lineament at 190m, directly over the lineament, indicative of a fault. The borehole is positioned near the premises of the old Mbhejeka Primary School.

Geological description

The hole was drilled through highly fractured and weathered greenish-grey meta-basalt of the Theespruit Formation. The fractures are filled with quartz and calcite. The first water strike was encountered at 15m with an associated blow yield of 0.3 l/s. There were no lithological changes, except in the physical character like the degree of fracturing and weathering. Another water strike of 0.2 l/s was obtained at 24m. Then, at 36m a highly fractured and weathered meta-basalt was penetrated, which displayed slickenside striations in some of the fractured rock chips. The striations suggest movements along the fracture plane. Therefore, the lineament is definitely a fault. A water strike of 5 l/s was encountered at this depth. Drilling continued through the alternating hard, soft and fractured meta-basaltic rock until 81m where another water strike of 4.5 l/sec was encountered. At this depth, fracturing is even more intensive with loose fractured rock chips of about 5cm, which suggest an open fracture. Drilling terminated when meta-basalt became uniformly hard and fresh and the final blow yield measured 10 l/s.

Borehole X12-02 on site BGB6

Borehole site

This site was mapped in the field as an E-W shear zone. The shear zones are of great significance with respect to mineral exploration for Au mineralisation in the greenstones, in particular. There is not much known about the groundwater potential of these structural features, however, the E-W orientation has been predicted to be under present day compression, or antithetic shear, depending on whether the orientation of maximum extension is E-W or SE-NW (4.5.3). As a result this site was chosen to verify whether the yield associated with shear zones is poor due to compression, or marginal due to rotational strike-slip shear . A poor geophysical response, especially with the HLEM was obtained (4.6.4), hence the borehole was sited based on field observation of the shear zone. The site is located on a flat plain, about 200m from the Mbhejeka stream that runs eastward from the site view. The hole was sited at 100m of the HLEM and magnetic traverses (Figure 4.22). The hole is positioned, next to the path that goes to Mbhejeka Primary school at Mbhejeka.

Geological description

The borehole was drilled through a mono-litho type, which changed mineralogical and in physical character as drilling proceeded. The rock type is the green, schistosed meta-basalt, that is a typical greenschist litho-type, with a great abundance of quartz veins. The first 20m were hard due to the presence of thick quartz vein. The rock chips were still weathered and fractured but not to a greater extent. At 24m, the rock became more fractured and weathered and a water strike was encountered with a blow yield of 0.3 l/s. Drilling continued to 54m, through a green, phyllitic rock which can be described from a hand specimen as a chlorite-phyllite schist. This rock type has a soapy feel and is rich in clay minerals. Because of the mineralogical content, it is thought that this metamorphic variety of meta-basalt has a low permeability. A more crystalline, light greenish-grey meta-basalt was encountered at 55m and a water strike with a blow yield of 1 l/s was obtained. Surface striations were observed on fracture faces of rock chips at this depth, which indicates some form of movement along the fracture planes. The drilling terminated within this rock type at 102m and the final blow yield measured as 1 l/s.

Borehole X12-03 on site BGB 2

Borehole site

Borehole X12-03 was selected to investigate a NW trending fault, an orientation presumed to be poor due to compression in spite of the intrusion of NW trending diabase dykes. The borehole was sited on the basis of geophysical traverse BGB 2. The site is located in an E-W depression adjacent to a minor perennial stream. The geophysical response (Figure 4.19) suggests the fault is located at 100m of the survey line and the borehole was positioned directly over the fault line. The borehole is located at Hoegenoeg.

Geological description

The borehole was drilled through a crystalline, fractured Komatiite or meta-basalt. A dolerite sill outcrops very close to the borehole locality. The main lithological units in the borehole vicinity are dolerite and meta-basalt. The first water strike of 0.1 l/s was encountered at 12m depth. The rock formation was very hard to drill even though it was fractured. Crysotile asbestos covered the fractured faces of large rock chips and these were first observed at 20m. Fractured dolerite was encountered at 32m, however, the contact zone was not water bearing. There was a great abundance of green and white quartz crystals at 41m after a lithological change at this depth to a greenish-grey meta-basalt. At 58m, the rock became soft to drill, since a highly weathered greenish – grey meta-basalt was encountered. A second water strike of 0.2 l/s was encountered at 97m where large fractured meta-basalt chips, which display striations, were observed. Drilling terminated at 120m after penetrating through a fractured and weathered meta-basalt with a great abundance of crysotile asbestos, green and white quartz crystals. The final blow yield was measured as 0.3 l/s.

Borehole X12-04 on site BGB3

Borehole site

Borehole X12-04 targeted an E-W trending fault marked on the ground by an almost 1m thick quartz veins. This orientation has been identified as being under compression or antithetic shear. The borehole is positioned at 110m of geophysical traverse BGB3 and the position was selected based on observations of the fault in the field. The site is located in a relatively flat topography almost central between the two parallel dykes with E-W orientation. The two dykes are about 300m apart and approximately 20m in thickness. The site locality is Tjakastad East.

Geological description

The hole was drilled through highly fractured and highly weathered meta-basalt of the Theespruit Formation, Onverwacht Group and encountered numerous quartz veins. The meta-basalt weathers to a saprolite clay matrix. The first water strike of 0.5 l/s was intersected at 19m. Drilling operation continued through soft fractured and weathered greenish-grey meta-basalt with a great abundance of quartz veins. A 2m thick open cavity was encountered at 47 and 48m. It was expected that a water strike would be intersected at the cavity, but it was a dry cavity. Drilling continued through soft greenish-grey basalt, until a fractured dolerite was encountered at 61m, with another water strike of 0.8 l/s at 62m. Drilling continued through the fractured and weathered meta-basalt and quartz veins from 63 to 120m. Drilling terminated at 120m, with a final measured blow yield of 1.2 l/s. After careful observation of the shear zone, which is parallel to the drilling target, the fault in which X12-04 is drilled through has strike-slip movements.

Borehole X12-05

Borehole site

This site was drilled on an identified shear zone. The E – W trending shear zone coincides with a strike slip fault (BGB3) on which X12-04 was drilled. It can be deduced that the E – W trending fault is a response to shear deformation. Borehole X12-05 is positioned on the flat plain, a mere 10m from the deep gullies where a highly sheared meta-basalt outcrop is evident at Tjakastad East.

Geological description

The first 12m was drilled through a hard milky quartz vein, which was followed by soft greenschist amphibolite with granules of quartz vein. Seepage was obtained at 18m. From 18-24 m, drilling continued through a more siliceous meta-basalt. Subsequently, the rock changed to a dark grey with greenish tint, highly foliated and highly weathered phyllite schist with abundant quartz veining. This rock formation remained the same until 120m except for minor changes like the proportion of quartz crystals. In some places the rock sample became more granular with greater abundance of quartz grains and additive seepage strikes are obtained in those places. There were two such water strikes at 32 and 66m depths. These two water strikes occur in places where the sample was more granular. Au was observed in association with quartz grains from 80m up to 120m. It was observed that the phyllite-schist units are not water yielding and instead absorb water in the course of drilling. The final blow yield was measured 0.1 l/s.

Borehole X12-06 on site BGB26

Borehole site

Borehole X12-06 was chosen to investigate the contact between a xenolith of greenschist, a N- S striking dolerite dyke and a granitic pluton (i.e. the Stolzburg gneiss). This orientation has been predicted as one under extension. The dolerite – gneiss contact was identified on the basis of geophysical traverse BGB 26. The site is located on a footslope of a hill, which descends northwards in the direction of the Theespruit River. The borehole site is positioned at 90m of the E-M traverse. The borehole site is located at Nhlazatje.

Geological description

The hole was drilled through highly weathered granite with pink and white quartz in the first 5 m. Drilling continued through fractured granite with quartz veining. Fractured dolerite was first intersected at 13m, however, the contact was dry. Drilling continued through light grey, fresh granite gneiss with quartz veins. Seepage was attained at 27m. The granite was more weathered and foliated at this depth. A dolerite dyke was intersected again at 31m and drilling continued through hard, light grey fresh granite gneiss up to 39m. Another dolerite dyke was intersected at 40m depth, but the contact was also dry. Drilling continued to 48m through hard light grey granite – gneiss. The granite was more fine-grained and no quartz veins were observed. Seepage was attained at 49m where the granite was relatively weathered and fractured. Drilling continued through an extremely hard, very fine grained, light grey granite and was terminated at 74m as a result of hard rock. The final measured blow yield was 0.1 l/s.

Borehole X12-07 on site BGB-27

Borehole Site

Borehole X12-07 is in a similar geological setting to X12-06; a granite pluton where greenschist and dolerite dykes occur in one locality. The site is located in a depression that runs NE – SW, intersecting a N-S trending dolerite ridge. The geophysical response was not conclusive, however, borehole X12-07 was proposed at 130m on the traverse (Appendix 4-A) based on the observed NE trending linear contact between granite gneiss and greenschist. The hole is located at Ntlazatshe, about 170m from the settlement area.

Geological description

The first metre of drilling penetrated through both the weathered and fractured greenschist and granite gneiss. Drilling then continued through highly fractured and weathered light grey granite with abundant quartz veins. The dolerite was encountered at 13 to 16m and drilling continued through light coloured micaceous granite with quartz veining. Seepage was obtained at 23m. Drilling was terminated at 47m when penetration rates decreased dramatically due to the hardness of the granite gneiss. The blow yield was below measurable limits and as such the borehole was regarded as dry.

Borehole X12-08 on site BGB13

Borehole site

Borehole X12-08 was chosen to investigate a NE striking lineament related to a dolerite dyke intruding amphibolite schist. This is the orientation of maximum extension (4.5.3). The borehole site is located in a flat plain at Steynsdorp village.

Geological description

The first 20 metres were drilled through a highly foliated, weathered and fractured greenschist (amphibolite). The first water strike of 0.5 l/s was obtained at 19m, where the greenschist had abundant quartz grains. Drilling continued through weathered and fractured light greenish-grey meta-basalt with green and white quartz crystals. Another water strike was obtained at 53m with a blow yield of 1.5 l/s. Highly fractured and weathered dolerite was intersected at 54m, showing slickenside striations in some of the fracture surfaces. It can therefore be deduced that there had been post dolerite intrusion movements and that the NE orientation is presumably in an antithetic strike-slip setting. Quartz veins are also more abundant at this depth. Drilling continued from 73 to 120m, through a green to dark grey, weathered basalt with quartz and calcite grains. Drilling was terminated at 120m, and the final measured blow yield was 2 l/s.

Borehole X12-09 on site BGB24

Borehole site

The borehole site was selected to investigate a long lineament with a NNE – SSW trend, which corresponds to the orientation presumed to be under maximum extension and in a dip-slip fault setting. The borehole site is located on a flat plain, on a bank of a minor stream. This borehole site is positioned opposite the turn-off road that goes to Natuurskoon at Stynsdorp. Hills facing site X12-09 are made up of granite–gneiss of the Stynsdorp pluton. However, the site is located in the greenschist terrain that consists of highly foliated, talc-chlorite schist and meta-basalt.

Geological description

Drilling progressed through a highly fractured, medium to coarse-grained meta-basalt. Most of the fracture faces display pronounced striations. A water strike of 0.5 l/s was obtained at 40m. Drilling terminated at 120m, with no lithological changes, except the proportion of quartz veins. Since the striations are common to most of the fracture faces, it can be deduced that the lineament observed from the LANDSAT image is a fault. The final blow yield was measured as 1.0 l/s.

Conclusions

The NE to NNE baring structures proved to be the highest yielding structural features in the Barberton Greenstone Belt. These features can be presumed to be faults in a dip-slip setting. This supports the theory that such features are open to due to E to SE oriented extension. The N-S striking structural features proved to be low yielding in contrast to the structural analysis of joints, which suggested that the N-S structures are open. The poor results from N-S targets suggests that this orientation is under a present day synthetic strike-slip setting, with the NE structures being the other conjugate set. Hence the NNE structures appear to be the preferred setting. The contact between N-S dolerite dykes and host rocks proved not to be water bearing. However, all such targets were located in granitic plutons, which generally have low yielding boreholes and are extremely hard to drill.

The E-W shear zones that consist of talc-chlorite schist are soft to drill through but because of the mineralogical composition, these zones are not transmissive enough to bear water. In general, high yields occur in such zones, which have been rejuvenated by antithetic strike slip faulting.

4.8 Test Pumping

Constant rate discharge tests were carried out on 7 of the 9 newly drilled boreholes in order to characterise hydraulic properties of the penetrated lithologies; to assist with conceptual model of aquifers and to determine sustainable borehole yields. The test pumping and recovery data are presented in Appendix 4-C.

Borehole X12-01

Borehole X12-01 had water strikes at depths of 15, 24, 36 and 81m, which is indicative of a multi-layered aquifer between basaltic flows. The total blow yield was 10 l/s with 36m being the main water strike. The static water level of the hole is 3.38m below surface, giving an available drawdown of 32.62m. The pump was set at 37.2 m below surface during the test. The borehole was then pumped at a rate of 2.5l/s for 720m.

Radial flow occurs until the drawdown curve shows an increasing rate of drawdown after 70 minutes. The slope of this line is 0.25 on the derivative of drawdown curve, indicating a finite fracture and that boundary conditions are present. This suggests that one of the main water strikes is bounded.

The recovery of the borehole was monitored for 480 minutes. The data shows that after 480 minutes since pumping was stopped, the water level has recovered to within 0.28 m. No evidence of leakage from an overlying weathered zone can be detected, hence storage is limited to fractures.

Table 4.6 presents the calculated transmissivity values on the basis of early (radial flow) and late time data. The sustainable yield calculated on the basis of the various methods is shown

in Table 4.7. The various parameters utilised for each of these methods are illustrated in Table 4.8.

Table 4-6 Transmissivity values for X12-01

Borehole Number	T_{early} (m^2/d)	T_{late} (m^2/d)	$T_{recovery}$ (m^2/d)
X12-01	132	54	132

Table 4-7 Recommended borehole yield values for X12-01 method

Method	m^3/d
Drawdown to boundary	142
Distance to boundary	67
Flow characteristic	685
Max. Drawdown	170

Table 4-8 Critical parameters for sustainable yield estimation

Parameter	X12-01	X12-02	X12-03	X12-04	X12-05	X12-08	X12-09
T_{early}	132	1.4	0.8	8.3	1.6	11.9	1.9
T_{late}	54	1.9	0.8	12.4	0.9	39.1	0.3
$S_{fracture}$	0.001	0.001	0.001	0.001	0.001	0.001	0.001
S_{matrix}	0.01	0.01	0.01	0.01	0.01	0.01	0.01
Boundary(m)	1.78	12.00					4.24
Boundary(d)	0.375	0.0347					0.000486
Lithology	Meta-basalt	Meta-basalt	Meta-basalt	Meta-basalt	Schist	Schist	Meta-basalt
F2	3	2	2	2	3	1.6	4
Yield (m^3/d)	685	60	47	145	20	~400	8
Conceptual Model	Weathered multi-layered Finite aquifer	Confined, double porosity aquifer	Confined, leaky, Double porosity aquifer	Confined, double porosity aquifer	Confined, multi-layered aquifer	Weathered, Leaky, double-porosity aquifer	Finite fracture aquifer

The sustainable borehole yield estimate varies from 142 to 685 m^3/day for the different methods. Since insufficient drawdown was achieved, the drawdown and distance to boundary methods are considered underestimates. The flow characteristic method estimate of 685 m^3/d is considered to be the best approximation of sustainable yield.

Borehole X12-02

The borehole had a water strike of 66m, which gave a blow yield of 1.0 l/s. The static water level of this borehole is 10.76m below surface and therefore an available drawdown is calculated to be 55m. The pump was set at 27.20m below surface. The borehole was then pumped at a rate of 0.52 l/s for 360 minutes.

The semi-log drawdown curve is characterised by parallel early and late time drawdown, separated by a horizontal line in the middle. This can be interpreted to represent leakage from a double porosity system. However, at this point the water level drops below a highly fractured and weathered basalt horizon into fractured and weathered basalt, a contact zone where seepage was encountered during drilling. This suggests that the flattening of the drawdown curve could be related to the initiation of unconfined conditions in this seepage zone. After borehole completion this seepage zone probably gained water through the borehole from the confined higher yielding fracture zone below. During pumping, this water

returns to the borehole, resulting in dewatering of this seepage zone and a reduction in the rate of drawdown.

No significant boundary conditions can be observed. Since this borehole is drilled through a shear zone, it is possible to have both matrix (primary) porosity in the gouge material as well as fracture (secondary) permeability through the fault system.

The recovery of the borehole was monitored for 252 minutes. The semi-log time-residual drawdown curve indicates that the rate of recovery decreases towards the end of the test. The recovery shows that the borehole have fully recovered before t/t' = 2, hence dewatering seems not to have taken place.

The calculated transmissivity values are presented in Table 4.9. The early time transmissivity was calculated from 1.5 to 7 minutes, when the derivative curve indicates radial flow conditions exist prior to the water level reaching the seepage zone at 25 m. Late time transmissivity was calculated from 70 to 360 minutes of the time-drawdown curve, after leakage from the matrix, or dewatering of the seepage zone, reaches pseudo steady-state. The sustainable yield calculated on the basis of the various methods is shown in Table 4.10. The various parameters for each of these methods are listed in Table 4.7.

Table 4-9 Transmissivity values for X12-02

Borehole Number	T_{early} (m^2/d)	T_{late} (m^2/d)	$T_{recovery}$ (m^2/d)
X12-02	1.4	1.9	0.9

Table 4-10 Recommended borehole yield values for X12-02

Method	m^3/d
Late T	75.7
Drawdown to boundary	12.1
Distance to boundary	6.1
Flow characteristic	60.0
Max. Drawdown	15.0

The sustainable yield for the borehole X12-02 varies from 6 to 76 m^3/d for the different methods. The distance and drawdown to boundary methods could not be adequately applied since no boundary conditions were observed, hence these methods provide underestimates of yield. The flow characteristic method estimate of 60 m^3/d is considered to be the best approximation since all the parameters can be defined and a conservative approach is adopted.

Borehole X12-03

The main water strike occurred at 97m in a deep fracture yielding 0.3 l/s. The static water level is at 1.61m below surface, giving an available drawdown of 95.4m. A pumping test was carried out at 0.61l/s for 540minutes.

The semi-log drawdown curve displays a horizontal line after 20 min, which is indicative of significant recharge, or can be associated with the early part of a double porosity aquifer system. At this point the water level drops below a fractured basalt into a weathered basalt and seepage was encountered during drilling. This suggests that the flattening of the drawdown curve could be related to the initiation of unconfined conditions in the weathered zone. Since the water level is significantly higher than the seepage zone, it probably gained water through the borehole from the confined fracture zone below at 97 m. Once this

weathered zone begins to release water to the borehole, a reduction in the rate of drawdown occurs. Such a system can be described as a double porosity or leaky, confined aquifer system.

The derivative curve, however, shows a steep increase after 200 minutes, indicating that boundary conditions have been reached, or that the late time of a double porosity system is encountered.

The recovery test shows that after 112 minutes since pumping stopped, at t/t' = 6, no residual drawdown remains, indicating that significant leakage from the weathered zone has taken place.

Table 4.11 presents the calculated transmissivity values for this borehole and the recommended yields by the various methods are shown in Table 4.12.

Table 4-11 Transmissivity values for X12-03

Borehole Number	T_{early} (m^2/d)	T_{late} (m^2/d)	$T_{recovery}$ (m^2/d)
X12-03	0.8	0.8	0.7

Table 4-12 Recommended borehole yield values for X12-03

Method	m^3/d
Recovery	44.2
Flow characteristic	47

Since no boundaries were encountered only the flow characteristic and recovery methods could be applied. These suggest that the recommended sustainable yield is approximately $45m^3$/day.

Borehole X12-04

A water strike of 1.2l/s was encountered at 62m. A 2m open cavity was observed at 47 and 48m, above the main water strike. The static water level is at 11.08m, giving an available drawdown of 50.92m. The pump was set at 17.43m and the borehole was pumped for 720 minutes at a rate of 0.80 l/s. Due to the presence of the dry cavity, it is expected that significant water losses occur from the borehole and that the yield is significantly higher than that recorded.

The semi-log drawdown curve suggests the aquifer is of the double porosity type. The calculated transmissivity values for boreholes X12-04 are presented in Table 4.13.

Table 4-13 Transmissivity values for X12-04

Borehole Number	T_{early} (m^2/d)	T_{late} (m^2/d)	$T_{recovery}$ (m^2/d)
X12-04	8.3	12.4	12.2

Only the flow characteristic method could be applied to estimate sustainable yield, since no boundary conditions were observed. The estimated yield is 145 m^3/d.

Borehole X12-05

Seepage was encountered at 18 and 32 m, with the main water strike of 0.1 l/s at 66m. The static water level was at 13.95m, giving an available drawdown of 52m. The pump was set at 29.06m and the borehole was pumped for 360 minutes at a rate of 0.48 l/s.

The semi-log plot of the time–drawdown curve shows radial flow without boundary effects, until pump suction was reached at approximately 120 minutes. An inflection point is seen at 4 m of drawdown, where the water level reaches the first seepage zone. The increased rate of drawdown thereafter suggests that this seepage zone contributes water to the borehole, consequently, the early time transmissivity was calculated from 2-9 minutes. The calculated early and late time transmissivity are listed in Table 4.14.

The recovery of borehole X12-05 was monitored for 210 minutes ($t/t' = 3.3$), at which time the water level recovered to within 0.02m of the original static water level.

Since no boundary conditions were encountered, the drawdown to boundary and distance to boundary methods could not be applied. The sustainable yield estimates varied from 20-28m^3 d (Table 4.15).

Table 4-14 Transmissivity values for X12-05

Borehole Number	T_{early} (m^2/d)	T_{late} (m^2/d)	$T_{recovery}$ (m^2/d)
X12-05	1.6	0.9	0.7

Table 4-15 Recommended borehole yield values for X12-05

Method	m^3/d
Flow characteristic	20
Max. Drawdown	22
Recovery	28

Borehole X12-08

The main water strike occurred at 53m, with seepage at 19m. The blow yield was measured to be 2 l/s. The static water level was at 7.86m, giving an available drawdown of 45m. The pump was set at 12.43m and the borehole pumped at 720 minutes at a rate of 1.86 l/s.

The semi-log plot of the time-drawdown curve exhibits a horizontal line, separated by an early and late drawdown curve. The shape of the curve suggests a double porosity aquifer system, with leakage affecting the late time drawdown, since this segment has a smaller slope.

The calculated early and late time transmissivity values for boreholes X12-08 are presented in Table 4.16. Recommended borehole yields estimated by various methods are in Table 4.17.

Table 4-16 Transmissivity values for X12-08

Borehole Number	T_{early} (m^2/d)	T_{late} (m^2/d)	$T_{recovery}$ (m^2/d)
X12-08	11.9	39.1	9.5

Table 4-17 Recommended borehole yield values for X12-08

Method	m^3/d
Late T	348
Flow characteristic	450

Since no boundary conditions were encountered, the drawdown and distance to boundary methods could not be applied. The sustainable yield is estimated to range from 350-450 m^3 d.

however, this cannot be verified, as it is significantly higher than the rate at which the borehole was tested.

Borehole X12-09

Seepage strike occurred at 12m and the main water strike of 1.2 l/sec was attained at 40m. The static water level was at 4.34m, giving an available drawdown of 35.66m. The pump was set at 21.43m. The borehole could only be pumped for 30 minutes at a rate of 0.55 l/s before pump suction was reached.

The semi-log time-drawdown curve indicates that a closed boundary condition is encountered after 9 minutes. The derivative of drawdown curve suggests that the aquifer is a finite fracture and that radial flow conditions are never encountered.

The recovery test of borehole X12-09 was monitored for 300 minutes and the water level recovered to within 0.30m of the original static water level. An extrapolation of recovery suggests that the borehole will not fully recover by t/t' = 1, hence dewatering seems to have taken place. Calculated transmissivities are shown in table 4-18, and sustainable yields are in table 4-19. The sustainable yield varies from 3 to 14 m^3/day, and is probably around 8 m^3/day. However, this low yield is anomalous given the blow yield. It is possible that significant water losses are occurring to the formation, since highly fractured meta-basalts, which were not water bearing, occurred at 96 m.

Table 4-18 Transmissivity values for X12-09

Borehole Number	T_{early} (m^2/d)	T_{late} (m^2/d)	$T_{recovery}$ (m^2/d)
X12-09	1.9	0.3	1.8

Table 4-19 Recommended borehole values for X12-09

Method	m^3/d
Late T	8.6
Drawdown to boundary	7.2
Distance to boundary	8.2
Flow characteristic	2.9
Max. Drawdown	14

Conclusions

Table 4-20 is a summary of the results of the constant discharge tests in relation to the calculated transmissivities, blow yield, sustainable yield and pressure head.

Table 4-20 Results of the seven constant discharge rate tests.

B/H No.	T_{early}/T_{late} (m^2/day)	Sustainable Yield (m^3/d)	Blow Yield (l/s)	Sustainable Yield (% blow yield)	Pressure head (m)
X12-01	132/64	685	10	79	32.62
X12-02	1.4/1.9	60	1.0	69	55
X12-03	0.8/0.8	47	0.3	181	95.4
X12-04	8.3/12.4	145	1.2	140	50.92
X12-05	1.6/0.9	20	0.1	232	52
X12-08	13.1/39.1	400	2.0	232	45
X12-09	1.9/0.3	8	1.2	8	35.66

4.9 Evaluation of Climatic Data

Only one rainfall station occurs in close proximity to the study area: Badplaas police station, 10 km from the study area. The distribution of estimated mean annual precipitation (MAP) of the study area is shown in Figure 4-29.

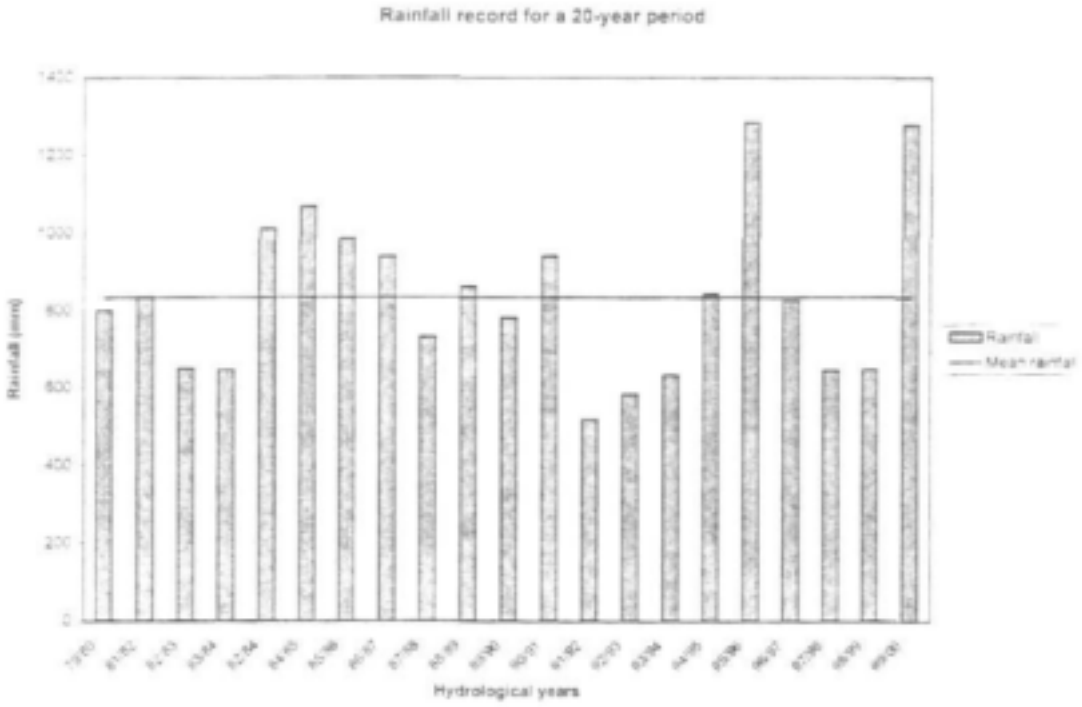

Figure 4-29 Annual time series of rainfall of Badplaas hydrological station.

The MAP of the study area calculated on the basis of Figure 4-29 is 834.1mm. This figure is not significantly different from 836mm recorded by Midgley et al. (1990). The monthly rainfall distribution in the area is characterised by summer rainfall and almost dry winter seasons (Figure 4-30). Mean annual S-pan evaporation is 1632mm (Midgley et. al., 1990), distributed monthly as shown Figure 4-31.

4.10 Financial Analysis

The financial analysis compared two different scenarios:

- Scenario 1 is based on historic drilling records as recorded in the NGDB, which are assumed to represent random drilling or boreholes. In the study area 219 boreholes have been drilled, of which 71% have no recorded discharge, 15% yield water and 145 are recorded as dry. For this investigation, only boreholes with a recorded discharge were considered, giving a success rate of 50%. This success record was used to estimate the number of holes and associated costs required to establish 10 yielding boreholes.

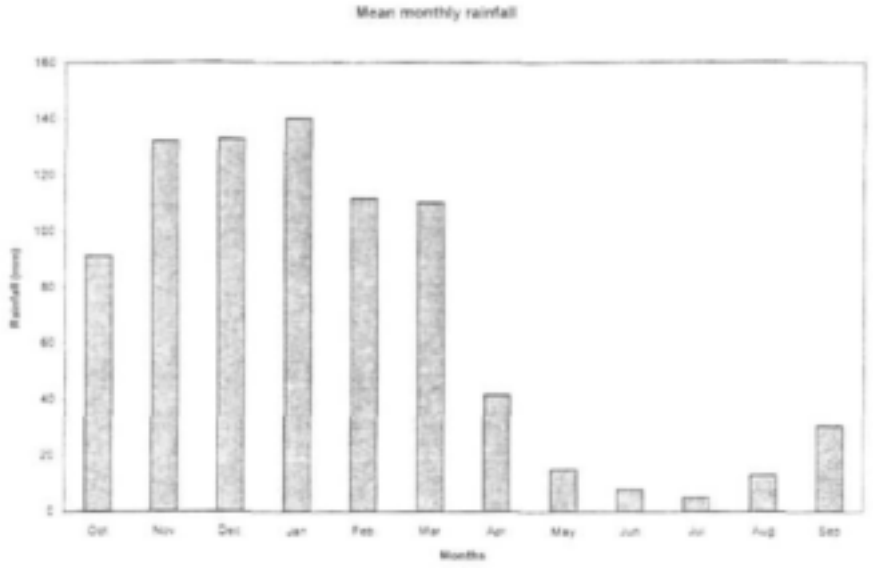

Figure 4-30 Mean monthly rainfall distribution, based on data recorded at the Badplaas Police Station.

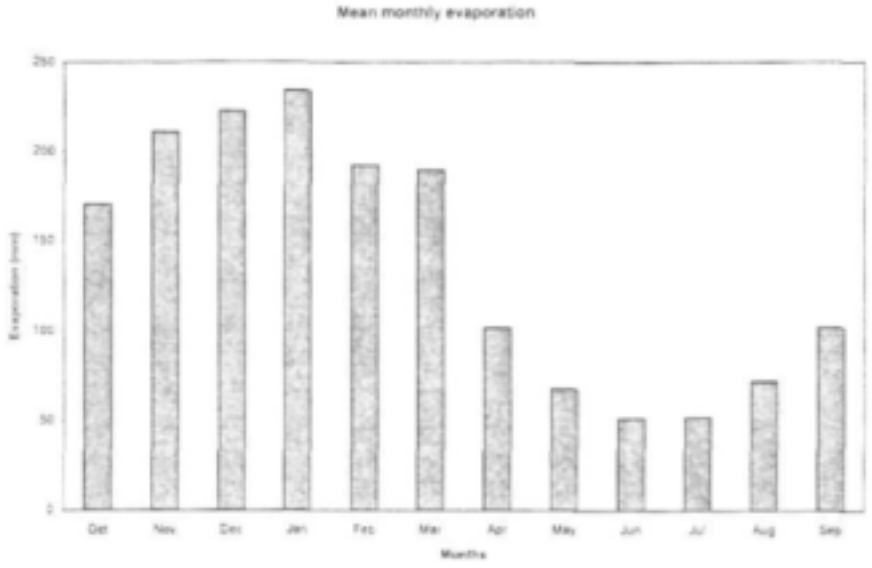

Figure 4-31 Mean monthly distribution of S-pan evaporation at Badplaas Police station.

- Scenario 2 is based on the methodology adopted for this project, where geophysical methods (MAX-MIN EM, Magnetic and Electrical Soundings), as well as geological observations, were used to site boreholes on lineaments identified from LANDSAT and aerial photo interpretation, and field observations. The investigation drilled 9 holes, of which 8 were successful. Costs were extrapolated to estimate costs required to achieve 10 yielding boreholes so that they could be compared to scenario 1.

ITEM		Units	Rate	Scenario 1		Scenario3	
				Qty	Cost	Qty	Cost
Desk Study[1]	EXPLORATION	Day	1600			5	8000
EM34 survey[2]		Day	1500				
Max Min survey[4]		Day	2500			5.5	13750
Resistivity survey[3]		Day	2500			5.5	13750
Geophysical interp.		Line	100			33	3300
Accommodation		Day	150			11	1650
LANDSAT image[5]		Each	2500			1	2500
LANDSAT interp.		Day	1200			3	3600
Structural mapping[6]		Day	1350			3	4050
Sub total - Exploration					0		50600
Community liaison[7]		Hr	100	20[10]	2000	11[11]	1100
Drilling[8]		Hole	11000	20	220000	11	121000
Drill supervision		Day	1000	20	20000	11	11000
TOTAL					242000		183700
Per successful site					24200		18370
Median yield		L/s			0.4		1.0
R/l/s per site					60500		18370

Historic success rates have resulted in an expenditure of approximately R24200 for the establishment of each successful borehole. If at least R50 000 were expended on geologically based, success rates of nearly 90% could be expected: hence the drilling budget could be greatly reduced. Expenditure would then be about R18500 per successful borehole.

This analysis suggests that a more comprehensive exploration program and a larger exploration budget could in the long-term result in significant cost savings, especially in large regional programs where the costs of regional geological exploration are spread over many boreholes. In such cases dedicating a larger proportion of the budget to exploration than is currently the case may result in more efficient drilling and a net reduction in establishment costs per site. For such an exploration program to be successful it must incorporate field geological mapping, remote sensing and appropriate geophysical based on identified hydrogeological regime.

In some cases, such as reticulated systems where production rates are more important than the number of water points established, it may be beneficial to evaluate program efficiency in terms of costs per unit yield of water. In the greenschists costs per unit yield are less relevant as the low yield of boreholes and the rugged topography constrain borehole schemes which supply several communities, hence the number of individual developed water sources is a more important indicator of success. Nevertheless, it is possible to measure the costs of water production in terms of R/l/s of water produced. Minimal exploration (scenario 1) results in costs of R60500/l/s of water produced. The data suggests that the proposed methodology would reduce production costs to R18500/l/sec.

4.11 Conclusions and Recommendations

The geology of the area consists of impermeable granites and meta-basalts (i.e. basalt metamorphosed at a low grade to an amphibolite schist or greenschist). The granites contain widespread quartz veining, which often fill the fractures, hence the granitic plutons are poor

geological terrains for groundwater exploration. The meta-basalts are the best targets for groundwater exploration, especially when fractured by faults and dykes.

The following conclusions can be drawn regarding the potential of structures in the study area:

- Fractures follow a distinct joint set, with four dominant strike orientations: NW – SE, N – S, E-W and NE – SW. This joint pattern is exhibited by various morphological features in the Barberton greenstone belt, which include gorges, straight valleys and other depressions that are surface expression of buried structural features. The N-S to NE-SW faults show evidence of being in a dip-slip setting and hence being open structures, however, the E-W and NW joints are dominant in terms of frequency.

- The best geological features for groundwater exploration in the Barberton Greenstone Belt are the NNE tending dip-faults. E-W strike-slip faults have also been shown to be water bearing and are associated with formation of deep open cavities that enhance the permeability of the greenstones.

- The joint analysis of the study area shows that lineaments that have a NW – SE strike direction is more likely to be compressional and therefore closed. The E-W striking lineaments are more likely to be strike-slip faults and are also the hydrogeological targets if there is no shear zone associated with the lineament.

- The shear zones also proved to be of low potential due to the generated clay minerals, which reduces the transmissivity of the sheared greenstones.

- Aerial photographs and LANDSAT imagery indicate that NW trending lineaments are the longest and most frequent structures, however, these represent Archean shears or pre and post Transvaal dykes under present day compression. Hence they are poor targets. Longer NE trending lineaments represent Archean compressional structures rejuvenated as shears; these are moderately high yielding structures. Shorter structures trending more to the NNE represent dip-slip structures under present day extension. Remote sensing should therefore target the north-easterly trending structures.

- The dykes and sills do not seem to be important groundwater exploration targets in the study area. This is proven by low yielding holes that were sunk through the dyke contacts that were thought to be fractured. This can be associated with the compressional nature of diabase dyke contacts. Dolerite dykes in granite batholiths also proved to be low yielding.

- The electromagnetic method was able to detect water bearing structural features, which appeared as ridge of valley discontinuities.

In conclusion, the research study showed that successful groundwater exploration for the study area is possible. An evaluation of structural geology and hydrogeology conditions of the area with suitable geophysical methods for the environment increased the success rate from 50% to over 80%. High yielding holes are limited to major faults with deep open cavities that are located in the greenstones.

4.12 References

Andreoli, M. A. G., Doucoure M., Van Bever Donker J., Brandt, D. and Andersen, N.J.B. (1996). Neotectonics of Southern Africa – a review. *Africa geoscience*, vol **3**, 1, pp 1- 16.

Anhaeusser, C.R., Robb, L.J. and Viljoen, M.J. (1981). Provisional geological map of Barberton greenstone belt and surrounding granitic terrane, eastern Transvaal and swaziland. Geol. Soc. of S.A., Scale 1:250 000.

Anheausser, C.R. (1986). Archean gold mineralisation in the Barberton Mountain Land. In: Mineral deposits of Southern Africa. P 113 – 154.

Cleverly, R.W. and Bristow, J. W. (1979). Revised volcanic stratigraphy of the Lebombo monocline. *Trans. Geol. Soc. S. Africa*, vol **82**, pp 227 – 230.

Davis, G.H. (1984). Structural geology of rocks and regions. John-Willey & Sons, New York, pp 491.

de Ronde, C.E.J. and de Wit, M. (1994). Tectonic history of the Barberton greenstone belt, S.A.: 490 million years of Archean crustal evolution. *Tectonics*, vol **13**, 4, pp 983 – 1005.

de Wit, M.J. (1982). Gliding and overthrust nappe tectonics in the Barbeton greenstone belt. *Journal of Structural geology*, vol **4**, pp 117 – 136.

de Wit, M.J., Fripp, R.E.P. and Stanistreet, I.G. (1983). Tectonic and stratigraphic implications of new field observations along the southern part of Barberton greenstone belt. Spec. Publi. Geol. Soc. S. Africa, 9, pp 21 – 29.

de Wit, M. J. (1986). Extensional tectonics during igneous emplacement of the mafic-ultramafic rocks of the Barberton greenstone belt. Lunar and Planetary Institute Technical Report No. 86-10, pp 84 – 85.

de Wit, M.J., Roering, C., Hart, J.R. Armstrong, R.A., de Ronde, C.E.J., Green, R.W.E., Tredoux, M., Peberdy, E. And Hart, R.A. (1992). Formation of an Archean continent. *Nature*, vol. **357**, pp 553 –562.

Driscoll, F.G. (1986). Groundwater and Wells , 2nd edition. Johnson Division, St. Paul, Minnesota.

Flinn, D. (1962). On folding during 3-D progressive deformation. Q. J. Geol. Soc. London, vol **135**, pp291 – 305.

Heubeck, C. and Lowe D.R. (1999). Sedimentary petrography and provenance of Archean Moodies Group, Barberton greenstone belt. *Geol. Soc. of America*, Special paper 329.

Heubeck, C., Wendt, J.I., Toulkeridis, T., Kroner, A. And Lowe, D.R. (1993). Timing of deformation of the Archean Barberton greenstone belt, S.A. *Tectonics*, vol **13**, pp 1514 – 1536.

Kisters, A.F.M.and Anhaeusser, C.R. (1994). The structural significance of the Stynsdorp pluton and anticline within the tectono-magmatic framework of the Barberton Mountain Land, S.A. Economic Geology Research Unit Information Circular no. 279.

Kruseman, G.P. and de Ridder, N.A. (1994). Analysis and evaluation of pumping test data. ILRI publicationj 47, Wageningen, The Netherlands.

Lageat, Y. and Robb, L. J. (1984). The relationship between structural landforms, erosion surfaces and the geology of the Archean granite basement in the Baberton region, eastern Transvaal. *Transactions of the Geol. Soc. of S.A.*, vol **87**, 2, pp 141 – 159.

Low, A.B. and Rabelo, A. (1996). Vegetation of S.A., Lesotho and Swaziland. Special publication of the Dept of Environmental Affairs and Tourism, Pretoria.

Lowe, D.R. (1999). Geological evolution of the Barberton greenstone belt and vicinity. Geol. Soc. of America, Special paper 329.

Lowe, D.R., Byerly G.R. and Heubeck, C. (1999). Structural divisions and development of the west central part of the Barberton greenstone belt. Geol. Soc. of America, Special paper 329.

Lowe, D.R. and Nochita, B.W. (1999). Foreland basin sedimentation in the Mapepe Formation, southern-facies Fig Tree Group. Geol. Soc. of America, Special paper 329.

Midgley, D.C., Pitman, W.V. and Middleton, B.J. (1994). Surface Water Resources of S.A., Water Research Commission Report No. 298/6.1/94, Vol **VI**, eds 1.

Nochita, B.R. and Lowe, D.R. (1990). Fan delta Sequence in the Archean Fig Tree Group, Barberton greenstone belt, S.A. *Precambrian Research*, vol **48**, pp 375 – 393.

Ramsay, J.G. (1963). Structural investigations in the Barberton Mountain Land, eastern Transvaal. *Transactions of the Geol. Soc. of S.A.*, vol **66**, pp 353 – 401.

Ramsay, J.G. (1967). Folding and Fracturing of Rocks. Mc-Graw Hill, New York, pp 568.

Ramsay, J.G. and Huber, M. I. (1987). The techniques of Modern Structural Geology: vol 2, Folds and Fractures. Academic Press, London, pp 309 – 700.

Robb, L.J. (1983). The nature, origin and significance of Archean migmatites in the Barberton Mountain Land, A new approach in the assessment of early crustal evolution. In: Anhaesser C.R. (eds): Contributions to the geology of the Barberton Mountain Land, Special publications 9, The Geological Society of S.A.

SACS (South African Commitee on Stratigrphy) (1980). Stratigraphy of S.A., Part1. Lithostratigraphy of the Republics of S.A., South West Africa / Namibia and the Republics of Bophuthatswana, Transkei, Ciskei and Venda. Geological Survey of S.A. Handbook 8, pp 690.

Sami, K. and Murray, E.C. (1997). Guidelines for the evaluation of Water Resources for the development with an emphasis on groundwater. Water Research Commission, Pretoria, S.A.

Sami, K , Crail, C. and Prinsloo, M. (1998). Groundwater exploration in sections 16 & 17 – Maputo Corridor Road. Unpublished Report Number 1998-0070, Council for Geoscience, Pretoria.

Tankard, A.J., Jackson, M.P.A., Erikson, K.A., Hobday, D.K., Hunter, D.R. and Minter, W.E.L (1982). Crustal evolution of Southern Africa. pub. By Springler-Verlag, New York, Heidelberg, Berlin.

Van Zijl, J.S.V. (1985). A practical manual on the resistivity method. CSIR Report K79, CSIR, Geophysics Division, Pretoria, S.A.

Van Zijl, J.S.V. and Kostlin, E.O. (1985). The electromagnetic method. Soth African Geophysical Association, Witwatersrand University, Johannesburg, pp 302.

Visser, D.J.L. (1989). The geology of the Republics of S.A., Transkei, Bophuthatswana, Venda and Ciskei and Kingdoms of Lesotho and Swaziland. Explanation of the 1:1000000 geological map, 4th edition, Geological Survey of S.A., Pretoria, S.A.

Ward, J.H.W. (1999). The metallogeny of the Barberton greenstone belt, S.A. and Swaziland. Memoir 86, Council for Geoscience, Prtoria, S.A.

Ward, J.H.W. (2001). The metallogeny of sheet 2530 Barberton, map explanation 1:250000 metallogenic series, Council for Geoscience, Pretoria.

Watkeys, M.K. and Sokoutis, D. (1998). Transtension in South Eastern Africa associated with Godwana break-up. In: Holdsworth, R.E., Strachan, R.A. and Dewey, J.F. (eds) (1998): Continental Transpressional and Transtensional Tectonics, Geol. Soc., London, Special publ., 135, pp 203 – 214.

APPENDIX 4-A
GEOPHYSICAL DATA

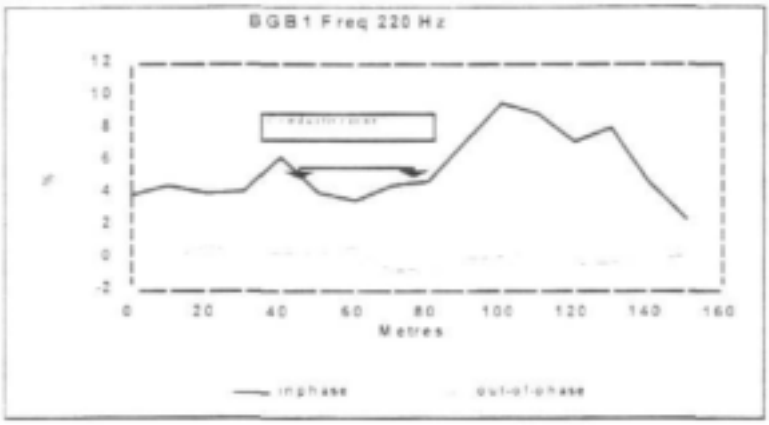
BGB1 Freq 220 Hz
%
12
10
8
6
4
2
0
-2
0
20
40
60
80
100
120
140
160
Metres
inphase
out-of-phase

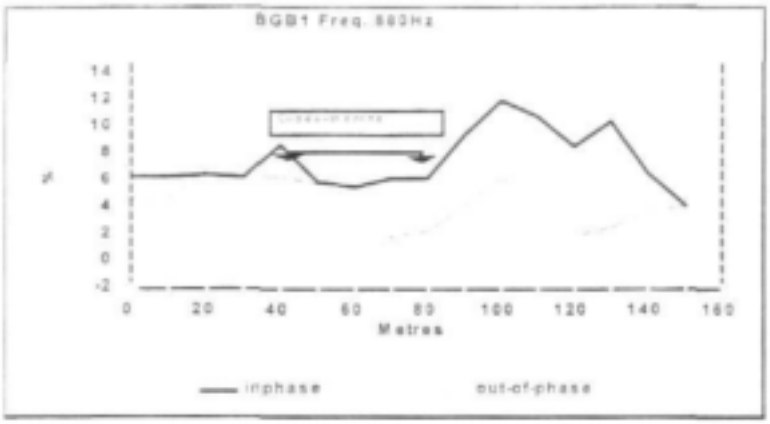
BGB1 Freq. 880Hz
%
14
12
10
8
6
4
2
0
-2
0
20
40
60
80
100
120
140
160
Metres
inphase
out-of-phase

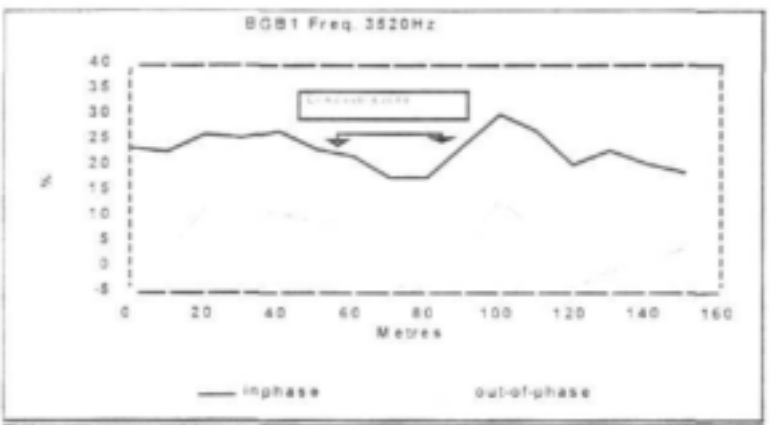
BGB1 Freq. 3520Hz
%
40
35
30
25
20
15
10
5
0
-5
0
20
40
60
80
100
120
140
160
Metres
inphase
out-of-phase

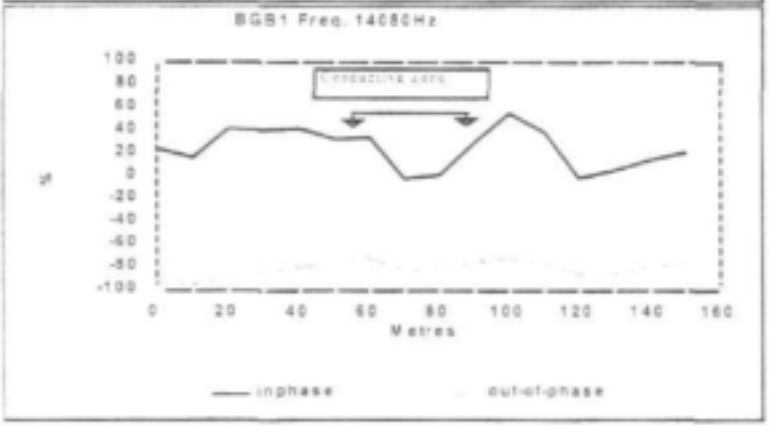
BGB1 Freq. 14080Hz
%
100
80
60
40
20
0
-20
-40
-60
-80
-100
0
20
40
60
80
100
120
140
160
Metres
inphase
out-of-phase

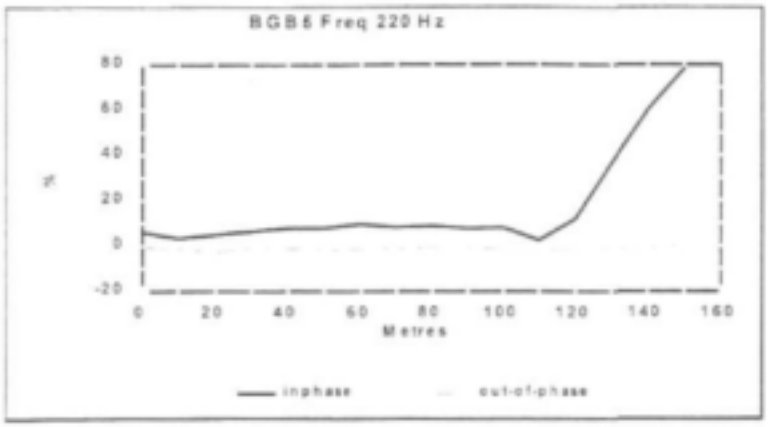
BGB5 Freq. 220 Hz
80
60
40
20
0
-20
0
20
40
60
80
100
120
140
160
Metres
inphase
out-of-phase

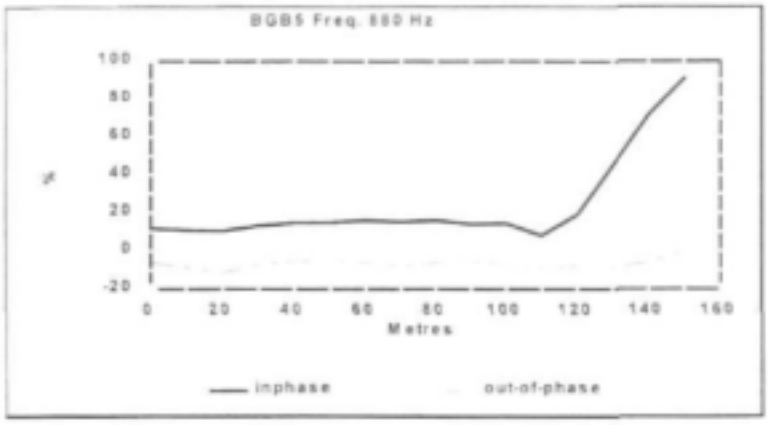
BGB5 Freq. 880 Hz
100
80
60
40
20
0
-20
0
20
40
60
80
100
120
140
160
Metres
inphase
out-of-phase

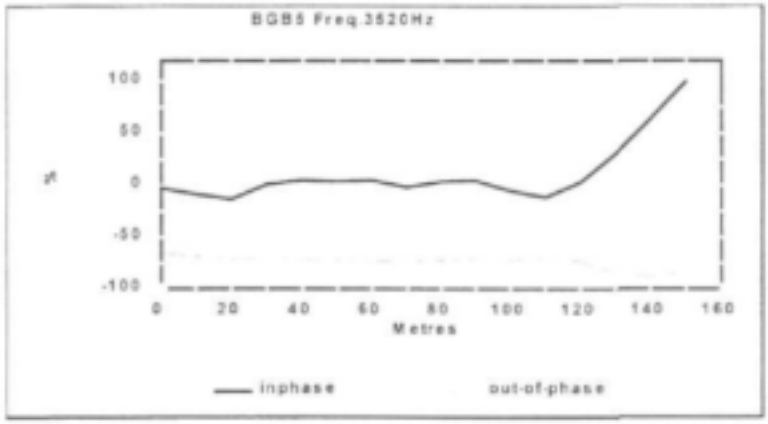
BGB5 Freq.3520Hz
100
50
0
-50
-100
0
20
40
60
80
100
120
140
160
Metres
inphase
out-of-phase

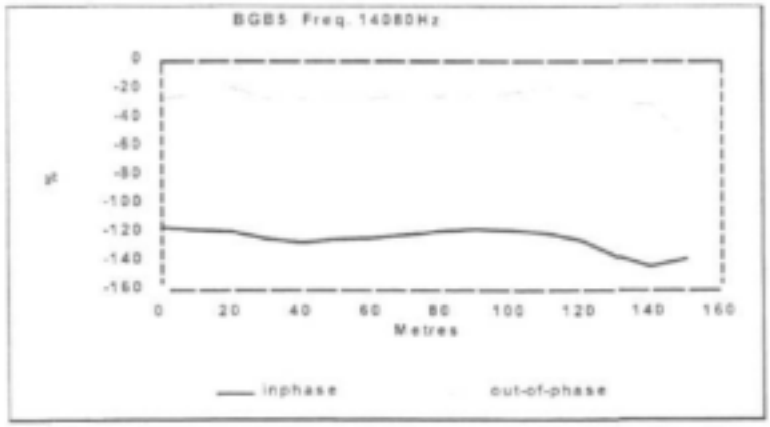
BGB5 Freq. 14080Hz
0
-20
-40
-60
-80
-100
-120
-140
-160
0
20
40
60
80
100
120
140
160
Metres
inphase
out-of-phase

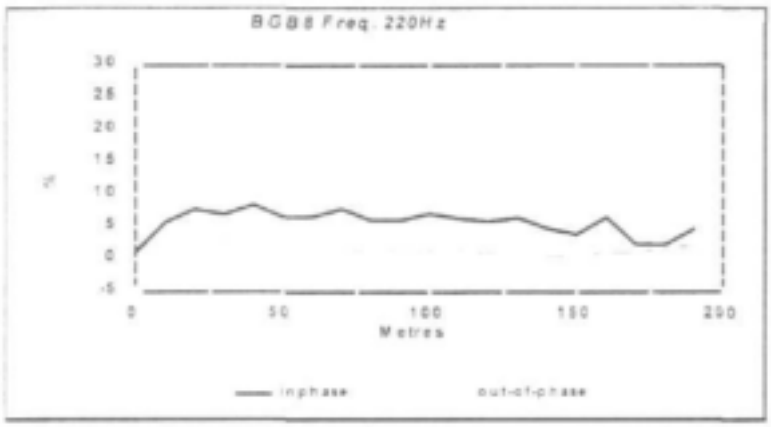
BGB8 Freq. 220Hz
30
25
20
15
10
5
0
-5
0
50
100
150
200
Metres
inphase
out-of-phase

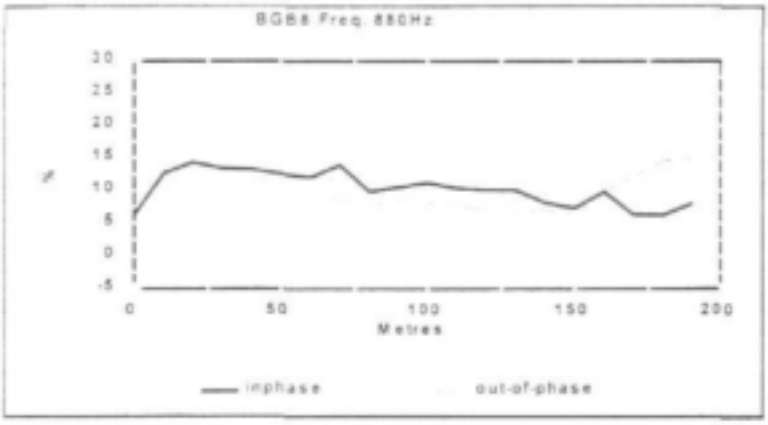
BGB8 Freq. 880Hz
30
25
20
15
10
5
0
-5
0
50
100
150
200
Metres
inphase
out-of-phase

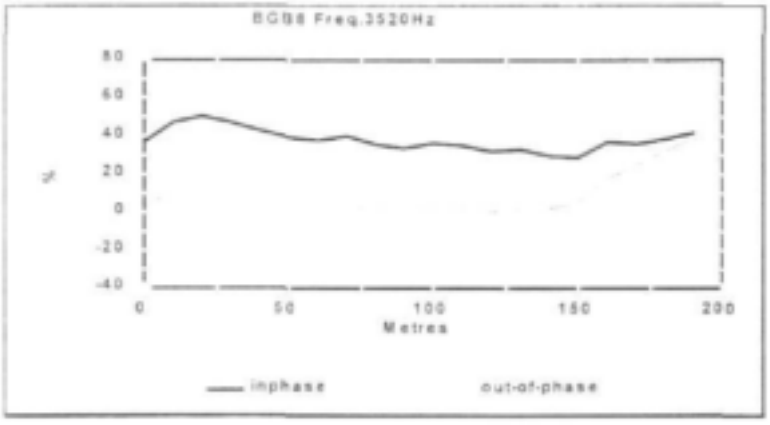
BGB8 Freq.3520Hz
80
60
40
20
0
-20
-40
0
50
100
150
200
Metres
inphase
out-of-phase

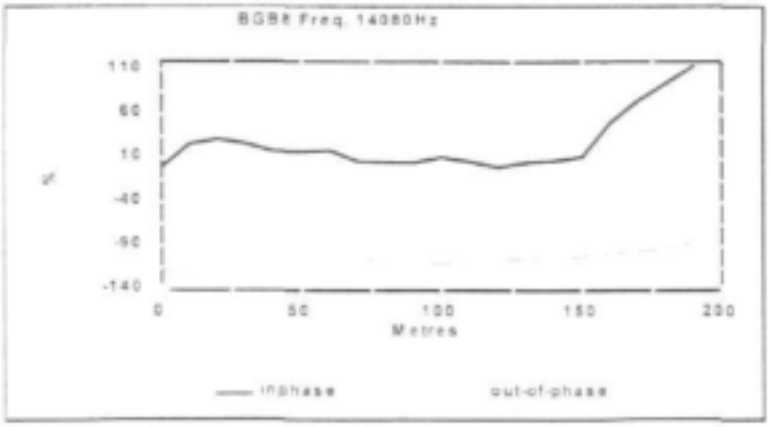
BGB8 Freq. 14080Hz
110
60
10
-40
-90
-140
0
50
100
150
200
Metres
inphase
out-of-phase

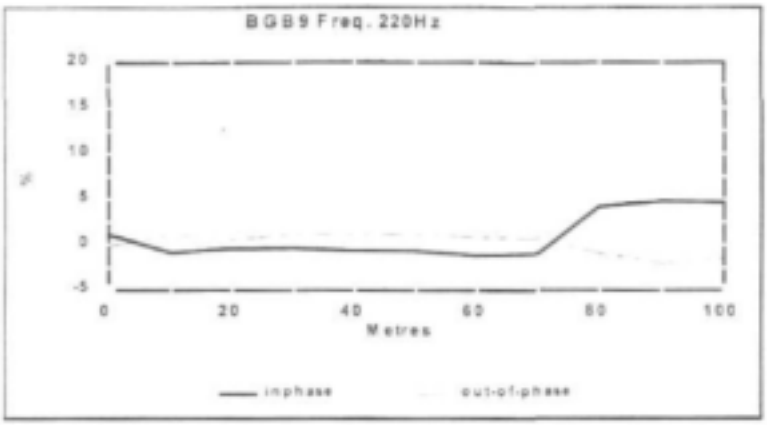
BGB9 Freq. 220Hz
20
15
10
5
0
-5
0
20
40
60
80
100
Metres
inphase
out-of-phase

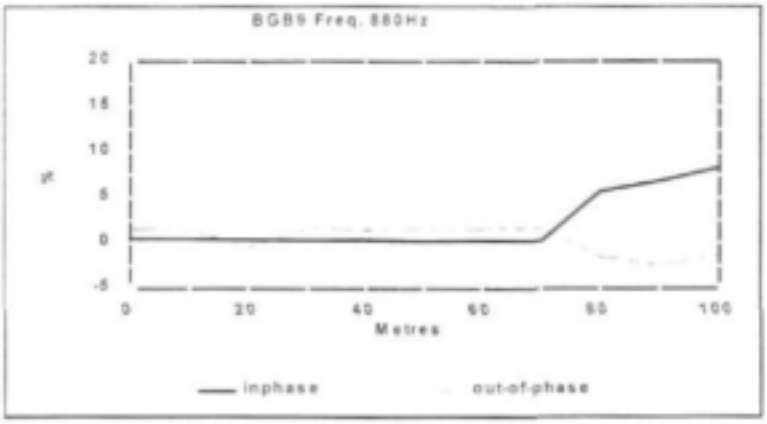
BGB9 Freq. 880Hz
20
15
10
5
0
-5
0
20
40
60
80
100
Metres
inphase
out-of-phase

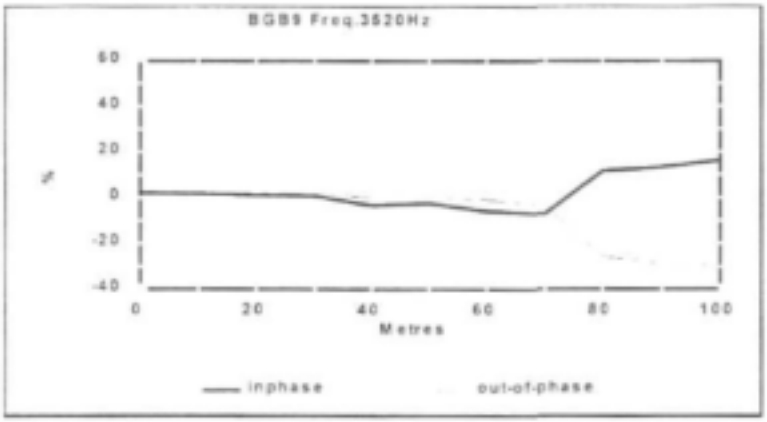
BGB9 Freq.3520Hz
60
40
20
0
-20
-40
0
20
40
60
80
100
Metres
inphase
out-of-phase

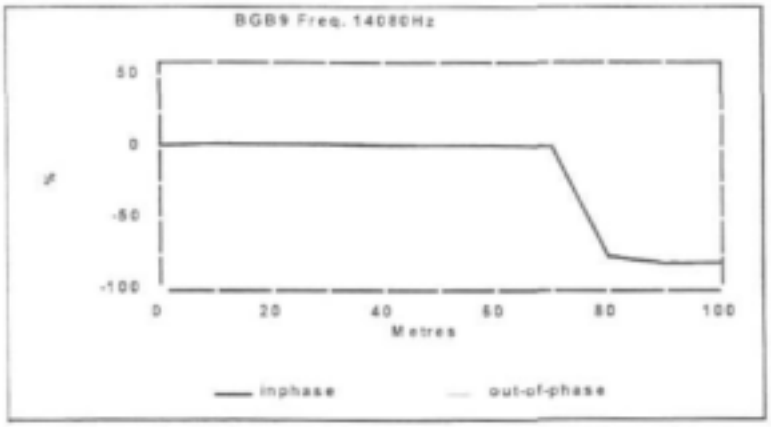
BGB9 Freq. 14080Hz
50
0
-50
-100
0
20
40
60
80
100
Metres
inphase
out-of-phase

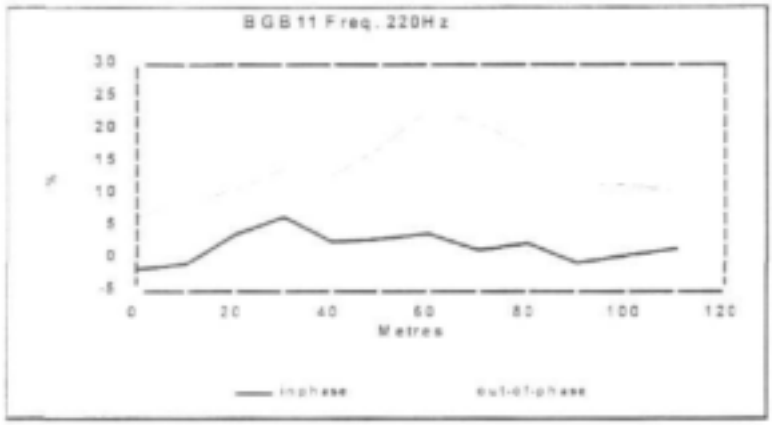
BGB11 Freq. 220Hz
30
25
20
15
10
5
0
-5
%
0
20
40
60
80
100
120
Metres
inphase
out-of-phase

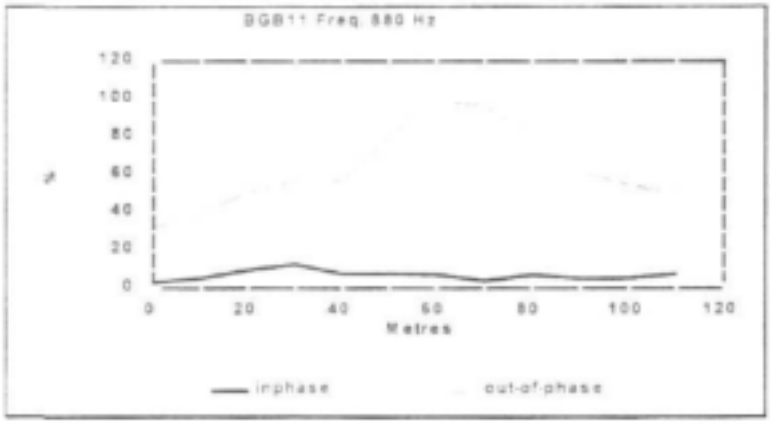
BGB11 Freq. 880 Hz
120
100
80
60
40
20
0
%
0
20
40
60
80
100
120
Metres
inphase
out-of-phase

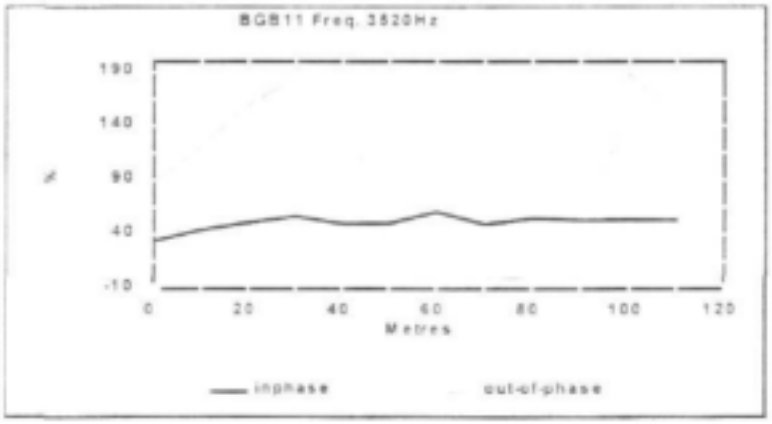
BGB11 Freq. 3520Hz
190
140
90
40
-10
%
0
20
40
60
80
100
120
Metres
inphase
out-of-phase

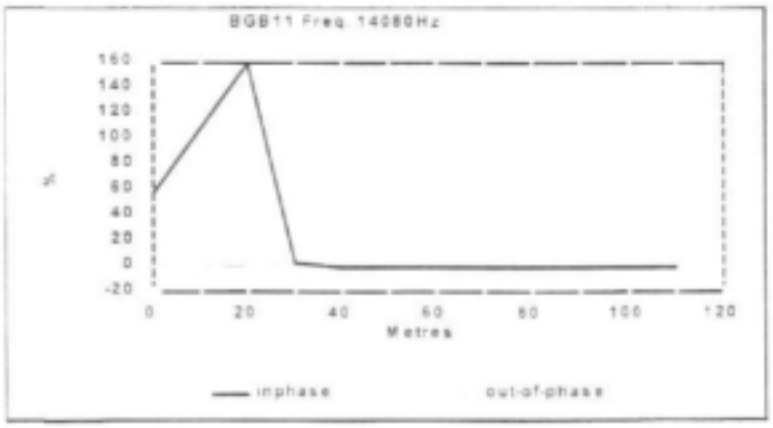
BGB11 Freq. 14080Hz
160
140
120
100
80
60
40
20
0
-20
%
0
20
40
60
80
100
120
Metres
inphase
out-of-phase

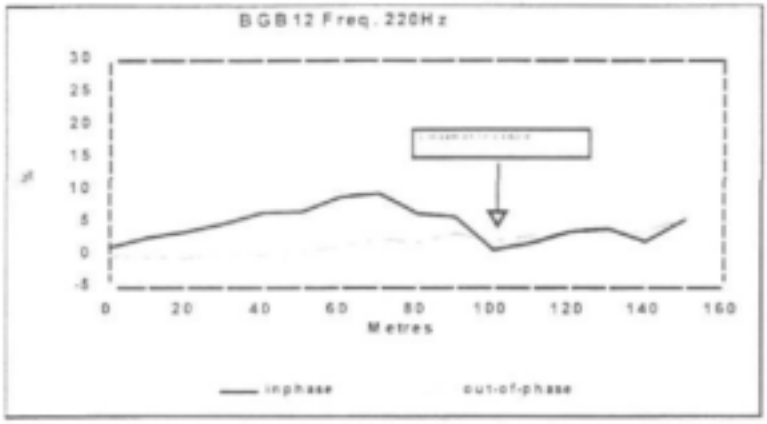
BGB12 Freq. 220Hz
30
25
20
15
10
5
0
-5
0
20
40
60
80
100
120
140
160
Metres
inphase
out-of-phase

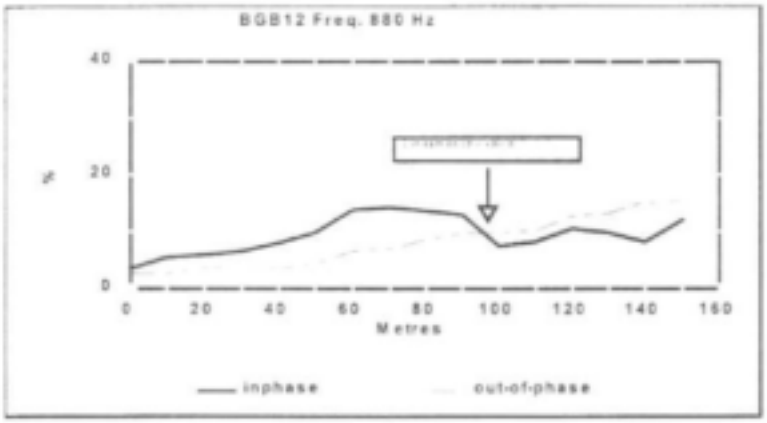
BGB12 Freq. 880 Hz
40
20
0
0
20
40
60
80
100
120
140
160
Metres
inphase
out-of-phase

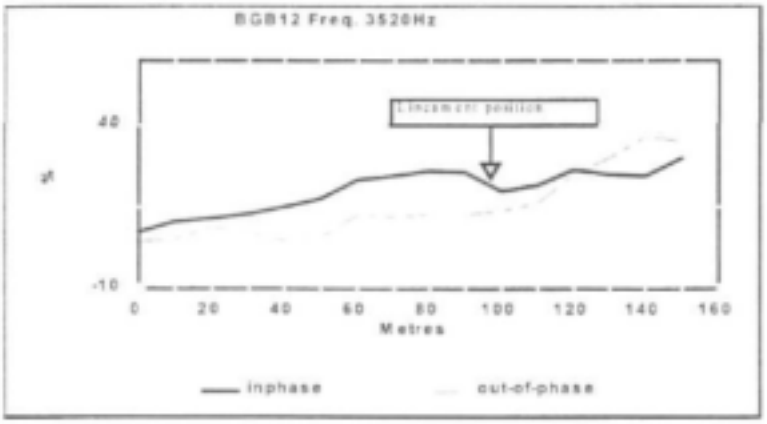
BGB12 Freq. 3520Hz
40
-10
0
20
40
60
80
100
120
140
160
Metres
inphase
out-of-phase

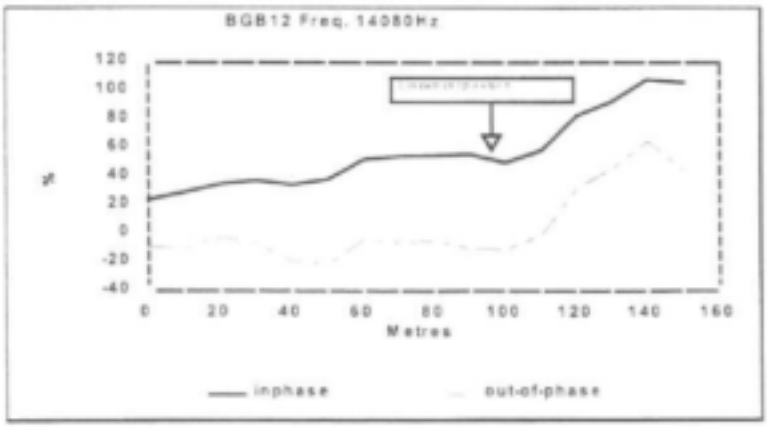
BGB12 Freq. 14080Hz
120
100
80
60
40
20
0
-20
-40
0
20
40
60
80
100
120
140
160
Metres
inphase
out-of-phase

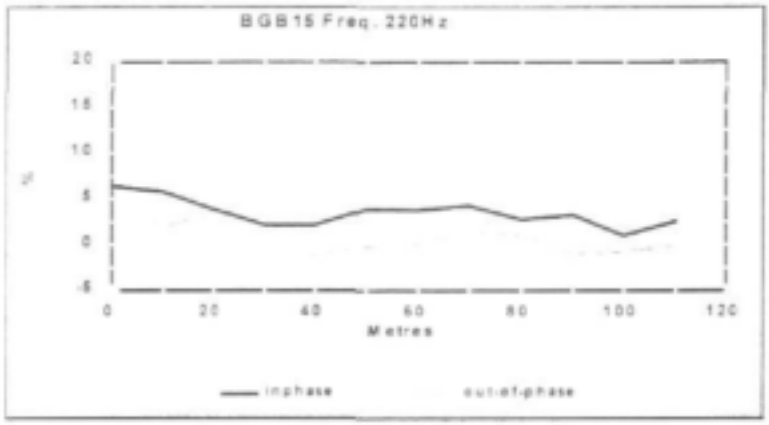
BGB15 Freq. 220Hz
20
15
10
5
0
-5
0
20
40
60
80
100
120
Metres
inphase
out-of-phase

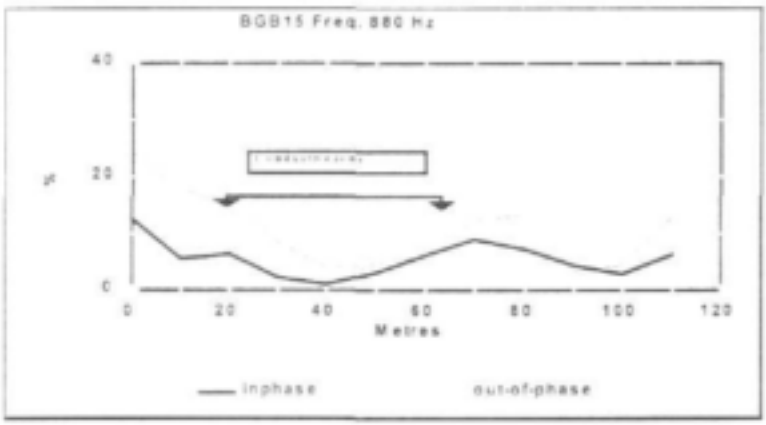
BGB15 Freq. 880 Hz
40
20
0
0
20
40
60
80
100
120
Metres
inphase
out-of-phase

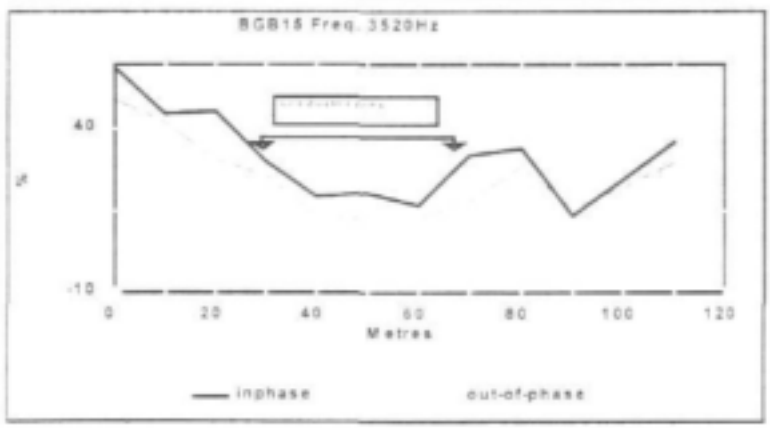
BGB15 Freq. 3520Hz
40
-10
0
20
40
60
80
100
120
Metres
inphase
out-of-phase

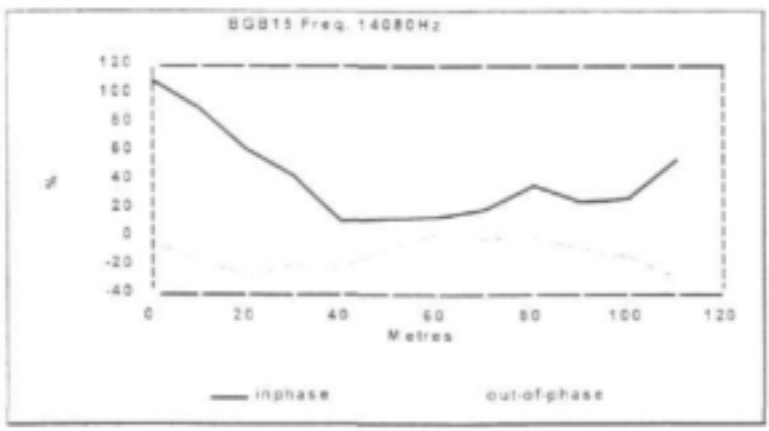
BGB15 Freq. 14080Hz
120
100
80
60
40
20
0
-20
-40
0
20
40
60
80
100
120
Metres
inphase
out-of-phase

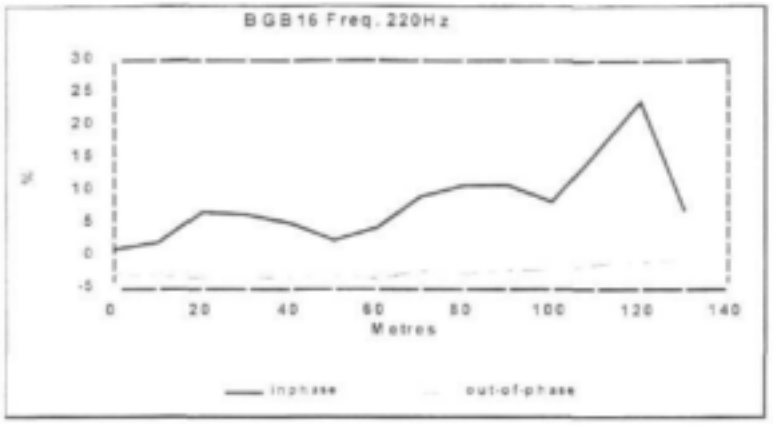
BGB16 Freq. 220Hz
30
25
20
15
10
5
0
-5
0
20
40
60
80
100
120
140
Metres
inphase
out-of-phase

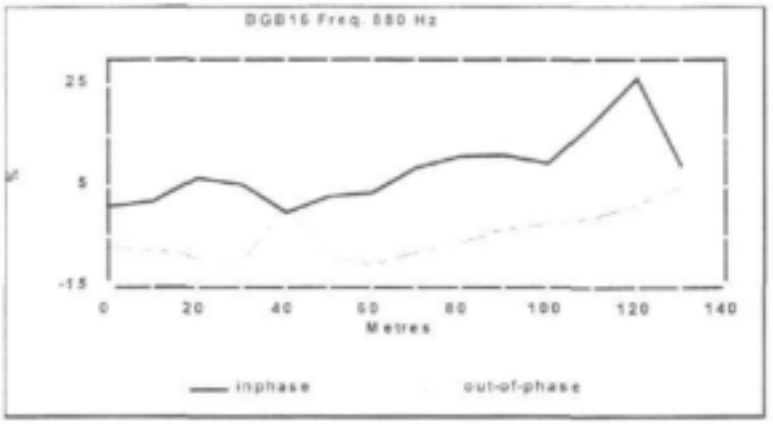
BGB16 Freq. 880 Hz
25
5
-15
0
20
40
60
80
100
120
140
Metres
inphase
out-of-phase

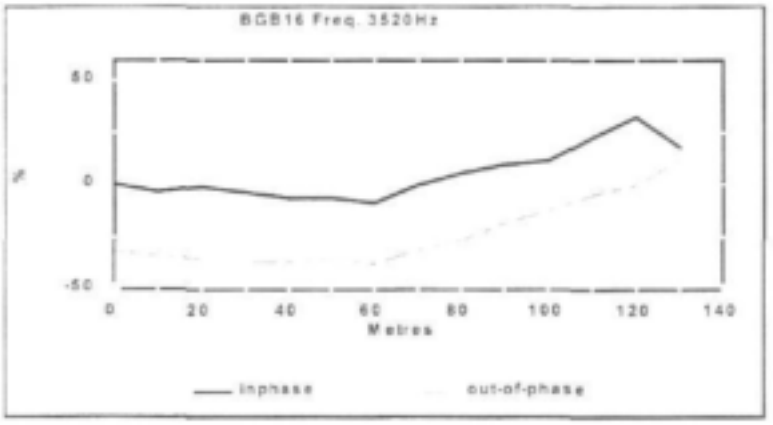
BGB16 Freq. 3520Hz
50
0
-50
0
20
40
60
80
100
120
140
Metres
inphase
out-of-phase

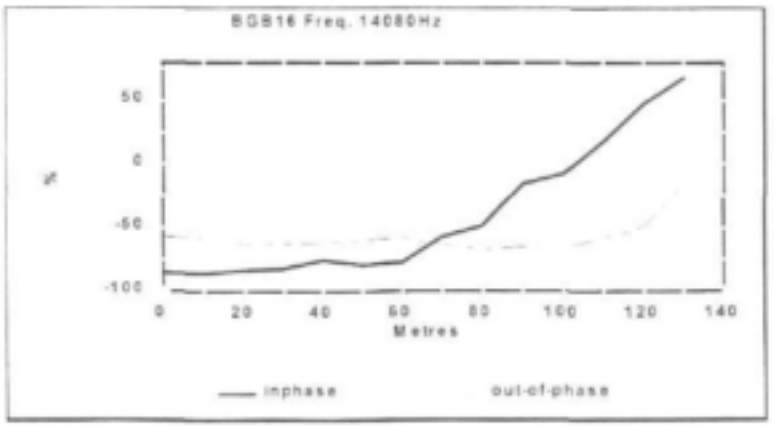
BGB16 Freq. 14080Hz
50
0
-50
-100
0
20
40
60
80
100
120
140
Metres
inphase
out-of-phase

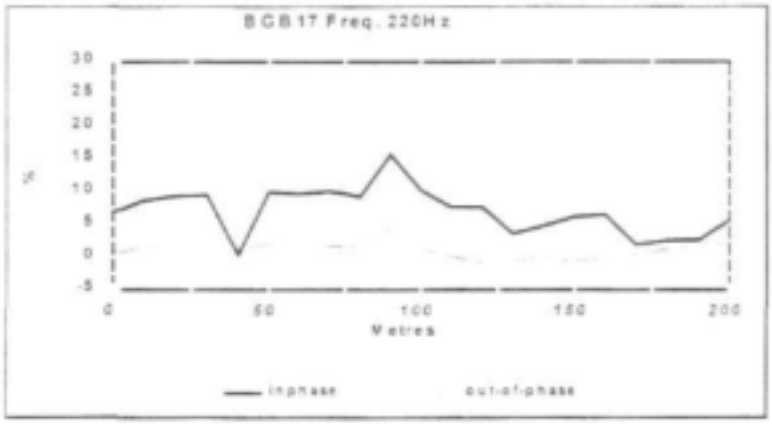
BGB17 Freq. 220Hz
30
25
20
15
10
5
0
-5
%
0
50
100
150
200
Metres
inphase
out-of-phase

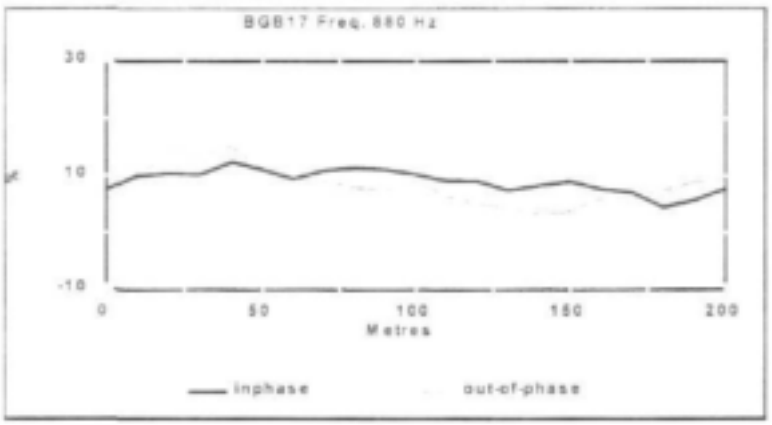
BGB17 Freq. 880 Hz
30
10
-10
%
0
50
100
150
200
Metres
inphase
out-of-phase

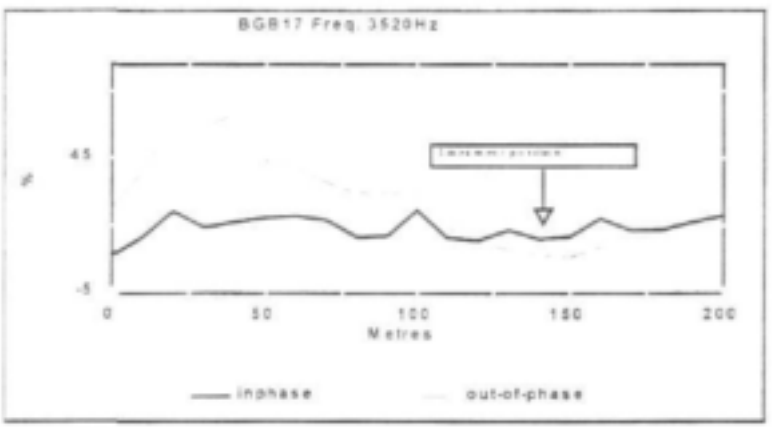
BGB17 Freq. 3520Hz
45
-5
%
0
50
100
150
200
Metres
inphase
out-of-phase

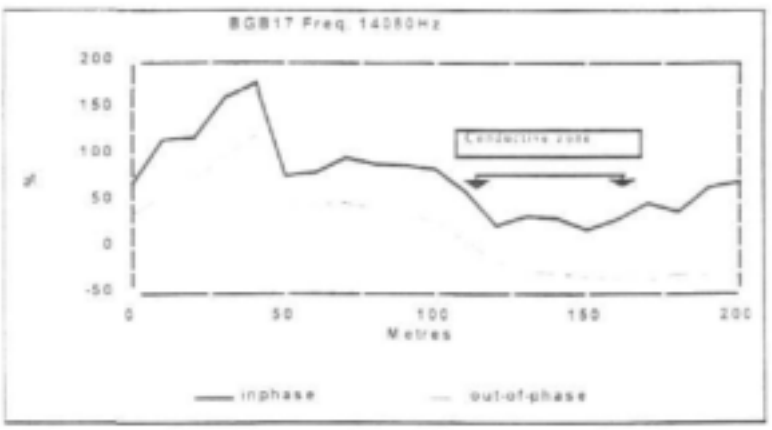
BGB17 Freq. 14080Hz
200
150
100
50
0
-50
%
0
50
100
150
200
Metres
inphase
out-of-phase

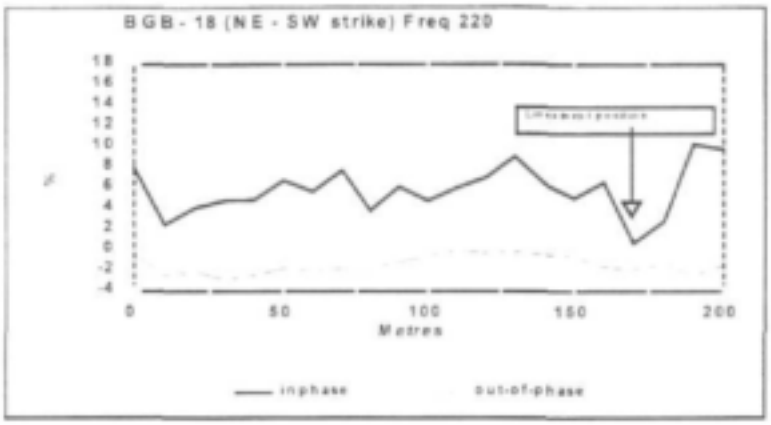
BGB - 18 (NE - SW strike) Freq 220
18
16
14
12
10
8
6
4
2
0
-2
-4
%
0
50
100
150
200
Metres
inphase
out-of-phase

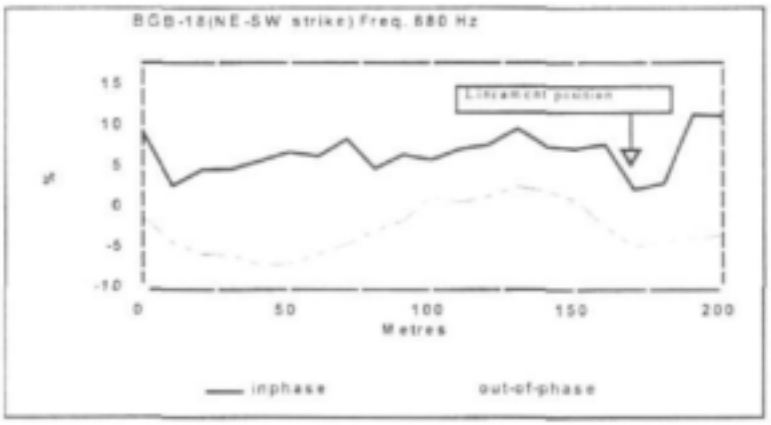
BGB-18(NE-SW strike) Freq. 880 Hz
15
10
5
0
-5
-10
%
0
50
100
150
200
Metres
inphase
out-of-phase

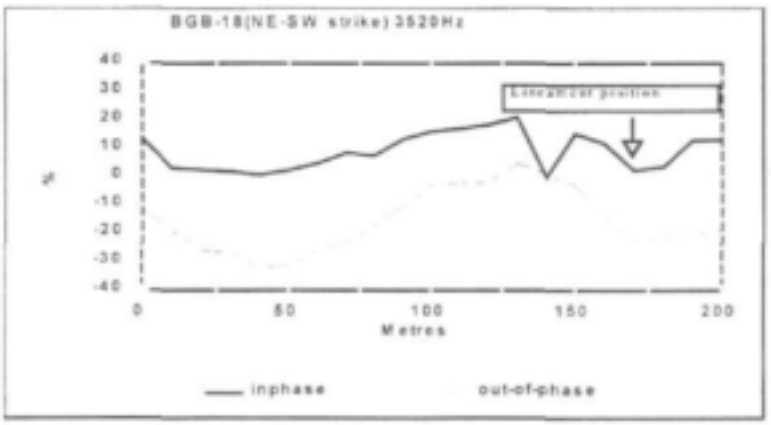
BGB-18(NE-SW strike) 3520Hz
40
30
20
10
0
-10
-20
-30
-40
%
0
50
100
150
200
Metres
inphase
out-of-phase

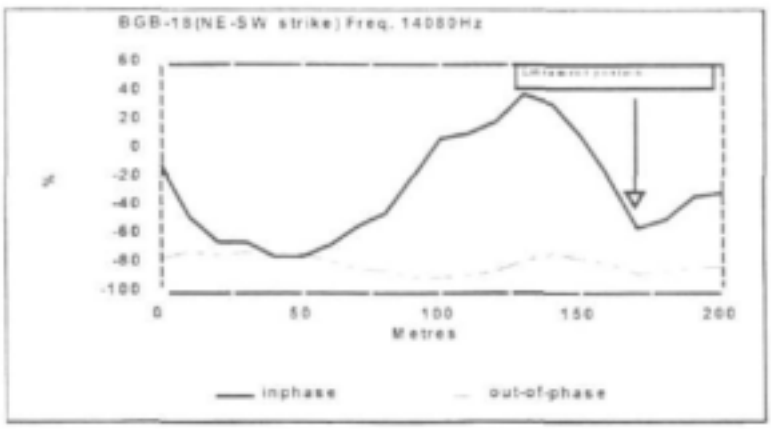
BGB-18(NE-SW strike) Freq. 14080Hz
60
40
20
0
-20
-40
-60
-80
-100
%
0
50
100
150
200
Metres
inphase
out-of-phase

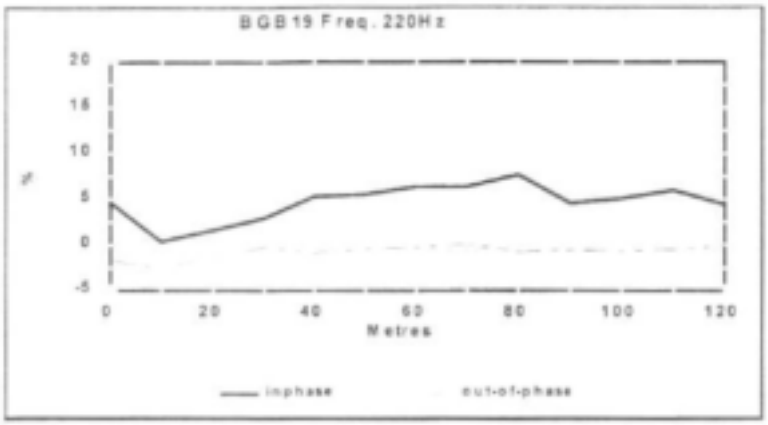
BGB19 Freq. 220Hz
20
15
10
5
0
-5
%
0
20
40
60
80
100
120
Metres
inphase
out-of-phase

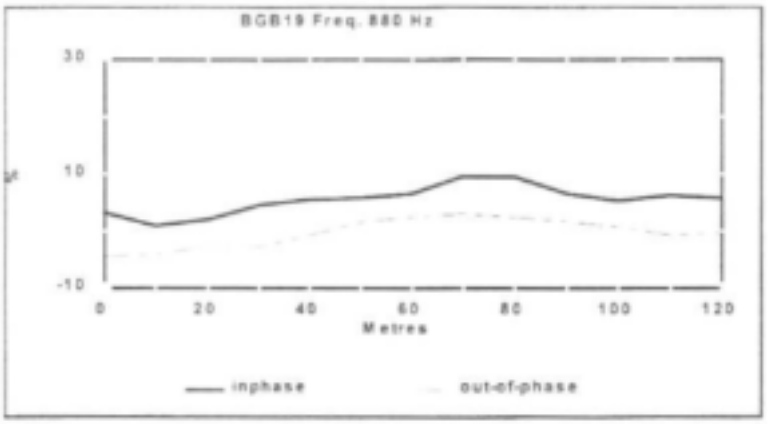
BGB19 Freq. 880 Hz
30
10
-10
%
0
20
40
60
80
100
120
Metres
inphase
out-of-phase

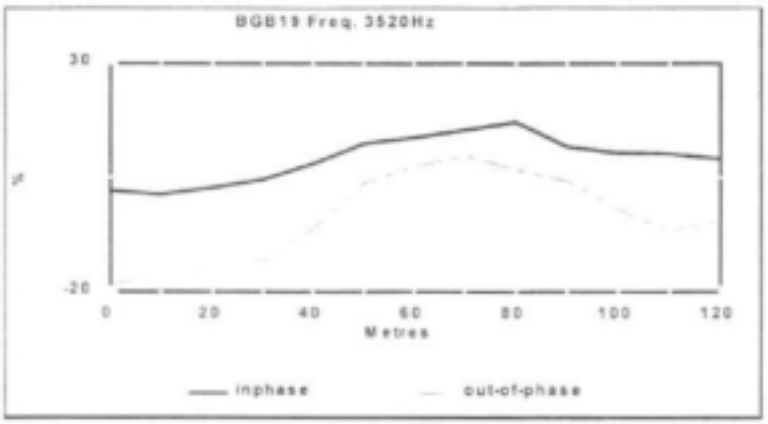
BGB19 Freq. 3520Hz
30
-20
%
0
20
40
60
80
100
120
Metres
inphase
out-of-phase

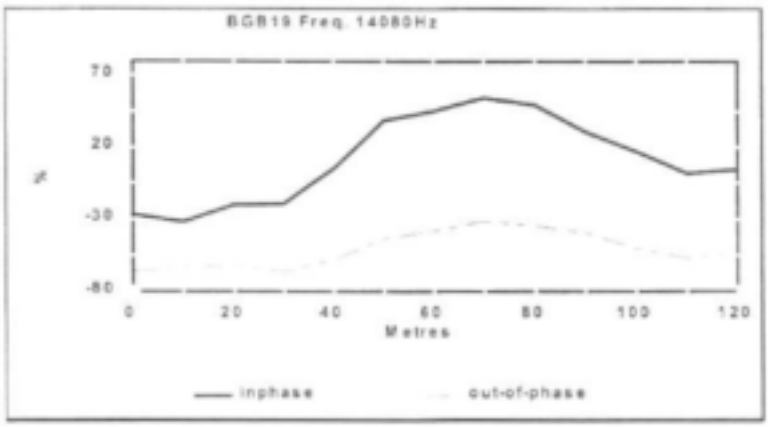
BGB19 Freq. 14080Hz
70
20
-30
-80
%
0
20
40
60
80
100
120
Metres
inphase
out-of-phase

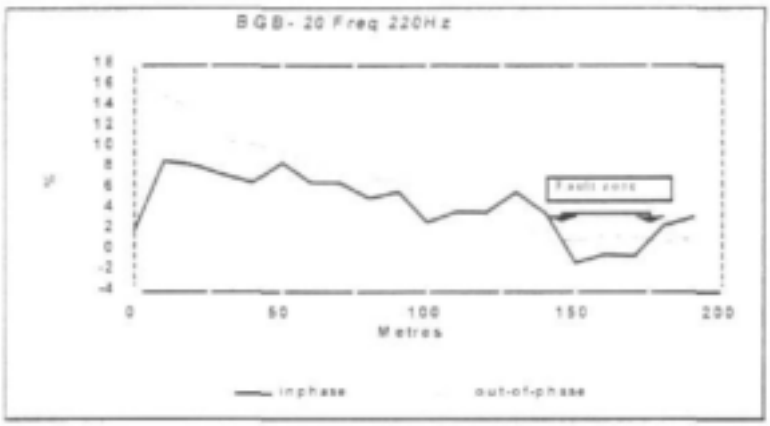
BGB- 20 Freq 220Hz
18
16
14
12
10
8
6
4
2
0
-2
-4
%
Fault zone
0
50
100
150
200
Metres
inphase
out-of-phase

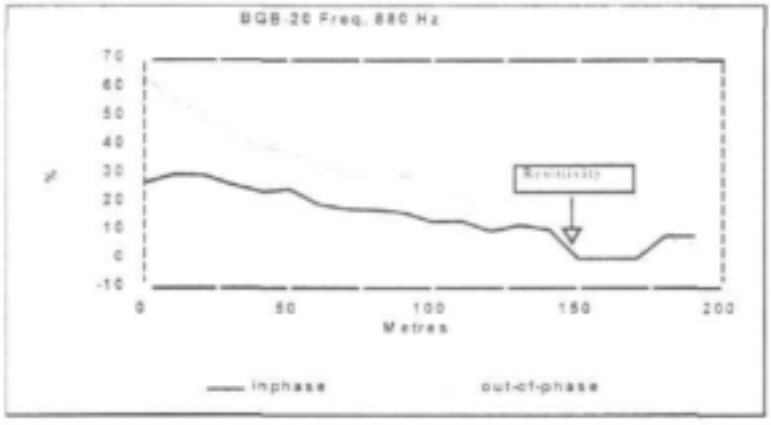
BGB-20 Freq. 880 Hz
70
60
50
40
30
20
10
0
-10
%
Resistivity
0
50
100
150
200
Metres
inphase
out-of-phase

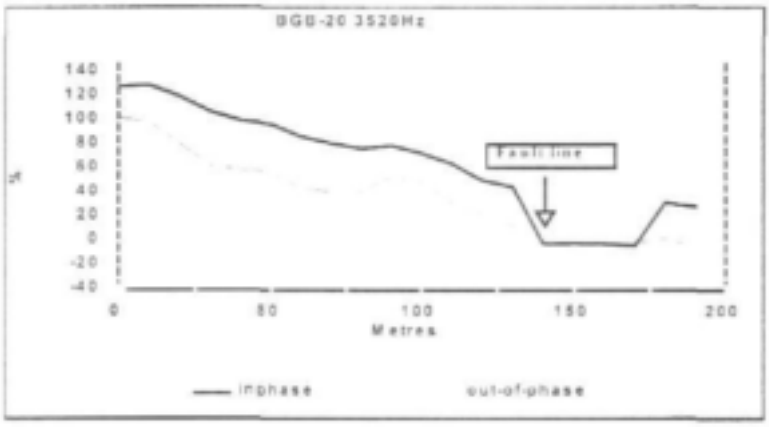
BGB-20 3520Hz
140
120
100
80
60
40
20
0
-20
-40
%
Fault line
0
50
100
150
200
Metres
inphase
out-of-phase

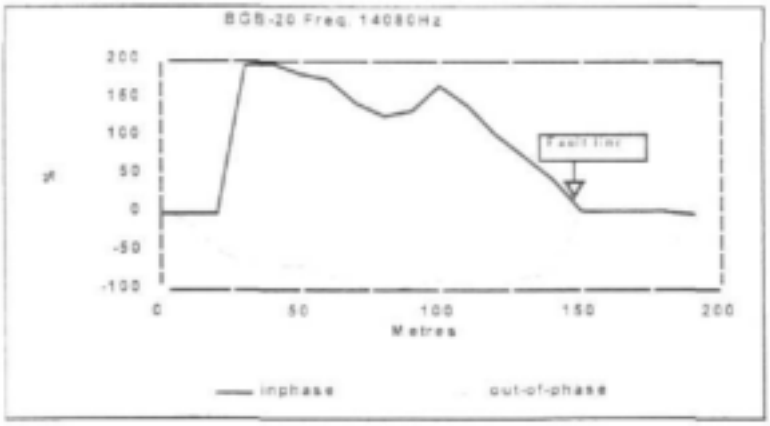
BGB-20 Freq. 14080Hz
200
150
100
50
0
-50
-100
%
Fault line
0
50
100
150
200
Metres
inphase
out-of-phase

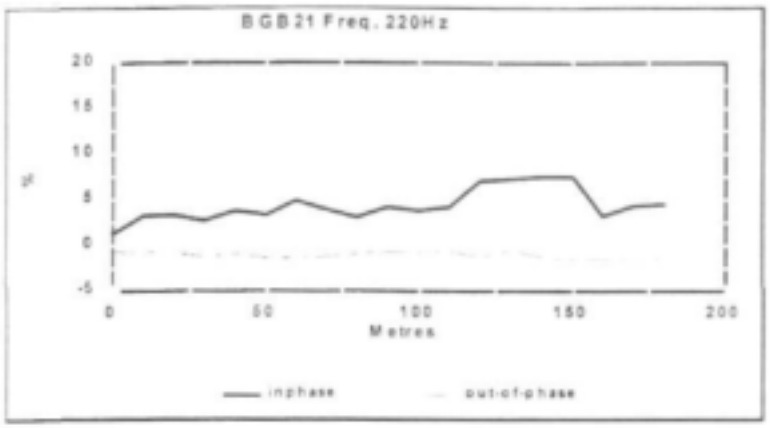
BGB21 Freq. 220Hz
20
15
10
5
0
-5
0
50
100
150
200
Metres
inphase
out-of-phase

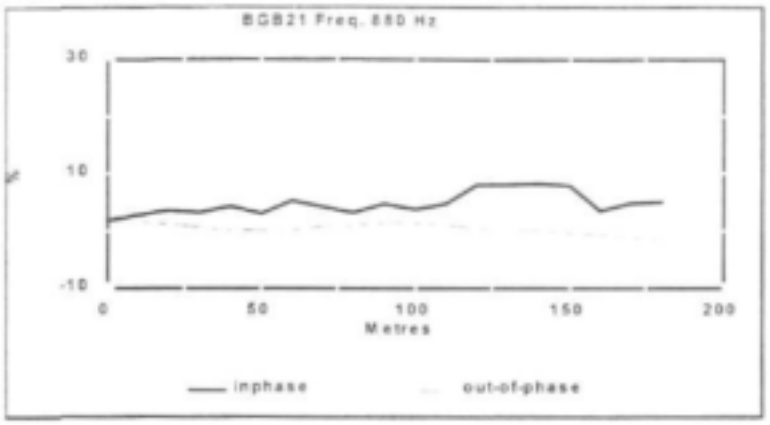
BGB21 Freq. 880 Hz
30
10
-10
0
50
100
150
200
Metres
inphase
out-of-phase

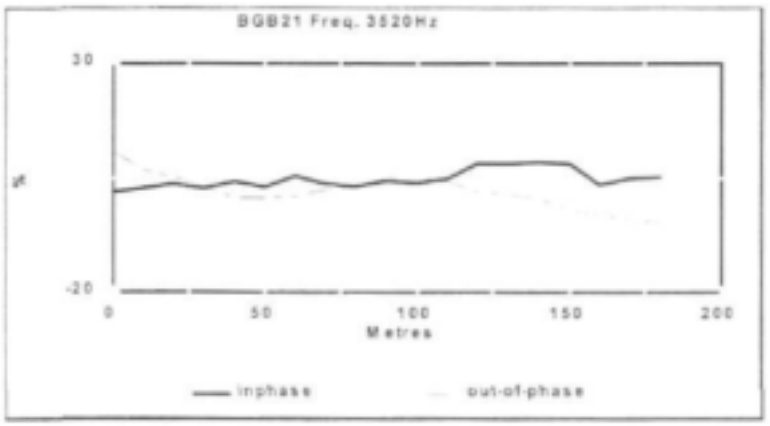
BGB21 Freq. 3520Hz
30
-20
0
50
100
150
200
Metres
inphase
out-of-phase

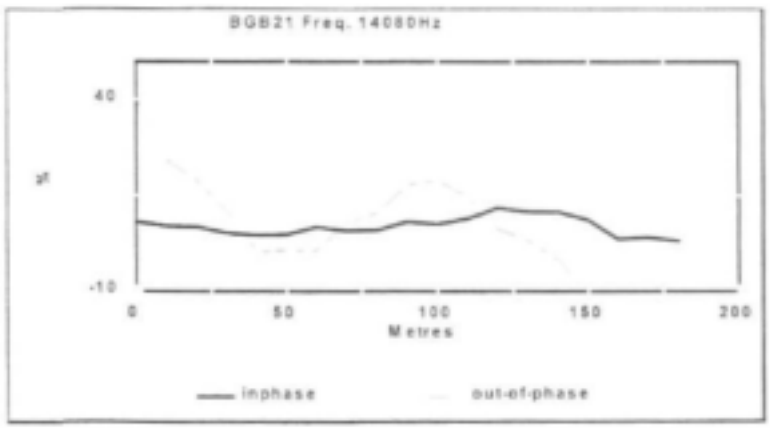
BGB21 Freq. 14080Hz
40
-10
0
50
100
150
200
Metres
inphase
out-of-phase

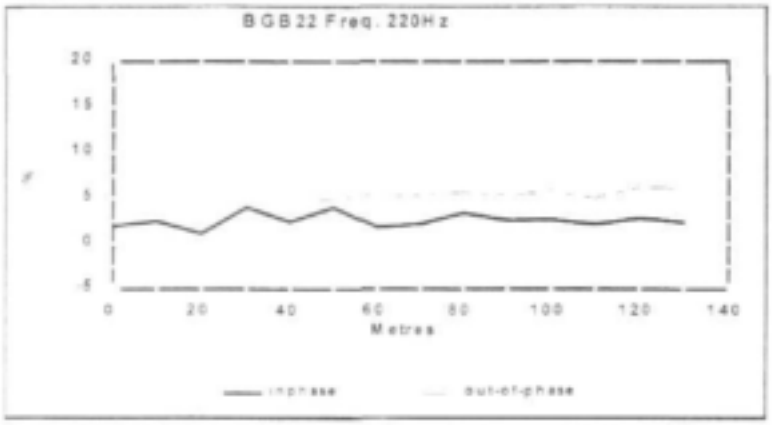
BGB22 Freq. 220Hz
20
15
10
5
0
-5
0
20
40
60
80
100
120
140
Metres
inphase
out-of-phase

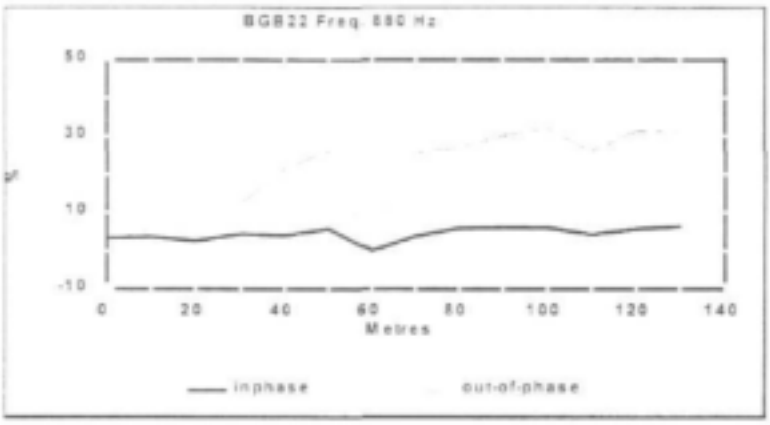
BGB22 Freq. 880 Hz
50
30
10
-10
0
20
40
60
80
100
120
140
Metres
inphase
out-of-phase

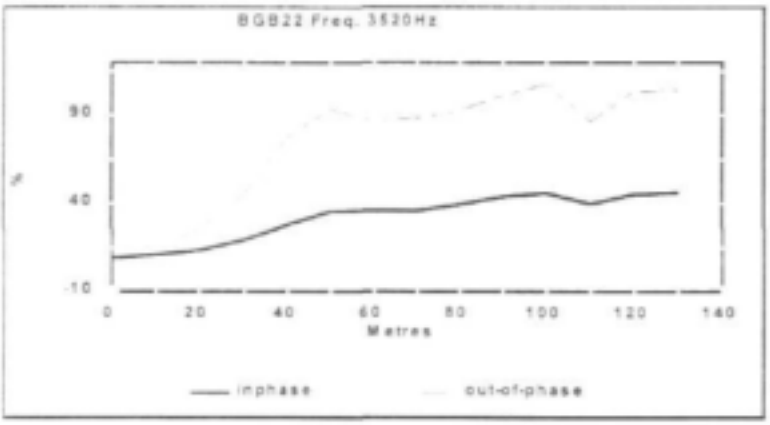
BGB22 Freq. 3520Hz
90
40
-10
0
20
40
60
80
100
120
140
Metres
inphase
out-of-phase

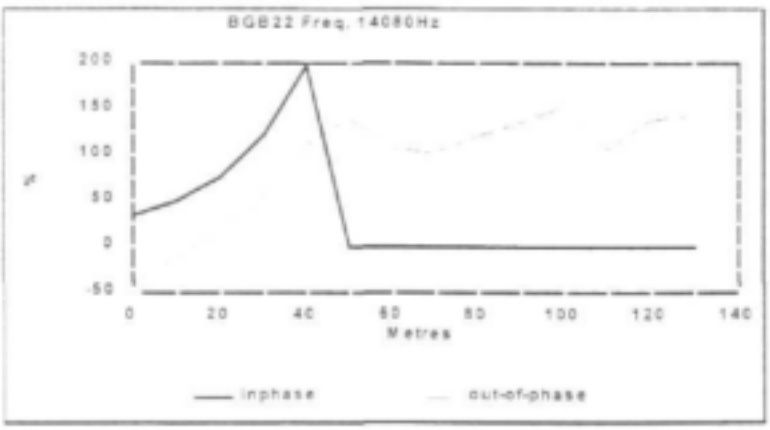
BGB22 Freq. 14080Hz
200
150
100
50
0
-50
0
20
40
60
80
100
120
140
Metres
inphase
out-of-phase

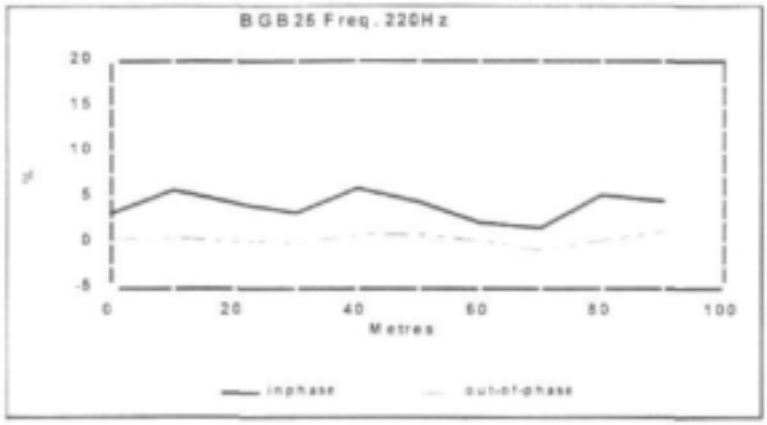
BGB26 Freq. 220Hz
20
15
10
5
0
-5
0
20
40
60
80
100
Metres
inphase
out-of-phase

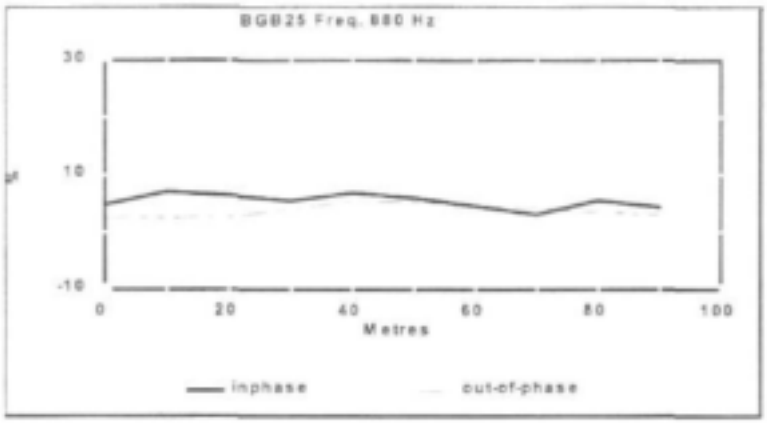
BGB25 Freq. 880 Hz
30
10
-10
0
20
40
60
80
100
Metres
inphase
out-of-phase

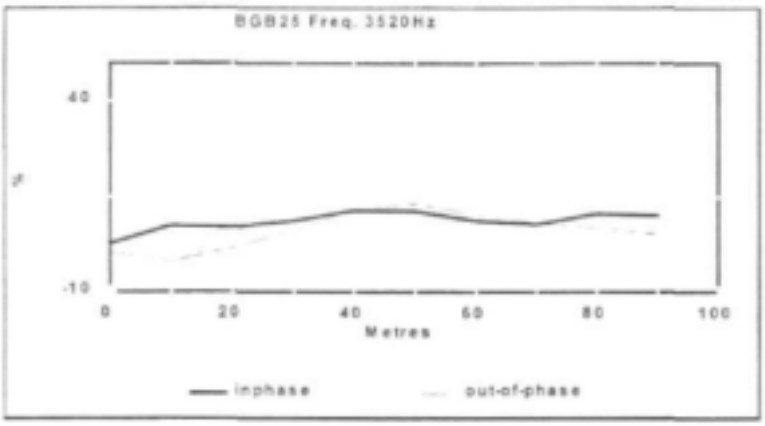
BGB25 Freq. 3520Hz
40
-10
0
20
40
60
80
100
Metres
inphase
out-of-phase

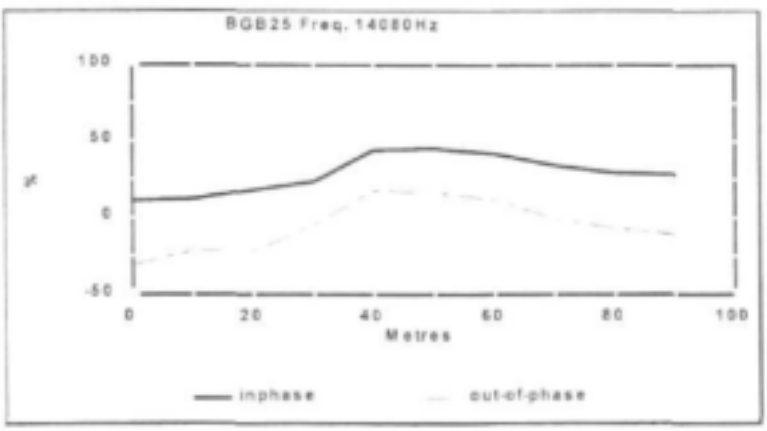
BGB25 Freq. 14080Hz
100
50
0
-50
0
20
40
60
80
100
Metres
inphase
out-of-phase

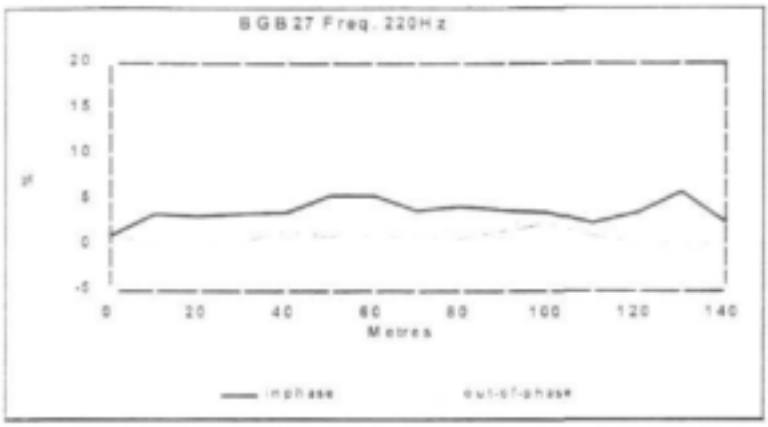
BGB27 Freq. 220Hz
20
15
10
5
0
-5
%
0
20
40
60
80
100
120
140
Metres
inphase
out-of-phase

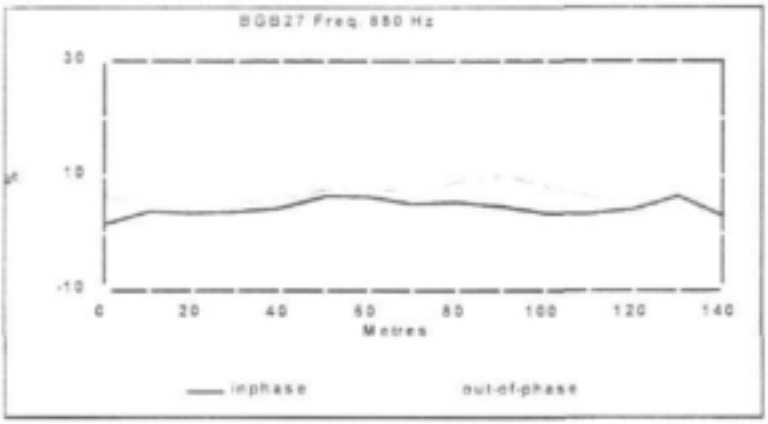
BGB27 Freq. 880 Hz
30
10
-10
%
0
20
40
60
80
100
120
140
Metres
inphase
out-of-phase

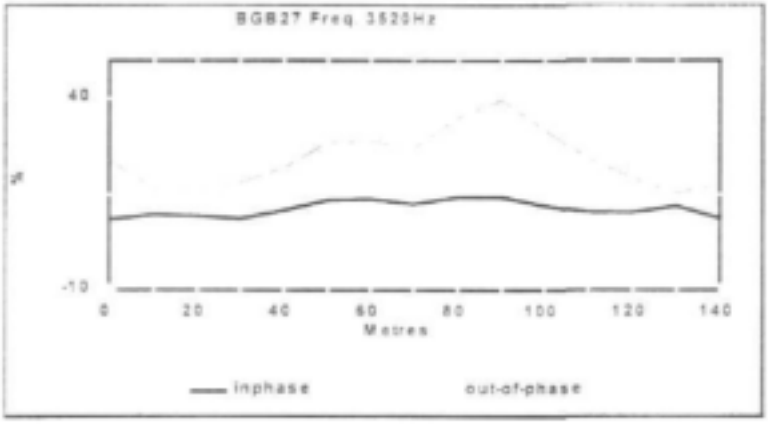
BGB27 Freq. 3520Hz
40
-10
%
0
20
40
60
80
100
120
140
Metres
inphase
out-of-phase

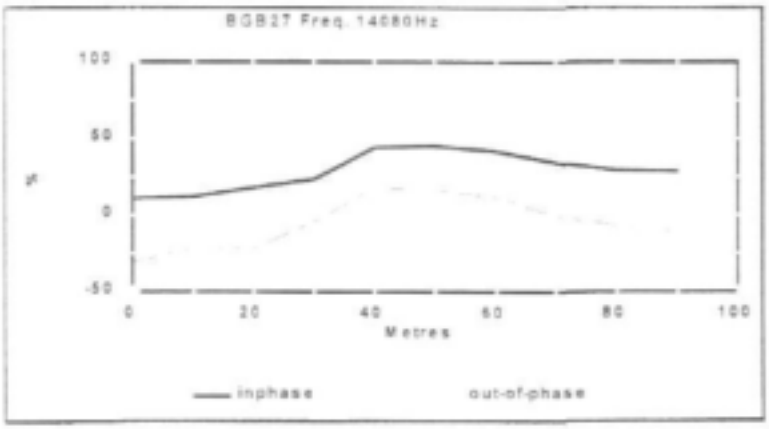
BGB27 Freq. 14080Hz
100
50
0
-50
%
0
20
40
60
80
100
Metres
inphase
out-of-phase

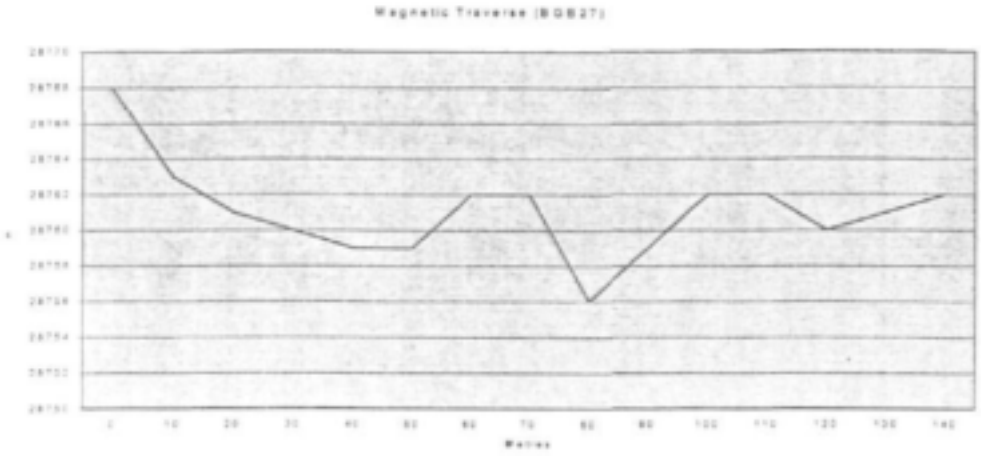
Magnetic Traverse (BGB27)
Metres

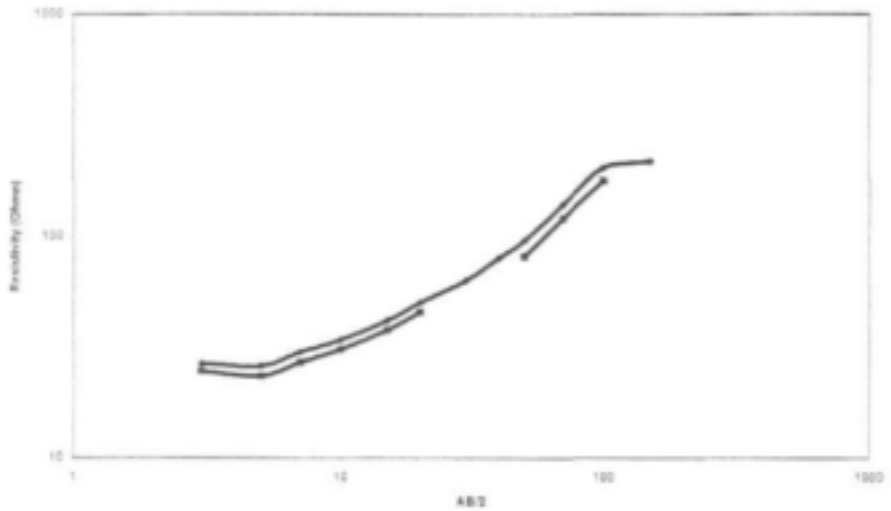
Electrical Sounding (BGB2)
Resistivity (Ohmm)
1000
100
10
1
10
100
1000
AB/2

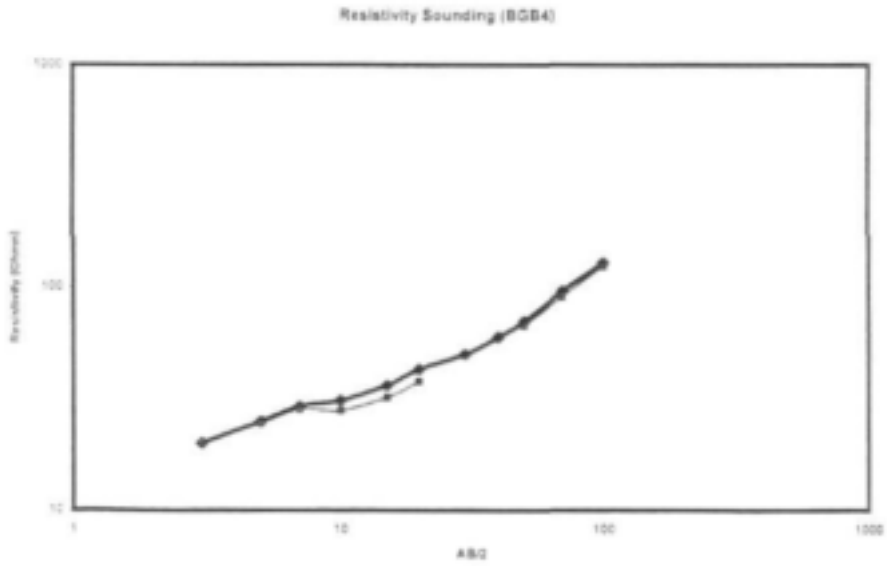
Resistivity Sounding (BGB4)
Resistivity (Ohmm)
1000
100
10
1
10
100
1000
AB/2

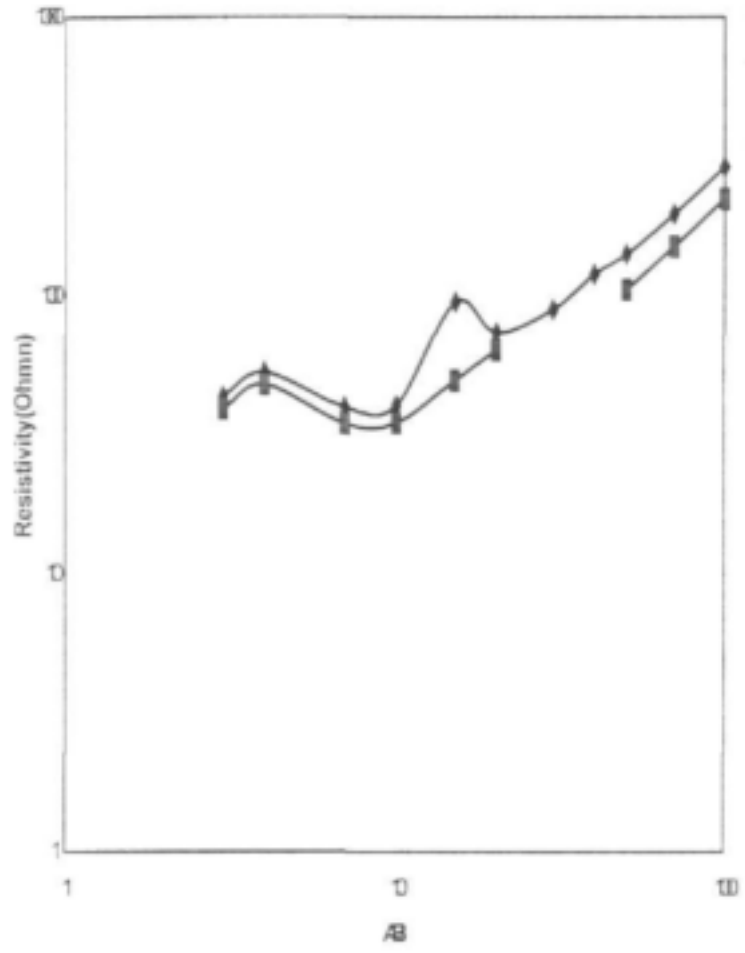

Resistivity Sounding (BGB13

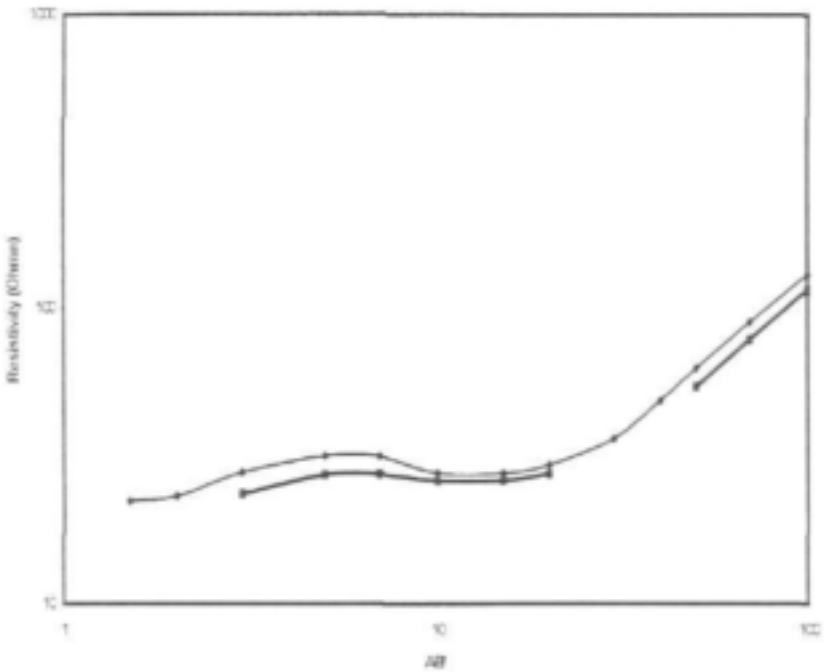

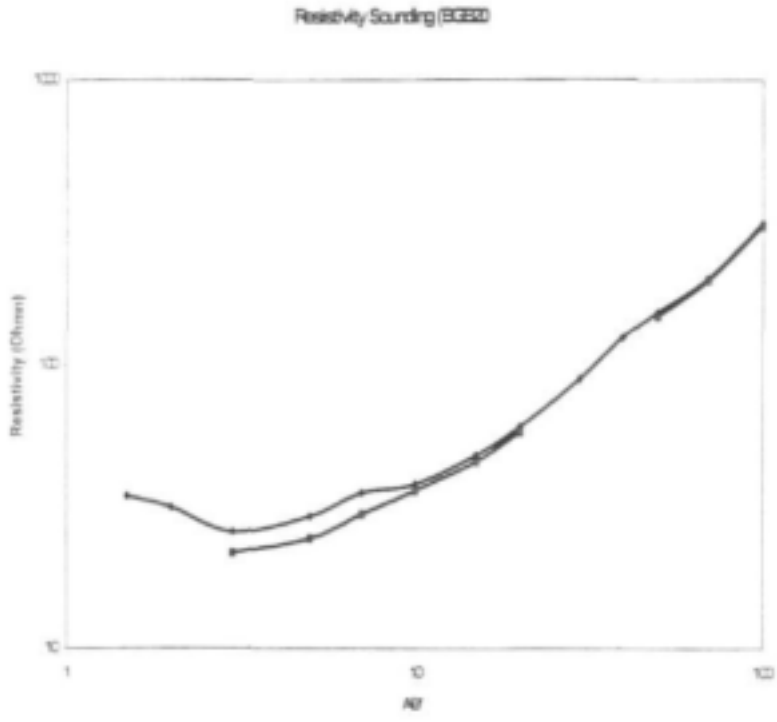
Resistivity Sounding (BGE30
Resistivity (Ohmm)
AB

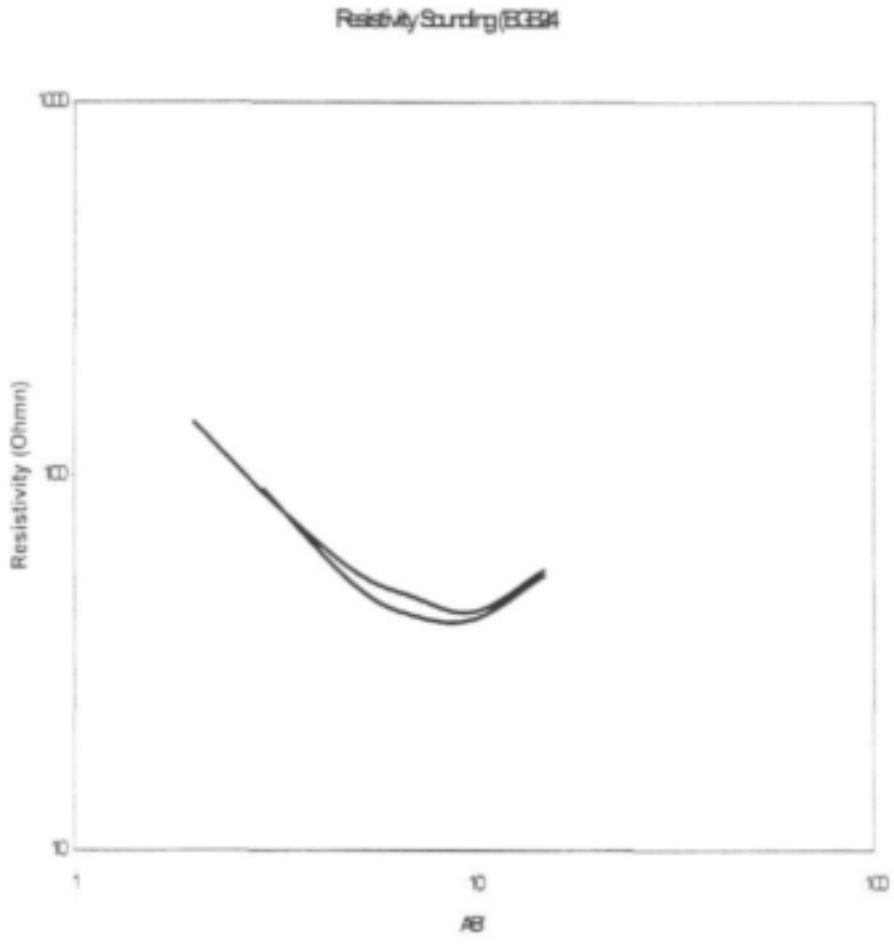
Resistivity Sounding (BGE34
Resistivity (Ohmm)
AB

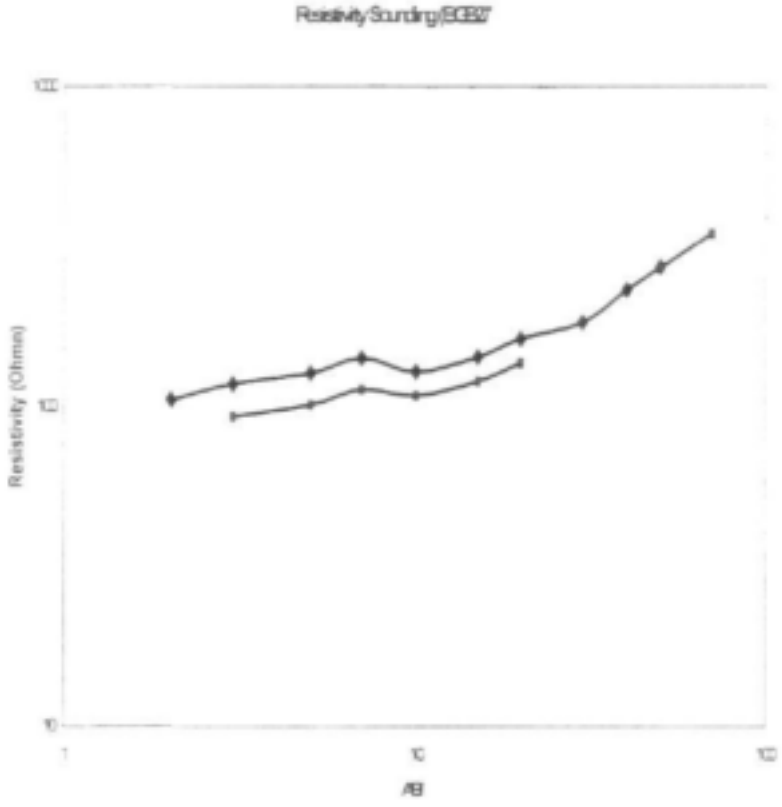
Resistivity Sounding (BGB27
Resistivity (Ohmm)
AB

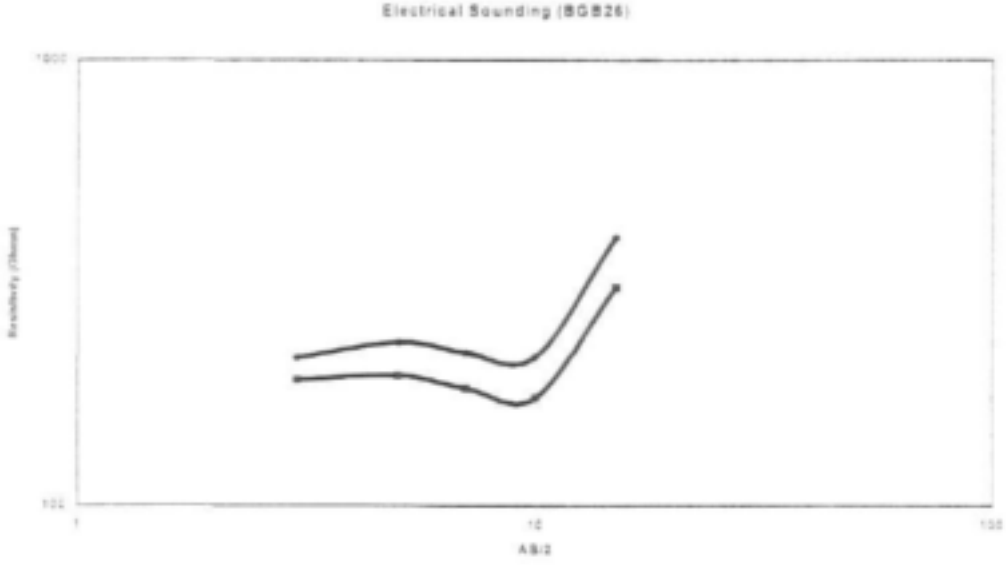
Electrical Sounding (BGB26)
AB/2

APPENDIX 4-B
DRILLING LOGS

COUNCIL FOR GEOSCIENCE
Private Bag X112
PRETORIA 0001
REPUBLIC OF SOUTH AFRICA

GROUNDWATER DEVELOPMENT IN COMPLEX TERRAIN

HOLE No: X12-01
Sheet 1 of 2

PROJECT NUMBER: K5/966

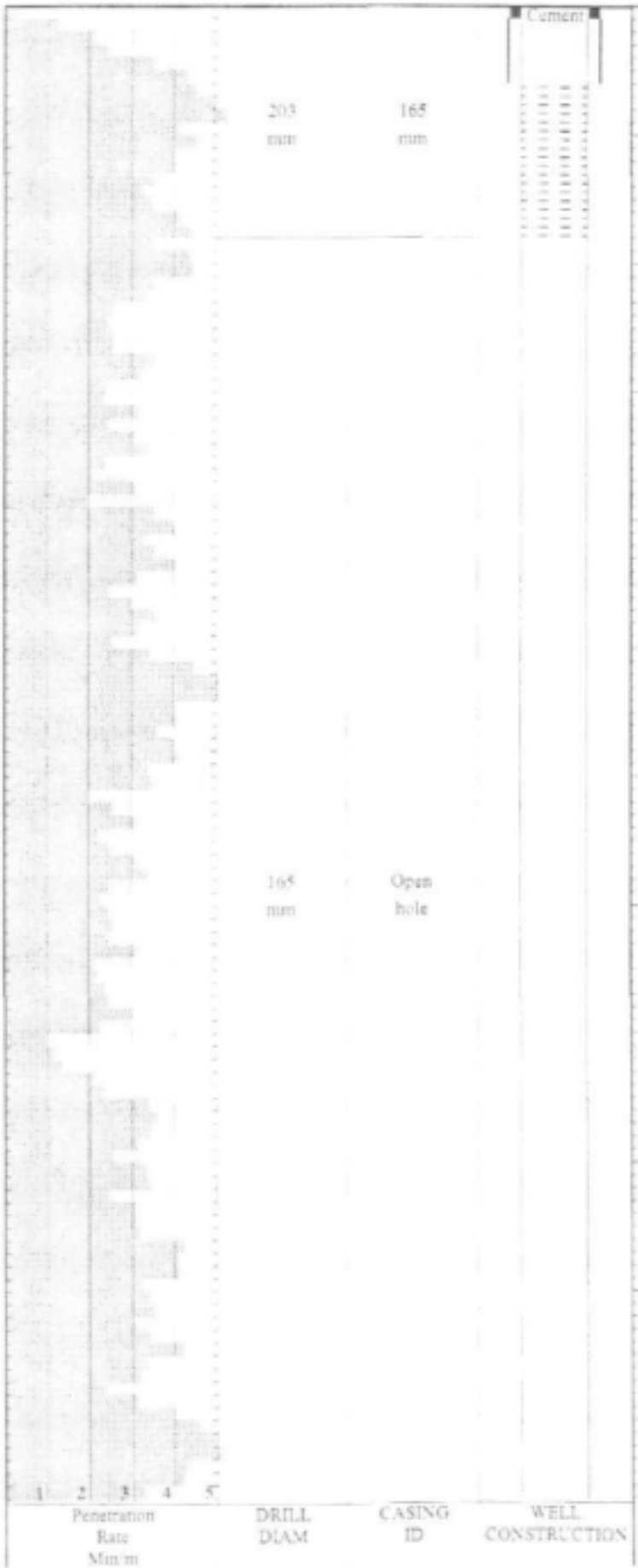

:Highly fractured and weathered med-fine grained grey metabasalt

:Highly fractured and weathered yellowish brown saprolite abd grey metabasalt BASALT

Highly fractured and weathered greenish grey metabasalt BASALT

Highly fractured grey metabasalt BASALT

Highly weathered greenish-grey basalt with highly weathered zone at 24 m BASALT

Highly weathered grey diabase/basalt with slickenslides at 36 m BASALT

Fractured dark grey metabasalt BASALT

Fractured and weathered dark grey metabasalt with stringers BASALT

:Highly weathered light grey metabasalt with quartz with sporadic fractures BASALT

:Higly fractured dark grey metabasalt BASALT

:Highly weathered and fractured fine grained metabasalt with crystals BASALT

Dark green-grey basalt and quartz vein, mid to fine grained BASALT

COUNCIL FOR GEOSCIENCE
Private Bag X112
PRETORIA 0001
REPUBLIC OF SOUTH AFRICA

GROUNDWATER DEVELOPMENT IN COMPLEX TERRAIN

PROJECT NUMBER: K5/966

120

Highly fractured and weathered fine grained dark grey metabasalt BASALT

96.00

Fractured and weathered mid to fine grained dark grey-green striated BASALT

120.00

NOTES

1) Seepage at 81 m

2) First Water strike at 15 m

3) Second water strike at 24 m

4) Third water strike at 36 m

5) Rest water level at 7.25 m

1 2 3 4 5			
Penetration Rate Min/m	DRILL DIAM	CASING ID	WELL CONSTRUCTION

CONTRACTOR : DWAF
DRILLED BY : Mr. Legodi
DRILL METHOD : DTH HAMMER
SAMPLING : BLOWN CUTTINGS

INCLINATION :
DIAMETER :
DRILL DATE : 27 November 2000
CASING TYPE : 4,5 mm steel

ELEVATION : 948 m
COLLAR HEIGHT : 25 cm
BLOW YIELD : 10 l/s

LOGGED BY : D. Gqiba
SETUP FILE : STANDARD SET

DATE : 03/01/02 14:24
TEXT : C:\DOTPLOT\DATA\X12-01.TXT

HOLE No: X12-01
Mbhejeka, Tjakastad

COUNCIL FOR GEOSCIENCE
Private Bag X112
PRETORIA 0001
REPUBLIC OF SOUTH AFRICA

GROUNDWATER DEVELOPMENT IN COMPLEX TERRAIN

HOLE No: X12-02

PROJECT NUMBER: K5/966

COUNCIL FOR GEOSCIENCE
Private Bag X112
PRETORIA 0001
REPUBLIC OF SOUTH AFRICA

GROUNDWATER DEVELOPMENT IN COMPLEX TERRAIN

HOLE No: X12-02
Sheet 2 of 2

PROJECT NUMBER: K5/966

NOTES

1) Seepage at 25 m

2) Water strike at 55 m

3) Rest water level at 10.25 m

1 2 3 4 5

Penetration Rate Min m	DRILL DIAM	CASING ID	WELL CONSTRUCTION

CONTRACTOR : DWAF
DRILLED BY : Mr. Legodi
DRILL METHOD : DTH HAMMER
SAMPLING : BLOWN CUTTINGS

LOGGED BY : D. Gqiba
SETUP FILE : STANDARD.SET

INCLINATION :
DIAMETER :
DRILL DATE : 14 January 2001
CASING TYPE : 4.5 mm steel

DATE : 03/01/02 14:25
TEXT : C:\DOTPLOT\DATA\X12-02.TXT

ELEVATION : 871 m
COLLAR HEIGHT : 30 cm
BLOW YIELD : 1 l/s

HOLE No: X12-02
Mbhojeka, Tshakastad

COUNCIL FOR GEOSCIENCE

Private Bag X112
PRETORIA 0001
REPUBLIC OF SOUTH AFRICA

GROUNDWATER DEVELOPMENT IN COMPLEX TERRAIN

HOLE No. X12-03
Sheet 1 of 2

PROJECT NUMBER: K5/966

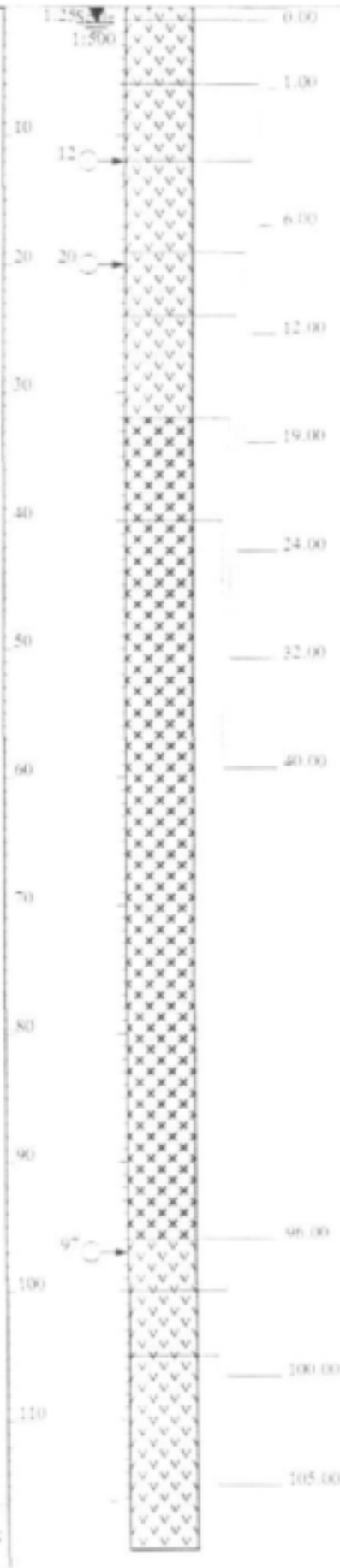

Weathered coarse grained basalt (komatiite

Highly fractured and weathered greyish khaki basalt (komatiite BASALT

Fractured med-fine grained grey komatiite basalt BASALT

Weathered med-fine grained dark grey basalt BASALT

Fractured light grey basalt with asbestos crystals BASALT

Weathered greensih grey basalt, less abundant asbestos BASALT

Weathered fine grained dark-grey dolerite with SiO2 crystals DOLERITE

Mid-fine grained dolerite, weathered DOLERITE

Highly weathered lightly fractured greenish grey 45% crystals, greenstone BASALT

Weathered dark grey mid-fine grained basalt BASALT

COUNCIL FOR GEOSCIENCE
Private Bag X112
PRETORIA 0001
REPUBLIC OF SOUTH AFRICA

GROUNDWATER DEVELOPMENT IN COMPLEX TERRAIN

HOLE No: X12-03
Sheet 2 of 2

PROJECT NUMBER: K5/966

120

:Highly weathered and fractured greenish grey greenstone with abundant minerals 'BASALT

120.00

NOTES

1) First Water strike at 12 m

2) Second water strike at 20 m

3) Third water strike at 97 m

4) Rest water level at 1.25 m

1 2 3 4 5

Penetration Rate Min m	DRILL DIAM	CASING ID	WELL CONSTRUCTION

CONTRACTOR : DWAF
DRILLED BY : Mr. Legodi
DRILL METHOD : DTH HAMMER
SAMPLING : BLOWN CUTTINGS

INCLINATION :
DIAMETER :
DRILL DATE : 27 November 2000
CASING TYPE : 4.5 mm steel

ELEVATION : 982 m
COLLAR HEIGHT : 45 cm
BLOW YIELD : 0.3 l/s

LOGGED BY : D. Gqiba
SETUP FILE : STANDARD.SET

DATE : 03/01/02 14:26
TEXT : C:\DOTPLOT DATA\X12-03.TXT

HOLE No: X12-03
Mbhejeka, Tjakastad

COUNCIL FOR GEOSCIENCE
Private Bag X112
PRETORIA 0001
REPUBLIC OF SOUTH AFRICA

GROUNDWATER DEVELOPMENT IN COMPLEX TERRAIN

HOLE No: X12/04
Sheet 1 of 2

PROJECT NUMBER: K5/966

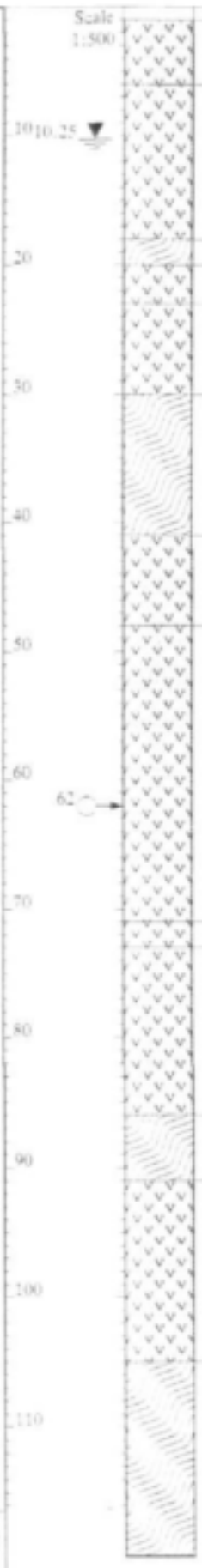

0.00 :Weathered khaki grey clay saporpeline :Soil

1.00 :Highly fractured and weathered greenish grey metabasalt with quartz vein BASALT

6.00 :Highly weathered greenish grey metabasalt and clay BASALT

18.00 :Highly fractured and weathered medium to fine grained Schist

20.00 :Fractured greenish grey metabasalt BASALT

23.00 :Highly weathered green to dark grey metabasalt with quartz veins BASALT

30.00 :Fractured and weathered phillyte schist :Schist

41.00 :Fractured and weathered medium to fine grained dark grey metabasalt with green quartz crystals BASALT

48.00 :Highly fractured light grey metabasalt with quartz veins BASALT

71.00 :Fractured and weathered greenish grey foliated metabasalt with green quartz crystals :BASALT

73.00 :Fractured medium to fine grained dark grey metabasalt with crystals BASALT

86.00 :Weathered mid to fine grained phyllite schist :Schist

91.00

COUNCIL FOR GEOSCIENCE
Private Bag X112
PRETORIA 0001
REPUBLIC OF SOUTH AFRICA

GROUNDWATER DEVELOPMENT IN COMPLEX TERRAIN

HOLE No: X12-04
Sheet 2 of 2

PROJECT NUMBER: K5/966

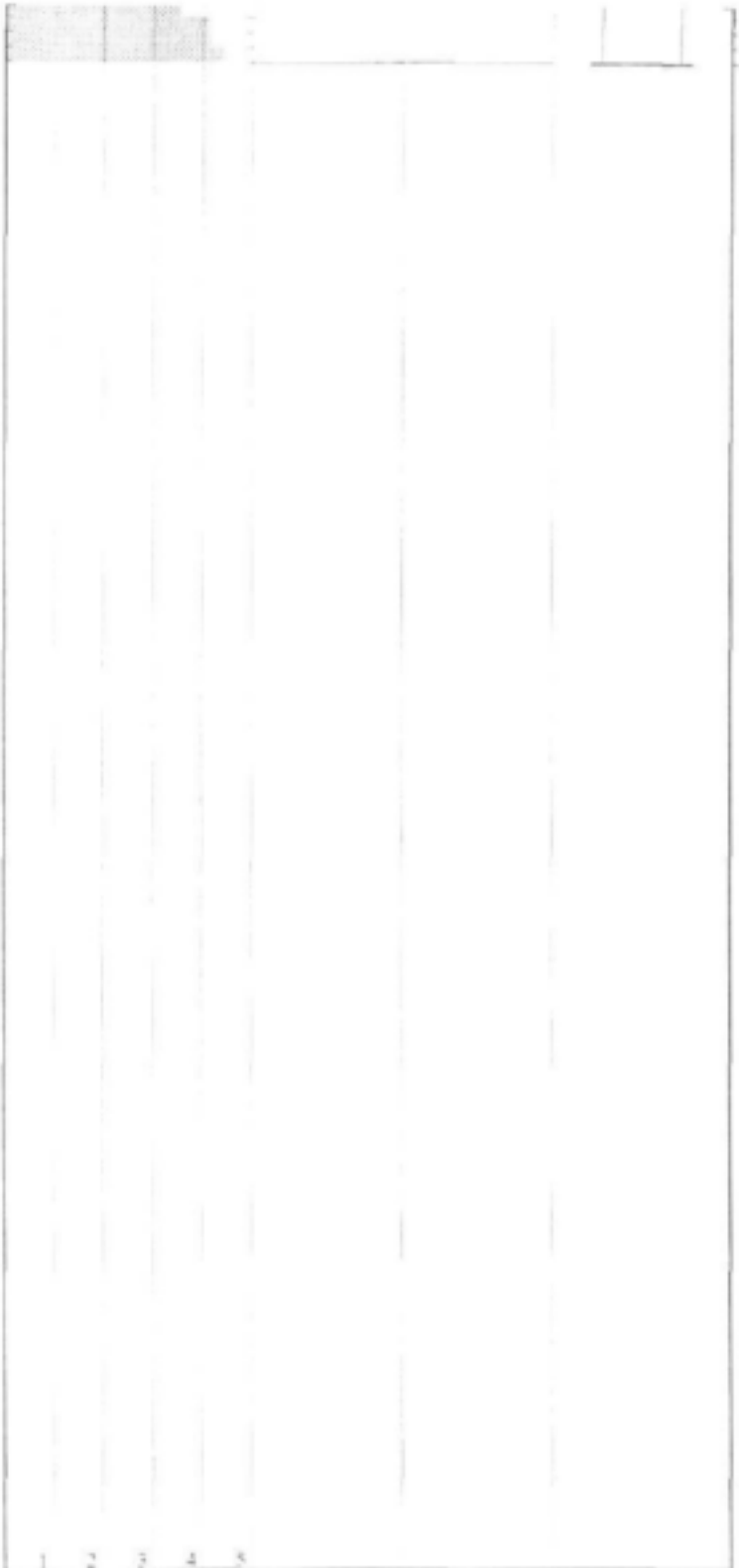

120

:Fractured and highly weathered mid to fine grained greenish grey metabasalt with quartz veins 'BASALT

105.00

:Highly weathered fine green matrix of schist with quartz veins 'Schist

120.00

NOTES

1) Seepage at 19 m

2) Water strike at 62 m

3) Rest water level at 10.25 m

CONTRACTOR : DWAF
DRILLED BY : Mr. Legodi
DRILL METHOD : DTH HAMMER
SAMPLING : BLOWN CUTTINGS

INCLINATION :
DIAMETER :
DRILL DATE : 30 November 2000
CASING TYPE : 4.5 mm steel

ELEVATION : 863 m
COLLAR HEIGHT : 52 cm
BLOW YIELD : 1-2 l/s

LOGGED BY : D. Gqiba
SETUP FILE : STANDARD SET

DATE : 03/01/02 14:27
TEXT : C:\DOTPLOT\DATA\X12-04.TXT

HOLE No: X12-04
Main Township, Tjakastad

COUNCIL FOR GEOSCIENCE
Private Bag X112
PRETORIA 0001
REPUBLIC OF SOUTH AFRICA

GROUNDWATER DEVELOPMENT IN COMPLEX TERRAIN

HOLE No: X12-05
Sheet 1 of 2

PROJECT NUMBER: K5/906

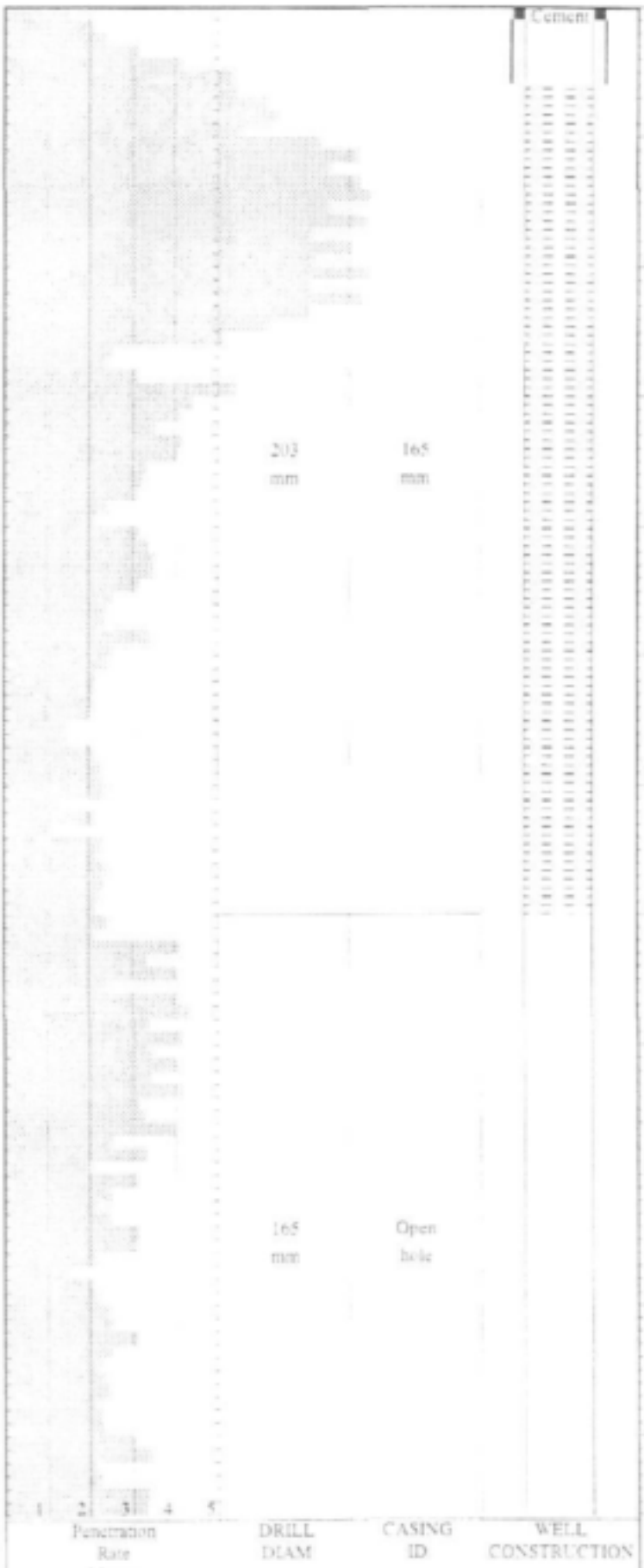

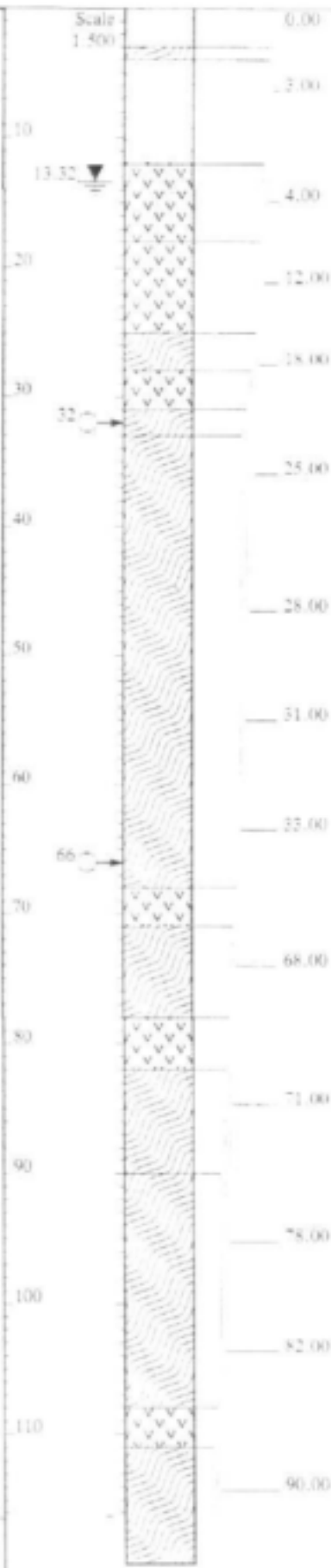

0.00	Light brown sand with quartz pebbles Sand
2.00	Quartz vein with siliceous weathered schist Schist
4.00	Light brown sand with quartz vein pebbles Sand
12.00	Highly weathered fine grained metabasalt Basalt
18.00	Highly weathered dark grey metabasalt with quartz crystals BASALT
25.00	Highly weathered greenish grey phyllite schist with quartz vein Schist
28.00	Highly weathered dark grey metabasalt with quartz veins Basalt
31.00	Highly weathered greenish grey chlorite phyllite schist Schist
33.00	Highly weathered greenish grey phyllite schist matrix (clay) with quartz grains Schist
68.00	Highly weathered greenish grey fine grained metabasalt with green quartz crystals BASALT
71.00	Highly weathered greenish grey phyllite schist matrix (clay) with quartz grains Schist
78.00	Highly weathered fine grained light grey metabasalt Basalt
82.00	Highly weathered greenish grey phyllite schist matrix (clay) with quartz grains Schist
90.00	

COUNCIL FOR GEOSCIENCE
Private Bag X112
PRETORIA 0001
REPUBLIC OF SOUTH AFRICA

GROUNDWATER DEVELOPMENT IN COMPLEX TERRAIN

HOLE No: X12-05
Sheet 2 of 2

PROJECT NUMBER: K5/966

120

:Highly weathered greenish grey talc chlorite schist with quartz veins
'Schist

108.00

:Highly weathered greenish grey fine grained metabasalt with quartz and gold mineralisation
'Basalt

111.00

:Highly weathered greenish grey talc chlorite schist with quartz crystals
'Schist

120.00

NOTES

1) Seepage at 18 m

2) Water strike at 32 m

3) Water strike at 66 m

4) Rest water level at 13.32

1 2 3 4 5

Penetration Rate Min/m	DRILL DIAM	CASING ID	WELL CONSTRUCTION

CONTRACTOR : DWAF
DRILLED BY : Mr. Legodi
DRILL METHOD : DTH HAMMER
SAMPLING : BLOWN CUTTINGS

LOGGED BY : D. Gqiba
SETUP FILE : STANDARD.SET

INCLINATION :
DIAMETER :
DRILL DATE : 04 December 2000
CASING TYPE : 4.5 mm steel

DATE : 03/01/02 14:27
TEXT : C:\DOTPLOT\DATA\X12-05.TXT

ELEVATION : 871 m
COLLAR HEIGHT : 30 cm
BLOW YIELD : 0.25 l/s

HOLE No: X12-05
Main Township, Tjakastad

dot PLOT 3027 J&W Inc

COUNCIL FOR GEOSCIENCE
Private Bag X112
PRETORIA 0001
REPUBLIC OF SOUTH AFRICA

GROUNDWATER DEVELOPMENT IN COMPLEX TERRAIN

HOLE No: X12-06
Sheet 1 of 2

PROJECT NUMBER: K5/966

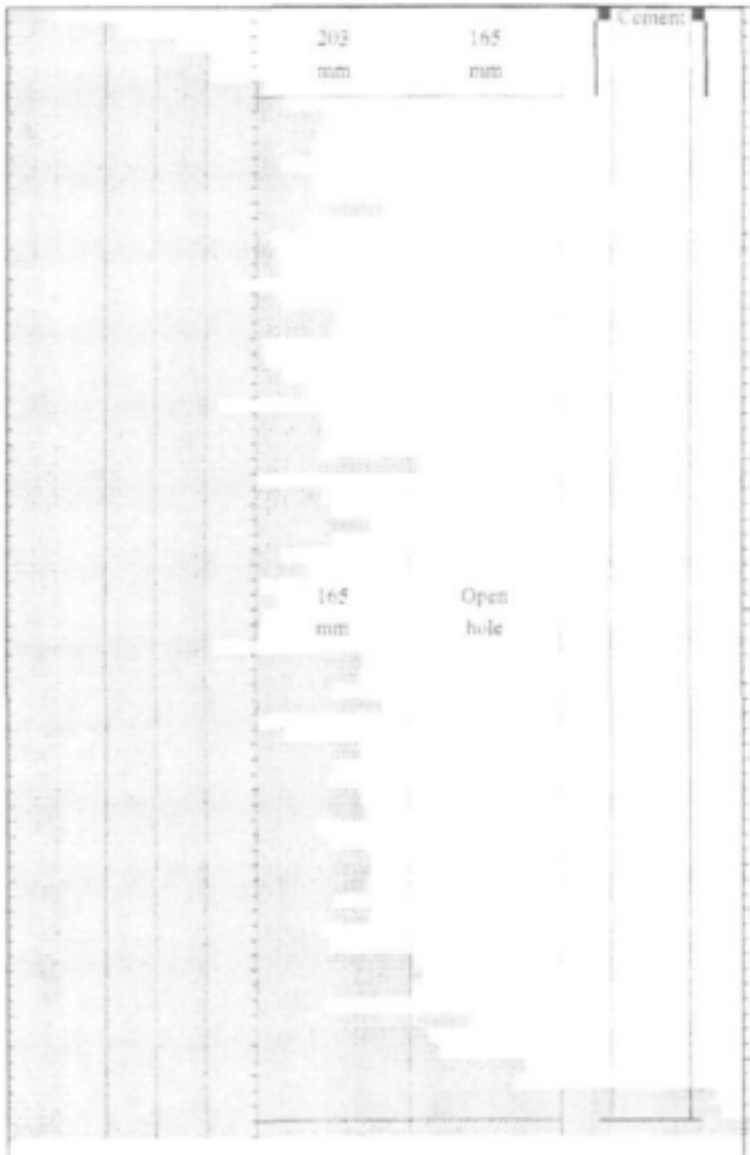

0.00	Brown clay sand with quartz pebbles Sand
2.00	Fractured and weathered granite with pink and white quartz Granite
11.00	Fractured dark grey dolerite dyke Dolerite
12.00	Weathered light grey with pinkish coloured minerals granite Granite
16.00	Weathered light grey granite with quartz veins Granite
20.00	Fine grained dark grey fresh dolerite Dolerite
21.00	Weathered and unfractured light grey granite gneiss with quartz vein Granite
26.00	Weathered light grey foliated granite gneiss Granite
31.00	Fine grained dark grey dolerite Dolerite
33.00	Weathered grey banded granite gneiss Granite
35.00	Weathered light grey foliated granite gneiss Granite
39.00	Fine grained dark grey dolerite Dolerite
40.00	Weathered light grey granite with quartz vein Granite
54.00	

1	2	3	4	5
Penetration Rate Min/m		DRILL DIAM	CASING ID	WELL CONSTRUCTION

COUNCIL FOR GEOSCIENCE
Private Bag X112
PRETORIA 0001
REPUBLIC OF SOUTH AFRICA

GROUNDWATER DEVELOPMENT IN COMPLEX TERRAIN

HOLE No: X12-06
Sheet 2 of 2

PROJECT NUMBER: K5/966

74.00	Fine grained dark grey siliceous hard granite'Granite

NOTES

1) Seepage at 27 m

2) Rest water level at 46.60 m

1 2 3 4 5

Penetration Rate Min/m	DRILL DIAM	CASING ID	WELL CONSTRUCTION

CONTRACTOR : DWAF
DRILLED BY : Mr. Legodi
DRILL METHOD : DTH HAMMER
SAMPLING : BLOWN CUTTINGS

INCLINATION :
DIAMETER :
DRILL DATE : 08 December 2000
CASING TYPE : 4.5 mm steel

ELEVATION : 920 m
COLLAR HEIGHT : 35 cm
BLOW YIELD : 0.001 l/s

LOGGED BY : D. Gqiba
SETUP FILE : STANDARD SET

DATE : 03/01/02 14:27
TEXT : C:\DOTPLOT\DATA\X12-06.TXT

HOLE No: X12-06
Ntlazatshe

COUNCIL FOR GEOSCIENCE
Private Bag X112
PRETORIA 0001
REPUBLIC OF SOUTH AFRICA

GROUNDWATER DEVELOPMENT IN COMPLEX TERRAIN

HOLE No: X12-07
Sheet 1 of 2

PROJECT NUMBER: K5/966

DRILL DIAM	CASING ID	WELL CONSTRUCTION
203 mm	165 mm	Cement
165 mm	Open hole	

Scale 1:500

17.72 ▼

Penetration Rate Min/m	
3	0.00
6	1.00
90	6.00
15	10.00
	11.00
	13.00
	16.00
	20.00
	30.00
	32.00
	33.00
	35.00
	37.00
	38.00

Weathered greyish greenschist Schist

Weathered mid to coarse grained granite with quartz veins Granite

Highly fractured and highly weathered dark grey granite Granite

Light brown sand with fractured pebbles of banded granite Sand

Fractured coarse grained banded granite Granite

Fractured dark grey fine grained dolerite Dolerite

Fine grained fractured light brown granite with quatz vein Granite

Mid to course grained hard light coloured granite Granite

Weathered mid to coarse grained dark grey foliated granite Granite

Fine grained dark grey dolerite Dolerite

Weathered mid to coarse grained foliated granite Granite

Fine grained dark grey dolerite with greenish tint Dolerite

Mid to coarse grained foliated dark grey granite Granite

COUNCIL FOR GEOSCIENCE
Private Bag X112
PRETORIA 0001
REPUBLIC OF SOUTH AFRICA

GROUNDWATER DEVELOPMENT IN COMPLEX TERRAIN

HOLE No: X12-07
Sheet 2 of 2

PROJECT NUMBER: K5/966

	:Hard fine grained siliceous dark grey dolerite with greenish tint 'Dolerite
47.00	

NOTES

1) Seepage at 37 m

2) Rest water level at 17.72 m

3 6 10 15

Penetration Rate Min/m	DRILL DIAM	CASING ID	WELL CONSTRUCTION

CONTRACTOR : DWAF
DRILLED BY : Mr. Legodi
DRILL METHOD : DTH HAMMER
SAMPLING : BLOWN CUTTINGS

INCLINATION :
DIAMETER :
DRILL DATE : 07 January 2001
CASING TYPE : 4.5 mm steel

ELEVATION : 1063 m
COLLAR HEIGHT : 30 cm
BLOW YIELD : 0.001 l/s

LOGGED BY : D. Gqiba
SETUP FILE : STANDARD SET

DATE : 05/01/02 14:58
TEXT : C:\DOTPLOT\DATA\X12-07.TXT

HOLE No: X12-07
NTlazatshe

COUNCIL FOR GEOSCIENCE
Private Bag X112
PRETORIA 0001
REPUBLIC OF SOUTH AFRICA

GROUNDWATER DEVELOPMENT IN COMPLEX TERRAIN

HOLE No: X12-08
Sheet 1 of 2

PROJECT NUMBER: K5/966

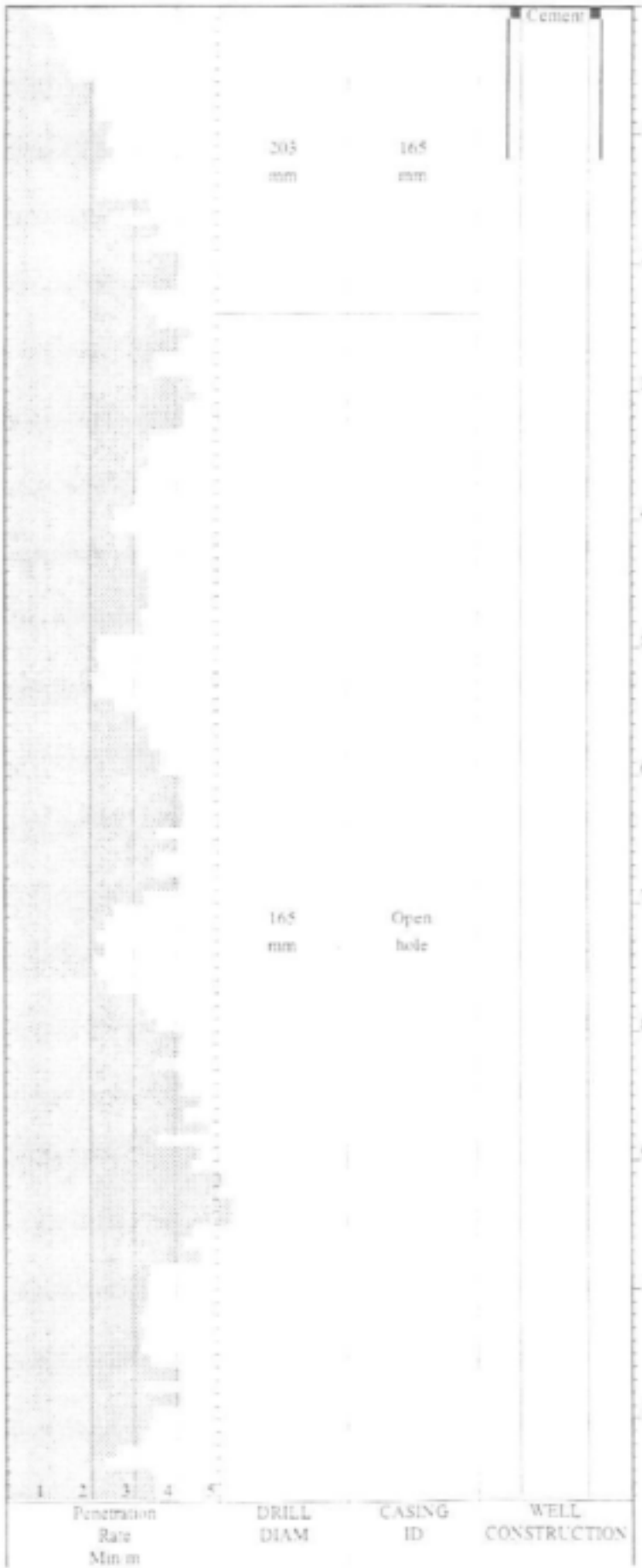

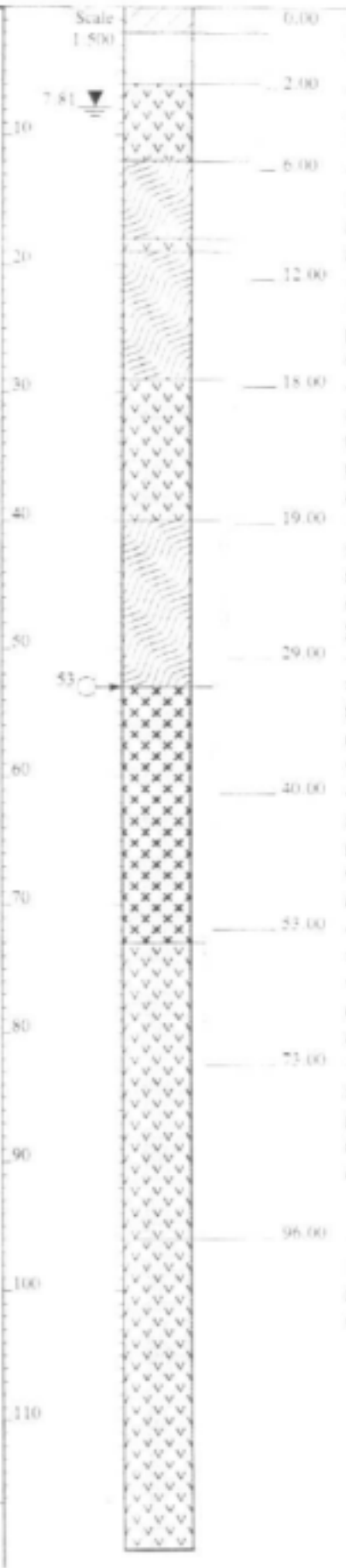

0.00 :Dark brown silty clay Clay

2.00 :Reddish brown clay sand Sand

6.00 :Highly weathered light grey mid to coarse grained metabasalt Basalt

12.00 :Fractured and weathered phyllite-talc schist greenschist Schist

18.00 :Highly fractured mid to fine grained dark grey metabasalt with quartz crystals BASALT

19.00 :Highly weathered and fractured striated phyllite schist with quartz veins Schist

29.00 :Weathered and fractured fine grained light grey metabasalt with quartz veins Basalt

40.00 :Highly weathered greenish grey schist with white and green quartz crystals Schist

53.00 :Highly Fractured and weathered dark striated dolerite with quartz crystals Dolerite

73.00 :Weathered mid to fine grained greenish grey metabasalt with green quartz crystals BASALT

96.00 :Weathered mid to fine grained metabasalt with calcite crystals Basalt

COUNCIL FOR GEOSCIENCE
Private Bag X112
PRETORIA 0001
REPUBLIC OF SOUTH AFRICA

GROUNDWATER DEVELOPMENT IN COMPLEX TERRAIN

HOLE No: X12-08
Sheet 2 of 2

PROJECT NUMBER: K5/966

120 120.00

NOTES

1) Seepage at 19 m

2) Water strike at 52 m

3) Rest water level at 7.81 m

1 2 3 4 5			
Penetration Rate Min/m	DRILL DIAM	CASING ID	WELL CONSTRUCTION

CONTRACTOR : DWAF
DRILLED BY : Mr. Monenyama
DRILL METHOD : DTH HAMMER
SAMPLING : BLOWN CUTTINGS

INCLINATION :
DIAMETER :
DRILL DATE : 09 January 2001
CASING TYPE : 4.5 mm steel

ELEVATION : 871 m
COLLAR HEIGHT : 30 cm
BLOW YIELD : 2.0 l/s

LOGGED BY : D. Gqiba
SETUP FILE : STANDARD.SET

DATE : 03/01/02 14:28
TEXT : C:\DOTPLOT DATA\X12-08.TXT

HOLE No: X12-08
Main Township, Stynsdorp

COUNCIL FOR GEOSCIENCE
Private Bag X112
PRETORIA 0001
REPUBLIC OF SOUTH AFRICA

GROUNDWATER DEVELOPMENT IN COMPLEX TERRAIN

HOLE No: X12499
Sheet 1 of 2

PROJECT NUMBER: K5/966

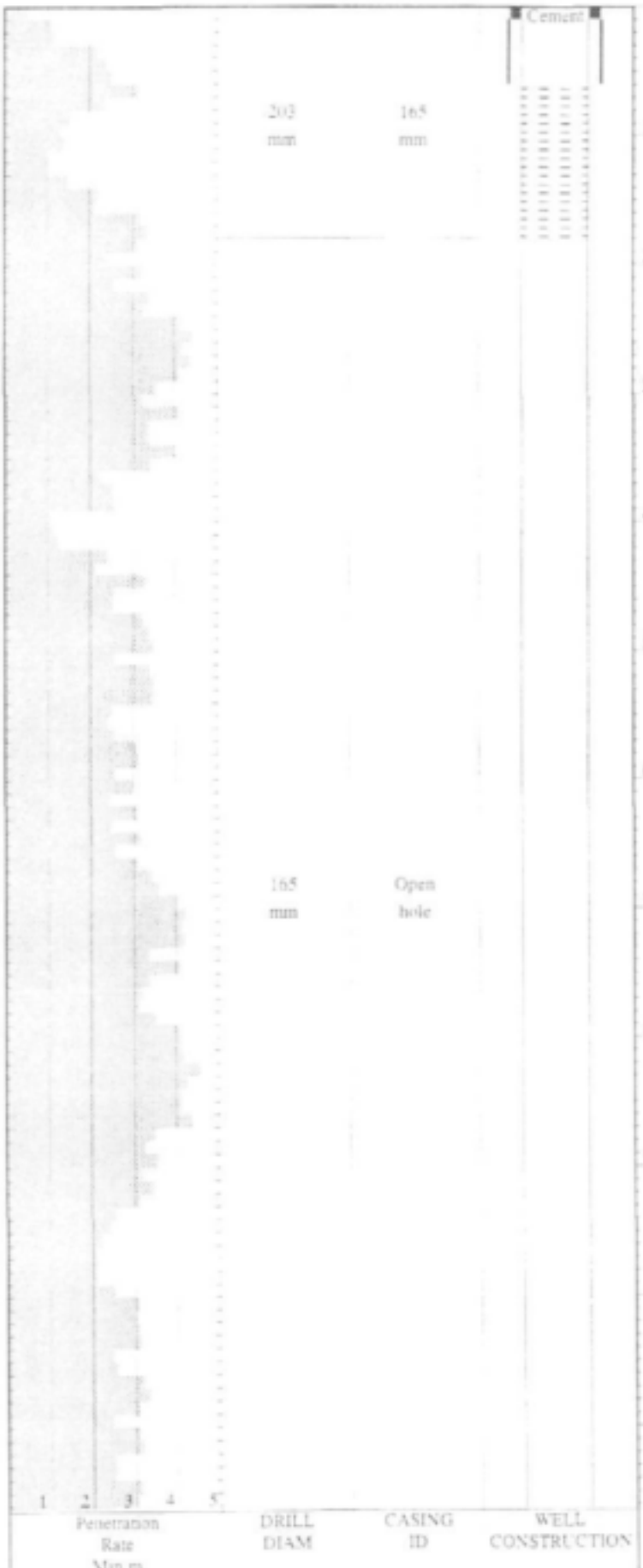

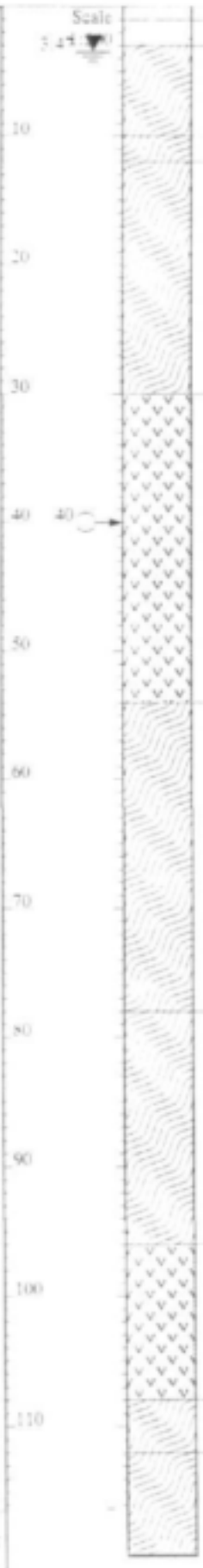

0.00 Coarse grained dark grey clay sand Sand

1.00 Coarse grained brown with greenish tinge clay sand Sand

5.00 Fractured and weathered coarse grained greyish greenschist Schist

10.00 Fractured and weathered mid to fine grained greenschist with quartz veins Schist

12.00 Fractured and weathered mid to fine grained striated greenschist Schist

30.00 Fractured and weathered mid to fine grained light grey striated metabasalt Basalt

54.00 Fracture and weathered striated chlorite-talc phyllite schist with quartz veins Schist

78.00 Highly weathered chlorite phyllite schist Schist

96.00 Highly fractured mid to fine grained metabasalt with quartz veins Basalt

108.00

COUNCIL FOR GEOSCIENCE
Private Bag X112
PRETORIA 0001
REPUBLIC OF SOUTH AFRICA

GROUNDWATER DEVELOPMENT IN COMPLEX TERRAIN

HOLE No: X12-09
Sheet 2 of 2

PROJECT NUMBER: K5/966

120

Weathered mid to coarse grained striated greenschist 'Schist

112.00

Highly weathered mid to coarse grained greenschist with quartz grains 'Schist

120.00

NOTES

1) Seepage at 12 m

2) Water strike at 40 m

3) Rest water level at 3.47 m

1 2 3 4 5

Penetration Rate Min/m	DRILL DIAM	CASING ID	WELL CONSTRUCTION

CONTRACTOR : DWAF
DRILLED BY : Mr. Motsonyana
DRILL METHOD : DTH HAMMER
SAMPLING : BLOWN CUTTINGS

INCLINATION :
DIAMETER :
DRILL DATE : 14 January 2001
CASING TYPE : 4.5 mm steel

ELEVATION : 871 m
COLLAR HEIGHT : 30 cm
BLOW YIELD : 0.25 l/s

LOGGED BY : D. Gqiba
SETUP FILE : STANDARD.SET

DATE : 03/01/02 14:29
TEXT : C:\DOTPLOT\DATA\X12-09.TXT

HOLE No: X12-09
Main Township, Stynsdorp

APPENDIX 4-C
PUMPING TEST GRAPHS

X12-01

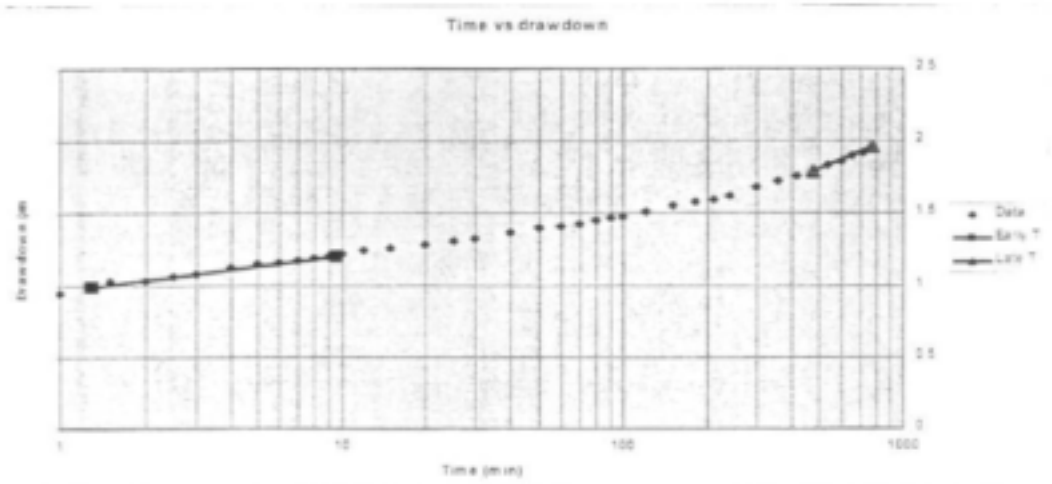
Time vs drawdown
Drawdown (m)
Time (min)
Data
Early T
Late T

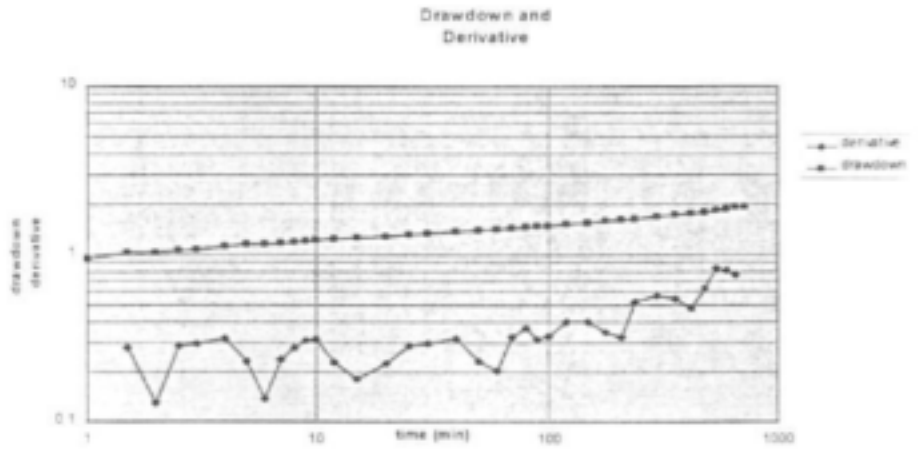
Drawdown and Derivative
drawdown derivative
time (min)
derivative
drawdown

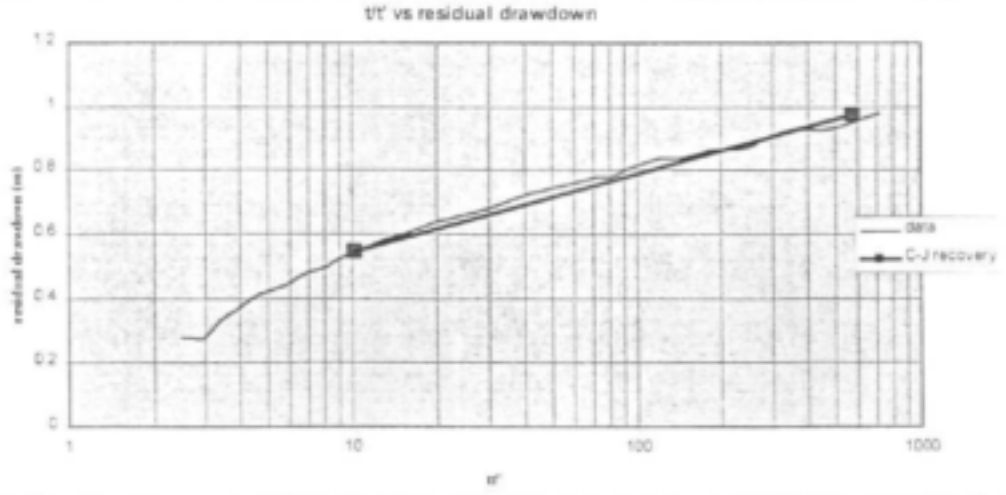
t/t' vs residual drawdown
residual drawdown (m)
t/t'
data
C-J recovery

X12-02

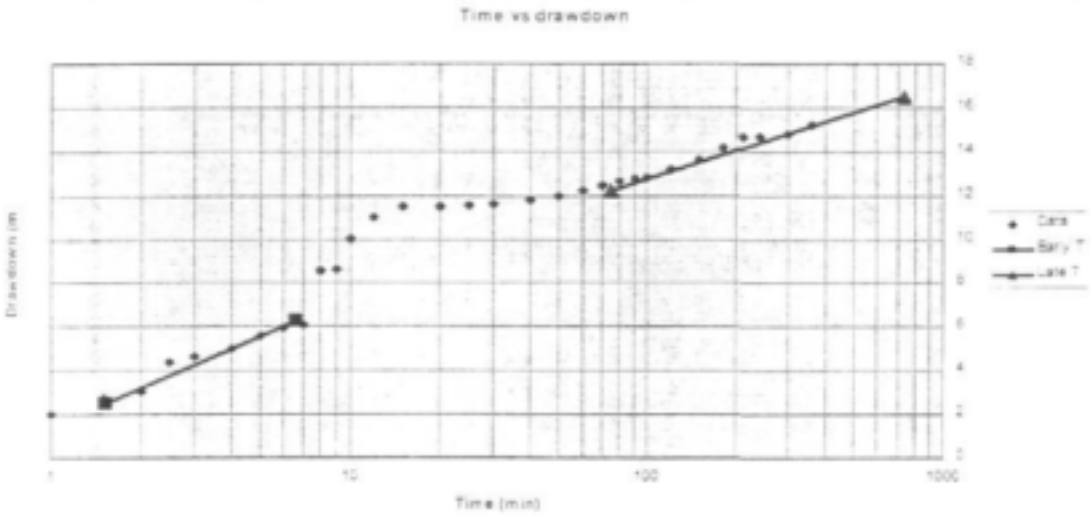
Time vs drawdown
Drawdown (m)
Time (min)
1
10
100
1000
0
2
4
6
8
10
12
14
16
18
Data
Barry T
Jake T

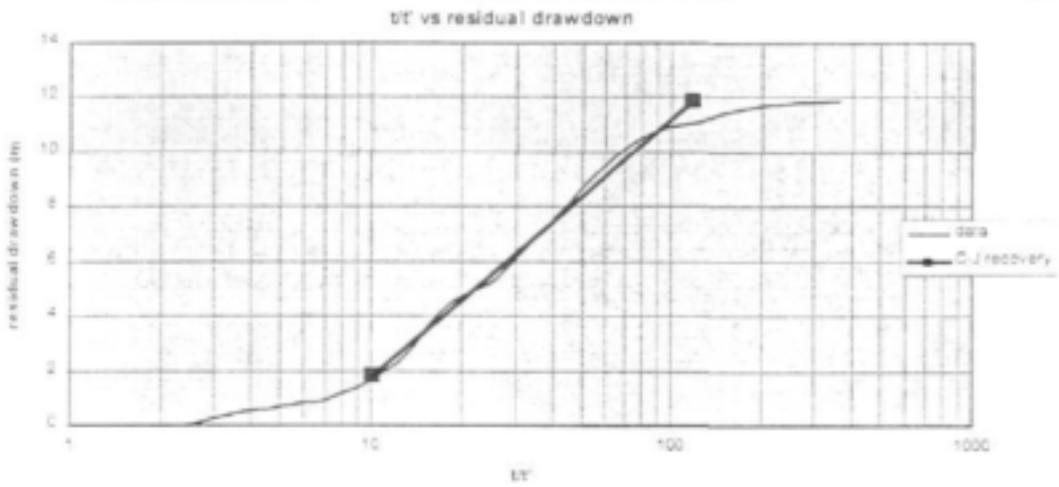
t/t' vs residual drawdown
residual drawdown (m)
t/t'
1
10
100
1000
0
2
4
6
8
10
12
14
data
Barry recovery

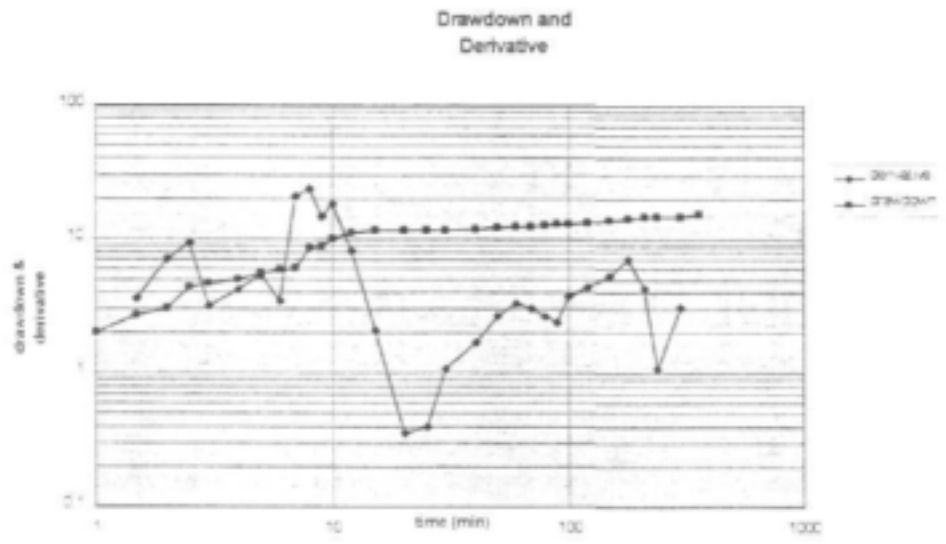
Drawdown and
Derivative
drawdown & derivative
time (min)
1
10
100
1000
0.1
1
10
100

X12-03

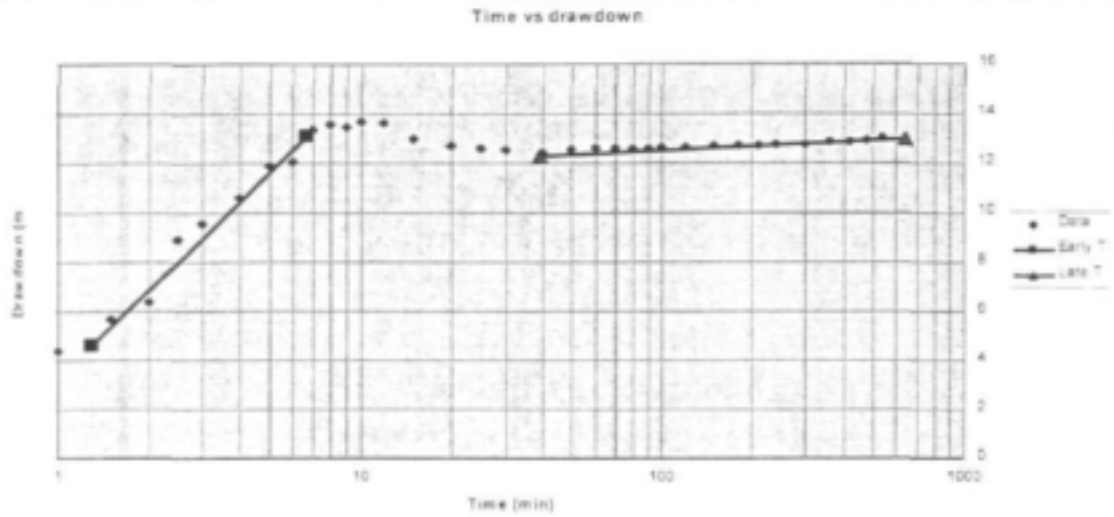
Time vs drawdown
Drawdown (m
Time (min)
Data
Early T
Late T

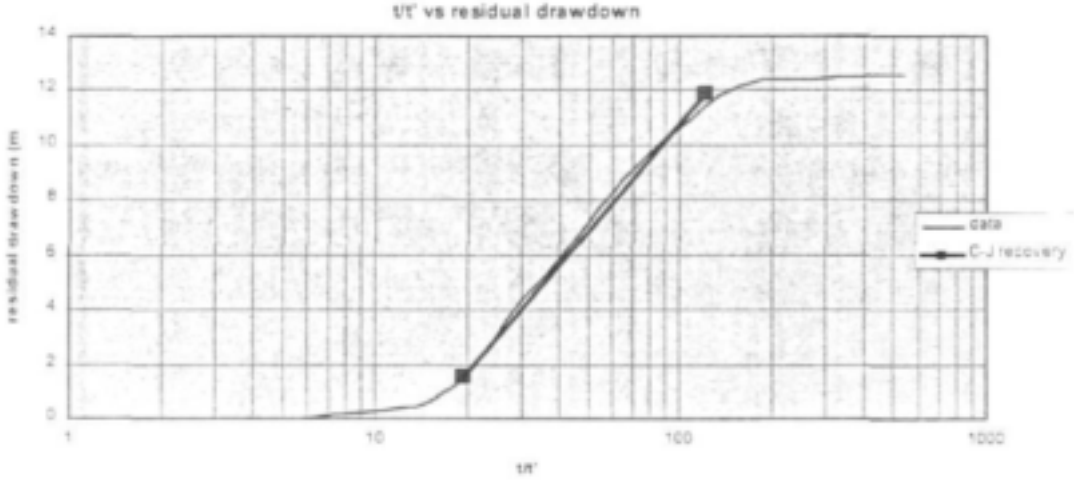
t/t' vs residual drawdown
residual drawdown (m
t/t'
data
C-J recovery

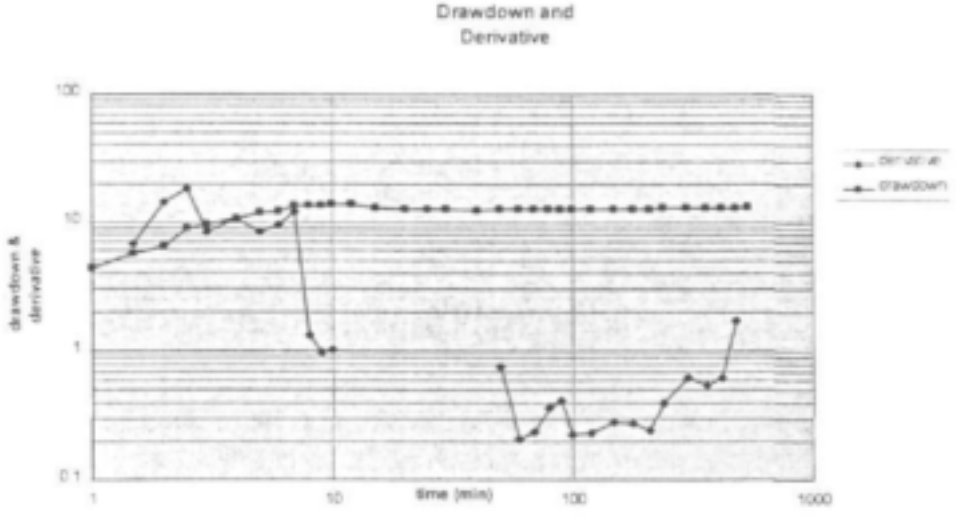
Drawdown and
Derivative
drawdown & derivative
time (min)
drawdown

X12-04

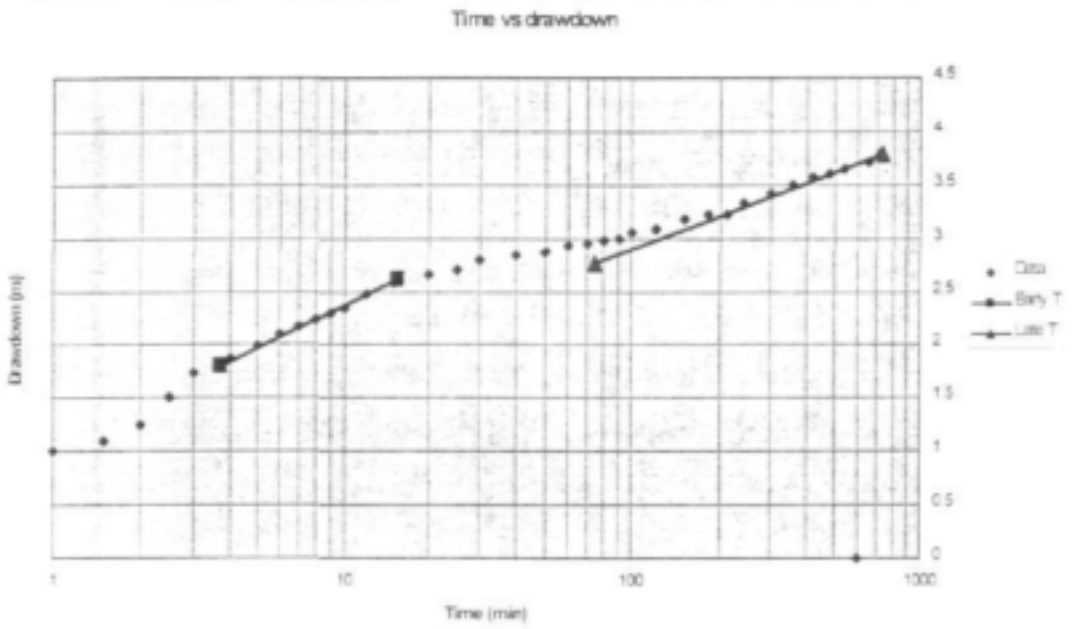
Time vs drawdown
Drawdown (m)
Time (min)
Data
Early T
Late T

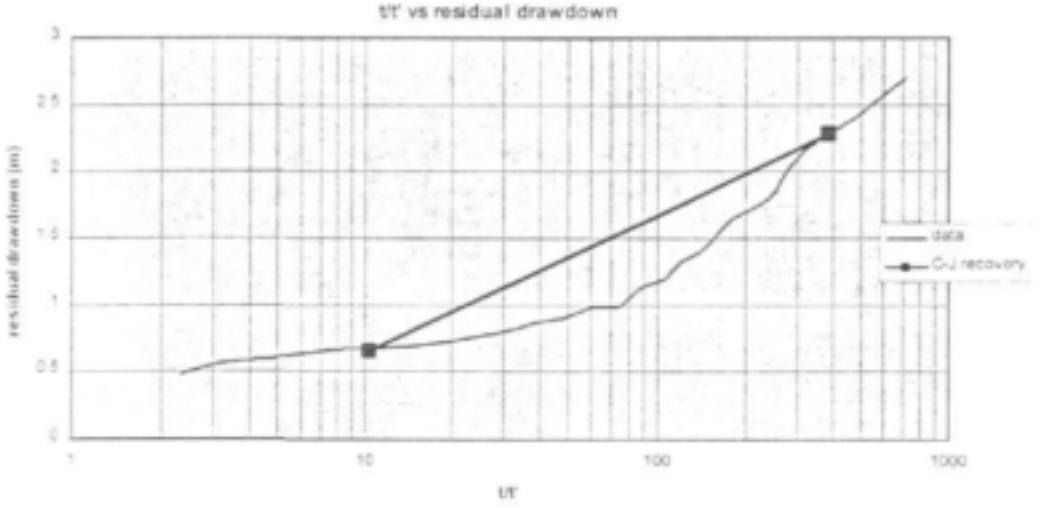
t/t' vs residual drawdown
residual drawdown (m)
t/t'
data
Cvj recovery

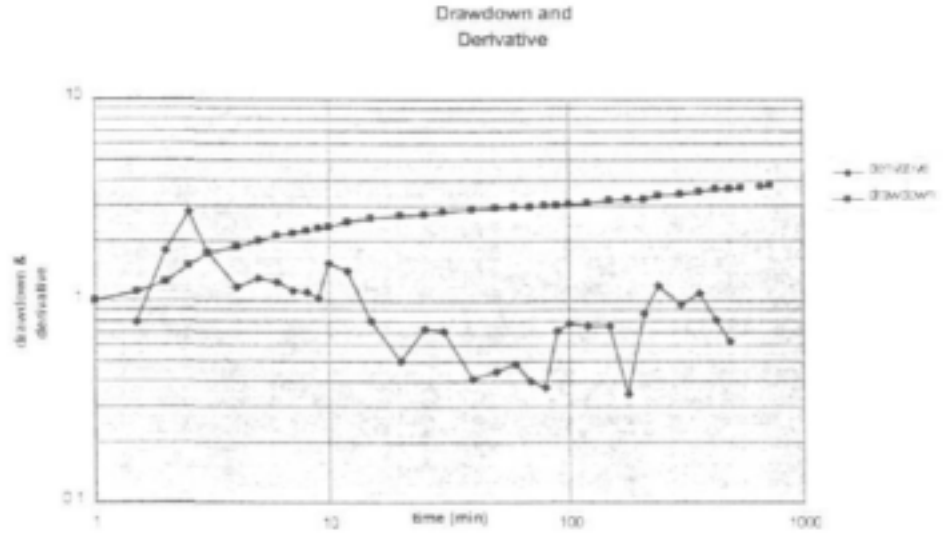
Drawdown and
Derivative
drawdown & derivative
time (min)

X12-05

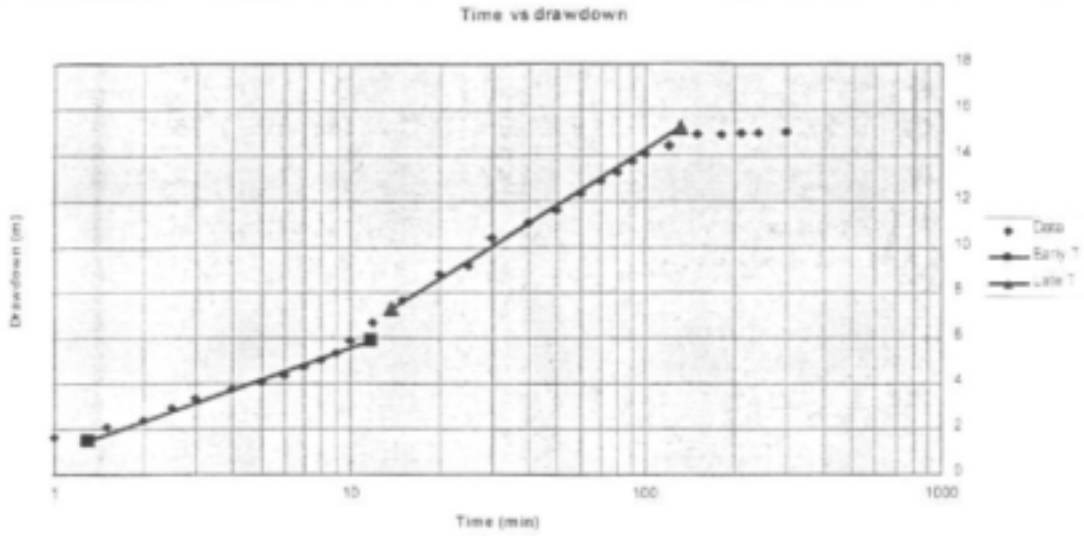
Time vs drawdown
Drawdown (m)
Time (min)
Data
Early T
Late T

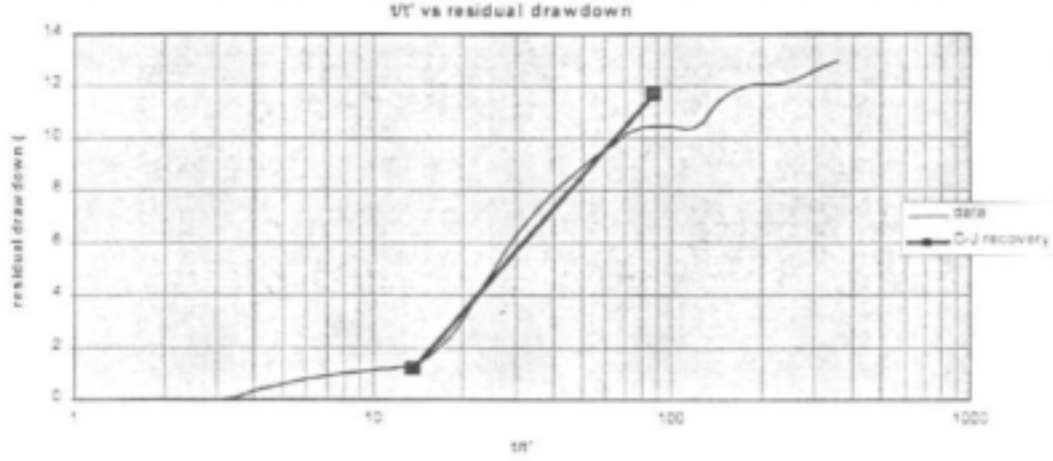
t/t' vs residual drawdown
residual drawdown (
t/t'
data
C-J recovery

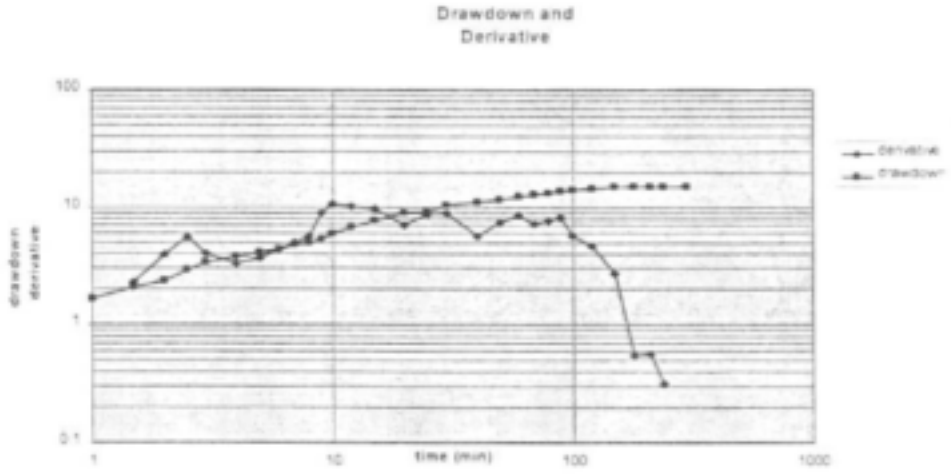
Drawdown and
Derivative
drawdown
derivative
time (min)
derivative
drawdown

X12-08

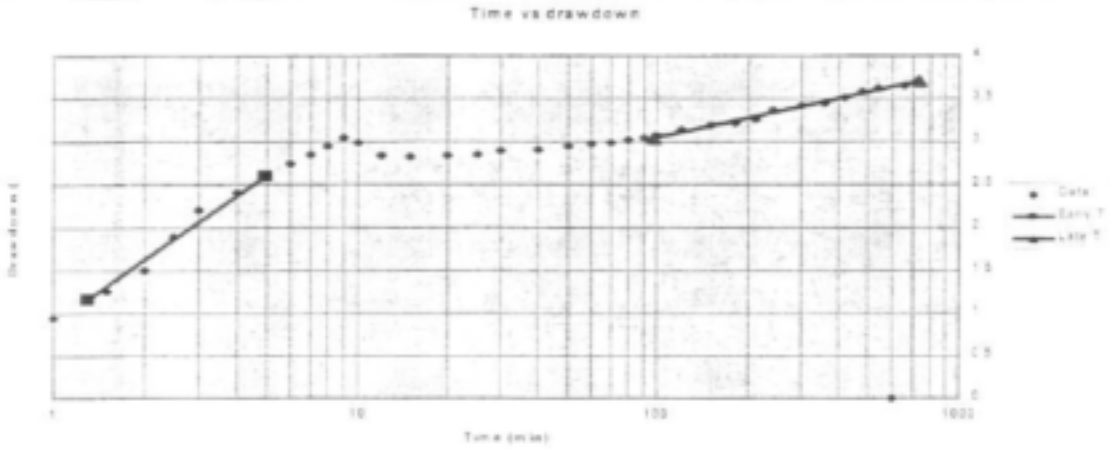
Time vs drawdown
Drawdown
Time (mins)
1
10
100
1000
Data
Early T
Late T

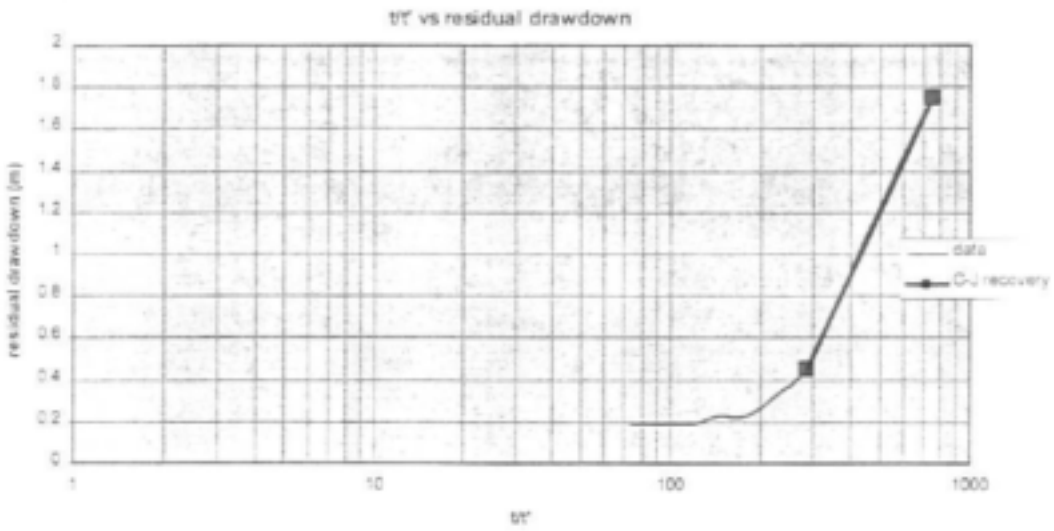
t/t' vs residual drawdown
residual drawdown (m)
t/t'
1
10
100
1000
data
C-J recovery

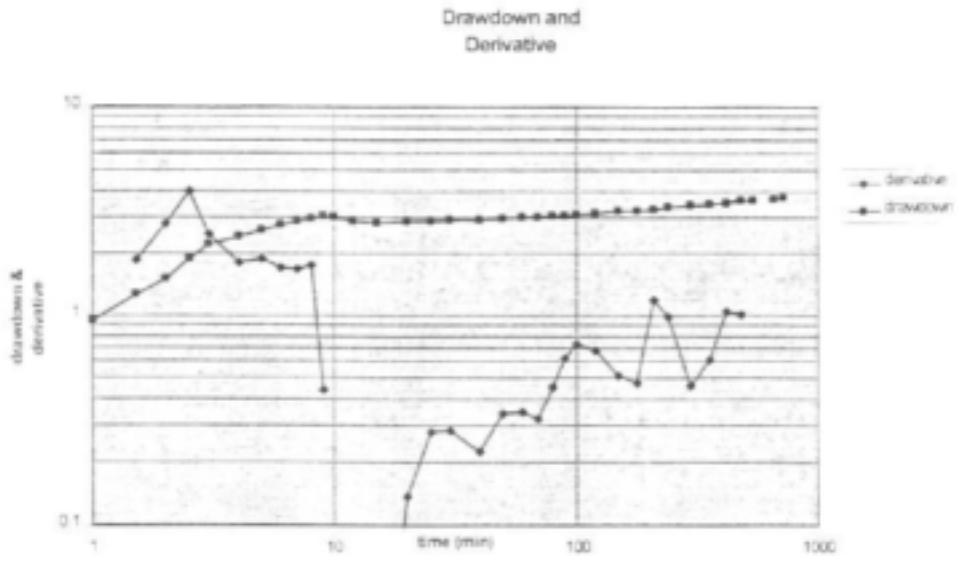
Drawdown and
Derivative
drawdown & derivative
time (min)
1
10
100
1000
0.1
Derivative
Drawdown

X12-09

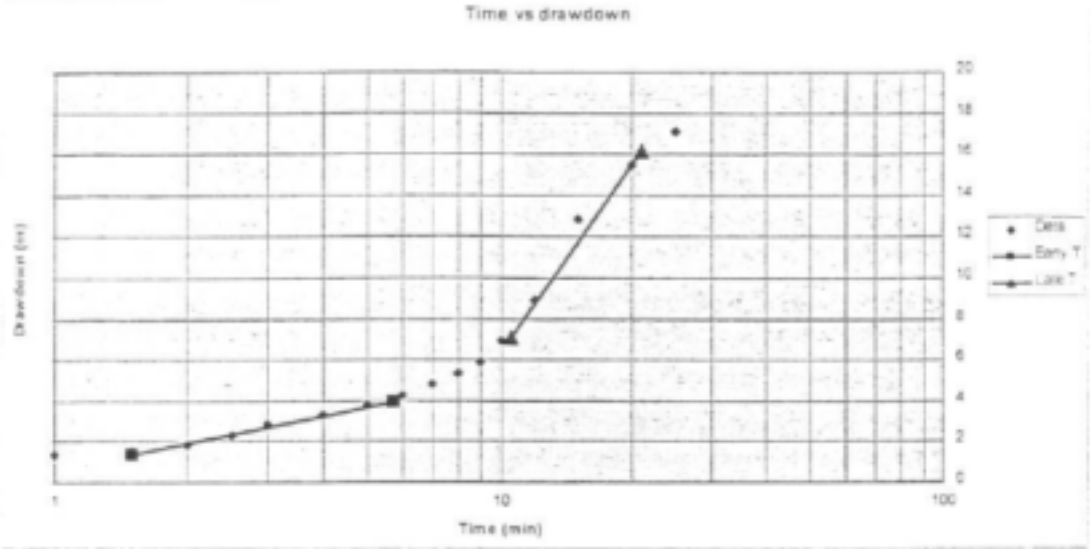
Time vs drawdown
Drawdown (m)
Time (min)
1
10
100
0
2
4
6
8
10
12
14
16
18
20
Data
Early T
Late T

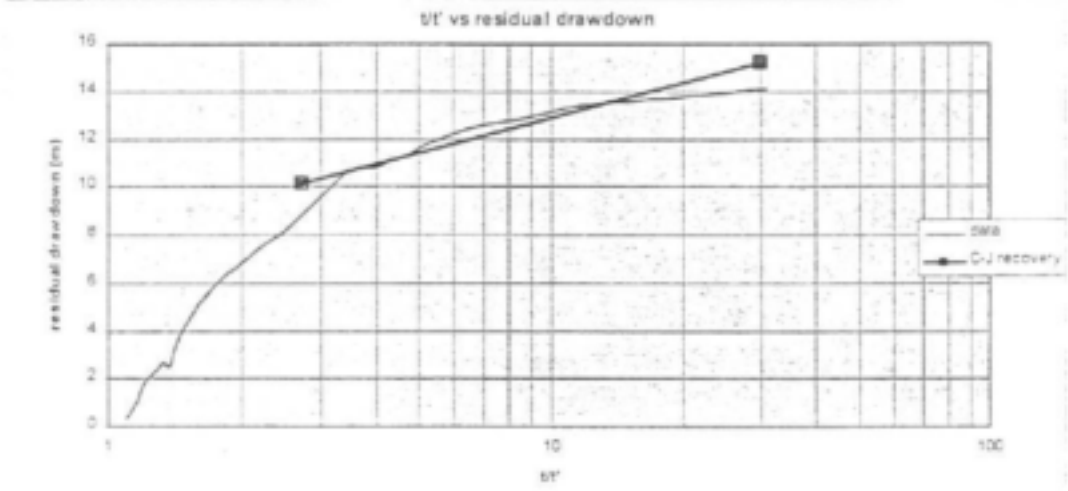
t/t' vs residual drawdown
residual drawdown (m)
t/t'
1
10
100
0
2
4
6
8
10
12
14
16
Data
C-J recovery

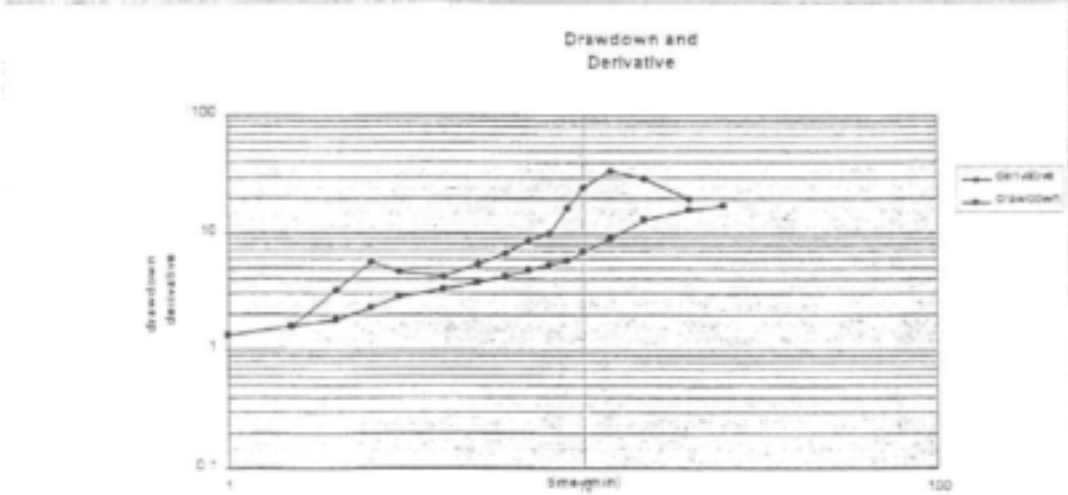
Drawdown and
Derivative
drawdown
derivative
1
10
100
0.1
derivative
drawdown

Other related WRC reports available

A synthesis of the hydrogeology of the Table Mountain Group – formation of a research strategy

Kevin Pietersen and Roger Parsons

A project was initiated during 2000 to synthesize the current knowledge about the Table Mountain Group (TMG) aquifer systems. This resulted in a document on the "Synthesis of the Hydrogeology of TMG – Formation of a Research Strategy." The document is subdivided into technical papers and appropriate case studies. This exercise resulted in the understanding that to realize the potential, of this groundwater supply, many uncertainties and barriers need to be overcome, including: deficient understanding of the occurrence, attributes and dynamics of TMG aquifer systems; lack of understanding of environmental impacts of exploitation; and uncertainties about how best to manage the resource within a multi-objective environment. Research of a multi-disciplinary nature is thus needed to find appropriate answers to questions concerning the water resource potential and optimal management of TMG aquifers, in the interest of furthering integrated water resource management in the region.

Report Number: TT 158/01 **ISBN 1 86845 804 0**

Grounwater vulnerability to pollution in urban catchments

OTN Sililo, IC Saayman, MV Fey

This report lists a number of methods for vulnerability assessments, which include empirical, deterministic, probabilistic and stochastic methods. A serious omission is risk-based approaches to pollution risk. The report further discusses current techniques used in South Africa and the limitations of these techniques. However, adoption of "classical" vulnerability mapping methods may cause problems, because they do not deal with fractured rock systems. Further attention is given to soils, and its role in vulnerability assessments. Finally a research strategy is formulated which should form the core of a research programme to be developed on "Groundwater Quality Impacts and Protection".

Report Number: 1008/01 **ISBN 1 86845 783 4**

Water Research Commissio
Private Bag X03, Gezina, 0031, South Africa
Tel: +27 12 330 0340, Fax: +27 12 331 2565
Web: http://www.wrc.org.za